

RESERVOIR

FOURTH EDITION

Remove Watermark Now

TAREK AHMED

ENGINEERING

HANDBOOK

pdfelement



Gulf Professional Publishing is an imprint of Elsevier
 30 Corporate Drive, Suite 400, Burlington, MA 01803, USA
 The Boulevard, Langford Lane, Kidlington, Oxford, OX5 1GB, UK

© 2010 ELSEVIER Inc. All rights reserved.

No part of this publication may be reproduced or transmitted in any form or by any means, electronic or mechanical, including photocopying, recording, or any information storage and retrieval system, without permission in writing from the publisher. Details on how to seek permission, further information about the Publisher's permissions policies and our arrangements with organizations such as the Copyright Clearance Center and the Copyright Licensing Agency, can be found at our website: www.elsevier.com/permissions.

This book and the individual contributions contained in it are protected under copyright by the Publisher (other than as may be noted herein).

Notices

Knowledge and best practice in this field are constantly changing. As new research and experience broaden our understanding, changes in research methods, professional practices, or medical treatment may become necessary.

Practitioners and researchers must always rely on their own experience and knowledge in evaluating and using any information, methods, compounds, or experiments described herein. In using such information or methods they should be mindful of their own safety and the safety of others, including parties for whom they have a professional responsibility.

To the fullest extent of the law, neither the Publisher nor the authors, contributors, or editors, assume any liability for any injury and/or damage to persons or property as a matter of products liability, negligence or otherwise, or from any use or operation of any methods, products, instructions, or ideas contained in the material herein.

Library of Congress Cataloging-in-Publication Data

Ahmed, Tarek H., 1946–

Reservoir engineering handbook / Tarek Ahmed.—4th ed.

p. cm.

Includes bibliographical references and index.

ISBN 978-1-85617-803-7 (alk. paper)

1. Oil reservoir engineering. 2. Oil fields. 3. Gas reservoirs. I. Title.

TN871.A337 2010

622'.3382—dc22

2009039148

British Library Cataloguing-in-Publication Data

A catalogue record for this book is available from the British Library.

For information on all Gulf Professional Publishing publications visit our Web site at www.elsevierdirect.com

10 11 12 13 8 7 6 5 4 3 2 1

Printed in the United States of America.

Working together to grow
 libraries in developing countries

www.elsevier.com | www.bookaid.org | www.sabre.org

ELSEVIER

BOOK AID
 International

Sabre Foundation

*This book is dedicated to my children,
Jennifer, Justin, Brittany, and Carsen Ahmed.*

The book is also dedicated to a very special person, "Wendy."



ACKNOWLEDGMENTS

Much of the material on which this book is based was drawn from the publications of the Society of Petroleum Engineers (SPE). Tribute is due to the SPE and the petroleum engineers, scientists, and authors who have made numerous and significant contributions to the field of reservoir engineering. This book reflects my style of teaching during my tenure at Montana Tech of the University of Montana and my understanding of the subject of reservoir engineering. I would like to thank all my former students at Montana Tech for putting up with me and my Egyptian temper.

I hope that my friends and colleagues in academia will enjoy this edition of the book. Special thanks to Dr. Bob Chase, Dr. Tom Blasingame, Dr. J. Tiab, Dr. F. Civan, and Dr. Nathan Meehan for their constructive (I think) criticisms and discussions. I would like also to thank the Petroleum faculty and their students at Cairo University and Suez Canal University for their suggestions for updating and improving the book.

It was my pleasure to spend the past 7 years with Anadarko Petroleum and work with an outstanding group of professionals. Special thanks to Kevin Corrigan, Brian Roux, Diana McCranie, and Aydin Centilmen.

I would like to thank the editorial and production staff of Elsevier for their work and professionalism, particularly Ken McCombs and Sarah Binns.

PREFACE TO THE FOURTH EDITION

To make the fourth edition of this textbook as complete as possible, I have added Chapter 17 that deals with the topics of Fracture Reservoirs and Hydraulically Fracture Wells. The book documents the technical materials that have published and addressed this subject over the last 20 years, particularly the research work that has been authored by Dr. H. Kazemi and Dr. Steve Holditch.

PREFACE TO THE THIRD EDITION

To make the third edition of this textbook as complete as possible, I have included the following: a new chapter on decline curve and type curve analysis, a section on tight and shallow gas reservoirs, and water-flood surveillance techniques.

Many of my colleagues have provided me with valuable recommendations and suggestions that I have included through the textbook to make it more comprehensive in treating the subject of reservoir engineering.

PREFACE TO THE SECOND EDITION

I have attempted to construct the chapters following a sequence that I have used for several years in teaching three undergraduate courses in reservoir engineering. Two new chapters have been included in this second edition; Chapters 14 and 15. Chapter 14 reviews principles of waterflooding with emphasis on the design of a waterflooding project. Chapter 15 is intended to introduce and document the practical applications of equations of state in the area of vapor-liquid phase equilibria. A comprehensive review of different equations of state is presented with an emphasis on the Peng-Robinson equation of state.

PREFACE TO THE FIRST EDITION

This book explains the fundamentals of reservoir engineering and their practical application in conducting a comprehensive field study. Chapter 1 reviews fundamentals of reservoir fluid behavior with an emphasis on the classification of reservoir and reservoir fluids. Chapter 2 documents reservoir-fluid properties, while Chapter 3 presents a comprehensive treatment and description of the routine and specialized PVT laboratory tests. The fundamentals of rock properties are discussed in Chapter 4 and numerous methodologies for generating those properties are reviewed. Chapter 5 focuses on presenting the concept of relative permeability and its applications in fluid flow calculations.

The fundamental mathematical expressions that are used to describe the reservoir fluid flow behavior in porous media are discussed in Chapter 6, while Chapters 7 and 8 describe the principle of oil and gas well performance calculations, respectively. Chapter 9 provides the theoretical analysis of coning and outlines many of the practical solutions for calculating water and gas coning behavior. Various water influx calculation models are shown in Chapter 10, along with detailed descriptions of the computational steps involved in applying these models. The objective of Chapter 11 is to introduce the basic principle of oil recovery mechanisms and to present the generalized form of the material balance equation. Chapters 12 and 13 focus on illustrating the practical applications of the material balance equation in oil and gas reservoirs.

ABOUT THE AUTHOR

Tarek Ahmed, Ph.D., P.E. is a Senior Reservoir Engineering Advisor with Baker Hughes International at the Reservoir Engineering Technology Center. Before joining BHI, Dr. Ahmed was a professor and the head of the Petroleum Engineering Department at Montana Tech of University of Montana. Until recently he was a Reservoir Engineering Advisor with Anadarko Petroleum. He holds a Ph.D. from Oklahoma University, an M.S. from the University of Missouri-Rolla, and a B.S. from the Faculty of Petroleum (Egypt)—all degrees in Petroleum Engineering. Dr. Ahmed is also the author of other textbooks including *Hydrocarbon Phase Behavior* (Gulf Publishing Company, 1989), *Advanced Reservoir Engineering* (Elsevier, 2005), and *Equations of State and PVT Analysis* (Gulf Publishing, 2007).

C H A P T E R 1

FUNDAMENTALS OF RESERVOIR FLUID BEHAVIOR

Naturally occurring hydrocarbon systems found in petroleum reservoirs are mixtures of organic compounds that exhibit multiphase behavior over wide ranges of pressures and temperatures. These hydrocarbon accumulations may occur in the gaseous state, the liquid state, the solid state, or in various combinations of gas, liquid, and solid.

These differences in phase behavior, coupled with the physical properties of reservoir rock that determine the relative ease with which gas and liquid are transmitted or retained, result in many diverse types of hydrocarbon reservoirs with complex behaviors. Frequently, petroleum engineers have the task to study the behavior and characteristics of a petroleum reservoir and to determine the course of future development and production that would maximize the profit.

The objective of this chapter is to review the basic principles of reservoir fluid phase behavior and illustrate the use of phase diagrams in classifying types of reservoirs and the native hydrocarbon systems.

CLASSIFICATION OF RESERVOIRS AND RESERVOIR FLUIDS

Petroleum reservoirs are broadly classified as oil or gas reservoirs. These broad classifications are further subdivided depending on:

- The composition of the reservoir hydrocarbon mixture
- Initial reservoir pressure and temperature
- Pressure and temperature of the surface production

The conditions under which these phases exist are a matter of considerable practical importance. The experimental or the mathematical determinations of these conditions are conveniently expressed in different types of diagrams commonly called *phase diagrams*. One such diagram is called the *pressure-temperature diagram*.

Pressure-Temperature Diagram

Figure 1-1 shows a typical pressure-temperature diagram of a multi-component system with a specific overall composition. Although a different hydrocarbon system would have a different phase diagram, the general configuration is similar.

These multicomponent pressure-temperature diagrams are essentially used to:

- Classify reservoirs
- Classify the naturally occurring hydrocarbon systems
- Describe the phase behavior of the reservoir fluid

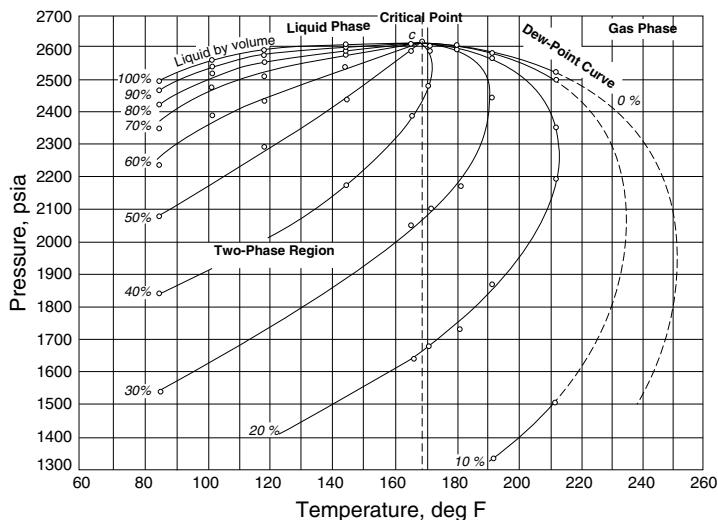


Figure 1-1. Typical p-T diagram for a multicomponent system.

To fully understand the significance of the pressure-temperature diagrams, it is necessary to identify and define the following key points on these diagrams:

- **Cricodentherm (T_{ct})**—The Cricodentherm is defined as the maximum temperature above which liquid cannot be formed regardless of pressure (point E). The corresponding pressure is termed the Cricodentherm pressure p_{ct} .
- **Cricodenbar (p_{cb})**—The Cricodenbar is the maximum pressure above which no gas can be formed regardless of temperature (point D). The corresponding temperature is called the Cricodenbar temperature T_{cb} .
- **Critical point**—The critical point for a multicomponent mixture is referred to as the state of pressure and temperature at which all intensive properties of the gas and liquid phases are equal (point C). At the critical point, the corresponding pressure and temperature are called the critical pressure p_c and critical temperature T_c of the mixture.
- **Phase envelope (two-phase region)**—The region enclosed by the bubble-point curve and the dew-point curve (line BCA), wherein gas and liquid coexist in equilibrium, is identified as the phase envelope of the hydrocarbon system.
- **Quality lines**—The dashed lines within the phase diagram are called quality lines. They describe the pressure and temperature conditions for equal volumes of liquids. Note that the quality lines converge at the critical point (point C).
- **Bubble-point curve**—The bubble-point curve (line BC) is defined as the line separating the liquid-phase region from the two-phase region.
- **Dew-point curve**—The dew-point curve (line AC) is defined as the line separating the vapor-phase region from the two-phase region.

In general, reservoirs are conveniently classified on the basis of the location of the point representing the initial reservoir pressure p_i and temperature T with respect to the pressure-temperature diagram of the reservoir fluid. Accordingly, reservoirs can be classified into basically two types. These are:

- **Oil reservoirs**—If the reservoir temperature T is less than the critical temperature T_c of the reservoir fluid, the reservoir is classified as an oil reservoir.

- **Gas reservoirs**—If the reservoir temperature is greater than the critical temperature of the hydrocarbon fluid, the reservoir is considered a gas reservoir.

Oil Reservoirs

Depending upon initial reservoir pressure p_i , oil reservoirs can be sub-classified into the following categories:

1. **Undersaturated oil reservoir.** If the initial reservoir pressure p_i (as represented by point 1 on Figure 1-1), is greater than the bubble-point pressure p_b of the reservoir fluid, the reservoir is labeled an undersaturated oil reservoir.
2. **Saturated oil reservoir.** When the initial reservoir pressure is equal to the bubble-point pressure of the reservoir fluid, as shown on Figure 1-1 by point 2, the reservoir is called a saturated oil reservoir.
3. **Gas-cap reservoir.** If the initial reservoir pressure is below the bubble-point pressure of the reservoir fluid, as indicated by point 3 on Figure 1-1, the reservoir is termed a gas-cap or two-phase reservoir, in which the gas or vapor phase is underlain by an oil phase. The appropriate quality line gives the ratio of the gas-cap volume to reservoir oil volume.

Crude oils cover a wide range in physical properties and chemical compositions, and it is often important to be able to group them into broad categories of related oils. In general, crude oils are commonly classified into the following types:

- Ordinary black oil
- Low-shrinkage crude oil
- High-shrinkage (volatile) crude oil
- Near-critical crude oil

The above classifications are essentially based upon the properties exhibited by the crude oil, including physical properties, composition, gas-oil ratio, appearance, and pressure-temperature phase diagrams.

1. **Ordinary black oil.** A typical pressure-temperature phase diagram for ordinary black oil is shown in Figure 1-2. It should be noted that quality lines, which are approximately equally spaced, characterize this black oil phase diagram. Following the pressure reduction path as indicated by the vertical line EF on Figure 1-2, the liquid shrinkage curve, as shown in Figure 1-3, is prepared by plotting the liquid volume percent as a function of pressure. The liquid shrinkage curve approxi-

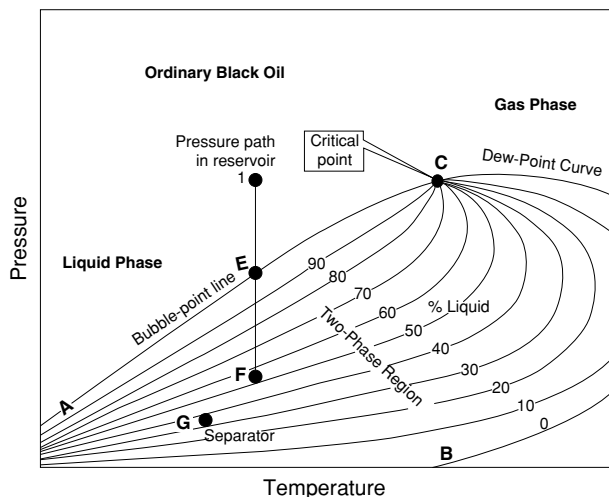


Figure 1-2. A typical p-T diagram for an ordinary black oil.

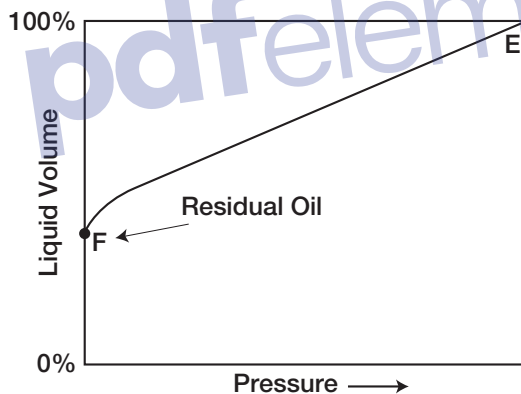


Figure 1-3. Liquid-shrinkage curve for black oil.

mates a straight line except at very low pressures. When produced, ordinary black oils usually yield gas-oil ratios between 200 and 700 scf/STB and oil gravities of 15° to 40° API. The stock tank oil is usually brown to dark green in color.

2. **Low-shrinkage oil.** A typical pressure-temperature phase diagram for low-shrinkage oil is shown in Figure 1-4. The diagram is characterized by quality lines that are closely spaced near the dew-point curve. The liquid-shrinkage curve, as given in Figure 1-5, shows the shrinkage characteristics of this category of crude oils. The other associated properties of this type of crude oil are:

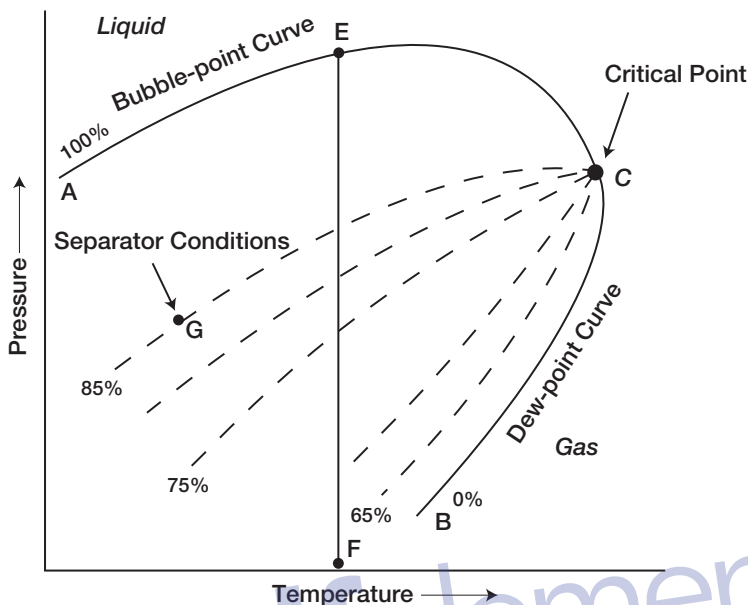


Figure 1-4. A typical phase diagram for a low-shrinkage oil.

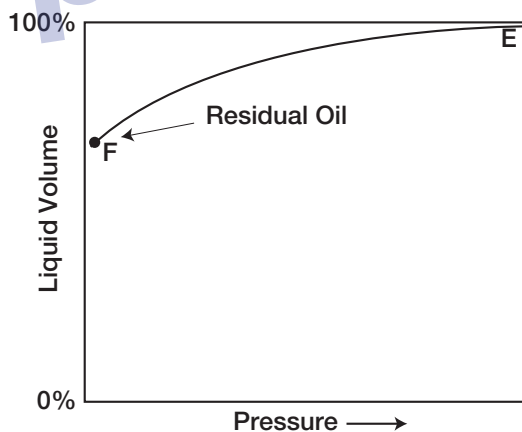


Figure 1-5. Oil-shrinkage curve for low-shrinkage oil.

- Oil formation volume factor less than 1.2 bbl/STB
- Gas-oil ratio less than 200 scf/STB
- Oil gravity less than 35° API
- Black or deeply colored
- Substantial liquid recovery at separator conditions as indicated by point G on the 85% quality line of Figure 1-4

3. **Volatile crude oil.** The phase diagram for a volatile (high-shrinkage) crude oil is given in Figure 1-6. Note that the quality lines are close together near the bubble-point and are more widely spaced at lower pressures. This type of crude oil is commonly characterized by a high liquid shrinkage immediately below the bubble-point as shown in Figure 1-7. The other characteristic properties of this oil include:

- Oil formation volume factor less than 2 bbl/STB
- Gas-oil ratios between 2,000 and 3,200 scf/STB
- Oil gravities between 45° and 55° API

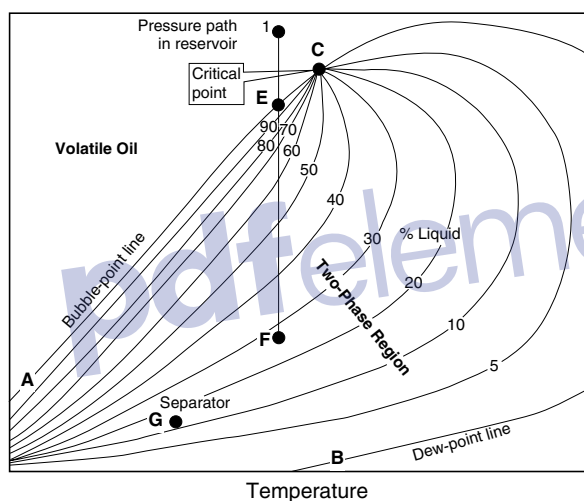


Figure 1-6. A typical p-T diagram for a volatile crude oil.

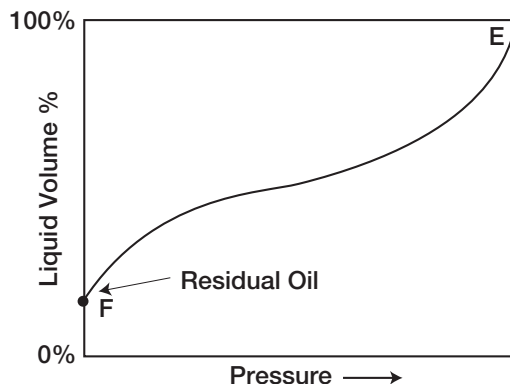


Figure 1-7. A typical liquid-shrinkage curve for a volatile crude oil.

- Lower liquid recovery of separator conditions as indicated by point G on Figure 1-6
- Greenish to orange in color

Another characteristic of volatile oil reservoirs is that the API gravity of the stock-tank liquid will increase in the later life of the reservoirs.

4. **Near-critical crude oil.** If the reservoir temperature T is near the critical temperature T_c of the hydrocarbon system, as shown in Figure 1-8, the hydrocarbon mixture is identified as a near-critical crude oil. Because all the quality lines converge at the critical point, an isothermal pressure drop (as shown by the vertical line EF in Figure 1-8) may shrink the crude oil from 100% of the hydrocarbon pore volume at the bubble-point to 55% or less at a pressure 10 to 50 psi below the bubble-point. The shrinkage characteristic behavior of the near-critical crude oil is shown in Figure 1-9. The near-critical crude oil is characterized by a high GOR in excess of 3,000 scf/STB with an oil formation volume factor of 2.0 bbl/STB or higher. The compositions of near-critical oils are usually characterized by 12.5 to 20 mol% heptanes-plus, 35% or more of ethane through hexanes, and the remainder methane.

Figure 1-10 compares the characteristic shape of the liquid-shrinkage curve for each crude oil type.

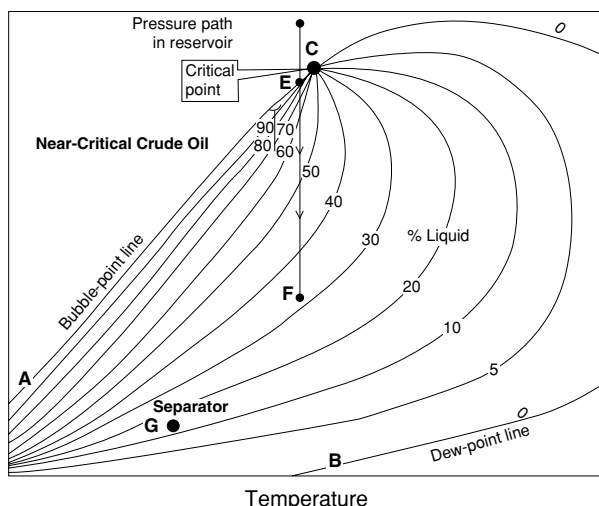


Figure 1-8. A schematic phase diagram for the near-critical crude oil.

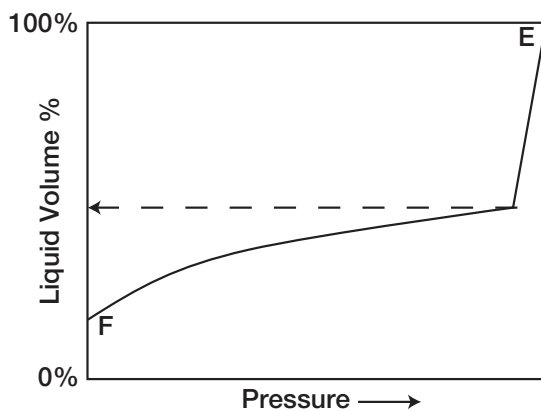


Figure 1-9. A typical liquid-shrinkage curve for the near-critical crude oil.

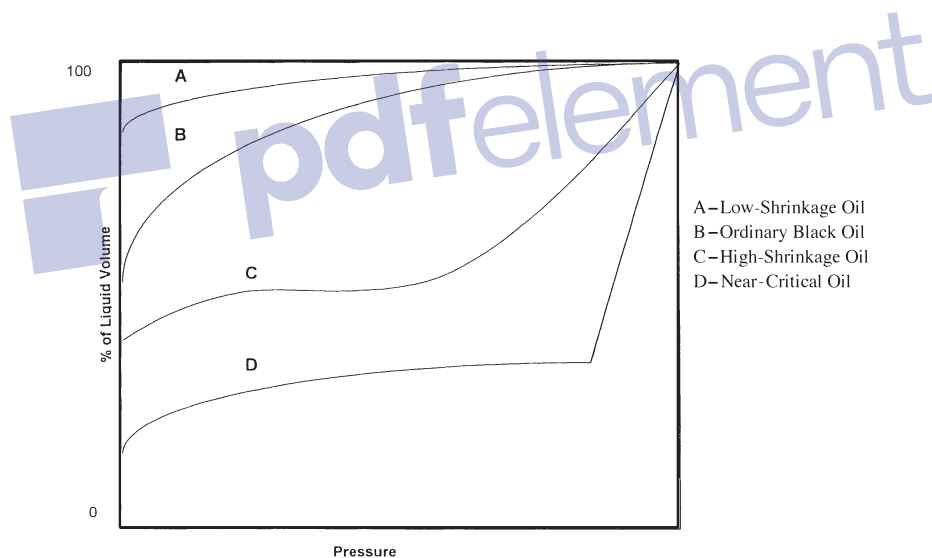


Figure 1-10. Liquid shrinkage for crude oil systems.

Gas Reservoirs

In general, if the reservoir temperature is above the critical temperature of the hydrocarbon system, the reservoir is classified as a natural gas reservoir. On the basis of their phase diagrams and the prevailing reservoir conditions, natural gases can be classified into four categories:

- Retrograde gas-condensate
- Near-critical gas-condensate
- Wet gas
- Dry gas

Retrograde gas-condensate reservoir. If the reservoir temperature T lies between the critical temperature T_c and cricondentherm T_{ct} of the reservoir fluid, the reservoir is classified as a retrograde gas-condensate reservoir. This category of gas reservoir is a unique type of hydrocarbon accumulation in that the special thermodynamic behavior of the reservoir fluid is the controlling factor in the development and the depletion process of the reservoir. When the pressure is decreased on these mixtures, instead of expanding (if a gas) or vaporizing (if a liquid) as might be expected, they vaporize instead of condensing.

Consider that the initial condition of a retrograde gas reservoir is represented by point 1 on the pressure-temperature phase diagram of Figure 1-11. Because the reservoir pressure is above the upper dew-point pressure, the hydrocarbon system exists as a single phase (i.e., vapor phase) in the reservoir. As the reservoir pressure declines isothermally during production from the initial pressure (point 1) to the upper dew-point pressure (point 2), the attraction between the molecules of the light and heavy components causes them to move farther apart. As this occurs,

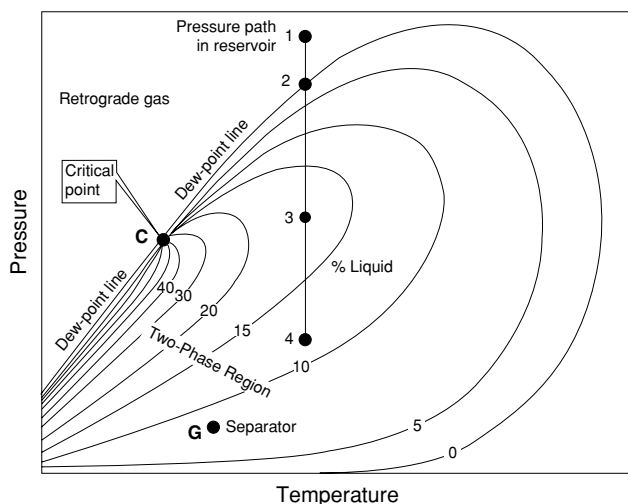


Figure 1-11. A typical phase diagram of a retrograde system.

attraction between the heavy component molecules becomes more effective; thus, liquid begins to condense.

This retrograde condensation process continues with decreasing pressure until the liquid dropout reaches its maximum at point 3. Further reduction in pressure permits the heavy molecules to commence the normal vaporization process. This is the process whereby fewer gas molecules strike the liquid surface, which causes more molecules to leave than enter the liquid phase. The vaporization process continues until the reservoir pressure reaches the lower dew-point pressure. This means that all the liquid that formed must vaporize because the system is essentially all vapors at the lower dew point.

Figure 1-12 shows a typical liquid shrinkage volume curve for a condensate system. The curve is commonly called the **liquid dropout curve**. In most gas-condensate reservoirs, the condensed liquid volume seldom exceeds more than 15% to 19% of the pore volume. This liquid saturation is not large enough to allow any liquid flow. It should be recognized, however, that around the wellbore where the pressure drop is high, enough liquid dropout might accumulate to give two-phase flow of gas and retrograde liquid.

The associated physical characteristics of this category are:

- Gas-oil ratios between 8,000 and 70,000 scf/STB. Generally, the gas-oil ratio for a condensate system increases with time due to the liquid dropout and the loss of heavy components in the liquid.

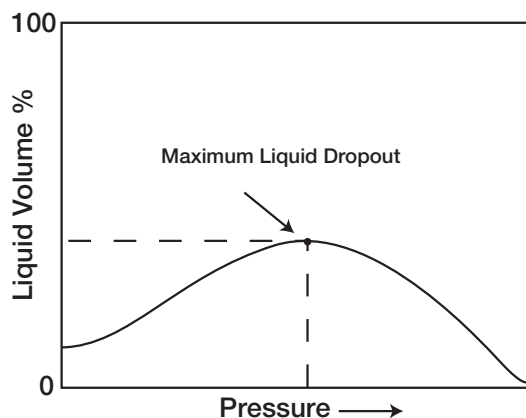


Figure 1-12. A typical liquid dropout curve.

- Condensate gravity above 50° API
- Stock-tank liquid is usually water-white or slightly colored.

There is a fairly sharp dividing line between oils and condensates from a compositional standpoint. Reservoir fluids that contain heptanes and are heavier in concentrations of more than 12.5 mol% are almost always in the liquid phase in the reservoir. Oils have been observed with heptanes and heavier concentrations as low as 10% and condensates as high as 15.5%. These cases are rare, however, and usually have very high tank liquid gravities.

Near-critical gas-condensate reservoir. If the reservoir temperature is near the critical temperature, as shown in Figure 1-13, the hydrocarbon mixture is classified as a near-critical gas condensate. The volumetric behavior of this category of natural gas is described through the isothermal pressure declines as shown by the vertical line 1-3 in Figure 1-13 and also by the corresponding liquid dropout curve of Figure 1-14. Because all the quality lines converge at the critical point, a rapid liquid buildup will immediately occur below the dew point (Figure 1-14) as the pressure is reduced to point 2.

This behavior can be justified by the fact that several quality lines are crossed very rapidly by the isothermal reduction in pressure. At the point where the liquid ceases to build up and begins to shrink again, the

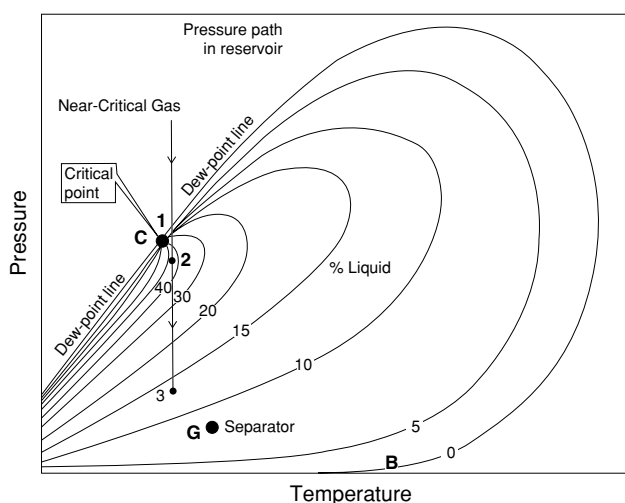


Figure 1-13. A typical phase diagram for a near-critical gas condensate reservoir.

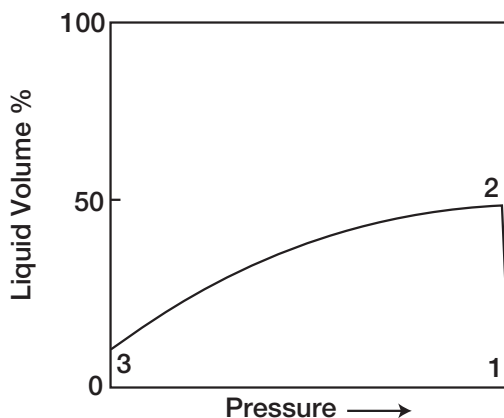


Figure 1-14. Liquid-shrinkage curve for a near-critical gas-condensate system.

reservoir goes from the retrograde region to a normal vaporization region.

Wet-gas reservoir. A typical phase diagram of a wet gas is shown in Figure 1-15, where reservoir temperature is above the cricondentherm of the hydrocarbon mixture. Because the reservoir temperature exceeds the cricondentherm of the hydrocarbon system, the reservoir fluid will always remain in the vapor phase region as the reservoir is depleted isothermally, along the vertical line A-B.

As the produced gas flows to the surface, however, the pressure and temperature of the gas will decline. If the gas enters the two-phase region, a liquid phase will condense out of the gas and be produced from the surface separators. This is caused by a sufficient decrease in the kinetic energy of heavy molecules with temperature drop and their subsequent change to liquid through the attractive forces between molecules.

Wet-gas reservoirs are characterized by the following properties:

- Gas oil ratios between 60,000 and 100,000 scf/STB
- Stock-tank oil gravity above 60° API
- Liquid is water-white in color
- Separator conditions, i.e., separator pressure and temperature, lie within the two-phase region

Dry-gas reservoir. The hydrocarbon mixture exists as a gas both in the reservoir and in the surface facilities. The only liquid associated

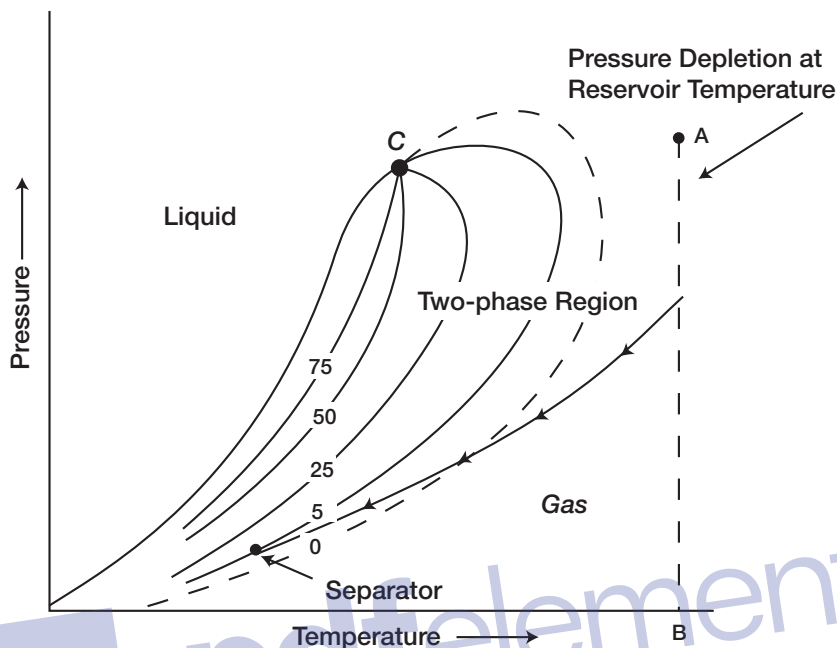


Figure 1-15. Phase diagram for a wet gas. (After Clark, N.J. Elements of Petroleum Reservoirs, SPE, 1969.)

with the gas from a dry-gas reservoir is water. A phase diagram of a dry-gas reservoir is given in Figure 1-16. Usually a system having a gas-oil ratio greater than 100,000 scf/STB is considered to be a dry gas.

Kinetic energy of the mixture is so high and attraction between molecules so small that none of them coalesces to a liquid at stock-tank conditions of temperature and pressure.

It should be pointed out that the classification of hydrocarbon fluids might also be characterized by the initial composition of the system. McCain (1994) suggested that the heavy components in the hydrocarbon mixtures have the strongest effect on fluid characteristics. The ternary diagram, as shown in Figure 1-17, with equilateral triangles can be conveniently used to roughly define the compositional boundaries that separate different types of hydrocarbon systems.

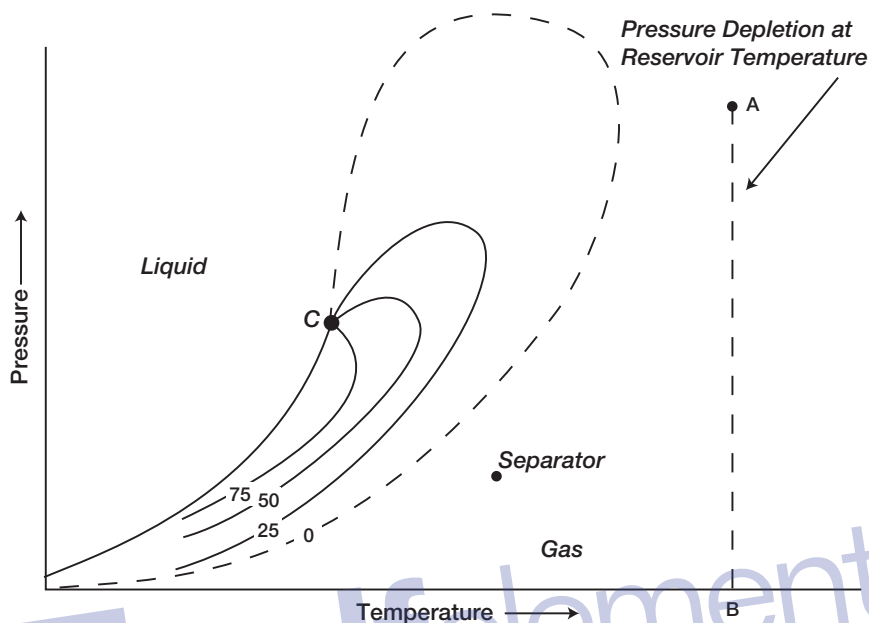
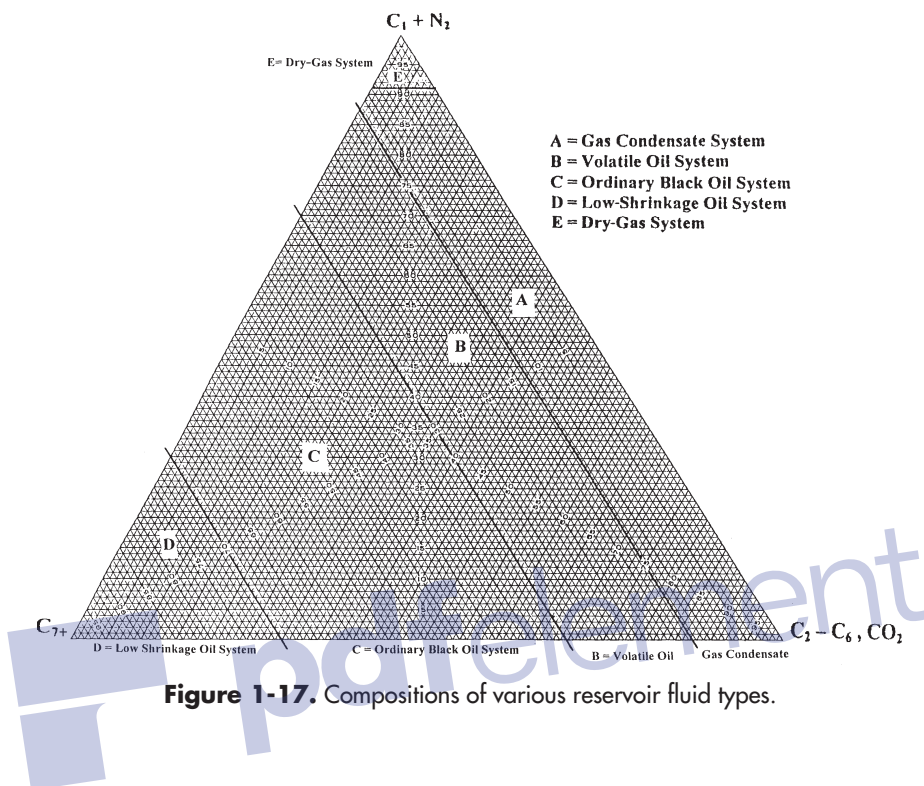


Figure 1-16. Phase diagram for a dry gas. (After Clark, N.J. Elements of Petroleum Reservoirs, SPE, 1969.)

From the foregoing discussion, it can be observed that hydrocarbon mixtures may exist either the gaseous or liquid state, depending on the reservoir and operating conditions to which they are subjected. The qualitative concepts presented may be of aid in developing quantitative analyses. Empirical equations of state are commonly used as a quantitative tool in describing and classifying the hydrocarbon system. These equations of state require:

- Detailed compositional analyses of the hydrocarbon system
- Complete descriptions of the physical and critical properties of the mixture individual components

Many characteristic properties of these individual components (in other words, pure substances) have been measured and compiled over the years. These properties provide vital information for calculating the



thermodynamic properties of pure components, as well as their mixtures. The most important of these properties are:

- Critical pressure, p_c
- Critical temperature, T_c
- Critical volume, V_c
- Critical compressibility factor, z_c
- Acentric factor, T
- Molecular weight, M

Table 1-2 documents the above-listed properties for a number of hydrocarbon and nonhydrocarbon components.

Katz and Firoozabadi (1978) presented a generalized set of physical properties for the petroleum fractions C_6 through C_{45} . The tabulated properties include the average boiling point, specific gravity, and molecular weight. The authors proposed a set of tabulated properties

that were generated by analyzing the physical properties of 26 condensates and crude oil systems. These generalized properties are given in Table 1-1.

Ahmed (1985) correlated the Katz-Firoozabadi-tabulated physical properties with the number of carbon atoms of the fraction by using a regression model. The generalized equation has the following form:

$$\theta = a_1 + a_2 n + a_3 n^2 + a_4 n^3 + (a_5/n) \quad (1-1)$$

where θ = any physical property
 n = number of carbon atoms, i.e., 6, 7, . . . , 45
 a_1 – a_5 = coefficients of the equation and are given in Table 1-3

Undefined Petroleum Fractions

Nearly all naturally occurring hydrocarbon systems contain a quantity of heavy fractions that are not well defined and are not mixtures of discretely identified components. These heavy fractions are often lumped together and identified as the plus fraction, e.g., C_{7+} fraction.

A proper description of the physical properties of the plus fractions and other undefined petroleum fractions in hydrocarbon mixtures is essential in performing reliable phase behavior calculations and compositional modeling studies. Frequently, a distillation analysis or a chromatographic analysis is available for this undefined fraction. Other physical properties, such as molecular weight and specific gravity, may also be measured for the entire fraction or for various cuts of it.

To use any of the thermodynamic property-prediction models, e.g., equation of state, to predict the phase and volumetric behavior of complex hydrocarbon mixtures, one must be able to provide the acentric factor, along with the critical temperature and critical pressure, for both the defined and undefined (heavy) fractions in the mixture. The problem of how to adequately characterize these undefined plus fractions in terms of their critical properties and acentric factors has been long recognized in the petroleum industry. Whitson (1984) presented an excellent documentation on the influence of various heptanes-plus (C_{7+}) characterization schemes on predicting the volumetric behavior of hydrocarbon mixtures by equations-of-state.

(text continued on page 24)

Table 1-1
Generalized Physical Properties

| Group | T _b (°R) | γ | K | M | T _c (°R) | P _c (psia) | ω | V _c (ft ³ /lb) | Group |
|-----------------|---------------------|-------|-------|-----|---------------------|-----------------------|-------|--------------------------------------|-----------------|
| C ₆ | 607 | 0.690 | 12.27 | 84 | 923 | 483 | 0.250 | 0.06395 | C ₆ |
| C ₇ | 658 | 0.727 | 11.96 | 96 | 985 | 453 | 0.280 | 0.06289 | C ₇ |
| C ₈ | 702 | 0.749 | 11.87 | 107 | 1,036 | 419 | 0.312 | 0.06264 | C ₈ |
| C ₉ | 748 | 0.768 | 11.82 | 121 | 1,085 | 383 | 0.348 | 0.06258 | C ₉ |
| C ₁₀ | 791 | 0.782 | 11.83 | 134 | 1,128 | 351 | 0.385 | 0.06273 | C ₁₀ |
| C ₁₁ | 829 | 0.793 | 11.85 | 147 | 1,166 | 325 | 0.419 | 0.06291 | C ₁₁ |
| C ₁₂ | 867 | 0.804 | 11.86 | 161 | 1,203 | 302 | 0.454 | 0.06306 | C ₁₂ |
| C ₁₃ | 901 | 0.815 | 11.85 | 175 | 1,236 | 286 | 0.484 | 0.06311 | C ₁₃ |
| C ₁₄ | 936 | 0.826 | 11.84 | 190 | 1,270 | 270 | 0.516 | 0.06316 | C ₁₄ |
| C ₁₅ | 971 | 0.836 | 11.84 | 206 | 1,304 | 255 | 0.550 | 0.06325 | C ₁₅ |
| C ₁₆ | 1,002 | 0.843 | 11.87 | 222 | 1,332 | 241 | 0.582 | 0.06342 | C ₁₆ |
| C ₁₇ | 1,032 | 0.851 | 11.87 | 237 | 1,360 | 230 | 0.613 | 0.06350 | C ₁₇ |
| C ₁₈ | 1,055 | 0.856 | 11.89 | 251 | 1,380 | 222 | 0.638 | 0.06362 | C ₁₈ |
| C ₁₉ | 1,077 | 0.861 | 11.91 | 263 | 1,400 | 214 | 0.662 | 0.06372 | C ₁₉ |
| C ₂₀ | 1,101 | 0.866 | 11.92 | 275 | 1,421 | 207 | 0.690 | 0.06384 | C ₂₀ |
| C ₂₁ | 1,124 | 0.871 | 11.94 | 291 | 1,442 | 200 | 0.717 | 0.06394 | C ₂₁ |
| C ₂₂ | 1,146 | 0.876 | 11.95 | 300 | 1,461 | 193 | 0.743 | 0.06402 | C ₂₂ |
| C ₂₃ | 1,167 | 0.881 | 11.95 | 312 | 1,480 | 188 | 0.768 | 0.06408 | C ₂₃ |
| C ₂₄ | 1,187 | 0.885 | 11.96 | 324 | 1,497 | 182 | 0.793 | 0.06417 | C ₂₄ |

| | | | | | | | | | |
|-----------------|-------|-------|-------|-----|-------|-----|-------|---------|-----------------|
| C ₂₅ | 1,207 | 0.888 | 11.99 | 337 | 1,515 | 177 | 0.819 | 0.06431 | C ₂₅ |
| C ₂₆ | 1,226 | 0.892 | 12.00 | 349 | 1,531 | 173 | 0.844 | 0.06438 | C ₂₆ |
| C ₂₇ | 1,244 | 0.896 | 12.00 | 360 | 1,547 | 169 | 0.868 | 0.06443 | C ₂₇ |
| C ₂₈ | 1,262 | 0.899 | 12.02 | 372 | 1,562 | 165 | 0.894 | 0.06454 | C ₂₈ |
| C ₂₉ | 1,277 | 0.902 | 12.03 | 382 | 1,574 | 161 | 0.915 | 0.06459 | C ₂₉ |
| C ₃₀ | 1,294 | 0.905 | 12.04 | 394 | 1,589 | 158 | 0.941 | 0.06468 | C ₃₀ |
| C ₃₁ | 1,310 | 0.909 | 12.04 | 404 | 1,603 | 143 | 0.897 | 0.06469 | C ₃₁ |
| C ₃₂ | 1,326 | 0.912 | 12.05 | 415 | 1,616 | 138 | 0.909 | 0.06475 | C ₃₂ |
| C ₃₃ | 1,341 | 0.915 | 12.05 | 426 | 1,629 | 134 | 0.921 | 0.06480 | C ₃₃ |
| C ₃₄ | 1,355 | 0.917 | 12.07 | 437 | 1,640 | 130 | 0.932 | 0.06489 | C ₃₄ |
| C ₃₅ | 1,368 | 0.920 | 12.07 | 445 | 1,651 | 127 | 0.942 | 0.06490 | C ₃₅ |
| C ₃₆ | 1,382 | 0.922 | 12.08 | 456 | 1,662 | 124 | 0.954 | 0.06499 | C ₃₆ |
| C ₃₇ | 1,394 | 0.925 | 12.08 | 464 | 1,673 | 121 | 0.964 | 0.06499 | C ₃₇ |
| C ₃₈ | 1,407 | 0.927 | 12.09 | 475 | 1,683 | 118 | 0.975 | 0.06506 | C ₃₈ |
| C ₃₉ | 1,419 | 0.929 | 12.10 | 484 | 1,693 | 115 | 0.985 | 0.06511 | C ₃₉ |
| C ₄₀ | 1,432 | 0.931 | 12.11 | 495 | 1,703 | 112 | 0.997 | 0.06517 | C ₄₀ |
| C ₄₁ | 1,442 | 0.933 | 12.11 | 502 | 1,712 | 110 | 1.006 | 0.06520 | C ₄₁ |
| C ₄₂ | 1,453 | 0.934 | 12.13 | 512 | 1,720 | 108 | 1.016 | 0.06529 | C ₄₂ |
| C ₄₃ | 1,464 | 0.936 | 12.13 | 521 | 1,729 | 105 | 1.026 | 0.06532 | C ₄₃ |
| C ₄₄ | 1,477 | 0.938 | 12.14 | 531 | 1,739 | 103 | 1.038 | 0.06538 | C ₄₄ |
| C ₄₅ | 1,487 | 0.940 | 12.14 | 539 | 1,747 | 101 | 1.048 | 0.06540 | C ₄₅ |

Table 1-2
Physical Properties for Pure Components

| Number | Compound | Formula | A. | | | B. | | | C. | | | D. | | | Critical constants | | |
|--------|---------------------|--------------------------------|----------------------------------|-------------------|--------------------------------|--------------------|----------------------------------|----------------|-----------------|------------------------------|----|----|--|--|--------------------|--|--|
| | | | Molar mass (molecular weight) | Boiling point, °F | Vapor pressure, psia 100 °F | Freezing point, °F | Refractive index, n_D 60 °F | Pressure, psia | Temperature, °F | Volume, ft ³ /lbm | | | | | | | |
| 1 | Methane | CH ₄ | 16.043 | -258.73 | (5000)* | -296.44* | 1.00042* | 666.4 | -116.67 | 0.0988 | 1 | | | | | | |
| 2 | Ethane | C ₂ H ₆ | 30.070 | -127.49 | (800)* | -297.04* | 1.20971* | 706.5 | 89.92 | 0.0783 | 2 | | | | | | |
| 3 | Propane | C ₃ H ₈ | 44.097 | -43.75 | 188.64 | -305.73* | 1.28480* | 616.0 | 206.06 | 0.0727 | 3 | | | | | | |
| 4 | Isobutane | C ₄ H ₁₀ | 58.123 | 10.78 | 72.581 | -255.28 | 1.3245* | 527.9 | 274.46 | 0.0714 | 4 | | | | | | |
| 5 | n-Butane | C ₄ H ₁₀ | 58.123 | 31.08 | 51.706 | -217.05 | 1.35588* | 550.8 | 305.62 | 0.0703 | 5 | | | | | | |
| 6 | Isopentane | C ₅ H ₁₂ | 72.150 | 82.12 | 20.445 | -255.82 | 1.35631 | 490.4 | 369.10 | 0.0679 | 6 | | | | | | |
| 7 | n-Pentane | C ₅ H ₁₂ | 72.150 | 96.92 | 15.574 | -201.51 | 1.35992 | 488.6 | 385.8 | 0.0675 | 7 | | | | | | |
| 8 | Neopentane | C ₅ H ₁₂ | 72.150 | 49.10 | 36.69 | 2.17 | 1.342* | 464.0 | 321.13 | 0.0673 | 8 | | | | | | |
| 9 | n-Hexane | C ₆ H ₁₄ | 86.177 | 155.72 | 4.9597 | -139.58 | 1.37708 | 436.9 | 453.6 | 0.0688 | 9 | | | | | | |
| 10 | 2-Methylpentane | C ₆ H ₁₄ | 86.177 | 140.47 | 6.769 | -244.62 | 1.37387 | 436.6 | 435.83 | 0.0682 | 10 | | | | | | |
| 11 | 3-Methylpentane | C ₆ H ₁₄ | 86.177 | 145.89 | 6.103 | -177.72 | 1.37898 | 453.1 | 448.4 | 0.0682 | 11 | | | | | | |
| 12 | Neohexane | C ₆ H ₁₄ | 86.177 | 121.52 | 9.859 | -147.72 | 1.37126 | 446.8 | 420.13 | 0.0667 | 12 | | | | | | |
| 13 | 2,3-Dimethylbutane | C ₆ H ₁₄ | 86.177 | 136.36 | 7.406 | -199.38 | 1.37730 | 453.5 | 440.29 | 0.0665 | 13 | | | | | | |
| 14 | n-Heptane | C ₇ H ₁₆ | 100.204 | 209.16 | 1.620 | -131.05 | 1.38989 | 396.8 | 512.7 | 0.0691 | 14 | | | | | | |
| 15 | 2-Methylhexane | C ₇ H ₁₆ | 100.204 | 194.09 | 2.272 | -180.89 | 1.38714 | 396.5 | 495.00 | 0.0673 | 15 | | | | | | |
| 16 | 3-Methylhexane | C ₇ H ₁₆ | 100.204 | 197.33 | 2.131 | -181.48 | 1.39091 | 408.1 | 503.80 | 0.0645 | 16 | | | | | | |
| 17 | 3-Ethylpentane | C ₇ H ₁₆ | 100.204 | 200.25 | 2.013 | -181.48 | 1.38566 | 419.3 | 513.39 | 0.0665 | 17 | | | | | | |
| 18 | 2,2-Dimethylpentane | C ₇ H ₁₆ | 100.204 | 174.54 | 3.494 | -190.86 | 1.38446 | 402.2 | 477.23 | 0.0665 | 18 | | | | | | |
| 19 | 2,4-Dimethylpentane | C ₇ H ₁₆ | 100.204 | 176.89 | 3.293 | -182.63 | 1.38379 | 396.9 | 475.95 | 0.0668 | 19 | | | | | | |
| 20 | 3,3-Dimethylpentane | C ₇ H ₁₆ | 100.204 | 186.91 | 2.774 | -210.01 | 1.38564 | 427.2 | 505.87 | 0.0662 | 20 | | | | | | |
| 21 | Triptane | C ₇ H ₁₆ | 100.204 | 177.58 | 3.375 | -12.81 | 1.39168 | 428.4 | 496.44 | 0.0636 | 21 | | | | | | |
| 22 | n-Octane | C ₈ H ₁₈ | 114.231 | 258.21 | 0.53694 | -70.18 | 1.39956 | 360.7 | 564.22 | 0.0690 | 22 | | | | | | |
| 23 | Dioctbutyl | C ₈ H ₁₈ | 114.231 | 228.39 | 1.102 | -132.11 | 1.39481 | 360.6 | 530.44 | 0.0678 | 23 | | | | | | |
| 24 | Isooctane | C ₈ H ₁₈ | 114.231 | 210.63 | 1.709 | -161.27 | 1.38624 | 372.4 | 519.46 | 0.0656 | 24 | | | | | | |

| | | | | | | | | | |
|----|--------------------|---------|-----------|-----------|----------|---------|---------|---------------------|----|
| 25 | n-Nonane | 128.258 | 303.47 | -64.28 | 1.40746 | 331.8 | 610.68 | 0.0684 | 25 |
| 26 | n-Decane | 142.285 | 345.48 | -21.36 | 1.41385 | 305.2 | 652.0 | 0.0679 | 26 |
| 27 | Cyclopentane | 70.134 | 9.915 | -136.91 | 1.40896 | 653.8 | 481.2 | 0.0594 | 27 |
| 28 | Methylcyclopentane | 84.161 | 161.25 | -224.40 | 1.41210 | 548.9 | 499.35 | 0.0607 | 28 |
| 29 | Cyclohexane | 84.161 | 177.29 | 43.77 | 1.42862 | 580.8 | 536.6 | 0.0586 | 29 |
| 30 | Methylcyclohexane | 98.188 | 213.68 | -195.87 | 1.42538 | 503.5 | 570.27 | 0.0600 | 30 |
| 31 | Ethene(Ethylene) | 28.054 | -154.73 | -272.47* | (1.228)* | 731.0 | 48.54 | 0.0746 | 31 |
| 32 | Propene(Propylene) | 42.081 | -53.84 | -301.45* | 1.3130* | 668.6 | 197.17 | 0.0689 | 32 |
| 33 | 1-Butene(Butylene) | 56.108 | 20.79 | -301.63* | 1.3494* | 583.5 | 295.48 | 0.0685 | 33 |
| 34 | cis-2-Butene | 56.108 | 38.69 | -218.06 | 1.3665* | 612.1 | 324.37 | 0.0688 | 34 |
| 35 | trans-2-Butene | 56.108 | 33.58 | -157.96 | 1.3563* | 587.4 | 311.86 | 0.0679 | 35 |
| 36 | Isobutene | 56.108 | 19.59 | -220.65 | 1.3512* | 580.2 | 292.55 | 0.0682 | 36 |
| 37 | 1-Pentene | 70.134 | 85.93 | -265.39 | 1.37426 | 511.8 | 376.93 | 0.0676 | 37 |
| 38 | 1,2-Butadiene | 54.092 | 51.53 | -213.16 | (340.)* | (653.)* | (340.)* | (0.065)* | 38 |
| 39 | 1,3-Butadiene | 54.092 | 24.06 | -164.02 | 1.3975* | 627.5 | 305 | 0.0654 | 39 |
| 40 | Isoprene | 68.119 | 93.31 | -230.73 | 1.42498 | (558.)* | (412.)* | (0.065)* | 40 |
| 41 | Acetylene | 26.038 | -120.49* | -114.5* | — | 890.4 | 95.34 | 0.0695 | 41 |
| 42 | Benzene | 78.114 | 176.18 | 41.95 | 1.50396 | 710.4 | 552.22 | 0.0531 | 42 |
| 43 | Toluene | 92.141 | 231.13 | -139.00 | 1.49942 | 595.5 | 605.57 | 0.0550 | 43 |
| 44 | Ethylbenzene | 106.167 | 277.16 | -138.966 | 1.49826 | 523.0 | 651.29 | 0.0565 | 44 |
| 45 | o-Xylene | 106.167 | 291.97 | -43.59 | 1.50767 | 541.6 | 674.92 | 0.0557 | 45 |
| 46 | m-Xylene | 106.167 | 282.41 | -54.18 | 1.49951 | 512.9 | 651.02 | 0.0567 | 46 |
| 47 | p-Xylene | 106.167 | 281.07 | 55.85 | 1.49810 | 509.2 | 649.54 | 0.0570 | 47 |
| 48 | Styrene | 104.152 | 293.25 | -23.10 | 1.54937 | 587.8 | (703.)* | 0.0534 | 48 |
| 49 | Isopropylbenzene | 120.194 | 306.34 | -140.814 | 1.49372 | 465.4 | 676.3 | 0.0572 | 49 |
| 50 | Methyl alcohol | 32.042 | 148.44 | -143.79 | 1.33034 | 1174. | 463.08 | 0.0590 | 50 |
| 51 | Ethyl alcohol | 46.069 | 172.90 | -173.4 | 1.36346 | 890.1 | 465.39 | 0.0581 | 51 |
| 52 | Carbon monoxide | 28.010 | -312.68* | -357.00* | 1.00036* | 507.5 | -220.43 | 0.0532 | 52 |
| 53 | Carbon dioxide | 44.010 | -109.257* | -69.83* | 1.00043* | 1071. | 87.91 | 0.0344 | 53 |
| 54 | Hydrogen sulfide | 34.08 | -76.497 | -121.88 | 1.00060* | 1300. | 212.45 | 0.0461 | 54 |
| 55 | Sulfur dioxide | 64.06 | 14.11 | -103.86* | 1.00062* | 1143. | 315.8 | 0.0305 | 55 |
| 56 | Ammonia | 17.0305 | -27.99 | -107.88* | 1.00036* | 1646. | 270.2 | 0.0681 | 56 |
| 57 | Air | 28.9625 | -317.8 | — | 1.00028* | 546.9 | -221.31 | 0.0517 | 57 |
| 58 | Hydrogen | 2.0159 | -422.955* | -435.26* | 1.00013* | 188.1 | -399.9 | 0.0165 | 58 |
| 59 | Oxygen | 31.9988 | -297.332* | -361.820* | 1.00027* | 731.4 | -181.43 | 0.0367 | 59 |
| 60 | Nitrogen | 28.0134 | -320.451 | -346.00* | 1.00028* | 483.1 | -232.51 | 0.0510 | 60 |
| 61 | Chlorine | 70.906 | -29.13 | -149.73* | 1.3878* | 1157. | 290.75 | 0.0280 | 61 |
| 62 | Water | 18.0153 | 212.000* | 32.00 | 1.33335 | 3198.8 | 705.16 | 0.0497 ^s | 62 |
| 63 | Helium | 4.0026 | -452.09 | — | 1.00003* | 32.89 | -450.31 | 0.2300 | 63 |
| 64 | Hydrogen chloride | 36.461 | -121.27 | -173.52* | 1.00042* | 1205. | 124.77 | 0.0356 | 64 |

(table continued on next page)

Table 1-2 (continued)

Physical Constants

*See the Table of Notes and References.

| Number | E. | | F. | G. | H. | I. | | | J. | | Number |
|--------|---|----------|-----------|--------|--------|--------------------------------|--------------------------------|---|-------------------------|------------------------------------|--------|
| | Density of liquid 14,696 psia, 60°F | | | | | Ideal gas 14,696 psia, 60°F | Ideal gas 14,696 psia, 60°F | | Specific Heat 60°F | | |
| | Relative density (specific gravity) 60°F/60°F | lbm/gal. | | | | | gal./lb mole | Relative density (specific gravity) Air = 1 | ft ³ gas/lbm | ft ³ liquid gas/gal. | |
| 1 | (0.3)* | (2.5)* | — | 0.0104 | 0.9980 | 23.654 | 0.5539 | 23.654 | 0.52668 | — | 1 |
| 2 | 0.3619* | 2.9696* | — | 0.9979 | 0.9918 | 12.620 | 1.0382 | 12.620 | 0.40782 | 0.97225 | 2 |
| 3 | 0.5089* | 4.2288* | -0.00162* | 0.1522 | 0.9825 | 8.6059 | 1.5226 | 8.6059 | 0.38852 | 0.61996 | 3 |
| 4 | 0.5628* | 4.6927* | -0.00119* | 0.1852 | 0.9711 | 6.5291 | 2.0068 | 6.5291 | 0.38669 | 0.57066 | 4 |
| 5 | 0.5840* | 4.8690* | -0.00106* | 0.1995 | 0.9667 | 6.5291 | 2.0068 | 6.5291 | 0.39499 | 0.57272 | 5 |
| 6 | 0.62470 | 5.2082 | -0.00090 | 0.2280 | — | 5.2596 | 2.4912 | 5.2596 | 0.38440 | 0.53331 | 6 |
| 7 | 0.63112 | 5.2617 | -0.00086 | 0.2514 | — | 5.2596 | 2.4912 | 5.2596 | 0.38825 | 0.54363 | 7 |
| 8 | 0.59666 | 4.9744* | -0.00106* | 0.1963 | 0.9582 | 5.2596 | 2.4912 | 5.2596 | 0.39038 | 0.55021 | 8 |
| 9 | 0.66383 | 5.5344 | -0.00075 | 0.2994 | — | 4.4035 | 2.9755 | 4.4035 | 0.38628 | 0.53327 | 9 |
| 10 | 0.65785 | 5.4846 | -0.00076 | 0.2780 | — | 4.4035 | 2.9755 | 4.4035 | 0.38526 | 0.52732 | 10 |
| 11 | 0.66901 | 5.5776 | -0.00076 | 0.2732 | — | 4.4035 | 2.9755 | 4.4035 | 0.37902 | 0.51876 | 11 |
| 12 | 0.65385 | 5.4512 | -0.00076 | 0.2326 | — | 4.4035 | 2.9755 | 4.4035 | 0.38231 | 0.51367 | 12 |
| 13 | 0.66631 | 5.5551 | -0.00076 | 0.2469 | — | 4.4035 | 2.9755 | 4.4035 | 0.37762 | 0.51308 | 13 |
| 14 | 0.68820 | 5.7376 | -0.00068 | 0.3494 | — | 3.7872 | 3.4598 | 3.7872 | 0.38447 | 0.52802 | 14 |
| 15 | 0.68310 | 5.6951 | -0.00070 | 0.3298 | — | 3.7872 | 3.4598 | 3.7872 | 0.38041 | 0.52199 | 15 |
| 16 | 0.69165 | 5.7684 | -0.00070 | 0.3232 | — | 3.7872 | 3.4598 | 3.7872 | 0.37882 | 0.51019 | 16 |
| 17 | 0.70276 | 5.8590 | -0.00069 | 0.3105 | — | 3.7872 | 3.4598 | 3.7872 | 0.38646 | 0.51410 | 17 |
| 18 | 0.67829 | 5.6720 | -0.00070 | 0.2871 | — | 3.7872 | 3.4598 | 3.7872 | 0.38594 | 0.51678 | 18 |
| 19 | 0.67733 | 5.6470 | -0.00073 | 0.3026 | — | 3.7872 | 3.4598 | 3.7872 | 0.39414 | 0.52440 | 19 |
| 20 | 0.69722 | 5.8170 | -0.00067 | 0.2674 | — | 3.7872 | 3.4598 | 3.7872 | 0.38306 | 0.50138 | 20 |
| 21 | 0.69457 | 5.7907 | -0.00068 | 0.2503 | — | 3.7872 | 3.4598 | 3.7872 | 0.37724 | 0.49920 | 21 |
| 22 | 0.70696 | 5.8940 | -0.00064 | 0.3977 | — | 3.3220 | 3.9441 | 3.3220 | 0.38331 | 0.52406 | 22 |
| 23 | 0.69793 | 5.8187 | -0.00067 | 0.3564 | — | 3.3220 | 3.9441 | 3.3220 | 0.37571 | 0.51130 | 23 |
| 24 | 0.69624 | 5.8046 | -0.00065 | 0.3035 | — | 3.3220 | 3.9441 | 3.3220 | 0.38222 | 0.48951 | 24 |
| 25 | 0.72187 | 6.0183 | -0.00061 | 0.4445 | — | 2.6671 | 4.4284 | 2.6671 | 0.38246 | 0.52244 | 25 |
| 26 | 0.73421 | 6.1212 | -0.00057 | 0.4898 | — | 2.6671 | 4.9127 | 2.6671 | 0.38179 | 0.52103 | 26 |

| | | | | | | | | | | | |
|----|-----------|----------|---------|-----------|----------|----------|---------|--------|---------|---------|---------|
| 27 | 0.75050 | 6.2570 | 11.209 | -0.00073 | 0.1950 | — | 2.4215 | 5.4110 | 33.856 | 0.27199 | 0.42182 |
| 28 | 0.75349 | 6.2819 | 13.397 | -0.00069 | 0.2302 | — | 1.9599 | 4.5090 | 28.325 | 0.30100 | 0.44126 |
| 29 | 0.78347 | 6.5319 | 12.885 | -0.00065 | 0.2096 | — | 2.9059 | 4.5090 | 29.452 | 0.28817 | 0.43584 |
| 30 | 0.77400 | 6.4529 | 15.216 | -0.00062 | 0.2358 | — | 3.3902 | 3.8649 | 24.940 | 0.31700 | 0.44012 |
| 31 | — | — | — | — | — | — | — | — | — | — | — |
| 32 | 0.52095 | 4.3432 | 9.6889 | -0.00173* | 0.0865 | 0.9936 | 1.9586 | 13.527 | — | 0.35697 | — |
| 33 | 0.60107 | 5.0112 | 11.197 | -0.00112* | 0.1356 | 0.9944 | 1.4529 | 9.0179 | 39.167* | 0.35714 | 0.57116 |
| 34 | 0.62717 | 5.2288 | 10.731 | -0.00105* | 0.1941 | 0.9699 | 1.9373 | 6.7636 | 33.894* | 0.35446 | 0.54533 |
| 35 | 0.60996 | 5.0853 | 11.033 | -0.00106* | 0.2029 | 0.9665 | 1.9373 | 6.7636 | 35.366* | 0.33754 | 0.52980 |
| 36 | 0.60040 | 5.0056 | 11.209 | -0.00117* | 0.2128 | 0.9667 | 1.9373 | 6.7636 | 34.395* | 0.35574 | 0.54215 |
| 37 | 0.64571 | 5.3834 | 13.028 | -0.00089 | 0.1999 | 0.9700 | 1.9373 | 6.7636 | 33.856* | 0.37690 | 0.54839 |
| 38 | 0.65799 | 5.4857 | 9.8605 | -0.00101* | 0.2333 | (0.969) | 2.4215 | 5.4110 | 29.129 | 0.36351 | 0.51782 |
| 39 | 0.62723 | 5.2293 | 10.344* | -0.00110* | 0.2007 | (0.965) | 1.8577 | 7.0156 | 38.485* | 0.34347 | 0.54029 |
| 40 | 0.68615 | 5.7205 | 11.908 | -0.00082 | 0.1568 | — | 2.3520 | 5.5710 | 31.869 | 0.34120 | 0.53447 |
| 41 | (0.41796) | (3.4842) | (7.473) | — | 0.1949 | 0.9930 | 0.8990 | 14.574 | — | 0.39754 | — |
| 42 | 0.88448 | 7.3740 | 10.593 | -0.00067 | 0.2093 | — | 2.6971 | 4.8581 | 35.824 | 0.24296 | 0.40989 |
| 43 | 0.87190 | 7.2691 | 12.676 | -0.00059 | 0.2633 | — | 3.1814 | 4.1184 | 29.937 | 0.26370 | 0.40095 |
| 44 | 0.87158 | 7.2673 | 14.509 | -0.00056 | 0.3027 | — | 3.6557 | 3.5744 | 25.976 | 0.27792 | 0.41139 |
| 45 | 0.88467 | 7.3756 | 14.594 | -0.00052 | 0.3942 | — | 3.6657 | 3.5744 | 26.365 | 0.28964 | 0.41620 |
| 46 | 0.86875 | 7.2429 | 14.658 | -0.00053 | 0.3257 | — | 3.6657 | 3.5744 | 25.889 | 0.27427 | 0.40545 |
| 47 | 0.86578 | 7.2181 | 14.708 | -0.00056 | 0.3216 | — | 3.6657 | 3.5744 | 25.800 | 0.27471 | 0.40255 |
| 48 | 0.91108 | 7.5958 | 13.712 | -0.00053 | (0.2412) | — | 3.5961 | 3.6435 | 27.675 | 0.27110 | 0.41220 |
| 49 | 0.86634 | 7.2228 | 16.641 | -0.00055 | 0.3260 | — | 4.1500 | 3.1573 | 22.804 | 0.29170 | 0.42053 |
| 50 | 0.79626 | 6.6385 | 4.8267 | -0.00066 | 0.5649 | — | 1.1063 | 11.843 | 78.622 | 0.32316 | 0.59187 |
| 51 | 0.79399 | 6.6196 | 6.9595 | -0.00058 | 0.6438 | — | 1.5906 | 8.2372 | 54.527 | 0.33222 | 0.56610 |
| 52 | 0.78939 | 6.5812 | 4.2561* | — | 0.0481 | 0.9959 | 0.9671 | 13.548 | 89.163* | 0.24847 | — |
| 53 | 0.81802 | 6.8199 | 6.4532* | -0.00583* | 0.2667 | 0.9943 | 1.5196 | 8.6229 | 58.807* | 0.19911 | — |
| 54 | 0.80144 | 6.6817 | 5.1005 | -0.00157* | 0.0948 | 0.9846 | 1.1767 | 11.135 | 74.401* | 0.23827 | 0.50418 |
| 55 | 1.3974* | 11.650* | 5.4987* | — | 0.2548 | 0.9802 | 2.2118 | 5.9238 | 69.012* | 0.14804 | 0.32460 |
| 56 | 0.61832* | 5.1550* | 3.3037* | — | 0.2557 | 0.9877 | 0.5880 | 22.283 | 114.87* | 0.49677 | — |
| 57 | 0.87476* | 7.2930* | 3.9713* | — | — | 1.0000 | 1.0000 | 13.103 | 95.557* | 0.23988 | — |
| 58 | 0.071070* | 0.59252* | 3.4022* | -0.202 | — | 1.0006 | 0.06960 | 188.25 | 111.54* | 3.4038 | — |
| 59 | 1.1421* | 8.5221* | 3.3605* | — | 0.0216 | 0.9892 | 1.1048 | 11.859 | 112.93* | 0.21892 | — |
| 60 | 0.80940* | 6.7481* | 4.1513* | — | 0.0372 | 0.9997 | 0.9674 | 13.546 | 91.413* | 0.24828 | — |
| 61 | 1.4244* | 11.875* | 5.9710* | — | 0.0878 | (0.9875) | 2.4482 | 5.3519 | 63.554* | 0.11377 | — |
| 62 | 1.00000 | 8.33712 | 2.1609 | -0.00009 | 0.3443 | — | 0.62202 | 175.62 | 0.44457 | 0.99974 | — |
| 63 | 0.12510* | 1.0430* | 3.8376* | — | 0. | 1.0006 | 0.1382 | 94.814 | 98.891* | 1.2404 | — |
| 64 | 0.85129* | 7.0973* | 5.1373* | -0.00300* | 0.1259 | 0.9923 | 1.2589 | 10.408 | 73.869* | 0.19086 | — |

12/12/86

(text continued from page 17)

Table 1-3
Coefficients of Equation 1-1

| θ | a_1 | a_2 | a_3 | a_4 | a_5 |
|-----------------------------|---------------------------|-----------------------------|-----------------------------|-----------------------------|----------------------------|
| M | -131.11375 | 24.96156 | -0.34079022 | 2.4941184×10^{-3} | 468.32575 |
| T_c , °R | 915.53747 | 41.421337 | -0.7586859 | 5.8675351×10^{-3} | -1.3028779×10^3 |
| P_c , psia | 275.56275 | -12.522269 | 0.29926384 | $-2.8452129 \times 10^{-3}$ | 1.7117226×10^{-3} |
| T_b , °R | 434.38878 | 50.125279 | -0.9097293 | 7.0280657×10^{-3} | -601.85651 |
| T | -0.50862704 | 8.700211×10^{-2} | $-1.8484814 \times 10^{-3}$ | 1.4663890×10^{-5} | 1.8518106 |
| γ | 0.86714949 | 3.4143408×10^{-3} | -2.839627×10^{-5} | 2.4943308×10^{-8} | -1.1627984 |
| V_c , ft ³ /lb | 5.223458×10^{-2} | $7.87091369 \times 10^{-4}$ | $-1.9324432 \times 10^{-5}$ | 1.7547264×10^{-7} | 4.4017952×10^{-2} |

Riazi and Daubert (1987) developed a simple two-parameter equation for predicting the physical properties of pure compounds and undefined hydrocarbon mixtures. The proposed generalized empirical equation is based on the use of the molecular weight M and specific gravity γ of the undefined petroleum fraction as the correlating parameters. Their mathematical expression has the following form:

$$\theta = a (M)^b \gamma^c \text{EXP} [d (M) + e \gamma + f (M) \gamma] \quad (1-2)$$

where θ = any physical property

a–f = constants for each property as given in Table 1-4

γ = specific gravity of the fraction

M = molecular weight

T_c = critical temperature, °R

P_c = critical pressure, psia (Table 1-4)

Table 1-4
Correlation Constants for Equation 1-2

| θ | a | b | c | d | e | f |
|-----------------------------|------------------------|----------|----------|--------------------------|----------|---------------------------|
| T_c , °R | 544.4 | 0.2998 | 1.0555 | -1.3478×10^{-4} | -0.61641 | 0.0 |
| P_c , psia | 4.5203×10^4 | -0.8063 | 1.6015 | -1.8078×10^{-3} | -0.3084 | 0.0 |
| V_c , ft ³ /lb | 1.206×10^{-2} | 0.20378 | -1.3036 | -2.657×10^{-3} | 0.5287 | 2.6012×10^{-3} |
| T_b , °R | 6.77857 | 0.401673 | -1.58262 | 3.77409×10^{-3} | 2.984036 | -4.25288×10^{-3} |

T_b = boiling point temperature, °R
 V_c = critical volume, ft³/lb

Edmister (1958) proposed a correlation for estimating the acentric factor T of pure fluids and petroleum fractions. The equation, widely used in the petroleum industry, requires boiling point, critical temperature, and critical pressure. The proposed expression is given by the following relationship:

$$\omega = \frac{3[\log(p_c/14.70)]}{7[(T_c/T_b - 1)]} - 1 \quad (1-3)$$

where T = acentric factor

p_c = critical pressure, psia

T_c = critical temperature, °R

T_b = normal boiling point, °R

If the acentric factor is available from another correlation, the Edmister equation can be rearranged to solve for any of the three other properties (providing the other two are known).

The critical compressibility factor is another property that is often used in thermodynamic-property prediction models. It is defined as the component compressibility factor calculated at its critical point. This property can be conveniently computed by the real gas equation-of-state at the critical point, or

$$z_c = \frac{p_c V_c M}{R T_c} \quad (1-4)$$

where R = universal gas constant, 10.73 psia-ft³/lb-mol. °R

V_c = critical volume, ft³/lb

M = molecular weight

The accuracy of Equation 1-4 depends on the accuracy of the values of p_c , T_c , and V_c used in evaluating the critical compressibility factor. Table 1-5 presents a summary of the critical compressibility estimation methods.

Table 1-5
Critical Compressibility Estimation Methods

| Method | Year | z_c | Equation No. |
|-------------------------------|------|---|--------------|
| Haugen | 1959 | $z_c = 1/(1.28 \omega + 3.41)$ | 1-5 |
| Reid, Prausnitz, and Sherwood | 1977 | $z_c = 0.291 - 0.080 \omega$ | 1-6 |
| Salerno et al. | 1985 | $z_c = 0.291 - 0.080 \omega - 0.016 \omega^2$ | 1-7 |
| Nath | 1985 | $z_c = 0.2918 - 0.0928 \omega$ | 1-8 |

Example 1-1

Estimate the critical properties and the acentric factor of the heptanes-plus fraction, i.e., C_{7+} , with a measured molecular weight of 150 and specific gravity of 0.78.

Solution

Step 1. Use Equation 1-2 to estimate T_c , p_c , V_c , and T_b :

- $T_c = 544.2 (150)^{.2998} (.78)^{1.0555} \exp[-1.3478 \times 10^{-4} (150) - 0.61641 (.78) + 0] = 1139.4 \text{ }^\circ\text{R}$
- $p_c = 4.5203 \times 10^4 (150)^{-.8063} (.78)^{1.6015} \exp[-1.8078 \times 10^{-3} (150) - 0.3084 (.78) + 0] = 320.3 \text{ psia}$
- $V_c = 1.206 \times 10^{-2} (150)^{.20378} (.78)^{-1.3036} \exp[-2.657 \times 10^{-3} (150) + 0.5287 (.78)] = 2.6012 \times 10^{-3} (150) (.78) = .06035 \text{ ft}^3/\text{lb}$
- $T_b = 6.77857 (150)^{.401673} (.78)^{-1.58262} \exp[3.77409 \times 10^{-3} (150) + 2.984036 (0.78) - 4.25288 \times 10^{-3} (150) (0.78)] = 825.26 \text{ }^\circ\text{R}$

Step 2. Use Edmister's Equation (Equation 1-3) to estimate the acentric factor:

$$\omega = \frac{3 [\log (320.3/14.7)]}{7 [1139.4/825.26 - 1]} - 1 = 0.5067$$

PROBLEMS

1. The following is a list of the compositional analysis of different hydrocarbon systems. The compositions are expressed in the terms of mol%.

| Component | System #1 | System #2 | System #3 | System #4 |
|-----------------|-----------|-----------|-----------|-----------|
| C ₁ | 68.00 | 25.07 | 60.00 | 12.15 |
| C ₂ | 9.68 | 11.67 | 8.15 | 3.10 |
| C ₃ | 5.34 | 9.36 | 4.85 | 2.51 |
| C ₄ | 3.48 | 6.00 | 3.12 | 2.61 |
| C ₅ | 1.78 | 3.98 | 1.41 | 2.78 |
| C ₆ | 1.73 | 3.26 | 2.47 | 4.85 |
| C ₇₊ | 9.99 | 40.66 | 20.00 | 72.00 |

Classify these hydrocarbon systems.

2. If a petroleum fraction has a measured molecular weight of 190 and a specific gravity of 0.8762, characterize this fraction by calculating the boiling point, critical temperature, critical pressure, and critical volume of the fraction. Use the Riazi and Daubert correlation.
3. Calculate the acentric factor and critical compressibility factor of the component in the above problem.

REFERENCES

1. Ahmed, T., "Composition Modeling of Tyler and Mission Canyon Formation Oils with CO₂ and Lean Gases," final report submitted to the Montana's on a New Track for Science (MONTS) program (Montana National Science Foundation Grant Program), 1985.
2. Edmister, W. C., "Applied Hydrocarbon Thermodynamic, Part 4: Compressibility Factors and Equations of State," *Petroleum Refiner*, April 1958, Vol. 37, pp. 173–179.
3. Haugen, O. A., Watson, K. M., and Ragatz R. A., *Chemical Process Principles*, 2nd ed. New York: Wiley, 1959, p. 577.
4. Katz, D. L., and Firoozabadi, A., "Predicting Phase Behavior of Condensate/ Crude-oil Systems Using Methane Interaction Coefficients," *JPT*, Nov. 1978, pp. 1649–1655.
5. McCain, W. D., "Heavy Components Control Reservoir Fluid Behavior," *JPT*, September 1994, pp. 746–750.
6. Nath, J., "Acentric Factor and Critical Volumes for Normal Fluids," *Ind. Eng. Chem. Fundam.*, 1985, Vol. 21, No. 3, pp. 325–326.

7. Reid, R., Prausnitz, J. M., and Sherwood, T., *The Properties of Gases and Liquids*, 3rd ed., p. 21. McGraw-Hill, 1977.
8. Riazi, M. R., and Daubert, T. E., "Characterization Parameters for Petroleum Fractions," *Ind. Eng. Chem. Res.*, 1987, Vol. 26, No. 24, pp. 755–759.
9. Salerno, S., et al., "Prediction of Vapor Pressures and Saturated Vol.," *Fluid Phase Equilibria*, June 10, 1985, Vol. 27, pp. 15–34.



C H A P T E R 2

RESERVOIR-FLUID PROPERTIES

To understand and predict the volumetric behavior of oil and gas reservoirs as a function of pressure, knowledge of the physical properties of reservoir fluids must be gained. These fluid properties are usually determined by laboratory experiments performed on samples of actual reservoir fluids. In the absence of experimentally measured properties, it is necessary for the petroleum engineer to determine the properties from empirically derived correlations. The objective of this chapter is to present several of the well-established physical property correlations for the following reservoir fluids:

- Natural gases
- Crude oil systems
- Reservoir water systems

PROPERTIES OF NATURAL GASES

A gas is defined as a homogeneous fluid of low viscosity and density that has no definite volume but expands to completely fill the vessel in which it is placed. Generally, the natural gas is a mixture of hydrocarbon and nonhydrocarbon gases. The hydrocarbon gases that are normally found in a natural gas are methanes, ethanes, propanes, butanes, pentanes, and small amounts of hexanes and heavier. The nonhydrocarbon gases (i.e., impurities) include carbon dioxide, hydrogen sulfide, and nitrogen.

Knowledge of pressure-volume-temperature (PVT) relationships and other physical and chemical properties of gases is essential for solving problems in natural gas reservoir engineering. These properties include:

- Apparent molecular weight, M_a
- Specific gravity, γ_g
- Compressibility factor, z
- Density, ρ_g
- Specific volume, v
- Isothermal gas compressibility coefficient, c_g
- Gas formation volume factor, B_g
- Gas expansion factor, E_g
- Viscosity, μ_g

The above gas properties may be obtained from direct laboratory measurements or by prediction from generalized mathematical expressions. This section reviews laws that describe the volumetric behavior of gases in terms of pressure and temperature and also documents the mathematical correlations that are widely used in determining the physical properties of natural gases.

BEHAVIOR OF IDEAL GASES

The kinetic theory of gases postulates that gases are composed of a very large number of particles called molecules. For an ideal gas, the volume of these molecules is insignificant compared with the total volume occupied by the gas. It is also assumed that these molecules have no attractive or repulsive forces between them, and that all collisions of molecules are perfectly elastic.

Based on the above kinetic theory of gases, a mathematical equation called *equation-of-state* can be derived to express the relationship existing between pressure p , volume V , and temperature T for a given quantity of moles of gas n . This relationship for perfect gases is called the **ideal gas law** and is expressed mathematically by the following equation:

$$pV = nRT \quad (2-1)$$

where p = absolute pressure, psia

V = volume, ft^3

T = absolute temperature, $^{\circ}\text{R}$

n = number of moles of gas, lb-mole
 R = the universal gas constant, which, for the above units, has the value 10.730 psia ft³/lb-mole °R

The number of pound-moles of gas, i.e., n , is defined as the weight of the gas m divided by the molecular weight M , or:

$$n = \frac{m}{M} \quad (2-2)$$

Combining Equation 2-1 with 2-2 gives:

$$pV = \left(\frac{m}{M}\right)RT \quad (2-3)$$

where m = weight of gas, lb
 M = molecular weight, lb/lb-mol

Since the density is defined as the mass per unit volume of the substance, Equation 2-3 can be rearranged to estimate the gas density at any pressure and temperature:

$$\rho_g = \frac{m}{V} = \frac{pM}{RT} \quad (2-4)$$

where ρ_g = density of the gas, lb/ft³

It should be pointed out that lb refers to lbs mass in any of the subsequent discussions of density in this text.

Example 2-1

Three pounds of n-butane are placed in a vessel at 120°F and 60 psia. Calculate the volume of the gas assuming an ideal gas behavior.

Solution

Step 1. Determine the molecular weight of n-butane from Table 1-1 to give:

$$M = 58.123$$

Step 2. Solve Equation 2-3 for the volume of gas:

$$V = \left(\frac{m}{M} \right) \frac{RT}{p}$$

$$V = \left(\frac{3}{58.123} \right) \frac{(10.73)(120 + 460)}{60} = 5.35 \text{ ft}^3$$

Example 2-2

Using the data given in the above example, calculate the density of n-butane.

Solution

Solve for the density by applying Equation 2-4:

$$\rho_g = \frac{(60)(58.123)}{(10.73)(580)} = 0.56 \text{ lb/ft}^3$$

Petroleum engineers are usually interested in the behavior of mixtures and rarely deal with pure component gases. Because natural gas is a mixture of hydrocarbon components, the overall physical and chemical properties can be determined from the physical properties of the individual components in the mixture by using appropriate mixing rules.

The basic properties of gases are commonly expressed in terms of the apparent molecular weight, standard volume, density, specific volume, and specific gravity. These properties are defined as follows.

Apparent Molecular Weight

One of the main gas properties that is frequently of interest to engineers is the apparent molecular weight. If y_i represents the mole fraction of the i th component in a gas mixture, the apparent molecular weight is defined mathematically by the following equation:

$$M_a = \sum_{i=1} y_i M_i \quad (2-5)$$

where M_a = apparent molecular weight of a gas mixture

M_i = molecular weight of the i th component in the mixture

y_i = mole fraction of component i in the mixture

Standard Volume

In many natural gas engineering calculations, it is convenient to measure the volume occupied by 1 lb-mole of gas at a reference pressure and temperature. These reference conditions are usually 14.7 psia and 60°F, and are commonly referred to as *standard conditions*. The standard volume is then defined as the volume of gas occupied by 1 lb-mol of gas at standard conditions. Applying the above conditions to Equation 2-1 and solving for the volume, i.e., the standard volume, gives:

$$V_{sc} = \frac{(1) RT_{sc}}{p_{sc}} = \frac{(1)(10.73)(520)}{14.7}$$

or

$$V_{sc} = 379.4 \text{ scf/lb-mol} \quad (2-6)$$

where V_{sc} = standard volume, scf/lb-mol

scf = standard cubic feet

T_{sc} = standard temperature, °R

p_{sc} = standard pressure, psia

Density

The density of an ideal gas mixture is calculated by simply replacing the molecular weight of the pure component in Equation 2-4 with the apparent molecular weight of the gas mixture to give:

$$\rho_g = \frac{pM_a}{RT} \quad (2-7)$$

where ρ_g = density of the gas mixture, lb/ft³

M_a = apparent molecular weight

Specific Volume

The specific volume is defined as the volume occupied by a unit mass of the gas. For an ideal gas, this property can be calculated by applying Equation 2-3:

$$v = \frac{V}{m} = \frac{RT}{p M_a} = \frac{1}{\rho_g} \quad (2-8)$$

where v = specific volume, ft^3/lb
 ρ_g = gas density, lb/ft^3

Specific Gravity

The specific gravity is defined as the ratio of the gas density to that of the air. Both densities are measured or expressed at the same pressure and temperature. Commonly, the standard pressure p_{sc} and standard temperature T_{sc} are used in defining the gas specific gravity:

$$\gamma_g = \frac{\rho_g}{\rho_{\text{air}}} \quad (2-9)$$

Assuming that the behavior of both the gas mixture and the air is described by the ideal gas equation, the specific gravity can then be expressed as:

$$\gamma_g = \frac{\frac{p_{sc} M_a}{RT_{sc}}}{\frac{p_{sc} M_{\text{air}}}{RT_{sc}}}$$

or

$$\gamma_g = \frac{M_a}{M_{\text{air}}} = \frac{M_a}{28.96} \quad (2-10)$$

where γ_g = gas specific gravity

ρ_{air} = density of the air

M_{air} = apparent molecular weight of the air = 28.96

M_a = apparent molecular weight of the gas

p_{sc} = standard pressure, psia

T_{sc} = standard temperature, °R

Example 2-3

A gas well is producing gas with a specific gravity of 0.65 at a rate of 1.1 MMscf/day. The average reservoir pressure and temperature are 1,500 psi and 150°F. Calculate:

- Apparent molecular weight of the gas
- Gas density at reservoir conditions
- Flow rate in lb/day

Solution

a. From Equation 2-10, solve for the apparent molecular weight:

$$M_a = 28.96 \gamma_g$$

$$M_a = (28.96) (0.65) = 18.82$$

b. Apply Equation 2-7 to determine gas density:

$$\rho_g = \frac{(1500)(18.82)}{(10.73)(610)} = 4.31 \text{ lb/ft}^3$$

c. *Step 1.* Because 1 lb-mol of any gas occupies 379.4 scf at standard conditions, then the daily number of moles that the gas well is producing can be calculated from:

$$n = \frac{(1.1)(10)^6}{379.4} = 2899 \text{ lb-mol}$$

Step 2. Determine the daily mass m of the gas produced from Equation 2-2:

$$m = (n) (M_a)$$

$$m = (2899) (18.82) = 54559 \text{ lb/day}$$

Example 2-4

A gas well is producing a natural gas with the following composition:

| Component | y_i |
|-----------------|-------|
| CO ₂ | 0.05 |
| C ₁ | 0.90 |
| C ₂ | 0.03 |
| C ₃ | 0.02 |

Assuming an ideal gas behavior, calculate:

- Apparent molecular weight
- Specific gravity
- Gas density at 2,000 psia and 150°F
- Specific volume at 2,000 psia and 150°F

Solution

| Component | y_i | M_i | $y_i \cdot M_i$ |
|-----------------|-------|-------|-----------------|
| CO ₂ | 0.05 | 44.01 | 2.200 |
| C ₁ | 0.90 | 16.04 | 14.436 |
| C ₂ | 0.03 | 30.07 | 0.902 |
| C ₃ | 0.02 | 44.11 | 0.882 |

$$M_a = 18.42$$

- Apply Equation 2-5 to calculate the apparent molecular weight:

$$M_a = 18.42$$

- Calculate the specific gravity by using Equation 2-10:

$$\gamma_g = M_a / 28.96 = 18.42 / 28.96 = 0.636$$

- Solve for the density by applying Equation 2-7:

$$\rho_g = \frac{PM_a}{RT} = \frac{(2000)(18.42)}{(10.73)(610)} = 5.628 \text{ lb/ft}^3$$

- Determine the specific volume from Equation 2-8:

$$v = \frac{1}{\rho} = \frac{1}{5.628} = 0.178 \text{ ft}^3/\text{lb}$$

BEHAVIOR OF REAL GASES

In dealing with gases at a very low pressure, the ideal gas relationship is a convenient and generally satisfactory tool. At higher pressures, the use of the ideal gas equation-of-state may lead to errors as great as 500%, as compared to errors of 2–3% at atmospheric pressure.

Basically, the magnitude of deviations of real gases from the conditions of the ideal gas law increases with increasing pressure and temperature and varies widely with the composition of the gas. Real gases behave differently from ideal gases. The reason for this is that the perfect gas law was derived under the assumption that the volume of molecules is insignificant and that no molecular attraction or repulsion exists between them. This is not the case for real gases.

Numerous equations-of-state have been developed in the attempt to correlate the pressure-volume-temperature variables for real gases with experimental data. In order to express a more exact relationship between the variables p , V , and T , a correction factor called the *gas compressibility factor*, *gas deviation factor*, or simply the *z-factor*, must be introduced into Equation 2-1 to account for the departure of gases from ideality. The equation has the following form:

$$pV = znRT \quad (2-11)$$

where the gas compressibility factor z is a dimensionless quantity and is defined as the ratio of the actual volume of n -moles of gas at T and p to the ideal volume of the same number of moles at the same T and p :

$$z = \frac{V_{\text{actual}}}{V_{\text{ideal}}} = \frac{V}{(nRT)/p}$$

Studies of the gas compressibility factors for natural gases of various compositions have shown that compressibility factors can be generalized with sufficient accuracies for most engineering purposes when they are expressed in terms of the following two dimensionless properties:

- Pseudo-reduced pressure
- Pseudo-reduced temperature

These dimensionless terms are defined by the following expressions:

$$p_{\text{pr}} = \frac{p}{p_{\text{pc}}} \quad (2-12)$$

$$T_{\text{pr}} = \frac{T}{T_{\text{pc}}} \quad (2-13)$$

where p = system pressure, psia

p_{pr} = pseudo-reduced pressure, dimensionless

T = system temperature, °R

T_{pr} = pseudo-reduced temperature, dimensionless

p_{pc} , T_{pc} = pseudo-critical pressure and temperature, respectively, and defined by the following relationships:

$$p_{pc} = \sum_{i=1} y_i p_{ci} \quad (2-14)$$

$$T_{pc} = \sum_{i=1} y_i T_{ci} \quad (2-15)$$

It should be pointed out that these pseudo-critical properties, i.e., p_{pc} and T_{pc} , do not represent the actual critical properties of the gas mixture. These pseudo properties are used as correlating parameters in generating gas properties.

Based on the concept of pseudo-reduced properties, Standing and Katz (1942) presented a generalized gas compressibility factor chart as shown in Figure 2-1. The chart represents compressibility factors of sweet natural gas as a function of p_{pr} and T_{pr} . This chart is generally reliable for natural gas with minor amount of nonhydrocarbons. It is one of the most widely accepted correlations in the oil and gas industry.

Example 2-5

A gas reservoir has the following gas composition: the initial reservoir pressure and temperature are 3,000 psia and 180°F, respectively.

| Component | y_i |
|--------------------|-------|
| CO ₂ | 0.02 |
| N ₂ | 0.01 |
| C ₁ | 0.85 |
| C ₂ | 0.04 |
| C ₃ | 0.03 |
| i - C ₄ | 0.03 |
| n - C ₄ | 0.02 |

Calculate the gas compressibility factor under initial reservoir conditions.

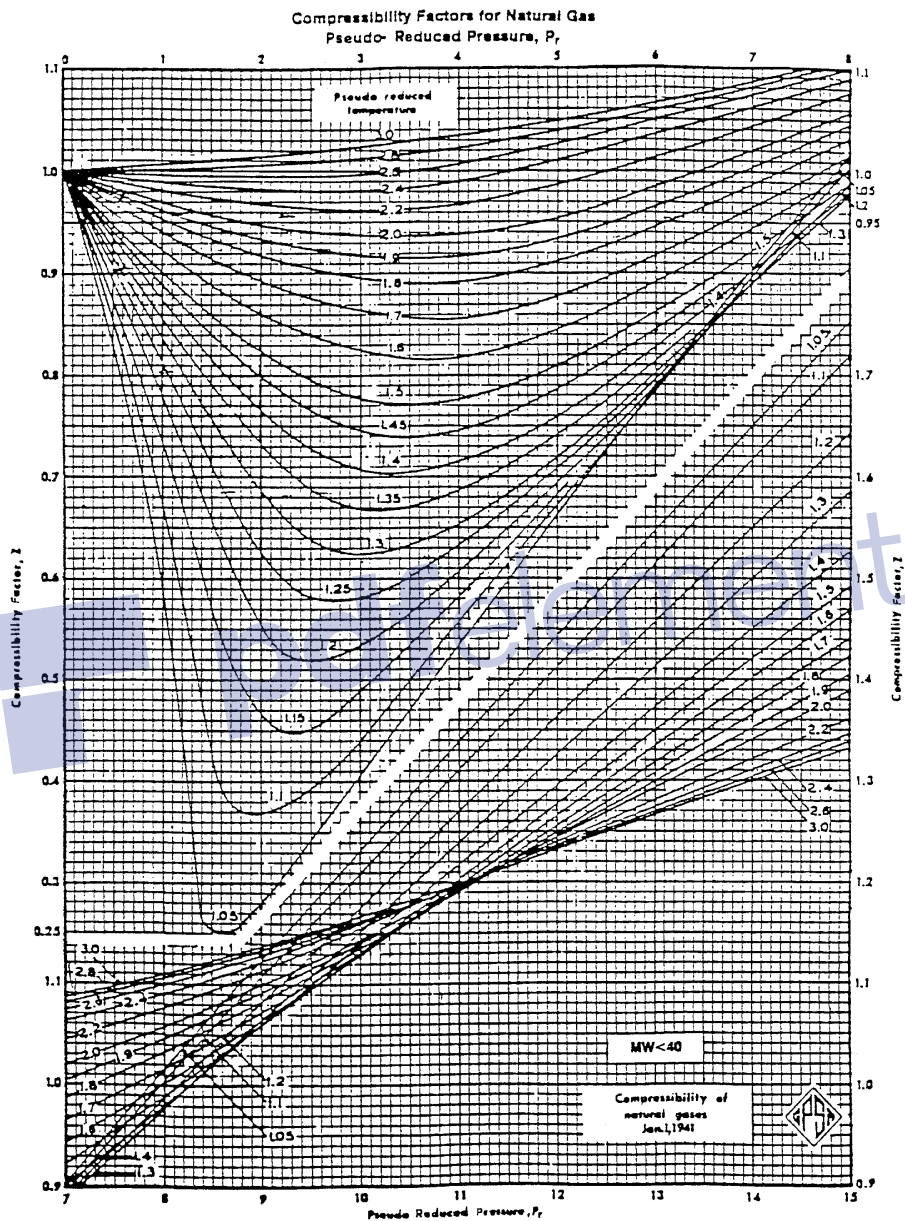


Figure 2-1. Standing and Katz compressibility factors chart. (Courtesy of GPSA and GPA Engineering Data Book, EO Edition, 1987.)

Solution

| Component | y_i | $T_{ci}, ^\circ R$ | $y_i T_{ci}$ | P_{ci} | $y_i P_{ci}$ |
|--------------------|-------|--------------------|-------------------|-------------------|--------------|
| CO ₂ | 0.02 | 547.91 | 10.96 | 1071 | 21.42 |
| N ₂ | 0.01 | 227.49 | 2.27 | 493.1 | 4.93 |
| C ₁ | 0.85 | 343.33 | 291.83 | 666.4 | 566.44 |
| C ₂ | 0.04 | 549.92 | 22.00 | 706.5 | 28.26 |
| C ₃ | 0.03 | 666.06 | 19.98 | 616.4 | 18.48 |
| i - C ₄ | 0.03 | 734.46 | 22.03 | 527.9 | 15.84 |
| n - C ₄ | 0.02 | 765.62 | 15.31 | 550.6 | 11.01 |
| | | | $T_{pc} = 383.38$ | $P_{pc} = 666.38$ | |

Step 1. Determine the pseudo-critical pressure from Equation 2-14:

$$P_{pc} = 666.18$$

Step 2. Calculate the pseudo-critical temperature from Equation 2-15:

$$T_{pc} = 383.38$$

Step 3. Calculate the pseudo-reduced pressure and temperature by applying Equations 2-12 and 2-13, respectively:

$$P_{pr} = \frac{3000}{666.38} = 4.50$$

$$T_{pr} = \frac{640}{383.38} = 1.67$$

Step 4. Determine the z-factor from Figure 2-1, to give:

$$z = 0.85$$

Equation 2-11 can be written in terms of the apparent molecular weight M_a and the weight of the gas m :

$$pV = z \left(\frac{m}{M_a} \right) RT$$

Solving the above relationship for the gas specific volume and density, give:

$$v = \frac{V}{m} = \frac{zRT}{pM_a} \quad (2-16)$$

$$\rho_g = \frac{1}{v} = \frac{pM_a}{zRT} \quad (2-17)$$

where v = specific volume, ft^3/lb
 ρ_g = density, lb/ft^3

Example 2-6

Using the data in Example 2-5 and assuming real gas behavior, calculate the density of the gas phase under initial reservoir conditions. Compare the results with that of ideal gas behavior.

Solution

| Component | y_i | M_i | $y_i \cdot M_i$ | $T_{ci}, ^\circ\text{R}$ | $y_i T_{ci}$ | P_{ci} | $y_i P_{ci}$ |
|--------------------|-------|-------|-------------------|--------------------------|-------------------|----------|--------------|
| CO ₂ | 0.02 | 44.01 | 0.88 | 547.91 | 10.96 | 1071 | 21.42 |
| N ₂ | 0.01 | 28.01 | 0.28 | 227.49 | 2.27 | 493.1 | 4.93 |
| C ₁ | 0.85 | 16.04 | 13.63 | 343.33 | 291.83 | 666.4 | 566.44 |
| C ₂ | 0.04 | 30.1 | 1.20 | 549.92 | 22.00 | 706.5 | 28.26 |
| C ₃ | 0.03 | 44.1 | 1.32 | 666.06 | 19.98 | 616.40 | 18.48 |
| i - C ₄ | 0.03 | 58.1 | 1.74 | 734.46 | 22.03 | 527.9 | 15.84 |
| n - C ₄ | 0.02 | 58.1 | 1.16 | 765.62 | 15.31 | 550.6 | 11.01 |
| $M_a = 20.23$ | | | $T_{pc} = 383.38$ | | $P_{pc} = 666.38$ | | |

Step 1. Calculate the apparent molecular weight from Equation 2-5:

$$M_a = 20.23$$

Step 2. Determine the pseudo-critical pressure from Equation 2-14:

$$p_{pc} = 666.18$$

Step 3. Calculate the pseudo-critical temperature from Equation 2-15:

$$T_{pc} = 383.38$$

Step 4. Calculate the pseudo-reduced pressure and temperature by applying Equations 2-12 and 2-13, respectively:

$$p_{pr} = \frac{3000}{666.38} = 4.50$$

$$T_{pr} = \frac{640}{383.38} = 1.67$$

Step 5. Determine the z-factor from Figure 2-1:

$$z = 0.85$$

Step 6. Calculate the density from Equation 2-17:

$$\rho_g = \frac{(3000)(20.23)}{(0.85)(10.73)(640)} = 10.4 \text{ lb/ft}^3$$

Step 7. Calculate the density of the gas assuming an ideal gas behavior from Equation 2-7:

$$\rho_g = \frac{(3000)(20.23)}{(10.73)(640)} = 8.84 \text{ lb/ft}^3$$

The results of the above example show that the ideal gas equation estimated the gas density with an absolute error of 15% when compared with the density value as predicted with the real gas equation.

In cases where the composition of a natural gas is not available, the pseudo-critical properties, i.e., p_{pc} and T_{pc} , can be predicted solely from the specific gravity of the gas. Brown et al. (1948) presented a graphical method for a convenient approximation of the pseudo-critical pressure and pseudo-critical temperature of gases when only the specific gravity of the gas is available. The correlation is presented in Figure 2-2. Standing (1977) expressed this graphical correlation in the following mathematical forms:

Case 1: Natural Gas Systems

$$T_{pc} = 168 + 325 \gamma_g - 12.5 \gamma_g^2 \quad (2-18)$$

$$p_{pc} = 677 + 15.0 \gamma_g - 37.5 \gamma_g^2 \quad (2-19)$$

Case 2: Gas-Condensate Systems

$$T_{pc} = 187 + 330 \gamma_g - 71.5 \gamma_g^2 \quad (2-20)$$

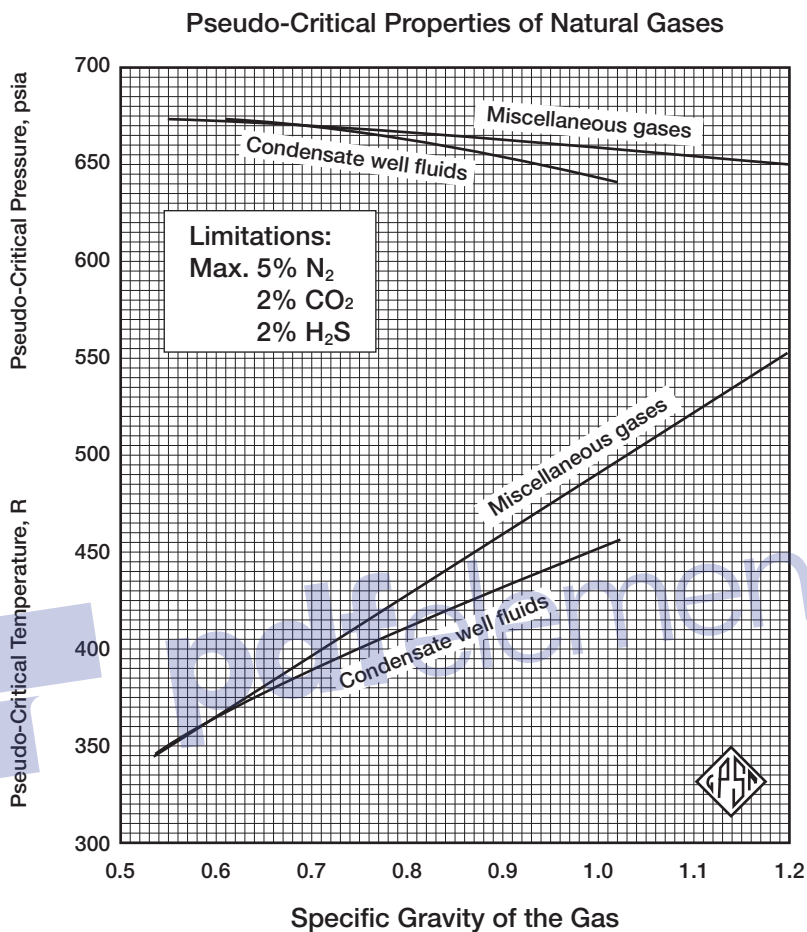


Figure 2-2. Pseudo-critical properties of natural gases. (Courtesy of GPSA and GPA Engineering Data Book, 10th Edition, 1987.)

$$p_{pc} = 706 - 51.7 \gamma_g - 11.1 \gamma_g^2 \quad (2-21)$$

where T_{pc} = pseudo-critical temperature, °R

p_{pc} = pseudo-critical pressure, psia

γ_g = specific gravity of the gas mixture

Example 2-7

Rework Example 2-5 by calculating the pseudo-critical properties from Equations 2-18 and 2-19.

Solution

Step 1. Calculate the specific gravity of the gas:

$$\gamma_g = \frac{M_a}{28.96} = \frac{20.23}{28.96} = 0.699$$

Step 2. Solve for the pseudo-critical properties by applying Equations 2-18 and 2-19:

$$T_{pc} = 168 + 325 (0.699) - 12.5 (0.699)^2 = 389.1^\circ\text{R}$$

$$p_{pc} = 677 + 15 (0.699) - 37.5 (0.699)^2 = 669.2 \text{ psia}$$

Step 3. Calculate p_{pr} and T_{pr} .

$$p_{pr} = \frac{3000}{669.2} = 4.48$$

$$T_{pr} = \frac{640}{389.1} = 1.64$$

Step 4. Determine the gas compressibility factor from Figure 2-1:

$$z = 0.824$$

Step 5. Calculate the density from Equation 2-17:

$$\rho_g = \frac{(3000)(20.23)}{(0.845)(10.73)(640)} = 10.46 \text{ lb/ft}^3$$

EFFECT OF NONHYDROCARBON COMPONENTS ON THE Z-FACTOR

Natural gases frequently contain materials other than hydrocarbon components, such as nitrogen, carbon dioxide, and hydrogen sulfide. Hydrocarbon gases are classified as sweet or sour depending on the hydrogen sulfide content. Both sweet and sour gases may contain nitrogen, carbon dioxide, or both. A hydrocarbon gas is termed a *sour gas* if it contains one grain of H_2S per 100 cubic feet.

The common occurrence of small percentages of nitrogen and carbon dioxide is, in part, considered in the correlations previously cited. Con-

centrations of up to 5 percent of these nonhydrocarbon components will not seriously affect accuracy. Errors in compressibility factor calculations as large as 10 percent may occur in higher concentrations of nonhydrocarbon components in gas mixtures.

Nonhydrocarbon Adjustment Methods

There are two methods that were developed to adjust the pseudo-critical properties of the gases to account for the presence of the nonhydrocarbon components. These two methods are the:

- Wichert-Aziz correction method
- Carr-Kobayashi-Burrows correction method

The Wichert-Aziz Correction Method

Natural gases that contain H₂S and or CO₂ frequently exhibit different compressibility-factor behavior than do sweet gases. Wichert and Aziz (1972) developed a simple, easy-to-use calculation procedure to account for these differences. This method permits the use of the Standing-Katz chart, i.e., Figure 2-1, by using a pseudo-critical temperature adjustment factor, which is a function of the concentration of CO₂ and H₂S in the sour gas. This correction factor is then used to adjust the pseudo-critical temperature and pressure according to the following expressions:

$$T'_{pc} = T_{pc} - \epsilon \quad (2-22)$$

$$p'_{pc} = \frac{p_{pc} T'_{pc}}{T_{pc} + B(1 - B)\epsilon} \quad (2-23)$$

where T_{pc} = pseudo-critical temperature, °R

p_{pc} = pseudo-critical pressure, psia

T'_{pc} = corrected pseudo-critical temperature, °R

p'_{pc} = corrected pseudo-critical pressure, psia

B = mole fraction of H₂S in the gas mixture

ϵ = pseudo-critical temperature adjustment factor and is defined mathematically by the following expression

$$\epsilon = 120 [A^{0.9} - A^{1.6}] + 15 (B^{0.5} - B^{4.0}) \quad (2-24)$$

where the coefficient A is the sum of the mole fraction H₂S and CO₂ in the gas mixture, or:

$$A = Y_{\text{H}_2\text{S}} + Y_{\text{CO}_2}$$

The computational steps of incorporating the adjustment factor ϵ into the z-factor calculations are summarized below:

Step 1. Calculate the pseudo-critical properties of the whole gas mixture by applying Equations 2-18 and 2-19 or Equations 2-20 and 2-21.

Step 2. Calculate the adjustment factor ϵ from Equation 2-24.

Step 3. Adjust the calculated p_{pc} and T_{pc} (as computed in Step 1) by applying Equations 2-22 and 2-23.

Step 4. Calculate the pseudo-reduced properties, i.e., p_{pr} and T_{pr} , from Equations 2-11 and 2-12.

Step 5. Read the compressibility factor from Figure 2-1.

Example 2-8

A sour natural gas has a specific gravity of 0.7. The compositional analysis of the gas shows that it contains 5% CO_2 and 10% H_2S . Calculate the density of the gas at 3,500 psia and 160°F.

Solution

Step 1. Calculate the uncorrected pseudo-critical properties of the gas from Equations 2-18 and 2-19:

$$T_{\text{pc}} = 168 + 325 (0.7) - 12.5 (0.7)^2 = 389.38^\circ\text{R}$$

$$p_{\text{pc}} = 677 + 15 (0.7) - 37.5 (0.7)^2 = 669.1 \text{ psia}$$

Step 2. Calculate the pseudo-critical temperature adjustment factor from Equation 2-24:

$$\epsilon = 120 (0.15^{0.9} - 0.15^{1.6}) + 15 (0.1^{0.5} - 0.1^4) = 20.735$$

Step 3. Calculate the corrected pseudo-critical temperature by applying Equation 2-22:

$$T'_{pc} = 389.38 - 20.735 = 368.64$$

Step 4. Adjust the pseudo-critical pressure p_{pc} by applying Equation 2-23:

$$p'_{pc} = \frac{(669.1)(368.64)}{389.38 + 0.1(1 - 0.1)(20.635)}$$

Step 5. Calculate p_{pr} and T_{pr} :

$$p_{pr} = \frac{3500}{630.44} = 5.55$$

$$T_{pr} = \frac{160 + 460}{368.64} = 1.68$$

Step 6. Determine the z -factor from Figure 2-1:

$$z = 0.89$$

Step 7. Calculate the apparent molecular weight of the gas from Equation 2-10:

$$M_a = (28.96)(0.7) = 20.27$$

Step 8. Solve for gas density:

$$\rho_g = \frac{(3500)(20.27)}{(0.89)(10.73)(620)} = 11.98 \text{ lb/ft}^3$$

The Carr-Kobayashi-Burrows Correction Method

Carr, Kobayashi, and Burrows (1954) proposed a simplified procedure to adjust the pseudo-critical properties of natural gases when nonhydrocarbon components are present. The method can be used when the composition of the natural gas is not available. The proposed procedure is summarized in the following steps:

Step 1. Knowing the specific gravity of the natural gas, calculate the pseudo-critical temperature and pressure by applying Equations 2-18 and 2-19.

Step 2. Adjust the estimated pseudo-critical properties by using the following two expressions:

$$T'_{pc} = T_{pc} - 80 y_{CO_2} + 130 y_{H_2S} - 250 y_{N_2} \quad (2-25)$$

$$p'_{pc} = p_{pc} + 440 y_{CO_2} + 600 y_{H_2S} - 170 y_{N_2} \quad (2-26)$$

where T'_{pc} = the adjusted pseudo-critical temperature, °R
 T_{pc} = the unadjusted pseudo-critical temperature, °R
 y_{CO_2} = mole fraction of CO₂
 y_{H_2S} = mole fraction of H₂S in the gas mixture
 y_{N_2} = mole fraction of nitrogen
 p'_{pc} = the adjusted pseudo-critical pressure, psia
 p_{pc} = the unadjusted pseudo-critical pressure, psia

Step 3. Use the adjusted pseudo-critical temperature and pressure to calculate the pseudo-reduced properties.

Step 4. Calculate the z-factor from Figure 2-1.

Example 2-9

Using the data in Example 2-8, calculate the density by employing the above correction procedure.

Solution

Step 1. Determine the corrected pseudo-critical properties from Equations 2-25 and 2-26:

$$T'_{pc} = 389.38 - 80 (0.05) + 130 (0.10) - 250 (0) = 398.38^\circ\text{R}$$

$$p'_{pc} = 669.1 + 440 (0.05) + 600 (0.10) - 170 (0) = 751.1 \text{ psia}$$

Step 2. Calculate p_{pr} and T_{pr} :

$$p_{pr} = \frac{3500}{751.1} = 4.56$$

$$T_{pr} = \frac{620}{398.38} = 1.56$$

Step 3. Determine the gas compressibility factor from Figure 2-1:

$$z = 0.820$$

Step 4. Calculate the gas density:

$$\rho_g = \frac{(3500)(20.27)}{(0.82)(10.73)(620)} = 13.0 \text{ lb/ft}^3$$

CORRECTION FOR HIGH-MOLECULAR-WEIGHT GASES

It should be noted that the Standing and Katz compressibility factor chart (Figure 2-1) was prepared from data on binary mixtures of methane with propane, ethane, and butane, and on natural gases, thus covering a wide range in composition of hydrocarbon mixtures containing methane. No mixtures having molecular weights in excess of 40 were included in preparing this plot.

Sutton (1985) evaluated the accuracy of the Standing-Katz compressibility factor chart using laboratory-measured gas compositions and z -factors, and found that the chart provides satisfactory accuracy for engineering calculations. However, Kay's mixing rules, i.e., Equations 2-13 and 2-14 (or comparable gravity relationships for calculating pseudo-critical pressure and temperature), result in unsatisfactory z -factors for high-molecular-weight reservoir gases. The author observed that large deviations occur to gases with high heptanes-plus concentrations. He pointed out that Kay's mixing rules should not be used to determine the pseudo-critical pressure and temperature for reservoir gases with specific gravities greater than about 0.75.

Sutton proposed that this deviation can be minimized by utilizing the mixing rules developed by Stewart et al. (1959), together with newly introduced empirical adjustment factors (F_J , E_J , and E_K) that are related to the presence of the heptane-plus fraction in the gas mixture. The proposed approach is outlined in the following steps:

Step 1. Calculate the parameters J and K from the following relationships:

$$J = \frac{1}{3} \left[\sum_i y_i (T_{ci}/p_{ci}) \right] + \frac{2}{3} \left[\sum_i y_i (T_{ci}/p_{ci})^{0.5} \right]^2 \quad (2-27)$$

$$K = \sum_i [y_i T_{ci} / \sqrt{p_{ci}}] \quad (2-28)$$

where J = Stewart-Burkhardt-Voo correlating parameter, °R/psia
 K = Stewart-Burkhardt-Voo correlating parameter, °R/psia
 y_i = mole fraction of component i in the gas mixture.

Step 2. Calculate the adjustment parameters F_J , E_J , and E_K from the following expressions:

$$F_J = \frac{1}{3} [Y(T_c/p_c)]_{C_{7+}} + \frac{2}{3} [Y(T_c/p_c)^{0.5}]_{C_{7+}}^2 \quad (2-29)$$

$$E_J = 0.6081 F_J + 1.1325 F_J^2 - 14.004 F_J y_{C_{7+}} + 64.434 F_J y_{C_{7+}}^2 \quad (2-30)$$

$$E_K = [T_c/\sqrt{P_c}]_{C_{7+}} [0.3129 y_{C_{7+}} - 4.8156 (y_{C_{7+}})^2 + 27.3751 (y_{C_{7+}})^3] \quad (2-31)$$

where $y_{C_{7+}}$ = mole fraction of the heptanes-plus component
 $(T_c)_{C_{7+}}$ = critical temperature of the C_{7+}
 $(p_c)_{C_{7+}}$ = critical pressure of the C_{7+}

Step 3. Adjust the parameters J and K by applying the adjustment factors E_J and E_K , according to the relationships:

$$J' = J - E_J \quad (2-32)$$

$$K' = K - E_K \quad (2-33)$$

where J, K = calculated from Equations 2-27 and 2-28
 E_J, E_K = calculated from Equations 2-30 and 2-31

Step 4. Calculate the adjusted pseudo-critical temperature and pressure from the expressions:

$$T'_{pc} = \frac{(K')^2}{J'} \quad (2-34)$$

$$p'_{pc} = \frac{T'_{pc}}{J'} \quad (2-35)$$

Step 5. Having calculated the adjusted T_{pc} and p_{pc} , the regular procedure of calculating the compressibility factor from the Standing and Katz chart is followed.

Sutton's proposed mixing rules for calculating the pseudo-critical properties of high-molecular-weight reservoir gases, i.e., $\gamma_g > 0.75$, should significantly improve the accuracy of the calculated z -factor.

Example 2-10

A hydrocarbon gas system has the following composition:

| Component | y |
|------------------|------|
| C ₁ | 0.83 |
| C ₂ | 0.06 |
| C ₃ | 0.03 |
| n-C ₄ | 0.02 |
| n-C ₅ | 0.02 |
| C ₆ | 0.01 |
| C ₇₊ | 0.03 |

The heptanes-plus fraction is characterized by a molecular weight and specific gravity of 161 and 0.81, respectively.

- Using Sutton's methodology, calculate the density of the gas 2,000 psi and 150°F.
- Recalculate the gas density without adjusting the pseudo-critical properties.

Solution

Part A.

Step 1. Calculate the critical properties of the heptanes-plus fraction by the Riazi-Daubert correlation (Chapter 1, Equation 1-2):

$$(T_c)_{C_{7+}} = 544.2 \cdot 161^{0.2998} \cdot 0.81^{1.0555} \cdot \exp^{[-1.3478(10)^{-4}(150) - 0.61641(0.81)]} = 1189^\circ\text{R}$$

$$(p_c)_{C_{7+}} = 4.5203(10)^4 \cdot 161^{-.8063} \cdot 0.81^{1.6015} \cdot \exp^{[-1.8078(10)^{-3}(150) - 0.3084(0.81)]} = 318.4 \text{ psia}$$

Step 2. Construct the following table:

| Component | y_i | M_i | T_{ci} | p_{ci} | $y_i M_i$ | $y_i(T_{ci}/p_{ci})$ | $y_i z(\overline{T_c}/\overline{p_c})_i$ | $y_i(T_{ci}/z\overline{p_c})_i$ |
|------------------|-------|-------|----------|----------|-----------|----------------------|--|---------------------------------|
| C ₁ | 0.83 | 16.0 | 343.33 | 666.4 | 13.31 | .427 | .596 | 11.039 |
| C ₂ | 0.06 | 30.1 | 549.92 | 706.5 | 1.81 | .047 | .053 | 1.241 |
| C ₃ | 0.03 | 44.1 | 666.06 | 616.4 | 1.32 | .032 | .031 | .805 |
| n-C ₄ | 0.02 | 58.1 | 765.62 | 550.6 | 1.16 | .028 | .024 | .653 |
| n-C ₅ | 0.02 | 72.2 | 845.60 | 488.6 | 1.45 | .035 | .026 | .765 |
| C ₆ | 0.01 | 84.0 | 923.00 | 483.0 | 0.84 | .019 | .014 | .420 |
| C ₇₊ | 0.03 | 161. | 1189.0 | 318.4 | 4.83 | .112 | .058 | 1.999 |
| Total | | | | | 27.72 | 0.700 | 0.802 | 16.972 |

Step 3. Calculate the parameters J and K from Equations 2-27 and 2-28:

$$J = (1/3) [0.700] + (2/3) [0.802]^2 = 0.662$$

$$K = 16.922$$

Step 4. Determine the adjustment factors F_J , E_J and E_K by applying Equations 2-29 through 2-31:

$$F_J = \frac{1}{3}[0.112] + \frac{2}{3}[0.058]^2 = 0.0396$$

$$E_J = 0.6081 (0.04) + 1.1325 (0.04)^2 - 14.004 (0.04) (0.03) + 64.434 (0.04) 0.3^2 = 0.012$$

$$E_K = 66.634 [0.3129 (0.03) - 4.8156 (0.03)^2 + 27.3751 (0.03)^3] = 0.386$$

Step 5. Calculate the parameters J' and K' from Equations 2-32 and 2-33:

$$J' = 0.662 - 0.012 = 0.650$$

$$K' = 16.922 - 0.386 = 16.536$$

Step 6. Determine the adjusted pseudo-critical properties from Equations 2-33 and 2-36:

$$T'_{pc} = \frac{(16.536)^2}{0.65} = 420.7$$

$$p'_{pc} = \frac{420.7}{0.65} = 647.2$$

Step 7. Calculate the pseudo-reduced properties of the gas by applying Equations 2-11 and 2-12, to give:

$$p_{pr} = \frac{2000}{647.2} = 3.09$$

$$T_{pr} = \frac{610}{420.7} = 1.45$$

Step 8. Calculate the z-factor from Figure 2-1 to give:

$$z = 0.745$$

Step 9. From Equation 2-16, calculate the density of the gas:

$$\rho_g = \frac{(2000)(24.73)}{(10.73)(610)(.745)} = 10.14 \text{ lb/ft}^3$$

Part B.

Step 1. Calculate the specific gravity of the gas:

$$\gamma_g = \frac{M_a}{28.96} = \frac{24.73}{28.96} = 0.854$$

Step 2. Solve for the pseudo-critical properties by applying Equations 2-18 and 2-19:

$$T_{pc} = 168 + 325 (0.854) - 12.5 (0.854)^2 = 436.4^\circ\text{R}$$

$$p_{pc} = 677 + 15 (0.854) - 37.5 (0.854)^2 = 662.5 \text{ psia}$$

Step 3. Calculate p_{pr} and T_{pr} :

$$p_{pr} = \frac{2000}{662.5} = 3.02$$

$$T_{pr} = \frac{610}{436.4} = 1.40$$

Step 4. Calculate the z-factor from Figure 2-1 to give:

$$z = 0.710$$

Step 5. From Equation 2-16, calculate the density of the gas:

$$\rho_g = \frac{(2000)(24.73)}{(10.73)(610)(.710)} = 10.64 \text{ lb/ft}^3$$

DIRECT CALCULATION OF COMPRESSIBILITY FACTORS

After four decades of existence, the Standing-Katz z-factor chart is still widely used as a practical source of natural gas compressibility factors. As a result, there has been an apparent need for a simple mathematical description of that chart. Several empirical correlations for calculating z-factors have been developed over the years. The following three empirical correlations are described below:

- Hall-Yarborough
- Dranchuk-Abu-Kassem
- Dranchuk-Purvis-Robinson

The Hall-Yarborough Method

Hall and Yarborough (1973) presented an equation-of-state that accurately represents the Standing and Katz z-factor chart. The proposed expression is based on the Starling-Carnahan equation-of-state. The coefficients of the correlation were determined by fitting them to data taken from the Standing and Katz z-factor chart. Hall and Yarborough proposed the following mathematical form:

$$z = \left[\frac{0.06125 p_{pr} t}{Y} \right] \exp[-1.2(1-t)^2] \quad (2-36)$$

where p_{pr} = pseudo-reduced pressure

t = reciprocal of the pseudo-reduced temperature, i.e., T_{pc}/T

Y = the reduced density that can be obtained as the solution of the following equation:

$$F(Y) = X1 + \frac{Y + Y^2 + Y^3 + Y^4}{(1 - Y)^3} - (X2) Y^2 + (X3) Y^{X4} = 0 \quad (2-37)$$

where $X1 = -0.06125 p_{pr} t \exp [-1.2 (1 - t)^2]$

$$X2 = (14.76 t - 9.76 t^2 + 4.58 t^3)$$

$$X3 = (90.7 t - 242.2 t^2 + 42.4 t^3)$$

$$X4 = (2.18 + 2.82 t)$$

Equation 2-37 is a nonlinear equation and can be conveniently solved for the reduced density Y by using the Newton-Raphson iteration technique. The computational procedure of solving Equation 2-37 at any specified pseudo-reduced pressure p_{pr} and temperature T_{pr} is summarized in the following steps:

Step 1. Make an initial guess of the unknown parameter, Y^k , where k is an iteration counter. An appropriate initial guess of Y is given by the following relationship:

$$Y^k = 0.0125 p_{pr} t \exp [-1.2 (1 - t)^2]$$

Step 2. Substitute this initial value in Equation 2-37 and evaluate the nonlinear function. Unless the correct value of Y has been initially selected, Equation 2-37 will have a nonzero value of $F(Y)$:

Step 3. A new improved estimate of Y , i.e., Y^{k+1} , is calculated from the following expression:

$$Y^{k+1} = Y^k - \frac{f(Y^k)}{f'(Y^k)} \quad (2-38)$$

where $f'(Y^k)$ is obtained by evaluating the derivative of Equation 2-37 at Y^k , or:

$$f'(Y) = \frac{1 + 4Y + 4Y^2 - 4Y^3 + Y^4}{(1 - Y)^4} - 2(X2) Y + (X3)(X4) Y^{(X4-1)} \quad (2-39)$$

Step 4. Steps 2–3 are repeated n times, until the error, i.e., $\text{abs}(Y^k - Y^{k+1})$, becomes smaller than a preset tolerance, e.g., 10^{-12} .

Step 5. The correct value of Y is then used to evaluate Equation 2-36 for the compressibility factor.

Hall and Yarborough pointed out that the method is not recommended for application if the pseudo-reduced temperature is less than one.

The Dranchuk-Abu-Kassem Method

Dranchuk and Abu-Kassem (1975) derived an analytical expression for calculating the reduced gas density that can be used to estimate the gas compressibility factor. The reduced gas density ρ_r is defined as the ratio of the gas density at a specified pressure and temperature to that of the gas at its critical pressure or temperature, or:

$$\rho_r = \frac{\rho}{\rho_c} = \frac{p M_a / [zRT]}{p_c M_a / [z_c R T_c]} = \frac{p / [zT]}{p_c / [z_c T_c]}$$

The critical gas compressibility factor z_c is approximately 0.27, which leads to the following simplified expression for the reduced gas density:

$$\rho_r = \frac{0.27 p_{pr}}{z T_{pr}} \quad (2-40)$$

The authors proposed the following eleven-constant equation-of-state for calculating the reduced gas density:

$$\begin{aligned} f(\rho_r) = & (R_1) \rho_r - \frac{R_2}{\rho_r} + (R_3) \rho_r^2 - (R_4) \rho_r^5 \\ & + (R_5) (1 + A_{11} \rho_r^2) \rho_r^2 \exp[-A_{11} \rho_r^2] + 1 = 0 \end{aligned} \quad (2-41)$$

With the coefficients R_1 through R_5 as defined by the following relations:

$$R_1 = \left[A_1 + \frac{A_2}{T_{pr}} + \frac{A_3}{T_{pr}^3} + \frac{A_r}{T_{pr}^4} + \frac{A_t}{T_{pr}^5} \right]$$

$$R_2 = \left[\frac{0.27 p_{pr}}{T_{pr}} \right]$$

$$R_3 = \left[A_6 + \frac{A_7}{T_{pr}} + \frac{A_8}{T_{pr}^2} \right]$$

$$R_4 = A_9 \left[\frac{A_7}{T_{pr}} + \frac{A_8}{T_{pr}^2} \right]$$

$$R_5 = \left[\frac{A_{10}}{T_{pr}^3} \right]$$

The constants A_1 through A_{11} were determined by fitting the equation, using nonlinear regression models, to 1,500 data points from the Standing and Katz z-factor chart. The coefficients have the following values:

$$\begin{array}{llll} A_1 = 0.3265 & A_2 = -1.0700 & A_3 = -0.5339 & A_4 = 0.01569 \\ A_5 = -0.05165 & A_6 = 0.5475 & A_7 = -0.7361 & A_8 = 0.1844 \\ A_9 = 0.1056 & A_{10} = 0.6134 & A_{11} = 0.7210 & \end{array}$$

Equation 2-41 can be solved for the reduced gas density ρ_r by applying the Newton-Raphson iteration technique as summarized in the following steps:

Step 1. Make an initial guess of the unknown parameter, ρ_r^k , where k is an iteration counter. An appropriate initial guess of ρ_r^k is given by the following relationship:

$$\rho_r = \frac{0.27 p_{pr}}{T_{pr}}$$

Step 2. Substitute this initial value in Equation 2-41 and evaluate the nonlinear function. Unless the correct value of ρ_r^k has been initially selected, Equation 2-41 will have a nonzero value for the function $f(\rho_r^k)$.

Step 3. A new improved estimate of ρ_r , i.e., ρ_r^{k+1} , is calculated from the following expression:

$$\rho_r^{k+1} = \rho_r^k - \frac{f(\rho_r^k)}{f'(\rho_r^k)}$$

where

$$f'(\rho_r) = (R_1) + \frac{R_2}{\rho_r^2} + 2(R_3)\rho_r - 5(R_4)\rho_r^4 + 2(R_5)\rho_r \exp[-A_{11}\rho_r^2][(1 + 2A_{11}\rho_r^3) - A_{11}\rho_r^2(1 + A_{11}\rho_r^2)]$$

Step 4. Steps 2–3 are repeated n times, until the error, i.e., $\text{abs}(\rho_r^k - \rho_r^{k+1})$, becomes smaller than a preset tolerance, e.g., 10^{-12} .

Step 5. The correct value of ρ_r is then used to evaluate Equation 2-40 for the compressibility factor, i.e.:

$$z = \frac{0.27 p_{pr}}{\rho_r T_{pr}}$$

The proposed correlation was reported to duplicate compressibility factors from the Standing and Katz chart with an average absolute error of 0.585 percent and is applicable over the ranges:

$$0.2 < p_{pr} < 15$$

$$1.0 < T_{pr} < 3.0$$

The Dranchuk-Purvis-Robinson Method

Dranchuk, Purvis, and Robinson (1974) developed a correlation based on the Benedict-Webb-Rubin type of equation-of-state. Fitting the equation to 1,500 data points from the Standing and Katz z -factor chart optimized the eight coefficients of the proposed equations. The equation has the following form:

$$1 + T_1 \rho_r + T_2 \rho_r^2 + T_3 \rho_r^5 + [T_4 \rho_r^2 (1 + A_8 \rho_r^2) \exp(-A_8 \rho_r^2)] - \frac{T_5}{\rho_r} = 0 \quad (2-42)$$

with

$$T_1 = \left[A_1 + \frac{A_2}{T_{pr}} + \frac{A_3}{T_{pr}^3} \right]$$

$$T_2 = \left[A_4 + \frac{A_5}{T_{pr}} \right]$$

$$T_3 = [A_5 A_6 / T_{pr}]$$

$$T_4 = [A_7 / T_{pr}^3]$$

$$T_5 = [0.27 p_{pr} / T_{pr}]$$

where ρ_r is defined by Equation 2-41 and the coefficients A_1 through A_8 have the following values:

$$A_1 = 0.31506237$$

$$A_5 = -0.61232032$$

$$A_2 = -1.0467099$$

$$A_6 = -0.10488813$$

$$A_3 = -0.57832720$$

$$A_7 = 0.68157001$$

$$A_4 = 0.53530771$$

$$A_8 = 0.68446549$$

The solution procedure of Equation 2-43 is similar to that of Dranchuk and Abu-Kassem.

The method is valid within the following ranges of pseudo-reduced temperature and pressure:

$$1.05 < T_{pr} < 3.0$$

$$0.2 < p_{pr} < 3.0$$

COMPRESSIBILITY OF NATURAL GASES

Knowledge of the variability of fluid compressibility with pressure and temperature is essential in performing many reservoir engineering calculations. For a liquid phase, the compressibility is small and usually assumed to be constant. For a gas phase, the compressibility is neither small nor constant.

By definition, the isothermal gas compressibility is the change in volume per unit volume for a unit change in pressure or, in equation form:

$$c_g = -\frac{1}{V} \left(\frac{\partial V}{\partial p} \right)_T \quad (2-44)$$

where c_g = isothermal gas compressibility, 1/psi.

From the real gas equation-of-state:

$$V = \frac{nRTz}{p}$$

Differentiating the above equation with respect to pressure at constant temperature T gives:

$$\left(\frac{\partial V}{\partial p}\right)_T = nRT \left[\frac{1}{p} \left(\frac{\partial z}{\partial p}\right) - \frac{z}{p^2} \right]$$

Substituting into Equation 2-44 produces the following generalized relationship:

$$c_g = \frac{1}{p} - \frac{1}{z} \left(\frac{\partial z}{\partial p}\right)_T \quad (2-45)$$

For an ideal gas, $z = 1$ and $(\partial z/\partial p)_T = 0$, therefore:

$$c_g = \frac{1}{p} \quad (2-46)$$

It should be pointed out that Equation 2-46 is useful in determining the expected order of magnitude of the isothermal gas compressibility.

Equation 2-45 can be conveniently expressed in terms of the pseudo-reduced pressure and temperature by simply replacing p with $(p_{pr} p_{pc})$, or:

$$c_g = \frac{1}{p_{pr} p_{pc}} - \frac{1}{z} \left[\frac{\partial z}{\partial (p_{pr} p_{pc})} \right]_{T_{pr}}$$

Multiplying the above equation by p_{pc} yields:

$$c_g p_{pc} = c_{pr} = \frac{1}{p_{pr}} - \frac{1}{z} \left[\frac{\partial z}{\partial p_{pr}} \right]_{T_{pr}} \quad (2-47)$$

The term c_{pr} is called the isothermal pseudo-reduced compressibility and is defined by the relationship:

$$c_{pr} = c_g p_{pc} \quad (2-48)$$

where c_{pr} = isothermal pseudo-reduced compressibility
 c_g = isothermal gas compressibility, psi^{-1}
 p_{pc} = pseudo-reduced pressure, psi

Values of $(\partial z / \partial p_{pr})_{T_{pr}}$ can be calculated from the slope of the T_{pr} isotherm on the Standing and Katz z -factor chart.

Example 2-11

A hydrocarbon gas mixture has a specific gravity of 0.72. Calculate the isothermal gas compressibility coefficient at 2,000 psia and 140°F by assuming:

- An ideal gas behavior
- A real gas behavior

Solution

- Assuming an ideal gas behavior, determine c_g by applying Equation 2-45:

$$c_g = \frac{1}{2000} = 500 \times 10^{-6} \text{psi}^{-1}$$

- Assuming a real gas behavior

Step 1. Calculate T_{pc} and p_{pc} by applying Equations 2-17 and 2-18

$$T_{pc} = 168 + 325 (0.72) - 12.5 (0.72)^2 = 395.5 \text{ }^\circ\text{R}$$

$$p_{pc} = 677 + 15 (0.72) - 37.5 (0.72)^2 = 668.4 \text{ psia}$$

Step 2. Compute p_{pr} and T_{pr} from Equations 2-11 and 2-12.

$$p_{pr} = \frac{2000}{668.4} = 2.99$$

$$T_{pr} = \frac{600}{395.5} = 1.52$$

Step 3. Determine the z -factor from Figure 2-1:

$$z = 0.78$$

Step 4. Calculate the slope $[\partial z / \partial p_{pr}]_{T_{pr} = 1.52}$:

$$\left[\frac{\partial z}{\partial p_{pr}} \right]_{T_{pr}} = -0.022$$

Step 5. Solve for c_{pr} by applying Equation 2-47:

$$c_{pr} = \frac{1}{2.99} - \frac{1}{0.78} [-0.022] = 0.3627$$

Step 6. Calculate c_g from Equation 2-48:

$$c_g = \frac{0.327}{668.4} = 543 \times 10^{-6} \text{ psi}^{-1}$$

Trube (1957) presented graphs from which the isothermal compressibility of natural gases may be obtained. The graphs, as shown in Figures 2-3 and 2-4, give the isothermal pseudo-reduced compressibility as a function of pseudo-reduced pressure and temperature.

Example 2-12

Using Trube's generalized charts, rework Example 2-11.

Solution

Step 1. From Figure 2-3, find c_{pr} :

$$c_{pr} = 0.36$$

Step 2. Solve for c_g by applying Equation 2-49:

$$c_g = \frac{0.36}{668.4} = 539 \times 10^{-6} \text{ psi}^{-1}$$

Matter, Brar, and Aziz (1975) presented an analytical technique for calculating the isothermal gas compressibility. The authors expressed c_{pr} as a function of $\partial p / \partial \rho_r$ rather than $\partial p / \partial p_{pr}$.

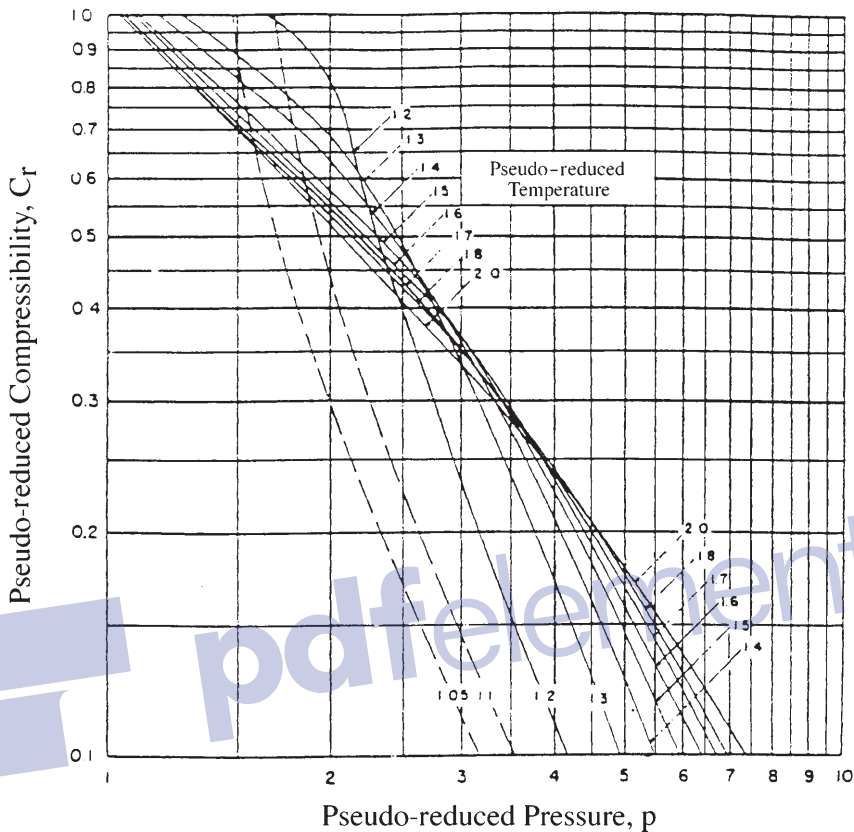


Figure 2-3. Trube's pseudo-reduced compressibility for natural gases. (Permission to publish by the Society of Petroleum Engineers of AIME. Copyright SPE-AIME.)

Equation 2-41 is differentiated with respect to p_{pr} to give:

$$\left[\frac{\partial z}{\partial p_{pr}} \right] = \frac{0.27}{z T_{pr}} \left[\frac{(\partial z / \partial p_r)_{T_{pr}}}{1 + \frac{p_r}{z} (\partial z / \partial p_r)_{T_{pr}}} \right] \quad (2-49)$$

Equation 2-49 may be substituted into Equation 2-47 to express the pseudo-reduced compressibility as:

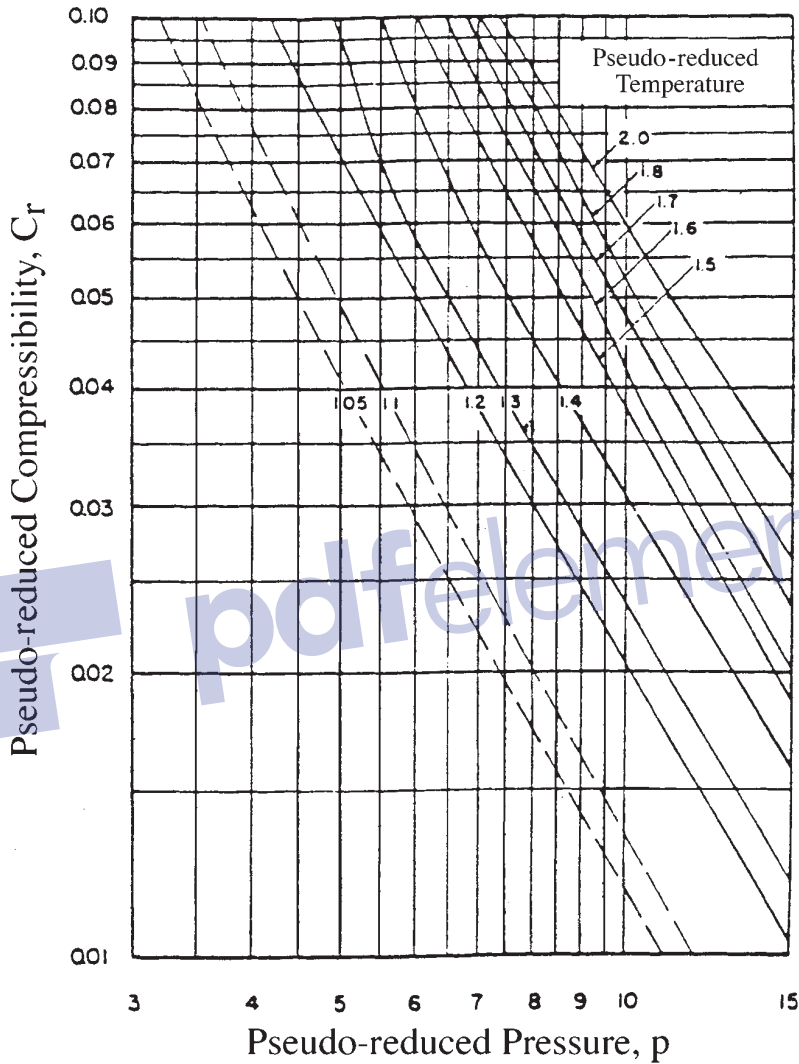


Figure 2-4. Trube's pseudo-reduced compressibility for natural gases. (Permission to publish by the Society of Petroleum Engineers of AIME. Copyright SPE-AIME.)

$$c_{pr} = \frac{1}{p_{pr}} - \frac{0.27}{z^2 T_{pr}} \left[\frac{(\partial z \partial p_r)_{T_{pr}}}{1 + \frac{\rho_r}{z} (\partial z \partial p_r)_{T_{pr}}} \right] \quad (2-50)$$

where ρ_r = pseudo-reduced gas density.

The partial derivative appearing in Equation 2-50 is obtained from Equation 2-43 to give:

$$\left[\frac{\partial z}{\partial \rho_r} \right]_{T_{pr}} = T_1 + 2 T_2 \rho_r + 5 T_3 \rho_r^4 + 2 T_4 \rho_r (1 + A_8 \rho_r^2 - A_8^2 \rho_r^4) \times \exp(-A_8 \rho_r^2) \quad (2-51)$$

where the coefficients T_1 through T_4 and A_1 through A_8 are defined previously by Equation 2-43.

GAS FORMATION VOLUME FACTOR

The gas formation volume factor is used to relate the volume of gas, as measured at reservoir conditions, to the volume of the gas as measured at standard conditions, i.e., 60°F and 14.7 psia. This gas property is then defined as the actual volume occupied by a certain amount of gas at a specified pressure and temperature, divided by the volume occupied by the same amount of gas at standard conditions. In an equation form, the relationship is expressed as

$$B_g = \frac{V_{p,T}}{V_{sc}} \quad (2-52)$$

where B_g = gas formation volume factor, ft³/scf

$V_{p,T}$ = volume of gas at pressure p and temperature, T , ft³

V_{sc} = volume of gas at standard conditions, scf

Applying the real gas equation-of-state, i.e., Equation 2-11, and substituting for the volume V , gives:

$$B_g = \frac{z_n RT}{z_{sc} n R T_{sc}} = \frac{p_{sc}}{p} \frac{zT}{T_{sc}}$$

where z_{sc} = z -factor at standard conditions = 1.0

p_{sc}, T_{sc} = standard pressure and temperature

Assuming that the standard conditions are represented by $p_{sc} = 14.7$ psia and $T_{sc} = 520$, the above expression can be reduced to the following relationship:

$$B_g = 0.02827 \frac{zT}{p} \quad (2-53)$$

where B_g = gas formation volume factor, ft^3/scf
 z = gas compressibility factor
 T = temperature, $^\circ\text{R}$

Equation 2-53 can be expressed in terms of the gas density ρ_g if combined with Equation 2-17, to give:

$$B_g = 0.02827 \frac{M_a}{R\rho_g} = 0.002635 \frac{M_a}{\rho_g}; \quad \text{ft}^3/\text{scf}$$

where ρ_g = gas density, lb/ft^3
 M_a = apparent molecular weight of gas

In other field units, the gas formation volume factor can be expressed in bbl/scf to give:

$$B_g = 0.005035 \frac{zT}{p} \quad (2-54)$$

Similarly, Equation 2-54 can be expressed in terms of the gas density ρ_g by:

$$B_g = 0.00504 \frac{M_a}{R\rho_g} = 0.000469 \frac{M_a}{\rho_g}; \quad \text{bbl}/\text{scf}$$

The reciprocal of the gas formation volume factor is called the *gas expansion factor* and is designated by the symbol E_g , or:

$$E_g = 35.37 \frac{p}{zT}; \quad \text{scf}/\text{ft}^3 \quad (2-55)$$

or in terms of the gas density ρ_g :

$$E_g = 35.37 \frac{R\rho_g}{M_a} = 379.52 \frac{\rho_g}{M_a}; \quad \text{scf}/\text{ft}^3$$

In other units:

$$E_g = 198.6 \frac{p}{zT}; \quad \text{scf}/\text{bbl} \quad (2-56)$$

or:

$$E_g = 198.6 \frac{R\rho_g}{M_a} = 2131.0 \frac{\rho_g}{M_a}; \quad \text{scf/bbl}$$

Example 2-13

A gas well is producing at a rate of 15,000 ft³/day from a gas reservoir at an average pressure of 2,000 psia and a temperature of 120°F. The specific gravity is 0.72. Calculate the gas flow rate in scf/day.

Solution

Step 1. Calculate the pseudo-critical properties from Equations 2-17 and 2-18 to give:

$$T_{pc} = 395.5 \text{ } ^\circ\text{R} \quad p_{pc} = 668.4 \text{ psia}$$

Step 2. Calculate the p_{pr} and T_{pr} :

$$p_{pr} = \frac{2000}{668.4} = 2.29$$

$$T_{pr} = \frac{600}{395.5} = 1.52$$

Step 3. Determine the z-factor from Figure 2-1:

$$z = 0.78$$

Step 4. Calculate the gas expansion factor from Equation 2-55:

$$E_g = 35.37 \frac{2000}{(0.78)(600)} = 151.15 \text{ scf/ft}^3$$

Step 5. Calculate the gas flow rate in scf/day by multiplying the gas flow rate (in ft³/day) by the gas expansion factor E_g as expressed in scf/ft³:

$$\text{Gas flow rate} = (151.15)(15,000) = 2.267 \text{ MMscf/day}$$

GAS VISCOSITY

The viscosity of a fluid is a measure of the internal fluid friction (resistance) to flow. If the friction between layers of the fluid is small, i.e., low viscosity, an applied shearing force will result in a large velocity gradi-

ent. As the viscosity increases, each fluid layer exerts a larger frictional drag on the adjacent layers and velocity gradient decreases.

The viscosity of a fluid is generally defined as the ratio of the shear force per unit area to the local velocity gradient. Viscosities are expressed in terms of poises, centipoise, or micropoises. One poise equals a viscosity of 1 dyne-sec/cm² and can be converted to other field units by the following relationships:

$$\begin{aligned} 1 \text{ poise} &= 100 \text{ centipoises} \\ &= 1 \times 10^6 \text{ micropoises} \\ &= 6.72 \times 10^{-2} \text{ lb mass/ft-sec} \\ &= 2.09 \times 10^{-3} \text{ lb-sec/ft}^2 \end{aligned}$$

The gas viscosity is not commonly measured in the laboratory because it can be estimated precisely from empirical correlations. Like all intensive properties, viscosity of a natural gas is completely described by the following function:

$$\mu_g = (p, T, y_i)$$

where μ_g = the viscosity of the gas phase. The above relationship simply states that the viscosity is a function of pressure, temperature, and composition. Many of the widely used gas viscosity correlations may be viewed as modifications of that expression.

METHODS OF CALCULATING THE VISCOSITY OF NATURAL GASES

Two popular methods that are commonly used in the petroleum industry are the:

- Carr-Kobayashi-Burrows Correlation Method
- Lee-Gonzalez-Eakin Method

The Carr-Kobayashi-Burrows Correlation Method

Carr, Kobayashi, and Burrows (1954) developed graphical correlations for estimating the viscosity of natural gas as a function of temperature, pressure, and gas gravity. The computational procedure of applying the proposed correlations is summarized in the following steps:

Step 1. Calculate the pseudo-critical pressure, pseudo-critical temperature, and apparent molecular weight from the specific gravity or the composition of the natural gas. Corrections to these pseudo-critical properties for the presence of the nonhydrocarbon gases (CO_2 , N_2 , and H_2S) should be made if they are present in concentrations greater than 5 mole percent.

Step 2. Obtain the viscosity of the natural gas at one atmosphere and the temperature of interest from Figure 2-5. This viscosity, as denoted by μ_1 , must be corrected for the presence of nonhydrocarbon components by using the inserts of Figure 2-5. The nonhydrocarbon fractions tend to increase the viscosity of the gas phase. The effect of nonhydrocarbon components on the viscosity of the natural gas can be expressed mathematically by the following relationships:

$$\mu_1 = (\mu_1)_{\text{uncorrected}} + (\Delta\mu)_{\text{N}_2} + (\Delta\mu)_{\text{CO}_2} + (\Delta\mu)_{\text{H}_2\text{S}} \quad (2-57)$$

where μ_1 = "corrected" gas viscosity at one atmospheric pressure and reservoir temperature, cp
 $(\Delta\mu)_{\text{N}_2}$ = viscosity corrections due to the presence of N_2
 $(\Delta\mu)_{\text{CO}_2}$ = viscosity corrections due to the presence of CO_2
 $(\Delta\mu)_{\text{H}_2\text{S}}$ = viscosity corrections due to the presence of H_2S
 $(\mu_1)_{\text{uncorrected}}$ = uncorrected gas viscosity, cp

Step 3. Calculate the pseudo-reduced pressure and temperature.

Step 4. From the pseudo-reduced temperature and pressure, obtain the viscosity ratio (μ_g/μ_1) from Figure 2-6. The term μ_g represents the viscosity of the gas at the required conditions.

Step 5. The gas viscosity, μ_g , at the pressure and temperature of interest is calculated by multiplying the viscosity at one atmosphere and system temperature, μ_1 , by the viscosity ratio.

The following examples illustrate the use of the proposed graphical correlations:

Example 2-14

Using the data given in Example 2-13, calculate the viscosity of the gas.

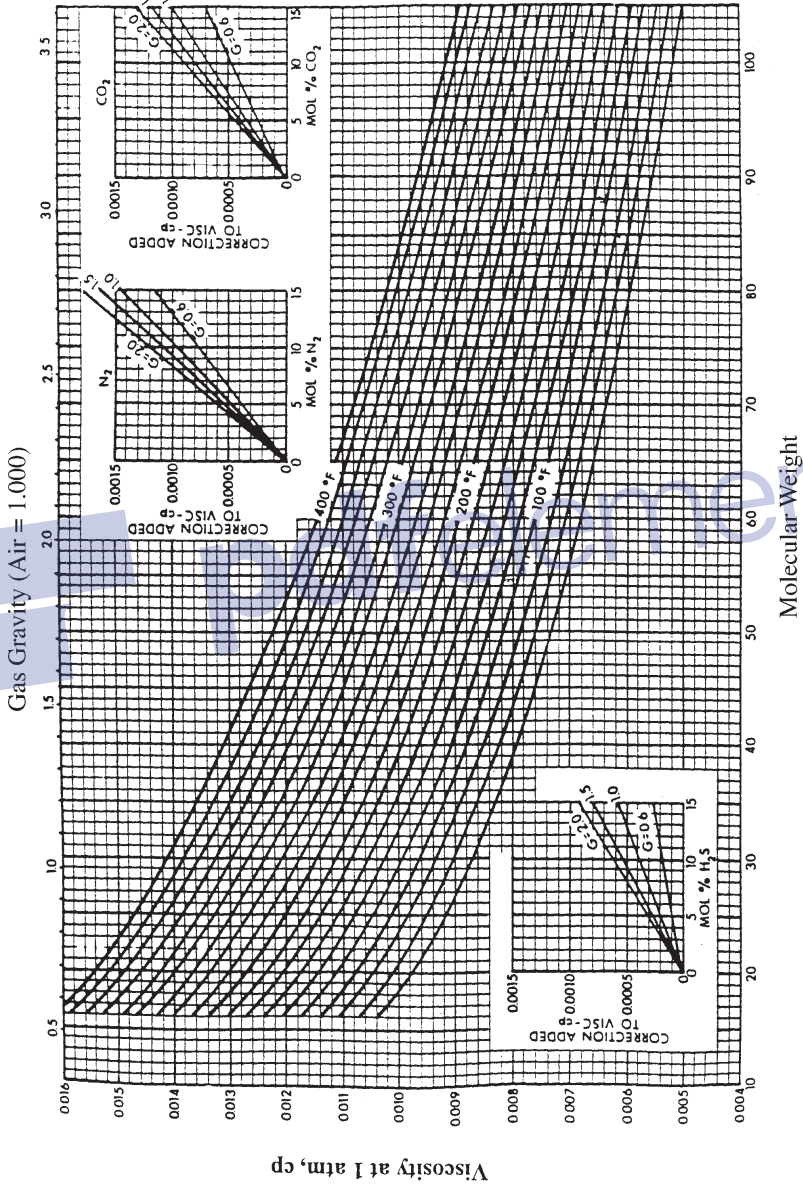


Figure 2-5. Carr's atmospheric gas viscosity correlation. (Permission to publish by the Society of Petroleum Engineers of AIME. Copyright SPE-AIME.)

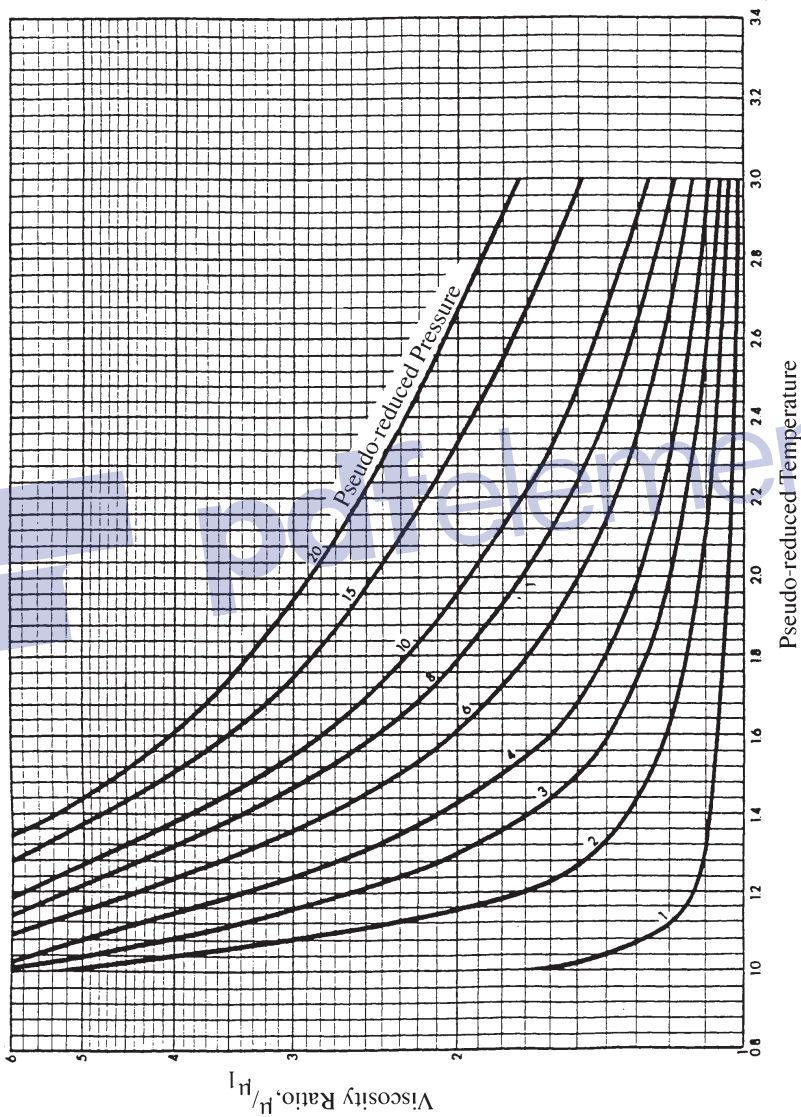


Figure 2-6. Carr's viscosity ratio correlation. (Permission to publish by the Society of Petroleum Engineers of AIME. Copyright SPE-AIME.)

Solution

Step 1. Calculate the apparent molecular weight of the gas:

$$M_a = (0.72)(28.96) = 20.85$$

Step 2. Determine the viscosity of the gas at 1 atm and 140°F from Figure 2-5:

$$\mu_1 = 0.0113$$

Step 3. Calculate p_{pr} and T_{pr} :

$$p_{pr} = 2.99$$

$$T_{pr} = 1.52$$

Step 4. Determine the viscosity rates from Figure 2-6:

$$\frac{\mu_g}{\mu_1} = 1.5$$

Step 5. Solve for the viscosity of the natural gas:

$$\mu_g = \frac{\mu_g}{\mu_1}(\mu_1) = (1.5)(0.0113) = 0.01695 \text{ cp}$$

Standing (1977) proposed a convenient mathematical expression for calculating the viscosity of the natural gas at atmospheric pressure and reservoir temperature, μ_1 . Standing also presented equations for describing the effects of N_2 , CO_2 , and H_2S on μ_1 . The proposed relationships are:

$$\mu_1 = (\mu_1)_{\text{uncorrected}} + (\Delta\mu)_{CO_2} + (\Delta\mu)_{H_2S} + (\Delta\mu)_{N_2}$$

where:

$$\begin{aligned} (\mu_1)_{\text{uncorrected}} = & [1.709(10^{-5} - 2.062 \cdot 10^{-6} \gamma_g)(T - 460) \\ & + 8.118(10^{-3}) - 6.15(10^{-3}) \log(\gamma_g)] \end{aligned} \quad (2-58)$$

$$(\Delta\mu)_{CO_2} = y_{CO_2} [(9.08 \times 10^{-3}) \log \gamma_g + (6.24 \times 10^{-3})]$$

$$(\Delta\mu)_{N_2} = y_{N_2} [8.48(10^{-3}) \log(\gamma_g) + 9.59(10^{-3})] \quad (2-59)$$

$$(\Delta\mu)_{\text{H}_2\text{S}} = y_{\text{H}_2\text{S}} [8.49(10^{-3}) \log(\gamma_g) + 3.73(10^{-3})] \quad (2-60)$$

where μ_1 = viscosity of the gas at atmospheric pressure and reservoir temperature, cp
 T = reservoir temperature, °R
 γ_g = gas gravity
 $y_{\text{N}_2}, y_{\text{CO}_2}, y_{\text{H}_2\text{S}}$ = mole fraction of $\text{N}_2, \text{CO}_2,$ and H_2S , respectively

Dempsey (1965) expressed the viscosity ratio μ_g/μ_1 by the following relationship:

$$\begin{aligned} \ln \left[T_{\text{pr}} \left(\frac{\mu_g}{\mu_1} \right) \right] = & a_0 + a_1 p_{\text{pr}} + a_2 p_{\text{pr}}^2 + a_3 p_{\text{pr}}^3 + T_{\text{pr}} (a_4 + a_5 p_{\text{pr}} \\ & + a_6 p_{\text{pr}}^2 + a_7 p_{\text{pr}}^3) + T_{\text{pr}}^2 (a_8 + a_9 p_{\text{pr}} + a_{10} p_{\text{pr}}^2 + a_{11} p_{\text{pr}}^3) \\ & + T_{\text{pr}}^3 (a_{12} + a_{13} p_{\text{pr}} + a_{14} p_{\text{pr}}^2 + a_{15} p_{\text{pr}}^3) \end{aligned} \quad (2-61)$$

where T_{pr} = pseudo-reduced temperature of the gas mixture, °R
 p_{pr} = pseudo-reduced pressure of the gas mixture, psia
 $a_0 \dots a_{17}$ = coefficients of the equations are given below:

| | |
|-------------------------------|----------------------------------|
| $a_0 = -2.46211820$ | $a_8 = -7.93385648 (10^{-1})$ |
| $a_1 = 2.970547414$ | $a_9 = 1.39643306$ |
| $a_2 = -2.86264054 (10^{-1})$ | $a_{10} = -1.49144925 (10^{-1})$ |
| $a_3 = 8.05420522 (10^{-3})$ | $a_{11} = 4.41015512 (10^{-3})$ |
| $a_4 = 2.80860949$ | $a_{12} = 8.39387178 (10^{-2})$ |
| $a_5 = -3.49803305$ | $a_{13} = -1.86408848 (10^{-1})$ |
| $a_6 = 3.60373020 (10^{-1})$ | $a_{14} = 2.03367881 (10^{-2})$ |
| $a_7 = -1.044324 (10^{-2})$ | $a_{15} = -6.09579263 (10^{-4})$ |

The Lee-Gonzalez-Eakin Method

Lee, Gonzalez, and Eakin (1966) presented a semi-empirical relationship for calculating the viscosity of natural gases. The authors expressed the gas viscosity in terms of the reservoir temperature, gas density, and the molecular weight of the gas. Their proposed equation is given by:

$$\mu_g = 10^{-4} K \exp \left[X \left(\frac{\rho_g}{62.4} \right)^Y \right] \quad (2-62)$$

where

$$K = \frac{(9.4 + 0.02 M_a) T^{1.5}}{209 + 19 M_a + T} \quad (2-63)$$

$$X = 3.5 + \frac{986}{T} + 0.01 M_a \quad (2-64)$$

$$Y = 2.4 - 0.2 X \quad (2-65)$$

ρ_g = gas density at reservoir pressure and temperature, lb/ft³

T = reservoir temperature, °R

M_a = apparent molecular weight of the gas mixture

The proposed correlation can predict viscosity values with a standard deviation of 2.7% and a maximum deviation of 8.99%. The correlation is less accurate for gases with higher specific gravities. The authors pointed out that the method cannot be used for sour gases.

Example 2-15

Rework Example 2-14 and calculate the gas viscosity by using the Lee-Gonzalez-Eakin method.

Step 1. Calculate the gas density from Equation 2-16:

$$\rho_g = \frac{(2000)(20.85)}{(10.73)(600)(0.78)} = 8.3 \text{ lb/ft}^3$$

Step 2. Solve for the parameters K, X, and Y by using Equations 2-64, 2-65, and 2-66, respectively:

$$K = \frac{[9.4 + 0.02(20.85)](600)^{1.5}}{209 + 19(20.85) + 600} = 119.72$$

$$X = 3.5 + \frac{986}{600} + 0.01(20.85) = 5.35$$

$$Y = 2.4 - 0.2(5.35) = 1.33$$

Step 3. Calculate the viscosity from Equation 2-63:

$$\mu_g = 10^{-4} (119.72) \exp \left[5.35 \left(\frac{8.3}{62.4} \right)^{1.33} \right] = 0.0173 \text{ cp}$$

PROPERTIES OF CRUDE OIL SYSTEMS

Petroleum (an equivalent term is *crude oil*) is a complex mixture consisting predominantly of hydrocarbons and containing sulfur, nitrogen, oxygen, and helium as minor constituents. The physical and chemical properties of crude oils vary considerably and are dependent on the concentration of the various types of hydrocarbons and minor constituents present.

An accurate description of physical properties of crude oils is of a considerable importance in the fields of both applied and theoretical science and especially in the solution of petroleum reservoir engineering problems. Physical properties of primary interest in petroleum engineering studies include:

- Fluid gravity
- Specific gravity of the solution gas
- Gas solubility
- Bubble-point pressure
- Oil formation volume factor
- Isothermal compressibility coefficient of undersaturated crude oils
- Oil density
- Total formation volume factor
- Crude oil viscosity
- Surface tension

Data on most of these fluid properties are usually determined by laboratory experiments performed on samples of actual reservoir fluids. In the absence of experimentally measured properties of crude oils, it is necessary for the petroleum engineer to determine the properties from empirically derived correlations.

Crude Oil Gravity

The crude oil density is defined as the mass of a unit volume of the crude at a specified pressure and temperature. It is usually expressed in pounds per cubic foot. The specific gravity of a crude oil is defined as the

ratio of the density of the oil to that of water. Both densities are measured at 60°F and atmospheric pressure:

$$\gamma_o = \frac{\rho_o}{\rho_w} \quad (2-66)$$

where γ_o = specific gravity of the oil
 ρ_o = density of the crude oil, lb/ft³
 ρ_w = density of the water, lb/ft³

It should be pointed out that the liquid specific gravity is dimensionless, but traditionally is given the units 60°/60° to emphasize the fact that both densities are measured at standard conditions. The density of the water is approximately 62.4 lb/ft³, or:

$$\gamma_o = \frac{\rho_o}{62.4}, 60^\circ/60^\circ$$

Although the density and specific gravity are used extensively in the petroleum industry, the API gravity is the preferred gravity scale. This gravity scale is precisely related to the specific gravity by the following expression:

$$^\circ\text{API} = \frac{141.5}{\gamma_o} - 131.5 \quad (2-67)$$

The API gravities of crude oils usually range from 47° API for the lighter crude oils to 10° API for the heavier asphaltic crude oils.

Example 2-16

Calculate the specific gravity and the API gravity of a crude oil system with a measured density of 53 lb/ft³ at standard conditions.

Solution

Step 1. Calculate the specific gravity from Equation 2-67:

$$\gamma_o = \frac{53}{62.4} = 0.849$$

Step 2. Solve for the API gravity:

$$\text{API} = \frac{141.5}{0.849} - 131.5 = 35.2^\circ \text{ API}$$

Specific Gravity of the Solution Gas

The specific gravity of the solution gas γ_g is described by the weighted average of the specific gravities of the separated gas from each separator. This weighted-average approach is based on the separator gas-oil ratio, or:

$$\gamma_g = \frac{\sum_{i=1}^n (R_{\text{sep}})_i (\gamma_{\text{sep}})_i + R_{\text{st}} \gamma_{\text{st}}}{\sum_{i=1}^n (R_{\text{sep}})_i + R_{\text{st}}} \quad (2-68)$$

where n = number of separators

R_{sep} = separator gas-oil ratio, scf/STB

γ_{sep} = separator gas gravity

R_{st} = gas-oil ratio from the stock tank, scf/STB

γ_{st} = gas gravity from the stock tank

Example 2-17

Separator tests were conducted on a crude oil sample. Results of the test in terms of the separator gas-oil ratio and specific gravity of the separated gas are given below:

| Separator # | Pressure psig | Temperature °F | Gas-Oil Ratio scf/STB | Gas Specific Gravity |
|--------------|---------------|----------------|-----------------------|----------------------|
| Primary | 660 | 150 | 724 | 0.743 |
| Intermediate | 75 | 110 | 202 | 0.956 |
| Stock tank | 0 | 60 | 58 | 1.296 |

Calculate the specific gravity of the separated gas.

Solution

Estimate the specific gravity of the solution by using Equation 2-69:

$$\gamma_g = \frac{(724)(0.743) + (202)(0.956) + (58)(1.296)}{724 + 202 + 58} = 0.819$$

Gas Solubility

The gas solubility R_s is defined as the number of standard cubic feet of gas that will dissolve in one stock-tank barrel of crude oil at certain pressure and temperature. The solubility of a natural gas in a crude oil is a strong function of the pressure, temperature, API gravity, and gas gravity.

For a particular gas and crude oil to exist at a constant temperature, the solubility increases with pressure until the saturation pressure is reached. At the saturation pressure (bubble-point pressure) all the available gases are dissolved in the oil and the gas solubility reaches its maximum value. Rather than measuring the amount of gas that will dissolve in a given stock-tank crude oil as the pressure is increased, it is customary to determine the amount of gas that will come out of a sample of reservoir crude oil as pressure decreases.

A typical gas solubility curve, as a function of pressure for an undersaturated crude oil, is shown in Figure 2-7. As the pressure is reduced from the initial reservoir pressure p_i to the bubble-point pressure p_b , no gas evolves from the oil and consequently the gas solubility remains constant at its maximum value of R_{sb} . Below the bubble-point pressure, the solution gas is liberated and the value of R_s decreases with pressure. The following five empirical correlations for estimating the gas solubility are given below:

- Standing's correlation
- The Vasquez-Beggs correlation
- Glaso's correlation
- Marhoun's correlation
- The Petrosky-Farshad correlation

Standing's Correlation

Standing (1947) proposed a graphical correlation for determining the gas solubility as a function of pressure, gas specific gravity, API gravity, and system temperature. The correlation was developed from a total of 105 experimentally determined data points on 22 hydrocarbon mixtures from California crude oils and natural gases. The proposed correlation has an average error of 4.8%. Standing (1981) expressed his proposed graphical correlation in the following more convenient mathematical form:

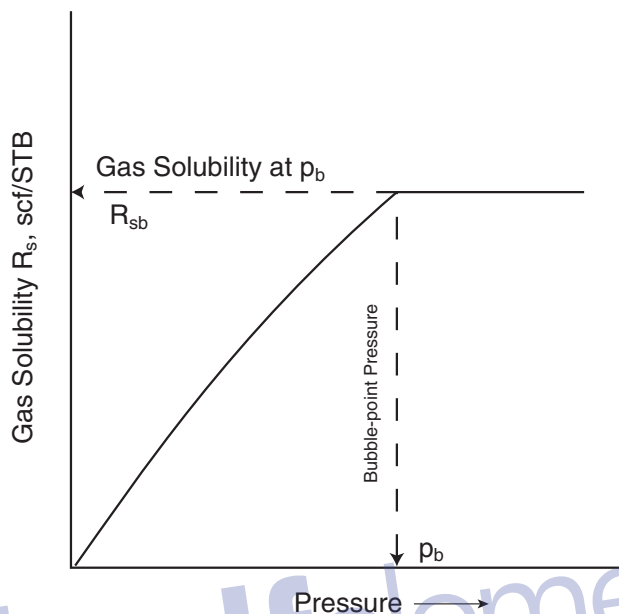


Figure 2-7. Gas-solubility pressure diagram.

$$R_s = \gamma_{\text{sg}} \left[\left(\frac{p}{18.2} + 1.4 \right) 10^x \right]^{1.2048} \quad (2-69)$$

with

$$x = 0.0125 \text{ API} - 0.00091(T - 460)$$

where T = temperature, °R

p = system pressure, psia

γ_{sg} = solution gas specific gravity

It should be noted that Standing's equation is valid for applications at and below the bubble-point pressure of the crude oil.

Example 2-18

The following experimental PVT data on six different crude oil systems are available. Results are based on two-stage surface separation.

| Oil # | T | p_b | R_s | B_o | ρ_o | c_o at $p > p_b$ | p_{sep} | T_{sep} | API | γ_g |
|-------|-----|-------|-------|-------|----------|--------------------------------|-----------|-----------|------|------------|
| 1 | 250 | 2377 | 751 | 1.528 | 38.13 | 22.14×10^{-6} at 2689 | 150 | 60 | 47.1 | 0.851 |
| 2 | 220 | 2620 | 768 | 1.474 | 40.95 | 18.75×10^{-6} at 2810 | 100 | 75 | 40.7 | 0.855 |
| 3 | 260 | 2051 | 693 | 1.529 | 37.37 | 22.69×10^{-6} at 2526 | 100 | 72 | 48.6 | 0.911 |
| 4 | 237 | 2884 | 968 | 1.619 | 38.92 | 21.51×10^{-6} at 2942 | 60 | 120 | 40.5 | 0.898 |
| 5 | 218 | 3045 | 943 | 1.570 | 37.70 | 24.16×10^{-6} at 3273 | 200 | 60 | 44.2 | 0.781 |
| 6 | 180 | 4239 | 807 | 1.385 | 46.79 | 11.45×10^{-6} at 4370 | 85 | 173 | 27.3 | 0.848 |

where T = reservoir temperature, °F
 p_b = bubble-point pressure, psig
 B_o = oil formation volume factor, bbl/STB
 p_{sep} = separator pressure, psig
 T_{sep} = separator temperature, °F
 c_o = isothermal compressibility coefficient of the oil at a specified pressure, psi^{-1}

Using Standing's correlation, estimate the gas solubility at the bubble-point pressure and compare with the experimental value in terms of the absolute average error (AAE).

Solution

Apply Equation 2-70 to determine the gas solubility. Results of the calculations are given in the following tabulated form:

| Oil # | X | 10^X | Predicted R_s Equation 2-70 | Measured R_s | % Error |
|-------|-------|--------|----------------------------------|----------------|---------|
| 1 | 0.361 | 2.297 | 838 | 751 | 11.6 |
| 2 | 0.309 | 2.035 | 817 | 768 | 6.3 |
| 3 | 0.371 | 2.349 | 774 | 693 | 11.7 |
| 4 | 0.312 | 2.049 | 969 | 968 | 0.108 |
| 5 | 0.322 | 2.097 | 1012 | 943 | 7.3 |
| 6 | 0.177 | 1.505 | 998 | 807 | 23.7 |

AAE = 10.1%

The Vasquez-Beggs Correlation

Vasquez and Beggs (1980) presented an improved empirical correlation for estimating R_s . The correlation was obtained by regression analy-

sis using 5,008 measured gas solubility data points. Based on oil gravity, the measured data were divided into two groups. This division was made at a value of oil gravity of 30°API. The proposed equation has the following form:

$$R_s = C_1 \gamma_{gs} p^{C_2} \exp \left[C_3 \left(\frac{\text{API}}{T} \right) \right] \quad (2-70)$$

Values for the coefficients are as follows:

| Coefficient | API ≤ 30 | API > 30 |
|----------------|----------|----------|
| C ₁ | 0.0362 | 0.0178 |
| C ₂ | 1.0937 | 1.1870 |
| C ₃ | 25.7240 | 23.931 |

Realizing that the value of the specific gravity of the gas depends on the conditions under which it is separated from the oil, Vasquez and Beggs proposed that the value of the gas specific gravity as obtained from a separator pressure of 100 psig be used in the above equation. This reference pressure was chosen because it represents the average field separator conditions. The authors proposed the following relationship for adjustment of the gas gravity γ_g to the reference separator pressure:

$$\gamma_{gs} = \gamma_g \left[1 + 5.912 (10^{-5}) (\text{API}) (T_{\text{sep}} - 460) \log \left(\frac{p_{\text{sep}}}{114.7} \right) \right] \quad (2-71)$$

where γ_{gs} = gas gravity at the reference separator pressure

γ_g = gas gravity at the actual separator conditions of p_{sep} and T_{sep}

p_{sep} = actual separator pressure, psia

T_{sep} = actual separator temperature, °R

The gas gravity used to develop all the correlations reported by the authors was that which would result from a two-stage separation. The first-stage pressure was chosen as 100 psig and the second stage was the stock tank. If the separator conditions are unknown, the unadjusted gas gravity may be used in Equation 2-71.

An independent evaluation of the above correlation by Sutton and Farashad (1984) shows that the correlation is capable of predicting gas solubilities with an average absolute error of 12.7%.

Example 2-19

Using the PVT of the six crude oil systems of Example 2-18, solve for the gas solubility.

Solution

| Oil # | γ_{gs} From Equation 2-72 | Predicted R_s Equation 2-71 | Measured R_s | % Error |
|-------|-------------------------------------|----------------------------------|-------------------|------------|
| 1 | 0.8731 | 779 | 751 | 3.76 |
| 2 | 0.855 | 733 | 768 | -4.58 |
| 3 | 0.911 | 702 | 693 | 1.36 |
| 4 | 0.850 | 820 | 968 | 15.2 |
| 5 | 0.814 | 947 | 943 | 0.43 |
| 6 | 0.834 | 841 | 807 | 4.30 |

AAE = 4.9%

Glaser's Correlation

Glaser (1980) proposed a correlation for estimating the gas solubility as a function of the API gravity, pressure, temperature, and gas specific gravity. The correlation was developed from studying 45 North Sea crude oil samples. Glaser reported an average error of 1.28% with a standard deviation of 6.98%. The proposed relationship has the following form:

$$R_s = \gamma_g \left[\left(\frac{API^{0.989}}{(T - 460)^{0.172}} \right) (p_b^*) \right]^{1.2255} \quad (2-72)$$

where p_b^* is a correlating number and is defined by the following expression:

$$p_b^* = 10^x$$

with

$$x = 2.8869 - [14.1811 - 3.3093 \log(p)]^{0.5}$$

Example 2-20

Rework Example 2-18 and solve for the gas solubility by using Glaser's correlation.

Solution

| Oil # | x | p^*_g | Predicted R_s Equation 2-73 | Measured R_s | % Error |
|-------|-------|---------|----------------------------------|-------------------|------------|
| 1 | 1.155 | 14.286 | 737 | 751 | -1.84 |
| 2 | 1.196 | 15.687 | 714 | 768 | -6.92 |
| 3 | 1.095 | 12.450 | 686 | 693 | -0.90 |
| 4 | 1.237 | 17.243 | 843 | 968 | -12.92 |
| 5 | 1.260 | 18.210 | 868 | 943 | -7.95 |
| 6 | 1.413 | 25.883 | 842 | 807 | 4.34 |

AAE = 5.8%

Marhoun's Correlation

Marhoun (1988) developed an expression for estimating the saturation pressure of the Middle Eastern crude oil systems. The correlation originates from 160 experimental saturation pressure data. The proposed correlation can be rearranged and solved for the gas solubility to give:

$$R_s = [a \gamma_g^b \gamma_o^c T^d p]^e \quad (2-73)$$

where γ_g = gas specific gravity
 γ_o = stock-tank oil gravity
 T = temperature, °R

a–e = coefficients of the above equation having these values:

$$a = 185.843208$$

$$b = 1.877840$$

$$c = -3.1437$$

$$d = -1.32657$$

$$e = 1.398441$$

Example 2-21

Resolve Example 2-18 by using Marhoun's correlation.

Solution

| Oil # | Predicted R_s Equation 2-74 | Measured R_s | % Error |
|-------|----------------------------------|-------------------|------------|
| 1 | 740 | 751 | -1.43 |
| 2 | 792 | 768 | 3.09 |
| 3 | 729 | 693 | 5.21 |
| 4 | 1041 | 968 | 7.55 |
| 5 | 845 | 943 | -10.37 |
| 6 | 1186 | 807 | 47.03 |

AAE = 12.4%

The Petrosky-Farshad Correlation

Petrosky and Farshad (1993) used a nonlinear multiple regression software to develop a gas solubility correlation. The authors constructed a PVT database from 81 laboratory analyses from the Gulf of Mexico crude oil system. Petrosky and Farshad proposed the following expression:

$$R_s = \left[\left(\frac{p}{112.727} + 12.340 \right) \gamma_g^{0.8439} 10^x \right]^{1.73184} \quad (2-74)$$

with

$$x = 7.916 (10^{-4}) (\text{API})^{1.5410} - 4.561(10^{-5}) (T - 460)^{1.3911}$$

where p = pressure, psia

T = temperature, °R

Example 2-22

Test the predictive capability of the Petrosky and Farshad equation by resolving Example 2-18.

Solution

| Oil # | x | Predicted R_s Equation 2-75 | Measured R_s | % Error |
|-------|--------|----------------------------------|-------------------|------------|
| 1 | 0.2008 | 772 | 751 | 2.86 |
| 2 | 0.1566 | 726 | 768 | -5.46 |
| 3 | 0.2101 | 758 | 693 | 9.32 |
| 4 | 0.1579 | 875 | 968 | -9.57 |
| 5 | 0.1900 | 865 | 943 | -8.28 |
| 6 | 0.0667 | 900 | 807 | 11.57 |

AAE = 7.84%

The gas solubility can also be calculated rigorously from the experimental measured PVT data at the specified pressure and temperature. The following expression relates the gas solubility R_s to oil density, specific gravity of the oil, gas gravity, and the oil formation volume factor:

$$R_s = \frac{B_o \rho_o - 62.4 \gamma_o}{0.0136 \gamma_g} \quad (2-75)$$

where ρ_o = oil density, lb/ft³

B_o = oil formation volume factor, bbl/STB

γ_o = specific gravity of the stock-tank oil

γ_g = specific gravity of the solution gas

McCain (1991) pointed out that the weight average of separator and stock-tank gas specific gravities should be used for γ_g . The error in calculating R_s by using the above equation will depend only on the accuracy of the available PVT data.

Example 2-23

Using the data of Example 2-18, estimate R_s by applying Equation 2-76.

Solution

| Oil # | Predicted R_s Equation 2-76 | Measured R_s | % Error |
|-------|----------------------------------|-------------------|------------|
| 1 | 762 | 751 | 1.53 |
| 2 | 781 | 768 | 1.73 |
| 3 | 655 | 693 | -5.51 |
| 4 | 956 | 968 | -1.23 |
| 5 | 841 | 943 | -10.79 |
| 6 | 798 | 807 | -1.13 |

AAE = 3.65%

Bubble-Point Pressure

The bubble-point pressure p_b of a hydrocarbon system is defined as the highest pressure at which a bubble of gas is first liberated from the oil. This important property can be measured experimentally for a crude oil system by conducting a constant-composition expansion test.

In the absence of the experimentally measured bubble-point pressure, it is necessary for the engineer to make an estimate of this crude oil property from the readily available measured producing parameters. Several graphical and mathematical correlations for determining p_b have been proposed during the past four decades. These correlations are essentially based on the assumption that the bubble-point pressure is a strong function of gas solubility R_s , gas gravity γ_g , oil gravity API, and temperature T, or:

$$p_b = f(R_s, \gamma_g, \text{API}, T)$$

Several ways of combining the above parameters in a graphical form or a mathematical expression are proposed by numerous authors, including:

- Standing
- Vasquez and Beggs
- Glaso
- Marhoun
- Petrosky and Farshad

The empirical correlations for estimating the bubble-point pressure proposed by the above-listed authors are given below.

Standing's Correlation

Based on 105 experimentally measured bubble-point pressures on 22 hydrocarbon systems from California oil fields, Standing (1947) proposed a graphical correlation for determining the bubble-point pressure of crude oil systems. The correlating parameters in the proposed correlation are the gas solubility R_s , gas gravity γ_g , oil API gravity, and the system temperature. The reported average error is 4.8%.

In a mathematical form, Standing (1981) expressed the graphical correlation by the following expression:

$$p_b = 18.2 [(R_s/\gamma_g)^{0.83} (10)^a - 1.4] \quad (2-76)$$

with

$$a = 0.00091 (T - 460) - 0.0125 (\text{API}) \quad (2-77)$$

where p_b = bubble-point pressure, psia

T = system temperature, °R

Standing's correlation should be used with caution if nonhydrocarbon components are known to be present in the system.

Example 2-24

The experimental data given in Example 2-18 are repeated here for convenience.

| Oil # | T | p_b | R_s | B_o | ρ_o | c_o at $p > p_b$ | P_{sep} | T_{sep} | API | γ_g |
|-------|-----|-------|-------|-------|----------|--------------------------------|-----------|-----------|------|------------|
| 1 | 250 | 2377 | 751 | 1.528 | 38.13 | 22.14×10^{-6} at 2689 | 150 | 60 | 47.1 | 0.851 |
| 2 | 220 | 2620 | 768 | 1.474 | 40.95 | 18.75×10^{-6} at 2810 | 100 | 75 | 40.7 | 0.855 |
| 3 | 260 | 2051 | 693 | 1.529 | 37.37 | 22.69×10^{-6} at 2526 | 100 | 72 | 48.6 | 0.911 |
| 4 | 237 | 2884 | 968 | 1.619 | 38.92 | 21.51×10^{-6} at 2942 | 60 | 120 | 40.5 | 0.898 |
| 5 | 218 | 3065 | 943 | 1.570 | 37.70 | 24.16×10^{-6} at 3273 | 200 | 60 | 44.2 | 0.781 |
| 6 | 180 | 4239 | 807 | 1.385 | 46.79 | 11.65×10^{-6} at 4370 | 85 | 173 | 27.3 | 0.848 |

Predict the bubble-point pressure by using Standing's correlation.

Solution

| Oil # | Coeff. a Equation 2-78 | Predicted p_b Equation 2-77 | Measured p_b | % Error |
|-------|-----------------------------|----------------------------------|-------------------|------------|
| 1 | -0.3613 | 2181 | 2392 | -8.8 |
| 2 | -0.3086 | 2503 | 2635 | -5.0 |
| 3 | -0.3709 | 1883 | 2066 | -8.8 |
| 4 | -0.3115 | 2896 | 2899 | -0.1 |
| 5 | -0.3541 | 2884 | 3060 | -5.7 |
| 6 | -0.1775 | 3561 | 4254 | -16.3 |

AAE = 7.4%

McCain (1991) suggested that by replacing the specific gravity of the gas in Equation 2-77 with that of the separator gas, i.e., excluding the gas from the stock tank, would improve the accuracy of the equation.

Example 2-25

Using the data of Example 2-24 and given the following separator gas gravities, estimate the bubble-point pressure by applying Standing's correlation.

| Oil # | Separator Gas Gravity |
|-------|-----------------------|
| 1 | 0.755 |
| 2 | 0.786 |
| 3 | 0.801 |
| 4 | 0.888 |
| 5 | 0.705 |
| 6 | 0.813 |

Solution

| Oil # | Predicted p_b | Measured p_b | % Error |
|-------|-----------------|----------------|---------|
| 1 | 2411 | 2392 | 0.83 |
| 2 | 2686 | 2635 | 1.93 |
| 3 | 2098 | 2066 | 1.53 |
| 4 | 2923 | 2899 | 0.84 |
| 5 | 3143 | 3060 | 2.70 |
| 6 | 3689 | 4254 | -13.27 |

AAE = 3.5%

The Vasquez-Beggs Correlation

Vasquez and Beggs' gas solubility correlation as presented by Equation 2-71 can be solved for the bubble-point pressure p_b to give:

$$p_b = [(C_1 R_s / \gamma_{gs}) (10)^a]^{C_2} \quad (2-78)$$

with

$$a = -C_3 \text{ API}/T$$

The gas specific gravity γ_{gs} at the reference separator pressure is defined by Equation 2-72. The coefficients C_1 , C_2 , and C_3 have the following values:

| Coefficient | API \leq 30 | API $>$ 30 |
|-------------|---------------|------------|
| C_1 | 27.624 | 56.18 |
| C_2 | 0.914328 | 0.84246 |
| C_3 | 11.172 | 10.393 |

Example 2-26

Rework Example 2-24 by applying Equation 2-79.

Solution

| Oil # | γ_{gs} Equation 2-72 | a | Predicted p_b | Measured p_b | % Error |
|-------|--------------------------------|--------|--------------------|-------------------|------------|
| 1 | 0.873 | -0.689 | 2319 | 2392 | -3.07 |
| 2 | 0.855 | -0.622 | 2741 | 2635 | 4.03 |
| 3 | 0.911 | -0.702 | 2043 | 2066 | -1.14 |
| 4 | 0.850 | -0.625 | 3331 | 2899 | 14.91 |
| 5 | 0.814 | -0.678 | 3049 | 3060 | -0.36 |
| 6 | 0.834 | -0.477 | 4093 | 4254 | -3.78 |

AAE = 4.5%

Glaso's Correlation

Glaso (1980) used 45 oil samples, mostly from the North Sea hydrocarbon system, to develop an accurate correlation for bubble-point pressure prediction. Glaso proposed the following expression:

$$\log(p_b) = 1.7669 + 1.7447 \log(p_b^*) - 0.30218 [\log(p_b^*)]^2 \quad (2-79)$$

where p_b^* is a correlating number and defined by the following equation:

$$p_b^* = (R_s/\gamma_g)^a (t)^b (\text{API})^c \quad (2-80)$$

where R_s = gas solubility, scf/STB

t = system temperature, °F

γ_g = average specific gravity of the total surface gases

a , b , c = coefficients of the above equation having the following values:

$$a = 0.816$$

$$b = 0.172$$

$$c = -0.989$$

For volatile oils, Glaso recommends that the temperature exponent b of Equation 2-81 be slightly changed, to the value of 0.130.

Example 2-27

Resolve Example 2-24 by using Glaso's correlation.

Solution

| Oil # | p_b^* Equation 2-81 | p_b Equation 2-80 | Measured p_b | % Error |
|-------|--------------------------|------------------------|-------------------|------------|
| 1 | 14.51 | 2431 | 2392 | 1.62 |
| 2 | 16.63 | 2797 | 2635 | 6.14 |
| 3 | 12.54 | 2083 | 2066 | 0.82 |
| 4 | 19.30 | 3240 | 2899 | 11.75 |
| 5 | 19.48 | 3269 | 3060 | 6.83 |
| 6 | 25.00 | 4125 | 4254 | -3.04 |

AAE = 5.03%

Marhoun's Correlation

Marhoun (1988) used 160 experimentally determined bubble-point pressures from the PVT analysis of 69 Middle Eastern hydrocarbon mixtures to develop a correlation for estimating p_b . The author correlated the bubble-point pressure with the gas solubility R_s , temperature T , and specific gravity of the oil and the gas. Marhoun proposed the following expression:

$$p_b = a R_s^b \gamma_g^c \gamma_o^d T^e \quad (2-81)$$

where T = temperature, °R

γ_o = stock-tank oil specific gravity

γ_g = gas specific gravity

a–e = coefficients of the correlation having the following values:

$$a = 5.38088 \times 10^{-3}$$

$$b = 0.715082$$

$$c = -1.87784$$

$$d = 3.1437$$

$$e = 1.32657$$

The reported average absolute relative error for the correlation is 3.66% when compared with the experimental data used to develop the correlation.

Example 2-28

Using Equation 2-82, rework Example 2-24.

Solution

| Oil # | Predicted p_b | Measured p_b | % Error |
|-------|-----------------|----------------|---------|
| 1 | 2417 | 2392 | 1.03 |
| 2 | 2578 | 2635 | -2.16 |
| 3 | 1992 | 2066 | -3.57 |
| 4 | 2752 | 2899 | -5.07 |
| 5 | 3309 | 3060 | 8.14 |
| 6 | 3229 | 4254 | -24.09 |

$$AAE = 7.3\%$$

The Petrosky-Farshad Correlation

The Petrosky and Farshad gas solubility equation, i.e., Equation 2-75, can be solved for the bubble-point pressure to give:

$$p_b = \left[\frac{112.727 R_s^{0.577421}}{\gamma_g^{0.8439} (10)^x} \right] - 1391.051 \quad (2-82)$$

where the correlating parameter x is previously defined by Equation 2-75.

The authors concluded that the correlation predicts measured bubble-point pressures with an average absolute error of 3.28%.

Example 2-29

Use the Petrosky and Farshad correlation to predict the bubble-point pressure data given in Example 2-24.

Solution

| Oil # | X | Predicted p_b | Measured p_b | % Error |
|-------|--------|-----------------|----------------|---------|
| 1 | 0.2008 | 2331 | 2392 | -2.55 |
| 2 | 0.1566 | 2768 | 2635 | 5.04 |
| 3 | 0.2101 | 1893 | 2066 | -8.39 |
| 4 | 0.1579 | 3156 | 2899 | 8.86 |
| 5 | 0.1900 | 3288 | 3060 | 7.44 |
| 6 | 0.0667 | 3908 | 4254 | -8.13 |

AAE = 6.74%

Oil Formation Volume Factor

The oil formation volume factor, B_o , is defined as the ratio of the volume of oil (plus the gas in solution) at the prevailing reservoir temperature and pressure to the volume of oil at standard conditions. B_o is always greater than or equal to unity. The oil formation volume factor can be expressed mathematically as:

$$B_o = \frac{(V_o)_{p,T}}{(V_o)_{sc}} \quad (2-83)$$

where B_o = oil formation volume factor, bbl/STB

$(V_o)_{p,T}$ = volume of oil under reservoir pressure p and temperature T ,
bbl

$(V_o)_{sc}$ = volume of oil is measured under standard conditions, STB

A typical oil formation factor curve, as a function of pressure for an undersaturated crude oil ($p_i > p_b$), is shown in Figure 2-8. As the pressure is reduced below the initial reservoir pressure p_i , the oil volume increases due to the oil expansion. This behavior results in an increase in the oil formation volume factor and will continue until the bubble-point pressure is reached. At p_b , the oil reaches its maximum expansion and consequently attains a maximum value of B_{ob} for the oil formation volume factor. As the pressure is reduced below p_b , volume of the oil and B_o are decreased as the solution gas is liberated. When the pressure is reduced to atmospheric pressure and the temperature to 60°F, the value of B_o is equal to one.

Most of the published empirical B_o correlations utilize the following generalized relationship:

$$B_o = f(R_s, \gamma_g, \gamma_o, T)$$

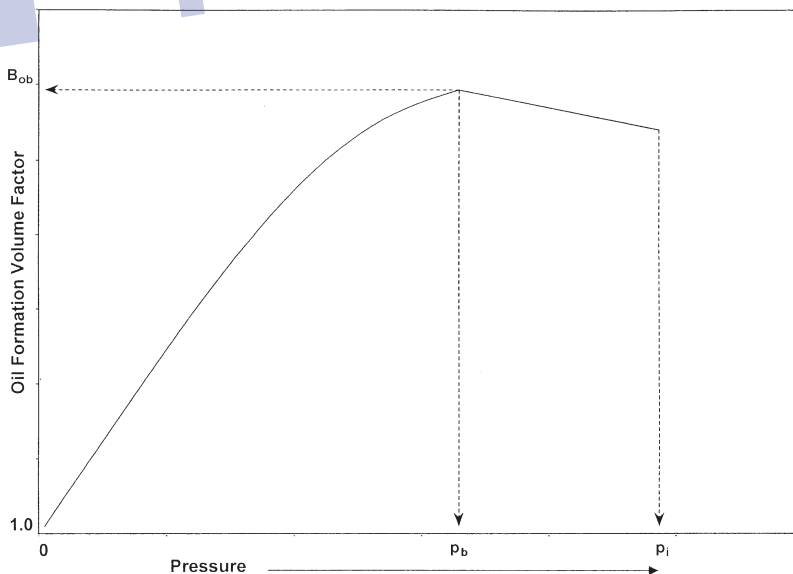


Figure 2-8. Oil formation volume factor versus pressure.

Six different methods of predicting the oil formation volume factor are presented below:

- Standing's correlation
- The Vasquez-Beggs correlation
- Glaso's correlation
- Marhoun's correlation
- The Petrosky-Farshad correlation
- Other correlations

It should be noted that all the correlations could be used for any pressure equal to or below the bubble-point pressure.

Standing's Correlation

Standing (1947) presented a graphical correlation for estimating the oil formation volume factor with the gas solubility, gas gravity, oil gravity, and reservoir temperature as the correlating parameters. This graphical correlation originated from examining a total of 105 experimental data points on 22 different California hydrocarbon systems. An average error of 1.2% was reported for the correlation.

Standing (1981) showed that the oil formation volume factor can be expressed more conveniently in a mathematical form by the following equation:

$$B_o = 0.9759 + 0.000120 \left[R_s \left(\frac{\gamma_g}{\gamma_o} \right)^{0.5} + 1.25(T - 460) \right]^{1.2} \quad (2-84)$$

where T = temperature, °R

γ_o = specific gravity of the stock-tank oil

γ_g = specific gravity of the solution gas

The Vasquez-Beggs Correlation

Vasquez and Beggs (1980) developed a relationship for determining B_o as a function of R_s , γ_o , γ_g , and T . The proposed correlation was based on 6,000 measurements of B_o at various pressures. Using the regression

analysis technique, Vasquez and Beggs found the following equation to be the best form to reproduce the measured data:

$$B_o = 1.0 + C_1 R_s + (T - 520) \left(\frac{API}{\gamma_{gs}} \right) [C_2 + C_3 R_s] \quad (2-85)$$

where R = gas solubility, scf/STB

T = temperature, °R

γ_{gs} = gas specific gravity as defined by Equation 2-72

Values for the coefficients C_1 , C_2 , and C_3 are given below:

| Coefficient | API ≤ 30 | API > 30 |
|-------------|-------------------------|------------------------|
| C_1 | 4.677×10^{-4} | 4.670×10^{-4} |
| C_2 | 1.751×10^{-5} | 1.100×10^{-5} |
| C_3 | -1.811×10^{-8} | 1.337×10^{-9} |

Vasquez and Beggs reported an average error of 4.7% for the proposed correlation.

Glaso's Correlation

Glaso (1980) proposed the following expressions for calculating the oil formation volume factor:

$$B_o = 1.0 + 10^A \quad (2-86)$$

where

$$A = -6.58511 + 2.91329 \log B_{ob}^* - 0.27683 (\log B_{ob}^*)^2 \quad (2-87)$$

B_{ob}^* is a *correlating number* and is defined by the following equation:

$$B_{ob}^* = R_s \left(\frac{\gamma_g}{\gamma_o} \right)^{0.526} + 0.968(T - 460) \quad (2-88)$$

where T = temperature, °R

γ_o = specific gravity of the stock-tank oil

The above correlations were originated from studying PVT data on 45 oil samples. The average error of the correlation was reported at -0.43% with a standard deviation of 2.18% .

Sutton and Farshad (1984) concluded that Glaso's correlation offers the best accuracy when compared with the Standing and Vasquez-Beggs correlations. In general, Glaso's correlation underpredicts formation volume factor. Standing's expression tends to overpredict oil formation volume factors greater than 1.2 bbl/STB. The Vasquez-Beggs correlation typically overpredicts the oil formation volume factor.

Marhoun's Correlation

Marhoun (1988) developed a correlation for determining the oil formation volume factor as a function of the gas solubility, stock-tank oil gravity, gas gravity, and temperature. The empirical equation was developed by use of the nonlinear multiple regression analysis on 160 experimental data points. The experimental data were obtained from 69 Middle Eastern oil reserves. The author proposed the following expression:

$$B_o = 0.497069 + 0.862963 \times 10^{-3} T + 0.182594 \times 10^{-2} F + 0.318099 \times 10^{-5} F^2 \quad (2-89)$$

with the correlating parameter F as defined by the following equation:

$$F = R_s^a \gamma_g^b \gamma_o^c \quad (2-90)$$

The coefficients a , b , and c have the following values:

$$\begin{aligned} a &= 0.742390 \\ b &= 0.323294 \\ c &= -1.202040 \end{aligned}$$

where T is the system temperature in $^{\circ}\text{R}$.

The Petrosky-Farshad Correlation

Petrosky and Farshad (1993) proposed a new expression for estimating B_o . The proposed relationship is similar to the equation developed by Standing; however, the equation introduces three additional fitting parameters in order to increase the accuracy of the correlation.

The authors used a nonlinear regression model to match experimental crude oil from the Gulf of Mexico hydrocarbon system. Their correlation has the following form:

$$B_o = 1.0113 + 7.2046 (10^{-5}) \left[R_s^{0.3738} \left(\frac{\gamma_g^{0.2914}}{\gamma_o^{0.6265}} \right) + 0.24626 (T - 460)^{0.5371} \right]^{3.0936} \quad (2-91)$$

where T = temperature, °R
 γ_o = specific gravity of the stock-tank oil

Material Balance Equation

Following the definition of B_o as expressed mathematically by Equation 2-84, it can be shown that:

$$B_o = \frac{62.4 \gamma_o + 0.0136 R_s \gamma_g}{\rho_o} \quad (2-92)$$

where ρ_o = density of the oil at the specified pressure and temperature, lb/ft³.

The error in calculating B_o by using Equation 2-93 will depend only on the accuracy of the input variables (R_s , γ_g , and γ_o) and the method of calculating ρ_o .

Example 2-30

The following experimental PVT data on six different crude oil systems are available. Results are based on two-stage surface separation.

| Oil # | T | p_b | R_s | B_o | ρ_o | c_o at $p > p_b$ | p_{sep} | T_{sep} | API | γ_g |
|-------|-----|-------|-------|-------|----------|--------------------------------|-----------|-----------|------|------------|
| 1 | 250 | 2377 | 751 | 1.528 | 38.13 | 22.14×10^{-6} at 2689 | 150 | 60 | 47.1 | 0.851 |
| 2 | 220 | 2620 | 768 | 1.474 | 40.95 | 18.75×10^{-6} at 2810 | 100 | 75 | 40.7 | 0.855 |
| 3 | 260 | 2051 | 693 | 1.529 | 37.37 | 22.69×10^{-6} at 2526 | 100 | 72 | 48.6 | 0.911 |
| 4 | 237 | 2884 | 968 | 1.619 | 38.92 | 21.51×10^{-6} at 2942 | 60 | 120 | 40.5 | 0.898 |
| 5 | 218 | 3065 | 943 | 1.570 | 37.70 | 24.16×10^{-6} at 3273 | 200 | 60 | 44.2 | 0.781 |
| 6 | 180 | 4239 | 807 | 1.385 | 46.79 | 11.65×10^{-6} at 4370 | 85 | 173 | 27.3 | 0.848 |

Calculate the oil formation volume factor at the bubble-point pressure by using the six different correlations. Compare the results with the experimental values and calculate the absolute average error (AAE).

Solution

| Crude Oil | Exp. B_o | Method 1 | Method 2 | Method 3 | Method 4 | Method 5 | Method 6 |
|-----------|------------|----------|----------|----------|----------|----------|----------|
| 1 | 1.528 | 1.506 | 1.474 | 1.473 | 1.516 | 1.552 | 1.525 |
| 2 | 1.474 | 1.487 | 1.450 | 1.459 | 1.477 | 1.508 | 1.470 |
| 3 | 1.529 | 1.495 | 1.451 | 1.461 | 1.511 | 1.556 | 1.542 |
| 4 | 1.619 | 1.618 | 1.542 | 1.589 | 1.575 | 1.632 | 1.623 |
| 5 | 1.570 | 1.571 | 1.546 | 1.541 | 1.554 | 1.584 | 1.599 |
| 6 | 1.385 | 1.461 | 1.389 | 1.438 | 1.414 | 1.433 | 1.387 |
| %AAE | — | 1.7 | 2.8 | 2.8 | 1.3 | 1.8 | 0.6 |

where Method 1 = Standing's correlation
 Method 2 = Vasquez-Beggs' correlation
 Method 3 = Glaso's correlation
 Method 4 = Marhoun's correlation
 Method 5 = Petrosky-Farshad correlation
 Method 6 = Material balance equation

Isothermal Compressibility Coefficient of Crude Oil

Isothermal compressibility coefficients are required in solving many reservoir engineering problems, including transient fluid flow problems, and they are also required in the determination of the physical properties of the undersaturated crude oil.

By definition, the isothermal compressibility of a substance is defined mathematically by the following expression:

$$c = -\frac{1}{V} \left(\frac{\partial V}{\partial p} \right)_T$$

For a crude oil system, the isothermal compressibility coefficient of the oil phase c_o is defined for *pressures above the bubble-point* by one of the following equivalent expressions:

$$c_o = -(1/V)(\partial V/\partial p)_T \quad (2-93)$$

$$c_o = -(1/B_o)(\partial B_o/\partial p)_T \quad (2-94)$$

$$c_o = (1/\rho_o)(\partial \rho_o/\partial p)_T \quad (2-95)$$

where c_o = isothermal compressibility, psi^{-1}

ρ_o = oil density lb/ft^3

B_o = oil formation volume factor, bbl/STB

At pressures below the bubble-point pressure, the oil compressibility is defined as:

$$c_o = \frac{-1}{B_o} \frac{\partial B_o}{\partial p} + \frac{B_g}{B_o} \frac{\partial R_s}{\partial p} \quad (2-96)$$

where B_g = gas formation volume factor, bbl/scf

There are several correlations that are developed to estimate the oil compressibility at pressures *above* the bubble-point pressure, i.e., undersaturated crude oil system. Three of these correlations are presented below:

- The Vasquez-Beggs correlation
- The Petrosky-Farshad correlation
- McCain's correlation

The Vasquez-Beggs Correlation

From a total of 4,036 experimental data points used in a linear regression model, Vasquez and Beggs (1980) correlated the isothermal oil compressibility coefficients with R_s , T , $^\circ\text{API}$, γ_g , and p . They proposed the following expression:

$$c_o = \frac{-1,433 + 5R_{sb} + 17.2(T - 460) - 1,180 \gamma_{gs} + 12.61^\circ\text{API}}{10^5 p} \quad (2-97)$$

where T = temperature, $^\circ\text{R}$

p = pressure above the bubble-point pressure, psia

R_{sb} = gas solubility at the bubble-point pressure

γ_{gs} = corrected gas gravity as defined by Equation 2-72

The Petrosky-Farshad Correlation

Petrosky and Farshad (1993) proposed a relationship for determining the oil compressibility for undersaturated hydrocarbon systems. The equation has the following form:

$$c_o = 1.705 \times 10^{-7} R_{sb}^{0.69357} \gamma_g^{0.1885} \text{API}^{0.3272} (T - 460)^{0.6729} p^{-0.5906} \quad (2-98)$$

where T = temperature, °R

R_{sb} = gas solubility at the bubble-point pressure, scf/STB

Example 2-31

Using the experimental data given in Example 2-30, estimate the undersaturated oil compressibility coefficient by using the Vasquez-Beggs and the Petrosky-Farshad correlations. Calculate the AAE.

Solution

| Oil # | Pressure | Measured c_o 10 ⁻⁶ psi | Vasquez-Beggs 10 ⁻⁶ psi | Petrosky-Farshad 10 ⁻⁶ psi |
|-------|----------|--|---------------------------------------|--|
| 1 | 2689 | 22.14 | 22.88 | 22.24 |
| 2 | 2810 | 18.75 | 20.16 | 19.27 |
| 3 | 2526 | 22.60 | 23.78 | 22.92 |
| 4 | 2942 | 21.51 | 22.31 | 21.78 |
| 5 | 3273 | 24.16 | 20.16 | 20.39 |
| 6 | 4370 | 11.45 | 11.54 | 11.77 |
| AAE | | | 6.18% | 4.05% |

Below the bubble-point pressure, McCain and coauthors (1988) correlated the oil compressibility with pressure p , the oil API gravity, gas solubility at the bubble-point R_{sb} , and the temperature T in °R. Their proposed relationship has the following form:

$$c_o = \exp(A) \quad (2-99)$$

where the correlating parameter A is given by the following expression:

$$A = -7.633 - 1.497 \ln(p) + 1.115 \ln(T) + 0.533 \ln(\text{API}) + 0.184 \ln(R_{sp}) \quad (2-100)$$

The authors suggested that the accuracy of the Equation 2-100 can be substantially improved if the bubble-point pressure is known. They improved correlating parameter A by including the bubble-point pressure p_b as one of the parameters in the above equation, to give:

$$A = -7.573 - 1.45 \ln(p) - 0.383 \ln(P_b) + 1.402 \ln(T) + 0.256 \ln(\text{API}) + 0.449 \ln(R_{sb}) \quad (2-101)$$

Analytically, Standing's correlations for R_s (Equation 2-70) and β_o (Equation 2-85) can be differentiated with respect to the pressure p to give:

$$\frac{\partial R_s}{\partial p} = \frac{R_s}{0.83p + 21.75} \quad (2-102)$$

$$\frac{\partial B_o}{\partial p} = \left[\frac{0.000144 R_s}{0.83p + 21.75} \right] \left(\frac{\gamma_g}{\gamma_o} \right)^{0.5} \times \left[R_s \left(\frac{\gamma_g}{\gamma_o} \right)^{0.5} + 1.25(T - 460) \right]^{0.12} \quad (2-103)$$

The above two expressions can be substituted into Equation 2-97 to give the following relationship:

$$c_o = \frac{-R_s}{B_o(0.83p + 21.75)} \times \left\{ 0.00014 \sqrt{\frac{\gamma_g}{\gamma_o}} \left[R_s \sqrt{\frac{\gamma_g}{\gamma_o}} + 1.25(T - 460) \right]^{0.12} - B_g \right\} \quad (2-104)$$

where p = pressure, psia

T = temperature, °R

B_g = gas formation volume factor at pressure p , bbl/scf

R_s = gas solubility at pressure p , scf/STB

B_o = oil formation volume factor at p , bbl/STB

γ_o = specific gravity of the stock-tank oil

γ_g = specific gravity of the solution gas

Example 2-32

A crude oil system exists at 1,650 psi and a temperature of 250°F. The system has the following PVT properties:

$$\begin{aligned} \text{API} &= 47.1 & p_b &= 2377 & \gamma_g &= 0.851 & \gamma_{gs} &= 0.873 \\ R_{sb} &= 751 \text{ scf/STB} & B_{ob} &= 1.528 \text{ bbl/STB} \end{aligned}$$

The laboratory measured oil PVT data at 1,650 psig are listed below:

$$\begin{aligned} B_o &= 1.393 \text{ bbl/STB} & R_s &= 515 \text{ scf/STB} \\ B_g &= 0.001936 \text{ bbl/scf} & c_o &= 324.8 \times 10^{-6} \text{ psi}^{-1} \end{aligned}$$

Estimate the oil compressibility by using:

- McCain's correlation
- Equation 2-105

Solution

McCain's Correlation:

- Calculate the correlating parameter A by applying Equation 2-102

$$\begin{aligned} A &= -7.573 - 1.45 \ln(1665) - 0.383 \ln(2392) + 1.402 \ln(710) \\ &\quad + 0.256 \ln(47.1) + 0.449 \ln(451) = -8.1445 \end{aligned}$$

- Solve for c_o by using Equation 2-100

$$c_o = \exp(-8.1445) = 290.3 \times 10^{-6} \text{ psi}^{-1}$$

Oil Compressibility Using Equation 2-105:

$$\begin{aligned} c_o &= \frac{-515}{1.393[0.83(1665) + 21.75]} \\ &\quad \times \left\{ 0.00014 \sqrt{\frac{0.851}{0.792}} \left[515 \sqrt{\frac{.851}{.792}} + 1.25(250) \right]^{0.12} - 0.001936 \right\} \end{aligned}$$

$$c_o = 424 \times 10^{-6} \text{ psi}^{-1}$$

It should be pointed out that when it is necessary to establish PVT relationships for the hydrocarbon system through correlations or by extrapolation, care should be exercised to see that the PVT functions are consistent.

This consistency is assured if the increase in oil volume with increasing pressure is less than the decrease in volume associated with the gas going into solution. Since the oil compressibility coefficient c_o as expressed by Equation 2-97 must be positive, that leads to the following consistency criteria:

$$\frac{\partial B_o}{\partial p} < B_g \frac{\partial R_s}{\partial p} \quad (2-105)$$

This consistency can easily be checked in the tabular form of PVT data. The PVT consistency errors most frequently occur at higher pressures where the gas formation volume factor, B_g , assumes relatively small values.

Oil Formation Volume Factor for Undersaturated Oils

With increasing pressures above the bubble-point pressure, the oil formation volume factor decreases due to the compression of the oil, as illustrated schematically in Figure 2-9.

To account for the effects of oil compression on B_o , the oil formation volume factor at the bubble-point pressure is first calculated by using any of the methods previously described. The calculated B_o is then adjusted to account for the effect of increasing the pressure above the bubble-point pressure. This adjustment step is accomplished by using the isothermal compressibility coefficient as described below.

The isothermal compressibility coefficient (as expressed mathematically by Equation 2-94) can be equivalently written in terms of the oil formation volume factor:

$$c_o = \frac{-1}{B_o} \frac{\partial B_o}{\partial p}$$

The above relationship can be rearranged and integrated to produce

$$\int_{p_b}^p -c_o \, dp = \int_{B_{ob}}^{B_o} \frac{1}{B_o} dB_o \quad (2-106)$$

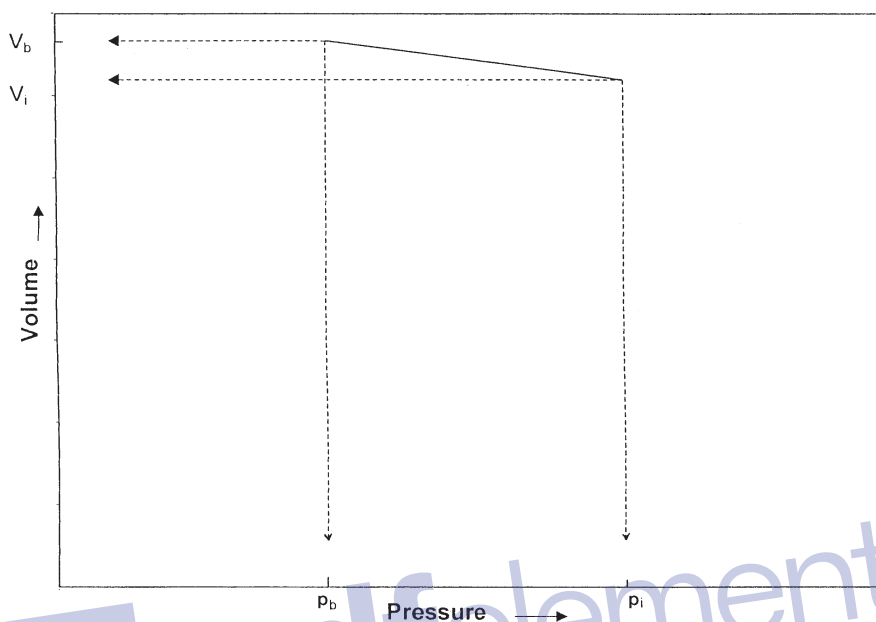


Figure 2-9. Volume versus pressure relationship.

Evaluating c_o at the arithmetic average pressure and concluding the integration procedure give:

$$B_o = B_{ob} \exp [-c_o (p - p_b)] \quad (2-107)$$

where B_o = oil formation volume factor at the pressure of interest,
bbl/STB

B_{ob} = oil formation volume factor at the bubble-point pressure,
bbl/STB

p = pressure of interest, psia

p_b = bubble-point pressure, psia

Replacing with the Vasquez-Beggs c_o expression, i.e., Equation 2-98, and integrating the resulting equation give:

$$B_o = B_{ob} \exp \left[-A \ln \left(\frac{p}{p_b} \right) \right] \quad (2-108)$$

where

$$A = 10^{-5} [-1433 + 5 R_{sb} + 17.2(T - 460) - 1180 \gamma_{gs} + 12.61 \text{ API}]$$

Replacing c_o in Equation 2-107 with the Petrosky-Farshad expression (i.e., Equation 2-99) and integrating give:

$$B_o = B_{ob} \exp[-A (p^{0.4094} - p_b^{0.4094})] \quad (2-109)$$

with the correlating parameter A as defined by:

$$A = 4.1646 (10^{-7}) R_{sb}^{0.69357} \gamma_g^{0.1885} (\text{API})^{0.3272} (T - 460)^{0.6729} \quad (2-110)$$

where T = temperature, °R

p = pressure, psia

R_{sb} = gas solubility at the bubble-point pressure

Example 2-33

Using the PVT data given in Example 2-32, calculate the oil formation volume factor at 5000 psig by using:

- Equation 2-109
- Equation 2-110

The experimental measured B_o is 1.457 bbl/STB.

Solution

Using Equation 2-109:

- Calculate the parameter A:

$$A = 10^{-5} [-1433 + 5 (751) + 17.2 (250) - 1180 (0.873) + 12.61 (47.1)] = 0.061858$$

- Apply Equation 2-109:

$$B_o = 1.528 \exp \left[-0.061858 \ln \left(\frac{5015}{2392} \right) \right] = 1.459 \text{ bbl/STB}$$

Using Equation 2-110:

- Calculate the correlating parameter A from Equation 2-111:

$$A = 4.1646 \times 10^{-7} (751)^{0.69357} (0.851)^{0.1885} (47.1)^{0.3272} \\ \times (250)^{0.6729} = 0.005778$$

- Solve for B_o by applying Equation 2-110:

$$B_o = 1.528 \exp [-0.005778 (50150^{0.4094} - 23920^{0.4096})] = 1.453 \text{ bbl/STB}$$

Crude Oil Density

The crude oil density is defined as the mass of a unit volume of the crude at a specified pressure and temperature. It is usually expressed in pounds per cubic foot. Several empirical correlations for calculating the density of liquids of unknown compositional analysis have been proposed. The correlations employ limited PVT data such as gas gravity, oil gravity, and gas solubility as correlating parameters to estimate liquid density at the prevailing reservoir pressure and temperature.

Equation 2-93 may be used to calculate the density of the oil at pressure below or equal to the bubble-point pressure. Solving Equation 2-93 for the oil density gives:

$$\rho_o = \frac{62.4 \gamma_o + 0.0136 R_s \gamma_g}{B_o} \quad (2-111)$$

where γ_o = specific gravity of the stock-tank oil

R_s = gas solubility, scf/STB

ρ_o = oil density, lb/ft³

Standing (1981) proposed an empirical correlation for estimating the oil formation volume factor as a function of the gas solubility R_s , the specific gravity of stock-tank oil γ_o , the specific gravity of solution gas γ_g , and the system temperature T. By coupling the mathematical definition of the oil formation volume factor (as discussed in a later section) with Standing's correlation, the density of a crude oil at a specified pressure and temperature can be calculated from the following expression:

$$\rho_o = \frac{62.4 \gamma_o + 0.0136 R_s \gamma_g}{0.972 + 0.000147 \left[R_s \left(\frac{\gamma_g}{\gamma_o} \right)^5 + 1.25 (T - 460) \right]^{1.175}} \quad (2-112)$$

where T = system temperature, °R
 γ_o = specific gravity of the stock-tank oil

Example 2-34

Using the experimental PVT data given in Example 2-30 for the six different crude oil systems, calculate the oil density by using Equations 2-112 and 2-113. Compare the results with the experimental values and calculate the absolute average error (AAE).

Solution

| Crude Oil | Measured Oil Density | Equation 2-112 | Equation 2-113 |
|-----------|----------------------|----------------|----------------|
| 1 | 38.13 | 38.04 | 38.31 |
| 2 | 40.95 | 40.85 | 40.18 |
| 3 | 37.37 | 37.68 | 38.26 |
| 4 | 42.25 | 41.52 | 40.39 |
| 5 | 37.70 | 38.39 | 38.08 |
| 6 | 46.79 | 46.86 | 44.11 |
| AAE | | 0.84% | 2.65% |

Density of the oil at pressures above the bubble-point pressure can be calculated with:

$$\rho_o = \rho_{ob} \exp [c_o (p - p_b)] \quad (2-113)$$

where ρ_o = density of the oil at pressure p , lb/ft³

ρ_{ob} = density of the oil at the bubble-point pressure, lb/ft³

c_o = isothermal compressibility coefficient at average pressure, psi⁻¹

Vasquez-Beggs' oil compressibility correlation and the Petrosky-Farshad c_o expression can be incorporated in Equation 2-114 to give:

For the Vasquez-Beggs c_o equation:

$$\rho_o = \rho_{ob} \exp \left[A \ln \left(\frac{p}{p_b} \right) \right] \quad (2-114)$$

where

$$A = 10^{-5} [-1433 + 5 R_{sb} + 17.2 (T - 460) - 1180 \gamma_{gs} + 12.61 \text{ }^\circ\text{API}]$$

For the Petrosky-Farshad c_o expression:

$$\rho_o = \rho_{ob} \exp [A (p^{0.4094} - p_b^{0.4094})] \quad (2-115)$$

with the correlating parameter A as given by Equation 2-111.

Total Formation Volume Factor

To describe the pressure-volume relationship of hydrocarbon systems below their bubble-point pressure, it is convenient to express this relationship in terms of the total formation volume factor as a function of pressure. This property defines the total volume of a system regardless of the number of phases present. The total formation volume factor, denoted B_t , is defined as the ratio of the total volume of the hydrocarbon mixture (i.e., oil and gas, if present), at the prevailing pressure and temperature per unit volume of the stock-tank oil. Because naturally occurring hydrocarbon systems usually exist in either one or two phases, the term *two-phase formation volume factor* has become synonymous with the total formation volume.

Mathematically, B_t is defined by the following relationship:

$$B_t = \frac{(V_o)_{p,T} + (V_g)_{p,T}}{(V_o)_{sc}}$$

where B_t = total formation volume factor, bbl/STB

$(V_o)_{p,T}$ = volume of the oil at p and T, bbl

$(V_g)_{p,T}$ = volume of the liberated gas at p and T, bbl

$(V_o)_{sc}$ = volume of the oil at standard conditions, STB

Notice that above the bubble point pressure, no free gas exists and the expression is reduced to the equation that describes the oil formation volume factor, that is:

$$B_t = \frac{(V_o)_{p,T} + 0}{(V_o)_{sc}} = \frac{(V_o)_{p,T}}{(V_o)_{sc}} = B_o$$

A typical plot of B_t as a function of pressure for an undersaturated crude oil is shown in Figure 2-10. The oil formation volume factor curve is also included in the illustration. As pointed out above, B_o and B_t are identical at pressures above or equal to the bubble-point pressure because only one phase, the oil phase, exists at these pressures. It should also be noted that at pressures below the bubble-point pressure, the difference in the values of the two oil properties represents the volume of the evolved solution gas as measured at system conditions per stock-tank barrel of oil.

Consider a crude oil sample placed in a PVT cell at its bubble-point pressure, p_b , and reservoir temperature. Assume that the volume of the oil sample is sufficient to yield one stock-tank barrel of oil at standard conditions. Let R_{sb} represent the gas solubility at p_b . If the cell pressure is lowered to p , a portion of the solution gas is evolved and occupies a certain volume of the PVT cell. Let R_s and B_o represent the corresponding gas solubility and oil formation volume factor at p . Obviously, the term $(R_{sb} - R_s)$ represents the volume of the free gas as measured in scf per stock-tank barrel of oil. The volume of the free gas at the cell conditions is then

$$(V_g)_{p,T} = (R_{sb} - R_s)B_g$$

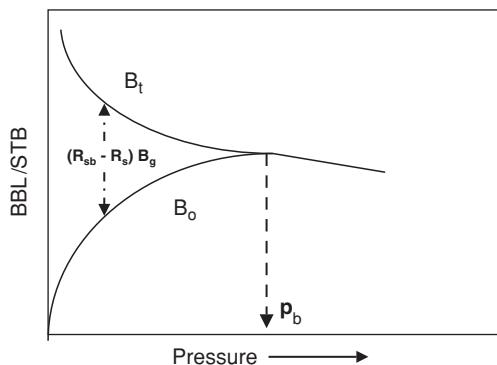


Figure 2-10. B_t and B_o vs. Pressure

where $(V_g)_{p,T}$ = volume of the free gas at p and T, bbl of gas/STB of oil
 B_g = gas formation volume factor, bbl/scf

The volume of the remaining oil at the cell condition is

$$(V)_{p,T} = B_o$$

From the definition of the two-phase formation volume factor

$$B_t = B_o + (R_{sb} - R_s)B_g$$

where R_{sb} = gas solubility at the bubble-point pressure, scf/STB
 R_s = gas solubility at any pressure, scf/STB
 B_o = oil formation volume factor at any pressure, bbl/STB
 B_g = gas formation volume factor, bbl/scf

There are several correlations that can be used to estimate the two-phase formation volume factor when the experimental data are not available; three of these methods are presented below:

- Standing's correlations
- Glaso's method
- Marhoun's correlation

Standing's Correlation

Standing (1947) used a total of 387 experimental data points to develop a graphical correlation for predicting the two-phase formation volume factor with a reported average error of 5%. The proposed correlation uses the following parameters for estimating the two-phase formation volume factor:

The gas solubility at pressure of interest, R_s
 Solution gas gravity,
 Oil gravity, $60^\circ/60^\circ$
 Reservoir temperature, T
 Pressure of interest, p

In developing his graphical correlation, Standing used a combined correlating parameter that is given by:

$$\log(A^*) = \log \left[R_s \frac{(T - 460)^{0.5} (\gamma_o)^C}{(\gamma_g)^{0.3}} \right] - \left(10.1 - \frac{96.8}{6.604 + \log(p)} \right)$$

with the exponent C defined as follows:

$$C = (2.9) 10^{-0.00027R_s}$$

Whitson and Brule (2000) expressed Standing's graphical correlation by the following mathematical form:

$$\log(B_t) = -5.223 - \frac{47.4}{-12.22 + \log(A^*)}$$

Glaso's Correlation

The experimental data on 45 crude oil samples from the North Sea were used by Glaso (1980) in developing a generalized correlation for estimating B_t . Glaso modified Standing's correlating parameter A^* and used a regression analysis model to develop the following expression for B_t :

$$\log(B_t) = 0.080135 + 0.47257 \log(A^*) + 0.17351 [\log(A^*)]^2$$

The author included the pressure in Standing's correlating parameter A^* , to give:

$$A^* = \left[\frac{R_s (T - 460)^{0.5} (\gamma_o)^C}{(\gamma_g)^{0.3}} \right] p^{-1.1089}$$

with the exponent C given by:

$$C = (2.9) 10^{-0.00027R_s}$$

Glaso reported a standard deviation of 6.54% for the total formation volume factor correlation.

Marhoun's Correlation

Based on 1,556 experimentally determined total formation volume factors, Marhoun (1988) used a nonlinear multiple-regression model to develop a mathematical expression for B_t . The empirical equation has the following form:

$$B_t = 0.314693 + 0.106253 \times 10^{-4}F + 0.18883 \times 10^{-10}F^2$$

with the correlating parameter F given by:

$$F = R_s^a \gamma_g^b \gamma_o^c T^d p^e$$

$$\begin{aligned} \text{where } a &= 0.644516 \\ b &= -1.079340 \\ c &= 0.724874 \\ d &= 2.006210 \\ e &= -0.761910 \end{aligned}$$

Marhoun reported an average absolute error of 4.11% with a standard deviation of 4.94% for the correlation.

Example 2-35

Given the following PVT data:

$$p_b = 2,744 \text{ psia}$$

$$T = 600^\circ\text{R}$$

$$\gamma_g = 0.6744$$

$$R_s = 444 \text{ scf/STB}$$

$$R_{sb} = 603 \text{ scf/STB}$$

$$\gamma_o = 0.843 \text{ } 60^\circ/60^\circ$$

$$p = 2,000 \text{ psia}$$

$$B_o = 1.1752 \text{ bbl/STB}$$

calculate B_t at 2,000 psia by using

- Definition of B_t
- Standing's correlation
- Glasco's correlation
- Marhoun's correlation

Solutions

Solution by Using Definition of B_t

Step 1. Calculate T_{pc} and p_{pc} of the solution gas from its specific gravity by applying Equations 2-18 and 2-19, to give:

$$T_{pc} = 168 + 325 \gamma_g - 12.5(\gamma_g)^2$$

$$T_{pc} = 168 + 325 (0.6744) - 12.5(0.6744)^2 = 381.49 \text{ }^\circ\text{R}$$

$$p_{pc} = 677 + 15 \gamma_g - 37.5(\gamma_g)^2 = 670.06 \text{ psia}$$

Step 2. Calculate p_{pr} and T_{pr} :

$$p_{pr} = \frac{2000}{670.06} = 2.986$$

$$T_{pr} = \frac{600}{381.49} = 1.57$$

Step 3. Determine the gas compressibility factor from Figure 2-1. $Z = 0.81$

Step 4. Calculate B_g from Equation 2-54:

$$B_g = 0.00504 \frac{(0.81)(600)}{2000} = 0.001225 \text{ bbl/scf}$$

Step 5. Solve for B_t from:

$$B_t = B_o + (R_{sb} - R_s) B_g$$

$$B_t = 1.1752 + 0.0001225 (603 - 444) = 1.195 \text{ bbl/STB}$$

Solution by Using Standing's Correlation

Step 1. Calculate the correlating parameters C and A^* :

$$C = (2.9) 10^{-0.00027R_s}$$

$$C = (2.9) 10^{-0.00027(444)} = 2.20$$

$$\log(A^*) = \log \left[R_s \frac{(T - 460)^{0.5} (\gamma_o)^C}{(\gamma_g)^{0.3}} \right] - \left(10.1 - \frac{96.8}{6.604 + \log(p)} \right)$$

$$\begin{aligned} \log(A^*) &= \log \left[(444) \frac{(140)^{0.5} (0.843)^{2.2}}{(0.6744)^{0.3}} \right] - \left(10.1 - \frac{96.8}{6.604 + \log(2000)} \right) \\ &= 3.281 \end{aligned}$$

Step 2. Estimate B_t from Standing's equation:

$$\log(B_t) = -5.223 - \frac{47.4}{-12.22 + \log(A^*)}$$

$$\log(B_t) = -5.223 - \frac{47.4}{-12.22 + 3.281} = 0.0792$$

to give:

$$B_t = 10^{0.0792} = 1.200 \text{ bb/STB}$$

Solution by Using Glaso's Correlation

Step 1. Determine the coefficient C:

$$C = (2.9) 10^{-0.00027(444)} = 2.2$$

Step 2. Calculate the correlating parameter A^* to give:

$$A^* = \left[\frac{R_s (T - 460)^{0.5} (\gamma_o)^C}{(\gamma_g)^{0.3}} \right] p^{-1.1089}$$

$$A^* = \left[\frac{(444) (140)^{0.5} (0.843)^{2.2}}{(0.6744)^{0.3}} \right] 2000^{-1.1089} = 0.8873$$

Step 3. Solve for B_t by applying Glaso's expression to yield:

$$\log(B_t) = 0.080135 + 0.47257 \log(A^*) + 0.17351 [\log(A^*)]^2$$

$$\log(B_t) = 0.080135 + 0.47257 \log(0.8873) + 0.17351$$

$$[\log(0.8873)]^2 = 0.0561$$

to give:

$$B_t = 10^{0.0561} = 1.138$$

Solution by Using Marhoun's Correlation

Step 1. Determine the correlating parameter, F to give:

$$F = R_s^a \gamma_g^b \gamma_o^c T^d p^e = 78,590.6789$$

Step 2. Solve for B_t by applying Marhoun's equation:

$$B_t = 0.314693 + 0.106253 \times 10^{-4} F + 0.18883 \times 10^{-10} F^2$$

$$B_t = 0.314693 + 0.106253 \times 10^{-4} (78590.6789) + 0.18883$$

$$\times 10^{-10} (78590.6789)^2$$

$$B_t = 1.2664 \text{ bbl/STB}$$

Crude Oil Viscosity

Crude oil viscosity is an important physical property that controls and influences the flow of oil through porous media and pipes. The viscosity, in general, is defined as the internal resistance of the fluid to flow.

The oil viscosity is a strong function of the temperature, pressure, oil gravity, gas gravity, and gas solubility. Whenever possible, oil viscosity should be determined by laboratory measurements at reservoir temperature and pressure. The viscosity is usually reported in standard PVT analyses. If such laboratory data are not available, engineers may refer to published correlations, which usually vary in complexity and accuracy depending upon the available data on the crude oil.

According to the pressure, the viscosity of crude oils can be classified into three categories:

- **Dead-Oil Viscosity**

The dead-oil viscosity is defined as the viscosity of crude oil at atmospheric pressure (no gas in solution) and system temperature.

- **Saturated-Oil Viscosity**

The saturated (bubble-point)-oil viscosity is defined as the viscosity of the crude oil at the bubble-point pressure and reservoir temperature.

- **Undersaturated-Oil Viscosity**

The undersaturated-oil viscosity is defined as the viscosity of the crude oil at a pressure above the bubble-point and reservoir temperature.

Estimation of the oil viscosity at pressures equal to or below the bubble-point pressure is a two-step procedure:

Step 1. Calculate the viscosity of the oil without dissolved gas (dead oil), μ_{ob} , at the reservoir temperature.

Step 2. Adjust the dead-oil viscosity to account for the effect of the gas solubility at the pressure of interest.

At pressures greater than the bubble-point pressure of the crude oil, another adjustment step, i.e., Step 3, should be made to the bubble-point oil viscosity, μ_{ob} , to account for the compression and the degree of undersaturation in the reservoir. A brief description of several correlations that are widely used in estimating the oil viscosity in the above three steps is given below.

METHODS OF CALCULATING VISCOSITY OF THE DEAD OIL

Several empirical methods are proposed to estimate the viscosity of the dead oil, including:

- Beal's correlation
- The Beggs-Robinson correlation
- Glaso's correlation

These three methods are presented below.

Beal's Correlation

From a total of 753 values for dead-oil viscosity at and above 100°F, Beal (1946) developed a graphical correlation for determining the viscosity of the dead oil as a function of temperature and the API gravity of the crude. Standing (1981) expressed the proposed graphical correlation in a mathematical relationship as follows:

$$\mu_{od} = \left(0.32 + \frac{1.8(10^7)}{API^{4.53}} \right) \left(\frac{360}{T-260} \right)^a \quad (2-116)$$

with

$$a = 10^{(0.43 + 8.33/API)}$$

where μ_{od} = viscosity of the dead oil as measured at 14.7 psia and reservoir temperature, cp
 T = temperature, °R

The Beggs-Robinson Correlation

Beggs and Robinson (1975) developed an empirical correlation for determining the viscosity of the dead oil. The correlation originated from analyzing 460 dead-oil viscosity measurements. The proposed relationship is expressed mathematically as follows:

$$\mu_{od} = 10^X - 1 \quad (2-117)$$

where $X = Y(T - 460)^{-1.163}$

$$Y = 10^Z$$

$$Z = 3.0324 - 0.02023^\circ API$$

An average error of -0.64% with a standard deviation of 13.53% was reported for the correlation when tested against the data used for its development. Sutton and Farshad (1980) reported an error of 114.3% when the correlation was tested against 93 cases from the literature.

Glaso's Correlation

Glaso (1980) proposed a generalized mathematical relationship for computing the dead-oil viscosity. The relationship was developed from experimental measurements on 26 crude oil samples. The correlation has the following form:

$$\mu_{od} = [3.141 (10^{10})] (T - 460)^{-3.444} [\log(\text{API})]^a \quad (2-118)$$

where the coefficient a is given by:

$$a = 10.313 [\log(T - 460)] - 36.447$$

The above expression can be used within the range of 50–300°F for the system temperature and 20–48° for the API gravity of the crude.

Sutton and Farshad (1986) concluded that Glaso's correlation showed the best accuracy of the three previous correlations.

METHODS OF CALCULATING THE SATURATED OIL VISCOSITY

Several empirical methods are proposed to estimate the viscosity of the saturated oil, including:

- The Chew-Connally correlation
- The Beggs-Robinson correlation

These two correlations are presented below.

The Chew-Connally Correlation

Chew and Connally (1959) presented a graphical correlation to adjust the dead-oil viscosity according to the gas solubility at saturation pressure. The correlation was developed from 457 crude oil samples. Standing (1977) expressed the correlation in a mathematical form as follows:

$$\mu_{ob} = (10)^a (\mu_{od})^b \quad (2-119)$$

with $a = R_s [2.2(10^{-7}) R_s - 7.4(10^{-4})]$

$$b = \frac{0.68}{10^c} + \frac{0.25}{10^d} + \frac{0.062}{10^e}$$

$$c = 8.62(10^{-5})R_s$$

$$d = 1.1(10^{-3})R_s$$

$$e = 3.74(10^{-3})R_s$$

where μ_{ob} = viscosity of the oil at the bubble-point pressure, cp
 μ_{od} = viscosity of the dead oil at 14.7 psia and reservoir temperature, cp

The experimental data used by Chew and Connally to develop their correlation encompassed the following ranges of values for the independent variables:

Pressure, psia: 132–5,645

Temperature, °F: 72–292

Gas solubility, scf/STB: 51–3,544

Dead oil viscosity, cp: 0.377–50

The Beggs-Robinson Correlation

From 2,073 saturated oil viscosity measurements, Beggs and Robinson (1975) proposed an empirical correlation for estimating the saturated-oil viscosity. The proposed mathematical expression has the following form:

$$\mu_{ob} = a(\mu_{od})^b \quad (2-120)$$

where $a = 10.715(R_s + 100)^{-0.515}$

$$b = 5.44(R_s + 150)^{-0.338}$$

The reported accuracy of the correlation is -1.83% with a standard deviation of 27.25% .

The ranges of the data used to develop Beggs and Robinson's equation are:

Pressure, psia: 132–5,265

Temperature, °F: 70–295

API gravity: 16–58

Gas solubility, scf/STB: 20–2,070

METHODS OF CALCULATING THE VISCOSITY OF THE UNDERSATURATED OIL

Oil viscosity at pressures above the bubble point is estimated by first calculating the oil viscosity at its bubble-point pressure and adjusting the bubble-point viscosity to higher pressures. Vasquez and Beggs proposed a simple mathematical expression for estimating the viscosity of the oil above the bubble-point pressure. This method is discussed below.

The Vasquez-Beggs Correlation

From a total of 3,593 data points, Vasquez and Beggs (1980) proposed the following expression for estimating the viscosity of undersaturated crude oil:

$$\mu_o = \mu_{ob} \left(\frac{p}{p_b} \right)^m \quad (2-121)$$

where

$$m = 2.6 p^{1.187} 10^a$$

with

$$a = -3.9(10^{-5}) p - 5$$

The data used in developing the above correlation have the following ranges:

Pressure, psia: 141–9,151

Gas solubility, scf/STB: 9.3–2,199

Viscosity, cp: 0.117–148

Gas gravity: 0.511–1.351

API gravity: 15.3–59.5

The average error of the viscosity correlation is reported as -7.54% .

Example 2-36

In addition to the experimental PVT data given in Example 2-30, the following viscosity data are available:

| Oil # | Dead Oil μ_{od} @ T | Saturated Oil μ_{ob} cP | Undersaturated Oil μ_o @ p |
|-------|----------------------------|--------------------------------|-----------------------------------|
| 1 | 0.765 @ 250°F | 0.224 | 0.281 @ 5000 psi |
| 2 | 1.286 @ 220°F | 0.373 | 0.450 @ 5000 psi |
| 3 | 0.686 @ 260°F | 0.221 | 0.292 @ 5000 psi |
| 4 | 1.014 @ 237°F | 0.377 | 0.414 @ 6000 psi |
| 5 | 1.009 @ 218°F | 0.305 | 0.394 @ 6000 psi |
| 6 | 4.166 @ 180°F | 0.950 | 1.008 @ 5000 psi |

Using all the oil viscosity correlations discussed in this chapter, please calculate μ_{od} , μ_{ob} , and the viscosity of the undersaturated oil.

Solution

Dead-oil viscosity

| Oil # | Measured μ_{od} | Beal's | Beggs-Robinson | Glaso's |
|-------|---------------------|--------|----------------|---------|
| 1 | 0.765 | 0.322 | 0.568 | 0.417 |
| 2 | 0.286 | 0.638 | 1.020 | 0.775 |
| 3 | 0.686 | 0.275 | 0.493 | 0.363 |
| 4 | 1.014 | 0.545 | 0.917 | 0.714 |
| 5 | 1.009 | 0.512 | 0.829 | 0.598 |
| 6 | 4.166 | 4.425 | 4.246 | 4.536 |
| AAE | | 44.9% | 17.32% | 35.26% |

Saturated-oil viscosity

| Oil # | Measured μ_{ob} | Chew-Connally | Beggs-Robinson |
|-------|---------------------|---------------|----------------|
| 1 | 0.224 | 0.313* | 0.287* |
| 2 | 0.373 | 0.426 | 0.377 |
| 3 | 0.221 | 0.308 | 0.279 |
| 4 | 0.377 | 0.311 | 0.297 |
| 5 | 0.305 | 0.316 | 0.300 |
| 6 | 0.950 | 0.842 | 0.689 |
| AAE | | 21% | 17% |

*Using the measured μ_{od} .

Undersaturated-oil viscosity

| Oil # | Measured μ_o | Beal's | Vasquez-Beggs |
|-------|------------------|--------|---------------|
| 1 | 0.281 | 0.273* | 0.303* |
| 2 | 0.450 | 0.437 | 0.485 |
| 3 | 0.292 | 0.275 | 0.318 |
| 4 | 0.414 | 0.434 | 0.472 |
| 5 | 0.396 | 0.373 | 0.417 |
| 6 | 1.008 | 0.945 | 1.016 |
| AAE | | 3.8% | 7.5% |

Using the measured μ_{ob} .

Surface/Interfacial Tension

The surface tension is defined as the force exerted on the boundary layer between a liquid phase and a vapor phase per unit length. This force is caused by differences between the molecular forces in the vapor phase and those in the liquid phase, and also by the imbalance of these forces at the interface. The surface can be measured in the laboratory and is unusually expressed in dynes per centimeter. The surface tension is an important property in reservoir engineering calculations and designing enhanced oil recovery projects.

Sugden (1924) suggested a relationship that correlates the surface tension of a pure liquid in equilibrium with its own vapor. The correlating parameters of the proposed relationship are molecular weight M of the pure component, the densities of both phases, and a newly introduced temperature-independent parameter P_{ch} . The relationship is expressed mathematically in the following form:

$$\sigma = \left[\frac{P_{ch} (\rho_L - \rho_v)}{M} \right]^4 \quad (2-122)$$

where σ is the surface tension and P_{ch} is a temperature-independent parameter and is called the *parachor*.

The parachor is a dimensionless constant characteristic of a pure compound and is calculated by imposing experimentally measured surface tension and density data on Equation 2-124 and solving for P_{ch} . The parachor values for a selected number of pure compounds are given in Table 2-1 as reported by Weinaug and Katz (1943).

Table 2-1
Parachor for Pure Substances

| Component | Parachor | Component | Parachor |
|------------------|----------|------------------|----------|
| CO ₂ | 78.0 | n-C ₄ | 189.9 |
| N ₂ | 41.0 | i-C ₅ | 225.0 |
| C ₁ | 77.0 | n-C ₅ | 231.5 |
| C ₂ | 108.0 | n-C ₆ | 271.0 |
| C ₃ | 150.3 | n-C ₇ | 312.5 |
| i-C ₄ | 181.5 | n-C ₈ | 351.5 |

Fanchi (1985) correlated the parachor with molecular weight with a simple linear equation. This equation is only valid for components heavier than methane. Fanchi's linear equation has the following form:

$$(P_{ch})_i = 69.9 + 2.3 M_i \quad (2-123)$$

where M_i = molecular weight of component i

$(P_{ch})_i$ = parachor of component i

For a complex hydrocarbon mixture, Katz et al. (1943) employed the Sugden correlation for mixtures by introducing the compositions of the two phases into Equation 2-124. The modified expression has the following form:

$$\sigma^{1/4} = \sum_{i=1}^n [(P_{ch})_i (Ax_i - By_i)] \quad (2-124)$$

with the parameters A and B as defined by:

$$A = \frac{\rho_o}{62.4M_o}$$

$$B = \frac{\rho_g}{62.4M_g}$$

where ρ_o = density of the oil phase, lb/ft³

M_o = apparent molecular weight of the oil phase

ρ_g = density of the gas phase, lb/ft³

M_g = apparent molecular weight of the gas phase

x_i = mole fraction of component i in the oil phase

y_i = mole fraction of component i in the gas phase
 n = total number of components in the system

Example 2-37

The composition of a crude oil and the associated equilibrium gas is given below. The reservoir pressure and temperature are 4,000 psia and 160°F, respectively.

| Component | x_i | y_i |
|------------------|-------|-------|
| C ₁ | 0.45 | 0.77 |
| C ₂ | 0.05 | 0.08 |
| C ₃ | 0.05 | 0.06 |
| n-C ₄ | 0.03 | 0.04 |
| n-C ₅ | 0.01 | 0.02 |
| C ₆ | 0.01 | 0.02 |
| C ₇₊ | 0.40 | 0.01 |

The following additional PVT data are available:

Oil density = 46.23 lb/ft³

Gas density = 18.21 lb/ft³

Molecular weight of C₇₊ = 215

Calculate the surface tension.

Solution

Step 1. Calculate the apparent molecular weight of the liquid and gas phase:

$$M_o = 100.253 \quad M_g = 24.99$$

Step 2. Calculate the coefficients A and B:

$$A = \frac{46.23}{(62.4)(100.253)} = 0.00739$$

$$B = \frac{18.21}{(62.4)(24.99)} = 0.01168$$

Step 3. Calculate the parachor of C_{7+} from Equation 2-125:

$$(P_{ch})_{C_{7+}} = 69.9 + (2.3)(215) = 564.4$$

Step 4. Construct the following working table:

| Component | P_{ch} | Ax_i | By_i | $P_{ch}(Ax_i - By_i)$ |
|-----------|----------|----------|----------|-----------------------|
| C_1 | 77 | 0.00333 | 0.0090 | -0.4361 |
| C_2 | 108 | 0.00037 | 0.00093 | -0.0605 |
| C_3 | 150.3 | 0.00037 | 0.00070 | -0.0497 |
| n- C_4 | 189.9 | 0.00022 | 0.00047 | -0.0475 |
| n- C_5 | 231.5 | 0.00007 | 0.00023 | -0.0370 |
| C_6 | 271.0 | 0.000074 | 0.00023 | -0.0423 |
| C_{7+} | 564.4 | 0.00296 | 0.000117 | 1.6046 |
| | | | | 0.9315 |

Step 5. $\sigma = (0.9315)^4 = 0.753$ dynes/cm

PROPERTIES OF RESERVOIR WATER

Water Formation Volume Factor

The water formation volume factor can be calculated by the following mathematical expression:*

$$B_w = A_1 + A_2 p + A_3 p^2 \quad (2-125)$$

where the coefficients $A_1 - A_3$ are given by the following expression:

$$A_i = a_1 + a_2(T - 460) + a_3(T - 460)^2$$

with $a_1 - a_3$ given for gas-free and gas-saturated water:

Gas-Free Water

| A_i | a_1 | a_2 | a_3 |
|-------|--------------------|----------------------|--------------------|
| A_1 | 0.9947 | $5.8 (10^{-6})$ | $1.02 (10^{-6})$ |
| A_2 | $-4.228 (10^{-6})$ | $1.8376 (10^{-8})$ | $-6.77 (10^{-11})$ |
| A_3 | $1.3 (10^{-10})$ | $-1.3855 (10^{-12})$ | $4.285 (10^{-15})$ |

Gas-Saturated Water

| A_i | α_1 | α_2 | α_3 |
|-------|--------------------|--------------------|--------------------|
| A_1 | 0.9911 | $6.35 (10^{-5})$ | $8.5 (10^{-7})$ |
| A_2 | $-1.093 (10^{-6})$ | $-3.497 (10^{-9})$ | $4.57 (10^{-12})$ |
| A_3 | $-5.0 (10^{-11})$ | $6.429 (10^{-13})$ | $-1.43 (10^{-15})$ |

*Hewlett-Packard H.P. 41C Petroleum Fluids PAC manual, 1982.

The temperature T in Equation 2-127 is in °R.

Water Viscosity

Meehan (1980) proposed a water viscosity correlation that accounts for both the effects of pressure and salinity:

$$\mu_{wT} = (109.574 - 8.40564w_s + 0.313314w_s^2 + 8.72213 \times 10^{-3}w_s^3)(T - 460)^{-D} \quad (2-126)$$

With:

$$D = 1.12166 - 0.0263951w_s + 6.79461 \times 10^{-4}w_s^2 + 5.47119 \times 10^{-5}w_s^3 - 1.55586 \times 10^{-6}w_s^4$$

where μ_{wT} = brine viscosity at 14.7 psi and reservoir temperature T, cp
 w_s = weight percent of salt in brine
 T = temperature in °R

The effect of pressure “p” on the brine viscosity can be estimated from:

$$\mu_w = \mu_{wT} (0.9994 + 4.0295 \times 10^{-5} P + 3.1062 \times 10^{-9} P^2)$$

where μ_w = viscosity of the brine at pressure and temperature

Brill and Beggs (1978) presented a simpler equation, which considers only temperature effects:

$$\mu_w = \exp[1.003 - 1.479 \times 10^{-2} (T-460) + 1.982 \times 10^{-5} (T-460^2)] \quad (2-127)$$

where T is in °F and μ_w is in cp.

Gas Solubility in Water

The following correlation can be used to determine the gas solubility in water:

$$R_{sw} = A + B p + C p^2 \quad (2-128)$$

$$\begin{aligned} \text{where } A &= 2.12 + 3.45 (10^{-3}) T - 3.59 (10^{-5}) T^2 \\ B &= 0.0107 - 5.26 (10^{-5}) T + 1.48 (10^{-7}) T^2 \\ C &= 8.75 (10^{-7}) + 3.9 (10^{-9}) T - 1.02 (10^{-11}) T^2 \end{aligned}$$

The temperature T in above equations is expressed in $^{\circ}\text{F}$.

Water Isothermal Compressibility

Brill and Beggs (1978) proposed the following equation for estimating water isothermal compressibility, ignoring the corrections for dissolved gas and solids:

$$C_w = (C_1 + C_2 T + C_3 T^2) \times 10^{-6} \quad (2-129)$$

$$\begin{aligned} \text{where } C_1 &= 3.8546 - 0.000134 p \\ C_2 &= -0.01052 + 4.77 \times 10^{-7} p \\ C_3 &= 3.9267 \times 10^{-5} - 8.8 \times 10^{-10} p \\ T &= ^{\circ}\text{F} \\ p &= \text{psia} \\ C_w &= \text{psi}^{-1} \end{aligned}$$

PROBLEMS

1. Assuming an ideal gas behavior, calculate the density of n-butane at 220°F and 50 psia .
2. Show that:

$$y_i = \frac{(w_i/M_i)}{\sum_i (w_i/M_i)}$$

3. Given the following gas:

| Component | Weight Fraction |
|-----------|-----------------|
| C_1 | 0.65 |
| C_2 | 0.15 |
| C_3 | 0.10 |
| n- C_4 | 0.06 |
| n- C_5 | 0.04 |

calculate:

- a. Mole fraction of the gas
 - b. Apparent molecular weight
 - c. Specific gravity
 - d. Specific volume at 300 psia and 120°F by assuming an ideal gas behavior
4. An ideal gas mixture has a density of 1.92 lb/ft³ at 500 psia and 100°F. Calculate the apparent molecular weight of the gas mixture.
 5. Using the gas composition as given in Problem 3, and assuming real gas behavior, calculate:
 - a. Gas density at 2,000 psia and 150°F
 - b. Specific volume at 2,000 psia and 150°F
 - c. Gas formation volume factor in scf/ft³
 6. A natural gas with a specific gravity of 0.75 has a gas formation volume factor of 0.00529 ft³/scf at the prevailing reservoir pressure and temperature. Calculate the density of the gas.
 7. A natural gas has the following composition:

| Component | y_i |
|------------------|-------|
| C ₁ | 0.75 |
| C ₂ | 0.10 |
| C ₃ | 0.05 |
| i-C ₄ | 0.04 |
| n-C ₄ | 0.03 |
| i-C ₅ | 0.02 |
| n-C ₅ | 0.01 |

Reservoir conditions are 3,500 psia and 200°F. Calculate:

- a. Isothermal gas compressibility coefficient
- b. Gas viscosity by using the
 1. Carr-Kobayashi-Burrows method
 2. Lee-Gonzales-Eakin method

8. Given the following gas composition:

| Component | y_i |
|------------------|-------|
| CO ₂ | 0.06 |
| N ₂ | 0.03 |
| C ₁ | 0.75 |
| C ₂ | 0.07 |
| C ₃ | 0.04 |
| n-C ₄ | 0.03 |
| n-C ₅ | 0.02 |

If the reservoir pressure and temperature are 2,500 psia and 175°F, respectively, calculate:

- a. Gas density by accounting for the presence of nonhydrocarbon components by using the
 1. Wichert-Aziz method
 2. Carr-Kobayashi-Burrows method
 - b. Isothermal gas compressibility coefficient
 - c. Gas viscosity by using the
 1. Carr-Kobayashi-Burrows method
 2. Lee-Gonzales-Eakin method
9. A crude oil system exists at its bubble-point pressure of 1,708.7 psia and a temperature of 131°F. Given the following data:
- API = 40°
- Average specific gravity of separator gas = 0.85
- Separator pressure = 100 psig
- a. Calculate R_{sb} by using
 1. Standing's correlation
 2. The Vasquez-Beggs method
 3. Glaso's correlation
 4. Marhoun's equation
 5. The Petrosky-Farshad correlation
 - b. Calculate B_{ob} by applying methods listed in Part a.
10. Estimate the bubble-point pressure of a crude oil system with the following limited PVT data:
- API = 35° T = 160°F $R_{sb} = 700$ scf/STB $\gamma_g = 0.75$
- Use the six different methods listed in Problem 9.

11. A crude oil system exists at an initial reservoir pressure of 4,500 psi and 85°F. The bubble-point pressure is estimated at 2,109 psi. The oil properties at the bubble-point pressure are as follows:

$$B_{ob} = 1.406 \text{ bbl/STB} \quad R_{sb} = 692 \text{ scf/STB}$$

$$\gamma_g = 0.876 \quad \text{API} = 41.9^\circ$$

Calculate:

- Oil density at the bubble-point pressure
 - Oil density at 4,500 psi
 - B_o at 4,500 psi
12. A high-pressure cell has a volume of 0.33 ft³ and contains gas at 2,500 psia and 130°F, at which conditions its z-factor is 0.75. When 43.6 scf of the gas are bled from the cell, the pressure dropped to 1,000 psia, the temperature remaining at 130°F. What is the gas deviation factor at 1,000 psia and 130°F?
13. A hydrocarbon gas mixture with a specific gravity of 0.7 has a density of 9 lb/ft³ at the prevailing reservoir pressure and temperature. Calculate the gas formation volume factor in bbl/scf.
14. A gas reservoir exists at a 150°F. The gas has the following composition:

| Component | Mole% |
|----------------|-------|
| C ₁ | 89 |
| C ₂ | 7 |
| C ₃ | 4 |

The gas expansion factor E_g was calculated as 204.648 scf/ft³ at the existing reservoir pressure and temperature. Calculate the viscosity of the gas.

15. A 20 ft³ tank at a pressure of 2,500 psia and 212°F contains ethane gas. How many pounds of ethane are in the tank?
16. The PVT data as shown below were obtained on a crude oil sample taken from the Nameless Field. The initial reservoir pressure was 3,600 psia at 160°F. The average specific gravity of the solution gas is 0.65. The reservoir contains 250 mm bbl of oil initially in place. The oil has a bubble-point pressure of 2,500 psi.
- Calculate the two-phase oil formation volume factor at:
 - 3,200 psia
 - 2,800 psia
 - 1,800 psia

- b. What is the initial volume of dissolved gas in the reservoir?
 c. Oil compressibility coefficient at 3,200 psia.

| Pressure, psia | Solution Gas, scf/STB at 1407 psia and 60°F | Formation Volume Factor, bbl/STB |
|-------------------|---|--|
| 3600 | | 1.310 |
| 3200 | | 1.317 |
| 2800 | | 1.325 |
| 2500 | 567 | 1.333 |
| 2400 | 554 | 1.310 |
| 1800 | 436 | 1.263 |
| 1200 | 337 | 1.210 |
| 600 | 223 | 1.140 |
| 200 | 143 | 1.070 |

17. The following PVT data were obtained from the analysis of a bottom-hole sample.

| p psia | Relative Volume V/V_{sat} |
|-----------|--------------------------------|
| 3000 | 1.0000 |
| 2927 | 1.0063 |
| 2703 | 1.0286 |
| 2199 | 1.1043 |
| 1610 | 1.2786 |
| 1206 | 1.5243 |
| 999 | 1.7399 |

- a. Plot the Y-function versus pressure on rectangular coordinate paper, see Equation 3-3.
 b. Determine the constants in the equation

$$Y = mp + b$$

by using the method of least squares.

- c. Recalculate relative oil volume from the equation (see Equation 3-5).

18. A 295-cc crude oil sample was placed in a PVT at an *initial* pressure of 3,500 psi. The cell temperature was held at a constant temperature of 220°F. A differential liberation test was then performed on the crude oil sample with the recorded measurements as given below:

| p, psi | T, °F | Total Volume, cc | Vol. of Liquids, cc | Vol. of Liberated Gas, scf | Specific Gravity of Liberated Gas |
|-----------|----------|---------------------|------------------------|----------------------------------|---|
| 3500 | 220 | 290 | 290 | 0 | — |
| 3300 | 220 | 294 | 294 | 0 | — |
| *3000 | 220 | 300 | 300 | 0 | — |
| 2000 | 220 | 323.2 | 286.4 | 0.1627 | 0.823 |
| 1000 | 220 | 375.2 | 271.5 | 0.1840 | 0.823 |
| 14.7 | 60 | — | 179.53 | 0.5488 | 0.823 |

*Bubble-point pressure

Using the bore-recorded measurements and assuming an oil gravity of 40° API, calculate the following PVT properties:

- a. Oil formation volume factor at 3,500 psi
 - b. Gas solubility at 3,500 psi
 - c. Oil viscosity at 3,500 psi
 - d. Isothermal compressibility coefficient at 3,300 psi
 - e. Oil density at 1,000 psi
19. Experiments were made on a bottom-hole crude oil sample taken from the North Grieve Field to determine the gas solubility and oil formation volume factor as a function of pressure. The initial reservoir pressure was recorded as 3,600 psia and reservoir temperature was 130°F. The following data were obtained from the measurements:

| Pressure, psia | R _s , scf/STB | B _o , bbl/STB |
|-------------------|-----------------------------|-----------------------------|
| 3600 | 567 | 1.310 |
| 3200 | 567 | 1.317 |
| 2800 | 567 | 1.325 |
| 2500 | 567 | 1.333 |
| 2400 | 554 | 1.310 |
| 1800 | 436 | 1.263 |
| 1200 | 337 | 1.210 |
| 600 | 223 | 1.140 |
| 200 | 143 | 1.070 |

At the end of the experiments, the API gravity of the oil was measured as 40°. If the average specific gravity of the solution gas is 0.7, calculate:

- a. Total formation volume factor at 3,200 psia
 - b. Oil viscosity at 3,200 psia
 - c. Isothermal compressibility coefficient at 1,800 psia
20. You are producing a 35°API crude oil from a reservoir at 5,000 psia and 140°F. The bubble-point pressure of the reservoir liquids is 4,000 psia at 140°F. Gas with a gravity of 0.7 is produced with the oil at a rate of 900 scf/STB. Calculate:
- a. Density of the oil at 5,000 psia and 140°F
 - b. Total formation volume factor at 5,000 psia and 140°F
21. An undersaturated-oil reservoir exists at an initial reservoir pressure 3,112 psia and a reservoir temperature of 125°F. The bubble point of the oil is 1,725 psia. The crude oil has the following pressure versus oil formation volume factor relationship:

| Pressure, psia | B_{or} , bbl/STB |
|-------------------|-----------------------|
| 3112 | 1.4235 |
| 2800 | 1.4290 |
| 2400 | 1.4370 |
| 2000 | 1.4446 |
| 1725 | 1.4509 |
| 1700 | 1.4468 |
| 1600 | 1.4303 |
| 1500 | 1.4139 |
| 1400 | 1.3978 |

The API gravity of the crude oil and the specific gravity of the solution gas are 40° and 0.65, respectively. Calculate the density of the crude oil at 3,112 psia and 125°F.

22. A PVT cell contains 320 cc of oil and its bubble-point pressure of 2,500 psia and 200°F. When the pressure was reduced to 2,000 psia, the volume increased to 335.2 cc. The gas was bled off and found to occupy a volume of 0.145 scf. The volume of the oil was recorded as 303 cc. The pressure was reduced to 14.7 psia and the temperature to 60°F while 0.58 scf of gas was evolved leaving 230 cc of oil with a gravity of 42°API. Calculate:
- a. Gas compressibility factor at 2,000 psia
 - b. Gas solubility at 2,000 psia

REFERENCES

1. Ahmed, T., "Compositional Modeling of Tyler and Mission Canyon Formation Oils with CO₂ and Lean Gases," final report submitted to Montana's on a New Track for Science (MONTS) (Montana National Science Foundation Grant Program), 1985–1988.
2. Baker, O., and Swerdloff, W., "Calculations of Surface Tension-3: Calculations of Surface Tension Parachor Values," *OGJ*, December 5, 1955, Vol. 43, p. 141.
3. Beal, C., "The Viscosity of Air, Water, Natural Gas, Crude Oils and its Associated Gases at Oil Field Temperatures and Pressures," *Trans. AIME*, 1946, Vol. 165, pp. 94–112.
4. Beggs, H. D., and Robinson, J. R., "Estimating the Viscosity of Crude Oil Systems," *JPT*, September 1975, pp. 1140–1141.
5. Brill, J., and Beggs, H., *Two-Phase Flow in Pipes*. Tulsa, OK: The University of Tulsa, 1978.
6. Brown, et al., "Natural Gasoline and the Volatile Hydrocarbons," Tulsa: NGAA, 1948.
7. Carr, N., Kobayashi, R., and Burrows, D., "Viscosity of Hydrocarbon Gases Under Pressure," *Trans. AIME*, 1954, Vol. 201, pp. 270–275.
8. Chew, J., and Connally, Jr., C. A., "A Viscosity Correlation for Gas-Saturated Crude Oils," *Trans. AIME*, 1959, Vol. 216, pp. 23–25.
9. Dean, D. E., and Stiel, L. I., "The Viscosity of Non-polar Gas Mixtures at Moderate and High Pressure," *AIChE Jour.*, 1958, Vol. 4, pp. 430–436.
10. Dempsey, J. R., "Computer Routine Treats Gas Viscosity as a Variable," *Oil and Gas Journal*, Aug. 16, 1965, pp. 141–143.
11. Dranchuk, P. M., and Abu-Kassem, J. H., "Calculation of Z-factors for Natural Gases Using Equations-of-State," *JCPT*, July–Sept. 1975, pp. 34–36.
12. Dranchuk, P. M., Purvis, R. A., and Robinson, D. B., "Computer Calculations of Natural Gas Compressibility Factors Using the Standing and Katz Correlation," *Inst. of Petroleum Technical Series*, No. IP 74-008, 1974.
13. Fanchi, J. R., "Calculation of Parachors for Composition Simulation," *JPT*, November 1985, pp. 2049–2050.
14. Glaso, O., "Generalized Pressure-Volume-Temperature Correlations," *JPT*, May 1980, pp. 785–795.
15. Hall, K. R., and Yarborough, L., "A New Equation-of-State for Z-factor Calculations," *Oil and Gas Journal*, June 18, 1973, pp. 82–92.

16. Hankinson, R. W., Thomas, L. K., and Phillips, K. A., "Predict Natural Gas Properties," *Hydrocarbon Processing*, April 1969, pp. 106–108.
17. Kay, W. B., "Density of Hydrocarbon Gases and Vapor," *Industrial and Engineering Chemistry*, 1936, Vol. 28, pp. 1014–1019.
18. Lee, A. L., Gonzalez, M. H., and Eakin, B. E., "The Viscosity of Natural Gases," *JTP*, August 1966, pp. 997–1000.
19. Marhoun, M. A., "PVT Correlation for Middle East Crude Oils," *JPT*, May 1988, pp. 650–665.
20. Mattar, L. G., Brar, S., and Aziz, K., "Compressibility of Natural Gases," *Journal of Canadian Petroleum Technology*, October–November 1975, pp. 77–80.
21. Meehan, D. N., "A Correlation for Water Compressibility," *Petroleum Engineer*, November 1980, pp. 125–126.
22. Papay, J., "A Termelestechnologiai Parameterek Valtozasa a Gazleplek Muvelese Soran," *OGIL MUSZ*, Tud, Kuzl., Budapest, 1968, pp. 267–273.
23. Petrosky, G. E., and Farshad, F., "Pressure-Volume-Temperature Correlations for Gulf of Mexico Crude Oils," SPE Paper 26644, presented at the 68th Annual Technical Conference of the SPE in Houston, Texas, 3–6 October, 1993.
24. Standing, M. B., *Volumetric and Phase Behavior of Oil Field Hydrocarbon Systems*, pp. 125–126. Dallas: Society of Petroleum Engineers, 1977.
25. Standing, M. B., and Katz, D. L., "Density of Natural Gases," *Trans. AIME*, 1942, Vol. 146, pp. 140–149.
26. Stewart, W. F., Burkhard, S. F., and Voo, D., "Prediction of Pseudo-Critical Parameters for Mixtures," paper presented at the AIChE Meeting, Kansas City, MO, 1959.
27. Sugden, S., "The Variation of Surface Tension, VI. The Variation of Surface Tension with Temperature and Some Related Functions," *J. Chem. Soc.*, 1924, Vol. 125, pp. 32–39.
28. Sutton, R. P., "Compressibility Factors for High-Molecular-Weight Reservoir Gases," SPE Paper 14265, presented at the 60th Annual Technical Conference and Exhibition of the Society of Petroleum Engineers, Las Vegas, Sept. 22–25, 1985.
29. Sutton, R. P., and Farshad, F. F., "Evaluation of Empirically Derived PVT Properties for Gulf of Mexico Crude Oils," SPE Paper 13172, presented at the 59th Annual Technical Conference, Houston, Texas, 1984.
30. Takacs, G., "Comparisons Made for Computer Z-Factor Calculation," *Oil and Gas Journal*, Dec. 20, 1976, pp. 64–66.

31. Trube, A. S., "Compressibility of Undersaturated Hydrocarbon Reservoir Fluids," *Trans. AIME*, 1957, Vol. 210, pp. 341–344.
32. Trube, A. S., "Compressibility of Natural Gases," *Trans. AIME*, 1957, Vol. 210, pp. 355–357.
33. Vasquez, M., and Beggs, D., "Correlations for Fluid Physical Properties Prediction," *JPT*, June 1980, pp. 968–970.
34. Weinaug, C., and Katz, D. L., "Surface Tension of Methane-Propane Mixtures," *Ind. Eng. Chem.*, 1943, Vol. 25, pp. 35–43.
35. Wichert, E., and Aziz, K., "Calculation of Z's for Sour Gases," *Hydrocarbon Processing*, 1972, Vol. 51, No. 5, pp. 119–122.
36. Yarborough, L., and Hall, K. R., "How to Solve Equation-of-State for Z-factors," *Oil and Gas Journal*, Feb. 18, 1974, pp. 86–88.



LABORATORY ANALYSIS OF RESERVOIR FLUIDS

Accurate laboratory studies of PVT and phase-equilibria behavior of reservoir fluids are necessary for characterizing these fluids and evaluating their volumetric performance at various pressure levels. There are many laboratory analyses that can be made on a reservoir fluid sample. The amount of data desired determines the number of tests performed in the laboratory. In general, there are three types of laboratory tests used to measure hydrocarbon reservoir samples:

1. Primary tests

These are simple, routine field (on-site) tests involving the measurements of the specific gravity and the gas-oil ratio of the produced hydrocarbon fluids.

2. Routine laboratory tests

These are several laboratory tests that are routinely conducted to characterize the reservoir hydrocarbon fluid. They include:

- Compositional analysis of the system
- Constant-composition expansion
- Differential liberation
- Separator tests
- Constant-volume depletion

3. Special laboratory PVT tests

These types of tests are performed for very specific applications. If a reservoir is to be depleted under miscible gas injection or a gas cycling scheme, the following tests may be performed:

- Slim-tube test
- Swelling test

The objective of this chapter is to review the PVT laboratory tests and to illustrate the proper use of the information contained in PVT reports.

COMPOSITION OF THE RESERVOIR FLUID

It is desirable to obtain a fluid sample as early in the life of a field as possible so that the sample will closely approximate the original reservoir fluid. Collection of a fluid sample early in the life of a field reduces the chances of free gas existing in the oil zone of the reservoir.

Most of the parameters measured in a reservoir fluid study can be calculated with some degree of accuracy from the composition. It is the most complete description of reservoir fluid that can be made. In the past, reservoir fluid compositions were usually measured to include separation of the component methane through hexane, with the heptanes and heavier components grouped as a single component reported with the average molecular weight and density.

With the development of more sophisticated equations-of-state to calculate fluid properties, it was learned that a more complete description of the heavy components was necessary. It is recommended that compositional analyses of the reservoir fluid should include a separation of components through C_{10} as a minimum. The more sophisticated research laboratories now use equations-of-state that require compositions through C_{30} or higher.

Table 3-1 shows a chromatographic “fingerprint” compositional analysis of the Big Butte crude oil system. The table includes the mole fraction, weight fraction, density, and molecular weight of the individual component.

CONSTANT-COMPOSITION EXPANSION TESTS

Constant-composition expansion experiments are performed on gas condensates or crude oil to simulate the pressure-volume relations of these hydrocarbon systems. The test is conducted for the purposes of determining:

- Saturation pressure (bubble-point or dew-point pressure)
- Isothermal compressibility coefficients of the single-phase fluid in excess of saturation pressure
- Compressibility factors of the gas phase
- Total hydrocarbon volume as a function of pressure

(text continued on page 140)

Table 3-1
Hydrocarbon Analysis of Reservoir Fluid Sample

| Composition of Reservoir Fluid Sample (by Flash, Extended-Capillary Chromatography) | | | | |
|--|-------|------|------------------------|--------|
| Component Name | Mol % | Wt % | Liquid Density (gm/cc) | MW |
| Hydrogen Sulfide | 0.00 | 0.00 | 0.8006 | 34.08 |
| Carbon Dioxide | 0.25 | 0.11 | 0.8172 | 44.01 |
| Nitrogen | 0.88 | 0.25 | 0.8086 | 28.013 |
| Methane | 23.94 | 3.82 | 0.2997 | 16.043 |
| Ethane | 11.67 | 3.49 | 0.3562 | 30.07 |
| Propane | 9.36 | 4.11 | 0.5070 | 44.097 |
| iso-Butane | 1.39 | 0.81 | 0.5629 | 58.123 |
| n-Butane | 4.61 | 2.66 | 0.5840 | 58.123 |
| iso-Pentane | 1.50 | 1.07 | 0.6244 | 72.15 |
| n-Pentane | 2.48 | 1.78 | 0.6311 | 72.15 |
| Hexanes | 3.26 | 2.73 | 0.6850 | 84 |
| Heptanes | 5.83 | 5.57 | 0.7220 | 96 |
| Octanes | 5.52 | 5.88 | 0.7450 | 107 |
| Nonanes | 3.74 | 4.50 | 0.7640 | 121 |
| Decanes | 3.38 | 4.50 | 0.7780 | 134 |

Total Sample Properties

Molecular Weight 100.55
 Equivalent Liquid Density, gm/scs 0.7204

(text continued from page 137)

The experimental procedure, as shown schematically in Figure 3-1, involves placing a hydrocarbon fluid sample (oil or gas) in a visual PVT cell at reservoir temperature and at a pressure in excess of the initial reservoir pressure (Figure 3-1, Section A). The pressure is reduced in steps at constant temperature by removing mercury from the cell, and the change in the *total* hydrocarbon volume V_t is measured for each pressure increment.

The saturation pressure (bubble-point or dew-point pressure) and the corresponding volume are observed and recorded and used as a reference volume V_{sat} (Figure 3-1, Section C). The volume of the hydrocarbon system as a function of the cell pressure is reported as the ratio of the reference volume. This volume is termed the *relative volume* and is expressed mathematically by the following equation:

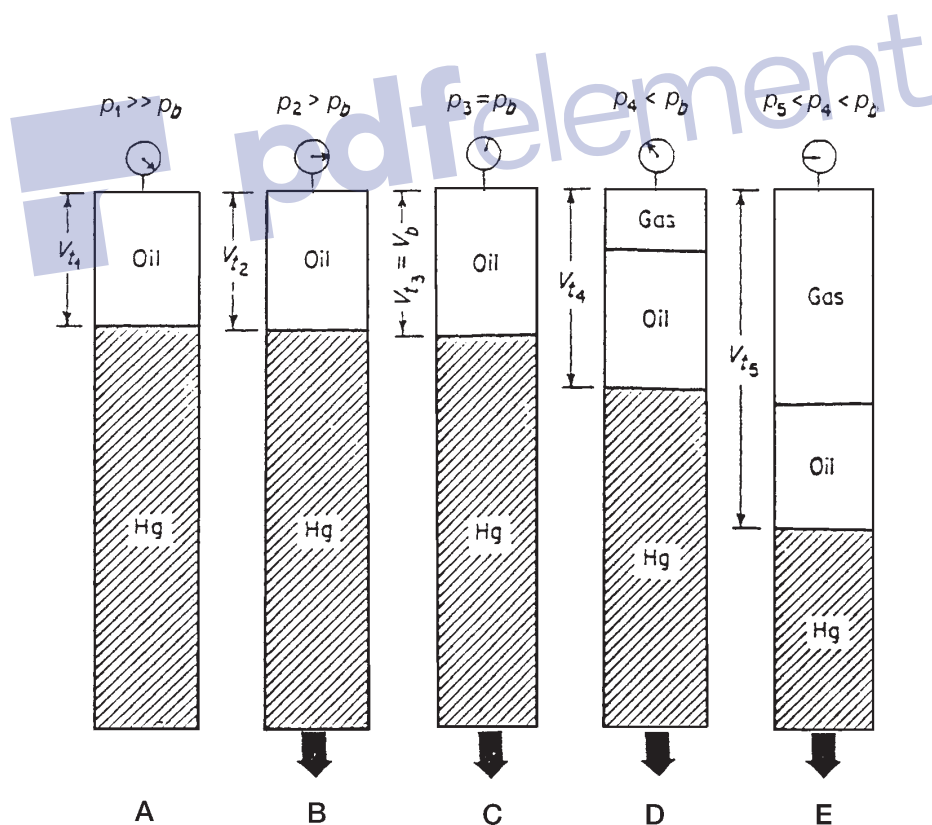


Figure 3-1. Constant-composition expansion test.

$$V_{\text{rel}} = \frac{V_t}{V_{\text{sat}}} \quad (3-1)$$

where V_{rel} = relative volume
 V_t = total hydrocarbon volume
 V_{sat} = volume at the saturation pressure

The relative volume is equal to **one** at the saturation pressure. This test is commonly called pressure-volume relations, flash liberation, flash vaporization, or flash expansion.

It should be noted that no hydrocarbon material is removed from the cell; thus, the composition of the total hydrocarbon mixture in the cell remains fixed at the original composition.

Table 3-2 shows the results of the flash liberation test (the constant composition expansion test) for the Big Butte crude oil system. The bubble-point pressure of the hydrocarbon system is 1,930 psi at 247°F. In addition to the reported values of the relative volume, the table includes the measured values of the oil density at and above the saturation pressure.

The density of the oil at the saturation pressure is 0.6484 gm/cc and is determined from direct weight-volume measurements on the sample in the PVT cell. Above the bubble-point pressure, the density of the oil can be calculated by using the recorded relative volume:

$$\rho = \rho_{\text{sat}}/V_{\text{rel}} \quad (3-2)$$

where ρ = density at any pressure above the saturation pressure
 ρ_{sat} = density at the saturation pressure
 V_{rel} = relative volume at the pressure of interest

Example 3-1

Given the experimental data in Table 3-2, verify the oil density values at 4,000 and 6,500 psi.

Solution

Using Equation 3-2 gives:

- At 4,000 psi

Table 3-2
Constant-Composition Expansion Data

| Pressure-Volume Relations (at 247°F) | | | |
|--|------------------------|-------------------|-------------------|
| Pressure, psig | Relative Volume (A) | Y-Function (B) | Density, gm/cc |
| 6500 | 0.9371 | | 0.6919 |
| 6000 | 0.9422 | | 0.6882 |
| 5500 | 0.9475 | | 0.6843 |
| 5000 | 0.9532 | | 0.6803 |
| 4500 | 0.9592 | | 0.6760 |
| 4000 | 0.9657 | | 0.6714 |
| 3500 | 0.9728 | | 0.6665 |
| 3000 | 0.9805 | | 0.6613 |
| 2500 | 0.9890 | | 0.6556 |
| 2400 | 0.9909 | | 0.6544 |
| 2300 | 0.9927 | | 0.6531 |
| 2200 | 0.9947 | | 0.6519 |
| 2100 | 0.9966 | | 0.6506 |
| 2000 | 0.9987 | | 0.6493 |
| b>>1936 | 1.0000 | | 0.6484 |
| 1930 | 1.0014 | | |
| 1928 | 1.0018 | | |
| 1923 | 1.0030 | | |
| 1918 | 1.0042 | | |
| 1911 | 1.0058 | | |
| 1878 | 1.0139 | | |
| 1808 | 1.0324 | | |
| 1709 | 1.0625 | 2.108 | |
| 1600 | 1.1018 | 2.044 | |
| 1467 | 1.1611 | 1.965 | |
| 1313 | 1.2504 | 1.874 | |
| 1161 | 1.3694 | 1.784 | |
| 1035 | 1.5020 | 1.710 | |
| 782 | 1.9283 | 1.560 | |
| 600 | 2.4960 | 1.453 | |
| 437 | 3.4464 | 1.356 | |

(A) Relative volume: V/V_{sat} or volume at indicated pressure per volume at saturation pressure

(B) Where Y-function
$$\frac{(P_{sat} - P)}{(P_{abs}) \cdot (V/V_{sat} - 1)}$$

$$\rho_o = \frac{0.6484}{0.9657} = 0.6714 \text{ gm/cc}$$

- At 6,500 psi

$$\rho_o = \frac{0.6484}{0.9371} = 0.6919$$

The relative volume data frequently require smoothing to correct for laboratory inaccuracies in measuring the total hydrocarbon volume just below the saturation pressure and also at lower pressures. A dimensionless compressibility function, commonly called the *Y-function*, is used to smooth the values of the relative volume. The function in its mathematical form is only defined below the saturation pressure and is given by the following expression:

$$Y = \frac{p_{\text{sat}} - p}{p(V_{\text{rel}} - 1)} \quad (3-3)$$

where p_{sat} = saturation pressure, psia

p = pressure, psia

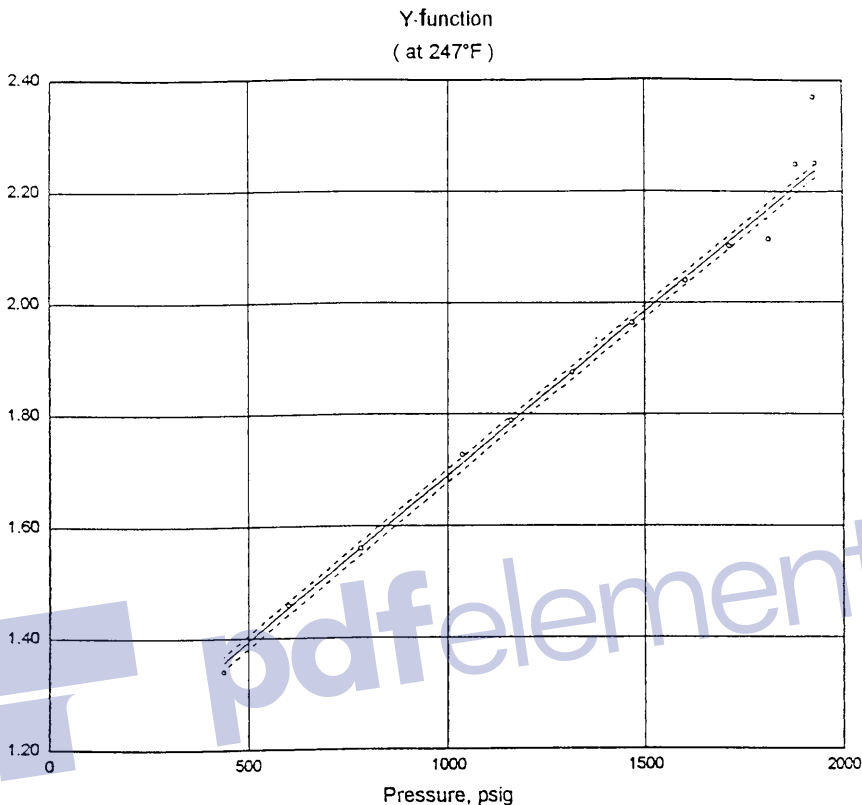
V_{rel} = relative volume at pressure p

Column 3 in Table 3-2 lists the computed values of the Y-function as calculated by using Equation 3-3. To smooth the relative volume data below the saturation pressure, the Y-function is plotted as a function of pressure on a Cartesian scale. When plotted, the Y-function forms a straight line or has only a small curvature. Figure 3-2 shows the Y-function versus pressure for the Big Butte crude oil system. The figure illustrates the erratic behavior of the data near the bubble-point pressure.

The following steps summarize the simple procedure of smoothing and correcting the relative volume data:

Step 1. Calculate the Y-function for all pressures below the saturation pressure by using Equation 3-3.

Step 2. Plot the Y-function versus pressure on a Cartesian scale.



| | |
|---|---|
| <p>Y-function Expression : $y = a + b (X_d)^i$</p> | <p>LEGEND</p> |
| <p>where: $a = 1.09810e+ 00$ $i = 1.000$ $b = 1.14439e+ 00$</p> <p>Note: X_d (dimensionless 'X') = P_i / P_{sat}, psig</p> | <p>○ Laboratory Data - - - - - Confidence Limits _____ Analytical Expression</p> <p>Saturation Pressure: 1.936 psig Current Reservoir Pressure: 2.900 psig</p> |
| <p>Confidence level: 99 % Confidence interval: +/- 0.012 'r squared': .999133</p> | <p>Pressure-Volume Relations Figure A-2</p> |

Figure 3-2. Y-function versus pressure.

Step 3. Determine the coefficients of the best straight fit of the data, or:

$$Y = a + bp \quad (3-4)$$

where a and b are the intercept and slope of the lines, respectively.

Step 4. Recalculate the relative volume at all pressure below the saturation pressure from the following expression:

$$V_{rel} = 1 + \frac{P_{sat} - P}{p(a + bp)} \quad (3-5)$$

Example 3-2

The best straight fit of the Y -function as a function of pressure for the Big Butte oil system is given by:

$$Y = a + bp$$

where $a = 1.0981$
 $b = 0.000591$

Smooth the recorded relative volume data of Table 3-2.

Solution

| Pressure | Measured V_{rel} | Smoothed V_{rel} Equation 3-5 |
|----------|--------------------|------------------------------------|
| 1936 | — | — |
| 1930 | — | 1.0014 |
| 1928 | — | 1.0018 |
| 1923 | — | 1.0030 |
| 1918 | — | 1.0042 |
| 1911 | — | 1.0058 |
| 1878 | — | 1.0139 |
| 1808 | — | 1.0324 |
| 1709 | 1.0625 | 1.0630 |
| 1600 | 1.1018 | 1.1028 |
| 1467 | 1.1611 | 1.1626 |
| 1313 | 1.2504 | 1.2532 |
| 1161 | 1.3696 | 1.3741 |
| 1035 | 1.5020 | 1.5091 |
| 782 | 1.9283 | 1.9458 |
| 600 | 2.4960 | 2.5328 |
| 437 | 3.4464 | 3.5290 |

The oil compressibility coefficient c_o above the bubble-point pressure is also obtained from the relative volume data as listed in Table 3-3 for the Big Butte oil system.

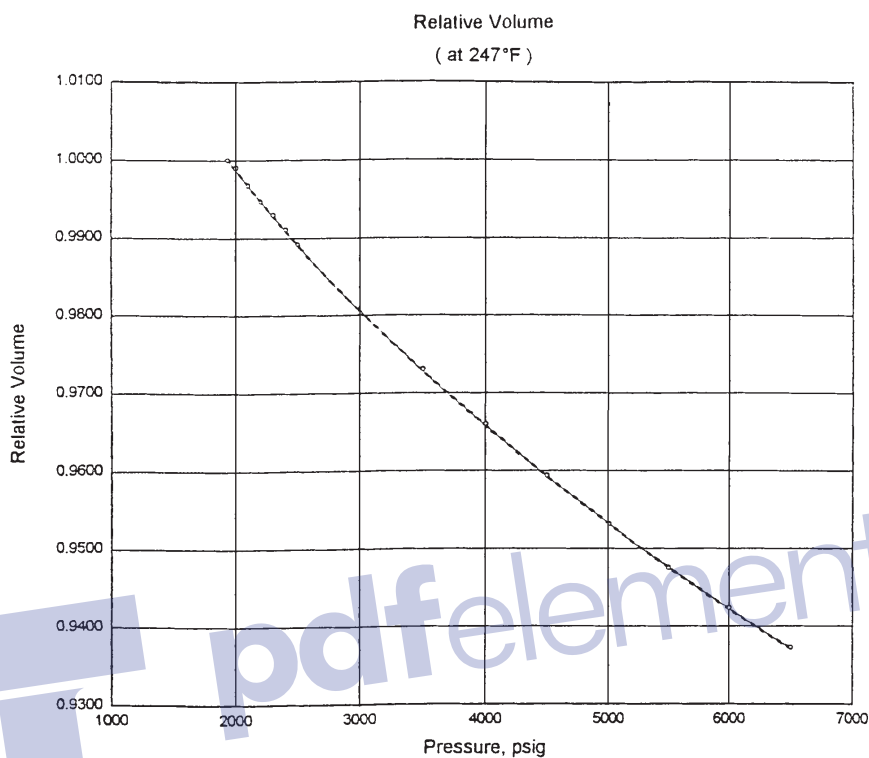
Table 3-3
Undersaturated Compressibility Data

| Volumetric Data (at 247°F) | |
|--|---|
| Saturation Pressure (p_{sat}) | 1936 psig |
| Density at p_{sat} | 0.6484 gm/cc |
| Thermal Exp @ 6500 psig | 1.10401 V at 247°F/V at 60°F |
| Average Single-Phase Compressibilities | |
| Pressure Range, psig | Single-Phase Compressibility, V/V/psi |
| 6500 to 6000 | 10.73 E-6 |
| 6000 to 5500 | 11.31 E-6 |
| 5500 to 5000 | 11.96 E-6 |
| 5000 to 4500 | 12.70 E-6 |
| 4500 to 4000 | 13.57 E-6 |
| 4000 to 3500 | 14.61 E-6 |
| 3500 to 3000 | 15.86 E-6 |
| 3000 to 2500 | 17.43 E-6 |
| 2500 to 2000 | 19.47 E-6 |
| 2000 to 1936 | 20.79 E-6 |

The oil compressibility is defined by Equations 2-94 through 2-96 and equivalently can be written in terms of the relative volume as:

$$c_o = \frac{-1}{V_{rel}} \frac{\partial V_{rel}}{\partial p} \quad (3-6)$$

Commonly, the relative volume data above the bubble-point pressure is plotted as a function of pressure as shown in Figure 3-3. To evaluate c_o at any pressure p , it is only necessary to graphically differentiate the curve by drawing a tangent line and determining the slope of the line, i.e., $\partial V_{rel}/\partial p$.



| | |
|--|---|
| <p>Relative Volume Expression:</p> $y = a + b (Xd)^i + c (Xd)^j + d \log(Xd)^k$ | LEGEND |
| <p>where:</p> <p>a= 1.11371e+ 00 i= 0.500 b= -1.48699e- 01 j= 0.750' c= 3.49924e- 02 k= 1.000 d= 1.73284e- 02</p> <p>Note: Xd (dimensionless 'X') = Pi / Psat, psig</p> | <p>○ Laboratory Data ----- Confidence Limits ----- Analytical Expression</p> <p>Saturation Pressure: 1,936 psig Current Reservoir Pressure: 2,900 psig</p> |
| <p>Confidence level: 99 % Confidence interval: +/- 0.00015 'r squared': .999928</p> | <p>Pressure-Volume Relations Figure A-1</p> |

Figure 3-3. Relative volume data above the bubble-point pressure.

Example 3-3

Using Figure 3-3, evaluate c_o at 3,000 psi.

Solution

- Draw a tangent line to the curve and determine the slope.

$$\partial V_{\text{rel}}/\partial p = -14.92 \times 10^{-6}$$

- Apply Equation 3-6 to give

$$c_o = \left(\frac{-1}{0.98} \right) (-14.92 \times 10^{-6}) = 15.23 \times 10^{-6} \text{ psi}^{-1}$$

It should be noted that Table 3-3 lists the compressibility coefficient at several ranges of pressure, e.g., 6,500–6,000. These values are determined by calculating the changes in the relative volume at the indicated pressure interval and evaluating the relative volume at the lower pressure, or

$$c_o = \frac{-1}{[V_{\text{rel}}]_2} \frac{(V_{\text{rel}})_1 - (V_{\text{rel}})_2}{p_1 - p_2} \quad (3-7)$$

where the subscripts 1 and 2 represent the corresponding values at the higher and lower pressure range, respectively.

Example 3-4

Using the measured relative volume data in Table 3-2 for the Big Butte crude oil system, calculate the average oil compressibility in the pressure range of 2,500 to 2,000 psi.

Solution

Apply Equation 3-7 to give

$$c_o = \frac{-1}{0.9987} \frac{0.9890 - 0.9987}{2500 - 2000} = 19.43 \times 10^{-6} \text{ psi}^{-1}$$

DIFFERENTIAL LIBERATION (VAPORIZATION) TEST

In the differential liberation process, the solution gas that is liberated from an oil sample during a decline in pressure is continuously removed from contact with the oil, and before establishing equilibrium with the liquid phase. This type of liberation is characterized by a varying composition of the total hydrocarbon system.

The experimental data obtained from the test include:

- Amount of gas in solution as a function of pressure
- The shrinkage in the oil volume as a function of pressure
- Properties of the evolved gas including the composition of the liberated gas, the gas compressibility factor, and the gas specific gravity
- Density of the remaining oil as a function of pressure

The differential liberation test is considered to better describe the separation process taking place in the reservoir and is also considered to simulate the flowing behavior of hydrocarbon systems at conditions above the critical gas saturation. As the saturation of the liberated gas reaches the critical gas saturation, the liberated gas begins to flow, leaving behind the oil that originally contained it. This is attributed to the fact that gases have, in general, higher mobility than oils. Consequently, this behavior follows the differential liberation sequence.

The test is carried out on reservoir oil samples and involves charging a visual PVT cell with a liquid sample at the bubble-point pressure and at reservoir temperature. As shown schematically in Figure 3-4, the pressure is reduced in steps, usually 10 to 15 pressure levels, and all the liberated gas is removed and its volume is measured at standard conditions. The volume of oil remaining V_L is also measured at each pressure level. It should be noted that the remaining oil is subjected to continual compositional changes as it becomes progressively richer in the heavier components.

The above procedure is continued to atmospheric pressure where the volume of the residual (remaining) oil is measured and converted to a volume at 60°F, V_{sc} . The differential oil formation volume factors B_{od} (commonly called the *relative oil volume factors*) at all the various pressure levels are calculated by dividing the recorded oil volumes V_L by the volume of residual oil V_{sc} , or:

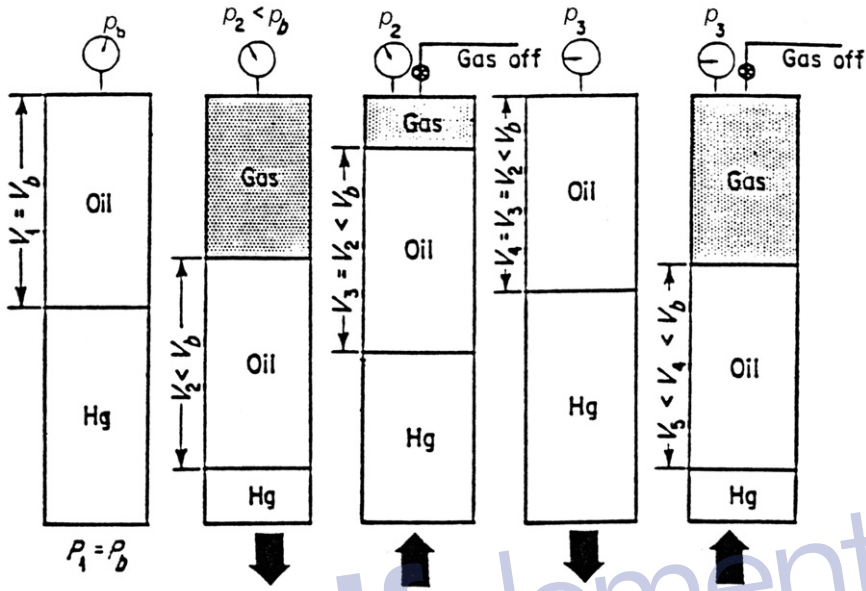


Figure 3-4. Differential vaporization test.

$$B_{od} = \frac{V_L}{V_{sc}} \quad (3-8)$$

The differential solution gas-oil ratio R_{sd} is also calculated by dividing the volume of gas in solution by the residual oil volume.

Table 3-4 shows the results of a differential liberation test for the Big Butte crude. The test indicates that the differential gas-oil ratio and differential relative oil volume at the bubble-point pressure are 933 scf/STB and 1.730 bbl/STB, respectively. The symbols R_{sdb} and B_{odb} are used to represent these two values, i.e.:

$$R_{sdb} = 933 \text{ scf/STB} \quad \text{and} \quad B_{odb} = 1.730 \text{ bbl/STB}$$

Column C of Table 3-4 shows the relative total volume B_{td} from differential liberation as calculated from the following expression:

$$B_{td} = B_{od} + (R_{sdb} - R_{sd}) B_g \quad (3-9)$$

where B_{td} = relative total volume, bbl/STB

B_g = gas formation volume factor, bbl/scf

Table 3-4
Differential Liberation Data

| Pressure, psig | Solution Gas/Oil Ratio, R _{sd} (A) | Relative Oil Volume, B _{od} (B) | Relative Total Volume, B _{td} (C) | Differential Vaporization (at 247°F) | | Gas Formation Volume Factor, (D) | Incremental Gas Gravity (Air = 1.000) |
|-------------------|--|---|---|---|---------------------------|--|--|
| | | | | Oil Density, gm/cc | Deviation Factor, z | | |
| b>>1936 | 933 | 1.730 | 1.730 | 0.6484 | | | |
| 1700 | 841 | 1.679 | 1.846 | 0.6577 | 0.864 | 0.01009 | 0.885 |
| 1500 | 766 | 1.639 | 1.982 | 0.6650 | 0.869 | 0.01149 | 0.894 |
| 1300 | 693 | 1.600 | 2.171 | 0.6720 | 0.876 | 0.01334 | 0.901 |
| 1100 | 622 | 1.563 | 2.444 | 0.6790 | 0.885 | 0.01591 | 0.909 |
| 900 | 551 | 1.525 | 2.862 | 0.6863 | 0.898 | 0.01965 | 0.927 |
| 700 | 479 | 1.486 | 3.557 | 0.6944 | 0.913 | 0.02559 | 0.966 |
| 500 | 400 | 1.440 | 4.881 | 0.7039 | 0.932 | 0.03626 | 1.051 |
| 300 | 309 | 1.382 | 8.138 | 0.7161 | 0.955 | 0.06075 | 1.230 |
| 185 | 242 | 1.335 | 13.302 | 0.7256 | 0.970 | 0.09727 | 1.423 |
| 120 | 195 | 1.298 | 20.439 | 0.7328 | 0.979 | 0.14562 | 1.593 |
| 0 | 0 | 1.099 | | 0.7745 | | | 2.375 |
| @ 60°F = 1.000 | | | | | | | |

Gravity of residual oil = 34.6°API at 60°F

Density of residual oil = 0.8511 gm/cc at 60°F

(A) Cubic feet of gas at 14.73 psia and 60°F per barrel of residual oil at 60°F

(B) Barrels of oil at indicated pressure and temperature per barrel of residual oil at 60°F

(C) Barrels of oil plus liberated gas at indicated pressure and temperature per barrel of residual oil at 60°F

(D) Cubic feet of gas at indicated pressure and temperature per cubic feet at 14.73 psia and 60°F

The gas deviation z-factor listed in column 6 of Table 3-4 represents the z-factor of the liberated (removed) solution gas at the specific pressure and these values are calculated from the recorded gas volume measurements as follows:

$$z = \left(\frac{Vp}{T} \right) \left(\frac{T_{sc}}{V_{sc} p_{sc}} \right) \quad (3-10)$$

where V = volume of the liberated gas in the PVT cell at p and T
 V_{sc} = volume of the removed gas at standard column 7 of Table 3-4 contains the gas formation volume factor B_g as expressed by the following equation:

$$B_g = \left(\frac{p_{sc}}{T_{sc}} \right) \frac{zT}{p} \quad (3-11)$$

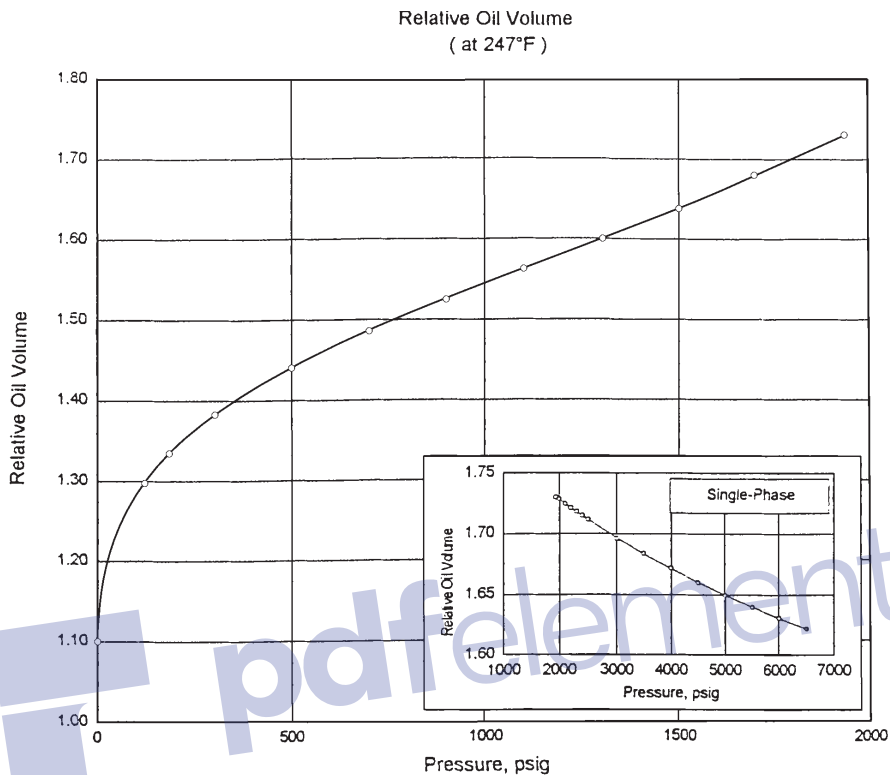
where B_g = gas formation volume factor, ft³/scf
 T = temperature, °R
 p = cell pressure, psia
 T_{sc} = standard temperature, °R
 p_{sc} = standard pressure, psia

Moses (1986) pointed out that reporting the experimental data in relation to the residual oil volume at 60°F (as shown graphically in Figures 3-5 and 3-6) gives the relative oil volume B_{od} and that the differential gas-oil ratio R_{sd} curves the appearance of the oil formation volume factor B_o and the solution gas solubility R_s curves, leading to their misuse in reservoir calculations.

It should be pointed out that the differential liberation test represents the behavior of the oil in the reservoir as the pressure declines. We must find a way of bringing this oil to the surface through separators and into the stock tank. This process is a flash or separator process.

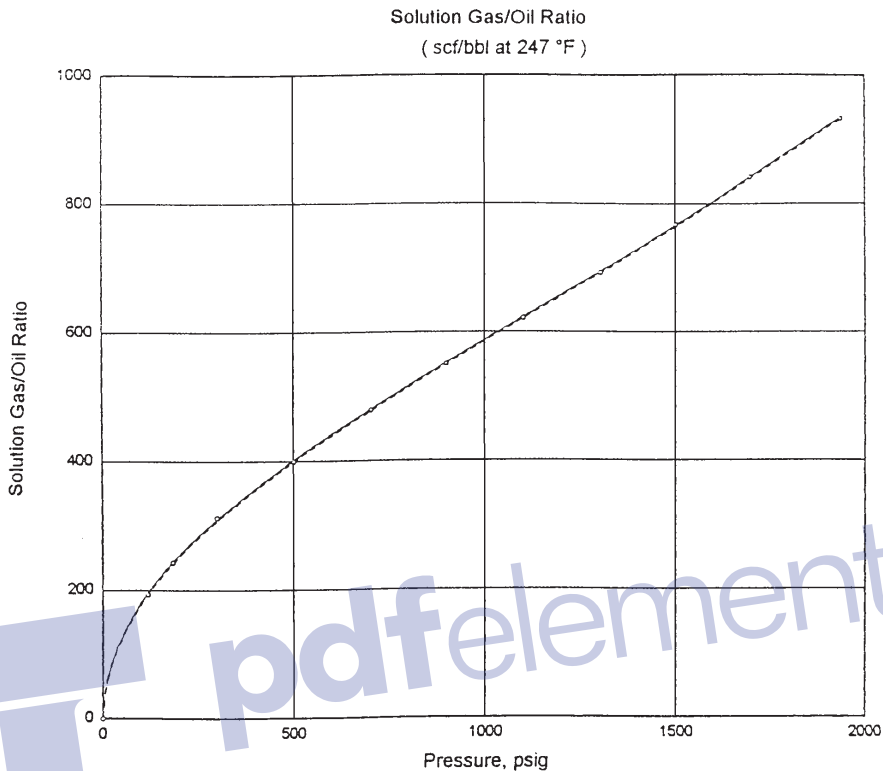
SEPARATOR TESTS

Separator tests are conducted to determine the changes in the volumetric behavior of the reservoir fluid as the fluid passes through the separator (or separators) and then into the stock tank. The resulting volumetric behavior is influenced to a large extent by the operating conditions, i.e., pressures and temperatures, of the surface separation facilities. The primary objective of conducting separator tests, therefore, is to provide the essential laboratory information necessary for determining the optimum surface separation conditions, which in turn will maximize the stock-tank oil production. In addition, the results of the test, when appropriately combined with the differential liberation test data, provide a means of obtaining the PVT parameters (B_o , R_s , and B_i) required for petroleum engineering calculations. These separator tests are performed only on the original oil at the bubble point.



| | | | | | | | | | |
|---|-------------------|----------|----------------------|-------------|-----------------|----------|--|--|--|
| <p>Relative Oil Volume Expression:</p> $y = a + b (Xi)^i + c (Xi)^j + d (Xi)^k$ <p>where:</p> <table style="width: 100%;"> <tr> <td>a= 1.09883e+ 00</td> <td>i= 1.075</td> </tr> <tr> <td>b= -1.08945e- 04</td> <td>j= 0.449</td> </tr> <tr> <td>c= 2.52865e- 02</td> <td>k= 2.000</td> </tr> <tr> <td>d= 6.59813e- 08</td> <td></td> </tr> </table> <p>Note: Xi (incremental 'X') = pressure, psig</p> | a= 1.09883e+ 00 | i= 1.075 | b= -1.08945e- 04 | j= 0.449 | c= 2.52865e- 02 | k= 2.000 | d= 6.59813e- 08 | | <p style="text-align: center;">LEGEND</p> <p style="text-align: center;">○ Laboratory Data</p> <p style="text-align: center;">- - - - - Confidence Limits</p> <p style="text-align: center;">————— Analytical Expression</p> <p style="text-align: center;">Saturation Pressure: 1,936 psig</p> |
| a= 1.09883e+ 00 | i= 1.075 | | | | | | | | |
| b= -1.08945e- 04 | j= 0.449 | | | | | | | | |
| c= 2.52865e- 02 | k= 2.000 | | | | | | | | |
| d= 6.59813e- 08 | | | | | | | | | |
| <table style="width: 100%;"> <tr> <td>Confidence level:</td> <td style="text-align: right;">99 %</td> </tr> <tr> <td>Confidence interval:</td> <td style="text-align: right;">+/- 0.00028</td> </tr> <tr> <td>'r squared':</td> <td style="text-align: right;">.999997</td> </tr> </table> | Confidence level: | 99 % | Confidence interval: | +/- 0.00028 | 'r squared': | .999997 | <p>Differential Vaporization</p> <p>Figure B-1</p> | | |
| Confidence level: | 99 % | | | | | | | | |
| Confidence interval: | +/- 0.00028 | | | | | | | | |
| 'r squared': | .999997 | | | | | | | | |

Figure 3-5. Relative volume versus pressure.



| | |
|---|---|
| <p>Solution Gas/Oil Ratio Expression:</p> $y = a + b (Xi)^i + c (Xi)^j + d (Xi)^k$ | <p>LEGEND</p> |
| <p>where:</p> <p>a= -2.13685e- 01 i= 0.515 b= 1.69108e+ 01 j= 1.482 c= -5.05326e- 03 k= 1.906 d= 2.58392e- 04</p> <p>Note: Xi (incremental 'X') = pressure, psig</p> | <p>○ Laboratory Data - - - - - Confidence Limits ———— Analytical Expression</p> <p>Saturation Pressure: 1936 psig</p> |
| <p>Confidence level: 99 % Confidence interval: +/- 1.47 scf/bbl 'r squared': .999966</p> | <p>Differential Vaporization Figure B-2</p> |

Figure 3-6. Solution gas-oil ratio versus pressure.

The test involves placing a hydrocarbon sample at its saturation pressure and reservoir temperature in a PVT cell. The volume of the sample is measured as V_{sat} . The hydrocarbon sample is then displaced and flashed through a laboratory multistage separator system—commonly one to three stages. The pressure and temperature of these stages are set to represent the desired or actual surface separation facilities. The gas liberated from each stage is removed and its specific gravity and volume at standard conditions are measured. The volume of the remaining oil in the last stage (representing the stock-tank condition) is measured and recorded as $(V_o)_{\text{st}}$. These experimental measured data can then be used to determine the oil formation volume factor and gas solubility at the bubble-point pressure as follows:

$$B_{\text{ofb}} = \frac{V_{\text{sat}}}{(V_o)_{\text{st}}} \quad (3-12)$$

$$R_{\text{sfb}} = \frac{(V_g)_{\text{sc}}}{(V_o)_{\text{st}}} \quad (3-13)$$

where B_{ofb} = bubble-point oil formation volume factor, as measured by flash liberation, bbl of the bubble-point oil/STB

R_{sfb} = bubble-point solution gas-oil ratio as measured by flash liberation, scf/STB

$(V_g)_{\text{sc}}$ = total volume of gas removed from separators, scf

The above laboratory procedure is repeated at a series of different separator pressures and at a fixed temperature. It is usually recommended that four of these tests be used to determine the optimum separator pressure, which is usually considered the separator pressure that results in minimum oil formation volume factor. At the same pressure, the stock-tank oil gravity will be a maximum and the total evolved gas, i.e., the separator gas and the stock-tank gas will be at a minimum.

A typical example of a set of separator tests for a two-stage separation system, as reported by Moses (1986), is shown in Table 3-5. By examining the laboratory results reported in Table 3-5, it should be noted that

Table 3-5
Separator Tests

| Separator Pressure (psig) | Temperature (°F) | GOR, R_{stb} * | Stock-Tank Oil Gravity (°API at 60°F) | FVF, B_{otb} ** |
|---------------------------|------------------|-------------------|---------------------------------------|-------------------|
| 50 | 75 | 737 | | |
| to 0 | 75 | <u>41</u> 778 | 40.5 | 1.481 |
| 100 | 75 | 676 | | |
| to 0 | 75 | <u>92</u> 768 | 40.7 | 1.474 |
| 200 | 75 | 602 | | |
| to 0 | 75 | <u>178</u> 780 | 40.4 | 1.483 |
| 300 | 75 | 549 | | |
| to 0 | 75 | <u>246</u> 795 | 40.1 | 1.495 |

*GOR in cubic feet of gas at 14.65 psia and 60°F per barrel of stock-tank oil at 60°F

**FVF is barrels of saturated oil at 2.620 psig and 220°F per barrel of stock-tank oil at 60°F
(Permission to publish by the Society of Petroleum Engineers of AIME. Copyright SPE-AIME.)

the optimum separator pressure is 100 psia, considered to be the separator pressure that results in the minimum oil formation volume factor. It is important to notice that the oil formation volume factor varies from 1.474 bbl/STB to 1.495 bbl/STB while the gas solubility ranges from 768 scf/STB to 795 scf/STB.

Table 3-5 indicates that the values of the crude oil PVT data are dependent on the method of surface separation. Table 3-6 presents the results of performing a separator test on the Big Butte crude oil. The differential liberation data, as expressed in Table 3-4, show that the solution gas-oil ratio at the bubble point is 933 scf/STB as compared with the measured value of 646 scf/STB from the separator test. This significant difference is attributed to the fact that the processes of obtaining residual oil and stock-tank oil from bubble-point oil are different.

The differential liberation is considered as a multiple series of flashes at the elevated reservoir temperatures. The separator test is generally a one- or two-stage flash at low pressure and low temperature. The quantity of gas released will be different and the quantity of final liquid will be different. Again, it should be pointed out that the oil formation volume

Table 3-6
Separator Test Data

| Separator Flash Analysis | | | | | | | | |
|--------------------------|-----|---------------|---------------|------------------------|-------------------------|-------------------------|---------------------------------|-------------------|
| Flash Conditions | | Gas-Oil Ratio | Gas-Oil Ratio | Stock-Tank Oil Gravity | Formation Volume Factor | Separator Volume Factor | Specific Gravity of Flashed Gas | Oil Phase Density |
| psig | °F | (A) | (B) | at 60°F (°API) | Bofb (C) | (D) | (Air = 1.000) | |
| 1936 | 247 | | | | | | | 0.6484 |
| 28 | 130 | 593 | 632 | | | 1.066 | 1.132* | 0.7823 |
| 0 | 80 | 13 | 13 | 38.8 | 1.527 | 1.010 | ** | 0.8220 |
| Rsfb = 646 | | | | | | | | |

*Collected and analyzed in the laboratory by gas chromatography

**Insufficient quantity for measurement

(A) Cubic feet of gas at 14.73 psia and 60°F per barrel of oil at indicated pressure and temperature

(B) Cubic feet of gas at 14.73 psia and 60°F per barrel of stock-tank oil at 60°F

(C) Barrels of saturated oil at 1936 psig and 247°F per barrel of stock-tank oil at 60°F

(D) Barrels of oil at indicated pressure and temperature per barrel of stock-tank oil at 60°F

factor, as expressed by Equation 3-12, is defined as “the volume of oil at reservoir pressure and temperature divided by the resulting stock-tank oil volume after it passes through the surface separators.”

Adjustment of Differential Liberation Data to Separator Conditions

To perform material balance calculations, the oil formation volume factor B_o and gas solubility R_s as a function of the reservoir pressure must be available. The ideal method of obtaining these data is to place a large crude oil sample in a PVT cell at its bubble-point pressure and reservoir temperature. At some pressure a few hundred psi below the bubble-point pressure, a small portion of the oil is removed and flashed at temperatures and pressures equal to those in the surface separators and stock tank. The liberated gas volume and stock-tank oil volume are measured to obtain B_o and R_s . This process is repeated at several progressively lower reservoir pressures until complete curves of B_o and R_s versus pressure have been obtained. This procedure is occasionally conducted in the laboratory. This experimental methodology was originally proposed by Dodson (1953) and is called the Dodson Method.

Amyx et al. (1960) and Dake (1978) proposed a procedure for constructing the oil formation volume factor and gas solubility curves by using the differential liberation data (as shown in Table 3-4) in conjunction

with the experimental separator flash data (as shown in Table 3-6) for a given set of separator conditions. The method is summarized in the following steps:

Step 1. Calculate the differential shrinkage factors at various pressures by dividing each relative oil volume factor B_{od} by the relative oil volume factor at the bubble-point B_{odb} , or:

$$S_{od} = \frac{B_{od}}{B_{odb}} \quad (3-14)$$

where B_{od} = differential relative oil volume factor at pressure p , bbl/STB

B_{odb} = differential relative oil volume factor at the bubble-point pressure p_b , psia, bbl/STB

S_{od} = differential oil shrinkage factor, bbl/bbl of bubble-point oil

The differential oil shrinkage factor has a value of one at the bubble-point and a value less than one at subsequent pressures below p_b .

Step 2. Adjust the relative volume data by multiplying the separator (flash) formation volume factor at the bubble-point B_{ofb} (as defined by Equation 3-12) by the differential oil shrinkage factor S_{od} (as defined by Equation 3-14) at various reservoir pressures. Mathematically, this relationship is expressed as follows:

$$B_o = B_{ofb} S_{od} \quad (3-15)$$

where B_o = oil formation volume factor, bbl/STB

B_{ofb} = bubble-point oil formation volume factor, bbl of the bubble-point oil/STB (as obtained from the separator test)

S_{od} = differential oil shrinkage factor, bbl/bbl of bubble-point oil

Step 3. Calculate the oil formation volume factor at pressures above the bubble-point pressure by multiplying the relative oil volume data V_{rel} , as generated from the constant-composition expansion test, by B_{ofb} , or:

$$B_o = (V_{rel}) (B_{ofb}) \quad (3-16)$$

where B_o = oil formation volume factor above the bubble-point pressure, bbl/STB

V_{rel} = relative oil volume, bbl/bbl

Step 4. Adjust the differential gas solubility data R_{sd} to give the required gas solubility factor R_s

$$R_s = R_{sfb} - (R_{sdb} - R_{sd}) \frac{B_{ofb}}{B_{odb}} \quad (3-17)$$

where R_s = gas solubility, scf/STB

R_{sfb} = bubble-point solution gas-oil ratio from the separator test, scf/STB

R_{sdb} = solution gas-oil ratio at the bubble-point pressure as measured by the differential liberation test, scf/STB

R_{sd} = solution gas-oil ratio at various pressure levels as measured by the differential liberation test, scf/STB

These adjustments will typically produce lower formation volume factors and gas solubilities than the differential liberation data.

Step 5. Obtain the two-phase (total) formation volume factor B_t by multiplying values of the relative oil volume V_{rel} below the bubble-point pressure by B_{ofb} , or:

$$B_t = (B_{ofb}) (V_{rel}) \quad (3-18)$$

where B = two-phase formation volume factor, bbl/STB

V_{rel} = relative oil volume below the p_b , bbl/bbl

Similar values for B_t can be obtained from the differential liberation test by multiplying the relative total volume B_{td} (see Table 3-4, Column C) by B_{ofb} , or

$$B_t = (B_{td}) (B_{ofb})/B_{odb} \quad (3-19)$$

It should be pointed out that Equations 3-16 and 3-17 usually produce values less than one for B_o and negative values for R_s at low pressures. The calculated curves of B_o and R_s versus pressures must be manually drawn to $B_o = 1.0$ and $R_s = 0$ at atmospheric pressure.

Example 3-5

The constant-composition expansion test, differential liberation test, and separator test for the Big Butte crude oil system are given in Tables 3-2, 3-4, and 3-6, respectively. Calculate:

- Oil formation volume factor at 4,000 and 1,100 psi
- Gas solubility at 1,100 psi
- The two-phase formation volume factor at 1,300 psi

Solution

Step 1. Determine B_{odb} , R_{sdb} , B_{ofb} , and R_{sfb} from Tables 3-4 and 3-6:

$$B_{odb} = 1.730 \text{ bbl/STB} \quad R_{sdb} = 933 \text{ scf/STB}$$

$$B_{ofb} = 1.527 \text{ bbl/STB} \quad R_{sfb} = 646 \text{ scf/STB}$$

Step 2. Calculate B_o at 4,000 by applying Equation 3-16:

$$B_o = (0.9657) (1.57) = 1.4746 \text{ bbl/STB}$$

Step 3. Calculate B_o at 1,100 psi by applying Equations 3-14 and 3-15.

$$S_{od} = \frac{1.563}{1.730} = 0.9035$$

$$B_o = (0.9035) (1.527) = 1.379 \text{ bbl/STB}$$

Step 4. Calculate the gas solubility at 1,100 psi by using Equation 3-17:

$$R_s = 646 - (933 - 622) \left(\frac{1.527}{1.730} \right) = 371 \text{ scf/STB}$$

Step 5. From the pressure-volume relations (i.e., constant-composition data) of Table 3-2 the relative volume at 1,300 PSI in 1.2579 bbl/bbl. Using Equation 3-18, calculate B_t to give:

$$B_t = (1.527) (1.2579) = 1.921 \text{ bbl/STB}$$

Applying Equation 3-19 gives:

$$B_t = (2.171) (1.527)/1.73 = 1.916 \text{ bbl/STB}$$

Table 3-7 presents a complete documentation of the adjusted differential vaporization data for the Big Butte crude oil system. Figures 3-7 and 3-8 compare graphically the adjusted values of R_s

Table 3-7
Adjusted Differential Liberation Data

| Differential Vaporization Adjusted to Separator Conditions* | | | | | |
|--|--|---|---|--------------------------|-------------------------------|
| Pressure, psig | Solution Gas-Oil Ratio, R_s (A) | Formation Volume Factor, B_o (B) | Gas Formation Volume Factor (C) | Oil Density, gm/cc | Oil-Gas Viscosity Ratio |
| 6500 | 646 | 1.431 | | 0.6919 | |
| 6000 | 646 | 1.439 | | 0.6882 | |
| 5500 | 646 | 1.447 | | 0.6843 | |
| 5000 | 646 | 1.456 | | 0.6803 | |
| 4500 | 646 | 1.465 | | 0.6760 | |
| 4000 | 646 | 1.475 | | 0.6714 | |
| 3500 | 646 | 1.486 | | 0.6665 | |
| 3000 | 646 | 1.497 | | 0.6613 | |
| 2500 | 646 | 1.510 | | 0.6556 | |
| 2400 | 646 | 1.513 | | 0.6544 | |
| 2300 | 646 | 1.516 | | 0.6531 | |
| 2200 | 646 | 1.519 | | 0.6519 | |
| 2100 | 646 | 1.522 | | 0.6506 | |
| 2000 | 646 | 1.525 | | 0.6493 | |
| b>>1936 | 646 | 1.527 | | 0.6484 | |
| 1700 | 564 | 1.482 | 0.01009 | 0.6577 | 19.0 |
| 1500 | 498 | 1.446 | 0.01149 | 0.6650 | 21.3 |
| 1300 | 434 | 1.412 | 0.01334 | 0.6720 | 23.8 |
| 1100 | 371 | 1.379 | 0.01591 | 0.6790 | 26.6 |
| 900 | 309 | 1.346 | 0.01965 | 0.6863 | 29.8 |
| 700 | 244 | 1.311 | 0.02559 | 0.6944 | 33.7 |
| 500 | 175 | 1.271 | 0.03626 | 0.7039 | 38.6 |
| 300 | 95 | 1.220 | 0.06075 | 0.7161 | 46.0 |
| 185 | 36 | 1.178 | 0.09727 | 0.7256 | 52.8 |
| 120 | | 1.146 | 0.14562 | 0.7328 | 58.4 |
| 0 | | | | 0.7745 | |

***Separator Conditions**

| | |
|------------|------------------|
| Fist Stage | 28 psig at 130°F |
| Stock Tank | 0 psig at 80°F |

(A) Cubic feet of gas at 14.73 psia and 60°F per barrel of stock-tank oil at 60°F

(B) Barrel of oil at indicated pressure and temperature per barrel of stock-tank oil at 60°F

(C) Cubic feet of gas at indicated pressure and temperature per cubic feet at 14.73 psia and 60°F

and B_o with those of the unadjusted PVT data. It should be noted that no adjustments are needed for the gas formation volume factor, oil density, or viscosity data.

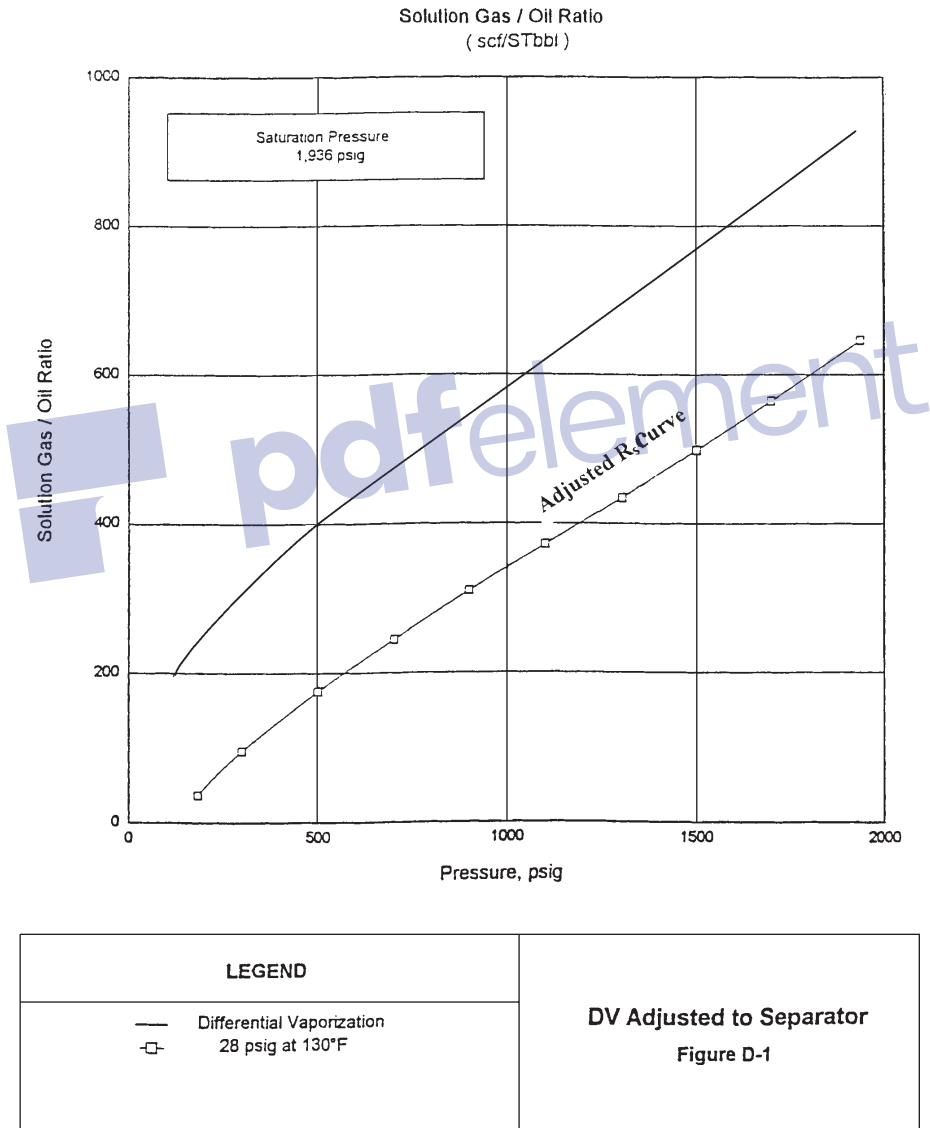
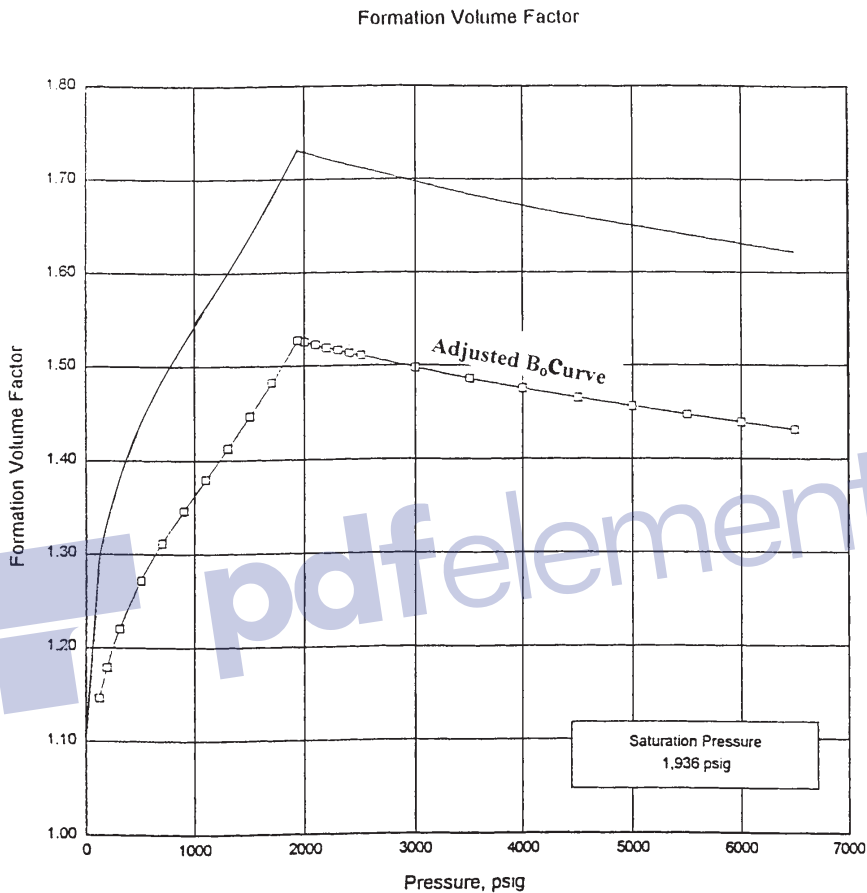


Figure 3-7. Adjusted gas solubility versus pressure.



| LEGEND | | DV Adjusted to Separator Figure D-2 |
|--------|---------------------------|--|
| — | Differential Vaporization | |
| □ | 28 psig at 130°F | |

Figure 3-8. Adjusted oil formation volume factor versus pressure.

EXTRAPOLATION OF RESERVOIR FLUID DATA

In partially depleted reservoirs or in fields that originally existed at the bubble-point pressure, it is difficult to obtain a fluid sample, which usually represents the original oil in the reservoir at the time of discovery. Also, in collecting fluid samples from oil wells, the possibility exists of obtaining samples with a saturation pressure that might be lower than or higher than the actual saturation pressure of the reservoir. In these cases, it is necessary to correct or adjust the laboratory PVT measured data to reflect the actual saturation pressure. The proposed correction procedure for adjusting the following laboratory test data is described in the subsequent sections:

- Constant-composition expansion (CCE) test
- Differential expansion (DE) test
- Oil viscosity test
- Separator tests

Correcting Constant-Composition Expansion Data

The correction procedure, summarized in the following steps, is based on calculating the Y-function value for each point below the “old” saturation pressure.

Step 1. Calculate the Y-function, as expressed by Equation 3-3, for each point by using the old saturation pressure.

Step 2. Plot the values of the Y-function versus pressure on a Cartesian scale and draw the best straight line. Points in the neighborhood of the saturation pressure may be erratic and need not be used.

Step 3. Calculate the coefficients a and b of the straight-line equation, i.e.:

$$Y = a + bp$$

Step 4. Recalculate the relative volume V_{rel} values by applying Equation 3-5 and using the “new” saturation pressure, or:

$$V_{\text{rel}} = 1 + \frac{p_{\text{sat}}^{\text{new}} - p}{p(a + bp)} \quad (3-20)$$

To determine points above the “new” saturation pressure, apply the following steps:

Step 1. Plot the “old” relative volume values above the “old” saturation pressure versus pressure on a regular scale and draw the best straight line through these points.

Step 2. Calculate the slope of the Line S. It should be noted that the slope is negative, i.e., $S < 0$.

Step 3. Draw a straight line that passes through the point ($V_{\text{rel}} = 1$, $p_{\text{sat}}^{\text{new}}$) and parallel to the line of Step 1.

Step 4. Relative volume data above the new saturation pressure are read from the straight line or determined from the following expression at any pressure p :

$$V_{\text{rel}} = 1 - S(p_{\text{sat}}^{\text{new}} - p) \quad (3-21)$$

where S = slope of the line
 p = pressure

Example 3-6

The pressure-volume relations of the Big Butte crude oil system is given in Table 3-2. The test indicates that the oil has a bubble-point pressure of 1,930 psig at 247°F. The Y-function for the oil system is expressed by the following linear equation:

$$Y = 1.0981 + 0.000591p$$

Above the bubble-point pressure, the relative volume data versus pressure exhibit a straight-line relationship with a slope of -0.0000138 .

The surface production data of the field suggest that the actual bubble-point pressure is approximately 2,500 psig. Reconstruct the pressure-volume data using the new reported saturation pressure.

Solution

Using Equations 3-30 and 3-31, gives:

| Pressure, psig | Old V_{rel} | New V_{rel} | Comments |
|--------------------|---------------|---------------|---------------|
| 6500 | 0.9371 | 0.9448 | Equation 3-21 |
| 6000 | 0.9422 | 0.9517 | |
| 5000 | 0.9532 | 0.9655 | |
| 4000 | 0.9657 | 0.9793 | |
| 3000 | 0.9805 | 0.9931 | |
| $p_b^{new} = 2500$ | 0.9890 | 1.0000 | Equation 3-20 |
| 2000 | 0.9987 | 1.1096 | |
| $p_b^{old} = 1936$ | 1.0000 | 1.1299 | |
| 1911 | 1.0058 | 1.1384 | |
| 1808 | 1.0324 | 1.1767 | |
| 1600 | 1.1018 | 1.1018 | |
| 600 | 2.4960 | 2.4960 | |
| 437 | 3.4404 | 3.4404 | |

Correcting Differential Liberation Data

Relative oil volume B_{od} versus pressure:

The laboratory-measured B_{od} data must be corrected to account for the new bubble-point pressure p_b^{new} . The proposed procedure is summarized in the following steps:

- Step 1.* Plot the B_{od} data versus gauge pressure on a regular scale.
- Step 2.* Draw the best straight line through the *middle pressure range* of 30%–90% p_b .
- Step 3.* Extend the straight line to the new bubble-point pressure, as shown schematically in Figure 3-9.

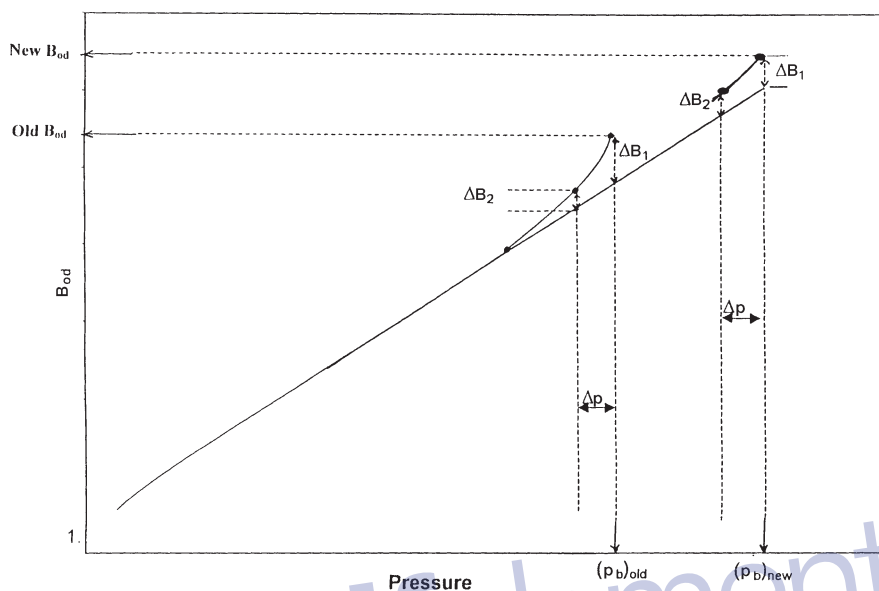


Figure 3-9. Correcting B_{od} for the new p_b .

Step 4. Transfer any curvature at the end of the original curve, i.e., ΔB_{o1} at p_b^{old} , to the new bubble-point pressure by placing ΔB_{o1} above or below the straight line at p_b^{new} .

Step 5. Select any differential pressure Δp below the p_b^{old} and transfer the corresponding curvature to the pressure $(p_b^{new} - \Delta p)$.

Step 6. Repeat the above process and draw a curve that connects the generated B_{od} points with original curve at the point of intersection with the straight line. Below this point, no change is needed.

Solution gas-oil ratio:

The correction procedure for the isolation gas-oil ratio R_{sd} data is identical to that of the relative oil volume data.

Correcting Oil Viscosity Data

The oil viscosity data can be extrapolated to a new higher bubble-point pressure by applying the following steps:

- Step 1.* Defining the *fluidity* as the reciprocal of the oil viscosity, i.e., $1/\mu_o$, calculate the fluidity for each point *below* the original saturation pressure.
- Step 2.* Plot fluidity versus pressure on a Cartesian scale (see Figure 3-10).
- Step 3.* Draw the best straight line through the points and extend it to the new saturation pressure p_b^{old} .
- Step 4.* New oil viscosity values above p_b^{old} are read from the straight line.

To obtain the oil viscosity for pressures above the new bubble-point pressure p_b^{new} , follow these steps:

- Step 1.* Plot the viscosity values for all points *above* the old saturation pressure on a Cartesian coordinate as shown schematically in Figure 3-11, and draw the best straight line through them, as Line A.
- Step 2.* Through the point on the extended viscosity curve at p_b^{new} , draw a straight line (Line B) parallel to A.

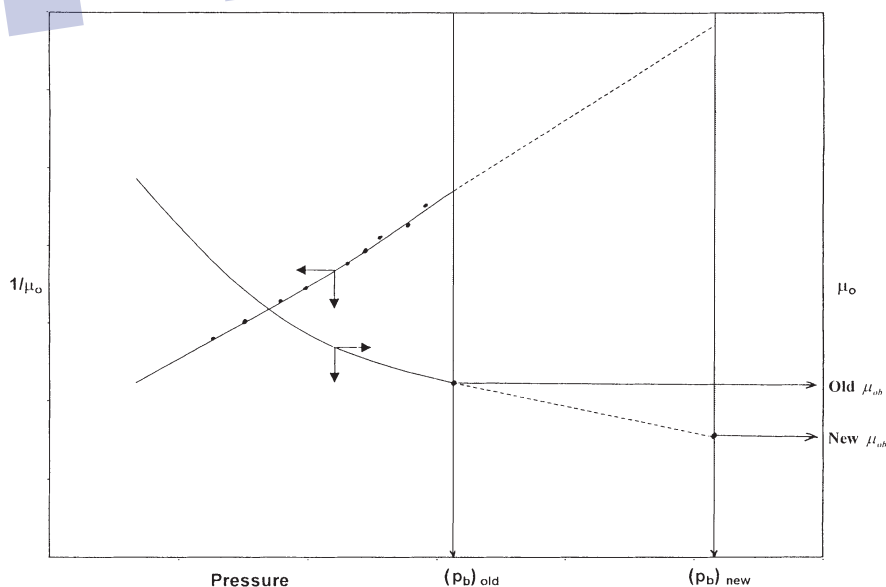


Figure 3-10. Extrapolating μ_o to new p_b .

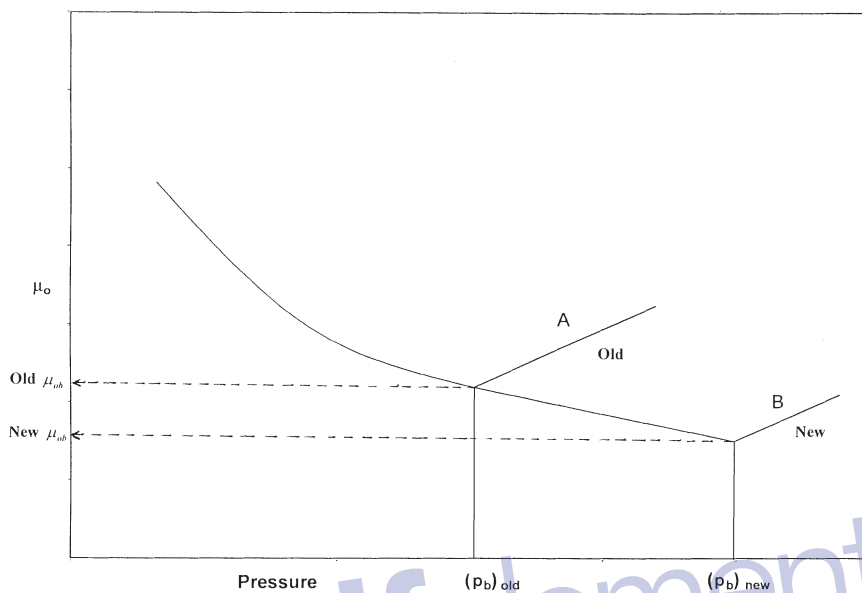


Figure 3-11. Extrapolating oil viscosity above new p_b .

Step 3. Viscosities above the new saturation pressure are then read from Line A.

Correcting the Separator Tests Data

Stock-tank gas-oil ratio and gravity:

No corrections are needed for the stock-tank gas-oil ratio and the stock-tank API gravity.

Separator gas-oil ratio:

The *total* gas-oil ratio R_{sfb} is changed in the same proportion as the differential ratio was changed, or

$$R_{sfb}^{new} = R_{sfb}^{old} (R_{sdb}^{new} / R_{sdb}^{old}) \quad (3-22)$$

The *separator* gas-oil ratio is then the difference between the new (corrected) gas solubility R_{sfb}^{new} and the unchanged stock-tank gas-oil ratio.

Formation volume factor:

The separator oil formation volume factor B_{ofb} is adjusted in the same proportion as the differential liberation values:

$$B_{\text{ofb}}^{\text{new}} = B_{\text{ofb}}^{\text{old}} (B_{\text{odb}}^{\text{new}} / B_{\text{odb}}^{\text{old}}) \quad (3-23)$$

Example 3-7

Results of the differential liberation and the separator tests on the Big Butte crude oil system are given in Tables 3-4 and 3-6, respectively. New field and production data indicate that the bubble-point pressure is better described by a value of 2,500 psi as compared with the laboratory-reported value of 1,936 psi. The correction procedure for B_{od} and R_{sd} as described previously was applied to give the following values at the new bubble point:

$$B_{\text{odb}}^{\text{new}} = 2.013 \text{ bbl/STB} \quad R_{\text{sbd}}^{\text{new}} = 1,134 \text{ scf/STB}$$

Using the separator test data as given in Table 3-6, calculate the gas solubility and the oil formation volume factor at the new bubble-point pressure.

Solution

- Gas solubility: from Equation 3-22

$$R_{\text{sb}} = 646 \left(\frac{1134}{933} \right) = 785 \text{ scf/STB}$$

$$\text{Separator GOR} = 785 - 13 = 772 \text{ scf/STB}$$

- Oil formation volume factor

Applying Equation 3-23 gives

$$B_{\text{ob}} = 1.527 \left(\frac{2.013}{1.730} \right) = 1.777 \text{ bbl/STB}$$

LABORATORY ANALYSIS OF GAS-CONDENSATE SYSTEMS

In the laboratory, a standard analysis of a gas-condensate sample consists of:

- Recombination and analysis of separator samples
- Measuring the pressure-volume relationship, i.e., constant-composition expansion test
- Constant-volume depletion test (CVD)

Recombination of Separator Samples

Obtaining a representative sample of the reservoir fluid is considerably more difficult for a gas-condensate fluid than for a conventional black-oil reservoir. The principal reason for this difficulty is that liquid may condense from the reservoir fluid during the sampling process, and if representative proportions of both liquid and gas are not recovered then an erroneous composition will be calculated.

Because of the possibility of erroneous compositions and also because of the limited volumes obtainable, subsurface sampling is seldom used in gas-condensate reservoirs. Instead, surface sampling techniques are used, and samples are obtained only after long stabilized flow periods. During this stabilized flow period, volumes of liquid and gas produced in the surface separation facilities are accurately measured, and the fluid samples are then recombined in these proportions.

The hydrocarbon composition of separator samples is also determined by chromatography or low-temperature fractional distillation or a combination of both. Table 3-7 shows the hydrocarbon analyses of the separator liquid and gas samples taken from the Nameless Field. The gas and liquid samples are recombined in the proper ratio to obtain the well-stream composition as given in Table 3-8. The laboratory data indicate that the overall well-stream system contains 63.71 mol% methane and 10.75 mol% heptanes-plus.

Frequently, the surface gas is processed to remove and liquefy all hydrocarbon components that are heavier than methane, i.e., ethane, propanes, etc. These liquids are called *plant products*. These quantities of

Table 3-8
Hydrocarbon Analyses of Separator Products
and Calculated Wellstream

| Component | Separator | Separator Gas | | Wellstream | |
|--|---------------------|---------------|--------------|--------------|--------------|
| | mol % | mol % | GPM | mol % | GPM |
| Hydrogen Sulfide | Nil | Nil | | Nil | |
| Carbon Dioxide | 0.29 | 1.17 | | 0.92 | |
| Nitrogen | 0.13 | 0.38 | | 0.31 | |
| Methane | 18.02 | 81.46 | | 63.71 | |
| Ethane | 12.08 | 11.46 | | 11.63 | |
| Propane | 11.40 | 3.86 | 1.083 | 5.97 | 1.675 |
| iso-Butane | 3.05 | 0.49 | 0.163 | 1.21 | 0.404 |
| n-Butane | 5.83 | 0.71 | 0.228 | 2.14 | 0.688 |
| iso-Pentane | 3.07 | 0.18 | 0.067 | 0.99 | 0.369 |
| Pentane | 2.44 | 0.12 | 0.044 | 0.77 | 0.284 |
| Hexanes | 5.50 | 0.09 | 0.037 | 1.60 | 0.666 |
| Heptanes-plus | <u>38.19</u> | <u>0.08</u> | <u>0.037</u> | <u>10.75</u> | <u>7.944</u> |
| | 100.00 | 100.00 | 1.659 | 100.00 | 12.030 |
| Properties of Heptanes-plus | | | | | |
| API gravity @ 60°F | 43.4 | | | | |
| Specific gravity @ 60/60°F | 0.8091 | | | 0.809 | |
| Molecular weight | 185 | 103 | | 185 | |
| Calculated separator gas gravity (air = 1.000) = 0.687 | | | | | |
| Calculated gross heating value for separator gas = 1209 BTU per cubic foot of dry gas @ 15.025 psia and 60°F | | | | | |
| Primary separator gas collected @ 745 psig and 74°F | | | | | |
| Primary separator liquid collected @ 745 psig and 74°F | | | | | |
| Primary separator gas/separator liquid ratio | 2413 scf/bbl @ 60°F | | | | |
| Primary separator liquid/stock-tank liquid ratio | 1.360 bbl @ 60°F | | | | |
| Primary separator gas/wellstream ratio | 720.13 Mscf/MMscf | | | | |
| Stock-tank liquid/wellstream ratio | 219.4 bbl/MMscf | | | | |

liquid products are expressed in gallons of liquid per thousand standard cubic feet of gas processed, i.e., gal/Mscf, or GPM. McCain (1990) derived the following expression for calculating the anticipated GPM for each component in the gas phase:

$$\text{GPM}_i = 11.173 \left(\frac{p_{sc}}{T_{sc}} \right) \left(\frac{y_i M_i}{\gamma_{oi}} \right) \quad (3-24)$$

where p_{sc} = standard pressure, psia
 T_{sc} = standard temperature, °R
 y_i = mole fraction of component i in the gas phase
 M_i = molecular weight of component i
 γ_{oi} = specific gravity of component i as a liquid at standard conditions (Chapter 1, Table 1-1, Column E)

McCain pointed out that the complete recovery of these products is not feasible. He proposed that, as a rule of thumb, 5 to 25% of ethane, 80 to 90% of the propane, 95% or more of the butanes, and 100% of the heavier components can be recovered from a simple surface facility.

Example 3-8

Table 3-8 shows the wellstream compositional analysis of the Nameless Field. Using Equation 3-24, calculate the maximum available liquid products assuming 100% plant efficiency.

Solution

- Using the standard conditions as given in Table 3-8 gives:

$$\text{GPM} = 11.173 \left(\frac{15.025}{520} \right) \left(\frac{y_i M_i}{\gamma_{oi}} \right) = 0.3228 \left(\frac{y_i M_i}{\gamma_{oi}} \right)$$

- Construct the following working table:

| Component | y_i | M_i | γ_{oi} | GPM _{i} |
|-----------------------------|--------|--------|---------------|-------------------------------|
| CO ₂ | 0.0092 | | | |
| N ₂ | 0.0031 | | | |
| C ₁ | 0.6371 | | | |
| C ₂ | 0.1163 | 30.070 | 0.35619 | 1.069 |
| C ₃ | 0.0597 | 44.097 | 0.50699 | 1.676 |
| i-C ₄ | 0.0121 | 58.123 | 0.56287 | 0.403 |
| n-C ₄ | 0.0214 | 58.123 | 0.58401 | 0.688 |
| i-C ₅ | 0.0099 | 72.150 | 0.63112 | 0.284 |
| n-C ₅ | 0.0077 | 72.150 | 0.63112 | 0.284 |
| C ₆ | 0.0160 | 86.177 | 0.66383 | 0.670 |
| C ₇ ⁺ | 0.1075 | 185.00 | 0.809 | 7.936 |

15.20 GPM

Constant-Composition Test

This test involves measuring the pressure-volume relations of the reservoir fluid at reservoir temperature with a visual cell. This usual PVT cell allows the visual observation of the condensation process that results from changing the pressures. The experimental test procedure is similar to that conducted on crude oil systems. The CCE test is designed to provide the dew-point pressure p_d at reservoir temperature and the total relative volume V_{rel} of the reservoir fluid (relative to the dew-point volume) as a function of pressure. The relative volume is equal to one at p_d . The gas compressibility factor at pressures greater than or equal to the saturation pressure is also reported. It is only necessary to experimentally measure the z -factor at one pressure p_1 and determine the gas deviation factor at the other pressure p from:

$$z = z_1 \left(\frac{p}{p_1} \right) \frac{V_{rel}}{(V_{rel})_1} \quad (3-25)$$

where z = gas deviation factor at p
 V_{rel} = relative volume at pressure p
 $(V_{rel})_1$ = relative volume at pressure p_1

If the gas compressibility factor is measured at the dew-point pressure, then:

$$z = z_d \left(\frac{p}{p_d} \right) (V_{rel}) \quad (3-26)$$

where z_d = gas compressibility factor at the dew-point pressure p_d
 p_d = dew-point pressure, psia
 p = pressure, psia

Table 3-9 shows the dew-point determination and the pressure-volume relations of the Nameless Field. The dew-point pressure of the system is reported as 4,968 psi at 262°F. The measured gas compressibility factor at the dew point is 1.043.

Example 3-9

Using Equation 3-26 and the data in Table 3-9, calculate the gas deviation factor at 6,000 and 8,100 psi.

Table 3-9
Pressure-Volume Relations of Reservoir Fluid at 262°F
(Constant-Composition Expansion)

| Pressure, psig | Relative Volume | Deviation Factor, z |
|-------------------------|--------------------|------------------------|
| 8100 | 0.8733 | 1.484 |
| 7800 | 0.8806 | 1.441 |
| 7500 | 0.8880 | 1.397 |
| 7000 | 0.9036 | 1.327 |
| 6500 | 0.9195 | 1.254 |
| 6000 | 0.9397 | 1.184 |
| 5511 | 0.9641 | 1.116 |
| 5309 | 0.9764 | 1.089 |
| 5100 | 0.9909 | 1.061 |
| 5000 | 0.9979 | 1.048 |
| 4968 Dew-point pressure | 1.0000 | 1.043 |
| 4905 | 1.0057 | |
| 4800 | 1.0155 | |
| 4600 | 1.0369 | |
| 4309 | 1.0725 | |
| 4000 | 1.1177 | |
| 3600 | 1.1938 | |
| 3200 | 1.2970 | |
| 2830 | 1.4268 | |
| 2400 | 1.6423 | |
| 2010 | 1.9312 | |
| 1600 | 2.4041 | |
| 1230 | 3.1377 | |
| 1000 | 3.8780 | |
| 861 | 4.5249 | |
| 770 | 5.0719 | |

*Gas Expansion Factor = 1.2854 Mscf/bbl

Solution

- At 6,000 psi

$$z = 1.043 \left(\frac{6000 + 15.025}{4968 + 15.025} \right) (0.9397) = 1.184$$

- At 8,100 psi

$$z = 1.043 \left(\frac{8100 + 15.025}{4968 + 15.025} \right) (0.8733) = 1.483$$

Constant-Volume Depletion (CVD) Test

Constant-volume depletion (CVD) experiments are performed on gas condensates and volatile oils to simulate reservoir depletion performance and compositional variation. The test provides a variety of useful and important information that is used in reservoir engineering calculations.

The laboratory procedure of the test is shown schematically in Figure 3-12 and is summarized in the following steps:

Step 1. A measured amount of a representative sample of the original reservoir fluid with a known overall composition of z_i is charged to a visual PVT cell at the dew-point pressure p_d ("a" in Figure 3-12). The temperature of the PVT cell is maintained at the reservoir temperature T throughout the experiment. The initial volume V_i of the saturated fluid is used as a reference volume.

Step 2. The initial gas compressibility factor is calculated from the real gas equation

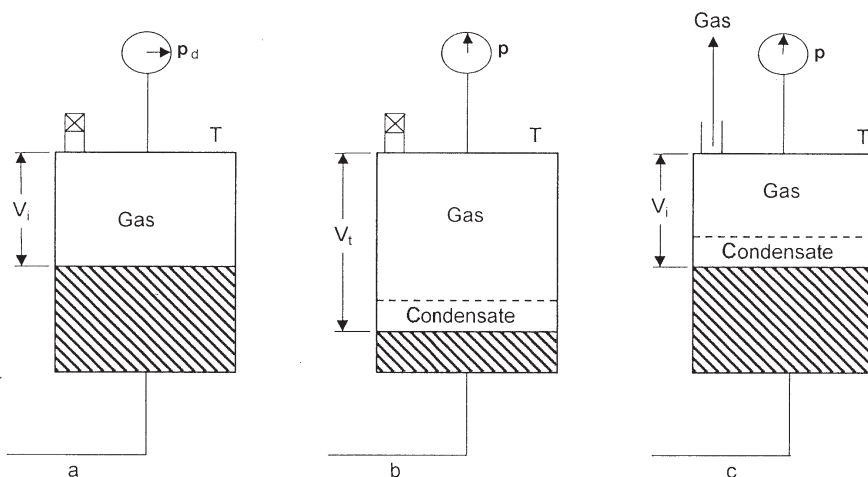


Figure 3-12. A schematic illustration of the constant-volume depletion test.

$$z_d = \frac{p_d V_i}{n_i RT} \quad (3-27)$$

where p_d = dew-point pressure, psia
 V_i = initial gas volume, ft³
 n_i = initial number of moles of the gas = m/M_a
 R = gas constant, 10.73
 T = temperature, °R
 z_d = compressibility factor at dew-point pressure

Step 3. The cell pressure is reduced from the saturation pressure to a pre-determined level P . This can be achieved by withdrawing mercury from the cell, as illustrated in column b of Figure 3-12. During the process, a second phase (retrograde liquid) is formed. The fluid in the cell is brought to equilibrium and the gas volume V_g and volume of the retrograde liquid V_L are visually measured. This retrograde volume is reported as a percent of the initial volume V_i , which basically represents the retrograde liquid saturation S_L :

$$S_L = \left(\frac{V_L}{V_i} \right) 100$$

Step 4. Mercury is reinjected into the PVT cell at constant pressure P while an equivalent volume of gas is simultaneously removed. When the initial volume V_i is reached, mercury injection is ceased, as illustrated in column c of Figure 3-12. This step simulates a reservoir producing only gas, with retrograde liquid remaining immobile in the reservoir.

Step 5. The removed gas is charged to analytical equipment where its composition y_i is determined, and its volume is measured at standard conditions and recorded as $(V_{gp})_{sc}$. The corresponding moles of gas produced can be calculated from the expression

$$n_p = \frac{p_{sc} (V_{gp})_{sc}}{R T_{sc}} \quad (3-28)$$

where n_p = moles of gas produced
 $(V_{gp})_{sc}$ = volume of gas produced measured at standard conditions, scf
 T_{sc} = standard temperature, °R
 p_{sc} = standard pressure, psia
 $R = 10.73$

Step 6. The gas compressibility factor at cell pressure and temperature is calculated from the real gas equation-of-state as follows:

$$z = \frac{p(V_g)}{n_p R T} \quad (3-29)$$

Another property, the two-phase compressibility factor, is also calculated. The two-phase compressibility factor represents the total compressibility of all the remaining fluid (gas and retrograde liquid) in the cell and is computed from the real gas law as

$$z_{\text{two-phase}} = \frac{p V_i}{(n_i - n_p) RT} \quad (3-30)$$

where $(n_i - n_p)$ = the remaining moles of fluid in the cell
 n_i = initial moles in the cell
 n_p = cumulative moles of gas removed

The two-phase z -factor is a significant property because it is used when the p/z versus cumulative-gas produced plot is constructed for evaluating gas-condensate production.

Equation 3-30 can be expressed in a more convenient form by replacing moles of gas, i.e., n_i and n_p , with their equivalent gas volumes, or:

$$z_{\text{two-phase}} = \left(\frac{z_d}{P_d} \right) \left[\frac{P}{1 - (G_p/GIIP)} \right] \quad (3-31)$$

where z_d = gas deviation factor at the dew-point pressure
 P_d = dew-point pressure, psia
 P = reservoir pressure, psia
 $GIIP$ = initial gas in place, scf
 G_p = cumulative gas produced at pressure p , scf

Step 7. The volume of gas produced as a percentage of gas initially in place is calculated by dividing the cumulative volume of the produced gas by the gas initially in place, both at standard conditions

$$\% G_p = \left[\frac{\sum (V_{gp})_{sc}}{GIIP} \right] 100 \quad (3-32)$$

or

$$\% G_p = \left[\frac{\sum n_p}{(n_i)_{\text{original}}} \right] 100$$

The above experimental procedure is repeated several times until a minimum test pressure is reached, after which the quantity and composition of the gas and retrograde liquid remaining in the cell are determined.

The test procedure can also be conducted on a volatile oil sample. In this case, the PVT cell initially contains liquid, instead of gas, at its bubble-point pressure.

The results of the pressure-depletion study for the Nameless Field are illustrated in Tables 3-10 and 3-11. Note that the composition listed in the 4,968 psi pressure column in Table 3-10 is the composition of the reservoir fluid at the dew point and exists in the reservoir in the gaseous state. Table 3-10 and Figure 3-13 show the changing composition of the well-stream during depletion. Notice the progressive reduction of C_{7+} below the dew point and increase in the methane fraction, i.e., C_1 .

The concentrations of *intermediates*, i.e., C_2 – C_6 , are also seen to decrease (they condense) as pressure drops down to about 2,000 psi and then increase as they revaporize at the lower pressures. The final column shows the composition of the liquid remaining in the cell (or reservoir) at the abandonment pressure of 700 psi; the predominance of C_{7+} components in the liquid is apparent.

The z -factor of the equilibrium gas and the two-phase z are presented. (Note: if a (p/z) versus G_p analysis is to be done, the two-phase compressibility factors are the appropriate values to use.)

(text continued on page 182)

| | | | | | | | | |
|---|--------|-------|--------|--------|--------|--------|--------|-------|
| Molecular weight of heptanes- plus | 185 | 143 | 133 | 125 | 118 | 114 | 112 | 203 |
| Specific gravity of heptanes- plus | 0.809 | 0.777 | 0.768 | 0.760 | 0.753 | 0.749 | 0.747 | 0.819 |
| Deviation factor-z | | | | | | | | |
| Equilibrium gas | 1.043 | 0.927 | 0.874 | 0.862 | 0.879 | 0.908 | 0.946 | |
| Two-phase | 1.043 | 0.972 | 0.897 | 0.845 | 0.788 | 0.720 | 0.603 | |
| Wellstream produced— | | | | | | | | |
| Cumulative percent of initial GPM from smooth compositions | 0.000 | 7.021 | 17.957 | 30.268 | 46.422 | 61.745 | 75.172 | |
| Propane-plus | 12.030 | 7.303 | 5.623 | 4.855 | 4.502 | 4.624 | 5.329 | |
| Butanes-plus | 10.354 | 5.683 | 4.054 | 3.301 | 2.916 | 2.946 | 3.421 | |
| Pentanes-plus | 9.263 | 4.664 | 3.100 | 2.378 | 2.004 | 1.965 | 2.261 | |

*Equilibrium liquid phase, representing 13.323 percent of original wellstream.

Table 3-11
Retrograde Condensation During Gas Depletion at 262°F

| Pressure, psig | Retrograde Liquid Volume Percent of Hydrocarbon Pore Space |
|----------------------------|---|
| 4968 Dew-point pressure | 0.0 |
| 4905 | 19.3 |
| 4800 | 25.0 |
| 4600 | 29.9 |
| 4300 First depletion level | 33.1 |
| 3500 | 34.4 |
| 2800 | 34.1 |
| 2000 | 32.5 |
| 1300 | 30.2 |
| 700 | 27.3 |
| 0 | 21.8 |

(text continued from page 179)

The row in the table, "Wellstream Produced, % of initial GPM from smooth compositions," gives the fraction of the total moles (of scf) in the cell (or reservoir) that has been produced. This is *total* recovery of wellstream and has not been separated here into surface gas and oil recoveries.

In addition to the composition of the produced wellstream at the final depletion pressure, the composition of the retrograde liquid is also measured. The composition of the liquid is reported in the last column of Table 3-10 at 700 psi. These data are included as a control composition in the event the study is used for compositional material-balance purposes.

The volume of the retrograde liquid, i.e., liquid dropout, measured during the course of the depletion study is shown in Table 3-11. The data are reshown as a percent of hydrocarbon pore space. The measurements indicate that the maximum liquid dropout of 34.4% occurs at 3,500 psi. The liquid dropout can be expressed as a percent of the pore volume, i.e., saturation, by adjusting the reported values to account for the presence of the initial water saturation, or

$$S_o = (\text{LDO}) (1 - S_{wi}) \quad (3-33)$$

where S_o = retrograde liquid (oil) saturation, %

LDO = liquid dropout, %

S_{wi} = initial water saturation, fraction

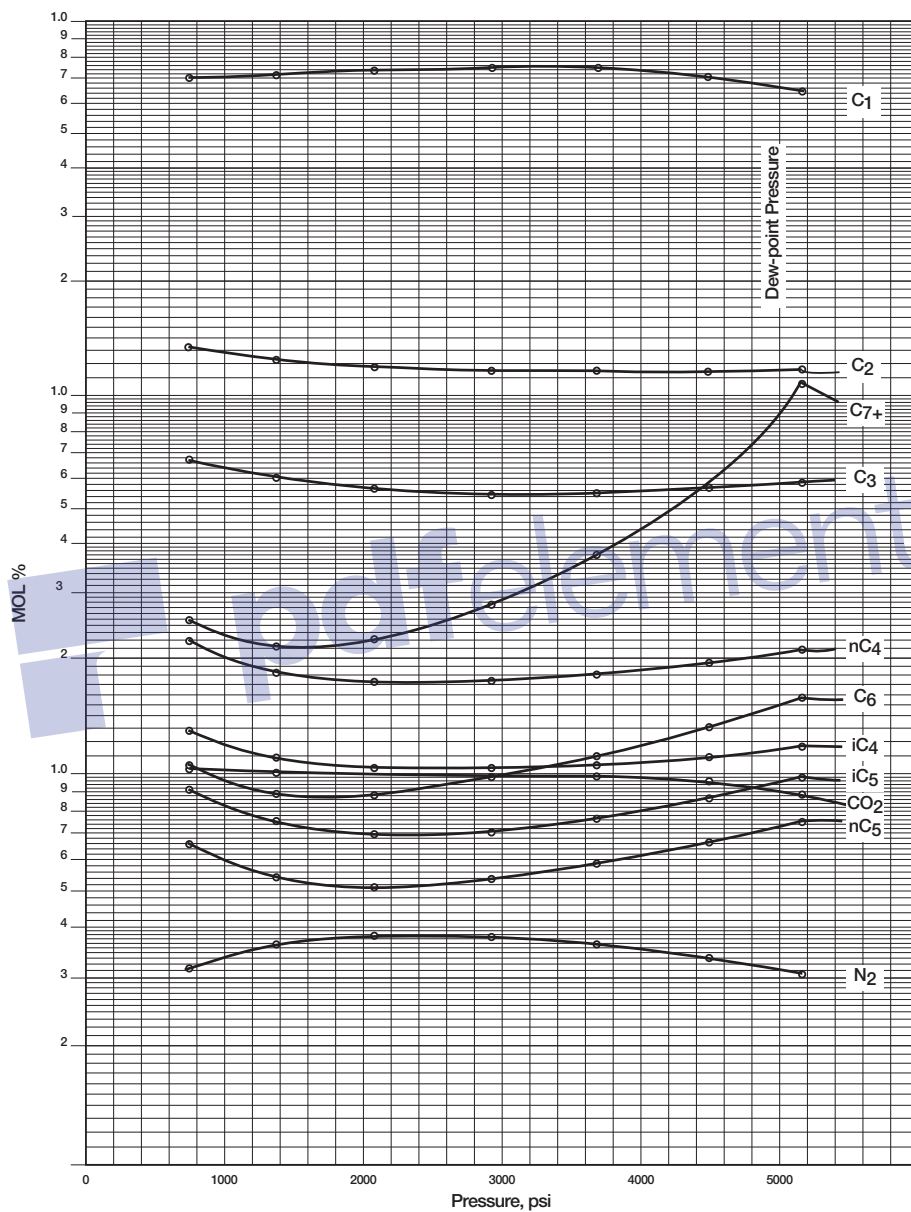


Figure 3-13. Hydrocarbon analysis during depletion.

Example 3-10

Using the experimental data of the Nameless gas-condensate field given in Table 3-10, calculate the two-phase compressibility factor at 2,000 psi by applying Equation 3-31.

Solution

The laboratory report indicates that the base (standard) pressure is 15.025 psia. Applying Equation 3-31 gives:

$$z_{2\text{-phase}} = \left[\frac{1.043}{4968 + 15.025} \right] \left[\frac{2000 + 15.025}{1 - 0.46422} \right] = 0.787$$

PROBLEMS

Table 3-12 shows the experimental results performed on a crude oil sample taken from the Mtech field. The results include the CCE, DE, and separator tests.

- Select the optimum separator conditions and generate B_o , R_s , and B_t values for the crude oil system. Plot your results and compare with the unadjusted values.
- Assume that new field indicates that the bubble-point pressure is better described by a value of 2,500 psi. Adjust the PVT to reflect the new bubble-point pressure.

(text continued on page 188)

Table 3-12
Pressure-Volume Relations of Reservoir Fluid at 260°F
(Constant-Composition Expansion)

| Pressure, psig | Relative Volume |
|-------------------|--------------------|
| 5000 | 0.9460 |
| 4500 | 0.9530 |
| 4000 | 0.9607 |
| 3500 | 0.9691 |
| 3000 | 0.9785 |
| 2500 | 0.9890 |
| 2300 | 0.9938 |
| 2200 | 0.9962 |
| 2100 | 0.9987 |
| 2051 | 1.0000 |
| 2047 | 1.0010 |
| 2041 | 1.0025 |
| 2024 | 1.0069 |
| 2002 | 1.0127 |
| 1933 | 1.0320 |
| 1843 | 1.0602 |
| 1742 | 1.0966 |
| 1612 | 1.1524 |
| 1467 | 1.2299 |
| 1297 | 1.3431 |
| 1102 | 1.5325 |
| 862 | 1.8992 |
| 653 | 2.4711 |
| 482 | 3.4050 |

**Table 3-12 (Continued)
Differential Vaporization at 260°F**

| Pressure, psig | Solution Gas-Oil Ratio (1) | Relative Oil Volume (2) | Relative Total Volume (3) | Oil Density, gm/cc | Deviation Factor, z | Gas Formation Volume Factor (4) | Incremental Gas Gravity |
|-------------------|----------------------------------|-------------------------------|---------------------------------|--------------------------|---------------------------|---------------------------------------|-------------------------------|
| 2051 | 1004 | 1.808 | 1.808 | 0.5989 | | | |
| 1900 | 930 | 1.764 | 1.887 | 0.6063 | 0.880 | 0.00937 | 0.843 |
| 1700 | 838 | 1.708 | 2.017 | 0.6165 | 0.884 | 0.01052 | 0.840 |
| 1500 | 757 | 1.660 | 2.185 | 0.6253 | 0.887 | 0.01194 | 0.844 |
| 1300 | 678 | 1.612 | 2.413 | 0.6348 | 0.892 | 0.01384 | 0.857 |
| 1100 | 601 | 1.566 | 2.743 | 0.6440 | 0.899 | 0.01644 | 0.876 |
| 900 | 529 | 1.521 | 3.229 | 0.6536 | 0.906 | 0.02019 | 0.901 |
| 700 | 456 | 1.476 | 4.029 | 0.6635 | 0.917 | 0.02616 | 0.948 |
| 500 | 379 | 1.424 | 5.537 | 0.6755 | 0.933 | 0.03695 | 0.018 |
| 300 | 291 | 1.362 | 9.214 | 0.6896 | 0.955 | 0.06183 | 1.188 |
| 170 | 223 | 1.309 | 16.246 | 0.7020 | 0.974 | 0.10738 | 1.373 |
| 0 | 0 | 1.110 | | 0.7298 | | | 2.230 |

at 60°F = 1.000

Gravity of Residual Oil = 43.1°API at 60°F

(1) Cubic feet of gas at 14.73 psia and 60°F per barrel of residual oil at 60°F

(2) Barrels of oil at indicated pressure and temperature per barrel of residual oil at 60°F

(3) Barrels of oil plus liberated gas at indicated pressure and temperature per barrel of residual oil at 60°F

(4) Cubic feet of gas at indicated pressure and temperature per cubic foot at 14.73 psia and 60°F

Table 3-12 (Continued)
Separator Tests of Reservoir Fluid Sample

| Separator Pressure PSI Gauge | Separator Temperature, °F | Gas-Oil Ratio (1) | Gas-Oil Ratio (2) | Stock-Tank Gravity, °API @ 60°F | Formation Volume Factor (3) | Separator Volume Factor (4) | Specific Gravity of Flashed Gas |
|---------------------------------|------------------------------|----------------------|----------------------|------------------------------------|--------------------------------|--------------------------------|---------------------------------|
| 200 to 0 | 71 | 431 | 490 | | | 1.138 | 0.739* |
| | 71 | 222 | 223 | 48.2 | 1.549 | 1.006 | 1.367 |
| 100 to 0 | 72 | 522 | 566 | | | 1.083 | 0.801* |
| | 72 | 126 | 127 | 48.6 | 1.529 | 1.006 | 1.402 |
| 50 to 0 | 71 | 607 | 632 | | | 1.041 | 0.869* |
| | 71 | 54 | 54 | 48.6 | 1.532 | 1.006 | 1.398 |
| 25 to 0 | 70 | 669 | 682 | | | 1.020 | 0.923* |
| | 70 | 25 | 25 | 48.4 | 1.558 | 1.006 | 1.340 |

*Collected and analyzed in the laboratory

(1) Gas-oil ratio in cubic feet of gas @ 60°F and 14.75 psi absolute per barrel of oil @ indicated pressure and temperature

(2) Gas-oil ratio in cubic feet of gas @ 60°F and 14.73 psi absolute per barrel of stock-tank oil @ 60°F

(3) Formation volume factor in barrels of saturated oil @ 2051 psi gauge and 260°F per barrel of stock-tank oil @ 60°F

(4) Separator volume factor in barrels of oil @ indicated pressure and temperature per barrel of stock-tank oil @ 60°F

(text continued from page 184)

REFERENCES

1. Amyx, J. M., Bass, D. M., and Whiting, R., *Petroleum Reservoir Engineering-Physical Properties*. New York: McGraw-Hill Book Company, 1960.
2. Dake, L. P., *Fundamentals of Reservoir Engineering*. Amsterdam: Elsevier Scientific Publishing Company, 1978.
3. Dodson, L. P., "Application of Laboratory PVT Data to Reservoir Engineering Problems," *JPT*, December 1953, pp. 287–298.
4. McCain, W., *The Properties of Petroleum Fluids*. Tulsa, OK: PennWell Publishing Company, 1990.
5. Moses, P., "Engineering Application of Phase Behavior of Crude Oil and Condensate Systems," *JPT*, July 1986, pp. 715–723.



C H A P T E R 4

FUNDAMENTALS OF ROCK PROPERTIES

The material of which a petroleum reservoir rock may be composed can range from very loose and unconsolidated sand to a very hard and dense sandstone, limestone, or dolomite. The grains may be bonded together with a number of materials, the most common of which are silica, calcite, or clay. Knowledge of the physical properties of the rock and the existing interaction between the hydrocarbon system and the formation is essential in understanding and evaluating the performance of a given reservoir.

Rock properties are determined by performing laboratory analyses on cores from the reservoir to be evaluated. The cores are removed from the reservoir environment, with subsequent changes in the core bulk volume, pore volume, reservoir fluid saturations, and, sometimes, formation wettability. The effect of these changes on rock properties may range from negligible to substantial, depending on characteristics of the formation and property of interest, and should be evaluated in the testing program.

There are basically two main categories of core analysis tests that are performed on core samples regarding physical properties of reservoir rocks. These are:

Routine core analysis tests

- Porosity
- Permeability
- Saturation

Special tests

- Overburden pressure
- Capillary pressure
- Relative permeability
- Wettability
- Surface and interfacial tension

The above rock property data are essential for reservoir engineering calculations as they directly affect both the quantity and the distribution of hydrocarbons and, when combined with fluid properties, control the flow of the existing phases (i.e., gas, oil, and water) within the reservoir.

POROSITY

The porosity of a rock is a measure of the storage capacity (pore volume) that is capable of holding fluids. Quantitatively, the porosity is the ratio of the pore volume to the total volume (bulk volume). This important rock property is determined mathematically by the following generalized relationship:

$$\phi = \frac{\text{pore volume}}{\text{bulk volume}}$$

where ϕ = porosity

As the sediments were deposited and the rocks were being formed during past geological times, some void spaces that developed became isolated from the other void spaces by excessive cementation. Thus, many of the void spaces are interconnected while some of the pore spaces are completely isolated. This leads to two distinct types of porosity, namely:

- Absolute porosity
- Effective porosity

Absolute porosity

The absolute porosity is defined as the ratio of the total pore space in the rock to that of the bulk volume. A rock may have considerable absolute porosity and yet have no conductivity to fluid for lack of pore

interconnection. The absolute porosity is generally expressed mathematically by the following relationships:

$$\phi_a = \frac{\text{total pore volume}}{\text{bulk volume}} \quad (4-1)$$

or

$$\phi_a = \frac{\text{bulk volume} - \text{grain volume}}{\text{bulk volume}} \quad (4-2)$$

where ϕ_a = absolute porosity.

Effective porosity

The effective porosity is the percentage of *interconnected* pore space with respect to the bulk volume, or

$$\phi = \frac{\text{interconnected pore volume}}{\text{bulk volume}} \quad (4-3)$$

where ϕ = effective porosity.

The effective porosity is the value that is used in all reservoir engineering calculations because it represents the interconnected pore space that contains the recoverable hydrocarbon fluids.

Porosity may be classified according to the mode of origin as originally induced.

The *original* porosity is that developed in the deposition of the material, while *induced* porosity is that developed by some geological process subsequent to deposition of the rock. The intergranular porosity of sandstones and the intercrystalline and oolitic porosity of some limestones typify original porosity. Induced porosity is typified by fracture development as found in shales and limestones and by the slugs or solution cavities commonly found in limestones. Rocks having original porosity are more uniform in their characteristics than those rocks in which a large part of the porosity is included. For direct quantitative measurement of porosity, reliance must be placed on formation samples obtained by coring.

Since effective porosity is the porosity value of interest to the petroleum engineer, particular attention should be paid to the methods used to

determine porosity. For example, if the porosity of a rock sample was determined by saturating the rock sample 100% with a fluid of known density and then determining, by weighing, the increased weight due to the saturating fluid, this would yield an effective porosity measurement because the saturating fluid could enter only the interconnected pore spaces. On the other hand, if the rock sample were crushed with a mortar and pestle to determine the actual volume of the solids in the core sample, then an absolute porosity measurement would result because the identity of any isolated pores would be lost in the crushing process.

One important application of the effective porosity is its use in determining the original hydrocarbon volume in place. Consider a reservoir with an areal extent of A acres and an average thickness of h feet. The total bulk volume of the reservoir can be determined from the following expressions:

$$\text{Bulk volume} = 43,560 Ah, \text{ ft}^3 \quad (4-4)$$

or

$$\text{Bulk volume} = 7,758 Ah, \text{ bbl} \quad (4-5)$$

where A = areal extent, acres
 h = average thickness

The reservoir pore volume PV can then be determined by combining Equations 4-4 and 4-5 with 4-3. Expressing the reservoir pore volume in cubic feet gives:

$$PV = 43,560 Ah\phi, \text{ ft}^3 \quad (4-6)$$

Expressing the reservoir pore volume in barrels gives:

$$PV = 7,758 Ah\phi, \text{ bbl} \quad (4-7)$$

Example 4-1

An oil reservoir exists at its bubble-point pressure of 3,000 psia and temperature of 160°F. The oil has an API gravity of 42° and gas-oil ratio of 600 scf/STB. The specific gravity of the solution gas is 0.65. The following additional data are also available:

- Reservoir area = 640 acres
- Average thickness = 10 ft
- Connate water saturation = 0.25
- Effective porosity = 15%

Calculate the initial oil in place in STB.

Solution

Step 1. Determine the specific gravity of the stock-tank oil from Equation 2-68.

$$\gamma_o = \frac{141.5}{42 + 131.5} = 0.8156$$

Step 2. Calculate the initial oil formation volume factor by applying Standing's equation, i.e., Equation 2-85, to give:

$$B_o = 0.9759 + 0.00012 \left[600 \left(\frac{0.65}{0.8156} \right)^{0.5} + 1.25(160) \right]^{1.2}$$

$$= 1,396 \text{ bbl/STB}$$

Step 3. Calculate the pore volume from Equation 4-7.

$$\text{Pore volume} = 7758 (640) (10) (0.15) = 7,447,680 \text{ bbl}$$

Step 4. Calculate the initial oil in place.

$$\text{Initial oil in place} = 12,412,800 (1 - 0.25)/1.306 = 4,276,998 \text{ STB}$$

The reservoir rock may generally show large variations in porosity vertically but does not show very great variations in porosity parallel to the bedding planes. In this case, the arithmetic average porosity or the thickness-weighted average porosity is used to describe the average reservoir porosity. A change in sedimentation or depositional conditions, however, can cause the porosity in one portion of the reservoir to be greatly different from that in another area. In such cases, the areal-weighted average or the volume-weighted average porosity is used to characterize the average rock porosity. These averaging techniques are expressed mathematically in the following forms:

$$\text{Arithmetic average} \quad \phi = \Sigma\phi_i/n \quad (4-8)$$

$$\text{Thickness-weighted average} \quad \phi = \Sigma\phi_i h_i / \Sigma h_i \quad (4-9)$$

$$\text{Areal-weighted average} \quad \phi = \Sigma\phi_i A_i / \Sigma A_i \quad (4-10)$$

$$\text{Volumetric-weighted average} \quad \phi = \Sigma\phi_i A_i h_i / \Sigma A_i h_i \quad (4-11)$$

where n = total number of core samples

h_i = thickness of core sample i or reservoir area i

ϕ_i = porosity of core sample i or reservoir area i

A_i = reservoir area i

Example 4-2

Calculate the arithmetic average and thickness-weighted average from the following measurements:

| Sample | Thickness, ft | Porosity, % |
|--------|---------------|-------------|
| 1 | 1.0 | 10 |
| 2 | 1.5 | 12 |
| 3 | 1.0 | 11 |
| 4 | 2.0 | 13 |
| 5 | 2.1 | 14 |
| 6 | 1.1 | 10 |

Solution

- Arithmetic average

$$\phi = \frac{10 + 12 + 11 + 13 + 14 + 10}{6} = 11.67\%$$

- Thickness-weighted average

$$\phi = \frac{(1)(10) + (1.5)(12) + (1)(11) + (2)(13) + (2.1)(14) + (1.1)(10)}{1 + 1.5 + 1 + 2 + 2.1 + 1.1} = 12.11\%$$

SATURATION

Saturation is defined as that fraction, or percent, of the pore volume occupied by a particular fluid (oil, gas, or water). This property is expressed mathematically by the following relationship:

$$\text{fluid saturation} = \frac{\text{total volume of the fluid}}{\text{pore volume}}$$

Applying the above mathematical concept of saturation to each reservoir fluid gives

$$S_o = \frac{\text{volume of oil}}{\text{pore volume}} \quad (4-12)$$

$$S_g = \frac{\text{volume of gas}}{\text{pore volume}} \quad (4-13)$$

$$S_w = \frac{\text{volume of water}}{\text{pore volume}} \quad (4-14)$$

where S_o = oil saturation
 S_g = gas saturation
 S_w = water saturation

Thus, all saturation values are based on *pore volume* and not on the gross reservoir volume.

The saturation of each individual phase ranges between zero to 100%. By definition, the sum of the saturations is 100%, therefore

$$S_g + S_o + S_w = 1.0 \quad (4-15)$$

The fluids in most reservoirs are believed to have reached a state of equilibrium and, therefore, will have become separated according to their

density, i.e., oil overlain by gas and underlain by water. In addition to the bottom (or edge) water, there will be connate water distributed throughout the oil and gas zones. The water in these zones will have been reduced to some irreducible minimum. The forces retaining the water in the oil and gas zones are referred to as *capillary forces* because they are important only in pore spaces of capillary size.

Connate (interstitial) water saturation S_{wc} is important primarily because it reduces the amount of space available between oil and gas. It is generally not uniformly distributed throughout the reservoir but varies with permeability, lithology, and height above the free water table.

Another particular phase saturation of interest is called the *critical saturation*, and it is associated with each reservoir fluid. The definition and the significance of the critical saturation for each phase are described below.

Critical oil saturation, S_{oc}

For the oil phase to flow, the saturation of the oil must exceed a certain value, which is termed critical oil saturation. At this particular saturation, the oil remains in the pores and, for all practical purposes, will not flow.

Residual oil saturation, S_{or}

During the displacing process of the crude oil system from the porous media by water or gas injection (or encroachment), there will be some remaining oil left that is quantitatively characterized by a saturation value that is larger than the *critical oil saturation*. This saturation value is called the *residual oil saturation*, S_{or} . The term residual saturation is usually associated with the nonwetting phase when it is being displaced by a wetting phase.

Movable oil saturation, S_{om}

Movable oil saturation S_{om} is another saturation of interest and is defined as the fraction of pore volume occupied by movable oil as expressed by the following equation:

$$S_{om} = 1 - S_{wc} - S_{oc}$$

where S_{wc} = connate water saturation

S_{oc} = critical oil saturation

Critical gas saturation, S_{gc}

As the reservoir pressure declines below the bubble-point pressure, gas evolves from the oil phase and consequently the saturation of the gas increases as the reservoir pressure declines. The gas phase remains immobile until its saturation exceeds a certain saturation, called *critical gas saturation*, above which gas begins to move.

Critical water saturation, S_{wc}

The critical water saturation, connate water saturation, and irreducible water saturation are extensively used interchangeably to define the maximum water saturation at which the water phase will remain immobile.

Average Saturation

Proper averaging of saturation data requires that the saturation values be weighted by both the interval *thickness* h_i and interval *porosity* ϕ . The average saturation of each reservoir fluid is calculated from the following equations:

$$S_o = \frac{\sum_{i=1}^n \phi_i h_i S_{oi}}{\sum_{i=1}^n \phi_i h_i} \quad (4-16)$$

$$S_w = \frac{\sum_{i=1}^n \phi_i h_i S_{wi}}{\sum_{i=1}^n \phi_i h_i} \quad (4-17)$$

$$S_g = \frac{\sum_{i=1}^n \phi_i h_i S_{gi}}{\sum_{i=1}^n \phi_i h_i} \quad (4-18)$$

where the subscript i refers to any individual measurement and h_i represents the depth interval to which ϕ_i , S_{oi} , S_{gi} , and S_{wi} apply.

Example 4-3

Calculate average oil and connate water saturation from the following measurements:

| Sample | h_i , ft | ϕ , % | S_{oi} , % | S_{wci} , % |
|--------|------------|------------|--------------|---------------|
| 1 | 1.0 | 10 | 75 | 25 |
| 2 | 1.5 | 12 | 77 | 23 |
| 3 | 1.0 | 11 | 79 | 21 |
| 4 | 2.0 | 13 | 74 | 26 |
| 5 | 2.1 | 14 | 78 | 22 |
| 6 | 1.1 | 10 | 75 | 25 |

Solution

Construct the following table and calculate the average saturation for the oil and water phase:

| Sample | h_i , ft | ϕ | ϕh | S_o | $S_o \phi h$ | S_{wc} | $S_{wc} \phi h$ |
|--------|------------|--------|----------|-------|--------------|----------|-----------------|
| 1 | 1.0 | .10 | .100 | .75 | .0750 | .25 | .0250 |
| 2 | 1.5 | .12 | .180 | .77 | .1386 | .23 | .0414 |
| 3 | 1.0 | .11 | .110 | .79 | .0869 | .21 | .0231 |
| 4 | 2.0 | .13 | .260 | .74 | .1924 | .26 | .0676 |
| 5 | 2.1 | .14 | .294 | .78 | .2293 | .22 | .0647 |
| 6 | 1.1 | .10 | .110 | .75 | .0825 | .25 | .0275 |
| | | | 1.054 | | 0.8047 | | 0.2493 |

Calculate average oil saturation by applying Equation 4-16:

$$S_o = \frac{.8047}{1.054} = 0.7635$$

Calculate average water saturation by applying Equation 4-17:

$$S_w = \frac{0.2493}{1.054} = 0.2365$$

WETTABILITY

Wettability is defined as the tendency of one fluid to spread on or adhere to a solid surface in the presence of other immiscible fluids. The concept of wettability is illustrated in Figure 4-1. Small *drops* of three liquids—mercury, oil, and water—are placed on a clean glass plate. The three droplets are then observed from one side as illustrated in Figure 4-1. It is noted that the mercury retains a spherical shape, the oil droplet develops an approximately hemispherical shape, but the water tends to spread over the glass surface.

The tendency of a liquid to spread over the surface of a solid is an indication of the *wetting* characteristics of the liquid for the solid. This spreading tendency can be expressed more conveniently by measuring the angle of contact at the *liquid-solid* surface. This angle, which is always measured through the liquid to the solid, is called the contact angle θ .

The contact angle θ has achieved significance as a measure of wettability. As shown in Figure 4-1, as the contact angle decreases, the wetting characteristics of the liquid increase. Complete wettability would be evidenced by a zero contact angle, and complete nonwetting would be evidenced by a contact angle of 180° . There have been various definitions of *intermediate* wettability but, in much of the published literature, contact angles of 60° to 90° will tend to repel the liquid.

The wettability of reservoir rocks to the fluids is important in that the distribution of the fluids in the porous media is a function of wettability. Because of the attractive forces, the wetting phase tends to occupy the smaller pores of the rock and the nonwetting phase occupies the more open channels.

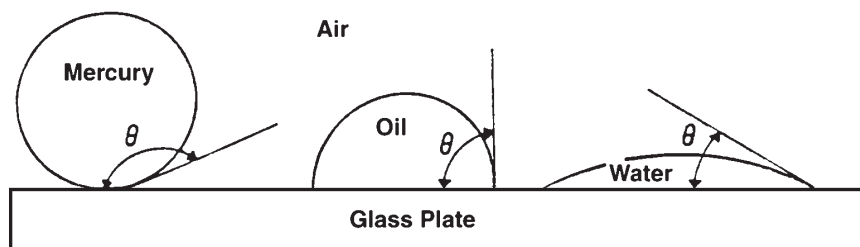


Figure 4-1. Illustration of wettability.

SURFACE AND INTERFACIAL TENSION

In dealing with multiphase systems, it is necessary to consider the effect of the forces at the interface when two immiscible fluids are in contact. When these two fluids are liquid and gas, the term *surface tension* is used to describe the forces acting on the interface. When the interface is between two liquids, the acting forces are called *interfacial tension*.

Surfaces of liquids are usually blanketed with what acts as a thin film. Although this apparent film possesses little strength, it nevertheless acts like a thin membrane and resists being broken. This is believed to be caused by attraction between molecules within a given system. All molecules are attracted one to the other in proportion to the product of their masses and inversely as the squares of the distance between them.

Consider the two immiscible fluids, air (or gas) and water (or oil), as shown schematically in Figure 4-2. A liquid molecule, which is remote from the interface, is surrounded by other liquid molecules, thus having a resulting net attractive force on the molecule of zero. A molecule at the interface, however, has a force acting on it from the air (gas) molecules lying immediately above the interface and from liquid molecules lying below the interface.

Resulting forces are unbalanced and give rise to surface tension. The unbalanced attraction force between the molecules creates a membrane-like surface with a measurable tension, i.e., surface tension. As a matter

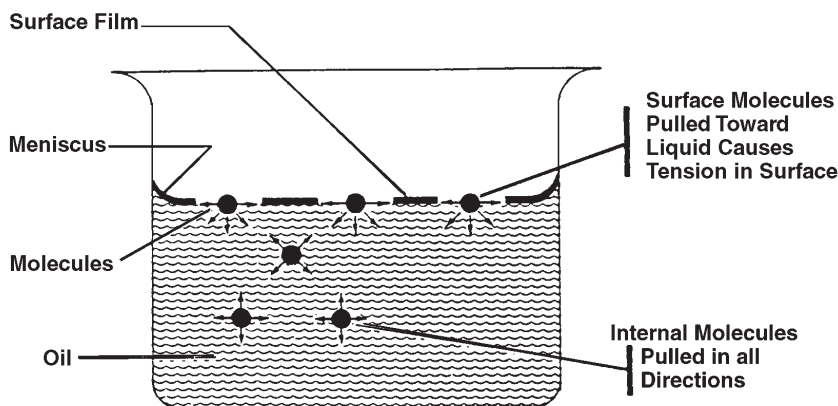


Figure 4-2. Illustration of surface tension. (After Clark, N. J., Elements of Petroleum Reservoirs, SPE, 1969.)

of fact, if carefully placed, a needle will float on the surface of the liquid, supported by the thin membrane even though it is considerably more dense than the liquid.

The surface or interfacial tension has the units of force per unit of length, e.g., dynes/cm, and is usually denoted by the symbol σ .

If a glass capillary tube is placed in a large open vessel containing water, the combination of surface tension and wettability of tube to water will cause water to rise in the tube above the water level in the container outside the tube as shown in Figure 4-3.

The water will rise in the tube until the total force acting to pull the liquid upward is balanced by the weight of the column of liquid being

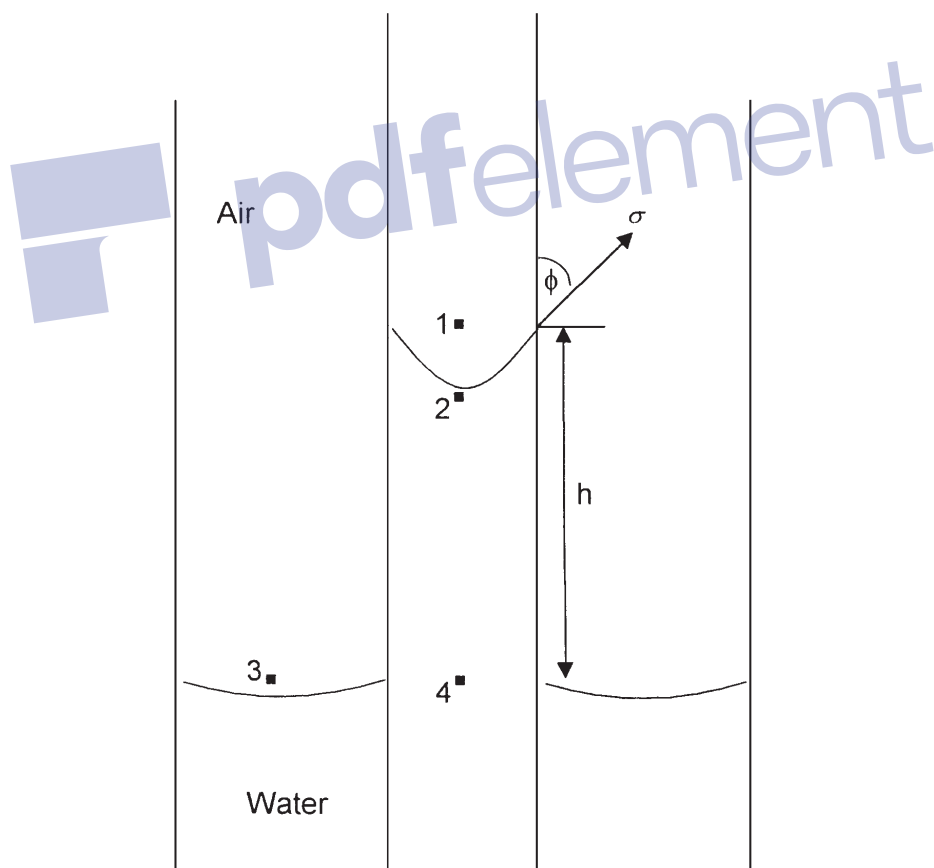


Figure 4-3. Pressure relations in capillary tubes.

supported in the tube. Assuming the radius of the capillary tube is r , the total upward force F_{up} , which holds the liquid up, is equal to the force per unit length of surface times the total length of surface, or

$$F_{\text{up}} = (2\pi r) (\sigma_{\text{gw}}) (\cos \theta) \quad (4-19)$$

where σ_{gw} = surface tension between air (gas) and water (oil), dynes/cm

θ = contact angle

r = radius, cm

The upward force is counteracted by the weight of the water, which is equivalent to a downward force of mass times acceleration, or

$$F_{\text{down}} = \pi r^2 h (\rho_w - \rho_{\text{air}}) g \quad (4-20)$$

where h = height to which the liquid is held, cm

g = acceleration due to gravity, cm/sec²

ρ_w = density of water, gm/cm³

ρ_{air} = density of gas, gm/cm³

Because the density of air is negligible in comparison with the density of water, Equation 4-20 is reduced to:

$$F_{\text{down}} = \pi r^2 \rho_w g \quad (4-21)$$

Equating Equation 4-19 with 4-21 and solving for the surface tension gives:

$$\sigma_{\text{gw}} = \frac{r h \rho_w g}{2 \cos \theta} \quad (4-22)$$

The generality of Equations 4-19 through 4-22 will not be lost by applying them to the behavior of two liquids, i.e., water and oil. Because the density of oil is not negligible, Equation 4-22 becomes

$$\sigma_{\text{ow}} = \frac{r h g (\rho_w - \rho_o)}{2 \cos \theta} \quad (4-23)$$

where ρ_o = density of oil, gm/cm³

σ_{ow} = interfacial tension between the oil and the water, dynes/cm

CAPILLARY PRESSURE

The capillary forces in a petroleum reservoir are the result of the combined effect of the surface and interfacial tensions of the rock and fluids, the pore size and geometry, and the wetting characteristics of the system. Any curved surface between two immiscible fluids has the tendency to contract into the smallest possible area per unit volume. This is true whether the fluids are oil and water, water and gas (even air), or oil and gas. When two immiscible fluids are in contact, a discontinuity in pressure exists between the two fluids, which depends upon the curvature of the interface separating the fluids. We call this pressure difference the *capillary pressure*, and it is referred to by p_c .

The displacement of one fluid by another in the pores of a porous medium is either aided or opposed by the surface forces of capillary pressure. As a consequence, in order to maintain a porous medium partially saturated with nonwetting fluid and while the medium is also exposed to wetting fluid, it is necessary to maintain the pressure of the nonwetting fluid at a value greater than that in the wetting fluid.

Denoting the pressure in the wetting fluid by p_w and that in the nonwetting fluid by p_{nw} , the capillary pressure can be expressed as:

Capillary pressure = (pressure of the nonwetting phase) – (pressure of the wetting phase)

$$P_c = P_{nw} - P_w \quad (4-24)$$

That is, the pressure excess in the nonwetting fluid is the capillary pressure, and this quantity is a function of saturation. This is the defining equation for capillary pressure in a porous medium.

There are three types of capillary pressure:

- Water-oil capillary pressure (denoted as P_{cwo})
- Gas-oil capillary pressure (denoted as P_{cgo})
- Gas-water capillary pressure (denoted as P_{cgw})

Applying the mathematical definition of the capillary pressure as expressed by Equation 4-24, the three types of the capillary pressure can be written as:

$$P_{cwo} = p_o - p_w$$

$$p_{cgo} = p_g - p_o$$

$$p_{cgw} = p_g - p_w$$

where p_g , p_o , and p_w represent the pressure of gas, oil, and water, respectively.

If all the three phases are continuous, then:

$$p_{cgw} = p_{cgo} + p_{cwo}$$

Referring to Figure 4-3, the pressure difference across the interface between Points 1 and 2 is essentially the capillary pressure, i.e.:

$$p_c = p_1 - p_2 \quad (4-25)$$

The pressure of the water phase at Point 2 is equal to the pressure at point 4 minus the head of the water, or:

$$p_2 = p_4 - gh\rho_w \quad (4-26)$$

The pressure just above the interface at Point 1 represents the pressure of the air and is given by:

$$p_1 = p_3 - gh\rho_{air} \quad (4-27)$$

It should be noted that the pressure at Point 4 within the capillary tube is the same as that at Point 3 outside the tube. Subtracting Equation 4-26 from 4-27 gives:

$$p_c = gh(\rho_w - \rho_{air}) = gh\Delta\rho \quad (4-28)$$

where $\Delta\rho$ is the density difference between the wetting and nonwetting phase. The density of the air (gas) is negligible in comparison with the water density.

In practical units, Equation 4-28 can be expressed as:

$$p_c = \left(\frac{h}{144} \right) \Delta\rho$$

where p_c = capillary pressure, psi

h = capillary rise, ft

$\Delta\rho$ = density difference, lb/ft³

In the case of an oil-water system, Equation 4-28 can be written as:

$$p_c = gh (\rho_w - \rho_o) = gh\Delta\rho \quad (4-29)$$

and in practical units

$$p_c = \left(\frac{h}{144} \right) (\rho_w - \rho_o)$$

The capillary pressure equation can be expressed in terms of the surface and interfacial tension by combining Equations 4-28 and 4-29 with Equations 4-22 and 4-23 to give:

• **Gas-liquid system**

$$P_c = \frac{2 \sigma_{gw} (\cos \theta)}{r} \quad (4-30)$$

and

$$h = \frac{2 \sigma_{gw} (\cos \theta)}{r g (\rho_w - \rho_{gas})} \quad (4-31)$$

where ρ_w = water density, gm/cm³

σ_{gw} = gas-water surface tension, dynes/cm

r = capillary radius, cm

θ = contact angle

h = capillary rise, cm

g = acceleration due to gravity, cm/sec²

p_c = capillary pressure, dynes/cm²

• **Oil-water system**

$$p_c = \frac{2 \sigma_{ow} (\cos \theta)}{r} \quad (4-32)$$

and

$$h = \frac{2 \sigma_{wo} (\cos \theta)}{r g (\rho_w - \rho_o)} \quad (4-33)$$

where σ_{wo} is the water-oil interfacial tension.

Example 4-4

Calculate the pressure difference, i.e., capillary pressure, and capillary rise in an oil-water system from the following data:

$$\begin{aligned} \theta &= 30^\circ & \rho_w &= 1.0 \text{ gm/cm}^3 & \rho_o &= 0.75 \text{ gm/cm}^3 \\ r &= 10^{-4} \text{ cm} & \sigma_{ow} &= 25 \text{ dynes/cm} \end{aligned}$$

Solution

Step 1. Apply Equation 4-32 to give

$$p_c = \frac{(2)(25)(\cos 30^\circ)}{0.0001} = 4.33 \times 10^5 \text{ dynes/cm}^2$$

Since $1 \text{ dyne/cm}^2 = 1.45 \times 10^{-5} \text{ psi}$, then

$$p_c = 6.28 \text{ psi}$$

This result indicates that the oil-phase pressure is 6.28 psi higher than the water-phase pressure.

Step 2. Calculate the capillary rise by applying Equation 4-33.

$$h = \frac{(2)(25)(\cos 30^\circ)}{(0.0001)(980.7)(1.0 - 0.75)} = 1766 \text{ cm} = 75.9 \text{ ft}$$

Capillary Pressure of Reservoir Rocks

The interfacial phenomena described above for a single capillary tube also exist when bundles of interconnected capillaries of varying sizes exist in a porous medium. The capillary pressure that exists within a porous medium between two immiscible phases is a function of the interfacial tensions and the average size of the capillaries, which, in turn, control the curvature of the interface. In addition, the curvature is also a function of the saturation distribution of the fluids involved.

Laboratory experiments have been developed to simulate the displacing forces in a reservoir in order to determine the magnitude of the capillary forces in a reservoir and, thereby, determine the fluid saturation distributions and connate water saturation. One such experiment is called the *restored*

capillary pressure technique, which was developed primarily to determine the magnitude of the connate water saturation. A diagrammatic sketch of this equipment is shown in Figure 4-4.

Briefly, this procedure consists of saturating a core 100% with the reservoir water and then placing the core on a porous membrane, which is saturated 100% with water and is permeable to the water only, under the pressure drops imposed during the experiment. Air is then admitted into the core chamber and the pressure is increased until a small amount of water is displaced through the porous, semi-permeable membrane into the graduated cylinder. Pressure is held constant until no more water is displaced, which may require several days or even several weeks, after which the core is removed from the apparatus and the water saturation is

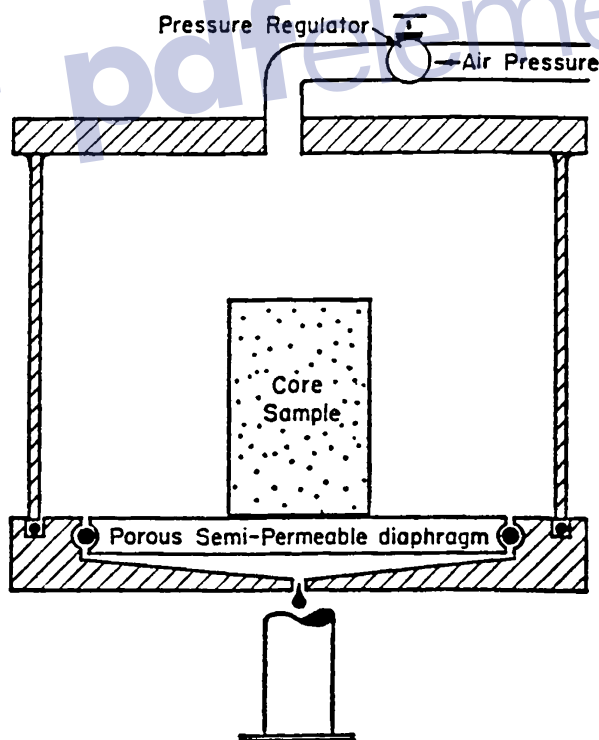


Figure 4-4. Capillary pressure equipment. (After Cole, F., 1969.)

determined by weighing. The core is then replaced in the apparatus, the pressure is increased, and the procedure is repeated until the water saturation is reduced to a minimum.

The data from such an experiment are shown in Figure 4-5. Since the pressure required to displace the wetting phase from the core is exactly equal to the capillary forces holding the remaining water within the core after equilibrium has been reached, the pressure data can be plotted as capillary pressure data. Two important phenomena can be observed in Figure 4-5. First, there is a finite capillary pressure at 100% water saturation that is necessary to force the nonwetting phase into a capillary filled with the wetting phase. This minimum capillary pressure is known as the *displacement pressure*, p_d .

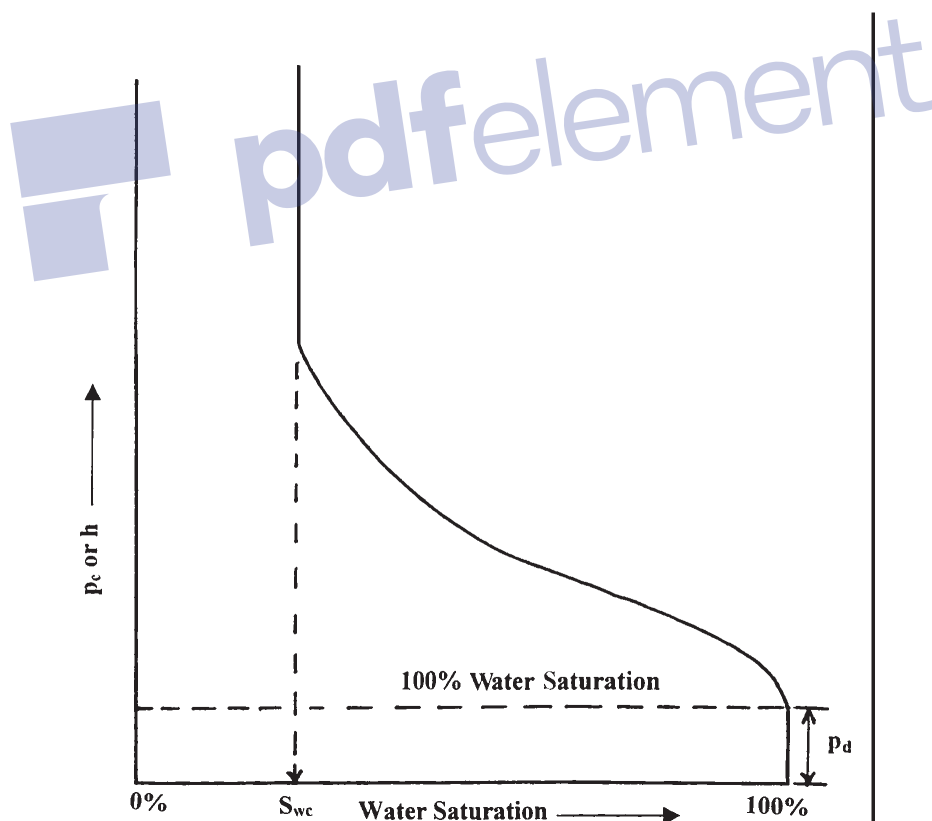


Figure 4-5. Capillary pressure curve.

If the largest capillary opening is considered as circular with a radius of r , the pressure needed for forcing the nonwetting fluid out of the core is:

$$P_c = \frac{2 \sigma (\cos \theta)}{r}$$

This is the minimum pressure that is required to displace the wetting phase from the largest capillary pore because any capillary of smaller radius will require a higher pressure.

As the wetting phase is displaced, the second phenomenon of any immiscible displacement process is encountered, that is, the reaching of some finite minimum irreducible saturation. This irreducible water saturation is referred to as connate water.

It is possible from the capillary pressure curve to calculate the average size of the pores making up a stated fraction of the total pore space. Let p_c be the average capillary pressure for the 10% between saturation of 40% and 50%. The average capillary radius is obtained from

$$r = \frac{2 \sigma (\cos \theta)}{p_c}$$

The above equation may be solved for r providing that the interfacial tension σ , and the angle of contact θ may be evaluated.

Figure 4-6 is an example of typical oil-water capillary pressure curves. In this case, capillary pressure is plotted versus water saturation for four rock samples with permeabilities increasing from k_1 to k_4 . It can be seen that, for decreases in permeability, there are corresponding increases in capillary pressure at a constant value of water saturation. This is a reflection of the influence of pore size since the smaller diameter pores will invariably have the lower permeabilities. Also, as would be expected, the capillary pressure for any sample increases with decreasing water saturation, another indication of the effect of the radius of curvature of the water-oil interface.

Capillary Hysteresis

It is generally agreed that the pore spaces of reservoir rocks were originally filled with water, after which oil moved into the reservoir, displacing some of the water and reducing the water to some residual saturation. When discovered, the reservoir pore spaces are filled with a connate-water saturation and an oil saturation. All laboratory experiments are

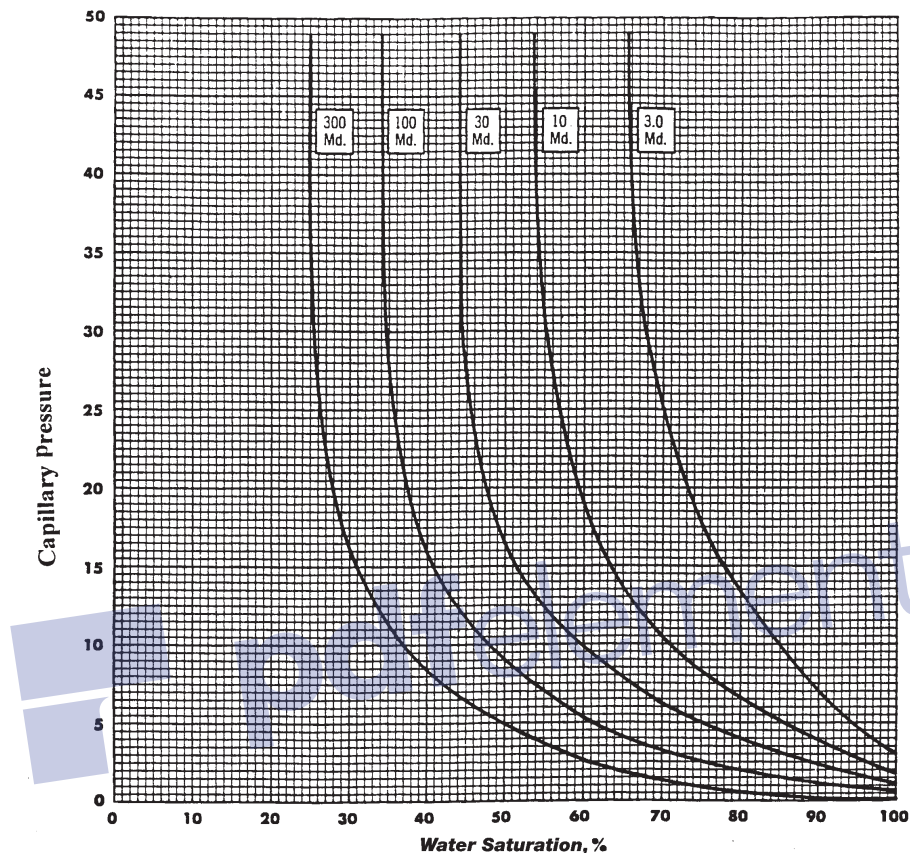


Figure 4-6. Variation of capillary pressure with permeability.

designed to duplicate the saturation history of the reservoir. The process of generating the capillary pressure curve by displacing the wetting phase, i.e., water, with the nonwetting phase (such as with gas or oil), is called the *drainage process*.

This drainage process establishes the fluid saturations, which are found when the reservoir is discovered. The other principal flow process of interest involves reversing the drainage process by displacing the nonwetting phase (such as with oil) with the wetting phase (e.g., water). This displacing process is termed the *imbibition process* and the resulting curve is termed the *capillary pressure imbibition curve*. The process of *saturation* and *desaturation* a core with the nonwetting phase is called *capillary hysteresis*. Figure 4-7 shows typical drainage and imbibition

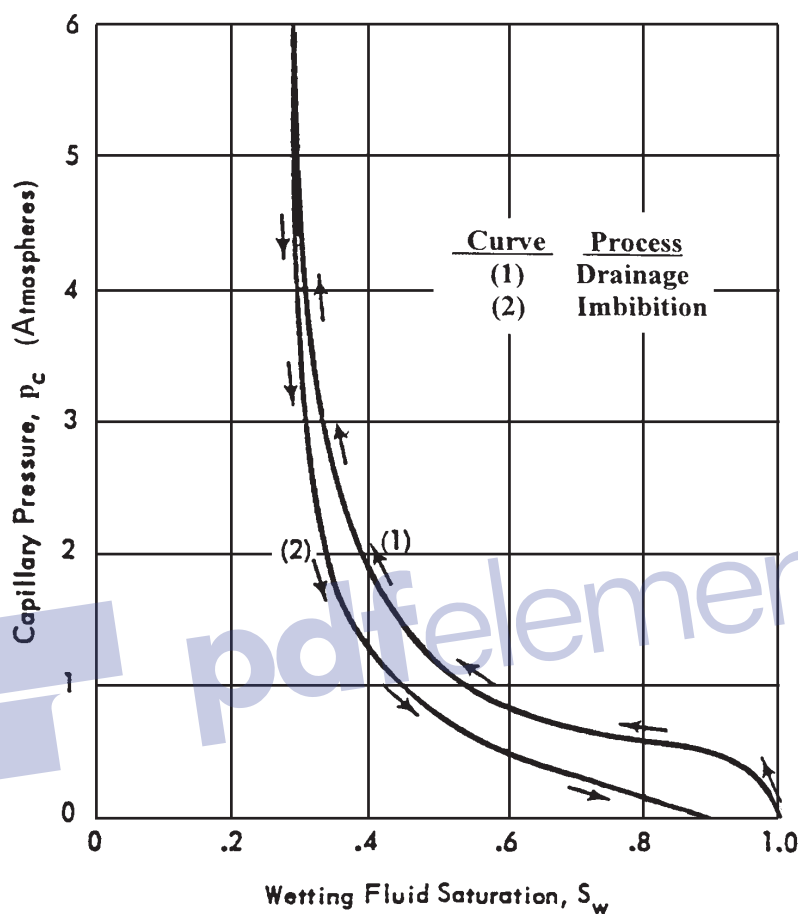


Figure 4-7. Capillary pressure hysteresis.

capillary pressure curves. The two capillary pressure-saturation curves are not the same.

This difference in the saturating and desaturating of the capillary-pressure curves is closely related to the fact that the advancing and receding contact angles of fluid interfaces on solids are different. Frequently, in natural crude oil-brine systems, the contact angle or wettability may change with time. Thus, if a rock sample that has been thoroughly cleaned with volatile solvents is exposed to crude oil for a period of time, it will behave as though it were oil wet. But if it is exposed to brine after

cleaning, it will appear water wet. At the present time, one of the greatest unsolved problems in the petroleum industry is that of wettability of reservoir rock.

Another mechanism that has been proposed by McCardell (1955) to account for capillary hysteresis is called the *ink-bottle effect*. This phenomenon can be easily observed in a capillary tube having variations in radius along its length. Consider a capillary tube of axial symmetry having roughly sinusoidal variations in radius. When such a tube has its lower end immersed in water, the water will rise in the tube until the hydrostatic fluid head in the tube becomes equal to the capillary pressure. If then the tube is lifted to a higher level in the water, some water will drain out, establishing a new equilibrium level in the tube.

When the meniscus is advancing and it approaches a constriction, it *jumps* through the neck, whereas when receding, it halts without passing through the neck. This phenomenon explains why a given capillary pressure corresponds to a higher saturation on the drainage curve than on the imbibition curve.

Initial Saturation Distribution in a Reservoir

An important application of the concept of capillary pressures pertains to the fluid distribution in a reservoir prior to its exploitation. The capillary pressure-saturation data can be converted into height-saturation data by arranging Equation 4-29 and solving for the height h above the free-water level.

$$h = \frac{144 p_c}{\Delta \rho} \quad (4-34)$$

where p_c = capillary pressure, psia

$\Delta \rho$ = density difference between the wetting and nonwetting phase, lb/ft³

H = height above the free-water level, ft

Figure 4-8 shows a plot of the water saturation distribution as a function of distance from the free-water level in an oil-water system.

It is essential at this point to introduce and define four important concepts:

- Transition zone
- Water-oil contact (WOC)
- Gas-oil contact (GOC)
- Free water level (FWL)

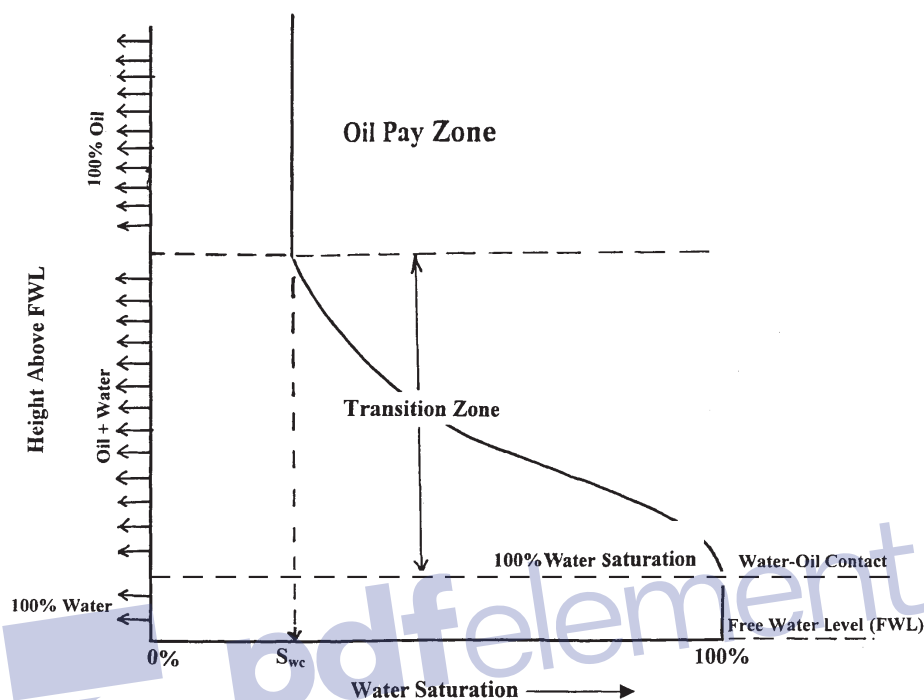


Figure 4-8. Water saturation profile.

Figure 4-9 illustrates an idealized gas, oil, and water distribution in a reservoir. The figure indicates that the saturations are gradually changing from 100% water in the water zone to irreducible water saturation some vertical distance above the water zone. This vertical area is referred to as the *transition zone*, which must exist in any reservoir where there is a bottom water table. The transition zone is then defined as the vertical thickness over which the water saturation ranges from 100% saturation to irreducible water saturation S_{wc} . The important concept to be gained from Figure 4-9 is that there is no abrupt change from 100% water to maximum oil saturation. The creation of the oil-water transition zone is one of the major effects of capillary forces in a petroleum reservoir.

Similarly, the total liquid saturation (i.e., oil and water) is smoothly changing from 100% in the oil zone to the connate water saturation in the gas cap zone. A similar transition exists between the oil and gas zone. Figure 4-8 serves as a definition of what is meant by gas-oil and water-oil contacts. The WOC is defined as the “uppermost depth in the reservoir where a 100% water saturation exists.” The GOC is defined as the “mini-

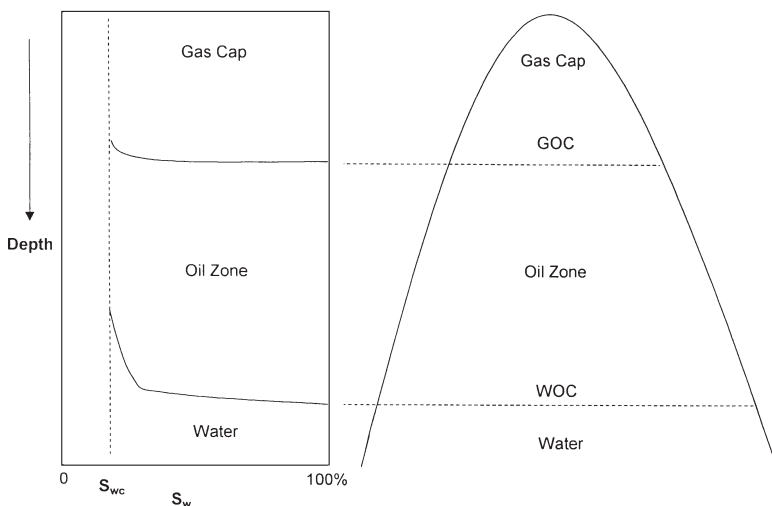


Figure 4-9. Initial saturation profile in a combination-drive reservoir.

imum depth at which a 100% liquid, i.e., oil + water, saturation exists in the reservoir.”

Section A of Figure 4-10 shows a schematic illustration of a core that is represented by five different pore sizes and completely saturated with water, i.e., wetting phase. Assume that we subject the core to oil (the nonwetting phase) with increasing pressure until some water is displaced from the core, i.e., displacement pressure p_d . This water displacement will occur from the largest pore size. The oil pressure will have to increase to displace the water in the second largest pore. This sequential process is shown in sections B and C of Figure 4-10.

It should be noted that there is a difference between the free water level (FWL) and the depth at which 100% water saturation exists. From a reservoir engineering standpoint, the free water level is defined by *zero capillary pressure*. Obviously, if the largest pore is so large that there is no capillary rise in this size pore, then the free water level and 100% water saturation level, i.e., WOC, will be the same. This concept can be expressed mathematically by the following relationship:

$$\text{FWL} = \text{WOC} + \frac{144 p_d}{\Delta \rho} \quad (4-35)$$

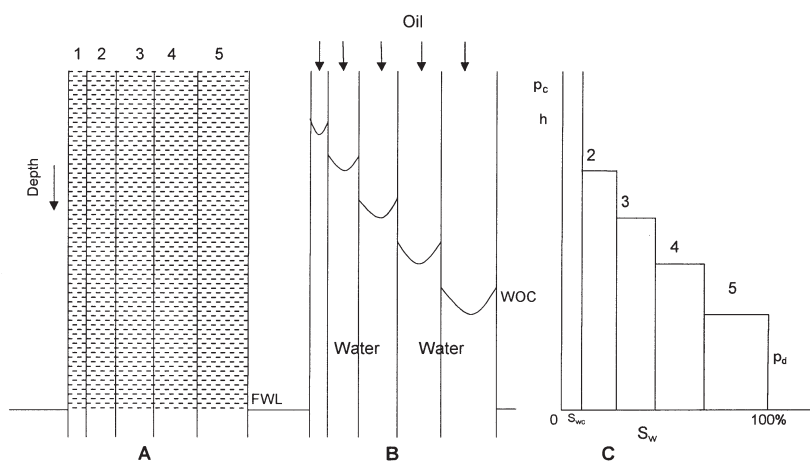


Figure 4-10. Relationship between saturation profile and pore-size distribution.

where p_d = displacement pressure, psi

$\Delta\rho$ = density difference, lb/ft³

FWL = free water level, ft

WOC = water-oil contact, ft

Example 4-5

The reservoir capillary pressure-saturation data of the Big Butte Oil reservoir is shown graphically in Figure 4-11. Geophysical log interpretations and core analysis establish the WOC at 5,023 ft. The following additional data are available:

- Oil density = 43.5 lb/ft³
- Water density = 64.1 lb/ft³
- Interfacial tension = 50 dynes/cm

Calculate:

- Connate water saturation (S_{wc})
- Depth to FWL
- Thickness of the transition zone
- Depth to reach 50% water saturation

Solution

- From Figure 4-11, connate-water saturation is 20%.
- Applying Equation 4-35 with a displacement pressure of 1.5 psi gives

$$\text{FWL} = 5023 + \frac{(144)(1.5)}{(64.1 - 43.5)} = 5033.5 \text{ ft}$$

- Thickness of transition zone = $\frac{144(6.0 - 1.5)}{(64.1 - 43.5)} = 31.5 \text{ ft}$

- P_c at 50% water saturation = 3.5 psia

$$\text{Equivalent height above the FWL} = (144)(3.5)/(64.1 - 43.5) = 24.5 \text{ ft}$$

$$\text{Depth to 50\% water saturation} = 5033.5 - 24.5 = 5009 \text{ ft}$$

The above example indicates that only oil will flow in the interval between the top of the pay zone and depth of 4,991.5 ft. In the transition zone, i.e., the interval from 4,991.5 ft to the WOC, oil production would be accompanied by simultaneous water production.

It should be pointed out that the thickness of the transition zone may range from a few feet to several hundred feet in some reservoirs. Recalling the capillary rise equation, i.e., height above FWL,

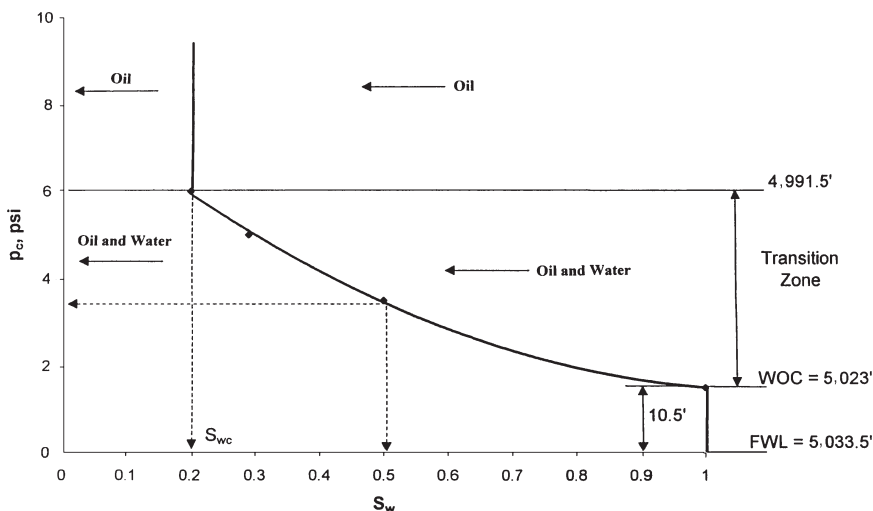


Figure 4-11. Capillary pressure saturation data.

$$h = \frac{2\sigma(\cos\phi)}{rg\Delta\rho}$$

The above relationship suggests that the height above FWL increases with decreasing the density difference $\Delta\rho$.

From a practical standpoint, this means that in a gas reservoir having a gas-water contact, the thickness of the transition zone will be a minimum since $\Delta\rho$ will be large. Also, if all other factors remain unchanged, a low API gravity oil reservoir with an oil-water contact will have a longer transition zone than a high API gravity oil reservoir. Cole (1969) illustrated this concept graphically in Figure 4-12.

The above expression also shows that as the radius of the pore r increases the volume of h decreases. Therefore, a reservoir rock system with small pore sizes will have a longer transition zone than a reservoir rock system comprised of large pore sizes.

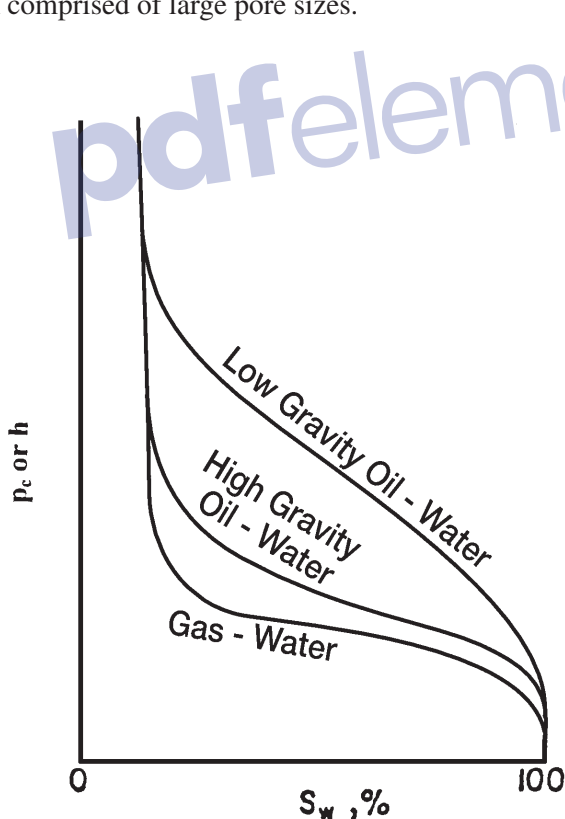


Figure 4-12. Variation of transition zone with fluid gravity. (After Cole, F., 1969.)

The reservoir pore size can often be related approximately to permeability, and where this applies, it can be stated that high permeability reservoirs will have shorter transition zones than low permeability reservoirs as shown graphically in Figure 4-13. As shown by Cole (Figure 4-14), a tilted water-oil contact could be caused by a change in permeability across the reservoir. It should be emphasized that the factor responsible for this change in the location of the water-oil contact is actually a change in the size of the pores in the reservoir rock system.

The previous discussion of capillary forces in reservoir rocks has assumed that the reservoir pore sizes, i.e., permeabilities, are essentially uniform. Cole (1969) discussed the effect of reservoir non-uniformity on the distribution of the fluid saturation through the formation. Figure 4-15 shows a hypothetical reservoir rock system that is comprised of seven layers. In addition, the seven layers are characterized by only two different pore sizes, i.e., permeabilities, and corresponding capillary pressure

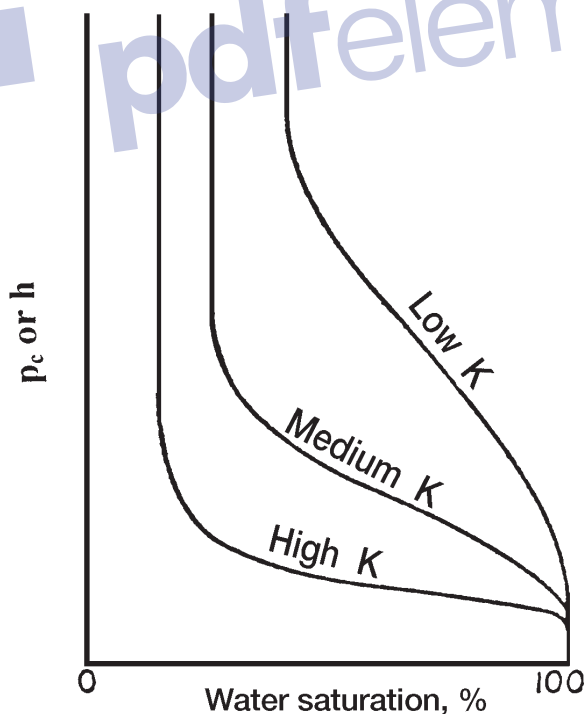


Figure 4-13. Variation of transition zone with permeability.

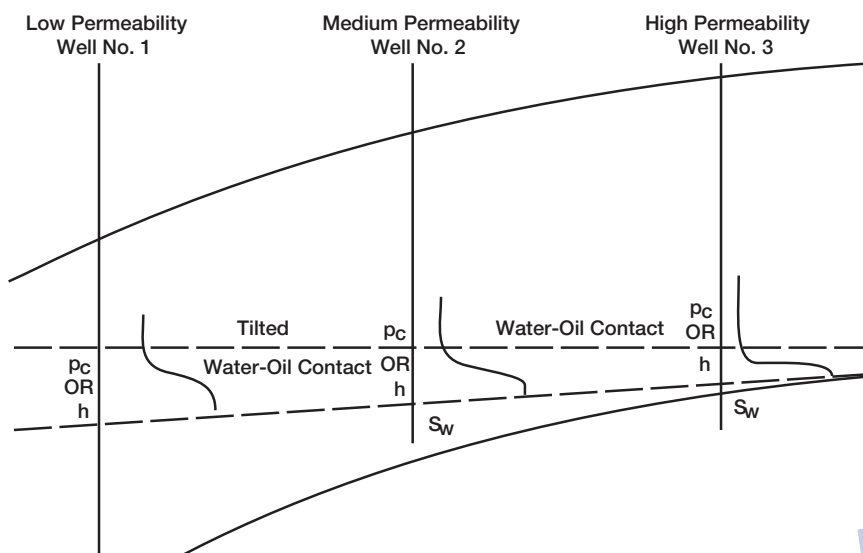


Figure 4-14. Tilted WOC. (After Cole, F., 1969.)

curves as shown in section A of Figure 4-15. The resulting capillary pressure curve for the layered reservoir would resemble that shown in section B of Figure 4-15. If a well were drilled at the point shown in section B of Figure 4-15, Layers 1 and 3 would not produce water, while Layer 2, which is above Layer 3, would produce water since it is located in the transition zone.

Example 4-6

A four-layer oil reservoir is characterized by a set of reservoir capillary pressure-saturation curves as shown in Figure 4-16. The following additional data are also available.

| Layer | Depth, ft | Permeability, md |
|-------|-----------|------------------|
| 1 | 4000–4010 | 80 |
| 2 | 4010–4020 | 190 |
| 3 | 4020–4035 | 70 |
| 4 | 4035–4060 | 100 |

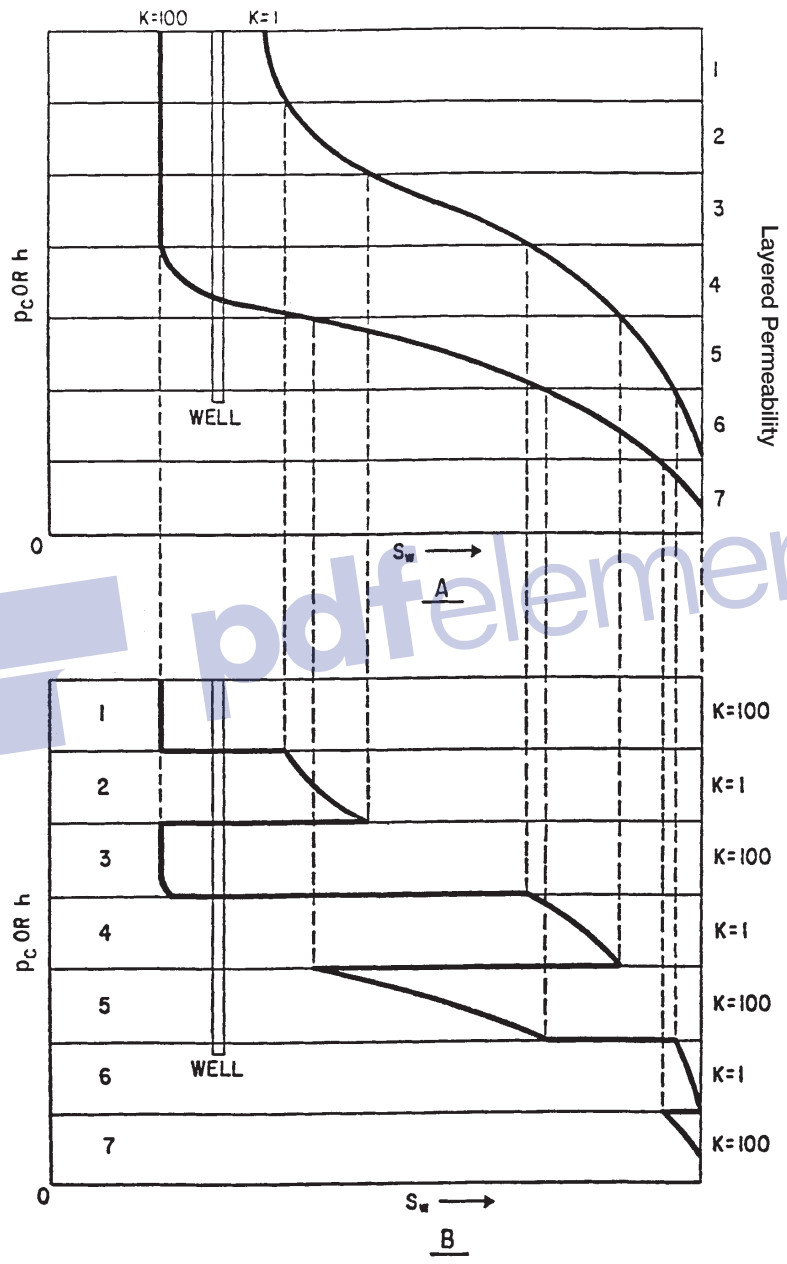


Figure 4-15. Effect of permeability on water saturation profile. (After Cole, F., 1969.)

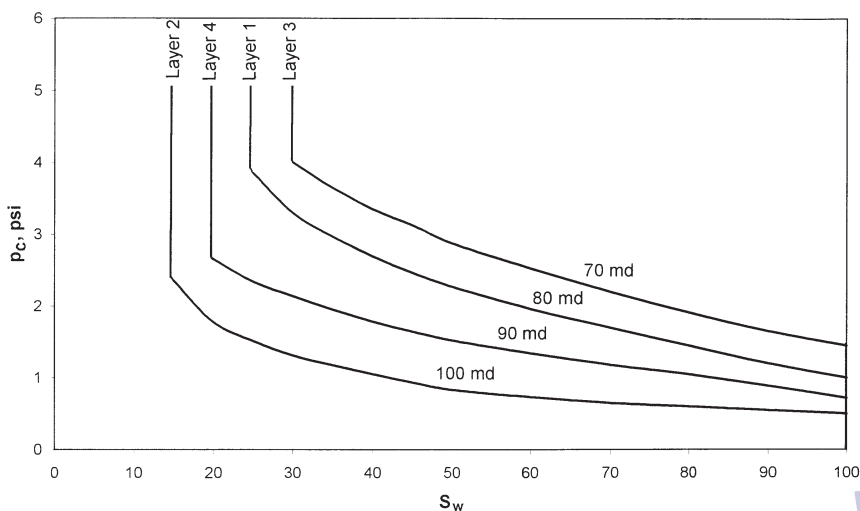


Figure 4-16. Variation of p_c with k .

WOC = 4060 ft

Water density = 65.2 lb/ft³

Oil density = 55.2 lb/ft³

Calculate and plot water saturation versus depth for this reservoir.

Solution

Step 1. Establish the FWL by determining the displacement pressure p_d for the bottom layer, i.e., Layer 4, and apply Equation 4-37:

- $p_d = 0.75$ psi

$$\text{FWL} = 4060 + \frac{(144)(0.75)}{(65.2 - 55.2)} = 4070.8 \text{ ft}$$

Step 2. The top of the bottom layer is located at a depth of 4,035 ft, which is 35.8 ft above the FWL. Using that height h of 35.8 ft, calculate the capillary pressure at the top of the bottom layer.

$$p_c = \left(\frac{h}{144} \right) \Delta \rho = \left(\frac{35.8}{144} \right) (65.2 - 55.2) = 2.486 \text{ psi}$$

- From the capillary pressure-saturation curve designated for Layer 4, read the water saturation that corresponds to a p_c of 2.486 to give $S_w = 0.23$.
- Assume different values of water saturations and convert the corresponding capillary pressures into height above the FWL by applying Equation 4-34.

$$h = \frac{144 p_c}{\rho_w - \rho_o}$$

| S_w | p_c , psi | h , ft | Depth = FWL - h |
|-------|-------------|----------|-------------------|
| 0.23 | 2.486 | 35.8 | 4035 |
| 0.25 | 2.350 | 33.84 | 4037 |
| 0.30 | 2.150 | 30.96 | 4040 |
| 0.40 | 1.800 | 25.92 | 4045 |
| 0.50 | 1.530 | 22.03 | 4049 |
| 0.60 | 1.340 | 19.30 | 4052 |
| 0.70 | 1.200 | 17.28 | 4054 |
| 0.80 | 1.050 | 15.12 | 4056 |
| 0.90 | 0.900 | 12.96 | 4058 |

Step 3. The top of Layer 3 is located at a distance of 50.8 ft from the FWL (i.e., $h = 4070.8 - 4,020 = 50.8$ ft). Calculate the capillary pressure at the top of the third layer:

- $p_c = \left(\frac{50.8}{144} \right) (65.2 - 55.2) = 3.53$ psi
- The corresponding water saturation as read from the curve designated for Layer 3 is 0.370.
- Construct the following table for Layer 3.

| S_w | p_c , psi | h , ft | Depth = FWL - h |
|-------|-------------|----------|-------------------|
| 0.37 | 3.53 | 50.8 | 4020 |
| 0.40 | 3.35 | 48.2 | 4023 |
| 0.50 | 2.75 | 39.6 | 4031 |
| 0.60 | 2.50 | 36.0 | 4035 |

Step 4. • Distance from the FWL to the top of Layer 2 is:

$$h = 4070.8 - 4010 = 60.8 \text{ ft}$$

$$\bullet p_c = \left(\frac{60.8}{144} \right) (65.2 - 55.2) = 4.22 \text{ psi}$$

- S_w at p_c of 4.22 psi is 0.15.
- Distance from the FWL to the bottom of the layer is 50.8 ft that corresponds to a p_c of 3.53 psi and S_w of 0.15. This indicates that the second layer has a uniform water saturation of 15%.

Step 5. For Layer 1, distance from the FWL to the top of the layer:

$$\bullet h = 4070.8 - 4000 = 70.8 \text{ ft}$$

$$\bullet p_c = \left(\frac{70.8}{144} \right) (10) = 4.92 \text{ psi}$$

- S_w at the top of Layer 1 = 0.25
- The capillary pressure at the bottom of the layer is 3.53 psi with a corresponding water saturation of 0.27.

Step 6. Figure 4-17 documents the calculated results graphically. The figure indicates that Layer 2 will produce 100% oil while all remaining layers produce oil and water simultaneously.

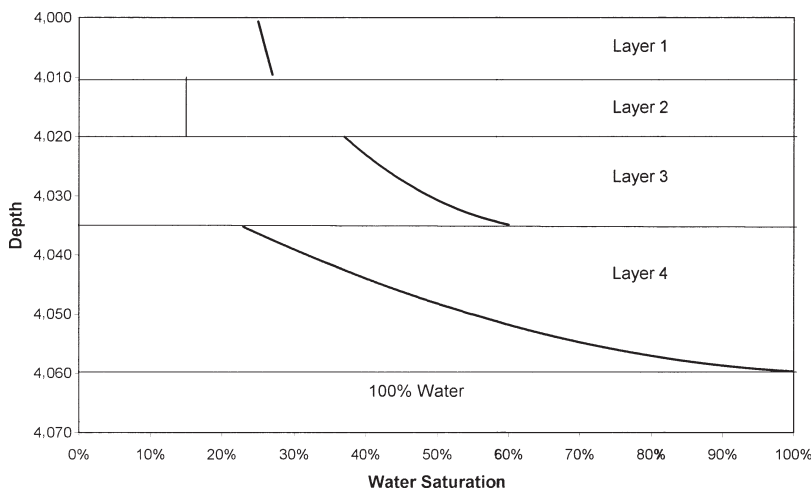


Figure 4-17. Water saturation profile.

Leverett J-Function

Capillary pressure data are obtained on small core samples that represent an extremely small part of the reservoir, and, therefore, it is necessary to combine all capillary data to classify a particular reservoir. The fact that the capillary pressure-saturation curves of nearly all naturally porous materials have many features in common has led to attempts to devise some general equation describing all such curves. Leverett (1941) approached the problem from the standpoint of dimensional analysis.

Realizing that capillary pressure should depend on the porosity, interfacial tension, and mean pore radius, Leverett defined the dimensionless function of saturation, which he called the J-function, as

$$J(S_w) = 0.21645 \frac{p_c}{\sigma} \sqrt{\frac{k}{\phi}} \quad (4-36)$$

where $J(S_w)$ = Leverett J-function

p_c = capillary pressure, psi

σ = interfacial tension, dynes/cm

k = permeability, md

ϕ = fractional porosity

In doing so, Leverett interpreted the ratio of permeability, k , to porosity, ϕ , as being proportional to the square of a mean pore radius.

The J-function was originally proposed as a means of converting all capillary-pressure data to a universal curve. There are significant differences in correlation of the J-function with water saturation from formation to formation, so that no universal curve can be obtained. For the same formation, however, this dimensionless capillary-pressure function serves quite well in many cases to remove discrepancies in the p_c versus S_w curves and reduce them to a common curve. This is shown for various unconsolidated sands in Figure 4-18.

Example 4-7

A laboratory capillary pressure test was conducted on a core sample taken from the Nameless Field. The core has a porosity and permeability of 16% and 80 md, respectively. The capillary pressure-saturation data are given as follows:

| S_w | p_c , psi |
|-------|-------------|
| 1.0 | 0.50 |
| 0.8 | 0.60 |
| 0.6 | 0.75 |
| 0.4 | 1.05 |
| 0.2 | 1.75 |

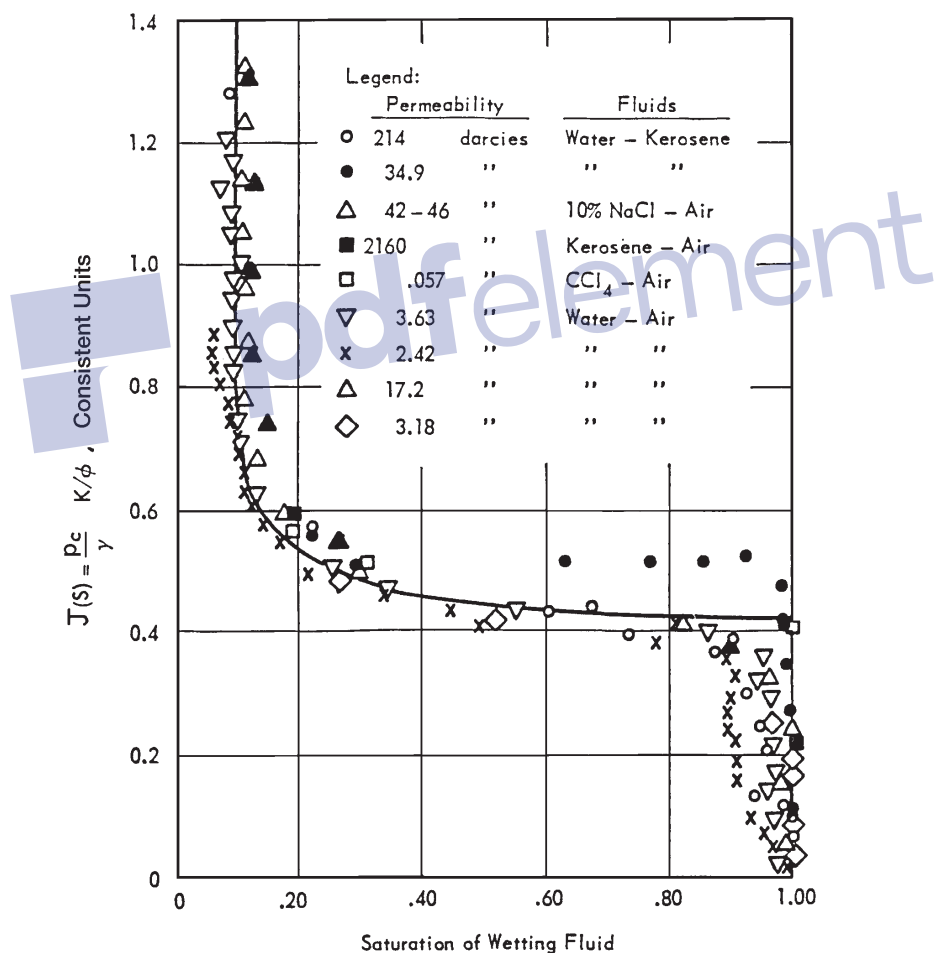


Figure 4-18. The Leverett J-function for unconsolidated sands. (After Leverett, 1941.)

The interfacial tension is measured at 50 dynes/cm. Further reservoir engineering analysis indicated that the reservoir is better described at a porosity value of 19% and an absolute permeability of 120 md. Generate the capillary pressure data for the reservoir.

Solution

Step 1. Calculate the J-function using the measured capillary pressure data.

$$J(S_w) = 0.21645 (p_c/50) \sqrt{80/0.16} = 0.096799 p_c$$

| S_w | p_c , psi | $J(S_w) = 0.096799 (p_c)$ |
|-------|-------------|---------------------------|
| 1.0 | 0.50 | 0.048 |
| 0.8 | 0.60 | 0.058 |
| 0.6 | 0.75 | 0.073 |
| 0.4 | 1.05 | 0.102 |
| 0.2 | 1.75 | 0.169 |

Step 2. Using the new porosity and permeability values, solve Equation 4-36 for the capillary pressure p_c .

$$p_c = J(S_w) \sigma / \left[0.21645 \sqrt{\frac{k}{\phi}} \right]$$

$$p_c = J(S_w) 50 / \left[0.21645 \sqrt{\frac{120}{0.19}} \right]$$

$$p_c = 9.192 J(S_w)$$

Step 3. Reconstruct the capillary pressure-saturation table.

| S_w | $J(S_w)$ | $p_c = 9.192 J(S_w)$ |
|-------|----------|----------------------|
| 1.0 | 0.048 | 0.441 |
| 0.8 | 0.058 | 0.533 |
| 0.6 | 0.073 | 0.671 |
| 0.4 | 0.102 | 0.938 |
| 0.2 | 0.169 | 1.553 |

Converting Laboratory Capillary Pressure Data

For experimental convenience, it is common in the laboratory determination of capillary pressure to use air-mercury or air-brine systems, rather than the actual water-oil system characteristic of the reservoir. Since the laboratory fluid system does not have the same surface tension as the reservoir system, it becomes necessary to convert laboratory capillary pressure to reservoir capillary pressure. By assuming that the Leverett J-function is a property of rock and does not change from the laboratory to the reservoir, we can calculate reservoir capillary pressure as shown below.

$$(p_c)_{\text{res}} = (p_c)_{\text{lab}} \frac{\sigma_{\text{res}}}{\sigma_{\text{lab}}}$$

Even after the laboratory capillary pressure has been corrected for surface tension, it may be necessary to make further corrections for permeability and porosity. The reason for this is that the core sample that was used in performing the laboratory capillary pressure test may not be representative of the average reservoir permeability and porosity. If we assume that the J-function will be invariant for a given rock type over a range of porosity and permeability values, then the reservoir capillary pressure can be expressed as

$$(p_c)_{\text{res}} = (p_c)_{\text{lab}} \frac{\sigma_{\text{res}}}{\sigma_{\text{lab}}} \sqrt{(\phi_{\text{res}} k_{\text{core}})/(\phi_{\text{core}} k_{\text{res}})} \quad (4-37)$$

where $(p_c)_{\text{res}}$ = reservoir capillary pressure
 σ_{res} = reservoir surface or interfacial tension
 k_{res} = reservoir permeability
 ϕ_{res} = reservoir porosity
 $(p_c)_{\text{lab}}$ = laboratory measured capillary pressure
 ϕ_{core} = core porosity
 k_{core} = core permeability

PERMEABILITY

Permeability is a property of the porous medium that measures the capacity and ability of the formation to transmit fluids. The rock permeability, k , is a very important rock property because it controls the directional

movement and the flow rate of the reservoir fluids in the formation. This rock characterization was first defined mathematically by Henry Darcy in 1856. In fact, the equation that defines permeability in terms of measurable quantities is called **Darcy's Law**.

Darcy developed a fluid flow equation that has since become one of the standard mathematical tools of the petroleum engineer. If a horizontal linear flow of an incompressible fluid is established through a core sample of length L and a cross-section of area A , then the governing fluid flow equation is defined as

$$v = -\frac{k}{\mu} \frac{dp}{dL} \quad (4-38)$$

where v = apparent fluid flowing velocity, cm/sec

k = proportionality constant, or permeability, Darcy's

μ = viscosity of the flowing fluid, cp

dp/dL = pressure drop per unit length, atm/cm

The velocity, v , in Equation 4-38 is not the actual velocity of the flowing fluid but is the apparent velocity determined by dividing the flow rate by the cross-sectional area across which fluid is flowing. Substituting the relationship, q/A , in place of v in Equation 4-38 and solving for q results in

$$q = -\frac{kA}{\mu} \frac{dp}{dL} \quad (4-39)$$

where q = flow rate through the porous medium, cm³/sec

A = cross-sectional area across which flow occurs, cm²

With a flow rate of one cubic centimeter per second across a cross-sectional area of one square centimeter with a fluid of one centipoise viscosity and a pressure gradient at one atmosphere per centimeter of length, it is obvious that k is unity. For the units described above, k has been arbitrarily assigned a unit called *Darcy* in honor of the man responsible for the development of the theory of flow through porous media. Thus, when all other parts of Equation 4-39 have values of unity, k has a value of one Darcy.

One Darcy is a relatively high permeability as the permeabilities of most reservoir rocks are less than one Darcy. In order to avoid the use of

fractions in describing permeabilities, the term *millidarcy* is used. As the term indicates, one millidarcy, i.e., 1 md, is equal to one-thousandth of one Darcy or,

$$1 \text{ Darcy} = 1000 \text{ md}$$

The negative sign in Equation 4-39 is necessary as the pressure increases in one direction while the length increases in the opposite direction.

Equation 4-39 can be integrated when the geometry of the system through which fluid flows is known. For the simple linear system shown in Figure 4-19, the integration is performed as follows:

$$q \int_0^L dL = -\frac{kA}{\mu} \int_{p_1}^{p_2} dp$$

Integrating the above expression yields:

$$qL = -\frac{kA}{\mu} (p_2 - p_1)$$

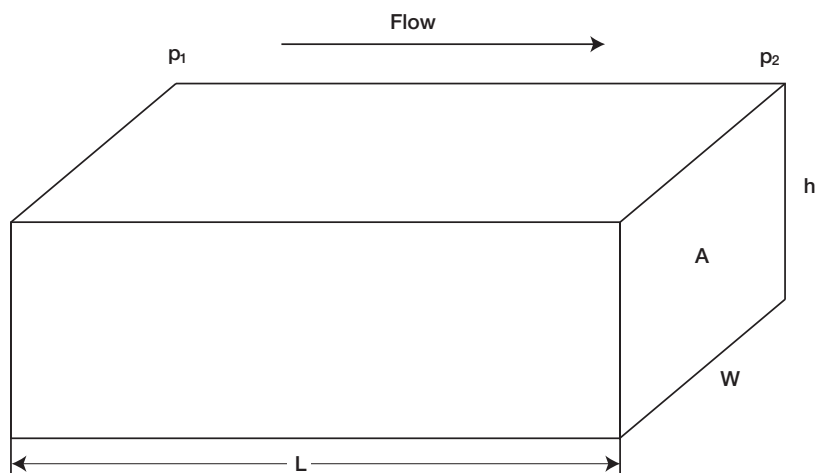


Figure 4-19. Linear flow model.

It should be pointed out that the volumetric flow rate, q , is constant for liquids because the density does not change significantly with pressure.

Since p_1 is greater than p_2 , the pressure terms can be rearranged, which will eliminate the negative term in the equation. The resulting equation is:

$$q = \frac{kA (p_1 - p_2)}{\mu L} \quad (4-40)$$

Equation 4-40 is the conventional linear flow equation used in fluid flow calculations.

Standard laboratory analysis procedures will generally provide reliable data on permeability of core samples. If the rock is not homogeneous, the whole core analysis technique will probably yield more accurate results than the analysis of core plugs (small pieces cut from the core). Procedures that have been used for improving the accuracy of the permeability determination include cutting the core with an oil-base mud, employing a pressure-core barrel, and conducting the permeability tests with reservoir oil.

Permeability is reduced by overburden pressure, and this factor should be considered in estimating permeability of the reservoir rock in deep wells because permeability is an isotropic property of porous rock in some defined regions of the system; that is, it is directional. Routine core analysis is generally concerned with plug samples drilled parallel to bedding planes and, hence, parallel to direction of flow in the reservoir. These yield horizontal permeabilities (k_h).

The measured permeability on plugs that are drilled perpendicular to bedding planes is referred to as vertical permeability (k_v). Figure 4-20 shows a schematic illustration of the concept of the core plug and the associated permeability.

As shown in Figure 4-20, there are several factors that must be considered as possible sources of error in determining reservoir permeability. These factors are:

1. Core sample may not be representative of the reservoir rock because of reservoir heterogeneity.
2. Core recovery may be incomplete.
3. Permeability of the core may be altered when it is cut, or when it is cleaned and dried in preparation for analysis. This problem is likely to occur when the rock contains reactive clays.
4. Sampling process may be biased. There is a temptation to select the best parts of the core for analysis.

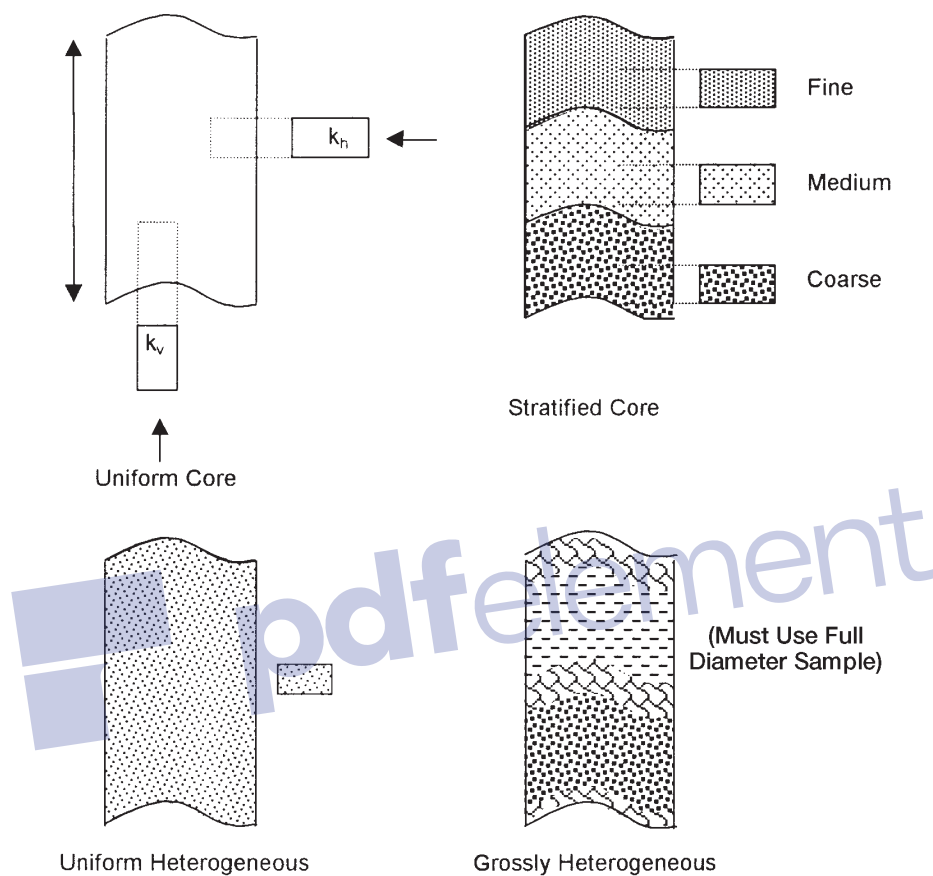


Figure 4-20. Representative samples of porous media.

Permeability is measured by passing a fluid of known viscosity μ through a core plug of measured dimensions (A and L) and then measuring flow rate q and pressure drop Δp . Solving Equation 4-40 for the permeability, gives:

$$k = \frac{q \mu L}{A \Delta p}$$

where L = length of core, cm
 A = cross-sectional area, cm^2

The following conditions must exist during the measurement of permeability:

- Laminar (viscous) flow
- No reaction between fluid and rock
- Only single phase present at 100% pore space saturation

This measured permeability at 100% saturation of a single phase is called the *absolute permeability* of the rock.

Example 4-8

A brine is used to measure the absolute permeability of a core plug. The rock sample is 4 cm long and 3 cm^2 in cross section. The brine has a viscosity of 1.0 cp and is flowing a constant rate of 0.5 cm^3/sec under a 2.0 atm pressure differential. Calculate the absolute permeability.

Solution

Applying Darcy's equation, i.e., Equation 4-40, gives:

$$0.5 = \frac{(k) (3) (2)}{(1) (4)}$$

$$k = 0.333 \text{ Darcys}$$

Example 4-9

Rework the above example assuming that an oil of 2.0 cp is used to measure the permeability. Under the same differential pressure, the flow rate is 0.25 cm^3/sec .

Solution

Applying Darcy's equation yields:

$$0.25 = \frac{(k) (3) (2)}{(2) (4)}$$

$$k = 0.333 \text{ Darcys}$$

Dry gas is usually used (air, N₂, He) in permeability determination because of its convenience and availability and to minimize fluid-rock reaction.

The measurement of the permeability should be restricted to the low (laminar/viscous) flow rate region, where the pressure remains proportional to flow rate within the experimental error. For high flow rates, Darcy's equation as expressed by Equation 4-40 is inappropriate to describe the relationship of flow rate and pressure drop.

In using dry gas in measuring the permeability, the gas volumetric flow rate q varies with pressure because the gas is a highly compressible fluid. Therefore, the value of q at the average pressure in the core must be used in Equation 4-40. Assuming the used gases follow the ideal gas behavior (at low pressures), the following relationships apply:

$$p_1 V_1 = p_2 V_2 = p_m V_m$$

In terms of the flow rate q , the above equation can be equivalently expressed as:

$$p_1 q_1 = p_2 q_2 = p_m q_m \quad (4-41)$$

with the mean pressure p_m expressed as:

$$p_m = \frac{p_1 + p_2}{2}$$

where p_1, p_2, p_m = inlet, outlet, and mean pressures, respectively, atm
 V_1, V_2, V_m = inlet, outlet, and mean gas volume, respectively, cm³
 q_1, q_2, q_m = inlet, outlet, and mean gas flow rate, respectively, cm³/sec

The gas flow rate is usually measured at base (atmospheric) pressure p_b and, therefore, the term Q_{gsc} is introduced into Equation 4-41 to produce:

$$Q_{gsc} p_b = q_m p_m$$

where Q_{gsc} = gas flow rate at standard conditions, cm^3/sec
 p_b = base pressure (atmospheric pressure), atm

Substituting Darcy's Law in the above expression gives

$$Q_{gsc} p_b = \frac{k A (p_1 - p_2)}{\mu_g L} \left(\frac{p_1 + p_2}{2} \right)$$

or

$$Q_{gsc} = \frac{k A (p_1^2 - p_2^2)}{2 \mu_g L p_b} \quad (4-42)$$

where k = absolute permeability, Darcys

μ_g = gas viscosity, cp

p_b = base pressure, atm

p_1 = inlet (upstream) pressure, atm

p_2 = outlet (downstream) pressure, atm

L = length of the core, cm

A = cross-sectional area, cm^2

Q_{gsc} = gas flow rate at standard conditions, cm^3/sec

The Klinkenberg Effect

Klinkenberg (1941) discovered that permeability measurements made with air as the flowing fluid showed different results from permeability measurements made with a liquid as the flowing fluid. The permeability of a core sample measured by flowing air is always greater than the permeability obtained when a liquid is the flowing fluid. Klinkenberg postulated, on the basis of his laboratory experiments, that liquids had a zero velocity at the sand grain surface, while gases exhibited some finite velocity at the sand grain surface. In other words, the gases exhibited *slippage* at the sand grain surface. This slippage resulted in a higher flow rate for the gas at a given pressure differential. Klinkenberg also found that for a given porous medium as the mean pressure increased the calculated permeability decreased.

Mean pressure is defined as upstream flowing plus downstream flowing pressure divided by two, [$p_m = (p_1 + p_2)/2$]. If a plot of measured permeability versus $1/p_m$ were extrapolated to the point where $1/p_m = 0$, in other words, where $p_m = \text{infinity}$, this permeability would be approximately equal to the liquid permeability. A graph of this nature is shown in Figure 4-21. The absolute permeability is determined by extrapolation as shown in Figure 4-21.

The magnitude of the Klinkenberg effect varies with the core permeability and the type of the gas used in the experiment as shown in Figures 4-22 and 4-23. The resulting straight-line relationship can be expressed as

$$k_g = k_L + c \left[\frac{1}{p_m} \right] \quad (4-43)$$

where k_g = measured gas permeability

p_m = mean pressure

k_L = equivalent liquid permeability, i.e., absolute permeability, k

c = slope of the line

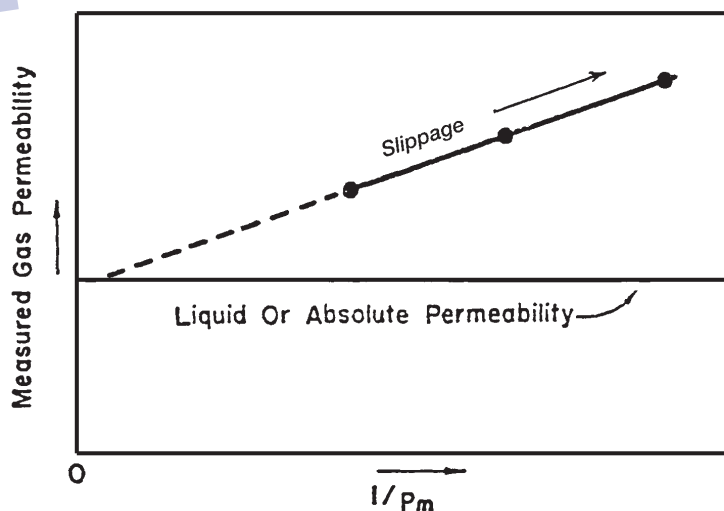


Figure 4-21. The Klinkenberg effect in gas permeability measurements.

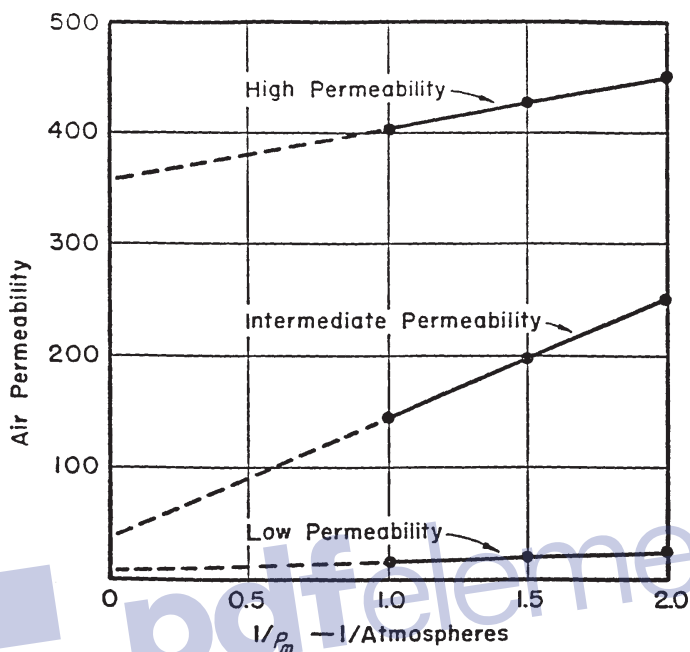


Figure 4-22. Effect of permeability on the magnitude of the Klinkenberg effect. (After Cole, F., 1969.)

Klinkenberg suggested that the slope c is a function of the following factors:

- Absolute permeability k , i.e., permeability of medium to a single phase completely filling the pores of the medium k_L .
- Type of the gas used in measuring the permeability, e.g., air.
- Average radius of the rock capillaries.

Klinkenberg expressed the slope c by the following relationship:

$$c = bk_L \quad (4-44)$$

where k_L = equivalent liquid permeability, i.e., absolute permeability, k
 b = constant that depends on the size of the pore openings and is inversely proportional to radius of capillaries.

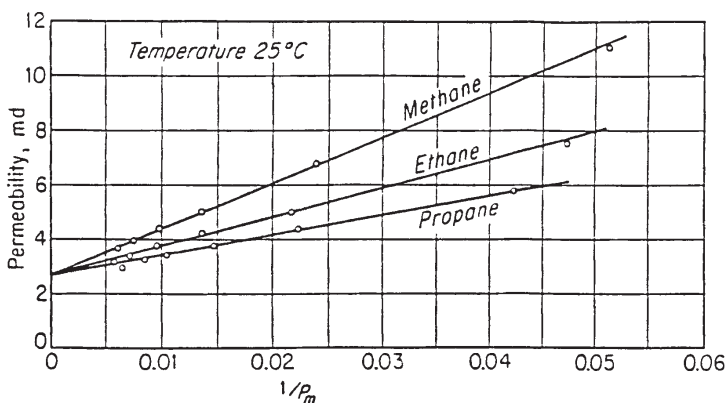


Figure 4-23. Effect of gas pressure on measured permeability for various gases. (After Calhoun, J., 1976.)

Combining Equation 4-44 with 4-43 gives:

$$k_g = k_L + (b k_L) \left[\frac{1}{p_m} \right] \quad (4-45)$$

where k_g is the gas permeability as measured at the average pressure p_m .

Jones (1972) studied the gas slip phenomena for a group of cores for which porosity, liquid permeability k_L (absolute permeability), and air permeability were determined. He correlated the parameter b with the liquid permeability by the following expression:

$$b = 6.9 k_L^{-0.36} \quad (4-46)$$

The usual measurement of permeability is made with air at mean pressure just above atmospheric pressure (1 atm). To evaluate the slip phenomenon and the Klinkenberg effect, it is necessary to at least measure the gas permeability at two mean-pressure levels. In the absence of such data, Equations 4-45 and 4-46 can be combined and arranged to give:

$$6.9 k_L^{0.64} + p_m k_L - p_m k_g = 0 \quad (4-47)$$

where p_m = mean pressure, psi

k_g = air permeability at p_m , psi

k_L = absolute permeability (k), md

Equation 4-47 can be used to calculate the absolute permeability when only one gas permeability measurement (k_g) of a core sample is made at p_m . This nonlinear equation can be solved iteratively by using the Newton-Raphson iterative methods. The proposed solution method can be conveniently written as

$$k_{i+1} = k_i - \frac{f(k_i)}{f'(k_i)}$$

where k_i = initial guess of the absolute permeability, md

k_{i+1} = new permeability value to be used for the next iteration

i = iteration level

$f(k_i)$ = Equation 4-47 as evaluated by using the assumed value of k_i

$f'(k_i)$ = first-derivative of Equation 4-47 as evaluated at k_i

The first derivative of Equation 4-47 with respect to k_i is:

$$f'(k_i) = 4.416 k_i^{-0.36} + p_m \quad (4-48)$$

The iterative procedure is repeated until convergence is achieved when $f(k_i)$ approaches zero or when no changes in the calculated values of k_i are observed.

Example 4-10

The permeability of a core plug is measured by air. Only one measurement is made at a mean pressure of 2.152 psi. The air permeability is 46.6 md. Estimate the absolute permeability of the core sample. Compare the result with the actual absolute permeability of 23.66 md.

Solution

Step 1. Substitute the given values of p_m and k_g into Equations 4-47 and 4-48, to give:

$$f(k_i) = 6.9 k_i^{0.64} + 2.152 k_i - (2.152)(46.6) \quad f'(k_i) = 4.416 k_i^{-0.36} + 2.152$$

Step 2. Assume $k_i = 30$ and apply the Newton-Raphson method to find the required solution as shown below.

| i | k_i | $f(k_i)$ | $f'(k_i)$ | k_{i+1} |
|-----|--------|----------|-----------|-----------|
| 1 | 30.000 | 25.12 | 3.45 | 22.719 |
| 2 | 22.719 | -0.466 | 3.29 | 22.861 |
| 3 | 22.861 | 0.414 | 3.29 | 22.848 |

After three iterations, the Newton-Raphson method converges to an absolute value for the permeability of 22.848 md.

Equation 4-39 can be expanded to describe flow in any porous medium where the geometry of the system is not too complex to integrate. For example, the flow into a well bore is not linear, but is more often radial. Figure 4-24 illustrates the type of flow that is typical of that occurring in the vicinity of a producing well. For a radial flow, Darcy's equation in a differential form can be written as:

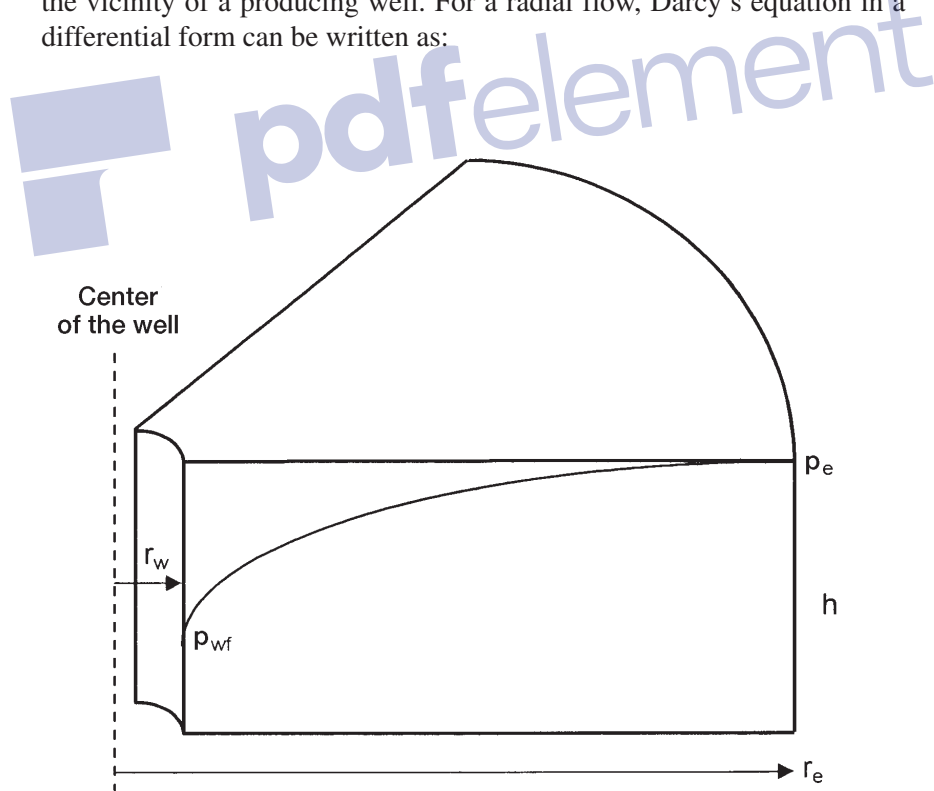


Figure 4-24. Radial flow model.

$$q = \frac{k A}{\mu} \frac{dp}{dr}$$

Integrating Darcy's equation gives:

$$q \int_{r_w}^{r_e} dr = \frac{kA}{\mu} \int_{P_{wf}}^{P_e} dp$$

The term dL has been replaced by dr as the length term has now become a radius term. The minus sign is no longer required for the radial system shown in Figure 4-24 as the radius increases in the same direction as the pressure. In other words, as the radius increases going away from the well bore, the pressure also increases. At any point in the reservoir, the cross-sectional area across which flow occurs will be the surface area of a cylinder, which is $2\pi rh$. Since the cross-sectional area is related to r , then A must be included within the integral sign as follows:

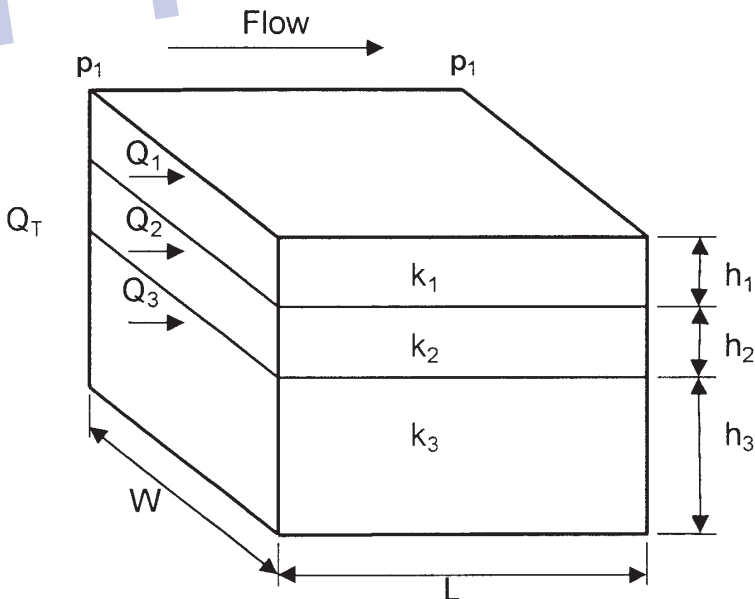


Figure 4-25. Linear flow through layered beds.

$$q \int_{r_w}^{r_e} \frac{dr}{2 \pi r h} = \frac{k}{\mu} \int_{p_{wf}}^{p_e} dp$$

rearranging

$$\frac{q}{2 \pi h} \int_{r_w}^{r_e} \frac{dr}{r} = \frac{k}{\mu} \int_{p_{wf}}^{p_e} dp$$

and integrating

$$\frac{q}{2 \pi h} (\ln r_e - \ln r_w) = \frac{k}{\mu} (p_e - p_{wf})$$

Solving for the flow rate, q , results in:

$$q = \frac{2 \pi k h (p_e - p_{wf})}{\mu \ln (r_e/r_w)} \quad (4-49)$$

The above equation assumes that the reservoir is homogeneous and is completely saturated with a single liquid phase (appropriate modifications will be discussed in later sections to account for the presence of other fluids), where:

q = flow rate, reservoir cm^3/sec

k = absolute permeability, Darcy

h = thickness, cm

r_e = drainage radius, cm

r_w = well bore radius, cm

p_e = pressure at drainage radius, atm

p_{wf} = bottom-hole flowing pressure

μ = viscosity, cp

Averaging Absolute Permeabilities

The most difficult reservoir properties to determine usually are the level and distribution of the absolute permeability throughout the reservoir. They are more variable than porosity and more difficult to measure. Yet an adequate knowledge of permeability distribution is critical to the

prediction of reservoir depletion by any recovery process. It is rare to encounter a homogeneous reservoir in actual practice. In many cases, the reservoir contains distinct layers, blocks, or concentric rings of varying permeabilities. Also, because smaller-scale heterogeneities always exist, core permeabilities must be averaged to represent the flow characteristics of the entire reservoir or individual reservoir layers (units). The proper way of averaging the permeability data depends on how permeabilities were distributed as the rock was deposited.

There are three simple permeability-averaging techniques that are commonly used to determine an appropriate average permeability to represent an equivalent homogeneous system. These are:

- Weighted-average permeability
- Harmonic-average permeability
- Geometric-average permeability

Weighted-Average Permeability

This averaging method is used to determine the average permeability of layered-parallel beds with different permeabilities. Consider the case where the flow system is comprised of three parallel layers that are separated from one another by thin impermeable barriers, i.e., no cross-flow, as shown in Figure 4-25. All the layers have the same width w with a cross-sectional area of A .

The flow from each layer can be calculated by applying Darcy's equation in a linear form as expressed by Equation 4-40, to give:

Layer 1

$$q_1 = \frac{k_1 w h_1 \Delta p}{\mu L}$$

Layer 2

$$q_2 = \frac{k_2 w h_2 \Delta p}{\mu L}$$

Layer 3

$$q_3 = \frac{k_3 w h_3 \Delta p}{\mu L}$$

The total flow rate from the entire system is expressed as

$$q_t = \frac{k_{\text{avg}} w h_t \Delta p}{\mu L}$$

where q_t = total flow rate

k_{avg} = average permeability for the entire model

w = width of the formation

$\Delta p = p_1 - p_2$

h_t = total thickness

The total flow rate q_t is equal to the sum of the flow rates through each layer or:

$$q_t = q_1 + q_2 + q_3$$

Combining the above expressions gives:

$$\frac{k_{\text{avg}} w h_t \Delta p}{\mu L} = \frac{k_1 w h_1 \Delta p}{\mu L} + \frac{k_2 w h_2 \Delta p}{\mu L} + \frac{k_3 w h_3 \Delta p}{\mu L}$$

or

$$k_{\text{avg}} h_t = k_1 h_1 + k_2 h_2 + k_3 h_3$$

$$k_{\text{avg}} = \frac{k_1 h_1 + k_2 h_2 + k_3 h_3}{h_t}$$

The average absolute permeability for a parallel-layered system can be expressed in the following form:

$$k_{\text{avg}} = \frac{\sum_{j=1}^n k_j h_j}{\sum_{j=1}^n h_j} \quad (4-50)$$

Equation 4-50 is commonly used to determine the average permeability of a reservoir from core analysis data.

Figure 4-26 shows a similar layered system with variable layers width. Assuming no cross-flow between the layers, the average permeability can be approximated in a manner similar to the above derivation to give:

$$k_{\text{avg}} = \frac{\sum_{j=1}^n k_j A_j}{\sum_{j=1}^n A_j} \quad (4-51)$$

with

$$A_j = h_j w_j$$

where A_j = cross-sectional area of layer j

w_j = width of layer j

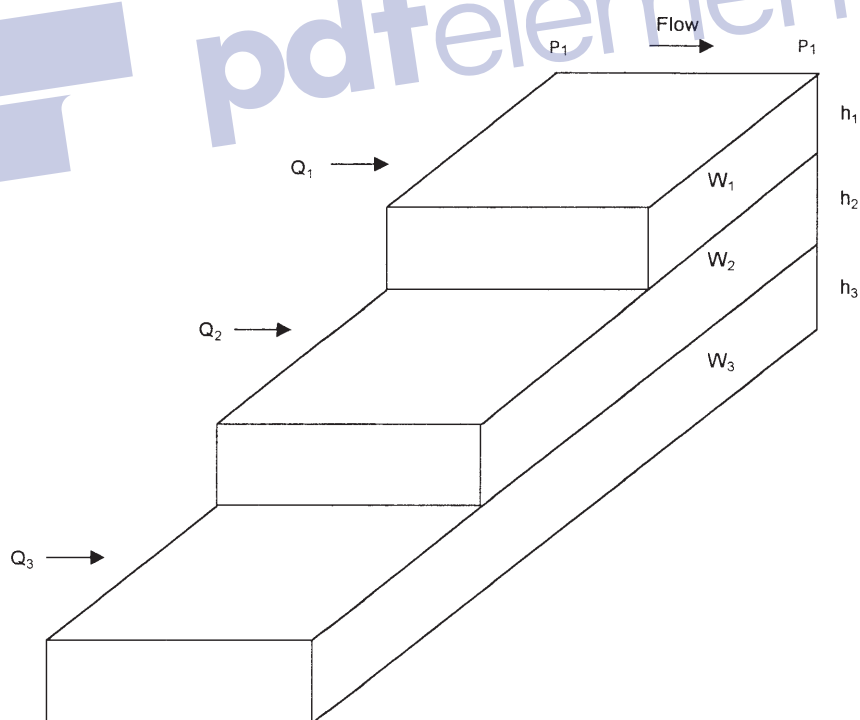


Figure 4-26. Linear flow through layered beds with variable area.

Example 4-11

Given the following permeability data from a core analysis report, calculate the average permeability of the reservoir.

| Depth, ft | Permeability, md |
|-----------|------------------|
| 3998-4002 | 200 |
| 4002-4004 | 130 |
| 4004-4006 | 170 |
| 4006-4008 | 180 |
| 4008-4010 | 140 |

Solution

| h_i , ft | k_i | $h_i k_i$ |
|------------|-------|-----------------------|
| 4 | 200 | 800 |
| 2 | 130 | 260 |
| 2 | 170 | 340 |
| 2 | 180 | 360 |
| 2 | 140 | 280 |
| $h_t = 12$ | | $\sum h_i k_i = 2040$ |

$$k_{\text{avg}} = \frac{2040}{12} = 170 \text{ md}$$

Harmonic-Average Permeability

Permeability variations can occur laterally in a reservoir as well as in the vicinity of a well bore. Consider Figure 4-27, which shows an illustration of fluid flow through a series combination of beds with different permeabilities.

For a steady-state flow, the flow rate is constant and the total pressure drop Δp is equal to the sum of the pressure drops across each bed, or

$$\Delta p = \Delta p_1 + \Delta p_2 + \Delta p_3$$

Substituting for the pressure drop by applying Darcy's equation, i.e., Equation 4-40, gives:

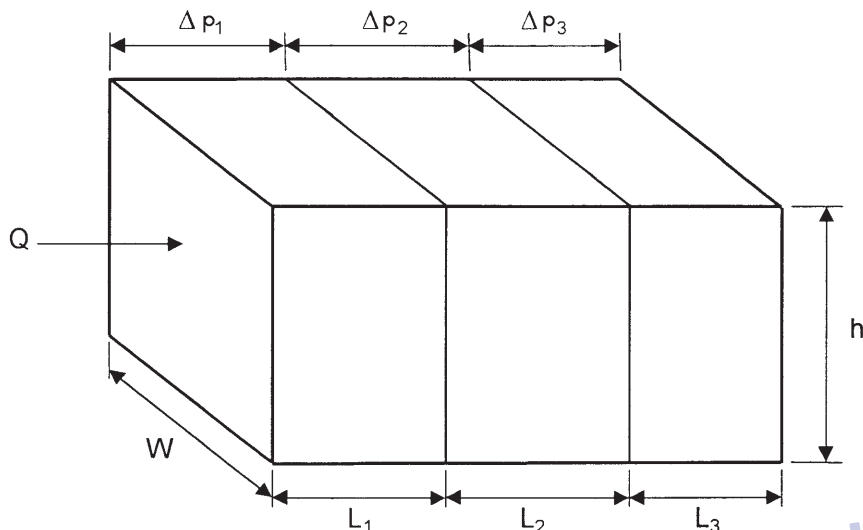


Figure 4-27. Linear flow through series beds.

$$\frac{q\mu L}{A k_{\text{avg}}} = \frac{q\mu L_1}{A k_1} + \frac{q\mu L_2}{A k_2} + \frac{q\mu L_3}{A k_3}$$

Canceling the identical terms and simplifying gives:

$$k_{\text{avg}} = \frac{L}{(L/k)_1 + (L/k)_2 + (L/k)_3}$$

The above equation can be expressed in a more generalized form to give:

$$k_{\text{avg}} = \frac{\sum_{i=1}^n L_i}{\sum_{i=1}^n (L/k)_i} \quad (4-52)$$

where L_i = length of each bed

k_i = absolute permeability of each bed

In the radial system shown in Figure 4-28, the above averaging methodology can be applied to produce the following generalized expression:

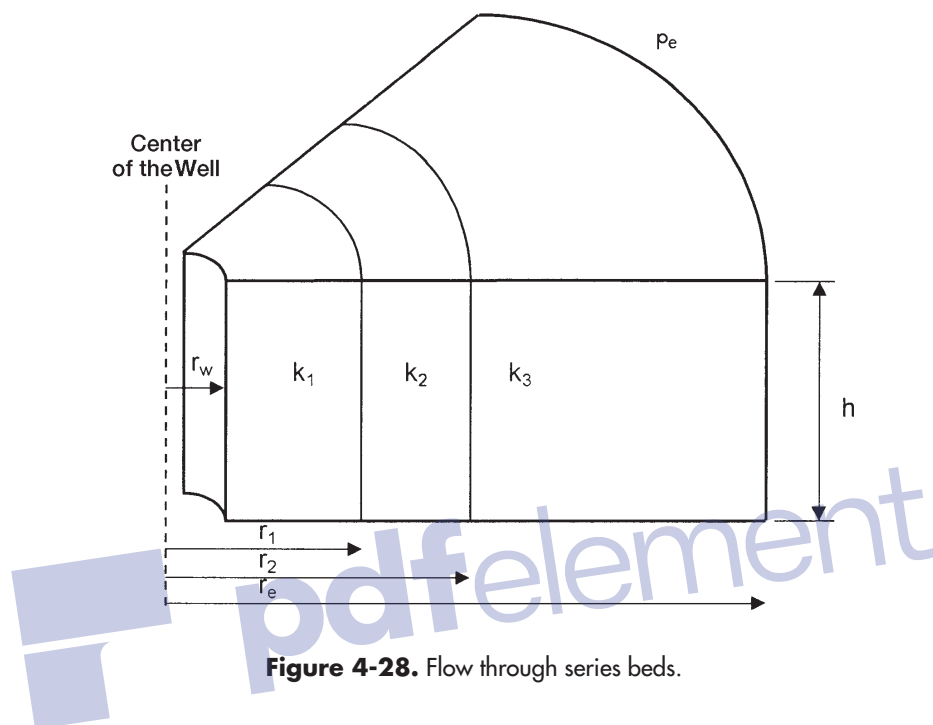


Figure 4-28. Flow through series beds.

$$k_{avg} = \frac{\ln(r_e/r_w)}{\sum_{j=1}^n \left[\frac{\ln(r_j/r_{j-1})}{k_j} \right]} \quad (4-53)$$

The relationship in Equation 4-53 can be used as a basis for estimating a number of useful quantities in production work. For example, the effects of mud invasion, acidizing, or well shooting can be estimated from it.

Example 4-12

A hydrocarbon reservoir is characterized by five distinct formation segments that are connected in series. Each segment has the same formation thickness. The length and permeability of each section of the five-bed reservoir are given below:

| Length, ft | Permeability, md |
|------------|------------------|
| 150 | 80 |
| 200 | 50 |
| 300 | 30 |
| 500 | 20 |
| 200 | 10 |

Calculate the average permeability of the reservoir by assuming:

- Linear flow system
- Radial flow system

Solution

For a linear system:

| L_i , ft | k_i | L_i/k_i |
|------------|-------|---------------------------|
| 150 | 80 | 1.8750 |
| 200 | 50 | 4.0000 |
| 300 | 30 | 10.0000 |
| 500 | 20 | 25.0000 |
| 200 | 10 | 20.0000 |
| 1350 | | $\Sigma L_i/k_i = 60.875$ |

Using Equation 4-52 gives:

$$k_{\text{avg}} = \frac{1350}{60.875} = 22.18 \text{ md}$$

For a radial system:

The solution of the radial system can be conveniently expressed in the following tabulated form. The solution is based on Equation 4-53 and assuming a well bore radius of 0.25 ft:

| Segment | r_i , ft | $\ln(r_i/r_{iB1})$ | k_i | $[\ln(r_i/r_{iB1})]/k_i$ |
|-----------|------------|--------------------|-------|--------------------------|
| well bore | 0.25 | — | — | — |
| 1 | 150 | 6.397 | 80 | 0.080 |
| 2 | 350 | 0.847 | 50 | 0.017 |
| 3 | 650 | 0.619 | 30 | 10.021 |
| 4 | 1150 | 0.571 | 20 | 0.029 |
| 5 | 1350 | 0.160 | 10 | 0.016 |

0.163

From Equation 4-53,

$$k_{\text{avg}} = \frac{\ln(1350/0.25)}{0.163} = 52.72 \text{ md}$$

Geometric-Average Permeability

Warren and Price (1961) illustrated experimentally that the most probable behavior of a heterogeneous formation approaches that of a uniform system having a permeability that is equal to the geometric average. The geometric average is defined mathematically by the following relationship:

$$k_{\text{avg}} = \exp \left[\frac{\sum_{i=1}^n (h_i \ln(k_i))}{\sum_{i=1}^n h_i} \right] \quad (4-54)$$

where k_i = permeability of core sample i
 h_i = thickness of core sample i
 n = total number of samples

If the thicknesses (h_i) of all core samples are the same, Equation 4-57 can be simplified as follows:

$$k_{\text{avg}} = (k_1 k_2 k_3 \dots k_n)^{\frac{1}{n}} \quad (4-55)$$

Example 4-13

Given the following core data, calculate the geometric average permeability:

| Sample | h_i , ft | k_i , md |
|--------|------------|------------|
| 1 | 1.0 | 10 |
| 2 | 1.0 | 30 |
| 3 | 0.5 | 100 |
| 4 | 1.5 | 40 |
| 5 | 2.0 | 80 |
| 6 | 1.5 | 70 |
| 7 | 1.0 | 15 |
| 8 | 1.0 | 50 |
| 9 | 1.5 | 35 |
| 10 | 0.5 | 20 |

Solution

| Sample | h_i , ft | k_i , md | $h_i * \ln(k_i)$ |
|--------|------------|------------|------------------|
| 1 | 1.0 | 10 | 2.303 |
| 2 | 1.0 | 30 | 3.401 |
| 3 | 0.5 | 100 | 2.303 |
| 4 | 1.5 | 40 | 5.533 |
| 5 | 2.0 | 80 | 8.764 |
| 6 | 1.5 | 70 | 6.373 |
| 7 | 1.0 | 15 | 2.708 |
| 8 | 1.0 | 50 | 3.912 |
| 9 | 1.5 | 35 | 5.333 |
| 10 | 0.5 | 20 | 1.498 |
| 11.5 | | | 42.128 |

$$k_{\text{avg}} = \exp \left[\frac{42.128}{11.5} \right] = 39 \text{ md}$$

Absolute Permeability Correlations

The determination of connate water by capillary-pressure measurements has allowed the evaluation of connate-water values on samples of varying permeability and within a given reservoir to a wider extent and to a greater accuracy than was possible beforehand. These measurements have accumulated to the point where it is possible to correlate connate-water content with the permeability of the sample in a given reservoir and to a certain extent between reservoirs.

Calhoun (1976) suggested that in an ideal pore configuration of uniform structure, the irreducible connate water would be independent of permeability, lower permeabilities being obtained merely by a scaled reduction in particle size. In an actual porous system formed by deposition of graded particles or by some other natural means, the connate water might be expected to increase as permeability decreases. This conclusion results from the thought that lower permeabilities result from increasing non-uniformity of pore structure by a gradation of particles rather than by a scaled reduction of particles. In this sense, connate-water content is a function of permeability only insofar as permeability is dependent upon the variation of pore structure. Thus, for unconsolidated sands formed of uniform particles of one size, the connate-water content would be independent of permeability.

Calhoun (1976) pointed out that any correlation found between various reservoir properties would be anticipated to apply only within the rather narrow limits of a single reservoir or perhaps of a given formation. Beyond these bounds, a general correspondence between permeability and pore structure would not be known. It would be anticipated, however, that for formations of similar characteristics, a similar dependence of permeability on pore structure and, consequently, similar correlation of connate water and permeability would be found.

It has been generally considered for many years that connate water reached higher values in lower permeabilities. This observation amounted to nothing more than a trend. The data from capillary pressure measurements have indicated that the relationship is semi-logarithmic, although it is not yet certain from published data that this is the exact relationship. No generalizations are apparent from this amount of data, although it can now be quite generally stated that within a given reservoir the connate water (if an irreducible value) will increase proportionally to the decrease in the logarithm of the permeability. It is apparent, moreover, that one cannot state the value of connate water expected in any new formation unless one knows something of its pore makeup.

Experience indicates a general relationship between reservoir porosity (ϕ) and irreducible water saturation (S_{wc}) provided the rock type and/or the grain size does not vary over the zone of interest. This relationship is defined by the equation

$$C = (S_{wi}) (\phi)$$

where C is a constant for a particular rock type and/or grain size.

Several investigators suggest that the constant C that describes the rock type can be correlated with the absolute permeability of the rock. Two commonly used empirical methods are the Timur equation and the Morris-Biggs equation.

The Timur Equation

Timur (1968) proposed the following expression for estimating the permeability from connate-water saturation and porosity:

$$k = 8.58102 \frac{\phi^{4.4}}{S_{wc}^2} \quad (4-56)$$

The Morris-Biggs Equation

Morris and Biggs (1967) presented the following two expressions for estimating the permeability if oil and gas reservoirs:

For an oil reservoir:

$$k = 62.5 \left(\frac{\phi^3}{S_{wc}} \right)^2 \quad (4-57)$$

For a gas reservoir:

$$k = 2.5 \left(\frac{\phi^3}{S_{wc}} \right)^2 \quad (4-58)$$

where k = absolute permeability, Darcy

ϕ = porosity, fraction

S_{wc} = connate-water saturation, fraction

Example 4-14

Estimate the absolute permeability of an oil zone with a connate-water saturation and average porosity of 25% and 19%, respectively.

Solution

Applying the Timur equation:

$$k = 8.58102 \frac{(0.19)^{4.4}}{(0.25)^2} = 0.0921 \text{ Darcy}$$

From the Morris and Biggs correlation:

$$k = 62.5 \left[\frac{(0.29)^3}{0.25} \right]^2 = 0.047 \text{ Darcy}$$

In the previous discussion of Darcy's Law and absolute permeability measurements, it was assumed that the entire porous medium is fully saturated with a single phase, i.e., 100% saturation. In a hydrocarbon reservoir, however, the rocks are usually saturated with two or more fluids.

Therefore, the concept of absolute permeability must be modified to describe the fluid flowing behavior when more than one fluid is present

in the reservoir. If a core sample is partially saturated with a fluid (other than the test fluid) and both saturations are maintained constant throughout the flow, the measured permeability to the test fluid will be reduced below the permeability, which could be measured if the core were 100 percent saturated with the test fluid.

As the saturation of a particular phase decreases, the permeability to that phase also decreases. The measured permeability is referred to as the *effective permeability* and is a relative measure of the conductance of the porous medium for one fluid when the medium is saturated with more than one fluid. This implies that the effective permeability is an associated property with each reservoir fluid, i.e., gas, oil, and water. These effective permeabilities for the three reservoir fluids are represented by:

$$\begin{aligned}k_g &= \text{effective gas permeability} \\k_o &= \text{effective oil permeability} \\k_w &= \text{effective water permeability}\end{aligned}$$

One of the phenomena of multiphase effective permeabilities is that the sum of the effective permeabilities is always less than or equal to the absolute permeability, i.e.,

$$k_g + k_o + k_w \leq k$$

The effective permeability is used mathematically in Darcy's Law in place of the absolute permeability. For example, the expression for flow through the linear system under a partial saturation of oil is written

$$q_o = \frac{k_o A (p_1 - p_2)}{\mu_o L} \quad (4-59)$$

where q_o = oil flow rate, cc/sec

μ_o = oil viscosity, cm

k_o = oil effective permeability, Darcys

Effective permeabilities are normally measured directly in the laboratory on small core samples. Owing to the many possible combinations of saturation for a single medium, however, laboratory data are usually summarized and reported as relative permeability. Relative permeability is defined as the ratio of the effective permeability to a given fluid at a definite saturation to the permeability at 100% saturation. The terminology

most widely used is simply k_g/k , k_o/k , k_w/k , meaning the relative permeability to gas, oil, and water, respectively. Since k is a constant for a given porous material, the relative permeability varies with the fluid saturation in the same fashion as does the effective permeability. The relative permeability to a fluid will vary from a value of zero at some low saturation of that fluid to a value of 1.0 at 100% saturation of that fluid. Thus, the relative permeability can be expressed symbolically as

$$k_{rg} = \frac{k_g}{k}$$

$$k_{ro} = \frac{k_o}{k}$$

$$k_{rw} = \frac{k_w}{k}$$

which are relative permeabilities to gas, oil, and water, respectively. A comprehensive treatment of the relative permeability is presented in Chapter 5.

ROCK COMPRESSIBILITY

A reservoir thousands of feet underground is subjected to an overburden pressure caused by the weight of the overlying formations. Overburden pressures vary from area to area depending on factors such as depth, nature of the structure, consolidation of the formation, and possibly the geologic age and history of the rocks. Depth of the formation is the most important consideration, and a typical value of overburden pressure is approximately one psi per foot of depth.

The weight of the overburden simply applies a compressive force to the reservoir. The pressure in the rock pore spaces does not normally approach the overburden pressure. A typical pore pressure, commonly referred to as the reservoir pressure, is approximately 0.5 psi per foot of depth, assuming that the reservoir is sufficiently consolidated so the overburden pressure is not transmitted to the fluids in the pore spaces.

The pressure difference between overburden and internal pore pressure is referred to as the *effective overburden* pressure. During pressure depletion operations, the internal pore pressure decreases and, therefore, the effective overburden pressure increases. This increase causes the following effects:

- The bulk volume of the reservoir rock is reduced.
- Sand grains within the pore spaces expand.

These two volume changes tend to reduce the pore space and, therefore, the porosity of the rock. Often these data exhibit relationships with both porosity and the effective overburden pressure. Compressibility typically decreases with increasing porosity and effective overburden pressure.

Geertsma (1957) points out that there are three different types of compressibility that must be distinguished in rocks:

- **Rock-matrix compressibility, c_r**

Is defined as the fractional change in volume of the solid rock material (grains) with a unit change in pressure. Mathematically, the rock compressibility coefficient is given by

$$c_r = -\frac{1}{V_r} \left(\frac{\partial V_r}{\partial p} \right)_T \quad (4-60)$$

where c_r = rock-matrix compressibility, psi^{-1}
 V_r = volume of solids

The subscript T indicates that the derivative is taken at constant temperature.

- **Rock-bulk compressibility, c_B**

Is defined as the fractional change in volume of the bulk volume of the rock with a unit change in pressure. The rock-bulk compressibility is defined mathematically by:

$$c_B = -\frac{1}{V_B} \left(\frac{\partial V_B}{\partial p} \right)_T \quad (4-61)$$

where c_B = rock-bulk compressibility coefficient, psi^{-1}
 V_B = bulk volume

- **Pore compressibility, c_p**

The pore compressibility coefficient is defined as the fractional change in pore volume of the rock with a unit change in pressure and given by the following relationship:

$$c_p = \frac{-1}{V_p} \left(\frac{\partial V_p}{\partial p} \right)_T \quad (4-62)$$

where p = pore pressure, psi
 c_p = pore compressibility coefficient, psi^{-1}
 V_p = pore volume

Equation 4-62 can be expressed in terms of the porosity ϕ by noting that ϕ increases with the increase in the pore pressure; or:

$$c_p = \frac{1}{\phi} \frac{\partial \phi}{\partial p}$$

For most petroleum reservoirs, the rock and bulk compressibility are considered small in comparison with the pore compressibility c_p . The *formation compressibility* c_f is the term commonly used to describe the total compressibility of the formation and is set equal to c_p , i.e.:

$$c_f = c_p = \frac{1}{\phi} \frac{\partial \phi}{\partial p} \quad (4-63)$$

Typical values for the formation compressibility range from 3×10^{-6} to $25 \times 10^{-6} \text{psi}^{-1}$. Equation 4-62 can be rewritten as:

$$c_f = \frac{1}{V_p} \frac{\Delta V_p}{\Delta p}$$

or

$$\Delta V_p = c_f V_p \Delta p \quad (4-64)$$

where ΔV_p and Δp are the change in the pore volume and pore pressure, respectively.

Geertsma (1957) suggested that the bulk compressibility c_B is related to the pore compressibility c_p by the following expression.

$$c_B \cong c_p \phi \quad (4-65)$$

Geertsma has stated that in a reservoir only the vertical component of hydraulic stress is constant and that the stress components in the horizontal plane are characterized by the boundary condition that there is no bulk deformation in those directions. For those boundary conditions, he developed the following approximation for sandstones:

$$c_p (\text{reservoir}) = 1/2 c_p (\text{laboratory})$$

Example 4-15

Calculate the reduction in the pore volume of a reservoir due to a pressure drop of 10 psi. The reservoir original pore volume is one million barrels with an estimated formation compressibility of $10 \times 10^{-6} \text{ psi}^{-1}$.

Solution

Applying Equation 4-64 gives

$$\Delta V_p = (10 \times 10^{-6}) (1 \times 10^6) (10) = 100 \text{ bbl}$$

Although the above value is small, it becomes an important factor in undersaturated reservoirs when calculations are made to determine initial oil-in-place and aquifer contents.

The reduction in the pore volume due to pressure decline can also be expressed in terms of the changes in the reservoir porosity. Equation 4-63 can be rearranged, to give:

$$c_f \partial p = \left(\frac{1}{\phi} \right) \partial \phi$$

Integrating the above relation gives:

$$c_f \int_{p_o}^p \partial p = \int_{\phi_o}^{\phi} \frac{\partial \phi}{\phi}$$

$$c_f (p - p_o) = \ln \left(\frac{\phi}{\phi_o} \right)$$

or:

$$\phi = \phi_o e^{c_f(p - p_o)} \quad (4-66)$$

where p_o = original pressure, psi
 ϕ_o = original porosity
 p = current pressure, psi
 ϕ = porosity at pressure p

Noting that the e^x expansion series is expressed as:

$$e^x = 1 + x + \frac{x^2}{2!} + \frac{x^3}{3!} + \dots$$

Using the expansion series and truncating the series after the first two terms, gives:

$$\phi = \phi_o [1 + c_f (p - p_o)] \quad (4-67)$$

Example 4-16

Given the following data:

- $c_f = 10 \times 10^{-6}$
- original pressure = 5000 psi
- original porosity = 18%
- current pressure = 4500 psi

Calculate the porosity at 4,500 psi.

Solution

$$\phi = 0.18 [1 + (10 \times 10^{-6})(4500 - 5000)] = 0.179$$

It should be pointed out that the total reservoir compressibility c_t is extensively used in the transient flow equation and the material balance equation as defined by the following expression:

$$c_t = S_o c_o + S_w c_s + S_g c_g + c_f \quad (4-68)$$

where S_o , S_w , S_g = oil, water, and gas saturation
 c_o = oil compressibility, psi^{-1}
 c_w = water compressibility, psi^{-1}
 c_g = gas compressibility, psi^{-1}
 c_t = total reservoir compressibility

For undersaturated oil reservoirs, the reservoir pressure is above the bubble-point pressure, i.e., no initial gas cap, which reduces Equation 4-68 to:

$$c_t = S_o c_o + S_w c_w + c_f$$

In general, the formation compressibility c_f is the same order of magnitude as the compressibility of the oil and water and, therefore, cannot be regulated.

Several authors have attempted to correlate the pore compressibility with various parameters including the formation porosity. Hall (1953) correlated the pore compressibility with porosity as given by the following relationship:

$$c_f = (1.782/\phi^{0.438}) 10^{-6} \quad (4-69)$$

where c_f = formation compressibility, psi^{-1}
 ϕ = porosity, fraction

Newman (1973) used 79 samples for consolidated sandstones and limestones to develop a correlation between the formation compressibility and porosity. The proposed generalized hyperbolic form of the equation is:

$$c_f = \frac{a}{[1 + cb\phi]}$$

where

For consolidated sandstones

$$\begin{aligned} a &= 97.32 \times 10^{-6} \\ b &= 0.699993 \\ c &= 79.8181 \end{aligned}$$

For limestones

$$\begin{aligned} a &= 0.8535 \\ b &= 1.075 \\ c &= 2.202 \times 10^6 \end{aligned}$$

Example 4-17

Estimate the compressibility coefficient of a sandstone formation that is characterized by a porosity of 0.2, using:

- a. Hall's correlation
- b. Newman's correlation

Solution

a. Hall's correlations:

$$c_f = (1.782/0.2^{0.438}) 10^{-6} = 3.606 \times 10^{-6} \text{ psi}^{-1}$$

b. Newman's correlation:

$$c_f = \frac{97.32 \times 10^{-6}}{[1 + (0.699993)(79.8181)(0.2)]^{1/0.699993}} = 2.74 \times 10^{-6} \text{ psi}^{-1}$$

NET PAY THICKNESS

A fundamental prerequisite to reservoir performance prediction is a satisfactory knowledge of the volume of oil originally in place. The reservoir is necessarily confined to certain geologic and fluid boundaries, i.e., GOC, WOC, and GWC, so accuracy is imperative. Within the confines of such boundaries, oil is contained in what is commonly referred to as *Gross Pay*. *Net Pay* is that part of the reservoir thickness that contributes to oil recovery and is defined by imposing the following criteria:

- Lower limit of porosity
- Lower limit of permeability
- Upper limit of water saturation

All available measurements performed on reservoir samples and in wells, such as core analysis and well logs, are extensively used in evaluating the reservoir net thickness.

The choice of lower limits of porosity and permeability will depend upon such individual characteristics as

- Total reservoir volume
- Total range of permeability values
- Total range of porosity values
- Distribution of the permeability and porosity values

RESERVOIR HETEROGENEITY

It has been proposed that most reservoirs are laid down in a body of water by a long-term process, spanning a variety of depositional environments, in both time and space. As a result of subsequent physical and chemical reorganization, such as compaction, solution, dolomitization, and cementation, the reservoir characteristics are further changed. Thus, the heterogeneity of reservoirs is, for the most part, dependent upon the depositional environments and subsequent events.

The main geologic characteristic of all the physical rock properties that have a bearing on reservoir behavior when producing oil and gas is the extreme variability in such properties within the reservoir itself, both laterally and vertically, and within short distances. It is important to recognize that there are no homogeneous reservoirs, only varying degrees of heterogeneity.

The reservoir heterogeneity is then defined as a variation in reservoir properties as a function of space. Ideally, if the reservoir is homogeneous, measuring a reservoir property at any location will allow us to fully describe the reservoir. The task of reservoir description is very simple for homogeneous reservoirs. On the other hand, if the reservoir is heterogeneous, the reservoir properties vary as a function of a spatial location. These properties may include permeability, porosity, thickness, saturation, faults and fractures, rock facies, and rock characteristics. For a proper reservoir description, we need to predict the variation in these reservoir properties as a function of spatial locations. There are essentially two types of heterogeneity:

- Vertical heterogeneity
- Areal heterogeneity

Geostatistical methods are used extensively in the petroleum industry to quantitatively describe the two types of the reservoir heterogeneity. It is obvious that the reservoir may be nonuniform in all intensive properties such as permeability, porosity, wettability, and connate-water saturation. We will discuss heterogeneity of the reservoir in terms of permeability.

Vertical Heterogeneity

One of the first problems encountered by the reservoir engineer in predicting or interpreting fluid displacement behavior during secondary recovery and enhanced oil recovery processes is that of organizing and using the large amount of data available from core analysis. Permeabilities pose particular problems in organization because they usually vary by more than an order of magnitude between different strata. The engineer must be able then to:

- Describe the degree of the vertical heterogeneity in mathematical terms, and
- Describe and define the proper permeability stratification of the pay zone. This task is commonly called the *zoning or layering problem*.

It is appropriate to be able to describe the degree of heterogeneity within a particular system in quantitative terms. The *degree of homogeneity* of a reservoir property is a number that characterizes the departure from uniformity or constancy of that particular measured property through the thickness of the reservoir. A formation is said to have a uniformity coefficient of zero in a specified property when that property is constant throughout the formation thickness. A completely heterogeneous formation has a uniformity coefficient of unity. Between the two extremes, formations have uniformity coefficients comprised between zero and one. The following are the two most widely used descriptors of the vertical heterogeneity of the formation:

- Dykstra-Parsons permeability variation V
- Lorenz coefficient L

The Dykstra-Parsons Permeability Variation

Dykstra and Parsons (1950) introduced the concept of the permeability variation coefficient V , which is a statistical measure of non-uniformity of a set of data. It is generally applied to the property of permeability but can be extended to treat other rock properties. It is generally recognized that the permeability data are log-normally distributed. That is, the geologic processes that create permeability in reservoir rocks appear to leave permeabilities distributed around the geometric mean. Dykstra and Parsons recognized this feature and introduced the permeability variation that characterizes a particular distribution. The required computational steps for determining the coefficient V are summarized below:

- Step 1.* Arrange the core samples in decreasing permeability sequence, i.e., descending order.
- Step 2.* For each sample, calculate the percentage of thickness with permeability greater than this sample.
- Step 3.* Using a log-probability graph paper, plot permeability values on the log scale and the % of thickness on the probability scale. This special graph paper is shown in Figure 4-29.
- Step 4.* Draw the best straight line through the points.
- Step 5.* Read the corresponding permeability values at 84.1% and 50% of thickness. These two values are designated as $k_{84.1}$ and k_{50} .
- Step 6.* The Dykstra-Parsons permeability variation is defined by the following expression:

$$V = \frac{k_{50} - k_{84.1}}{k_{50}} \quad (4-70)$$

Example 4-18

The following conventional core analysis data are available from three wells:

| Well #1 | | | Well #2 | | | Well #3 | | |
|-------------|---------|-------------|-------------|---------|-------------|------------|---------|-------------|
| Depth ft | k md | ϕ % | Dept ft | k md | ϕ % | Dept ft | k md | ϕ % |
| 5389–5391 | 166 | 17.4 | 5397–5398.5 | 72 | 15.7 | 5401–5403 | 28 | 14.0 |
| –5393 | 435 | 18.0 | –539.95 | 100 | 15.6 | –5405 | 40 | 13.7 |
| –5395 | 147 | 16.7 | –5402 | 49 | 15.2 | –5407 | 20 | 12.2 |
| –5397 | 196 | 17.4 | –5404.5 | 90 | 15.4 | –5409 | 32 | 13.6 |
| –5399 | 254 | 19.2 | –5407 | 91 | 16.1 | –5411 | 35 | 14.2 |
| –5401 | 105 | 16.8 | –5409 | 44 | 14.1 | –5413 | 27 | 12.6 |
| –5403 | 158 | 16.8 | –5411 | 62 | 15.6 | –5415 | 27 | 12.3 |
| –5405 | 153 | 15.9 | –5413 | 49 | 14.9 | –5417 | 9 | 10.6 |
| –5406 | 128 | 17.6 | –5415 | 49 | 14.8 | –5419 | 30 | 14.1 |
| –5409 | 172 | 17.2 | –5417 | 83 | 15.2 | | | |

Calculate the Dykstra-Parsons permeability variation.

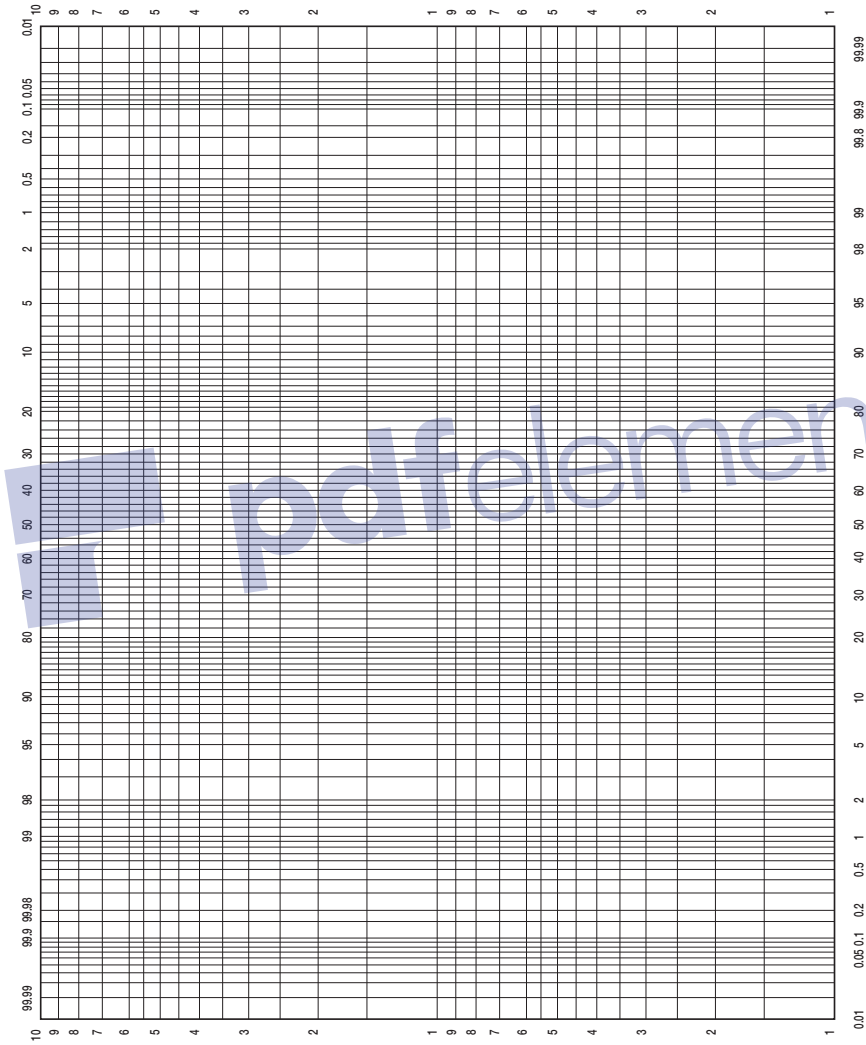


Figure 4-29. Probability-log scale.

Solution

Step 1. Arrange the entire permeability data in a descending order and calculate % of thickness with greater permeability as shown below:

| k md | h ft | h with greater k | % of h with greater k |
|---------|---------|------------------|-----------------------|
| 435 | 2 | 0 | 0 |
| 254 | 2 | 2 | 3.6 |
| 196 | 2 | 4 | 7.1 |
| 172 | 3 | 6 | 10.7 |
| 166 | 2 | 9 | 16.1 |
| 158 | 2 | 11 | 19.6 |
| 153 | 2 | 13 | 23.2 |
| 147 | 2 | 15 | 26.8 |
| 128 | 1 | 17 | 30.4 |
| 105 | 2 | 18 | 32.1 |
| 100 | 1 | 20 | 35.7 |
| 91 | 2.5 | 21 | 37.5 |
| 90 | 2.5 | 23.5 | 42.0 |
| 83 | 2 | 26 | 46.4 |
| 72 | 1.5 | 28 | 50 |
| 62 | 2 | 29.5 | 52.7 |
| 49 | 6.5 | 31.5 | 56.3 |
| 44 | 2 | 38 | 67.9 |
| 40 | 2 | 40 | 71.4 |
| 35 | 2 | 42 | 75.0 |
| 32 | 2 | 44 | 78.6 |
| 30 | 2 | 46 | 82.1 |
| 28 | 2 | 48 | 85.7 |
| 27 | 2 | 50 | 89.3 |
| 20 | 2 | 52 | 92.9 |
| 9 | 2 | 54 | 96.4 |

Total = 56'

Step 2. Plot the permeability versus % of thickness with greater k on a log-probability scale as shown in Figure 4-30 and read

$$k_{50} = 68 \text{ md}$$

$$k_{84.1} = 29.5$$

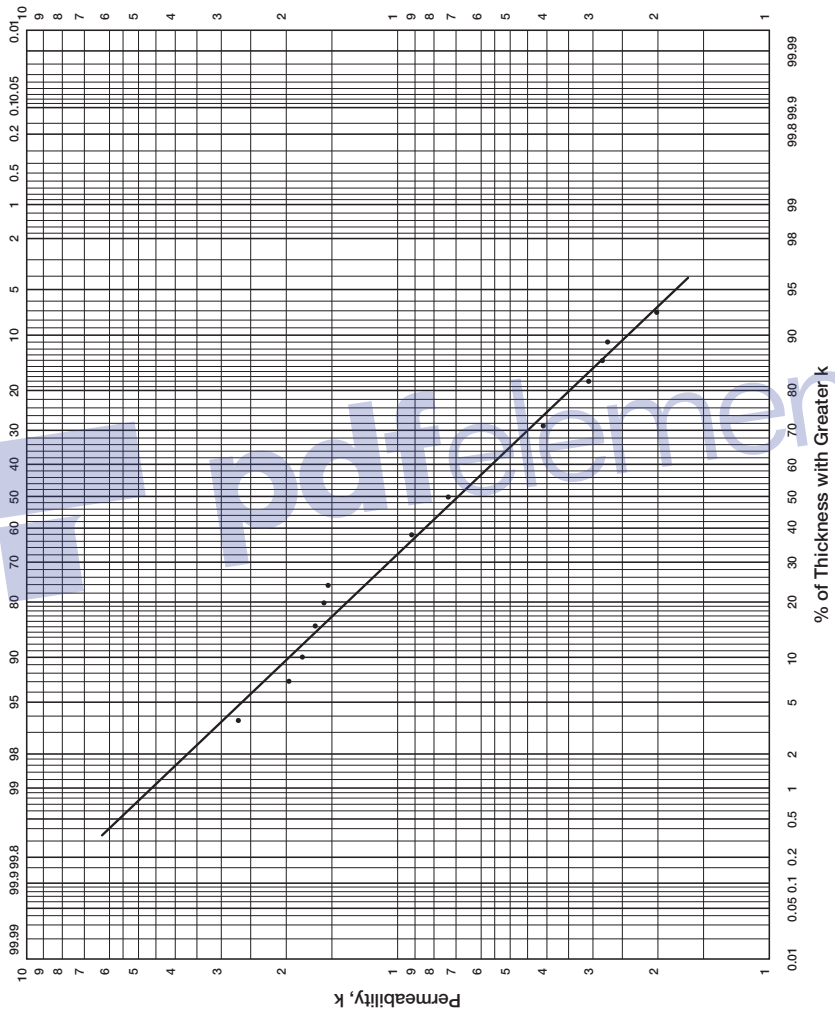


Figure 4-30. % of h vs. k.

Step 3. Calculate V by applying Equation 4-70.

$$V = \frac{68 - 29.5}{68} = 0.57$$

It should be noted that if all the permeabilities are equal, the numerator or Equation 4-70 would be zero, and the V would also be zero. This would be the case for a completely homogeneous system. The Dykstra-Parsons method is commonly referred to as a *Permeability Ordering Technique*.

In water flooding calculations, it is frequently desired to divide the reservoir into layers that have equal thickness and different permeability. The log-probability scale can be used in this case to assign the permeability scale into equal percent increments and to read the corresponding permeability at the midpoint of each interval.

Example 4-19

Using the data given in Example 4-18, determine the average layer permeability for a 10-layered system, assuming a uniform porosity.

Solution

Using the Dykstra-Parsons's log-probability plot as shown in Figure 4-30, determine the permeability for the 10-layered system as follows:

| Layer | % Probability | k, md |
|-------|---------------|-------|
| 1 | 5 | 265 |
| 2 | 15 | 160 |
| 3 | 25 | 120 |
| 4 | 35 | 94 |
| 5 | 45 | 76 |
| 6 | 55 | 60 |
| 7 | 65 | 49 |
| 8 | 75 | 39 |
| 9 | 85 | 29 |
| 10 | 95 | 18 |

Although permeability and porosity are not related in a strict technical sense, they should correlate in rock of similar lithology and pore size

distribution. In many cases, the logarithm of permeability versus porosity plots is frequently made and the best straight line is drawn through the points.

Lorenz Coefficient L

Schmalz and Rahme (1950) introduced a single parameter that describes the degree of heterogeneity within a pay zone section. The term is called *Lorenz coefficient* and varies between zero, for a completely homogeneous system, to one for a completely heterogeneous system.

The following steps summarize the methodology of calculating the Lorenz coefficient:

Step 1. Arrange all the available permeability values in a descending order.

Step 2. Calculate the cumulative permeability capacity Σkh and cumulative volume capacity $\Sigma \phi h$.

Step 3. Normalize both cumulative capacities such that each cumulative capacity ranges from 0 to 1.

Step 4. Plot the normalized cumulative permeability capacity versus the normalized cumulative volume capacity on a Cartesian scale.

Figure 4-31 shows an illustration of the flow capacity distribution. A completely uniform system would have all permeabilities equal, and a plot of the normalized Σkh versus $\Sigma \phi h$ would be a straight line. Figure 4-31 indicates that as the degree of contrast between high and low values of permeability increases the plot exhibits greater concavity toward the upper left corner. This would indicate more heterogeneity, i.e., the severity of deviation from a straight line is an indication of the degree of heterogeneity. The plot can be used to describe the reservoir heterogeneity quantitatively by calculating the Lorenz coefficient. The coefficient is defined by the following expression:

$$L = \frac{\text{Area above the straight line}}{\text{Area below the straight line}} \quad (4-71)$$

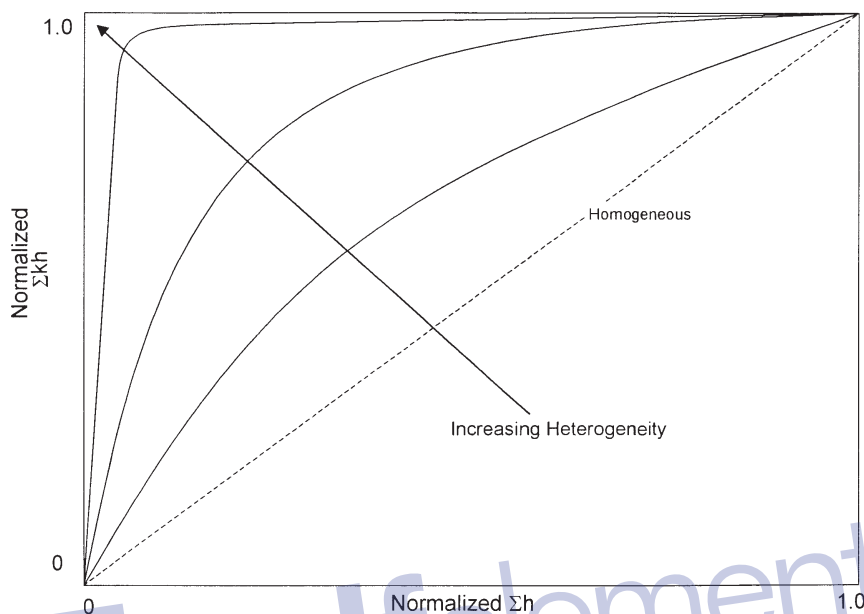


Figure 4-31. Normalized flow capacity.

where the Lorenz coefficient L can vary between 0 and 1.

0 = completely homogeneous

1 = completely heterogeneous

Figure 4-32 shows the relation of the permeability variation V and Lorenz coefficient L for log-normal permeability distributions as proposed by Warren and Price (1961). This relationship can be expressed mathematically by the following two expressions:

Lorenz coefficient in terms of permeability variation:

$$L = 0.0116356 + 0.339794V + 1.066405V^2 - 0.3852407V^3 \quad (4-72)$$

Permeability variation in terms of Lorenz coefficient:

$$V = -5.05971(10^{-4}) + 1.747525L - 1.468855L^2 + 0.701023L^3 \quad (4-73)$$

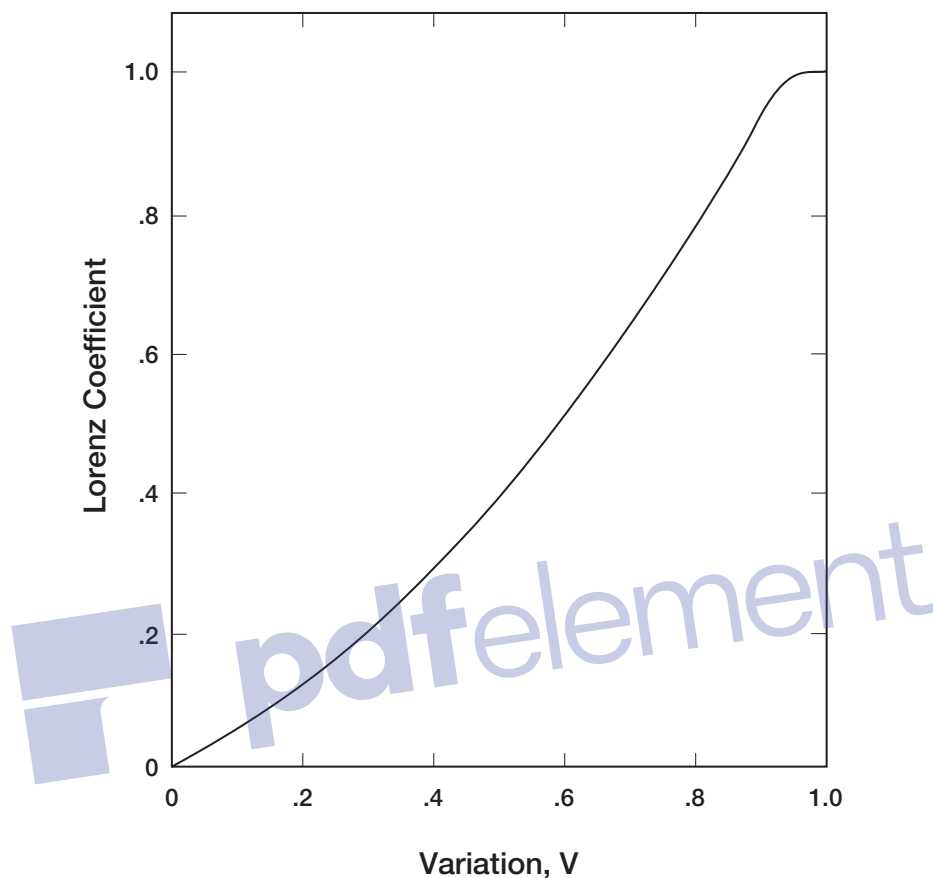


Figure 4-32. Correlation of Lorenz coefficient and permeability variation.

The above two expressions are applicable between $0 < L < 1$ and $0 < V < 1$.

Example 4-20

Using the data given in Example 4-18, calculate the Lorenz coefficient assuming a uniform porosity.

Solution

Step 1. Tabulate the permeability data in a descending order and calculate the normalized Σkh and Σh as shown below:

| k, md | h, ft | kh | Σkh | $\Sigma kh/5646.5$ | Σh | $\Sigma h/56$ |
|-------|-------|-------|-------------|--------------------|------------|---------------|
| 435 | 2 | 870 | 870 | 0.154 | 2 | 0.036 |
| 254 | 2 | 508 | 1378 | 0.244 | 4 | 0.071 |
| 196 | 2 | 392 | 1770 | 0.313 | 6 | 0.107 |
| 172 | 3 | 516 | 2286 | 0.405 | 9 | 0.161 |
| 166 | 2 | 332 | 2618 | 0.464 | 11 | 0.196 |
| 158 | 2 | 316 | 2934 | 0.520 | 13 | 0.232 |
| 153 | 2 | 306 | 3240 | 0.574 | 15 | 0.268 |
| 147 | 2 | 294 | 3534 | 0.626 | 17 | 0.304 |
| 128 | 1 | 128 | 3662 | 0.649 | 18 | 0.321 |
| 105 | 2 | 210 | 3872 | 0.686 | 20 | 0.357 |
| 100 | 1 | 100 | 3972 | 0.703 | 21 | 0.375 |
| 91 | 2.5 | 227.5 | 4199.5 | 0.744 | 23.5 | 0.420 |
| 90 | 2.5 | 225 | 4424.5 | 0.784 | 26 | 0.464 |
| 83 | 2 | 166 | 4590.5 | 0.813 | 28 | 0.50 |
| 72 | 1.5 | 108 | 4698.5 | 0.832 | 29.5 | 0.527 |
| 62 | 2 | 124 | 4822.5 | 0.854 | 31.5 | 0.563 |
| 49 | 6.5 | 294 | 5116.5 | 0.906 | 38.0 | 0.679 |
| 44 | 2 | 88 | 5204.5 | 0.922 | 40.0 | 0.714 |
| 40 | 2 | 80 | 5284.5 | 0.936 | 42 | 0.750 |
| 35 | 2 | 70 | 5354.4 | 0.948 | 44 | 0.786 |
| 32 | 2 | 64 | 5418.5 | 0.960 | 46 | 0.821 |
| 30 | 2 | 60 | 5478.5 | 0.970 | 48 | 0.857 |
| 28 | 2 | 56 | 5534.5 | 0.980 | 50 | 0.893 |
| 27 | 2 | 54 | 5588.5 | 0.990 | 52 | 0.929 |
| 20 | 2 | 40 | 5628.5 | 0.997 | 54 | 0.964 |
| 9 | 2 | 18 | 5646.5 | 1.000 | 56 | 1.000 |

Step 2. Plot the normalized capacities on a Cartesian scale as shown in Figure 4-33.

Step 3. Calculate the Lorenz coefficient by dividing the area above the straight line (area A) by the area under the straight line (area B) to give:

$$L = 0.42$$

A plot of the cumulative permeability capacity Σkh versus Σh (without normalization) is commonly constructed, as shown in Figure 4-34, and used to assign average permeability values for a selected number of reservoir layers. If the intervals of the thickness are chosen, as shown in Figure 4-34, then the average values of permeability for each thickness interval (layer) can be calculated by dividing the incremental (kh) by the incremental thickness.

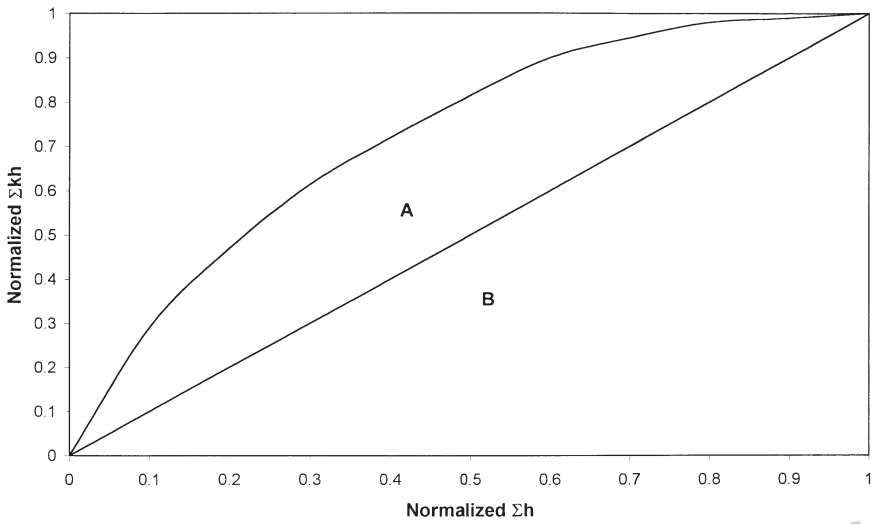


Figure 4-33. Normalized flow capacity for Example 4-20.

pdfelement

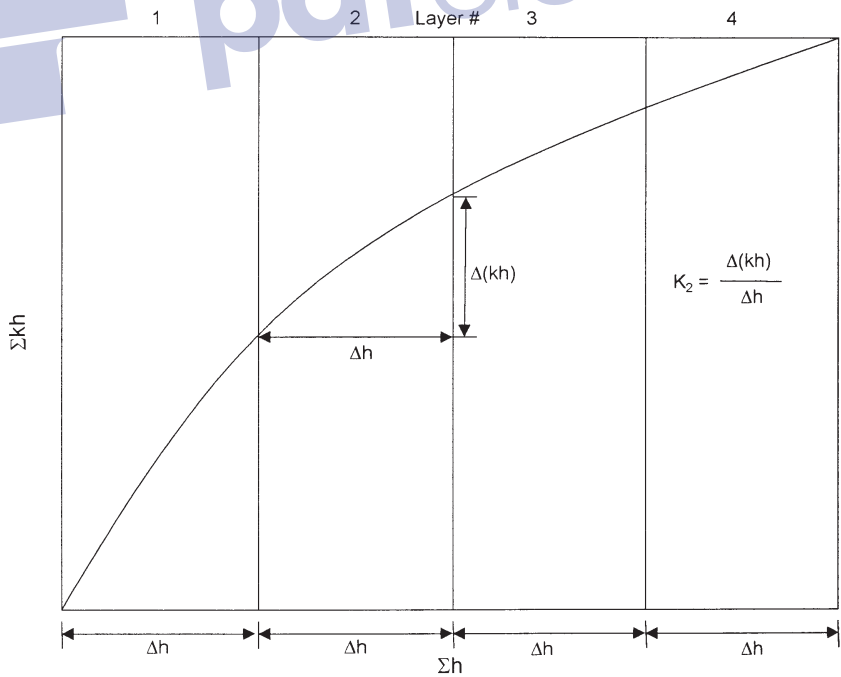


Figure 4-34. Cumulative permeability capacity vs. cumulative thickness.

It should be noted that it is not necessary that equal thickness sections be chosen. They may be selected at irregular increments as desired. There are also some advantages of selecting layer properties so that each layer has the same permeability thickness product.

Example 4-21

Using the data given in Example 4-18, calculate the average permeability for a 10-layered system reservoir. Compare the results with those of the Dykstra-Parsons method.

Solution

Step 1. Using the calculated values of Σkh and Σh of Example 4-20, plot Σkh versus Σh on a Cartesian coordinate as shown in Figure 4-35.

Step 2. Divide the x-axis into 10 equal segments*, each with 5.6 ft.

Step 3. Calculate the average permeability \bar{k} for each interval, to give:

| Layer | \bar{k} | \bar{k} from Dykstra-Parsons, Example 4-19 |
|-------|-----------|--|
| 1 | 289 | 265 |
| 2 | 196.4 | 160 |
| 3 | 142.9 | 120 |
| 4 | 107.1 | 94 |
| 5 | 83.9 | 76 |
| 6 | 67.9 | 60 |
| 7 | 44.6 | 49 |
| 8 | 35.7 | 39 |
| 9 | 32.1 | 29 |
| 10 | 17.2 | 18 |

The permeability sequencing (ordering) methods of zonation do not consider the physical location of the rocks with the vertical column. All the data are considered to be a statistical sampling, which will describe the statistical distribution of permeability, porosity, and thickness within the reservoir. All the values of equal permeability are presumed to be in communication with each other.

*It should be noted that the 56 feet *do not* equal the reservoir net thickness. It essentially represents the cumulative thickness of the core samples.

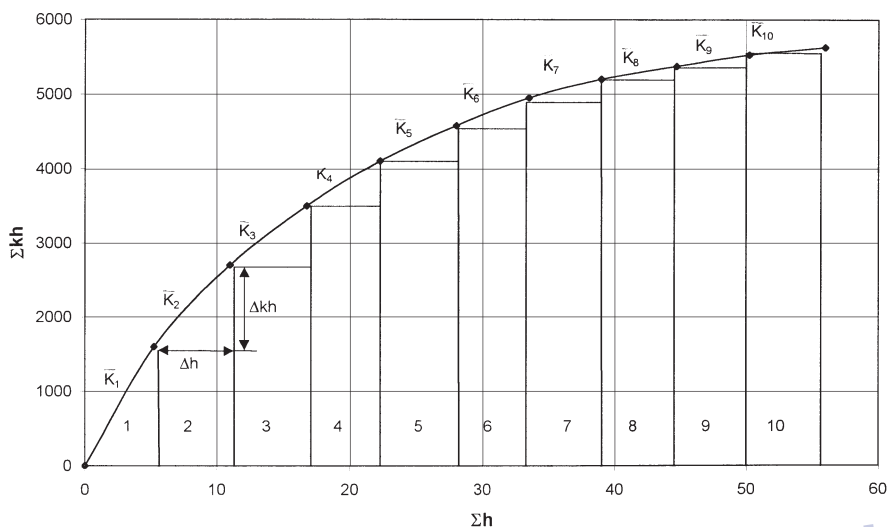


Figure 4-35. Cumulative kh vs. cumulative h (Example 4-21).

Miller and Lents (1947) suggested that the fluid movement in the reservoir remains in the same relative vertical position, i.e., remains in the same elevation, and that the permeability in this elevation (layer) is better described by the *geometric mean average permeability*. This method is called the *positional method*. Thus, to describe the layering system, or a reservoir using the positional approach, it is necessary to calculate the geometric mean average permeability (Equations 4-54 and 4-55) for each elevation and treat each of these as an individual layer.

AREAL HETEROGENEITY

Since the early stages of oil production, engineers have recognized that most reservoirs vary in permeability and other rock properties in the lateral direction. To understand and predict the behavior of an underground reservoir, one must have as accurate and detailed knowledge as possible of the subsurface. Indeed, water and gas displacement is conditioned by the storage geometry (structural shape, thickness of strata) and the local values of the physical parameters (variable from one point to another) characteristic of the porous rock. Hence, prediction accuracy is closely related to the detail in which the reservoir is described.

Johnson and co-workers (1966) devised a well testing procedure, called *pulse testing*, to generate rock properties data between wells. In this procedure, a series of producing rate changes or pluses is made at one well with the response being measured at adjacent wells. The technique provides a measure of the formation flow capacity (kh) and storage capacity (ϕh). The most difficult reservoir properties to define usually are the level and distribution of permeability. They are more variable than porosity and more difficult to measure. Yet an adequate knowledge of permeability distribution is critical to the prediction of reservoir depletion by any recovery process.

A variety of geostatistical estimation techniques has been developed in an attempt to describe accurately the spatial distribution of rock properties. The concept of spatial continuity suggests that data points close to one another are more likely to be similar than are data points farther apart from one another. One of the best geostatistical tools to represent this continuity is a visual map showing a data set value with regard to its location. Automatic or computer contouring and girding is used to prepare these maps. These methods involve interpolating between known data points, such as elevation or permeability, and extrapolating beyond these known data values. These rock properties are commonly called regionalized variables. These variables usually have the following contradictory characteristics:

- A random characteristic showing erratic behavior from point to point
- A structural characteristic reflecting the connections among data points

For example, net thickness values from a limited number of wells in a field may show randomness or erratic behavior. They also can display a connecting or smoothing behavior as more wells are drilled or spaced close together.

To study regionalized variables, a proper formulation must take this double aspect of randomness and structure into account. In geostatistics, a variogram is used to describe the randomness and spatial correlations of the regionalized variables.

There are several conventional interpolation and extrapolation methods that can be applied to values of a regionalized variable at different locations. Most of these methods use the following generalized expression:

$$Z^*(x) = \sum_{i=1}^n \lambda_i Z(x_i) \quad (4-74)$$

with

$$\sum_{i=1}^R \lambda_i = 1 \quad (4-75)$$

where $Z^*(x)$ = estimate of the regionalized variable at location x

$Z(x_i)$ = measured value of the regionalized variable at position x_i

λ_i = weight factor

n = number of nearby data points

The difference between the commonly used interpolation and extrapolation methods is in the mathematical algorithm employed to compute the weighting factors λ_i . Compared to other interpolation methods, the geostatistical originality stems from the intuition that the accuracy of the estimation at a given point (and the λ_i) depends on two factors, the first one being of geometrical nature, the second related to the statistical spatial characteristics of the considered phenomenon.

The first factor is the geometry of the problem that is the relative positions of the measured points to the one to be estimated. When a point is well surrounded by experimental points, it can be estimated with more accuracy than one located in an isolated area. This fact is taken into account by classical interpolation methods (polynomial, multiple regression, least-squares) but these appear to be inapplicable as soon as the studied phenomenon shows irregular variations or measurement errors.

Five simple conventional interpolation and/or extrapolation methods are briefly discussed below:

- **The Polygon Method**

This technique is essentially based on assigning the nearest measured value of the regionalized variable to the designated location. This implies that all the weighting factors, i.e., λ_i , in Equation 4-72 are set equal to zero except the corresponding λ_i for the nearest point is set equal to one.

- **The Inverse Distance Method**

With *inverse distance*, data points are weighted during interpolation such that the influences of one data point relative to another declines with distance from the desired location.

The inverse distance method assigns a weight factor λ_i to each measured regionalized variable by the inverse distance between the measured value and the point being estimated, or

$$\lambda_i = \left(\frac{1}{d_i} \right) / \sum_{i=1}^n \left(\frac{1}{d_i} \right) \quad (4-76)$$

where d_i = distance between the measured value and location of interest
 n = number of nearby points

- **The Inverse Distance Squared Method**

The method assigns a weight to each measured regionalized variable by the inverse distance squared of the sample to the point being estimated, i.e.,

$$\lambda_i = \left(\frac{1}{d_i} \right)^2 / \sum_{i=1}^n \left(\frac{1}{d_i} \right)^2 \quad (4-77)$$

While this method accounts for all nearby wells with recorded rock properties, it gives proportionately more weight to near wells than the previous method.

Example 4-22

Figure 4-36 shows a schematic illustration of the locations of four wells and distances between the wells and point x. The average permeability in each well location is given below:

| Well # | Permeability, md |
|--------|------------------|
| 1 | 73 |
| 2 | 110 |
| 3 | 200 |
| 4 | 140 |

Estimate the permeability at location x by the polygon and the two inverse distance methods.

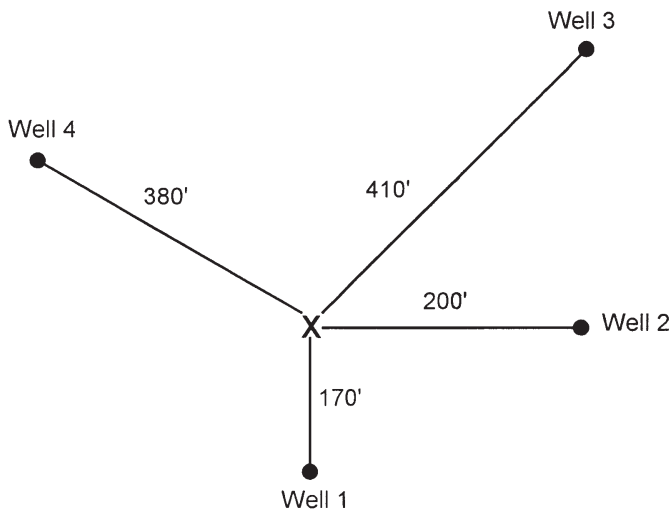


Figure 4-36. Well locations for Example 4-22.

Solution

The Polygon Method

The nearest well location to point x is Well #1 with a distance of 170 ft. The recorded average permeability at this well is 73 md; therefore, the permeability in location x is

$$k = (1) (73) + (0) (110) + (0) (200) + (0) (140) = 73 \text{ md}$$

The Inverse Distance Method

Step 1. Calculate the weighting factors by applying Equation 4-76.

| Distance d_i ft | $1/d_i$ | $\lambda_i = \left(\frac{1}{d_i}\right) / 0.0159$ | k, md |
|----------------------|---------|---|-------|
| 170 | 0.0059 | 0.3711 | 73 |
| 200 | 0.0050 | 0.3145 | 110 |
| 410 | 0.0024 | 0.1509 | 200 |
| 380 | 0.0026 | 0.1635 | 140 |

$$\text{Sum} = 0.0159$$

Step 2. Estimate the permeability at location x by applying Equation 4-74

$$k = (0.3711) (73) + (0.3145) (110) + (0.1509) (200) + (0.1635) (140) = 114.8 \text{ md}$$

The Inverse Distance Squared

Step 1. Apply Equation 4-77 to determine the weighting factors.

| d_i ft | $\left(\frac{1}{d_i}\right)^2$ | $\lambda_i = \left(\frac{1}{d_i}\right)^2 / 0.00007$ | k, md |
|-------------|--------------------------------|--|-------|
| 170 | 0.000035 | 0.4795 | 73 |
| 200 | 0.000025 | 0.3425 | 110 |
| 410 | 0.000006 | 0.0822 | 200 |
| 380 | 0.000007 | 0.958 | 140 |

Sum = 0.000073

Step 2. Estimate the permeability in location x by using Equation 4-72

$$k = (0.4795) (73) + (0.3425) (110) + (0.0822) (200) + (0.0958) (140) = 102.5 \text{ md}$$

• The Triangulation Method

The triangulation method is designed to remove possible discontinuities between adjacent points by fitting a plane through three samples that surround the point being estimated. The method is based on selecting the nearest three locations with measured data values that form a triangle, as shown in Figure 4-37.

The equation of the plane can be expressed generally as

$$Z = a x + b y + c$$

where Z is a regionalized value, for example, permeability, k, at the coordinate “x and y.” Given the coordinates and the regionalized value of three nearby samples, as shown in Figure 4-37 for absolute permeabilities, the coefficients a, b, and c can be determined by solving the following three equations:

$$k_1 = a x_1 + b y_1 + c$$

$$k_2 = a x_2 + b y_2 + c$$

$$k_3 = a x_3 + b y_3 + c$$

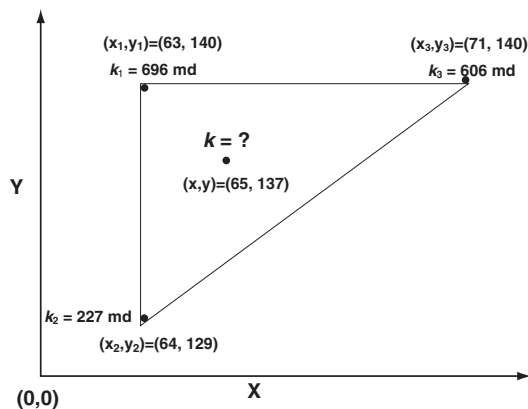


Figure 4-37. Triangulation method.

Substituting permeability values and coordinates into this system of equations gives:

$$63 a + 140 b + c = 696$$

$$64 a + 129 b + c = 227$$

$$71 a + 140 b + c = 606$$

Solving these three expressions yields:

$$a = -11.25 \quad b = 41.614 \quad c = -4421.159$$

or:

$$k = -11.25 x + 41.614 y - 4421.159$$

This relationship estimates the value of permeability at any location within that specific triangular. To estimate the permeability at the coordinates $(x, y) = (65, 137)$, then:

$$k = -11.25 (65) + 41.614 (137) - 4421.159 = 548.7 \text{ md}$$

• Delaunay Triangulation

Figure 4-38 shows the Delaunay triangle for the same samples given in Figure 4-37 for the triangulation method. The sample permeability values at these locations are k_1 , k_2 , and k_3 . Instead of solving the three simultaneous equations and substituting the coordinates of the point of interest into the solution, the permeability value can be directly calculated from:

$$k = \frac{(k_1)(\text{area I}) + (k_1)(\text{area II}) + (k_3)(\text{area III})}{(\text{area I}) + (\text{area II}) + (\text{area III})}$$

The triangulation method is essentially a weighted linear combination in which each value is weighted according to the *area of the opposite triangle*. Using the data given in Figure 4-38, the permeability value at the designated location is:

$$k = \frac{(k_1)(\text{area I}) + (k_1)(\text{area II}) + (k_3)(\text{area III})}{(\text{area I}) + (\text{area II}) + (\text{area III})}$$

$$k = \frac{(696)(22.25) + (227)(12.) + (606)(9.5)}{(22.25) + (12) + (9.5)} = 548.7 \text{ md}$$

PROBLEMS

1. Given:

$$p_i = 3500$$

$$A = 1000 \text{ acres}$$

$$\phi = 12\%$$

$$\gamma_g = 0.7$$

$$p_b = 3500$$

$$h = 25 \text{ ft}$$

$$\text{API} = 45^\circ$$

$$T = 160^\circ\text{F}$$

$$S_{wi} = 30\%$$

$$R_{sb} = 750 \text{ scf/STB}$$

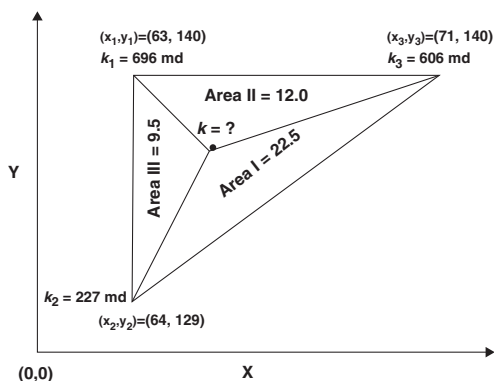


Figure 4-38. Delaunay triangulation method.

Calculate:

- a. Initial oil in place as expressed in STB
- b. Volume of gas originally dissolved in the oil

2. The following measurements on pay zone are available:

| Sample | Thickness, ft | ϕ , % | S_{oir} % |
|--------|---------------|------------|--------------------|
| 1 | 2 | 12 | 75 |
| 2 | 3 | 16 | 74 |
| 3 | 1 | 10 | 73 |
| 4 | 4 | 14 | 76 |
| 5 | 2 | 15 | 75 |
| 6 | 2 | 15 | 72 |

Calculate:

- a. Average porosity
- b. Average oil and water saturations (assuming no gas)

3. The capillary pressure data for a water-oil system are given below:

| S_w | p_c |
|-------|-------|
| 0.25 | 35 |
| 0.30 | 16 |
| 0.40 | 8.5 |
| 0.50 | 5 |
| 1.0 | 0 |

The core sample used in generalizing the capillary pressure data was taken from a layer that is characterized by an absolute permeability of 300 md and a porosity of 17%. Generate the capillary pressure data for a different layer that is characterized by a porosity and permeability of 15%, 200 md, respectively. The interfacial tension is measured at 35 dynes/cm.

4. A five-layer oil reservoir is characterized by a set of capillary pressure-saturation curves as shown in Figure 4-6. The following additional data are also available:

| Layer | Depth, ft | Permeability |
|-------|-----------|--------------|
| 1 | 6000–6016 | 10 |
| 2 | 6016–6025 | 300 |
| 3 | 6025–6040 | 100 |
| 4 | 6040–6055 | 30 |
| 5 | 6055–6070 | 3 |

- WOC = 6,070 ft
- Water density = 65 lb/ft³
- Oil density = 32 lb/ft³

Calculate and plot the water and oil saturation profiles for this reservoir.

5. Assuming a steady-state laminar flow, calculate the permeability from the following measurement made on a core sample by using air.

flow rate = 2 cm³/sec T = 65°F
 upstream pressure = 2 atm downstream pressure = 1 atm
 A = 2 cm² L = 3 cm viscosity = 0.018 cp

6. Calculate average permeability from the following core analysis data.

| Depth, ft | k, md |
|-----------|-------|
| 4000–4002 | 50 |
| 4002–4005 | 20 |
| 4005–4006 | 70 |
| 4006–4008 | 100 |
| 4008–4010 | 85 |

7. Calculate the average permeability of a formation that consists of four beds in series, assuming:

- Linear system
- Radial system with $r_w = 0.3$ and $r_e = 1,450$ ft

| Bed | Length of bed Linear or radial | k, md |
|-----|-----------------------------------|-------|
| 1 | 400 | 70 |
| 2 | 250 | 400 |
| 3 | 300 | 100 |
| 4 | 500 | 60 |

8. Estimate the absolute permeability of a formation that is characterized by an average porosity and connate water saturation of 15% and 20% md, respectively.
9. Given:

| Depth, ft | k, md |
|-----------|-------|
| 4100–4101 | 295 |
| 4101–4102 | 262 |
| 4102–4103 | 88 |
| 4103–4104 | 87 |
| 4104–4105 | 168 |
| 4105–4106 | 71 |
| 4106–4107 | 62 |
| 4107–4108 | 187 |
| 4108–4109 | 369 |
| 4109–4110 | 77 |
| 4110–4111 | 127 |
| 4111–4112 | 161 |
| 4112–4113 | 50 |
| 4113–4114 | 58 |
| 4114–4115 | 109 |
| 4115–4116 | 228 |
| 4116–4117 | 282 |
| 4117–4118 | 776 |
| 4118–4119 | 87 |
| 4119–4120 | 47 |
| 4120–4121 | 16 |
| 4121–4122 | 35 |
| 4122–4123 | 47 |
| 4123–4124 | 54 |
| 4124–4125 | 273 |
| 4125–4126 | 454 |
| 4126–4127 | 308 |
| 4127–4128 | 159 |
| 4128–4129 | 178 |

Calculate:

- Average permeability
- Permeability variation
- Lorenz coefficient
- Assuming four-layer reservoir system with equal length, calculate the permeability for each layer

10. Three layers of 4, 6, and 10 feet thick, respectively, are conducting fluid in parallel flow.

The depth to the top of the first layer is recorded as 5,012 feet. The core analysis report shows the following permeability data for each layer.

| Layer #1 | | Layer #2 | | Layer #3 | |
|-------------|--------------------|-------------|--------------------|-------------|--------------------|
| Depth ft | Permeability md | Depth ft | Permeability md | Depth ft | Permeability md |
| 5012–5013 | 485 | 5016–5017 | 210 | 5022–5023 | 100 |
| 5013–5014 | 50 | 5017–5018 | 205 | 5023–5024 | 95 |
| 5014–5015 | 395 | 5018–5019 | 60 | 5024–5025 | 20 |
| 5015–5016 | 110 | 5019–5020 | 203 | 5025–5026 | 96 |
| | | 5020–5021 | 105 | 5026–5027 | 98 |
| | | 5021–5022 | 195 | 5027–5028 | 30 |
| | | | | 5028–5029 | 89 |
| | | | | 5029–5030 | 86 |
| | | | | 5030–5031 | 90 |
| | | | | 5031–5032 | 10 |

Calculate the *average* permeability of the entire pay zone (i.e., 5,012–5,032').

11. A well has a radius of 0.25 ft and a drainage radius of 660 ft. The sand that penetrates is 15 ft thick and has an absolute permeability of 50 md. The sand contains crude oil with the following PVT properties.

| Pressure psia | B_o bbl/STB | μ_o cp |
|------------------|------------------|---------------|
| 3500 | 1.827 | 1.123 |
| 3250 | 1.842 | 1.114 |
| 3000 | 1.858 | 1.105 |
| 2746* | 1.866 | 1.100 |
| 2598 | 1.821 | 1.196 |
| 2400 | 1.771 | 1.337 |
| 2200 | 1.725 | 1.497 |
| 600 | 1.599 | 2.100 |

*Bubble point

The reservoir pressure (i.e., p_e) and the bubble-point pressure are 3,500 and 2,746 psia, respectively. If the bottom-hole flowing pressure is 2,500 psia, calculate the oil-flow rate.

12. Test runs on three core samples from three wells in the mythical field yielded the following three sets of values for water saturation (S_w), porosity (ϕ), and permeability (k). It is believed that these three properties can be used to determine the recovery fraction (RF).

| | Core 1 | Core 2 | Core 3 |
|-----------------|--------|--------|--------|
| ϕ | .185 | .157 | .484 |
| S_w | 0.476 | .527 | .637 |
| k | .614 | .138 | .799 |
| Recovery factor | .283 | .212 | .141 |

The recovery factor can be expressed by the following equation:

$$RF = a_0 \phi + a_1 S_w + a_2 k$$

where a_0 , a_1 , and a_2 are constants.

Calculate RF if:

$$S_w = .75, \phi = .20, \text{ and } k = .85$$

REFERENCES

1. Calhoun, J. R., *Fundamentals of Reservoir Engineering*. University of Oklahoma Press, 1976.
2. Cole, Frank, *Reservoir Engineering Manual*. Houston: Gulf Publishing Company, 1969.
3. Dykstra, H., and Parsons, R. L., "The Prediction of Oil Recovery by Water Flood," *In Secondary Recovery of Oil in the United States*, 2nd ed., pp. 160–174. API, 1950.
4. Geertsma, J., "The Effect of Fluid Pressure Decline on Volumetric Changes of Porous Rocks," *Trans. AIME*, 1957, pp. 210, 331–340.
5. Hall, H. N., "Compressibility of Reservoir Rocks," *Trans. AIME*, 1953, p. 309.
6. Hustad, O., and Holt, H., "Gravity Stable Displacement of Oil by Gas after Water Flooding," SPE Paper 24116, SPE/DOE Symposium on EOR, Tulsa, OK, April 22–24, 1972.
7. Johnson C. R., Careenkorn, R. A., and Woods, E. G., "Pulse Testing: A New Method for Describing Reservoir Flow Properties Between Wells," *JPT*, Dec. 1966, pp. 1599–1604

8. Jones, S. C., "A Rapid Accurate Unsteady State Klinkenberg Parameter," *SPEJ*, 1972, Vol. 12, No. 5, pp. 383–397.
9. Klinkenberg, L. J., "The Permeability of Porous Media to Liquids and Gases," *API Drilling and Production Practice*, 1941, p. 200.
10. Leverett, M. C., "Capillary Behavior in Porous Solids," *Trans. AIME*, 1941.
11. McCardell, W. M., "A Review of the Physical Basis for the Use of the J-Function," Eighth Oil Recovery Conference, Texas Petroleum Research Committee, 1955.
12. Miller, M. G., and Lents, M. R., "Performance of Bodcaw Reservoir, Cotton Valley Field Cycling Project: New Methods of Predicting Gas-Condensate Reservoir," *SPEJ*, Sept. 1966, pp. 239.
13. Morris, R. L., and Biggs, W. P., "Using Log-Derived Values of Water Saturation and Porosity." *SPWLA*, Paper X, 1967.
14. Newman, G. H., "Pore-Volume Compressibility," *JPT*, Feb. 1973, pp. 129–134
15. Schmalz, J. P., and Rahme, H. D., "The Variation of Waterflood Performance With Variation in Permeability Profile," *Prod. Monthly*, 1950, Vol. 15, No. 9, pp. 9–12.
16. Timur, A., "An Investigation of Permeability, Porosity, and Residual Water Saturation Relationships," *AIME*, June 1968.
17. Warren, J. E., and Price, H. S., "Flow in Heterogeneous Porous Media," *SPEJ*, Sept. 1961, pp. 153–169.

C H A P T E R 5

RELATIVE PERMEABILITY CONCEPTS

Numerous laboratory studies have concluded that the effective permeability of any reservoir fluid is a function of the reservoir fluid saturation and the wetting characteristics of the formation. It becomes necessary, therefore, to specify the fluid saturation when stating the effective permeability of any particular fluid in a given porous medium. Just as k is the accepted universal symbol for the absolute permeability, k_o , k_g , and k_w are the accepted symbols for the effective permeability to oil, gas, and water, respectively. The saturations, i.e., S_o , S_g , and S_w , must be specified to completely define the conditions at which a given effective permeability exists.

Effective permeabilities are normally measured directly in the laboratory on small core plugs. Owing to many possible combinations of saturation for a single medium, however, laboratory data are usually summarized and reported as relative permeability.

The absolute permeability is a property of the porous medium and is a measure of the capacity of the medium to transmit fluids. When two or more fluids flow at the same time, the relative permeability of each phase at a specific saturation is the ratio of the effective permeability of the phase to the absolute permeability, or:

$$k_{ro} = \frac{k_o}{k}$$

$$k_{rg} = \frac{k_g}{k}$$

$$k_{rw} = \frac{k_w}{k}$$

where k_{ro} = relative permeability to oil
 k_{rg} = relative permeability to gas
 k_{rw} = relative permeability to water
 k = absolute permeability
 k_o = effective permeability to oil for a given oil saturation
 k_g = effective permeability to gas for a given gas saturation
 k_w = effective permeability to water at some given water saturation

For example, if the absolute permeability k of a rock is 200 md and the effective permeability k_o of the rock at an oil saturation of 80% is 60 md, the relative permeability k_{ro} is 0.30 at $S_o = 0.80$.

Since the effective permeabilities may range from zero to k , the relative permeabilities may have any value between zero and one, or:

$$0 \leq k_{rw}, k_{ro}, k_{rg} \leq 1.0$$

It should be pointed out that when three phases are present the *sum of the relative permeabilities* ($k_{ro} + k_{rg} + k_{rw}$) *is both variable and always less than or equal to unity*. An appreciation of this observation and of its physical causes is a prerequisite to a more detailed discussion of two- and three-phase relative permeability relationships.

It has become a common practice to refer to the relative permeability curve for the nonwetting phase as k_{nw} and the relative permeability for the wetting phase as k_w .

TWO-PHASE RELATIVE PERMEABILITY

When a wetting and a nonwetting phase flow together in a reservoir rock, each phase follows separate and distinct paths. The distribution of the two phases according to their wetting characteristics results in characteristic wetting and nonwetting phase relative permeabilities. Since the wetting phase occupies the smaller pore openings at small saturations, and these pore openings do not contribute materially to flow, it follows that the presence of a small wetting phase saturation will affect the nonwetting

phase permeability only to a limited extent. Since the nonwetting phase occupies the central or larger pore openings that contribute materially to fluid flow through the reservoir, however, a small nonwetting phase saturation will drastically reduce the wetting phase permeability.

Figure 5-1 presents a typical set of relative permeability curves for a water-oil system with the water being considered the wetting phase. Figure 5-1 shows the following four distinct and significant observations:

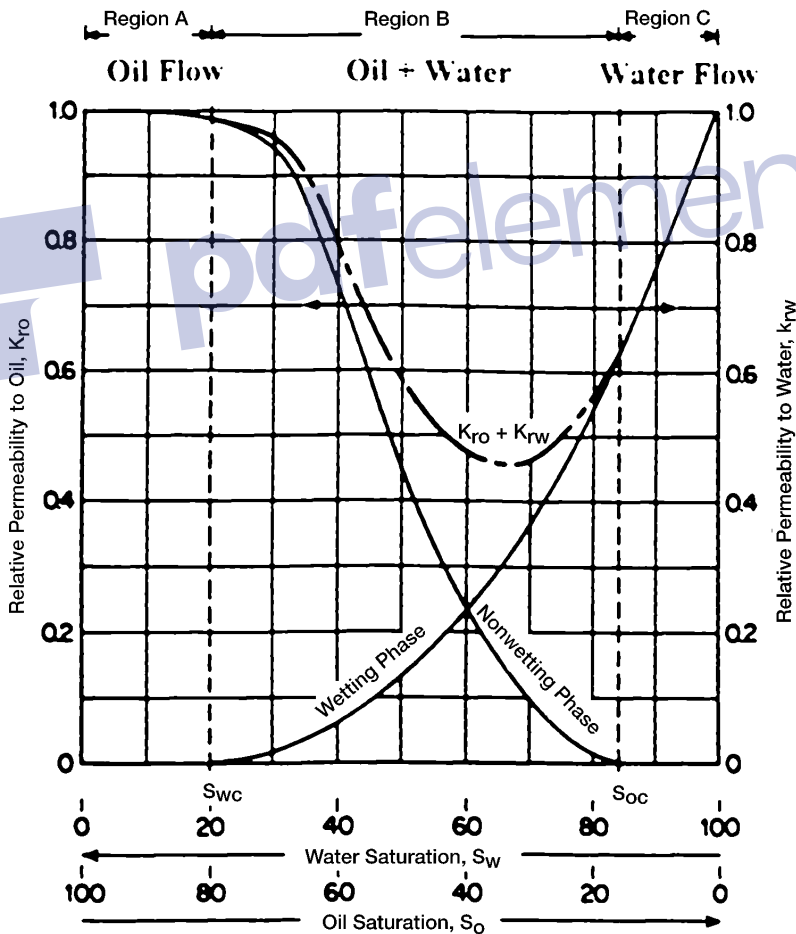


Figure 5-1. Typical two-phase flow behavior.

- **Observation 1**

The wetting phase relative permeability shows that a small saturation of the nonwetting phase will drastically reduce the relative permeability of the wetting phase. The reason for this is that the nonwetting phase occupies the larger pore spaces, and it is in these large pore spaces that flow occurs with the least difficulty.

- **Observation 2**

The nonwetting phase relative permeability curve shows that the nonwetting phase begins to flow at the relatively low saturation of the nonwetting phase. The saturation of the oil at this point is called *critical oil saturation* S_{oc} .

- **Observation 3**

The wetting phase relative permeability curve shows that the wetting phase will cease to flow at a relatively large saturation. This is because the wetting phase preferentially occupies the smaller pore spaces, where capillary forces are the greatest. The saturation of the water at this point is referred to as the *irreducible water saturation* S_{wir} or *connate-water saturation* S_{wi} —both terms are used interchangeably.

- **Observation 4**

The nonwetting phase relative permeability curve shows that, at the lower saturations of the wetting phase, changes in the wetting phase saturation have only a small effect on the magnitude of the nonwetting phase relative permeability curve. The reason for the phenomenon at Point 4 is that at the low saturations, the wetting phase fluid occupies the small pore spaces that do not contribute materially to flow, and therefore changing the saturation, in these small pore spaces has a relatively small effect on the flow of the nonwetting phase.

This process could have been visualized in reverse just as well. It should be noted that this example portrays oil as nonwetting and water as wetting. The curve shapes shown are typical for wetting and nonwetting phases and may be mentally reversed to visualize the behavior of an oil-wet system. Note also that the total permeability to both phases, $k_{rw} + k_{ro}$, is less than 1, in regions B and C.

The above discussion may be also applied to gas-oil relative permeability data, as can be seen for a typical set of data in Figure 5-2. Note that this might be termed gas-liquid relative permeability since it is plotted versus the liquid saturation. This is typical of gas-oil relative permeability data in the presence of connate-water. Since the connate (irreducible) water normally occupies the smallest pores in the presence of oil

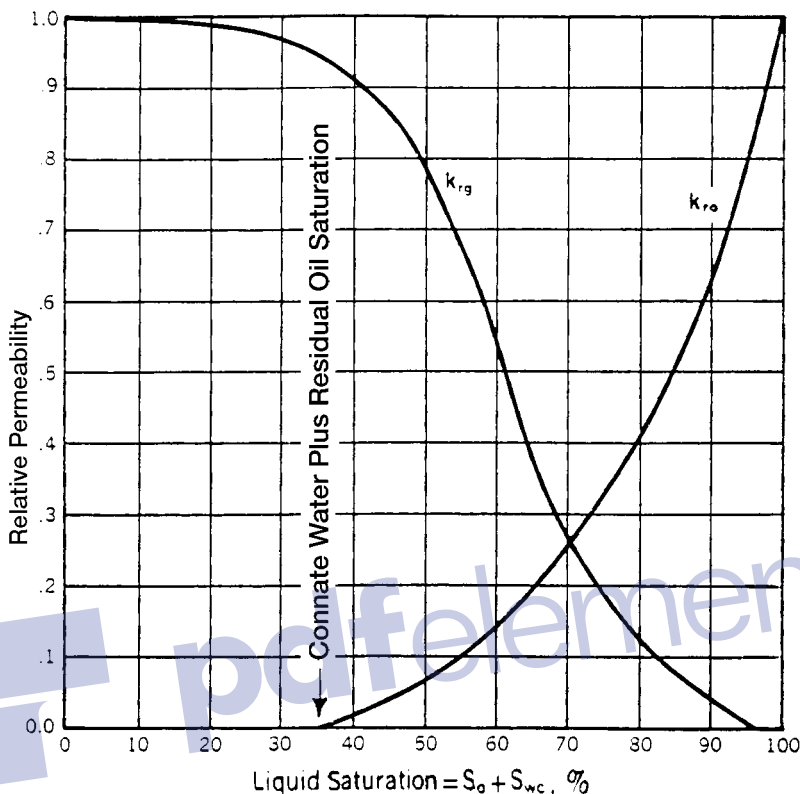


Figure 5-2. Gas-oil relative permeability curves.

and gas, it appears to make little difference whether water or oil that would also be immobile in these small pores occupies these pores. Consequently, in applying the gas-oil relative permeability data to a reservoir, the total liquid saturation is normally used as a basis for evaluating the relative permeability to the gas and oil.

Note that the relative permeability curve representing oil changes completely from the shape of the relative permeability curve for oil in the water-oil system. In the water-oil system, as noted previously, oil is normally the nonwetting phase, whereas in the presence of gas the oil is the wetting phase. Consequently, in the presence of water only, the oil relative permeability curve takes on an S shape whereas in the presence of gas the oil relative permeability curve takes on the shape of the wetting phase, or is concave upward. Note further that the critical gas saturation S_{gc} is generally very small.

Another important phenomenon associated with fluid flow through porous media is the concept of residual saturations. As when one immiscible fluid is displacing another, it is impossible to reduce the saturation of the displaced fluid to zero. At some small saturation, which is presumed to be the saturation at which the displaced phase ceases to be continuous, flow of the displaced phase will cease. This saturation is often referred to as the *residual* saturation. This is an important concept as it determines the maximum recovery from the reservoir. Conversely, a fluid must develop a certain minimum saturation before the phase will begin to flow. This is evident from an examination of the relative permeability curves shown in Figure 5-1. The saturation at which a fluid will just begin to flow is called the *critical* saturation.

Theoretically, the critical saturation and the residual saturation should be exactly equal for any fluid; however, they are not identical. **Critical saturation is measured in the direction of increasing saturation, while irreducible saturation is measured in the direction of reducing saturation.** Thus, the saturation histories of the two measurements are different.

As was discussed for capillary pressure data, there is also a saturation history effect for relative permeability. The effect of saturation history on relative permeability is illustrated in Figure 5-3. If the rock sample is initially saturated with the wetting phase (e.g., water) and relative permeability data are obtained by decreasing the wetting phase saturation while flowing nonwetting fluid (e.g., oil) in the core, the process is classified as *drainage* or *desaturation*.

If the data are obtained by increasing the saturation of the wetting phase, the process is termed *imbibition* or *resaturation*. The nomenclature is consistent with that used in connection with capillary pressure. This difference in permeability when changing the saturation history is called *hysteresis*. Since relative permeability measurements are subject to hysteresis, it is important to duplicate, in the laboratory, the saturation history of the reservoir.

Drainage Process

It is generally agreed that the pore spaces of reservoir rocks were originally filled with water, after which oil moved into the reservoir, displacing some of the water, and reducing the water to some residual saturation. When discovered, the reservoir pore spaces are filled with a connate-water saturation and an oil saturation. If gas is the displacing agent, then gas moves into the reservoir, displacing the oil.

This same history must be duplicated in the laboratory to eliminate the effects of hysteresis. The laboratory procedure is to first saturate the core with water, then displace the water to a residual, or connate, water saturation with oil after which the oil in the core is displaced by gas. This flow process is called the gas drive, or drainage, depletion process. In the gas drive depletion process, the nonwetting phase fluid is continuously increased, and the wetting phase fluid is continuously decreased.

Imbibition Process

The *imbibition process* is performed in the laboratory by first saturating the core with the water (wetting phase), then displacing the water to its irreducible (connate) saturation by injection oil. This “drainage” procedure is designed to establish the original fluid saturations that are found when the reservoir is discovered. The wetting phase (water) is reintroduced into the core and the water (wetting phase) is continuously increased. This is the imbibition process and is intended to produce the relative permeability data needed for water drive or water flooding calculations.

Figure 5-3 schematically illustrates the difference in the drainage and imbibition processes of measuring relative permeability. It is noted that the imbibition technique causes the nonwetting phase (oil) to lose its mobility at higher values of water saturation than does the drainage process. The two processes have similar effects on the wetting phase (water) curve. The drainage method causes the wetting phase to lose its mobility at higher values of wetting phase saturation than does the imbibition method.

There are several important differences between oil-wet and water-wet relative permeability curves that are generally observed; these are as follows:

1. The water saturation at which oil and water permeabilities are equal, that is, the intersection point of the two curves, will generally be greater than 50% for water-wet systems and less than 50% for oil-wet systems.
2. The relative permeability to water at maximum water saturation (i.e., $(1-S_{or})$), will be less than 0.3 for water-wet systems and is roughly greater than 0.5 for oil-wet systems.
3. The connate-water saturation for a water-wet system, S_{wc} , is generally greater than 25%, whereas for oil-wet systems it is generally less than 15%.

Frequently, summary water-oil permeability tests are conducted on core samples. These summary tests are often referred to as **end-point** tests

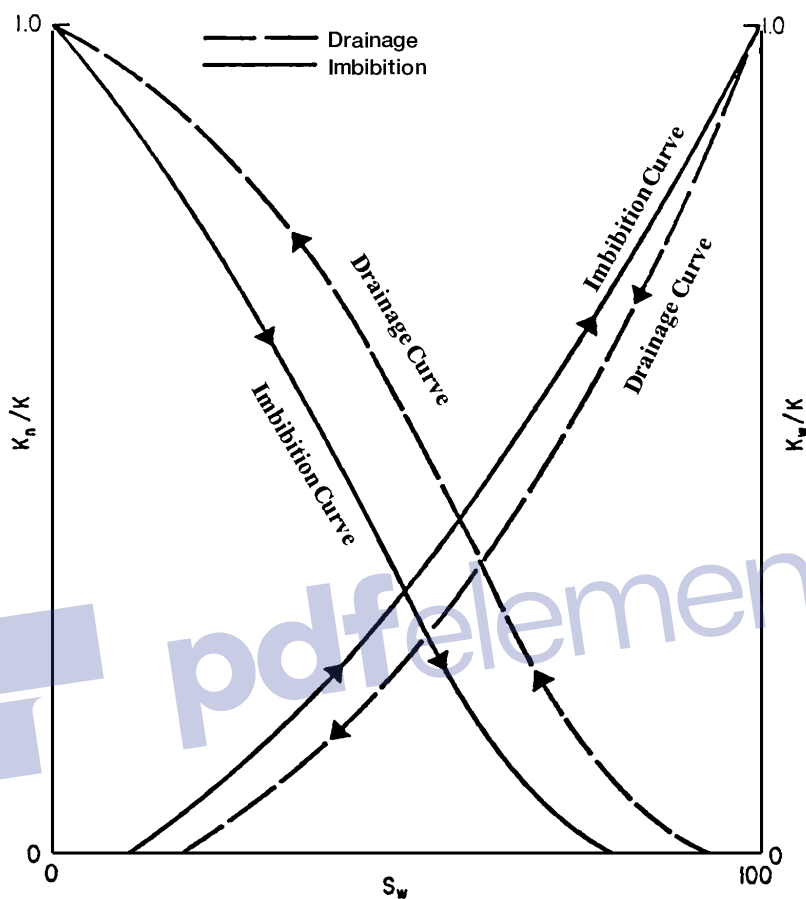


Figure 5-3. Hysteresis effects in relative permeability.

because they only provide the values of S_{wc} , S_{or} , $(k_{ro})_{S_{wc}}$, and $(k_{rw})_{S_{or}}$. Results of these tests are less expensive than normal relative permeability tests; however, they can provide useful information on reservoir characteristics. Listed below are end-point test data for three sandstone cores:

| Sample | ϕ , % | k , md | S_{wc} , % | S_{or} , % | $(k_{ro})_{S_{wc}}$ | $(k_{rw})_{S_{or}}$ |
|--------|------------|----------|--------------|--------------|---------------------|---------------------|
| 1 | 15 | 10 | 28 | 35 | 0.70 | 0.20 |
| 2 | 16 | 5 | 35 | 34 | 0.65 | 0.25 |
| 3 | 12 | 20 | 25 | 40 | 0.75 | 0.27 |

Two-Phase Relative Permeability Correlations

In many cases, relative permeability data on actual samples from the reservoir under study may not be available, in which case it is necessary to obtain the desired relative permeability data in some other manner. Field relative permeability data can usually be calculated, and the procedure will be discussed more fully in Chapter 6. The field data are unavailable for future production, however, and some substitute must be devised. Several methods have been developed for calculating relative permeability relationships. Various parameters have been used to calculate the relative permeability relationships, including:

- Residual and initial saturations
- Capillary pressure data

In addition, most of the proposed correlations use the effective phase saturation as a correlating parameter. The effective phase saturation is defined by the following set of relationships:

$$S_o^* = \frac{S_o}{1 - S_{wc}} \quad (5-1)$$

$$S_w^* = \frac{S_w - S_{wc}}{1 - S_{wc}} \quad (5-2)$$

$$S_g^* = \frac{S_g}{1 - S_{wc}} \quad (5-3)$$

where S_o^* , S_w^* , S_g^* = effective oil, water, and gas saturation, respectively
 S_o , S_w , S_g = oil, water, and gas saturation, respectively
 S_{wc} = connate (irreducible) water saturation

1. Wyllie and Gardner Correlation

Wyllie and Gardner (1958) observed that, in some rocks, the relationship between the reciprocal capillary pressure squared ($1/P_c^2$) and the effective water saturation S_w^* is linear over a wide range of saturation. Honapour et al. (1988) conveniently tabulated Wyllie and Gardner correlations as shown below:

| Drainage Oil-Water Relative Permeabilities | | | |
|--|----------------------------------|-----------------|----------|
| Type of formation | k_{ro} | k_{rw} | Equation |
| Unconsolidated sand, well sorted | $(1 - S_w^*)$ | $(S_w^*)^3$ | (5-4) |
| Unconsolidated sand, poorly sorted | $(1 - S_w^*)^2 (1 - S_w^{*1.5})$ | $(S_o^*)^{3.5}$ | (5-5) |
| Cemented sandstone, oolitic limestone | $(1 - S_w^*)^2 (1 - S_w^{*2})$ | $(S_o^*)^4$ | (5-6) |

| Drainage Gas-Oil Relative Permeabilities | | | |
|---|-----------------|----------------------------------|----------|
| Type of formation | k_{ro} | k_{rg} | Equation |
| Unconsolidated sand, well sorted | $(S_o^*)^3$ | $(1 - S_o^*)^3$ | (5-7) |
| Unconsolidated sand, poorly sorted | $(S_o^*)^{3.5}$ | $(1 - S_o^*)^2 (1 - S_o^{*1.5})$ | (5-8) |
| Cemented sandstone, oolitic limestone, rocks with vugular porosity | $(S_o^*)^4$ | $(1 - S_o^*)^2 (1 - S_o^{*2})$ | (5-9) |

Wyllie and Gardner have also suggested the following two expressions that can be used when one relative permeability is available:

- **Oil-water system**

$$k_{rw} = (S_w^*)^2 - k_{ro} \left[\frac{S_w^*}{1 - S_w^*} \right] \quad (5-10)$$

- **Gas-oil system**

$$k_{ro} = (S_o^*) - k_{rg} \left[\frac{S_o^*}{1 - S_o^*} \right] \quad (5-11)$$

2. Torcaso and Wyllie Correlation

Torcaso and Wyllie (1958) developed a simple expression to determine the relative permeability of the oil phase in a gas-oil system. The expression permits the calculation of k_{ro} from the measurements of k_{rg} . The equation has the following form:

$$k_{ro} = k_{rg} \left[\frac{(S_o^*)^4}{(1 - S_o^*)^2 (1 - (S_o^*)^2)} \right] \quad (5-12)$$

The above expression is very useful since k_{rg} measurements are easily made and k_{ro} measurements are usually made with difficulty.

3. Pirson's Correlation

From petrophysical considerations, Pirson (1958) derived generalized relationships for determining the wetting and nonwetting phase relative permeability for both imbibition and drainage processes. The generalized expressions are applied for water-wet rocks.

For the Water (Wetting) Phase

$$k_{rw} = \sqrt{S_w^*} S_w^3 \quad (5-13)$$

The above expression is valid for both the imbibition and drainage processes.

For the Nonwetting Phase

• Imbibition

$$(k_r)_{\text{nonwetting}} = \left[1 - \left(\frac{S_w - S_{wc}}{1 - S_{wc} - S_{nw}} \right) \right]^2 \quad (5-14)$$

• Drainage

$$(k_r)_{\text{nonwetting}} = (1 - S_w^*) \left[1 - (S_w^*)^{0.25} \sqrt{S_w} \right]^{0.5} \quad (5-15)$$

where S_{nw} = saturation of the nonwetting phase

S_w = water saturation

S_w^* = effective water saturation as defined by Equation 5-2

Example 5-1

Generate the drainage relative permeability data for an unconsolidated well-sorted sand by using the Wyllie and Gardner method. Assume the following critical saturation values:

$$S_{oc} = 0.3, \quad S_{wc} = 0.25, \quad S_{gc} = 0.05$$

Solution

Generate the oil-water relative permeability data by applying Equation 5-4 in conjunction with Equation 5-2, to give:

| S_w | $S_w^* = \frac{S_w - S_{wc}}{1 - S_{wc}}$ | $k_{ro} = (1 - S_w^*)^3$ | $K_{rw} = (S_w^*)^3$ |
|-------|---|--------------------------|----------------------|
| 0.25 | 0.0000 | 1.000 | 0.0000 |
| 0.30 | 0.0667 | 0.813 | 0.0003 |
| 0.35 | 0.1333 | 0.651 | 0.0024 |
| 0.40 | 0.2000 | 0.512 | 0.0080 |
| 0.45 | 0.2667 | 0.394 | 0.0190 |
| 0.50 | 0.3333 | 0.296 | 0.0370 |
| 0.60 | 0.4667 | 0.152 | 0.1017 |
| 0.70 | 0.6000 | 0.064 | 0.2160 |

Apply Equation 5-7 in conjunction with Equation 5-1 to generate relative permeability data for the gas-oil system.

| S_g | $S_o = 1 - S_g - S_{wc}$ | $S_o^* = \frac{S_o}{1 - S_{wc}}$ | $k_{ro} = (S_o^*)^3$ | $k_{rg} = (1 - S_o^*)^3$ |
|-------|--------------------------|----------------------------------|----------------------|--------------------------|
| 0.05 | 0.70 | 0.933 | 0.813 | — |
| 0.10 | 0.65 | 0.867 | 0.651 | 0.002 |
| 0.20 | 0.55 | 0.733 | 0.394 | 0.019 |
| 0.30 | 0.45 | 0.600 | 0.216 | 0.064 |
| 0.40 | 0.35 | 0.467 | 0.102 | 0.152 |
| 0.50 | 0.25 | 0.333 | 0.037 | 0.296 |
| 0.60 | 0.15 | 0.200 | 0.008 | 0.512 |
| 0.70 | 0.05 | 0.067 | 0.000 | 0.813 |

Example 5-2

Resolve Example 5-1 by using Pirson's correlation for the water-oil system.

Solution

| S_w | $S_w^* = \frac{S_w - S_{wc}}{1 - S_{wc}}$ | $k_{rw} = \sqrt{S_w^* S_w^3}$ | $k_{ro} = (1 - S_w^*) \left[1 - (S_w^*)^{2.5} \sqrt{S_w} \right]^{0.5}$ |
|-------|---|-------------------------------|--|
| 0.25 | 0.0000 | 0.000 | 1.000 |
| 0.30 | 0.0667 | 0.007 | 0.793 |
| 0.35 | 0.1333 | 0.016 | 0.695 |
| 0.40 | 0.2000 | 0.029 | 0.608 |
| 0.45 | 0.2667 | 0.047 | 0.528 |
| 0.50 | 0.3333 | 0.072 | 0.454 |
| 0.60 | 0.4667 | 0.148 | 0.320 |
| 0.70 | 0.6000 | 0.266 | 0.205 |

4. Corey's Method

Corey (1954) proposed a simple mathematical expression for generating the relative permeability data of the gas-oil system. The approximation is good for drainage processes, i.e., gas-displacing oil.

$$k_{ro} = (1 - S_g^*)^4 \quad (5-16)$$

$$k_{rg} = (S_g^*) (2 - S_g^*) \quad (5-17)$$

where the effective gas saturation S_g^* is defined in Equation 5-3.

Corey (1954) proposed that the water-oil relative permeability can be represented as follows:

$$k_{ro} = \left(\frac{1 - S_w}{1 - S_{wc}} \right)^4$$

$$k_{rw} = \left(\frac{S_w - S_{wc}}{1 - S_{wc}} \right)^4$$

or:

$$(k_{ro})^{0.25} = \left(\frac{1 - S_w}{1 - S_{wc}} \right)$$

$$(k_{rw})^{0.25} = \left(\frac{S_w - S_{wc}}{1 - S_{wc}} \right)$$

The last two expressions suggest that a plot of $K_{ro}^{0.25}$ and $K_{rw}^{0.25}$ versus S_w would produce straight lines with the following end values:

$$\begin{aligned}k_{ro} &= 1.0 @ S_{wc} \\k_{rw} &= 1.0 @ S_w = 1.0 \\k_{ro} &= 0.0 @ S_w = 1.0 \\k_{rw} &= 0.0 @ S_{wc}\end{aligned}$$

It should be pointed out that Corey's equations apply only to well-sorted homogeneous rocks. To account for the degree of consolidation, the exponent of the relationships (i.e., 4) can be expressed in a more generalized way:

$$k_{ro} = \left(\frac{1 - S_w}{1 - S_{wc}} \right)^n$$

$$k_{rw} = \left[\frac{S_w - S_{wc}}{1 - S_{wc}} \right]^m$$

Taking the logarithm of both sides of the previous two expressions gives:

$$\log(k_{ro}) = n \log \left(\frac{1 - S_w}{1 - S_{wc}} \right)$$

$$\log(k_{rw}) = m \log \left(\frac{S_w - S_{wc}}{1 - S_{wc}} \right)$$

The exponents n and m represent slopes of the two straight lines resulting from plotting k_{ro} and k_{rw} versus the term in parentheses on a log-log scale.

Example 5-3

Use Corey's approximation to generate the gas-oil relative permeability for a formation with a connate-water saturation of 0.25.

Solution

| S_g | $S_g^* = \frac{S_g}{1 - S_{wc}}$ | $k_{ro} = (1 - S_g^*)^4$ | $k_{rg} = (S_g^*)^3 (2 - S_g^*)$ |
|-------|----------------------------------|--------------------------|----------------------------------|
| 0.05 | 0.0667 | 0.759 | 0.001 |
| 0.10 | 0.1333 | 0.564 | 0.004 |
| 0.20 | 0.2667 | 0.289 | 0.033 |
| 0.30 | 0.4000 | 0.130 | 0.102 |
| 0.40 | 0.5333 | 0.047 | 0.222 |
| 0.50 | 0.6667 | 0.012 | 0.395 |
| 0.60 | 0.8000 | 0.002 | 0.614 |
| 0.70 | 0.9333 | 0.000 | 0.867 |

5. Relative Permeability from Capillary Pressure Data

Rose and Bruce (1949) showed that capillary pressure p_c is a measure of the fundamental characteristics of the formation and could also be used to predict the relative permeabilities. Based on the concepts of tortuosity, Wyllie and Gardner (1958) developed the following mathematical expression for determining the drainage water-oil relative permeability from capillary pressure data:

$$k_{rw} = \left(\frac{S_w - S_{wc}}{1 - S_{wc}} \right)^2 \frac{\int_{S_{wc}}^{S_w} dS_w / p_c^2}{\int_{S_{wc}}^1 dS_w / p_c^2} \quad (5-18)$$

$$k_{ro} = \left(\frac{1 - S_w}{1 - S_{wc}} \right)^2 \frac{\int_{S_w}^1 dS_w / p_c^2}{\int_{S_{wc}}^1 dS_w / (p_c)^2} \quad (5-19)$$

Wyllie and Gardner also presented two expressions for generating the oil and gas relative permeabilities in the presence of the connate-water saturation. The authors considered the connate-water as part of the rock matrix to give:

$$k_{ro} = \left(\frac{S_o - S_{or}}{1 - S_{or}} \right)^2 \frac{\int_0^{S_o} dS_o / p_c^2}{\int_0^1 dS_o / p_c^2} \quad (5-20)$$

$$k_{rg} = \left(1 - \frac{S_o - S_{or}}{S_g - S_{gc}} \right)^2 \frac{\int_{S_o}^1 dS_o / p_c^2}{\int_0^1 dS_o / p_c^2} \quad (5-21)$$

where S_{gc} = critical gas saturation
 S_{wc} = connate-water saturation
 S_{or} = residual oil saturation

Corey observed that the plot of $1/p_c^2$ versus effective water saturation S_w^* may produce or yield a straight line over a considerable range of saturations. By applying this observation and making further simplifications, Corey reduced Equations 5-20 and 5-21 to:

$$k_{ro} = (S_w^*)^4$$

$$k_{rg} = (1 - S_w^*)^2 [1 - (S_w^*)^2]$$

Example 5-4

The laboratory capillary pressure curve for a water-oil system between the connate-water saturation and a water saturation of 100% is represented by the following linear equation:

$$P_c = 22 - 20 S_w$$

The connate-water saturation is 30%. Using Wyllie and Gardner methods, generate the relative permeability data for the oil-water system.

Solution

Step 1. Integrate the capillary pressure equation, to give:

$$I = \int_a^b \frac{dS_w}{(22 - 20S_w)^2} = \left[\frac{1}{440 - 400b} \right] - \left[\frac{1}{440 - 400a} \right]$$

Step 2. Evaluate the above integral at the following limits:

$$\bullet \int_{0.3}^1 \frac{dS_w}{(22 - 20S_w)^2} = \left[\frac{1}{440 - 400(1)} - \frac{1}{440 - 400(0.3)} \right] = 0.02188$$

$$\bullet \int_{.3}^{S_w} \frac{dS_w}{(22 - 20S_w)^2} = \left[\frac{1}{440 - 400S_w} - 0.00313 \right]$$

$$\bullet \int_{S_w}^1 \frac{dS_w}{(22 - 20S_w)^2} = \left[0.025 - \frac{1}{440 - 400S_w} \right]$$

Step 3. Construct the following working table:

| S_w | k_{rw} Equation 5-18 | k_{ro} Equation 5-19 |
|-------|---------------------------|---------------------------|
| 0.3 | 0.0000 | 1.0000 |
| 0.4 | 0.0004 | 0.7195 |
| 0.5 | 0.0039 | 0.4858 |
| 0.6 | 0.0157 | 0.2985 |
| 0.7 | 0.0466 | 0.1574 |

6. Relative Permeability from Analytical Equations

Analytical representations for individual-phase relative permeabilities are commonly used in numerical simulators. The most frequently used functional forms for expressing the relative permeability and capillary pressure data are given below:

Oil-Water Systems:

$$k_{ro} = (k_{ro})_{S_{wc}} \left[\frac{1 - S_w - S_{orw}}{1 - S_{wc} - S_{orw}} \right]^{n_o} \quad (5-22)$$

$$k_{rw} = (k_{rw})_{S_{orw}} \left[\frac{S_w - S_{wc}}{1 - S_{wc} - S_{orw}} \right]^{n_w} \quad (5-23)$$

$$p_{cwo} = (p_c)_{S_{wc}} \left(\frac{1 - S_w - S_{orw}}{1 - S_{wc} - S_{orw}} \right)^{n_p} \quad (5-24)$$

Gas-Oil Systems:

$$k_{ro} = (k_{ro})_{S_{gc}} \left[\frac{1 - S_g - S_{lc}}{1 - S_{gc} - S_{lc}} \right]^{n_{go}} \quad (5-25)$$

$$k_{rg} = (k_{rg})_{S_{wc}} \left[\frac{S_g - S_{gc}}{1 - S_{lc} - S_{gc}} \right]^{n_g} \quad (5-26)$$

$$p_{cgo} = (p_c)_{S_{lc}} \left[\frac{S_g - S_{gc}}{1 - S_{lc} - S_{gc}} \right]^{n_{pg}} \quad (5-27)$$

with

$$S_{lc} = S_{wc} + S_{org}$$

where S_{lc} = total critical liquid saturation

$(k_{ro})_{S_{wc}}$ = oil relative permeability at connate-water saturation

$(k_{ro})_{S_{gc}}$ = oil relative permeability at critical gas saturation

S_{orw} = residual oil saturation in the water-oil system

S_{org} = residual oil saturation in the gas-oil system

S_{gc} = critical gas saturation

$(k_{rw})_{S_{orw}}$ = water relative permeability at the residual oil saturation

n_o, n_w, n_g, n_{go} = exponents on relative permeability curves

p_{cwo} = capillary pressure of water-oil systems

$(p_c)_{S_{wc}}$ = capillary pressure at connate-water saturation

n_p = exponent of the capillary pressure curve for the oil-water system

p_{cgo} = capillary pressure of gas-oil system

n_{pg} = exponent of the capillary pressure curve in gas-oil system

$(p_c)_{S_{lc}}$ = capillary pressure at critical liquid saturation.

The exponents and coefficients of Equations 5-22 through 5-26 are usually determined by the least-squares method to match the experimental or field relative permeability and capillary pressure data.

Figures 5-4 and 5-5 schematically illustrate the key critical saturations and the corresponding relative permeability values that are used in Equations 5-22 through 5-27.

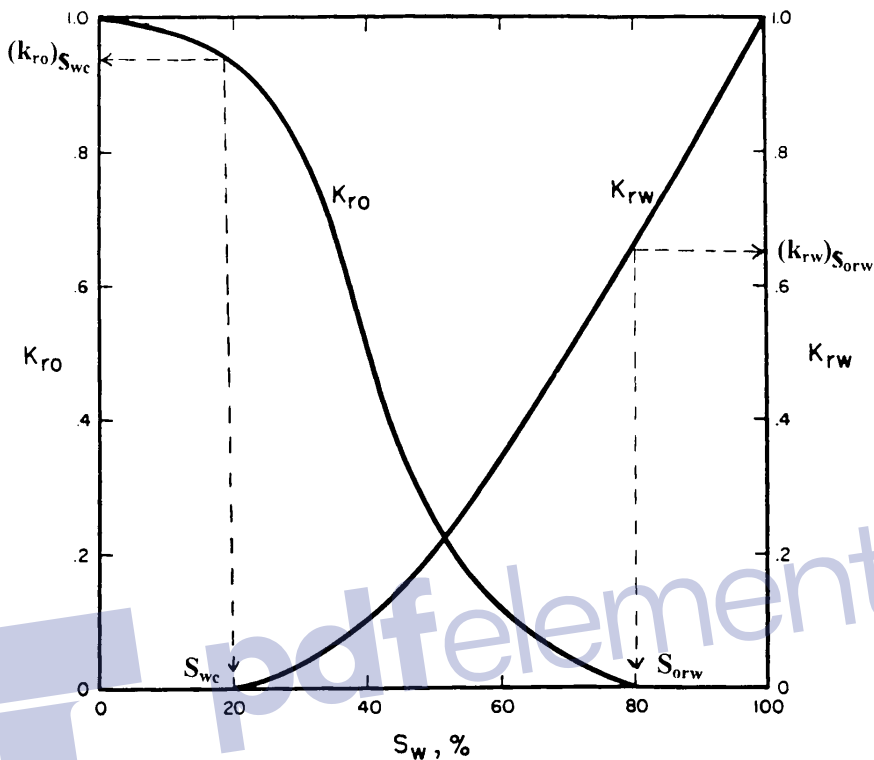


Figure 5-4. Water-oil relative permeability curves.

Example 5-5

Using the analytical expressions of Equations 5-22 through 5-27, generate the relative permeability and capillary pressure data. The following information on the water-oil and gas-oil systems is available:

| | | | |
|----------------------------|----------------------------|---------------------------|-----------------|
| $S_{wc} = 0.25$ | $S_{orw} = 0.35$ | $S_{gc} = 0.05$ | $S_{org} = .23$ |
| $(k_{ro})_{S_{wc}} = 0.85$ | $(k_{rw})_{S_{orw}} = 0.4$ | $(P_c)_{S_{wc}} = 20$ psi | |
| $(k_{ro})_{S_{gc}} = 0.60$ | $(k_{rg})_{S_{wc}} = 0.95$ | | |
| $n_o = 0.9$ | $n_w = 1.5$ | $n_p = 0.71$ | |
| $n_{go} = 1.2$ | $n_g = 0.6$ | $(p_c)_{S_{lc}} = 30$ psi | |
| $n_{pg} = 0.51$ | | | |

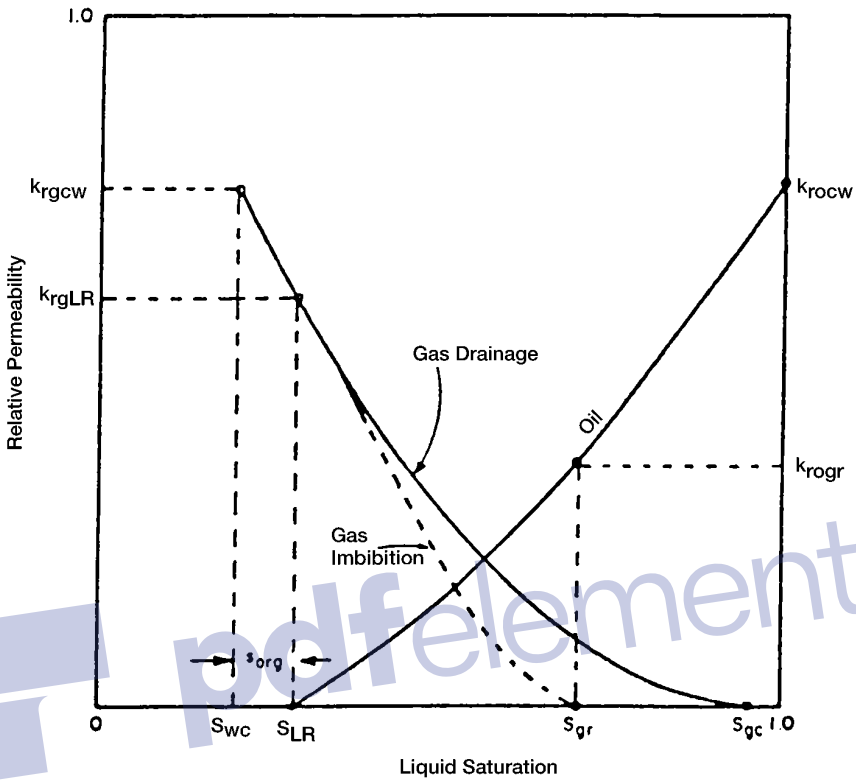


Figure 5-5. Gas-oil relative permeability curves.

Solution

Step 1. Calculate residual liquid saturation S_{lc} .

$$\begin{aligned} S_{lc} &= S_{wc} + S_{org} \\ &= 0.25 + 0.23 = 0.48 \end{aligned}$$

Step 2. Generate relative permeability and capillary pressure data for oil-water system by applying Equations 5-22 through 5-24.

| S_w | k_{ro} Equation 5-22 | k_{rw} Equation 5-23 | P_c Equation 5-24 |
|-------|---------------------------|---------------------------|------------------------|
| 0.25 | 0.850 | 0.000 | 20.00 |
| 0.30 | 0.754 | 0.018 | 18.19 |
| 0.40 | 0.557 | 0.092 | 14.33 |
| 0.50 | 0.352 | 0.198 | 9.97 |
| 0.60 | 0.131 | 0.327 | 4.57 |
| 0.65 | 0.000 | 0.400 | 0.00 |

Step 3. Apply Equations 5-25 through 5-27 to determine the relative permeability and capillary data for the gas-oil system.

| S_g | k_{ro} Equation 5-25 | k_{rg} Equation 5-26 | P_c Equation 5-27 |
|-------|---------------------------|---------------------------|------------------------|
| 0.05 | 0.600 | 0.000 | 0.000 |
| 0.10 | 0.524 | 0.248 | 9.56 |
| 0.20 | 0.378 | 0.479 | 16.76 |
| 0.30 | 0.241 | 0.650 | 21.74 |
| 0.40 | 0.117 | 0.796 | 25.81 |
| 0.52 | 0.000 | 0.95 | 30.00 |

RELATIVE PERMEABILITY RATIO

Another useful relationship that derives from the relative permeability concept is the relative (or effective) permeability ratio. This quantity lends itself more readily to analysis and to the correlation of flow performances than does relative permeability itself. The relative permeability ratio expresses the ability of a reservoir to permit flow of one fluid as related to its ability to permit flow of another fluid under the same circumstances. The two most useful permeability ratios are k_{rg}/k_{ro} , the relative permeability to gas with respect to that to oil, and k_{rw}/k_{ro} , the relative permeability to water with respect to that to oil, it being understood that both quantities in the ratio are determined simultaneously on a given system. The relative permeability ratio may vary in magnitude from zero to infinity.

In describing two-phase flow mathematically, it is always the relative permeability ratio (e.g., k_{rg}/k_{ro} or k_{ro}/k_{rw}) that is used in the flow equations. Because of the wide range of the relative permeability ratio values, the permeability ratio is usually plotted on the log scale of semilog paper as a function of the saturation. Like many relative permeability ratio curves, the central or the main portion of the curve is quite linear.

Figure 5-6 shows a plot of k_{rg}/k_{ro} versus gas saturation. It has become common usage to express the central straight-line portion of the relationship in the following analytical form:

$$\frac{k_{rg}}{k_{ro}} = a e^{bS_g} \quad (5-28)$$

The constants a and b may be determined by selecting the coordinate of two different points on the straight-line portion of the curve and substituting in Equation 5-28. The resulting two equations can be solved simultaneously for the constants a and b . To find the coefficients of Equation 5-28 for the straight-line portion of Figure 5-6, select the following two points:

Point 1: at $S_g = 0.2$, the relative permeability ratio $k_{rg}/k_{ro} = 0.07$

Point 2: at $S_g = 0.4$, the relative permeability ratio $k_{rg}/k_{ro} = 0.70$

Imposing the above points on Equation 5-28, gives:

$$0.07 = a e^{0.2b}$$

$$0.70 = a e^{0.4b}$$

Solving simultaneously gives:

- The intercept $a = 0.0070$
- The slope $b = 11.513$

or

$$\frac{k_{rg}}{k_{ro}} = 0.0070 e^{11.513S_g}$$

In a similar manner, Figure 5-7 shows a semilog plot of k_{ro}/k_{rw} versus water saturation.

The middle straight-line portion of the curve is expressed by a relationship similar to that of Equation 5-28.

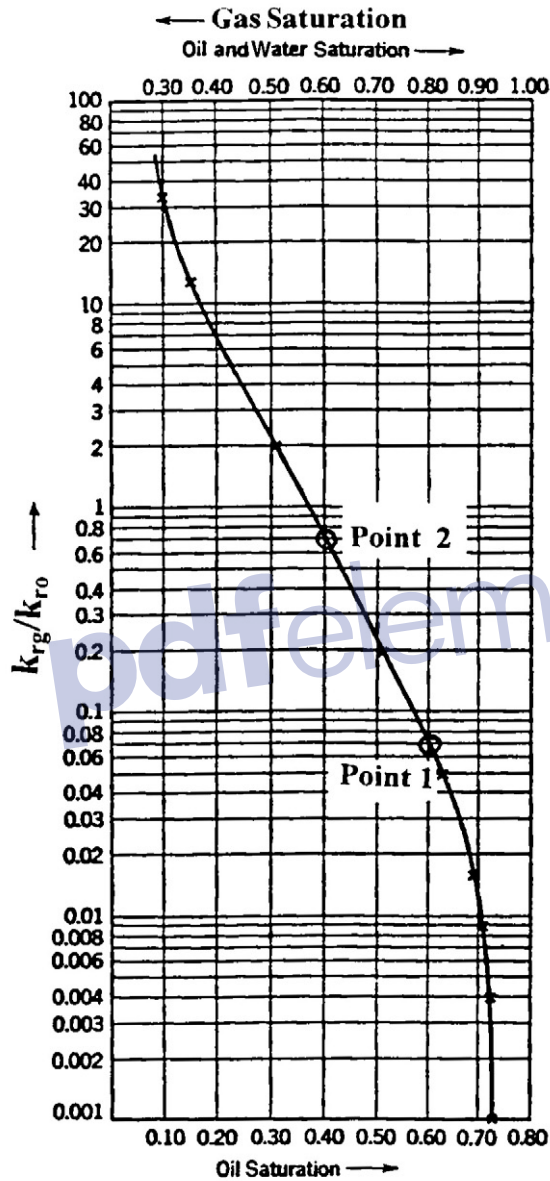


Figure 5-6. k_{rg}/k_{ro} as a function of saturation.

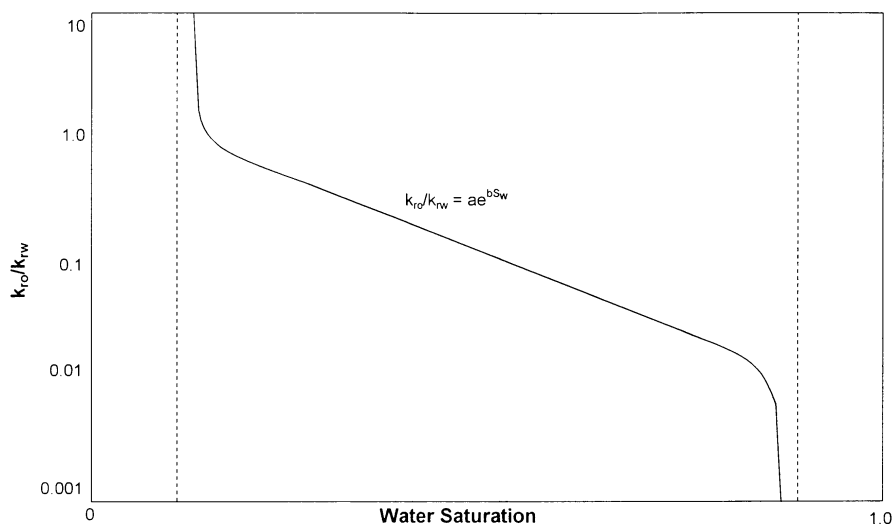


Figure 5-7. Semilog plot of relative permeability ratio vs. saturation.

$$\frac{k_{ro}}{k_{rw}} = a e^{b S_w} \quad (5-29)$$

where the slope b has a negative value.

DYNAMIC PSEUDO-RELATIVE PERMEABILITIES

For a multilayered reservoir with each layer as described by a set of relative permeability curves, it is possible to treat the reservoir by a single layer that is characterized by a weighted-average porosity, absolute permeability, and a set of dynamic pseudo-relative permeability curves. These averaging properties are calculated by applying the following set of relationships:

Average Porosity

$$\phi_{\text{avg}} = \frac{\sum_{i=1}^N \phi_i h_i}{\sum h_i} \quad (5-30)$$

Average Absolute Permeability

$$k_{\text{avg}} = \frac{\sum_{i=1}^N k_i h_i}{\sum_{i=1}^N h_i} \quad (5-31)$$

Average Relative Permeability for the Wetting Phase

$$\bar{k}_{\text{rw}} = \frac{\sum_{i=1}^N (k h)_i (k_{\text{rw}})_i}{\sum_{i=1}^N (k h)_i} \quad (5-32)$$

Average Relative Permeability for the Nonwetting Phase

$$\bar{k}_{\text{rnw}} = \frac{\sum_{i=1}^N (k h)_i (k_{\text{rnw}})_i}{\sum_{i=1}^N (k h)_i} \quad (5-33)$$

The corresponding average saturations should be determined by using Equations 4-16 through 4-18. These equations are given below for convenience:

Average Oil Saturation

$$\bar{S}_o = \frac{\sum_{i=1}^n \phi_i h_i S_{o_i}}{\sum_{i=1}^n \phi_i h_i}$$

Average Water Saturation

$$\bar{S}_w = \frac{\sum_{i=1}^n \phi_i h_i S_{wi}}{\sum_{i=1}^n \phi_i h_i}$$

Average Gas Saturation

$$\bar{S}_g = \frac{\sum_{i=1}^n \phi_i h_i S_{gi}}{\sum_{i=1}^n \phi_i h_i}$$

where n = total number of layers

h_i = thickness of layer i

k_i = absolute permeability of layer i

k_{rw} = average relative permeability of the wetting phase

k_{rnw} = average relative permeability of the nonwetting phase

In Equations 5-22 and 5-23, the subscripts w and n_w represent wetting and nonwetting, respectively. The resulting dynamic pseudo-relative permeability curves are then used in a single-layer model. The objective of the single-layer model is to produce results similar to those from the multilayered, cross-sectional model.

NORMALIZATION AND AVERAGING RELATIVE PERMEABILITY DATA

Results of relative permeability tests performed on several core samples of a reservoir rock often vary. Therefore, it is necessary to average the relative permeability data obtained on individual rock samples. Prior to usage for oil recovery prediction, the relative permeability curves should first be normalized to remove the effect of different initial water and critical oil saturations. The relative permeability can then be de-normalized and assigned to different regions of the reservoir based on the existing critical fluid saturation for each reservoir region.

The most generally used method adjusts all data to reflect assigned end values, determines an average adjusted curve, and finally constructs an average curve to reflect reservoir conditions. These procedures are commonly described as normalizing and de-normalizing the relative permeability data.

To perform the normalization procedure, it is helpful to set up the calculation steps for each core sample i in a tabulated form as shown below:

| Relative Permeability Data for Core Sample i | | | | | |
|--|----------|----------|--|---|---|
| (1) | (2) | (3) | (4) | (5) | (6) |
| S_w | k_{ro} | k_{rw} | $S_w^* = \frac{S_w - S_{wc}}{1 - S_{wc} - S_{oc}}$ | $k_{ro}^* = \frac{k_{ro}}{(k_{ro})_{S_{wc}}}$ | $k_{rw}^* = \frac{k_{rw}}{(k_{rw})_{S_{oc}}}$ |

The following normalization methodology describes the necessary steps for a water-oil system as outlined in the above table.

Step 1. Select several values of S_w starting at S_{wc} (column 1), and list the corresponding values of k_{ro} and k_{rw} in columns 2 and 3.

Step 2. Calculate the normalized water saturation S_w^* for each set of relative permeability curves and list the calculated values in column 4 by using the following expression:

$$S_w^* = \frac{S_w - S_{wc}}{1 - S_{wc} - S_{oc}} \quad (5-34)$$

where S_{oc} = critical oil saturation

S_{wc} = connate-water saturation

S_w^* = normalized water saturation

Step 3. Calculate the normalized relative permeability for the oil phase at different water saturation by using the relation (column 5):

$$k_{ro}^* = \frac{k_{ro}}{(k_{ro})_{S_{wc}}} \quad (5-35)$$

where k_{ro} = relative permeability of oil at different S_w

$(k_{ro})_{S_{wc}}$ = relative permeability of oil at connate-water saturation

k_{ro}^* = normalized relative permeability of oil

Step 4. Normalize the relative permeability of the water phase by applying the following expression and document results of the calculation in column 6:

$$k_{rw}^* = \frac{k_{rw}}{(k_{rw})_{S_{oc}}} \quad (5-36)$$

where $(k_{rw})_{S_{oc}}$ is the relative permeability of water at the critical oil saturation.

Step 5. Using regular Cartesian coordinates, plot the normalized k_{ro}^* and k_{rw}^* versus S_w^* for *all* core samples on the same graph.

Step 6. Determine the average normalized relative permeability values for oil and water as a function of the normalized water saturation by select arbitrary values of S_w^* and calculate the average of k_{ro}^* and k_{rw}^* by applying the following relationships:

$$(k_{ro}^*)_{avg} = \frac{\sum_{i=1}^n (h k k_{ro}^*)_i}{\sum_{i=1}^n (h k)_i} \quad (5-37)$$

$$(k_{rw}^*)_{avg} = \frac{\sum_{i=1}^n (h k k_{rw}^*)_i}{\sum_{i=1}^n (h k)_i} \quad (5-38)$$

where n = total number of core samples

h_i = thickness of sample i

k_i = absolute permeability of sample i

Step 7. The last step in this methodology involves de-normalizing the average curve to reflect actual reservoir and conditions of S_{wc} and S_{oc} . These parameters are the most critical part of the methodology and, therefore, a major effort should be spent in determining representative values. The S_{wc} and S_{oc} are usually determined by averaging the core data, log analysis, or correlations, versus graphs, such as: $(k_{ro})_{S_{wc}}$ vs. S_{wc} , $(k_{rw})_{S_{oc}}$ vs. S_{oc} , and S_{oc} vs. S_{wc} , which should be constructed to determine if a significant correlation

exists. Often, plots of S_{wc} and S_{or} versus $\log Z\bar{k}/\bar{\phi}$ may demonstrate a reliable correlation to determine end-point saturations as shown schematically in Figure 5-8. When representative end values have been estimated, it is again convenient to perform the denormalization calculations in a tabular form as illustrated below:

| (1) | (2) | (3) | (4) | (5) | (6) |
|---------|------------------|------------------|--|---|---|
| S_w^* | $(k_{ro})_{avg}$ | $(k_{rw})_{avg}$ | $S_w = S_w^* (1 - S_{wc} - S_{oc}) + S_{wc}$ | $k_{ro} = (k_{ro})_{avg} (\bar{k}_{ro})_{S_{wc}}$ | $k_{rw} = (k_{rw})_{avg} (\bar{k}_{rw})_{S_{oc}}$ |

Where $(k_{ro})_{S_{wc}}$ and $(k_{ro})_{S_{oc}}$ are the average relative permeability of oil and water at connate-water and critical oil, respectively, and given by:

$$(\bar{k}_{ro})_{S_{wc}} = \frac{\sum_{i=1}^n [hk(k_{ro})_{S_{wc}}]_i}{\sum_{i=1}^n (hk)_i} \quad (5-39)$$

$$(\bar{k}_{rw})_{S_{oc}} = \frac{\sum_{i=1}^n [hk(k_{rw})_{S_{oc}}]_i}{\sum_{i=1}^n (hk)_i} \quad (5-40)$$

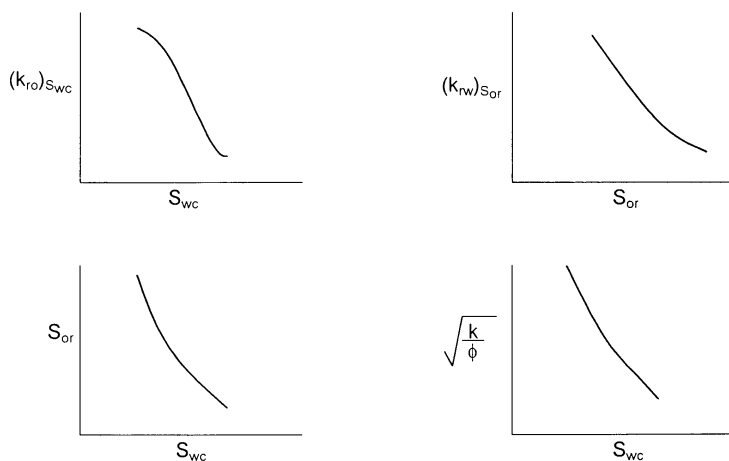


Figure 5-8. Critical saturation relationships.

Example 5-6

Relative permeability measurements are made on three core samples. The measured data are summarized below:

| Core Sample #1 | | | Core Sample #2 | | Core Sample #3 | |
|-----------------|----------|----------|-----------------|----------|-----------------|----------|
| h = 1 ft | | | h = 1 ft | | h = 1 ft | |
| k = 100 md | | | k = 80 md | | k = 150 md | |
| $S_{oc} = 0.35$ | | | $S_{oc} = 0.28$ | | $S_{oc} = 0.35$ | |
| $S_{wc} = 0.25$ | | | $S_{wc} = 0.30$ | | $S_{wc} = 0.20$ | |
| S_w | k_{ro} | k_{rw} | k_{ro} | k_{rw} | k_{ro} | k_{rw} |
| 0.20 | — | — | — | — | 1.000* | 0.000 |
| 0.25 | 0.850* | 0.000 | — | — | 0.872 | 0.008 |
| 0.30 | 0.754 | 0.018 | 0.800 | 0 | 0.839 | 0.027 |
| 0.40 | 0.557 | 0.092 | 0.593 | 0.077 | 0.663 | 0.088 |
| 0.50 | 0.352 | 0.198 | 0.393 | 0.191 | 0.463 | 0.176 |
| 0.60 | 0.131 | 0.327 | 0.202 | 0.323 | 0.215 | 0.286 |
| 0.65 | 0.000 | 0.400* | 0.111 | 0.394 | 0.000 | 0.350* |
| 0.72 | — | — | 0.000 | 0.500* | — | — |

*Values at critical saturations

It is believed that a connate-water saturation of 0.27 and a critical oil saturation of 30% better describe the formation. Generate the oil and water relative permeability data using the new critical saturations.

Solution

Step 1. Calculate the normalized water saturation for each core sample by using Equation 5-36.

| S_w^* | Core Sample #1 S_w^* | Core Sample #2 S_w^* | Core Sample #3 S_w^* |
|---------|---------------------------|---------------------------|---------------------------|
| 0.20 | — | — | 0.000 |
| 0.25 | 0.000 | — | 0.111 |
| 0.30 | 0.125 | 0.000 | 0.222 |
| 0.40 | 0.375 | 0.238 | 0.444 |
| 0.50 | 0.625 | 0.476 | 0.667 |
| 0.60 | 0.875 | 0.714 | 0.889 |
| 0.65 | 1.000 | 0.833 | 1.000 |
| 0.72 | — | 1.000 | — |

Step 2. Determine relative permeability values at critical saturation for each core sample.

| | Core 1 | Core 2 | Core 3 |
|---------------------|--------|--------|--------|
| $(k_{ro})_{S_{wc}}$ | 0.850 | 0.800 | 1.000 |
| $(k_{rw})_{S_{or}}$ | 0.400 | 0.500 | 0.35 |

Step 3. Calculate $(\bar{k}_{ro})_{S_{wc}}$ and $(\bar{k}_{rw})_{S_{or}}$ by applying Equations 5-39 and 5-40 to give:

$$(\bar{k}_{ro})_{S_{wc}} = 0.906$$

$$(\bar{k}_{rw})_{S_{oc}} = 0.402$$

Step 4. Calculate the normalized k_{ro}^* and k_{rw}^* for all core samples:

| S_w | Core 1 | | | Core 2 | | | Core 3 | | |
|-------|---------|------------|------------|---------|------------|------------|---------|------------|------------|
| | S_w^* | k_{ro}^* | k_{rw}^* | S_w^* | k_{ro}^* | k_{rw}^* | S_w^* | k_{ro}^* | k_{rw}^* |
| 0.20 | — | — | — | — | — | — | 0.000 | 1.000 | 0 |
| 0.25 | 0.000 | 1.000 | 0 | — | — | — | 0.111 | 0.872 | 0.023 |
| 0.30 | 0.125 | 0.887 | 0.045 | 0.000 | 1.000 | 0 | 0.222 | 0.839 | 0.077 |
| 0.40 | 0.375 | 0.655 | 0.230 | 0.238 | 0.741 | 0.154 | 0.444 | 0.663 | 0.251 |
| 0.50 | 0.625 | 0.414 | 0.495 | 0.476 | 0.491 | 0.382 | 0.667 | 0.463 | 0.503 |
| 0.60 | 0.875 | 0.154 | 0.818 | 0.714 | 0.252 | 0.646 | 0.889 | 0.215 | 0.817 |
| 0.65 | 1.000 | 0.000 | 1.000 | 0.833 | 0.139 | 0.788 | 1.000 | 0.000 | 1.000 |
| 0.72 | — | — | — | 1.000 | 0.000 | 1.000 | — | — | — |

Step 5. Plot the normalized values of k_{ro}^* and k_{rw}^* versus S_w^* for each core on a regular graph paper as shown in Figure 5-9.

Step 6. Select arbitrary values of S_w^* and calculate the average k_{ro}^* and k_{rw}^* by applying Equations 5-37 and 5-38.

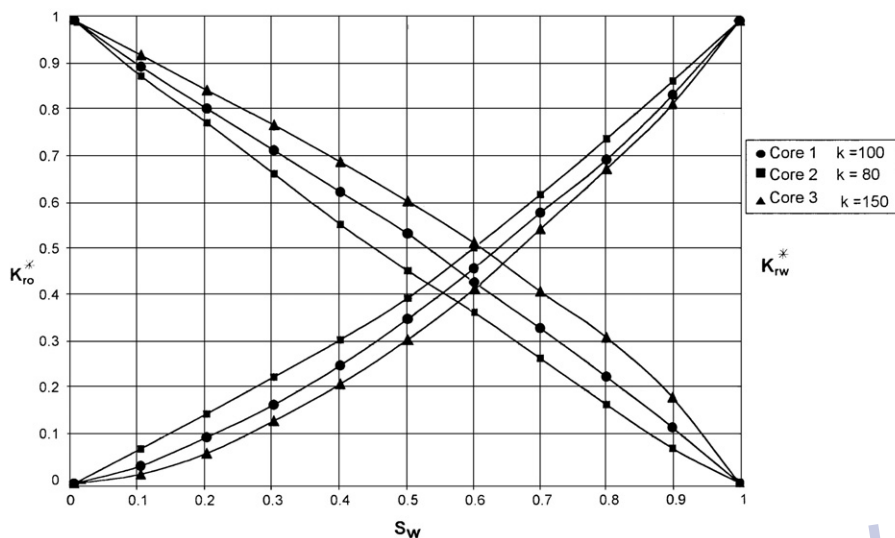


Figure 5-9. Averaging relative permeability data.

| S_w | k^*_{ro} | | | $(k^*_{ro})_{Avg}$ | k^*_{rw} | | | $(k^*_{rw})_{avg}$ |
|-------|------------|--------|--------|--------------------|------------|--------|--------|--------------------|
| | Core 1 | Core 2 | Core 3 | | Core 1 | Core 2 | Core 3 | |
| 0.1 | 0.91 | 0.88 | 0.93 | 0.912 | 0.035 | 0.075 | 0.020 | 0.038 |
| 0.2 | 0.81 | 0.78 | 0.85 | 0.821 | 0.100 | 0.148 | 0.066 | 0.096 |
| 0.3 | 0.72 | 0.67 | 0.78 | 0.735 | 0.170 | 0.230 | 0.134 | 0.168 |
| 0.4 | 0.63 | 0.51 | 0.70 | 0.633 | 0.255 | 0.315 | 0.215 | 0.251 |
| 0.5 | 0.54 | 0.46 | 0.61 | 0.552 | 0.360 | 0.405 | 0.310 | 0.348 |
| 0.6 | 0.44 | 0.37 | 0.52 | 0.459 | 0.415 | 0.515 | 0.420 | 0.442 |
| 0.7 | 0.33 | 0.27 | 0.42 | 0.356 | 0.585 | 0.650 | 0.550 | 0.585 |
| 0.8 | 0.23 | 0.17 | 0.32 | 0.256 | 0.700 | 0.745 | 0.680 | 0.702 |
| 0.9 | 0.12 | 0.07 | 0.18 | 0.135 | 0.840 | 0.870 | 0.825 | 0.833 |

Step 7. Using the desired formation S_{oc} and S_{wc} (i.e., $S_{oc} = 0.30$, $S_{wc} = 0.27$), de-normalize the data to generate the required relative permeability data as shown below:

| S_w^* | $(k_{ro}^*)_{avg}$ | $(k_{rw}^*)_{avg}$ | $S_w = S_w^* (1 - S_{wc} - S_{oc}) + S_{wc}$ | $k_{ro} = 0.906 (k_{ro}^*)_{avg}$ | $k_{rw} = 0.402 (k_{rw}^*)_{avg}$ |
|---------|--------------------|--------------------|--|-----------------------------------|-----------------------------------|
| 0.1 | 0.912 | 0.038 | 0.313 | 0.826 | 0.015 |
| 0.2 | 0.821 | 0.096 | 0.356 | 0.744 | 0.039 |
| 0.3 | 0.735 | 0.168 | 0.399 | 0.666 | 0.068 |
| 0.4 | 0.633 | 0.251 | 0.442 | 0.573 | 0.101 |
| 0.5 | 0.552 | 0.368 | 0.485 | 0.473 | 0.140 |
| 0.6 | 0.459 | 0.442 | 0.528 | 0.416 | 0.178 |
| 0.7 | 0.356 | 0.585 | 0.571 | 0.323 | 0.235 |
| 0.8 | 0.256 | 0.702 | 0.614 | 0.232 | 0.282 |
| 0.9 | 0.135 | 0.833 | 0.657 | 0.122 | 0.335 |

It should be noted that the proposed normalization procedure for water-oil systems as outlined above could be extended to other systems, i.e., gas-oil or gas-water.

THREE-PHASE RELATIVE PERMEABILITY

The relative permeability to a fluid is defined as the ratio of effective permeability at a given saturation of that fluid to the absolute permeability at 100% saturation. Each porous system has unique relative permeability characteristics, which must be measured experimentally. Direct experimental determination of three-phase relative permeability properties is extremely difficult and involves rather complex techniques to determine the fluid saturation distribution along the length of the core. For this reason, the more easily measured two-phase relative permeability characteristics are experimentally determined.

In a three-phase system of this type, it is found that the relative permeability to water depends only upon the water saturation. Since the water can flow only through the smallest interconnect pores that are present in the rock and able to accommodate its volume, it is hardly surprising that the flow of water does not depend upon the nature of the fluids occupying the other pores. Similarly, the gas relative permeability depends only upon the gas saturation. This fluid, like water, is restricted to a particular range of pore sizes and its flow is not influenced by the nature of the fluid or fluids that fill the remaining pores.

The pores available for flow of oil are those that, in size, are larger than pores passing only water, and smaller than pores passing only gas. The number of pores occupied by oil depends upon the particular size

distribution of the pores in the rock in which the three phases coexist and upon the oil saturation itself.

In general, the relative permeability of each phase, i.e., water, gas, and oil, in a three-phase system is essentially related to the existing saturation by the following functions:

$$k_{rw} = f(S_w) \quad (5-41)$$

$$k_{rg} = f(S_g) \quad (5-42)$$

$$k_{ro} = f(S_w, S_g) \quad (5-43)$$

Function 5-43 is rarely known and, therefore, several practical approaches are proposed and based on estimating the three-phase relative permeability from two sets of two-phase data:

Set 1: Oil-Water System

$$k_{row} = f(S_w)$$

$$k_{rw} = f(S_w)$$

Set 2: Oil-Gas System

$$k_{rog} = f(S_g)$$

$$k_{rg} = f(S_g)$$

where k_{row} and k_{rog} are defined as the relative permeability to oil in the water-oil two-phase system and similarly k_{rog} is the relative permeability of oil in the gas-oil system. The symbol k_{ro} is reserved for the oil relative permeability in the three-phase system.

The triangular graph paper is commonly used to illustrate the changes in the relative permeability values when three phases are flowing simultaneously, as illustrated in Figures 5-10 and 5-11. The relative permeability data are plotted as lines of constant percentage relative permeability (oil, water, and gas isoperms). Figures 5-10 and 5-11 show that the relative permeability data, expressed as isoperms, are dependent on the saturation values for all three phases in the rock.

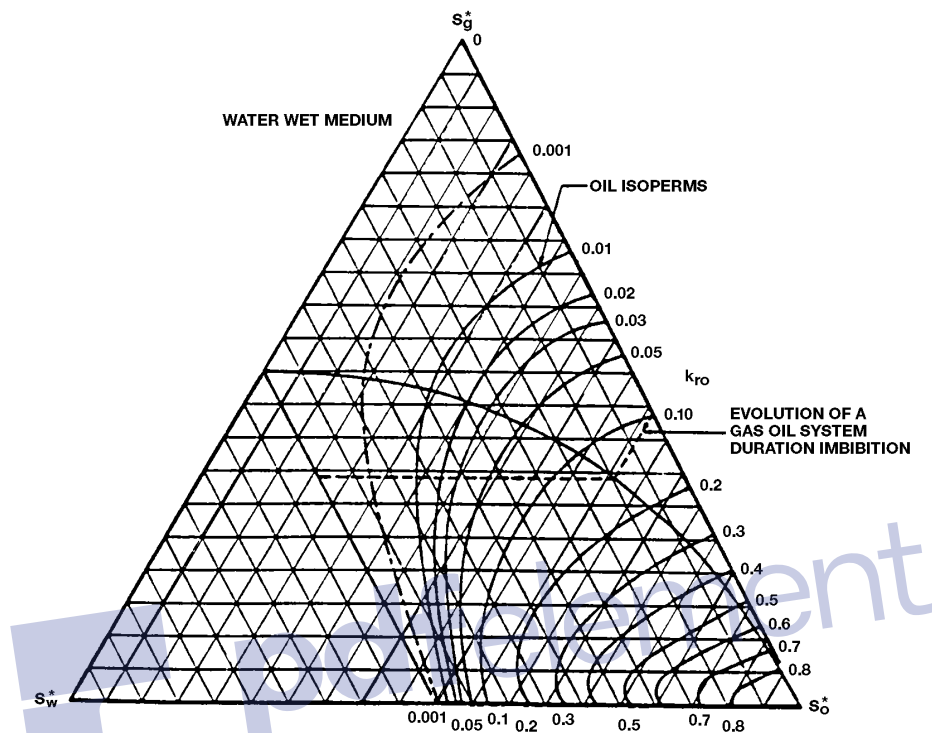


Figure 5-10. Three-phase relative permeability imbibition. (After Honarpour et al., 1988.)

Three-Phase Relative Permeability Correlations

Honarpour, Keoderitz, and Harvey (1988) provided a comprehensive treatment of the two- and three-phase relative permeabilities. The authors listed numerous correlations for estimating relative permeabilities. The simplest approach to predict the relative permeability to the oil phase in a three-phase system is defined as:

$$k_{ro} = k_{row} k_{rog} \quad (5-44)$$

There are several practical and more accurate correlations that have developed over the years, including:

- Wyllie's Correlations
- Stone's Model I
- Stone's Model II
- The Hustad-Holt Correlation

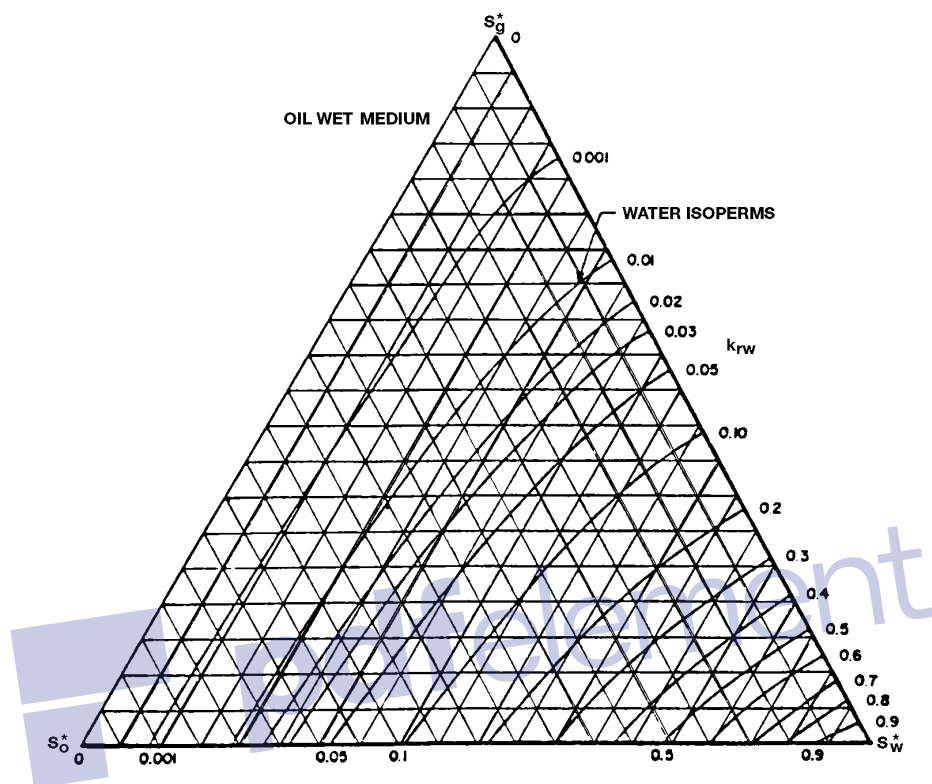


Figure 5-11. Three-phase drainage. (After Honarpour et al., 1988.)

Wyllie's Correlations

Wyllie (1961) proposed the following equations for three-phase relative permeabilities in a water-wet system:

In a cemented sandstone, vugular rock, or oolitic limestone:

$$k_{rg} = \frac{S_g^2 \left[(1 - S_{wc})^2 - (S_w + S_o - S_{wc})^2 \right]}{(1 - S_{wc})^4} \quad (5-45)$$

$$k_{ro} = \frac{S_o^3 (2S_w + S_o - 2S_{wc})}{(1 - S_{wc})^4} \quad (5-46)$$

$$k_{rw} = \left(\frac{S_w - S_{wc}}{1 - S_{wc}} \right)^4 \quad (5-47)$$

In unconsolidated, well-sorted sand:

$$k_{rw} = \left(\frac{S_w - S_{wc}}{1 - S_{wi}} \right)^3 \quad (5-48)$$

$$k_{ro} = \frac{(S_o)^3}{(1 - S_{wc})^3} \quad (5-49)$$

$$k_{rg} = \frac{(S_o)^3 (2S_w + S_o - 2S_{wc})^4}{(1 - S_{wi})^4} \quad (5-50)$$

Stone's Model I

Stone (1970) developed a probability model to estimate three-phase relative permeability data from the laboratory-measured two-phase data. The model combines the channel flow theory in porous media with probability concepts to obtain a simple result for determining the relative permeability to oil in the presence of water and gas flow. The model accounts for hysteresis effects when water and gas saturations are changing in the same direction of the two sets of data.

The use of the channel flow theory implies that water-relative permeability and water-oil capillary pressure in the three-phase system are functions of water saturation alone, irrespective of the relative saturations of oil and gas. Moreover, they are the same function in the three-phase system as in the two-phase water-oil system. Similarly, the gas-phase relative permeability and gas-oil capillary pressure are the same functions of gas saturation in the three-phase system as in the two-phase gas-oil system.

Stone suggested that a nonzero residual oil saturation, called *minimum oil saturation*, S_{om} exists when oil is displaced simultaneously by water and gas. It should be noted that this minimum oil saturation S_{om} is different than the critical oil saturation in the oil-water system (i.e., S_{orw}) and the residual oil saturation in the gas-oil system, i.e., S_{org} . Stone introduced the following normalized saturations:

$$S_o^* = \frac{S_o - S_{om}}{(1 - S_{wc} - S_{om})}, \text{ for } S_o \geq S_{om} \quad (5-51)$$

$$S_w^* = \frac{S_w - S_{wc}}{(1 - S_{wc} - S_{om})}, \text{ for } S_w \geq S_{wc} \quad (5-52)$$

$$S_g^* = \frac{S_g}{(1 - S_{wc} - S_{om})} \quad (5-53)$$

The oil-relative permeability in a three-phase system is then defined as:

$$k_{ro} = S_o^* \beta_w \beta_g \quad (5-54)$$

The two multipliers β_w and β_g are determined from:

$$\beta_w = \frac{k_{row}}{1 - S_w^*} \quad (5-55)$$

$$\beta_g = \frac{k_{rog}}{1 - S_g^*} \quad (5-56)$$

where S_{om} = minimum oil saturation

k_{row} = oil relative permeability as determined from the oil-water two-phase relative permeability at S_w

k_{rog} = oil relative permeability as determined from the gas-oil two-phase relative permeability at S_g

The difficulty in using Stone's first model is selecting the minimum oil saturation S_{om} . Fayers and Mathews (1984) suggested an expression for determining S_{om} .

$$S_{om} = \alpha S_{orw} + (1 - \alpha) S_{org} \quad (5-57)$$

with

$$\alpha = 1 - \frac{S_g}{1 - S_{wc} - S_{org}} \quad (5-58)$$

where S_{orw} = residual oil saturation in the oil-water relative permeability system

S_{org} = residual oil saturation in the gas-oil relative permeability system

Aziz and Sattari (1979) pointed out that Stone's correlation could give k_{ro} values greater than unity. The authors suggested the following normalized form of Stone's model:

$$k_{ro} = \frac{S_o^*}{(1-S_w^*)(1-S_g^*)} \left(\frac{k_{row} k_{rog}}{(k_{ro})_{S_{wc}}} \right) \quad (5-59)$$

where $(k_{ro})_{S_{wc}}$ is the value of the relative permeability of the oil at the connate-water saturation as determined from the oil-water relative permeability system. It should be noted that it is usually assumed that k_{rg} and k_{rog} curves are measured in the presence of connate-water.

Stone's Model II

It was the difficulties in choosing S_{om} that led to the development of Stone's Model II. Stone (1973) proposed the following normalized expression:

$$k_{ro} = (k_{ro})_{S_{wc}} \left[\left(\frac{k_{row}}{(k_{ro})_{S_{wc}}} + k_{rw} \right) \left(\frac{k_{rog}}{(k_{ro})_{S_{wc}}} + k_{rg} \right) - (k_{rw} + k_{rg}) \right] \quad (5-60)$$

This model gives a reasonable approximation to the three-phase relative permeability.

The Hustad-Holt Correlation

Hustad and Holt (1992) modified Stone's Model I by introducing an exponent term n to the normalized saturations to give:

$$k_{ro} = \left[\frac{k_{row} k_{rog}}{(k_{ro})_{S_{wc}}} \right] (\beta)^n \quad (5-61)$$

where

$$\beta = \frac{S_o^*}{(1 - S_w^*)(1 - S_g^*)} \quad (5-62)$$

$$S_o^* = \frac{S_o - S_{om}}{1 - S_{wc} - S_{om} - S_{gc}} \quad (5-63)$$

$$S_g^* = \frac{S_g - S_{gc}}{1 - S_{wc} - S_{om} - S_{gc}} \quad (5-64)$$

$$S_w^* = \frac{S_w - S_{wc}}{1 - S_{wc} - S_{om} - S_{gc}} \quad (5-65)$$

The β term may be interpreted as a variable that varies between zero and one for low- and high-oil saturations, respectively. If the exponent n is one, the correlation is identical to Stone's first model. Increasing n above unity causes the oil isoperms at low oil saturations to spread from one another. n values below unity have the opposite effect.

Example 5-7

Two-phase relative permeability tests were conducted on a core sample to generate the permeability data for oil-water and oil-gas systems. The following information is obtained from the test:

$$\begin{aligned} S_{gc} &= 0.10 & S_{wc} &= 0.15 \\ S_{orw} &= 0.15 & S_{org} &= 0.05 \\ (k_{ro})_{S_{wc}} &= 0.88 \end{aligned}$$

At the existing saturation values of $S_o = 40\%$, $S_w = 30\%$, and $S_g = 30\%$ the two-phase relative permeabilities are listed below:

$$\begin{aligned} k_{row} &= 0.403 \\ k_{rw} &= 0.030 \end{aligned}$$

$$k_{rg} = 0.035$$

$$k_{rog} = 0.175$$

Estimate the three-phase relative permeability at the existing saturations by using:

- a. Stone's Model I
- b. Stone's Model II

Solution

a. Stone's Model I

Step 1. Calculate S_{om} by applying Equations 5-58 and 5-57, to give:

$$\alpha = 1 - \frac{0.3}{1 - 0.15 - 0.05} = 0.625$$

$$S_{om} = (0.625)(0.15) + (1 - 0.625)(0.05) = 0.1125$$

Step 2. Calculate the normalized saturations by applying Equations 5-51 through 5-53.

$$S_o^* = \frac{0.4 - 0.1125}{1 - 0.15 - 0.1125} = 0.3898$$

$$S_w^* = \frac{0.30 - 0.15}{1 - 0.15 - 0.1125} = 0.2034$$

$$S_g^* = \frac{0.3}{1 - 0.15 - 0.1125} = 0.4068$$

Step 3. Estimate k_{ro} by using Equation 5-59.

$$k_{ro} = \frac{0.3898}{(1 - 0.2034)(1 - 0.4068)} \left[\frac{(0.406)(0.175)}{0.88} \right] = 0.067$$

b. Stone's Model II

Apply Equation 5-60 to give:

$$k_{ro} = 0.88 \left[\left(\frac{0.406}{0.88} + 0.03 \right) \left(\frac{0.175}{0.88} + 0.035 \right) - (0.03 + 0.035) \right] = 0.044$$

PROBLEMS

1. Given:

- $S_{wc} = 0.30$ $S_{gc} = 0.06$ $S_{oc} = 0.35$
- unconsolidated well-sorted sand

Generate the drainage relative permeability data by using:

- The Wyllie-Gardner correlation
- Pirson's correlation
- Corey's method

2. The capillary pressure data for an oil-water system are given below:

| S_w | p_c , psi |
|-------|-------------|
| 0.25 | 35 |
| 0.30 | 16 |
| 0.40 | 8.5 |
| 0.50 | 5 |
| 1.00 | 0 |

- Generate the relative permeability data for this system.
- Using the relative permeability ratio concept, plot k_{ro}/k_{rw} versus S_w on a semi log scale and determine the coefficients of the following expression:

$$k_{ro}/k_{rw} = ae^{bS_w}$$

3. Using the relative permeability data of Example 5-6, generate the relative permeability values for a layer in the reservoir that is characterized by the following critical saturations:

$$S_{oc} = 0.25 \quad S_{wc} = 0.25 \quad h = 1$$

4. Prepare a k_{rg}/k_{ro} versus S_g plot for the following laboratory data:

| k_{rg}/k_{ro} | S_g |
|-----------------|-------|
| 1.9 | 0.50 |
| 0.109 | 0.30 |

Find the coefficients of the following relationship:

$$k_{rg}/k_{ro} = ae^b S_g$$

REFERENCES

1. Aziz, K., and Sattari, A., *Petroleum Reservoir Simulation*. London: Applied Science Publishers Ltd., 1979.
2. Corey, A. T., and Rathjens, C. H., "Effect of Stratification on Relative Permeability," *Trans. AIME*, 1956, pp. 207, 358.
3. Corey, A. T., "The Interrelation Between Gas and Oil Relative Permeabilities," *Prod. Mon.*, 1954, pp. 19, 38, 1954.
4. Fayers, F., and Matthews, J. D., "Evaluation of Normalized Stone's Method for Estimating Three-Phase Relative Permeabilities," *SPEJ*, April 1984, pp. 224–239.
5. Honarpour, M. M., Koederitz, L. F., and Harvey, A. H., "Empirical Equations for Estimating Two-Phase Relative Permeability in Consolidated Rock," *Trans. AIME*, 1982, pp. 273, 290.
6. Honarpour, M. M., Koederitz, L. F., and Harvey, A. H., *Relative Permeability of Petroleum Reservoirs*. CRC Press, Inc., 1988.
7. Hustad, O. S., and Holt, T., "Gravity Stable Displacement of Oil by Hydrocarbon Gas after Waterflooding," SPE Paper 24116, EOR Symposium, Tulsa, OK, 1992.
8. Pirson, S. J. (ed.), *Oil Reservoir Engineering*. New York: McGraw-Hill, 1958.
9. Rose, W. D., and Bruce, W. A., "Evaluation of Capillary Character in Petroleum Reservoir Rock," *Trans. AIME*, 1949, pp. 127, 186.
10. Stone, H. L., "Estimation of Three-Phase Relative Permeability and Residual Oil Data," *J. of Can. Pet. Technol.*, 1973, pp. 12, 53.
11. Stone, H. L., "Estimation of Three-Phase Relative Permeability," *JPT*, 1970, pp. 2, 214.
12. Torcaso, M. A., and Wyllie, M. R. J., "A Comparison of Calculated k_{rg}/k_{ro} Ratios with Field Data," *JPT*, 1958, pp. 6, 57.
13. Wyllie, M. R. J., and Gardner, G. H. F., "The Generalized Kozeny-Carmen Equation—Its Application to Problems of Multi-Phase Flow in Porous Media," *World Oil*, 1958, pp. 121, 146.
14. Wyllie, M. R. J., "Interrelationship Between Wetting and Nonwetting Phase Relative Permeability," *Trans. AIME*, 1961, pp. 83, 192.

C H A P T E R 6

FUNDAMENTALS OF RESERVOIR FLUID FLOW

Flow in porous media is a very complex phenomenon and as such cannot be described as explicitly as flow through pipes or conduits. It is rather easy to measure the length and diameter of a pipe and compute its flow capacity as a function of pressure; in porous media, however, flow is different in that there are no clear-cut flow paths that lend themselves to measurement.

The analysis of fluid flow in porous media has evolved throughout the years along two fronts—the experimental and the analytical. Physicists, engineers, hydrologists, and the like have examined experimentally the behavior of various fluids as they flow through porous media ranging from sand packs to fused Pyrex glass. On the basis of their analyses, they have attempted to formulate laws and correlations that can then be utilized to make analytical predictions for similar systems.

The main objective of this chapter is to present the mathematical relationships that are designed to describe the flow behavior of the reservoir fluids. The mathematical forms of these relationships will vary depending upon the characteristics of the reservoir. The primary reservoir characteristics that must be considered include:

- Types of fluids in the reservoir
- Flow regimes
- Reservoir geometry
- Number of flowing fluids in the reservoir

TYPES OF FLUIDS

The isothermal compressibility coefficient is essentially the controlling factor in identifying the type of the reservoir fluid. In general, reservoir fluids are classified into three groups:

- Incompressible fluids
- Slightly compressible fluids
- Compressible fluids

As described in Chapter 2, the isothermal compressibility coefficient c is described mathematically by the following two equivalent expressions:

- In terms of fluid volume:

$$c = \frac{-1}{V} \frac{\partial V}{\partial p} \quad (6-1)$$

- In terms of fluid density:

$$c = \frac{1}{\rho} \frac{\partial \rho}{\partial p} \quad (6-2)$$

where V and ρ are the volume and density of the fluid, respectively.

Incompressible Fluids

An incompressible fluid is defined as the fluid whose volume (or density) does not change with pressure, i.e.:

$$\frac{\partial V}{\partial p} = 0$$

$$\frac{\partial \rho}{\partial p} = 0$$

Incompressible fluids do not exist; this behavior, however, may be assumed in some cases to simplify the derivation and the final form of many flow equations.

Slightly Compressible Fluids

These “slightly” compressible fluids exhibit small changes in volume, or density, with changes in pressure. Knowing the volume V_{ref} of a slightly compressible liquid at a reference (initial) pressure p_{ref} , the changes in the volumetric behavior of this fluid as a function of pressure p can be mathematically described by integrating Equation 6-1 to give:

$$-c \int_{p_{\text{ref}}}^p dp = \int_{V_{\text{ref}}}^V \frac{dV}{V}$$

$$e^{c(p_{\text{ref}}-p)} = \frac{V}{V_{\text{ref}}}$$

$$V = V_{\text{ref}} e^{c(p_{\text{ref}}-p)} \quad (6-3)$$

where p = pressure, psia

V = volume at pressure p , ft³

p_{ref} = initial (reference) pressure, psia

V_{ref} = fluid volume at initial (reference) pressure, psia

The e^x may be represented by a series expansion as:

$$e^x = 1 + x + \frac{x^2}{2!} + \frac{x^3}{3!} + \dots + \frac{x^n}{n!} \quad (6-4)$$

Because the exponent x [which represents the term $c(p_{\text{ref}}-p)$] is very small, the e^x term can be approximated by truncating Equation 6-4 to:

$$e^x = 1 + x \quad (6-5)$$

Combining Equation 6-5 with Equation 6-3 gives:

$$V = V_{\text{ref}} [1 + c(p_{\text{ref}} - p)] \quad (6-6)$$

A similar derivation is applied to Equation 6-2 to give:

$$\rho = \rho_{\text{ref}} [1 - c(p_{\text{ref}} - p)] \quad (6-7)$$

where V = volume at pressure p
 ρ = density at pressure p
 V_{ref} = volume at initial (reference) pressure p_{ref}
 ρ_{ref} = density at initial (reference) pressure p_{ref}

It should be pointed out that crude oil and water systems fit into this category.

Compressible Fluids

These are fluids that experience large changes in volume as a function of pressure. All gases are considered compressible fluids. The truncation of the series expansion, as given by Equation 6-5, is not valid in this category and the complete expansion as given by Equation 6-4 is used. As shown previously in Chapter 2 in Equation 2-45, the isothermal compressibility of any compressible fluid is described by the following expression:

$$c_g = \frac{1}{p} - \frac{1}{z} \left(\frac{\partial z}{\partial p} \right)_T \quad (6-8)$$

Figures 6-1 and 6-2 show schematic illustrations of the volume and density changes as a function of pressure for the three types of fluids.

FLOW REGIMES

There are basically three types of flow regimes that must be recognized in order to describe the fluid flow behavior and reservoir pressure distribution as a function of time. There are three flow regimes:

- Steady-state flow
- Unsteady-state flow
- Pseudosteady-state flow

Steady-State Flow

The flow regime is identified as a steady-state flow if the pressure at every location in the reservoir remains constant, i.e., does not change with time. Mathematically, this condition is expressed as:

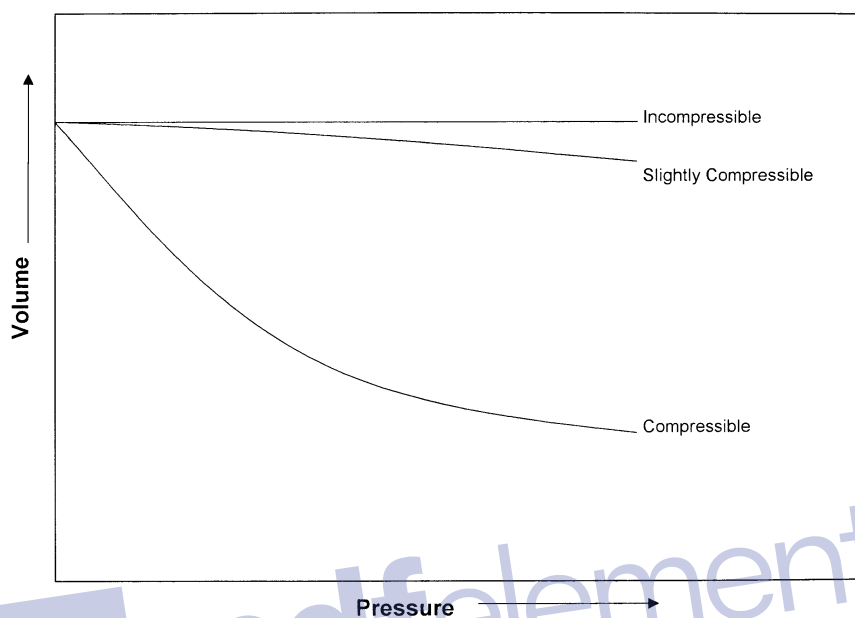


Figure 6-1. Pressure-volume relationship.

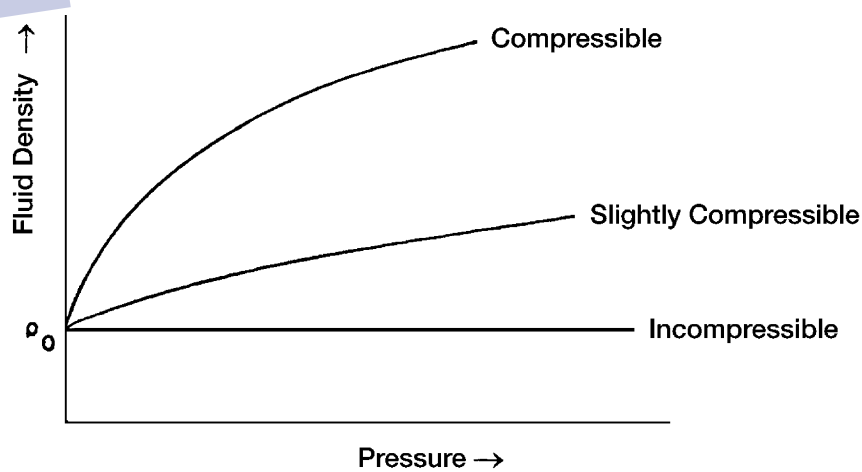


Figure 6-2. Fluid density versus pressure for different fluid types.

$$\left(\frac{\partial p}{\partial t}\right)_i = 0 \quad (6-9)$$

The above equation states that the rate of change of pressure p with respect to time t at any location i is zero. In reservoirs, the steady-state flow condition can only occur when the reservoir is completely recharged and supported by strong aquifer or pressure maintenance operations.

Unsteady-State Flow

The unsteady-state flow (frequently called *transient flow*) is defined as the fluid flowing condition at which the rate of change of pressure with respect to time at any position in the reservoir is not zero or constant. This definition suggests that the pressure derivative with respect to time is essentially a function of both position i and time t , thus

$$\left(\frac{\partial p}{\partial t}\right)_i = f(i, t) \quad (6-10)$$

Pseudosteady-State Flow

When the pressure at different locations in the reservoir is declining linearly as a function of time, i.e., at a constant declining rate, the flowing condition is characterized as the pseudosteady-state flow. Mathematically, this definition states that the rate of change of pressure with respect to time at every position is constant, or

$$\left(\frac{\partial p}{\partial t}\right)_i = \text{constant} \quad (6-11)$$

It should be pointed out that the pseudosteady-state flow is commonly referred to as semisteady-state flow and quasisteady-state flow.

Figure 6-3 shows a schematic comparison of the pressure declines as a function of time of the three flow regimes.

RESERVOIR GEOMETRY

The shape of a reservoir has a significant effect on its flow behavior. Most reservoirs have irregular boundaries and a rigorous mathematical

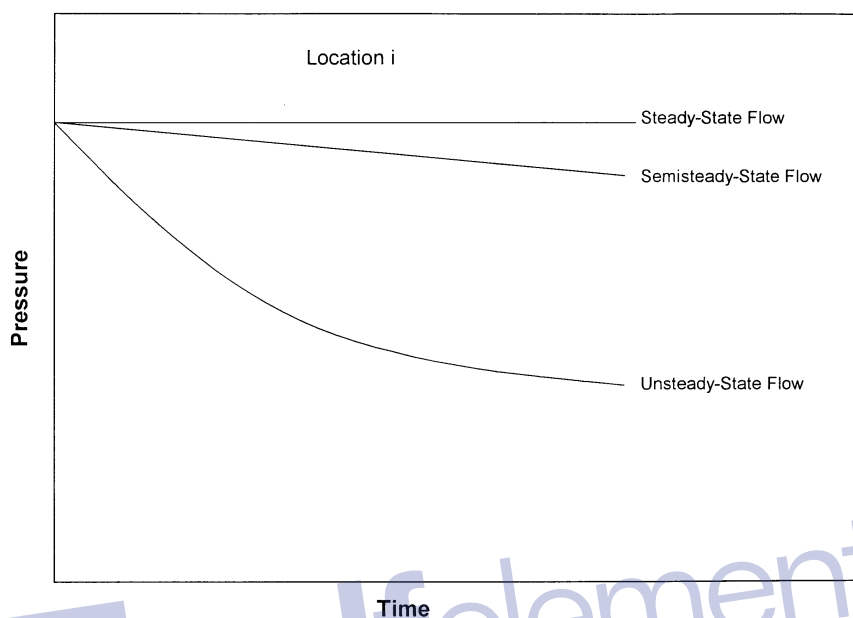


Figure 6-3. Flow regimes.

description of geometry is often possible only with the use of numerical simulators. For many engineering purposes, however, the actual flow geometry may be represented by one of the following flow geometries:

- Radial flow
- Linear flow
- Spherical and hemispherical flow

Radial Flow

In the absence of severe reservoir heterogeneities, flow into or away from a wellbore will follow radial flow lines from a substantial distance from the wellbore. Because fluids move toward the well from all directions and coverage at the wellbore, the term *radial flow* is given to characterize the flow of fluid into the wellbore. Figure 6-4 shows idealized flow lines and iso-potential lines for a radial flow system.

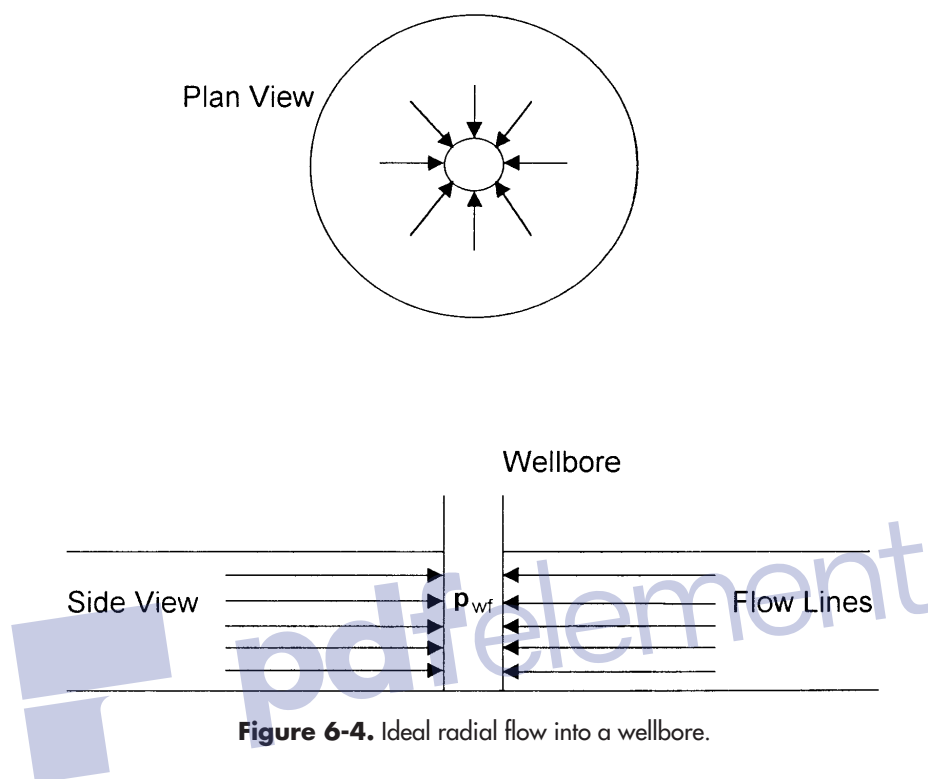


Figure 6-4. Ideal radial flow into a wellbore.

Linear Flow

Linear flow occurs when flow paths are parallel and the fluid flows in a single direction. In addition, the cross-sectional area to flow must be constant. Figure 6-5 shows an idealized linear flow system. A common application of linear flow equations is the fluid flow into vertical hydraulic fractures as illustrated in Figure 6-6.

Spherical and Hemispherical Flow

Depending upon the type of wellbore completion configuration, it is possible to have a spherical or hemispherical flow near the wellbore. A well with a limited perforated interval could result in spherical flow in the vicinity of the perforations as illustrated in Figure 6-7. A well that only partially penetrates the pay zone, as shown in Figure 6-8, could result in hemispherical flow. The condition could arise where coning of bottom water is important.

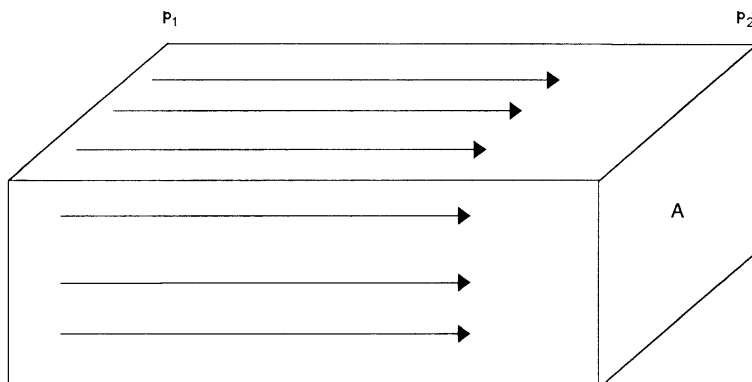


Figure 6-5. Linear flow.

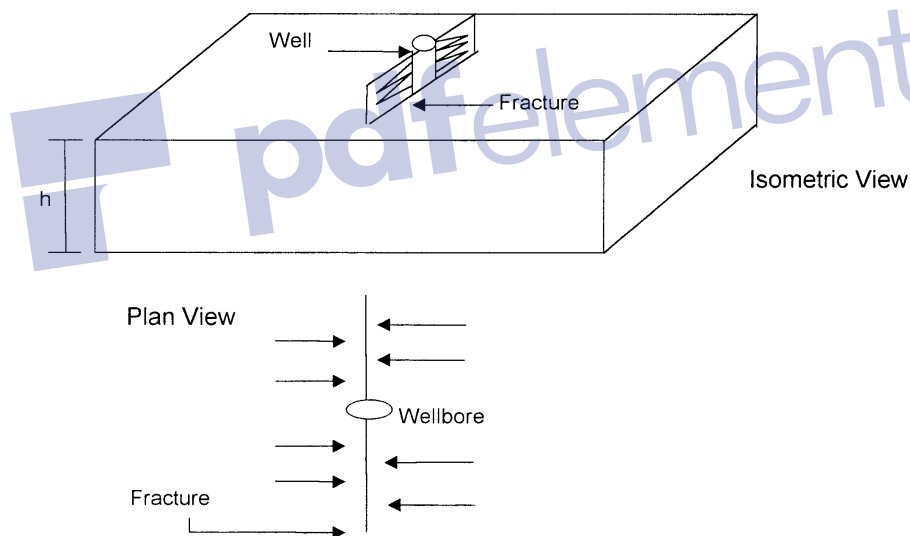


Figure 6-6. Ideal linear flow into vertical fracture.

NUMBER OF FLOWING FLUIDS IN THE RESERVOIR

The mathematical expressions that are used to predict the volumetric performance and pressure behavior of the reservoir vary in forms and complexity depending upon the number of mobile fluids in the reservoir. There are generally three cases of flowing systems:

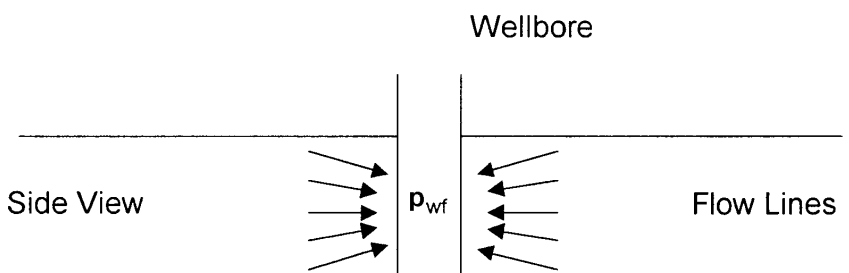


Figure 6-7. Spherical flow due to limited entry.

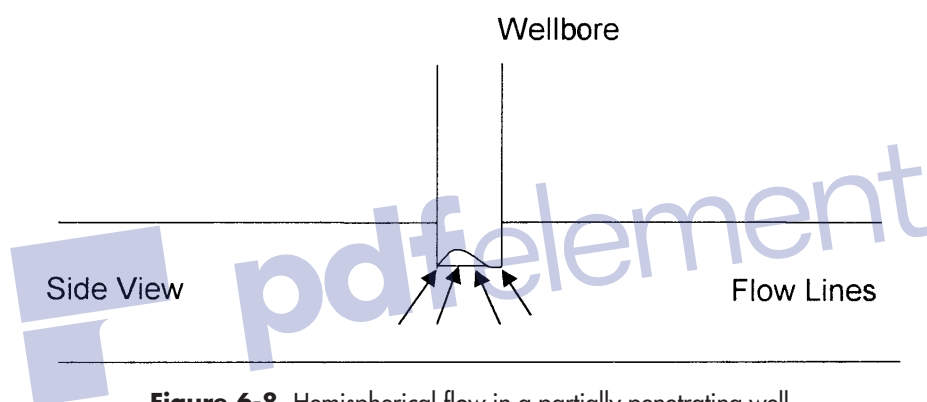


Figure 6-8. Hemispherical flow in a partially penetrating well.

- Single-phase flow (oil, water, or gas)
- Two-phase flow (oil-water, oil-gas, or gas-water)
- Three-phase flow (oil, water, and gas)

The description of fluid flow and subsequent analysis of pressure data becomes more difficult as the number of mobile fluids increases.

FLUID FLOW EQUATIONS

The fluid flow equations that are used to describe the flow behavior in a reservoir can take many forms depending upon the combination of variables presented previously (i.e., types of flow, types of fluids, etc.). By combining the conservation of mass equation with the transport equation (Darcy's equation) and various equations-of-state, the necessary flow equations can be developed. Since all flow equations to be consid-

ered depend on Darcy's Law, it is important to consider this transport relationship first.

Darcy's Law

The fundamental law of fluid motion in porous media is Darcy's Law. The mathematical expression developed by Henry Darcy in 1856 states the velocity of a homogeneous fluid in a porous medium is proportional to the pressure gradient and inversely proportional to the fluid viscosity. For a horizontal linear system, this relationship is:

$$v = \frac{q}{A} = -\frac{k}{\mu} \frac{dp}{dx} \quad (6-12)$$

v is the **apparent** velocity in centimeters per second and is equal to q/A , where q is the volumetric flow rate in cubic centimeters per second and A is total cross-sectional area of the rock in square centimeters. In other words, A includes the area of the rock material as well as the area of the pore channels. The fluid viscosity, μ , is expressed in centipoise units, and the pressure gradient, dp/dx , is in atmospheres per centimeter, taken in the same direction as v and q . The proportionality constant, k , is the *permeability* of the rock expressed in Darcy units.

The negative sign in Equation 6-12 is added because the pressure gradient is negative in the direction of flow as shown in Figure 6-9.

For a horizontal-radial system, the pressure gradient is positive (see Figure 6-10) and Darcy's equation can be expressed in the following generalized radial form:

$$v = \frac{q_r}{A_r} = \frac{k}{\mu} \left(\frac{\partial p}{\partial r} \right)_r \quad (6-13)$$

where q_r = volumetric flow rate at radius r

A_r = cross-sectional area to flow at radius r

$(\partial p/\partial r)_r$ = pressure gradient at radius r

v = apparent velocity at radius r

The cross-sectional area at radius r is essentially the surface area of a cylinder. For a fully penetrated well with a net thickness of h , the cross-sectional area A_r is given by:

$$A_r = 2 \pi r h$$

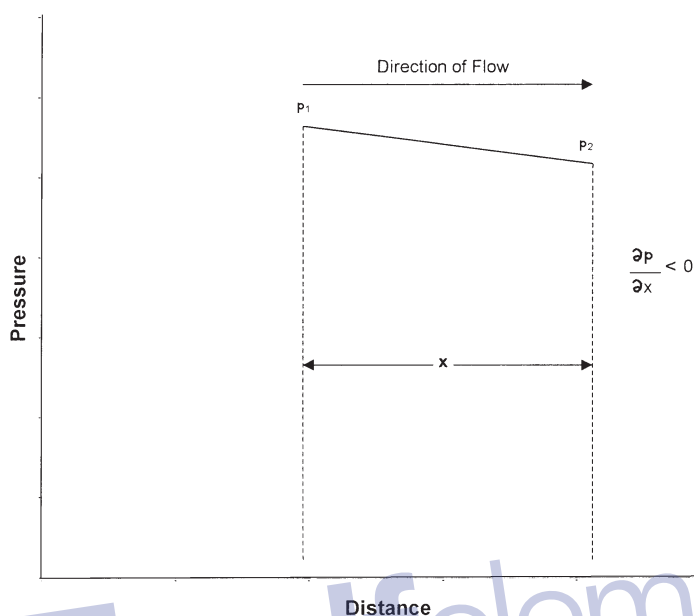


Figure 6-9. Pressure vs. distance in a linear flow.

Darcy's Law applies only when the following conditions exist:

- Laminar (viscous) flow
- Steady-state flow
- Incompressible fluids
- Homogeneous formation

For turbulent flow, which occurs at higher velocities, the pressure gradient increases at a greater rate than does the flow rate and a special modification of Darcy's equation is needed. When turbulent flow exists, the application of Darcy's equation can result in serious errors. Modifications for turbulent flow will be discussed later in this chapter.

STEADY-STATE FLOW

As defined previously, steady-state flow represents the condition that exists when the pressure throughout the reservoir does not change with time. The applications of the steady-state flow to describe the flow behavior of several types of fluid in different reservoir geometries are presented below. These include:

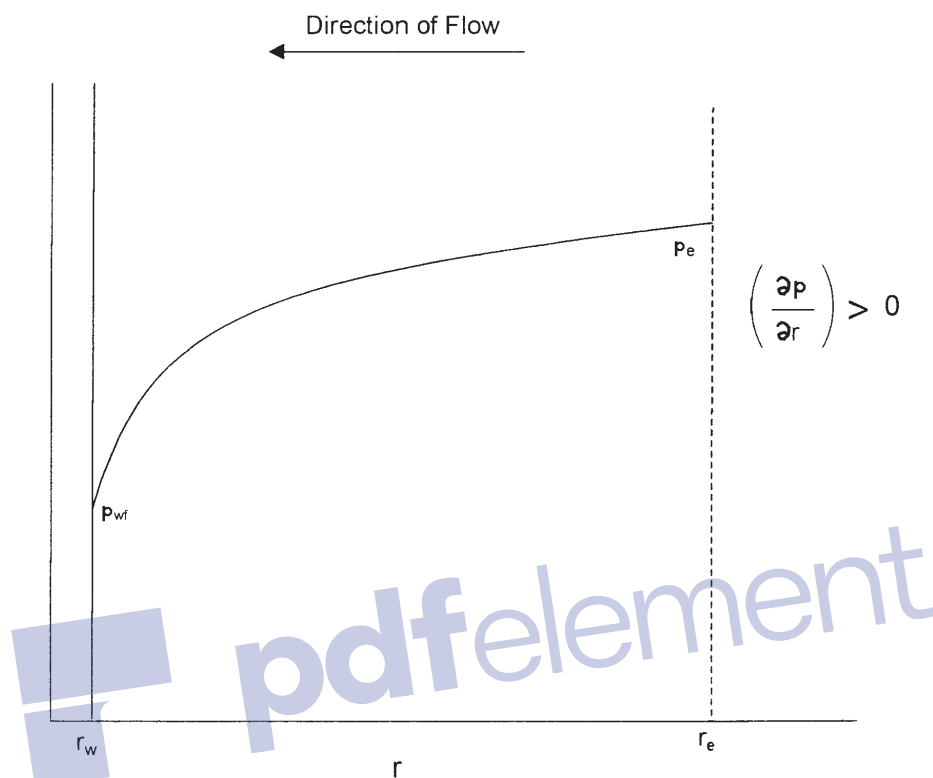


Figure 6-10. Pressure gradient in radial flow.

- Linear flow of incompressible fluids
- Linear flow of slightly compressible fluids
- Linear flow of compressible fluids
- Radial flow of incompressible fluids
- Radial flow of slightly compressible fluids
- Radial flow of compressible fluids
- Multiphase flow

Linear Flow of Incompressible Fluids

In the linear system, it is assumed the flow occurs through a constant cross-sectional area A , where both ends are entirely open to flow. It is also assumed that no flow crosses the sides, top, or bottom as shown in Figure 6-11.

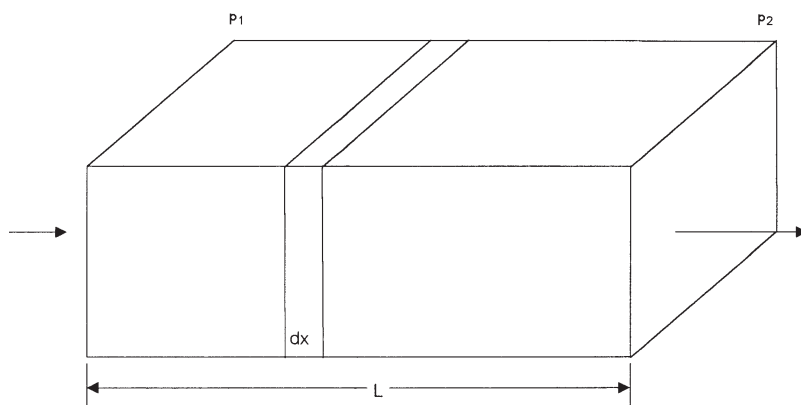


Figure 6-11. Linear flow model.

If an incompressible fluid is flowing across the element dx , then the fluid velocity v and the flow rate q are constants at all points. The flow behavior in this system can be expressed by the differential form of Darcy's equation, i.e., Equation 6-12. Separating the variables of Equation 6-12 and integrating over the length of the linear system gives:

$$\frac{q}{A} \int_0^L dx = -\frac{k}{\mu} \int_{P_1}^{P_2} dp$$

or:

$$q = \frac{kA(p_1 - p_2)}{\mu L}$$

It is desirable to express the above relationship in customary field units, or:

$$q = \frac{0.001127 kA(p_1 - p_2)}{\mu L} \quad (6-14)$$

where q = flow rate, bbl/day

k = absolute permeability, md

p = pressure, psia

μ = viscosity, cp

L = distance, ft

A = cross-sectional area, ft^2

Example 6-1

An incompressible fluid flows in a linear porous media with the following properties:

$$\begin{array}{lll} L = 2000 \text{ ft} & h = 20' & \text{width} = 300' \\ k = 100 \text{ md} & \phi = 15\% & \mu = 2 \text{ cp} \\ p_1 = 2000 \text{ psi} & p_2 = 1990 \text{ psi} & \end{array}$$

Calculate:

- Flow rate in bbl/day
- Apparent fluid velocity in ft/day
- Actual fluid velocity in ft/day

Solution

Calculate the cross-sectional area A:

$$A = (h) (\text{width}) = (20) (300) = 6000 \text{ ft}^2$$

- Calculate the flow rate from Equation 6-14:

$$q = \frac{(0.001127) (100) (6000) (2000 - 1990)}{(2) (2000)} = 1.6905 \text{ bbl/day}$$

- Calculate the apparent velocity:

$$v = \frac{q}{A} = \frac{(1.6905)(5.615)}{6000} = 0.0016 \text{ ft/day}$$

- Calculate the actual fluid velocity:

$$v = \frac{q}{\phi A} = \frac{(1.6905)(5.615)}{(0.15)(6000)} = 0.0105 \text{ ft/day}$$

The difference in the pressure ($p_1 - p_2$) in Equation 6-14 is not the only driving force in a tilted reservoir. The gravitational force is the other important driving force that must be accounted for to determine the direction and rate of flow. The fluid gradient force (gravitational force) is always directed *vertically downward* while the force that results from an applied pressure drop may be in any direction. The force causing flow

would then be the *vector sum* of these two. In practice, we obtain this result by introducing a new parameter, called fluid potential, which has the same dimensions as pressure, e.g., psi. Its symbol is Φ . The fluid potential at any point in the reservoir is defined as the pressure at that point less the pressure that would be exerted by a fluid head extending to an arbitrarily assigned datum level. Letting Δz_i be the vertical distance from a point i in the reservoir to this datum level

$$\Phi_i = p_i - \left(\frac{\rho}{144} \right) \Delta z_i \quad (6-15)$$

where ρ is the density in lb/ft³.

Expressing the fluid density in gm/cc in Equation 6-15 gives:

$$\Phi_i = p_i - 0.433 \gamma \Delta z_i \quad (6-16)$$

where Φ_i = fluid potential at point i , psi

p_i = pressure at point i , psi

Δz_i = vertical distance from point i to the selected datum level

ρ = fluid density, lb/ft³

γ = fluid density, gm/cm³

The datum is usually selected at the gas-oil contact, oil-water contact, or at the highest point in formation. In using Equations 6-15 or 6-16 to calculate the fluid potential Φ_i at location i , **the vertical distance Δz_i is assigned as a positive value when the point i is below the datum level and as a negative when it is above the datum level, i.e.:**

If point i is above the datum level:

$$\Phi_i = p_i + \left(\frac{\rho}{144} \right) \Delta z_i$$

and

$$\Phi_i = p_i - 0.433 \gamma \Delta z_i$$

If point i is below the datum level:

$$\Phi_i = p_i - \left(\frac{\rho}{144} \right) \Delta z_i$$

and

$$\Phi_1 = p_1 - 0.433 \gamma \Delta z_1$$

Applying the above-generalized concept to Darcy's equation (Equation 6-14) gives:

$$q = \frac{0.001127 kA (\Phi_1 - \Phi_2)}{\mu L} \quad (6-17)$$

It should be pointed out that the fluid potential drop ($\Phi_1 - \Phi_2$) is equal to the pressure drop ($p_1 - p_2$) only when the flow system is horizontal.

Example 6-2

Assume that the porous media with the properties as given in the previous example is tilted with a dip angle of 5° as shown in Figure 6-12. The incompressible fluid has a density of 42 lb/ft^3 . Resolve Example 6-1 using this additional information.

Solution

Step 1. For the purpose of illustrating the concept of fluid potential, select the datum level at half the vertical distance between the two points, i.e., at 87.15 feet, as shown in Figure 6-12.

Step 2. Calculate the fluid potential at Points 1 and 2.

Since Point 1 is below the datum level, then:

$$\Phi_1 = p_1 - \left(\frac{\rho}{144}\right) \Delta z_1 = 2000 - \left(\frac{42}{144}\right) (87.15) = 1974.58 \text{ psi}$$

Since Point 2 is above the datum level, then:

$$\Phi_2 = p_2 + \left(\frac{\rho}{144}\right) \Delta z_2 = 1990 + \left(\frac{42}{144}\right) (87.15) = 2015.42 \text{ psi}$$

Because $\Phi_2 > \Phi_1$, the fluid flows downward from Point 2 to Point 1. The difference in the fluid potential is:

$$\Delta\Phi = 2015.42 - 1974.58 = 40.84 \text{ psi}$$

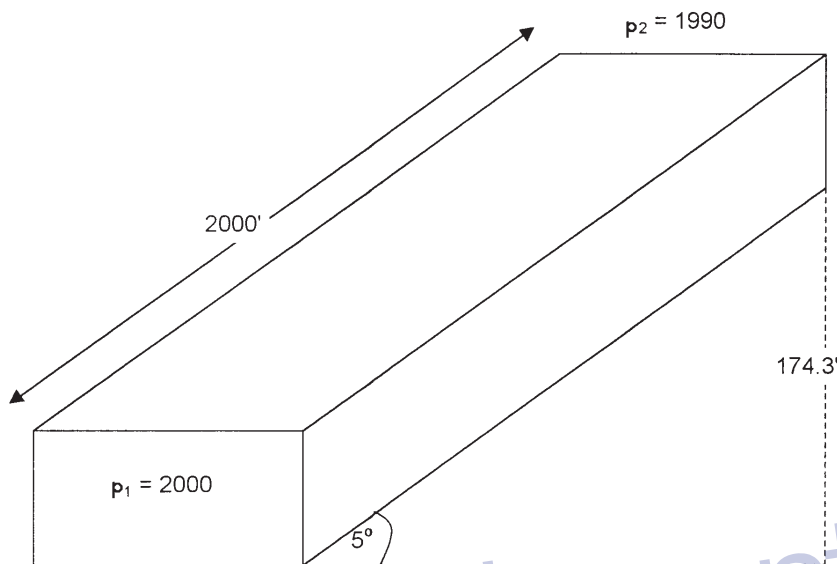


Figure 6-12. Example of a tilted layer.

- Notice, if we select Point 2 for the datum level, then

$$\Phi_1 = 2000 - \left(\frac{42}{144} \right) (174.3) = 1949.16 \text{ psi}$$

$$\Phi_2 = 1990 + \left(\frac{42}{144} \right) (0) = 1990 \text{ psi}$$

The above calculations indicate that regardless of the position of the datum level, the flow is downward from 2 to 1 with:

$$\Delta\Phi = 1990 - 1949.16 = 40.84 \text{ psi}$$

Step 3. Calculate the flow rate

$$q = \frac{(0.001127)(100)(6000)(40.84)}{(2)(2000)} = 6.9 \text{ bbl/day}$$

Step 4. Calculate the velocity:

$$\text{Apparent velocity} = \frac{(6.9)(5.615)}{6000} = 0.0065 \text{ ft/day}$$

$$\text{Actual velocity} = \frac{(6.9)(5.615)}{(0.15)(6000)} = 0.043 \text{ ft/day}$$

Linear Flow of Slightly Compressible Fluids

Equation 6-6 describes the relationship that exists between pressure and volume for slightly compressible fluids, or:

$$V = V_{\text{ref}} [1 + c (p_{\text{ref}} - p)]$$

The above equation can be modified and written in terms of flow rate as:

$$q = q_{\text{ref}} [1 + c (p_{\text{ref}} - p)] \quad (6-18)$$

where q_{ref} is the flow rate at some reference pressure p_{ref} . Substituting the above relationship in Darcy's equation gives:

$$\frac{q}{A} = \frac{q_{\text{ref}} [1 + c (p_{\text{ref}} - p)]}{A} = -0.001127 \frac{k}{\mu} \frac{dp}{dx}$$

Separating the variables and arranging:

$$\frac{q_{\text{ref}}}{A} \int_0^L dx = -0.001127 \frac{k}{\mu} \int_{p_1}^{p_2} \left[\frac{dp}{1 + c(p_{\text{ref}} - p)} \right]$$

Integrating gives:

$$q_{\text{ref}} = \left[\frac{0.001127 kA}{\mu c L} \right] \ln \left[\frac{1 + c(p_{\text{ref}} - p_2)}{1 + c(p_{\text{ref}} - p_1)} \right] \quad (6-19)$$

where q_{ref} = flow rate at a reference pressure p_{ref} , bbl/day
 p_1 = upstream pressure, psi

p_2 = downstream pressure, psi
 k = permeability, md
 μ = viscosity, cp
 c = average liquid compressibility, psi^{-1}

Selecting the upstream pressure p_1 as the reference pressure p_{ref} and substituting in Equation 6-19 gives the flow rate at Point 1 as:

$$q_1 = \left[\frac{0.001127 kA}{\mu cL} \right] \ln [1 + c (p_1 - p_2)] \quad (6-20)$$

Choosing the downstream pressure p_2 as the reference pressure and substituting in Equation 6-19 gives:

$$q_2 = \left[\frac{0.001127 kA}{\mu cL} \right] \ln \left[\frac{1}{1 + c(p_2 - p_1)} \right] \quad (6-21)$$

where q_1 and q_2 are the flow rates at Points 1 and 2, respectively.

Example 6-3

Consider the linear system given in Example 6-1 and, assuming a slightly compressible liquid, calculate the flow rate at both ends of the linear system. The liquid has an average compressibility of $21 \times 10^{-5} \text{ psi}^{-1}$.

Solution

- Choosing the upstream pressure as the reference pressure gives:

$$\begin{aligned}
 q_1 &= \left[\frac{(0.001127)(100)(6000)}{(2)(21 \times 10^{-5})(2000)} \right] \ln [1 + (21 \times 10^{-5})(2000 - 1990)] \\
 &= 1.689 \text{ bbl/day}
 \end{aligned}$$

- Choosing the downstream pressure, gives:

$$\begin{aligned}
 q_2 &= \left[\frac{(0.001127)(100)(6000)}{(2)(21 \times 10^{-5})(2000)} \right] \ln \left[\frac{1}{1 + (21 \times 10^{-5})(1990 - 2000)} \right] \\
 &= 1.692 \text{ bbl/day}
 \end{aligned}$$

The above calculations show that q_1 and q_2 are not largely different, which is due to the fact that the liquid is slightly incompressible and its volume is not a strong function of pressure.

Linear Flow of Compressible Fluids (Gases)

For a viscous (laminar) gas flow in a homogeneous-linear system, the real-gas equation-of-state can be applied to calculate the number of gas moles n at pressure p , temperature T , and volume V :

$$n = \frac{pV}{zRT}$$

At standard conditions, the volume occupied by the above n moles is given by:

$$V_{sc} = \frac{n z_{sc} R T_{sc}}{p_{sc}}$$

Combining the above two expressions and assuming $z_{sc} = 1$ gives:

$$\frac{pV}{zT} = \frac{p_{sc} V_{sc}}{T_{sc}}$$

Equivalently, the above relation can be expressed in terms of the flow rate as:

$$\frac{5.615pq}{zT} = \frac{p_{sc} Q_{sc}}{T_{sc}}$$

Rearranging:

$$\left(\frac{p_{sc}}{T_{sc}}\right) \left(\frac{zT}{p}\right) \left(\frac{Q_{sc}}{5.615}\right) = q \quad (6-22)$$

where q = gas flow rate at pressure p in bbl/day

Q_{sc} = gas flow rate at standard conditions, scf/day

z = gas compressibility factor

T_{sc} , p_{sc} = standard temperature and pressure in °R and psia, respectively

Replacing the gas flow rate q with that of Darcy's Law, i.e., Equation 6-12, gives:

$$\frac{q}{A} = \left(\frac{p_{sc}}{T_{sc}} \right) \left(\frac{zT}{p} \right) \left(\frac{Q_{sc}}{5.615} \right) \left(\frac{1}{A} \right) = -0.001127 \frac{k}{\mu} \frac{dp}{dx}$$

The constant 0.001127 is to convert from Darcy's units to field units. Separating variables and arranging yields:

$$\left[\frac{q_{sc} p_{sc} T}{0.006328 k T_{sc} A} \right] \int_0^L dx = - \int_{p_1}^{p_2} \frac{p}{z \mu_g} dp$$

Assuming constant z and μ_g over the specified pressures, i.e., p_1 and p_2 , and integrating gives:

$$Q_{sc} = \frac{0.003164 T_{sc} A k (p_1^2 - p_2^2)}{p_{sc} T L z \mu_g}$$

where Q_{sc} = gas flow rate at standard conditions, scf/day

k = permeability, md

T = temperature, °R

μ_g = gas viscosity, cp

A = cross-sectional area, ft²

L = total length of the linear system, ft

Setting $p_{sc} = 14.7$ psi and $T_{sc} = 520^\circ\text{R}$ in the above expression gives:

$$Q_{sc} = \frac{0.111924 A k (p_1^2 - p_2^2)}{T L z \mu_g} \quad (6-23)$$

It is essential to notice that those gas properties z and μ_g are a very strong function of pressure, but they have been removed from the integral to simplify the final form of the gas flow equation. The above equation is valid for applications when the pressure $< 2,000$ psi. The gas properties must be evaluated at the average pressure \bar{p} as defined below.

$$\bar{p} = \sqrt{\frac{p_1^2 + p_2^2}{2}} \quad (6-24)$$

Example 6-4

A linear porous media is flowing a 0.72 specific gravity gas at 120°F. The upstream and downstream pressures are 2,100 psi and 1,894.73 psi, respectively. The cross-sectional area is constant at 4,500 ft². The total length is 2,500 feet with an absolute permeability of 60 md. Calculate the gas flow rate in scf/day ($p_{sc} = 14.7$ psia, $T_{sc} = 520^\circ\text{R}$).

Solution

Step 1. Calculate average pressure by using Equation 6-24.

$$\bar{p} = \sqrt{\frac{2100^2 + 1894.73^2}{2}} = 2000 \text{ psi}$$

Step 2. Using the specific gravity of the gas, calculate its pseudo-critical properties by applying Equations 2-17 and 2-18.

$$T_{pc} = 395.5^\circ\text{R} \quad p_{pc} = 668.4 \text{ psia}$$

Step 3. Calculate the pseudo-reduced pressure and temperature.

$$p_{pr} = \frac{2000}{668.4} = 2.99$$

$$T_{pr} = \frac{600}{395.5} = 1.52$$

Step 4. Determine the z -factor from the Standing-Katz chart (Figure 2-1) to give:

$$z = 0.78$$

Step 5. Solve for the viscosity of the gas by applying the Lee-Gonzalez-Eakin method (Equations 2-63 through 2-66) to give:

$$\mu_g = 0.0173 \text{ cp}$$

Step 6. Calculate the gas flow rate by applying Equation 6-23.

$$Q_{sc} = \frac{(0.111924)(4500)(60)(2100^2 - 1894.73^2)}{(600)(0.78)(2500)(0.0173)}$$

$$= 1,224,242 \text{ scf/day}$$

Radial Flow of Incompressible Fluids

In a radial flow system, all fluids move toward the producing well from all directions. Before flow can take place, however, a pressure differential must exist. Thus, if a well is to produce oil, which implies a flow of fluids through the formation to the wellbore, the pressure in the formation at the wellbore must be less than the pressure in the formation at some distance from the well.

The pressure in the formation at the wellbore of a producing well is known as the *bottom-hole flowing pressure* (flowing BHP, p_{wf}).

Consider Figure 6-13, which schematically illustrates the radial flow of an incompressible fluid toward a vertical well. The formation is considered to a uniform thickness h and a constant permeability k . Because the fluid is incompressible, the flow rate q must be constant at all radii. Due to the steady-state flowing condition, the pressure profile around the wellbore is maintained constant with time.

Let p_{wf} represent the maintained bottom-hole flowing pressure at the wellbore radius r_w and p_e denote the external pressure at the external or drainage radius. Darcy's equation as described by Equation 6-13 can be used to determine the flow rate at any radius r :

$$v = \frac{q}{A_r} = 0.001127 \frac{k}{\mu} \frac{dp}{dr} \quad (6-25)$$

where v = apparent fluid velocity, bbl/day-ft²

q = flow rate at radius r , bbl/day

k = permeability, md

μ = viscosity, cp

0.001127 = conversion factor to express the equation in field units

A_r = cross-sectional area at radius r

The minus sign is no longer required for the radial system shown in Figure 6-13 as the radius increases in the same direction as the pressure. In other words, as the radius increases going away from the wellbore the

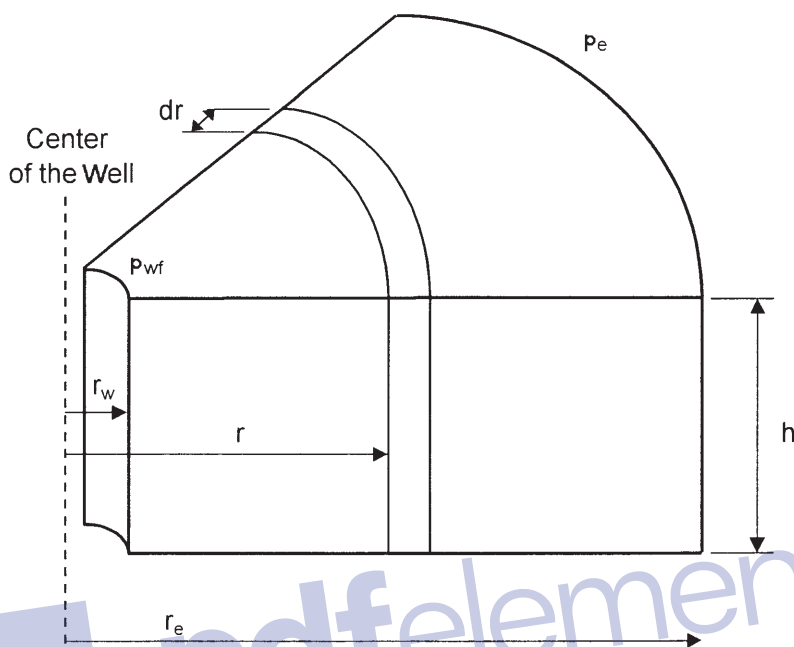


Figure 6-13. Radial flow model.

pressure also increases. At any point in the reservoir the cross-sectional area across which flow occurs will be the surface area of a cylinder, which is $2\pi rh$, or:

$$v = \frac{q}{A_r} = \frac{q}{2\pi rh} = 0.001127 \frac{k}{\mu} \frac{dp}{dr}$$

The flow rate for a crude oil system is customarily expressed in surface units, i.e., stock-tank barrels (STB), rather than reservoir units. Using the symbol Q_o to represent the oil flow as expressed in STB/day, then:

$$q = B_o Q_o$$

where B_o is the oil formation volume factor bbl/STB. The flow rate in Darcy's equation can be expressed in STB/day to give:

$$\frac{Q_o B_o}{2\pi rh} = 0.001127 \frac{k}{\mu_o} \frac{dp}{dr}$$

Integrating the above equation between two radii, r_1 and r_2 , when the pressures are p_1 and p_2 yields:

$$\int_{r_1}^{r_2} \left(\frac{Q_o}{2\pi h} \right) \frac{dr}{r} = 0.001127 \int_{p_1}^{p_2} \left(\frac{k}{\mu_o B_o} \right) dp \quad (6-26)$$

For an incompressible system in a uniform formation, Equation 6-26 can be simplified to:

$$\frac{Q_o}{2\pi h} \int_{r_1}^{r_2} \frac{dr}{r} = \frac{0.001127 k}{\mu_o B_o} \int_{p_1}^{p_2} dp$$

Performing the integration gives:

$$Q_o = \frac{0.00708 k h (p_2 - p_1)}{\mu_o B_o \ln (r_2/r_1)}$$

Frequently the two radii of interest are the wellbore radius r_w and the *external* or *drainage* radius r_e . Then:

$$Q_o = \frac{0.00708 k h (p_e - p_w)}{\mu_o B_o \ln (r_e/r_w)} \quad (6-27)$$

where Q_o = oil, flow rate, STB/day

p_e = external pressure, psi

p_{wf} = bottom-hole flowing pressure, psi

k = permeability, md

μ_o = oil viscosity, cp

B_o = oil formation volume factor, bbl/STB

h = thickness, ft

r_e = external or drainage radius, ft

r_w = wellbore radius, ft

The external (drainage) radius r_e is usually determined from the well spacing by equating the area of the well spacing with that of a circle, i.e.,

$$\pi r_e^2 = 43,560 A$$

or

$$r_e = \sqrt{\frac{43,560 A}{\pi}} \quad (6-28)$$

where A is the well spacing in acres.

In practice, neither the external radius nor the wellbore radius is generally known with precision. Fortunately, they enter the equation as a logarithm, so that the error in the equation will be less than the errors in the radii.

Equation 6-27 can be arranged to solve for the pressure p at any radius r to give:

$$p = p_{wf} + \left[\frac{Q_o B_o \mu_o}{0.00708 kh} \right] \ln \left(\frac{r}{r_w} \right) \quad (6-29)$$

Example 6-5

An oil well in the Nameless Field is producing at a stabilized rate of 600 STB/day at a stabilized bottom-hole flowing pressure of 1,800 psi. Analysis of the pressure buildup test data indicates that the pay zone is characterized by a permeability of 120 md and a uniform thickness of 25 ft. The well drains an area of approximately 40 acres. The following additional data are available:

$$\begin{aligned} r_w &= 0.25 \text{ ft} & A &= 40 \text{ acres} \\ B_o &= 1.25 \text{ bbl/STB} & \mu_o &= 2.5 \text{ cp} \end{aligned}$$

Calculate the pressure profile (distribution) and list the pressure drop across 1 ft intervals from r_w to 1.25 ft, 4 to 5 ft, 19 to 20 ft, 99 to 100 ft, and 744 to 745 ft.

Solution

Step 1. Rearrange Equation 6-27 and solve for the pressure p at radius r.

$$p = p_{wf} + \left[\frac{\mu_o B_o Q_o}{0.00708 kh} \right] \ln (r/r_w)$$

$$p = 1800 + \left[\frac{(2.5)(1.25)(600)}{(0.00708)(120)(25)} \right] \ln \left(\frac{r}{0.25} \right)$$

$$p = 1800 + 88.28 \ln \left(\frac{r}{0.25} \right)$$

Step 2. Calculate the pressure at the designated radii.

| r, ft | p, psi | Radius Interval | Pressure drop |
|-------|--------|-----------------|---------------------------|
| 0.25 | 1800 | | |
| 1.25 | 1942 | 0.25–1.25 | 1942 – 1800 = 142 psi |
| 4 | 2045 | | |
| 5 | 2064 | 4–5 | 2064 – 2045 = 19 psi |
| 19 | 2182 | | |
| 20 | 2186 | 19–20 | 2186 – 2182 = 4 psi |
| 99 | 2328 | | |
| 100 | 2329 | 99–100 | 2329 – 2328 = 1 psi |
| 744 | 2506.1 | | |
| 745 | 2506.2 | 744–745 | 2506.2 – 2506.1 = 0.1 psi |

Figure 6-14 shows the pressure profile on a function of radius for the calculated data.

Results of the above example reveal that the pressure drop just around the wellbore (i.e., 142 psi) is 7.5 times greater than at the 4–5 ft interval, 36 times greater than at 19–20 ft, and 142 times than that at the 99–100 ft interval. The reason for this large pressure drop around the wellbore is that the fluid is flowing in from a large drainage of 40 acres.

The external pressure p_e used in Equation 6-27 cannot be measured readily, but P_e does not deviate substantially from initial reservoir pressure if a strong and active aquifer is present.

Several authors have suggested that the average reservoir pressure p_r , which often is reported in well test results, should be used in performing material balance calculations and flow rate prediction. Craft and Hawkins (1959) showed that the average pressure is located at about 61% of the drainage radius r_e for a steady-state flow condition. Substitute $0.61 r_e$ in Equation 6-29 to give:

$$p(\text{at } r=0.61r_e) = p_r = p_{wf} + \left[\frac{Q_o B_o \mu_o}{7.08 kh} \right] \ln \left(\frac{0.61 r_e}{r_w} \right)$$

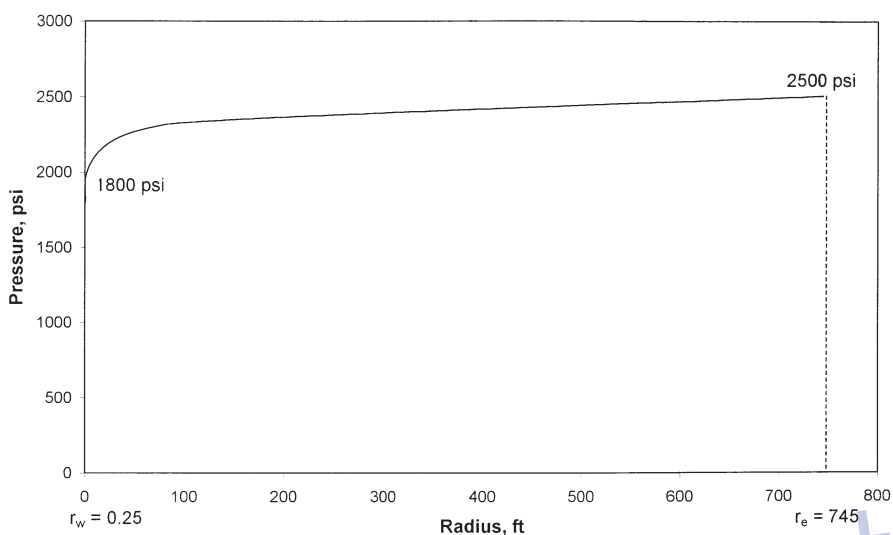


Figure 6-14. Pressure profile around the wellbore.

or in terms of flow rate:

$$Q_o = \frac{0.00708 kh(p_r - p_{wf})}{\mu_o B_o \ln \left(\frac{0.61r_e}{r_w} \right)} \quad (6-30)$$

But, since $\ln(0.61r_e/r_w) = \ln \left(\frac{r_e}{r_w} \right) - 0.5$, then:

$$Q_o = \frac{0.00708 kh(p_r - p_{wf})}{\mu_o B_o \left[\ln \left(\frac{r_e}{r_w} \right) - 0.5 \right]} \quad (6-31)$$

Golan and Whitson (1986) suggest a method for approximating drainage area of wells producing from a common reservoir. The authors assume that the volume drained by a single well is proportional to its rate of flow. Assuming constant reservoir properties and a uniform thickness, the approximate drainage area of a single well, A_w , is:

$$A_w = A_T \left(\frac{q_w}{q_T} \right) \quad (6-32)$$

where A_w = drainage area
 A_T = total area of the field
 q_T = total flow rate of the field
 q_w = well flow rate

Radial Flow of Slightly Compressible Fluids

Craft et al. (1990) used Equation 6-18 to express the dependency of the flow rate on pressure for slightly compressible fluids. If this equation is substituted into the radial form of Darcy's Law, the following is obtained:

$$\frac{q}{A_r} = \frac{q_{\text{ref}} [1 + c(p_{\text{ref}} - p)]}{2\pi r h} = 0.001127 \frac{k}{\mu} \frac{dp}{dr}$$

where q_{ref} is the flow rate at some reference pressure p_{ref} .

Separating the variables in the above equation and integrating over the length of the porous medium gives:

$$\frac{q_{\text{ref}} \mu}{2\pi k h} \int_{r_w}^{r_e} \frac{dr}{r} = 0.001127 \int_{p_{\text{wf}}}^{p_e} \frac{dp}{1 + c(p_{\text{ref}} - p)}$$

or:

$$q_{\text{ref}} = \left[\frac{0.00708 kh}{\mu c \ln \left(\frac{r_e}{r_w} \right)} \right] \ln \left[\frac{1 + c(p_e - p_{\text{ref}})}{1 + c(p_{\text{wf}} - p_{\text{ref}})} \right]$$

where q_{ref} is oil flow rate at a reference pressure p_{ref} . Choosing the bottom-hole flow pressure p_{wf} as the reference pressure and expressing the flow rate in STB/day gives:

$$Q_o = \left[\frac{0.00708 kh}{\mu_o B_o c_o \ln \left(\frac{r_e}{r_w} \right)} \right] \ln [1 + c_o (p_e - p_{wf})] \quad (6-33)$$

where c_o = isothermal compressibility coefficient, psi^{-1}

Q_o = oil flow rate, STB/day

k = permeability, md

Example 6-6

The following data are available on a well in the Red River Field:

$$\begin{array}{ll} p_e = 2506 \text{ psi} & p_{wf} = 1800 \\ r_e = 745' & r_w = 0.25 \\ B_o = 1.25 & \mu_o = 2.5 & c_o = 25 \times 10^{-6} \text{ psi}^{-1} \\ k = 0.12 \text{ Darcy} & h = 25 \text{ ft.} \end{array}$$

Assuming a slightly compressible fluid, calculate the oil flow rate. Compare the result with that of incompressible fluid.

Solution

For a slightly compressible fluid, the oil flow rate can be calculated by applying Equation 6-33:

$$\begin{aligned} Q_o &= \left[\frac{(0.00708)(120)(25)}{(2.5)(1.25)(25 \times 10^{-6}) \ln(745/0.25)} \right] \\ &\times \ln [1 + (25 \times 10^{-6})(2506 - 1800)] = 595 \text{ STB/day} \end{aligned}$$

Assuming an incompressible fluid, the flow rate can be estimated by applying Darcy's equation, i.e., Equation 6-27:

$$Q_o = \frac{(0.00708)(120)(25)(2506 - 1800)}{(2.5)(1.25) \ln(745/0.25)} = 600 \text{ STB/day}$$

Radial Flow of Compressible Gases

The basic differential form of Darcy's Law for a horizontal laminar flow is valid for describing the flow of both gas and liquid systems. For a radial gas flow, the Darcy's equation takes the form:

$$q_{gr} = \frac{0.001127 (2\pi rh) k}{\mu_g} \frac{dp}{dr} \quad (6-34)$$

where q_{gr} = gas flow rate at radius r , bbl/day

r = radial distance, ft

h = zone thickness, ft

μ_g = gas viscosity, cp

p = pressure, psi

0.001127 = conversion constant from Darcy units to field units

The gas flow rate is usually expressed in scf/day. Referring to the gas flow rate at standard condition as Q_g , the gas flow rate q_{gr} under pressure and temperature can be converted to that of standard condition by applying the real gas equation-of-state to both conditions, or

$$\frac{5.615 q_{gr} p}{zRT} = \frac{Q_g p_{sc}}{z_{sc} R T_{sc}}$$

or

$$\left(\frac{p_{sc}}{5.615 T_{sc}} \right) \left(\frac{zT}{p} \right) Q_g = q_{gr} \quad (6-35)$$

where p_{sc} = standard pressure, psia

T_{sc} = standard temperature, °R

Q_g = gas flow rate, scf/day

q_{gr} = gas flow rate at radius r , bbl/day

p = pressure at radius r , psia

T = reservoir temperature, °R

z = gas compressibility factor at p and T

z_{sc} = gas compressibility factor at standard condition $\cong 1.0$

Combining Equations 6-34 and 6-35 yields:

$$\left(\frac{p_{sc}}{5.615 T_{sc}}\right)\left(\frac{zT}{p}\right)Q_g = \frac{0.001127(2\pi rh)k}{\mu_g} \frac{dp}{dr}$$

Assuming that $T_{sc} = 520^\circ R$ and $p_{sc} = 14.7$ psia:

$$\left(\frac{T Q_g}{kh}\right) \frac{dr}{r} = 0.703 \left(\frac{2p}{\mu_g z}\right) dp \quad (6-36)$$

Integrating Equation 6-36 from the wellbore conditions (r_w and p_{wf}) to any point in the reservoir (r and p) gives:

$$\int_{r_w}^r \left(\frac{T Q_g}{kh}\right) \frac{dr}{r} = 0.703 \int_{p_{wf}}^p \left(\frac{2p}{\mu_g z}\right) dp \quad (6-37)$$

Imposing Darcy's Law conditions on Equation 6-37, i.e.:

- **Steady-state flow**, which requires that Q_g is constant at all radii
- **Homogeneous formation**, which implies that k and h are constant

gives:

$$\left(\frac{T Q_g}{kh}\right) \ln\left(\frac{r}{r_w}\right) = 0.703 \int_{p_{wf}}^p \left(\frac{2p}{\mu_g z}\right) dp$$

The term $\int_{p_{wf}}^p \left(\frac{2p}{\mu_g z}\right) dp$ can be expanded to give:

$$\int_{p_{wf}}^p \left(\frac{2p}{\mu_g z}\right) dp = \int_0^p \left(\frac{2p}{\mu_g z}\right) dp - \int_0^{p_{wf}} \left(\frac{2p}{\mu_g z}\right) dp$$

Combining the above relationships yields:

$$\left(\frac{TQ_g}{kh} \right) \ln \left(\frac{r}{r_w} \right) = 0.703 \left[\int_0^p \left(\frac{2p}{\mu_g z} \right) dp - \int_0^{p_{wf}} \left(\frac{2p}{\mu_g z} \right) dp \right] \quad (6-38)$$

The integral $\int_0^p 2p/(\mu_g z) dp$ is called the *real gas potential* or *real gas pseudopressure*, and it is usually represented by $m(p)$ or ψ . Thus

$$m(p) = \psi = \int_0^p \left(\frac{2p}{\mu_g z} \right) dp \quad (6-39)$$

Equation 6-38 can be written in terms of the real gas potential to give:

$$\left(\frac{TQ_g}{kh} \right) \ln \frac{r}{r_w} = 0.703 (\psi - \psi_w)$$

or

$$\psi = \psi_w + \frac{Q_g T}{0.703 kh} \ln \frac{r}{r_w} \quad (6-40)$$

Equation 6-40 indicates that a graph of ψ vs. $\ln r/r_w$ yields a straight line of slope $(Q_g T/0.703 kh)$ and intercepts ψ_w (Figure 6-15).

The flow rate is given exactly by

$$Q_g = \frac{0.703 kh (\psi - \psi_w)}{T \ln \frac{r}{r_w}} \quad (6-41)$$

In the particular case when $r = r_e$, then:

$$Q_g = \frac{0.703 kh (\psi_e - \psi_w)}{T \left(\ln \frac{r_e}{r_w} \right)} \quad (6-42)$$

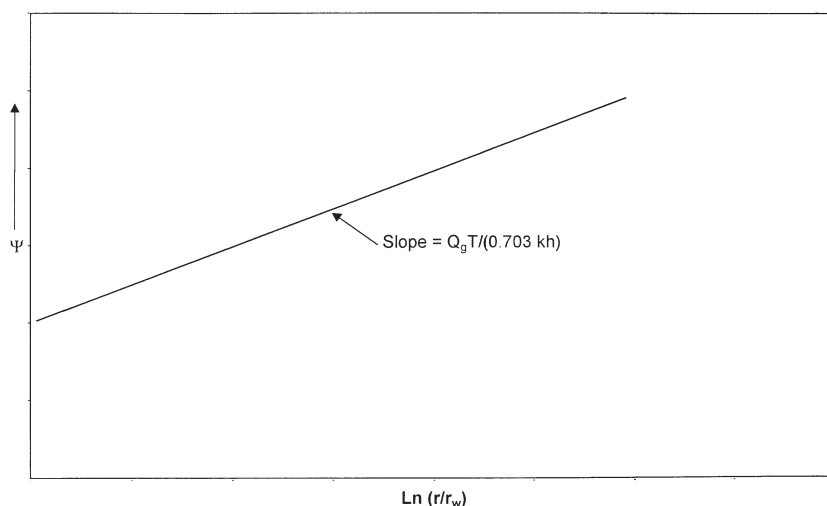


Figure 6-15. Graph of Ψ vs. $\ln (r/r_w)$.

where ψ_e = real gas potential as evaluated from 0 to p_e , psi^2/cp
 ψ_w = real gas potential as evaluated from 0 to P_w , psi^2/cp
 k = permeability, md
 h = thickness, ft
 r_e = drainage radius, ft
 r_w = wellbore radius, ft
 Q_g = gas flow rate, scf/day

The gas flow rate is commonly expressed in Mscf/day, or

$$Q_g = \frac{kh(\psi_e - \psi_w)}{1422 T \left(\ln \frac{r_e}{r_w} \right)} \quad (6-43)$$

where Q_g = gas flow rate, Mscf/day.

Equation 6-43 can be expressed in terms of the average reservoir pressure p_r instead of the initial reservoir pressure p_e as:

$$Q_g = \frac{kh(\psi_r - \psi_w)}{1422 T \left[\ln \left(\frac{r_e}{r_w} \right) - 0.5 \right]} \quad (6-44)$$

To calculate the integral in Equation 6-43, the values of $2p/\mu_g z$ are calculated for several values of pressure p . Then $(2p/\mu_g z)$ versus p is plotted on a Cartesian scale and the area under the curve is calculated either numerically or graphically, where the area under the curve from $p = 0$ to any pressure p represents the value of ψ corresponding to p . The following example will illustrate the procedure.

Example 6-7

The following PVT data from a gas well in the Anaconda Gas Field is given below¹:

| p (psi) | μ_g (cp) | z |
|-----------|--------------|-------|
| 0 | 0.0127 | 1.000 |
| 400 | 0.01286 | 0.937 |
| 800 | 0.01390 | 0.882 |
| 1200 | 0.01530 | 0.832 |
| 1600 | 0.01680 | 0.794 |
| 2000 | 0.01840 | 0.770 |
| 2400 | 0.02010 | 0.763 |
| 2800 | 0.02170 | 0.775 |
| 3200 | 0.02340 | 0.797 |
| 3600 | 0.02500 | 0.827 |
| 4000 | 0.02660 | 0.860 |
| 4400 | 0.02831 | 0.896 |

The well is producing at a stabilized bottom-hole flowing pressure of 3,600 psi. The wellbore radius is 0.3 ft. The following additional data are available:

$$\begin{array}{lll}
 k = 65 \text{ md} & h = 15 \text{ ft} & T = 600^\circ\text{R} \\
 p_e = 4400 \text{ psi} & r_e = 1000 \text{ ft} &
 \end{array}$$

Calculate the gas flow rate in Mscf/day.

Solution

Step 1. Calculate the term $\left(\frac{2p}{\mu_g z} \right)$ for each pressure as shown below:

¹Data from "Gas Well Testing, Theory, Practice & Regulations," Donohue and Ertekin, IHRDC Corporation (1982).

| p (psi) | μ_g (cp) | z | $\frac{2p}{\mu_g z} \left(\frac{\text{psia}}{\text{cp}} \right)$ |
|---------|--------------|-------|---|
| 0 | 0.0127 | 1.000 | 0 |
| 400 | 0.01286 | 0.937 | 66,391 |
| 800 | 0.01390 | 0.882 | 130,508 |
| 1200 | 0.01530 | 0.832 | 188,537 |
| 1600 | 0.01680 | 0.794 | 239,894 |
| 2000 | 0.01840 | 0.770 | 282,326 |
| 2400 | 0.02010 | 0.763 | 312,983 |
| 2800 | 0.02170 | 0.775 | 332,986 |
| 3200 | 0.02340 | 0.797 | 343,167 |
| 3600 | 0.02500 | 0.827 | 348,247 |
| 4000 | 0.02660 | 0.860 | 349,711 |
| 4400 | 0.02831 | 0.896 | 346,924 |

Step 2. Plot the term $\left(\frac{2p}{\mu_g z} \right)$ versus pressure as shown in Figure 6-16.

Step 3. Calculate numerically the area under the curve for each value of p. These areas correspond to the real gas potential ψ at each pressure. These ψ values are tabulated below (ψ versus p is also plotted in the figure).

| p (psi) | $\psi \left(\frac{\text{psi}^2}{\text{cp}} \right)$ |
|---------|--|
| 400 | 13.2×10^6 |
| 800 | 52.0×10^6 |
| 1200 | 113.1×10^6 |
| 1600 | 198.0×10^6 |
| 2000 | 304.0×10^6 |
| 2400 | 422.0×10^6 |
| 2800 | 542.4×10^6 |
| 3200 | 678.0×10^6 |
| 3600 | 816.0×10^6 |
| 4000 | 950.0×10^6 |
| 4400 | 1089.0×10^6 |

Step 4. Calculate the flow rate by applying Equation 6-41.

$$p_w = 816.0 \times 10^6 \quad p_e = 1089 \times 10^6$$

$$Q_g = \frac{(65)(15)(1089 - 816)10^6}{(1422)(600) \ln(1000/0.25)} = 37,614 \text{ Mscf/day}$$

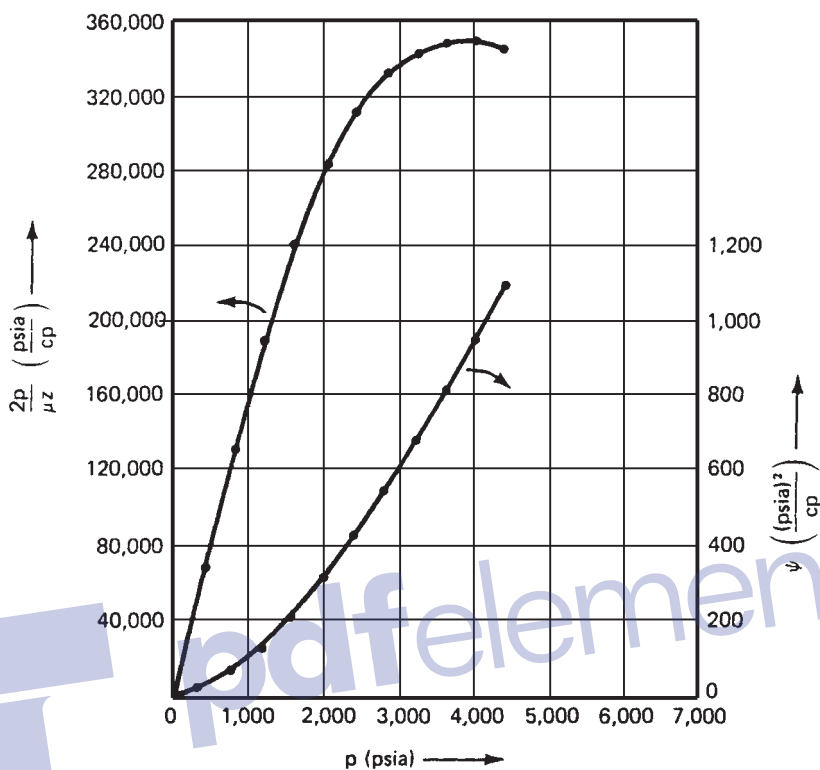


Figure 6-16. Real gas pseudopressure data for Example 6-7 (After Donohue and Erekin, 1982).

Approximation of the Gas Flow Rate

The exact gas flow rate as expressed by the different forms of Darcy's Law, i.e., Equations 6-37 through 6-44, can be approximated by removing the term $\frac{2}{\mu_g z}$ outside the integral as a constant. It should be pointed out that the $z\mu_g$ is considered constant only under a pressure range of < 2,000 psi. Equation 6-43 can be rewritten as:

$$Q_g = \left[\frac{kh}{1422 T \ln \left(\frac{r_e}{r_w} \right)} \right] \int_{P_{wf}}^{P_e} \left(\frac{2p}{\mu_g z} \right) dp$$

Removing the term and integrating gives:

$$Q_g = \frac{kh (p_c^2 - p_{wf}^2)}{1422 T (\mu_g z)_{avg} \ln\left(\frac{r_e}{r_w}\right)} \quad (6-45)$$

where Q_g = gas flow rate, Mscf/day
 k = permeability, md

The term $(\mu_g z)_{avg}$ is evaluated at an average pressure \bar{p} that is defined by the following expression:

$$\bar{p} = \sqrt{\frac{p_{wf}^2 + p_c^2}{2}}$$

The above approximation method is called the *pressure-squared* method and is limited to flow calculations when the reservoir pressure is less than 2,000 psi. Other approximation methods are discussed in Chapter 7.

Example 6-8

Using the data given in Example 6-7, re-solve for the gas flow rate by using the pressure-squared method. Compare with the exact method (i.e., real gas potential solution).

Solution

Step 1. Calculate the arithmetic average pressure.

$$\bar{p} = \left[\frac{4400^2 + 3600^2}{2} \right]^{.5} = 4020 \text{ psi}$$

Step 2. Determine gas viscosity and gas compressibility factor at 4,020 psi.

$$\begin{aligned} \mu_g &= 0.0267 \\ z &= 0.862 \end{aligned}$$

Step 3. Apply Equation 6-45:

$$Q_g = \frac{(65)(15)[4400^2 - 3600^2]}{(1422)(600)(0.0267)(0.862)\ln(1000/0.25)}$$

$$= 38,314 \text{ Mscf/day}$$

Step 4. Results show that the pressure-squared method approximates the exact solution of 37,614 with an absolute error of 1.86%. This error is due to the limited applicability of the pressure-squared method to a pressure range of < 2,000 psi.

Horizontal Multiple-Phase Flow

When several fluid phases are flowing simultaneously in a horizontal porous system, the concept of the effective permeability to each phase and the associated physical properties must be used in Darcy's equation. For a radial system, the generalized form of Darcy's equation can be applied to each reservoir as follows:

$$q_o = 0.001127 \left(\frac{2\pi r h}{\mu_o} \right) k_o \frac{dp}{dr}$$

$$q_w = 0.001127 \left(\frac{2\pi r h}{\mu_w} \right) k_w \frac{dp}{dr}$$

$$q_g = 0.001127 \left(\frac{2\pi r h}{\mu_g} \right) k_g \frac{dp}{dr}$$

where k_o, k_w, k_g = effective permeability to oil, water, and gas, md

μ_o, μ_w, μ_g = viscosity to oil, water, and gas, cp

q_o, q_w, q_g = flow rates for oil, water, and gas, bbl/day

k = absolute permeability, md

The effective permeability can be expressed in terms of the relative and absolute permeability, as presented by Equations 5-1 through 5-2, to give:

$$k_o = k_{ro} k$$

$$k_w = k_{rw} k$$

$$k_g = k_{rg} k$$

Using the above concept in Darcy's equation and expressing the flow rate in standard conditions yield:

$$Q_o = 0.00708 (rhk) \left(\frac{k_{ro}}{\mu_o \beta_o} \right) \frac{dp}{dr} \quad (6-46)$$

$$Q_w = 0.00708 (rhk) \left(\frac{k_{rw}}{\mu_w \beta_w} \right) \frac{dp}{dr} \quad (6-47)$$

$$Q_g = 0.00708 (rhk) \left(\frac{k_{rg}}{\mu_g \beta_g} \right) \frac{dp}{dr} \quad (6-48)$$

where Q_o, Q_w = oil and water flow rates, STB/day

B_o, B_w = oil and water formation volume factor, bbl/STB

Q_g = gas flow rate, scf/day

B_g = gas formation volume factor, bbl/scf

k = absolute permeability, md

The gas formation volume factor B_g is previously expressed by Equation 2-54 as:

$$B_g = 0.005035 \frac{zT}{p}, \text{ bbl/scf}$$

Performing the regular integration approach on Equations 6-46 through 6-48 yields:

• **Oil Phase**

$$Q_o = \frac{0.00708 (kh) (k_{ro}) (p_e - p_{wf})}{\mu_o B_o \ln(r_e/r_w)} \quad (6-49)$$

• **Water Phase**

$$Q_w = \frac{0.00708 (kh) (k_{rw}) (p_e - p_{wf})}{\mu_w B_w \ln(r_e/r_w)} \quad (6-50)$$

• Gas Phase

In terms of the real gas potential:

$$Q_g = \frac{(kh) k_{rg} (\Psi_c - \Psi_w)}{1422 T \ln (r_c/r_w)} \quad (6-51)$$

In terms of the pressure-squared:

$$Q_g = \frac{(kh) k_{rg} (p_c^2 - p_{wf}^2)}{1422 (\mu_g z)_{avg} T \ln (r_c/r_w)} \quad (6-52)$$

where Q_g = gas flow rate, Mscf/day
 k = absolute permeability, md
 T = temperature, °R

In numerous petroleum engineering calculations, it is convenient to express the flow rate of any phase as a ratio of other flowing phase. Two important flow ratios are the “instantaneous” water-oil ratio (WOR) and “instantaneous” gas-oil ratio (GOR). The generalized form of Darcy’s equation can be used to determine both flow ratios.

The water-oil ratio is defined as the ratio of the water flow rate to that of the oil. Both rates are expressed in stock-tank barrels per day, or:

$$WOR = \frac{Q_w}{Q_o}$$

Dividing Equation 6-46 by Equation 6-48 gives:

$$WOR = \left(\frac{k_{rw}}{k_{ro}} \right) \left(\frac{\mu_o B_o}{\mu_w B_w} \right) \quad (6-53)$$

where WOR = water-oil ratio, STB/STB.

The instantaneous GOR, as expressed in scf/STB, is defined as the total gas flow rate, i.e., free gas and solution gas, divided by the oil flow rate, or

$$GOR = \frac{Q_o R_s + Q_g}{Q_o}$$

or

$$\text{GOR} = R_s + \frac{Q_g}{Q_o} \quad (6-54)$$

where GOR = “instantaneous” gas-oil ratio, scf/STB

R_s = gas solubility, scf/STB

Q_g = free gas flow rate, scf/day

Q_o = oil flow rate, STB/day

Substituting Equations 6-46 and 6-48 into Equation 6-54 yields:

$$\text{GOR} = R_s + \left(\frac{k_{rg}}{k_{ro}} \right) \left(\frac{\mu_o B_o}{\mu_g B_g} \right) \quad (6-55)$$

where B_g is the gas formation volume factor as expressed in bbl/scf.

A complete discussion of the practical applications of the water-oil and gas-oil ratios is given in the subsequent chapters.

UNSTEADY-STATE FLOW

Consider Figure 6-17A, which shows a shut-in well that is centered in a homogeneous circular reservoir of radius r_e with a uniform pressure p_i throughout the reservoir. This initial reservoir condition represents the zero producing time. If the well is allowed to flow at a constant flow rate of q , a pressure disturbance will be created at the sand face. The pressure at the wellbore, i.e., p_{wf} , will drop instantaneously as the well is opened. The pressure disturbance will move away from the wellbore at a rate that is determined by:

- Permeability
- Porosity
- Fluid viscosity
- Rock and fluid compressibilities

Section B in Figure 6-17 shows that at time t_1 , the pressure disturbance has moved a distance r_1 into the reservoir. Notice that the pressure disturbance radius is continuously increasing with time. This radius is commonly called *radius of investigation* and referred to as r_{inv} . It is also

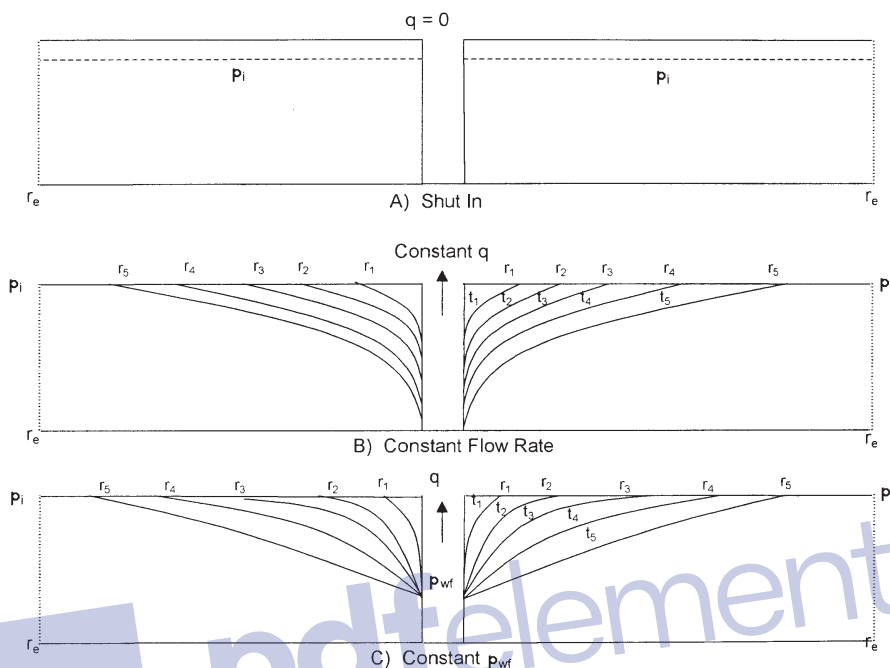


Figure 6-17. Pressure disturbance as a function of time.

important to point out that as long as the radius of investigation has not reached the reservoir boundary, i.e., r_e , the reservoir will be acting as if it is *infinite* in size. During this time we say that the reservoir is *infinite acting* because the outer drainage radius r_e can be mathematically *infinite*.

A similar discussion to the above can be used to describe a well that is producing at a constant bottom-hole flowing pressure. Section C in Figure 6-17 schematically illustrates the propagation of the radius of investigation with respect to time. At time t_4 , the pressure disturbance reaches the boundary, i.e., $r_{inv} = r_e$. This causes the pressure behavior to change.

Based on the above discussion, the transient (unsteady-state) flow is defined as **that time period during which the boundary has no effect on the pressure behavior in the reservoir and the reservoir will behave as its infinite in size**. Section B in Figure 6-17 shows that the transient flow period occurs during the time interval $0 < t < t_1$ for the constant flow rate scenario and during the time period $0 < t < t_4$ during the constant p_{wf} scenario as depicted by Section C in Figure 6-17.

Basic Transient Flow Equation

Under the steady-state flowing condition, the same quantity of fluid enters the flow system as leaves it. In the unsteady-state flow condition, the flow rate into an element of volume of a porous media may not be the same as the flow rate out of that element. Accordingly, the fluid content of the porous medium changes with time. The variables in unsteady-state flow additional to those already used for steady-state flow, therefore, become:

- Time, t
- Porosity, ϕ
- Total compressibility, c_t

The mathematical formulation of the transient flow equation is based on combining three independent equations and a specifying set of boundary and initial conditions that constitute the unsteady-state equation. These equations and boundary conditions are briefly described below:

a. Continuity Equation

The continuity equation is essentially a material balance equation that accounts for every pound mass of fluid produced, injected, or remaining in the reservoir.

b. Transport Equation

The continuity equation is combined with the equation for fluid motion (transport equation) to describe the fluid flow rate “in” and “out” of the reservoir. Basically, the transport equation is Darcy’s equation in its generalized differential form.

c. Compressibility Equation

The fluid compressibility equation (expressed in terms of density or volume) is used in formulating the unsteady-state equation with the objective of describing the changes in the fluid volume as a function of pressure.

d. Initial and Boundary Conditions

There are two boundary conditions and one initial condition required to complete the formulation and the solution of the transient flow equation. The two boundary conditions are:

- The formation produces at a constant rate into the wellbore.
- There is no flow across the outer boundary and the reservoir behaves as if it were infinite in size, i.e., $r_e = \infty$.

The initial condition simply states the reservoir is at a uniform pressure when production begins, i.e., time = 0.

Consider the flow element shown in Figure 6-18. The element has a width of dr and is located at a distance of r from the center of the well. The porous element has a differential volume of dV . According to the concept of the material-balance equation, the rate of mass flow into an element minus the rate of mass flow out of the element during a differential time Δt must be equal to the mass rate of accumulation during that time interval, or:

$$\begin{aligned} & \left[\begin{array}{l} \text{mass entering} \\ \text{volume element} \\ \text{during interval } \Delta t \end{array} \right] - \left[\begin{array}{l} \text{mass leaving} \\ \text{volume element} \\ \text{during interval } \Delta t \end{array} \right] \\ & = \left[\begin{array}{l} \text{rate of mass} \\ \text{accumulation} \\ \text{during interval } \Delta t \end{array} \right] \end{aligned} \quad (6-56)$$

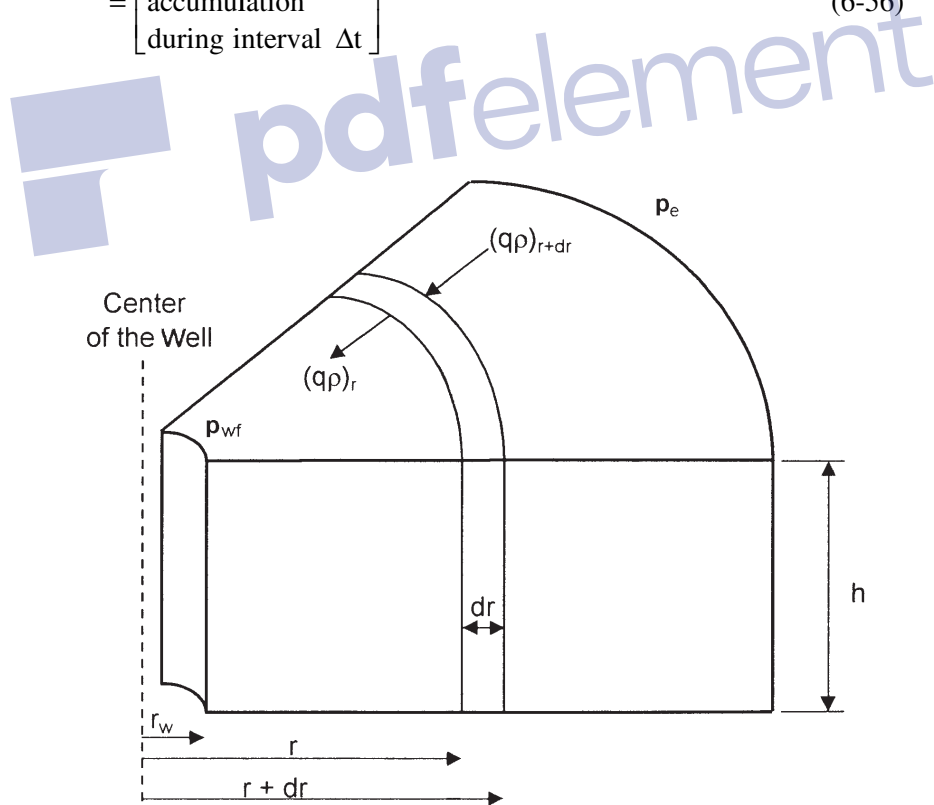


Figure 6-18. Illustration of radial flow.

The individual terms of Equation 6-56 are described below:

Mass Entering the Volume Element During Time Interval Δt

$$(\text{Mass})_{\text{in}} = \Delta t [Av\rho]_{r+dr} \quad (6-57)$$

where v = velocity of flowing fluid, ft/day

ρ = fluid density at $(r + dr)$, lb/ft³

A = Area at $(r + dr)$

Δt = time interval, days

The area of an element at the entering side is:

$$A_{r+dr} = 2\pi(r + dr) h \quad (6-58)$$

Combining Equation 6-58 with 6-47 gives:

$$[\text{Mass}]_{\text{in}} = 2\pi \Delta t (r + dr) h (v\rho)_{r+dr} \quad (6-59)$$

Mass Leaving the Volume Element

Adopting the same approach as that of the leaving mass gives:

$$[\text{Mass}]_{\text{out}} = 2\pi \Delta t rh (v\rho)_r \quad (6-60)$$

Total Accumulation of Mass

The volume of some element with a radius of r is given by:

$$V = \pi r^2 h$$

Differentiating the above equation with respect to r gives:

$$\frac{dV}{dr} = 2\pi rh$$

or:

$$dV = (2\pi rh)dr \quad (6-61)$$

Total mass accumulation during $\Delta t = dV [(\phi\rho)_{t+\Delta t} - (\phi\rho)_t]$

Substituting for dV yields:

$$\text{Total mass accumulation} = (2\pi rh) dr [(\phi\rho)_{t+\Delta t} - (\phi\rho)_t] \quad (6-62)$$

Replacing terms of Equation 6-56 with those of the calculated relationships gives:

$$2\pi h (r + dr) \Delta t (\phi\rho)_{r+dr} - 2\pi hr \Delta t (\phi\rho)_r = (2\pi rh) dr [(\phi\rho)_{t+\Delta t} - (\phi\rho)_t]$$

Dividing the above equation by $(2\pi rh) dr$ and simplifying gives:

$$\frac{1}{(r)dr} [(r + dr) (v\rho)_{r+dr} - r (v\rho)_r] = \frac{1}{\Delta t} [(\phi\rho)_{t+\Delta t} - (\phi\rho)_t]$$

or

$$\frac{1}{r} \frac{\partial}{\partial r} [r(v\rho)] = \frac{\partial}{\partial t} (\phi\rho) \quad (6-63)$$

where ϕ = porosity

ρ = density, lb/ft³

v = fluid velocity, ft/day

Equation 6-63 is called the *continuity equation*, and it provides the principle of conservation of mass in radial coordinates.

The transport equation must be introduced into the continuity equation to relate the fluid velocity to the pressure gradient within the control volume dV . Darcy's Law is essentially the basic motion equation, which states that the velocity is proportional to the pressure gradient ($\partial p/\partial r$). From Equation 6-25:

$$v = (5.615) (0.001127) \frac{k}{\mu} \frac{\partial p}{\partial r}$$

$$v = (0.006328) \frac{k}{\mu} \frac{\partial p}{\partial r} \quad (6-64)$$

where k = permeability, md

v = velocity, ft/day

Combining Equation 6-64 with Equation 6-63 results in:

$$\frac{0.006328}{r} \frac{\partial}{\partial r} \left(\frac{k}{\mu} (\rho r) \frac{\partial p}{\partial r} \right) = \frac{\partial}{\partial t} (\phi \rho) \quad (6-65)$$

Expanding the right-hand side by taking the indicated derivatives eliminates the porosity from the partial derivative term on the right-hand side:

$$\frac{\partial}{\partial t} (\phi \rho) = \phi \frac{\partial \rho}{\partial t} + \rho \frac{\partial \phi}{\partial t} \quad (6-66)$$

As shown in Chapter 4, porosity is related to the formation compressibility by the following:

$$c_f = \frac{1}{\phi} \frac{\partial \phi}{\partial p} \quad (6-67)$$

Applying the chain rule of differentiation to $\partial \phi / \partial t$,

$$\frac{\partial \phi}{\partial t} = \frac{\partial \phi}{\partial p} \frac{\partial p}{\partial t}$$

Substituting Equation 6-67 into this equation,

$$\frac{\partial \phi}{\partial t} = \phi c_f \frac{\partial p}{\partial t}$$

Finally, substituting the above relation into Equation 6-66 and the result into Equation 6-65 gives:

$$\frac{0.006328}{r} \frac{\partial}{\partial r} \left(\frac{k}{\mu} (\rho r) \frac{\partial p}{\partial r} \right) = \rho \phi c_f \frac{\partial p}{\partial t} + \phi \frac{\partial \rho}{\partial t} \quad (6-68)$$

Equation 6-68 is the general partial differential equation used to describe the flow of any fluid flowing in a radial direction in porous media. In addition to the initial assumptions, Darcy's equation has been added, which implies that the flow is laminar. Otherwise, the equation is not restricted to any type of fluid and is equally valid for gases or liquids. Compressible and slightly compressible fluids, however, must be treated

separately in order to develop practical equations that can be used to describe the flow behavior of these two fluids. The treatments of the following systems are discussed below:

- Radial flow of slightly compressible fluids
- Radial flow of compressible fluids

Radial Flow of Slightly Compressible Fluids

To simplify Equation 6-68, assume that the permeability and viscosity are constant over pressure, time, and distance ranges. This leads to:

$$\left[\frac{0.006328 k}{\mu r} \right] \frac{\partial}{\partial r} \left(r \rho \frac{\partial p}{\partial r} \right) = \rho \phi c_f \frac{\partial p}{\partial t} + \phi \frac{\partial \rho}{\partial t} \quad (6-69)$$

Expanding the above equation gives:

$$0.006328 \left(\frac{k}{\mu} \right) \left[\frac{\rho}{r} \frac{\partial p}{\partial r} + \rho \frac{\partial^2 p}{\partial r^2} + \frac{\partial p}{\partial r} \frac{\partial \rho}{\partial r} \right] = \rho \phi c_f \left(\frac{\partial p}{\partial t} \right) + \phi \left(\frac{\partial \rho}{\partial t} \right)$$

Using the chain rule in the above relationship yields:

$$0.006328 \left(\frac{k}{\mu} \right) \left[\frac{\rho}{r} \frac{\partial p}{\partial r} + \rho \frac{\partial^2 p}{\partial r^2} + \left(\frac{\partial \rho}{\partial r} \right)^2 \frac{\partial p}{\partial \rho} \right] = \rho \phi c_f \left(\frac{\partial p}{\partial t} \right) + \phi \left(\frac{\partial p}{\partial t} \right) \left(\frac{\partial \rho}{\partial p} \right)$$

Dividing the above expression by the fluid density ρ gives

$$0.006328 \left(\frac{k}{\mu} \right) \left[\frac{1}{r} \frac{\partial p}{\partial r} + \frac{\partial^2 p}{\partial r^2} + \left(\frac{\partial p}{\partial r} \right)^2 \left(\frac{1}{\rho} \frac{\partial \rho}{\partial p} \right) \right] = \phi c_f \left(\frac{\partial p}{\partial t} \right) + \phi \frac{\partial p}{\partial t} \left(\frac{1}{\rho} \frac{\partial \rho}{\partial p} \right)$$

Recall that the compressibility of any fluid is related to its density by:

$$c = \frac{1}{\rho} \frac{\partial \rho}{\partial p}$$

Combining the above two equations gives:

$$0.006328 \left(\frac{k}{\mu} \right) \left[\frac{\partial^2 p}{\partial r^2} + \frac{1}{r} \frac{\partial p}{\partial r} + c \left[\frac{\partial p}{\partial r} \right]^2 \right] = \phi c_f \left(\frac{\partial p}{\partial t} \right) + \phi c \left(\frac{\partial p}{\partial t} \right)$$

The term $c \left(\frac{\partial p}{\partial r} \right)^2$ is considered very small and may be ignored:

$$0.006328 \left(\frac{k}{\mu} \right) \left[\frac{\partial^2 p}{\partial r^2} + \frac{1}{r} \frac{\partial p}{\partial r} \right] = \phi (c_f + c) \frac{\partial p}{\partial t} \quad (6-70)$$

Define total compressibility, c_t , as:

$$c_t = c + c_f \quad (6-71)$$

Combining Equations 6-69 with 6-70 and rearranging gives:

$$\frac{\partial^2 p}{\partial r^2} + \frac{1}{r} \frac{\partial p}{\partial r} = \frac{\phi \mu c_t}{0.006328 k} \frac{\partial p}{\partial t} \quad (6-72)$$

where the time t is expressed in days.

Equation 6-72 is called the *diffusivity equation*. It is one of the most important equations in petroleum engineering. The equation is particularly used in analysis well testing data where the time t is commonly recorded in hours. The equation can be rewritten as:

$$\frac{\partial^2 p}{\partial r^2} + \frac{1}{r} \frac{\partial p}{\partial r} = \frac{\phi \mu c_t}{0.000264 k} \frac{\partial p}{\partial t} \quad (6-73)$$

where k = permeability, md
 r = radial position, ft
 p = pressure, psia
 c_t = total compressibility, psi^{-1}
 t = time, hrs
 ϕ = porosity, fraction
 μ = viscosity, cp

When the reservoir contains more than one fluid, total compressibility should be computed as

$$c_t = c_o S_o + c_w S_w + c_g S_g + c_f \quad (6-74)$$

where c_o , c_w , and c_g refer to the compressibility of oil, water, and gas, respectively, while S_o , S_w , and S_g refer to the fractional saturation of these fluids. Note that the introduction of c_t into Equation 6-72 does not make Equation 6-72 applicable to multiphase flow; the use of c_t , as defined by Equation 6-73, simply accounts for the compressibility of any *immobile* fluids that may be in the reservoir with the fluid that is flowing.

The term $[0.000264 k/\phi\mu c_t]$ (Equation 6-73) is called the diffusivity constant and is denoted by the symbol η , or:

$$\eta = \frac{0.000264 k}{\phi\mu c_t} \quad (6-75)$$

The diffusivity equation can then be written in a more convenient form as:

$$\frac{\partial^2 p}{\partial r^2} + \frac{1}{r} \frac{\partial p}{\partial r} = \frac{1}{\eta} \frac{\partial p}{\partial t} \quad (6-76)$$

The diffusivity equation as represented by Equation 6-76 is essentially designed to determine the pressure as a function of time t and position r .

Before discussing and presenting the different solutions to the diffusivity equation, it is necessary to summarize the assumptions and limitations used in developing Equation 6-76:

1. Homogeneous and isotropic porous medium
2. Uniform thickness
3. Single phase flow
4. Laminar flow
5. Rock and fluid properties independent of pressure

Notice that for a steady-state flow condition, the pressure at any point in the reservoir is constant and does not change with time, i.e., $\partial p/\partial t = 0$, and therefore Equation 6-76 reduces to:

$$\frac{\partial^2 p}{\partial r^2} + \frac{1}{r} \frac{\partial p}{\partial r} = 0 \quad (6-77)$$

Equation 6-77 is called Laplace's equation for steady-state flow.

Example 6-9

Show that the radial form of Darcy's equation is the solution to Equation 6-77.

Solution

Step 1. Start with Darcy's Law as expressed by Equation 6-29

$$p = p_{wf} + \left[\frac{Q_o B_o u_o}{0.00708 k h} \right] \ln \left(\frac{r}{r_w} \right)$$

Step 2. For a steady-state incompressible flow, the term between the two brackets is constant and labeled as C, or:

$$p = p_{wf} + [C] \ln \left(\frac{r}{r_w} \right)$$

Step 3. Evaluate the above expression for the first and second derivative to give:

$$\frac{\partial p}{\partial r} = [C] \left(\frac{1}{r} \right)$$

$$\frac{\partial^2 p}{\partial r^2} = [C] \left(\frac{-1}{r^2} \right)$$

Step 4. Substitute the above two derivatives in Equation 6-77

$$\frac{-1}{r^2} [C] + \left(\frac{1}{r} \right) [C] \left(\frac{-1}{r} \right) = 0$$

Step 5. Results of Step 4 indicate that Darcy's equation satisfies Equation 6-77 and is indeed the solution to Laplace's equation.

To obtain a solution to the diffusivity equation (Equation 6-76), it is necessary to specify an initial condition and impose two boundary conditions. The initial condition simply states that the reservoir is at a uniform pressure p_i when production begins. The two boundary conditions require that the well is producing at a constant production rate and that the reservoir behaves as if it were infinite in size, i.e., $r_e = \infty$.

Based on the boundary conditions imposed on Equation 6-76, there are two generalized solutions to the diffusivity equation:

- Constant-terminal-pressure solution
- Constant-terminal-rate solution

The **constant-terminal-pressure solution** is designed to provide the cumulative flow at any particular time for a reservoir in which the pressure at one boundary of the reservoir is held constant. This technique is frequently used in water influx calculations in gas and oil reservoirs.

The **constant-terminal-rate solution** of the radial diffusivity equation solves for the pressure change throughout the radial system providing that the flow rate is held constant at one terminal end of the radial system, i.e., at the producing well. These are two commonly used forms of the constant-terminal-rate solution:

- The E_i -function solution
- The dimensionless pressure p_D solution

CONSTANT-TERMINAL-PRESSURE SOLUTION

In the constant-rate solution to the radial diffusivity equation, the flow rate is considered to be constant at a certain radius (usually wellbore radius) and the pressure profile around that radius is determined as a function of time and position. In the constant-terminal-pressure solution, the pressure is known to be constant at some particular radius and the solution is designed to provide the cumulative fluid movement across the specified radius (boundary).

The constant-pressure solution is widely used in water influx calculations. A detailed description of the solution and its practical reservoir engineering applications is appropriately discussed in the water influx chapter of the book (Chapter 10).

CONSTANT-TERMINAL-RATE SOLUTION

The constant-terminal-rate solution is an integral part of most transient test analysis techniques, such as with drawdown and pressure buildup analyses. Most of these tests involve producing the well at a **constant flow rate** and recording the flowing pressure as a function of time, i.e.,

$p(r_w, t)$. There are two commonly used forms of the constant-terminal-rate solution:

- The E_i -function solution
- The dimensionless pressure p_D solution

These two popular forms of solution are discussed below.

The E_i -Function Solution

Matthews and Russell (1967) proposed a solution to the diffusivity equation that is based on the following assumptions:

- Infinite acting reservoir, i.e., the reservoir is infinite in size
- The well is producing at a constant flow rate
- The reservoir is at a uniform pressure, p_i , when production begins
- The well, with a wellbore radius of r_w , is centered in a cylindrical reservoir of radius r_e
- No flow across the outer boundary, i.e., at r_e

Employing the above conditions, the authors presented their solution in the following form:

$$p(r, t) = p_i + \left[\frac{70.6 Q_o \mu_o b_o}{kh} \right] E_i \left[\frac{-948 \phi \mu_o c_t r^2}{kt} \right] \quad (6-78)$$

where $p(r, t)$ = pressure at radius r from the well after t hours

t = time, hrs

k = permeability, md

Q_o = flow rate, STB/day

The mathematical function, E_i , is called the **exponential integral** and is defined by:

$$E_i(-x) = - \int_x^\infty \frac{e^{-u}}{u} du = \left[\ln x - \frac{x}{1!} + \frac{x^2}{2(2!)} - \frac{x^3}{3(3!)} + \text{etc.} \right] \quad (6-79)$$

Craft, Hawkins, and Terry (1991) presented the values of the E_i -function in tabulated and graphical forms as shown in Table 6-1 and Figure 6-19, respectively.

The E_i solution, as expressed by Equation 6-78, is commonly referred to as the **line-source solution**. The exponential integral E_i can be approximated by the following equation when its argument x is less than 0.01:

$$E_i(-x) = \ln(1.781x) \quad (6-80)$$

where the argument x in this case is given by:

$$x = \frac{948\phi\mu c_t r^2}{kt}$$

Equation 6-80 approximates the E_i -function with less than 0.25% error. Another expression that can be used to approximate the E_i -function for the range $0.01 < x < 3.0$ is given by:

$$E_i(-x) = a_1 + a_2 \ln(x) + a_3 [\ln(x)]^2 + a_4 [\ln(x)]^3 + a_5 x + a_6 x^2 + a_7 x^3 + a_8 / x \quad (6-81)$$

With the coefficients a_1 through a_8 having the following values:

$$\begin{aligned} a_1 &= -0.33153973 & a_2 &= -0.81512322 & a_3 &= 5.22123384(10^{-2}) \\ a_4 &= 5.9849819(10^{-3}) & a_5 &= 0.662318450 & a_6 &= -0.12333524 \\ a_7 &= 1.0832566(10^{-2}) & a_8 &= 8.6709776(10^{-4}) \end{aligned}$$

The above relationship approximated the E_i -values with an average error of 0.5%.

It should be pointed out that for $x > 10.9$, the $E_i(-x)$ can be considered zero for all practical reservoir engineering calculations.

Example 6-10

An oil well is producing at a constant flow rate of 300 STB/day under unsteady-state flow conditions. The reservoir has the following rock and fluid properties:

$$\begin{aligned} B_o &= 1.25 \text{ bbl/STB} & \mu_o &= 1.5 \text{ cp} & c_t &= 12 \times 10^{-6} \text{ psi}^{-1} \\ k_o &= 60 \text{ md} & h &= 15 \text{ ft} & p_i &= 4000 \text{ psi} \\ \phi &= 15\% & r_w &= 0.25 \text{ ft} & & \end{aligned}$$

Table 6-1
Values of the $-E_i(-x)$ as a Function of x
(After Craft, Hawkins, and Terry, 1991)

| x | $-E_i(-x)$ | x | $-E_i(-x)$ | x | $-E_i(-x)$ |
|-----|------------|-----|------------|------|------------|
| 0.1 | 1.82292 | 4.3 | 0.00263 | 8.5 | 0.00002 |
| 0.2 | 1.22265 | 4.4 | 0.00234 | 8.6 | 0.00002 |
| 0.3 | 0.90568 | 4.5 | 0.00207 | 8.7 | 0.00002 |
| 0.4 | 0.70238 | 4.6 | 0.00184 | 8.8 | 0.00002 |
| 0.5 | 0.55977 | 4.7 | 0.00164 | 8.9 | 0.00001 |
| 0.6 | 0.45438 | 4.8 | 0.00145 | 9.0 | 0.00001 |
| 0.7 | 0.37377 | 4.9 | 0.00129 | 9.1 | 0.00001 |
| 0.8 | 0.31060 | 5.0 | 0.00115 | 9.2 | 0.00001 |
| 0.9 | 0.26018 | 5.1 | 0.00102 | 9.3 | 0.00001 |
| 1.0 | 0.21938 | 5.2 | 0.00091 | 9.4 | 0.00001 |
| 1.1 | 0.18599 | 5.3 | 0.00081 | 9.5 | 0.00001 |
| 1.2 | 0.15841 | 5.4 | 0.00072 | 9.6 | 0.00001 |
| 1.3 | 0.13545 | 5.5 | 0.00064 | 9.7 | 0.00001 |
| 1.4 | 0.11622 | 5.6 | 0.00057 | 9.8 | 0.00001 |
| 1.5 | 0.10002 | 5.7 | 0.00051 | 9.9 | 0.00000 |
| 1.6 | 0.08631 | 5.8 | 0.00045 | 10.0 | 0.00000 |
| 1.7 | 0.07465 | 5.9 | 0.00040 | | |
| 1.8 | 0.06471 | 6.0 | 0.00036 | | |
| 1.9 | 0.05620 | 6.1 | 0.00032 | | |
| 2.0 | 0.04890 | 6.2 | 0.00029 | | |
| 2.1 | 0.04261 | 6.3 | 0.00026 | | |
| 2.2 | 0.03719 | 6.4 | 0.00023 | | |
| 2.3 | 0.03250 | 6.5 | 0.00020 | | |
| 2.4 | 0.02844 | 6.6 | 0.00018 | | |
| 2.5 | 0.02491 | 6.7 | 0.00016 | | |
| 2.6 | 0.02185 | 6.8 | 0.00014 | | |
| 2.7 | 0.01918 | 6.9 | 0.00013 | | |
| 2.8 | 0.01686 | 7.0 | 0.00012 | | |
| 2.9 | 0.01482 | 7.1 | 0.00010 | | |
| 3.0 | 0.01305 | 7.2 | 0.00009 | | |
| 3.1 | 0.01149 | 7.3 | 0.00008 | | |
| 3.2 | 0.01013 | 7.4 | 0.00007 | | |
| 3.3 | 0.00894 | 7.5 | 0.00007 | | |
| 3.4 | 0.00789 | 7.6 | 0.00006 | | |
| 3.5 | 0.00697 | 7.7 | 0.00005 | | |
| 3.6 | 0.00616 | 7.8 | 0.00005 | | |
| 3.7 | 0.00545 | 7.9 | 0.00004 | | |
| 3.8 | 0.00482 | 8.0 | 0.00004 | | |
| 3.9 | 0.00427 | 8.1 | 0.00003 | | |
| 4.0 | 0.00378 | 8.2 | 0.00003 | | |
| 4.1 | 0.00335 | 8.3 | 0.00003 | | |
| 4.2 | 0.00297 | 8.4 | 0.00002 | | |

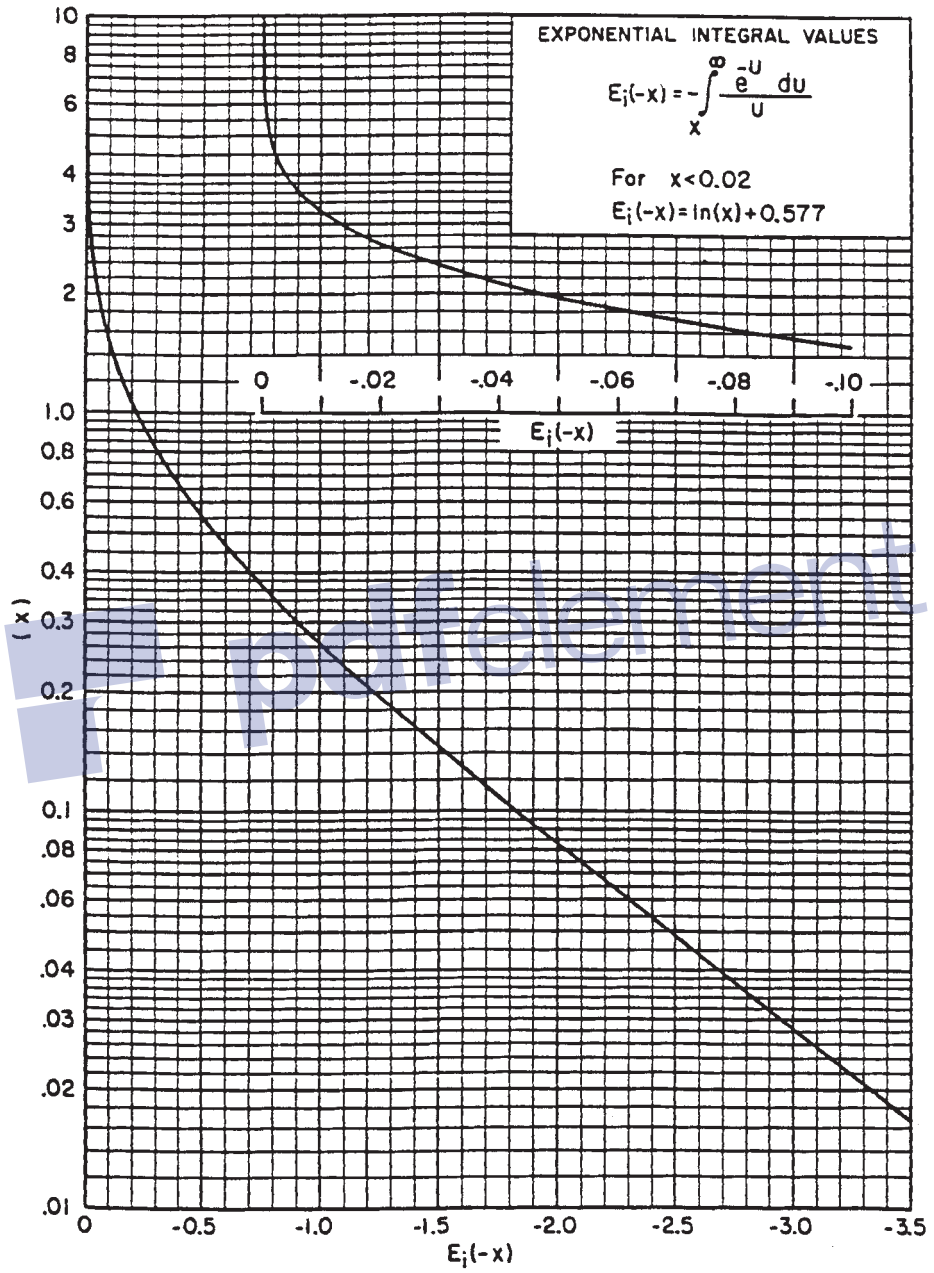


Figure 6-19. The E_i-function. (After Craft, Hawkins, and Terry, 1991.)

1. Calculate pressure at radii of 0.25, 5, 10, 50, 100, 500, 1,000, 1,500, 2,000, and 2,500 feet, for 1 hour.

Plot the results as:

- Pressure versus logarithm of radius
- Pressure versus radius

2. Repeat part 1 for $t = 12$ hours and 24 hours. Plot the results as pressure versus logarithm of radius.

Solution

Step 1. From Equation 6-78:

$$p(r,t) = 4000 + \left[\frac{70.6(300)(1.5)(1.25)}{(60)(15)} \right]$$

$$\times E_i \left[\frac{-948(.15)(1.5)(12 \times 10^{-6})r^2}{(60)(t)} \right]$$

$$p(r,t) = 4000 + 44.125 E_i \left[-42.6(10^{-6}) \frac{r^2}{t} \right]$$

Step 2. Perform the required calculations after one hour in the following tabulated form:

Elapsed Time $t = 1$ hr

| r , ft | $x = -42.6(10^{-6}) \frac{r^2}{1}$ | $E_i(-x)$ | $p(r,1) = 4000 + 44.125 E_i(-x)$ |
|----------|------------------------------------|-----------------|----------------------------------|
| 0.25 | $-2.6625(10^{-6})$ | -12.26^* | 3459 |
| 5 | -0.001065 | -6.27^* | 3723 |
| 10 | -0.00426 | -4.88^* | 3785 |
| 50 | -0.1065 | -1.76^\dagger | 3922 |
| 100 | -0.4260 | -0.75^\dagger | 3967 |
| 500 | -10.65 | 0 | 4000 |
| 1000 | -42.60 | 0 | 4000 |
| 1500 | -95.85 | 0 | 4000 |
| 2000 | -175.40 | 0 | 4000 |
| 2500 | -266.25 | 0 | 4000 |

*As calculated from Equation 6-29

†From Figure 6-19

Step 3. Show results of the calculation graphically as illustrated in Figures 6-20 and 6-21.

Step 4. Repeat the calculation for $t = 12$ and 24 hrs.

Elapsed Time $t = 12$ hrs

| r , ft | $x = 42.6(10^{-6}) \frac{r^2}{12}$ | $E_i(-x)$ | $p(r, 12) = 4000 + 44.125 E_i(-x)$ |
|----------|------------------------------------|--------------------|------------------------------------|
| 0.25 | $0.222 (10^{-6})$ | -14.74* | 3350 |
| 5 | $88.75 (10^{-6})$ | -8.75* | 3614 |
| 10 | $355.0 (10^{-6})$ | -7.37* | 3675 |
| 50 | 0.0089 | -4.14* | 3817 |
| 100 | 0.0355 | -2.81 [†] | 3876 |
| 500 | 0.888 | -0.269 | 3988 |
| 1000 | 3.55 | -0.0069 | 4000 |
| 1500 | 7.99 | $-3.77(10^{-5})$ | 4000 |
| 2000 | 14.62 | 0 | 4000 |
| 2500 | 208.3 | 0 | 4000 |

*As calculated from Equation 6-29

[†]From Figure 6-19

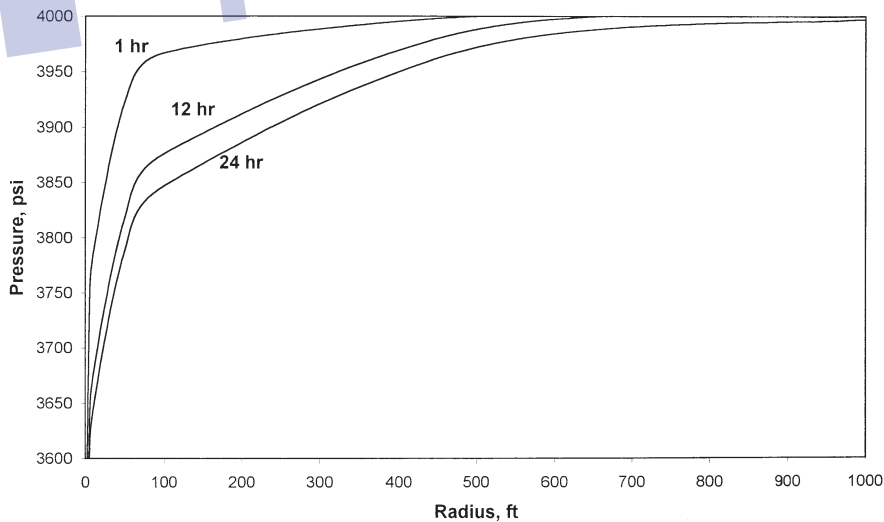


Figure 6-20. Pressure profiles as a function of time.

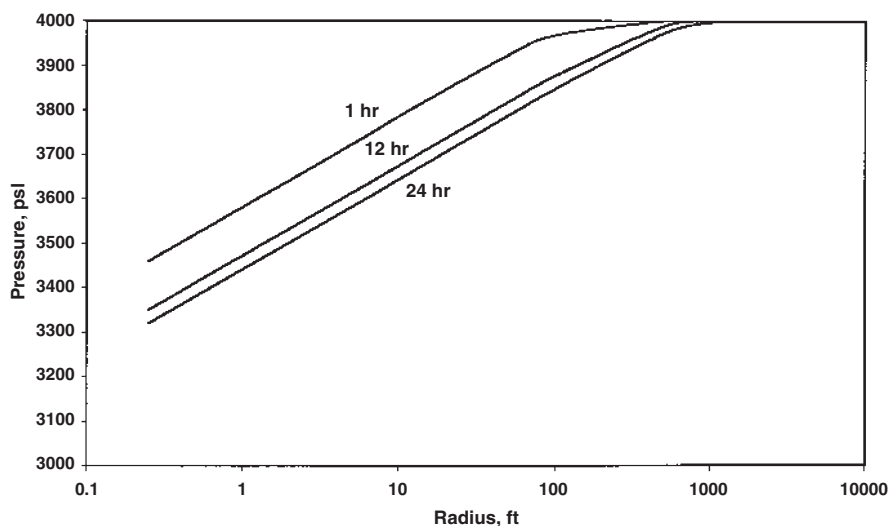


Figure 6-21. Pressure profiles as a function of time on a semi log scale.

Elapsed Time $t = 24$ hrs

| r, ft | $x = 42.6(10^{-6}) \frac{r^2}{24}$ | $E_i(-x)$ | $p(r,24) = 4000 + 44.125 E_i(-x)$ |
|----------------|------------------------------------|------------------|-----------------------------------|
| 0.25 | $-0.111 (10^{-6})$ | -15.44^* | 3319 |
| 5 | $-44.38 (10^{-6})$ | -9.45^* | 3583 |
| 10 | $-177.5 (10^{-6})$ | -8.06^* | 3644 |
| 50 | -0.0045 | -4.83^* | 3787 |
| 100 | -0.0178 | -3.458^\dagger | 3847 |
| 500 | -0.444 | -0.640 | 3972 |
| 1000 | -1.775 | -0.067 | 3997 |
| 1500 | -3.995 | -0.0427 | 3998 |
| 2000 | -7.310 | $8.24 (10^{-6})$ | 4000 |
| 2500 | -104.15 | 0 | 4000 |

*As calculated from Equation 6-29

†From Figure 6-19

Step 5. Results of Step 4 are shown graphically in Figure 6-21.

The above example shows that most of the pressure loss occurs close to the wellbore; accordingly, near-wellbore conditions will exert the

greatest influence on flow behavior. Figure 6-21 shows that the pressure profile and the drainage radius are continuously changing with time.

When the parameter x in the E_i -function is less than 0.01, the log approximation as expressed by Equation 6-80 can be used in Equation 6-78 to give:

$$p(r,t) = p_i - \frac{162.6 Q_o B_o m_o}{k h} \left[\log \left(\frac{k t}{\phi \mu_o c_t r^2} \right) - 3.23 \right] \quad (6-82)$$

For most of the transient flow calculations, engineers are primarily concerned with the behavior of the bottom-hole flowing pressure at the wellbore, i.e., $r = r_w$. Equation 6-82 can be applied at $r = r_w$ to yield:

$$p_{wf} = p_i - \frac{162.6 Q_o B_o m_o}{k h} \left[\log \left(\frac{k t}{\phi \mu_o c_t r_w^2} \right) - 3.23 \right] \quad (6-83)$$

where k = permeability, md

t = time, hr

c_t = total compressibility, psi^{-1}

It should be noted that Equations 6-82 and 6-83 cannot be used until the flow time t exceeds the limit imposed by the following constraint:

$$t > 9.48 \times 10^4 \frac{\phi \mu_o c_t r^2}{k} \quad (6-84)$$

where t = time, hr

k = permeability, md

Example 6-11

Using the data in Example 6-10, estimate the bottom-hole flowing pressure after 10 hours of production.

Solution

Step 1. Equation 6-83 can be used to calculate p_{wf} only if the time exceeds the time limit imposed by Equation 6-84, or:

$$t = 9.48(10^4) \frac{(0.15)(1.5)(12 \times 10^{-6})(0.25)^2}{60} = 0.000267 \text{ hr} \\ = 0.153 \text{ sec}$$

For all practical purposes, Equation 6-83 can be used anytime during the transient flow period to estimate the bottom-hole pressure.

Step 2. Since the specified time of 10 hr is greater than 0.000267 hr, the p_{wf} can be estimated by applying Equation 6-83.

$$p_{wf} = 4000 - \frac{162.6(300)(1.25)(1.5)}{(60)(15)} \\ \times \left[\log \left(\frac{(60)(10)}{(0.15)(1.5)(12 \times 10^{-6})(0.25)^2} \right) - 3.23 \right] = 3358 \text{ psi}$$

The second form of solution to the diffusivity equation is called the *dimensionless pressure drop* and is discussed below.

The Dimensionless Pressure Drop (p_D) Solution

Well test analysis often makes use of the concept of the dimensionless variables in solving the unsteady-state flow equation. The importance of dimensionless variables is that they simplify the diffusivity equation and its solution by combining the reservoir parameters (such as permeability, porosity, etc.) and thereby reduce the total number of unknowns.

To introduce the concept of the dimensionless pressure drop solution, consider for example Darcy's equation in a radial form as given previously by Equation 6-27.

$$Q_o = 0.00708 \frac{kh(p_e - p_{wf})}{\mu_o B_o \ln(r_e / r_w)}$$

Rearrange the above equation to give:

$$\frac{p_e - p_{wf}}{\left(\frac{Q_o B_o \mu_o}{0.00708 kh} \right)} = \ln \left(\frac{r_e}{r_w} \right) \quad (6-85)$$

It is obvious that the right-hand side of the above equation has no units (i.e., dimensionless) and, accordingly, the left-hand side must be dimensionless. Since the left-hand side is dimensionless, and $(p_e - p_{wf})$ has the units of psi, it follows that the term $[Q_o B_o \mu_o / (0.00708kh)]$ has units of pressure. In fact, any pressure difference divided by $[Q_o B_o \mu_o / (0.00708kh)]$ is a dimensionless pressure. Therefore, Equation 6-85 can be written in a dimensionless form as:

$$p_D = \ln(r_{eD})$$

where

$$p_D = \frac{p_e - p_{wf}}{\left(\frac{Q_o B_o \mu_o}{0.00708 kh} \right)}$$

This concept can be extended to consider unsteady-state equations where the time is a variable. Defining:

$$r_{eD} = \frac{r_e}{r_w}$$

In transient flow analysis, the dimensionless pressure p_D is always a function of dimensionless time that is defined by the following expression:

$$p_D = \frac{p_i - p(r,t)}{\left(\frac{Q_o B_o \mu_o}{0.00708 kh} \right)} \quad (6-86)$$

In transient flow analysis, the dimensionless pressure p_D is always a function of dimensionless time that is defined by the following expression:

$$t_D = \frac{0.000264 kt}{\phi \mu c_t r_w^2} \quad (6-87)$$

The above expression is only one form of the dimensionless time. Another definition in common usage is t_{DA} , the dimensionless time based on total drainage area.

$$t_{DA} = \frac{0.000264 kt}{\phi \mu c_t A} = t_D \left(\frac{r_w^2}{A} \right) \quad (6-87a)$$

where A = total drainage area = πr_e^2
 r_e = drainage radius, ft
 r_w = wellbore radius, ft

The dimensionless pressure p_D also varies with location in the reservoir as represented by the dimensionless radial distances r_D and r_{eD} that are defined by:

$$r_D = \frac{r}{r_w} \quad (6-88)$$

and

$$r_{eD} = \frac{r_e}{r_w} \quad (6-89)$$

where p_D = dimensionless pressure drop
 r_{eD} = dimensionless external radius
 t_D = dimensionless time
 r_D = dimensionless radius
 t = time, hr
 $p(r,t)$ = pressure at radius r and time t
 k = permeability, md
 μ = viscosity, cp

The above dimensionless groups (i.e., p_D , t_D , and r_D) can be introduced into the diffusivity equation (Equation 6-76) to transform the equation into the following dimensionless form:

$$\frac{\partial^2 p_D}{\partial r_D^2} + \frac{1}{r_D} \frac{\partial p_D}{\partial r_D} = \frac{\partial p_D}{\partial t_D} \quad (6-90)$$

Van Everdingen and Hurst (1949) proposed an analytical solution to the above equation by assuming:

- Perfectly radial reservoir system
- The producing well is in the center and producing at a constant production rate of Q
- Uniform pressure p_i throughout the reservoir before production
- No flow across the external radius r_e

Van Everdingen and Hurst presented the solution to Equation 6-89 in a form of infinite series of exponential terms and Bessel functions. The authors evaluated this series for several values of r_{eD} over a wide range of values for t_D . Chatas (1953) and Lee (1982) conveniently tabulated these solutions for the following two cases:

- Infinite-acting reservoir
- Finite-radial reservoir

Infinite-Acting Reservoir

When a well is put on production at a constant flow rate after a shut-in period, the pressure in the wellbore begins to drop and causes a pressure disturbance to spread in the reservoir. The influence of the reservoir boundaries or the shape of the drainage area does not affect the rate at which the pressure disturbance spreads in the formation. That is why the transient state flow is also called the *infinite acting state*. During the infinite acting period, the declining rate of wellbore pressure and the manner by which the pressure disturbance spreads through the reservoir are determined by reservoir and fluid characteristics such as:

- Porosity, ϕ
- Permeability, k
- Total compressibility, c_t
- Viscosity, μ

For an infinite-acting reservoir, i.e., $r_{eD} = \infty$, the dimensionless pressure drop function p_D is strictly a function of the dimensionless time t_D , or:

$$p_D = f(t_D)$$

Chatas and Lee tabulated the p_D values for the infinite-acting reservoir as shown in Table 6-2. The following mathematical expressions can be used to approximate these tabulated values of p_D :

Table 6-2
 p_D vs. t_D —Infinite-Radial System, Constant-Rate at the Inner
Boundary (After Lee, J., Well Testing, SPE Textbook Series.)
(Permission to publish by the SPE, copyright SPE, 1982)

| t_D | p_D | t_D | p_D | t_D | p_D |
|--------|--------|-------|--------|---------|--------|
| 0 | 0 | 0.15 | 0.3750 | 60.0 | 2.4758 |
| 0.0005 | 0.0250 | 0.2 | 0.4241 | 70.0 | 2.5501 |
| 0.001 | 0.0352 | 0.3 | 0.5024 | 80.0 | 2.6147 |
| 0.002 | 0.0495 | 0.4 | 0.5645 | 90.0 | 2.6718 |
| 0.003 | 0.0603 | 0.5 | 0.6167 | 100.0 | 2.7233 |
| 0.004 | 0.0694 | 0.6 | 0.6622 | 150.0 | 2.9212 |
| 0.005 | 0.0774 | 0.7 | 0.7024 | 200.0 | 3.0636 |
| 0.006 | 0.0845 | 0.8 | 0.7387 | 250.0 | 3.1726 |
| 0.007 | 0.0911 | 0.9 | 0.7716 | 300.0 | 3.2630 |
| 0.008 | 0.0971 | 1.0 | 0.8019 | 350.0 | 3.3394 |
| 0.009 | 0.1028 | 1.2 | 0.8672 | 400.0 | 3.4057 |
| 0.01 | 0.1081 | 1.4 | 0.9160 | 450.0 | 3.4641 |
| 0.015 | 0.1312 | 2.0 | 1.0195 | 500.0 | 3.5164 |
| 0.02 | 0.1503 | 3.0 | 1.1665 | 550.0 | 3.5643 |
| 0.025 | 0.1669 | 4.0 | 1.2750 | 600.0 | 3.6076 |
| 0.03 | 0.1818 | 5.0 | 1.3625 | 650.0 | 3.6476 |
| 0.04 | 0.2077 | 6.0 | 1.4362 | 700.0 | 3.6842 |
| 0.05 | 0.2301 | 7.0 | 1.4997 | 750.0 | 3.7184 |
| 0.06 | 0.2500 | 8.0 | 1.5557 | 800.0 | 3.7505 |
| 0.07 | 0.2680 | 9.0 | 1.6057 | 850.0 | 3.7805 |
| 0.08 | 0.2845 | 10.0 | 1.6509 | 900.0 | 3.8088 |
| 0.09 | 0.2999 | 15.0 | 1.8294 | 950.0 | 3.8355 |
| 0.1 | 0.3144 | 20.0 | 1.9601 | 1,000.0 | 3.8584 |
| | | 30.0 | 2.1470 | | |
| | | 40.0 | 2.2824 | | |
| | | 50.0 | 2.3884 | | |

Notes: For $t_D < 0.01$, $p_D \cong 2 \sqrt{2t_D/x}$.

For $100 < t_D < 0.25 r_{eD}^2$, $p_D \cong 0.5 (\ln t_D + 0.80907)$.

- For $t_D < 0.01$:

$$p_D = 2 \sqrt{\frac{t_D}{\pi}} \quad (6-91)$$

- For $t_D > 100$:

$$p_D = 0.5[\ln(t_D) + 0.80907] \quad (6-92)$$

- For $0.02 < t_D < 1000$:

$$p_D = a_1 + a_2 \ln(t_D) + a_3 [\ln(t_D)]^2 + a_4 [\ln(t_D)]^3 + a_5 t_D + a_6 (t_D)^2 + a_7 (t_D)^3 + a_8/t_D \quad (6-93)$$

where

$$\begin{aligned} a_1 &= 0.8085064 & a_2 &= 0.29302022 & a_3 &= 3.5264177(10^{-2}) \\ a_4 &= -1.4036304(10^{-3}) & a_5 &= -4.7722225(10^{-4}) & a_6 &= 5.1240532(10^{-7}) \\ a_7 &= -2.3033017(10^{-10}) & a_8 &= -2.6723117(10^{-3}) \end{aligned}$$

Finite-Radial Reservoir

The arrival of the pressure disturbance at the well drainage boundary marks the end of the transient flow period and the beginning of the semi (pseudo)-steady state. During this flow state, the reservoir boundaries and the shape of the drainage area influence the wellbore pressure response as well as the behavior of the pressure distribution throughout the reservoir. Intuitively, one should not expect the change from the transient to the semi-steady state in this bounded (finite) system to occur instantaneously. There is a short period of time that separates the transient state from the semi-steady state that is called *late-transient state*. Due to its complexity and short duration, the late transient flow is not used in practical well test analysis.

For a finite radial system, the p_D -function is a function of both the dimensionless time and radius, or:

$$p_D = f(t_D, r_{eD})$$

where

$$r_{eD} = \frac{\text{external radius}}{\text{wellbore radius}} = \frac{r_e}{r_w} \quad (6-94)$$

Table 6-3 presents p_D as a function of t_D for $1.5 < r_{eD} < 10$. It should be pointed out that Van Everdingen and Hurst principally applied the p_D -function solution to model the performance of water influx into oil reservoirs. Thus, the authors' wellbore radius r_w was in this case the external radius of the reservoir and the r_e was essentially the external boundary radius of the aquifer. Therefore, the range of the r_{eD} values in Table 6-3 is practical for this application.

Table 6-3
 p_D vs. t_D —Finite-Radial System, Constant-Rate at the Inner Boundary
(After Lee, J., Well Testing, SPE Textbook Series.)
(Permission to publish by the SPE, copyright SPE, 1982)

| $r_{eD} = 1.5$ | | $r_{eD} = 2.0$ | | $r_{eD} = 2.5$ | | $r_{eD} = 3.0$ | | $r_{eD} = 3.5$ | | $r_{eD} = 4.0$ | |
|----------------|-------|----------------|-------|----------------|-------|----------------|-------|----------------|-------|----------------|-------|
| t_D | p_D | t_D | p_D | t_D | p_D | t_D | p_D | t_D | p_D | t_D | p_D |
| 0.06 | 0.251 | 0.22 | 0.443 | 0.40 | 0.565 | 0.52 | 0.627 | 1.0 | 0.802 | 1.5 | 0.927 |
| 0.08 | 0.288 | 0.24 | 0.459 | 0.42 | 0.576 | 0.54 | 0.636 | 1.1 | 0.830 | 1.6 | 0.948 |
| 0.10 | 0.322 | 0.26 | 0.476 | 0.44 | 0.587 | 0.56 | 0.645 | 1.2 | 0.857 | 1.7 | 0.968 |
| 0.12 | 0.355 | 0.28 | 0.492 | 0.46 | 0.598 | 0.60 | 0.662 | 1.3 | 0.882 | 1.8 | 0.988 |
| 0.14 | 0.387 | 0.30 | 0.507 | 0.48 | 0.608 | 0.65 | 0.683 | 1.4 | 0.906 | 1.9 | 1.007 |
| 0.16 | 0.420 | 0.32 | 0.522 | 0.50 | 0.618 | 0.70 | 0.703 | 1.5 | 0.929 | 2.0 | 1.025 |
| 0.18 | 0.452 | 0.34 | 0.536 | 0.52 | 0.628 | 0.75 | 0.721 | 1.6 | 0.951 | 2.2 | 1.059 |
| 0.20 | 0.484 | 0.36 | 0.551 | 0.54 | 0.638 | 0.80 | 0.740 | 1.7 | 0.973 | 2.4 | 1.092 |
| 0.22 | 0.516 | 0.38 | 0.565 | 0.56 | 0.647 | 0.85 | 0.758 | 1.8 | 0.994 | 2.6 | 1.123 |
| 0.24 | 0.548 | 0.40 | 0.579 | 0.58 | 0.657 | 0.90 | 0.776 | 1.9 | 1.014 | 2.8 | 1.154 |
| 0.26 | 0.580 | 0.42 | 0.593 | 0.60 | 0.666 | 0.95 | 0.791 | 2.0 | 1.034 | 3.0 | 1.184 |
| 0.28 | 0.612 | 0.44 | 0.607 | 0.65 | 0.688 | 1.0 | 0.806 | 2.25 | 1.083 | 3.5 | 1.255 |
| 0.30 | 0.644 | 0.46 | 0.621 | 0.70 | 0.710 | 1.2 | 0.865 | 2.50 | 1.130 | 4.0 | 1.324 |
| 0.35 | 0.724 | 0.48 | 0.634 | 0.75 | 0.731 | 1.4 | 0.920 | 2.75 | 1.176 | 4.5 | 1.392 |
| 0.40 | 0.804 | 0.50 | 0.648 | 0.80 | 0.752 | 1.6 | 0.973 | 3.0 | 1.221 | 5.0 | 1.460 |
| 0.45 | 0.884 | 0.60 | 0.715 | 0.85 | 0.772 | 2.0 | 1.076 | 4.0 | 1.401 | 5.5 | 1.527 |
| 0.50 | 0.964 | 0.70 | 0.782 | 0.90 | 0.792 | 3.0 | 1.328 | 5.0 | 1.579 | 6.0 | 1.594 |
| 0.55 | 1.044 | 0.80 | 0.849 | 0.95 | 0.812 | 4.0 | 1.578 | 6.0 | 1.757 | 6.5 | 1.660 |
| 0.60 | 1.124 | 0.90 | 0.915 | 1.0 | 0.832 | 5.0 | 1.828 | | | 7.0 | 1.727 |
| 0.65 | 1.204 | 1.0 | 0.982 | 2.0 | 1.215 | | | | | 8.0 | 1.861 |
| 0.70 | 1.284 | 2.0 | 1.649 | 3.0 | 1.506 | | | | | 9.0 | 1.994 |
| 0.75 | 1.364 | 3.0 | 2.316 | 4.0 | 1.977 | | | | | 10.0 | 2.127 |
| 0.80 | 1.444 | 5.0 | 3.649 | 5.0 | 2.398 | | | | | | |

| $r_{eD} = 4.5$ | | $r_{eD} = 5.0$ | | $r_{eD} = 6.0$ | | $r_{eD} = 7.0$ | | $r_{eD} = 8.0$ | | $r_{eD} = 9.0$ | | $r_{eD} = 10.0$ | |
|----------------|-------|----------------|-------|----------------|-------|----------------|-------|----------------|-------|----------------|-------|-----------------|-------|
| t_D | p_D | t_D | p_D | t_D | p_D | t_D | p_D | t_D | p_D | t_D | p_D | t_D | p_D |
| 2.0 | 1.023 | 3.0 | 1.167 | 4.0 | 1.275 | 6.0 | 1.436 | 8.0 | 1.556 | 10.0 | 1.651 | 12.0 | 1.732 |
| 2.1 | 1.040 | 3.1 | 1.180 | 4.5 | 1.322 | 6.5 | 1.470 | 8.5 | 1.582 | 10.5 | 1.673 | 12.5 | 1.750 |
| 2.2 | 1.056 | 3.2 | 1.192 | 5.0 | 1.364 | 7.0 | 1.501 | 9.0 | 1.607 | 11.0 | 1.693 | 13.0 | 1.768 |
| 2.3 | 1.702 | 3.3 | 1.204 | 5.5 | 1.404 | 7.5 | 1.531 | 9.5 | 1.631 | 11.5 | 1.713 | 13.5 | 1.784 |
| 2.4 | 1.087 | 3.4 | 1.215 | 6.0 | 1.441 | 8.0 | 1.559 | 10.0 | 1.653 | 12.0 | 1.732 | 14.0 | 1.801 |
| 2.5 | 1.102 | 3.5 | 1.227 | 6.5 | 1.477 | 8.5 | 1.586 | 10.5 | 1.675 | 12.5 | 1.750 | 14.5 | 1.817 |
| 2.6 | 1.116 | 3.6 | 1.238 | 7.0 | 1.511 | 9.0 | 1.613 | 11.0 | 1.697 | 13.0 | 1.768 | 15.0 | 1.832 |
| 2.7 | 1.130 | 3.7 | 1.249 | 7.5 | 1.544 | 9.5 | 1.638 | 11.5 | 1.717 | 13.5 | 1.786 | 15.5 | 1.847 |
| 2.8 | 1.144 | 3.8 | 1.259 | 8.0 | 1.576 | 10.0 | 1.663 | 12.0 | 1.737 | 14.0 | 1.803 | 16.0 | 1.862 |
| 2.9 | 1.158 | 3.9 | 1.270 | 8.5 | 1.607 | 11.0 | 1.711 | 12.5 | 1.757 | 14.5 | 1.819 | 17.0 | 1.890 |
| 3.0 | 1.171 | 4.0 | 1.281 | 9.0 | 1.638 | 12.0 | 1.757 | 13.0 | 1.776 | 15.0 | 1.835 | 18.0 | 1.917 |

(table continued on next page)

Table 6-3 (continued)

| $r_{eD} = 4.5$ | | $r_{eD} = 5.0$ | | $r_{eD} = 6.0$ | | $r_{eD} = 7.0$ | | $r_{eD} = 8.0$ | | $r_{eD} = 9.0$ | | $r_{eD} = 10.0$ | |
|----------------|-------|----------------|-------|----------------|-------|----------------|-------|----------------|-------|----------------|-------|-----------------|-------|
| t_D | p_D | t_D | p_D | t_D | p_D | t_D | p_D | t_D | p_D | t_D | p_D | t_D | p_D |
| 3.2 | 1.197 | 4.2 | 1.301 | 9.5 | 1.668 | 13.0 | 1.810 | 13.5 | 1.795 | 15.5 | 1.851 | 19.0 | 1.943 |
| 3.4 | 1.222 | 4.4 | 1.321 | 10.0 | 1.698 | 14.0 | 1.845 | 14.0 | 1.813 | 16.0 | 1.867 | 20.0 | 1.968 |
| 3.6 | 1.246 | 4.6 | 1.340 | 11.0 | 1.757 | 15.0 | 1.888 | 14.5 | 1.831 | 17.0 | 1.897 | 22.0 | 2.017 |
| 3.8 | 1.269 | 4.8 | 1.360 | 12.0 | 1.815 | 16.0 | 1.931 | 15.0 | 1.849 | 18.0 | 1.926 | 24.0 | 2.063 |
| 4.0 | 1.292 | 5.0 | 1.378 | 13.0 | 1.873 | 17.0 | 1.974 | 17.0 | 1.919 | 19.0 | 1.955 | 26.0 | 2.108 |
| 4.5 | 1.349 | 5.5 | 1.424 | 14.0 | 1.931 | 18.0 | 2.016 | 19.0 | 1.986 | 20.0 | 1.983 | 28.0 | 2.151 |
| 5.0 | 1.403 | 6.0 | 1.469 | 15.0 | 1.988 | 19.0 | 2.058 | 21.0 | 2.051 | 22.0 | 2.037 | 30.0 | 2.194 |
| 5.5 | 1.457 | 6.5 | 1.513 | 16.0 | 2.045 | 20.0 | 2.100 | 23.0 | 2.116 | 24.0 | 2.906 | 32.0 | 2.236 |
| 6.0 | 1.510 | 7.0 | 1.556 | 17.0 | 2.103 | 22.0 | 2.184 | 25.0 | 2.180 | 26.0 | 2.142 | 34.0 | 2.278 |
| 7.0 | 1.615 | 7.5 | 1.598 | 18.0 | 2.160 | 24.0 | 2.267 | 30.0 | 2.340 | 28.0 | 2.193 | 36.0 | 2.319 |
| 8.0 | 1.719 | 8.0 | 1.641 | 19.0 | 2.217 | 26.0 | 2.351 | 35.0 | 2.499 | 30.0 | 2.244 | 38.0 | 2.360 |
| 9.0 | 1.823 | 9.0 | 1.725 | 20.0 | 2.274 | 28.0 | 2.434 | 40.0 | 2.658 | 34.0 | 2.345 | 40.0 | 2.401 |
| 10.0 | 1.927 | 10.0 | 1.808 | 25.0 | 2.560 | 30.0 | 2.517 | 45.0 | 2.817 | 38.0 | 2.446 | 50.0 | 2.604 |
| 11.0 | 2.031 | 11.0 | 1.892 | 30.0 | 2.846 | | | | | 40.0 | 2.496 | 60.0 | 2.806 |
| 12.0 | 2.135 | 12.0 | 1.975 | | | | | | | 45.0 | 2.621 | 70.0 | 3.008 |
| 13.0 | 2.239 | 13.0 | 2.059 | | | | | | | 50.0 | 2.746 | 80.0 | 3.210 |
| 14.0 | 2.343 | 14.0 | 2.142 | | | | | | | 60.0 | 2.996 | 90.0 | 3.412 |
| 15.0 | 2.447 | 15.0 | 2.225 | | | | | | | 70.0 | 3.246 | 100.0 | 3.614 |

Notes: For t_D smaller than values listed in this table for a given r_{eD} , reservoir is infinite acting.

Find p_D in Table 6-2.

For $25 < t_D$ and t_D larger than values in table.

$$p_D \cong \frac{(\frac{1}{2} + 2t_D)}{(r_{eD}^2 - 1)} - \frac{3r_{eD}^4 - 4r_{eD}^2 \ln r_{eD} - 2r_{eD}^2 - 1}{4(r_{eD}^2 - 1)^2}$$

For wells in rebounded reservoirs with

$r_{eD}^2 \gg 1$

$$p_D \cong \frac{2t_D}{r_{eD}^2} + \ln r_{eD} - \frac{3}{4}$$

Chatas (1953) proposed the following mathematical expression for calculating p_D :

For $25 < t_D$ and $0.25 r_{eD}^2 < t_D$

$$p_D = \frac{0.5 + 2t_D}{r_{eD}^2 - 1} - \frac{r_{eD}^4 [3 - 4 \ln(r_{eD})] - 2r_{eD}^2 - 1}{4(r_{eD}^2 - 1)^2} \quad (6-95)$$

A special case of Equation 6-95 arises when $r_{eD}^2 \gg 1$, then:

$$p_D = \frac{2t_D}{r_{eD}^2} + \ln(r_{eD}) - 0.75 \quad (6-96)$$

The computational procedure of using the p_D -function in determining the bottom-hole flowing pressure changing the transient flow period is summarized in the following steps:

Step 1. Calculate the dimensionless time t_D by applying Equation 6-87.

Step 2. Calculate the dimensionless radius r_{eD} from Equation 6-89.

Step 3. Using the calculated values of t_D and r_{eD} , determine the corresponding pressure function p_D from the appropriate table or equation.

Step 4. Solve for the pressure at the desired radius, i.e., r_w , by applying Equation 6-86, or:

$$p(r_w, t) = p_i - \left(\frac{Q_o B_o \mu_o}{0.00708 k h} \right) p_D \quad (6-97)$$

Example 6-12

A well is producing at a constant flow rate of 300 STB/day under unsteady-state flow condition. The reservoir has the following rock and fluid properties (see Example 6-10):

| | | |
|----------------------|------------------|---|
| $B_o = 1.25$ bbl/STB | $\mu_o = 1.5$ cp | $c_t = 12 \times 10^{-6}$ psi ⁻¹ |
| $k = 60$ md | $h = 15$ ft | $p_i = 4000$ psi |
| $\phi = 15\%$ | $r_w = 0.25'$ | |

Assuming an infinite acting reservoir, i.e., $r_{eD} = \infty$, calculate the bottom-hole flowing pressure after one hour of production by using the dimensionless pressure approach.

Solution

Step 1. Calculate the dimensionless time t_D from Equation 6-87.

$$t_D = \frac{0.000264 (60) (1)}{(0.15)(1.5)(12 \times 10^{-6})(0.25)^2} = 93,866.67$$

Step 2. Since $t_D > 100$, use Equation 6-92 to calculate the dimensionless pressure drop function:

$$p_D = 0.5 [\ln(93,866.67) + 0.80907] = 6.1294$$

Step 3. Calculate the bottom-hole pressure after 1 hour by applying Equation 6-97:

$$p(0.25, 1) = 4000 - \left[\frac{(300)(1.25)(1.5)}{0.00708(60)(15)} \right] (6.1294) = 3459 \text{ psi}$$

The above example shows that the solution as given by the p_D -function technique is identical to that of the E_i -function approach. The main difference between the two formulations is that **the p_D -function can be used only to calculate the pressure at radius r when the flow rate Q is constant and known.** In that case, the p_D -function application is essentially restricted to the wellbore radius because the rate is usually known. On the other hand, the E_i -function approach can be used to calculate the pressure at any radius in the reservoir by using the well flow rate Q .

It should be pointed out that, for an infinite-acting reservoir with $t_D > 100$, the p_D -function is related to the E_i -function by the following relation:

$$p_D = 0.5 \left[-E_i \left(\frac{-1}{4t_D} \right) \right] \quad (6-98)$$

The previous example, i.e., Example 6-12, is not a practical problem, but it is essentially designed to show the physical significance of the p_D solution approach. In transient flow testing, we normally record the bottom-hole flowing pressure as a function of time. Therefore, the dimensionless pressure drop technique can be used to determine one or more of the reservoir properties, e.g., k or kh , as discussed later in this chapter.

Radial Flow of Compressible Fluids

Gas viscosity and density vary significantly with pressure and therefore the assumptions of Equation 6-76 are not satisfied for gas systems, i.e., compressible fluids. In order to develop the proper mathematical function for describing the flow of compressible fluids in the reservoir, the following two additional gas equations must be considered:

- Real density equation

$$\rho = \frac{pM}{zRT}$$

- Gas compressibility equation

$$c_g = \frac{1}{p} - \frac{1}{z} \frac{dz}{dp}$$

Combining the above two basic gas equations with that of Equation 6-68 gives:

$$\frac{1}{r} \frac{\partial}{\partial r} \left(r \frac{p}{\mu z} \frac{\partial p}{\partial r} \right) = \frac{\phi \mu c_t}{0.000264 k} \frac{p}{\mu z} \frac{\partial p}{\partial t} \quad (6-99)$$

where t = time, hr

k = permeability, md

c_t = total isothermal compressibility, psi^{-1}

ϕ = porosity

Al-Hussainy, Ramey, and Crawford (1966) linearize the above basic flow equation by introducing the real gas potential $m(p)$ to Equation 6-99. Recall the previously defined $m(p)$ equation:

$$m(p) = \int_0^p \frac{2p}{\mu z} dp \quad (6-100)$$

Differentiating the above relation with respect to p gives:

$$\frac{\partial m(p)}{\partial p} = \frac{2p}{\mu z} \quad (6-101)$$

Obtain the following relationships by applying the chain rule:

$$\frac{\partial m(p)}{\partial r} = \frac{\partial m(p)}{\partial p} \frac{\partial p}{\partial r} \quad (6-102)$$

$$\frac{\partial m(p)}{\partial t} = \frac{\partial m(p)}{\partial p} \frac{\partial p}{\partial t} \quad (6-103)$$

Substituting Equation 6-101 into Equations 6-102 and 6-103 gives:

$$\frac{\partial p}{\partial r} = \frac{\mu z}{2p} \frac{\partial m(p)}{\partial r} \quad (6-104)$$

and

$$\frac{\partial p}{\partial t} = \frac{\mu z}{2p} \frac{\partial m(p)}{\partial t} \quad (6-105)$$

Combining Equations 6-104 and 6-105 with 6-99 yields:

$$\frac{\partial^2 m(p)}{\partial r^2} + \frac{1}{r} \frac{\partial m(p)}{\partial r} = \frac{\phi \mu c_t}{0.000264k} \frac{\partial m(p)}{\partial t} \quad (6-106)$$

Equation 6-106 is the radial diffusivity equation for compressible fluids. This differential equation relates the real gas pseudopressure (real gas potential) to the time t and the radius r . Al-Hussainy, Ramey, and Crawford (1966) pointed out that in gas well testing analysis, the constant-rate solution has more practical applications than that provided by the constant-pressure solution. The authors provided the exact solution to Equation 6-106 that is commonly referred to as the $m(p)$ -solution method. There are also two other solutions that approximate the exact solution. These two approximation methods are called the pressure-squared method and the *pressure-approximation method*. In general, there are three forms of the mathematical solution to the diffusivity equation:

- The $m(p)$ -Solution Method (Exact Solution)
- The Pressure-Squared Method (p^2 -Approximation Method)
- The Pressure Method (p -Approximation Method)

These three methods are presented as follows:

The $m(p)$ -Solution Method (Exact-Solution)

Imposing the constant-rate condition as one of the boundary conditions required to solve Equation 6-106, Al-Hussainy, et al. (1966) proposed the following exact solution to the diffusivity equation:

$$m(p_{wf}) = m(p_i) - 57,895.3 \left(\frac{p_{sc}}{T_{sc}} \right) \left(\frac{Q_g T}{kh} \right) \left[\log \left(\frac{kt}{\phi \mu_i c_{ti} r_w^2} \right) - 3.23 \right] \quad (6-107)$$

where p_{wf} = bottom-hole flowing pressure, psi

p_e = initial reservoir pressure

Q_g = gas flow rate, Mscf/day

t = time, hr

k = permeability, md

p_{sc} = standard pressure, psi

T_{sc} = standard temperature, °R

T = reservoir temperature

r_w = wellbore radius, ft

h = thickness, ft

μ_i = gas viscosity at the initial pressure, cp

c_{ti} = total compressibility coefficient at p_i , psi⁻¹

ϕ = porosity

When $p_{sc} = 14.7$ psia and $T_{sc} = 520^\circ\text{R}$, Equation 6-107 reduces to:

$$m(p_{wf}) = m(p_i) - \left(\frac{1637 Q_g T}{kh} \right) \left[\log \left(\frac{kt}{\phi \mu_i c_{ti} r_w^2} \right) - 3.23 \right] \quad (6-108)$$

Equation 6-108 can be written equivalently in terms of the dimensionless time t_D as:

$$m(p_{wf}) = m(p_i) - \left(\frac{1637 Q_g T}{kh} \right) \left[\log \left(\frac{4t_D}{\gamma} \right) \right] \quad (6-109)$$

The dimensionless time is defined previously by Equation 6-86 as:

$$t_D = \frac{0.000264 kt}{\phi \mu_i c_{ti} r_w^2}$$

The parameter γ is called Euler's constant and given by:

$$\gamma = e^{0.5772} = 1.781 \quad (6-110)$$

The solution to the diffusivity equation as given by Equations 6-108 and 6-109 expresses the bottom-hole real gas pseudopressure as a function of the transient flow time t . The solution as expressed in terms of $m(p)$ is recommended mathematical expression for performing gas-well pressure analysis due to its applicability in all pressure ranges.

The radial gas diffusivity equation can be expressed in a dimensionless form in terms of the dimensionless real gas pseudopressure drop ψ_D . The solution to the dimensionless equation is given by:

$$m(p_{wf}) = m(p_i) - \left(\frac{1422 Q_g T}{kh} \right) \psi_D \quad (6-111)$$

where Q_g = gas flow rate, Mscf/day
 k = permeability, md

The dimensionless pseudopressure drop ψ_D can be determined as a function of t_D by using the appropriate expression of Equations 6-91 through 6-96. When $t_D > 100$, the ψ_D can be calculated by applying Equation 6-82, or:

$$\psi_D = 0.5 [\ln(t_D) + 0.80907] \quad (6-112)$$

Example 6-13

A gas well with a wellbore radius of 0.3 ft is producing at a constant flow rate of 2,000 Mscf/day under transient flow conditions. The initial reservoir pressure (shut-in pressure) is 4,400 psi at 140°F. The formation permeability and thickness are 65 md and 15 ft, respectively. The porosity is recorded as 15%. Example 6-7 documents the properties of the gas as well as values of $m(p)$ as a function of pressures. The table is reproduced below for convenience:

| p | μ_g (cp) | z | m(p), psi ² /cp |
|------|--------------|-------|----------------------------|
| 0 | 0.01270 | 1.000 | 0.000 |
| 400 | 0.01286 | 0.937 | 13.2×10^6 |
| 800 | 0.01390 | 0.882 | 52.0×10^6 |
| 1200 | 0.01530 | 0.832 | 113.1×10^6 |
| 1600 | 0.01680 | 0.794 | 198.0×10^6 |
| 2000 | 0.01840 | 0.770 | 304.0×10^6 |
| 2400 | 0.02010 | 0.763 | 422.0×10^6 |
| 2800 | 0.02170 | 0.775 | 542.4×10^6 |
| 3200 | 0.02340 | 0.797 | 678.0×10^6 |
| 3600 | 0.02500 | 0.827 | 816.0×10^6 |
| 4000 | 0.02660 | 0.860 | 950.0×10^6 |
| 4400 | 0.02831 | 0.896 | 1089.0×10^6 |

Assuming that the initial total isothermal compressibility is 3×10^{-4} psi⁻¹, calculate the bottom-hole flowing pressure after 1.5 hours.

Step 1. Calculate the dimensionless time t_D

$$t_D = \frac{(0.000264)(65)(1.5)}{(0.15)(0.02831)(3 \times 10^{-4})(0.3^2)} = 224,498.6$$

Step 2. Solve for $m(p_{wf})$ by using Equation 6-109

$$\begin{aligned} m(p_{wf}) &= 1089 \times 10^6 - \frac{(1637)(2000)(600)}{(65)(15)} \left[\log \left(\frac{(4)224,498.6}{e^{0.5772}} \right) \right] \\ &= 1077.5 (10^6) \end{aligned}$$

Step 3. From the given PVT data, interpolate using the value of $m(p_{wf})$ to give a corresponding p_{wf} of 4,367 psi.

An identical solution can be obtained by applying the ψ_D approach as shown below:

Step 1. Calculate ψ_D from Equation 6-112

$$\psi_D = 0.5 [\ln (224,498.6) + 0.8090] = 6.565$$

Step 2. Calculate $m(p_{wf})$ by using Equation 6-111

$$m(p_{wf}) = 1089 \times 10^6 - \left(\frac{1422(2000)(600)}{(65)(15)} \right) (6.565) = 1077.5 \times 10^6$$

The Pressure-Squared Approximation Method (p²-method)

The first approximation to the exact solution is to remove the pressure-dependent term (μz) outside the integral that defines $m(p_{wf})$ and $m(p_i)$ to give:

$$m(p_i) - m(p_{wf}) = \frac{2}{\bar{\mu} \bar{z}} \int_{p_{wf}}^{p_i} p dp \quad (6-113)$$

or

$$m(p_i) - m(p_{wf}) = \frac{p_i^2 - p_{wf}^2}{\bar{\mu} \bar{z}} \quad (6-114)$$

The bars over μ and z represent the values of the gas viscosity and deviation factor as evaluated at the average pressure \bar{p} . This average pressure is given by:

$$\bar{p} = \sqrt{\frac{p_i^2 + p_{wf}^2}{2}} \quad (6-115)$$

Combining Equation 6-114 with Equation 6-108, 6-109, or 6-111 gives:

$$p_{wf}^2 = p_i^2 - \left(\frac{1637Q_g T \bar{\mu} \bar{z}}{kh} \right) \left[\log \left(\frac{kt}{\phi \mu_i c_{ti} r_w^2} \right) - 3.23 \right] \quad (6-116)$$

or

$$p_{wf}^2 = p_i^2 - \left(\frac{1637Q_g T \bar{\mu} \bar{z}}{kh} \right) \left[\log \left(\frac{4t_D}{\gamma} \right) \right] \quad (6-117)$$

or, equivalently:

$$p_{wf}^2 = p_i^2 - \left(\frac{1422 Q_g T \bar{\mu} \bar{z}}{kh} \right) \Psi_D \quad (6-118)$$

The above approximation solution forms indicate that the product (μz) is assumed constant at the average pressure \bar{p} . This effectively limits the applicability of the p^2 -method to reservoir pressures < 2000 . It should be pointed out that when the p^2 -method is used to determine p_{wf} it is perhaps sufficient to set $\bar{\mu} \bar{z} = \mu_i z$.

Example 6-14

A gas well is producing at a constant rate of 7,454.2 Mscf/day under transient flow conditions. The following data are available:

$$\begin{array}{llll} k = 50 \text{ md} & h = 10 \text{ ft} & \phi = 20\% & p_i = 1600 \text{ psi} \\ T = 600^\circ\text{R} & r_w = 0.3 \text{ ft} & c_{fi} = 6.25 \times 10^{-4} \text{ psi}^{-1} & \end{array}$$

The gas properties are tabulated below:

| p | $\mu_g, \text{ cp}$ | z | $m(p), \text{ psi}^2/\text{cp}$ |
|------|---------------------|-------|---------------------------------|
| 0 | 0.01270 | 1.000 | 0.000 |
| 400 | 0.01286 | 0.937 | 13.2×10^6 |
| 800 | 0.01390 | 0.882 | 52.0×10^6 |
| 1200 | 0.01530 | 0.832 | 113.1×10^6 |
| 1600 | 0.01680 | 0.794 | 198.0×10^6 |

Calculate the bottom-hole flowing pressure after 4 hours by using:

- The $m(p)$ -method
- The p^2 -method

Solution

a. The $m(p)$ -method

Step 1. Calculate t_D

$$t_D = \frac{0.000264(50)(4)}{(0.2)(0.0168)(6.25 \times 10^{-4})(0.3^2)} = 279,365.1$$

Step 2. Calculate ψ_D :

$$\psi_D = 0.5 [\ln(279365.1) + 0.80907] = 6.6746$$

Step 3. Solve for $m(p_{wf})$ by applying Equation 6-111:

$$m(p_{wf}) = (198 \times 10^6) - \left[\frac{1422 (7454.2) (600)}{(50) (10)} \right] 6.6746 = 113.1 \times 10^6$$

The corresponding value of $p_{wf} = 1200$ psi.

b. The p^2 -method

Step 1. Calculate ψ_D by applying Equation 6-112:

$$\psi_D = 0.5 [\ln(279365.1) + 0.80907] = 6.6477$$

Step 2. Calculate p_{wf}^2 by applying Equation 6-118:

$$p_{wf}^2 = 1600^2 - \left[\frac{(1422) (7454.2) (600) (0.0168) (0.794)}{(50) (10)} \right] \\ \times 6.6477 = 1,427,491$$

$$p_{wf} = 1195 \text{ psi}$$

Step 3. The absolute average error is 0.4%

The Pressure-Approximation Method

The second method of approximation to the exact solution of the radial flow of gases is to treat the gas as a *pseudoliquid*.

Recalling the gas formation volume factor B_g as expressed in bbl/scf is given by:

$$B_g = \left(\frac{P_{sc}}{5.615 T_{sc}} \right) \left(\frac{zT}{p} \right)$$

Solving the above expression for p/z gives:

$$\frac{p}{z} = \left(\frac{T p_{sc}}{5.615 T_{sc}} \right) \left(\frac{1}{B_g} \right)$$

The difference in the real gas pseudopressure is given by:

$$m(p_i) - m(p_{wf}) = \int_{p_{wf}}^{p_i} \frac{2p}{\mu z} dp$$

Combining the above two expressions gives:

$$m(p_i) - m(p_{wf}) = \frac{2T p_{sc}}{5.615 T_{sc}} \int_{p_{wf}}^{p_i} \left(\frac{1}{\mu B_g} \right) dp \quad (6-119)$$

Fetkovich (1973) suggested that at high pressures ($p > 3,000$), $1/\mu B_g$ is nearly constant as shown schematically in Figure 6-22. Imposing Fetkovich's condition on Equation 6-119 and integrating gives:

$$m(p_i) - m(p_{wf}) = \frac{2T p_{sc}}{5.615 T_{sc} \bar{\mu} B_g} (p_i - p_{wf}) \quad (6-120)$$

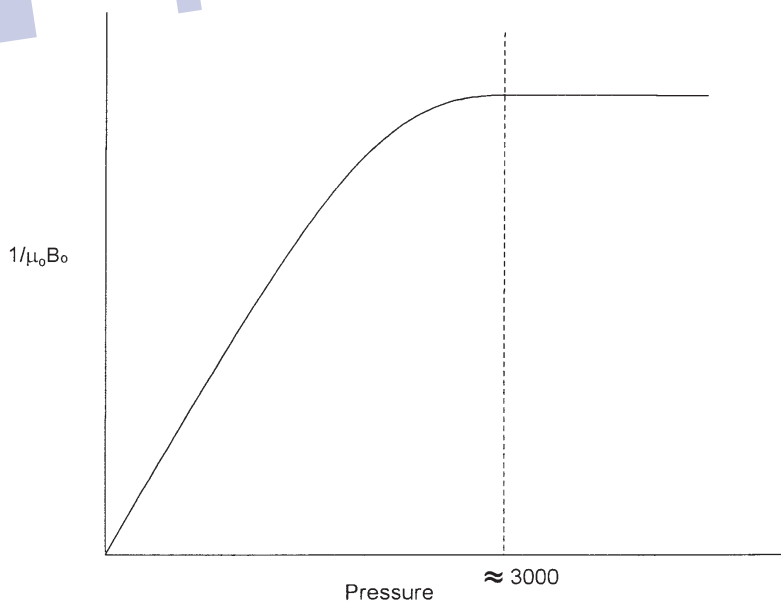


Figure 6-22. $1/\mu_0 B_0$ vs. pressure.

Combining Equation 6-120 with Equation 6-108, 6-109, or 6-111 gives:

$$p_{wf} = p_i - \left(\frac{162.5 \times 10^3 Q_g \bar{\mu} \bar{B}_g}{kh} \right) \left[\log \left(\frac{kt}{\phi \bar{\mu} \bar{c}_i r_w^2} \right) - 3.23 \right] \quad (6-121)$$

or

$$p_{wf} = p_i - \left(\frac{162.5 (10^3) Q_g \bar{\mu} \bar{B}_g}{kh} \right) \left[\log \left(\frac{4t_D}{\gamma} \right) \right] \quad (6-122)$$

or equivalently in terms of dimensionless pressure drop:

$$p_{wf} = p_i - \left(\frac{141.2 (10^3) Q_g \bar{\mu} \bar{B}_g}{kh} \right) p_D \quad (6-123)$$

where Q_g = gas flow rate, Mscf/day
 k = permeability, md
 \bar{B}_g = gas formation volume factor, bbl/scf
 t = time, hr
 p_D = dimensionless pressure drop
 t_D = dimensionless time

It should be noted that the gas properties, i.e., μ , B_g , and c_i , are evaluated at pressure \bar{p} as defined below:

$$\bar{p} = \frac{p_i + p_{wf}}{2} \quad (6-124)$$

Again, this method is only limited to applications above 3,000 psi. When solving for p_{wf} , it might be sufficient to evaluate the gas properties at p_i .

Example 6-15

Resolve Example 6-13 by using the p-approximation method and compare with the exact solution.

Solution

Step 1. Calculate the dimensionless time t_D .

$$t_D = \frac{(0.000264)(65)(1.5)}{(0.15)(0.02831)(3 \times 10^{-4})(0.3^2)} = 224,498.6$$

Step 2. Calculate B_g at p_i .

$$B_g = 0.00504 \frac{(0.896)(600)}{4400} = 0.0006158 \text{ bbl/scf}$$

Step 3. Calculate the dimensionless pressure p_D by applying Equation 6-92.

$$p_D = 0.5[\ln(224,498.6) + 0.80907] = 6.565$$

Step 4. Approximate p_{wf} from Equation 6-123.

$$p_{wf} = 4400 - \left[\frac{141.2 \times 10^3 (2000)(0.02831)(0.0006158)}{(65)(15)} \right] 6.565$$

$$= 4367 \text{ psi}$$

The solution is identical to that of the exact solution.

It should be pointed that Examples 6-10 through 6-15 are designed to illustrate the use of different solution methods. These examples are not practical, however, because in transient flow analysis, the bottom-hole flowing pressure is usually available as a function of time. All the previous methodologies are essentially used to characterize the reservoir by determining the permeability k or the permeability-thickness product (kh).

PSEUDOSTEADY-STATE FLOW

In the unsteady-state flow cases discussed previously, it was assumed that a well is located in a very large reservoir and producing at a constant flow rate. This rate creates a pressure disturbance in the reservoir that travels throughout this infinite-size reservoir. During this transient flow period, reservoir boundaries have no effect on the pressure behavior of the well. Obviously, the time period where this assumption can be imposed is

often very short in length. As soon as the pressure disturbance reaches all drainage boundaries, it ends the transient (unsteady-state) flow regime. A different flow regime begins that is called **pseudosteady (semisteady)-state flow**. It is necessary at this point to impose different boundary conditions on the diffusivity equation and derive an appropriate solution to this flow regime.

Consider Figure 6-23, which shows a well in radial system that is producing at a constant rate for a long enough period that eventually affects the entire drainage area. During this semisteady-state flow, the change in pressure with time becomes the same throughout the drainage area. Section B in Figure 6-23 shows that the pressure distributions become paralleled at successive time periods. Mathematically, this important condition can be expressed as:

$$\left(\frac{\partial p}{\partial t} \right)_r = \text{constant}$$

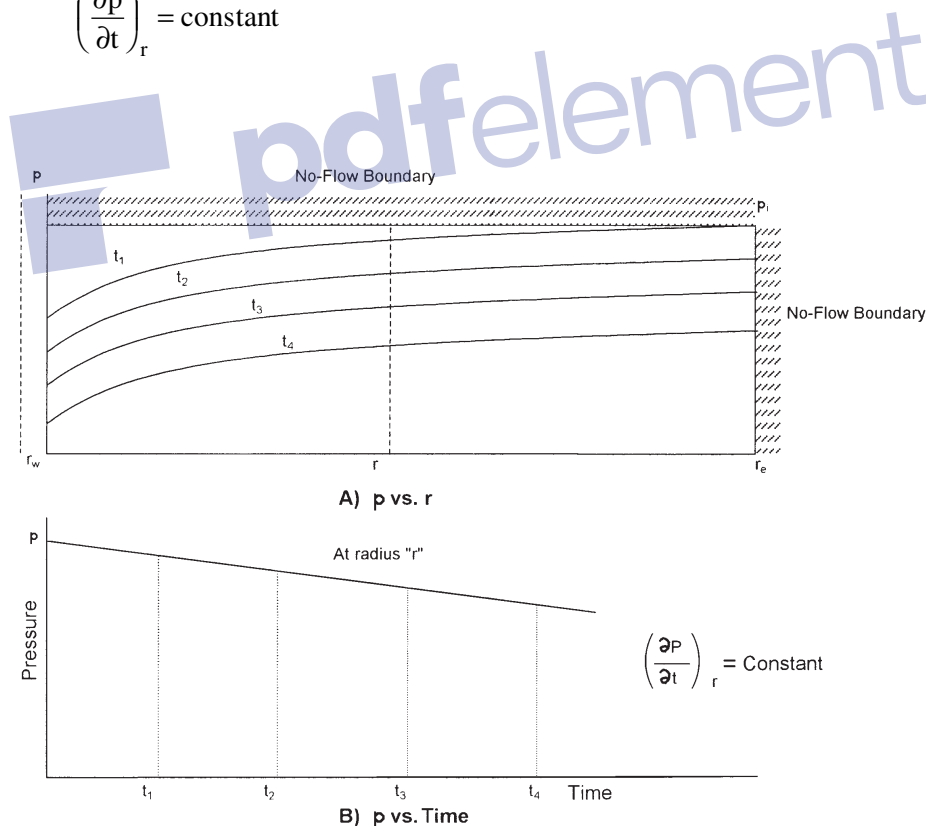


Figure 6-23. Semisteady-state flow regime.

The constant referred to in the above equation can be obtained from a simple material balance using the definition of the compressibility, thus:

$$c = \frac{-1}{V} \frac{dV}{dp}$$

Arranging:

$$cVdp = -dV$$

Differentiating with respect to time t :

$$cV \frac{dp}{dt} = - \frac{dV}{dt} = q$$

or

$$\frac{dp}{dt} = - \frac{q}{cV}$$

Expressing the pressure decline rate dp/dt in the above relation in psi/hr gives:

$$\frac{dp}{dt} = - \frac{q}{24cV} = - \frac{Q_o B_o}{24cV} \quad (6-125)$$

where q = flow rate, bbl/day
 Q_o = flow rate, STB/day
 dp/dt = pressure decline rate, psi/hr
 V = pore volume, bbl

For a radial drainage system, the pore volume is given by:

$$V = \frac{\pi r_c^2 h \phi}{5.615} = \frac{Ah\phi}{5.615} \quad (6-126)$$

where A = drainage area, ft^2

Combining Equation 6-127 with Equation 6-126 gives:

$$\frac{dp}{dt} = -\frac{0.23396q}{c_t \pi r_c^2 h \phi} = \frac{-0.23396q}{c_t Ah \phi} \quad (6-127)$$

Examination of the above expression reveals the following important characteristics of the behavior of the pressure decline rate dp/dt during the semisteady-state flow:

- The reservoir pressure declines at a higher rate with an increase in the fluids production rate
- The reservoir pressure declines at a slower rate for reservoirs with higher total compressibility coefficients
- The reservoir pressure declines at a lower rate for reservoirs with larger pore volumes

Example 6-16

An oil well is producing at a constant oil flow rate of 1,200 STB/day under a semisteady-state flow regime. Well testing data indicate that the pressure is declining at a constant rate of 4.655 psi/hr. The following additional data are available:

$$h = 25 \text{ ft} \quad \phi = 15\% \quad B_o = 1.3 \text{ bbl/STB}$$

$$c_t = 12 \times 10^{-6} \text{ psi}^{-1}$$

Calculate the well drainage area.

Solution

- $q = Q_o B_o$
- $q = (1200)(1.3) = 1560 \text{ bb/day}$
- Apply Equation 6-128 to solve for A.

$$-4.655 = -\frac{0.23396(1560)}{(12 \times 10^{-6})(A)(25)(0.15)}$$

$$A = 1,742,400 \text{ ft}^2$$

or

$$A = 1,742,400 / 43,560 = 40 \text{ acres}$$

Matthews, Brons, and Hazebroek (1954) pointed out that once the reservoir is producing under the *semisteady-state condition*, each well will drain from within its own no-flow boundary independently of the other wells. For this condition to prevail, the pressure decline rate dp/dt must be approximately constant throughout the entire reservoir, otherwise flow would occur across the boundaries causing a readjustment in their positions. Because the pressure at every point in the reservoir is changing at the same rate, it leads to the conclusion that the average reservoir pressure is changing at the same rate. This average reservoir pressure is essentially set equal to the volumetric average reservoir pressure \bar{p}_r . It is the pressure that is used to perform flow calculations during the semisteady state flowing condition. In the above discussion, \bar{p}_r indicates that, in principal, Equation 6-128 can be used to estimate by replacing the pressure decline rate dp/dt with $(p_i - \bar{p}_r)/t$, or:

$$p_i - \bar{p}_r = \frac{0.23396qt}{c_t Ah\phi}$$

or

$$\bar{p}_r = p_i - \frac{0.23396qt}{c_t Ah\phi} \quad (6-128)$$

where t is approximately the elapsed time since the end of the transient flow regime to the time of interest.

It should be noted that when performing material balance calculations, the volumetric average pressure of the entire reservoir is used to calculate the fluid properties. This pressure can be determined from the individual well drainage properties as follows:

$$\bar{p}_r = \frac{\sum_i \bar{p}_r V_i}{\sum_i V_i} \quad (6-129)$$

in which V_i = pore volume of the i th drainage volume

\bar{p}_{ri} = volumetric average pressure within the i th drainage volume.

Figure 6-24 illustrates the concept of the volumetric average pressure. In practice, the V_i 's are difficult to determine and, therefore, it is common to use the flow rate q_i in Equation 6-129.

$$\bar{p}_r = \frac{\sum_i (\bar{p}_{ri} q_i)}{\sum_i q_i} \quad (6-130)$$

The flow rates are measured on a routing basis throughout the lifetime of the field, thus facilitating the calculation of the volumetric average reservoir pressure, \bar{p}_r . Alternatively, the average reservoir pressure can be expressed in terms of the individual well's average drainage pressure decline rates and fluid flow rates by:

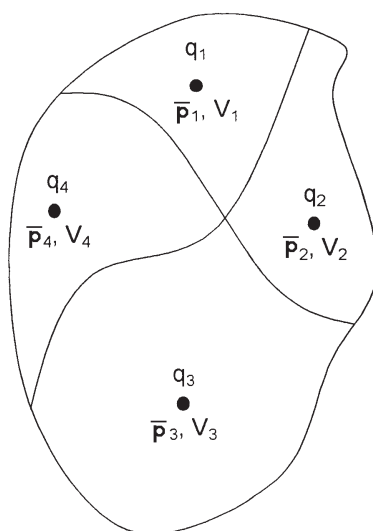


Figure 6-24. Volumetric average reservoir pressure.

$$\bar{p}_r = \frac{\sum_j [(\bar{p}q)_j / (\partial \bar{p} / \partial t)_j]}{\sum_j [q_j / (\partial \bar{p} / \partial t)_j]}$$

However, since the material balance equation is usually applied at regular intervals of 3 to 6 months (i.e., $\Delta t = 3\text{--}6$ months), throughout the life of the field, the average field pressure can be expressed in terms of the incremental net change in underground fluid withdrawal, $\Delta(F)$, as:

$$\bar{p}_r = \frac{\sum_j \frac{\bar{p}_j \Delta(F)_j}{\Delta \bar{p}_j}}{\sum_j \frac{\Delta(F)_j}{\Delta \bar{p}_j}}$$

Where the total underground fluid withdrawals at time t and $t + \Delta t$ are given by:

$$F_t = \int_0^t [Q_o B_o + Q_w B_w + (Q_g - Q_o R_s - Q_w R_{sw}) B_g] dt$$

$$F_{t+\Delta t} = \int_0^{t+\Delta t} [Q_o B_o + Q_w B_w + (Q_g - Q_o R_s - Q_w R_{sw}) B_g] dt$$

with

$$\Delta(F) = F_{t+\Delta t} - F_t$$

where R_s = gas solubility, scf/STB

R_{sw} = gas solubility in the water, scf/STB

B_g = gas formation volume factor, bbl/scf

Q_o = oil flow rate, STB/day

q_o = oil flow rate, bbl/day

Q_w = water flow rate, STB/day

q_w = water flow rate, bbl/day

Q_g = gas flow rate, scf/day

The practical applications of using the pseudosteady-state flow condition to describe the flow behavior of the following two types of fluids are presented below:

- Radial flow of slightly compressible fluids
- Radial flow of compressible fluids

Radial Flow of Slightly Compressible Fluids

The diffusivity equation as expressed by Equation 6-73 for the transient flow regime is:

$$\frac{\partial^2 p}{\partial r^2} + \frac{1}{r} \frac{\partial p}{\partial r} = \left(\frac{\phi \mu c_t}{0.000264k} \right) \frac{\partial p}{\partial t}$$

For the semisteady-state flow, the term $(\partial p / \partial t)$ is constant and is expressed by Equation 6-128. Substituting Equation 6-128 into the diffusivity equation gives:

$$\frac{\partial^2 p}{\partial r^2} + \frac{1}{r} \frac{\partial p}{\partial r} = \left(\frac{\phi \mu c_t}{0.000264k} \right) \left(\frac{-0.23396q}{c_t A h \phi} \right)$$

or

$$\frac{\partial^2 p}{\partial r^2} + \frac{1}{r} \frac{\partial p}{\partial r} = \frac{-887.22 q \mu}{A h k} \quad (6-131)$$

Equation 6-132 can be expressed as:

$$\frac{1}{r} \frac{\partial}{\partial r} \left(r \frac{\partial p}{\partial r} \right) = - \frac{887.22 q \mu}{(\pi r_e^2) h k}$$

Integrating the above equation gives:

$$r \frac{\partial p}{\partial r} = - \frac{887.22 q \mu}{(\pi r_e^2) h k} \left(\frac{r^2}{2} \right) + c_1$$

where c_1 is the constant of the integration and can be evaluated by imposing the outer no-flow boundary condition [i.e., $(\partial p / \partial r)_{r_e} = 0$] on the above relation to give:

$$c_1 = \frac{141.2 q \mu}{\pi h k}$$

Combining the above two expressions gives:

$$\frac{\partial p}{\partial r} = \frac{141.2 q \mu}{hk} \left(\frac{1}{r} - \frac{r}{r_e^2} \right)$$

Integrating again:

$$\int_{p_{wf}}^{p_i} dp = \frac{141.2 q \mu}{hk} \int_{r_w}^{r_e} \left(\frac{1}{r} - \frac{r}{r_e^2} \right) dr$$

Performing the above integration and assuming (r_w^2/r_e^2) is negligible gives:

$$(p_i - p_{wf}) = \frac{141.2 q \mu}{kh} \left[\ln \left(\frac{r_e}{r_w} \right) - \frac{1}{2} \right] \quad (6-132)$$

A more appropriate form of the above is to solve for the flow rate, to give:

$$Q = \frac{0.00708 kh (p_i - p_{wf})}{\mu B \left[\ln \left(\frac{r_e}{r_w} \right) - 0.5 \right]} \quad (6-133)$$

where Q = flow rate, STB/day

B = formation volume factor, bbl/STB

k = permeability, md

The volumetric average reservoir pressure \bar{p}_r is commonly used in calculating the liquid flow rate under the semisteady-state flowing condition. Introducing the \bar{p}_r into Equation 6-134 gives:

$$Q = \frac{0.00708 kh (\bar{p}_r - p_{wf})}{\mu B \left[\ln \left(\frac{r_e}{r_w} \right) - 0.75 \right]} \quad (6-134)$$

Note that:

$$\ln\left(\frac{0.471 r_e}{r_w}\right) = \ln\left(\frac{r_e}{r_w}\right) - 0.75$$

The above observation suggests that the volumetric average pressure \bar{p}_r occurs at about 47% of the drainage radius during the semisteady-state condition.

It is interesting to notice that the dimensionless pressure p_D solution to the diffusivity equation can be used to derive Equation 6-135. The p_D function for a bounded reservoir was given previously by Equation 6-96 for a bounded system as:

$$p_D = \frac{2t_D}{r_{eD}^2} + \ln(r_{eD}) - 0.75$$

where the above three dimensionless parameters are given by Equations 6-86 through 6-88 as:

$$p_D = \frac{(p_i - p_{wf})}{0.00708 k h} \frac{Q B \mu}{Q B \mu}$$

$$t_D = \frac{0.000264 k t}{\phi \mu c_t r_w^2}$$

$$r_{eD} = \frac{r_e}{r_w}$$

Combining the above four relationships gives:

$$p_{wf} = p_i - \frac{Q B \mu}{0.00708 k h} \left[\frac{0.0005274 k t}{\phi \mu c_t r_e^2} + \ln\left(\frac{r_e}{r_w}\right) - 0.75 \right]$$

Solving Equation 6-129 for the time t gives:

$$t = \frac{c_t A h \phi (p_i - \bar{p}_r)}{0.23396 Q B} = \frac{c_t (\pi r_e^2) h \phi (p_i - \bar{p}_r)}{0.23396 Q B}$$

Combining the above two equations and solving for the flow rate Q yields:

$$Q = \frac{0.00708 k h (\bar{p}_r - p_{wf})}{\mu B \left[\ln \left(\frac{r_e}{r_w} \right) - 0.75 \right]}$$

It should be pointed out that the pseudosteady-state flow occurs regardless of the geometry of the reservoir. Irregular geometries also reach this state when they have been produced long enough for the entire drainage area to be affected.

Rather than developing a separate equation for each geometry, Ramey and Cobb (1971) introduced a correction factor that is called the **shape factor**, C_A , which is designed to account for the deviation of the drainage area from the ideal circular form. The shape factor, as listed in Table 6-4, accounts also for the location of the well within the drainage area. Introducing C_A into Equation 6-132 and performing the solution procedure gives the following two solutions:

- In terms of the volumetric average pressure \bar{p}_r :

$$p_{wf} = \bar{p}_r - \frac{162.6 Q B \mu}{k h} \log \left[\frac{4A}{1.781 C_A r_w^2} \right] \quad (6-135)$$

- In terms of the initial reservoir pressure p_i :

The changes in the average reservoir pressure as a function of time and initial reservoir pressure p_i is given by Equation 6-129; as:

$$\bar{p}_r = p_i - \frac{0.23396 q t}{c_t A h \phi}$$

Combining the above equation with Equation 6-136 gives:

$$p_{wf} = \left[p_i - \frac{0.23396 Q B t}{A h \phi c_t} \right] - \frac{162.6 Q B \mu}{k h} \log \left[\frac{4A}{1.781 C_A r_w^2} \right] \quad (6-136)$$

where k = permeability, md
 A = drainage area, ft²
 C_A = shape factor
 Q = flow rate, STB/day
 t = time, hr
 c_t = total compressibility coefficient, psi⁻¹

Equation 6-136 can be arranged to solve for Q to give:

$$Q = \frac{k h (\bar{p}_r - p_{wf})}{162.6 B \mu \log \left[\frac{4A}{1.781 C_A r_w^2} \right]} \quad (6-137)$$

It should be noted that if Equation 6-138 is applied to a circular reservoir of a radius r_e , then:

$$A = \pi r_e^2$$

and the shape factor for a circular drainage area as given in Table 6-3 is:

$$C_A = 31.62$$




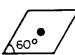



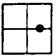
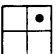
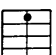
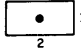


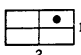
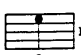
Substituting in Equation 6-138, it reduces to:

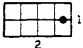
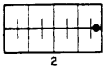
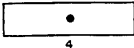

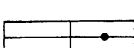
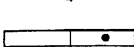

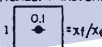
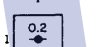
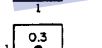
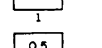
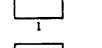
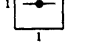


$$p_{wf} = \bar{p}_r - \left(\frac{Q B \mu}{0.00708 k h} \right) \left[\ln \left(\frac{r_e}{r_w} \right) - 0.75 \right]$$

The above equation is identical to that of Equation 6-135.

(text continued on page 427)

Table 6-4
Shape Factors for Various Single-Well Drainage Areas
(After Earlougher, R., Advances in Well Test Analysis, permission to publish by the SPE, copyright SPE, 1977)

| In Bounded Reservoirs | C_A | $\ln C_A$ | $\frac{1}{2} \ln \left(\frac{2.2458}{C_A} \right)$ | Exact for $t_{DA} >$ | Less Than 1% Error For $t_{DA} >$ | Use Infinite System Solution with Less Than 1% Error for $t_{DA} <$ |
|---|---------|-----------|---|----------------------|-----------------------------------|---|
|  | 31.62 | 3.4538 | -1.3224 | 0.1 | 0.06 | 0.10 |
|  | 31.6 | 3.4532 | -1.3220 | 0.1 | 0.06 | 0.10 |
|  | 27.6 | 3.3178 | -1.2544 | 0.2 | 0.07 | 0.09 |
|  | 27.1 | 3.2995 | -1.2452 | 0.2 | 0.07 | 0.09 |
|  | 21.9 | 3.0865 | -1.1387 | 0.4 | 0.12 | 0.08 |
|  | 0.098 | -2.3227 | +1.5659 | 0.9 | 0.60 | 0.015 |
|  | 30.8828 | 3.4302 | -1.3106 | 0.1 | 0.05 | 0.09 |
|  | 12.9851 | 2.5638 | -0.8774 | 0.7 | 0.25 | 0.03 |
|  | 4.5132 | 1.5070 | -0.3490 | 0.6 | 0.30 | 0.025 |
|  | 3.3351 | 1.2045 | -0.1977 | 0.7 | 0.25 | 0.01 |
|  | 21.8369 | 3.0836 | -1.1373 | 0.3 | 0.15 | 0.025 |
|  | 10.8374 | 2.3830 | -0.7870 | 0.4 | 0.15 | 0.025 |
|  | 4.5141 | 1.5072 | -0.3491 | 1.5 | 0.50 | 0.06 |
|  | 2.0769 | 0.7309 | -0.0391 | 1.7 | 0.50 | 0.02 |
|  | 3.1573 | 1.1497 | -0.1703 | 0.4 | 0.15 | 0.005 |

| In Bounded Reservoirs | C_A | $\ln C_A$ | $\frac{1}{2} \ln \left(\frac{2.2458}{C_A} \right)$ | Exact for $t_{DA} >$ | Less Than 1% Error For $t_{DA} >$ | Use Infinite System Solution with Less Than 1% Error for $t_{DA} <$ |
|---|--------|-----------|---|----------------------|-----------------------------------|---|
|  | 0.5813 | -0.5425 | +0.6758 | 2.0 | 0.60 | 0.02 |
|  | 0.1109 | -2.1991 | +1.5041 | 3.0 | 0.60 | 0.005 |
|  | 5.3790 | 1.6825 | -0.4367 | 0.8 | 0.30 | 0.01 |
|  | 2.6896 | 0.9894 | -0.0902 | 0.8 | 0.30 | 0.01 |
|  | 0.2318 | -1.4619 | +1.1355 | 4.0 | 2.00 | 0.03 |
|  | 0.1155 | -2.1585 | +1.4838 | 4.0 | 2.00 | 0.01 |
|  | 2.3606 | 0.8589 | -0.0249 | 1.0 | 0.40 | 0.025 |
| <i>IN VERTICALLY FRACTURED RESERVOIRS</i> Use $(x_e/x_f)^2$ in place of A/r_w^2 for fractured systems | | | | | | |
|  | 2.6541 | 0.9761 | -0.0835 | 0.175 | 0.08 | cannot use |
|  | 2.0348 | 0.7104 | +0.0493 | 0.175 | 0.09 | cannot use |
|  | 1.9986 | 0.6924 | +0.0583 | 0.175 | 0.09 | cannot use |
|  | 1.6620 | 0.5080 | +0.1505 | 0.175 | 0.09 | cannot use |
|  | 1.3127 | 0.2721 | +0.2685 | 0.175 | 0.09 | cannot use |
|  | 0.7887 | -0.2374 | +0.5232 | 0.175 | 0.09 | cannot use |
| <i>IN WATER-DRIVE RESERVOIRS</i> | | | | | | |
|  | 19.1 | 2.95 | -1.07 | — | — | — |
| <i>IN RESERVOIRS OF UNKNOWN PRODUCTION CHARACTER</i> | | | | | | |
|  | 25.0 | 3.22 | -1.20 | — | — | — |

(text continued from page 424)

Example 6-17

An oil well is developed on the center of a 40-acre square drilling pattern. The well is producing at a constant flow rate of 800 STB/day under a semisteady-state condition. The reservoir has the following properties:

$$\begin{array}{lll} \phi = 15\% & h = 30 \text{ ft} & k = 200 \text{ md} \\ \mu = 1.5 \text{ cp} & B_o = 1.2 \text{ bbl/STB} & c_t = 25 \times 10^{-6} \text{ psi}^{-1} \\ p_i = 4500 \text{ psi} & r_w = 0.25 \text{ ft} & A = 40 \text{ acres} \end{array}$$

- Calculate and plot the bottom-hole flowing pressure as a function of time.
- Based on the plot, calculate the pressure decline rate. What is the decline in the average reservoir pressure from $t = 10$ to $t = 200$ hr?

Solution

a. p_{wf} calculations:

Step 1. From Table 6-3, determine C_A :

$$C_A = 30.8828$$

Step 2. Convert the area A from acres to ft^2 :

$$A = (40) (43,560) = 1,742,400 \text{ ft}^2$$

Step 3. Apply Equation 6-137:

$$P_{wf} = 4500 - 1.719 t - 58.536 \log (2,027,436)$$

or

$$p_{wf} = 4493.69 - 1.719 t$$

Step 4. Calculate p_{wf} at different assumed times.

| $t, \text{ hr}$ | $P_{wf} = 44369 - 1.719 t$ |
|-----------------|----------------------------|
| 10 | 4476.50 |
| 20 | 4459.31 |
| 50 | 4407.74 |
| 100 | 4321.79 |
| 200 | 4149.89 |

Step 5. Present the results of Step 4 in a graphical form as shown in Figure 6-25.

- b. It is obvious from Figure 6-25 and the above calculation that the bottom-hole flowing pressure is declining at a rate of 1.719 psi/hr, or:

$$\frac{dp}{dt} = -1.719 \text{ psi/hr}$$

The significance of this example is that the rate of pressure decline during the pseudosteady state is the same throughout the drainage area. This means that the *average reservoir pressure*, p_r , is declining at the same rate of 1.719 psi, therefore the change in p_r from 10 to 200 hours is:

$$\Delta \bar{p}_r = (1.719)(200 - 10) = 326.6 \text{ psi}$$

Example 6-18

An oil well is producing under a constant bottom-hole flowing pressure of 1,500 psi. The current average reservoir pressure p_r is 3,200 psi.

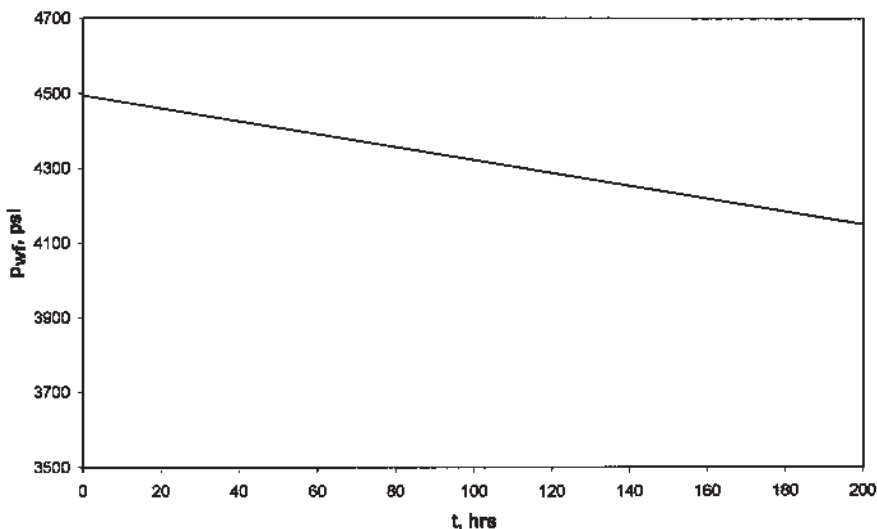


Figure 6-25. Bottom-hole flowing pressure as a function of time.

The well is developed in the center of a 40-acre square drilling pattern. Given the following additional information:

$$\begin{array}{lll} \phi = 16\% & h = 15 \text{ ft} & k = 50 \text{ md} \\ \mu = 26 \text{ cp} & B_o = 1.15 \text{ bbl/STB} & c_t = 10 \times 10^{-6} \text{ psi}^{-1} \\ r_w = 0.25 \text{ ft} & & \end{array}$$

calculate the flow rate.

Solution

Because the volumetric average pressure is given, solve for the flow rate by applying Equation 6-138.

$$\begin{aligned} Q &= \frac{(50)(15)(3200-1500)}{(162.6)(1.15)(2.6) \log \left[\frac{(4)(40)(43,560)}{1.781(30.8828)(0.25^2)} \right]} \\ &= 416 \text{ STB/day} \end{aligned}$$

Radial Flow of Compressible Fluids (Gases)

The radial diffusivity equation as expressed by Equation 6-106 was developed to study the performance of compressible fluid under unsteady-state conditions. The equation has the following form:

$$\frac{\partial^2 m(p)}{\partial r^2} + \frac{1}{r} \frac{\partial m(p)}{\partial r} = \frac{\phi \mu c_t}{0.000264 k} \frac{\partial m(p)}{\partial t}$$

For the semisteady-state flow, the rate of change of the real gas pseudopressure with respect to time is constant, i.e.,

$$\frac{\partial m(p)}{\partial t} = \text{constant}$$

Using the same technique identical to that described previously for liquids gives the following exact solution to the diffusivity equation:

$$Q_g = \frac{kh[m(\bar{p}_r) - m(p_{wf})]}{1422 T \left[\ln \left(\frac{r_e}{r_w} \right) - 0.75 \right]} \quad (6-138)$$

where Q_g = gas flow rate, Mscf/day

T = temperature, °R

k = permeability, md

Two approximations to the above solution are widely used. These approximations are:

- Pressure-squared approximation
- Pressure-approximation

Pressure-Squared Approximation Method

As outlined previously, the method provides us with compatible results to that of the exact solution approach when $p < 2,000$. The solution has the following familiar form:

$$Q_g = \frac{kh(\bar{p}_r^2 - p_{wf}^2)}{1422 T \bar{\mu} \bar{z} \left(\ln \frac{r_e}{r_w} - 0.75 \right)} \quad (6-139)$$

The gas properties \bar{z} and $\bar{\mu}$ are evaluated at:

$$\bar{p} = \sqrt{\frac{(\bar{p}_r)^2 + p_{wf}^2}{2}}$$

Pressure-Approximation Method

This approximation method is applicable at $p > 3,000$ psi and has the following mathematical form:

$$Q_g = \frac{kh(\bar{p}_r - p_{wf})}{1422 \bar{\mu} \bar{B}_g \left(\ln \frac{r_e}{r_w} - 0.75 \right)} \quad (6-140)$$

with the gas properties evaluated at:

$$\bar{p} = \frac{\bar{p}_r + p_{wf}}{2}$$

where Q_g = gas flow rate, Mscf/day

k = permeability, md

\bar{B}_g = gas formation volume factor at average pressure, bbl/scf

The gas formation volume factor is given by the following expression:

$$\bar{B}_g = 0.00504 \frac{\bar{z} T}{\bar{p}}$$

In deriving the flow equations, the following two main assumptions were made:

- Uniform permeability throughout the drainage area
- Laminar (viscous) flow

Before using any of the previous mathematical solutions to the flow equations, the solution must be modified to account for the possible deviation from the above two assumptions. Introducing the following two correction factors into the solution of the flow equation can eliminate the above two assumptions:

- Skin factor
- Turbulent flow factor

Skin Factor

It is not unusual for materials such as mud filtrate, cement slurry, or clay particles to enter the formation during drilling, completion, or workover operations and reduce the permeability around the wellbore. This effect is commonly referred to as a *wellbore damage* and the region of altered permeability is called the *skin zone*. This zone can extend from a few inches to several feet from the wellbore. Many other wells are stimulated by acidizing or fracturing, which in effect increase the permeability near the wellbore. Thus, the permeability near the wellbore is always different from the permeability away from the well where the formation has not been affected by drilling or stimulation. A schematic illustration of the skin zone is shown in Figure 6-26.

Those factors that cause damage to the formation can produce additional localized pressure drop during flow. This additional pressure drop is commonly referred to as Δp_{skin} . On the other hand, well stimulation techniques will normally enhance the properties of the formation and increase the permeability around the wellbore, so that a decrease in pressure

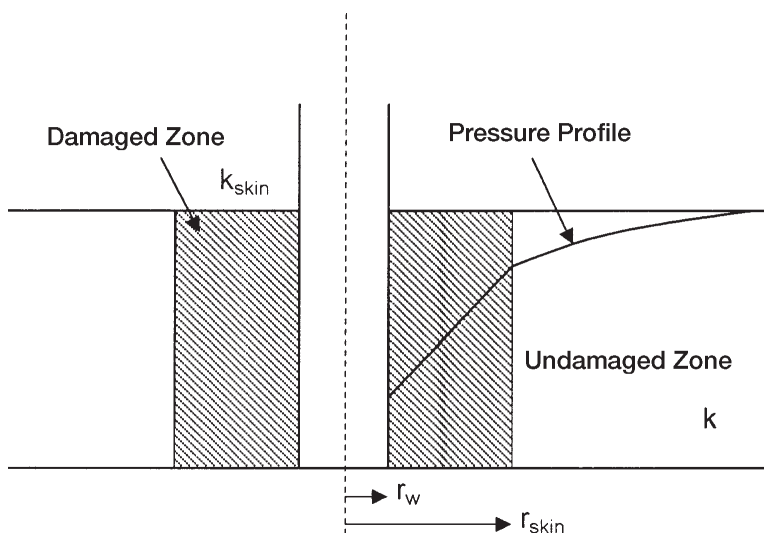


Figure 6-26. Near wellbore skin effect.

drop is observed. The resulting effect of altering the permeability around the well bore is called the *skin effect*.

Figure 6-27 compares the differences in the skin zone pressure drop for three possible outcomes:

- First Outcome:
 $\Delta p_{skin} > 0$, indicates an additional pressure drop due to wellbore damage, i.e., $k_{skin} < k$.
- Second Outcome:
 $\Delta p_{skin} < 0$, indicates less pressure drop due to wellbore improvement, i.e., $k_{skin} > k$.
- Third Outcome:
 $\Delta p_{skin} = 0$, indicates no changes in the wellbore condition, i.e., $k_{skin} = k$.

Hawkins (1956) suggested that the permeability in the skin zone, i.e., k_{skin} , is uniform and the pressure drop across the zone can be approximated by Darcy's equation. Hawkins proposed the following approach:

$$\Delta p_{skin} = \left[\Delta p \text{ in skin zone} \right]_{\text{due to } k_{skin}} - \left[\Delta p \text{ in the skin zone} \right]_{\text{due to } k}$$

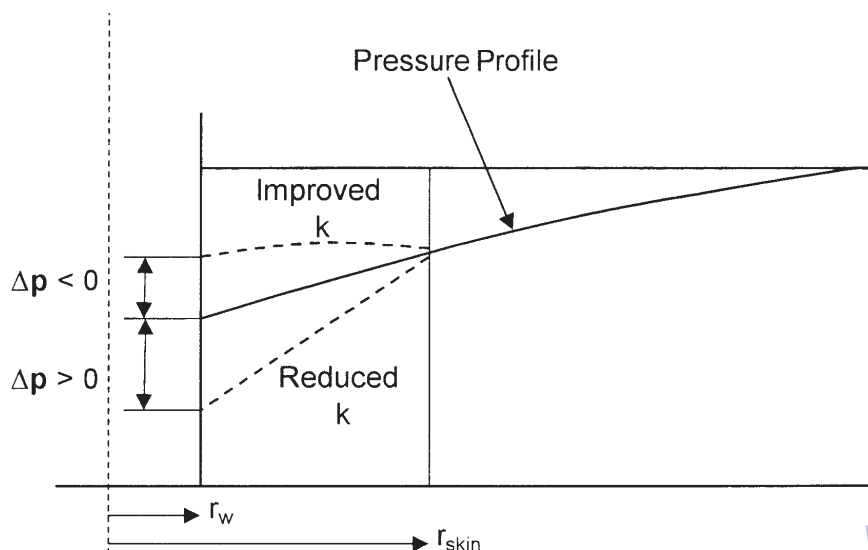


Figure 6-27. Representation of positive and negative skin effects.

Applying Darcy's equation gives:

$$\Delta p_{\text{skin}} = \left[\frac{Q_o B_o \mu_o}{0.00708 h k_{\text{skin}}} \right] \ln \left(\frac{r_{\text{skin}}}{r_w} \right) - \left[\frac{Q_o B_o \mu_o}{0.00708 h k} \right] \ln \left(\frac{r_{\text{skin}}}{r_w} \right)$$

or

$$\Delta p_{\text{skin}} = \left(\frac{Q_o B_o \mu_o}{0.00708 kh} \right) \left[\frac{k}{k_{\text{skin}}} - 1 \right] \ln \left(\frac{r_{\text{skin}}}{r_w} \right)$$

where k = permeability of the formation, md

k_{skin} = permeability of the skin zone, md

The above expression for determining the additional pressure drop in the skin zone is commonly expressed in the following form:

$$\Delta p_{\text{skin}} = \left[\frac{Q_o B_o \mu_o}{0.00708 kh} \right] s = 141.2 \left[\frac{Q_o B_o \mu_o}{kh} \right] s \quad (6-141)$$

where s is called the skin factor and defined as:

$$s = \left[\frac{k}{k_{\text{skin}}} - 1 \right] \ln \left(\frac{r_{\text{skin}}}{r_w} \right) \quad (6-142)$$

Equation 6-143 provides some insight into the physical significance of the sign of the skin factor. There are only three possible outcomes in evaluating the skin factor s :

- **Positive Skin Factor, $s > 0$**

When a damaged zone near the wellbore exists, k_{skin} is less than k and hence s is a positive number. The magnitude of the skin factor increases as k_{skin} decreases and as the depth of the damage r_{skin} increases.

- **Negative Skin Factor, $s < 0$**

When the permeability around the well k_{skin} is higher than that of the formation k , a negative skin factor exists. This negative factor indicates an improved wellbore condition.

- **Zero Skin Factor, $s = 0$**

Zero skin factor occurs when no alternation in the permeability around the wellbore is observed, i.e., $k_{\text{skin}} = k$.

Equation 6-143 indicates that a negative skin factor will result in a negative value of Δp_{skin} . This implies that a stimulated well will require less pressure drawdown to produce at rate q than an equivalent well with uniform permeability.

The proposed modification of the previous flow equation is based on the concept that the actual total pressure drawdown will increase or decrease by an amount of Δp_{skin} . Assuming that $(\Delta p)_{\text{ideal}}$ represents the pressure drawdown for a drainage area with a uniform permeability k , then:

$$(\Delta p)_{\text{actual}} = (\Delta p)_{\text{ideal}} + (\Delta p)_{\text{skin}}$$

or

$$(p_i - p_{wf})_{\text{actual}} = (p_i - p_{wf})_{\text{ideal}} + \Delta p_{\text{skin}} \quad (6-143)$$

The above concept as expressed by Equation 6-144 can be applied to all the previous flow regimes to account for the skin zone around the wellbore as follows:

Steady-State Radial Flow

Substituting Equations 6-27 and 6-142 into Equation 6-144 gives:

$$(p_i - p_{wf})_{\text{actual}} = \left[\frac{Q_o B_o \mu_o}{0.00708 kh} \right] \ln \left(\frac{r_e}{r_w} \right) + \left[\frac{Q_o B_o \mu_o}{0.00708 kh} \right] s$$

or

$$Q_o = \frac{0.00708 kh (p_i - p_{wf})}{\mu_o B_o \left[\ln \frac{r_e}{r_w} + s \right]} \quad (6-144)$$

where Q_o = oil flow rate, STB/day

k = permeability, md

h = thickness, ft

s = skin factor

B_o = oil formation volume factor, bbl/STB

μ_o = oil viscosity, cp

p_i = initial reservoir pressure, psi

p_{wf} = bottom hole flowing pressure, psi

Unsteady-State Radial Flow

• For Slightly Compressible Fluids:

Combining Equations 6-83 and 6-142 with that of Equation 6-144 yields:

$$p_i - p_{wf} = 162.6 \left(\frac{Q_o B_o \mu_o}{kh} \right) \left[\log \frac{kt}{\phi \mu c_t r_w^2} - 3.23 \right] + 141.2 \left(\frac{Q_o B_o \mu_o}{kh} \right) s$$

or

$$p_i - p_{wf} = 162.6 \left(\frac{Q_o B_o \mu_o}{kh} \right) \left[\log \frac{kt}{\phi \mu c_t r_w^2} - 3.23 + 0.87s \right] \quad (6-145)$$

• **For Compressible Fluids:**

A similar approach to that of the above gives:

$$m(p_{wf}) = m(p_i) - \frac{1637 Q_g T}{kh} \left[\log \frac{kt}{\phi \mu c_{ti} r_w^2} - 3.23 + 0.87s \right] \quad (6-146)$$

and, in terms of the pressure-squared approach, gives:

$$p_{wf}^2 = p_i^2 - \frac{1637 Q_g T \bar{\mu}}{kh} \left[\log \frac{kt}{\phi \mu_i c_{ti} r_w^2} - 3.23 + 0.87s \right] \quad (6-147)$$

Pseudosteady-State Flow

• **For Slightly Compressible Fluids:**

Introducing the skin factor into Equation 6-135 gives:

$$Q_o = \frac{0.00708 kh (\bar{p}_r - p_{wf})}{\mu_o B_o \left[\ln \left(\frac{r_c}{r_w} \right) - 0.75 + s \right]} \quad (6-148)$$

• **For Compressible Fluids:**

$$Q_g = \frac{kh [m(\bar{p}_r) - m(P_{wf})]}{1422 T \left[\ln \left(\frac{r_c}{r_w} \right) - 0.75 + s \right]} \quad (6-149)$$

or, in terms of the pressure-squared approximation, gives:

$$Q_g = \frac{kh (p_r^2 - p_{wf}^2)}{1422 T \bar{\mu} \bar{z} \left[\ln \left(\frac{r_c}{r_w} \right) - 0.75 + s \right]} \quad (6-150)$$

where Q_g = gas flow rate, Mscf/day
 k = permeability, md
 T = temperature, °R

$$\begin{aligned}(\bar{\mu}_g) &= \text{gas viscosity at average pressure } \bar{p}, \text{ cp} \\ \bar{z}_g &= \text{gas compressibility factor at average pressure } \bar{p}\end{aligned}$$

Example 6-19

Calculate the skin factor resulting from the invasion of the drilling fluid to a radius of 2 feet. The permeability of the skin zone is estimated at 20 md as compared with the unaffected formation permeability of 60 md. The wellbore radius is 0.25 ft.

Solution

Apply Equation 6-143 to calculate the skin factor:

$$s = \left[\frac{60}{20} - 1 \right] \ln \left(\frac{2}{0.25} \right) = 4.16$$

Matthews and Russell (1967) proposed an alternative treatment to the skin effect by introducing the **effective or apparent wellbore radius** r_{wa} that accounts for the pressure drop in the skin. They define r_{wa} by the following equation:

$$r_{wa} = r_w e^{-s} \quad (6-151)$$

All of the ideal radial flow equations can be also modified for the skin by simply replacing wellbore radius r_w with that of the apparent wellbore radius r_{wa} . For example, Equation 6-146 can be equivalently expressed as:

$$p_i - p_{wf} = 162.6 \left(\frac{Q_o B_o \mu_o}{kh} \right) \left[\log \frac{kt}{\phi \mu_o c_t r_{wa}^2} - 3.23 \right] \quad (6-152)$$

Turbulent Flow Factor

All of the mathematical formulations presented so far are based on the assumption that laminar flow conditions are observed during flow. During radial flow, the flow velocity increases as the wellbore is approached. This increase in the velocity might cause the development of a turbulent flow around the wellbore. If turbulent flow does exist, it is most likely to occur with gases and causes an additional pressure drop similar to that caused by

the skin effect. The term *non-Darcy flow* has been adopted by the industry to describe the additional pressure drop due to the turbulent (non-Darcy) flow.

Referring to the additional real gas pseudopressure drop due to non-Darcy flow as $\Delta\psi$ non-Darcy, the total (actual) drop is given by:

$$(\Delta\psi)_{\text{actual}} = (\Delta\psi)_{\text{ideal}} + (\Delta\psi)_{\text{skin}} + (\Delta\psi)_{\text{non-Darcy}}$$

Wattenburger and Ramey (1968) proposed the following expression for calculating $(\Delta\psi)_{\text{non-Darcy}}$:

$$(\Delta\psi)_{\text{non-Darcy}} = 3.161 \times 10^{-12} \left[\frac{\beta T \gamma_g}{\mu_{\text{gw}} h^2 r_w} \right] Q_g^2 \quad (6-153)$$

The above equation can be expressed in a more convenient form as:

$$(\Delta\psi)_{\text{non-Darcy}} = F Q_g^2 \quad (6-154)$$

where F is called the *non-Darcy flow coefficient* and is given by:

$$F = 3.161 \times 10^{-12} \left[\frac{\beta T \gamma_g}{\mu_{\text{gw}} h^2 r_w} \right] \quad (6-155)$$

where Q_g = gas flow rate, Mscf/day

μ_{gw} = gas viscosity as evaluated at p_{wf} , cp

γ_g = gas specific gravity

h = thickness, ft

F = non-Darcy flow coefficient, $\text{psi}^2/\text{cp}/(\text{Mscf}/\text{day})^2$

β = turbulence parameter

Jones (1987) proposed a mathematical expression for estimating the turbulence parameter β as:

$$\beta = 1.88 (10^{-10}) (k)^{-1.47} (\phi)^{-0.53} \quad (6-156)$$

where k = permeability, md

ϕ = porosity, fraction

The term $F Q_g^2$ can be included in all the compressible gas flow equations in the same way as the skin factor. This non-Darcy term is interpreted as being a *rate-dependent skin*. The modification of the gas flow equations to account for the turbulent flow condition is given below:

Unsteady-State Radial Flow

The gas flow equation for an unsteady-state flow is given by Equation 6-147 and can be modified to include the additional drop in the real gas potential as:

$$m(p_i) - m(p_{wf}) = \left(\frac{1637 Q_g T}{kh} \right) \left[\log \frac{kt}{\phi \mu_i c_{ti} r_w^2} - 3.23 + 0.87s \right] + FQ_g^2 \quad (6-157)$$

Equation 6-158 is commonly written in a more convenient form as:

$$m(p_i) - m(p_{wf}) = \left(\frac{1637 Q_g T}{kh} \right) \times \left[\log \frac{kt}{\phi \mu_i c_{ti} r_w^2} - 3.23 + 0.87s + 0.87 DQ_g \right] \quad (6-158)$$

where the term DQ_g is interpreted as the rate dependent skin factor. The coefficient D is called the **inertial** or **turbulent flow factor** and given by:

$$D = \frac{Fkh}{1422T} \quad (6-159)$$

The true skin factor s , which reflects the formation damage or stimulation, is usually combined with the non-Darcy rate dependent skin and labeled as the **apparent** or **total skin factor**:

$$s' = s + DQ_g \quad (6-160)$$

or

$$m(p_i) - m(p_{wf}) = \left[\frac{1637 Q_g T}{kh} \right] \times \left[\log \frac{kt}{\phi \mu_i c_{ti} r_w^2} - 3.23 + 0.87s' \right] \quad (6-161)$$

Equation 6-162 can be expressed in the pressure-squared approximation form as:

$$p_i^2 - p_{wf}^2 = \left[\frac{1637 Q_g T \bar{z} \bar{\mu}}{kh} \right] \left[\log \frac{kt}{\phi \mu_i c_{ti} r_w^2} - 3.23 + 0.87s' \right] \quad (6-162)$$

where Q_g = gas flow rate, Mscf/day

t = time, hr

k = permeability, md

μ_i = gas viscosity as evaluated at p_i , cp

Semisteady-State Flow

Equations 6-150 and 6-151 can be modified to account for the non-Darcy flow as follows:

$$Q_g = \frac{kh[m(\bar{p}_r) - m(p_{wf})]}{1422 T \left[\ln \left(\frac{r_c}{r_w} \right) - 0.75 + s + DQ_g \right]} \quad (6-163)$$

or in terms of the pressure-squared approach:

$$Q_g = \frac{kh(\bar{p}_r^2 - p_{wf}^2)}{1422 T \bar{\mu} \bar{z} \left[\ln \left(\frac{r_c}{r_w} \right) - 0.75 + s + DQ_g \right]} \quad (6-164)$$

where the coefficient D is defined as:

$$D = \frac{Fkh}{1422 T} \quad (6-165)$$

Steady-State Flow

Similar to the above modification procedure, Equations 6-44 and 6-45 can be expressed as:

$$Q_g = \frac{kh[m(p_i) - m(p_{wf})]}{1422 T \left[\ln \frac{r_e}{r_w} - 0.5 + s + DQ_g \right]} \quad (6-166)$$

$$Q_g = \frac{kh(p_e^2 - p_{wf}^2)}{1422 T \bar{\mu} \bar{z} \left[\ln \frac{r_e}{r_w} - 0.5 + s + DQ_g \right]} \quad (6-167)$$

where D is defined by Equation 6-166.

Example 6-20

A gas well has an estimated wellbore damage radius of 2 feet and an estimated reduced permeability of 30 md. The formation has a permeability and porosity of 55 md and 12%. The well is producing at a rate of 20 Mscf/day with a gas gravity of 0.6. The following additional data are available:

$$r_w = 0.25$$

$$h = 20'$$

$$T = 140^\circ\text{F}$$

$$\mu_{gw} = 0.013 \text{ cp}$$

Calculate the apparent skin factor.

Solution

Step 1. Calculate the skin factor from Equation 6-143

$$s = \left[\frac{55}{30} - 1 \right] \ln \left(\frac{2}{0.25} \right) = 1.732$$

Step 2. Calculate the turbulence parameter β by applying Equation 6-155:

$$\beta = 1.88 (10)^{-10} (55)^{-1.47} (0.12)^{-0.53} = 159.904 \times 10^6$$

Step 3. Calculate the non-Darcy flow coefficient from Equation 6-156:

$$F = 3.1612 \times 10^{-12} \left[\frac{159.904 \times 10^6 (600) (0.6)}{(0.013) (20)^2 (0.25)} \right] = 0.14$$

Step 4. Calculate the coefficient D from Equation 6-160:

$$D = \frac{(0.14)(55)(20)}{(1422)(600)} = 1.805 \times 10^{-4}$$

Step 5. Estimate the apparent skin factor by applying Equation 6-161:

$$s' = 1.732 + (1.805 \times 10^{-4})(20,000) = 5.342$$

PRINCIPLE OF SUPERPOSITION

The solutions to the radial diffusivity equation as presented earlier in this chapter appear to be applicable only for describing the pressure distribution in an infinite reservoir that was caused by a constant production from a single well. Since real reservoir systems usually have several wells that are operating at varying rates, a more generalized approach is needed to study the fluid flow behavior during the unsteady-state flow period.

The principle of superposition is a powerful concept that can be applied to remove the restrictions that have been imposed on various forms of solution to the transient flow equation. Mathematically the superposition theorem states that any sum of individual solutions to the diffusivity equation is also a solution to that equation. This concept can be applied to account for the following effects on the transient flow solution:

- Effects of multiple wells
- Effects of rate change
- Effects of the boundary
- Effects of pressure change

Slider (1976) presented an excellent review and discussion of the practical applications of the principle of superposition in solving a wide variety of unsteady-state flow problems.

Effects of Multiple Wells

Frequently, it is desired to account for the effects of more than one well on the pressure at some point in the reservoir. The superposition concept states that the total pressure drop at any point in the reservoir is the sum of the pressure changes at that point caused by flow in each of the wells in the reservoir. In other words, we simply superimpose one effect upon the other.

Consider Figure 6-28, which shows three wells that are producing at different flow rates from an infinite acting reservoir, i.e., unsteady-state

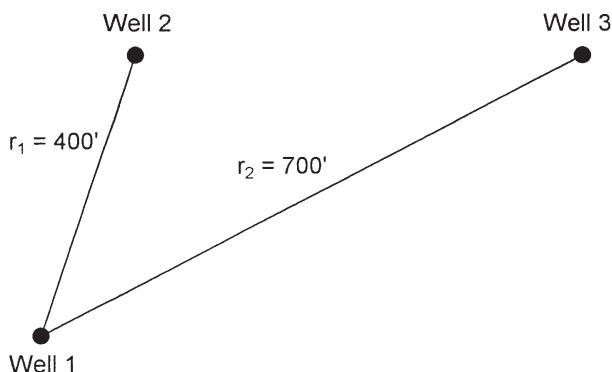


Figure 6-28. Well layout for Example 6-20.

flow reservoir. The principle of superposition shows that the total pressure drop observed at any well, e.g., Well 1, is:

$$\begin{aligned}
 (\Delta p)_{\text{total drop at well 1}} &= (\Delta p)_{\text{drop due to well 1}} \\
 &+ (\Delta p)_{\text{drop due to well 2}} \\
 &+ (\Delta p)_{\text{drop due to well 3}}
 \end{aligned}$$

The pressure drop at Well 1 due to its own production is given by the log-approximation to the E_i -function solution presented by Equation 6-146, or:

$$\begin{aligned}
 (p_i - p_{wf}) &= (\Delta p)_{\text{well1}} = \frac{162.6 Q_{o1} B_o \mu_o}{kh} \\
 &\times \left[\log \left(\frac{kt}{\phi \mu c_t r_w^2} \right) - 3.23 + 0.87s \right]
 \end{aligned}$$

where t = time, hr

s = skin factor

k = permeability, md

Q_{o1} = oil flow rate from Well 1

The pressure drop at Well 1 due to production at Wells 2 and 3 must be written in terms of the E_i -function solution as expressed by Equation 6-78. The log-approximation cannot be used because we are calculating the pressure at a large distance r from the well, i.e., the argument $x > 0.01$, or:

$$\begin{aligned}
 (p_i - p_{wf})_{\text{total at well 1}} &= \left(\frac{162.6 Q_{o1} B_o \mu_o}{kh} \right) \\
 &\times \left[\log \left(\frac{kt}{\phi \mu c_t r_w^2} \right) - 3.23 + 0.87s \right] - \left(\frac{70.6 Q_{o2} B_o \mu_o}{kh} \right) \\
 &\times E_i \left[- \frac{948 \phi \mu c_t r_1^2}{kt} \right] - \left(\frac{70.6 Q_{o3} B_o \mu_o}{kh} \right) E_i \left[- \frac{948 \phi \mu c_t r_2^2}{kt} \right]
 \end{aligned}$$

where Q_{o1} , Q_{o2} , and Q_{o3} refer to the respective producing rates of Wells 1, 2, and 3.

The above computational approach can be used to calculate the pressure at Wells 2 and 3. Further, it can be extended to include any number of wells flowing under the unsteady-state flow condition. It should also be noted that if the point of interest is an operating well, the skin factor s must be included for that well only.

Example 6-21

Assume that the three wells as shown in Figure 6-28 are producing under a transient flow condition for 15 hours. The following additional data are available:

| | |
|---|------------------|
| $Q_{o1} = 100$ STB/day | $h = 20'$ |
| $Q_{o2} = 160$ STB/day | $\phi = 15\%$ |
| $Q_{o3} = 200$ STB/day | $k = 40$ md |
| $p_i = 4500$ psi | $r_w = 0.25'$ |
| $B_o = 1.20$ bbl/STB | $\mu_o = 2.0$ cp |
| $c_t = 20 \times 10^{-6}$ psi ⁻¹ | $r_1 = 400'$ |
| $(s)_{\text{well 1}} = -0.5$ | $r_2 = 700'$ |

If the three wells are producing at a constant flow rate, calculate the sand face flowing pressure at Well 1.

Solution

Step 1. Calculate the pressure drop at Well 1 caused by its own production by using Equation 6-146.

$$\begin{aligned}
 (\Delta p)_{\text{well 1}} &= \frac{(162.6)(100)(1.2)(2.0)}{(40)(20)} \\
 &\times \left[\log \left(\frac{(40)(15)}{(0.15)(2)(20 \times 10^{-6})(0.25)^2} \right) - 3.23 + 0.87(0) \right] \\
 &= 270.2 \text{ psi}
 \end{aligned}$$

Step 2. Calculate the pressure drop at Well 1 due to the production from Well 2.

$$\begin{aligned}
 (\Delta p)_{\text{due to well 2}} &= -\frac{(70.6)(160)(1.2)(2)}{(40)(20)} \\
 &\times E_i \left[-\frac{(948)(0.15)(2.0)(20 \times 10^{-6})(400)^2}{(40)(15)} \right] \\
 &= 33.888 [-E_i (-1.5168)] \\
 &= (33.888)(0.13) = 4.41 \text{ psi}
 \end{aligned}$$

Step 3. Calculate pressure drop due to production from Well 3.

$$\begin{aligned}
 (\Delta p)_{\text{due to well 3}} &= -\frac{(70.6)(200)(1.2)(2)}{(40)(20)} \\
 &\times E_i \left[-\frac{(948)(0.15)(2.0)(20 \times 10^{-6})(700)^2}{(40)(15)} \right] \\
 &= (42.36)[-E_i (-4.645)] \\
 &= (42.36)(1.84 \times 10^{-3}) = 0.08 \text{ psi}
 \end{aligned}$$

Step 4. Calculate total pressure drop at Well 1.

$$(\Delta p)_{\text{total at well 1}} = 270.2 + 4.41 + 0.08 = 274.69 \text{ psi}$$

Step 5. Calculate p_{wf} at Well 1.

$$p_{\text{wf}} = 4500 - 274.69 = 4225.31 \text{ psi}$$

Effects of Variable Flow Rates

All of the mathematical expressions presented previously in this chapter require that the wells produce at a constant rate during the transient flow periods. Practically all wells produce at varying rates and, therefore, it is important that we be able to predict the pressure behavior when the rate changes. For this purpose, the concept of superposition states, “**Every flow rate change in a well will result in a pressure response which is independent of the pressure responses caused by other previous rate changes.**” Accordingly, the total pressure drop that has occurred at any time is the summation of pressure changes caused separately by each *net* flow rate change.

Consider the case of a shut-in well, i.e., $Q = 0$, that was then allowed to produce at a series of constant rates for the different time periods shown in Figure 6-29. To calculate the total pressure drop at the sand face at time t_4 , the composite solution is obtained by adding the individual constant-rate solutions at the specified rate-time sequence, or:

$$(\Delta p)_{\text{total}} = (\Delta p)_{\text{due to } (Q_{01} - 0)} + (\Delta p)_{\text{due to } (Q_{02} - Q_{01})} + (\Delta p)_{\text{due to } (Q_{03} - Q_{02})} + (\Delta p)_{\text{due to } (Q_{04} - Q_{03})}$$

The above expression indicates that there are four contributions to the total pressure drop resulting from the four individual flow rates.

The first contribution results from increasing the rate from 0 to Q_1 and is in effect over the entire time period t_4 , thus:

$$(\Delta p)_{Q_1-0} = \left[\frac{162.6 (Q_1 - 0) B \mu}{kh} \right] \left[\log \left(\frac{kt_4}{\phi \mu c_t r_w^2} \right) - 3.23 + 0.87s \right]$$

It is essential to notice the *change* in the rate, i.e., (new rate – old rate), that is used in the above equation. It is the change in the rate that causes the pressure disturbance. Further, it should be noted that the “time” in the equation represents the *total elapsed time* since the change in the rate has been in effect.

Second contribution results from decreasing the rate from Q_1 to Q_2 at t_1 , thus:

$$(\Delta p)_{Q_2-Q_1} = \left[\frac{162.6 (Q_2 - Q_1) B \mu}{kh} \right] \times \left[\log \left(\frac{k(t_4 - t_1)}{\phi \mu c_t r_w^2} \right) - 3.23 + 0.87s \right]$$

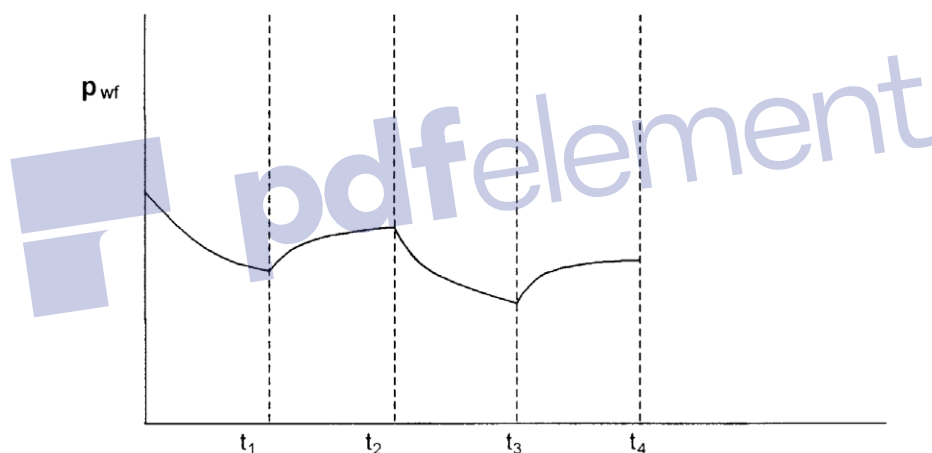
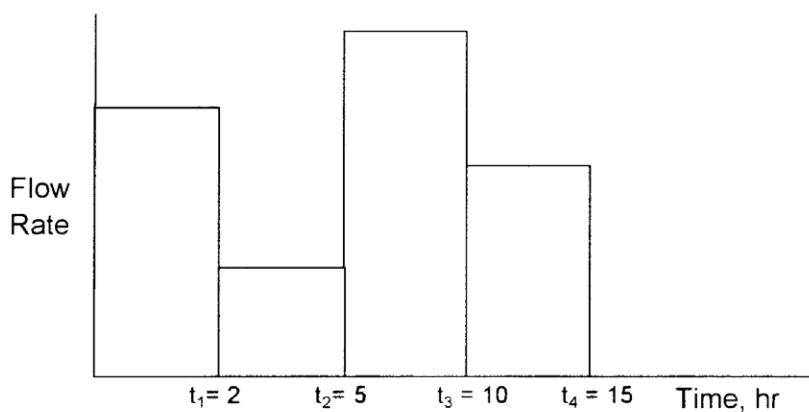


Figure 6-29. Production and pressure history of a well.

Using the same concept, the contributions from Q_2 to Q_3 and from Q_3 to Q_4 can be computed as:

$$(\Delta p)_{Q_3-Q_2} = \left[\frac{162.6 (Q_3 - Q_2) B \mu}{kh} \right] \times \left[\log \left(\frac{k(t_4 - t_2)}{\phi \mu c_t r_w^2} \right) - 3.23 + 0.87s \right]$$

$$(\Delta p)_{Q_4 - Q_3} = \left[\frac{162.6 (Q_4 - Q_3) B \mu}{kh} \right] \\ \times \left[\log \left(\frac{k(t_4 - t_3)}{\phi \mu c_t r_w^2} \right) - 3.23 + 0.87s \right]$$

The above approach can be extended to model a well with several rate changes. Note, however, the above approach is valid only if the well is flowing under the unsteady-state flow condition for the total time elapsed since the well began to flow at its initial rate.

Example 6-22

Figure 6-29 shows the rate history of a well that is producing under transient flow condition for 15 hours. Given the following data:

$$\begin{array}{ll} p_i = 5000 \text{ psi} & h = 20' \\ B_o = 1.1 \text{ bbl/STB} & \phi = 15\% \\ \mu_o = 2.5 \text{ cp} & r_w = 0.3' \\ c_t = 20 \times 10^{-6} \text{ psi}^{-1} & s = 0 \\ k = 40 \text{ md} & \end{array}$$

calculate the sand face pressure after 15 hours.

Solution

Step 1. Calculate the pressure drop due to the first flow rate for the entire flow period.

$$(\Delta p)_{Q_1 - 0} = \frac{(162.6)(100 - 0)(1.1)(2.5)}{(40)(20)} \\ \times \left[\log \left[\frac{(40)(15)}{(0.15)(2.5)(20 \times 10^{-6})(0.3)^2} \right] - 3.23 + 0 \right] = 319.6 \text{ psi}$$

Step 2. Calculate the additional pressure change due to the change of the flow rate from 100 to 70 STB/day.

$$\begin{aligned}
 (\Delta p)_{Q_2 - Q_1} &= \frac{(162.6)(70 - 100)(1.1)(2.5)}{(40)(20)} \\
 &\times \left[\log \left[\frac{(40)(15 - 2)}{(0.15)(2.5)(20 \times 10^{-6})(0.3)^2} \right] - 3.23 \right] = -94.85 \text{ psi}
 \end{aligned}$$

Step 3. Calculate the additional pressure change due to the change of the flow rate from 70 to 150 STB/day.

$$\begin{aligned}
 (\Delta p)_{Q_3 - Q_2} &= \frac{(162.6)(150 - 70)(1.1)(2.5)}{(40)(20)} \\
 &\times \left[\log \left[\frac{(40)(15 - 5)}{(0.15)(2.5)(20 \times 10^{-6})(0.3)^2} \right] - 3.23 \right] = 249.18 \text{ psi}
 \end{aligned}$$

Step 4. Calculate the additional pressure change due to the change of the flow rate from 150 to 85 STB/day.

$$\begin{aligned}
 (\Delta p)_{Q_4 - Q_3} &= \frac{(162.6)(85 - 150)(1.1)(2.5)}{(40)(20)} \\
 &\times \left[\log \left[\frac{(40)(15 - 10)}{(0.15)(2.5)(20 \times 10^{-6})(0.3)^2} \right] - 3.23 \right] = -190.44 \text{ psi}
 \end{aligned}$$

Step 5. Calculate the total pressure drop:

$$(\Delta p)_{\text{total}} = 319.6 + (-94.85) + 249.18 + (-190.44) = 283.49 \text{ psi}$$

Step 6. Calculate wellbore pressure after 15 hours of transient flow:

$$p_{\text{wf}} = 5000 - 283.49 = 4716.51 \text{ psi}$$

Effects of the Reservoir Boundary

The superposition theorem can also be extended to predict the pressure of a well in a bounded reservoir. Consider Figure 6-30, which shows a well that is located a distance r from the no-flow boundary, e.g., sealing fault.

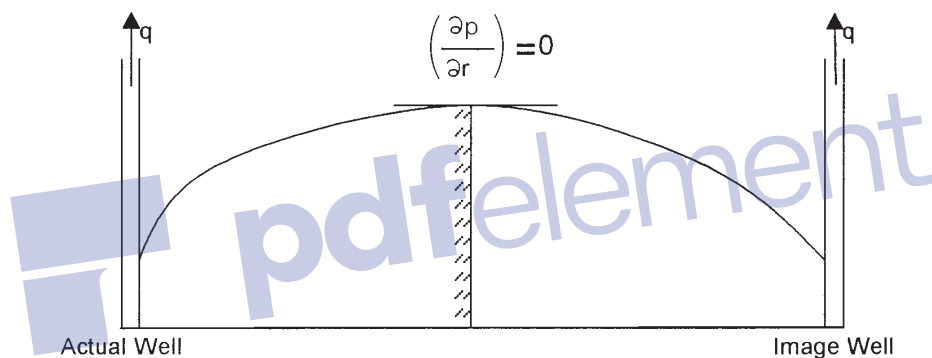
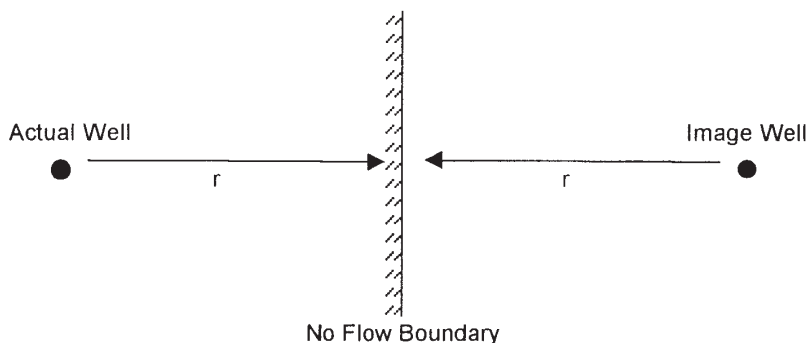


Figure 6-30. Method of images in solving boundary problems.

The no-flow boundary can be represented by the following pressure gradient expression:

$$\left(\frac{\partial p}{\partial r} \right)_{\text{Boundary}} = 0$$

Mathematically, the above boundary condition can be met by placing an *image* well, identical to that of the actual well, on the other side of the fault at exactly distance r . Consequently, the effect of the boundary on the pressure behavior of a well would be the same as the effect from an image well located a distance $2r$ from the actual well.

In accounting for the boundary effects, the superposition method is frequently called the *method of images*. Thus, for the problem of the system configuration given in Figure 6-30, the problem reduces to one of

determining the effect of the image well on the actual well. The total pressure drop at the actual well will be the pressure drop due to its own production plus the additional pressure drop caused by an identical well at a distance of $2r$, or:

$$(\Delta p)_{\text{total}} = (\Delta p)_{\text{actual well}} + (\Delta p)_{\text{due to image well}}$$

or

$$\begin{aligned} (\Delta p)_{\text{total}} = & \frac{162.6 Q_o B_o \mu_o}{kh} \left[\log \left(\frac{kt}{\phi \mu_o c_t r_w^2} \right) - 3.23 + 0.87s \right] \\ & - \left(\frac{70.6 Q_o B_o \mu_o}{kh} \right) E_i \left(- \frac{948 \phi \mu_o c_t (2r)^2}{kt} \right) \end{aligned} \quad (6-168)$$

Notice that this equation assumes the reservoir is infinite except for the indicated boundary. The effect of boundaries is always to cause greater pressure drop than those calculated for infinite reservoirs.

The concept of image wells can be extended to generate the pressure behavior of a well located within a variety of boundary configurations.

Example 6-23

Figure 6-31 shows a well located between two sealing faults at 200 and 100 feet from the two faults. The well is producing under a transient flow condition at a constant flow rate of 200 STB/day.

Given:

$$\begin{array}{ll} p_i = 500 \text{ psi} & k = 600 \text{ md} \\ B_o = 1.1 \text{ bbl/STB} & \phi = 17\% \\ \mu_o = 2.0 \text{ cp} & h = 25 \text{ ft} \\ r_w = 0.3 \text{ ft} & s = 0 \\ c_t = 25 \times 10^{-6} \text{ psi}^{-1} & \end{array}$$

calculate the sand face pressure after 10 hours.

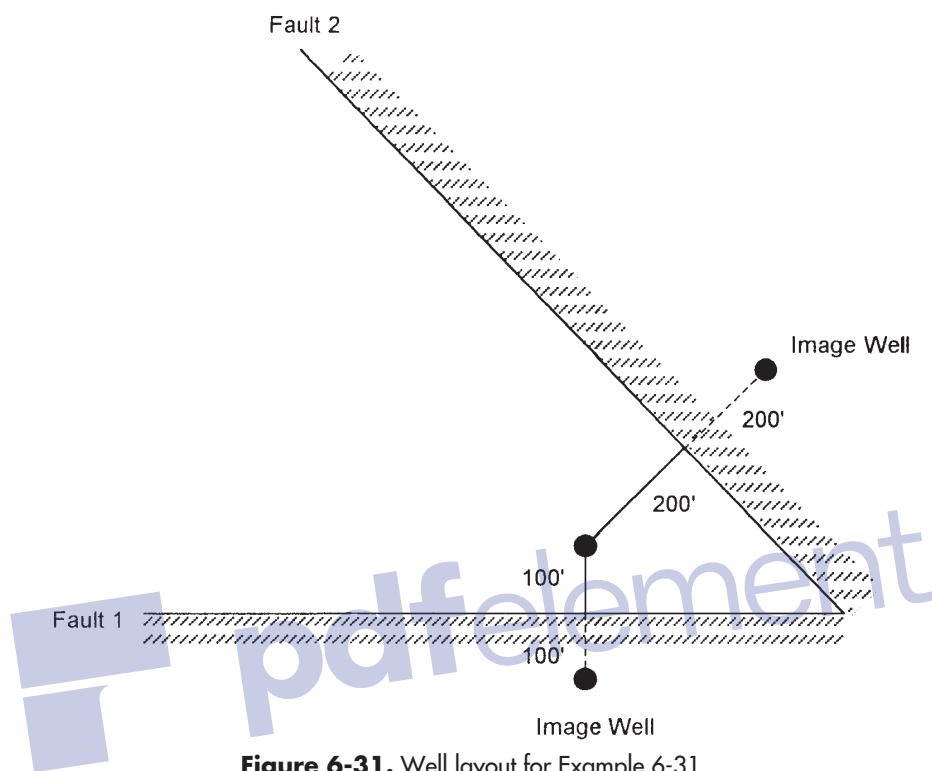


Figure 6-31. Well layout for Example 6-31.

Solution

Step 1. Calculate the pressure drop due to the actual well flow rate.

$$\begin{aligned}
 (\Delta p)_{\text{actual}} &= \frac{(162.6)(200)(1.1)(2.0)}{(60)(25)} \\
 &\times \left[\log \left[\frac{(60)(10)}{(0.17)(2)(0.17)(2)(25 \times 10^{-6})(0.3)^2} \right] - 3.23 + 0 \right] \\
 &= 270.17
 \end{aligned}$$

Step 2. Determine the additional pressure drop due to the first fault (i.e., image well 1):

$$\begin{aligned} (\Delta p)_{\text{image well 1}} &= -\frac{(70.6)(200)(1.1)(2.0)}{(60)(25)} \\ &\times E_i \left[-\frac{(948)(0.17)(2)(25 \times 10^{-6})(2 \times 100)^2}{(6)(10)} \right] \\ &= 20.71 [-E_i (-0.537)] = 10.64 \text{ psi} \end{aligned}$$

Step 3. Calculate the effect of the second fault (i.e., image well 2):

$$\begin{aligned} (\Delta p)_{\text{image well 2}} &= 20.71 \left[-E_i \left(\frac{-948(0.17)(2)(25 \times 10^{-6})(2 \times 200)^2}{(60)(10)} \right) \right] \\ &= 20.71 [-E_i (-2.15)] = 1.0 \text{ psi} \end{aligned}$$

Step 4. Total pressure drop is:

$$(\Delta p)_{\text{total}} = 270.17 + 10.64 + 1.0 = 281.8 \text{ psi}$$

Step 5. $p_{\text{wf}} = 5000 - 281.8 = 4718.2 \text{ psi}$

Accounting for Pressure-Change Effects

Superposition is also used in applying the constant-pressure case. Pressure changes are accounted for in this solution in much the same way that rate changes are accounted for in the constant rate case. The description of the superposition method to account for the pressure-change effect is fully described in the Water Influx section in this book.

TRANSIENT WELL TESTING

Detailed reservoir information is essential to the petroleum engineer in order to analyze the current behavior and future performance of the reservoir. Pressure transient testing is designed to provide the engineer with a quantitative analysis of the reservoir properties. A transient test is essentially conducted by creating a pressure disturbance in the reservoir and recording the pressure response at the wellbore, i.e., bottom-hole flowing

pressure p_{wf} , as a function of time. The pressure transient tests most commonly used in the petroleum industry include:

- Pressure drawdown
- Pressure buildup
- Multirate
- Interference
- Pulse
- Drill stem
- Fall off
- Injectivity
- Step rate

It has long been recognized that the pressure behavior of a reservoir following a rate change directly reflects the geometry and flow properties of the reservoir. Information available from a well test includes:

- Effective permeability
- Formation damage or stimulation
- Flow barriers and fluid contacts
- Volumetric average reservoir pressure
- Drainage pore volume
- Detection, length, capacity of fractures
- Communication between wells

Only the drawdown and buildup tests are briefly described in the following two sections. There are several excellent books that comprehensively address the subject of well testing, notably:

- John Lee, *Well Testing* (1982)
- C. S. Matthews and D. G. Russell, *Pressure Buildup and Flow Test in Wells* (1967)
- Robert Earlougher, *Advances in Well Test Analysis* (1977)
- Canadian Energy Resources Conservation Board, *Theory and Practice of the Testing of Gas Wells* (1975)
- Roland Horn, *Modern Well Test Analysis* (1995)

Drawdown Test

A pressure drawdown test is simply a series of bottom-hole pressure measurements made during a period of flow at constant producing rate.

Usually the well is shut-in prior to the flow test for a period of time sufficient to allow the pressure to equalize throughout the formation, i.e., to reach static pressure. A schematic of the ideal flow rate and pressure history is illustrated by Figure 6-32.

The fundamental objectives of drawdown testing are to obtain the average permeability, k , of the reservoir rock *within the drainage area of the well* and to assess the degree of damage or stimulation induced in the vicinity of the wellbore through drilling and completion practices. Other objectives are to determine the pore volume and to detect reservoir inhomogeneities *within the drainage area of the well*.

During flow at a constant rate of Q_o , the pressure behavior of a well in an infinite-acting reservoir (i.e., during the unsteady-state flow period) is given by Equation 6-146, as:

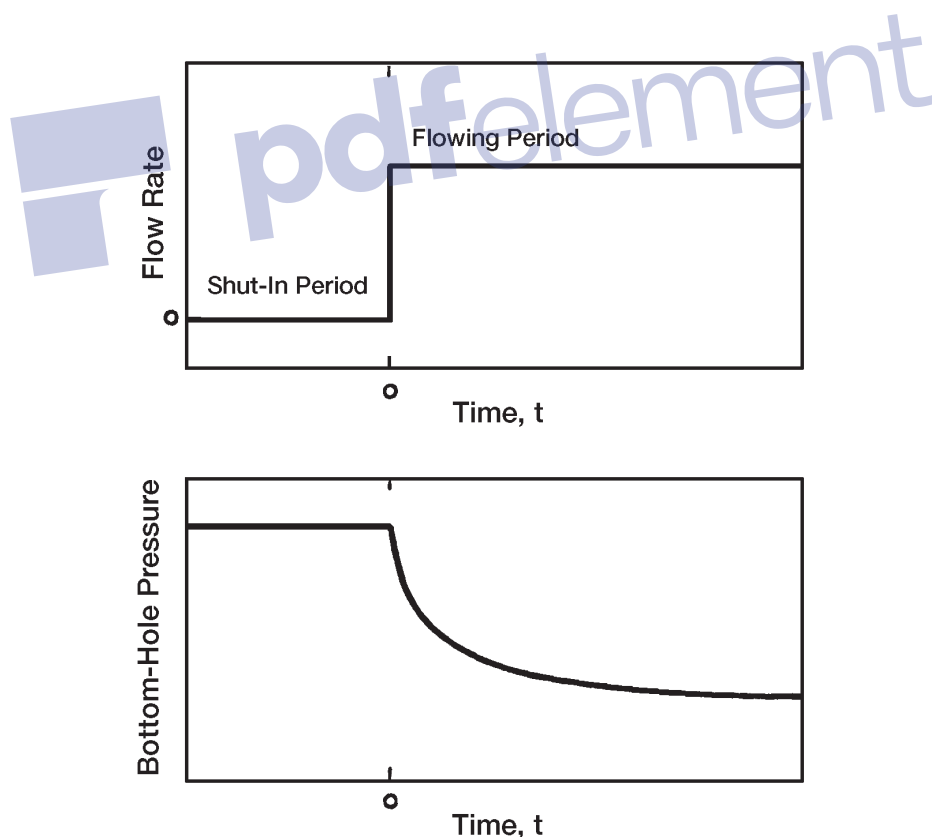


Figure 6-32. Idealized drawdown test.

$$p_{wf} = p_i - \frac{162.6 Q_o B_o \mu}{kh} \left[\log \left(\frac{kt}{\phi \mu c_t r_w^2} \right) - 3.23 + 0.87s \right]$$

where k = permeability, md

t = time, hr

r_w = wellbore radius

s = skin factor

The above expression can be written as:

$$p_{wf} = p_i - \frac{162.6 Q_o B_o \mu}{kh} \times \left[\log(t) + \log \left(\frac{k}{\phi \mu c_t r_w^2} \right) - 3.23 + 0.87s \right] \quad (6-169)$$

Equation 6-170 is essentially an equation of a straight line and can be expressed as:

$$p_{wf} = a + m \log(t) \quad (6-170)$$

where

$$a = p_i - \frac{162.6 Q_o B_o \mu}{kh} \left[\log \left(\frac{k}{\phi \mu c_t r_w^2} \right) - 3.23 + 0.87s \right]$$

The slope m is given by:

$$m = \frac{-162.6 Q_o B_o \mu_o}{kh} \quad (6-171)$$

Equation 6-171 suggests that a plot of p_{wf} versus time t on semilog graph paper would yield a straight line with a slope m in psi/cycle. This semilog straight-line relationship is illustrated by Figure 6-33.

Equation 6-172 can be also rearranged for the capacity kh of the drainage area of the well. If the thickness is known, then the average permeability is given by:

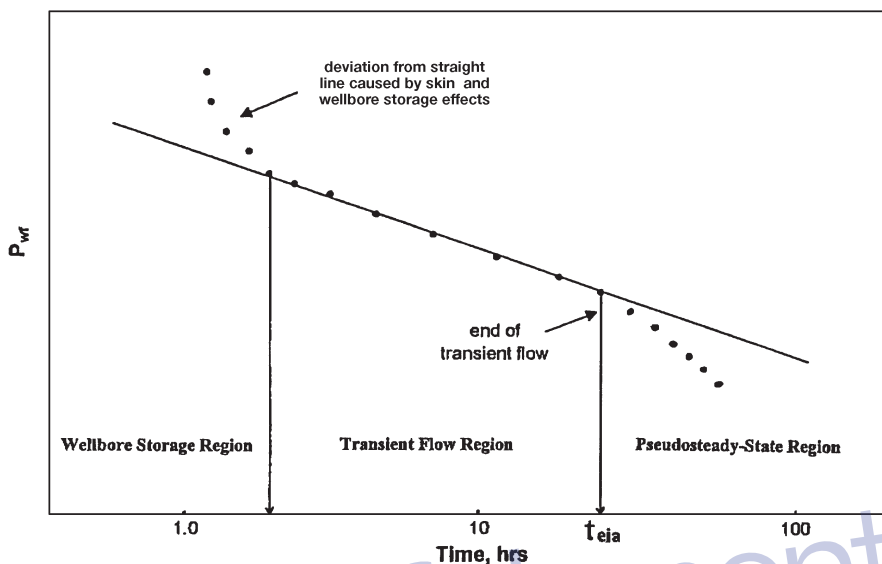


Figure 6-33. Semilog plot of pressure drawdown data.

$$k = \frac{-162.6 Q_o B_o \mu_o}{mh} \quad (6-172)$$

where k = average permeability, md
 m = slope, psi/cycle. Notice, slope m is negative.

Clearly, kh/μ or k/μ may be also estimated.

The skin effect can be obtained by rearranging Equation 6-170, as:

$$s = 1.151 \left(\frac{p_{wf} - p_i}{m} - \log t - \log \frac{k}{\phi \mu c_t r_w^2} + 3.23 \right)$$

or, more conveniently, if $p_{wf} = p_{1 \text{ hr}}$, which is found on the extension of the straight line at $\log t$ (1 hour), then:

$$s = 1.151 \left(\frac{p_{1 \text{ hr}} - p_i}{m} - \log \frac{k}{\phi \mu c_t r_w^2} + 3.23 \right) \quad (6-173)$$

In Equation 6-174, $p_{1 \text{ hr}}$ must be from the semilog straight line. If pressure data measured at 1 hour do not fall on that line, the line *must be extrapolated* to 1 hour and the extrapolated value of $p_{1 \text{ hr}}$ must be used in Equation 6-174. This procedure is necessary to avoid calculating an incorrect skin by using a wellbore-storage-influenced pressure. Figure 6-33 illustrates the extrapolation to $p_{1 \text{ hr}}$.

If the drawdown test is long enough, bottom-hole pressure will deviate from the semilog straight line and make the transition from infinite-acting to pseudosteady state.

It should be pointed out that the pressure drop due to the skin, as expressed by Equation 6-142, can be written in terms of the transient flow slope, m , by combining the equations:

$$m = 162.6 \frac{Q_o B_o \mu_o}{kh}$$

$$\Delta p_s = 141.2 \left[\frac{Q_o B_o \mu_o}{kh} \right] s$$

Combining the two expressions gives

$$\Delta p_s = 0.87 m s$$

Example 6-24²

Estimate oil permeability and skin factor from the drawdown data of Figure 6-34.

The following reservoir data are available:

| | |
|--|-----------------------------|
| $h = 130 \text{ ft}$ | $\phi = 20 \text{ percent}$ |
| $r_w = 0.25 \text{ ft}$ | $p_i = 1154 \text{ psi}$ |
| $Q_o = 348 \text{ STB/D}$ | $m = -22 \text{ psi/cycle}$ |
| $B_o = 1.14 \text{ bbl/STB}$ | |
| $\mu_o = 3.93 \text{ cp}$ | |
| $c_t = 8.74 \times 10^{-6} \text{ psi}^{-1}$ | |

Assuming that the wellbore storage effects are not significant, calculate:

- Permeability
- Skin factor

²This example problem and the solution procedure are given by Earlougher, R., "Advances in Well Test Analysis," Monograph Series, SPE, Dallas (1977).

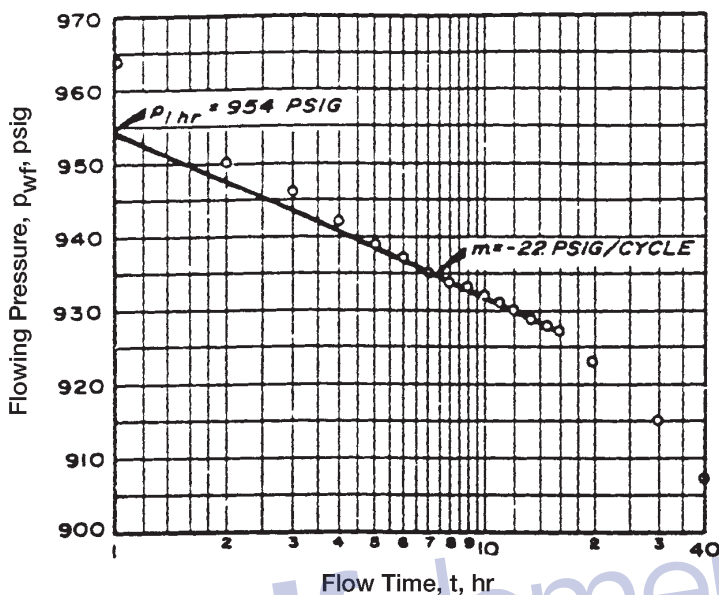


Figure 6-34. Earlougher's semilog data plot for the drawdown test. (Permission to publish by the SPE, copyright SPE, 1977.)

Solution

Step 1. From Figure 6-34, calculate $p_{1 \text{ hr}}$:

$$p_{1 \text{ hr}} = 954 \text{ psi}$$

Step 2. Determine the slope of the transient flow line:

$$m = -22 \text{ psi/cycle}$$

Step 3. Calculate the permeability by applying Equation 6-173:

$$k = \frac{-(162.6)(348)(1.14)(3.93)}{(-22)(130)} = 89 \text{ md}$$

Step 4. Solve for the skin factor s by using Equation 6-174:

$$s = 1.151 \left\{ \left(\frac{954 - 1,154}{-22} \right) - \log \left[\frac{89}{(0.2)(3.93)(8.74 \times 10^{-6})(0.25)^2} \right] + 3.2275 \right\} = 4.6$$

Basically, well test analysis deals with the interpretation of the wellbore pressure response to a given change in the flow rate (from zero to a constant value for a drawdown test, or from a constant rate to zero for a buildup test). Unfortunately, the producing rate is controlled at the surface, not at the sand face. Because of the wellbore volume, a constant surface flow rate does not ensure that the entire rate is being produced from the formation. This effect is due to **wellbore storage**. Consider the case of a drawdown test. When the well is first open to flow after a shut-in period, the pressure in the wellbore drops. This drop in the wellbore pressure causes the following two types of wellbore storage:

- Wellbore storage effect caused by **fluid expansion**
- Wellbore storage effect caused by **changing fluid level** in the casing-tubing annulus.

As the bottom hole pressure drops, the wellbore fluid expands and, thus, the initial surface flow rate is not from the formation, but essentially from the fluid that had been stored in the wellbore. This is defined as the wellbore storage due to fluid expansion.

The second type of wellbore storage is due to a changing of the annulus fluid level (falling level during a drawdown test and rising fluid level during a pressure buildup test). When the well is open to flow during a drawdown test, the reduction in pressure causes the fluid level in the annulus to fall. This annulus fluid production joins that from the formation and contributes to the total flow from the well. The falling fluid level is generally able to contribute more fluid than that by expansion.

The above discussion suggests that part of the flow will be contributed by the wellbore instead of the reservoir, i.e.,

$$q = q_f + q_{wb}$$

where q = surface flow rate, bbl/day

q_f = formation flow rate, bbl/day

q_{wb} = flow rate contributed by the wellbore, bbl/day

As production time increases, the wellbore contribution decreases, and the formation rate increases until it eventually equals the surface flow rate. During this period when the formation rate is changed, the measured drawdown pressures will not produce the ideal semilog straight-line behavior that is expected during transient flow. This indicates that the pressure data collected during the duration of the wellbore storage effect cannot be analyzed by using conventional methods.

Each of the above two effects can be quantified in terms of the wellbore storage factor C , which is defined as:

$$C = \frac{\Delta V_{wb}}{\Delta p}$$

where C = wellbore storage volume, bbl/psi

ΔV_{wb} = change in the volume of fluid in the wellbore, bbl

The above relationship can be applied to mathematically represent the individual effect of wellbore fluid expansion and falling (or rising) fluid level, to give:

- **Wellbore Storage Effect Due to Fluid Expansion**

$$C = V_{wb} c_{wb}$$

where V_{wb} = total wellbore fluid volume, bbl

c_{wb} = average compressibility of fluid in the wellbore, psi^{-1}

- **Wellbore Storage Effect Due to Changing Fluid Level**

If A_a is the cross-sectional area of the annulus, and ρ is the average fluid density in the wellbore, the wellbore storage coefficient is given by:

$$C = \frac{144 A_a}{5.615 \rho}$$

with:

$$A_a = \frac{\pi [(ID_c)^2 - (OD_T)^2]}{4 (144)}$$

where A_a = annulus cross-sectional area, ft^2

OD_T = outside diameter of the production tubing, in.

ID_C = inside diameter of the casing, in.

ρ = wellbore fluid density, lb/ft³

This effect is essentially small if a packer is placed near the producing zone. The total storage effect is the sum of both effects. It should be noted during oil well testing that the fluid expansion is generally insignificant due to the small compressibility of liquids. For gas wells, the primary storage effect is due to gas expansion.

To determine the duration of the wellbore storage effect, it is convenient to express the wellbore storage factor in a dimensionless form as:

$$C_D = \frac{5.615 C}{2 \pi h \phi c_t r_w^2} = \frac{0.894 C}{\phi h c_t r_w^2}$$

where C_D = dimensionless wellbore storage factor

C = wellbore storage factor, bbl/psi

c_t = total compressibility coefficient, psi⁻¹

r_w = wellbore radius, ft

h = thickness, ft

Horne (1995) and Earlougher (1977), among other authors, have indicated that the wellbore pressure is directly proportional to the time during the wellbore storage-dominated period of the test and is expressed by:

$$p_D = t_D / C_D$$

where p_D = dimensionless pressure during wellbore storage domination
time

t_D = dimensionless time

Taking the logarithm of both sides of the above relationship, gives:

$$\log(p_D) = \log(t_D) - \log(C_D)$$

The above expression has a characteristic that is diagnostic of wellbore storage effects. It indicates that a plot of p_D versus t_D on a log-log scale will yield as straight line of a unit slope during wellbore storage domination. Since p_D is proportional to Δp and t_D is proportional to time, it is convenient to log ($p_i - p_{wf}$) versus log (t) and observe where the plot has a slope of one cycle in pressure per cycle in time.

The log-log plot is a valuable aid for recognizing wellbore storage effects in transient tests (e.g., drawdown or buildup tests) when early-time pressure recorded data are available. It is recommended that this plot be made a part of transient test analysis. As wellbore storage effects become less severe, the formation begins to influence the bottom-hole pressure more and more, and the data points on the log-log plot fall below the unit-slope straight line and signify the end of the wellbore storage effect. At this point, wellbore storage is no longer important and standard semilog data-plotting analysis techniques apply. As a rule of thumb, that time usually occurs about 1 to 1½ cycles in time after the log-log data plot starts deviating significantly from the unit slope. This time may be estimated from:

$$t_D > (60 + 3.5s) C_D$$

or approximately:

$$t > \frac{(200,000 + 12,000 s)C}{(kh / \mu)}$$

where t = total time that marks the end of wellbore storage effect and the beginning of the semilog straight line, hr

k = permeability, md

s = skin factor

μ = viscosity, cp

C = wellbore storage coefficient, bbl/psi

Example 6-25

The following data are given for an oil well that is scheduled for a drawdown test:

- Volume of fluid in the wellbore = 180 bbls
- Tubing outside diameter = 2 inches
- Production casing inside diameter = 7.675 inches
- Average oil density in the wellbore = 45 lb/ft³
- $h = 20$ ft $\phi = 15\%$ $r_w = 0.25$ ft
- $\mu_o = 2$ cp $k = 30$ md $s = 0$
- $c_t = 20 \times 10^{-6}$ psi⁻¹ $c_o = 10 \times 10^{-6}$ psi⁻¹

If this well is placed under a constant production rate, how long will it take for wellbore storage effects to end?

Solution

Step 1. Calculate the cross-sectional area of the annulus A_a :

$$A_a = \frac{\pi [(7.675)^2 - (2)^2]}{(4)(144)} = 0.2995 \text{ ft}^2$$

Step 2. Calculate the wellbore storage factor caused by fluid expansion:

$$C = V_{wb} c_{wb}$$

$$C = (180)(10 \times 10^{-6}) = 0.0018 \text{ bbl/psi}$$

Step 3. Determine the wellbore storage factor caused by the falling fluid level:

$$C = \frac{144 A_a}{5.615 \rho}$$

$$C = \frac{144 (0.2995)}{(5.615)(45)} = 0.1707 \text{ bbl/psi}$$

Step 4. Calculate the total wellbore storage coefficient:

$$C = 0.0018 + 0.1707 = 0.1725 \text{ bbl/psi}$$

The above calculations show that the effect of fluid expansion can generally be neglected in crude oil systems.

Step 5. Determine the time required for wellbore storage influence to end from:

$$t = \frac{(200,000 + 12,000 \text{ s}) C \mu}{kh}$$

$$t = \frac{(200,000 + 0)(0.1725)(2)}{(30)(20)} = 115 \text{ hr}$$

The straight-line relationship as expressed by Equation 6-171 is only valid during the infinite-acting behavior of the well. Obviously, reservoirs are not infinite in extent, thus the infinite-acting radial flow period

cannot last indefinitely. Eventually the effects of the reservoir boundaries will be felt at the well being tested. The time at which the boundary effect is felt is dependent on the following factors:

- Permeability k
- Total compressibility c_t
- Porosity ϕ
- Viscosity μ
- Distance to the boundary
- Shape of the drainage area

Earlougher (1977) suggests the following mathematical expression for estimating the duration of the infinite-acting period.

$$t_{eia} = \left[\frac{\phi \mu c_t A}{0.000264 k} \right] (t_{DA})_{eia}$$

where t_{eia} = time to the end of infinite-acting period, hr

A = well drainage area, ft^2

c_t = total compressibility, psi^{-1}

$(t_{DA})_{eia}$ = dimensionless time to the end of the infinite-acting period

Earlougher's expression can be used to predict the end of transient flow in a drainage system of any geometry by obtaining the value of $(t_{DA})_{eia}$ from Table 6-3 as listed under "Use Infinite System Solution with Less Than 1% Error for $t_D <$." For example, for a well centered in a circular reservoir, $(t_{DA})_{eia} = 0.1$, and accordingly:

$$t_{eia} = \frac{380 \phi \mu c_t A}{k}$$

Hence, the specific steps involved in a drawdown test analysis are:

1. Plot $(p_i - p_{wf})$ versus t on a log-log scale.
2. Determine the time at which the unit slope line ends.
3. Determine the corresponding time at $1\frac{1}{2}$ log cycle, ahead of the observed time in Step 2. This is the time that marks the end of the wellbore storage effect and the start of the semilog straight line.
4. Estimate the wellbore storage coefficient from:

$$C = \frac{qt}{24\Delta p}$$

where t and Δp are values read from a point on the log-log unit-slope straight line and q is the flow rate in bbl/day.

5. Plot p_{wf} versus t on a semilog scale.
6. Determine the start of the straight-line portion as suggested in Step 3 and draw the best line through the points.
7. Calculate the slope of the straight line and determine the permeability k and skin factor s by applying Equations 6-173 and 6-174, respectively.
8. Estimate the time to the end of the infinite-acting (transient flow) period, i.e., t_{eia} , which marks the beginning of the pseudosteady-state flow.
9. Plot all the recorded pressure data after t_{eia} as a function of time on a regular Cartesian scale. These data should form a straight-line relationship.
10. Determine the **slope** of the pseudosteady-state line, i.e., dp/dt (commonly referred to as m') and use Equation 6-128 to solve for the drainage area "A,"

$$A = \frac{-0.23396 Q B}{c_t h \phi (dp/dt)} = \frac{-0.23396 Q B}{c_t h \phi m'}$$

where m' = slope of the semisteady-state Cartesian straight line

Q = fluid flow rate, STB/day

B = formation volume factor, bbl/STB

11. Calculate the shape factor C_A from an expression that has been developed by Earlougher (1977). Earlougher has shown that the reservoir shape factor can be estimated from the following relationship:

$$C_A = 5.456 \left(\frac{m}{m'} \right) \exp \left[\frac{2.303 (p_{1 \text{ hr}} - p_{\text{int}})}{m} \right]$$

where m = slope of transient semilog straight line, psi/log cycle

m' = slope of the semisteady-state Cartesian straight line

$p_{1 \text{ hr}}$ = pressure at $t = 1$ hr from semilog straight line, psi

p_{int} = pressure at $t = 0$ from semisteady-state Cartesian straight line, psi

12. Use Table 6-4 to determine the drainage configuration of the tested well that has a value of the shape factor C_A closest to that of the calculated one, i.e., Step 11.

Pressure Buildup Test

The use of pressure buildup data has provided the reservoir engineer with one more useful tool in the determination of reservoir behavior. Pressure buildup analysis describes the build up in wellbore pressure with time after a well has been shut-in. One of the principal objectives of this analysis is to determine the static reservoir pressure without waiting weeks or months for the pressure in the entire reservoir to stabilize. Because the buildup in wellbore pressure will generally follow some definite trend, it has been possible to extend the pressure buildup analysis to determine:

- Effective reservoir permeability
- Extent of permeability damage around the wellbore
- Presence of faults and to some degree the distance to the faults
- Any interference between producing wells
- Limits of the reservoir where there is not a strong water drive or where the aquifer is no larger than the hydrocarbon reservoir

Certainly all of this information will probably not be available from any given analysis, and the degree of usefulness of any of this information will depend on the experience in the area and the amount of other information available for correlation purposes.

The general formulas used in analyzing pressure buildup data come from a solution of the diffusivity equation. In pressure buildup and draw-down analyses, the following assumptions, with regard to the reservoir, fluid, and flow behavior, are usually made:

Reservoir:

- Homogeneous
- Isotropic
- Horizontal of uniform thickness

Fluid:

- Single phase
- Slightly compressible
- Constant μ_o and B_o

Flow:

- Laminar flow
- No gravity effects

Pressure buildup testing requires shutting in a producing well. The most common and the simplest analysis techniques require that the well produce at a constant rate, either from startup or long enough to establish a stabilized pressure distribution, before shut-in. Figure 6-35 schematically shows rate and pressure behavior for an ideal pressure buildup test. In that figure, t_p is the production time and Δt is running shut-in time. The pressure is measured immediately before shut-in and is recorded as a function of time during the shut-in period. The resulting pressure buildup curve is analyzed for reservoir properties and wellbore condition.

Stabilizing the well at a constant rate before testing is an important part of a pressure buildup test. If stabilization is overlooked or is impossible, standard data analysis techniques may provide erroneous information about the formation.

A pressure buildup test is described mathematically by using the principle of superposition. Before the shut-in, the well is allowed to flow at a constant flow rate of Q_0 STB/day for t_p days. At the time corresponding to the point of shut-in, i.e., t_p , a second well, superimposed over the location of the first well, is opened to flow at a constant rate equal to $-Q_0$ STB/day for Δt days. The first well is allowed to continue to flow at $+Q_0$ STB/day. When the effects of the two wells are added, the result is that a well has been allowed to flow at rate Q for time t_p and then shut-in for time Δt . This simulates the actual test procedure. The time corresponding to the point of shut-in, t_p , can be estimated from the following equation:

$$t_p = \frac{24 N_p}{Q_0} \quad (6-175)$$

where N_p = well cumulative oil produced before shut-in, STB

Q_0 = stabilized well flow rate before shut-in, STB/day

t_p = total production time, hr

Applying the superposition principle to a shut-in well, the total pressure change, i.e., $(p_i - p_{ws})$, which occurs at the wellbore during the shut-in time Δt , is essentially the sum of the pressure change caused by the constant flow rate Q and that of $-Q$, or:

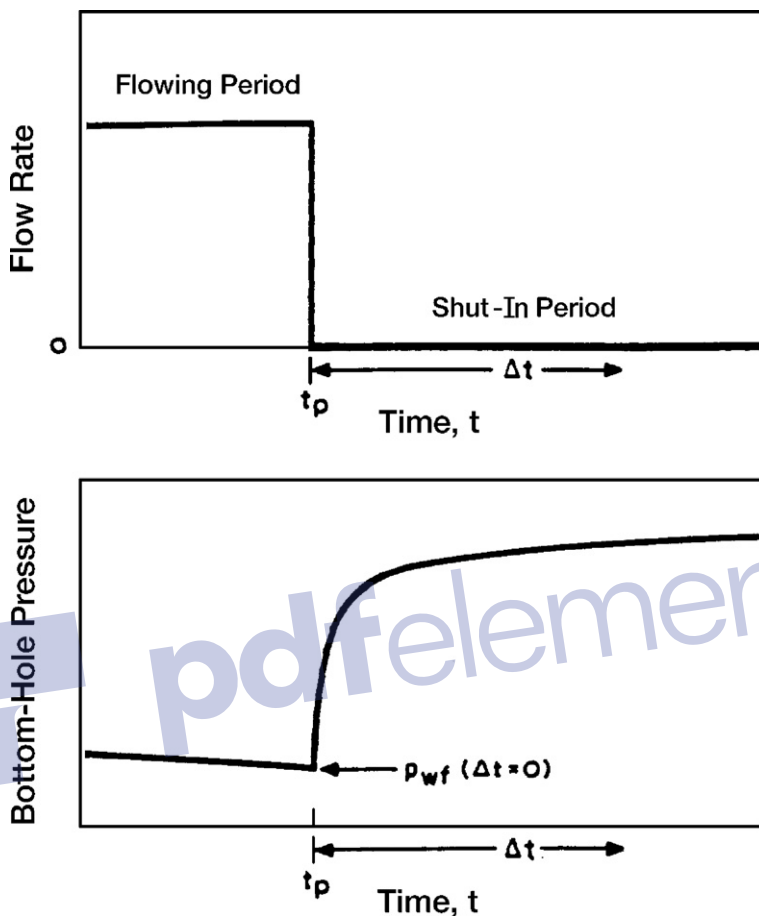


Figure 6-35. Idealized pressure buildup test.

$$p_i - p_{ws} = (p_i - p_{wf})Q_o - 0 + (p_i - p_{wf})0 - Q_o$$

Substituting Equation 6-146 for each of the terms on the right-hand side of the above relationship gives:

$$p_{ws} = p_i - \frac{162.6(Q_o - 0)\mu B_o}{kh} \left[\log \frac{k(t_p + \Delta t)}{\phi \mu c_t r_w^2} - 3.23 + 0.875 s \right] + \frac{162.6(0 - Q_o)\mu B_o}{kh} \left[\log \frac{k(\Delta t)}{\phi \mu c_t r_w^2} - 3.23 + 0.875 s \right] \quad (6-175)$$

Expanding this equation and canceling terms,

$$p_{ws} = p_i - \frac{162.6 Q_o \mu B}{kh} \left[\log \frac{(t_p + \Delta t)}{\Delta t} \right] \quad (6-176)$$

where p_i = initial reservoir pressure, psi

p_{ws} = sand-face pressure during pressure buildup, psi

t_p = flowing time before shut-in, hr

Δt = shut-in time, hr

The pressure buildup equation, i.e., Equation 6-176, was introduced by Horner (1951) and is commonly referred to as the Horner equation.

Equation 6-177 suggests that a plot of p_{ws} versus $(t_p + \Delta t)/\Delta t$ would produce a straight-line relationship with intercept p_i and slope of $-m$, where:

$$m = \frac{162.6 Q_o B_o \mu_o}{kh}$$

or

$$k = \frac{162.6 Q_o B_o \mu_o}{mh} \quad (6-177)$$

This plot, commonly referred to as the Horner plot, is illustrated in Figure 6-36. Note that on the Horner plot, the scale of time ratio increases from left to right. Because of the form of the ratio, however, the shut-in time Δt increases from right to left. It is observed from Equation 6-177 that $p_{ws} = p_i$ when the time ratio is unity. Graphically this means that the initial reservoir pressure, p_i , can be obtained by extrapolating the Horner plot straight line to $(t_p + \Delta t)/\Delta t = 1$.

Earlougher (1977) points out that a result of using the superposition principle is that skin factor, s , does not appear in the general pressure buildup equation, Equation 6-176. As a result, skin factor does not appear in the simplified equation for the Horner plot, Equation 6-177. That means the Horner-plot slope is not affected by the skin factor; however, the skin factor still does affect the shape of the pressure buildup data. In fact, an early-time deviation from the straight line can be caused by skin factor as well as by wellbore storage, as indicated in Figure 6-36. The deviation can be significant for the large negative skins that occur in hydraulically fractured wells. In any case, the skin factor does affect

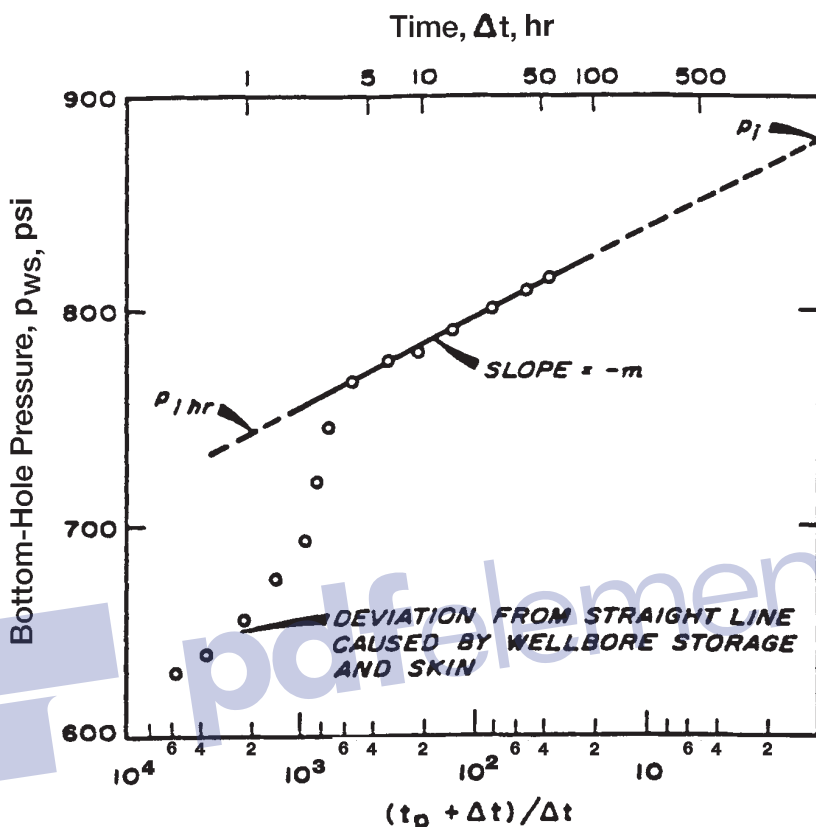


Figure 6-36. Horner plot. (After Earlougher, R. "Advances in Well Test Analysis.") (Permission to publish by the SPE, copyright SPE, 1977.)

flowing pressure before shut-in, so skin may be estimated from the buildup test data plus the flowing pressure immediately before the buildup test:

$$s = 1.151 \left[\frac{p_{1hr} - p_{wf}(\Delta t = 0)}{m} - \log \frac{k}{\phi \mu c_t r_w^2} + 3.23 \right] \quad (6-178)$$

where $p_{wf}(\Delta t = 0)$ = observed flowing bottom-hole pressure immediately before shut-in

m = slope of the Horner plot

k = permeability, md

$$\Delta p_{\text{skin}} = 0.87 \text{ m s} \quad (6-179)$$

The value of $p_{1 \text{ hr}}$ must be taken from the Horner straight line. Frequently, pressure data do not fall on the straight line at 1 hour because of wellbore storage effects or large negative skin factors. In that case, the semilog line must be extrapolated to 1 hour and the corresponding pressure is read.

It should be pointed out that when a well is shut in for a pressure buildup test, the well is usually closed at the surface rather than the sand face. Even though the well is shut-in, the reservoir fluid continues to flow and accumulates in the wellbore until the well fills sufficiently to transmit the effect of shut-in to the formation. This “after-flow” behavior is caused by the wellbore storage, and it has a significant influence on pressure buildup data. During the period of wellbore storage effects, the pressure data points fall below the semilog straight line. The duration of those effects may be estimated by making the log-log data plot described previously. For pressure buildup testing, plot $\log [p_{\text{ws}} - p_{\text{wf}}]$ versus $\log (\Delta t)$. The bottom-hole flow pressure p_{wf} is observed flowing pressure immediately before shut-in. When wellbore storage dominates, that plot will have a unit-slope straight line; as the semilog straight line is approached, the log-log plot bends over to a gently curving line with a low slope.

In all pressure buildup test analyses, the log-log data plot should be made before the straight line is chosen on the semilog data plot. This log-log plot is essential to avoid drawing a semilog straight line through the wellbore storage-dominated data. The beginning of the semilog line can be estimated by observing when the data points on the log-log plot reach the slowly curving low-slope line and adding 1 to 1.5 cycles in time after the end of the unit-slope straight line. Alternatively, the time to the beginning of the semilog straight line can be estimated from:

$$\Delta t > \frac{170,000 C e^{0.14s}}{(kh/\mu)}$$

where Δt = shut-in time, hr

C = calculated wellbore storage coefficient, bbl/psi

k = permeability, md

s = skin factor

h = thickness, ft

Example 6-26³

Table 6-5 shows pressure buildup data from an oil well with an estimated drainage radius of 2,640 ft.

Table 6-5
Earlougher's Pressure Buildup Data
(Permission to publish by the SPE, copyright SPE, 1977)

| Δt (hours) | $t_p + \Delta t$ (hours) | $\frac{(t_p + \Delta t)}{\Delta t}$ | P_{ws} (psig) |
|-----------------------|-----------------------------|-------------------------------------|--------------------|
| 0.0 | — | — | 2761 |
| 0.10 | 310.10 | 3101 | 3057 |
| 0.21 | 310.21 | 1477 | 3153 |
| 0.31 | 310.31 | 1001 | 3234 |
| 0.52 | 310.52 | 597 | 3249 |
| 0.63 | 310.63 | 493 | 3256 |
| 0.73 | 310.73 | 426 | 3260 |
| 0.84 | 310.84 | 370 | 3263 |
| 0.94 | 310.94 | 331 | 3266 |
| 1.05 | 311.05 | 296 | 3267 |
| 1.15 | 311.15 | 271 | 3268 |
| 1.36 | 311.36 | 229 | 3271 |
| 1.68 | 311.68 | 186 | 3274 |
| 1.99 | 311.99 | 157 | 3276 |
| 2.51 | 312.51 | 125 | 3280 |
| 3.04 | 313.04 | 103 | 3283 |
| 3.46 | 313.46 | 90.6 | 3286 |
| 4.08 | 314.08 | 77.0 | 3289 |
| 5.03 | 315.03 | 62.6 | 3293 |
| 5.97 | 315.97 | 52.9 | 3297 |
| 6.07 | 316.07 | 52.1 | 3297 |
| 7.01 | 317.01 | 45.2 | 3300 |
| 8.06 | 318.06 | 39.5 | 3303 |
| 9.00 | 319.00 | 35.4 | 3305 |
| 10.05 | 320.05 | 31.8 | 3306 |
| 13.09 | 323.09 | 24.7 | 3310 |
| 16.02 | 326.02 | 20.4 | 3313 |
| 20.00 | 330.00 | 16.5 | 3317 |
| 26.07 | 336.07 | 12.9 | 3320 |
| 31.03 | 341.03 | 11.0 | 3322 |
| 34.98 | 344.98 | 9.9 | 3323 |
| 37.54 | 347.54 | 9.3 | 3323 |

³This example problem and solution procedure are given by Earlougher, R., "Advanced Well Test Analysis," Monograph Series, SPE, Dallas (1977).

Before shut-in, the well had produced at a stabilized rate of 4,900 STB/day for 310 hours. Known reservoir data are:

$$\begin{aligned} r_e &= 2640 \text{ ft} \\ \text{depth} &= 10476 \text{ ft} \\ r_w &= 0.354 \text{ ft} \\ c_t &= 22.6 \times 10^{-6} \text{ psi}^{-1} \\ Q_o &= 4900 \text{ STB/D} \\ h &= 482 \text{ ft} \\ p_{wf}(\Delta t = 0) &= 2761 \text{ psig} \\ \mu_o &= 0.20 \text{ cp} \\ \phi &= 0.09 \\ B_o &= 1.55 \text{ bbl/STB} \\ \text{casing ID} &= 0.523 \text{ ft} \\ t_p &= 310 \text{ hours} \end{aligned}$$

Calculate

- Average permeability k
- Skin factor
- Pressure drop due to skin

Solution

Step 1. Plot p_{ws} versus $(t_p + \Delta t)/\Delta t$ on a semilog scale as shown in Figure 6-37.

Step 2. Identify the correct straight-line portion of the curve and determine the slope m to give:

$$m = 40 \text{ psi/cycle}$$

Step 3. Calculate the average permeability by using Equation 6-178 to give:

$$k = \frac{(162.6)(4,900)(1.55)(0.22)}{(40)(482)} = 12.8 \text{ md}$$

Step 4. Determine p_{wf} after 1 hour from the straight-line portion of the curve to give:

$$p_{1 \text{ hr}} = 3266 \text{ psi}$$

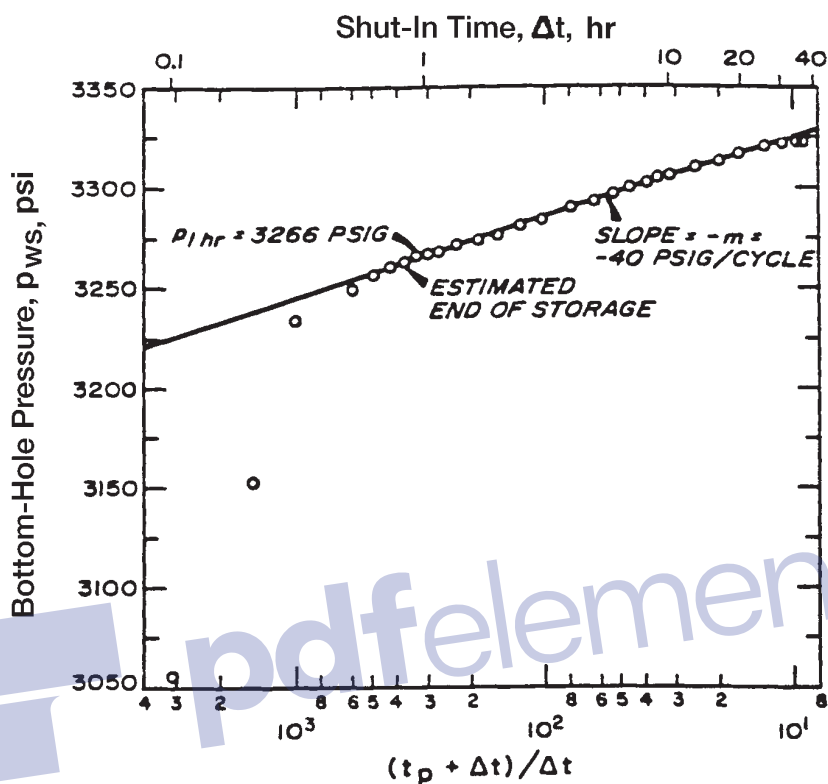


Figure 6-37. Earlougher's semilog data plot for the buildup test. (Permission to publish by the SPE, copyright SPE, 1977.)

Step 5. Calculate the skin factor by applying Equation 6-179.

$$s = 1.1513 \left[\frac{3,266 - 2,761}{40} - \log \left(\frac{(12.8)(12)^2}{(0.09)(0.20)(22.6 \times 10^{-6})(4.25)^2} \right) + 3.23 \right] = 8.6$$

Step 6. Calculate the pressure drop due to skin from:

$$\Delta p_{\text{skin}} = 0.87ms = 0.87(40)(8.6) = 299 \text{ psia}$$

PROBLEMS

1. An incompressible fluid flows in a linear porous media with the following properties.

$$\begin{array}{lll}
 L = 2500 \text{ ft} & h = 30 \text{ ft} & \text{width} = 500 \text{ ft} \\
 k = 50 \text{ md} & \phi = 17\% & \mu = 2 \text{ cp} \\
 \text{inlet pressure} = 2100 \text{ psi} & Q = 4 \text{ bbl/day} & \rho = 45 \text{ lb/ft}^3
 \end{array}$$

Calculate and plot the pressure profile throughout the linear system.

2. Assume the reservoir linear system as described in problem 1 is tilted with a dip angle of 7° . Calculate the fluid potential through the linear system.
3. A 0.7 specific gravity gas is flowing in a linear reservoir system at 150°F . The upstream and downstream pressures are 2,000 and 1,800 psi, respectively. The system has the following properties:

$$\begin{array}{lll}
 L = 2000 \text{ ft} & W = 300 \text{ ft} & h = 15 \text{ ft} \\
 k = 40 \text{ md} & \phi = 15\% &
 \end{array}$$

Calculate the gas flow rate.

4. An oil well is producing a crude oil system at 1,000 STB/day and 2,000 psi of bottom-hole flowing pressure. The pay zone and the producing well have the following characteristics:

$$\begin{array}{lll}
 h = 35 \text{ ft} & r_w = 0.25 \text{ ft} & \text{drainage area} = 40 \text{ acres} \\
 \text{API} = 45^\circ & \gamma_g = 0.72 & R_s = 700 \text{ scf/STB} \\
 k = 80 \text{ md} & T = 100^\circ\text{F} &
 \end{array}$$

Assuming steady-state flowing conditions, calculate and plot the pressure profile around the wellbore.

5. Assuming steady-state flow and incompressible fluid, calculate the oil flow rate under the following conditions:

$$\begin{array}{lll}
 p_e = 2500 \text{ psi} & p_{wf} = 2000 \text{ psi} & r_e = 745 \text{ ft} \\
 r_w = 0.3 \text{ ft} & \mu_o = 2 \text{ cp} & B_o = 1.4 \text{ bbl/STB} \\
 h = 30 \text{ ft} & k = 60 \text{ md} &
 \end{array}$$

6. A gas well is flowing under a bottom-hole flowing pressure of 900 psi. The current reservoir pressure is 1,300 psi. The following additional data are available:

$$\begin{array}{lll} T = 140^{\circ}\text{F} & \gamma_g = 0.65 & r_w = 0.3 \text{ ft} \\ k = 60 \text{ md} & h = 40 \text{ ft} & r_e = 1000 \text{ ft} \end{array}$$

Calculate the gas flow rate by using a:

- Real gas pseudo pressure approach
 - Pressure-squared method
7. An oil well is producing a stabilized flow rate of 500 STB/day under a transient flow condition. Given:

$$\begin{array}{lll} B_o = 1.1 \text{ bbl/STB} & \mu_o = 2 \text{ cp} & c_t = 15 \times 10^{-6} \text{ psi}^{-1} \\ k_o = 50 \text{ md} & h = 20 \text{ ft} & \phi = 20\% \\ r_w = 0.3 \text{ ft} & p_i = 3500 \text{ psi} & \end{array}$$

Calculate and plot the pressure profile after 1, 5, 10, 15, and 20 hours.

8. An oil well is producing at a constant flow rate of 800 STB/day under a transient flow condition. The following data are available:

$$\begin{array}{lll} B_o = 1.2 \text{ bbl/STB} & \mu_o = 3 \text{ cp} & c_t = 15 \times 10^{-6} \text{ psi}^{-1} \\ k_o = 100 \text{ md} & h = 25 \text{ ft} & \phi = 15\% \\ r_w = 0.5 & p_i = 4000 \text{ psi} & r_e = 1000 \text{ ft} \end{array}$$

Using the E_i -function approach and the p_D -method, calculate the bottom-hole flowing pressure after 1, 2, 3, 5, and 10 hr. Plot the results on a semi log scale and Cartesian scale.

9. A well is flowing under a drawdown pressure of 350 psi and produces at a constant flow rate of 300 STB/day. The net thickness is 25 ft. Given:

$$r_e = 660 \text{ ft} \quad r_w = 0.25 \text{ ft} \quad \mu_o = 1.2 \text{ cp} \quad B_o = 1.25 \text{ bbl/STB}$$

Calculate:

- Average permeability
- Capacity of the formation

10. An oil well is producing from the center of 40-acre-square drilling pattern. Given:

$$\begin{array}{lll} \phi = 20\% & h = 15 \text{ ft} & k = 60 \text{ md} \\ \mu_o = 1.5 \text{ cp} & B_o = 1.4 \text{ bbl/STB} & r_w = 0.25 \text{ ft} \\ p_r = 2000 \text{ psi} & p_{wf} = 1500 \text{ psi} & \end{array}$$

Calculate the oil flow rate.

11. A shut-in well is located at a distance of 700 ft from one well and 1100 ft from a second well. The first well flows for 5 days at 180 STB/day, at which time the second well begins to flow at 280 STB/day. Calculate the pressure drop in the shut-in well when the second well has been flowing for 7 days. The following additional data are given:

$$\begin{array}{llll} p_i = 3000 \text{ psi} & B_o = 1.3 \text{ bbl/STB} & \mu_o = 1.2 \text{ cp} & h = 60 \text{ ft} \\ c_t = 15 \times 10^{-6} \text{ psi}^{-1} & \phi = 15\% & k = 45 \text{ md} & \end{array}$$

12. A well is opened to flow at 150 STB/day for 24 hours. The flow rate is then increased to 360 STB/day and lasted for another 24 hours. The well flow rate is then reduced to 310 STB/day for 16 hours. Calculate the pressure drop in a shut-in well 700 ft away from the well given:

$$\begin{array}{lll} \phi = 15\% & h = 20 \text{ ft} & k = 100 \text{ md} \\ \mu_o = 2 \text{ cp} & B_o = 1.2 \text{ bbl/STB} & r_w = 0.25 \text{ ft} \\ p_i = 3000 \text{ psi} & c_t = 12 \times 10^{-6} \text{ psi}^{-1} & \end{array}$$

13. A well is flowing under unsteady-state flowing conditions for 5 days at 300 STB/day. The well is located at 350 ft and 420 ft distance from two sealing faults. Given:

$$\begin{array}{lll} \phi = 17\% & c_t = 16 \times 10^{-6} \text{ psi}^{-1} & k = 80 \text{ md} \\ p_i = 3000 \text{ psi} & B_o = 1.3 \text{ bbl/STB} & \mu_o = 1.1 \text{ cp} \\ r_w = 0.25 \text{ ft} & h = 25 \text{ ft} & \end{array}$$

Calculate the pressure in the well after 5 days.

14. A drawdown test was conducted on a new well with results as given below:

| $t, \text{ hr}$ | $p_{wfr}, \text{ psi}$ |
|-----------------|------------------------|
| 1.50 | 2978 |
| 3.75 | 2949 |
| 7.50 | 2927 |
| 15.00 | 2904 |
| 37.50 | 2876 |
| 56.25 | 2863 |
| 75.00 | 2848 |
| 112.50 | 2810 |
| 150.00 | 2790 |
| 225.00 | 2763 |

Given:

$$p_i = 3400 \text{ psi}$$

$$c_t = 18 \times 10^{-6} \text{ psi}^{-1}$$

$$r_w = 0.25 \text{ ft}$$

$$h = 25 \text{ ft}$$

$$\mu_o = 1.8 \text{ cp}$$

$$\phi = 12\%$$

$$Q = 300 \text{ STB/day}$$

$$B_o = 1.1 \text{ bbl/STB}$$

Assuming no wellbore storage, calculate:

- Average permeability
- Skin factor

15. A drawdown test was conducted on a discovery well. The well was flowed at a constant flow rate of 175 STB/day. The fluid and reservoir data are given below:

$$S_{wi} = 25\%$$

$$r_w = 0.25 \text{ ft}$$

$$\phi = 15\%$$

$$p_i = 4680 \text{ psi}$$

$$h = 30 \text{ ft}$$

$$\mu_o = 1.5 \text{ cp}$$

$$c_t = 18 \times 10^{-6} \text{ psi}^{-1}$$

$$B_o = 1.25 \text{ bbl/STB}$$

The drawdown test data are given below:

| $t, \text{ hr}$ | $p_{wf}, \text{ psi}$ |
|-----------------|-----------------------|
| 0.6 | 4388 |
| 1.2 | 4367 |
| 1.8 | 4355 |
| 2.4 | 4344 |
| 3.6 | 4334 |
| 6.0 | 4318 |
| 8.4 | 4309 |
| 12.0 | 4300 |
| 24.0 | 4278 |
| 36.0 | 4261 |
| 48.0 | 4258 |
| 60.0 | 4253 |
| 72.0 | 4249 |
| 84.0 | 4244 |
| 96.0 | 4240 |
| 108.0 | 4235 |
| 120.0 | 4230 |
| 144.0 | 4222 |
| 180.0 | 4206 |

Calculate:

- Drainage radius
- Skin factor
- Oil flow rate at a bottom-hole flowing pressure of 4,300 psi, assuming a semisteady-state flowing condition.

16. A pressure build up test was conducted on a well that had been producing at 146 STB/day for 53 hours. The reservoir and fluid data are given below.

$$B_o = 1.29 \text{ bbl/STB}$$

$$\phi = 10\%$$

$$\mu_o = 0.85 \text{ cp}$$

$$p_{wf} = 1426.9 \text{ psig}$$

$$c_t = 12 \times 10^{-6} \text{ psi}^{-1}$$

$$A = 20 \text{ acres}$$

The build up data are as follows:

| Time, hr | P_{wsr} psig |
|----------|----------------|
| 0.167 | 1451.5 |
| 0.333 | 1476.0 |
| 0.500 | 1498.6 |
| 0.667 | 1520.1 |
| 0.833 | 1541.5 |
| 1.000 | 1561.3 |
| 1.167 | 1581.9 |
| 1.333 | 1599.7 |
| 1.500 | 1617.9 |
| 1.667 | 1635.3 |
| 2.000 | 1665.7 |
| 2.333 | 1691.8 |
| 2.667 | 1715.3 |
| 3.000 | 1736.3 |
| 3.333 | 1754.7 |
| 3.667 | 1770.1 |
| 4.000 | 1783.5 |
| 4.500 | 1800.7 |
| 5.000 | 1812.8 |
| 5.500 | 1822.4 |
| 6.000 | 1830.7 |
| 6.500 | 1837.2 |
| 7.000 | 1841.1 |
| 7.500 | 1844.5 |
| 8.000 | 1846.7 |
| 8.500 | 1849.6 |
| 9.000 | 1850.4 |
| 10.000 | 1852.7 |
| 11.000 | 1853.5 |
| 12.000 | 1854.0 |
| 12.667 | 1854.0 |
| 14.620 | 1855.0 |

Calculate:

- Average reservoir pressure
- Skin factor
- Formation capacity

REFERENCES

1. Al-Hussainy, R., and Ramey, H. J., Jr., "Application of Real Gas Flow Theory to Well Testing and Deliverability Forecasting," *Jour. of Petroleum Technology*, May 1966; *Theory and Practice of the Testing of Gas Wells*, 3rd ed. Calgary, Canada: Energy Resources Conservation Board, 1975.
2. Al-Hussainy, R., Ramey, H. J., Jr., and Crawford, P. B., "The Flow of Real Gases Through Porous Media," *Trans. AIME*, 1966, pp. 237, 624.
3. Chatas, A. T., "A Practical Treatment of Nonsteady-state Flow Problems in Reservoir Systems," *Pet. Eng.*, Aug 1953, pp. B-44–56.
4. Craft, B., Hawkins, M., and Terry, R., *Applied Petroleum Reservoir Engineering*, 2nd ed. Prentice Hall, 1990.
5. Craft, B., and Hawkins, M., *Applied Petroleum Reservoir Engineering*. Prentice-Hall, 1959.
6. Dake, L. P., *The Practice of Reservoir Engineering*. Amsterdam: Elsevier, 1994.
7. Dake, L., *Fundamentals of Reservoir Engineering*. Amsterdam: Elsevier, 1978.
8. Davis, D. H., "Reduction in Permeability with Overburden Pressure," *Trans. AIME*, 1952, pp. 195, 329.
9. Donohue, D., and Erkekin, T., "Gas Well Testing, Theory and Practice," *IHRDC*, 1982.
10. Earlougher, Robert C., Jr., *Advances in Well Test Analysis*, Monograph Vol. 5, Society of Petroleum Engineers of AIME. Dallas, TX: Millet the Printer, 1977.
11. Fetkovich, M. J., "The Isochronal Testing of Oil Wells," SPE Paper 4529, presented at the SPE Annual Meeting, Las Vegas, September 30–October 3, 1973.
12. Golan, M., and Whitson, C., *Well Performance*, 2nd ed. Englewood Cliffs, NJ: Prentice-Hall, 1986.
13. Hawkins, M., "A Note on the Skin Effect," *Trans. AIME*, 1956, pp. 356.
14. Horne, R., *Modern Well Test Analysis*. Palo Alto, CA: Petroway, Inc., 1995.
15. Horner, D. R., "Pressure Build-Up in Wells," Proc., Third World Pet. Cong., The Hague (1951), Sec II, 503–523. Also *Reprint Series, No. 9—Pressure Analysis Methods*, pp. 25–43. Dallas: Society of Petroleum Engineers of AIME, 1967.
16. Hurst, W., "Establishment of the Skin Effect and Its Impediment to Fluid Flow into a Wellbore," *Petroleum Engineering*, Oct. 1953, p. 25, B-6.

17. Jones, S. C., "Using the Inertial Coefficient, b , to Characterize Heterogeneity in Reservoir Rock," SPE Paper 16949, presented at the SPE Conference, Dallas, TX, Sept. 27–30, 1987.
18. Joshi, S., *Horizontal Well Technology*. Pennwell Publishing Company, 1991.
19. Lee, J., and Wattenbarger, R., *Gas Reservoir Engineering*. SPE Textbook Series Vol. 5, SPE, 1996.
20. Lee, John W., *Well Testing*. Dallas: Society of Petroleum Engineers Textbook Series, 1982.
21. Matthews, S., Bronz, F., and Hazebroek, P. "A Method for the Determination of Average Pressure in a Bounded Reservoir," *Trans. AIME*, 1954, Vol. 201, pp. 82–191.
22. Matthews, C. S., and Russell, D. G., "Pressure Buildup and Flow Tests in Wells," Monograph Vol. 1, Society of Petroleum Engineers of AIME. Dallas, TX: Millet the Printer, 1967.
23. Ramey, H., and Cobb, W., "A General Pressure Buildup Theory for a Well in a Closed Drainage Area," *JPT*, December 1971, pp. 1493–1505.
24. Russell, D. G., Goodrich, J. H., Perry, G. E., and Bruskotter, J. F., "Methods for Predicting Gas Well Performance," *JPT*, Jan. 1966, pp. 99–108; *Trans. AIME*, p. 237.
25. Slider, H. C., *Practical Petroleum Reservoir Engineering Methods*. Tulsa, OK: Petroleum Publishing Co., 1976.
26. van Everdingen, A. F., "The Skin Effect and Its Influence on the Productive Capacity of a Well," *Trans. AIME*, 1953, pp. 171, 198.
27. van Everdingen, A. F., and Hurst, W., "The Application of the Laplace Transformation to Flow Problems in Reservoirs," *Trans. AIME*, 1949, pp. 186, 305–324.
28. Wattenbarger, Robert A., and Ramey, H. J., Jr., "Gas Well Testing With Turbulence. Damage and Wellbore Storage," *JPT*, 1968, pp. 877–887; *Trans. AIME*, p. 243.

C H A P T E R 7

OIL WELL PERFORMANCE

This chapter presents the practical reservoir engineering equations that are designed to predict the performance of vertical and horizontal oil wells. The chapter also describes some of the factors that are governing the flow of fluids from the formation to the wellbore and how these factors may affect the production performance of the well. The analysis of the production performance is essentially based on the following fluid and well characteristics:

- Fluid PVT properties
- Relative permeability data
- Inflow-performance-relationship (IPR)

VERTICAL OIL WELL PERFORMANCE

Productivity Index and IPR

A commonly used measure of the ability of the well to produce is the **productivity index**. Defined by the symbol J , the productivity index is the ratio of the total liquid flow rate to the pressure drawdown. For a water-free oil production, the productivity index is given by:

$$J = \frac{Q_o}{p_r - p_{wf}} = \frac{Q_o}{\Delta p} \quad (7-1)$$

where Q_o = oil flow rate, STB/day

J = productivity index, STB/day/psi

\bar{p}_r = volumetric average drainage area pressure (static pressure)

p_{wf} = bottom-hole flowing pressure
 Δp = drawdown, psi

The productivity index is generally measured during a production test on the well. The well is shut-in until the static reservoir pressure is reached. The well is then allowed to produce at a constant flow rate of Q and a stabilized bottom-hole flow pressure of p_{wf} . Since a stabilized pressure at surface does not necessarily indicate a stabilized p_{wf} , the bottom-hole flowing pressure should be recorded continuously from the time the well is to flow. The productivity index is then calculated from Equation 7-1.

It is important to note that the productivity index is a valid measure of the well productivity potential only if the well is flowing at pseudosteady-state conditions. Therefore, in order to accurately measure the productivity index of a well, it is essential that the well is allowed to flow at a constant flow rate for a sufficient amount of time to reach the pseudosteady-state as illustrated in Figure 7-1. The figure indicates that during the transient flow period, the calculated values of the productivity index will vary depending upon the time at which the measurements of p_{wf} are made.

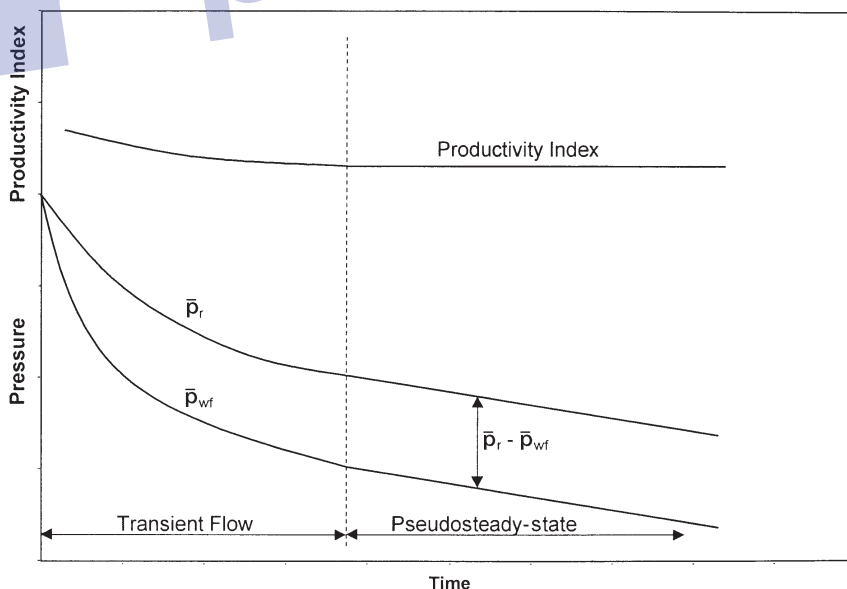


Figure 7-1. Productivity index during flow regimes.

The productivity index can be numerically calculated by recognizing that J must be defined in terms of semisteady-state flow conditions. Recalling Equation 6-149:

$$Q_o = \frac{0.00708 k_o h (\bar{p}_r - p_{wf})}{\mu_o B_o \left[\ln \left(\frac{r_c}{r_w} \right) - 0.75 + s \right]} \quad (7-2)$$

The above equation is combined with Equation 7-1 to give:

$$J = \frac{0.00708 k_o h}{\mu_o B_o \left[\ln \left(\frac{r_c}{r_w} \right) - 0.75 + s \right]} \quad (7-3)$$

where J = productivity index, STB/day/psi

k_o = effective permeability of the oil, md

s = skin factor

h = thickness, ft

The oil relative permeability concept can be conveniently introduced into Equation 7-3 to give:

$$J = \frac{0.00708 h k}{\left[\ln \left(\frac{r_c}{r_w} \right) - 0.75 + s \right]} \left(\frac{k_{ro}}{\mu_o B_o} \right) \quad (7-4)$$

Since most of the well life is spent in a flow regime that is approximating the pseudosteady-state, the productivity index is a valuable methodology for predicting the future performance of wells. Further, by monitoring the productivity index during the life of a well, it is possible to determine if the well has become damaged due to completion, workover, production, injection operations, or mechanical problems. If a measured J has an unexpected decline, one of the indicated problems should be investigated.

A comparison of productivity indices of different wells in the same reservoir should also indicate some of the wells might have experienced unusual difficulties or damage during completion. Since the productivity

indices may vary from well to well because of the variation in thickness of the reservoir, it is helpful to normalize the indices by dividing each by the thickness of the well. This is defined as the **specific productivity index J_s** , or:

$$J_s = \frac{J}{h} = \frac{Q_o}{h(\bar{p}_r - p_{wf})} \quad (7-5)$$

Assuming that the well's productivity index is constant, Equation 7-1 can be rewritten as:

$$Q_o = J(\bar{p}_r - p_{wf}) = J\Delta p \quad (7-6)$$

where Δp = drawdown, psi

J = productivity index

Equation 7-6 indicates that the relationship between Q_o and Δp is a straight line passing through the origin with a slope of J as shown in Figure 7-2.

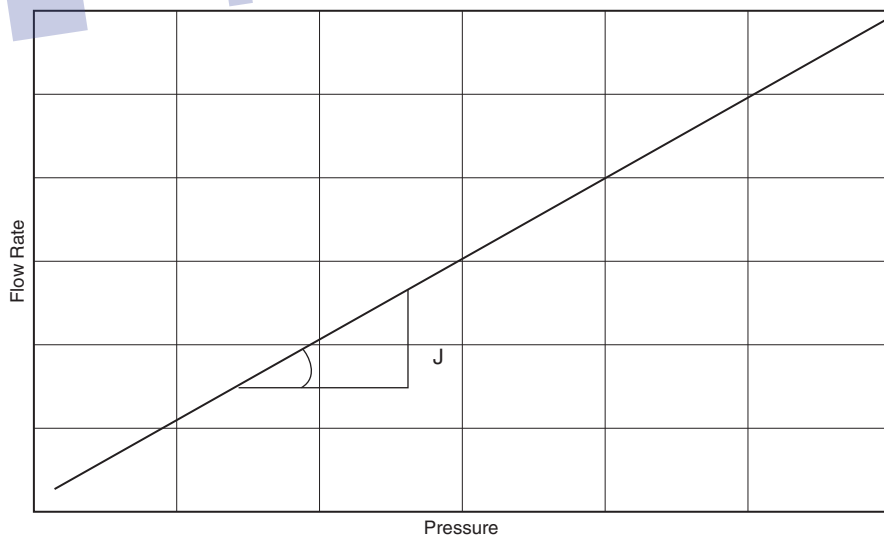


Figure 7-2. Q_o vs. Δp relationship.

Alternatively, Equation 7-1 can be written as:

$$p_{wf} = \bar{p}_r - \left(\frac{1}{J}\right) Q_o \quad (7-7)$$

The above expression shows that the plot p_{wf} against Q_o is a straight line with a slope of $(-1/J)$ as shown schematically in Figure 7-3. This graphical representation of the relationship that exists between the oil flow rate and bottom-hole flowing pressure is called the **inflow performance relationship** and referred to as **IPR**.

Several important features of the straight-line IPR can be seen in Figure 7-3:

- When p_{wf} equals average reservoir pressure, the flow rate is zero due to the absence of any pressure drawdown.
- Maximum rate of flow occurs when p_{wf} is zero. This maximum rate is called **absolute open flow** and referred to as **AOF**. Although in practice this may not be a condition at which the well can produce, it is a useful definition that has widespread applications in the petroleum industry

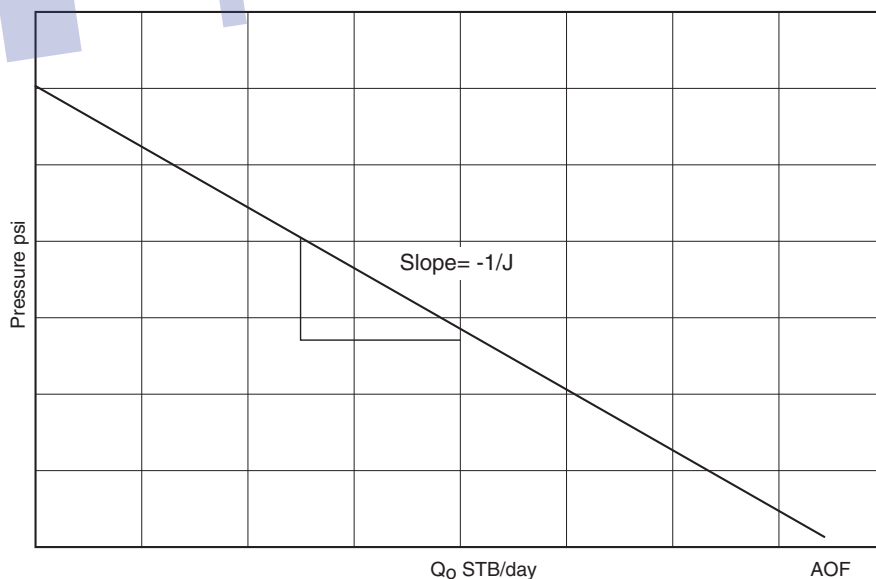


Figure 7-3. IPR.

(e.g., comparing flow potential of different wells in the field). The AOF is then calculated by:

$$\text{AOF} = J \bar{p}_r$$

- The slope of the straight line equals the reciprocal of the productivity index.

Example 7-1

A productivity test was conducted on a well. The test results indicate that the well is capable of producing at a stabilized flow rate of 110 STB/day and a bottom-hole flowing pressure of 900 psi. After shutting the well for 24 hours, the bottom-hole pressure reached a static value of 1,300 psi.

Calculate:

- Productivity index
- AOF
- Oil flow rate at a bottom-hole flowing pressure of 600 psi
- Wellbore flowing pressure required to produce 250 STB/day

Solution

- a. Calculate J from Equation 7-1:

$$J = \frac{110}{1300 - 900} = 0.275 \text{ STB/psi}$$

- b. Determine the AOF from:

$$\text{AOF} = J (\bar{p}_r - 0)$$

$$\text{AOF} = 0.275 (1300 - 0) = 375.5 \text{ STB/day}$$

- c. Solve for the oil flow rate by applying Equation 7-1:

$$Q_o = 0.275 (1300 - 600) = 192.5 \text{ STB/day}$$

- d. Solve for p_{wf} by using Equation 7-7:

$$p_{wf} = 1300 - \left(\frac{1}{0.275} \right) 250 = 390.9 \text{ psi}$$

Equation 7-6 suggests that the inflow into a well is directly proportional to the pressure drawdown and the constant of proportionality is the productivity index. Muskat and Evinger (1942) and Vogel (1968) observed that when the pressure drops below the bubble-point pressure, the IPR deviates from that of the simple straight-line relationship as shown in Figure 7-4.

Recalling Equation 7-4:

$$J = \left[\frac{0.00708 h k}{\ln\left(\frac{r_e}{r_w}\right) - 0.75 + s} \right] \left(\frac{k_{ro}}{\mu_o B_o} \right)$$

Treating the term between the two brackets as a constant c , the above equation can be written in the following form:

$$J = c \left(\frac{k_{ro}}{\mu_o B_o} \right) \quad (7-8)$$

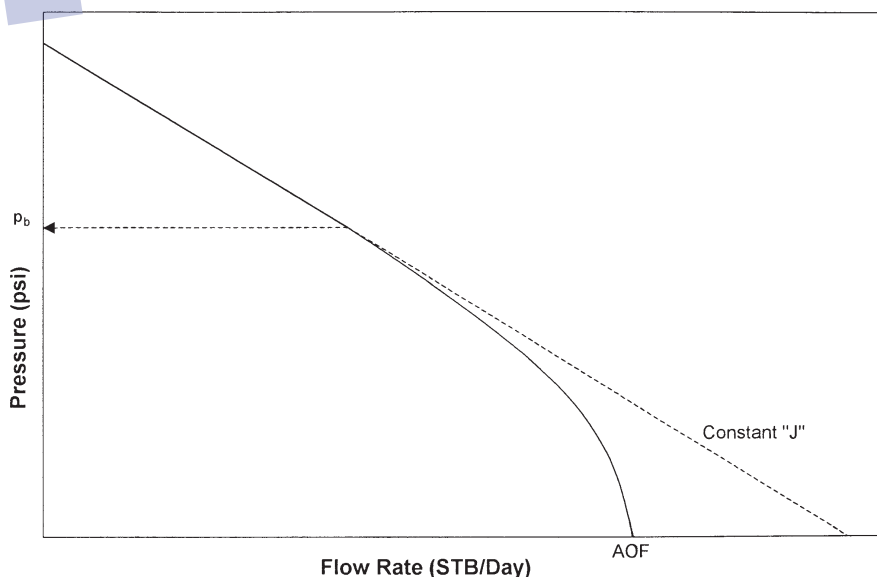


Figure 7-4. IPR below p_b .

with the coefficient c as defined by:

$$c = \frac{0.00708 k h}{\ln\left(\frac{r_e}{r_w}\right) - 0.75 + s}$$

Equation 7-8 reveals that the variables affecting the productivity index are essentially those that are pressure dependent, i.e.:

- Oil viscosity μ_o
- Oil formation volume factor B_o
- Relative permeability to oil k_{ro}

Figure 7-5 schematically illustrates the behavior of those variables as a function of pressure. Figure 7-6 shows the overall effect of changing the pressure on the term $(k_{ro}/\mu_o B_o)$. Above the bubble-point pressure p_b , the relative oil permeability k_{ro} equals unity ($k_{ro} = 1$) and the term $(k_{ro}/\mu_o B_o)$ is almost constant. As the pressure declines below p_b , the gas is released

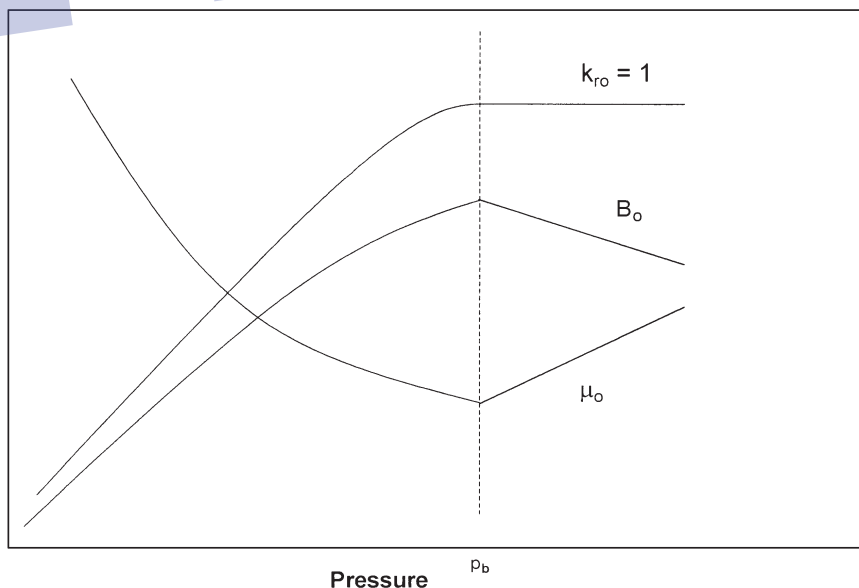


Figure 7-5. Effect of pressure on B_o , μ_o , and k_{ro} .

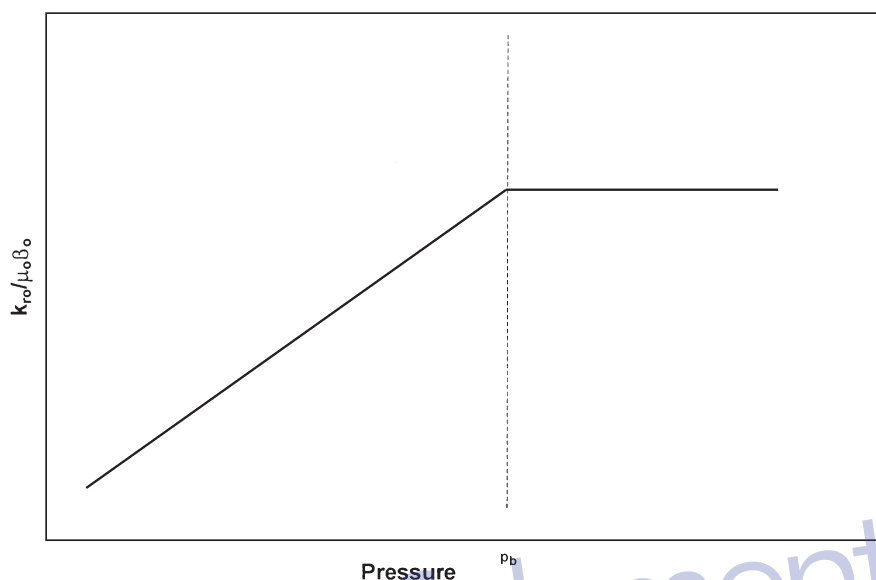


Figure 7-6. $k_{ro}/\mu_o B_o$ as a function of pressure.

from solution, which can cause a large decrease in both k_{ro} and $(k_{ro}/\mu_o B_o)$. Figure 7-7 shows qualitatively the effect of reservoir depletion on the IPR.

There are several empirical methods that are designed to predict the non-linearity behavior of the IPR for solution gas drive reservoirs. Most of these methods require at least one stabilized flow test in which Q_o and p_{wf} are measured. All the methods include the following two computational steps:

- Using the stabilized flow test data, construct the IPR curve at the current average reservoir pressure \bar{p}_r .
- Predict future inflow performance relationships as to the function of average reservoir pressures.

The following empirical methods that are designed to generate the current and future inflow performance relationships:

- Vogel's method
- Wiggins' method
- Standing's method
- Fetkovich's method
- The Klins-Clark method

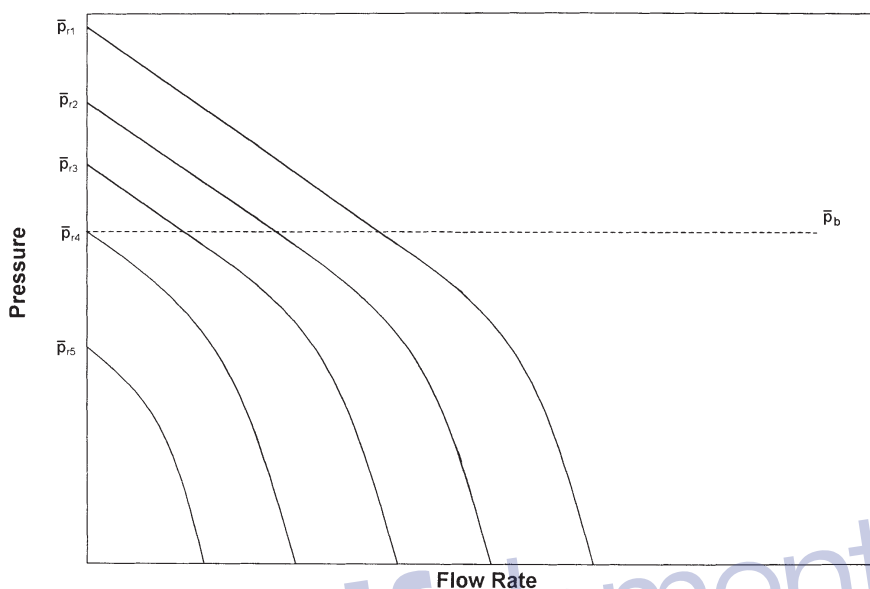


Figure 7-7. Effect of reservoir pressure on IPR.

Vogel's Method

Vogel (1968) used a computer model to generate IPRs for several hypothetical saturated oil reservoirs that are producing under a wide range of conditions. Vogel normalized the calculated IPRs and expressed the relationships in a dimensionless form. He normalized the IPRs by introducing the following dimensionless parameters:

$$\text{dimensionless pressure} = \frac{p_{wf}}{\bar{p}_r}$$

$$\text{dimensionless pressure} = \frac{Q_o}{(Q_o)_{\max}}$$

where $(Q_o)_{\max}$ is the flow rate at zero wellbore pressure, i.e., AOF.

Vogel plotted the dimensionless IPR curves for all the reservoir cases and arrived at the following relationship between the above dimensionless parameters:

$$\frac{Q_o}{(Q_o)_{\max}} = 1 - 0.2 \left(\frac{p_{wf}}{\bar{p}_r} \right) - 0.8 \left(\frac{p_{wf}}{\bar{p}_r} \right)^2 \quad (7-9)$$

where Q_o = oil rate at p_{wf}

$(Q_o)_{\max}$ = maximum oil flow rate at zero wellbore pressure, i.e., AOF

\bar{p}_r = current average reservoir pressure, psig

p_{wf} = wellbore pressure, psig

Notice that p_{wf} and \bar{p}_r must be expressed in psig.

Vogel's method can be extended to account for water production by replacing the dimensionless rate with $Q_L/(Q_L)_{\max}$ where $Q_L = Q_o + Q_w$. This has proved to be valid for wells producing at water cuts as high as 97%. The method requires the following data:

- Current average reservoir pressure \bar{p}_r
- Bubble-point pressure p_b
- Stabilized flow test data that include Q_o at p_{wf}

Vogel's methodology can be used to predict the IPR curve for the following two types of reservoirs:

- Saturated oil reservoirs $\bar{p}_r \leq p_b$
- Undersaturated oil reservoirs $\bar{p}_r > p_b$

Saturated Oil Reservoirs

When the reservoir pressure equals the bubble-point pressure, the oil reservoir is referred to as a *saturated oil reservoir*. The computational procedure of applying Vogel's method in a saturated oil reservoir to generate the IPR curve for a well with a stabilized flow data point, i.e., a recorded Q_o value at p_{wf} , is summarized below:

Step 1. Using the stabilized flow data, i.e., Q_o and p_{wf} , calculate:

$(Q_o)_{\max}$ from Equation 7-9, or

$$(Q_o)_{\max} = Q_o / \left[1 - 0.2 \left(\frac{p_{wf}}{p_r} \right) - 0.8 \left(\frac{p_{wf}}{p_r} \right)^2 \right]$$

Step 2. Construct the IPR curve by assuming various values for p_{wf} and calculating the corresponding Q_o from:

$$Q_o = (Q_o)_{\max} \left[1 - 0.2 \left(\frac{p_{wf}}{p_r} \right) - 0.8 \left(\frac{p_{wf}}{p_r} \right)^2 \right]$$

Example 7-2

A well is producing from a saturated reservoir with an average reservoir pressure of 2,500 psig. Stabilized production test data indicated that the stabilized rate and wellbore pressure are 350 STB/day and 2,000 psig, respectively. Calculate:

- Oil flow rate at $p_{wf} = 1850$ psig
- Calculate oil flow rate assuming constant J
- Construct the IPR by using Vogel's method and the constant productivity index approach.

Solution

Part A.

Step 1. Calculate $(Q_o)_{\max}$:

$$\begin{aligned} (Q_o)_{\max} &= 350 / \left[1 - 0.2 \left(\frac{2000}{2500} \right) - 0.8 \left(\frac{2000}{2500} \right)^2 \right] \\ &= 1067.1 \text{ STB/day} \end{aligned}$$

Step 2. Calculate Q_o at $p_{wf} = 1850$ psig by using Vogel's equation

$$Q_o = (Q_o)_{\max} \left[1 - 0.2 \left(\frac{p_{wf}}{p_r} \right) - 0.8 \left(\frac{p_{wf}}{p_r} \right)^2 \right]$$

$$= 1067.1 \left[1 - 0.2 \left(\frac{1850}{2500} \right) - 0.8 \left(\frac{1850}{2500} \right)^2 \right] = 441.7 \text{ STB/day}$$

Part B.

Calculating oil flow rate by using the constant J approach

Step 1. Apply Equation 7-1 to determine J

$$J = \frac{350}{2500 - 2000} = 0.7 \text{ STB/day/psi}$$

Step 2. Calculate Q_o

$$Q_o = J (\bar{p}_r - p_{wf}) = 0.7 (2500 - 1850) = 455 \text{ STB/day}$$

Part C.

Generating the IPR by using the constant J approach and Vogel's method:

Assume several values for p_{wf} and calculate the corresponding Q_o .

| p_{wf} | Vogel's | $Q_o = J (\bar{p}_r - p_{wf})$ |
|----------|---------|--------------------------------|
| 2500 | 0 | 0 |
| 2200 | 218.2 | 210 |
| 1500 | 631.7 | 700 |
| 1000 | 845.1 | 1050 |
| 500 | 990.3 | 1400 |
| 0 | 1067.1 | 1750 |

Undersaturated Oil Reservoirs

Beggs (1991) pointed out that in applying Vogel's method for undersaturated reservoirs, there are **two possible outcomes to the recorded stabilized flow test data** that must be considered, as shown schematically in Figure 7-8:

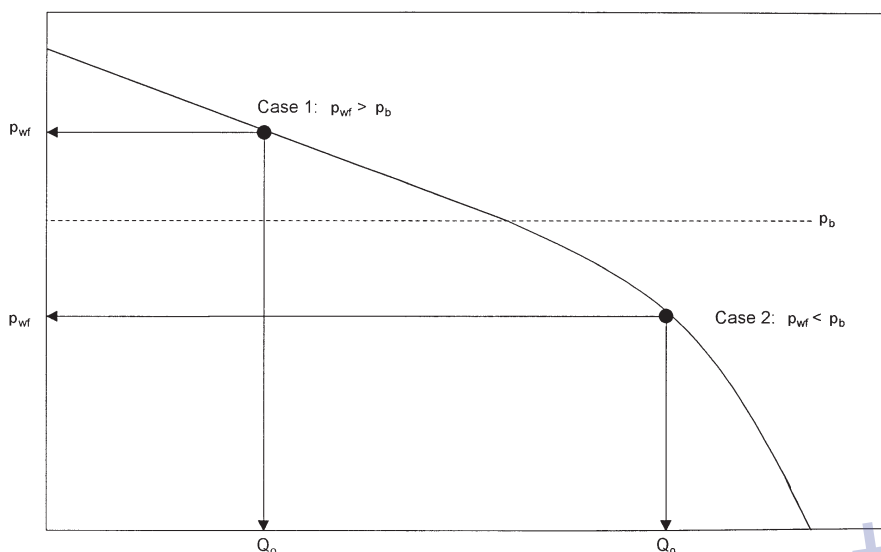


Figure 7-8. Stabilized flow test data.

- The recorded stabilized bottom-hole flowing pressure is greater than or equal to the bubble-point pressure, i.e. $p_{wf} \geq p_b$
- The recorded stabilized bottom-hole flowing pressure is less than the bubble-point pressure $p_{wf} < p_b$

Case 1. The Value of the Recorded Stabilized $p_{wf} \geq p_b$

Beggs outlined the following procedure for determining the IPR when the stabilized bottom-hole pressure is greater than or equal to the bubble-point pressure (Figure 7-8):

Step 1. Using the stabilized test data point (Q_o and p_{wf}) calculate the productivity index J :

$$J = \frac{Q_o}{\bar{p}_r - p_{wf}}$$

Step 2. Calculate the oil flow rate at the bubble-point pressure:

$$Q_{ob} = J (\bar{p}_r - P_b) \quad (7-10)$$

where Q_{ob} is the oil flow rate at p_b

Step 3. Generate the IPR values below the bubble-point pressure by assuming different values of $p_{wf} < p_b$ and calculating the corresponding oil flow rates by applying the following relationship:

$$Q_o = Q_{ob} + \frac{Jp_b}{1.8} \left[1 - 0.2 \left(\frac{p_{wf}}{p_b} \right) - 0.8 \left(\frac{p_{wf}}{p_b} \right)^2 \right] \quad (7-11)$$

The maximum oil flow rate ($Q_{o \max}$ or AOF) occurs when the bottom-hole flowing pressure is zero, i.e. $p_{wf} = 0$, which can be determined from the above expression as:

$$Q_{o \max} = Q_{ob} + \frac{Jp_b}{1.8}$$

It should be pointed out that when $p_{wf} \geq p_b$, the IPR is linear and is described by:

$$Q_o = J (\bar{p}_r - p_{wf}).$$

Example 7-3

An oil well is producing from an undersaturated reservoir that is characterized by a bubble-point pressure of 2,130 psig. The current average reservoir pressure is 3,000 psig. Available flow test data show that the well produced 250 STB/day at a stabilized p_{wf} of 2,500 psig. Construct the IPR data.

Solution

The problem indicates that the flow test data were recorded above the bubble-point pressure, therefore, the Case 1 procedure for undersaturated reservoirs as outlined previously must be used.

Step 1. Calculate J using the flow test data.

$$J = \frac{250}{3000 - 2500} = 0.5 \text{ STB/day/psi}$$

Step 2. Calculate the oil flow rate at the bubble-point pressure by applying Equation 7-10.

$$Q_{ob} = 0.5 (3000 - 2130) = 435 \text{ STB/day}$$

Step 3. Generate the IPR data by applying the constant J approach for all pressures above p_b and Equation 7-11 for all pressures below p_b .

| P_{wf} | Equation # | Q_o |
|----------|------------|-------|
| 3000 | (7-6) | 0 |
| 2800 | (7-6) | 100 |
| 2600 | (7-6) | 200 |
| 2130 | (7-6) | 435 |
| 1500 | (7-11) | 709 |
| 1000 | (7-11) | 867 |
| 500 | (7-11) | 973 |
| 0 | (7-11) | 1027 |

Case 2. The Value of the Recorded Stabilized $p_{wf} < p_b$

When the recorded p_{wf} from the stabilized flow test is below the bubble-point pressure, as shown in Figure 7-8, the following procedure for generating the IPR data is proposed:

Step 1. Using the stabilized well flow test data and combining Equation 7-10 with 7-11, solve for the productivity index J to give:

$$J = \frac{Q_o}{(\bar{p}_r - p_b) + \frac{p_b}{1.8} \left[1 - 0.2 \left(\frac{p_{wf}}{p_b} \right) - 0.8 \left(\frac{p_{wf}}{p_b} \right)^2 \right]} \quad (7-12)$$

Step 2. Calculate Q_{ob} by using Equation 7-10, or:

$$Q_{ob} = J (\bar{p}_r - p_b)$$

Step 3. Generate the IPR for $p_{wf} \geq p_b$ by assuming several values for p_{wf} above the bubble point pressure and calculating the corresponding Q_o from:

$$Q_o = J (\bar{p}_r - p_{wf})$$

Step 4. Use Equation 7-11 to calculate Q_o at various values of p_{wf} below p_b , or:

$$Q_o = Q_{ob} + \frac{Jp_b}{1.8} \left[1 - 0.2 \left(\frac{p_{wf}}{p_b} \right) - 0.8 \left(\frac{p_{wf}}{p_b} \right)^2 \right]$$

Example 7-4

The well described in Example 7-3 was retested and the following results obtained:

$$P_{wf} = 1700 \text{ psig}, Q_o = 630.7 \text{ STB/day}$$

Generate the IPR data using the new test data.

Solution

Notice that the stabilized p_{wf} is less than p_b .

Step 1. Solve for J by applying Equation 7-12.

$$J = \frac{630.7}{(3000 - 2130) + \frac{2130}{1.8} \left[1 - \left(\frac{1700}{2130} \right) - \left(\frac{1700}{2130} \right)^2 \right]}$$

Step 2. $Q_{ob} = 0.5 (3000 - 21,300) = 435 \text{ STB/day}$

Step 3. Generate the IPR data.

| P_{wf} | Equation # | Q_o |
|----------|------------|-------|
| 3000 | (7-6) | 0 |
| 2800 | (7-6) | 100 |
| 2600 | (7-6) | 200 |
| 2130 | (7-6) | 435 |
| 1500 | (7-11) | 709 |
| 1000 | (7-11) | 867 |
| 500 | (7-11) | 973 |
| 0 | (7-11) | 1027 |

Quite often it is necessary to predict the well's inflow performance for future times as the reservoir pressure declines. Future well performance calculations require the development of a relationship that can be used to predict future maximum oil flow rates.

There are several methods that are designed to address the problem of how the IPR might shift as the reservoir pressure declines. Some of these prediction methods require the application of the material balance equation to generate future oil saturation data as a function of reservoir pressure. In the absence of such data, there are two simple approximation methods that can be used in conjunction with Vogel's method to predict future IPRs.

First Approximation Method

This method provides a rough approximation of the future maximum oil flow rate $(Q_{\text{omax}})_f$ at the specified future average reservoir pressure $(\bar{p}_r)_f$. This future maximum flow rate $(Q_{\text{omax}})_f$ can be used in Vogel's equation to predict the future inflow performance relationships at $(\bar{p}_r)_f$. The following steps summarize the method:

Step 1. Calculate $(Q_{\text{omax}})_f$ at $(\bar{p}_r)_f$ from:

$$(Q_{\text{omax}})_f = (Q_{\text{omax}})_p \left(\frac{(\bar{p}_r)_f}{(\bar{p}_r)_p} \right) \left[0.2 + 0.8 \left(\frac{(\bar{p}_r)_f}{(\bar{p}_r)_p} \right) \right] \quad (7-13)$$

where the subscript f and p represent future and present conditions, respectively.

Step 2. Using the new calculated value of $(Q_{\text{omax}})_f$ and $(\bar{p}_r)_f$, generate the IPR by using Equation 7-9.

Second Approximation Method

A simple approximation for estimating future $(Q_{\text{omax}})_f$ at $(\bar{p}_r)_f$ is proposed by Fetkovich (1973). The relationship has the following mathematical form:

$$(Q_{\text{omax}})_f = (Q_{\text{omax}})_p \left[\frac{(\bar{p}_r)_f}{(\bar{p}_r)_p} \right]^{3.0}$$

where the subscripts f and p represent future and present conditions, respectively. The above equation is intended only to provide a rough estimation of future $(Q_o)_{\max}$.

Example 7-5

Using the data given in Example 7-2, predict the IPR where the average reservoir pressure declines from 2,500 psig to 2,200 psig.

Solution

Example 7-2 shows the following information:

- Present average reservoir pressure $(\bar{p}_r)_p = 2500$ psig
- Present maximum oil rate $(Q_{o\max})_p = 1067.1$ STB/day

Step 1. Solve for $(Q_{o\max})_f$ by applying Equation 7-13.

$$(Q_{o\max})_f = 1067.1 \left(\frac{2200}{2500} \right) \left[0.2 + 0.8 \left(\frac{2200}{2500} \right) \right] = 849 \text{ STB/day}$$

Step 2. Generate the IPR data by applying Equation 7-9.

| p_{wf} | $Q_o = 849 [1 - 0.2 (p_{wf}/2200) - 0.8 (p_{wf}/2200)^2]$ |
|----------|---|
| 2200 | 0 |
| 1800 | 255 |
| 1500 | 418 |
| 500 | 776 |
| 0 | 849 |

It should be pointed out that the main disadvantage of Vogel's methodology lies with its sensitivity to the match point, i.e., the stabilized flow test data point, used to generate the IPR curve for the well.

Wiggins' Method

Wiggins (1993) used four sets of relative permeability and fluid property data as the basic input for a computer model to develop equations to predict inflow performance. The generated relationships are limited by

the assumption that the reservoir initially exists at its bubble-point pressure. Wiggins proposed generalized correlations that are suitable for predicting the IPR during three-phase flow. His proposed expressions are similar to that of Vogel's and are expressed as:

$$Q_o = (Q_o)_{\max} \left[1 - 0.52 \left(\frac{p_{wf}}{p_r} \right) - 0.48 \left(\frac{p_{wf}}{p_r} \right)^2 \right] \quad (7-14)$$

$$Q_w = (Q_w)_{\max} \left[1 - 0.72 \left(\frac{p_{wf}}{p_r} \right) - 0.28 \left(\frac{p_{wf}}{p_r} \right)^2 \right] \quad (7-15)$$

where Q_w = water flow rate, STB/day

$(Q_w)_{\max}$ = maximum water production rate at $p_{wf} = 0$, STB/day

As in Vogel's method, data from a stabilized flow test on the well must be available in order to determine $(Q_o)_{\max}$ and $(Q_w)_{\max}$.

Wiggins extended the application of the above relationships to predict future performance by providing expressions for estimating future maximum flow rates. Wiggins expressed future maximum rates as a function of:

- Current (present) average pressure $(\bar{p}_r)_p$
- Future average pressure $(\bar{p}_r)_f$
- Current maximum oil flow rate $(Q_{o\max})_p$
- Current maximum water flow rate $(Q_{w\max})_p$

Wiggins proposed the following relationships:

$$(Q_{o\max})_f = (Q_{o\max})_p \left\{ 0.15 \left[\frac{(\bar{p}_r)_f}{(\bar{p}_r)_p} \right] + 0.84 \left[\frac{(\bar{p}_r)_f}{(\bar{p}_r)_p} \right]^2 \right\} \quad (7-16)$$

$$(Q_{w\max})_f = (Q_{w\max})_p \left\{ 0.59 \left[\frac{(\bar{p}_r)_f}{(\bar{p}_r)_p} \right] + 0.36 \left[\frac{(\bar{p}_r)_f}{(\bar{p}_r)_p} \right]^2 \right\} \quad (7-17)$$

Example 7-6

The information given in Examples 7-2 and 7-5 is repeated here for convenience:

- Current average pressure = 2500 psig
- Stabilized oil flow rate = 350 STB/day
- Stabilized wellbore pressure = 2000 psig

Generate the current IPR data and predict future IPR when the reservoir pressure declines from 2,500 to 2,000 psig by using Wiggins' method.

Solution

Step 1. Using the stabilized flow test data, calculate the current maximum oil flow rate by applying Equation 7-14.

$$\begin{aligned} (Q_{o\max})_p &= 350 / \left[1 - 0.52 \left(\frac{2000}{2500} \right) - 0.48 \left(\frac{2000}{2500} \right)^2 \right] \\ &= 1264 \text{ STB/day} \end{aligned}$$

Step 2. Generate the current IPR data by using Wiggins' method and compare the results with those of Vogel's.

Results of the two methods are shown graphically in Figure 7-9.

| P_{wf} | Wiggins' | Vogel's |
|----------|----------|---------|
| 2500 | 0 | 0 |
| 2200 | 216 | 218 |
| 1500 | 651 | 632 |
| 1000 | 904 | 845 |
| 500 | 1108 | 990 |
| 0 | 1264 | 1067 |

Step 3. Calculate future maximum oil flow rate by using Equation 7-16.

$$(Q_{o\max})_f = 11,264 \left[0.15 \left(\frac{2200}{2500} \right) + 0.84 \left(\frac{2200}{2500} \right)^2 \right] = 989 \text{ STB/day}$$

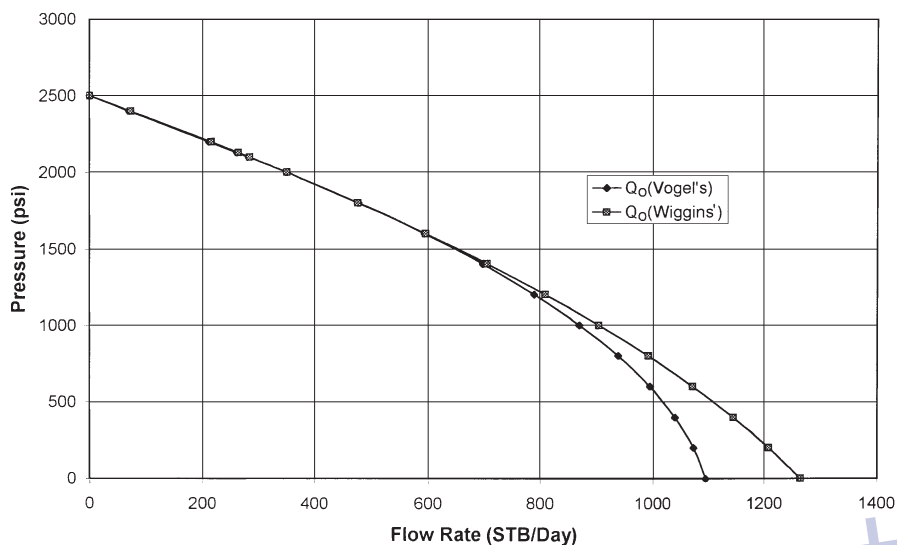


Figure 7-9. IPR curves.

Step 4. Generate future IPR data by using Equation 7-16

| p_{wf} | $Q_o = 989 \left[1 - 0.52 \left(\frac{p_{wf}}{2200} \right) - 0.48 \left(\frac{p_{wf}}{2200} \right)^2 \right]$ |
|----------|--|
| 2200 | 0 |
| 1800 | 250 |
| 1500 | 418 |
| 500 | 848 |
| 0 | 989 |

Standing's Method

Standing (1970) essentially extended the application of Vogel's to predict future inflow performance relationship of a well as a function of reservoir pressure. He noted that Vogel's equation (Equation 7-9) can be rearranged as:

$$\frac{Q_o}{(Q_o)_{\max}} = \left(1 - \frac{p_{wf}}{p_r} \right) \left[1 + 0.8 \left(\frac{p_{wf}}{p_r} \right) \right] \quad (7-18)$$

Standing introduced the productivity index J as defined by Equation 7-1 into Equation 7-18 to yield:

$$J = \frac{(Q_o)_{\max}}{p_r} \left[1 + 0.8 \left(\frac{p_{wf}}{p_r} \right) \right] \quad (7-19)$$

Standing then defined the present (current) zero drawdown productivity index as:

$$J_p^* = 1.8 \left[\frac{(Q_o)_{\max}}{p_r} \right] \quad (7-20)$$

where J_p^* is Standing's zero-drawdown productivity index. The J_p^* is related to the productivity index J by:

$$\frac{J}{J_p^*} = \frac{1}{1.8} \left[1 + 0.8 \left(\frac{p_{wf}}{p_r} \right) \right] \quad (7-21)$$

Equation 7-1 permits the calculation of J_p^* from a measured value of J .

To arrive at the final expression for predicting the desired IPR expression, Standing combines Equation 7-20 with Equation 7-18 to eliminate $(Q_o)_{\max}$ to give:

$$Q_o = \left[\frac{J_f^* (\bar{p}_r)_f}{1.8} \right] \left\{ 1 - 0.2 \left[\frac{p_{wf}}{(\bar{p}_r)_f} \right] - 0.8 \left[\frac{p_{wf}}{(\bar{p}_r)_f} \right]^2 \right\} \quad (7-22)$$

where the subscript f refers to future condition.

Standing suggested that J_p^* can be estimated from the present value of J_p^* by the following expression:

$$J_f^* = J_p^* \left(\frac{k_{ro}}{\mu_o B_o} \right)_f / \left(\frac{k_{ro}}{\mu_o B_o} \right)_p \quad (7-23)$$

where the subscript p refers to the present condition.

If the relative permeability data are not available, J_f^* can be roughly estimated from:

$$J_f^* = J_p^* \left[\frac{(\bar{p}_r)_f}{(\bar{p}_r)_p} \right]^2 \quad (7-24)$$

Standing's methodology for predicting a future IPR is summarized in the following steps:

Step 1. Using the current time condition and the available flow test data, calculate $(Q_o)_{\max}$ from Equation 7-9 or Equation 7-18.

Step 2. Calculate J^* at the present condition, i.e., J_p^* , by using Equation 7-20. Notice that other combinations of Equations 7-18 through 7-21 can be used to estimate J_p^* .

Step 3. Using fluid property, saturation, and relative permeability data, calculate both $(k_{ro}/\mu_o B_o)_p$ and $(k_{ro}/\mu_o B_o)_f$.

Step 4. Calculate J_f^* by using Equation 7-23. Use Equation 7-24 if the oil relative permeability data are not available.

Step 5. Generate the future IPR by applying Equation 7-22.

Example 7-7

A well is producing from a saturated oil reservoir that exists at its saturation pressure of 4,000 psig. The well is flowing at a stabilized rate of 600 STB/day and a p_{wf} of 3,200 psig. Material balance calculations provide the following current and future predictions for oil saturation and PVT properties.

| | Present | Future |
|-----------------|---------|--------|
| \bar{p}_r | 4000 | 3000 |
| μ_o , cp | 2.40 | 2.20 |
| B_o , bbl/STB | 1.20 | 1.15 |
| k_{ro} | 1.00 | 0.66 |

Generate the future IPR for the well at 3,000 psig by using Standing's method.

Solution

Step 1. Calculate the current $(Q_o)_{\max}$ from Equation 7-18.

$$(Q_o)_{\max} = 600 / \left[\left(1 - \frac{3200}{4000} \right) (1 + 0.8) \left(\frac{3200}{4000} \right) \right] = 1829 \text{ STB/day}$$

Step 2. Calculate J_p^* by using Equation 7-20.

$$J_p^* = 1.8 \left[\frac{1829}{4000} \right] = 0.823$$

Step 3. Calculate the following pressure function:

$$\left(\frac{k_{ro}}{\mu_o B_o} \right)_p = \frac{1}{(2.4)(1.20)} = 0.3472$$

$$\left(\frac{k_{ro}}{\mu_o B_o} \right)_f = \frac{0.66}{(2.2)(1.15)} = 0.2609$$

Step 4. Calculate J_f^* by applying Equation 7-23.

$$J_f^* = 0.823 \left(\frac{0.2609}{0.3472} \right) = 0.618$$

Step 5. Generate the IPR by using Equation 7-22.

| P_{wf} | Q_o , STB/day |
|----------|-----------------|
| 3000 | 0 |
| 2000 | 527 |
| 1500 | 721 |
| 1000 | 870 |
| 500 | 973 |
| 0 | 1030 |

It should be noted that one of the main disadvantages of Standing's methodology is that it requires reliable permeability information; in addition, it also requires material balance calculations to predict oil saturations at future average reservoir pressures.

Fetkovich's Method

Muskat and Evinger (1942) attempted to account for the observed non-linear flow behavior (i.e., IPR) of wells by calculating a theoretical productivity index from the pseudosteady-state flow equation. They expressed Darcy's equation as:

$$Q_o = \frac{0.00708 kh}{\left[\ln \frac{r_e}{r_w} - 0.75 + s \right]_{pwf}} \int_{p_{wf}}^{\bar{p}_r} f(p) dp \quad (7-25)$$

where the pressure function $f(p)$ is defined by:

$$f(p) = \frac{k_{ro}}{\mu_o B_o} \quad (7-26)$$

where k_{ro} = oil relative permeability
 k = absolute permeability, md
 B_o = oil formation volume factor
 μ_o = oil viscosity, cp

Fetkovich (1973) suggests that the pressure function $f(p)$ can basically fall into one of the following two regions:

Region 1: Undersaturated Region

The pressure function $f(p)$ falls into this region if $p > p_b$. Since oil relative permeability in this region equals unity (i.e., $k_{ro} = 1$), then:

$$f(p) = \left(\frac{1}{\mu_o B_o} \right)_p \quad (7-27)$$

Fetkovich observed that the variation in $f(p)$ is only slight and the pressure function is considered constant as shown in Figure 7-10.

Region 2: Saturated Region

In the saturated region where $p < p_b$, Fetkovich shows that the $(k_{ro}/\mu_o B_o)$ changes linearly with pressure and that the straight line passes through the origin. This linear is shown schematically in Figure 7-10 and can be expressed mathematically as:

$$f(p) = \left(\frac{1}{\mu_o B_o} \right)_{p_b} \left(\frac{P}{p_b} \right) \quad (7-28)$$

where μ_o and B_o are evaluated at the bubble-point pressure. In the application of the straight-line pressure function, there are three cases that must be considered:

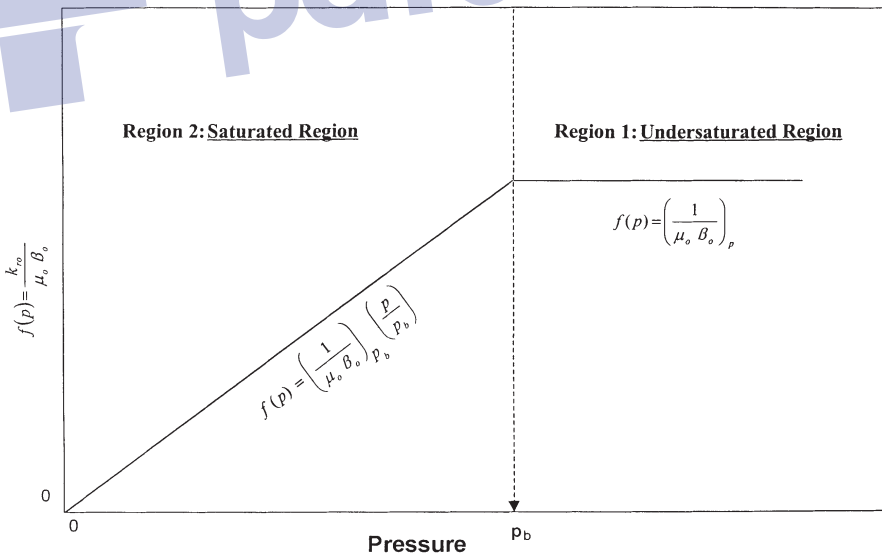


Figure 7-10. Pressure function concept.

- \bar{p}_r and $p_{wf} > p_b$
- \bar{p}_r and $p_{wf} < p_b$
- $\bar{p}_r > p_b$ and $p_{wf} < p_b$

All three cases are presented below.

Case 1: \bar{p}_r and $p_{wf} > p_b$

This is the case of a well producing from an undersaturated oil reservoir where both p_{wf} and \bar{p}_r are greater than the bubble-point pressure. The pressure function $f(p)$ in this case is described by Equation 7-27. Substituting Equation 7-27 into Equation 7-25 gives:

$$Q_o = \frac{0.00708 kh}{\ln\left(\frac{r_e}{r_w}\right) - 0.75 + s} \int_{p_{wf}}^{\bar{p}_r} \left(\frac{1}{\mu_o B_o}\right) dp$$

Since $\left(\frac{1}{\mu_o B_o}\right)$ is constant, then:

$$Q_o = \frac{0.00708 kh}{\mu_o B_o \left[\ln\left(\frac{r_e}{r_w}\right) - 0.75 + S \right]} (\bar{p}_r - p_{wf}) \quad (7-29)$$

or

$$Q_o = J (\bar{p}_r - p_{wf}) \quad (7-30)$$

The productivity index is defined in terms of the reservoir parameters as:

$$J = \frac{0.00708 kh}{\mu_o B_o \left[\ln\left(\frac{r_e}{r_w}\right) - 0.75 + s \right]} \quad (7-31)$$

where B_o and μ_o are evaluated at $(\bar{p}_r + p_{wf})/2$.

Example 7-8

A well is producing from an undersaturated oil reservoir that exists at an average reservoir pressure of 3,000 psi. The bubble-point pressure is recorded as 1,500 psi at 150°F. The following additional data are available:

- stabilized flow rate = 280 STB/day
- stabilized wellbore pressure = 2200 psi
- $h = 20'$ $r_w = 0.3'$ $r_e = 660'$ $s = -0.5$
- $k = 65$ md
- μ_o at 2600 psi = 2.4 cp
- B_o at 2600 psi = 1.4 bbl/STB

Calculate the productivity index by using both the reservoir properties (i.e., Equation 7-31) and flow test data (i.e., Equation 7-30).

Solution

- From Equation 7-31:

$$J = \frac{0.00708(65)(20)}{(2.4)(1.4) \left[\ln \left(\frac{660}{0.3} \right) - 0.75 - 0.5 \right]} = 0.42 \text{ STB/day/psi}$$

- From production data:

$$J = \frac{280}{3000 - 2200} = 0.35 \text{ STB/day/psi}$$

Results show a reasonable match between the two approaches. It should be noted, however, that there are several uncertainties in the values of the parameters used in Equation 7-31 to determine the productivity index. For example, changes in the skin factor k or drainage area would change the calculated value of J .

Case 2: \bar{p}_r and $p_{wf} < p_b$

When the reservoir pressure \bar{p}_r and bottom-hole flowing pressure p_{wf} are both below the bubble-point pressure p_b , the pressure function $f(p)$ is represented by the straight-line relationship as expressed by Equation 7-28. Combining Equation 7-28 with Equation 7-25 gives:

$$Q_o = \left[\frac{0.00708 kh}{\ln\left(\frac{r_e}{r_w}\right) - 0.75 + s} \right] \int_{p_{wf}}^{\bar{p}_r} \frac{1}{(\mu_o B_o)_{pb}} \left(\frac{p}{p_b}\right) dp$$

Since the term $\left[\frac{1}{(\mu_o B_o)_{pb}} \left(\frac{1}{p_b}\right) \right]$ is constant, then :

$$Q_o = \left[\frac{0.00708 kh}{\ln\left(\frac{r_e}{r_w}\right) - 0.75 + s} \right] \frac{1}{(\mu_o B_o)_{pb}} \left(\frac{1}{p_b}\right) \int_{p_{wf}}^{\bar{p}_r} p dp$$

Integrating gives:

$$Q_o = \frac{0.00708 kh}{(\mu_o B_o)_{pb} \left[\ln\left(\frac{r_e}{r_w}\right) - 0.75 + s \right]} \left(\frac{1}{2p_b}\right) (p_r^{-2} - p_{wf}^2) \quad (7-32)$$

Introducing the productivity index into the above equation gives:

$$Q_o = J \left(\frac{1}{2p_b}\right) (p_r^{-2} - p_{wf}^2) \quad (7-33)$$

The term $\left(\frac{J}{2p_b}\right)$ is commonly referred to as the **performance coefficient C**, or:

$$\left(\frac{J}{2p_b}\right)$$

$$Q_o = C (p_r^{-2} - p_{wf}^2) \quad (7-34)$$

To account for the possibility of non-Darcy flow (turbulent flow) in oil wells, Fetkovich introduced the exponent n in Equation 7-35 to yield:

$$Q_o = C \left(\bar{p}_r^{-2} - p_{wf}^2 \right)^n \quad (7-35)$$

The value of n ranges from 1.000 for a complete laminar flow to 0.5 for highly turbulent flow.

There are two unknowns in Equation 7-35: the performance coefficient C and the exponent n . At least two tests are required to evaluate these two parameters, assuming \bar{p}_r is known.

By taking the log of both sides of Equation 7-35 and solving for $\log(p_r^2 - p_{wf}^2)$, the expression can be written as:

$$\log(\bar{p}_r^{-2} - p_{wf}^2) = \frac{1}{n} \log Q_o - \frac{1}{n} \log C$$

A plot of $\bar{p}_r^{-2} - p_{wf}^2$ versus Q_o on log-log scales will result in a straight line having a slope of $1/n$ and an intercept of C at $\bar{p}_r^{-2} - p_{wf}^2 = 1$. The value of C can also be calculated using any point on the linear plot once n has been determined to give:

$$C = \frac{Q_o}{\left(\bar{p}_r^{-2} - p_{wf}^2 \right)^n}$$

Once the values of C and n are determined from test data, Equation 7-35 can be used to generate a complete IPR.

To construct the future IPR when the average reservoir pressure declines to $(\bar{p}_r)_f$, Fetkovich assumes that the performance coefficient C is a linear function of the average reservoir pressure and, therefore, the value of C can be adjusted as:

$$(C)_f = (C)_p [(\bar{p}_r)_f / (\bar{p}_r)_p] \quad (7-36)$$

where the subscripts f and p represent the future and present conditions.

Fetkovich assumes that the value of the exponent n would not change as the reservoir pressure declines. Beggs (1991) presented an excellent and comprehensive discussion of the different methodologies used in constructing the IPR curves for oil and gas wells.

The following example was used by Beggs (1991) to illustrate Fetkovich's method for generating the current and future IPR.

Example 7-9

A four-point stabilized flow test was conducted on a well producing from a saturated reservoir that exists at an average pressure of 3,600 psi.

| Q_o , STB/day | p_{wfr} , psi |
|-----------------|-----------------|
| 263 | 3170 |
| 383 | 2890 |
| 497 | 2440 |
| 640 | 2150 |

- Construct a complete IPR by using Fetkovich's method.
- Construct the IPR when the reservoir pressure declines to 2,000 psi.

Solution

Part A.

Step 1. Construct the following table:

| Q_o , STB/day | p_{wfr} , psi | $(\bar{p}_r^2 - p_{wfr}^2) \times 10^{-6}$, psi ² |
|-----------------|-----------------|---|
| 263 | 3170 | 2.911 |
| 383 | 2890 | 4.567 |
| 497 | 2440 | 7.006 |
| 640 | 2150 | 8.338 |

Step 2. Plot $(\bar{p}_r^2 - p_{wfr}^2)$ versus Q_o on log-log paper as shown in Figure 7-11 and determine the exponent n , or:

$$n = \frac{\log(750) - \log(105)}{\log(10^7) - \log(10^6)} = 0.854$$

Step 3. Solve for the performance coefficient C :

$$C = 0.00079$$

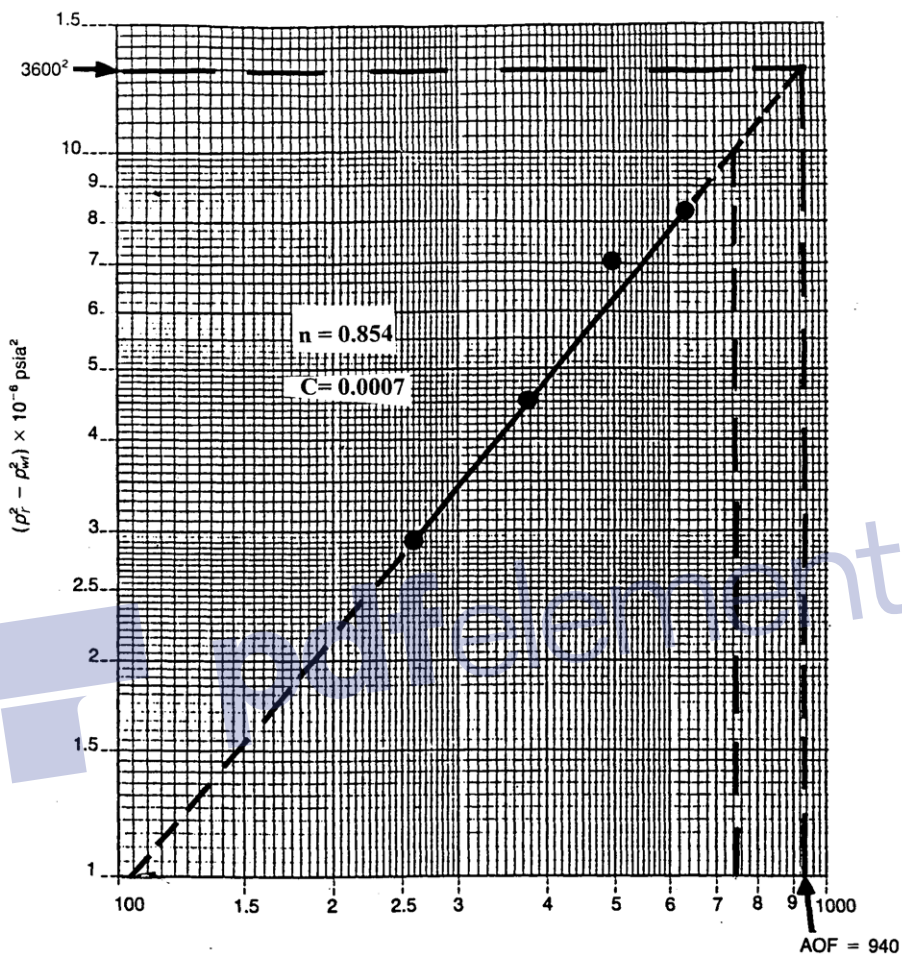


Figure 7-11. Flow-after-flow data for Example 7-9 (After Beggs, D., "Production Optimization Using Nodal Analysis," permission to publish by the OGCI, copyright OGCI, 1991.)

Step 4. Generate the IPR by assuming various values for p_{wf} and calculating the corresponding flow rate from Equation 7-25:

$$Q_o = 0.00079 (3600^2 - p_{wf}^2)^{0.854}$$

| P_{wf} | Q_o , STB/day |
|----------|-----------------|
| 3600 | 0 |
| 3000 | 340 |
| 2500 | 503 |
| 2000 | 684 |
| 1500 | 796 |
| 1000 | 875 |
| 500 | 922 |
| 0 | 937 |

The IPR curve is shown in Figure 7-12. Notice that the AOF, i.e., $(Q_o)_{max}$, is 937 STB/day.

Part B.

Step 1. Calculate future C by applying Equation 7-36:

$$(C)_f = 0.00079 \left(\frac{2000}{3600} \right) = 0.000439$$

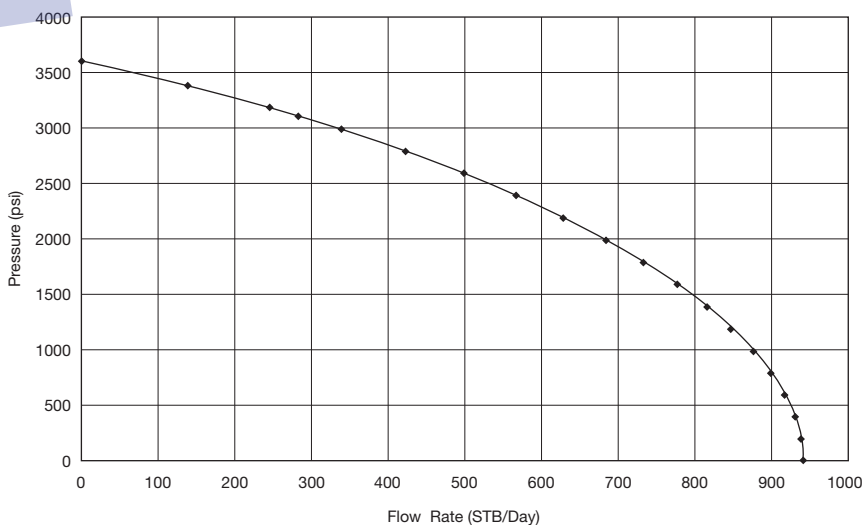


Figure 7-12. IPR using Fetkovich method.

Step 2. Construct the new IPR curve at 2,000 psi by using the new calculated C and applying the inflow equation.

$$Q_o = 0.000439 (20,002 - p_{wf}^2)^{0.854}$$

| P_{wf} | Q_o |
|----------|-------|
| 2000 | 0 |
| 1500 | 94 |
| 1000 | 150 |
| 500 | 181 |
| 0 | 191 |

Both the present time and future IPRs are plotted in Figure 7-13.

Klins and Clark (1993) developed empirical correlations that correlate the changes in Fetkovich's performance coefficient C and the flow exponent n with the decline in the reservoir pressure. The authors observed the exponent n changes considerably with reservoir pressure. Klins and Clark concluded the "future" values of $(n)_f$ and (C) at pressure $(\bar{p}_r)_f$ are related to the values of n and C at the bubble-point pressure. Denoting C_b

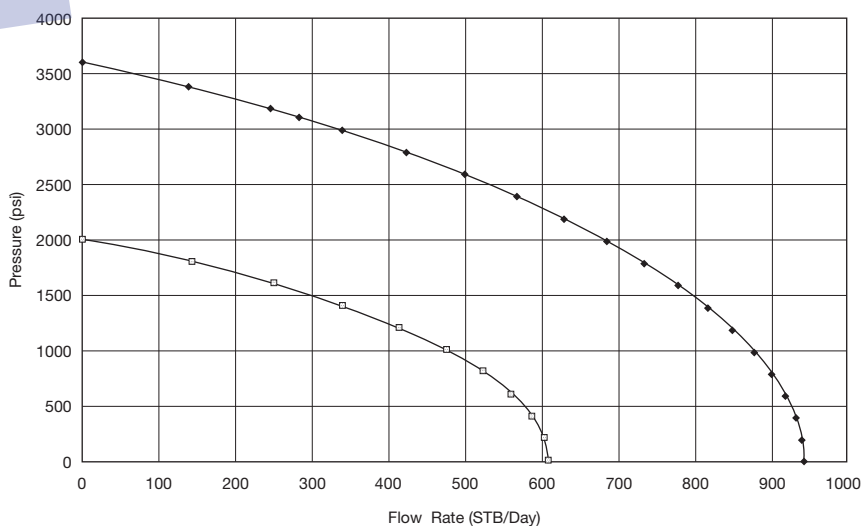


Figure 7-13. Future IPR at 2,000 psi.

and n_b as the values of the performance coefficient and the flow exponent at the bubble-point pressure p_b , Klins and Clark introduced the following dimensionless parameters:

- Dimensionless performance coefficient = C/C_b
- Dimensionless flow exponent = n/n_b
- Dimensionless average reservoir pressure = \bar{p}_r/p_b

The authors correlated (C/C_b) and (n/n_b) to the dimensionless pressure by the following two expressions:

$$\left(\frac{n}{n_b}\right) = 1 + 0.0577\left(1 - \frac{\bar{p}_r}{p_b}\right) - 0.2459\left(1 - \frac{\bar{p}_r}{p_b}\right)^2 + 0.503\left(1 - \frac{\bar{p}_r}{p_b}\right)^3 \quad (7-37)$$

and

$$\left(\frac{C}{C_b}\right) = 1 - 3.5718\left(1 - \frac{\bar{p}_r}{p_b}\right) + 4.7981\left(1 - \frac{\bar{p}_r}{p_b}\right)^2 - 2.3066\left(1 - \frac{\bar{p}_r}{p_b}\right)^3 \quad (7-38)$$

where C_b = performance coefficient at the bubble-point pressure
 n_b = flow exponent at the bubble-point pressure

The procedure of applying the above relationships in adjusting the coefficients C and n with changing average reservoir pressure is detailed below:

- Step 1.* Using the available flow test data in conjunction with Fetkovich's equation, i.e., Equation 7-34, calculate the present (current) values of n and C at the present average pressure \bar{p}_r .
- Step 2.* Using the current values of \bar{p}_r , calculate the dimensionless values of (n/n_b) and (C/C_b) by applying Equations 7-37 and 7-38, respectively.

Step 3. Solve for the constants n_b and C_b from:

$$n_b = \frac{n}{n/n_b} \quad (7-39)$$

and

$$C_b = \frac{C}{(C/C_b)} \quad (7-40)$$

It should be pointed out that if the present reservoir pressure equals the bubble-point pressure, the values of n and C as calculated in Step 1 are essentially n_b and C_b .

Step 4. Assume future average reservoir pressure \bar{p}_r and solve for the corresponding future dimensionless parameters (n_f/n_b) and (C_f/C_b) by applying Equations 7-37 and 7-38, respectively.

Step 5. Solve for future values of n_f and C_f from

$$n_f = n_b (n/n_b)$$

$$C_f = C_b (C/C_b)$$

Step 6. Use n_f and C_f in Fetkovich's equation to generate the well's future IPR at the desired average reservoir pressure $(\bar{p}_r)_f$. It should be noted that the maximum oil flow rate $(Q_o)_{\max}$ at $(\bar{p}_r)_f$ is given by:

$$(Q_o)_{\max} = C_f [(\bar{p}_r)^2]^{n_f} \quad (7-41)$$

Example 7-10

Using the data given in Example 7-9, generate the future IPR data when the reservoir pressure drops to 3,200 psi.

Solution

Step 1. Since the reservoir exists at its bubble-point pressure, then:

$$n_b = 0.854 \quad \text{and} \quad C_b = 0.00079 \quad \text{at} \quad p_b = 3600 \text{ psi}$$

Step 2. Calculate the future dimensionless parameters at 3,200 psi by applying Equations 7-37 and 7-38:

$$\left(\frac{n}{n_b}\right) = 1 + 0.0577\left(1 - \frac{3200}{3600}\right) - 0.2459\left(1 - \frac{3200}{3600}\right)^2$$

$$+ 0.5030\left(1 - \frac{3200}{3600}\right)^3 = 1.0041$$

$$\left(\frac{C}{C_b}\right) = 1 - 3.5718\left(1 - \frac{3200}{3600}\right) + 4.7981\left(1 - \frac{3200}{3600}\right)^2$$

$$- 2.3066\left(1 - \frac{3200}{3600}\right)^3 = 0.6592$$

Step 3. Solve for n_f and C_f :

$$n_f = (0.854) (1.0041) = 0.8575$$

$$C_f = (0.00079) (0.6592) = 0.00052$$

Therefore, the flow rate is expressed as:

$$Q_o = 0.00052 (32,002 - p_{wf}^2)^{0.8575}$$

When the maximum oil flow rate, i.e., AOF, occurs at $p_{wf} = 0$, then:

$$(Q_o)_{\max} = 0.00052 (3200^2 - 0^2)^{0.8575} = 534 \text{ STB/day}$$

Step 4. Construct the following table:

| P_{wf} | Q_o |
|----------|-------|
| 3200 | 0 |
| 2000 | 349 |
| 1500 | 431 |
| 500 | 523 |
| 0 | 534 |

Figure 7-14 compares current and future IPRs as calculated in Examples 7-9 and 7-10.

Case 3: $\bar{p}_r > p_b$ and $p_{wf} < p_b$

Figure 7-15 shows a schematic illustration of Case 3 in which it is assumed that $p_{wf} < p_b$ and $\bar{p}_r > p_b$. The integral in Equation 7-25 can be expanded and written as:

$$Q_o = \frac{0.00708 kh}{\ln\left(\frac{r_e}{r_w}\right) - 0.75 + s} \left[\int_{p_{wf}}^{p_b} f(p) dp + p_b \int_{p_b}^{\bar{p}_r} f(p) dp \right]$$

Substituting Equations 7-27 and 7-18 into the above expression gives:

$$Q_o = \frac{0.00708 kh}{\ln\left(\frac{r_e}{r_w}\right) - 0.75 + s} \left[\int_{p_{wf}}^{p_b} \left(\frac{1}{\mu_o B_o}\right) \left(\frac{p}{p_b}\right) dp + \int_{p_b}^{\bar{p}_r} \left(\frac{1}{\mu_o B_o}\right) dp \right]$$

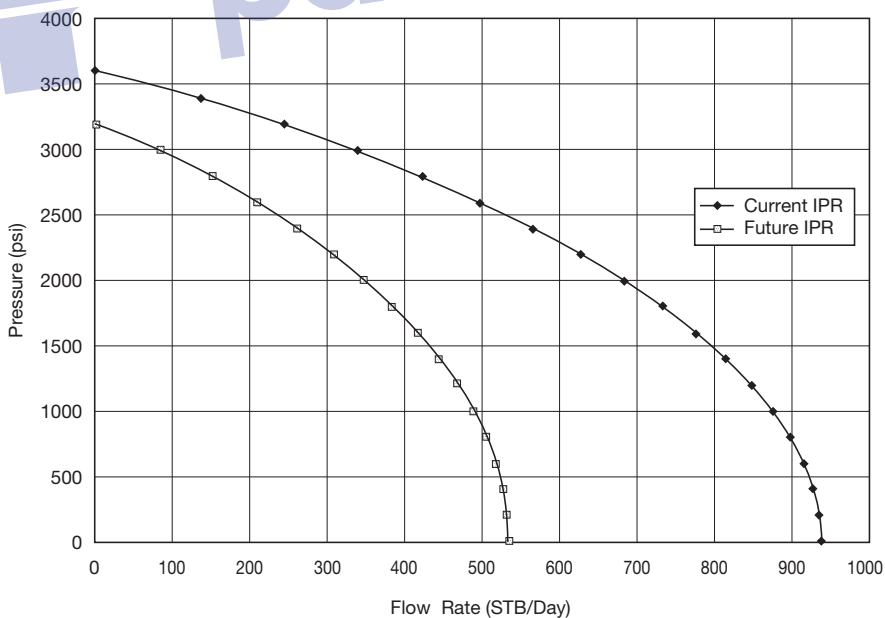


Figure 7-14. IPR.

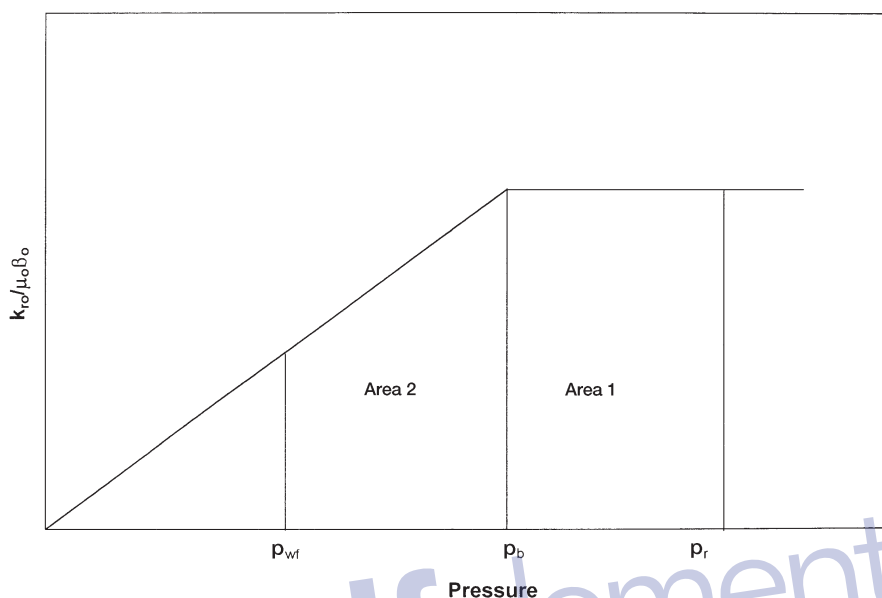


Figure 7-15. $(k_{ro}/\mu_o\beta_o)$ vs. pressure for Case 3.

where μ_o and B_o are evaluated at the bubble-point pressure p_b .

Arranging the above expression gives:

$$Q_o = \frac{0.00708kh}{\mu_o B_o \left[\ln\left(\frac{r_c}{r_w}\right) - 0.75 + s \right]} \left[\frac{1}{p_b} \int_{p_{wf}}^{p_b} p \, dp + \int_{p_b}^{\bar{p}_r} dp \right]$$

Integrating and introducing the productivity index J into the above relationship gives:

$$Q_o = J \left[\frac{1}{2p_b} (p_b^2 - p_{wf}^2) + (\bar{p}_r - p_b) \right]$$

or

$$Q_o = J(\bar{p}_r - p_b) + \frac{1}{2p_b}(p_b^2 - p_{wf}^2) \quad (7-42)$$

Example 7-11

The following reservoir and flow test data are available on an oil well:

- Pressure data: $\bar{p}_r = 4000$ psi $p_b = 3200$ psi
- Flow test data: $p_{wf} = 3600$ psi $Q_o = 280$ STB/day

Generate the IPR data of the well.

Solution

Step 1. Calculate the productivity index from the flow test data.

$$J = \frac{280}{4000 - 3600} = 0.7 \text{ STB/day/psi}$$

Step 2. Generate the IPR data by applying Equation 7-30 when the assumed $p_{wf} > p_b$ and using Equation 7-42 when $p_{wf} < p_b$.

| p_{wf} | Equation | Q_o |
|----------|----------|-------|
| 4000 | (7-30) | 0 |
| 3800 | (7-30) | 140 |
| 3600 | (7-30) | 280 |
| 3200 | (7-30) | 560 |
| 3000 | (7-42) | 696 |
| 2600 | (7-42) | 941 |
| 2200 | (7-42) | 1151 |
| 2000 | (7-42) | 1243 |
| 1000 | (7-42) | 1571 |
| 500 | (7-42) | 1653 |
| 0 | (7-42) | 1680 |

Results of the calculations are shown graphically in Figure 7-16.

It should be pointed out Fetkovich's method has the advantage over Standing's methodology in that it does not require the tedious material

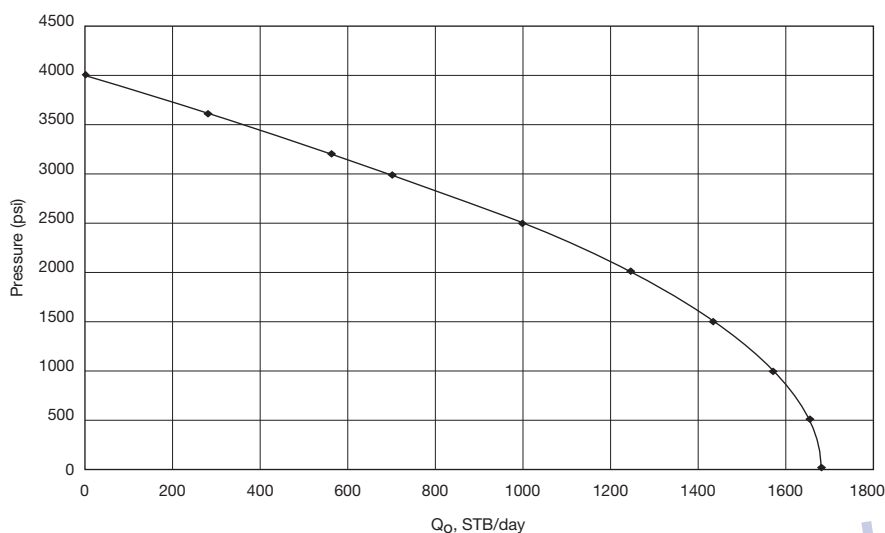


Figure 7-16. IPR using the Fetkovich method.

balance calculations to predict oil saturations at future average reservoir pressures.

The Klins-Clark Method

Klins and Clark (1993) proposed an inflow expression similar in form to that of Vogel's and which can be used to estimate future IPR data. To improve the predictive capability of Vogel's equation, the authors introduced a new exponent d to Vogel's expression. The authors proposed the following relationships:

$$\frac{Q_o}{(Q_o)_{\max}} = 1 - 0.295 \left(\frac{p_{wf}}{p_r} \right) - 0.705 \left(\frac{p_{wf}}{p_r} \right)^d \quad (7-43)$$

where

$$d = \left[0.28 + 0.72 \left(\frac{\bar{p}_r}{p_b} \right) \right] (1.24 + 0.001 p_b) \quad (7-44)$$

The computational steps of the Klins-Clark method are summarized below:

- Step 1.* Knowing the bubble-point pressure and the current reservoir pressure, calculate the exponent d from Equation 7-44.
- Step 2.* From the available stabilized flow data, i.e., Q_o at p_{wf} , solve Equation 7-43 for $(Q_o)_{max}$.
- Step 3.* Construct the current IPR by assuming several values of p_{wf} in Equation 7-43 and solving for Q_o .

Kelkar and Cox (1985) proposed a method for predicting future IPR. This method is a result of the unification of some methods discussed previously. Two sets of data points (each at different average reservoir pressures p_{r1} and p_{r2}) are required to predict future IPR curve, as summarized by the following steps:

Step 1. Calculate the maximum flow rate (Q_{max}) for both tests conducted by Vogel, Fetkovich, or Standing, i.e., $(Q_{max})_1$ and $(Q_{max})_2$.

Step 2. Calculate J^* from

$$J_1^* = \frac{(Q_{max})_1}{(p_r)_1} \quad \text{and} \quad J_2^* = \frac{(Q_{max})_2}{(p_r)_2}$$

Step 3. Determine the constants A and B , as defined by the following expressions:

$$A = \frac{J_1^* - J_2^*}{(p_r^2)_1 - (p_r^2)_2}$$

$$B = \frac{\frac{J_1^*}{(p_r^2)_1} - \frac{J_2^*}{(p_r^2)_2}}{\frac{1}{(p_r^2)_1} - \frac{1}{(p_r^2)_2}}$$

Step 4. Calculate the maximum flow rate of the corresponding future pressure, $(p_r)_f$, from:

$$(Q_{max})_f = A(p_r)_f^3 + B(p_r)_f$$

Step 5. Construct the IPR curve using the reference inflow equation used in Step 1 with calculated future values of $(p_r)_f$ and $(Q_{\max})_f$.

For example, consider a reservoir with the following data from two stabilized flow tests:

| Test | P_r , psia | Q_o , STB/day | P_{wf} , psia |
|--------|--------------|-----------------|-----------------|
| Test 1 | 2355.9 | 300 | 1300 |
| Test 2 | 2254.9 | 226.2 | 1300 |

To calculate future IPR at a reservoir pressure of 1,990 psia:

- Using Vogel's equation, Equation 7-9, solve for $(Q_o)_{\max}$ for the two stabilized test data points:

$$(Q_o)_{\max} = \frac{Q_o}{1 - 0.2 \left(\frac{p_{wf}}{p_r} \right) - 0.8 \left(\frac{p_{wf}}{p_r} \right)^2}$$

$$(Q_o)_{\max 1} = \frac{300}{1 - 0.2 \left(\frac{1300}{2355.9} \right) - 0.8 \left(\frac{1300}{2355.9} \right)^2} = 463.5 \text{ STB/day}$$

$$(Q_o)_{\max 2} = \frac{226.2}{1 - 0.2 \left(\frac{1300}{2254.9} \right) - 0.8 \left(\frac{1300}{2254.9} \right)^2} = 365.5 \text{ STB/day}$$

- Calculate J^* :

$$J_1^* = \frac{(Q_{\max})_1}{(p_r)_1} = \frac{463.5}{2355.4} = 0.197 \text{ STB/day}$$

$$J_2^* = \frac{(Q_{\max})_2}{(p_r)_2} = \frac{365.5}{2254.9} = 0.162 \text{ STB/day}$$

- Determine the constants A and B:

$$A = \frac{J_1^* - J_2^*}{(p_r)_1^2 - (p_r)_2^2} = \frac{0.197 - 0.162}{(2355.4)^2 - (2254.9)^2} = 7.55 \times 10^{-8}$$

$$B = \frac{\frac{J_1^*}{(p_r^2)_1} - \frac{J_2^*}{(p_r^2)_2}}{\frac{1}{(p_r^2)_1} - \frac{1}{(p_r^2)_2}} = \frac{\frac{0.197}{(2355.4)^2} - \frac{0.162}{(2254.9)^2}}{\frac{1}{(2355.4)^2} - \frac{1}{(2254.9)^2}} = -0.222$$

- Calculate the maximum flow rate of the corresponding future pressure, $(p_r)_f$, from:

$$(Q_{\max})_f = A(p_r)_f^3 + B(p_r)_f$$

$$(Q_{\max})_f = 7.554 \times 10^{-8} (1995)^3 + (-0.222)(1995) = 157 \text{ STB/day}$$

- Construct the IPR curve using Vogel's equation with the calculated future values of $(p_r)_f$ and $(Q_{\max})_f$:

$$Q_o = (Q_o)_{\max} \left[1 - 0.2 \left(\frac{p_{wf}}{p_r} \right) - 0.8 \left(\frac{p_{wf}}{p_r} \right)^2 \right]$$

$$Q_o = 157 \left[1 - 0.2 \left(\frac{p_{wf}}{1995} \right) - 0.8 \left(\frac{p_{wf}}{1995} \right)^2 \right]$$

HORIZONTAL OIL WELL PERFORMANCE

Since 1980, horizontal wells began capturing an ever-increasing share of hydrocarbon production. Horizontal wells offer the following advantages over those of vertical wells:

- A large volume of the reservoir can be drained by each horizontal well.
- Higher production is gained from thin pay zones.
- Horizontal wells minimize water and gas zoning problems.
- In high permeability reservoirs, where near-wellbore gas velocities are high in vertical wells, horizontal wells can be used to reduce near-wellbore velocities and turbulence.
- In secondary and enhanced oil recovery applications, long horizontal injection wells provide higher injectivity rates.

- The length of the horizontal well can provide contact with multiple fractures and greatly improve productivity.

The actual production mechanism and reservoir flow regimes around the horizontal well are considered more complicated than those for the vertical well, especially if the horizontal section of the well is of a considerable length. Some combination of both linear and radial flow actually exists, and the well may behave in a manner similar to that of a well that has been extensively fractured. Several authors reported that the shape of measured IPRs for horizontal wells is similar to those predicted by the Vogel or Fetkovich methods. The authors pointed out that the productivity gain from drilling 1,500-foot-long horizontal wells is two to four times that of vertical wells.

A horizontal well can be looked upon as a number of vertical wells drilling next to each other and completed in a limited pay zone thickness. Figure 7-17 shows the drainage area of a horizontal well of length L in a reservoir with a pay zone thickness of h . Each end of the horizontal well

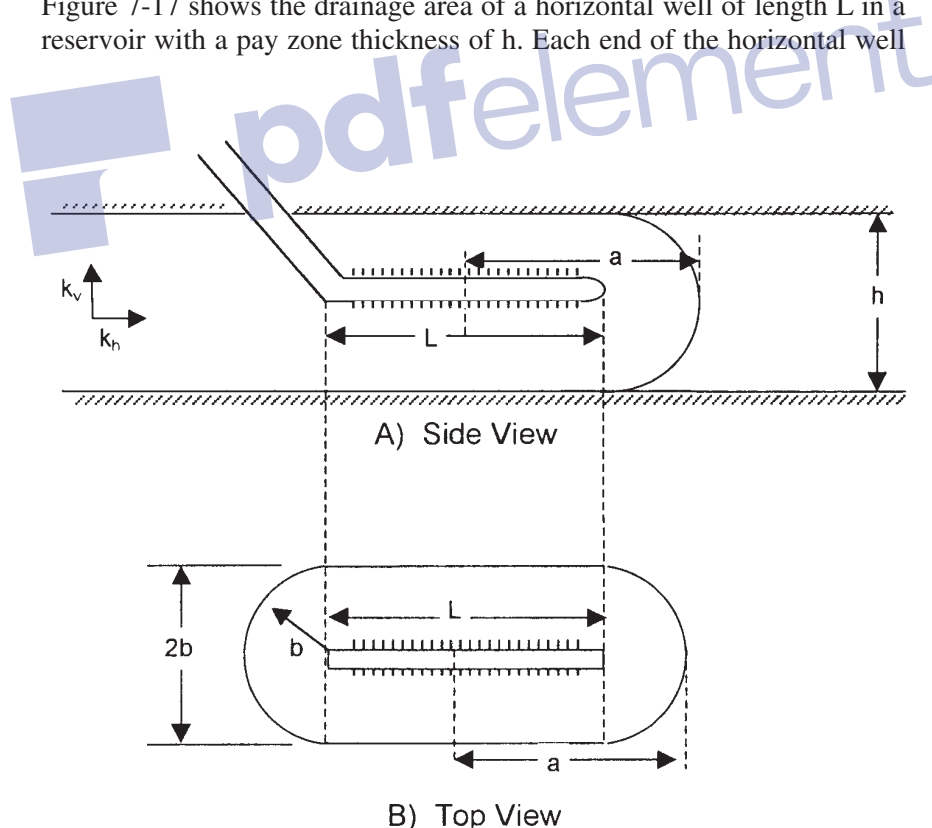


Figure 7-17. Horizontal well drainage area.

would drain a half-circular area of radius b , with a rectangular drainage shape of the horizontal well.

Assuming that each end of the horizontal well is represented by a vertical well that drains an area of a half circle with a radius of b , Joshi (1991) proposed the following two methods for calculating the drainage area of a horizontal well.

Method I

Joshi proposed that the drainage area is represented by two half circles of radius b (equivalent to a radius of a vertical well r_{ev}) at each end and a rectangle, of dimensions $L(2b)$, in the center. The drainage area of the horizontal well is given then by:

$$A = \frac{L(2b) + \pi b^2}{43,650} \quad (7-45)$$

where A = drainage area, acres
 L = length of the horizontal well, ft
 b = half minor axis of an ellipse, ft

Method II

Joshi assumed that the horizontal well drainage area is an ellipse and given by:

$$A = \frac{\pi ab}{43,560} \quad (7-46)$$

with

$$a = \frac{L}{2} + b \quad (7-47)$$

where a is the half major axis of an ellipse.

Joshi noted that the two methods give different values for the drainage area A and suggested assigning the average value for the drainage of the horizontal well. Most of the production rate equations require the value of the drainage radius of the horizontal well, which is given by:

$$r_{\text{eh}} = \sqrt{\frac{43,560 A}{\pi}}$$

where r_{eh} = drainage radius of the horizontal well, ft
 A = drainage area of the horizontal well, acres

Example 7-12

A 480-acre lease is to be developed by using 12 vertical wells. Assuming that each vertical well would effectively drain 40 acres, calculate the possible number of either 1,000- or 2,000-ft-long horizontal wells that will drain the lease effectively.

Solution

Step 1. Calculate the drainage radius of the vertical well:

$$r_{\text{cv}} = b = \sqrt{\frac{(40)(43,560)}{\pi}} = 745 \text{ ft}$$

Step 2. Calculate the drainage area of the 1,000- and 2,000-ft-long horizontal well using Joshi's two methods:

Method I

- For the 1,000-ft horizontal well using Equation 7-45:

$$A = \frac{(1000)(2 \times 745) + \pi(745)^2}{43,560} = 74 \text{ acres}$$

- For the 2,000-ft horizontal well:

$$A = \frac{(2000)(2 \times 745) + \pi(745)^2}{43,560} = 108 \text{ acres}$$

Method II

- For the 1,000-ft horizontal well using Equation 7-46:

$$a = \frac{1000}{2} + 745 = 1245'$$

$$A = \frac{\pi(1245)(745)}{43,560} = 67 \text{ acres}$$

- For the 2,000-ft horizontal well:

$$a = \frac{2000}{2} + 745 = 1745'$$

$$A = \frac{\pi(1745)(745)}{43,560} = 94 \text{ acres}$$

Step 3. Averaging the values from the two methods:

- Drainage area of 1,000-ft-long well

$$A = \frac{74 + 67}{2} = 71 \text{ acres}$$

- Drainage area of 2,000-ft-long well

$$A = \frac{108 + 94}{2} = 101 \text{ acres}$$

Step 4. Calculate the number of 1,000-ft-long horizontal wells:

$$= \frac{480}{71} = 7 \text{ wells}$$

Step 5. Calculate the number of 2,000-ft-long horizontal wells:

$$= \frac{480}{101} = 5 \text{ wells}$$

From a practical standpoint, inflow performance calculations for horizontal wells are presented here under the following two flowing conditions:

- Steady-state single-phase flow
- Pseudosteady-state two-phase flow

A reference textbook by Joshi (1991) provides an excellent treatment of horizontal well technology and it contains a detailed documentation of recent methodologies of generating inflow performance relationships.

Horizontal Well Productivity under Steady-State Flow

The steady-state analytical solution is the simplest solution to various horizontal well problems. The steady-state solution requires that the pressure at any point in the reservoir does not change with time. The flow rate equation in a steady-state condition is represented by:

$$Q_{oh} = J_h \Delta p \quad (7-48)$$

where Q_{oh} = horizontal well flow rate, STB/day

Δp = pressure drop from the drainage boundary to wellbore, psi

J_h = productivity index of the horizontal well, STB/day/psi

The productivity index of the horizontal well J_h can be always obtained by dividing the flow rate Q_{oh} by the pressure drop Δp , or:

$$J_h = \frac{Q_{oh}}{\Delta p}$$

There are several methods that are designed to predict the productivity index from the fluid and reservoir properties. Some of these methods include:

- Borisov's method
- The Giger-Reiss-Jourdan method
- Joshi's method
- The Renard-Dupuy method

Borisov's Method

Borisov (1984) proposed the following expression for predicting the productivity index of a horizontal well in an isotropic reservoir, i.e., $k_v = k_h$

$$J_h = \frac{0.00708 h k_h}{\mu_o B_o \left[\ln \left(\frac{4r_{eh}}{L} \right) + \left(\frac{h}{L} \right) \ln \left(\frac{h}{2\pi r_w} \right) \right]} \quad (7-49)$$

where h = thickness, ft

k_h = horizontal permeability, md

k_v = vertical permeability, md

L = length of the horizontal well, ft
 r_{ch} = drainage radius of the horizontal well, ft
 r_w = wellbore radius, ft
 J_h = productivity index, STB/day/psi

The Giger-Reiss-Jourdan Method

For an isotropic reservoir where the vertical permeability k_v equals the horizontal permeability k_h , Giger et al. (1984) proposed the following expression for determining J_h :

$$J_h = \frac{0.00708 L k_h}{\mu_o B_o \left[\left(\frac{L}{h} \right) \ln(X) + \ln \left(\frac{h}{2r_w} \right) \right]} \quad (7-50)$$

$$X = \frac{1 + \sqrt{1 + \left(\frac{L}{2r_{ch}} \right)^2}}{L / (2r_{ch})} \quad (7-51)$$

To account for the reservoir anisotropy, the authors proposed the following relationships:

$$J_h = \frac{0.00708 k_h}{\mu_o B_o \left[\left(\frac{1}{h} \right) \ln(X) + \left(\frac{B^2}{L} \right) \ln \left(\frac{h}{2r_w} \right) \right]} \quad (7-52)$$

with the parameter B as defined by:

$$B = \sqrt{\frac{K_h}{K_v}} \quad (7-53)$$

where k_v = vertical permeability, md
 L = length of the horizontal section, ft

Joshi's Method

Joshi (1991) presented the following expression for estimating the productivity index of a horizontal well in isotropic reservoirs:

$$J_h = \frac{0.00708 h k_h}{\mu_o B_o \left[\ln(R) + \left(\frac{h}{L} \right) \ln \left(\frac{h}{2r_w} \right) \right]} \quad (7-54)$$

with

$$R = \frac{a + \sqrt{a^2 - (L/2)^2}}{(L/2)} \quad (7-55)$$

and a is half the major axis of the drainage ellipse and given by:

$$a = (L/2) \left[0.5 + \sqrt{0.25 + (2r_{ch}/L)^4} \right]^{0.5} \quad (7-56)$$

Joshi accounted for the influence of the reservoir anisotropy by introducing the vertical permeability k_v into Equation 7-54, to give:

$$J_h = \frac{0.00708 h k_h}{\mu_o B_o \left[\ln(R) + \left(\frac{B^2 h}{L} \right) \ln \left(\frac{h}{2r_w} \right) \right]} \quad (7-57)$$

where the parameters B and R are defined by Equations 7-53 and 7-55, respectively.

The Renard-Dupuy Method

For an isotropic reservoir, Renard and Dupuy (1990) proposed the following expression:

$$J_h = \frac{0.00708 h k_h}{\mu_o B_o \left[\cosh^{-1} \left(\frac{2a}{L} \right) + \left(\frac{h}{L} \right) \ln \left(\frac{h}{2\pi r_w} \right) \right]} \quad (7-58)$$

where a is half the major axis of the drainage ellipse and given by Equation 7-56.

For anisotropic reservoirs, the authors proposed the following relationship:

$$J_h = \frac{0.00708 h k_h}{\mu_o B_o \left[\cosh^{-1} \left(\frac{2a}{L} \right) + \left(\frac{Bh}{L} \right) \ln \left(\frac{h}{2\pi r_w'} \right) \right]} \quad (7-59)$$

where

$$r_w' = \frac{(1+B)r_w}{2B} \quad (7-60)$$

with the parameter B as defined by Equation 7-53.

Example 7-13

A 2,000-foot-long horizontal well drains an estimated drainage area of 120 acres. The reservoir is characterized by an isotropic with the following properties:

$$\begin{aligned} k_v = k_h &= 100 \text{ md} & h &= 60 \text{ ft} \\ B_o &= 1.2 \text{ bbl/STB} & \mu_o &= 0.9 \text{ cp} \\ p_e &= 3000 \text{ psi} & p_{wf} &= 2500 \text{ psi} \\ r_w &= 0.30 \text{ ft} \end{aligned}$$

Assuming a steady-state flow, calculate the flow rate by using:

- Borisov's method
- The Giger-Reiss-Jourdan method
- Joshi's method
- The Renard-Dupuy method

Solution

a. Borisov's Method

Step 1. Calculate the drainage radius of the horizontal well:

$$r_{eh} = \sqrt{\frac{(120)(43,560)}{\pi}} = 1290 \text{ ft}$$

Step 2. Calculate J_h by using Equation 7-49:

$$J_h = \frac{(0.00708)(60)(100)}{(0.9)(1.2) \left[\ln \left(\frac{(4)(1290)}{2000} \right) + \left(\frac{60}{2000} \right) \ln \left(\frac{60}{2\pi(0.3)} \right) \right]}$$

$$= 37.4 \text{ STB/day/psi}$$

Step 3. Calculate the flow rate by applying Equation 7-48:

$$Q_{oh} = (37.4) (3000 - 2500) = 18,700 \text{ STB/day}$$

b. *The Giger-Reiss-Jourdan Method*

Step 1. Calculate the parameter X from Equation 7-51:

$$X = \frac{1 + \sqrt{1 + \left(\frac{2000}{(2)(1290)} \right)^2}}{2000 / [(2)(1290)]} = 2.105$$

Step 2. Solve for J_h by applying Equation 7-50:

$$J_h = \frac{(1.00708)(2000)(100)}{(0.9)(1.2) \left[\left(\frac{2000}{60} \right) \ln(2.105) + \ln \left(\frac{60}{2(0.3)} \right) \right]}$$

$$= 44.57 \text{ STB/day}$$

Step 3. Calculate flow rate:

$$Q_{oh} = 44.57 (3000 - 2500) = 22,286 \text{ STB/day}$$

c. *Joshi's Method*

Step 1. Calculate the half major axis of ellipse by using Equation 7-56:

$$a = \left(\frac{2000}{2} \right) \left[0.5 + \sqrt{0.25 + [2(1290)/2000]^2} \right]^{0.5} = 1372 \text{ ft}$$

Step 2. Calculate the parameter R from Equation 7-55:

$$R = \frac{1372 + \sqrt{(1372)^2 - (2000/2)^2}}{(2000/2)} = 2.311$$

Step 3. Solve for J_h by applying Equation 7-54:

$$J_h = \frac{0.00708(60)(100)}{(0.9)(1.2) \left[\ln(2.311) + \left(\frac{60}{2000} \right) \ln \left(\frac{60}{(2)(0.3)} \right) \right]} = 40.3 \text{ STB/day/psi}$$

Step 4. $Q_{oh} = (40.3)(3000 - 2500) = 20,154 \text{ STB/day}$

d. *The Renard-Dupuy Method*

Step 1. Calculate a from Equation 7-56:

$$a = 1372 \text{ ft}$$

Step 2. Apply Equation 7-58 to determine J_h :

$$J_h = \frac{0.00708(60)(100)}{(0.9)(1.2) \left[\cosh^{-1} \left(\frac{(2)(1372)}{2000} \right) + \left(\frac{60}{2000} \right) \ln \left(\frac{60}{2\pi(0.3)} \right) \right]} = 41.77 \text{ STB/day/psi}$$

Step 3. $Q_{oh} = 41.77(3000 - 2500) = 20,885 \text{ STB/day}$

Example 7-14

Using the data in Example 7-14 and assuming an isotropic reservoir with $k_h = 100 \text{ md}$ and $k_v = 10 \text{ md}$, calculate flow rate by using:

- The Giger-Reiss-Jourdan method
- Joshi's method
- The Renard-Dupuy method

Solution*a. The Giger-Reiss-Jourdan Method*

Step 1. Solve for the permeability ratio B by applying Equation 7-53.

$$\beta = \sqrt{\frac{100}{10}} = 3.162$$

Step 2. Calculate the parameter X as shown in Example 7-12 to give:

$$X = 2.105$$

Step 3. Determine J_h by using Equation 7-52.

$$J_h = \frac{0.00708(100)}{(0.9)(1.2) \left[\left(\frac{1}{60} \right) \ln(2.105) + \left(\frac{3.162^2}{2000} \right) \ln \left(\frac{60}{(2)(0.3)} \right) \right]}$$

$$= 18.50 \text{ STB/day/psi}$$

Step 4. Calculate Q_{oh}

$$Q_{oh} = (18.50)(3000 - 2500) = 9252 \text{ STB/day}$$

b. Joshi's Method

Step 1. Calculate the permeability ratio β .

$$\beta = 3.162$$

Step 2. Calculate the parameters a and R as given in Example 7-12.

$$A = 1372 \text{ ft} \quad R = 2.311$$

Step 3. Calculate J_h by using Equation 7-54.

$$J_h = \frac{0.00708(60)(100)}{(0.9)(1.2) \left[\ln(2.311) + \left(\frac{(3.162)^2(60)}{2000} \right) \ln \left(\frac{60}{(2)(0.3)} \right) \right]}$$

$$= 17.73 \text{ STB/day/psi}$$

$$\text{Step 4. } Q_{oh} = (17.73) (3000 - 2500) = 8863 \text{ STB/day}$$

c. *The Renard-Dupuy Method*

Step 1. Calculate r'_w from Equation 7-60.

$$r'_w = \frac{(1 + 3.162)(0.3)}{(2)(3.162)} = 0.1974$$

Step 2. Apply Equation 7-59.

$$J_h = \frac{0.00708(60)(100)}{(0.9)(1.2) \left[\cosh^{-1} \left(\frac{(2)(1372)}{2000} \right) + \left(\frac{(3.162)^2(60)}{2000} \right) \ln \left(\frac{60}{(2)\pi(0.1974)} \right) \right]}$$

$$= 19.65 \text{ STB/day/psi}$$

$$\text{Step 3. } Q_{oh} = 19.65(3000 - 2500) = 9825 \text{ STB/day}$$

Horizontal Well Productivity under Semisteady-State Flow

The complex flow regime existing around a horizontal wellbore probably precludes using a method as simple as that of Vogel to construct the IPR of a horizontal well in solution gas drive reservoirs. If at least two stabilized flow tests are available, however, the parameters J and n in the Fetkovich equation (Equation 7-35) could be determined and used to construct the IPR of the horizontal well. In this case, the values of J and n would not only account for effects of turbulence and gas saturation around the wellbore, but also for the effects of a nonradial flow regime existing in the reservoir.

Bendakhlia and Aziz (1989) used a reservoir model to generate IPRs for a number of wells and found that a combination of Vogel and Fetkovich equations would fit the generated data if expressed as:

$$\frac{Q_{oh}}{(Q_{oh})_{max}} = \left[1 - V \left(\frac{P_{wf}}{P_r} \right) - (1 - V) \left(\frac{P_{wf}}{P_r} \right)^2 \right]^n \quad (7-61)$$

where $(Q_{oh})_{max}$ = horizontal well maximum flow rate, STB/day

n = exponent in Fetkovich's equation

V = variable parameter

In order to apply the equation, at least three stabilized flow tests are required to evaluate the three unknowns $(Q_{oh})_{max}$, V , and n at any given average reservoir pressure \bar{p}_r . However, Bendakhlia and Aziz indicated that the parameters V and n are functions of the reservoir pressure or recovery factor and, thus, the use of Equation 7-61 is not convenient in a predictive mode.

Cheng (1990) presented a form of Vogel's equation for horizontal wells that is based on the results from a numerical simulator. The proposed expression has the following form:

$$\frac{Q_{oh}}{(Q_{oh})_{max}} = 1.0 + 0.2055 \left(\frac{P_{wf}}{p_r} \right) - 1.1818 \left(\frac{P_{wf}}{p_r} \right)^2$$

Example 7-15

A 1,000-foot-long horizontal well is drilled in a solution gas drive reservoir. The well is producing at a stabilized flow rate of 760 STB/day and wellbore pressure of 1,242 psi. The current average reservoir pressure is 2,145 psi. Generate the IPR data of this horizontal well by using Cheng's method.

Solution

Step 1. Use the given stabilized flow data to calculate the maximum flow rate of the horizontal well.

$$\frac{760}{(Q_{oh})_{max}} = 1 + 0.2055 \left(\frac{1242}{2145} \right) - 1.1818 \left(\frac{1242}{2145} \right)^2$$

$$(Q_{oh})_{max} = 1052 \text{ STB/day}$$

Step 2. Generate the IPR data by applying Equation 7-62.

| P_{wf} | Q_{oh} |
|----------|----------|
| 2145 | 0 |
| 1919 | 250 |
| 1580 | 536 |
| 1016 | 875 |
| 500 | 1034 |
| 0 | 1052 |

PROBLEMS

1. An oil well is producing under steady-state flow conditions at 300 STB/day. The bottom-hole flowing pressure is recorded at 2,500 psi. Given:

$$\begin{array}{llll} h = 23 \text{ ft} & k = 50 \text{ md} & \mu_o = 2.3 \text{ cp} & r_w = 0.25 \text{ ft} \\ B_o = 1.4 \text{ bbl/STB} & r_e = 660 \text{ ft} & s = 0.5 & \end{array}$$

Calculate:

- Reservoir pressure
 - AOF
 - Productivity index
2. A well is producing from a saturated oil reservoir with an average reservoir pressure of 3,000 psig. Stabilized flow test data indicate that the well is capable of producing 400 STB/day at a bottom-hole flowing pressure of 2,580 psig.
- Oil flow rate at $p_{wf} = 1950$ psig
 - Construct the IPR curve at the current average pressure.
 - Construct the IPR curve by assuming a constant J .
 - Plot the IPR curve when the reservoir pressure is 2,700 psig.
3. An oil well is producing from an undersaturated reservoir that is characterized by a bubble-point pressure of 2,230 psig. The current average reservoir pressure is 3,500 psig. Available flow test data show that the well produced 350 STB/day at a stabilized p_{wf} of 2,800 psig. Construct the current IPR data by using:
- Vogel's correlation
 - Wiggins' method
 - Generate the future IPR curve when the reservoir pressure declines from 3,500 psi to 2,230 and 2,000 psi.
4. A well is producing from a saturated oil reservoir that exists at its saturation pressure of 4,500 psig. The well is flowing at a stabilized rate of 800 STB/day and a p_{wf} of 3,700 psig. Material balance calculations provide the following current and future predictions for oil saturation and PVT properties.

| | Present | Future |
|-----------------|---------|--------|
| \bar{p}_r | 4500 | 3300 |
| μ_o , cp | 1.45 | 1.25 |
| B_o , bbl/STB | 1.23 | 1.18 |
| k_{ro} | 1.00 | 0.86 |

Generate the future IPR for the well at 3,300 psig by using Standing's method.

5. A four-point stabilized flow test was conducted on a well producing from a saturated reservoir that exists at an average pressure of 4,320 psi.

| Q_o , STB/day | p_{wfr} , psi |
|-----------------|-----------------|
| 342 | 3804 |
| 498 | 3468 |
| 646 | 2928 |
| 832 | 2580 |

- a. Construct a complete IPR using Fetkovich's method.
b. Construct the IPR when the reservoir pressure declines to 2,500 psi.

6. The following reservoir and flow test data are available on an oil well:

- Pressure data: $\bar{p}_r = 3280$ psi $p_b = 2624$ psi
- Flow test data: $p_{wf} = 2952$ psi $Q_o =$ STB/day

Generate the IPR data of the well.

7. A 2,500-foot-long horizontal well drains an estimated drainage area of 120 acres. The reservoir is characterized by an isotropic with the following properties:

$$\begin{aligned}
 k_v = k_h = 60 \text{ md} & & h = 70 \text{ ft} \\
 B_o = 1.4 \text{ bbl/STB} & & \mu_o = 1.9 \text{ cp} \\
 p_e = 3900 \text{ psi} & & p_{wf} = 3250 \text{ psi} \\
 r_w = 0.30 \text{ ft} & &
 \end{aligned}$$

Assuming a steady-state flow, calculate the flow rate by using:

- a. Borisov's method
b. The Giger-Reiss-Jourdan method
c. Joshi's method
d. The Renard-Dupuy method

8. A 2,000-foot-long horizontal well is drilled in a solution gas drive reservoir. The well is producing at a stabilized flow rate of 900 STB/day and wellbore pressure of 1,000 psi. The current average reservoir pressure is 2,000 psi. Generate the IPR data of this horizontal well by using Cheng's method.

REFERENCES

1. Beggs, D., "Gas Production Operations," *OGCI*, Tulsa, Oklahoma, 1984.
2. Beggs, D., "Production Optimization Using NODAL Analysis," *OGCI*, Tulsa, Oklahoma, 1991.
3. Bendakhlia, H., and Aziz, K., "IPR for Solution-Gas Drive Horizontal Wells," SPE Paper 19823, presented at the 64th Annual Meeting in San Antonio, Texas, October 8–11, 1989.
4. Borisov, Ju. P., "Oil Production Using Horizontal and Multiple Deviation Wells," Nedra, Moscow, 1964. Translated by J. Strauss. S. D. Joshi (ed.). Bartlesville, OK: Phillips Petroleum Co., the R & D Library Translation, 1984.
5. Cheng, A. M., "IPR For Solution Gas-Drive Horizontal Wells," SPE Paper 20720, presented at the 65th Annual SPE Meeting in New Orleans, September 23–26, 1990.
6. Fetkovich, M. J., "The Isochronal Testing of Oil Wells," SPE Paper 4529, presented at the SPE 48th Annual Meeting, Las Vegas, Sept. 30–Oct. 3, 1973.
7. Giger, F. M., Reiss, L. H., and Jourdan, A. P., "The Reservoir Engineering Aspect of Horizontal Drilling," SPE Paper 13024, presented at the SPE 59th Annual Technical Conference and Exhibition, Houston, Texas, September 16–19, 1984.
8. Golan, M., and Whitson, C. H., *Well Performance*, 2nd ed. Englewood Cliffs, NJ: Prentice-Hall, 1986.
9. Joshi, S., *Horizontal Well Technology*. Tulsa, OK: PennWell Publishing Company, 1991.
10. Klins, M., and Clark, L., "An Improved Method to Predict Future IPR Curves," *SPE Reservoir Engineering*, November 1993, pp. 243–248.
11. Muskat, M., and Evinger, H. H., "Calculations of Theoretical Productivity Factor," *Trans. AIME*, 1942, pp. 126–139, 146.
12. Renard, G. I., and Dupuy, J. M., "Influence of Formation Damage on the Flow Efficiency of Horizontal Wells," SPE Paper 19414, presented at the Formation Damage Control Symposium, Lafayette, Louisiana, Feb. 22–23, 1990.

13. Standing, M. B., "Inflow Performance Relationships for Damaged Wells Producing by Solution-Gas Drive," *JPT*, Nov. 1970, pp. 1399–1400.
14. Vogel, J. V., "Inflow Performance Relationships for Solution-Gas Drive Wells," *JPT*, Jan. 1968, pp. 86–92; *Trans. AIME*, p. 243.
15. Wiggins, M. L., "Generalized Inflow Performance Relationships for Three-Phase Flow," SPE Paper 25458, presented at the SPE Production Operations Symposium, Oklahoma City, March 21–23, 1993.



C H A P T E R 8

GAS WELL PERFORMANCE

Determination of the flow capacity of a gas well requires a relationship between the inflow gas rate and the sand face pressure or flowing bottom-hole pressure. This inflow performance relationship may be established by the proper solution of Darcy's equation. Solution of Darcy's Law depends on the conditions of the flow existing in the reservoir or the flow regime.

When a gas well is first produced after being shut-in for a period of time, the gas flow in the reservoir follows an unsteady-state behavior until the pressure drops at the drainage boundary of the well. Then the flow behavior passes through a short transition period, after which it attains a steady-state or semisteady (pseudosteady)-state condition. The objective of this chapter is to describe the empirical as well as analytical expressions that can be used to establish the inflow performance relationships under the pseudosteady-state flow condition.

VERTICAL GAS WELL PERFORMANCE

The exact solution to the differential form of Darcy's equation for compressible fluids under the pseudosteady-state flow condition was given previously by Equation 6-150 as:

$$Q_g = \frac{kh [\bar{\psi}_r - \psi_{wf}]}{1422 T \left[\ln \left(\frac{r_c}{r_w} \right) - 0.75 + s \right]} \quad (8-1)$$

where Q_g = gas flow rate, Mscf/day
 k = permeability, md
 $\bar{\Psi}_r$ = average reservoir real gas pseudopressure, psi^2/cp
 T = temperature, $^{\circ}\text{R}$
 s = skin factor
 h = thickness
 r_c = drainage radius
 r_w = wellbore radius

The productivity index J for a gas well can be written analogous to that for oil wells as:

$$J = \frac{Q_g}{\bar{\Psi}_r - \Psi_{wf}} = \frac{kh}{1422 T \left[\ln \left(\frac{r_c}{r_w} \right) - 0.75 + s \right]} \quad (8-2)$$

or

$$Q_g = J(\bar{\Psi}_r - \Psi_{wf}) \quad (8-3)$$

with the absolute open flow potential (AOF), i.e., maximum gas flow rate $(Q_g)_{\max}$, as calculated by:

$$(Q_g)_{\max} = J\bar{\Psi}_r \quad (8-4)$$

where J = productivity index, Mscf/day/ psi^2/cp

$$(Q_g)_{\max} = \text{AOF}$$

Equation 8-3 can be expressed in a linear relationship as:

$$\Psi_{wf} = \bar{\Psi}_r - \left(\frac{1}{J} \right) Q_g \quad (8-5)$$

Equation 8-5 indicates that a plot of Ψ_{wf} vs. Q_g would produce a straight line with a slope of $(1/J)$ and intercept of $\bar{\Psi}_r$, as shown in Figure 8-1. If two different stabilized flow rates are available, the line can be extrapolated and the slope is determined to estimate AOF, J , and $\bar{\Psi}_r$.

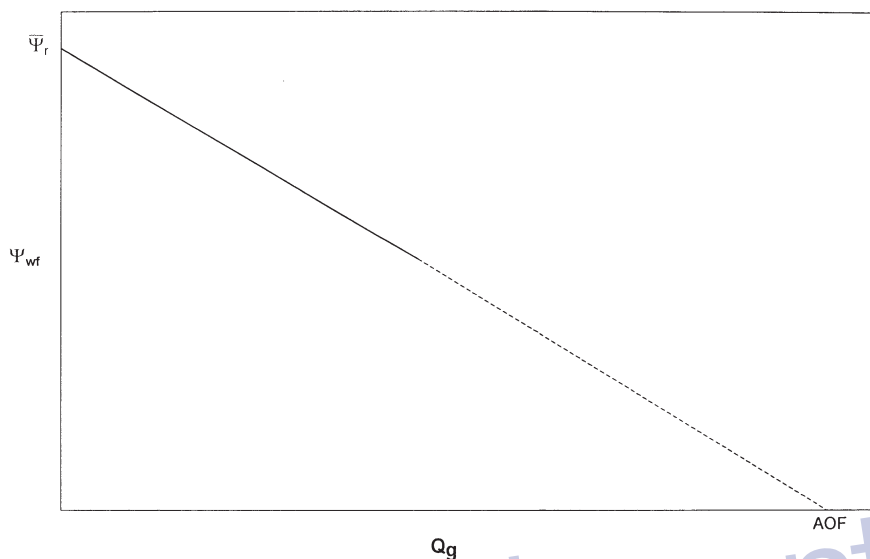


Figure 8-1. Steady-state gas well flow.

Equation 8-1 can be alternatively written in the following integral form:

$$Q_g = \frac{kh}{1422 T \left[\ln \left(\frac{r_e}{r_w} \right) - 0.75 + s \right]} \int_{p_{wf}}^{\bar{p}_r} \left(\frac{2p}{\mu_g z} \right) dp \quad (8-6)$$

Note that $(p/\mu_g z)$ is directly proportional to $(1/\mu_g B_g)$ where B_g is the gas formation volume factor and defined as:

$$B_g = 0.00504 \frac{zT}{p} \quad (8-7)$$

where B_g = gas formation volume factor, bbl/scf

z = gas compressibility factor

T = temperature, °R

Equation 8-6 can then be written in terms of B_g as:

$$Q_g = \left[\frac{7.08(10^{-6})kh}{\ln\left(\frac{r_e}{r_w}\right) - 0.75 + s} \right] \int_{p_{wf}}^{\bar{p}_r} \left(\frac{1}{\mu_g B_g} \right) dp \quad (8-8)$$

where Q_g = gas flow rate, Mscf/day
 μ_g = gas viscosity, cp
 k = permeability, md

Figure 8-2 shows a typical plot of the gas pressure functions ($2p/\mu_g z$) and ($1/\mu_g B_g$) versus pressure. The integral in Equations 8-6 and 8-8 represents the area under the curve between \bar{p}_r and p_{wf} .

As illustrated in Figure 8-2, the pressure function exhibits the following three distinct pressure application regions.

Region III. High-Pressure Region

When both p_{wf} and \bar{p}_r are higher than 3,000 psi, the pressure functions ($2p/\mu_g z$) and ($1/\mu_g B_g$) are nearly constants. This observation suggests that the pressure term ($1/\mu_g B_g$) in Equation 8-8 can be treated as a constant and removed outside the integral, to give the following approximation to Equation 8-6:

$$Q_g = \frac{7.08(10^{-6})kh(\bar{p}_r - p_{wf})}{(\mu_g B_g)_{avg} \left[\ln\left(\frac{r_e}{r_w}\right) - 0.75 + s \right]} \quad (8-9)$$

where Q_g = gas flow rate, Mscf/day
 B_g = gas formation volume factor, bbl/scf
 k = permeability, md

The gas viscosity μ_g and formation volume factor B_g should be evaluated at the average pressure p_{avg} as given by:

$$p_{avg} = \frac{\bar{p}_r + p_{wf}}{2} \quad (8-10)$$

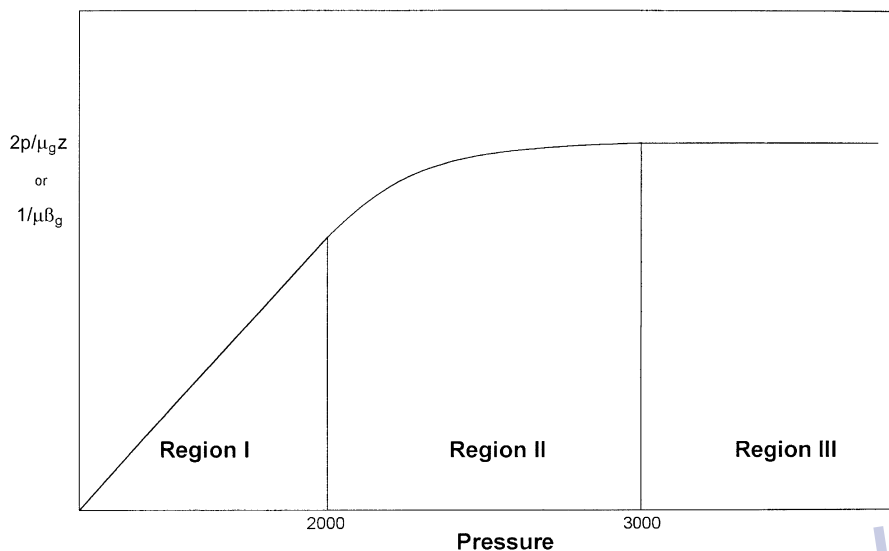


Figure 8-2. Gas PVT data.

The method of determining the gas flow rate by using Equation 8-9 is commonly called the **pressure-approximation method**.

It should be pointed out the concept of the productivity index J cannot be introduced into Equation 8-9 since Equation 8-9 is only valid for applications when both p_{wf} and \bar{p}_r are above 3,000 psi.

Region II. Intermediate-Pressure Region

Between 2,000 and 3,000 psi, the pressure function shows distinct curvature. When the bottom-hole flowing pressure and average reservoir pressure are both between 2,000 and 3,000 psi, the pseudopressure gas pressure approach (i.e., Equation 8-1) should be used to calculate the gas flow rate.

Region I. Low-Pressure Region

At low pressures, usually less than 2,000 psi, the pressure functions ($2p/\mu_g z$) and ($1/\mu_g B_g$) exhibit a linear relationship with pressure. Golan and Whitson (1986) indicated that the product ($\mu_g z$) is essentially constant when evaluating any pressure below 2,000 psi. Implementing this observation in Equation 8-6 and integrating gives:

$$Q_g = \frac{kh(\bar{p}_r^2 - p_{wf}^2)}{1422T(\mu_g z)_{avg} \left[\ln\left(\frac{r_e}{r_w}\right) - 0.75 + s \right]} \quad (8-11)$$

where Q_g = gas flow rate, Mscf/day
 k = permeability, md
 T = temperature, °R
 z = gas compressibility factor
 μ_g = gas viscosity, cp

It is recommended that the z -factor and gas viscosity be evaluated at the average pressure p_{avg} as defined by:

$$p_{avg} = \sqrt{\frac{\bar{p}_r^2 + p_{wf}^2}{2}}$$

The method of calculating the gas flow rate by Equation 8-11 is called the **pressure-squared approximation method**.

If both \bar{p}_r and p_{wf} are lower than 2000 psi, Equation 8-11 can be expressed in terms of the productivity index J as:

$$Q_g = J(\bar{p}_r^2 - p_{wf}^2) \quad (8-12)$$

with

$$(Q_g)_{max} = AOF = J\bar{p}_r^2 \quad (8-13)$$

where

$$J = \frac{kh}{1422T(\mu_g z)_{avg} \left[\ln\left(\frac{r_e}{r_w}\right) - 0.75 + s \right]} \quad (8-14)$$

Example 8-1

The PVT properties of a gas sample taken from a dry gas reservoir are given in the following table:

| p, psi | μ_g , cp | Z | ψ , psi ² /cp | B_g , bbl/scf |
|--------|--------------|-------|-------------------------------|-----------------|
| 0 | 0.01270 | 1.000 | 0 | — |
| 400 | 0.01286 | 0.937 | 13.2×10^6 | 0.007080 |
| 1200 | 0.01530 | 0.832 | 113.1×10^6 | 0.00210 |
| 1600 | 0.01680 | 0.794 | 198.0×10^6 | 0.00150 |
| 2000 | 0.01840 | 0.770 | 304.0×10^6 | 0.00116 |
| 3200 | 0.02340 | 0.797 | 678.0×10^6 | 0.00075 |
| 3600 | 0.02500 | 0.827 | 816.0×10^6 | 0.000695 |
| 4000 | 0.02660 | 0.860 | 950.0×10^6 | 0.000650 |

The reservoir is producing under the pseudosteady-state condition. The following additional data are available:

$$\begin{array}{lll}
 k = 65 \text{ md} & h = 15 \text{ ft} & T = 600^\circ\text{R} \\
 r_e = 1000 \text{ ft} & r_w = 0.25 \text{ ft} & s = 0.4
 \end{array}$$

Calculate the gas flow rate under the following conditions:

- $\bar{p}_r = 4000$ psi, $p_{wf} = 3200$ psi
- $\bar{p}_r = 2000$ psi, $p_{wf} = 1200$ psi

Use the appropriate approximation methods and compare results with the exact solution.

Solution

- Calculate Q_g at $\bar{p}_r = 4000$ and $p_{wf} = 3200$ psi:

Step 1. Select the approximation method. Because \bar{p}_r and p_{wf} are both > 3000 , the pressure-approximation method is used, i.e., Equation 8-9.

Step 2. Calculate average pressure and determine the corresponding gas properties.

$$\bar{p} = \frac{4000 + 3200}{2} = 3600 \text{ psi}$$

$$\mu_g = 0.025 \quad B_g = 0.000695$$

Step 3. Calculate the gas flow rate by applying Equation 8-9.

$$Q_g = \frac{7.08 (10^{-6}) (65) (15) (4000 - 3200)}{(0.025) (0.000695) \left[\ln \left(\frac{1000}{0.25} \right) - 0.75 - 0.4 \right]}$$

$$= 44,490 \text{ Mscf/day}$$

Step 4. Recalculate Q_g by using the pseudopressure equation, i.e., Equation 8-1.

$$Q_g = \frac{(65) (15) (950.0 - 678.0) (65) (15) 10^6}{(1422) (600) \left[\ln \left(\frac{1000}{0.25} \right) - 0.75 - 0.4 \right]} = 43,509 \text{ Mscf/day}$$

b. Calculate Q_g at $\bar{p}_r = 2000$ and $p_{wf} = 1058$:

Step 1. Select the appropriate approximation method. Because \bar{p}_r and $p_{wf} \leq 2000$, use the pressure-squared approximation.

Step 2. Calculate average pressure and the corresponding μ_g and z .

$$\bar{p} = \sqrt{\frac{2000^2 + 1200^2}{2}} = 1649 \text{ psi}$$

$$\mu_g = 0.017 \quad z = 0.791$$

Step 3. Calculate Q_g by using the pressure-squared equation, i.e., Equation 8-11.

$$Q_g = \frac{(65) (15) (2000^2 - 1200^2)}{1422 (600) (0.017) (0.791) \left[\ln \left(\frac{1000}{0.25} \right) - 0.75 - 0.4 \right]}$$

$$= 30,453 \text{ Mscf/day}$$

Step 4. Compare Q_g with the exact value from Equation 8-1:

$$Q_g = \frac{(65)(15)(304.0 - 113.1) 10^6}{(1422)(600) \left[\ln\left(\frac{1000}{0.25}\right) - 0.75 - 0.4 \right]}$$

$$= 30,536 \text{ Mscf/day}$$

All of the mathematical formulations presented thus far in this chapter are based on the assumption that laminar (viscous) flow conditions are observed during the gas flow. During radial flow, the flow velocity increases as the wellbore is approached. This increase of the gas velocity might cause the development of a turbulent flow around the wellbore. If turbulent flow does exist, it causes an additional pressure drop similar to that caused by the mechanical skin effect.

As presented in Chapter 6 by Equations 6-164 through 6-166, the semisteady-state flow equation for compressible fluids can be modified to account for the additional pressure drop due to the turbulent flow by including the rate-dependent skin factor DQ_g . The resulting pseudosteady-state equations are given in the following three forms:

First Form: Pressure-Squared Approximation Form

$$Q_g = \frac{kh(p_r^{-2} - p_{wf}^2)}{1422 T (\mu_g z)_{avg} \left[\ln\left(\frac{r_c}{r_w}\right) - 0.75 + s + DQ_g \right]} \quad (8-15)$$

where D is the **inertial** or **turbulent flow** factor and is given by Equation 6-160 as:

$$D = \frac{FKh}{1422 T} \quad (8-16)$$

where the non-Darcy flow coefficient F is defined by Equation 6-156 as:

$$F = 3.161 (10^{-12}) \left[\frac{\beta T \gamma_g}{\mu_g h^2 r_w} \right] \quad (8-17)$$

where F = non-Darcy flow coefficient
 k = permeability, md
 T = temperature, °R
 γ_g = gas gravity
 r_w = wellbore radius, ft
 h = thickness, ft
 β = turbulence parameter as given by Equation 6-157 as
 $\beta = 1.88 (10^{-10}) k^{-1.47} \phi^{-0.53}$

Second Form: Pressure-Approximation Form

$$Q_g = \frac{7.08 (10^{-6}) kh (\bar{p}_r - p_{wf})}{(\mu_g \beta_g)_{avg} T \left[\ln \left(\frac{r_e}{r_w} \right) - 0.75 + s + DQ_g \right]} \quad (8-18)$$

Third Form: Real Gas Potential (Pseudopressure) Form

$$Q_g = \frac{kh (\bar{\Psi}_r - \Psi_{wf})}{1422 T \left[\ln \left(\frac{r_e}{r_w} \right) - 0.75 + s + DQ_g \right]} \quad (8-19)$$

Equations 8-15, 8-18, and 8-19 are essentially quadratic relationships in Q_g and, thus, they do not represent explicit expressions for calculating the gas flow rate. There are two separate empirical treatments that can be used to represent the turbulent flow problem in gas wells. Both treatments, with varying degrees of approximation, are directly derived and formulated from the three forms of the pseudosteady-state equations, i.e., Equations 8-15 through 8-17. These two treatments are called:

- Simplified treatment approach
- Laminar-inertial-turbulent (LIT) treatment

The above two empirical treatments of the gas flow equation are presented on the following pages.

The Simplified Treatment Approach

Based on the analysis for flow data obtained from a large member of gas wells, Rawlins and Schellhardt (1936) postulated that the relationship between the gas flow rate and pressure can be expressed as:

$$Q_g = C(\bar{p}_r^2 - p_{wf}^2)^n \quad (8-20)$$

where Q_g = gas flow rate, Mscf/day
 \bar{p}_r = average reservoir pressure, psi
 n = exponent
 C = performance coefficient, Mscf/day/psi²

The exponent n is intended to account for the additional pressure drop caused by the high-velocity gas flow, i.e., turbulence. Depending on the flowing conditions, the exponent n may vary from 1.0 for completely laminar flow to 0.5 for fully turbulent flow. The performance coefficient C in Equation 8-20 is included to account for:

- Reservoir rock properties
- Fluid properties
- Reservoir flow geometry

Equation 8-20 is commonly called the **deliverability** or **back-pressure equation**. If the coefficients of the equation (i.e., n and C) can be determined, the gas flow rate Q_g at any bottom-hole flow pressure p_{wf} can be calculated and the IPR curve constructed.

Taking the logarithm of both sides of Equation 8-20 gives:

$$\log(Q_g) = \log(C) + n \log(\bar{p}_r^2 - p_{wf}^2) \quad (8-21)$$

Equation 8-22 suggests that a plot of Q_g versus $(\bar{p}_r^2 - p_{wf}^2)$ on log-log scales should yield a straight line having a slope of n . In the natural gas industry the plot is traditionally reversed by plotting $(\bar{p}_r^2 - p_{wf}^2)$ versus Q_g on the logarithmic scales to produce a straight line with a slope of $(1/n)$. This plot as shown schematically in Figure 8-3 is commonly referred to as the **deliverability graph** or the **back-pressure plot**.

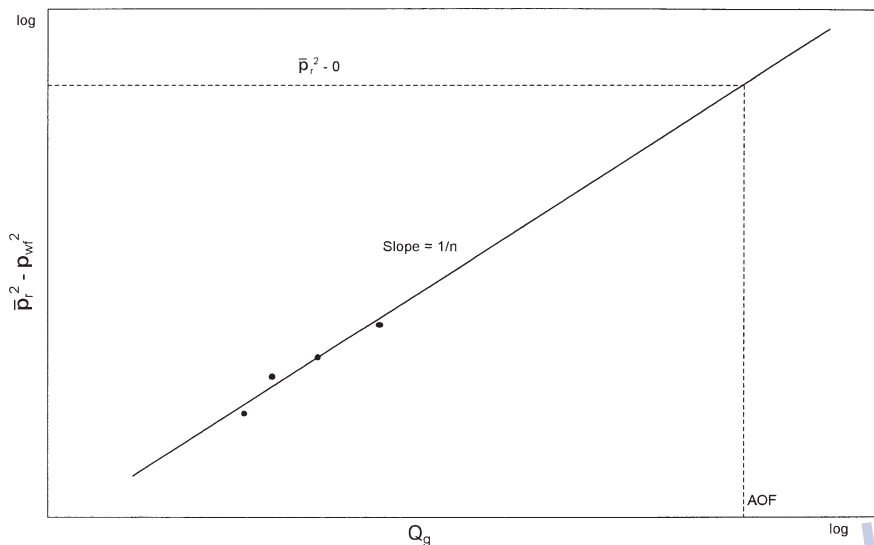


Figure 8-3. Well deliverability graph.

The deliverability exponent n can be determined from any two points on the *straight line*, i.e., $(Q_{g1}, \Delta p_1^2)$ and $(Q_{g2}, \Delta p_2^2)$, according to the flowing expression:

$$n = \frac{\log(Q_{g1}) - \log(Q_{g2})}{\log(\Delta p_1^2) - \log(\Delta p_2^2)} \quad (8-22)$$

Given n , any point on the straight line can be used to compute the performance coefficient C from:

$$C = \frac{Q_g}{(\bar{p}_r^2 - p_{wf}^2)^n} \quad (8-23)$$

The coefficients of the back-pressure equation or any of the other empirical equations are traditionally determined from analyzing gas well testing data. Deliverability testing has been used for more than sixty years by the petroleum industry to characterize and determine the flow potential of gas wells. There are essentially three types of deliverability tests and these are:

- Conventional deliverability (back-pressure) test
- Isochronal test
- Modified isochronal test

These tests basically consist of flowing wells at multiple rates and measuring the bottom-hole flowing pressure as a function of time. When the recorded data are properly analyzed, it is possible to determine the flow potential and establish the inflow performance relationships of the gas well. The deliverability test is discussed later in this chapter for the purpose of introducing basic techniques used in analyzing the test data.

The Laminar-Inertial-Turbulent (LIT) Approach

The three forms of the semisteady-state equation as presented by Equations 8-15, 8-18, and 8-19 can be rearranged in quadratic forms for the purpose of separating the *laminar* and *inertial-turbulent* terms composing these equations as follows:

a. Pressure-Squared Quadratic Form

Equation 8-15 can be written in a more simplified form as:

$$\bar{p}_r^2 - p_{wf}^2 = aQ_g + bQ_g^2 \quad (8-24)$$

with

$$a = \left(\frac{1422 T \mu_g z}{kh} \right) \left[\ln \left(\frac{r_e}{r_w} \right) - 0.75 + s \right] \quad (8-25)$$

$$b = \left(\frac{1422 T \mu_g z}{kh} \right) D \quad (8-26)$$

where a = laminar flow coefficient

b = inertial-turbulent flow coefficient

Q_g = gas flow rate, Mscf/day

z = gas deviation factor

k = permeability, md

μ_g = gas viscosity, cp

The term $(a Q_g)$ in Equation 8-26 represents the pressure-squared drop due to laminar flow while the term $(b Q_g^2)$ accounts for the pressure-squared drop due to inertial-turbulent flow effects.

Equation 8-24 can be linearized by dividing both sides of the equation by Q_g to yield:

$$\frac{\bar{p}_r^2 - p_{wf}^2}{Q_g} = a + b Q_g \quad (8-27)$$

The coefficients a and b can be determined by plotting $\left(\frac{\bar{p}_r^2 - p_{wf}^2}{Q_g} \right)$ versus Q_g on a Cartesian scale and should yield a straight line with a slope of b and intercept of a . As presented later in this chapter, data from deliverability tests can be used to construct the linear relationship as shown schematically in Figure 8-4.

Given the values of a and b , the quadratic flow equation, i.e., Equation 8-24, can be solved for Q_g at any p_{wf} from:

$$Q_g = \frac{-a + \sqrt{a^2 + 4b(\bar{p}_r^2 - p_{wf}^2)}}{2b} \quad (8-28)$$

Furthermore, by assuming various values of p_{wf} and calculating the corresponding Q_g from Equation 8-28, the current IPR of the gas well at the current reservoir pressure \bar{p}_r can be generated.

It should be pointed out the following assumptions were made in developing Equation 8-24:

- Single phase flow in the reservoir
- Homogeneous and isotropic reservoir system
- Permeability is independent of pressure
- The product of the gas viscosity and compressibility factor, i.e., $(\mu_g z)$ is constant

This method is recommended for applications at pressures below 2,000 psi.

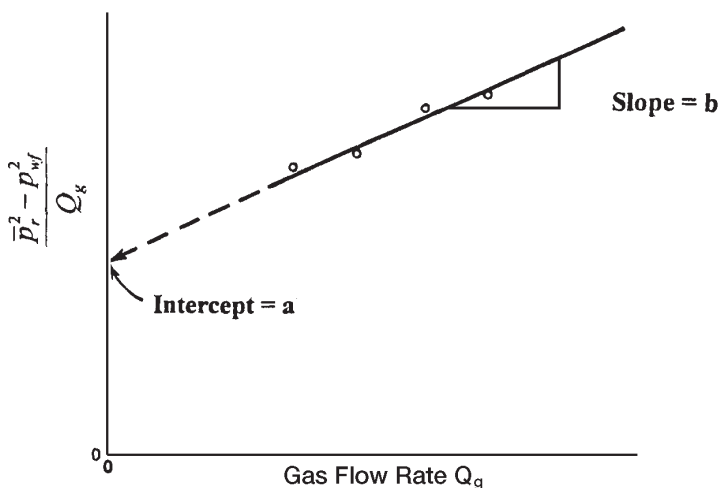


Figure 8-4. Graph of the pressure-squared data.

b. Pressure-Quadratic Form

The pressure-approximation equation, i.e., Equation 8-18, can be rearranged and expressed in the following quadratic form.

$$\bar{p}_r - p_{wf} = a_1 Q_g + b_1 Q_g^2 \quad (8-29)$$

where

$$a_1 = \frac{141.2 (10^{-3}) (\mu_g B_g)}{kh} \left[\ln \left(\frac{r_c}{r_w} \right) - 0.75 + s \right] \quad (8-30)$$

$$b_1 = \left[\frac{141.2 (10^{-3}) (\mu_g B_g)}{kh} \right] D \quad (8-31)$$

The term $(a_1 Q_g)$ represents the pressure drop due to laminar flow, while the term $(b_1 Q_g^2)$ accounts for the additional pressure drop due to

the turbulent flow condition. In a linear form, Equation 8-17 can be expressed as:

$$\frac{\bar{p}_r - p_{wf}}{Q_g} = a_1 + b_1 Q_g \quad (8-32)$$

The laminar flow coefficient a_1 and inertial-turbulent flow coefficient b_1 can be determined from the linear plot of the above equation as shown in Figure 8-5.

Having determined the coefficient a_1 and b_1 , the gas flow rate can be determined at any pressure from:

$$Q_g = \frac{-a_1 + \sqrt{a_1^2 + 4b_1(\bar{p}_r - p_{wf})}}{2b_1} \quad (8-33)$$

The application of Equation 8-29 is also restricted by the assumptions listed for the pressure-squared approach. However, the pressure method is applicable at pressures higher than 3,000 psi.

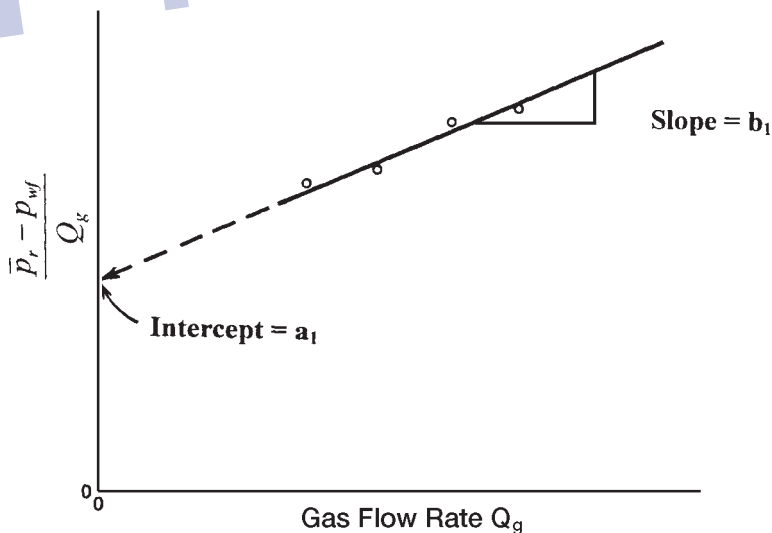


Figure 8-5. Graph of the pressure-method data.

c. Pseudopressure Quadratic Approach

Equation 8-19 can be written as:

$$\bar{\Psi}_r - \Psi_{wf} = a_2 Q_g + b_2 Q_g^2 \quad (8-34)$$

where

$$a_2 = \left(\frac{1422}{kh} \right) \left[\ln \left(\frac{r_e}{r_w} \right) - 0.75 + s \right] \quad (8-35)$$

$$b_2 = \left(\frac{1422}{kh} \right) D \quad (8-36)$$

The term ($a_2 Q_g$) in Equation 8-34 represents the pseudopressure drop due to laminar flow while the term ($b_2 Q_g^2$) accounts for the pseudopressure drop due to inertial-turbulent flow effects.

Equation 8-34 can be linearized by dividing both sides of the equation by Q_g to yield:

$$\frac{\bar{\Psi}_r - \Psi_{wf}}{Q_g} = a_2 + b_2 Q_g \quad (8-37)$$

The above expression suggests that a plot of $\left(\frac{\bar{\Psi}_r - \Psi_{wf}}{Q_g} \right)$ versus Q_g on a Cartesian scale should yield a straight line with a slope of b_2 and intercept of a_2 as shown in Figure 8-6.

Given the values of a_2 and b_2 , the gas flow rate at any p_{wf} is calculated from:

$$Q_g = \frac{-a_2 + \sqrt{a_2^2 + 4b_2(\bar{\Psi}_r - \Psi_{wf})}}{2b_2} \quad (8-38)$$

It should be pointed out that the pseudopressure approach is more rigorous than either the pressure-squared or pressure-approximation method and is applicable to all ranges of pressure.

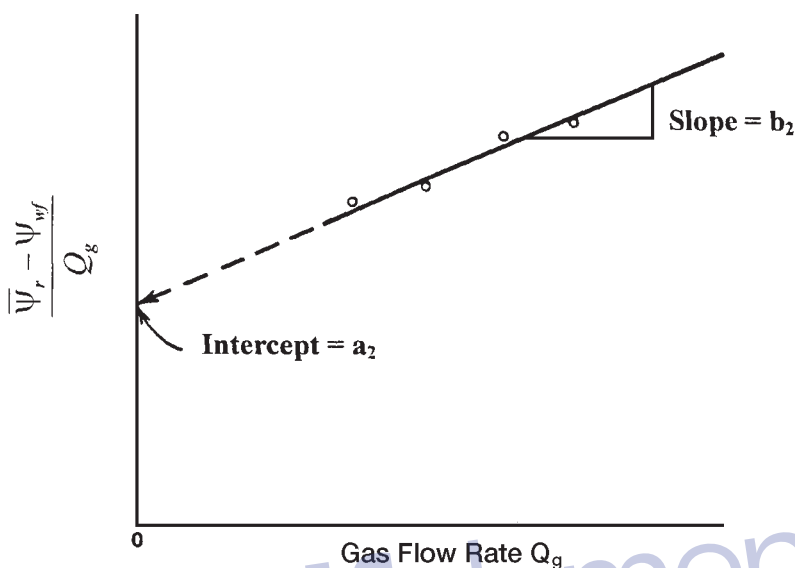


Figure 8-6. Graph of real gas pseudopressure data.

In the next section, the back-pressure test is introduced. The material, however, is intended only to be an introduction. There are several excellent books by the following authors that address transient flow and well testing in great detail:

- Earlougher (1977)
- Matthews and Russell (1967)
- Lee (1982)
- Canadian Energy Resources Conservation Board (1975)

The Back-Pressure Test

Rawlins and Schellhardt (1936) proposed a method for testing gas wells by gauging the ability of the well to flow against various back pressures. This type of flow test is commonly referred to as the *conventional deliverability test*. The required procedure for conducting this back-pressure test consists of the following steps:

- Step 1.* Shut in the gas well sufficiently long for the formation pressure to equalize at the volumetric average pressure \bar{p}_r .
- Step 2.* Place the well on production at a constant flow rate Q_{g1} for a sufficient time to allow the bottom-hole flowing pressure to stabilize at p_{wf1} , i.e., to reach the pseudosteady state.
- Step 3.* Repeat Step 2 for several rates and the stabilized bottom-hole flow pressure is recorded at each corresponding flow rate. If three or four rates are used, the test may be referred to as a three-point or four-point flow test.

The rate and pressure history of a typical four-point test is shown in Figure 8-7. The figure illustrates a normal sequence of rate changes where the rate is increased during the test. Tests may be also run, however, using a reverse sequence. Experience indicates that a normal rate sequence gives better data in most wells.

The most important factor to be considered in performing the conventional deliverability test is the length of the flow periods. It is required that each rate be maintained sufficiently long for the well to stabilize, i.e., to reach the pseudosteady state. The stabilization time for a well in the center of a circular or square drainage area may be estimated from:

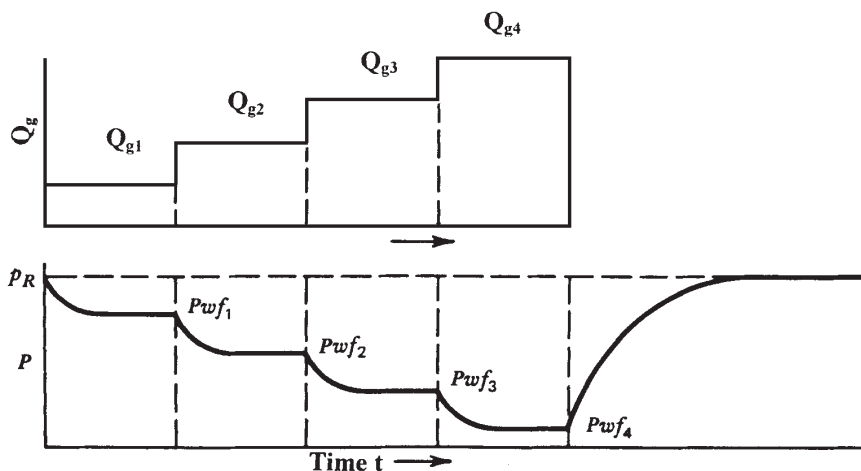


Figure 8-7. Conventional back-pressure test.

$$t_s = \frac{1200 \phi S_g \mu_g r_c^2}{k \bar{p}_r} \quad (8-39)$$

where t_s = stabilization time, hr
 ϕ = porosity, fraction
 μ_g = gas viscosity, cp
 S_g = gas saturation, fraction
 k = gas effective permeability, md
 \bar{p}_r = average reservoir pressure, psia
 r_c = drainage radius, ft

The application of the back-pressure test data to determine the coefficients of any of the empirical flow equations is illustrated in the following example.

Example 8-2

A gas well was tested using a three-point conventional deliverability test. Data recorded during the test are given below:

| p_{wfr} psia | ψ_{wfr} psi ² /cp | Q_g Mscf/day |
|--------------------|-----------------------------------|----------------|
| $\bar{p}_r = 1952$ | 316×10^6 | 0 |
| 1700 | 245×10^6 | 2624.6 |
| 1500 | 191×10^6 | 4154.7 |
| 1300 | 141×10^6 | 5425.1 |

Figure 8-8 shows the gas pseudopressure ψ as a function of pressure. Generate the current IPR by using the following methods.

- a. Simplified back-pressure equation
- b. Laminar-inertial-turbulent (LIT) methods:
 - i. Pressure-squared approach, Equation 8-29
 - ii. Pressure-approach, Equation 8-33
 - iii. Pseudopressure approach, Equation 8-26
- c. Compare results of the calculation.

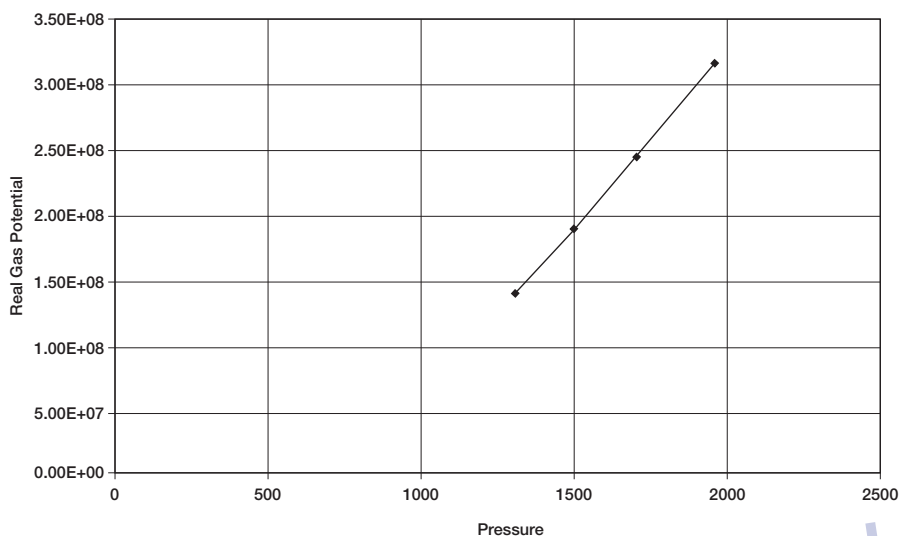


Figure 8-8. Real gas potential vs. pressure.

Solution

a. Back-Pressure Equation:

Step 1. Prepare the following table:

| p_{wf} | $p_{wf}^2, \text{psi}^2 \times 10^3$ | $(\bar{p}_r^2 - p_{wf}^2), \text{psi}^2 \times 10^3$ | $Q_g, \text{Mscf/day}$ |
|--------------------|--------------------------------------|--|------------------------|
| $\bar{p}_r = 1952$ | 3810 | 0 | 0 |
| 1700 | 2890 | 920 | 2624.6 |
| 1500 | 2250 | 1560 | 4154.7 |
| 1300 | 1690 | 2120 | 5425.1 |

Step 2. Plot $(\bar{p}_r^2 - p_{wf}^2)$ versus Q_g on a log-log scale as shown in Figure 8-9. Draw the best straight line through the points.

Step 3. Using any two points on the straight line, calculate the exponent n from Equation 8-22, as

$$n = \frac{\log(4000) - \log(1800)}{\log(1500) - \log(600)} = 0.87$$

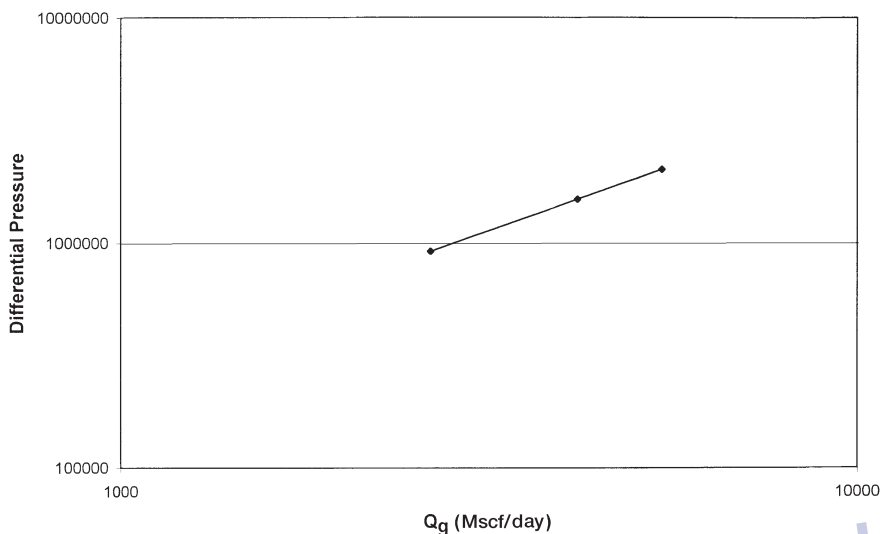


Figure 8-9. Back-pressure curve.

Step 4. Determine the performance coefficient C from Equation 8-23 by using the coordinate of any point on the straight line, or:

$$C = \frac{1800}{(600,000)^{0.87}} = 0.0169 \text{ Mscf/psi}^2$$

Step 5. The back-pressure equation is then expressed as:

$$Q_g = 0.0169 (3,810,000 - p_{wf}^2)^{0.87}$$

Step 6. Generate the IPR data by assuming various values of p_{wf} and calculate the corresponding Q_g .

| p_{wf} | Q_g , Mscf/day |
|----------|----------------------------|
| 1952 | 0 |
| 1800 | 1720 |
| 1600 | 3406 |
| 1000 | 6891 |
| 500 | 8465 |
| 0 | 8980 = AOF = $(Q_g)_{max}$ |

b. LIT Method

i. Pressure-squared method

Step 1. Construct the following table:

| p_{wf} | $(\bar{p}_r^2 - p_{wf}^2), \text{psi}^2 \times 10^3$ | $Q_g, \text{Mscf/day}$ | $(\bar{p}_r^2 - p_{wf}^2)/Q_g$ |
|--------------------|--|------------------------|--------------------------------|
| $\bar{p}_r = 1952$ | 0 | 0 | — |
| 1700 | 920 | 2624.6 | 351 |
| 1500 | 1560 | 4154.7 | 375 |
| 1300 | 2120 | 5425.1 | 391 |

Step 2. Plot $(\bar{p}_r^2 - p_{wf}^2)/Q_g$ versus Q_g on a Cartesian scale and draw the best straight line as shown in Figure 8-10.

Step 3. Determine the intercept and the slope of the straight line to give:

$$\text{intercept } a = 318$$

$$\text{slope } b = 0.01333$$

Step 4. The quadratic form of the pressure-squared approach can be expressed as:

$$(3,810,000 - p_{wf}^2) = 318 Q_g + 0.01333 Q_g^2$$

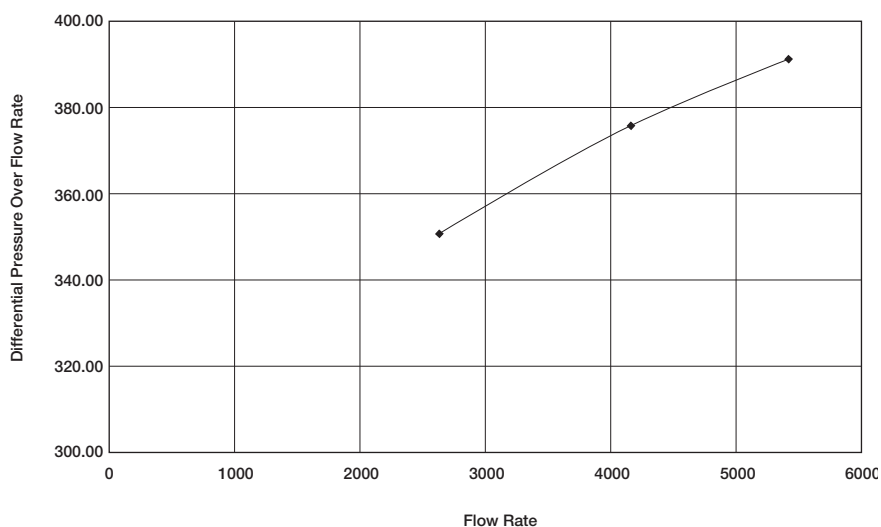


Figure 8-10. Pressure-squared method.

Step 5. Construct the IPR data by assuming various values of p_{wf} and solving for Q_g by using Equation 8-28.

| p_{wf} | $(\bar{p}_r^2 - p_{wf}^2), \text{psi}^2 \times 10^3$ | $Q_g, \text{Mscf/day}$ |
|--------------------|--|-----------------------------|
| $\bar{p}_r = 1952$ | 0 | 0 |
| 1800 | 570 | 1675 |
| 1600 | 1250 | 3436 |
| 1000 | 2810 | 6862 |
| 500 | 3560 | 8304 |
| 0 | 3810 | 8763 = AOF = $(Q_g)_{\max}$ |

ii. Pressure-approximation method

Step 1. Construct the following table:

| p_{wf} | $(\bar{p}_r - p_{wf})$ | $Q_g, \text{Mscf/day}$ | $(\bar{p}_r - p_{wf})/Q_g$ |
|--------------------|------------------------|------------------------|----------------------------|
| $\bar{p}_r = 1952$ | 0 | 0 | — |
| 1700 | 252 | 262.6 | 0.090 |
| 1500 | 452 | 4154.7 | 0.109 |
| 1300 | 652 | 5425.1 | 0.120 |

Step 2. Plot $(\bar{p}_r - p_{wf})/Q_g$ versus Q_g on a Cartesian scale as shown in Figure 8-11.

Draw the best straight line and determine the intercept and slope as:

$$\text{intercept } a_1 = 0.06$$

$$\text{slope } b_1 = 1.111 \times 10^{-5}$$

Step 3. The quadratic form of the pressure-approximation method is then given by:

$$(1952 - p_{wf}) = 0.06 Q_g + 1.111 (10^{-5}) Q_g^2$$

Step 4. Generate the IPR data by applying Equation 8-33:

| p_{wf} | $(\bar{p}_r - p_{wf})$ | $Q_g, \text{Mscf/day}$ |
|----------|------------------------|------------------------|
| 1952 | 0 | 0 |
| 1800 | 152 | 1879 |
| 1600 | 352 | 3543 |
| 1000 | 952 | 6942 |
| 500 | 1452 | 9046 |
| 0 | 1952 | 10,827 |

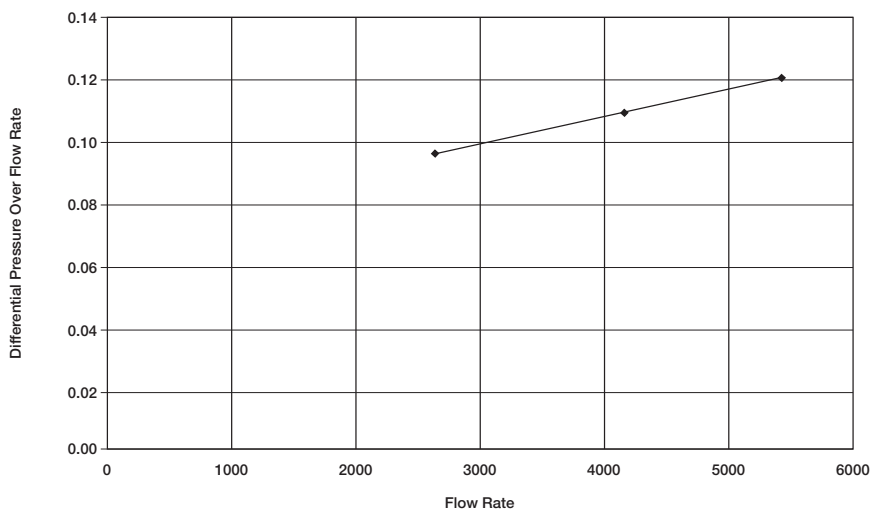


Figure 8-11. Pressure-approximation method.

iii. *Pseudopressure approach*

Step 1. Construct the following table:

| p_{wf} | $\psi, \text{psi}^2/\text{cp}$ | $(\bar{\psi}_r - \psi_{wf})$ | $Q_g, \text{Mscf/day}$ | $(\bar{\psi}_r - \psi_{wf})/Q_g$ |
|--------------------|--------------------------------|------------------------------|------------------------|----------------------------------|
| $\bar{p}_r = 1952$ | 316×10^6 | 0 | 0 | — |
| 1700 | 245×10^6 | 71×10^6 | 262.6 | 27.05×10^3 |
| 1500 | 191×10^6 | 125×10^6 | 4154.7 | 30.09×10^3 |
| 1300 | 141×10^6 | 175×10^6 | 5425.1 | 32.26×10^3 |

Step 2. Plot $(\bar{\psi}_r - \psi_{wf})/Q_g$ on a Cartesian scale as shown in Figure 8-12 and determine the intercept a_2 and slope b_2 , or:

$$a_2 = 22.28 \times 10^3$$

$$b_2 = 1.727$$

Step 3. The quadratic form of the gas pseudopressure method is given by:

$$(316 \times 10^6 - \psi_{wf}) = 22.28 \times 10^3 Q_g + 1.727 Q_g^2$$

Step 4. Generate the IPR data by assuming various values of p_{wf} , i.e., ψ_{wf} , and calculate the corresponding Q_g from Equation 8-38.

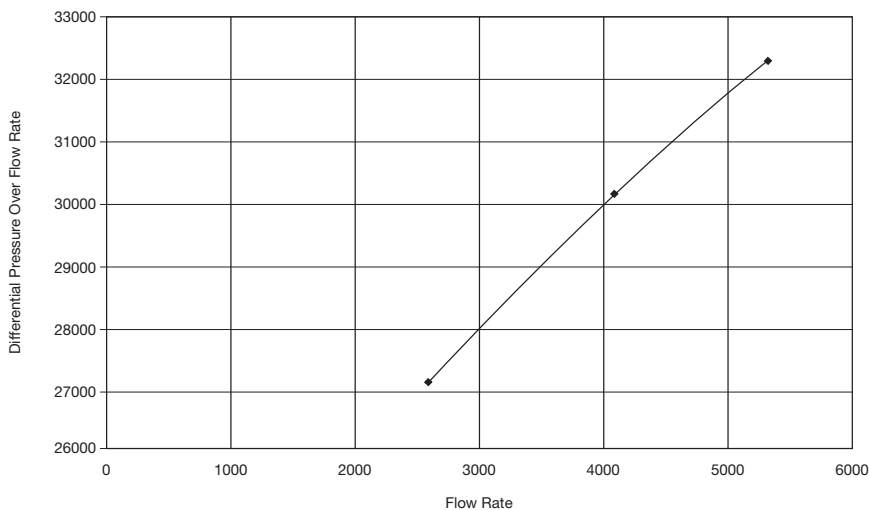


Figure 8-12. Pseudopressure method.

| P_{wf} | ψ | $\bar{\psi}_r - \psi_{wf}$ | Q_g , Mscf/day |
|----------|-------------------|----------------------------|-------------------------------------|
| 1952 | 316×10^6 | 0 | 0 |
| 1800 | 270×10^6 | 46×10^6 | 1794 |
| 1600 | 215×10^6 | 101×10^6 | 3503 |
| 1000 | 100×10^6 | 216×10^6 | 6331 |
| 500 | 40×10^6 | 276×10^6 | 7574 |
| 0 | 0 | 316×10^6 | 8342 = AOF (Q_g) _{max} |

c. Compare the gas flow rates as calculated by the four different methods. Results of the IPR calculation are documented below:

| Gas Flow Rate, Mscf/day | | | | |
|-------------------------|---------------|-----------------|---------------|------------------|
| Pressure | Back-Pressure | p^2 -Approach | p -Approach | ψ -Approach |
| 19,520 | 0 | 0 | 0 | 0 |
| 1800 | 1720 | 1675 | 1879 | 1811 |
| 1600 | 3406 | 3436 | 3543 | 3554 |
| 1000 | 6891 | 6862 | 6942 | 6460 |
| 500 | 8465 | 8304 | 9046 | 7742 |
| 0 | 8980 | 8763 | 10827 | 8536 |
| | 6.0% | 5.4% | 11% | — |

Since the pseudo-pressure analysis is considered more accurate and rigorous than the other three methods, the accuracy of each of the methods in predicting the IPR data is compared with that of the ψ -approach. Figure 8-13 compares graphically the performance of each method with that of the ψ -approach. Results indicate that the pressure-squared equation generated the IPR data with an absolute average error of 5.4% as compared with 6% and 11% for the back-pressure equation and the pressure-approximation method, respectively.

It should be noted that the pressure-approximation method is limited to applications for pressures greater than 3,000 psi.

Future Inflow Performance Relationships

Once a well has been tested and the appropriate deliverability or inflow performance equation established, it is essential to predict the IPR data as a function of average reservoir pressure. The gas viscosity μ_g and gas compressibility z -factor are considered the parameters that are subject to the greatest change as reservoir pressure \bar{p}_r changes.

Assume that the current average reservoir pressure is \bar{p}_r , with gas viscosity of μ_g and a compressibility factor of z_1 . At a selected future average reservoir pressure \bar{p}_{r2} , μ_{g2} and z_2 represent the corresponding gas properties. To approximate the effect of reservoir pressure changes, i.e. from \bar{p}_{r1}

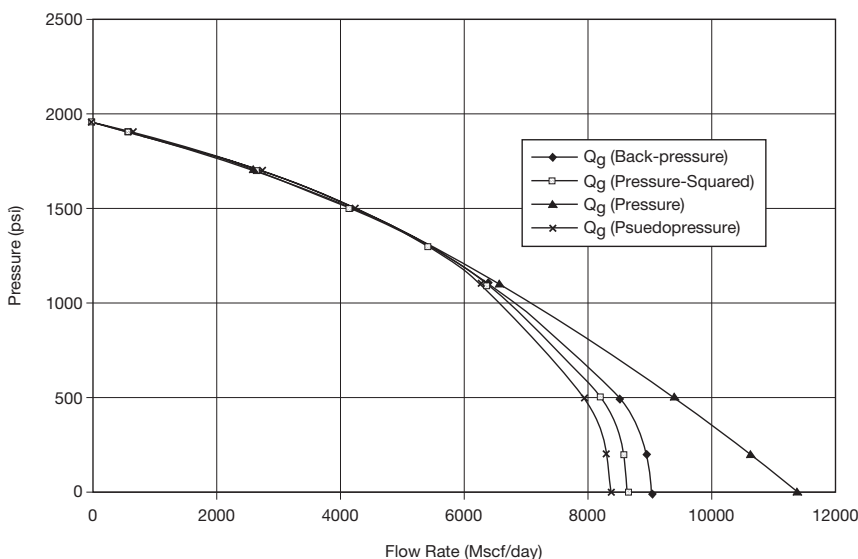


Figure 8-13. IPR for all methods.

to \bar{p}_{r2} , on the coefficients of the deliverability equation, the following methodology is recommended.

Back-Pressure Equation

The performance coefficient C is considered a pressure-dependent parameter and adjusted with each change of the reservoir pressure according to the following expression:

$$C_2 = C_1 \left[\frac{\mu_{g1} Z_1}{\mu_{g2} Z_2} \right] \quad (8-40)$$

The value of n is considered essentially constant.

LIT Methods

The laminar flow coefficient a and the inertial-turbulent flow coefficient b of any of the previous LIT methods, i.e., Equations 8-24, 8-29, and 8-34, are modified according to the following simple relationships:

• Pressure-Squared Method

The coefficients a and b of pressure-squared are modified to account for the change of the reservoir pressure from \bar{p}_{r1} to \bar{p}_{r2} by adjusting the coefficients as follows:

$$a_2 = a_1 \left[\frac{\mu_{g2} Z_2}{\mu_{g1} Z_1} \right] \quad (8-41)$$

$$b_2 = b_1 \left[\frac{\mu_{g2} Z_2}{\mu_{g1} Z_1} \right] \quad (8-42)$$

where the subscripts 1 and 2 represent conditions at reservoir pressure \bar{p}_{r1} to \bar{p}_{r2} , respectively.

• Pressure-Approximation Method

$$a_2 = a_1 \left[\frac{\mu_{g2} \beta_{g2}}{\mu_{g1} \beta_{g1}} \right] \quad (8-43)$$

$$b_2 = b_1 \left[\frac{\mu_{g2} \beta_{g2}}{\mu_{g1} \beta_{g1}} \right] \quad (8-44)$$

where B_g is the gas formation volume factor.

• Pseudopressure Approach

The coefficients a and b of the pseudopressure approach are essentially independent of the reservoir pressure and they can be treated as constants.

Example 8-3

In addition to the data given in Example 8-2, the following information is available:

- $(\mu_g z) = 0.01206$ at 1952 psi
- $(\mu_g z) = 0.01180$ at 1700 psi

Using the following methods:

- a. Back-pressure method
- b. Pressure-squared method
- c. Pseudopressure method

generate the IPR data for the well when the reservoir pressure drops from 1,952 to 1,700 psi.

Solution

Step 1. Adjust the coefficients a and b of each equation. For the:

• Back-pressure equation:

Using Equation 8-40, adjust C :

$$C = 0.0169 \left(\frac{0.01206}{0.01180} \right) = 0.01727$$

$$Q_g = 0.01727 (1700^2 - p_{wf}^2) 0.87$$

• Pressure-squared method:

Adjust a and b by applying Equations 8-41 and 8-42.

$$a = 318 \left(\frac{0.01180}{0.01206} \right) = 311.14$$

$$b = 0.01333 \left(\frac{0.01180}{0.01206} \right) = 0.01304$$

$$(1700^2 - p_{wf}^2) = 311.14 Q_g + 0.01304 Q_g^2$$

• **Pseudopressure method:**

No adjustments are needed.

$$(245 \times 10^6) - \psi_{wf} = (22.28 \times 10^3) Q_g + 1.727 Q_g^2$$

Step 2. Generate the IPR data:

| p _{wf} | Gas Flow Rate Q _g , Mscf/day | | |
|-----------------------|---|------------------------|----------|
| | Back-Pressure | p ² -Method | ψ-Method |
| p _r = 1700 | 0 | 0 | 0 |
| 1600 | 1092 | 1017 | 1229 |
| 1000 | 4987 | 5019 | 4755 |
| 500 | 6669 | 6638 | 6211 |
| 0 | 7216 | 7147 | 7095 |

Figure 8-14 compares graphically the IPR data as predicted by the above three methods.

Mishra and Caudle (1984) pointed out that when multipoint tests cannot be run due to economic or other reasons, single-point test data can be used to generate the IPR provided that a shut-in bottom-hole pressure, also known as average reservoir pressure, is known. The authors suggested the following relationship:

$$\frac{Q_g}{(Q_g)_{\max}} = 1.25 \left(1 - 5 \left[\frac{m(p_{wf}^2) - 1}{m(p_r^2)} \right] \right)$$

In terms of the pressure-squared method:

$$\frac{Q_g}{(Q_g)_{\max}} = 1.25 \left(1 - 5 \left[\frac{p_{wf}^2 - 1}{p_r^2} \right] \right)$$

And in terms of the pressure-approximation method:

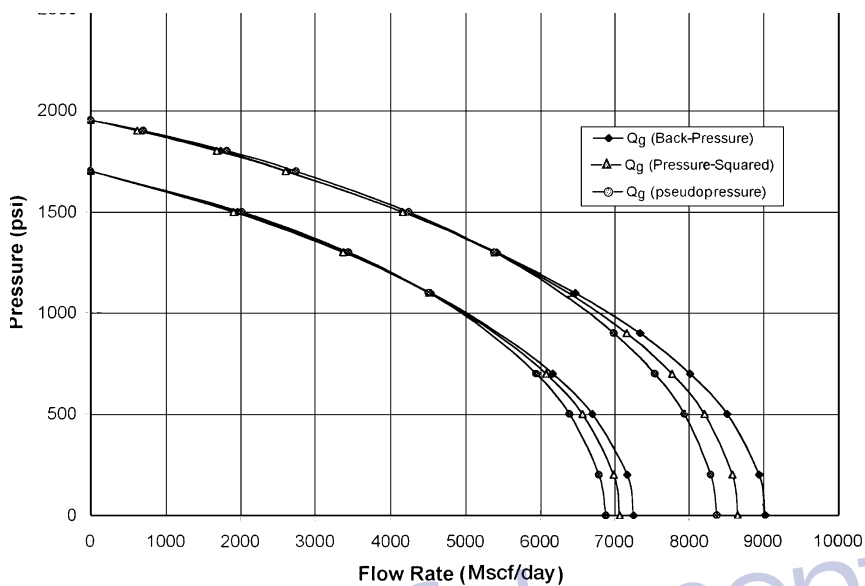


Figure 8-14. IPR comparison.

$$\frac{Q_g}{(Q_g)_{\max}} = 1.25 \left(1 - 5 \left[\frac{p_{wf}}{p_r} - 1 \right] \right)$$

For predicting future IPR, Mishra and Caudle proposed the following expression:

$$\frac{(Q_{\max})_f}{(Q_{\max})_P} = \frac{5}{3} \left(1 - 0.4 \left[\frac{m(p_{wf})_f}{m(p_r)_p} \right] \right)$$

where the subscripts f and p denote future and present, respectively.

HORIZONTAL GAS WELL PERFORMANCE

Many low permeability gas reservoirs are historically considered to be noncommercial due to low production rates. Most vertical wells drilled in tight gas reservoirs are stimulated using hydraulic fracturing and/or acidizing treatments to attain economical flow rates. In addition, to deplete a tight gas reservoir, vertical wells must be drilled at close spacing to efficiently drain the reservoir. This would require a large number of vertical wells. In such reservoirs, horizontal wells provide an attractive alternative to effectively deplete tight gas reservoirs and attain high flow rates. Joshi (1991) points out those horizontal wells are applicable in both low-permeability reservoirs as well as in high-permeability reservoirs.

An excellent reference textbook by Sada Joshi (1991) gives a comprehensive treatment of horizontal wells' performance in oil and gas reservoirs.

In calculating the gas flow rate from a horizontal well, Joshi introduced the concept of the **effective wellbore radius** r'_w into the gas flow equation. The effective wellbore radius is given by:

$$r'_w = \frac{r_{ch}(L/2)}{a[1 + \sqrt{1 - (L/2a)^2} [h/(2r_w)]^{h/L}]} \quad (8-45)$$

with

$$a = \left(\frac{L}{2}\right) \left[0.5 + \sqrt{0.25 + (2r_{ch}/L)^4}\right]^{0.5} \quad (8-46)$$

and

$$r_{ch} = \sqrt{\frac{43,560 A}{\pi}} \quad (8-47)$$

where L = length of the horizontal well, ft

h = thickness, ft

r_w = wellbore radius, ft

r_{ch} = horizontal well drainage radius, ft

a = half the major axis of drainage ellipse, ft

A = drainage area, acres

Methods of calculating the horizontal well drainage area A are presented in Chapter 7 by Equations 7-45 and 7-46.

For a pseudosteady-state flow, Joshi expressed Darcy's equation of a laminar flow in the following two familiar forms:

Pressure-Squared Form

$$Q_g = \frac{kh (\bar{p}_r^2 - p_{wf}^2)}{1422 T (\mu_g z)_{avg} [\ln(r_{eh}/r'_w) - 0.75 + s]} \quad (8-48)$$

where Q_g = gas flow rate, Mscf/day

s = skin factor

k = permeability, md

T = temperature, °R

Pseudopressure Form

$$Q_g = \frac{kh (\bar{\Psi}_r - \Psi_{wf})}{1422 T \left[\ln \left(\frac{r_{eh}}{r_w} \right) - 0.75 + s \right]}$$

Example 8-4

A 2,000-foot-long horizontal gas well is draining an area of approximately 120 acres. The following data are available:

$$\bar{p}_r = 2000 \text{ psi} \quad \bar{\Psi}_r = 340 \times 10^6 \text{ psi}^2/\text{cp}$$

$$p_{wf} = 1200 \text{ psi} \quad \Psi_{wf} = 128 \times 10^6 \text{ psi}^2/\text{cp}$$

$$\begin{aligned} (\mu_g z)_{avg} &= 0.011826 & r_w &= 0.3 \text{ ft} & s &= 0.5 \\ h &= 20 \text{ ft} & T &= 180^\circ\text{F} & k &= 1.5 \text{ md} \end{aligned}$$

Assuming a pseudosteady-state flow, calculate the gas flow rate by using the pressure-squared and pseudopressure methods.

Solution

Step 1. Calculate the drainage radius of the horizontal well:

$$r_{eh} = \sqrt{\frac{(43,560)(120)}{\pi}} = 1290 \text{ ft}$$

Step 2. Calculate half the major axis of drainage ellipse by using Equation 8-46:

$$a = \left[\frac{2000}{2} \right] \left[0.5 + \sqrt{0.25 + \left[\frac{(2)(1290)}{2000} \right]^4} \right]^{0.5} = 1495.8$$

Step 3. Calculate the effective wellbore radius r'_w from Equation 8-45:

$$(h/2r_w)^{h/L} = \left[\frac{20}{(2)(0.3)} \right]^{20/2000} = 1.0357$$

$$1 + \sqrt{1 - \left(\frac{L}{2a} \right)^2} = 1 + \sqrt{1 - \left(\frac{2000}{2(1495.8)} \right)^2} = 1.7437$$

Applying Equation 8-45 gives:

$$r'_w = \frac{1290(200/2)}{1495.8 (1.7437) (1.0357)} = 477.54 \text{ ft}$$

Step 4. Calculate the flow rate by using the pressure-squared approximation and ψ -approach.

- **Pressure-squared**

$$Q_g = \frac{(1.5)(20)(2000^2 - 1200^2)}{(1422)(640)(0.011826) \left[\ln \left(\frac{1290}{477.54} \right) - 0.75 + 0.5 \right]}$$

$$= 9594 \text{ Mscf/day}$$

• ψ -Method

$$Q_g = \frac{(1.5)(20)(340 - 128)(10^6)}{(1422)(640) \left[\ln \left(\frac{1290}{477.54} \right) - 0.75 + 0.5 \right]}$$

$$= 9396 \text{ Mscf/day}$$

For turbulent flow, Darcy's equation must be modified to account for the additional pressure caused by the non-Darcy flow by including the rate-dependent skin factor DQ_g . In practice, the back-pressure equation and the LIT approach are used to calculate the flow rate and construct the IPR curve for the horizontal well. Multirate tests, i.e., deliverability tests, must be performed on the horizontal well to determine the coefficients of the selected flow equation.

PROBLEMS

1. A gas well is producing under a constant bottom-hole flowing pressure of 1000 psi. The specific gravity of the produced gas is 0.65, given:

$$\begin{array}{llll} p_i = 1500 \text{ psi} & r_w = 0.33 \text{ ft} & r_e = 1000 \text{ ft} & k = 20 \text{ md} \\ h = 20 \text{ ft} & T = 140^\circ\text{F} & s = 0.40 & \end{array}$$

Calculate the gas flow rate by using:

- Real gas pseudopressure approach
 - Pressure-squared approximation
2. The following data¹ were obtained from a back-pressure test on a gas well.

| Q_g , Mscf/day | p_{wfr} , psi |
|------------------|-----------------|
| 0 | 481 |
| 4928 | 456 |
| 6479 | 444 |
| 8062 | 430 |
| 9640 | 415 |

¹Chi Ikoku, *Natural Gas Reservoir Engineering*, John Wiley and Sons, 1984.

- a. Calculate values of C and n.
 - b. Determine AOF.
 - c. Generate the IPR curves at reservoir pressures of 481 and 300 psi.
3. The following back-pressure test data are available:

| Q_{gr} Mscf/day | p_{wfr} psi |
|-------------------|---------------|
| 0 | 5240 |
| 1000 | 4500 |
| 1350 | 4191 |
| 2000 | 3530 |
| 2500 | 2821 |

Given:

gas gravity = 0.78

porosity = 12%

s_{wi} = 15%

T = 281°F

a. Generate the current IPR curve by using:

- i. Simplified back-pressure equation
- ii. Laminar-inertial-turbulent (LIT) methods:

- Pressure-squared approach
- Pressure-approximation approach
- Pseudopressure approach

b. Repeat part a for a future reservoir pressure of 4,000 psi.

4. A 3,000-foot horizontal gas well is draining an area of approximately 180 acres, given:

$$p_i = 2500 \text{ psi}$$

$$T = 120^\circ\text{F}$$

$$v_g = 0.65$$

$$p_{wf} = 1500 \text{ psi}$$

$$r_w = 0.25$$

$$k = 25 \text{ md}$$

$$h = 20 \text{ ft}$$

Calculate the gas flow rate.

REFERENCES

1. Earlougher, Robert C., Jr., *Advances in Well Test Analysis*. Mongraph Vol. 5, Society of Petroleum Engineers of AIME. Dallas, TX: Millet the Printer, 1977.

2. ERCB. *Theory and Practice of the Testing of Gas Wells*, 3rd ed. Calgary: Energy Resources Conservation Board, 1975.
3. Fetkovich, M. J., "Multipoint Testing of Gas Wells," SPE Mid-continent Section Continuing Education Course of Well Test Analysis, March 17, 1975.
4. Golan, M., and Whitson, C., *Well Performance*. International Human Resources Development Corporation, 1986.
5. Joshi, S., *Horizontal Well Technology*. Tulsa, OK: PennWell Publishing Company, 1991.
6. Lee, J., *Well Testing*. Dallas: Society of Petroleum Engineers of AIME, 1982.
7. Matthews, C., and Russell, D., "Pressure Buildup and Flow Tests in Wells." Dallas: SPE Monograph Series, 1967.
8. Rawlins, E. L., and Schellhardt, M. A., "Back-Pressure Data on Natural Gas Wells and Their Application to Production Practices." U.S. Bureau of Mines Monograph 7, 1936.



C H A P T E R 9

GAS AND WATER CONING

Coning is a term used to describe the mechanism underlying the upward movement of water and/or the down movement of gas into the perforations of a producing well. Coning can seriously impact the well productivity and influence the degree of depletion and the overall recovery efficiency of the oil reservoirs. The specific problems of water and gas coning are listed below.

- Costly added water and gas handling
- Gas production from the original or secondary gas cap reduces pressure without obtaining the displacement effects associated with gas drive
- Reduced efficiency of the depletion mechanism
- The water is often corrosive and its disposal costly
- The afflicted well may be abandoned early
- Loss of the total field overall recovery

Delaying the encroachment and production of gas and water are essentially the controlling factors in maximizing the field's ultimate oil recovery. Since coning can have an important influence on operations, recovery, and economics, it is the objective of this chapter to provide the theoretical analysis of coning and outline many of the practical solutions for calculating water and gas coning behavior.

CONING

Coning is primarily the result of movement of reservoir fluids in the direction of least resistance, balanced by a tendency of the fluids to maintain gravity equilibrium. The analysis may be made with respect to either gas or water. Let the original condition of reservoir fluids exist as shown schematically in Figure 9-1, water underlying oil and gas overlying oil. For the purposes of discussion, assume that a well is partially penetrating the formation (as shown in Figure 9-1) so that the production interval is halfway between the fluid contacts.

Production from the well would create pressure gradients that tend to lower the gas-oil contact and elevate the water-oil contact in the immediate vicinity of the well. Counterbalancing these flow gradients is the tendency of the gas to remain above the oil zone because of its lower density and of the water to remain below the oil zone because of its higher density. These counterbalancing forces tend to deform the gas-oil and water-oil contacts into a bell shape as shown schematically in Figure 9-2.

There are essentially three forces that may affect fluid flow distributions around the well bores. These are:

- Capillary forces
- Gravity forces
- Viscous forces

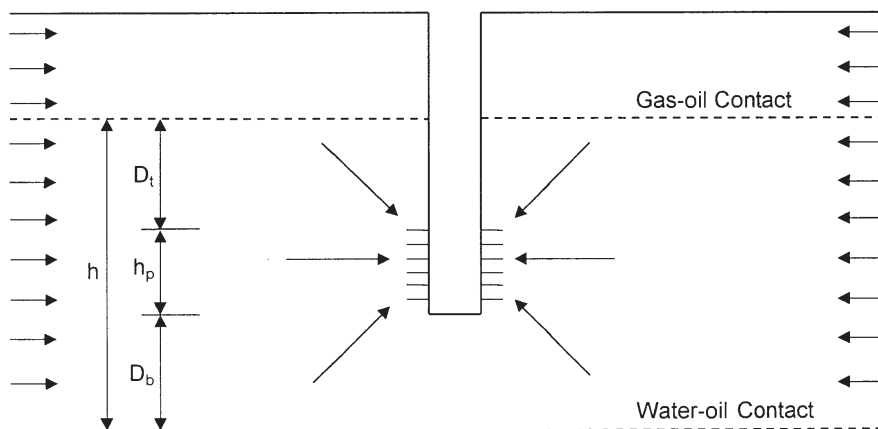


Figure 9-1. Original reservoir static condition.

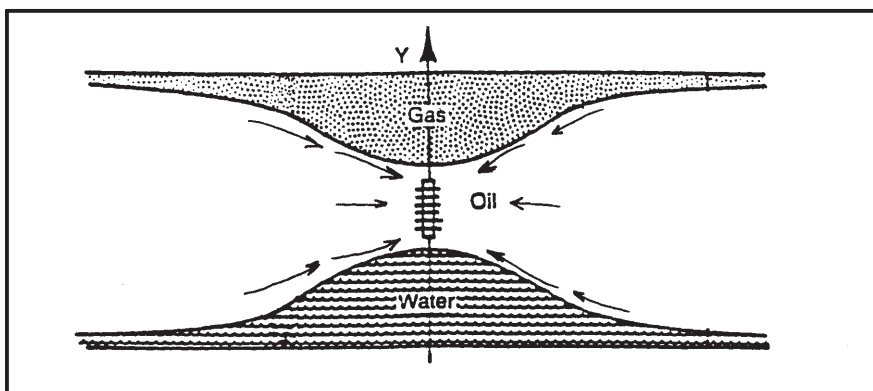


Figure 9-2. Gas and water coning.

Capillary forces usually have a negligible effect on coning and will be neglected. Gravity forces are directed in the vertical direction and arise from fluid density differences. The term *viscous forces* refers to the pressure gradients' associated fluid flow through the reservoir as described by Darcy's Law. Therefore, at any given time, there is a balance between gravitational and viscous forces at points on and away from the well completion interval. When the dynamic (viscous) forces at the wellbore exceed gravitational forces, a "cone" will ultimately break into the well.

We can expand on the above basic visualization of coning by introducing the concepts of:

- Stable cone
- Unstable cone
- Critical production rate

If a well is produced at a constant rate and the pressure gradients in the drainage system have become constant, a steady-state condition is reached. If at this condition the dynamic (viscous) forces at the well are less than the gravity forces, then the water or gas cone that has formed will not extend to the well. Moreover, the cone will neither advance nor recede, thus establishing what is known as a *stable cone*. Conversely, if the pressure in the system is an unsteady-state condition, then an *unstable cone* will continue to advance until steady-state conditions prevail.

If the flowing pressure drop at the well is sufficient to overcome the gravity forces, the unstable cone will grow and ultimately break into the

well. It is important to note that in a realistic sense, stable system cones may only be “pseudo-stable” because the drainage system and pressure distributions generally change. For example, with reservoir depletion, the water-oil contact may advance toward the completion interval, thereby increasing chances for coning. As another example, reduced productivity due to well damage requires a corresponding increase in the flowing pressure drop to maintain a given production rate. This increase in pressure drop may force an otherwise stable cone into a well.

The *critical production rate* is the rate above which the flowing pressure gradient at the well causes water (or gas) to cone into the well. It is, therefore, the maximum rate of oil production without concurrent production of the displacing phase by coning. At the critical rate, the built-up cone is stable but is at a position of incipient breakthrough.

Defining the conditions for achieving the maximum water-free and/or gas-free oil production rate is a difficult problem to solve. Engineers are frequently faced with the following specific problems:

1. Predicting the maximum flow rate that can be assigned to a completed well without the simultaneous production of water and/or free-gas
2. Defining the optimum length and position of the interval to be perforated in a well in order to obtain the maximum water and gas-free production rate

Calhoun (1960) pointed out that the rate at which the fluids can come to an equilibrium level in the rock may be so slow, due to the low permeability or to capillary properties, that the gradient toward the wellbore overcomes it. Under these circumstances, the water is lifted into the wellbore and the gas flows downward, creating a cone as illustrated in Figure 9-2. Not only is the direction of gradients reversed with gas and oil cones, but the rapidity with which the two levels will balance will differ. Also, the rapidity with which any fluid will move is inversely proportional to its viscosity, and, therefore, the gas has a greater tendency to cone than does water. For this reason, the amount of coning will depend upon the viscosity of the oil compared to that of water.

It is evident that the degree or rapidity of coning will depend upon the rate at which fluid is withdrawn from the well and upon the permeability in the vertical direction k_v , compared to that in the horizontal direction k_h . It will also depend upon the distance from the wellbore withdrawal point to the gas-oil or oil-water discontinuity.

The elimination of coning could be aided by shallower penetration of wells where there is a water zone or by the development of better horizontal permeability. Although the vertical permeability could not be lessened, the ratio of horizontal to vertical flow can be increased by such techniques as acidizing or pressure parting the formation. The application of such techniques needs to be controlled so that the effect occurs above the water zone or below the gas zone, whichever is the desirable case. This permits a more uniform rise of a water table.

Once either gas coning or water coning has occurred, it is possible to shut in the well and permit the contacts to restabilize. Unless conditions for rapid attainment of gravity equilibrium are present, restabilization will not be extremely satisfactory. Fortunately, bottom water is found often where favorable conditions for gravity separation do exist. Gas coning is more difficult to avoid because gas saturation, once formed, is difficult to eliminate.

There are essentially three categories of correlation that are used to solve the coning problem. These categories are:

- Critical rate calculations
- Breakthrough time predictions
- Well performance calculations after breakthrough

The above categories of calculations are applicable in evaluating the coning problem in vertical and horizontal wells.

CONING IN VERTICAL WELLS

Vertical Well Critical Rate Correlations

Critical rate Q_{oc} is defined as the maximum allowable oil flow rate that can be imposed on the well to avoid a cone breakthrough. The critical rate would correspond to the development of a stable cone to an elevation just below the bottom of the perforated interval in an oil-water system or to an elevation just above the top of the perforated interval in a gas-oil system. There are several empirical correlations that are commonly used to predict the oil critical rate, including the correlations of:

- Meyer-Garder
- Chierici-Ciucci
- Hoyland-Papatzacos-Skjaeveland

- Chaney et al.
- Chaperson
- Schols

The practical applications of these correlations in predicting the critical oil flow rate are presented over the following pages.

The Meyer-Garder Correlation

Meyer and Garder (1954) suggest that coning development is a result of the radial flow of the oil and associated pressure sink around the wellbore. In their derivations, Meyer and Garder assume a homogeneous system with a uniform permeability throughout the reservoir, i.e., $k_h = k_v$. It should be pointed out that the ratio k_h/k_v is the most critical term in evaluating and solving the coning problem. They developed three separate correlations for determining the critical oil flow rate:

- Gas coning
- Water coning
- Combined gas and water coning

Gas coning

Consider the schematic illustration of the gas coning problem shown in Figure 9-3.

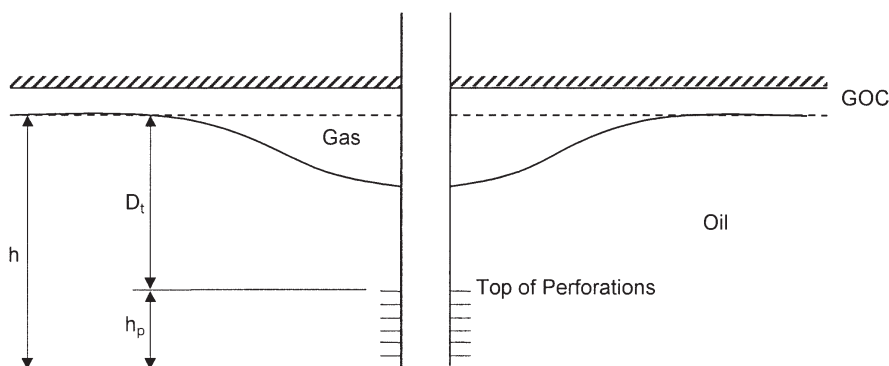


Figure 9-3. Gas coning.

Meyer and Garder correlated the critical oil rate required to achieve a stable gas cone with the following well penetration and fluid parameters:

- Difference in the oil and gas density
- Depth D_t from the original gas-oil contact to the top of the perforations
- The oil column thickness h

The well perforated interval h_p , in a gas-oil system, is essentially defined as

$$h_p = h - D_t$$

Meyer and Garder propose the following expression for determining the oil critical flow rate in a gas-oil system:

$$Q_{oc} = 0.246 \times 10^{-4} \left[\frac{\rho_o - \rho_g}{\ln(r_e / r_w)} \right] \left(\frac{k_o}{\mu_o B_o} \right) [h^2 - (h - D_t)^2] \quad (9-1)$$

where Q_{oc} = critical oil rate, STB/day

ρ_g, ρ_o = density of gas and oil, respectively, lb/ft³

k_o = effective oil permeability, md

r_e, r_w = drainage and wellbore radius, respectively, ft

h = oil column thickness, ft

D_t = distance from the gas-oil contact to the *top* of the perforations, ft

Water coning

Meyer and Garder propose a similar expression for determining the critical oil rate in the water coning system shown schematically in Figure 9-4.

The proposed relationship has the following form:

$$Q_{oc} = 0.246 \times 10^{-4} \left[\frac{\rho_w - \rho_o}{\ln(r_e / r_w)} \right] \left(\frac{k_o}{\mu_o B_o} \right) (h^2 - h_p^2) \quad (9-2)$$

where ρ_w = water density, lb/ft³

h_p = perforated interval, ft

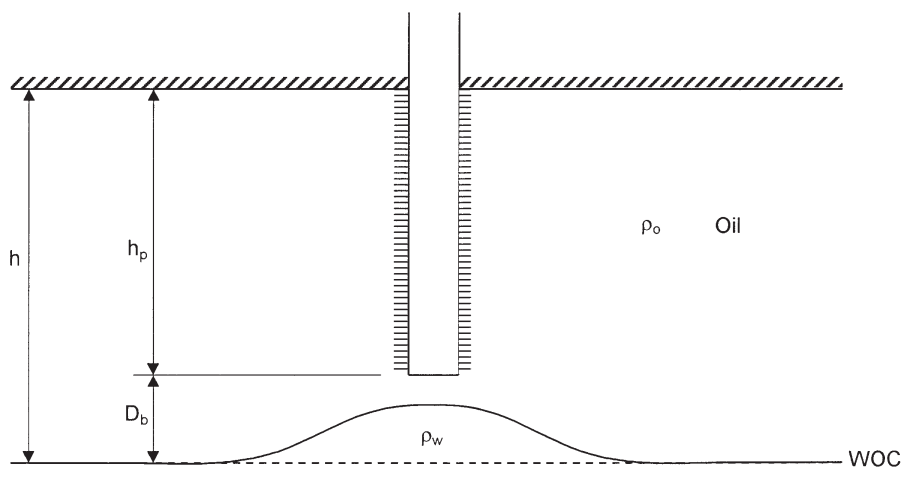


Figure 9-4. Water coning.

Simultaneous gas and water coning

If the effective oil-pay thickness h is comprised between a gas cap and a water zone (Figure 9-5), the completion interval h_p must be such as to permit maximum oil-production rate without having gas and water simultaneously produced by coning, gas breaking through at the top of the interval and water at the bottom.

This case is of particular interest in the production from a thin column underlaid by bottom water and overlaid by gas.

For this combined gas and water coning, Pirson (1977) combined Equations 9-1 and 9-2 to produce the following simplified expression for determining the maximum oil flow rate without gas and water coning:

$$Q_{oc} = 0.246 \times 10^{-4} \left[\frac{k_o}{\mu_o B_o} \right] \frac{h^2 - h_p^2}{\ln(r_e/r_w)} \times \left[(\rho_w - \rho_o) \left(\frac{\rho_o - \rho_g}{\rho_w - \rho_g} \right)^2 + (\rho_o - \rho_g) \left(1 - \frac{\rho_o - \rho_g}{\rho_w - \rho_g} \right)^2 \right] \quad (9-3)$$

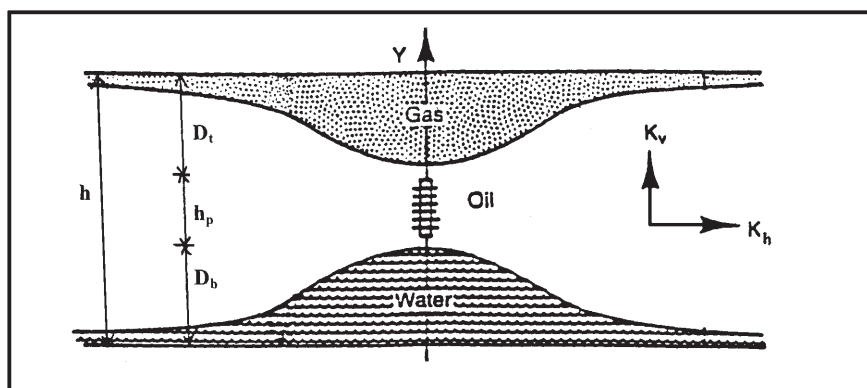


Figure 9-5. The development of gas and water coning.

Example 9-1

A vertical well is drilled in an oil reservoir overlaid by a gas cap. The related well and reservoir data are given below:

| | |
|--|---------------------------|
| horizontal and vertical permeability, i.e., k_h, k_v | = 110 md |
| oil relative permeability, k_{ro} | = 0.85 |
| oil density, ρ_o | = 47.5 lb/ft ³ |
| gas density, ρ_g | = 5.1 lb/ft ³ |
| oil viscosity, μ_o | = 0.73 cp |
| oil formation volume factor, B_o | = 1.1 bbl/STB |
| oil column thickness, h | = 40 ft |
| perforated interval, h_p | = 15 ft |
| depth from GOC to top of perforations, D_t | = 25 ft |
| wellbore radius, r_w | = 0.25 ft |
| drainage radius, r_e | = 660 ft |

Using the Meyer and Garder relationships, calculate the critical oil flow rate.

Solution

The critical oil flow rate for this gas coning problem can be determined by applying Equation 9-1. The following two steps summarize Meyer-Garder methodology:

Step 1. Calculate effective oil permeability k_o :

$$k_o = k_{ro} k = (0.85) (110) = 93.5 \text{ md}$$

Step 2. Solve for Q_{oc} by applying Equation 9-1:

$$\begin{aligned} Q_{oc} &= 0.246 \times 10^{-4} \frac{47.5 - 5.1}{\ln (660/0.25)} \frac{93.5}{(0.73)(1.1)} [40^2 - (40 - 25)^2] \\ &= 21.20 \text{ STB/day} \end{aligned}$$

Example 9-2

Resolve Example 9-1 assuming that the oil zone is underlaid by bottom water. The water density is given as 63.76 lb/ft^3 . The well completion interval is 15 feet as measured from the top of the formation (no gas cap) to the bottom of the perforations.

Solution

The critical oil flow rate for this water coning problem can be estimated by applying Equation 9-2. The equation is designed to determine the critical rate at which the water cone “touches” the bottom of the well to give

$$Q_{oc} = 0.246 \times 10^{-4} \left[\frac{(63.76 - 47.5)}{\ln (660 / 0.25)} \right] \left(\frac{93.5}{(0.73)(1.1)} \right) [40^2 - 15^2]$$

$$Q_{oc} = 8.13 \text{ STB/day}$$

The above two examples signify the effect of the fluid density differences on critical oil flow rate.

Example 9-3

A vertical well is drilled in an oil reservoir that is overlaid by a gas cap and underlaid by bottom water. Figure 9-6 shows an illustration of the simultaneous gas and water coning.

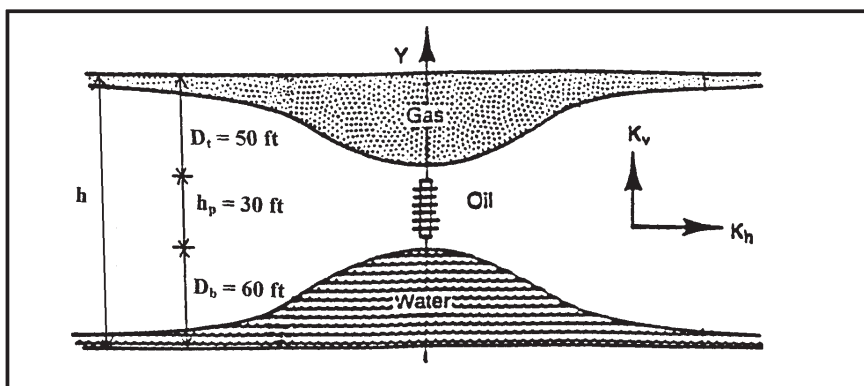


Figure 9-6. Gas and water coning problem (Example 9-3).

The following data are available:

| | |
|--|----------------------------------|
| oil density | $\rho_o = 47.5 \text{ lb/ft}^3$ |
| water density | $\rho_w = 63.76 \text{ lb/ft}^3$ |
| gas density | $\rho_g = 5.1 \text{ lb/ft}^3$ |
| oil viscosity | $\mu_o = 0.73 \text{ cp}$ |
| oil FVF | $B_o = 1.1 \text{ bbl/STB}$ |
| oil column thickness | $h = 65 \text{ ft}$ |
| depth from GOC to top of perforations | $D_t = 25 \text{ ft}$ |
| well perforated interval | $h_p = 15 \text{ ft}$ |
| wellbore radius | $r_w = 0.25 \text{ ft}$ |
| drainage radius | $r_e = 660 \text{ ft}$ |
| oil effective permeability | $k_o = 93.5 \text{ md}$ |
| horizontal and vertical permeability, i.e., k_h, k_v | $= 110 \text{ md}$ |
| oil relative permeability | $k_{ro} = 0.85$ |

Calculate the maximum permissible oil rate that can be imposed to avoid cones breakthrough, i.e., water and gas coning.

Solution

Apply Equation 9-3 to solve for the simultaneous gas and water coning problem, to give:

$$\begin{aligned}
 Q_{oc} &= 0.246 \times 10^{-4} \frac{93.5}{(0.73)(1.1)} \left[\frac{65^2 - 15^2}{\text{Ln}(660/0.25)} \right] \\
 &\times \left[(63.76 - 47.5) \left(\frac{47.5 - 5.1}{63.76 - 5.1} \right)^2 \right. \\
 &\quad \left. + (47.5 - 5.1) \left(1 - \frac{47.5 - 5.1}{63.76 - 5.1} \right)^2 \right] = 17.1 \text{ STB/day}
 \end{aligned}$$

Pirson (1977) derives a relationship for determining the optimum placement of the desired h_p feet of perforation in an oil zone with a gas cap above and a water zone below. Pirson proposes that the optimum distance D_t from the GOC to the top of the perforations can be determined from the following expression:

$$D_t = (h - h_p) \left[1 - \frac{\rho_o - \rho_g}{\rho_w - \rho_g} \right] \quad (9-4)$$

where the distance D_t is expressed in feet.

Example 9-4

Using the data given in Example 9-3, calculate the optimum distance for the placement of the 15-foot perforations.

Solution

Applying Equation 9-4 gives

$$D_t = (65 - 15) \left[1 - \frac{47.5 - 5.1}{63.76 - 5.1} \right] = 13.9 \text{ ft}$$

Slider (1976) presented an excellent overview of the coning problem and the above-proposed predictive expressions. Slider points out that Equations 9-1 through 9-4 are not based on realistic assumptions. One of the biggest difficulties is in the assumption that the permeability is the same in all directions. As noted, this assumption is seldom realistic. Since sedimentary formations were initially laid down in thin, horizontal

sheets, it is natural for the formation permeability to vary from one sheet to another vertically.

Therefore, there is generally quite a difference between the permeability measured in a vertical direction and the permeability measured in a horizontal direction. Furthermore, the permeability in the horizontal direction is normally considerably greater than the permeability in the vertical direction. This also seems logical when we recognize that very thin, even microscopic sheets of impermeable material, such as shale, may have been periodically deposited. These permeability barriers have a great effect on the vertical flow and have very little effect on the horizontal flow, which would be parallel to the plane of the sheets.

The Chierici-Ciucci Approach

Chierici and Ciucci (1964) used a potentiometric model to predict the coning behavior in vertical oil wells. The results of their work are presented in dimensionless graphs that take into account the vertical and horizontal permeability. The diagrams can be used for solving the following two types of problems:

- a. Given the reservoir and fluid properties, as well as the position of and length of the perforated interval, determine the maximum oil production rate without water and/or gas coning.
- b. Given the reservoir and fluids characteristics only, determine the optimum position of the perforated interval.

The authors introduced four dimensionless parameters that can be determined from a graphical correlation to determine the critical flow rates. The proposed four dimensionless parameters are shown in Figure 9-7 and defined as follows:

Effective dimensionless radius r_{De} :

The first dimensionless parameter that the authors used to correlate results of potentiometric model is called the *effective dimensionless radius* and is defined by:

$$r_{De} = \frac{r_e}{h} \sqrt{\frac{k_h}{k_v}} \quad (9-5)$$

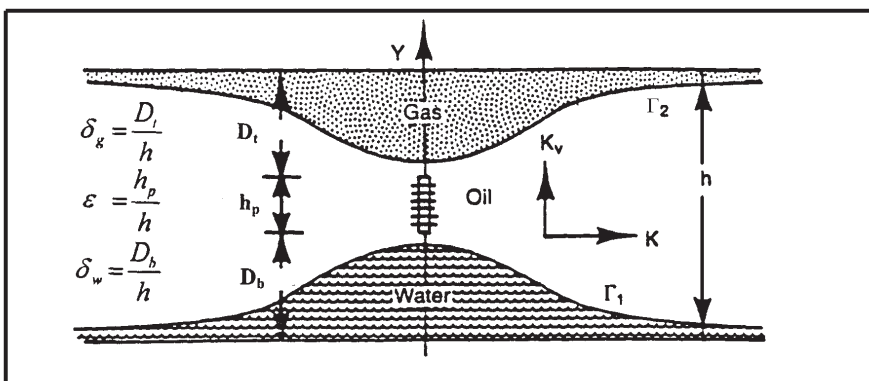


Figure 9-7. Water and gas coning in a homogeneous formation. (After Chierici, Ciucci, and Pizzi, courtesy JPT, August 1964.)

Meyer and Garder stated that the proposed graphical correlation is valid in the following range of r_{De} values:

$$5 \leq r_{De} \leq 80$$

where h = oil column thickness, ft

r_e = drainage radius, ft

k_v, k_h = vertical and horizontal permeability, respectively

Dimensionless perforated length ϵ :

The second dimensionless parameter that the authors used in developing their correlation is termed the *dimensionless perforated length* and is defined by:

$$\epsilon = h_p/h \quad (9-6)$$

The authors pointed out that the proposed graphical correlation is valid when the value of the dimensionless perforated length is in the following range:

$$0 \leq \epsilon \leq 0.75$$

Dimensionless gas cone ratio δ_g :

The authors introduced the *dimensionless gas cone ratio* as defined by the following relationship:

$$\delta_g = D_t/h \quad (9-7)$$

with

$$0.070 \leq \delta_g \leq 0.9$$

where D_t is the distance from the original GOC to the top of perforations, ft.

Dimensionless water cone ratio δ_w :

The last dimensionless parameter that Chierici et al. proposed in developing their correlation is called the *dimensionless water cone ratio* and is defined by:

$$\delta_w = D_b/h \quad (9-8)$$

with

$$0.07 \leq \delta_w \leq 0.9$$

where D_b = distance from the original WOC to the bottom of the perforations, ft

Chierici and coauthors proposed that the oil-water and gas-oil contacts are stable only if the oil production rate of the well is not higher than the following rates:

$$Q_{ow} = 0.492 \times 10^{-4} \frac{h^2 (\rho_w - \rho_o)}{B_o \mu_o} (k_{ro} k_h) \Psi_w(r_{De}, \epsilon, \delta_w) \quad (9-9)$$

$$Q_{og} = 0.492 \times 10^{-4} \frac{h^2 (\rho_o - \rho_g)}{B_o \mu_o} (k_{ro} k_h) \Psi_g(r_{De}, \epsilon, \delta_g) \quad (9-10)$$

where Q_{ow} = critical oil flow rate in oil-water system, STB/day

Q_{og} = critical oil flow rate in gas-oil system, STB/day

ρ_o, ρ_w, ρ_g = densities in lb/ft³

Ψ_w = water dimensionless function

Ψ_g = gas dimensionless function

k_h = horizontal permeability, md

The authors provided a set of working graphs for determining the dimensionless function ψ from the calculated dimensionless parameters r_{De} , ϵ , and δ . These graphs are shown in Figures 9-8 through 9-14. *This set of curves should be only applied to homogeneous formations.*

It should be noted that if a gas cap and an aquifer are present together, the following conditions must be satisfied in order to avoid water and free-gas production.

$$Q_o \leq Q_{ow}$$

and

$$Q_o \leq Q_{og}$$

(text continued on page 602)

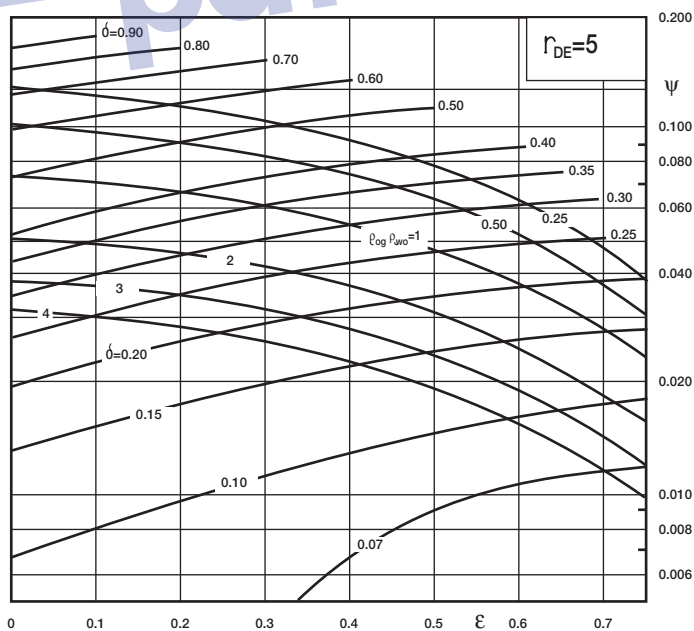


Figure 9-8. Dimensionless functions for $r_{De} = 5$. (After Chierici, Ciucci, and Pizzi, courtesy JPT, August 1964.)

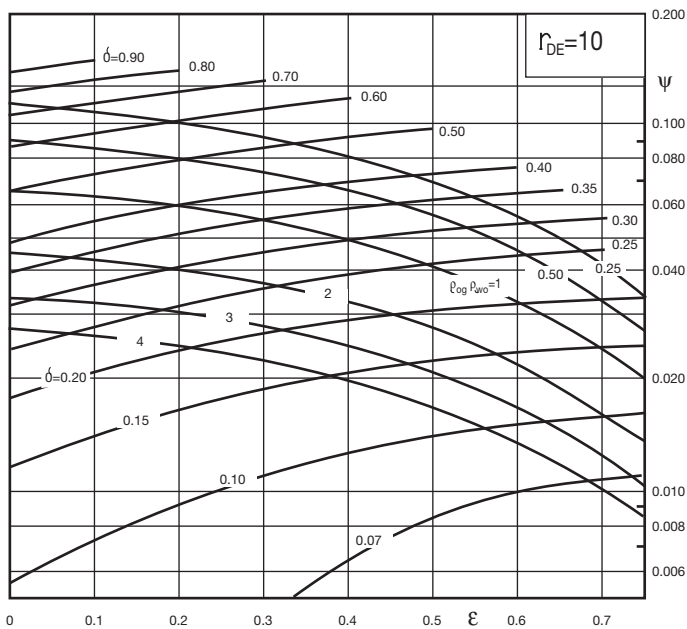


Figure 9-9. Dimensionless functions for $r_{De} = 10$. (After Chierici, Ciucci, and Pizzi, courtesy JPT, August 1964.)

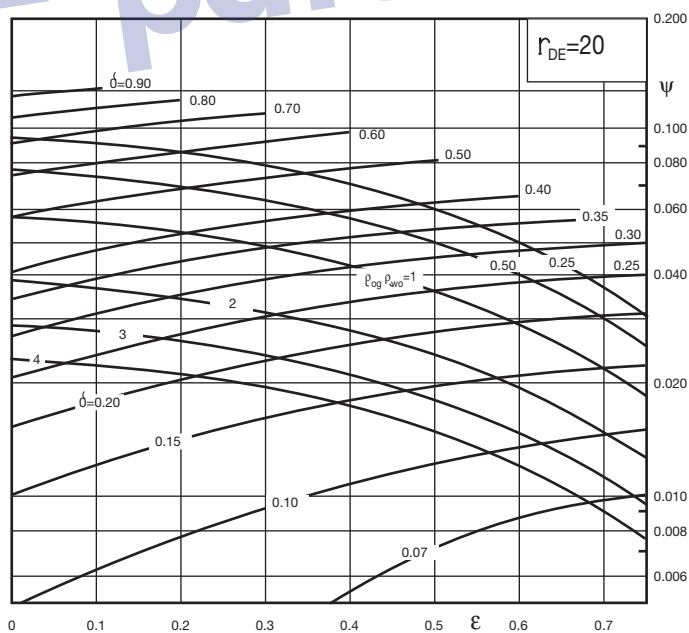


Figure 9-10. Dimensionless functions for $r_{De} = 20$. (After Chierici, Ciucci, and Pizzi, courtesy JPT, August 1964.)

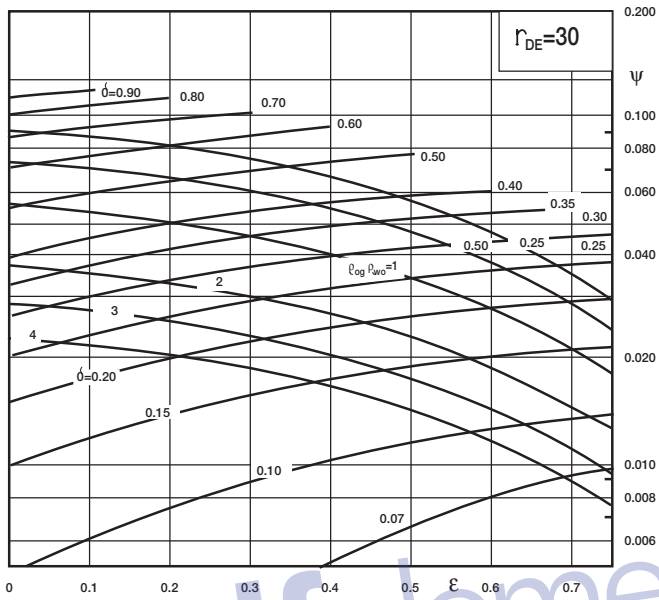


Figure 9-11. Dimensionless functions for $r_{De} = 30$. (After Chierici, Ciucci, and Pizzi, courtesy JPT, August 1964.)

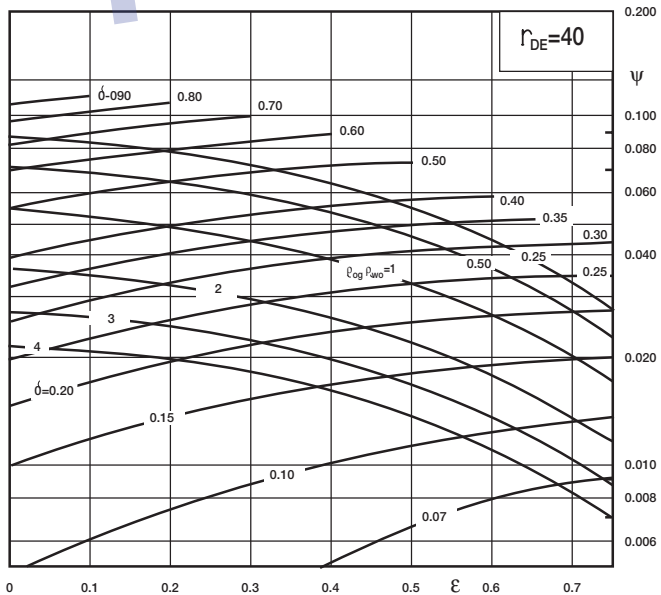


Figure 9-12. Dimensionless functions for $r_{De} = 40$. (After Chierici, Ciucci, and Pizzi, courtesy JPT, August 1964.)

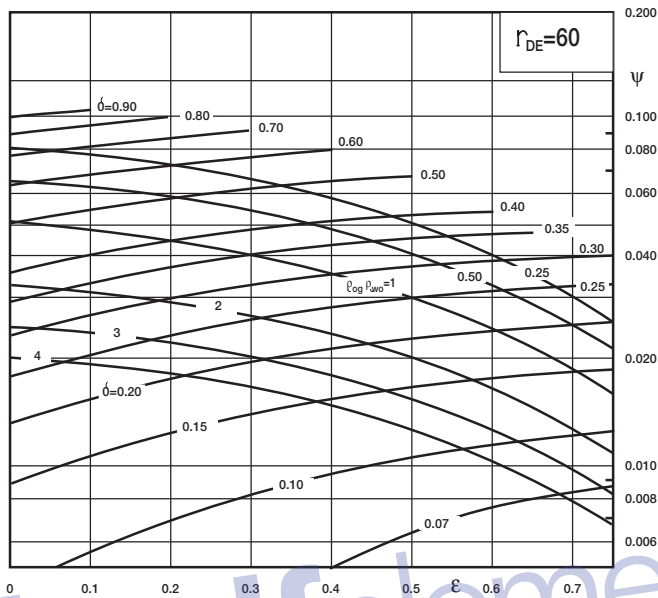


Figure 9-13. Dimensionless functions for $r_{De} = 60$. (After Chierici, Ciucci, and Pizzi, courtesy JPT, August 1964.)

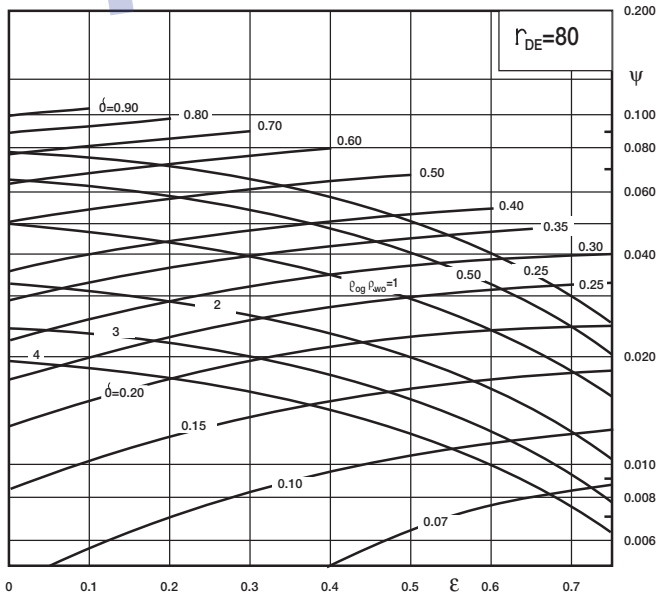


Figure 9-14. Dimensionless functions for $r_{De} = 80$. (After Chierici, Ciucci, and Pizzi, courtesy JPT, August 1964.)

(text continued from page 598)

Example 9-5

A vertical well is drilled on a regular 40-acre spacing in an oil reservoir that is overlaid by a gas cap and underlaid by an aquifer. The following data are available:

| | |
|--|-------------------------------------|
| Oil pay thickness | $h = 140$ ft |
| Distance from the GOC to the top of perforations | $D_t = 50$ ft |
| Length of the perforated interval | $h_p = 30$ ft |
| Horizontal permeability | $k_h = 300$ md |
| Relative oil permeability | $k_{ro} = 1.00$ |
| Vertical permeability | $k_v = 90$ md |
| Oil density | $\rho_o = 46.24$ lb/ft ³ |
| Water density | $\rho_w = 68.14$ lb/ft ³ |
| Gas density | $\rho_g = 6.12$ lb/ft ³ |
| Oil FVF | $B_o = 1.25$ bbl/STB |
| Oil viscosity | $\mu_o = 1.11$ cp |

A schematic representation of the given data is shown in Figure 9-15.

Calculate the maximum allowable oil flow rate without water and free-gas production.

Solution

Step 1. Calculate the drainage radius r_e :

$$\pi r_e^2 = (40)(43,560)$$

$$r_e = 745 \text{ ft}$$

Step 2. Compute the distance from the WOC to the bottom of the perforations D_b :

$$D_b = h - D_t - h_p$$

$$D_b = 140 - 50 - 30 = 60 \text{ ft}$$

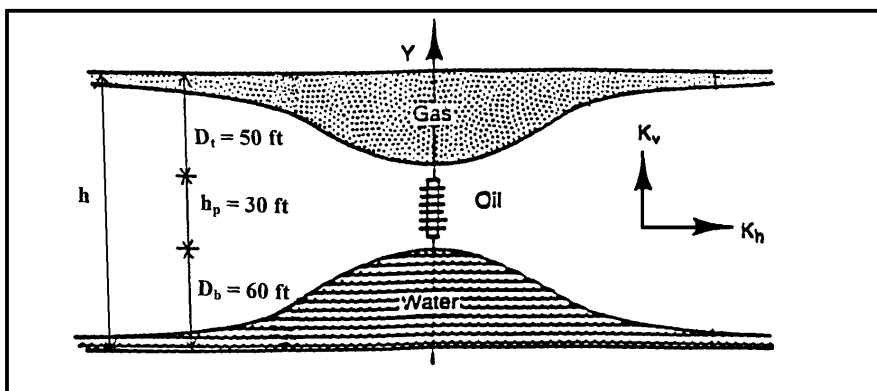


Figure 9-15. Gas and water coning problem (Example 9-5).

Step 3. Find the dimensionless radius r_{De} from Equation 9-5:

$$r_{De} = \frac{745}{140} \sqrt{\frac{300}{90}} = 9.72$$

Step 4. Calculate the dimensionless perforated length ε by applying Equation 9-6:

$$\varepsilon = \frac{30}{140} = 0.214$$

Step 5. Calculate the gas cone ratio δ_g from Equation 9-7:

$$\delta_g = \frac{50}{140} = 0.357$$

Step 6. Determine the water cone ratio δ_w by applying Equation 9-8:

$$\delta_w = \frac{60}{140} = 0.429$$

Step 7. Calculate the oil-gas and water-oil density differences:

$$\Delta\rho_{ow} = \rho_w - \rho_o = 68.14 - 46.24 = 21.90 \text{ lb/ft}^3$$

$$\Delta\rho_{og} = \rho_o - \rho_g = 46.24 - 6.12 = 40.12 \text{ lb/ft}^3$$

Step 8. Find the density differences ratio:

$$\Delta\rho_{og}/\Delta\rho_{ow} = \frac{40.12}{21.90} = 1.83$$

Step 9. From Figure 9-10, which corresponds to $r_{De} = 10$; approximate the dimensionless functions ψ_g and ψ_w :

$$\text{for } \varepsilon = 0.214 \text{ and } \delta_g = 0.357 \text{ to give } \psi_g = 0.051$$

and

$$\text{for } \varepsilon = 0.214 \text{ and } \delta_w = 0.429 \text{ to give } \psi_w = 0.065$$

Step 10. Estimate the oil critical rate by applying Equations 9-9 and 9-10:

$$Q_{ow} = 0.492 \times 10^{-4} \frac{140^2 (21.90)}{(1.25) (1.11)} [(1) (300)] 0.065 = 297 \text{ STB/day}$$

$$Q_{og} = 0.492 \times 10^{-4} \frac{140^2 (40.12)}{(1.25) (1.11)} [(1) (300)] 0.051 = 426 \text{ STB/day}$$

These calculations show that the water coning is the limiting condition for the oil flow rate. The maximum oil rate without water or free-gas production is, therefore, 297 STB/day.

Chierici and Ciucci (1964) proposed a methodology for determining the optimum completion interval in coning problems. The method is basically based on the "trial and error" approach.

For a given dimensionless radius r_{De} and knowing GOC, WOC, and fluids density, the specific steps of the proposed methodology are summarized below:

Step 1. Assume the length of the perforated interval h_p .

Step 2. Calculate the dimensionless perforated length $\varepsilon = h_p/h$.

Step 3. Select the appropriate family of curves that corresponds to r_{De} , interpolate if necessary, and enter the working charts with ε on the x-axis and move vertically to the calculated ratio $\Delta\rho_{og}/\Delta\rho_{ow}$. Estimate the corresponding δ and ψ . Designate these two dimen-

sionless parameters as the optimum gas cone ratio $\delta_{g,opt}$ and optimum dimensionless function ψ_{opt} .

Step 4. Calculate the distance from GOC to the top of the perforation,

$$D_t = (h) (\delta_{g,opt})$$

Step 5. Calculate the distance from the WOC to the bottom of the perforation, h_w ,

$$D_b = h - D_t - h_p$$

Step 6. Using the optimum dimensionless function ψ_{opt} in Equation 9-9, calculate the maximum allowable oil flow rate Q_{ow} .

Step 7. Repeat Steps 1 through 6.

Step 8. The calculated values of Q_{ow} at different assumed perforated intervals should be compared with those obtained from flow-rate equations, e.g., Darcy's equation, using the maximum drawdown pressure.

Example 9-6

Example 9-5 indicates that a vertical well is drilled in an oil reservoir that is overlaid by a gas cap and underlaid by an aquifer. Assuming that the pay thickness h is 200 feet and the rock and fluid properties are identical to those given in Example 9-5, calculate length and position of the perforated interval.

Solution

Step 1. Using the available data, calculate

$$r_{De} = \frac{745}{200} \sqrt{\frac{300}{90}} = 6.8$$

and

$$\Delta\rho_{og}/\Delta\rho_{wo} = 40.12 / 21.90 = 1.83$$

Step 2. Assume the length of the perforated interval is 40 feet; therefore,

$$h_p = 40'$$

$$\varepsilon = 40/200 = 0.2$$

Step 3. To obtain the values of ψ_{opt} and $\delta_{\text{g,opt}}$ for $r_{\text{De}} = 6.8$, interpolate between Figures 9-8 and 9-9 to give

$$\psi_{\text{opt}} = 0.043$$

$$\delta_{\text{g,opt}} = 0.317$$

Step 4. Calculate the distance from GOC to the top of the perforations.

$$D_t = (200) (0.317) = 63 \text{ ft}$$

Step 5. Determine the distance from the WOC to the bottom of the perforations.

$$D_b = 200 - 63 - 40 = 97 \text{ ft}$$

Step 6. Calculate the optimum oil flow rate.

$$\begin{aligned} (Q_o)_{\text{opt}} &= 0.492 \times 10^{-4} \frac{200^2 (40.12) (300) (0.043)}{(1.25) (1.11)} \\ &= 740 \text{ STB/day} \end{aligned}$$

Step 7. Repeat Steps 2 through 6 with the results of the calculation as shown below. The oil flow rates as calculated from appropriate flow equations are also included.

| | | | | | |
|-------------------------|--------|--------|--------|--------|--------|
| h_p | 20 | 40 | 60 | 80 | 100 |
| ε | 0.1 | 0.2 | 0.3 | 0.4 | 0.5 |
| ψ_{opt} | 0.0455 | 0.0430 | 0.0388 | 0.0368 | 0.0300 |
| $\delta_{\text{g,opt}}$ | 0.358 | 0.317 | 0.271 | 0.230 | 0.190 |
| D_t | 72 | 63 | 54 | 46 | 38 |
| D_b | 108 | 97 | 86 | 74 | 62 |
| $(Q_o)_{\text{opt}}$ | 786 | 740 | 669 | 600 | 516 |
| Expected Q_o | 525 | 890 | 1320 | 1540 | 1850 |

The maximum oil production rate that can be obtained from this well without coning breakthrough is 740 STB/day. This indicates that the optimum distance from the GOC to the top of the perforations is 63 ft and the optimum distance from the WOC to the bottom of the perforations is 97 ft. The total length of the perforated interval is $200 - 63 - 97 = 40$ ft.

The Hoyland-Papatzacos-Skjaveland Methods

Hoyland, Papatzacos, and Skjaveland (1989) presented two methods for predicting critical oil rate for bottom water coning in anisotropic, homogeneous formations with the well completed from the top of the formation. The first method is an analytical solution, and the second is a numerical solution to the coning problem. A brief description of the methods and their applications are presented below.

The Analytical Solution Method

The authors presented an analytical solution that is based on the Muskat-Wyckoff (1953) theory. In a steady-state flow condition, the solution takes a simple form when it is combined with the method of images to give the boundary conditions as shown in Figure 9-16.

To predict the critical rate, the authors superimpose the same criteria as those of Muskat and Wyckoff on the single-phase solution and, therefore, neglect the influence of cone shape on the potential distribution. Hoyland and his coworkers presented their analytical solution in the following form:

$$Q_{oc} = 0.246 \times 10^{-4} \left[\frac{h^2 (\rho_w - \rho_o) k_h}{\mu_o B_o} \right] q_{CD} \quad (9-11)$$

where Q_{oc} = critical oil rate, STB/day
 h = total thickness of the oil zone, ft
 ρ_w, ρ_o = water and oil density, lb/ft³
 k_h = horizontal permeability, md
 q_{CD} = dimensionless critical flow rate

The authors correlated the dimensionless critical rate q_{CD} with the dimensionless radius r_D and the fractional well penetration ratio h_p/h as shown in Figure 9-17.

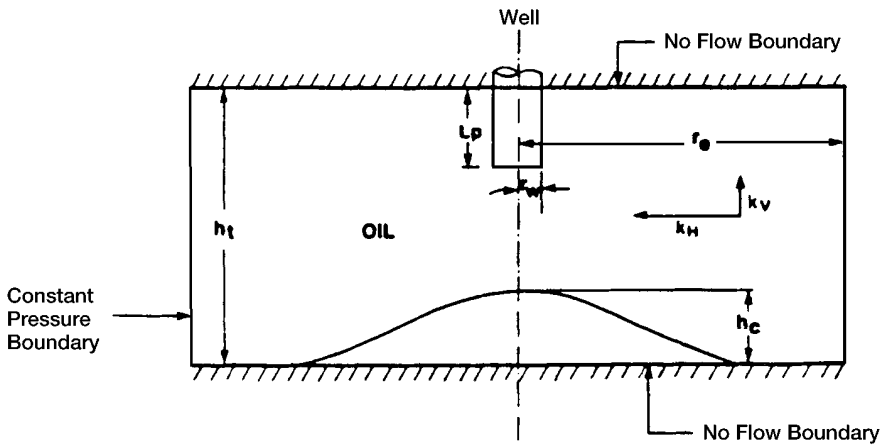


Figure 9-16. Illustration of the boundary condition for analytical solution. (After Hoyland, A. et al., courtesy SPE Reservoir Engineering, November 1989.)

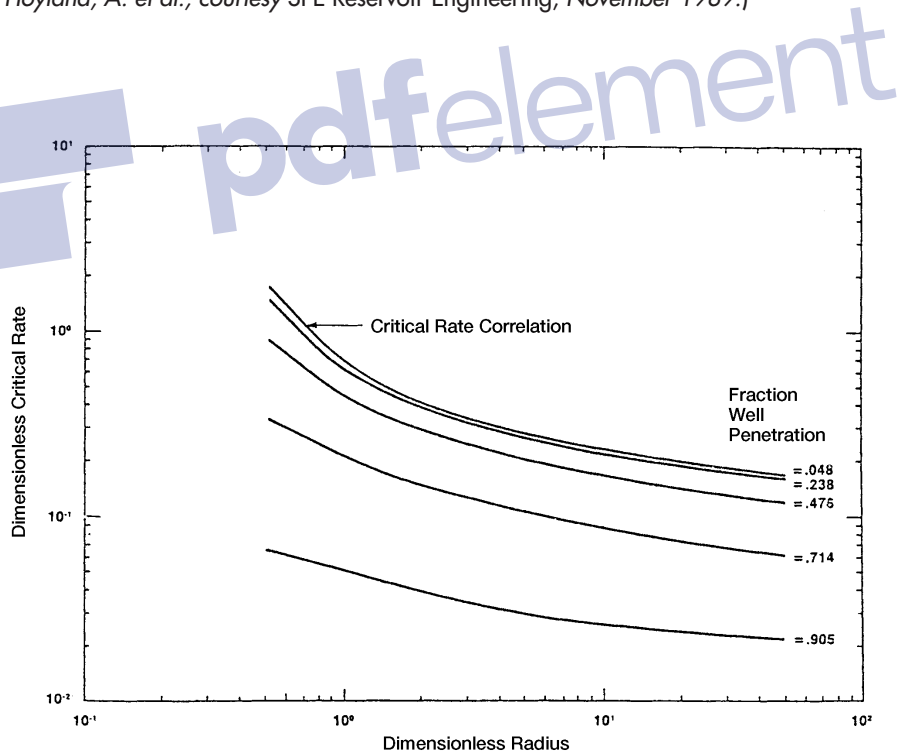


Figure 9-17. Critical rate correlation. (After Hoyland, A. et al., courtesy SPE Reservoir Engineering, November 1989.)

$$r_D = \frac{r_c}{h} \sqrt{\frac{k_v}{k_h}} \quad (9-12)$$

where r_c = drainage radius, ft
 k_v = vertical permeability, md
 k_h = horizontal permeability, md

The Numerical Solution Method

Based on a large number of simulation runs with more than 50 critical rate values, the authors used a regression analysis routine to develop the following relationships:

- For isotropic reservoirs with $k_h = k_v$, the following expression is proposed:

$$Q_{oc} = 0.924 \times 10^{-4} \frac{k_o(\rho_w - \rho_o)}{\mu_o B_o} \left[1 - \left(\frac{h_P}{h} \right)^2 \right]^{1.325} \times h^{2.238} [\ln(r_c)]^{-1.99} \quad (9-13)$$

- For anisotropic reservoirs, the authors correlated the dimensionless critical rate with the dimensionless radius r_D and five different fractional well penetrations. The correlation is presented in a graphical form as shown in Figure 9-18.

The authors illustrated their methodology through the following example.

Example 9-7

Given the following data, determine the oil critical rate:

| | |
|--|----------|
| Density differences (water/oil), lbm/ft ³ | = 17.4 |
| Oil FVF, RB/STB | = 1.376 |
| Oil viscosity, cp | = 0.8257 |
| Horizontal permeability, md | = 1000 |
| Vertical permeability, md | = 640 |
| Total oil thickness, ft | = 200 |
| Perforated thickness, ft | = 50 |
| External radius, ft | = 500 |

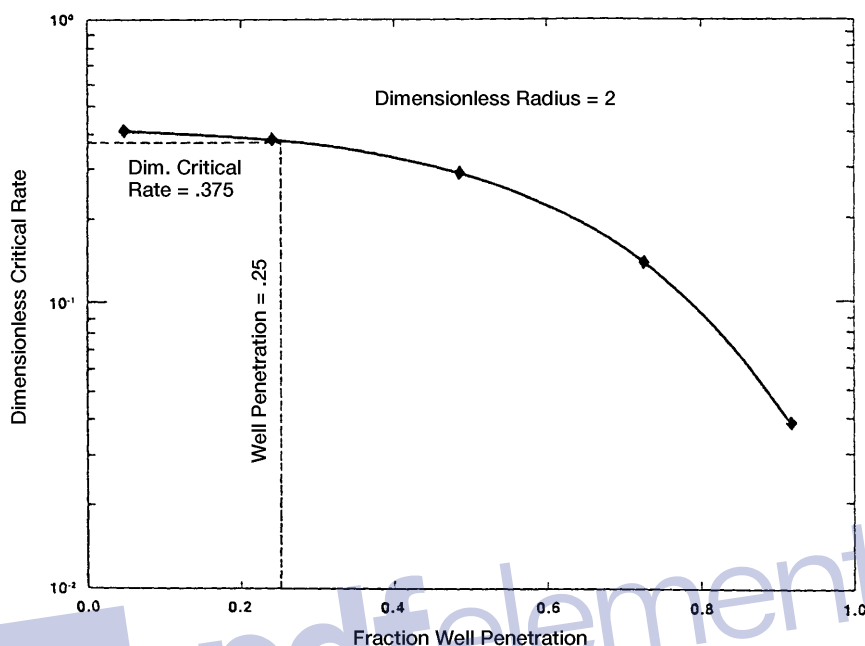


Figure 9-18. Critical rate calculation for Example 9-7. (After Hoyland, A. et al., courtesy SPE Reservoir Engineering, November 1989.)

Solution

Step 1. Calculate the dimensionless radius r_D by applying Equation 9-12.

$$r_D = \frac{r_e}{h} (k_v/k_h)^{0.5} = \frac{500}{200} (40/1000)^{0.5} = 2$$

Step 2. Determine dimensionless critical rate for several fractional well penetrations from Figure 9-17 for a dimensionless radius of 2.

Step 3. Plot dimensionless critical rate as a function of well penetration. The plot is shown in section A of Figure 9-17.

Step 4. Calculate fractional well penetration, $h_p/h = 50/200 = 0.25$.

Step 5. Interpolate in the plot in section A of Figure 9-17 to find dimensionless critical rate q_{Dc} equal to 0.375.

Step 6. Use Equation 9-11 and find the critical rate.

$$\begin{aligned} Q_{oc} &= 0.246 \times 10^{-4} \left[\frac{200^2 (17.4)}{(1.376) (0.8257)} \right] (1000) (0.375) \\ &= 5651 \text{ STB/day} \end{aligned}$$

Critical Rate Curves by Chaney et al.

Chaney et al. (1956) developed a set of working curves for determining oil critical flow rate. The authors proposed a set of working graphs that were generated by using a potentiometric analyzer study and applying the water coning mathematical theory as developed by Muskat-Wyckoff (1935).

The graphs, as shown in Figures 9-19 through 9-23, were generated using the following fluid and sand characteristics:

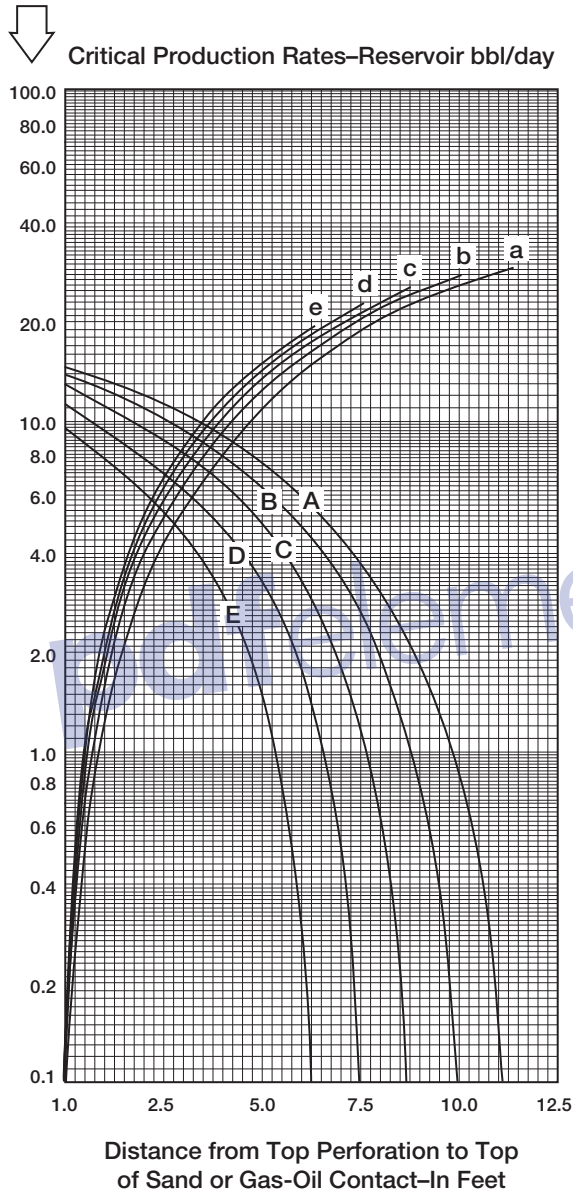
| | |
|----------------------|---|
| Drainage radius | $r_e = 1000 \text{ ft}$ |
| Wellbore radius | $r_w = 3''$ |
| Oil column thickness | $h = 12.5, 25, 50, 75, \text{ and } 100 \text{ ft}$ |
| Permeability | $k = 1000 \text{ md}$ |
| Oil viscosity | $\mu_o = 1 \text{ cp}$ |
| $\rho_o - \rho_w$ | $= 18.72 \text{ lb/ft}^3$ |
| $\rho_o - \rho_g$ | $= 37.44 \text{ lb/ft}^3$ |

The graphs are designed to determine the critical flow rate in oil-water, gas-oil, and gas-water systems with fluid and rock properties as listed above. The hypothetical rates as determined from the Chaney et al. curves (designated as Q_{curve}), are corrected to account for the actual reservoir rock and fluid properties by applying the following expressions:

In oil-water systems

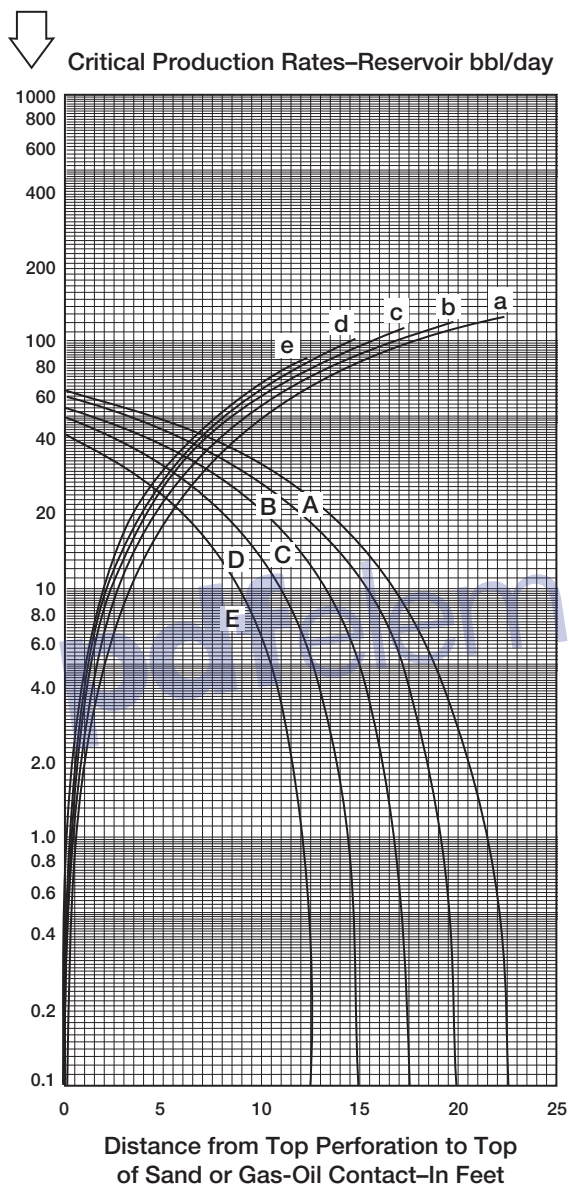
$$Q_{oc} = 0.5288 \times 10^{-4} \left[\frac{k_o (\rho_w - \rho_o)}{\mu_o B_o} \right] Q_{\text{curve}} \quad (9-14)$$

(text continued on page 617)



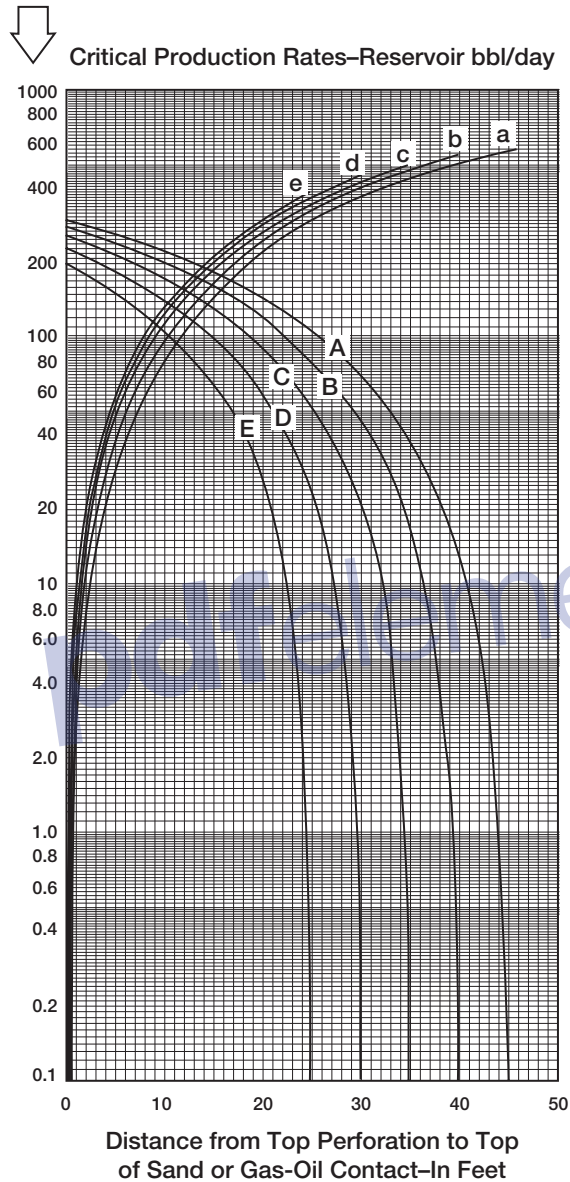
Critical-production-rate curves for sand thickness of 12.5 ft., well radius of 3 in., and drainage radius of 1,000 ft. Water coning curves: A, 1.25 ft. perforated interval; B, 2.5 ft.; C, 3.75 ft.; D, 5.00 ft.; and E, 6.25 ft. Gas coning curves: a, 1.25 ft. perforated interval; b, 2.5 ft.; c, 3.75 ft.; d, 5.00 ft., and e, 6.25 ft.

Figure 9-19. Critical production rate curves. (After Chaney et al., courtesy OGJ, May 1956.)



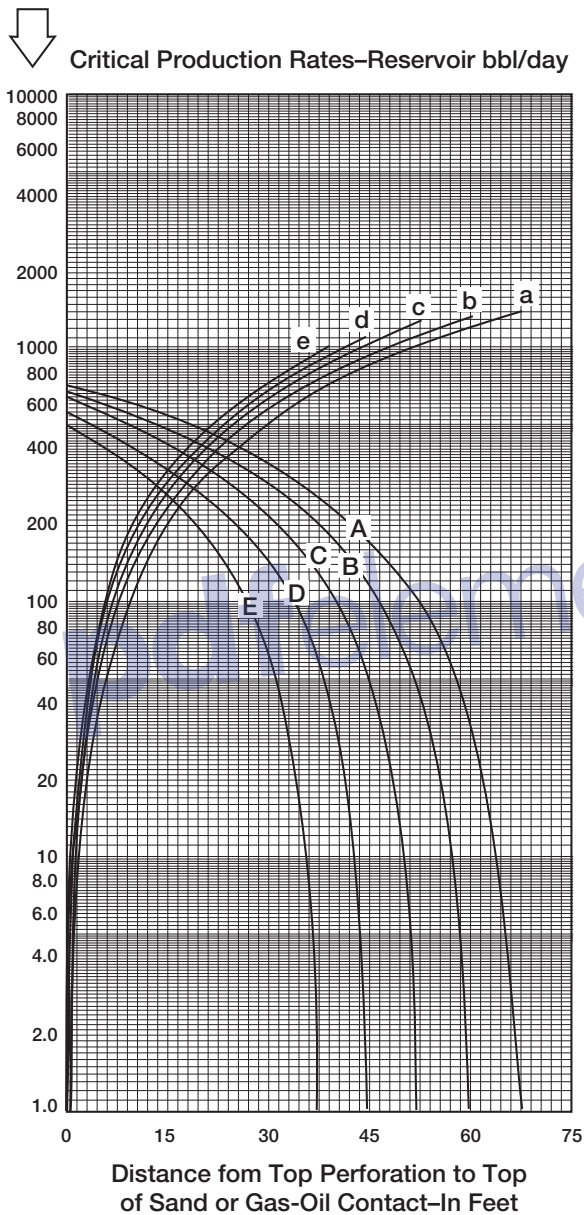
Critical-production-rate curves for sand thickness of 25 ft., well radius of 3 in., and drainage radius of 1,000 ft. Water coning curves: A, 2.5 ft. perforated interval; B, 5 ft.; C, 7.5 ft.; D, 10 ft.; and E, 12.5 ft. Gas coning curves: a, 2.5 ft. perforated interval; b, 5 ft.; c, 7.5 ft.; d, 10 ft., and e, 12.5 ft.

Figure 9-20. Critical production rate curves. (After Chaney et al., courtesy OGJ, May 1956.)



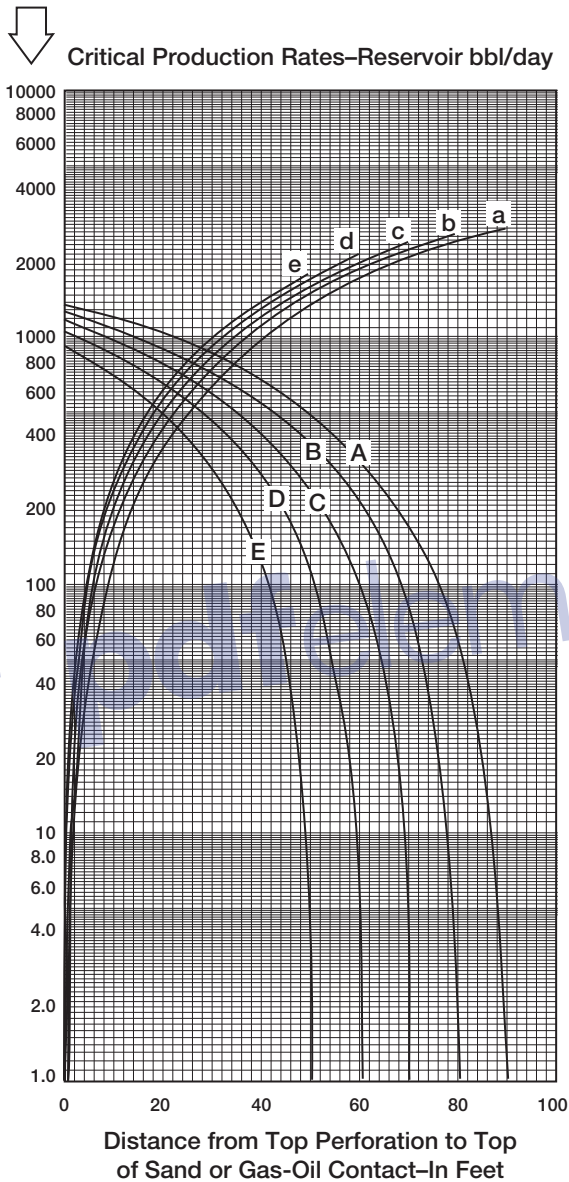
Critical-production-rate curves for sand thickness of 50 ft., well radius of 3 in., and drainage radius of 1,000 ft. Water coning curves: A, 5 ft. perforated interval; B, 10 ft.; C, 15 ft.; D, 20 ft.; and E, 25 ft. Gas coning curves: a, 5 ft. perforated interval; b, 10 ft.; c, 15 ft.; d, 20 ft., and e, 25 ft.

Figure 9-21. Critical production rate curves. (After Chaney et al., courtesy OGI, May 1956.)



Critical-production-rate curves for sand thickness of 75 ft., well radius of 3 in., and drainage radius of 1,000 ft. Water coning curves: A, 7.5 ft. perforated interval; B, 15 ft.; C, 22.5 ft.; D, 30 ft.; and E, 37.5 ft. Gas coning curves: a, 7.5 ft. perforated interval; b, 15 ft.; c, 22.5 ft.; d, 30 ft., and e, 37.5 ft.

Figure 9-22. Critical production rate curves. (After Chaney et al., courtesy OGJ, May 1956.)



Critical-production-rate curves for sand thickness of 100 ft., well radius of 3 in., and drainage radius of 1,000 ft. Water coning curves: A, 10 ft. perforated interval; B, 20 ft.; C, 30 ft.; D, 40 ft.; and E, 50 ft. Gas coning curves: a, 10 ft. perforated interval; b, 20 ft.; c, 30 ft.; d, 40 ft., and e, 50 ft.

Figure 9-23. Critical production rate curves. (After Chaney et al., courtesy OGJ, May 1956.)

(text continued from page 611)

where ρ_o = oil density, lb/ft³
 ρ_w = water density, lb/ft³
 Q_{oc} = critical oil flow rate, STB/day
 k_o = effective oil permeability, md

In gas-water systems

$$Q_{gc} = 0.5288 \times 10^{-4} \left[\frac{k_g (\rho_w - \rho_g)}{\mu_g B_g} \right] Q_{curve} \quad (9-15)$$

where ρ_g = gas density, lb/ft³
 ρ_w = water density, lb/ft³
 Q_{gc} = critical gas flow rate, Mscf/day
 β_g = gas FVF, bbl/Mscf
 k_g = effective gas permeability, md

In gas-oil systems

$$Q_{oc} = 0.2676 \times 10^{-4} \left[\frac{k_o (\rho_o - \rho_g)}{\mu_o B_o} \right] Q_{curve} \quad (9-16)$$

Example 9-8

In an oil-water system, the following fluid and sand data are available:

| | |
|---------------------------------|----------------------------------|
| $h = 50'$ | $h_p = 15'$ |
| $\rho_o = 47.5 \text{ lb/ft}^3$ | $\rho_w = 63.76 \text{ lb/ft}^3$ |
| $\mu_o = 0.73 \text{ cp}$ | $B_o = 1.1 \text{ bbl/STB}$ |
| $r_w = 3''$ | $r_e = 1000'$ |
| $k_o = 93.5 \text{ md}$ | |

Calculate the oil critical rate.

Solution

Step 1. Distance from the top of the perforations to top of the sand = 0'

Step 2. Using Figure 9-20, for $h = 50$, enter the graph with $0'$ and move vertically to curve C to give:

$$Q_{\text{curve}} = 270 \text{ bbl/day}$$

Step 3. Calculate critical oil rate from Equation 9-14.

$$Q_{\text{oc}} = 0.5288 \times 10^{-4} \left[\frac{93.5 (63.76 - 47.5)}{(1.1) (0.73)} \right] 270 = 27 \text{ STB/day}$$

The above method can be used through the trial-and-error procedure to optimize the location of the perforated interval in two-cone systems. It should be pointed out that Chaney's method was developed for a homogeneous, isotropic reservoir with $k_v = k_h$.

Chaperson's Method

Chaperson (1986) proposed a simple relationship to estimate the critical rate of a vertical well in an anisotropic formation ($k_v \neq k_h$). The relationship accounts for the distance between the production well and boundary. The proposed correlation has the following form:

$$Q_{\text{oc}} = 0.0783 \times 10^{-4} \frac{k_h (h - h_p)^2}{\mu_o B_o} [\Delta \rho] q_c^* \quad (9-17)$$

where Q_{oc} = critical oil rate, STB/day

k_h = horizontal permeability, md

$\Delta \rho = \rho_w - \rho_o$, density difference, lb/ft³

h = oil column thickness, ft

h_p = perforated interval, ft

Joshi (1991) correlated the coefficient q_c^* with the parameter α'' as

$$q_c^* = 0.7311 + (1.943/\alpha'') \quad (9-18)$$

$$\alpha'' = (r_c/h) \sqrt{k_v/k_h} \quad (9-19)$$

Example 9-9

The following data are available on an oil-water system:

$$\begin{array}{lll} h = 50' & r_c = 1000' & \mu_o = 0.73 \text{ cp} \\ B_o = 1.1 \text{ bbl/STB} & \rho_w = 63.76 \text{ lb/ft}^3 & k_h = 100 \text{ md} \\ \rho_o = 47.5 \text{ lb/ft}^3 & k_v = 10 \text{ md} & h_p = 15' \end{array}$$

Calculate the critical rate.

Solution

Step 1. Calculate α'' from Equation 9-19.

$$\alpha'' = (1000/50) \sqrt{10/100} = 6.324$$

Step 2. Solve for q_c^* by applying Equation 9-18.

$$q_c^* = 0.7311 + (1.943/6.324) = 1.0383$$

Step 3. Solve for the critical oil rate Q_{oc} by using Equation 9-17.

$$Q_{oc} = 0.0783 \times 10^{-4} \frac{(100) (50 - 15)^2}{(0.73) (1.1)} [63.76 - 47.5] (1.0383)$$

$$Q_{oc} = 20.16 \text{ STB/day}$$

Schols' Method

Schols (1972) developed an empirical equation based on results obtained from numerical simulator and laboratory experiments. His critical rate equation has the following form:

$$\begin{aligned} Q_{oc} = & 0.0783 \times 10^{-4} \left[\frac{(\rho_w - \rho_o) k_o (h^2 - h_p^2)}{u_o B_o} \right] \\ & \times \left[0.432 + \frac{3.142}{\ln(r_o/r_w)} \right] (ht_c)^{0.14} \end{aligned} \quad (9-20)$$

where k_o = effective oil permeability, md

r_w = wellbore radius, ft

h_p = perforated interval, ft

ρ = density, lb/ft³

Schols' equation is only valid for isotropic formation, i.e., $k_h = k_v$.

Example 9-10

In an oil-water system, the following fluid and rock data are available:

$$\begin{array}{llll} h = 50' & h_p = 15' & \rho_o = 47.5 \text{ lb/ft}^3 & \rho_w = 63.76 \text{ lb/ft}^3 \\ \mu_o = 0.73 \text{ cp} & B_o = 1.1 \text{ bbl/STB} & r_c = 1000' & r_w = 0.25' \\ k_o = k = 93.5 \text{ md} & & & \end{array}$$

Calculate the critical oil flow rate.

Solution

Applying Equation 9-20 gives

$$Q_{oc} = 0.0783 \times 10^{-4} \left[\frac{(63.76 - 47.5) (93.5) (50^2 - 15^2)}{(0.73) (1.1)} \right] \\ \times \left[0.432 + \frac{3.142}{\ln(1000/.25)} \right] (50/1000)^{0.14}$$

$$Q_{oc} = 18 \text{ STB/day}$$

BREAKTHROUGH TIME IN VERTICAL WELLS

Critical flow rate calculations frequently show low rates that, for economic reasons, cannot be imposed on production wells. Therefore, if a well produces above its critical rate, the cone will break through after a given time period. This time is called *time to breakthrough* t_{BT} . Two of the most widely used correlations are documented below.

The Sobocinski-Cornelius Method

Sobocinski and Cornelius (1965) developed a correlation for predicting water breakthrough time based on laboratory data and modeling results. The authors correlated the breakthrough time with two dimen-

sionless parameters, the dimensionless cone height and the dimensionless breakthrough time. Those two dimensionless parameters are defined by the following expressions:

Dimensionless cone height Z

$$Z = 0.492 \times 10^{-4} \frac{(\rho_w - \rho_o) k_h h (h - h_p)}{\mu_o B_o Q_o} \quad (9-21)$$

where ρ = density, lb/ft³

k_h = horizontal permeability, md

Q_o = oil production rate, STB/day

h_p = perforated interval, ft

h = oil column thickness, ft

Dimensionless breakthrough time $(t_D)_{BT}$

$$(t_D)_{BT} = \frac{4Z + 1.75Z^2 - 0.75Z^3}{7 - 2Z} \quad (9-22)$$

The authors proposed the following expression for predicting time to breakthrough from the calculated value of the dimensionless breakthrough time $(t_D)_{BT}$:

$$t_{BT} = \frac{20,325 \mu_o h \phi (t_D)_{BT}}{(\rho_w - \rho_o) k_v (1 + M^\alpha)} \quad (9-23)$$

where t_{BT} = time to breakthrough, days

ϕ = porosity, fraction

k_v = vertical permeability, md

M = water-oil mobility and is defined by:

$$M = \left[\frac{(k_{rw})_{sor}}{(k_{ro})_{swc}} \right] \left(\frac{\mu_o}{\mu_w} \right) \quad (9-24)$$

with $(k_{ro})_{swc}$ = oil relative permeability at connate water saturation

$(k_{rw})_{sor}$ = water relative permeability at residual oil saturation

$\alpha = 0.5$ for $M \leq 1$

$\alpha = 0.6$ for $1 < M \leq 10$

Joshi (1991) observed by examining Equation 9-22 that if $Z = 3.5$ or greater, there will be no water breakthrough. This observation can be

imposed on Equation 9-21 with $Z = 3.5$ to give an expression for calculating the critical oil flow rate, or

$$Q_{oc} = 0.141 \times 10^{-4} \frac{(\rho_w - \rho_o) k_h h (h - h_p)}{\mu_o B_o} \quad (9-25)$$

Example 9-11

Calculate the water breakthrough using the Sobocinski-Cornelius method for a vertical well producing at 250 STB/day. The following reservoir data are available:

$$\begin{aligned} Q_o &= 250 \text{ STB/day} & h &= 50 \text{ ft} & h_p &= 15 \text{ ft} & \rho_w &= 63.76 \text{ lb/ft}^3 \\ \rho_o &= 47.5 \text{ lb/ft}^3 & \mu_o &= 0.73 \text{ cp} & B_o &= 1.1 \text{ bbl/STB} & k_v &= 9 \text{ md} \\ k_h &= 93 \text{ md} & \phi &= 13\% & M &= 3 \end{aligned}$$

Solution

Step 1. Solve for the dimensionless cone height Z from Equation 9-21 to give

$$Z = 0.492 \times 10^{-4} \left[\frac{(63.76 - 47.5) (93) (50) (50 - 15)}{(0.73) (1.1) (250)} \right] = 0.6486$$

Step 2. Calculate the dimensionless breakthrough time by using Equation 9-22.

$$\begin{aligned} (t_D)_{BT} &= \frac{(4) (0.64866) + 1.75 (0.6486)^2 - 0.75 (0.6486)^3}{7 - 2 (0.6486)} \\ &= 0.5481 \end{aligned}$$

Step 3. Estimate time to breakthrough from Equation 9-23.

$$t_{BT} = \frac{20,325 (0.73) (0.13) (50) (0.5481)}{(63.76 - 47.5) (9) (1 + 3^6)} = 123 \text{ days}$$

Example 9-12

Using the data given in Example 9-11, approximate the critical oil flow rate by using Equation 9-25.

Solution

$$\begin{aligned} Q_{oc} &= 0.141 \times 10^{-4} \frac{(63.76 - 47.5) (93) (50) (50 - 15)}{(0.73) (1.1)} \\ &= 46.3 \text{ STB/day} \end{aligned}$$

The Bournazel-Jeanson Method

Based on experimental data, Bournazel and Jeanson (1971) developed a methodology that uses the same dimensionless groups proposed in the Sobocinski-Cornelius method. The procedure of calculating the time to breakthrough is given below.

Step 1. Calculate the dimensionless core height Z from Equation 9-21.

Step 2. Calculate the dimensionless breakthrough time by applying the following expression:

$$(t_D)_{BT} = \frac{Z}{3 - 0.7Z} \quad (9-26)$$

Step 3. Solve for the time to breakthrough t_{BT} by substituting the above-calculated dimensionless breakthrough time into Equation 9-23, i.e.,

$$t_{BT} = \frac{20,325 \mu_o h \phi (t_D)_{BT}}{(\rho_w - \rho_o) k_v (1 + M^\alpha)}$$

As pointed out by Joshi (1991), Equation 9-26 indicates that no breakthrough occurs if $Z \geq 4.286$. Imposing this value on Equation 9-21 gives a relationship for determining Q_{oc} .

$$Q_{oc} = 0.1148 \times 10^{-4} \frac{(\rho_w - \rho_o) k_h h (h - h_p)}{\mu_o B_o} \quad (9-27)$$

Example 9-13

Resolve Example 9-11 by using the Bournazel-Jeanson method.

Step 1. Solve for the dimensionless cone height $Z = 0.6486$

Step 2. Calculate the dimensionless breakthrough time from Equation 9-26.

$$(t_D)_{BT} = \frac{0.6486}{3 - 0.7 (.6486)} = 0.2548$$

Step 3. Calculate the time to breakthrough by applying Equation 9-23 to give

$$t_{BT} = \frac{20,325 (0.73) (0.13) (50) (0.2548)}{(63.76 - 47.5) (9) (1 + 3^6)} = 57.2 \text{ days}$$

Step 4. From Equation 9-27, the critical oil rate is

$$Q_{oc} = 37.8 \text{ STB/day}$$

AFTER BREAKTHROUGH PERFORMANCE

Once the water breakthrough occurs, it is important to predict the performance of water production as a function of time. Normally, using numerical radial models solves such a problem. Currently, no simple analytical solution exists to predict the performance of the vertical well after breakthrough. Kuo and Desbrisay (1983) applied the material balance equation to predict the rise in the oil-water contact in a homogeneous reservoir and correlated their numerical results in terms of the following dimensionless parameters:

- Dimensionless water cut $(f_w)_D$
- Dimensionless breakthrough time t_{DBT}
- Dimensionless limiting water cut $(WC)_{limit}$

The specific steps of the proposed procedure are given below.

Step 1. Calculate the time to breakthrough t_{BT} by using the Sobocinski-Cornelius method or the Bournazel-Jeanson correlation.

Step 2. Assume any time t after breakthrough.

Step 3. Calculate the dimensionless breakthrough time ratio t_{DBT} from:

$$t_{DBT} = t/t_{BT} \quad (9-28)$$

Step 4. Compute the dimensionless limiting water cut from:

$$(WC)_{limit} = \frac{M}{M + (h/h_w)} \quad (9-29)$$

with the parameters in Equation 9-29 as defined below:

$$M = \left[\frac{(k_{rw})_{sor}}{(k_{ro})_{swc}} \right] \frac{\mu_o}{\mu_w} \quad (9-30)$$

$$h = H_o (1 - R) \quad (9-31)$$

$$h_w = H_w + H_o R \quad (9-32)$$

$$R = (N_p/N) \left[\frac{1 - S_{wc}}{1 - S_{or} - S_{wc}} \right] \quad (9-33)$$

where $(WC)_{limit}$ = current limiting value for water cut

M = mobility ratio

$(k_{rw})_{sor}$ = relative permeability for the water and residual oil saturation (S_{or})

$(k_{ro})_{swc}$ = relative permeability for the oil at the connate water saturation (S_{wc})

μ_o, μ_w = oil and water viscosities, cp

H_o = initial oil zone thickness, ft

H_w = initial water zone thickness, ft

h = current oil zone thickness, ft

h_w = current water zone thickness, ft

N_p = cumulative oil production, STB

N = initial oil in place, STB

Step 5. Calculate the dimensionless water cut $(f_w)_D$ based upon the dimensionless breakthrough time ratio as given by the following relationships:

$$(f_w)_D = 0 \quad \text{for } t_{DBT} < 0.5 \quad (9-34)$$

$$(f_w)_D = 0.29 + 0.94 \log(t_{DBT}) \quad \text{for } 0.5 \leq t_{DBT} \leq 5.7 \quad (9-35)$$

$$(f_w)_D = 1.0 \quad \text{for } t_{DBT} > 5.7 \quad (9-36)$$

Step 6. Calculate the actual water cut f_w from the expression:

$$f_w = (f_w)_D (WC)_{\text{limit}} \quad (9-37)$$

Step 7. Calculate water and oil flow rate by using the following expressions:

$$Q_w = (f_w) Q_T \quad (9-38)$$

$$Q_o = Q_T - Q_w \quad (9-39)$$

where Q_w , Q_o , Q_T are the water, oil, and total flow rates, respectively.

It should be pointed out that as oil is recovered, the oil-water contact will rise and the limiting value for water cut will change. It also should be noted the limiting water cut value $(WC)_{\text{limit}}$ lags behind one time step when calculating future water cut.

Example 9-14

The rock, fluid, and the related reservoir properties of a bottom-water drive reservoir are given below:

well spacing = 80 acres

initial oil column thickness = 80 ft

| | | | |
|-----------------------|-------------------------------|-------------------------------|---------------------------|
| $h_p = 20'$ | $\rho_o = 47 \text{ lb/ft}^3$ | $\rho_w = 63 \text{ lb/ft}^3$ | $r_e = 1053'$ |
| $r_w = 0.25'$ | $M = 3.1$ | $\phi = 14\%$ | $S_{or} = 0.35$ |
| $S_{wc} = 0.25$ | $B_o = 1.2 \text{ bbl/STB}$ | $\mu_o = 1.6 \text{ cp}$ | $\mu_w = 0.82 \text{ cp}$ |
| $k_h = 60 \text{ md}$ | $k_v = 6 \text{ md}$ | | |

Calculate the water cut behavior of a vertical well in the reservoir assuming a total production rate of 500, 1,000, and 1,500 STB/day.

Solution

Step 1. Calculate the dimensionless cone height Z by using Equation 9-21.

$$Z = 0.492 \times 10^{-4} \frac{(63 - 47) (60) (80) (80 - 20)}{(1.6) (1.2) Q_o}$$

| | | | |
|-------|--------|--------|--------|
| Q_o | 500 | 1000 | 1500 |
| Z | 0.2362 | 0.1181 | 0.0787 |

Step 2. Calculate the dimensionless breakthrough time by applying Equation 9-26.

| | | | |
|--------------|---------|---------|---------|
| Q | 500 | 1000 | 1500 |
| Z | 0.2362 | 0.1181 | 0.0787 |
| $(t_D)_{BT}$ | 0.08333 | 0.04048 | 0.02672 |

Step 3. Calculate the time to breakthrough from Equation 9-23.

$$t_{BT} = \left[\frac{(20,325) (1.6) (0.14) (80)}{(63 - 47) (6) (1 + 3.1)^{-6}} \right] (t_D)_{BT}$$

$$t_{BT} = 1276.76 (t_D)_{BT}$$

| | | | |
|--------------|---------|---------|---------|
| Q | 500 | 1000 | 1500 |
| $(t_D)_{BT}$ | 0.08333 | 0.04048 | 0.02672 |
| t_{BT} | 106.40 | 51.58 | 34.11 |

Step 4. Calculate initial oil in place N .

$$N = 7758 A \phi h (1 - S_{wi}) / B_o$$

$$N = 7758 (80) (0.14) (80) (1 - 0.25) / 1.2 = 4,344,480 \text{ STB}$$

Step 5. Calculate the parameter R by applying Equation 9-33.

$$R = [N_p / (4,344,480)] \frac{1 - 0.25}{1 - 0.35 - 0.25} = 4.3158 \times 10^{-7} N_p$$

Step 6. Calculate the limiting water cut at breakthrough.

| | | | |
|----------------|---------|----------|----------|
| Q_o | 500 | 1000 | 1500 |
| t_{BT} | 106.4 | 51.58 | 34.11 |
| N_p | 53,200 | 51,580 | 51,165 |
| R | 0.02296 | 0.022261 | 0.022082 |
| h | 78.16 | 78.22 | 78.23 |
| h_w | 21.84 | 21.78 | 21.77 |
| $(WC)_{limit}$ | 0.464 | 0.463 | 0.463 |

Step 7. The water cut calculations after an assumed elapsed time of 120 days at a fixed total flow rate of 500 STB/days are given below:

- From Equation 9-28, calculate t_{DBT}

$$t_{DBT} = 120/106.4 = 1.1278$$

- Apply Equation 9-36 to find $(f_w)_D$:

$$(f_w)_D = 0.29 + 0.96 \log (1.1278) = 0.3391$$

- Solve for the present water cut from Equation 9-37:

$$f_w = (0.3391) (0.464) = 0.1573$$

Step 8. Calculate water and oil flow rate:

$$Q_w = (0.1573) (500) = 78.65 \text{ STB/day}$$

$$Q_o = 500 - 78.65 = 421.35 \text{ STB/day}$$

Step 9. Calculate cumulative oil produced from breakthrough to 120 days:

$$\Delta N_p = \left[\frac{500 + 421.35}{2} \right] (120 - 106.4) = 6265.18 \text{ STB}$$

Step 10. Calculate cumulative oil produced after 120 days:

$$N_p = 53,200 + 6265.18 = 59,465.18 \text{ STB}$$

Step 11. Find the recovery factory (RF):

$$RF = 59,465.18/4,344,480 = 0.0137$$

Step 12. Assume an elapsed time of 135 days, repeat the above steps at the same total rate of 500 STB/day:

- $R = 4.3158 \times 10^{-7} (59,465.18) = 0.020715$
- $h_w = 21.66$
- $h = 78.34$
- $(W_c)_{\text{limit}} = 0.4615$
- $(f_w)_D = 0.29 + 0.94 \log (135/106.4) = 0.3872$
- $f_w = (0.3872) (0.4615) = 0.1787$
- $Q_w = (500) (0.1787) = 89.34 \text{ STB/day}$
- $Q_o = 500 - 89.34 = 410.66 \text{ STB/day}$

$$\Delta N_p = \left[\frac{410.66 + 421.34}{2} \right] (135 - 120) = 6240.0 \text{ STB}$$

- $N_p = 59,465.18 + 6240.0 = 65,705.22$
- $RF = 0.0151$

Tables 9-1 through 9-3 summarize the calculations for water cut versus time for total flow rates of 500, 100, and 1,500 STB/day, respectively.

CONING IN HORIZONTAL WELLS

The applications of horizontal well technology in developing hydrocarbon reservoirs have been widely used in recent years. One of the main objectives of using this technology is to improve hydrocarbon recovery from water and/or gas-cap drive reservoirs. The advantages of using a horizontal well over a conventional vertical well are their larger capacity to produce oil at the same drawdown and a longer breakthrough time at a given production rate.

Many correlations to predict coning behavior in horizontal wells are available in the literature. Joshi (1991) provides a detailed treatment of the coning problem in horizontal wells. As in vertical wells, the coning problem in horizontal wells involves the following calculations:

- Determination of the critical flow rate
- Breakthrough time predictions
- Well performance calculations after breakthrough

Table 9-1
Results of Example 9-14
Total Production Rate Is 500 STB/day

| Time days | Oil Rate STB/day | Water Rate STB/day | Water Cut Fraction | Cum. Oil MSTB | Oil Rec. % |
|-----------|------------------|--------------------|--------------------|---------------|------------|
| 120 | 406.5 | 93.5 | 0.187 | 59.999 | 1.38 |
| 135 | 379.9 | 120.1 | 0.240 | 65.897 | 1.52 |
| 150 | 355.8 | 144.2 | 0.288 | 71.415 | 1.64 |
| 165 | 333.8 | 166.2 | 0.332 | 76.587 | 1.76 |
| 180 | 313.5 | 186.5 | 0.373 | 81.442 | 1.87 |
| 195 | 294.5 | 205.5 | 0.411 | 86.002 | 1.98 |
| 210 | 276.9 | 223.1 | 0.446 | 90.287 | 2.08 |
| 765 | 239.3 | 260.7 | 0.521 | 177.329 | 4.08 |
| 1020 | 226.4 | 273.6 | 0.547 | 236.676 | 5.45 |
| 1035 | 225.6 | 274.4 | 0.549 | 240.066 | 5.53 |
| 1575 | 202.4 | 297.6 | 0.595 | 355.425 | 8.18 |
| 2145 | 182.4 | 317.6 | 0.635 | 464.927 | 10.70 |
| 2415 | 174.2 | 325.8 | 0.652 | 513.062 | 11.81 |
| 2430 | 173.8 | 326.2 | 0.652 | 515.672 | 11.87 |
| 2445 | 173.4 | 326.6 | 0.653 | 518.276 | 11.93 |
| 3300 | 151.5 | 348.5 | 0.697 | 656.768 | 15.12 |
| 3615 | 144.6 | 355.4 | 0.711 | 703.397 | 16.19 |
| 3630 | 144.3 | 355.7 | 0.711 | 705.564 | 16.24 |
| 3645 | 144.0 | 356.0 | 0.712 | 707.727 | 16.29 |

Horizontal Well Critical Rate Correlations

The following four correlations for estimating critical flow rate in horizontal wells are discussed:

- Chaperson's method
- Efros' method
- Karcher's method
- Joshi's method

Chaperson's Method

Chaperson (1986) provides a simple and practical estimate of the critical rate under steady-state or pseudosteady-state flowing conditions for an isotropic formation. The author proposes the following two relationships for predicting water and gas coning:

Table 9-2
Results of Example 9-14
Total Production Rate Is 1,000 STB/day

| Time days | Oil Rate STB/day | Water Rate STB/day | Water Cut Fraction | Cum. Oil MSTB | Oil Rec. % |
|-----------|------------------|--------------------|--------------------|---------------|------------|
| 80 | 674.7 | 325.3 | 0.325 | 64.14 | 1.48 |
| 95 | 594.2 | 405.8 | 0.406 | 73.66 | 1.70 |
| 110 | 524.8 | 475.2 | 0.475 | 82.05 | 1.89 |
| 125 | 463.2 | 536.8 | 0.537 | 89.46 | 2.06 |
| 140 | 407.8 | 592.2 | 0.592 | 95.99 | 2.21 |
| 335 | 494.8 | 505.2 | 0.505 | 145.68 | 3.35 |
| 905 | 390.8 | 609.2 | 0.609 | 395.80 | 9.11 |
| 1115 | 362.4 | 637.6 | 0.638 | 474.81 | 10.93 |
| 1130 | 360.5 | 639.5 | 0.639 | 480.23 | 11.05 |
| 1475 | 321.8 | 678.2 | 0.678 | 597.70 | 13.76 |
| 1835 | 288.8 | 711.2 | 0.711 | 707.42 | 16.28 |
| 1850 | 287.5 | 712.5 | 0.712 | 711.74 | 16.38 |
| 1865 | 286.3 | 713.7 | 0.714 | 716.04 | 16.48 |
| 1880 | 285.1 | 714.9 | 0.715 | 720.33 | 16.58 |
| 1895 | 283.8 | 716.2 | 0.716 | 724.59 | 16.68 |
| 2615 | 234.4 | 765.6 | 0.766 | 910.20 | 20.95 |
| 2630 | 233.5 | 766.5 | 0.766 | 913.71 | 21.03 |
| 3065 | 210.4 | 789.6 | 0.790 | 1010.11 | 23.25 |
| 3080 | 209.6 | 790.4 | 0.790 | 1013.26 | 23.32 |
| 3620 | 185.8 | 814.2 | 0.814 | 1119.83 | 25.78 |
| 3635 | 185.2 | 814.8 | 0.815 | 1122.61 | 25.84 |
| 3650 | 184.6 | 815.4 | 0.815 | 1125.39 | 25.90 |

Water coning

$$Q_{oc} = 0.0783 - 10^{-4} \left(\frac{Lq_c^*}{y_c} \right) (\rho_w - \rho_o) \frac{k_h [h - (h - D_b)]^2}{\mu_o B_o} \quad (9-40)$$

Gas coning

$$Q_{oc} = 0.0783 - 10^{-4} \left(\frac{Lq_c^*}{y_c} \right) (\rho_o - \rho_g) \frac{k_h [h - (h - D_t)]^2}{\mu_o B_o} \quad (9-41)$$

The above two equations are applicable under the following constraint:

$$1 \leq \alpha'' < 70 \quad \text{and} \quad 2y_c < 4L \quad (9-42)$$

Table 9-3
Results of Example 9-14
Total Production Rate Is 1,500 STB/day

| Time days | Oil Rate STB/day | Water Rate STB/day | Water Cut Fraction | Cum. Oil MSTB | Oil Rec. % |
|-----------|------------------|--------------------|--------------------|---------------|------------|
| 80 | 742.1 | 757.9 | 0.505 | 67.98 | 1.56 |
| 260 | 734.6 | 765.4 | 0.510 | 160.34 | 3.69 |
| 275 | 727.1 | 772.9 | 0.515 | 171.31 | 3.94 |
| 290 | 719.6 | 780.4 | 0.520 | 182.16 | 4.19 |
| 770 | 541.8 | 958.2 | 0.639 | 481.00 | 11.07 |
| 785 | 537.6 | 962.4 | 0.642 | 489.10 | 11.26 |
| 800 | 533.5 | 966.5 | 0.644 | 497.13 | 11.44 |
| 1295 | 423.5 | 1076.5 | 0.718 | 732.08 | 16.85 |
| 1310 | 420.8 | 1079.2 | 0.719 | 738.42 | 17.00 |
| 1325 | 418.1 | 1081.9 | 0.721 | 744.71 | 17.14 |
| 2060 | 315.7 | 1184.3 | 0.790 | 1011.42 | 23.28 |
| 2075 | 314.0 | 1186.0 | 0.791 | 1016.14 | 23.39 |
| 2090 | 312.4 | 1187.6 | 0.792 | 1020.84 | 23.50 |
| 2105 | 310.8 | 1189.2 | 0.793 | 1025.51 | 23.60 |
| 2120 | 309.2 | 1190.8 | 0.794 | 1030.16 | 23.71 |
| 2135 | 307.6 | 1192.4 | 0.795 | 1034.79 | 23.82 |
| 2705 | 255.5 | 1244.5 | 0.830 | 1194.54 | 27.50 |
| 3545 | 200.1 | 1299.9 | 0.867 | 1384.48 | 31.87 |
| 3650 | 194.4 | 1305.6 | 0.870 | 1405.19 | 32.34 |

where

$$\alpha'' = \left(\frac{y_c}{h} \right) \sqrt{\frac{k_v}{k_h}} \quad (9-43)$$

D_b = distance between the WOC and the horizontal well

D_t = distance between the GOC and the horizontal well

Q_{oc} = critical oil rate, STB/day

ρ = density, lb/ft³

k_h = horizontal permeability, md

h = oil column thickness, ft

y_c = half distance between two lines of horizontal wells

(half drainage length perpendicular to the horizontal well)

L = length of the horizontal well

q_c^* = dimensionless function

Joshi (1991) correlated the dimensionless function F with the parameter α'' :

$$q_c^* = 3.9624955 + 0.0616438\alpha'' - 0.000504(\alpha'')^2 \quad (9-44)$$

Example 9-15

A 1,640-ft.-long horizontal well is drilled in the top elevation of the pay zone in a water-drive reservoir. The following data are available:

$$\begin{array}{llll} h = 50 \text{ ft} & k_h = 60 \text{ md} & k_v = 15 \text{ md} & B_o = 1.1 \text{ bbL/STB} \\ \mu_o = 0.73 \text{ cp} & r_w = 0.3 \text{ ft} & D_b = 50 \text{ ft} & \rho_o = 47.5 \text{ lb/ft}^3 \\ \rho_w = 63.76 \text{ lb/ft}^3 & y_e = 1320 \text{ ft} & & \end{array}$$

Using the Chaperson method, calculate:

- The oil critical flow rate for the horizontal well.
- Repeat the calculation assuming a vertical well with $h_p = 15'$ and $r_e = 1,489$ ft.

Solution

Critical rate for a horizontal well:

Step 1. Solve for α'' by applying Equation 9-43.

$$\alpha'' = \frac{1320}{50} \sqrt{\frac{15}{60}} = 13.20$$

Step 2. Solve for the dimensionless function q_c^* by applying Equation 9-44.

$$q_c^* = 4.6821$$

Step 3. Calculate the critical rate from Equation 9-41.

$$\begin{aligned} Q_{oc} &= 0.0783 \times 10^{-4} \left(\frac{1640 \times 4.6821}{1320} \right) (63.76 - 47.5) \left(\frac{60 \times 50^2}{.73 \times 1.1} \right) \\ &= 138.4 \text{ STB/day} \end{aligned}$$

Critical rate for a vertical well:

Step 1. Solve for α'' by using Equation 9-19.

$$\alpha'' = 14.89$$

Step 2. Solve for q_c^* by applying Equation 9-18.

$$q_c^* = 0.8616$$

Step 3. Calculate the critical rate for the vertical well from Equation 9-17.

$$\begin{aligned} Q_{oc} &= 0.0783 \times 10^{-4} \frac{60 \times (50 - 15)^2}{(0.73)(1.1)} (63.76 - 47.5)(0.8616) \\ &= 10 \text{ STB/day} \end{aligned}$$

The ratio of the two critical oil rates is

$$\text{Rate ratio} = \frac{138.4}{10} \cong 14$$

This rate ratio clearly shows the *critical rate improvement* in the case of the horizontal well over that of the vertical well.

Efros' Method

Efros (1963) proposed a critical flow rate correlation that is based on the assumption that the critical rate is nearly independent of drainage radius. The correlation does not account for the effect of the vertical permeability. Efros developed the following two relationships that are designed to calculate the critical rate in oil-water and gas-oil systems:

Water coning

$$Q_{oc} = 0.0783 \times 10^{-4} \frac{k_h (\rho_w - \rho_o) [h - (h - D_b)]^2 L}{\mu_o B_o \left[y_c + \sqrt{y_c^2 + (h^2/3)} \right]} \quad (9-45)$$

Gas coning

$$Q_{oc} = 0.0783 \times 10^{-4} \frac{k_h (\rho_o - \rho_g) [h - (h - D_t)]^2 L}{\mu_o B_o \left[y_e + \sqrt{y_e^2 + (h^2/3)} \right]} \quad (9-46)$$

where L = length of the horizontal well, ft

y_e = half distance between two lines of horizontal wells

ρ = density, lb/ft³

h = net pay thickness

k = permeability, md

Example 9-16

Using the horizontal well data given in Example 9-15, solve for the horizontal well critical flow rate by using Efros' correlation.

Solution

Step 1. Calculate the critical oil flow rate by applying Equation 9-45 to give

$$Q_{oc} = 0.0783 \times 10^{-4} \frac{60 (63.76 - 47.5) 50^2 (1640)}{(1.1) (0.73) \left[1320 + \sqrt{1320^2 + \frac{50^2}{3}} \right]}$$

$$\cong 15 \text{ STB/day}$$

Karcher's Method

Karcher (1986) proposed a correlation that produces a critical oil flow rate value similar to that of Efros' equation. Again, the correlation does not account for the vertical permeability.

Water coning

$$Q_{oc} = 0.0783 \times 10^{-4} \frac{k_h (\rho_w - \rho_o) (h - B)^2 L}{\mu_o B_o (2y_e)} \times \left[1 - \left(\frac{h - B}{y_e} \right)^2 (1/24) \right] \quad (9-47)$$

where $B = h - D_b$

D_b = distance between WOC and horizontal well, ft

Gas coning

$$Q_{oc} = 0.0783 \times 10^{-4} \frac{k_h(\rho_o - \rho_g)(h - T)^2 L}{\mu_o \beta_o (2y_e)} \times \left[1 - \left(\frac{h - T}{y_e} \right)^2 (1/24) \right] \quad (9-48)$$

where $T = h - D_t$

D_t = distance between GOC and horizontal well, ft

Example 9-17

Resolve example by using Karcher's method.

Solution

$$Q_{oc} = 0.0783 \times 10^{-4} \frac{60 (63.76 - 47.5) (50)^2 1640}{(1.1) (0.73) (2 \times 1320)} \times \left[1 - \left(\frac{50}{1320} \right)^2 (1/24) \right] \cong 15 \text{ STB/day}$$

Joshi's Method

Joshi (1988) suggests the following relationships for determining the critical oil flow rate in horizontal wells by defining the following parameters:

- Horizontal well drainage radius r_{eh}

$$r_{eh} = \sqrt{\frac{43,560 A}{\pi}}$$

where A is the horizontal well drainage area in acres.

- Half the major axis of drainage ellipse a

$$a = (L/2) \left[0.5 + \sqrt{0.25 + (2r_{ch}/L)^4} \right]^{0.5} \quad (9-49)$$

- Effective wellbore radius r'_w

$$r'_w = \frac{r_{ch} \left[\frac{L}{2a} \right]}{\left[1 + \sqrt{1 - [L/(2a)]^2} \right] \left[h/(2r_w) \right]^{h/L}} \quad (9-50)$$

For oil-water systems:

$$Q_{oc} = 0.0246 \times 10^{-3} \frac{(\rho_w - \rho_o) k_h [h^2 - (h - D_b)^2]}{\mu_o B_o \ln(r_{ch}/r'_w)} \quad (9-51)$$

For oil-gas systems:

$$Q_{oc} = 0.0246 \times 10^{-3} \frac{(\rho_o - \rho_g) k_h [h^2 - (h - D_t)^2]}{\mu_o B_o \ln(r_{ch}/r'_w)} \quad (9-52)$$

where ρ = density, lb/ft³

k_h = horizontal permeability, md

D_b = distance between the horizontal well and the WOC, ft

D_t = distance between the horizontal well and GOC, ft

r_w = wellbore radius, ft

Example 9-18

Resolve Example 9-17 by applying Joshi's approach.

Solution

Step 1. Solve for a by applying Equation 9-49

$$a = (1640/2) \left[0.5 + \sqrt{0.25 + (2 \times 1489/1640)^4} \right]^{0.5} = 1606 \text{ ft}$$

Step 2. Calculate r'_w from Equation 9-50.

$$r'_w = \frac{1489 \left[\frac{1640}{2(1606)} \right]}{\left[1 + \sqrt{1 - [1640 / (2 \times 1606)]^2} \right] [50 / (2 \times 0.3)]^{50/1640}} = 357 \text{ ft}$$

Step 3. Estimate the critical flow rate from Equation 9-51.

$$\begin{aligned} Q_{oc} &= 0.0246 \times 10^{-3} \frac{(63.76 - 47.5) (60) [50^2 - (50 - 50)^2]}{(0.73) (1.1) \ln (1489 / 357)} \\ &= 52 \text{ STB/day} \end{aligned}$$

HORIZONTAL WELL BREAKTHROUGH TIME

Several authors have proposed mathematical expressions for determining the time to breakthrough in horizontal wells. The following two methodologies are presented in the following sections:

- The Ozkan-Raghavan method
- Papatzacos' method

The Ozkan-Raghavan Method

Ozkan and Raghavan (1988) proposed a theoretical correlation for calculating time to breakthrough in a bottom-water-drive reservoir. The authors introduced the following dimensionless parameters:

$$L_D = \text{dimensionless well length} = [L / (2h)] \sqrt{k_v / k_h} \quad (9-53)$$

$$z_{WD} = \text{dimensionless vertical distance} = D_b / h \quad (9-54)$$

where L = well length, ft

D_b = distance between WOC and horizontal well

H = formation thickness, ft

k_v = vertical permeability, md

k_h = horizontal permeability, md

Ozkan and Raghavan expressed the water breakthrough time by the following equation:

$$t_{BT} = \left[\frac{f_d h^3 E_s}{5.615 Q_o B_o} \right] (k_h/k_v) \quad (9-55)$$

with the parameter f_d as defined by:

$$f_d = \phi (1 - S_{wc} - S_{or}) \quad (9-56)$$

where t_{BT} = time to breakthrough, days

k_v = vertical permeability, md

k_h = horizontal permeability, md

ϕ = porosity, fraction

S_{wc} = connate water saturation, fraction

S_{or} = residual oil saturation, fraction

Q_o = oil flow rate, STB/day

E_s = sweep efficiency, dimensionless

Ozkan and Raghavan graphically correlated the sweep efficiency with the dimensionless well length L_D and dimensionless vertical distance Z_{WD} as shown in Figure 9-24.

Example 9-19

A 1,640-foot-long horizontal well is drilled in a bottom-water-drive reservoir. The following data are available:

| | | | |
|-------------------|----------------|------------------------------------|-------------------------------------|
| $h = 50$ ft | $k_h = 60$ md | $k_v = 15$ md | $B_o = 1.1$ bbl/STB |
| $\mu_o = 0.73$ cp | $r_w = 0.3$ ft | $\rho_o = 47.5$ lb/ft ³ | $\rho_w = 63.76$ lb/ft ³ |
| $Z_{WD} = 1$ | $\phi = 15\%$ | $S_{wc} = 0.25$ | $S_{or} = 0.3$ |

The well is producing at 1,000 STB/day. Calculate time to breakthrough.

Solution

Step 1. Solve for L_D by using Equation 9-53.

$$L_D = \left[\frac{1640}{2(50)} \right] \sqrt{15/60} = 8.2$$

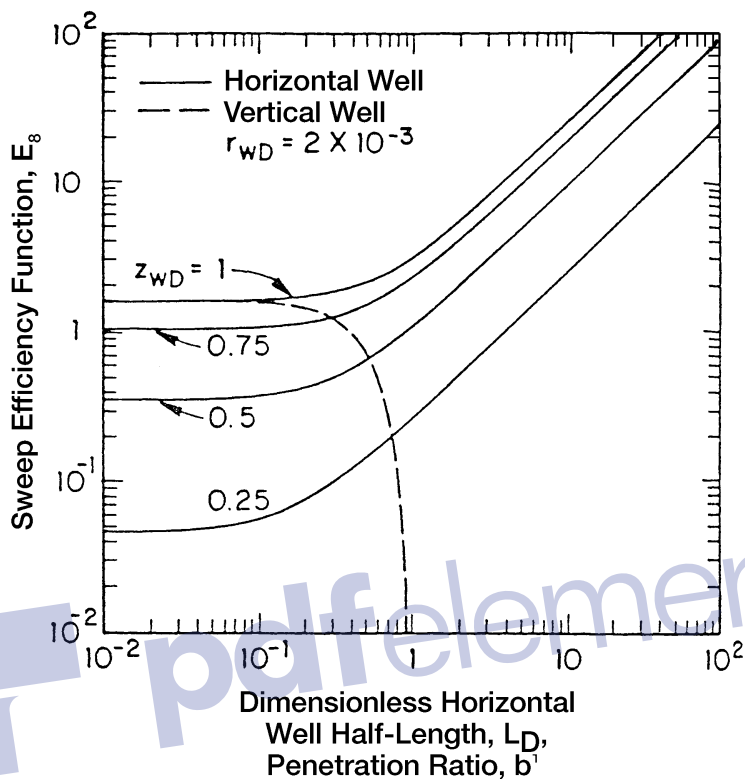


Figure 9-24. Sweep efficiency for horizontal and vertical wells. (After Ozkan, E., and Raghavan, R., courtesy SPE, 1988.)

Step 2. Calculate the parameter f_d from Equation 9-56.

$$f_d = 0.15 (1 - 0.25 - 0.30) = 0.0675$$

Step 3. Estimate the sweep efficiency E_s from Figure 9-24.

$$E_s \cong 21$$

Step 4. Solve for time to breakthrough by applying Equation 9-55.

$$t_{BT} = \left[\frac{0.0675 (50)^3 21}{5.615 \times 1000 \times 1.1} \right] (60/15) = 114.7 \text{ days}$$

Papatzacos' Method

Papatzacos et al. (1989) proposed a methodology that is based on semianalytical solutions for time development of a gas or water cone and simultaneous gas and water cones in an anisotropic, infinite reservoir with a horizontal well placed in the oil column.

Water coning

Step 1. Calculate the dimensionless rate q_D from the following expression:

$$q_D = 20,333.66 \mu_o B_o Q_o / [Lh (\rho_w - \rho_o) \sqrt{k_v k_h}] \quad (9-57)$$

where ρ = density, lb/ft³

k_v = vertical permeability, md

k_h = horizontal permeability, md

h = oil zone thickness, ft

L = length of horizontal well

Step 2. Solve for the dimensionless breakthrough time t_{DBT} by applying the following relationship:

$$t_{DBT} = 1 - (3q_D - 1) \ln \left[\frac{3q_D}{3q_D - 1} \right] \quad (9-58)$$

Step 3. Estimate the time to the water breakthrough t_{BT} by using the water and oil densities in the following expression:

$$t_{BT} = \frac{22,758.528 h \phi \mu_o t_{DBT}}{k_v (\rho_w - \rho_o)} \quad (9-59)$$

where t_{BT} = time to water breakthrough as expressed in days

ρ_o = oil density, lb/ft³

ρ_w = water density, lb/ft³

Gas coning

Step 1. Calculate the dimensionless flow rate q_D .

$$q_D = 20,333.66 \mu_o B_o Q_o / [Lh (\rho_o - \rho_g) \sqrt{k_v k_h}] \quad (9-60)$$

Step 2. Solve for t_{DBT} by applying Equation 9-58.

Step 3. Estimate the time to the gas breakthrough t_{BT} by using the gas and oil densities in the following expression:

$$t_{\text{BT}} = \frac{22,758.528 h \phi \mu_o t_{\text{DBT}}}{k_v (\rho_o - \rho_g)} \quad (9-61)$$

where t_{BT} = time to gas breakthrough as expressed in days

ρ_o = oil density, lb/ft³

ρ_g = gas density, lb/ft³

Water and gas coning

For the two-cone case, the authors developed two graphical correlations for determining the time to breakthrough and optimum placement of the horizontal well. The proposed method is summarized below:

Step 1. Calculate the gas coning dimensionless flow rate by applying Equation 9-60.

Step 2. Calculate the density difference ratio.

$$\psi = \frac{\rho_w - \rho_o}{\rho_o - \rho_g} \quad (9-62)$$

Step 3. Solve for the dimensionless breakthrough time by using Figure 9-25 or applying the following polynomial:

$$\ln(t_{\text{DBT}}) = c_0 + c_1 U + c_2 U^2 + c_3 U^3 \quad (9-63)$$

where $U = \ln(q_D)$

The coefficients $c_0 - c_3$ are tabulated in Table 9-4.

Step 4. Solve for the time to breakthrough by applying the gas coning Equation 9-61.

Step 5. Solve for the optimum placement of the horizontal above the WOC by applying the following expression:

$$D_b^{\text{opt}} = h \beta_{\text{opt}} \quad (9-64)$$

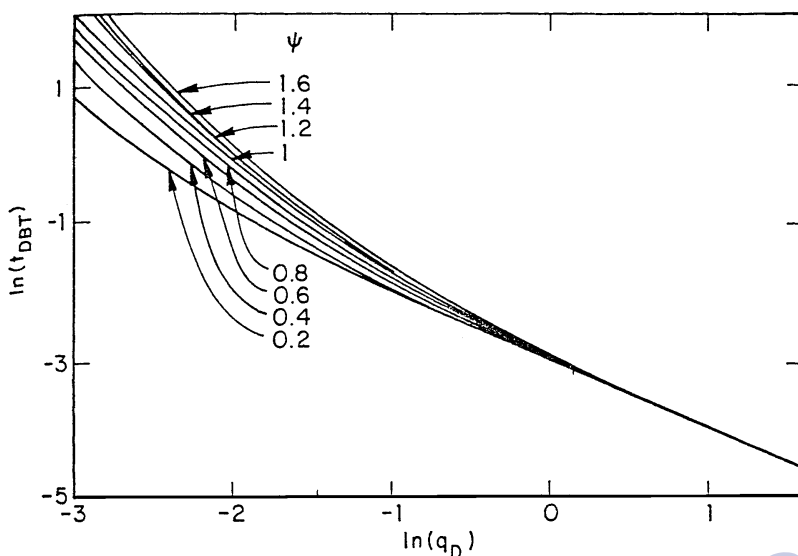


Figure 9-25. Dimensionless time for two-cone case. (After Papatzacos, P. et. al., courtesy SPE, 1989.)

where D_b^{opt} = optimum distance above the WOC, ft
 h = oil thickness, ft
 β_{opt} = optimum fractional well placement

The fractional well placement β_{opt} is determined from Figure 9-26 or the following relationship:

$$\beta_{\text{opt}} = c_0 + c_1U + c_2U^2 + c_3U^3 \quad (9-65)$$

The coefficients of the above polynomial are given in Table 9-5.

Example 9-20

Resolve Example 9-18 by using Papatzacos' method.

Solution

Step 1. Solve for the dimensionless flow rate by using Equation 9-57.

$$q_D = \frac{20,333.66 \times 0.73 \times 1.1 \times 1000}{\left[1640 \times 50 (63.76 - 47.5) \sqrt{60 \times 15}\right]} = 0.408$$

Table 9-4
Coefficients for Breakthrough Time, t_{DBT} (Equation 4-64)
(After Papatzacos, P. et al., SPE Paper 19822, 1989)

| ψ | C_0 | C_1 | C_2 | C_3 |
|--------|---------|----------|------------|-----------|
| 0.2 | -2.9494 | -0.94654 | -0.0028369 | -0.029879 |
| 0.4 | -2.9473 | -0.93007 | 0.016244 | -0.049687 |
| 0.6 | -2.9484 | -0.9805 | 0.050875 | -0.046258 |
| 0.8 | -2.9447 | -1.0332 | 0.075238 | -0.038897 |
| 1.0 | -2.9351 | -1.0678 | 0.088277 | -0.034931 |
| 1.2 | -2.9218 | -1.0718 | 0.091371 | -0.040743 |
| 1.4 | -2.9162 | -1.0716 | 0.093986 | -0.042933 |
| 1.6 | -2.9017 | -1.0731 | 0.094943 | -0.048212 |
| 1.8 | -2.8917 | -1.0856 | 0.096654 | -0.046621 |
| 2.0 | -2.8826 | -1.1103 | 0.10094 | -0.040963 |

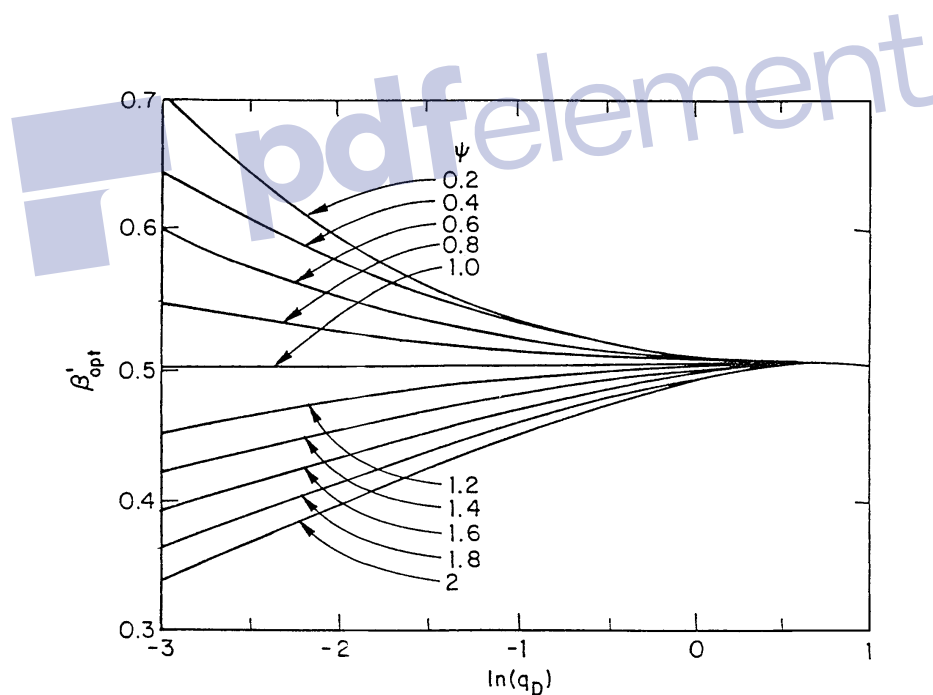


Figure 9-26. Optimum well placement for two-cone case. (After Papatzacos, P. et al., courtesy SPE, 1989.)

Table 9-5
Coefficients for Optimum Well Placement (Equation 4-66)
(After Papatzacos, P. et al., SPE Paper 19822, 1989)

| ψ | C_0 | C_1 | C_2 | C_3 |
|--------|-------|---------|----------|-----------|
| 0.2 | 0.507 | -0.0126 | 0.01055 | -0.002483 |
| 0.4 | 0.504 | -0.0159 | 0.01015 | -0.000096 |
| 0.6 | 0.503 | -0.0095 | 0.00624 | -0.000424 |
| 0.8 | 0.502 | -0.0048 | 0.00292 | -0.000148 |
| 1.0 | 0.500 | -0.0001 | 0.00004 | 0.000009 |
| 1.2 | 0.497 | 0.0042 | -0.00260 | 0.000384 |
| 1.4 | 0.495 | 0.0116 | -0.00557 | -0.000405 |
| 1.6 | 0.493 | 0.0178 | -0.00811 | -0.000921 |
| 1.8 | 0.490 | 0.0231 | -0.01020 | -0.001242 |
| 2.0 | 0.488 | 0.0277 | -0.01189 | -0.001467 |

Step 2. Calculate the dimensionless breakthrough time from Equation 9-58.

$$t_{DBT} = 1 - (3 \times 0.408 - 1) \ln \left[\frac{3 \times 0.408}{3 \times 0.408 - 1} \right] = 0.6191$$

Step 3. Estimate the time to breakthrough from Equation 9-59

$$t_{BT} = \frac{22,758.528 \times 50 \times .15 \times 0.73 \times 0.6191}{[15 (63.74 - 47.5)]} = 316 \text{ days}$$

Example 9-21

A 1,640-foot-long horizontal well is drilled in an oil reservoir with developing gas and water cones. The following data are available:

$$\begin{array}{llll} h = 50 \text{ ft} & k_h = 60 \text{ md} & k_v = 15 \text{ md} & B_o = 1.1 \text{ bbl/STB} \\ \mu_o = 0.73 \text{ cp} & r_w = 0.3 \text{ ft} & \rho_o = 47.5 \text{ lb/ft}^3 & \rho_w = 63.76 \text{ lb/ft}^3 \\ \rho_g = 9.1 \text{ lb/ft}^3 & \phi = 15\% & Q_o = 1000 \text{ STB/day} & \end{array}$$

Determine the optimum well placement and calculate the corresponding breakthrough time.

Solution

Step 1. Calculate the dimensionless flow rate from Equation 9-60.

$$q_D = \frac{20,333.66 \times 0.73 \times 1.1 \times 1000}{\left[1640 \times 50 (47.5 - 9.1) \sqrt{60 \times 15}\right]} = 0.1728$$

Step 2. Calculate the density difference ratio from Equation 9-62.

$$\psi = \frac{63.76 - 47.5}{47.5 - 9.1} = 0.4234$$

Step 3. Read the fraction well placement β_{opt} from Figure 9-26 by using the calculated values of ψ and q_D to give:

$$B_{opt} \cong 0.565$$

Step 4. Calculate the optimum well placement above the WOC from Equation 9-64.

$$D_b^{opt} = (0.565) (50) = 28.25 \text{ ft}$$

Step 5. From Figure 9-25, for $q_D = 0.1728$ and $\psi = 0.4234$, find the dimensionless breakthrough time t_{DBT} :

$$\begin{aligned} \text{Ln}(t_{DBT}) &= -0.8 \quad (\text{from Figure 9-25}) \\ t_{DBT} &= 0.449 \end{aligned}$$

Step 6. Estimate the time to breakthrough by applying Equation 9-61.

$$\begin{aligned} t_{BT} &= 22,758.528 \times 50 \times 0.15 \times 0.73 \times 0.449 / [15 (47.3 - 9.1)] \\ &= 97.71 \text{ days} \end{aligned}$$

PROBLEMS

1. In an oil-water system, the following fluid and rock data are available:

$$\begin{array}{llll} h = 60' & h_p = 25' & \rho_o = 47.5 \text{ lb/ft}^3 & \rho_w = 63.76 \text{ lb/ft}^3 \\ \mu_o = 0.85 \text{ cp} & B_o = 1.2 \text{ bbl/STB} & r_e = 660 & r_w = 0.25' \\ k_o = k = 90.0 \text{ md} & & & \end{array}$$

Calculate the critical oil flow rate, by using the following methods:

- Meyer-Garder
- Chierici-Ciucci
- Hoyland-Papatzacos-Skjaeveland
- Chaney
- Chaperson
- Schols

2. Given:

$$\begin{array}{llll} Q_o = 400 \text{ STB/day} & h = 60 \text{ ft} & h_p = 25 \text{ ft} & \rho_w = 63.76 \text{ lb/ft}^3 \\ \rho_o = 47.5 \text{ lb/ft}^3 & \mu_o = 0.85 \text{ cp} & B_o = 1.2 \text{ bbl/STB} & \\ k_v = 9 \text{ md} & k_h = 90 \text{ md} & \phi = 15\% & M = 3.5 \end{array}$$

Calculate the water breakthrough time by using the:

- a. Sobocinski-Cornelius method
 - b. Bournazel-Jeanson correlation
3. The rock, fluid, and the related reservoir properties of a bottom-water drive reservoir are given below:

well spacing = 80 acres
initial oil column thickness = 100 ft

$$\begin{array}{llll} h_p = 40' & \rho_o = 48 \text{ lb/ft}^3 & \rho_w = 63 \text{ lb/ft}^3 & r_e = 660' \\ r_w = 0.25' & M = 3.0 & \phi = 14\% & S_{or} = 0.25 \\ S_{wc} = 0.25 & B_o = 1.2 \text{ bbl/STB} & \mu_o = 2.6 \text{ cp} & \mu_w = 1.00 \text{ cp} \\ k_h = 80 \text{ md} & k_v = 16 \text{ md} & & \end{array}$$

Calculate the water-cut behavior of a vertical well in the reservoir assuming a total production rate of 500, 1,000, and 1,500 STB/day.

4. A 2,000-ft-long horizontal well is drilled in the top elevation of the pay zone in a water-drive reservoir. The following data are available:

$$\begin{array}{llll} h = 50 \text{ ft} & k_h = 80 \text{ md} & k_v = 25 \text{ md} & B_o = 1.2 \text{ bbl/STB} \\ \mu_o = 2.70 \text{ cp} & r_w = 0.3 \text{ ft} & D_b = 50 \text{ ft} & \rho_o = 48.5 \text{ lb/ft}^3 \\ \rho_w = 62.50 \text{ lb/ft}^3 & y_e = 1320 \text{ ft} & & \end{array}$$

Calculate the critical flow rate by using:

- a. Chaperson's method
- b. Efros' correlation
- c. Karcher's equation
- d. Joshi's method

5. A 2,000-foot-long horizontal well is producing at 1,500 STB/day. The following data are available:

$$\begin{array}{llll}
 h = 60 \text{ ft} & k_h = 80 \text{ md} & k_v = 15 \text{ md} & B_o = 1.2 \text{ bbl/STB} \\
 \mu_o = 2.70 \text{ cp} & r_w = 0.3 \text{ ft} & \rho_o = 47.5 \text{ lb/ft}^3 & \rho_w = 63.76 \text{ lb/ft}^3 \\
 z_{wD} = 1 & \phi = 15\% & S_{wc} = 0.25 & S_{or} = 0.25
 \end{array}$$

Calculate the time to breakthrough by using the:

- a. Ozkan-Raghavan method
- b. Papatzacos' method

REFERENCES

1. Bournazel, C., and Jeanson, B., "Fast Water Coning Evaluation," SPE Paper 3628 presented at the SPE 46th Annual Fall Meeting, New Orleans, Oct. 3–6, 1971.
2. Calhoun, John, *Fundamentals of Reservoir Engineering*. Norman, OK: The University of Oklahoma Press, 1960.
3. Chaney, P. E. et al., "How to Perforate Your Well to Prevent Water and Gas Coning," *OGJ*, May 1956, p. 108.
4. Chaperson, I., "Theoretical Study of Coning Toward Horizontal and Vertical Wells in Anisotropic Formations: Subcritical and Critical Rates," SPE Paper 15377, SPE 61st Annual Fall Meeting, New Orleans, LA, Oct. 5–8, 1986.
5. Chierici, G. L., Ciucci, G. M., and Pizzi, G., "A Systematic Study of Gas and Water Coning by Potentiometric Models," *JPT*, Aug. 1964, p. 923.
6. Efros, D. A., "Study of Multiphase Flows in Porous Media" (in Russian), *Gastotexizdat*, Leningrad, 1963.
7. Hoyland, L. A., Papatzacos, P., and Skjaeveland, S. M., "Critical Rate for Water Coning: Correlation and Analytical Solution," *SPE*, Nov. 1989, p. 495.

8. Joshi, S. D., "Augmentation of Well Productivity Using Slant and Horizontal Wells," *J. of Petroleum Technology*, June 1988, pp. 729–739.
9. Joshi, S., *Horizontal Well Technology*. Tulsa, OK: Pennwell Publishing Company, 1991.
10. Karcher, B., Giger, F., and Combe, J., "Some Practical Formulas to Predict Horizontal Well Behavior," SPE Paper 15430, presented at the SPE 61st Annual Conference, New Orleans, Oct. 5–8, 1986.
11. Kuo, C. T., and Desbrisay, C. L., "A Simplified Method for Water Coning Predictions," SPE Paper 12067, presented at the Annual SPE Technical Conference, San Francisco, Oct. 5–8, 1983.
12. Meyer, H. I., and Garder, A. O., "Mechanics of Two Immiscible Fluids in Porous Media," *J. Applied Phys.*, Nov. 1954, No. 11, p. 25.
13. Muskat, M., and Wyckoff, R. D., "An Approximate Theory of Water Coning in Oil Production," *Trans. AIME*, 1953, pp. 114, 144.
14. Ozkan, E., and Raghavan, R., "Performance of Horizontal Wells Subject to Bottom Water Drive," SPE Paper 18545, presented at the SPE Eastern Regional Meeting, Charleston, West Virginia, Nov. 2–4, 1988.
15. Papatzacos, P., Herring, T. U., Martinsen, R., and Skjaeveland, S. M., "Cone Breakthrough Time for Horizontal Wells," SPE Paper 19822, presented at the 64th SPE Annual Conference and Exhibition, San Antonio, TX, Oct. 8–11, 1989.
16. Pirson, S. J., *Oil Reservoir Engineering*. Huntington, NY: Robert E. Krieger Publishing Company, 1977.
17. Schols, R. S., "An Empirical Formula for the Critical Oil Production Rate," *Erdoel Erdgas*, A., January 1972, Vol. 88, No. 1, pp. 6–11.
18. Slider, H. C., *Practical Petroleum Reservoir Engineering Methods*. Tulsa, OK: Petroleum Publishing Company, 1976.
19. Sobocinski, D. P., and Cornelius, A. J., "A Correlation for Predicting Water Coning Time," *JPT*, May 1965, pp. 594–600.

C H A P T E R 1 0

WATER INFLUX

Nearly all hydrocarbon reservoirs are surrounded by water-bearing rocks called *aquifers*. These aquifers may be substantially larger than the oil or gas reservoirs they adjoin as to appear infinite in size, or they may be so small in size as to be negligible in their effect on reservoir performance.

As reservoir fluids are produced and reservoir pressure declines, a pressure differential develops from the surrounding aquifer into the reservoir. Following the basic law of fluid flow in porous media, the aquifer reacts by encroaching across the original hydrocarbon-water contact. In some cases, water encroachment occurs due to hydrodynamic conditions and recharge of the formation by surface waters at an outcrop.

In many cases, the pore volume of the aquifer is not significantly larger than the pore volume of the reservoir itself. Thus, the expansion of the water in the aquifer is negligible relative to the overall energy system, and the reservoir behaves volumetrically. In this case, the effects of water influx can be ignored. In other cases, the aquifer permeability may be sufficiently low such that a very large pressure differential is required before an appreciable amount of water can encroach into the reservoir. In this instance, the effects of water influx can be ignored as well.

This chapter focuses on those reservoir-aquifer systems in which the size of the aquifer is large enough and the permeability of the rock is high enough that water influx occurs as the reservoir is depleted. This chapter also provides various water influx calculation models and a detailed description of the computational steps involved in applying these models.

CLASSIFICATION OF AQUIFERS

Many gas and oil reservoirs are produced by a mechanism termed *water drive*. Often this is called *natural water drive* to distinguish it from *artificial water drive* that involves the injection of water into the formation. Hydrocarbon production from the reservoir and the subsequent pressure drop prompt a response from the aquifer to offset the pressure decline. This response comes in a form of *water influx*, commonly called *water encroachment*, which is attributed to:

- Expansion of the water in the aquifer
- Compressibility of the aquifer rock
- Artesian flow where the water-bearing formation outcrop is located structurally higher than the pay zone

Reservoir-aquifer systems are commonly classified on the basis of:

- Degree of pressure maintenance
- Outer boundary conditions
- Flow regimes
- Flow geometries

Degree of Pressure Maintenance

Based on the degree of the reservoir pressure maintenance provided by the aquifer, the natural water drive is often qualitatively described as:

- Active water drive
- Partial water drive
- Limited water drive

The term *active* water drive refers to the water encroachment mechanism in which the rate of water influx equals the reservoir *total* production rate. Active water-drive reservoirs are typically characterized by a gradual and slow reservoir pressure decline. If, during any long period, the production rate and reservoir pressure remain reasonably constant, the reservoir voidage rate must be equal to the water influx rate.

$$\left[\begin{array}{c} \text{water influx} \\ \text{rate} \end{array} \right] = \left[\begin{array}{c} \text{oil flow} \\ \text{rate} \end{array} \right] + \left[\begin{array}{c} \text{free gas} \\ \text{flow rate} \end{array} \right] + \left[\begin{array}{c} \text{water production} \\ \text{rate} \end{array} \right]$$

or

$$e_w = Q_o B_o + Q_g B_g + Q_w B_w \quad (10-1)$$

where e_w = water influx rate, bbl/day

Q_o = oil flow rate, STB/day

B_o = oil formation volume factor, bbl/STB

Q_g = **free** gas flow rate, scf/day

B_g = gas formation volume factor, bbl/scf

Q_w = water flow rate, STB/day

B_w = water formation volume factor, bbl/STB

Equation 10-1 can be equivalently expressed in terms of cumulative production by introducing the following derivative terms:

$$e_w = \frac{dW_e}{dt} = B_o \frac{dN_p}{dt} + (GOR - R_s) \frac{dN_p}{dt} B_g + \frac{dW_p}{dt} B_w \quad (10-2)$$

where

W_e = cumulative water influx, bbl

t = time, days

N_p = cumulative oil production, STB

GOR = current gas-oil ratio, scf/STB

R_s = current gas solubility, scf/STB

B_g = gas formation volume factor, bbl/scf

W_p = cumulative water production, STB

dN_p/dt = daily oil flow rate Q_o , STB/day

dW_p/dt = daily water flow rate Q_w , STB/day

dW_e/dt = daily water influx rate e_w , bbl/day

$(GOR - R_s)dN_p/dt$ = daily free gas flow rate, scf/day

Example 10-1

Calculate the water influx rate e_w in a reservoir whose pressure is stabilized at 3,000 psi.

Given: initial reservoir pressure = 3500 psi

dN_p/dt = 32,000 STB/day

B_o = 1.4 bbl/STB

GOR = 900 scf/STB

R_s = 700 scf/STB

B_g = 0.00082 bbl/scf

dW_p/dt = 0

B_w = 1.0 bbl/STB

Solution

Applying Equation 10-1 or 10-2 gives:

$$\begin{aligned} e_w &= (1.4) (32,000) + (900 - 700) (32,000) (0.00082) + 0 \\ &= 50,048 \text{ bbl/day} \end{aligned}$$

Outer Boundary Conditions

The aquifer can be classified as infinite or finite (bounded). Geologically all formations are finite, but may act as infinite if the changes in the pressure at the oil-water contact are not “felt” at the aquifer boundary. Some aquifers outcrop and are infinite acting because of surface replenishment. In general, the outer boundary governs the behavior of the aquifer and, therefore:

- a. Infinite system indicates that the effect of the pressure changes at the oil/aquifer boundary can never be felt at the outer boundary. This boundary is for all intents and purposes at a constant pressure equal to initial reservoir pressure.
- b. Finite system indicates that the aquifer outer limit is affected by the influx into the oil zone and that the pressure at this outer limit changes with time.

Flow Regimes

There are basically three flow regimes that influence the rate of water influx into the reservoir. As previously described in Chapter 6, those flow regimes are:

- a. Steady-state
- b. Semisteady (pseudosteady)-state
- c. Unsteady-state

Flow Geometries

Reservoir-aquifer systems can be classified on the basis of flow geometry as:

- a. Edge-water drive
- b. Bottom-water drive
- c. Linear-water drive

In edge-water drive, as shown in Figure 10-1, water moves into the flanks of the reservoir as a result of hydrocarbon production and pressure drop at the reservoir-aquifer boundary. The flow is essentially radial with negligible flow in the vertical direction.

Bottom-water drive occurs in reservoirs with large areal extent and gentle dip where the reservoir-water contact completely underlies the reservoir. The flow is essentially radial and, in contrast to the edge-water drive, the bottom-water drive has significant vertical flow.

In linear-water drive, the influx is from one flank of the reservoir. The flow is strictly linear with a constant cross-sectional area.

RECOGNITION OF NATURAL WATER INFLUX

Normally very little information is obtained during the exploration-development period of a reservoir concerning the presence or characteristics of an aquifer that could provide a source of water influx during the depletion period. Natural water drive may be assumed by analogy with nearby producing reservoirs, but early reservoir performance trends can provide clues. A comparatively low, and decreasing, rate of reservoir pressure decline with increasing cumulative withdrawals is indicative of fluid influx.

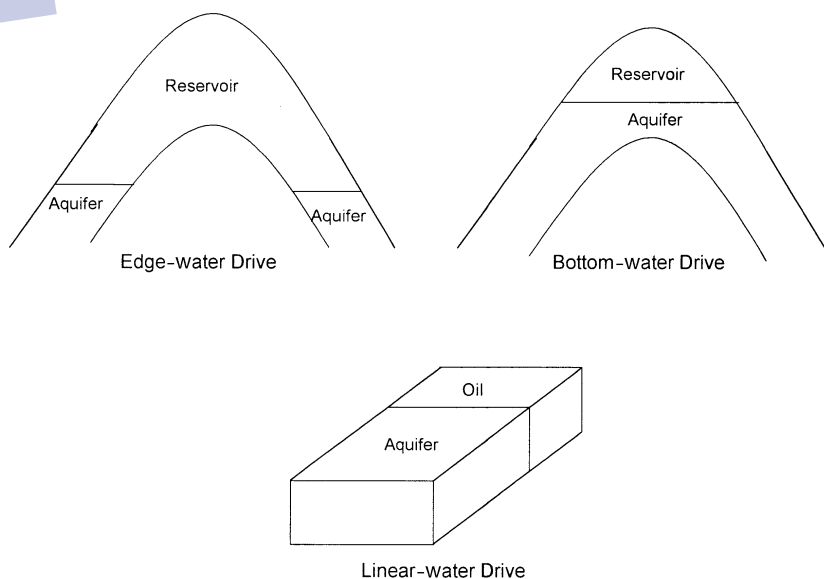


Figure 10-1. Flow geometries.

Successive calculations of barrels withdrawn per psi change in reservoir pressure can supplement performance graphs. If the reservoir limits have not been delineated by developed dry holes, however, the influx could be from an undeveloped area of the reservoir not accounted for in averaging reservoir pressure. If the reservoir pressure is below the oil saturation pressure, a low rate of increase in produced gas-oil ratio is also indicative of fluid influx.

Early water production from edge wells is indicative of water encroachment. Such observations must be tempered by the possibility that the early water production is due to formation fractures; thin, high permeability streaks; or to coning in connection with a limited aquifer. The water production may be due to casing leaks.

Calculation of increasing original oil in place from successive reservoir pressure surveys by using the material balance assuming no water influx is also indicative of fluid influx.

WATER INFLUX MODELS

It should be appreciated that in reservoir engineering there are more uncertainties attached to this subject than to any other. This is simply because one seldom drills wells into an aquifer to gain the necessary information about the porosity, permeability, thickness, and fluid properties. Instead, these properties frequently have to be inferred from what has been observed in the reservoir. Even more uncertain, however, is the geometry and areal continuity of the aquifer itself.

Several models have been developed for estimating water influx that are based on assumptions that describe the characteristics of the aquifer. Due to the inherent uncertainties in the aquifer characteristics, all of the proposed models require historical reservoir performance data to evaluate constants representing aquifer property parameters since these are rarely known from exploration-development drilling with sufficient accuracy for direct application. The material balance equation can be used to determine historical water influx provided original oil in place is known from pore volume estimates. This permits evaluation of the constants in the influx equations so that future water influx rate can be forecasted.

The mathematical water influx models that are commonly used in the petroleum industry include:

- Pot aquifer
- Schilthuis' steady-state

- Hurst's modified steady-state
- The van Everdingen-Hurst unsteady-state
 - Edge-water drive
 - Bottom-water drive
- The Carter-Tracy unsteady-state
- Fetkovich's method
 - Radial aquifer
 - Linear aquifer

The following sections describe these models and their practical applications in water influx calculations.

The Pot Aquifer Model

The simplest model that can be used to estimate the water influx into a gas or oil reservoir is based on the basic definition of compressibility. A drop in the reservoir pressure, due to the production of fluids, causes the aquifer water to expand and flow into the reservoir. The compressibility is defined mathematically as:

$$\Delta V = c V \Delta p \quad (10-3)$$

Applying the above basic compressibility definition to the aquifer gives:

$$\text{Water influx} = (\text{aquifer compressibility}) (\text{initial volume of water}) (\text{pressure drop})$$

or

$$W_e = (c_w + c_f) W_i (p_i - p) \quad (10-4)$$

where W_e = cumulative water influx, bbl

c_w = aquifer water compressibility, psi^{-1}

c_f = aquifer rock compressibility, psi^{-1}

W_i = initial volume of water in the aquifer, bbl

p_i = initial reservoir pressure, psi

p = current reservoir pressure (pressure at oil-water contact), psi

Calculating the initial volume of water in the aquifer requires the knowledge of aquifer dimension and properties. These, however, are seldom measured since wells are not deliberately drilled into the aquifer to obtain such information. For instance, if the aquifer shape is radial, then:

$$W_i = \left[\frac{\pi(r_a^2 - r_c^2)h\phi}{5.615} \right] \quad (10-5)$$

where r_a = radius of the aquifer, ft
 r_c = radius of the reservoir, ft
 h = thickness of the aquifer, ft
 ϕ = porosity of the aquifer

Equation 10-3 suggests that water is encroaching in a radial form from all directions. Quite often, water does not encroach on all sides of the reservoir, or the reservoir is not circular in nature.

To account for these cases, a modification to Equation 10-2 must be made in order to properly describe the flow mechanism. One of the simplest modifications is to include the fractional encroachment angle f in the equation, as illustrated in Figure 10-2, to give:

$$W_e = (c_w + c_f) W_i f (p_i - p) \quad (10-6)$$

where the fractional encroachment angle f is defined by:

$$f = \frac{(\text{encoachment angle})^\circ}{360^\circ} = \frac{\theta}{360^\circ} \quad (10-7)$$

The above model is only applicable to a small aquifer, i.e., pot aquifer, whose dimensions are of the same order of magnitude as the reservoir itself. Dake (1978) points out that because the aquifer is considered relatively small, a pressure drop in the reservoir is instantaneously transmitted throughout the entire reservoir-aquifer system. Dake suggests that for large aquifers, a mathematical model is required which includes time dependence to account for the fact that it takes a finite time for the aquifer to respond to a pressure change in the reservoir.

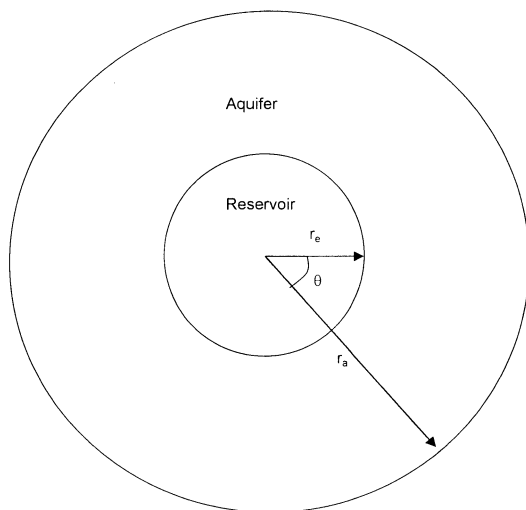


Figure 10-2. Radial aquifer geometries.

Example 10-2

Calculate the cumulative water influx that results from a pressure drop of 200 psi at the oil-water contact with an encroachment angle of 80° . The reservoir-aquifer system is characterized by the following properties:

| | Reservoir | Aquifer |
|---------------------------|--------------------|--------------------|
| radius, ft | 2600 | 10,000 |
| porosity | 0.18 | 0.12 |
| c_f , psi^{-1} | 4×10^{-6} | 3×10^{-6} |
| c_w , psi^{-1} | 5×10^{-6} | 4×10^{-6} |
| h, ft | 20 | 25 |

Solution

Step 1. Calculate the initial volume of water in the aquifer from Equation 10-4.

$$W_i = \left(\frac{\pi (10,000^2 - 2600^2) (25) (0.12)}{5.615} \right) = 156.5 \text{ MMbbl}$$

Step 2. Determine the cumulative water influx by applying Equation 10-5.

$$W_e = (4+3) 10^{-6} (156.5 \times 10^6) \left(\frac{80}{360} \right) (200) = 48,689 \text{ bbl}$$

Schilthuis' Steady-State Model

Schilthuis (1936) proposed that for an aquifer that is flowing under the steady-state flow regime, the flow behavior could be described by Darcy's equation. The rate of water influx e_w can then be determined by applying Darcy's equation:

$$\frac{dW_e}{dt} = e_w = \left[\frac{0.00708 kh}{\mu_w \ln \left(\frac{r_a}{r_e} \right)} \right] (p_i - p) \quad (10-8)$$

The above relationship can be more conveniently expressed as:

$$\frac{dW_e}{dt} = e_w = C (p_i - p) \quad (10-9)$$

where e_w = rate of water influx, bbl/day
 k = permeability of the aquifer, md
 h = thickness of the aquifer, ft
 r_a = radius of the aquifer, ft
 r_e = radius of the reservoir
 t = time, days

The parameter C is called the water influx constant and is expressed in bbl/day/psi. This water influx constant C may be calculated from the reservoir historical production data over a number of selected time intervals, provided that the rate of water influx e_w has been determined independently from a different expression. For instance, the parameter C may be estimated by combining Equation 10-1 with 10-8. Although the influx constant can only be obtained in this manner when the reservoir pressure stabilizes, once it has been found, it may be applied to both stabilized and changing reservoir pressures.

Example 10-3

The data given in Example 10-1 are used in this example:

$$\begin{array}{lll} p_i = 3500 \text{ psi} & p = 3000 \text{ psi} & Q_o = 32,000 \text{ STB/day} \\ B_o = 1.4 \text{ bbl/STB} & \text{GOR} = 900 \text{ scf/STB} & R_s = 700 \text{ scf/STB} \\ B_g = 0.00082 \text{ bbl/scf} & Q_w = 0 & B_w = 1.0 \text{ bbl/STB} \end{array}$$

Calculate Schilthuis' water influx constant.

Solution

Step 1. Solve for the rate of water influx e_w by using Equation 10-1.

$$\begin{aligned} e_w &= (1.4)(32,000) + (900 - 700)(32,000)(0.00082) + 0 \\ &= 50,048 \text{ bbl/day} \end{aligned}$$

Step 2. Solve for the water influx constant from Equation 10-8.

$$C = \frac{50,048}{(3500 - 3000)} = 100 \text{ bbl/day/psi}$$

If the steady-state approximation adequately describes the aquifer flow regime, the calculated water influx constant C values will be constant over the historical period.

Note that the pressure drops contributing to influx are the cumulative pressure drops from the initial pressure.

In terms of the cumulative water influx W_e , Equation 10-8 is integrated to give the common Schilthuis expression for water influx as:

$$\int_0^{W_e} dW_e = \int_0^t C (p_i - p) dt$$

or

$$W_e = C \int_0^t (p_i - p) dt \quad (10-10)$$

where W_e = cumulative water influx, bbl

C = water influx constant, bbl/day/psi

t = time, days
 p_i = initial reservoir pressure, psi
 p = pressure at the oil-water contact at time t , psi

When the pressure drop ($p_i - p$) is plotted versus the time t , as shown in Figure 10-3, the area under the curve represents the integral $\int_0^t (p_i - p) dt$.

This area at time t can be determined numerically by using the trapezoidal rule (or any other numerical integration method), as:

$$\int_0^t (p_i - p) dt = \text{area}_I + \text{area}_{II} + \text{area}_{III} + \text{etc.} = \left(\frac{p_i - p_1}{2} \right) (t_1 - 0) + \frac{(p_i - p_1) + (p_i - p_2)}{2} (t_2 - t_1) + \frac{(p_i - p_2) + (p_i - p_3)}{2} (t_3 - t_2) + \text{etc.}$$

Equation 10-9 can then be written as:

$$W_e = C \sum_0^t (\Delta p) \Delta t \quad (10-11)$$

Example 10-4

The pressure history of a water-drive oil reservoir is given below:

| t , days | p , psi |
|------------|----------------|
| 0 | 3500 (p_i) |
| 100 | 3450 |
| 200 | 3410 |
| 300 | 3380 |
| 400 | 3340 |

The aquifer is under a steady-state flowing condition with an estimated water influx constant of 130 bbl/day/psi. Calculate the cumulative water influx after 100, 200, 300, and 400 days using the steady-state model.

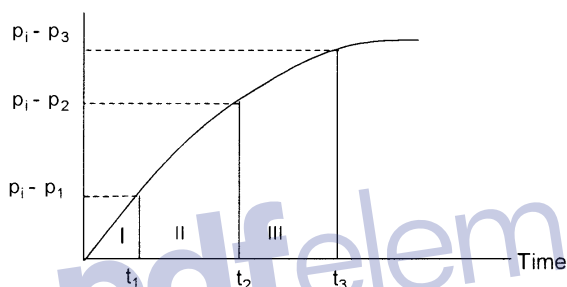
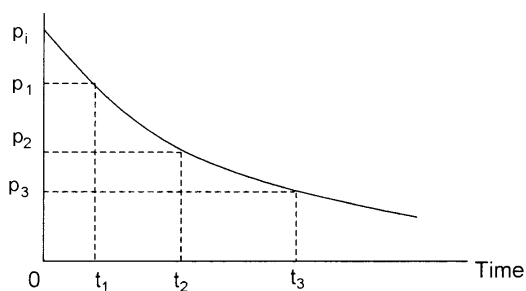


Figure 10-3. Calculating the area under the curve.

Solution

Step 1. Calculate the total pressure drop at each time t .

| t , days | p | $p_i - p$ |
|------------|------|-----------|
| 0 | 3500 | 0 |
| 100 | 3450 | 50 |
| 200 | 3410 | 90 |
| 300 | 3380 | 120 |
| 400 | 3340 | 160 |

Step 2. Calculate the cumulative water influx after 100 days:

$$W_e = 130 \left(\frac{50}{2} \right) (100 - 0) = 325,000 \text{ bbl}$$

Step 3. Determine W_e after 200 days.

$$W_e = 130 \left[\left(\frac{50}{2} \right) (100 - 0) + \left(\frac{50 + 90}{2} \right) (200 - 100) \right] = 1,235,000 \text{ bbl}$$

Step 4. W_e after 300 days.

$$W_e = 130 \left[\left(\frac{50}{2} \right) (100) + \left(\frac{50 + 90}{2} \right) (200 - 100) \right. \\ \left. + \left(\frac{120 + 90}{2} \right) (300 - 200) \right] = 2,600,000 \text{ bbl}$$

Step 5. Calculate W_e after 400 days.

$$W_e = 130 \left[2500 + 7000 + 10,500 + \left(\frac{160 + 120}{2} \right) (400 - 300) \right] \\ = 4,420,000 \text{ bbl}$$

Hurst's Modified Steady-State Model

One of the problems associated with the Schilthuis' steady-state model is that as the water is drained from the aquifer, the aquifer drainage radius r_a will increase as the time increases. Hurst (1943) proposed that the "apparent" aquifer radius r_a would increase with time and, therefore the dimensionless radius r_a/r_e may be replaced with a time dependent function, as:

$$r_a/r_e = at \quad (10-12)$$

Substituting Equation 10-11 into Equation 10-7 gives:

$$e_w = \frac{dW_e}{dt} = \frac{0.00708 kh(p_i - p)}{\mu_w \ln(at)} \quad (10-13)$$

The Hurst modified steady-state equation can be written in a more simplified form as:

$$e_w = \frac{dW_e}{dt} = \frac{C(p_i - p)}{\ln(at)} \quad (10-14)$$

and in terms of the cumulative water influx

$$W_e = C \int_0^t \left[\frac{p_i - p}{\ln(at)} \right] dt \quad (10-15)$$

or

$$W_e = C \sum_0^t \left[\frac{\Delta p}{\ln(at)} \right] \Delta t \quad (10-16)$$

The Hurst modified steady-state equation contains two unknown constants, i.e., a and C , that must be determined from the reservoir-aquifer pressure and water influx historical data. The procedure of determining the constants a and C is based on expressing Equation 10-13 as a linear relationship.

$$\left(\frac{p_i - p}{e_w} \right) = \frac{1}{C} \ln(at)$$

or

$$\frac{p_i - p}{e_w} = \left(\frac{1}{C} \right) \ln(a) + \left(\frac{1}{C} \right) \ln(t) \quad (10-17)$$

Equation 10-16 indicates that a plot of $(p_i - p)/e_w$ versus $\ln(t)$ will be a straight line with a slope of $1/C$ and intercept of $(1/C)\ln(a)$, as shown schematically in Figure 10-4.

Example 10-5

The following data, as presented by Craft and Hawkins (1959), documents the reservoir pressure as a function of time for a water-drive reservoir. Using the reservoir historical data, Craft and Hawkins calcu-

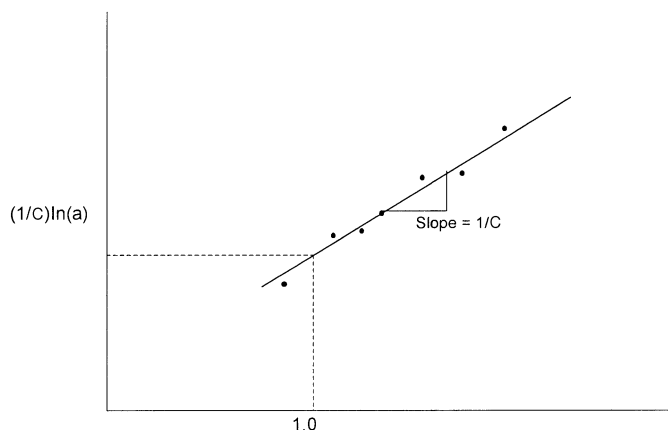


Figure 10-4. Graphical determination of C and a .

lated the water influx by applying the material balance equation (see Chapter 11). The rate of water influx was also calculated numerically at each time period.

| Time days | Pressure psi | W_e M bbl | e_w bbl/day | $p_i - p$ psi |
|--------------|-----------------|----------------|------------------|------------------|
| 0 | 3793 | 0 | 0 | 0 |
| 182.5 | 3774 | 24.8 | 389 | 19 |
| 365.0 | 3709 | 172.0 | 1279 | 84 |
| 547.5 | 3643 | 480.0 | 2158 | 150 |
| 730.0 | 3547 | 978.0 | 3187 | 246 |
| 912.5 | 3485 | 1616.0 | 3844 | 308 |
| 1095.0 | 3416 | 2388.0 | 4458 | 377 |

Assuming that the boundary pressure would drop to 3,379 psi after 1,186.25 days of production, calculate cumulative water influx at that time.

Solution

Step 1. Construct the following table:

| t , days | $\ln(t)$ | $p_i - p$ | e_w , bbl/day | $(p_i - p)/e_w$ |
|------------|----------|-----------|-----------------|-----------------|
| 0 | — | 0 | 0 | — |
| 182.5 | 5.207 | 19 | 389 | 0.049 |
| 365.0 | 5.900 | 84 | 1279 | 0.066 |
| 547.5 | 6.305 | 150 | 2158 | 0.070 |
| 730.0 | 6.593 | 246 | 31.87 | 0.077 |
| 912.5 | 6.816 | 308 | 3844 | 0.081 |
| 1095.0 | 6.999 | 377 | 4458 | 0.085 |

Step 2. Plot the term $(p_i - p)/e_w$ versus $\ln(t)$ and draw the best straight line through the points as shown in Figure 10-5, and determine the slope of the line to give:

$$\text{slope} = 0.020$$

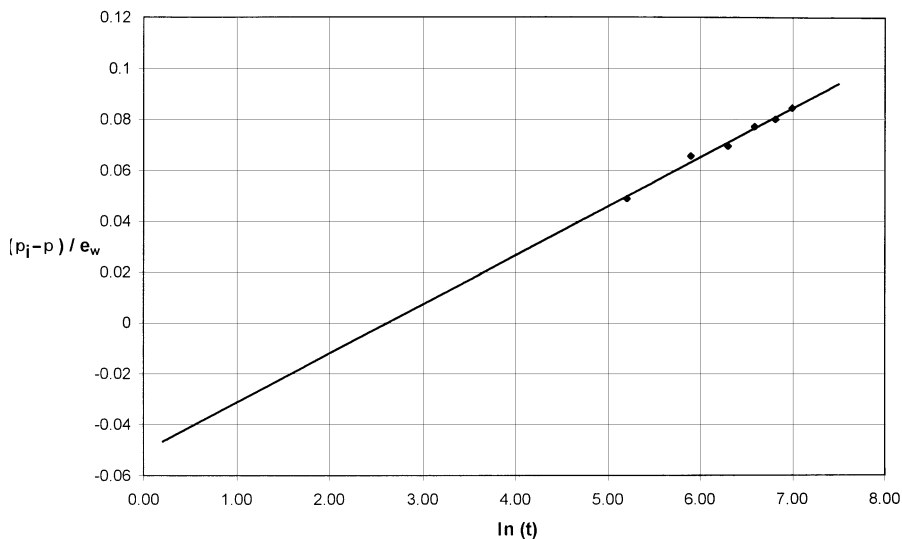


Figure 10-5. Determination of C and n for Example 10-5.

Step 3. Determine the coefficient C of the Hurst equation from the slope to give:

$$C = 1/0.02 = 50$$

Step 4. Using any point on the straight line, solve for the parameter a by applying Equation 10-13 to give:

$$a = 0.064$$

Step 5. The Hurst equation is represented by:

$$W_e = 50 \int_0^t \left[\frac{p_i - p}{\ln(0.064 t)} \right] dt$$

Step 6. Calculate the cumulative water influx after 1,186.25 days from:

pdfelement

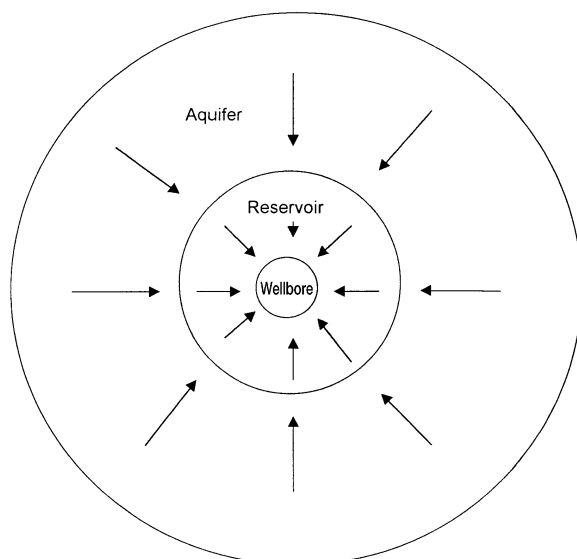


Figure 10-6. Water influx into a cylindrical reservoir.

$$W_e = 2388 \times 10^3 + \int_{1095}^{1186.25} 50 \left[\frac{P_i - P}{\ln(0.064t)} \right] dt$$

$$W_e = 2388 \times 10^3 + 50 \left[\frac{\frac{3793 - 3379}{\ln(0.064 \times 1186.25)} + \frac{3793 - 3416}{\ln(0.064 \times 1095)}}{2} \right]$$

$$\times (1186.25 - 1095)$$

$$W_e = 2388 \times 10^3 + 420.508 \times 10^3 = 2809 \text{ Mbbl}$$

The van Everdingen-Hurst Unsteady-State Model

The mathematical formulations that describe the flow of a crude oil system into a wellbore are identical in form to those equations that describe the flow of water from an aquifer into a cylindrical reservoir, as shown schematically in Figure 10-6.

When an oil well is brought on production at a constant flow rate after a shut-in period, the pressure behavior is essentially controlled by the transient (unsteady-state) flowing condition. This flowing condition is defined as the time period during which the boundary has no effect on the pressure behavior.

The dimensionless form of the diffusivity equation, as presented in Chapter 6 by Equation 6-90, is basically the general mathematical equation that is designed to model the transient flow behavior in reservoirs or aquifers. In a dimensionless form, the diffusivity equation takes the form:

$$\frac{\partial^2 P_D}{\partial r_D^2} + \frac{1}{r_D} \frac{\partial P_D}{\partial r_D} = \frac{\partial P_D}{\partial t_D}$$

Van Everdingen and Hurst (1949) proposed solutions to the dimensionless diffusivity equation for the following two reservoir-aquifer boundary conditions:

- Constant terminal rate
- Constant terminal pressure

For the constant-terminal-rate boundary condition, the rate of water influx is assumed constant for a given period; and the pressure drop at the reservoir-aquifer boundary is calculated.

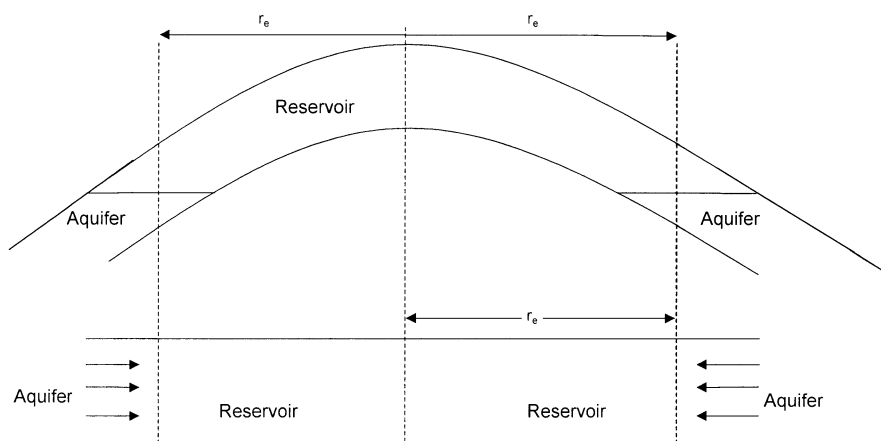


Figure 10-7. Idealized radial flow model.

For the constant-terminal-pressure boundary condition, a boundary pressure drop is assumed constant over some finite time period, and the water influx rate is determined.

In the description of water influx from an aquifer into a reservoir, there is greater interest in calculating the influx rate rather than the pressure. This leads to the determination of the water influx as a function of a given pressure drop at the inner boundary of the reservoir-aquifer system.

Van Everdingen and Hurst solved the diffusivity equation for the aquifer-reservoir system by applying the Laplace transformation to the equation. The authors' solution can be used to determine the water influx in the following systems:

- Edge-water-drive system (radial system)
- Bottom-water-drive system
- Linear-water-drive system

Edge-Water Drive

Figure 10-7 shows an idealized radial flow system that represents an edge-water-drive reservoir. The inner boundary is defined as the interface between the reservoir and the aquifer. The flow across this inner boundary is considered horizontal and encroachment occurs across a cylindrical plane encircling the reservoir. With the interface as the inner boundary, it is possible to impose a constant terminal pressure at the inner boundary and determine the rate of water influx across the interface.

Van Everdingen and Hurst proposed a solution to the dimensionless diffusivity equation that utilizes the constant terminal pressure condition in addition to the following initial and outer boundary conditions:

Initial conditions:

$$p = p_i \text{ for all values of radius } r$$

Outer boundary conditions

- For an infinite aquifer

$$p = p_i \text{ at } r = \infty$$

- For a bounded aquifer

$$\frac{\partial p}{\partial r} = 0 \text{ at } r = r_a$$

Van Everdingen and Hurst assumed that the aquifer is characterized by:

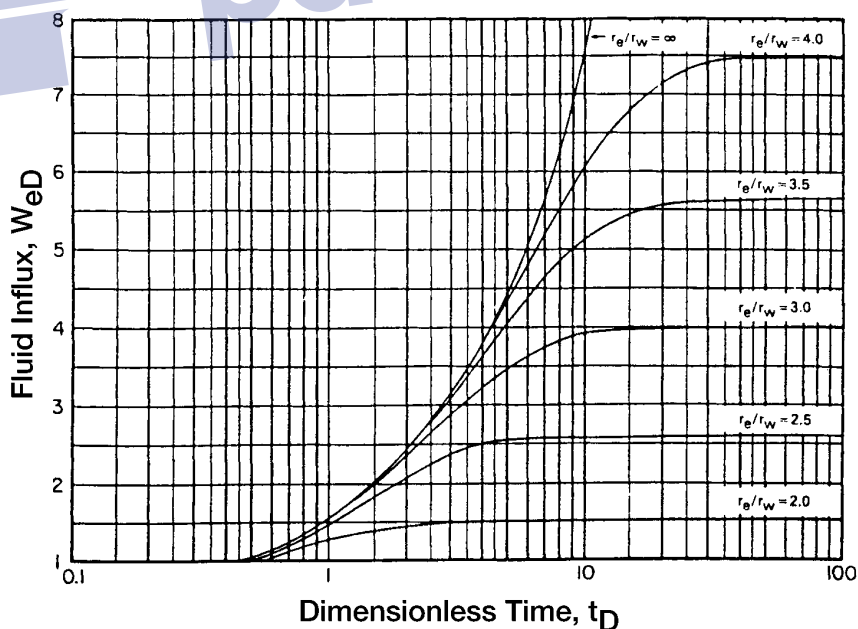


Figure 10-8. Dimensionless water influx W_{eD} for several values of r_e/r_w , i.e., r_a/r_e . (Van Everdingen and Hurst. Permission to publish by the SPE.)

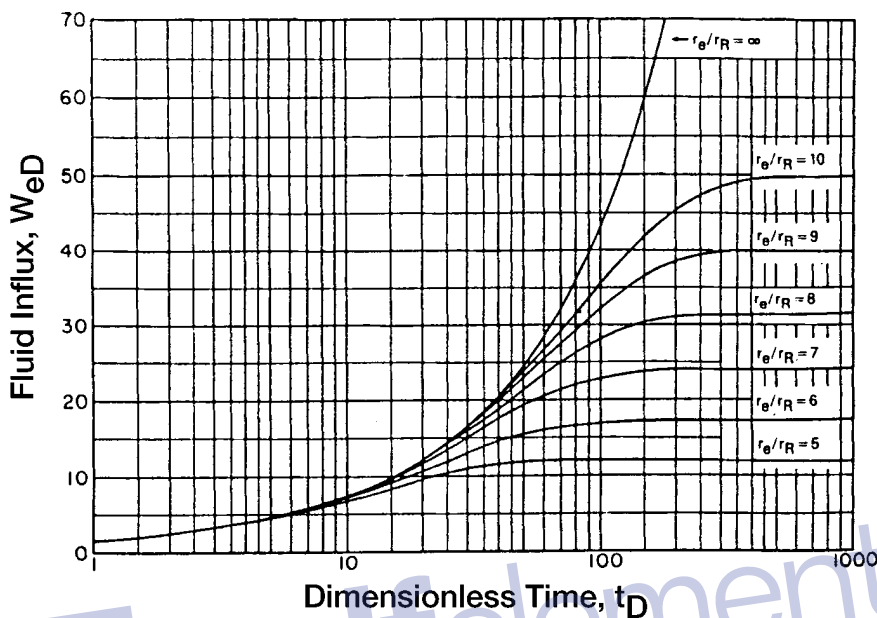


Figure 10-9. Dimensionless water influx W_{eD} for several values of r_e/r_R , i.e., r_a/r_e . (Van Everdingen and Hurst. Permission to publish by the SPE.)

- Uniform thickness
- Constant permeability
- Uniform porosity
- Constant rock compressibility
- Constant water compressibility

The authors expressed their mathematical relationship for calculating the water influx in a form of a dimensionless parameter that is called *dimensionless water influx* W_{eD} . They also expressed the dimensionless water influx as a function of the *dimensionless time* t_D and *dimensionless radius* r_D , thus they made the solution to the diffusivity equation generalized and applicable to any aquifer where the flow of water into the reservoir is essentially radial.

The solutions were derived for cases of bounded aquifers and aquifers of infinite extent. The authors presented their solution in tabulated and graphical forms as reproduced here in Figures 10-8 through 10-11 and Tables 10-1 and 10-2.

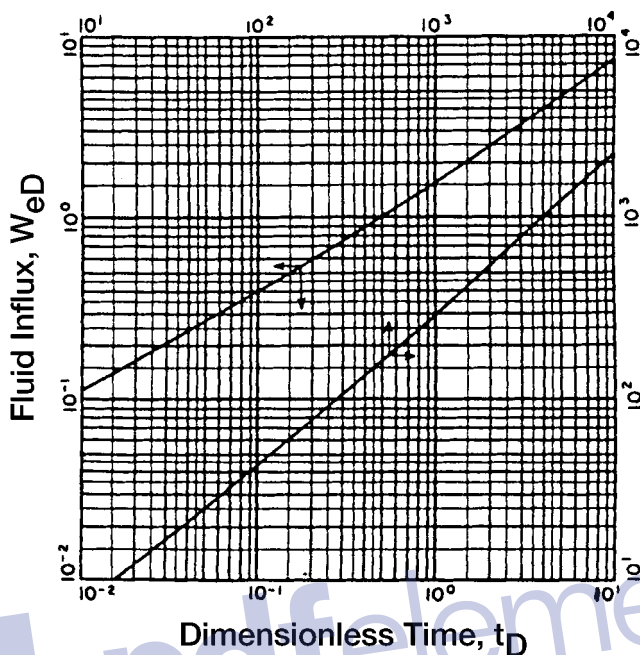


Figure 10-10. Dimensionless water influx W_{eD} for infinite aquifer. (Van Everdingen and Hurst. Permission to publish by the SPE.)

The two dimensionless parameters t_D and r_D are given by:

$$t_D = 6.328 \times 10^{-3} \frac{kt}{\phi \mu_w c_t r_c^2} \quad (10-18)$$

$$r_D = \frac{r_a}{r_c} \quad (10-19)$$

$$c_t = c_w + c_f \quad (10-20)$$

where t = time, days

k = permeability of the aquifer, md

ϕ = porosity of the aquifer

μ_w = viscosity of water in the aquifer, cp

r_a = radius of the aquifer, ft

r_c = radius of the reservoir, ft

c_w = compressibility of the water, psi^{-1}

c_f = compressibility of the aquifer formation, psi^{-1}

c_t = total compressibility coefficient, psi^{-1}

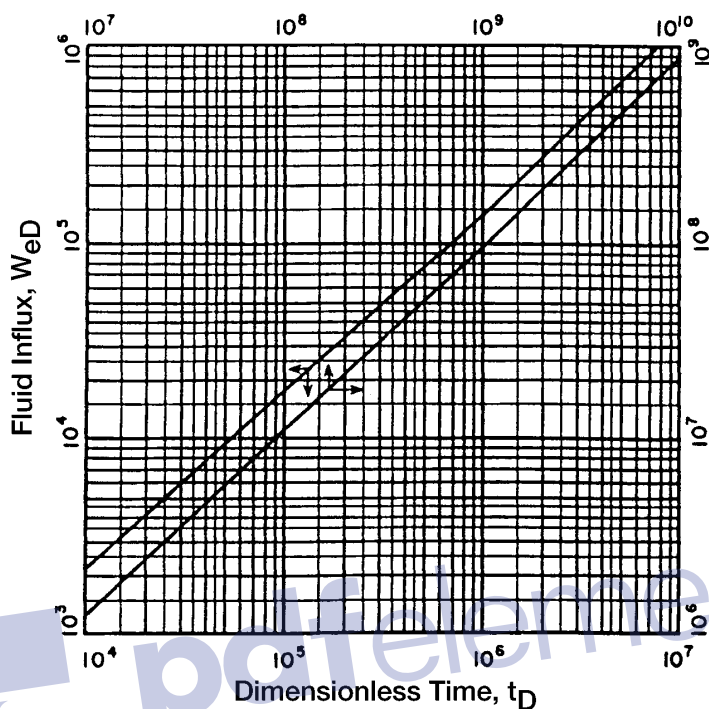


Figure 10-11. Dimensionless water influx W_{eD} for infinite aquifer. (Van Everdingen and Hurst. Permission to publish by the SPE.)

The water influx is then given by:

$$W_e = B \Delta p W_{eD} \quad (10-21)$$

with

$$B = 1.119 \phi c_t r_e^2 h \quad (10-22)$$

where W_e = cumulative water influx, bbl

B = water influx constant, bbl/psi

Δp = pressure drop at the boundary, psi

W_{eD} = dimensionless water influx

(text continued on page 682)

Water Influx

675

| | | | | | | | | | | | |
|----|--------|-----|--------|-----|---------|------|---------|------|----------|----------------------|------------------------|
| 10 | 7.411 | 110 | 46.574 | 620 | 195.208 | 1380 | 387.283 | 4400 | 1065.082 | 2.5" | 3.427" |
| 11 | 7.940 | 115 | 48.277 | 625 | 196.544 | 1390 | 389.705 | 4450 | 1075.743 | 3.0" | 4.064" |
| 12 | 8.457 | 120 | 49.968 | 630 | 197.878 | 1400 | 392.125 | 4500 | 1086.390 | 4.0" | 5.313" |
| 13 | 8.964 | 125 | 51.648 | 640 | 200.542 | 1410 | 394.543 | 4550 | 1097.024 | 5.0" | 6.544" |
| 14 | 9.461 | 130 | 53.317 | 650 | 203.201 | 1420 | 396.959 | 4600 | 1107.646 | 6.0" | 7.761" |
| 15 | 9.949 | 135 | 54.976 | 660 | 205.854 | 1425 | 398.167 | 4650 | 1118.257 | 7.0" | 8.965" |
| 16 | 10.434 | 140 | 56.625 | 670 | 208.502 | 1430 | 399.373 | 4700 | 1128.854 | 8.0" | 1.016(10) ⁶ |
| 17 | 10.913 | 145 | 58.265 | 675 | 209.825 | 1440 | 401.786 | 4750 | 1139.439 | 9.0" | 1.134" |
| 18 | 11.386 | 150 | 59.895 | 680 | 211.145 | 1450 | 404.197 | 4800 | 1150.012 | 1.0(10) ⁷ | 1.252" |
| 19 | 11.855 | 155 | 61.517 | 690 | 213.784 | 1460 | 406.606 | 4850 | 1160.574 | 1.5" | 1.828" |
| 20 | 12.319 | 160 | 63.131 | 700 | 216.417 | 1470 | 409.013 | 4900 | 1171.125 | 2.0" | 2.398" |
| 21 | 12.778 | 165 | 64.737 | 710 | 219.046 | 1475 | 410.214 | 4950 | 1181.666 | 2.5" | 2.961" |
| 22 | 13.233 | 170 | 66.336 | 720 | 221.670 | 1480 | 411.418 | 5000 | 1192.198 | 3.0" | 3.517" |
| 23 | 13.684 | 175 | 67.928 | 725 | 222.980 | 1490 | 413.820 | 5100 | 1213.222 | 4.0" | 4.610" |
| 24 | 14.131 | 180 | 69.512 | 730 | 224.289 | 1500 | 416.220 | 5200 | 1234.203 | 5.0" | 5.689" |
| 25 | 14.573 | 185 | 71.090 | 740 | 226.904 | 1525 | 422.214 | 5300 | 1255.141 | 6.0" | 6.758" |
| 26 | 15.013 | 190 | 72.661 | 750 | 229.514 | 1550 | 428.196 | 5400 | 1276.037 | 7.0" | 7.816" |
| 27 | 15.450 | 195 | 74.226 | 760 | 232.120 | 1575 | 434.168 | 5500 | 1296.893 | 8.0" | 8.866" |
| 28 | 15.883 | 200 | 75.785 | 770 | 234.721 | 1600 | 440.128 | 5600 | 1317.709 | 9.0" | 9.911" |
| 29 | 16.313 | 205 | 77.338 | 775 | 236.020 | 1625 | 446.077 | 5700 | 1338.486 | 1.0(10) ⁷ | 1.095(10) ⁷ |
| 30 | 16.742 | 210 | 78.886 | 780 | 237.318 | 1650 | 452.016 | 5800 | 1359.225 | 1.5" | 1.604" |
| 31 | 17.167 | 215 | 80.428 | 790 | 239.912 | 1675 | 457.945 | 5900 | 1379.927 | 2.0" | 2.108" |
| 32 | 17.590 | 220 | 81.965 | 800 | 242.501 | 1700 | 463.863 | 6000 | 1400.593 | 2.5" | 2.607" |
| 33 | 18.011 | 225 | 83.497 | 810 | 245.086 | 1725 | 469.771 | 6100 | 1421.224 | 3.0" | 3.100" |
| 34 | 18.429 | 230 | 85.023 | 820 | 247.668 | 1750 | 475.669 | 6200 | 1441.820 | 4.0" | 4.071" |
| 35 | 18.845 | 235 | 86.545 | 825 | 248.957 | 1775 | 481.558 | 6300 | 1462.383 | 5.0" | 5.032" |
| 36 | 19.259 | 240 | 88.062 | 830 | 250.245 | 1800 | 487.437 | 6400 | 1482.912 | 6.0" | 5.984" |
| 37 | 19.671 | 245 | 89.575 | 840 | 252.819 | 1825 | 493.307 | 6500 | 1503.408 | 7.0" | 6.928" |
| 38 | 20.080 | 250 | 91.084 | 850 | 255.388 | 1850 | 499.167 | 6600 | 1523.872 | 8.0" | 7.865" |
| 39 | 20.488 | 255 | 92.589 | 860 | 257.953 | 1875 | 505.019 | 6700 | 1544.305 | 9.0" | 8.797" |
| 40 | 20.894 | 260 | 94.090 | 870 | 260.515 | 1900 | 510.861 | 6800 | 1564.706 | 1.0(10) ⁹ | 9.725" |
| 41 | 21.298 | 265 | 95.588 | 875 | 261.795 | 1925 | 516.695 | 6900 | 1585.077 | 1.5" | 1.429(10) ⁸ |

(table continued on next page)

Table 10-1 (continued)

| Dimen- sionless Time t_b | Fluid Influx W_{eD} | Dimen- sionless Time t_b | Fluid Influx W_{eD} | Dimen- sionless Time t_b | Fluid Influx W_{eD} | Dimen- sionless Time t_b | Fluid Influx W_{eD} | Dimen- sionless Time t_b | Fluid Influx W_{eD} | Dimen- sionless Time t_b | Fluid Influx W_{eD} |
|-------------------------------------|-----------------------------|-------------------------------------|-----------------------------|-------------------------------------|-----------------------------|-------------------------------------|-----------------------------|-------------------------------------|-----------------------------|-------------------------------------|-----------------------------|
| 42 | 21.701 | 270 | 97.081 | 880 | 263.073 | 1950 | 522.520 | 7000 | 1605.418 | 2.0" | 1.880" |
| 43 | 22.101 | 275 | 98.571 | 890 | 265.629 | 1975 | 528.337 | 7100 | 1625.729 | 2.5" | 2.328" |
| 44 | 22.500 | 280 | 100.057 | 900 | 268.181 | 2000 | 534.145 | 7200 | 1646.011 | 3.0" | 2.771" |
| 45 | 22.897 | 285 | 101.540 | 910 | 270.729 | 2025 | 539.945 | 7300 | 1666.265 | 4.0" | 3.645" |
| 46 | 23.291 | 290 | 103.019 | 920 | 273.274 | 2050 | 545.737 | 7400 | 1686.490 | 5.0" | 4.510" |
| 47 | 23.684 | 295 | 104.495 | 925 | 274.545 | 2075 | 551.522 | 7500 | 1706.688 | 6.0" | 5.368" |
| 48 | 24.076 | 300 | 105.968 | 930 | 275.815 | 2100 | 557.299 | 7600 | 1726.859 | 7.0" | 6.220" |
| 49 | 24.466 | 305 | 107.437 | 940 | 278.353 | 2125 | 563.068 | 7700 | 1747.002 | 8.0" | 7.066" |
| 50 | 24.855 | 310 | 108.904 | 950 | 280.888 | 2150 | 568.830 | 7800 | 1767.120 | 9.0" | 7.909" |
| 51 | 25.244 | 315 | 110.367 | 960 | 283.420 | 2175 | 574.585 | 7900 | 1787.212 | 1.0(10) ¹⁰ | 8.747" |
| 52 | 25.633 | 320 | 111.827 | 970 | 285.948 | 2200 | 580.332 | 8000 | 1807.278 | 1.5" | 1.288"(10) ⁹ |
| 53 | 26.020 | 325 | 113.284 | 975 | 287.211 | 2225 | 586.072 | 8100 | 1827.319 | 2.0" | 1.697" |
| 54 | 26.406 | 330 | 114.738 | 980 | 288.473 | 2250 | 591.806 | 8200 | 1847.336 | 2.5" | 2.103" |
| 55 | 26.791 | 335 | 116.189 | 990 | 290.995 | 2275 | 597.532 | 8300 | 1867.329 | 3.0" | 2.505" |
| 56 | 27.174 | 340 | 117.638 | 1000 | 293.514 | 2300 | 603.252 | 8400 | 1887.298 | 4.0" | 3.299" |
| 57 | 27.555 | 345 | 119.083 | 1010 | 296.030 | 2325 | 608.965 | 8500 | 1907.243 | 5.0" | 4.087" |
| 58 | 27.935 | 350 | 120.526 | 1020 | 298.543 | 2350 | 614.672 | 8600 | 1927.166 | 6.0" | 4.868" |

Water Influx

677

| | | | | | | | | | | | |
|----|--------|-----|---------|------|---------|------|---------|--------|----------|-----------------------|------------------------|
| 59 | 28.314 | 355 | 121.966 | 1025 | 299.799 | 2375 | 620.372 | 8700 | 1947.065 | 7.0" | 5.643" |
| 60 | 28.691 | 360 | 123.403 | 1030 | 301.053 | 2400 | 626.066 | 8800 | 1966.942 | 8.0" | 6.414" |
| 61 | 29.068 | 365 | 124.838 | 1040 | 303.560 | 2425 | 631.755 | 8900 | 1986.796 | 9.0" | 7.183" |
| 62 | 29.443 | 370 | 126.720 | 1050 | 306.065 | 2450 | 637.437 | 9000 | 2006.628 | 1.0(10) ¹¹ | 7.948" |
| 63 | 29.818 | 375 | 127.699 | 1060 | 308.567 | 2475 | 643.113 | 9100 | 2026.438 | 1.5" | 1.17(10) ¹⁰ |
| 64 | 30.192 | 380 | 129.126 | 1070 | 311.066 | 2500 | 648.781 | 9200 | 2046.227 | 2.0" | 1.55" |
| 65 | 30.565 | 385 | 130.550 | 1075 | 312.314 | 2550 | 660.093 | 9300 | 2065.996 | 2.5" | 1.92" |
| 66 | 30.937 | 390 | 131.972 | 1080 | 313.562 | 2600 | 671.379 | 9400 | 2085.744 | 3.0" | 2.29" |
| 67 | 31.308 | 395 | 133.391 | 1090 | 316.055 | 2650 | 682.640 | 9500 | 2105.473 | 4.0" | 3.02" |
| 68 | 31.679 | 400 | 134.808 | 1100 | 318.545 | 2700 | 693.877 | 9600 | 2125.184 | 5.0" | 3.75" |
| 69 | 32.048 | 405 | 136.223 | 1110 | 321.032 | 2750 | 705.090 | 9700 | 2144.878 | 6.0" | 4.47" |
| 70 | 32.417 | 410 | 137.635 | 1120 | 323.517 | 2800 | 716.280 | 9800 | 2164.555 | 7.0" | 5.19" |
| 71 | 32.785 | 415 | 139.045 | 1125 | 324.760 | 2850 | 727.449 | 9900 | 2184.216 | 8.0" | 5.89" |
| 72 | 33.151 | 420 | 140.453 | 1130 | 326.000 | 2900 | 738.598 | 10,000 | 2203.861 | 9.0" | 6.58" |
| 73 | 33.517 | 425 | 141.859 | 1140 | 328.480 | 2950 | 749.725 | 12,500 | 2688.967 | 1.0(10) ¹² | 7.28" |
| 74 | 33.883 | 430 | 143.262 | 1150 | 330.958 | 3000 | 760.833 | 15,000 | 3164.780 | 1.5" | 1.08(10) ¹¹ |
| 75 | 34.247 | 435 | 144.664 | 1160 | 333.433 | 3050 | 771.922 | 17,500 | 3633.368 | 2.0" | 1.42" |
| 76 | 34.611 | 440 | 146.064 | 1170 | 335.906 | 3100 | 782.992 | 20,000 | 4095.800 | | |
| 77 | 34.974 | 445 | 147.461 | 1175 | 337.142 | 3150 | 794.042 | 25,000 | 5005.726 | | |
| 78 | 35.336 | 450 | 148.856 | 1180 | 338.376 | 3200 | 805.075 | 30,000 | 5899.508 | | |

Table 10-2
Dimensionless Water Influx W_{eD} for Several Values of r_e/r_R , i.e., r_d/r_e
(Van Everdingen and Hurst. Permission to publish by the SPE.)

| Dimensionless Time t_D | $r_e/r_R = 1.5$ | | $r_e/r_R = 2.0$ | | $r_e/r_R = 2.5$ | | $r_e/r_R = 3.0$ | | $r_e/r_R = 3.5$ | | $r_e/r_R = 4.0$ | | $r_e/r_R = 4.5$ | |
|--------------------------|-----------------------|--------------------------|-----------------------|--------------------------|-----------------------|--------------------------|-----------------------|--------------------------|-----------------------|--------------------------|-----------------------|--------------------------|-----------------------|--------------------------|
| | Fluid Influx W_{eD} | Dimensionless Time t_D | Fluid Influx W_{eD} | Dimensionless Time t_D | Fluid Influx W_{eD} | Dimensionless Time t_D | Fluid Influx W_{eD} | Dimensionless Time t_D | Fluid Influx W_{eD} | Dimensionless Time t_D | Fluid Influx W_{eD} | Dimensionless Time t_D | Fluid Influx W_{eD} | Dimensionless Time t_D |
| 5.0(10) ⁻² | 0.276 | 5.0(10) ⁻² | 0.278 | 1.0(10) ⁻¹ | 0.408 | 3.0(10) ⁻¹ | 0.755 | 1.00 | 1.571 | 2.00 | 2.442 | 2.5 | 2.835 | 2.5 |
| 6.0" | 0.304 | 7.5" | 0.345 | 1.5" | 0.509 | 4.0" | 0.895 | 1.20 | 1.761 | 2.20 | 2.598 | 3.0 | 3.196 | 3.0 |
| 7.0" | 0.330 | 1.0(10) ⁻¹ | 0.404 | 2.0" | 0.599 | 5.0" | 1.023 | 1.40 | 1.940 | 2.40 | 2.748 | 3.5 | 3.537 | 3.5 |
| 8.0" | 0.354 | 1.25" | 0.458 | 2.5" | 0.681 | 6.0" | 1.143 | 1.60 | 2.111 | 2.60 | 2.893 | 4.0 | 3.859 | 4.0 |
| 9.0" | 0.375 | 1.50" | 0.507 | 3.0" | 0.758 | 7.0" | 1.256 | 1.80 | 2.273 | 2.80 | 3.034 | 4.5 | 4.165 | 4.5 |
| 1.0(10) ⁻¹ | 0.395 | 1.75" | 0.553 | 3.5" | 0.829 | 8.0" | 1.363 | 2.00 | 2.427 | 3.00 | 3.170 | 5.0 | 4.454 | 5.0 |
| 1.1" | 0.414 | 2.00" | 0.597 | 4.0" | 0.897 | 9.0" | 1.465 | 2.20 | 2.574 | 3.25 | 3.334 | 5.5 | 4.727 | 5.5 |
| 1.2" | 0.431 | 2.25" | 0.638 | 4.5" | 0.962 | 1.00 | 1.563 | 2.40 | 2.715 | 3.50 | 3.493 | 6.0 | 4.986 | 6.0 |
| 1.3" | 0.446 | 2.50" | 0.678 | 5.0" | 1.024 | 1.25 | 1.791 | 2.60 | 2.849 | 3.75 | 3.645 | 6.5 | 5.231 | 6.5 |
| 1.4" | 0.461 | 2.75" | 0.715 | 5.5" | 1.083 | 1.50 | 1.997 | 2.80 | 2.976 | 4.00 | 3.792 | 7.0 | 5.464 | 7.0 |
| 1.5" | 0.474 | 3.00" | 0.751 | 6.0" | 1.140 | 1.75 | 2.184 | 3.00 | 3.098 | 4.25 | 3.932 | 7.5 | 5.684 | 7.5 |
| 1.6" | 0.486 | 3.25" | 0.785 | 6.5" | 1.195 | 2.00 | 2.353 | 3.25 | 3.242 | 4.50 | 4.068 | 8.0 | 5.892 | 8.0 |
| 1.7" | 0.497 | 3.50" | 0.817 | 7.0" | 1.248 | 2.25 | 2.507 | 3.50 | 3.379 | 4.75 | 4.198 | 8.5 | 6.089 | 8.5 |
| 1.8" | 0.507 | 3.75" | 0.848 | 7.5" | 1.299 | 2.50 | 2.646 | 3.75 | 3.507 | 5.00 | 4.323 | 9.0 | 6.276 | 9.0 |
| 1.9" | 0.517 | 4.00" | 0.877 | 8.0" | 1.348 | 2.75 | 2.772 | 4.00 | 3.628 | 5.50 | 4.560 | 9.5 | 6.453 | 9.5 |
| 2.0" | 0.525 | 4.25" | 0.905 | 8.5" | 1.395 | 3.00 | 2.886 | 4.25 | 3.742 | 6.00 | 4.779 | 10 | 6.621 | 10 |
| 2.1" | 0.533 | 4.50" | 0.932 | 9.0" | 1.440 | 3.25 | 2.990 | 4.50 | 3.850 | 6.50 | 4.982 | 11 | 6.930 | 11 |
| 2.2" | 0.541 | 4.75" | 0.958 | 9.5" | 1.484 | 3.50 | 3.084 | 4.75 | 3.951 | 7.00 | 5.169 | 12 | 7.208 | 12 |

Water Influx

679

| | | | | | | | | | | | | | |
|------|-------|-------|-------|------|-------|-------|-------|-------|-------|------|-------|-----|-------|
| 2.3" | 0.548 | 5.00" | 0.993 | 1.0 | 1.526 | 3.75 | 3.170 | 5.00 | 4.047 | 7.50 | 5.343 | 13 | 7.457 |
| 2.4" | 0.554 | 5.50" | 1.028 | 1.1 | 1.605 | 4.00 | 3.247 | 5.50 | 4.222 | 8.00 | 5.504 | 14 | 7.680 |
| 2.5" | 0.559 | 6.00" | 1.070 | 1.2 | 1.679 | 4.25 | 3.317 | 6.00 | 4.378 | 8.50 | 5.653 | 15 | 7.880 |
| 2.6" | 0.565 | 6.50" | 1.108 | 1.3 | 1.747 | 4.50 | 3.381 | 6.50 | 4.516 | 9.00 | 5.790 | 16 | 8.060 |
| 2.8" | 0.574 | 7.00" | 1.143 | 1.4 | 1.811 | 4.75 | 3.439 | 7.00 | 4.639 | 9.50 | 5.917 | 18 | 8.365 |
| 3.0" | 0.582 | 7.50" | 1.174 | 1.5 | 1.870 | 5.00 | 3.491 | 7.50 | 4.749 | 10 | 6.035 | 20 | 8.611 |
| 3.2" | 0.588 | 8.00" | 1.203 | 1.6 | 1.924 | 5.50 | 3.581 | 8.00 | 4.846 | 11 | 6.246 | 22 | 8.809 |
| 3.4" | 0.594 | 9.00" | 1.253 | 1.7 | 1.975 | 6.00 | 3.656 | 8.50 | 4.932 | 12 | 6.425 | 24 | 8.968 |
| 3.6" | 0.599 | 1.00" | 1.295 | 1.8 | 2.022 | 6.50 | 3.717 | 9.00 | 5.009 | 13 | 6.580 | 26 | 9.097 |
| 3.8" | 0.603 | 1.1 | 1.330 | 2.0 | 2.106 | 7.00 | 3.767 | 9.50 | 5.078 | 14 | 6.712 | 28 | 9.200 |
| 4.0" | 0.606 | 1.2 | 1.358 | 2.2 | 2.178 | 7.50 | 3.809 | 10.00 | 5.138 | 15 | 6.825 | 30 | 9.283 |
| 4.5" | 0.613 | 1.3 | 1.382 | 2.4 | 2.241 | 8.00 | 3.843 | 11 | 5.241 | 16 | 6.922 | 34 | 9.404 |
| 5.0" | 0.617 | 1.4 | 1.402 | 2.6 | 2.294 | 9.00 | 3.894 | 12 | 5.321 | 17 | 7.004 | 38 | 9.481 |
| 6.0" | 0.621 | 1.6 | 1.432 | 2.8 | 2.340 | 10.00 | 3.928 | 13 | 5.385 | 18 | 7.076 | 42 | 9.532 |
| 7.0" | 0.623 | 1.7 | 1.444 | 3.0 | 2.380 | 11.00 | 3.951 | 14 | 5.435 | 20 | 7.189 | 46 | 9.565 |
| 8.0" | 0.624 | 1.8 | 1.453 | 3.4 | 2.444 | 12.00 | 3.967 | 15 | 5.476 | 22 | 7.272 | 50 | 9.586 |
| | | 2.0 | 1.468 | 3.8 | 2.491 | 14.00 | 3.985 | 16 | 5.506 | 24 | 7.332 | 60 | 9.612 |
| | | 2.5 | 1.487 | 4.2 | 2.525 | 16.00 | 3.993 | 17 | 5.531 | 26 | 7.377 | 70 | 9.621 |
| | | 3.0 | 1.495 | 4.6 | 2.551 | 18.00 | 3.997 | 18 | 5.551 | 30 | 7.434 | 80 | 9.623 |
| | | 4.0 | 1.499 | 5.0 | 2.570 | 20.00 | 3.999 | 20 | 5.579 | 34 | 7.464 | 90 | 9.624 |
| | | 5.0 | 1.500 | 6.0 | 2.599 | 22.00 | 3.999 | 25 | 5.611 | 38 | 7.481 | 100 | 9.625 |
| | | | | 7.0 | 2.613 | 24.00 | 4.000 | 30 | 5.621 | 42 | 7.490 | | |
| | | | | 8.0 | 2.619 | | | 35 | 5.624 | 46 | 7.494 | | |
| | | | | 9.0 | 2.622 | | | 40 | 5.625 | 50 | 7.499 | | |
| | | | | 10.0 | 2.624 | | | | | | | | |

(table continued on next page)

Table 10-2 (continued)

| $r_e/r_R = 5.0$ | | $r_e/r_R = 6.0$ | | $r_e/r_R = 7.0$ | | $r_e/r_R = 8.0$ | | $r_e/r_R = 9.0$ | | $r_e/r_R = 10.0$ | |
|--------------------------|-----------------------|--------------------------|-----------------------|--------------------------|-----------------------|--------------------------|-----------------------|--------------------------|-----------------------|--------------------------|-----------------------|
| Dimensionless Time t_b | Fluid Influx W_{ed} | Dimensionless Time t_b | Fluid Influx W_{ed} | Dimensionless Time t_b | Fluid Influx W_{ed} | Dimensionless Time t_b | Fluid Influx W_{ed} | Dimensionless Time t_b | Fluid Influx W_{ed} | Dimensionless Time t_b | Fluid Influx W_{ed} |
| 3.0 | 3.195 | 6.0 | 5.148 | 9.00 | 6.861 | 9 | 6.861 | 10 | 7.417 | 15 | 9.965 |
| 3.5 | 3.542 | 6.5 | 5.440 | 9.50 | 7.127 | 10 | 7.398 | 15 | 9.945 | 20 | 12.32 |
| 4.0 | 3.875 | 7.0 | 5.724 | 10 | 7.389 | 11 | 7.920 | 20 | 12.26 | 22 | 13.22 |
| 4.5 | 4.193 | 7.5 | 6.002 | 11 | 7.902 | 12 | 8.431 | 22 | 13.13 | 24 | 14.95 |
| 5.0 | 4.499 | 8.0 | 6.273 | 12 | 8.397 | 13 | 8.930 | 24 | 13.98 | 26 | 14.95 |
| 5.5 | 4.792 | 8.5 | 6.537 | 13 | 8.876 | 14 | 9.418 | 26 | 14.79 | 28 | 15.78 |
| 6.0 | 5.074 | 9.0 | 6.795 | 14 | 9.341 | 15 | 9.895 | 26 | 15.59 | 30 | 16.59 |
| 6.5 | 5.345 | 9.5 | 7.047 | 15 | 9.791 | 16 | 10.361 | 30 | 16.35 | 32 | 17.38 |
| 7.0 | 5.605 | 10.0 | 7.293 | 16 | 10.23 | 17 | 10.82 | 32 | 17.10 | 34 | 18.16 |
| 7.5 | 5.854 | 10.5 | 7.533 | 17 | 10.65 | 18 | 11.26 | 34 | 17.82 | 36 | 18.91 |
| 8.0 | 6.094 | 11 | 7.767 | 18 | 11.06 | 19 | 11.70 | 36 | 18.52 | 38 | 19.65 |
| 8.5 | 6.325 | 12 | 8.220 | 19 | 11.46 | 20 | 12.13 | 38 | 19.19 | 40 | 20.37 |
| 9.0 | 6.547 | 13 | 8.651 | 20 | 11.85 | 22 | 12.95 | 40 | 19.85 | 42 | 21.07 |
| 9.5 | 6.760 | 14 | 9.063 | 22 | 12.58 | 24 | 13.74 | 42 | 20.48 | 44 | 21.76 |
| 10 | 6.965 | 15 | 9.456 | 24 | 13.27 | 26 | 14.50 | 44 | 21.09 | 46 | 22.42 |
| 11 | 7.350 | 16 | 9.829 | 26 | 13.92 | 28 | 15.23 | 46 | 21.69 | 48 | 23.07 |
| 12 | 7.706 | 17 | 10.19 | 28 | 14.53 | 30 | 15.92 | 48 | 22.26 | 50 | 23.71 |

Water Influx

681

| | | | | | | | | | | | |
|-----|-------|-----|-------|-----|-------|-----|-------|-----|-------|-----|-------|
| 13 | 8.035 | 18 | 10.53 | 30 | 15.11 | 34 | 17.22 | 50 | 22.82 | 52 | 24.33 |
| 14 | 8.339 | 19 | 10.85 | 35 | 16.39 | 38 | 18.41 | 52 | 23.36 | 54 | 24.94 |
| 15 | 8.620 | 20 | 11.16 | 40 | 17.49 | 40 | 18.97 | 54 | 23.89 | 56 | 25.53 |
| 16 | 8.879 | 22 | 11.74 | 45 | 18.43 | 45 | 20.26 | 56 | 24.39 | 58 | 26.11 |
| 18 | 9.338 | 24 | 12.26 | 50 | 19.24 | 50 | 21.42 | 58 | 24.88 | 60 | 26.67 |
| 20 | 9.731 | 25 | 12.50 | 60 | 20.51 | 55 | 22.46 | 60 | 25.36 | 65 | 28.02 |
| 22 | 10.07 | 31 | 13.74 | 70 | 21.45 | 60 | 23.40 | 65 | 26.48 | 70 | 29.29 |
| 24 | 10.35 | 35 | 14.40 | 80 | 22.13 | 70 | 24.98 | 70 | 27.52 | 75 | 30.49 |
| 26 | 10.59 | 39 | 14.93 | 90 | 22.63 | 80 | 26.26 | 75 | 28.48 | 80 | 31.61 |
| 28 | 10.80 | 51 | 16.05 | 100 | 23.00 | 90 | 27.28 | 80 | 29.36 | 85 | 32.67 |
| 30 | 10.98 | 60 | 16.56 | 120 | 23.47 | 100 | 28.11 | 85 | 30.18 | 90 | 33.66 |
| 34 | 11.26 | 70 | 16.91 | 140 | 23.71 | 120 | 29.31 | 90 | 30.93 | 95 | 34.60 |
| 38 | 11.46 | 80 | 17.14 | 160 | 23.85 | 140 | 30.08 | 95 | 31.63 | 100 | 35.48 |
| 42 | 11.61 | 90 | 17.27 | 180 | 23.92 | 160 | 30.58 | 100 | 32.27 | 120 | 38.51 |
| 46 | 11.71 | 100 | 17.36 | 200 | 23.96 | 180 | 30.91 | 120 | 34.39 | 140 | 40.89 |
| 50 | 11.79 | 110 | 17.41 | 500 | 24.00 | 200 | 31.12 | 140 | 35.92 | 160 | 42.75 |
| 60 | 11.91 | 120 | 17.45 | | | 240 | 31.34 | 160 | 37.04 | 180 | 44.21 |
| 70 | 11.96 | 130 | 17.46 | | | 280 | 31.43 | 180 | 37.85 | 200 | 45.36 |
| 80 | 11.98 | 140 | 17.48 | | | 320 | 31.47 | 200 | 38.44 | 240 | 46.95 |
| 90 | 11.99 | 150 | 17.49 | | | 360 | 31.49 | 240 | 39.17 | 280 | 47.94 |
| 100 | 12.00 | 160 | 17.49 | | | 400 | 31.50 | 280 | 39.56 | 320 | 48.54 |
| 120 | 12.00 | 180 | 17.50 | | | 500 | 31.50 | 320 | 39.77 | 360 | 48.91 |
| | | 200 | 17.50 | | | | | 360 | 39.88 | 400 | 49.14 |
| | | 220 | 17.50 | | | | | 400 | 39.94 | 440 | 49.28 |
| | | | | | | | | 440 | 39.97 | 480 | 49.36 |
| | | | | | | | | 480 | 39.98 | | |

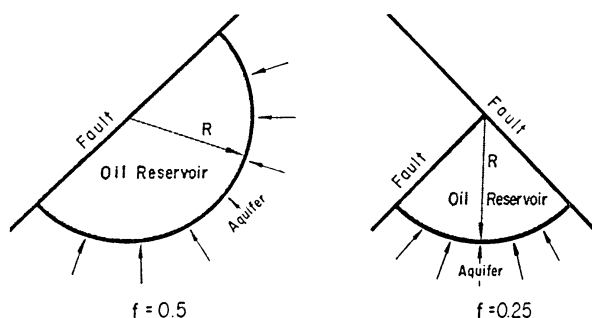


Figure 10-12. Gas cap drive reservoir. (After Cole, F., *Reservoir Engineering Manual*, Gulf Publishing Company, 1969.)

(text continued from page 673)

Equation 10-21 assumes that the water is encroaching in a radial form. Quite often, water does not encroach on all sides of the reservoir, or the reservoir is not circular in nature. In these cases, some modifications must be made in Equation 10-21 to properly describe the flow mechanism. One of the simplest modifications is to introduce the encroachment angle to the water influx constant B as:

$$f = \frac{\theta}{360} \quad (10-23)$$

$$B = 1.119\phi c_i r_e^2 hf \quad (10-24)$$

θ is the angle subtended by the reservoir circumference, i.e., for a full circle $\theta = 360^\circ$ and for semicircle reservoir against a fault $\theta = 180^\circ$, as shown in Figure 10-12.

Example 10-6¹

Calculate water influx at the end of 1, 2, and 5 years into a circular reservoir with an aquifer of infinite extent. The initial and current reservoir pressures are 2,500 and 2,490 psi, respectively. The reservoir-aquifer system has the following properties.

¹Data of this example was reported by Cole, F., *Reservoir Engineering Manual*, Gulf Publishing Company, 1969.

| | Reservoir | Aquifer |
|---------------------------|--------------------|----------------------|
| radius, ft | 2000 | ∞ |
| h, ft | 20 | 25 |
| k, md | 50 | 100 |
| ϕ , % | 15 | 20 |
| μ_w , cp | 0.5 | 0.8 |
| c_w , psi ⁻¹ | 1×10^{-6} | 0.7×10^{-6} |
| c_f , psi ⁻¹ | 2×10^{-6} | 0.3×10^{-6} |

Solution

Step 1. Calculate the total compressibility coefficient c_t .

$$c_t = 0.7 (10^{-6}) + 0.3 (10^{-3}) = 1 \times 10^{-6} \text{ psi}^{-1}$$

Step 2. Determine the water influx constant from Equation 10-23.

$$B = 1.119 (0.2) (1 \times 10^{-6}) (2000)^2 (25) (360/360) = 22.4$$

Step 3. Calculate the corresponding dimensionless time after 1, 2, and 5 years.

$$t_D = 6.328 \times 10^{-3} \frac{100 t}{(0.8)(0.2)(1 \times 10^{-6})(2000)^2}$$

$$t_D = 0.9888t$$

| t, days | $t_D = 0.9888 t$ |
|---------|------------------|
| 365 | 361 |
| 730 | 722 |
| 1825 | 1805 |

Step 4. Using Table 10-1, determine the dimensionless water influx W_{eD} .

| t, days | t_D | W_{eD} |
|---------|-------|----------|
| 365 | 361 | 123.5 |
| 730 | 722 | 221.8 |
| 1825 | 1805 | 484.6 |

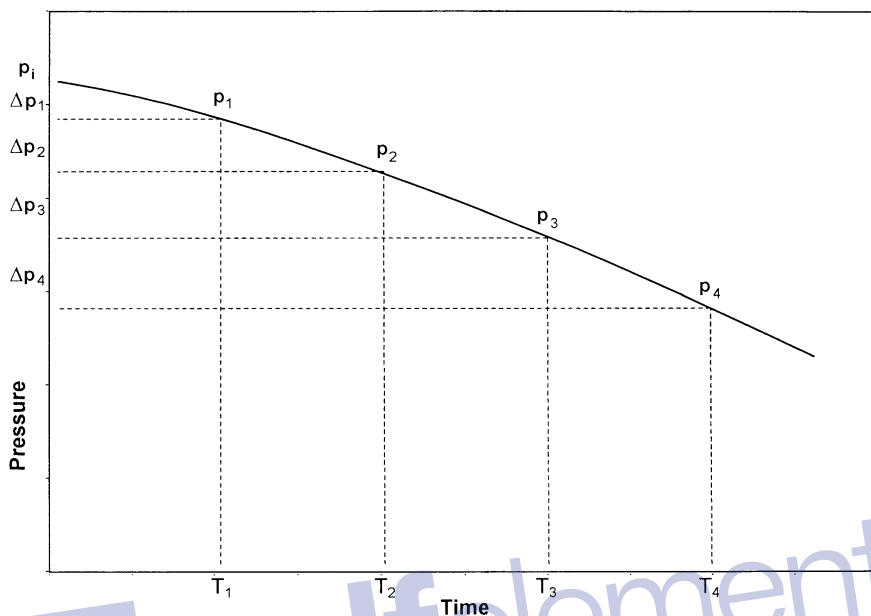


Figure 10-13. Boundary pressure versus time.

Step 5. Calculate the cumulative water influx by applying Equation 10-20.

| t , days | W_{eD} | $W_e = (20.4) (2500 - 2490) W_{eD}$ |
|------------|----------|-------------------------------------|
| 365 | 123.5 | 25,200 bbl |
| 730 | 221.8 | 45,200 bbl |
| 1825 | 484.6 | 98,800 bbl |

Example 10-6 shows that, for a given pressure drop, doubling the time interval will not double the water influx. This example also illustrates how to calculate water influx as a result of a single pressure drop. As there will usually be many of these pressure drops occurring throughout the prediction period, it is necessary to analyze the procedure to be used where these multiple pressure drops are present.

Consider Figure 10-13, which illustrates the decline in the boundary pressure as a function of time for a radial reservoir-aquifer system. If the boundary pressure in the reservoir shown in Figure 10-13 is suddenly reduced at time t , from p_i to p_1 , a pressure drop of $(p_i - p_1)$ will be imposed across the aquifer. Water will continue to expand and the new

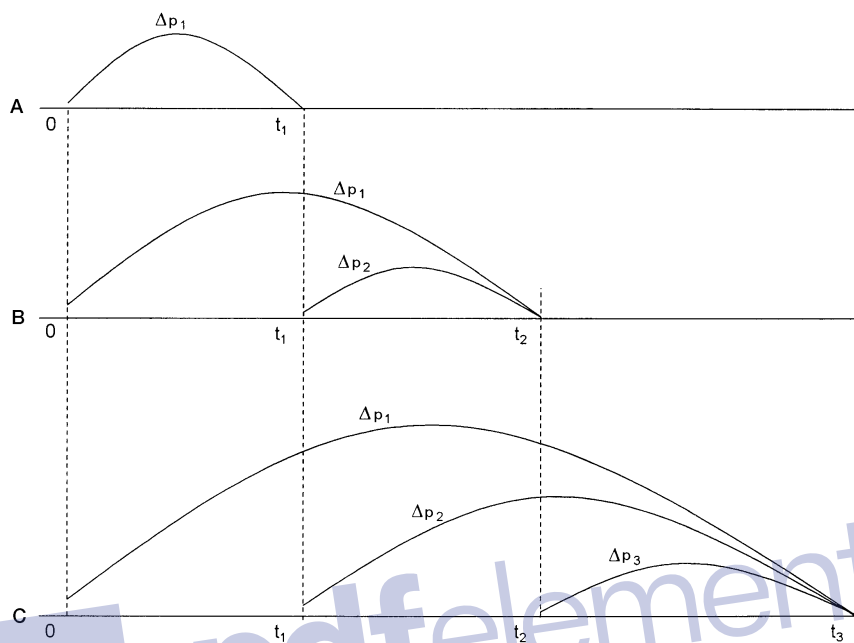


Figure 10-14. Illustration of the superposition concept.

reduced pressure will continue to move outward into the aquifer. Given a sufficient length of time the pressure at the outer edge of the aquifer will finally be reduced to p_1 .

If some time after the boundary pressure has been reduced to p_1 , a second pressure p_2 is suddenly imposed at the boundary, and a new pressure wave will begin moving outward into the aquifer. This new pressure wave will also cause water expansion and therefore encroachment into the reservoir. This new pressure drop, however, will not be $p_1 - p_2$, but will be $p_1 - p_2$. This second pressure wave will be moving behind the first pressure wave. Just ahead of the second pressure wave will be the pressure at the end of the first pressure drop, p_1 .

Since these pressure waves are assumed to occur at different times, they are entirely independent of each other. Thus, water expansion will continue to take place as a result of the first pressure drop, even though additional water influx is also taking place as a result of one or more later pressure drops. This is essentially an application of the **principle of superposition**.

In order to determine the total water influx into a reservoir at any given time, it is necessary to determine the water influx as a result of each successive pressure drop that has been imposed on the reservoir and aquifer.

In calculating cumulative water influx into a reservoir at successive intervals, it is necessary to calculate the total water influx from the beginning. This is required because of the different times during which the various pressure drops have been effective.

The van Everdingen-Hurst computational steps for determining the water influx are summarized below in conjunction with Figure 10-14:

Step 1. Assume that the boundary pressure has declined from its initial value of p_i to p_1 after t_1 days. To determine the cumulative water influx in response to this first pressure drop, $\Delta p_1 = p_i - p_1$ can be simply calculated from Equation 10-20, or:

$$W_e = B \Delta p_1 (W_{eD})_{t_1}$$

where W_e is the cumulative water influx due to the first pressure drop Δp_1 . The dimensionless influx $(W_{eD})_{t_1}$ is evaluated by calculating the dimensionless time at t_1 days. This simple calculation step is shown in section A of Figure 10-14.

Step 2. Let the boundary pressure decline again to p_2 after t_2 days with a pressure drop of $\Delta p_2 = p_1 - p_2$. The cumulative (total) water influx after t_2 days will result from the first pressure drop Δp_1 and the second pressure drop Δp_2 , or:

$$W_e = \text{water influx due to } \Delta p_1 + \text{water influx due to } \Delta p_2$$

$$W_e = (W_e)_{\Delta p_1} + (W_e)_{\Delta p_2}$$

where

$$(W_e)_{\Delta p_1} = B \Delta p_1 (W_{eD})_{t_2}$$

$$(W_e)_{\Delta p_2} = B \Delta p_2 (W_{eD})_{t_2 - t_1}$$

The above relationships indicate that the effect of the first pressure drop Δp_1 will continue for the entire time t_2 , while the effect of the second pressure drop will continue only for $(t_2 - t_1)$ days as shown in section B of Figure 10-14.

Step 3. A third pressure drop of $\Delta p_3 = p_2 - p_3$ would cause an additional water influx as illustrated in section C of Figure 10-14. The cumulative (total) water influx can then be calculated from:

$$W_e = (W_e)_{\Delta p_1} + (W_e)_{\Delta p_2} + (W_e)_{\Delta p_3}$$

where

$$(W_e)_{\Delta p_1} = B \Delta p_1 (W_{eD})_{t_3}$$

$$(W_e)_{\Delta p_2} = B \Delta p_2 (W_{eD})_{t_3 - t_1}$$

$$(W_e)_{\Delta p_3} = B \Delta p_3 (W_{eD})_{t_3 - t_2}$$

The van Everdingen-Hurst water influx relationship can then be expressed in a more generalized form as:

$$W_e = B \Sigma \Delta p W_{eD} \quad (10-24)$$

The authors also suggested that instead of using the entire pressure drop for the first period, a better approximation is to consider that one-half of the pressure drop, $\frac{1}{2}(p_i - p_1)$, is effective during the entire first period. For the second period, the effective pressure drop then is one-half of the pressure drop during the first period, $\frac{1}{2}(p_1 - p_2)$, which simplifies to:

$$\frac{1}{2}(p_i - p_1) + \frac{1}{2}(p_1 - p_2) = \frac{1}{2}(p_i - p_2)$$

Similarly, the effective pressure drop for use in the calculations for the third period would be one-half of the pressure drop during the second period, $\frac{1}{2}(p_1 - p_2)$, plus one-half of the pressure drop during the third period, $\frac{1}{2}(p_2 - p_3)$, which simplifies to $\frac{1}{2}(p_1 - p_3)$. The time intervals must all be equal in order to preserve the accuracy of these modifications.

Example 10-7

Using the data given in Example 10-6, calculate the cumulative water influx at the end of 6, 12, 18, and 24 months. The predicted boundary pressure at the end of each specified time period is given below:

| Time, months | Boundary pressure, psi |
|--------------|------------------------|
| 0 | 2500 |
| 6 | 2490 |
| 12 | 2472 |
| 18 | 2444 |
| 24 | 2408 |

Solution

Water influx at the end of 6 months

Step 1. Determine water influx constant B:

$$B = 22.4 \text{ bbl/psi}$$

Step 2. Calculate the dimensionless time t_D at 182.5 days.

$$\begin{aligned} t_D &= 0.9888t \\ &= 0.9888(182.5) = 180.5 \end{aligned}$$

Step 3. Calculate the first pressure drop Δp_1 . This pressure is taken as $\frac{1}{2}$ of the actual pressure drop, or:

$$\Delta p_1 = \frac{p_i - p_1}{2}$$

$$\Delta p_1 = \frac{2500 - 2490}{2} = 5 \text{ psi}$$

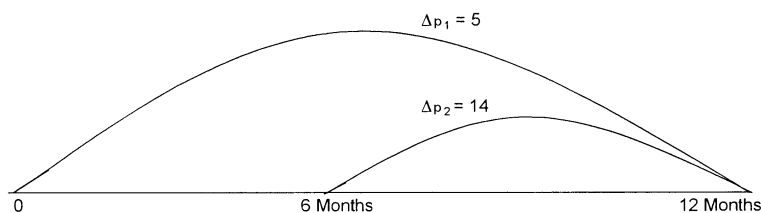


Figure 10-15. Duration of the pressure drop in Example 10-7.

Step 4. Determine the dimensionless water influx W_{eD} from Table 10-1 at $t_D = 180.5$ to give:

$$W_{eD} = 69.46$$

Step 5. Calculate the cumulative water influx at the end of 182.5 days due to the first pressure drop of 5 psi by using the van Everdingen-Hurst equation, or:

$$W_e = (20.4) (5) (69.46) = 7080 \text{ bbl}$$

Cumulative water influx after 12 months

Step 1. After an additional six months, the pressure has declined from 2,490 psi to 2,472 psi. This second pressure Δp_2 is taken as one-half the *actual* pressure drop during the first period, plus one-half the *actual* pressure drop during the second period, or:

$$\begin{aligned} \Delta p_2 &= \frac{P_i - P_2}{2} \\ &= \frac{2500 - 2472}{2} = 14 \text{ psi} \end{aligned}$$

Step 2. The cumulative (total) water influx at the end of 12 months would result from the first pressure drop Δp_1 and the second pressure drop Δp_2 .

The first pressure drop Δp_1 has been effective for one year, but the second pressure drop, Δp_2 , has been effective only 6 months, as shown in Figure 10-15.

Separate calculations must be made for the two pressure drops because of this time difference and the results added in order to determine the total water influx, i.e.:

$$W_e = (W_e)_{\Delta p_1} + (W_e)_{\Delta p_2}$$

Step 3. Calculate the dimensionless time at 365 days as:

$$\begin{aligned} t_D &= 0.9888t \\ &= 0.9888 (365) = 361 \end{aligned}$$

Step 4. Determine the dimensionless water influx at $t_D = 361$ from Table 10-1 to give:

$$W_{eD} = 123.5$$

Step 5. Calculate the water influx due to the first and second pressure drop, i.e., $(W_e)_{\Delta p_1}$ and $(W_e)_{\Delta p_2}$, or:

$$(W_e)_{\Delta p_1} = (20.4)(5)(123.5) = 12,597 \text{ bbl}$$

$$(W_e)_{\Delta p_2} = (20.4)(14)(69.46) = 19,838$$

Step 6. Calculate total (cumulative) water influx after one year.

$$W_e = 12,597 + 19,938 = 32,435 \text{ bbl}$$

Water influx after 18 months

Step 1. Calculate the third pressure drop Δp_3 , which is taken as $\frac{1}{2}$ of the *actual* pressure drop during the second period plus $\frac{1}{2}$ of the *actual* pressure drop during the third period, or:

$$\Delta p_3 = \frac{p_1 - p_3}{2}$$

$$\Delta p_3 = \frac{2490 - 2444}{2} = 23 \text{ psi}$$

Step 2. Calculate the dimensionless time after 6 months.

$$\begin{aligned} t_D &= 0.9888 t \\ &= 0.9888 (547.5) = 541.5 \end{aligned}$$

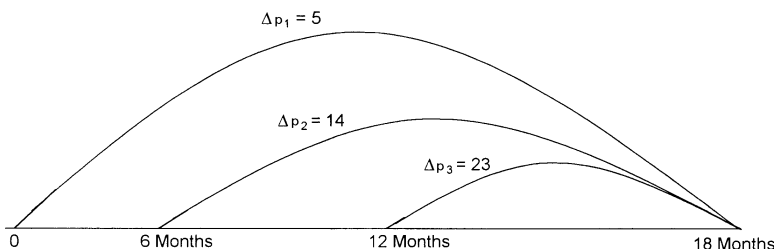


Figure 10-16. Pressure drop data for Example 10-7.

Step 3. Determine the dimensionless water influx at:

$$t_D = 541.5 \text{ from Table 10-1}$$

$$W_{eD} = 173.7$$

Step 4. The first pressure drop will have been effective the entire 18 months, the second pressure drop will have been effective for 12 months, and the last pressure drop will have been effective only 6 months, as shown in Figure 10-16. Therefore, the cumulative water influx is calculated below:

| Time, days | t_D | Δp | W_{eD} | $B\Delta p W_{eD}$ |
|------------|-------|------------|----------|--------------------|
| 547.5 | 541.5 | 5 | 173.7 | 17,714 |
| 365 | 361 | 14 | 123.5 | 35,272 |
| 182.5 | 180.5 | 23 | 69.40 | 32,291 |

$$W_e = 85,277 \text{ bbl}$$

Water influx after two years

The first pressure drop has now been effective for the entire two years, the second pressure drop has been effective for 18 months, the third pressure drop has been effective for 12 months, and the fourth pressure drop has been effective only 6 months. Summary of the calculations is given below:

| Time, days | t_D | Δp | W_{eD} | $B\Delta p W_{eD}$ |
|------------|-------|------------|----------|--------------------|
| 730 | 722 | 5 | 221.8 | 22,624 |
| 547.5 | 541.5 | 14 | 173.7 | 49,609 |
| 365 | 631 | 23 | 123.5 | 57,946 |
| 182.5 | 180.5 | 32 | 69.40 | 45,343 |

$$W_e = 175,522 \text{ bbl}$$

Edwardson and coworkers (1962) developed three sets of simple polynomial expressions for calculating the dimensionless water influx W_{eD} for infinite-acting aquifers. The proposed three expressions essentially approximate the W_{eD} values in three different dimensionless time regions.

- For $t_D < 0.01$

$$W_{eD} = 2 \left(\frac{t_D}{\pi} \right)^{0.5} \quad (10-26)$$

- For $0.01 < t_D < 200$

$$W_{eD} = \frac{1.2838\sqrt{t_D} + 1.19328t_D + 0.269872(t_D)^{3/2} + 0.00855294(t_D)^2}{1 + 0.616599\sqrt{t_D} + 0.0413008t_D} \quad (10-27)$$

- For $t_D > 200$

$$W_{eD} = \frac{-4.29881 + 2.02566t_D}{\ln(t_D)} \quad (10-28)$$

Bottom-Water Drive

The van Everdingen-Hurst solution to the *radial* diffusivity equation is considered the most rigorous aquifer influx model to date. The proposed solution technique, however, is not adequate to describe the vertical water encroachment in a bottom-water-drive system. Coats (1962) presented a mathematical model that takes into account the vertical flow effects from bottom-water aquifers. He correctly noted that in many cases reservoirs are situated on top of an aquifer with a continuous horizontal interface between the reservoir fluid and the aquifer water and with a significant aquifer thickness. He stated that in such situations significant bottom-water drive would occur. Coats modified the diffusivity equation to account for the vertical flow by including an additional term in the equation, to give:

$$\frac{\partial^2 p}{\partial r^2} + \frac{1}{r} \frac{\partial p}{\partial r} + F_k \frac{\partial^2 p}{\partial z^2} = \frac{\mu \phi c}{k} \frac{\partial p}{\partial t} \quad (10-29)$$

where F_k is the ratio of vertical to horizontal permeability, or:

$$F_k = k_v/k_h \quad (10-30)$$

where k_v = vertical permeability

k_h = horizontal permeability

Allard and Chen (1988) pointed out that there are an infinite number of solutions to Equation 10-28, representing all possible reservoir-aquifer configurations. They suggested that it is possible to derive a general solution that is applicable to a variety of systems by the solution to Equation 10-28 in terms of the dimensionless time t_D , dimensionless radius r_D , and a newly introduced dimensionless variable z_D .

$$z_D = \frac{h}{r_e \sqrt{F_k}} \quad (10-31)$$

where z_D = dimensionless vertical distance

h = aquifer thickness, ft

Allen and Chen used a numerical model to solve Equation 10-28. The authors developed a solution to the bottom-water influx that is comparable in form with that of van Everdingen and Hurst.

$$W_e = B \Delta p W_{eD} \quad (10-32)$$

They defined the water influx constant B identical to that of Equation 10-21, or

$$B = 1.119 \phi c_t r_e^2 h \quad (10-33)$$

Notice that the water influx constant B does not include the encroachment angle θ .

The actual values of W_{eD} are different from those of the van Everdingen-Hurst model because W_{eD} for the bottom-water drive is also a function of the vertical permeability. Allard and Chen tabulated the values of W_{eD} as a function of r_D , t_D , and z_D . These values are presented in Tables 10-3 through 10-7.

The solution procedure of a bottom-water influx problem is identical to the edge-water influx problem outlined in Example 10-7. Allard and Chen illustrated results of their method in the following example.

(text continued on page 716)

Table 10-3
Dimensionless Water Influx, W_{eD} , for Infinite Aquifer
(Permission to publish by the SPE)

| t_b | 0.05 | 0.1 | 0.3 | 0.5 | 0.7 | 0.9 | 1.0 |
|-------|-------|-------|-------|-------|-------|-------|-------|
| 0.1 | 0.700 | 0.677 | 0.508 | 0.349 | 0.251 | 0.195 | 0.176 |
| 0.2 | 0.793 | 0.786 | 0.696 | 0.547 | 0.416 | 0.328 | 0.295 |
| 0.3 | 0.936 | 0.926 | 0.834 | 0.692 | 0.548 | 0.440 | 0.396 |
| 0.4 | 1.051 | 1.041 | 0.952 | 0.812 | 0.662 | 0.540 | 0.486 |
| 0.5 | 1.158 | 1.155 | 1.059 | 0.918 | 0.764 | 0.631 | 0.569 |
| 0.6 | 1.270 | 1.268 | 1.167 | 1.021 | 0.862 | 0.721 | 0.651 |
| 0.7 | 1.384 | 1.380 | 1.270 | 1.116 | 0.953 | 0.806 | 0.729 |
| 0.8 | 1.503 | 1.499 | 1.373 | 1.205 | 1.039 | 0.886 | 0.803 |
| 0.9 | 1.621 | 1.612 | 1.477 | 1.286 | 1.117 | 0.959 | 0.872 |
| 1 | 1.743 | 1.726 | 1.581 | 1.347 | 1.181 | 1.020 | 0.932 |
| 2 | 2.402 | 2.393 | 2.288 | 2.034 | 1.827 | 1.622 | 1.509 |
| 3 | 3.031 | 3.018 | 2.895 | 2.650 | 2.408 | 2.164 | 2.026 |
| 4 | 3.629 | 3.615 | 3.477 | 3.223 | 2.949 | 2.669 | 2.510 |
| 5 | 4.217 | 4.201 | 4.048 | 3.766 | 3.462 | 3.150 | 2.971 |
| 6 | 4.784 | 4.766 | 4.601 | 4.288 | 3.956 | 3.614 | 3.416 |
| 7 | 5.323 | 5.303 | 5.128 | 4.792 | 4.434 | 4.063 | 3.847 |
| 8 | 5.829 | 5.808 | 5.625 | 5.283 | 4.900 | 4.501 | 4.268 |
| 9 | 6.306 | 6.283 | 6.094 | 5.762 | 5.355 | 4.929 | 4.680 |
| 10 | 6.837 | 6.816 | 6.583 | 6.214 | 5.792 | 5.344 | 5.080 |
| 11 | 7.263 | 7.242 | 7.040 | 6.664 | 6.217 | 5.745 | 5.468 |
| 12 | 7.742 | 7.718 | 7.495 | 7.104 | 6.638 | 6.143 | 5.852 |
| 13 | 8.196 | 8.172 | 7.943 | 7.539 | 7.052 | 6.536 | 6.231 |
| 14 | 8.648 | 8.623 | 8.385 | 7.967 | 7.461 | 6.923 | 6.604 |
| 15 | 9.094 | 9.068 | 8.821 | 8.389 | 7.864 | 7.305 | 6.973 |
| 16 | 9.534 | 9.507 | 9.253 | 8.806 | 8.262 | 7.682 | 7.338 |

 z_b

Water Influx

695

| | | | | | | | |
|----|--------|--------|--------|--------|--------|--------|--------|
| 17 | 9.969 | 9.942 | 9.679 | 9.218 | 8.656 | 8.056 | 7.699 |
| 18 | 10.399 | 10.371 | 10.100 | 9.626 | 9.046 | 8.426 | 8.057 |
| 19 | 10.823 | 10.794 | 10.516 | 10.029 | 9.432 | 8.793 | 8.411 |
| 20 | 11.241 | 11.211 | 10.929 | 10.430 | 9.815 | 9.156 | 8.763 |
| 21 | 11.664 | 11.633 | 11.339 | 10.826 | 10.194 | 9.516 | 9.111 |
| 22 | 12.075 | 12.045 | 11.744 | 11.219 | 10.571 | 9.874 | 9.457 |
| 23 | 12.486 | 12.454 | 12.147 | 11.609 | 10.944 | 10.229 | 9.801 |
| 24 | 12.893 | 12.861 | 12.546 | 11.996 | 11.315 | 10.581 | 10.142 |
| 25 | 13.297 | 13.264 | 12.942 | 12.380 | 11.683 | 10.931 | 10.481 |
| 26 | 13.698 | 13.665 | 13.336 | 12.761 | 12.048 | 11.279 | 10.817 |
| 27 | 14.097 | 14.062 | 13.726 | 13.140 | 12.411 | 11.625 | 11.152 |
| 28 | 14.493 | 14.458 | 14.115 | 13.517 | 12.772 | 11.968 | 11.485 |
| 29 | 14.886 | 14.850 | 14.501 | 13.891 | 13.131 | 12.310 | 11.816 |
| 30 | 15.277 | 15.241 | 14.884 | 14.263 | 13.488 | 12.650 | 12.145 |
| 31 | 15.666 | 15.628 | 15.266 | 14.634 | 13.843 | 12.990 | 12.473 |
| 32 | 16.053 | 16.015 | 15.645 | 15.002 | 14.196 | 13.324 | 12.799 |
| 33 | 16.437 | 16.398 | 16.023 | 15.368 | 14.548 | 13.659 | 13.123 |
| 34 | 16.819 | 16.780 | 16.398 | 15.732 | 14.897 | 13.992 | 13.446 |
| 35 | 17.200 | 17.160 | 16.772 | 16.095 | 15.245 | 14.324 | 13.767 |
| 36 | 17.579 | 17.538 | 17.143 | 16.456 | 15.592 | 14.654 | 14.088 |
| 37 | 17.956 | 17.915 | 17.513 | 16.815 | 15.937 | 14.983 | 14.406 |
| 38 | 18.331 | 18.289 | 17.882 | 17.173 | 16.280 | 15.311 | 14.724 |
| 39 | 18.704 | 18.662 | 18.249 | 17.529 | 16.622 | 15.637 | 15.040 |
| 40 | 19.088 | 19.045 | 18.620 | 17.886 | 16.964 | 15.963 | 15.356 |
| 41 | 19.450 | 19.407 | 18.982 | 18.240 | 17.305 | 16.288 | 15.671 |
| 42 | 19.821 | 19.777 | 19.344 | 18.592 | 17.644 | 16.611 | 15.985 |
| 43 | 20.188 | 20.144 | 19.706 | 18.943 | 17.981 | 16.933 | 16.297 |
| 44 | 20.555 | 20.510 | 20.065 | 19.293 | 18.317 | 17.253 | 16.608 |
| 45 | 20.920 | 20.874 | 20.424 | 19.641 | 18.651 | 17.573 | 16.918 |
| 46 | 21.283 | 21.237 | 20.781 | 19.988 | 18.985 | 17.891 | 17.227 |
| 47 | 21.645 | 21.598 | 21.137 | 20.333 | 19.317 | 18.208 | 17.535 |
| 48 | 22.006 | 21.958 | 21.491 | 20.678 | 19.648 | 18.524 | 17.841 |
| 49 | 22.365 | 22.317 | 21.844 | 21.021 | 19.978 | 18.840 | 18.147 |
| 50 | 22.722 | 22.674 | 22.196 | 21.363 | 20.307 | 19.154 | 18.452 |
| 51 | 23.081 | 23.032 | 22.547 | 21.704 | 20.635 | 19.467 | 18.757 |

(table continued on next page)

Table 10-3 (continued)

| t_b | z_b | | | | | | | | | |
|-------|--------|--------|--------|--------|--------|--------|--------|--|--|--|
| | 0.05 | 0.1 | 0.3 | 0.5 | 0.7 | 0.9 | 1.0 | | | |
| 52 | 23.436 | 23.387 | 22.897 | 22.044 | 20.962 | 19.779 | 19.060 | | | |
| 53 | 23.791 | 23.741 | 23.245 | 22.383 | 21.288 | 20.091 | 19.362 | | | |
| 54 | 24.145 | 24.094 | 23.593 | 22.721 | 21.613 | 20.401 | 19.664 | | | |
| 55 | 24.498 | 24.446 | 23.939 | 23.058 | 21.937 | 20.711 | 19.965 | | | |
| 56 | 24.849 | 24.797 | 24.285 | 23.393 | 22.260 | 21.020 | 20.265 | | | |
| 57 | 25.200 | 25.147 | 24.629 | 23.728 | 22.583 | 21.328 | 20.564 | | | |
| 58 | 25.549 | 25.496 | 24.973 | 24.062 | 22.904 | 21.636 | 20.862 | | | |
| 59 | 25.898 | 25.844 | 25.315 | 24.395 | 23.225 | 21.942 | 21.160 | | | |
| 60 | 26.246 | 26.191 | 25.657 | 24.728 | 23.545 | 22.248 | 21.457 | | | |
| 61 | 26.592 | 26.537 | 25.998 | 25.059 | 23.864 | 22.553 | 21.754 | | | |
| 62 | 26.938 | 26.883 | 26.337 | 25.390 | 24.182 | 22.857 | 22.049 | | | |
| 63 | 27.283 | 27.227 | 26.676 | 25.719 | 24.499 | 23.161 | 22.344 | | | |
| 64 | 27.627 | 27.570 | 27.015 | 26.048 | 24.816 | 23.464 | 22.639 | | | |
| 65 | 27.970 | 27.913 | 27.352 | 26.376 | 25.132 | 23.766 | 22.932 | | | |
| 66 | 28.312 | 28.255 | 27.688 | 26.704 | 25.447 | 24.068 | 23.225 | | | |
| 67 | 28.653 | 28.596 | 28.024 | 27.030 | 25.762 | 24.369 | 23.518 | | | |
| 68 | 28.994 | 28.936 | 28.359 | 27.356 | 26.075 | 24.669 | 23.810 | | | |
| 69 | 29.334 | 29.275 | 28.693 | 27.681 | 26.389 | 24.969 | 24.101 | | | |
| 70 | 29.673 | 29.614 | 29.026 | 28.006 | 26.701 | 25.268 | 24.391 | | | |
| 71 | 30.011 | 29.951 | 29.359 | 28.329 | 27.013 | 25.566 | 24.681 | | | |
| 72 | 30.349 | 30.288 | 29.691 | 28.652 | 27.324 | 25.864 | 24.971 | | | |
| 73 | 30.686 | 30.625 | 30.022 | 28.974 | 27.634 | 26.161 | 25.260 | | | |
| 74 | 31.022 | 30.960 | 30.353 | 29.296 | 27.944 | 26.458 | 25.548 | | | |
| 75 | 31.357 | 31.295 | 30.682 | 29.617 | 28.254 | 26.754 | 25.836 | | | |
| 76 | 31.692 | 31.629 | 31.012 | 29.937 | 28.562 | 27.049 | 26.124 | | | |
| 77 | 32.026 | 31.963 | 31.340 | 30.257 | 28.870 | 27.344 | 26.410 | | | |
| 78 | 32.359 | 32.296 | 31.668 | 30.576 | 29.178 | 27.639 | 26.697 | | | |
| 79 | 32.692 | 32.628 | 31.995 | 30.895 | 29.485 | 27.933 | 26.983 | | | |
| 80 | 33.024 | 32.959 | 32.322 | 31.212 | 29.791 | 28.226 | 27.268 | | | |
| 81 | 33.355 | 33.290 | 32.647 | 31.530 | 30.097 | 28.519 | 27.553 | | | |

| | | | | | | | |
|-----|--------|--------|--------|--------|--------|--------|--------|
| 82 | 33.686 | 33.621 | 32.973 | 31.846 | 30.402 | 28.812 | 27.837 |
| 83 | 34.016 | 33.950 | 33.297 | 32.163 | 30.707 | 29.104 | 28.121 |
| 84 | 34.345 | 34.279 | 33.622 | 32.478 | 31.011 | 29.395 | 28.404 |
| 85 | 34.674 | 34.608 | 33.945 | 32.793 | 31.315 | 29.686 | 28.687 |
| 86 | 35.003 | 34.935 | 34.268 | 33.107 | 31.618 | 29.976 | 28.970 |
| 87 | 35.330 | 35.263 | 34.590 | 33.421 | 31.921 | 30.266 | 29.252 |
| 88 | 35.657 | 35.589 | 34.912 | 33.735 | 32.223 | 30.556 | 29.534 |
| 89 | 35.984 | 35.915 | 35.233 | 34.048 | 32.525 | 30.845 | 29.815 |
| 90 | 36.310 | 36.241 | 35.554 | 34.360 | 32.826 | 31.134 | 30.096 |
| 91 | 36.636 | 36.566 | 35.874 | 34.672 | 33.127 | 31.422 | 30.376 |
| 92 | 36.960 | 36.890 | 36.194 | 34.983 | 33.427 | 31.710 | 30.656 |
| 93 | 37.285 | 37.214 | 36.513 | 35.294 | 33.727 | 31.997 | 30.935 |
| 94 | 37.609 | 37.538 | 36.832 | 35.604 | 34.026 | 32.284 | 31.215 |
| 95 | 37.932 | 37.861 | 37.150 | 35.914 | 34.325 | 32.570 | 31.493 |
| 96 | 38.255 | 38.183 | 37.467 | 36.223 | 34.623 | 32.857 | 31.772 |
| 97 | 38.577 | 38.505 | 37.785 | 36.532 | 34.921 | 33.142 | 32.050 |
| 98 | 38.899 | 38.826 | 38.101 | 36.841 | 35.219 | 33.427 | 32.327 |
| 99 | 39.220 | 39.147 | 38.417 | 37.149 | 35.516 | 33.712 | 32.605 |
| 100 | 39.541 | 39.467 | 38.733 | 37.456 | 35.813 | 33.997 | 32.881 |
| 105 | 41.138 | 41.062 | 40.305 | 38.987 | 37.290 | 35.414 | 34.260 |
| 110 | 42.724 | 42.645 | 41.865 | 40.508 | 38.758 | 36.821 | 35.630 |
| 115 | 44.299 | 44.218 | 43.415 | 42.018 | 40.216 | 38.221 | 36.993 |
| 120 | 45.864 | 45.781 | 44.956 | 43.520 | 41.666 | 39.612 | 38.347 |
| 125 | 47.420 | 47.334 | 46.487 | 45.012 | 43.107 | 40.995 | 39.694 |
| 130 | 48.966 | 48.879 | 48.009 | 46.497 | 44.541 | 42.372 | 41.035 |
| 135 | 50.504 | 50.414 | 49.523 | 47.973 | 45.967 | 43.741 | 42.368 |
| 140 | 52.033 | 51.942 | 51.029 | 49.441 | 47.386 | 45.104 | 43.696 |
| 145 | 53.555 | 53.462 | 52.528 | 50.903 | 48.798 | 46.460 | 45.017 |
| 150 | 55.070 | 54.974 | 54.019 | 52.357 | 50.204 | 47.810 | 46.333 |
| 155 | 56.577 | 56.479 | 55.503 | 53.805 | 51.603 | 49.155 | 47.643 |
| 160 | 58.077 | 57.977 | 56.981 | 55.246 | 52.996 | 50.494 | 48.947 |
| 165 | 59.570 | 59.469 | 58.452 | 56.681 | 54.384 | 51.827 | 50.247 |
| 170 | 61.058 | 60.954 | 59.916 | 58.110 | 55.766 | 53.156 | 51.542 |
| 175 | 62.539 | 62.433 | 61.375 | 59.534 | 57.143 | 54.479 | 52.832 |
| 180 | 64.014 | 63.906 | 62.829 | 60.952 | 58.514 | 55.798 | 54.118 |

(table continued on next page)

Table 10-3 (continued)

| f_b | 0.05 | 0.1 | 0.3 | 0.5 | 0.7 | 0.9 | 1.0 |
|-------|--------|--------|--------|--------|--------|--------|--------|
| 185 | 65.484 | 65.374 | 64.276 | 62.365 | 59.881 | 57.112 | 55.399 |
| 190 | 66.948 | 66.836 | 65.718 | 63.773 | 61.243 | 58.422 | 56.676 |
| 195 | 68.406 | 68.293 | 67.156 | 65.175 | 62.600 | 59.727 | 57.949 |
| 200 | 69.860 | 69.744 | 68.588 | 66.573 | 63.952 | 61.028 | 59.217 |
| 205 | 71.309 | 71.191 | 70.015 | 67.967 | 65.301 | 62.326 | 60.482 |
| 210 | 72.752 | 72.633 | 71.437 | 69.355 | 66.645 | 63.619 | 61.744 |
| 215 | 74.191 | 74.070 | 72.855 | 70.740 | 67.985 | 64.908 | 63.001 |
| 220 | 75.626 | 75.503 | 74.269 | 72.120 | 69.321 | 66.194 | 64.255 |
| 225 | 77.056 | 76.931 | 75.678 | 73.496 | 70.653 | 67.476 | 65.506 |
| 230 | 78.482 | 78.355 | 77.083 | 74.868 | 71.981 | 68.755 | 66.753 |
| 235 | 79.903 | 79.774 | 78.484 | 76.236 | 73.306 | 70.030 | 67.997 |
| 240 | 81.321 | 81.190 | 79.881 | 77.601 | 74.627 | 71.302 | 69.238 |
| 245 | 82.734 | 82.602 | 81.275 | 78.962 | 75.945 | 72.570 | 70.476 |
| 250 | 84.144 | 84.010 | 82.664 | 80.319 | 77.259 | 73.736 | 71.711 |
| 255 | 85.550 | 85.414 | 84.050 | 81.672 | 78.570 | 75.098 | 72.943 |
| 260 | 86.952 | 86.814 | 85.432 | 83.023 | 79.878 | 76.358 | 74.172 |
| 265 | 88.351 | 88.211 | 86.811 | 84.369 | 81.182 | 77.614 | 75.398 |
| 270 | 89.746 | 89.604 | 88.186 | 85.713 | 82.484 | 78.868 | 76.621 |
| 275 | 91.138 | 90.994 | 89.558 | 87.053 | 83.782 | 80.119 | 77.842 |
| 280 | 92.526 | 92.381 | 90.926 | 88.391 | 85.078 | 81.367 | 79.060 |
| 285 | 93.911 | 93.764 | 92.292 | 89.725 | 86.371 | 82.612 | 80.276 |
| 290 | 95.293 | 95.144 | 93.654 | 91.056 | 87.660 | 83.855 | 81.489 |
| 295 | 96.672 | 96.521 | 95.014 | 92.385 | 88.948 | 85.095 | 82.700 |
| 300 | 98.048 | 97.895 | 96.370 | 93.710 | 90.232 | 86.333 | 83.908 |
| 305 | 99.420 | 99.266 | 97.724 | 95.033 | 91.514 | 87.568 | 85.114 |

Water Influx

699

| | | | | | | | |
|-----|--------|--------|--------|--------|--------|--------|--------|
| 310 | 100.79 | 100.64 | 99.07 | 96.35 | 92.79 | 88.80 | 86.32 |
| 315 | 102.16 | 102.00 | 100.42 | 97.67 | 94.07 | 90.03 | 87.52 |
| 320 | 103.52 | 103.36 | 101.77 | 98.99 | 95.34 | 91.26 | 88.72 |
| 325 | 104.88 | 104.72 | 103.11 | 100.30 | 96.62 | 92.49 | 89.92 |
| 330 | 106.24 | 106.08 | 104.45 | 101.61 | 97.89 | 93.71 | 91.11 |
| 335 | 107.60 | 107.43 | 105.79 | 102.91 | 99.15 | 94.93 | 92.30 |
| 340 | 108.95 | 108.79 | 107.12 | 104.22 | 100.42 | 96.15 | 93.49 |
| 345 | 110.30 | 110.13 | 108.45 | 105.52 | 101.68 | 97.37 | 94.68 |
| 350 | 111.65 | 111.48 | 109.78 | 106.82 | 102.94 | 98.58 | 95.87 |
| 355 | 113.00 | 112.82 | 111.11 | 108.12 | 104.20 | 99.80 | 97.06 |
| 360 | 114.34 | 114.17 | 112.43 | 109.41 | 105.45 | 101.01 | 98.24 |
| 365 | 115.68 | 115.51 | 113.76 | 110.71 | 106.71 | 102.22 | 99.42 |
| 370 | 117.02 | 116.84 | 115.08 | 112.00 | 107.96 | 103.42 | 100.60 |
| 375 | 118.36 | 118.18 | 116.40 | 113.29 | 109.21 | 104.63 | 101.78 |
| 380 | 119.69 | 119.51 | 117.71 | 114.57 | 110.46 | 105.83 | 102.95 |
| 385 | 121.02 | 120.84 | 119.02 | 115.86 | 111.70 | 107.04 | 104.13 |
| 390 | 122.35 | 122.17 | 120.34 | 117.14 | 112.95 | 108.24 | 105.30 |
| 395 | 123.68 | 123.49 | 121.65 | 118.42 | 114.19 | 109.43 | 106.47 |
| 400 | 125.00 | 124.82 | 122.94 | 119.70 | 115.43 | 110.63 | 107.64 |
| 405 | 126.33 | 126.14 | 124.26 | 120.97 | 116.67 | 111.82 | 108.80 |
| 410 | 127.65 | 127.46 | 125.56 | 122.25 | 117.90 | 113.02 | 109.97 |
| 415 | 128.97 | 128.78 | 126.86 | 123.52 | 119.14 | 114.21 | 111.13 |
| 420 | 130.28 | 130.09 | 128.16 | 124.79 | 120.37 | 115.40 | 112.30 |
| 425 | 131.60 | 131.40 | 129.46 | 126.06 | 121.60 | 116.59 | 113.46 |
| 430 | 132.91 | 132.72 | 130.75 | 127.33 | 122.83 | 117.77 | 114.62 |
| 435 | 134.22 | 134.03 | 132.05 | 128.59 | 124.06 | 118.96 | 115.77 |
| 440 | 135.53 | 135.33 | 133.34 | 129.86 | 125.29 | 120.14 | 116.93 |
| 445 | 136.84 | 136.64 | 134.63 | 131.12 | 126.51 | 121.32 | 118.08 |
| 450 | 138.15 | 137.94 | 135.92 | 132.38 | 127.73 | 122.50 | 119.24 |
| 455 | 139.45 | 139.25 | 137.20 | 133.64 | 128.96 | 123.68 | 120.39 |
| 460 | 140.75 | 140.55 | 138.49 | 134.90 | 130.18 | 124.86 | 121.54 |
| 465 | 142.05 | 141.85 | 139.77 | 136.15 | 131.39 | 126.04 | 122.69 |
| 470 | 143.35 | 143.14 | 141.05 | 137.40 | 132.61 | 127.21 | 123.84 |
| 475 | 144.65 | 144.44 | 142.33 | 138.66 | 133.82 | 128.38 | 124.98 |
| 480 | 145.94 | 145.73 | 143.61 | 139.91 | 135.04 | 129.55 | 126.13 |

(table continued on next page)

Table 10-3 (continued)

| f_b | z_b | | | | | | | | | |
|-------|--------|--------|--------|--------|--------|--------|--------|--|--|--|
| | 0.05 | 0.1 | 0.3 | 0.5 | 0.7 | 0.9 | 1.0 | | | |
| 485 | 147.24 | 147.02 | 144.89 | 141.15 | 136.25 | 130.72 | 127.27 | | | |
| 490 | 148.53 | 148.31 | 146.16 | 142.40 | 137.46 | 131.89 | 128.41 | | | |
| 495 | 149.82 | 149.60 | 147.43 | 143.65 | 138.67 | 133.06 | 129.56 | | | |
| 500 | 151.11 | 150.89 | 148.71 | 144.89 | 139.88 | 134.23 | 130.70 | | | |
| 510 | 153.68 | 153.46 | 151.24 | 147.38 | 142.29 | 136.56 | 132.97 | | | |
| 520 | 156.25 | 156.02 | 153.78 | 149.85 | 144.70 | 138.88 | 135.24 | | | |
| 530 | 158.81 | 158.58 | 156.30 | 152.33 | 147.10 | 141.20 | 137.51 | | | |
| 540 | 161.36 | 161.13 | 158.82 | 154.79 | 149.49 | 143.51 | 139.77 | | | |
| 550 | 163.91 | 163.68 | 161.34 | 157.25 | 151.88 | 145.82 | 142.03 | | | |
| 560 | 166.45 | 166.22 | 163.85 | 159.71 | 154.27 | 148.12 | 144.28 | | | |
| 570 | 168.99 | 168.75 | 166.35 | 162.16 | 156.65 | 150.42 | 146.53 | | | |
| 580 | 171.52 | 171.28 | 168.85 | 164.61 | 159.02 | 152.72 | 148.77 | | | |
| 590 | 174.05 | 173.80 | 171.34 | 167.05 | 161.39 | 155.01 | 151.01 | | | |
| 600 | 176.57 | 176.32 | 173.83 | 169.48 | 163.76 | 157.29 | 153.25 | | | |
| 610 | 179.09 | 178.83 | 176.32 | 171.92 | 166.12 | 159.58 | 155.48 | | | |
| 620 | 181.60 | 181.34 | 178.80 | 174.34 | 168.48 | 161.85 | 157.71 | | | |
| 630 | 184.10 | 183.85 | 181.27 | 176.76 | 170.83 | 164.13 | 159.93 | | | |
| 640 | 186.60 | 186.35 | 183.74 | 179.18 | 173.18 | 166.40 | 162.15 | | | |
| 650 | 189.10 | 188.84 | 186.20 | 181.60 | 175.52 | 168.66 | 164.37 | | | |
| 660 | 191.59 | 191.33 | 188.66 | 184.00 | 177.86 | 170.92 | 166.58 | | | |
| 670 | 194.08 | 193.81 | 191.12 | 186.41 | 180.20 | 173.18 | 168.79 | | | |
| 680 | 196.57 | 196.29 | 193.57 | 188.81 | 182.53 | 175.44 | 170.99 | | | |
| 690 | 199.04 | 198.77 | 196.02 | 191.21 | 184.86 | 177.69 | 173.20 | | | |
| 700 | 201.52 | 201.24 | 198.46 | 193.60 | 187.19 | 179.94 | 175.39 | | | |
| 710 | 203.99 | 203.71 | 200.90 | 195.99 | 189.51 | 182.18 | 177.59 | | | |

Water Influx

701

| | | | | | | | |
|-----|--------|--------|--------|--------|--------|--------|--------|
| 720 | 206.46 | 206.17 | 203.34 | 198.37 | 191.83 | 184.42 | 179.78 |
| 730 | 208.92 | 208.63 | 205.77 | 200.75 | 194.14 | 186.66 | 181.97 |
| 740 | 211.38 | 211.09 | 208.19 | 203.13 | 196.45 | 188.89 | 184.15 |
| 750 | 213.83 | 213.54 | 210.62 | 205.50 | 198.76 | 191.12 | 186.34 |
| 760 | 216.28 | 215.99 | 213.04 | 207.87 | 201.06 | 193.35 | 188.52 |
| 770 | 218.73 | 218.43 | 215.45 | 210.24 | 203.36 | 195.57 | 190.69 |
| 780 | 221.17 | 220.87 | 217.86 | 212.60 | 205.66 | 197.80 | 192.87 |
| 790 | 223.61 | 223.31 | 220.27 | 214.96 | 207.95 | 200.01 | 195.04 |
| 800 | 226.05 | 225.74 | 222.68 | 217.32 | 210.24 | 202.23 | 197.20 |
| 810 | 228.48 | 228.17 | 225.08 | 219.67 | 212.53 | 204.44 | 199.37 |
| 820 | 230.91 | 230.60 | 227.48 | 222.02 | 214.81 | 206.65 | 201.53 |
| 830 | 233.33 | 233.02 | 229.87 | 224.36 | 217.09 | 208.86 | 203.69 |
| 840 | 235.76 | 235.44 | 232.26 | 226.71 | 219.37 | 211.06 | 205.85 |
| 850 | 238.18 | 237.86 | 234.65 | 229.05 | 221.64 | 213.26 | 208.00 |
| 860 | 240.59 | 240.27 | 237.04 | 231.38 | 223.92 | 215.46 | 210.15 |
| 870 | 243.00 | 242.68 | 239.42 | 233.72 | 226.19 | 217.65 | 212.30 |
| 880 | 245.41 | 245.08 | 241.80 | 236.05 | 228.45 | 219.85 | 214.44 |
| 890 | 247.82 | 247.49 | 244.17 | 238.37 | 230.72 | 222.04 | 216.59 |
| 900 | 250.22 | 249.89 | 246.55 | 240.70 | 232.98 | 224.22 | 218.73 |
| 910 | 252.62 | 252.28 | 248.92 | 243.02 | 235.23 | 226.41 | 220.87 |
| 920 | 255.01 | 254.68 | 251.28 | 245.34 | 237.49 | 228.59 | 223.00 |
| 930 | 257.41 | 257.07 | 253.65 | 247.66 | 239.74 | 230.77 | 225.14 |
| 940 | 259.80 | 259.46 | 256.01 | 249.97 | 241.99 | 232.95 | 227.27 |
| 950 | 262.19 | 261.84 | 258.36 | 252.28 | 244.24 | 235.12 | 229.39 |
| 960 | 264.57 | 264.22 | 260.72 | 254.59 | 246.48 | 237.29 | 231.52 |

(table continued on next page)

Table 10-3 (continued)

| b_b | z_b | | | | | | | | | |
|-------|--------|--------|--------|--------|--------|--------|--------|--|--|--|
| | 0.05 | 0.1 | 0.3 | 0.5 | 0.7 | 0.9 | 1.0 | | | |
| 970 | 266.95 | 266.60 | 263.07 | 256.89 | 248.72 | 239.46 | 233.65 | | | |
| 980 | 269.33 | 268.98 | 265.42 | 259.19 | 250.96 | 241.63 | 235.77 | | | |
| 990 | 271.71 | 271.35 | 267.77 | 261.49 | 253.20 | 243.80 | 237.89 | | | |
| 1000 | 274.08 | 273.72 | 270.11 | 263.79 | 255.44 | 245.96 | 240.00 | | | |
| 1010 | 276.35 | 275.99 | 272.35 | 265.99 | 257.58 | 248.04 | 242.04 | | | |
| 1020 | 278.72 | 278.35 | 274.69 | 268.29 | 259.81 | 250.19 | 244.15 | | | |
| 1030 | 281.08 | 280.72 | 277.03 | 270.57 | 262.04 | 252.35 | 246.26 | | | |
| 1040 | 283.44 | 283.08 | 279.36 | 272.86 | 264.26 | 254.50 | 248.37 | | | |
| 1050 | 285.81 | 285.43 | 281.69 | 275.15 | 266.49 | 256.66 | 250.48 | | | |
| 1060 | 288.16 | 287.79 | 284.02 | 277.43 | 268.71 | 258.81 | 252.58 | | | |
| 1070 | 290.52 | 290.14 | 286.35 | 279.71 | 270.92 | 260.95 | 254.69 | | | |
| 1080 | 292.87 | 292.49 | 288.67 | 281.99 | 273.14 | 263.10 | 256.79 | | | |
| 1090 | 295.22 | 294.84 | 290.99 | 284.26 | 275.35 | 265.24 | 258.89 | | | |
| 1100 | 297.57 | 297.18 | 293.31 | 286.54 | 277.57 | 267.38 | 260.98 | | | |
| 1110 | 299.91 | 299.53 | 295.63 | 288.81 | 279.78 | 269.52 | 263.08 | | | |
| 1120 | 302.26 | 301.87 | 297.94 | 291.07 | 281.98 | 271.66 | 265.17 | | | |
| 1130 | 304.60 | 304.20 | 300.25 | 293.34 | 284.19 | 273.80 | 267.26 | | | |
| 1140 | 306.93 | 306.54 | 302.56 | 295.61 | 286.39 | 275.93 | 269.35 | | | |
| 1150 | 309.27 | 308.87 | 304.87 | 297.87 | 288.59 | 278.06 | 271.44 | | | |
| 1160 | 311.60 | 311.20 | 307.18 | 300.13 | 290.79 | 280.19 | 273.52 | | | |
| 1170 | 313.94 | 313.53 | 309.48 | 302.38 | 292.99 | 282.32 | 275.61 | | | |
| 1180 | 316.26 | 315.86 | 311.78 | 304.64 | 295.19 | 284.44 | 277.69 | | | |
| 1190 | 318.59 | 318.18 | 314.08 | 306.89 | 297.38 | 286.57 | 279.77 | | | |
| 1200 | 320.92 | 320.51 | 316.38 | 309.15 | 299.57 | 288.69 | 281.85 | | | |
| 1210 | 323.24 | 322.83 | 318.67 | 311.39 | 301.76 | 290.81 | 283.92 | | | |
| 1220 | 325.56 | 325.14 | 320.96 | 313.64 | 303.95 | 292.93 | 286.00 | | | |
| 1230 | 327.88 | 327.46 | 323.25 | 315.89 | 306.13 | 295.05 | 288.07 | | | |
| 1240 | 330.19 | 329.77 | 325.54 | 318.13 | 308.32 | 297.16 | 290.14 | | | |
| 1250 | 332.51 | 332.08 | 327.83 | 320.37 | 310.50 | 299.27 | 292.21 | | | |
| 1260 | 334.82 | 334.39 | 330.11 | 322.61 | 312.68 | 301.38 | 294.28 | | | |

| | | | | | | | |
|------|--------|--------|--------|--------|--------|--------|--------|
| 1270 | 337.13 | 336.70 | 332.39 | 324.85 | 314.85 | 303.49 | 296.35 |
| 1280 | 339.44 | 339.01 | 334.67 | 327.08 | 317.03 | 305.60 | 298.41 |
| 1290 | 341.74 | 341.31 | 336.95 | 329.32 | 319.21 | 307.71 | 300.47 |
| 1300 | 344.05 | 343.61 | 339.23 | 331.55 | 321.38 | 309.81 | 302.54 |
| 1310 | 346.35 | 345.91 | 341.50 | 333.78 | 323.55 | 311.92 | 304.60 |
| 1320 | 348.65 | 348.21 | 343.77 | 336.01 | 325.72 | 314.02 | 306.65 |
| 1330 | 350.95 | 350.50 | 346.04 | 338.23 | 327.89 | 316.12 | 308.71 |
| 1340 | 353.24 | 352.80 | 348.31 | 340.46 | 330.05 | 318.22 | 310.77 |
| 1350 | 355.54 | 355.09 | 350.58 | 342.68 | 332.21 | 320.31 | 312.82 |
| 1360 | 357.83 | 357.38 | 352.84 | 344.90 | 334.38 | 322.41 | 314.87 |
| 1370 | 360.12 | 359.67 | 355.11 | 347.12 | 336.54 | 324.50 | 316.92 |
| 1380 | 362.41 | 361.95 | 357.37 | 349.34 | 338.70 | 326.59 | 318.97 |
| 1390 | 364.69 | 364.24 | 359.63 | 351.56 | 340.85 | 328.68 | 321.02 |
| 1400 | 366.98 | 366.52 | 361.88 | 353.77 | 343.01 | 330.77 | 323.06 |
| 1410 | 369.26 | 368.80 | 364.14 | 355.98 | 345.16 | 332.86 | 325.11 |
| 1420 | 371.54 | 371.08 | 366.40 | 358.19 | 347.32 | 334.94 | 327.15 |
| 1430 | 373.82 | 373.35 | 368.65 | 360.40 | 349.47 | 337.03 | 329.19 |
| 1440 | 376.10 | 375.63 | 370.90 | 362.61 | 351.62 | 339.11 | 331.23 |
| 1450 | 378.38 | 377.90 | 373.15 | 364.81 | 353.76 | 341.19 | 333.27 |
| 1460 | 380.65 | 380.17 | 375.39 | 367.02 | 355.91 | 343.27 | 335.31 |
| 1470 | 382.92 | 382.44 | 377.64 | 369.22 | 358.06 | 345.35 | 337.35 |
| 1480 | 385.19 | 384.71 | 379.88 | 371.42 | 360.20 | 347.43 | 339.38 |
| 1490 | 387.46 | 386.98 | 382.13 | 373.62 | 362.34 | 349.50 | 341.42 |
| 1500 | 389.73 | 389.25 | 384.37 | 375.82 | 364.48 | 351.58 | 343.45 |
| 1525 | 395.39 | 394.90 | 389.96 | 381.31 | 369.82 | 356.76 | 348.52 |
| 1550 | 401.04 | 400.55 | 395.55 | 386.78 | 375.16 | 361.93 | 353.59 |
| 1575 | 406.68 | 406.18 | 401.12 | 392.25 | 380.49 | 367.09 | 358.65 |
| 1600 | 412.32 | 411.81 | 406.69 | 397.71 | 385.80 | 372.24 | 363.70 |
| 1625 | 417.94 | 417.42 | 412.24 | 403.16 | 391.11 | 377.39 | 368.74 |
| 1650 | 423.55 | 423.03 | 417.79 | 408.60 | 396.41 | 382.53 | 373.77 |
| 1675 | 429.15 | 428.63 | 423.33 | 414.04 | 401.70 | 387.66 | 378.80 |
| 1700 | 434.75 | 434.22 | 428.85 | 419.46 | 406.99 | 392.78 | 383.82 |
| 1725 | 440.33 | 439.79 | 434.37 | 424.87 | 412.26 | 397.89 | 388.83 |
| 1750 | 445.91 | 445.37 | 439.89 | 430.28 | 417.53 | 403.00 | 393.84 |
| 1775 | 451.48 | 450.93 | 445.39 | 435.68 | 422.79 | 408.10 | 398.84 |

(table continued on next page)

Table 10-3 (continued)

| t_b | 0.05 | 0.1 | 0.3 | 0.5 | 0.7 | 0.9 | 1.0 |
|-------|--------|--------|--------|--------|--------|--------|--------|
| 1880 | 457.04 | 456.48 | 450.88 | 441.07 | 428.04 | 413.20 | 403.83 |
| 1825 | 462.59 | 462.03 | 456.37 | 446.46 | 433.29 | 418.28 | 408.82 |
| 1850 | 468.13 | 467.56 | 461.85 | 451.83 | 438.53 | 423.36 | 413.80 |
| 1875 | 473.67 | 473.09 | 467.32 | 457.20 | 443.76 | 428.43 | 418.77 |
| 1900 | 479.19 | 478.61 | 472.78 | 462.56 | 448.98 | 433.50 | 423.73 |
| 1925 | 484.71 | 484.13 | 478.24 | 467.92 | 454.20 | 438.56 | 428.69 |
| 1950 | 490.22 | 489.63 | 483.69 | 473.26 | 459.41 | 443.61 | 433.64 |
| 1975 | 495.73 | 495.13 | 489.13 | 478.60 | 464.61 | 448.66 | 438.59 |
| 2000 | 501.22 | 500.62 | 494.56 | 483.93 | 469.81 | 453.70 | 443.53 |
| 2025 | 506.71 | 506.11 | 499.99 | 489.26 | 475.00 | 458.73 | 448.47 |
| 2050 | 512.20 | 511.58 | 505.41 | 494.58 | 480.18 | 463.76 | 453.40 |
| 2075 | 517.67 | 517.05 | 510.82 | 499.89 | 485.36 | 468.78 | 458.32 |
| 2100 | 523.14 | 522.52 | 516.22 | 505.19 | 490.53 | 473.80 | 463.24 |
| 2125 | 528.60 | 527.97 | 521.62 | 510.49 | 495.69 | 478.81 | 468.15 |
| 2150 | 534.05 | 533.42 | 527.02 | 515.78 | 500.85 | 483.81 | 473.06 |
| 2175 | 539.50 | 538.86 | 532.40 | 521.07 | 506.01 | 488.81 | 477.96 |
| 2200 | 544.94 | 544.30 | 537.78 | 526.35 | 511.15 | 493.81 | 482.85 |
| 2225 | 550.38 | 549.73 | 543.15 | 531.62 | 516.29 | 498.79 | 487.74 |
| 2250 | 555.81 | 555.15 | 548.52 | 536.89 | 521.43 | 503.78 | 492.63 |
| 2275 | 561.23 | 560.56 | 553.88 | 542.15 | 526.56 | 508.75 | 497.51 |
| 2300 | 566.64 | 565.97 | 559.23 | 547.41 | 531.68 | 513.72 | 502.38 |
| 2325 | 572.05 | 571.38 | 564.58 | 552.66 | 536.80 | 518.69 | 507.25 |
| 2350 | 577.46 | 576.78 | 569.92 | 557.90 | 541.91 | 523.65 | 512.12 |
| 2375 | 582.85 | 582.17 | 575.26 | 563.14 | 547.02 | 528.61 | 516.98 |
| 2400 | 588.24 | 587.55 | 580.59 | 568.37 | 552.12 | 533.56 | 521.83 |
| 2425 | 593.63 | 592.93 | 585.91 | 573.60 | 557.22 | 538.50 | 526.68 |
| 2450 | 599.01 | 598.31 | 591.23 | 578.82 | 562.31 | 543.45 | 531.53 |
| 2475 | 604.38 | 603.68 | 596.55 | 584.04 | 567.39 | 548.38 | 536.37 |
| 2500 | 609.75 | 609.04 | 601.85 | 589.25 | 572.47 | 553.31 | 541.20 |
| 2550 | 620.47 | 619.75 | 612.45 | 599.65 | 582.62 | 563.16 | 550.86 |

| | | | | | | | |
|------|--------|--------|--------|--------|--------|--------|--------|
| 2600 | 631.17 | 630.43 | 623.03 | 610.04 | 592.75 | 572.99 | 560.50 |
| 2650 | 641.84 | 641.10 | 633.59 | 620.40 | 602.86 | 582.80 | 570.13 |
| 2700 | 652.50 | 651.74 | 644.12 | 630.75 | 612.95 | 592.60 | 579.73 |
| 2750 | 663.13 | 662.37 | 654.64 | 641.07 | 623.02 | 602.37 | 589.32 |
| 2800 | 673.75 | 672.97 | 665.14 | 651.38 | 633.07 | 612.13 | 598.90 |
| 2850 | 684.34 | 683.56 | 675.61 | 661.67 | 643.11 | 621.88 | 608.45 |
| 2900 | 694.92 | 694.12 | 686.07 | 671.94 | 653.12 | 631.60 | 617.99 |
| 2950 | 705.48 | 704.67 | 696.51 | 682.19 | 663.13 | 641.32 | 627.52 |
| 3000 | 716.02 | 715.20 | 706.94 | 692.43 | 673.11 | 651.01 | 637.03 |
| 3050 | 726.54 | 725.71 | 717.34 | 702.65 | 683.08 | 660.69 | 646.53 |
| 3100 | 737.04 | 736.20 | 727.73 | 712.85 | 693.03 | 670.36 | 656.01 |
| 3150 | 747.53 | 746.68 | 738.10 | 723.04 | 702.97 | 680.01 | 665.48 |
| 3200 | 758.00 | 757.14 | 748.45 | 733.21 | 712.89 | 689.64 | 674.93 |
| 3250 | 768.45 | 767.58 | 758.79 | 743.36 | 722.80 | 699.27 | 684.37 |
| 3300 | 778.89 | 778.01 | 769.11 | 753.50 | 732.69 | 708.87 | 693.80 |
| 3350 | 789.31 | 788.42 | 779.42 | 763.62 | 742.57 | 718.47 | 703.21 |
| 3400 | 799.71 | 798.81 | 789.71 | 773.73 | 752.43 | 728.05 | 712.62 |
| 3450 | 810.10 | 809.19 | 799.99 | 783.82 | 762.28 | 737.62 | 722.00 |
| 3500 | 820.48 | 819.55 | 810.25 | 793.90 | 772.12 | 747.17 | 731.38 |
| 3550 | 830.83 | 829.90 | 820.49 | 803.97 | 781.94 | 756.72 | 740.74 |
| 3600 | 841.18 | 840.24 | 830.73 | 814.02 | 791.75 | 766.24 | 750.09 |
| 3650 | 851.51 | 850.56 | 840.94 | 824.06 | 801.55 | 775.76 | 759.43 |
| 3700 | 861.83 | 860.86 | 851.15 | 834.08 | 811.33 | 785.27 | 768.76 |
| 3750 | 872.13 | 871.15 | 861.34 | 844.09 | 821.10 | 794.76 | 778.08 |
| 3800 | 882.41 | 881.43 | 871.51 | 854.09 | 830.86 | 804.24 | 787.38 |
| 3850 | 892.69 | 891.70 | 881.68 | 864.08 | 840.61 | 813.71 | 796.68 |
| 3900 | 902.95 | 901.95 | 891.83 | 874.05 | 850.34 | 823.17 | 805.96 |
| 3950 | 913.20 | 912.19 | 901.96 | 884.01 | 860.06 | 832.62 | 815.23 |
| 4000 | 923.43 | 922.41 | 912.09 | 893.96 | 869.77 | 842.06 | 824.49 |
| 4050 | 933.65 | 932.62 | 922.20 | 903.89 | 879.47 | 851.48 | 833.74 |
| 4100 | 943.86 | 942.82 | 932.30 | 913.82 | 889.16 | 860.90 | 842.99 |
| 4150 | 954.06 | 953.01 | 942.39 | 923.73 | 898.84 | 870.30 | 852.22 |
| 4200 | 964.25 | 963.19 | 952.47 | 933.63 | 908.50 | 879.69 | 861.44 |
| 4250 | 974.42 | 973.35 | 962.53 | 943.52 | 918.16 | 889.08 | 870.65 |
| 4300 | 984.58 | 983.50 | 972.58 | 953.40 | 927.80 | 898.45 | 879.85 |

(table continued on next page)

Table 10-3 (continued)

| t_b | 0.05 | 0.1 | 0.3 | 0.5 | 0.7 | 0.9 | 1.0 |
|-------|--------|--------|--------|--------|--------|--------|--------|
| 4350 | 994.73 | 993.64 | 982.62 | 963.27 | 937.43 | 907.81 | 889.04 |
| 4400 | 1004.9 | 1003.8 | 992.7 | 973.1 | 947.1 | 917.2 | 898.2 |
| 4450 | 1015.0 | 1013.9 | 1002.7 | 983.0 | 956.7 | 926.5 | 907.4 |
| 4500 | 1025.1 | 1024.0 | 1012.7 | 992.8 | 966.3 | 935.9 | 916.6 |
| 4550 | 1035.2 | 1034.1 | 1022.7 | 1002.6 | 975.9 | 945.2 | 925.7 |
| 4600 | 1045.3 | 1044.2 | 1032.7 | 1012.4 | 985.5 | 954.5 | 934.9 |
| 4650 | 1055.4 | 1054.2 | 1042.6 | 1022.2 | 995.0 | 963.8 | 944.0 |
| 4700 | 1065.5 | 1064.3 | 1052.6 | 1032.0 | 1004.6 | 973.1 | 953.1 |
| 4750 | 1075.5 | 1074.4 | 1062.6 | 1041.8 | 1014.1 | 982.4 | 962.2 |
| 4800 | 1085.6 | 1084.4 | 1072.5 | 1051.6 | 1023.7 | 991.7 | 971.4 |
| 4850 | 1095.6 | 1094.4 | 1082.4 | 1061.4 | 1033.2 | 1000.9 | 980.5 |
| 4900 | 1105.6 | 1104.5 | 1092.4 | 1071.1 | 1042.8 | 1010.2 | 989.5 |
| 4950 | 1115.7 | 1114.5 | 1102.3 | 1080.9 | 1052.3 | 1019.4 | 998.6 |
| 5000 | 1125.7 | 1124.5 | 1112.2 | 1090.6 | 1061.8 | 1028.7 | 1007.7 |
| 5100 | 1145.7 | 1144.4 | 1132.0 | 1110.0 | 1080.8 | 1047.2 | 1025.8 |
| 5200 | 1165.6 | 1164.4 | 1151.7 | 1129.4 | 1099.7 | 1065.6 | 1043.9 |
| 5300 | 1185.5 | 1184.3 | 1171.4 | 1148.8 | 1118.6 | 1084.0 | 1062.0 |
| 5400 | 1205.4 | 1204.1 | 1191.1 | 1168.2 | 1137.5 | 1102.4 | 1080.0 |
| 5500 | 1225.3 | 1224.0 | 1210.7 | 1187.5 | 1156.4 | 1120.7 | 1098.0 |
| 5600 | 1245.1 | 1243.7 | 1230.3 | 1206.7 | 1175.2 | 1139.0 | 1116.0 |
| 5700 | 1264.9 | 1263.5 | 1249.9 | 1226.0 | 1194.0 | 1157.3 | 1134.0 |
| 5800 | 1284.6 | 1283.2 | 1269.4 | 1245.2 | 1212.8 | 1175.5 | 1151.9 |
| 5900 | 1304.3 | 1302.9 | 1288.9 | 1264.4 | 1231.5 | 1193.8 | 1169.8 |
| 6000 | 1324.0 | 1322.6 | 1308.4 | 1283.5 | 1250.2 | 1211.9 | 1187.7 |
| 6100 | 1343.6 | 1342.2 | 1327.9 | 1302.6 | 1268.9 | 1230.1 | 1205.5 |
| 6200 | 1363.2 | 1361.8 | 1347.3 | 1321.7 | 1287.5 | 1248.3 | 1223.3 |
| 6300 | 1382.8 | 1381.4 | 1366.7 | 1340.8 | 1306.2 | 1266.4 | 1241.1 |
| 6400 | 1402.4 | 1400.9 | 1386.0 | 1359.8 | 1324.7 | 1284.5 | 1258.9 |
| 6500 | 1421.9 | 1420.4 | 1405.3 | 1378.8 | 1343.3 | 1302.5 | 1276.6 |
| 6600 | 1441.4 | 1439.9 | 1424.6 | 1397.8 | 1361.9 | 1320.6 | 1294.3 |

 z_b

| | | | | | | | |
|------|--------|--------|--------|--------|--------|--------|--------|
| 6700 | 1460.9 | 1459.4 | 1443.9 | 1416.7 | 1380.4 | 1338.6 | 1312.0 |
| 6800 | 1480.3 | 1478.8 | 1463.1 | 1435.6 | 1398.9 | 1356.6 | 1329.7 |
| 6900 | 1499.7 | 1498.2 | 1482.4 | 1454.5 | 1417.3 | 1374.5 | 1347.4 |
| 7000 | 1519.1 | 1517.5 | 1501.5 | 1473.4 | 1435.8 | 1392.5 | 1365.0 |
| 7100 | 1538.5 | 1536.9 | 1520.7 | 1492.3 | 1454.2 | 1410.4 | 1382.6 |
| 7200 | 1557.8 | 1556.2 | 1539.8 | 1511.1 | 1472.6 | 1428.3 | 1400.2 |
| 7300 | 1577.1 | 1575.5 | 1559.0 | 1529.9 | 1491.0 | 1446.2 | 1417.8 |
| 7400 | 1596.4 | 1594.8 | 1578.1 | 1548.6 | 1509.3 | 1464.1 | 1435.3 |
| 7500 | 1615.7 | 1614.0 | 1597.1 | 1567.4 | 1527.6 | 1481.9 | 1452.8 |
| 7600 | 1634.9 | 1633.2 | 1616.2 | 1586.1 | 1545.9 | 1499.7 | 1470.3 |
| 7700 | 1654.1 | 1652.4 | 1635.2 | 1604.8 | 1564.2 | 1517.5 | 1487.8 |
| 7800 | 1673.3 | 1671.6 | 1654.2 | 1623.5 | 1582.5 | 1535.3 | 1505.3 |
| 7900 | 1692.5 | 1690.7 | 1673.1 | 1642.2 | 1600.7 | 1553.0 | 1522.7 |
| 8000 | 1711.6 | 1709.9 | 1692.1 | 1660.8 | 1619.0 | 1570.8 | 1540.1 |
| 8100 | 1730.8 | 1729.0 | 1711.0 | 1679.4 | 1637.2 | 1588.5 | 1557.6 |
| 8200 | 1749.9 | 1748.1 | 1729.9 | 1698.0 | 1655.3 | 1606.2 | 1574.9 |
| 8300 | 1768.9 | 1767.1 | 1748.8 | 1716.6 | 1673.5 | 1623.9 | 1592.3 |
| 8400 | 1788.0 | 1786.2 | 1767.7 | 1735.2 | 1691.6 | 1641.5 | 1609.7 |
| 8500 | 1807.0 | 1805.2 | 1786.5 | 1753.7 | 1709.8 | 1659.2 | 1627.0 |
| 8600 | 1826.0 | 1824.2 | 1805.4 | 1772.2 | 1727.9 | 1676.8 | 1644.3 |
| 8700 | 1845.0 | 1843.2 | 1824.2 | 1790.7 | 1746.0 | 1694.4 | 1661.6 |
| 8800 | 1864.0 | 1862.1 | 1842.9 | 1809.2 | 1764.0 | 1712.0 | 1678.9 |
| 8900 | 1883.0 | 1881.1 | 1861.7 | 1827.7 | 1782.1 | 1729.6 | 1696.2 |
| 9000 | 1901.9 | 1900.0 | 1880.5 | 1846.1 | 1800.1 | 1747.1 | 1713.4 |
| 9100 | 1920.8 | 1918.9 | 1899.2 | 1864.5 | 1818.1 | 1764.7 | 1730.7 |
| 9200 | 1939.7 | 1937.4 | 1917.9 | 1882.9 | 1836.1 | 1782.2 | 1747.9 |
| 9300 | 1958.6 | 1956.6 | 1936.6 | 1901.3 | 1854.1 | 1799.7 | 1765.1 |
| 9400 | 1977.4 | 1975.4 | 1955.2 | 1919.7 | 1872.0 | 1817.2 | 1782.3 |
| 9500 | 1996.3 | 1994.3 | 1973.9 | 1938.0 | 1890.0 | 1834.7 | 1799.4 |
| 9600 | 2015.1 | 2013.1 | 1992.5 | 1956.4 | 1907.9 | 1852.1 | 1816.6 |
| 9700 | 2033.9 | 2031.9 | 2011.1 | 1974.7 | 1925.8 | 1869.6 | 1833.7 |
| 9800 | 2052.7 | 2050.6 | 2029.7 | 1993.0 | 1943.7 | 1887.0 | 1850.9 |
| 9900 | 2071.5 | 2069.4 | 2048.3 | 2011.3 | 1961.6 | 1904.4 | 1868.0 |

(table continued on next page)

Table 10-3 (continued)

| z_b | t_b | 0.05 | 0.1 | 0.3 | 0.5 | 0.7 | 0.9 | 1.0 |
|-------|--------------------|---------------------|---------------------|---------------------|---------------------|---------------------|---------------------|---------------------|
| | 1.00×10^4 | 2.090×10^3 | 2.088×10^3 | 2.067×10^3 | 2.029×10^3 | 1.979×10^3 | 1.922×10^3 | 1.885×10^3 |
| | 1.25×10^4 | 2.553×10^3 | 2.551×10^3 | 2.526×10^3 | 2.481×10^3 | 2.421×10^3 | 2.352×10^3 | 2.308×10^3 |
| | 1.50×10^4 | 3.009×10^3 | 3.006×10^3 | 2.977×10^3 | 2.925×10^3 | 2.855×10^3 | 2.775×10^3 | 2.724×10^3 |
| | 1.75×10^4 | 3.457×10^3 | 3.454×10^3 | 3.421×10^3 | 3.362×10^3 | 3.284×10^3 | 3.193×10^3 | 3.135×10^3 |
| | 2.00×10^4 | 3.900×10^3 | 3.897×10^3 | 3.860×10^3 | 3.794×10^3 | 3.707×10^3 | 3.605×10^3 | 3.541×10^3 |
| | 2.50×10^4 | 4.773×10^3 | 4.768×10^3 | 4.724×10^3 | 4.646×10^3 | 4.541×10^3 | 4.419×10^3 | 4.341×10^3 |
| | 3.00×10^4 | 5.630×10^3 | 5.625×10^3 | 5.574×10^3 | 5.483×10^3 | 5.361×10^3 | 5.219×10^3 | 5.129×10^3 |
| | 3.50×10^4 | 6.476×10^3 | 6.470×10^3 | 6.412×10^3 | 6.309×10^3 | 6.170×10^3 | 6.009×10^3 | 5.906×10^3 |
| | 4.00×10^4 | 7.312×10^3 | 7.305×10^3 | 7.240×10^3 | 7.125×10^3 | 6.970×10^3 | 6.790×10^3 | 6.675×10^3 |
| | 4.50×10^4 | 8.139×10^3 | 8.132×10^3 | 8.060×10^3 | 7.933×10^3 | 7.762×10^3 | 7.564×10^3 | 7.437×10^3 |
| | 5.00×10^4 | 8.959×10^3 | 8.951×10^3 | 8.872×10^3 | 8.734×10^3 | 8.548×10^3 | 8.331×10^3 | 8.193×10^3 |
| | 6.00×10^4 | 1.057×10^4 | 1.057×10^4 | 1.047×10^4 | 1.031×10^4 | 1.010×10^4 | 9.846×10^3 | 9.684×10^3 |
| | 7.00×10^4 | 1.217×10^4 | 1.217×10^4 | 1.206×10^4 | 1.188×10^4 | 1.163×10^4 | 1.134×10^4 | 1.116×10^4 |
| | 8.00×10^4 | 1.375×10^4 | 1.375×10^4 | 1.363×10^4 | 1.342×10^4 | 1.315×10^4 | 1.283×10^4 | 1.262×10^4 |
| | 9.00×10^4 | 1.532×10^4 | 1.531×10^4 | 1.518×10^4 | 1.496×10^4 | 1.465×10^4 | 1.430×10^4 | 1.407×10^4 |
| | 1.00×10^5 | 1.687×10^4 | 1.686×10^4 | 1.672×10^4 | 1.647×10^4 | 1.614×10^4 | 1.576×10^4 | 1.551×10^4 |
| | 1.25×10^5 | 2.071×10^4 | 2.069×10^4 | 2.052×10^4 | 2.023×10^4 | 1.982×10^4 | 1.936×10^4 | 1.906×10^4 |
| | 1.50×10^5 | 2.448×10^4 | 2.446×10^4 | 2.427×10^4 | 2.392×10^4 | 2.345×10^4 | 2.291×10^4 | 2.256×10^4 |
| | 2.00×10^5 | 3.190×10^4 | 3.188×10^4 | 3.163×10^4 | 3.119×10^4 | 3.059×10^4 | 2.989×10^4 | 2.945×10^4 |
| | 2.50×10^5 | 3.918×10^4 | 3.916×10^4 | 3.885×10^4 | 3.832×10^4 | 3.760×10^4 | 3.676×10^4 | 3.622×10^4 |
| | 3.00×10^5 | 4.636×10^4 | 4.633×10^4 | 4.598×10^4 | 4.536×10^4 | 4.452×10^4 | 4.353×10^4 | 4.290×10^4 |
| | 4.00×10^5 | 6.048×10^4 | 6.044×10^4 | 5.999×10^4 | 5.920×10^4 | 5.812×10^4 | 5.687×10^4 | 5.606×10^4 |
| | 5.00×10^5 | 7.436×10^4 | 7.431×10^4 | 7.376×10^4 | 7.280×10^4 | 7.150×10^4 | 6.998×10^4 | 6.900×10^4 |
| | 6.00×10^5 | 8.805×10^4 | 8.798×10^4 | 8.735×10^4 | 8.623×10^4 | 8.471×10^4 | 8.293×10^4 | 8.178×10^4 |
| | 7.00×10^5 | 1.016×10^5 | 1.015×10^5 | 1.008×10^5 | 9.951×10^4 | 9.777×10^4 | 9.573×10^4 | 9.442×10^4 |
| | 8.00×10^5 | 1.150×10^5 | 1.149×10^5 | 1.141×10^5 | 1.127×10^5 | 1.107×10^5 | 1.084×10^5 | 1.070×10^5 |
| | 9.00×10^5 | 1.283×10^5 | 1.282×10^5 | 1.273×10^5 | 1.257×10^5 | 1.235×10^5 | 1.210×10^5 | 1.194×10^5 |

Water Influx

709

| | | | | | | | |
|------------------------|-------------------------|-------------------------|-------------------------|-------------------------|-------------------------|-------------------------|-------------------------|
| 1.00 x 10 ⁶ | 1.415 x 10 ⁵ | 1.412 x 10 ⁵ | 1.404 x 10 ⁵ | 1.387 x 10 ⁵ | 1.363 x 10 ⁵ | 1.335 x 10 ⁵ | 1.317 x 10 ⁵ |
| 1.50 x 10 ⁶ | 2.059 x 10 ⁵ | 2.060 x 10 ⁵ | 2.041 x 10 ⁵ | 2.016 x 10 ⁵ | 1.982 x 10 ⁵ | 1.943 x 10 ⁵ | 1.918 x 10 ⁵ |
| 2.00 x 10 ⁶ | 2.695 x 10 ⁵ | 2.695 x 10 ⁵ | 2.676 x 10 ⁵ | 2.644 x 10 ⁵ | 2.601 x 10 ⁵ | 2.551 x 10 ⁵ | 2.518 x 10 ⁵ |
| 2.50 x 10 ⁶ | 3.320 x 10 ⁵ | 3.319 x 10 ⁵ | 3.296 x 10 ⁵ | 3.254 x 10 ⁵ | 3.202 x 10 ⁵ | 3.141 x 10 ⁵ | 3.101 x 10 ⁵ |
| 3.00 x 10 ⁶ | 3.937 x 10 ⁵ | 3.936 x 10 ⁵ | 3.909 x 10 ⁵ | 3.864 x 10 ⁵ | 3.803 x 10 ⁵ | 3.731 x 10 ⁵ | 3.684 x 10 ⁵ |
| 4.00 x 10 ⁶ | 5.154 x 10 ⁵ | 5.152 x 10 ⁵ | 5.118 x 10 ⁵ | 5.060 x 10 ⁵ | 4.981 x 10 ⁵ | 4.888 x 10 ⁵ | 4.828 x 10 ⁵ |
| 5.00 x 10 ⁶ | 6.352 x 10 ⁵ | 6.349 x 10 ⁵ | 6.308 x 10 ⁵ | 6.238 x 10 ⁵ | 6.142 x 10 ⁵ | 6.029 x 10 ⁵ | 5.956 x 10 ⁵ |
| 6.00 x 10 ⁶ | 7.536 x 10 ⁵ | 7.533 x 10 ⁵ | 7.485 x 10 ⁵ | 7.402 x 10 ⁵ | 7.290 x 10 ⁵ | 7.157 x 10 ⁵ | 7.072 x 10 ⁵ |
| 7.00 x 10 ⁶ | 8.709 x 10 ⁵ | 8.705 x 10 ⁵ | 8.650 x 10 ⁵ | 8.556 x 10 ⁵ | 8.427 x 10 ⁵ | 8.275 x 10 ⁵ | 8.177 x 10 ⁵ |
| 8.00 x 10 ⁶ | 9.872 x 10 ⁵ | 9.867 x 10 ⁵ | 9.806 x 10 ⁵ | 9.699 x 10 ⁵ | 9.555 x 10 ⁵ | 9.384 x 10 ⁵ | 9.273 x 10 ⁵ |
| 9.00 x 10 ⁶ | 1.103 x 10 ⁶ | 1.102 x 10 ⁶ | 1.095 x 10 ⁶ | 1.084 x 10 ⁶ | 1.067 x 10 ⁶ | 1.049 x 10 ⁶ | 1.036 x 10 ⁶ |
| 1.00 x 10 ⁷ | 1.217 x 10 ⁶ | 1.217 x 10 ⁶ | 1.209 x 10 ⁶ | 1.196 x 10 ⁶ | 1.179 x 10 ⁶ | 1.158 x 10 ⁶ | 1.144 x 10 ⁶ |
| 1.50 x 10 ⁷ | 1.782 x 10 ⁶ | 1.781 x 10 ⁶ | 1.771 x 10 ⁶ | 1.752 x 10 ⁶ | 1.727 x 10 ⁶ | 1.697 x 10 ⁶ | 1.678 x 10 ⁶ |
| 2.00 x 10 ⁷ | 2.337 x 10 ⁶ | 2.336 x 10 ⁶ | 2.322 x 10 ⁶ | 2.298 x 10 ⁶ | 2.266 x 10 ⁶ | 2.227 x 10 ⁶ | 2.202 x 10 ⁶ |
| 2.50 x 10 ⁷ | 2.884 x 10 ⁶ | 2.882 x 10 ⁶ | 2.866 x 10 ⁶ | 2.837 x 10 ⁶ | 2.797 x 10 ⁶ | 2.750 x 10 ⁶ | 2.720 x 10 ⁶ |
| 3.00 x 10 ⁷ | 3.425 x 10 ⁶ | 3.423 x 10 ⁶ | 3.404 x 10 ⁶ | 3.369 x 10 ⁶ | 3.323 x 10 ⁶ | 3.268 x 10 ⁶ | 3.232 x 10 ⁶ |
| 4.00 x 10 ⁷ | 4.493 x 10 ⁶ | 4.491 x 10 ⁶ | 4.466 x 10 ⁶ | 4.422 x 10 ⁶ | 4.361 x 10 ⁶ | 4.290 x 10 ⁶ | 4.244 x 10 ⁶ |
| 5.00 x 10 ⁷ | 5.547 x 10 ⁶ | 5.544 x 10 ⁶ | 5.514 x 10 ⁶ | 5.460 x 10 ⁶ | 5.386 x 10 ⁶ | 5.299 x 10 ⁶ | 5.243 x 10 ⁶ |
| 6.00 x 10 ⁷ | 6.590 x 10 ⁶ | 6.587 x 10 ⁶ | 6.551 x 10 ⁶ | 6.488 x 10 ⁶ | 6.401 x 10 ⁶ | 6.299 x 10 ⁶ | 6.232 x 10 ⁶ |
| 7.00 x 10 ⁷ | 7.624 x 10 ⁶ | 7.620 x 10 ⁶ | 7.579 x 10 ⁶ | 7.507 x 10 ⁶ | 7.407 x 10 ⁶ | 7.290 x 10 ⁶ | 7.213 x 10 ⁶ |
| 8.00 x 10 ⁷ | 8.651 x 10 ⁶ | 8.647 x 10 ⁶ | 8.600 x 10 ⁶ | 8.519 x 10 ⁶ | 8.407 x 10 ⁶ | 8.274 x 10 ⁶ | 8.188 x 10 ⁶ |
| 9.00 x 10 ⁷ | 9.671 x 10 ⁶ | 9.666 x 10 ⁶ | 9.615 x 10 ⁶ | 9.524 x 10 ⁶ | 9.400 x 10 ⁶ | 9.252 x 10 ⁶ | 9.156 x 10 ⁶ |
| 1.00 x 10 ⁸ | 1.069 x 10 ⁷ | 1.067 x 10 ⁷ | 1.062 x 10 ⁷ | 1.052 x 10 ⁷ | 1.039 x 10 ⁷ | 1.023 x 10 ⁷ | 1.012 x 10 ⁷ |
| 1.50 x 10 ⁸ | 1.567 x 10 ⁷ | 1.567 x 10 ⁷ | 1.555 x 10 ⁷ | 1.541 x 10 ⁷ | 1.522 x 10 ⁷ | 1.499 x 10 ⁷ | 1.483 x 10 ⁷ |
| 2.00 x 10 ⁸ | 2.059 x 10 ⁷ | 2.059 x 10 ⁷ | 2.048 x 10 ⁷ | 2.029 x 10 ⁷ | 2.004 x 10 ⁷ | 1.974 x 10 ⁷ | 1.954 x 10 ⁷ |
| 2.50 x 10 ⁸ | 2.546 x 10 ⁷ | 2.545 x 10 ⁷ | 2.531 x 10 ⁷ | 2.507 x 10 ⁷ | 2.476 x 10 ⁷ | 2.439 x 10 ⁷ | 2.415 x 10 ⁷ |
| 3.00 x 10 ⁸ | 3.027 x 10 ⁷ | 3.026 x 10 ⁷ | 3.010 x 10 ⁷ | 2.984 x 10 ⁷ | 2.947 x 10 ⁷ | 2.904 x 10 ⁷ | 2.875 x 10 ⁷ |
| 4.00 x 10 ⁸ | 3.929 x 10 ⁷ | 3.928 x 10 ⁷ | 3.958 x 10 ⁷ | 3.923 x 10 ⁷ | 3.875 x 10 ⁷ | 3.819 x 10 ⁷ | 3.782 x 10 ⁷ |
| 5.00 x 10 ⁸ | 4.920 x 10 ⁷ | 4.918 x 10 ⁷ | 4.894 x 10 ⁷ | 4.851 x 10 ⁷ | 4.793 x 10 ⁷ | 4.724 x 10 ⁷ | 4.679 x 10 ⁷ |
| 6.00 x 10 ⁸ | 5.852 x 10 ⁷ | 5.850 x 10 ⁷ | 5.821 x 10 ⁷ | 5.771 x 10 ⁷ | 5.702 x 10 ⁷ | 5.621 x 10 ⁷ | 5.568 x 10 ⁷ |

(table continued on next page)

Table 10-3 (continued)

| t_b | 0.05 | 0.1 | 0.3 | 0.5 | 0.7 | 0.9 | 1.0 |
|-----------------------|---------------------|---------------------|---------------------|---------------------|---------------------|---------------------|---------------------|
| 7.00×10^8 | 6.777×10^7 | 6.774×10^7 | 6.741×10^7 | 6.684×10^7 | 6.605×10^7 | 6.511×10^7 | 6.450×10^7 |
| 8.00×10^8 | 7.700×10^7 | 7.693×10^7 | 7.655×10^7 | 7.590×10^7 | 7.501×10^7 | 7.396×10^7 | 7.327×10^7 |
| 9.00×10^8 | 8.609×10^7 | 8.606×10^7 | 8.564×10^7 | 8.492×10^7 | 8.393×10^7 | 8.275×10^7 | 8.199×10^7 |
| 1.00×10^9 | 9.518×10^7 | 9.515×10^7 | 9.469×10^7 | 9.390×10^7 | 9.281×10^7 | 9.151×10^7 | 9.065×10^7 |
| 1.50×10^9 | 1.401×10^8 | 1.400×10^8 | 1.394×10^8 | 1.382×10^8 | 1.367×10^8 | 1.348×10^8 | 1.336×10^8 |
| 2.00×10^9 | 1.843×10^8 | 1.843×10^8 | 1.834×10^8 | 1.819×10^8 | 1.799×10^8 | 1.774×10^8 | 1.758×10^8 |
| 2.50×10^9 | 2.281×10^8 | 2.280×10^8 | 2.269×10^8 | 2.251×10^8 | 2.226×10^8 | 2.196×10^8 | 2.177×10^8 |
| 3.00×10^9 | 2.714×10^8 | 2.713×10^8 | 2.701×10^8 | 2.680×10^8 | 2.650×10^8 | 2.615×10^8 | 2.592×10^8 |
| 4.00×10^9 | 3.573×10^8 | 3.572×10^8 | 3.556×10^8 | 3.528×10^8 | 3.489×10^8 | 3.443×10^8 | 3.413×10^8 |
| 5.00×10^9 | 4.422×10^8 | 4.421×10^8 | 4.401×10^8 | 4.367×10^8 | 4.320×10^8 | 4.263×10^8 | 4.227×10^8 |
| 6.00×10^9 | 5.265×10^8 | 5.262×10^8 | 5.240×10^8 | 5.199×10^8 | 5.143×10^8 | 5.077×10^8 | 5.033×10^8 |
| 7.00×10^9 | 6.101×10^8 | 6.098×10^8 | 6.072×10^8 | 6.025×10^8 | 5.961×10^8 | 5.885×10^8 | 5.835×10^8 |
| 8.00×10^9 | 6.932×10^8 | 6.930×10^8 | 6.900×10^8 | 6.847×10^8 | 6.775×10^8 | 6.688×10^8 | 6.632×10^8 |
| 9.00×10^9 | 7.760×10^8 | 7.756×10^8 | 7.723×10^8 | 7.664×10^8 | 7.584×10^8 | 7.487×10^8 | 7.424×10^8 |
| 1.00×10^{10} | 8.583×10^8 | 8.574×10^8 | 8.543×10^8 | 8.478×10^8 | 8.389×10^8 | 8.283×10^8 | 8.214×10^8 |
| 1.50×10^{10} | 1.263×10^9 | 1.264×10^9 | 1.257×10^9 | 1.247×10^9 | 1.235×10^9 | 1.219×10^9 | 1.209×10^9 |
| 2.00×10^{10} | 1.666×10^9 | 1.666×10^9 | 1.659×10^9 | 1.646×10^9 | 1.630×10^9 | 1.610×10^9 | 1.596×10^9 |
| 2.50×10^{10} | 2.065×10^9 | 2.063×10^9 | 2.055×10^9 | 2.038×10^9 | 2.018×10^9 | 1.993×10^9 | 1.977×10^9 |
| 3.00×10^{10} | 2.458×10^9 | 2.458×10^9 | 2.447×10^9 | 2.430×10^9 | 2.405×10^9 | 2.376×10^9 | 2.357×10^9 |
| 4.00×10^{10} | 3.240×10^9 | 3.239×10^9 | 3.226×10^9 | 3.203×10^9 | 3.171×10^9 | 3.133×10^9 | 3.108×10^9 |

| | | | | | | |
|-----------------------|------------------------|------------------------|------------------------|------------------------|------------------------|------------------------|
| 5.00×10^{10} | 4.014×10^9 | 3.997×10^9 | 3.965×10^9 | 3.929×10^9 | 3.883×10^9 | 3.852×10^9 |
| 6.00×10^{10} | 4.782×10^9 | 4.762×10^9 | 4.728×10^9 | 4.682×10^9 | 4.627×10^9 | 4.591×10^9 |
| 7.00×10^{10} | 5.546×10^9 | 5.522×10^9 | 5.483×10^9 | 5.430×10^9 | 5.366×10^9 | 5.325×10^9 |
| 8.00×10^{10} | 6.305×10^9 | 6.278×10^9 | 6.234×10^9 | 6.174×10^9 | 6.102×10^9 | 6.055×10^9 |
| 9.00×10^{10} | 7.060×10^9 | 7.030×10^9 | 6.982×10^9 | 6.914×10^9 | 6.834×10^9 | 6.782×10^9 |
| 1.00×10^{11} | 7.813×10^9 | 7.780×10^9 | 7.726×10^9 | 7.652×10^9 | 7.564×10^9 | 7.506×10^9 |
| 1.50×10^{11} | 1.154×10^{10} | 1.149×10^{10} | 1.141×10^{10} | 1.130×10^{10} | 1.118×10^{10} | 1.109×10^{10} |
| 2.00×10^{11} | 1.522×10^{10} | 1.515×10^{10} | 1.505×10^{10} | 1.491×10^{10} | 1.474×10^{10} | 1.463×10^{10} |
| 2.50×10^{11} | 1.886×10^{10} | 1.878×10^{10} | 1.866×10^{10} | 1.849×10^{10} | 1.828×10^{10} | 1.814×10^{10} |
| 3.00×10^{11} | 2.248×10^{10} | 2.239×10^{10} | 2.224×10^{10} | 2.204×10^{10} | 2.179×10^{10} | 2.163×10^{10} |
| 4.00×10^{11} | 2.965×10^{10} | 2.953×10^{10} | 2.934×10^{10} | 2.907×10^{10} | 2.876×10^{10} | 2.855×10^{10} |
| 5.00×10^{11} | 3.677×10^{10} | 3.662×10^{10} | 3.638×10^{10} | 3.605×10^{10} | 3.566×10^{10} | 3.540×10^{10} |
| 6.00×10^{11} | 4.383×10^{10} | 4.365×10^{10} | 4.337×10^{10} | 4.298×10^{10} | 4.252×10^{10} | 4.221×10^{10} |
| 7.00×10^{11} | 5.085×10^{10} | 5.064×10^{10} | 5.032×10^{10} | 4.987×10^{10} | 4.933×10^{10} | 4.898×10^{10} |
| 8.00×10^{11} | 5.783×10^{10} | 5.760×10^{10} | 5.723×10^{10} | 5.673×10^{10} | 5.612×10^{10} | 5.572×10^{10} |
| 9.00×10^{11} | 6.478×10^{10} | 6.453×10^{10} | 6.412×10^{10} | 6.355×10^{10} | 6.288×10^{10} | 6.243×10^{10} |
| 1.00×10^{12} | 7.171×10^{10} | 7.143×10^{10} | 7.098×10^{10} | 7.035×10^{10} | 6.961×10^{10} | 6.912×10^{10} |
| 1.50×10^{12} | 1.060×10^{11} | 1.056×10^{11} | 1.050×10^{11} | 1.041×10^{11} | 1.030×10^{11} | 1.022×10^{11} |
| 2.00×10^{12} | 1.400×10^{11} | 1.394×10^{11} | 1.386×10^{11} | 1.374×10^{11} | 1.359×10^{11} | 1.350×10^{11} |

Table 10-7
Dimensionless Water Influx, W_{eD} , for $r_D = 10$
(Permission to publish by the SPE)

| t_D | z_D' | | | | | | |
|-------|--------|-------|-------|-------|-------|-------|-------|
| | 0.05 | 0.1 | 0.3 | 0.5 | 0.7 | 0.9 | 1.0 |
| 22 | 12.07 | 12.04 | 11.74 | 11.21 | 10.56 | 9.865 | 9.449 |
| 24 | 12.86 | 12.83 | 12.52 | 11.97 | 11.29 | 10.55 | 10.12 |
| 26 | 13.65 | 13.62 | 13.29 | 12.72 | 12.01 | 11.24 | 10.78 |
| 28 | 14.42 | 14.39 | 14.04 | 13.44 | 12.70 | 11.90 | 11.42 |
| 30 | 15.17 | 15.13 | 14.77 | 14.15 | 13.38 | 12.55 | 12.05 |
| 32 | 15.91 | 15.87 | 15.49 | 14.85 | 14.05 | 13.18 | 12.67 |
| 34 | 16.63 | 16.59 | 16.20 | 15.54 | 14.71 | 13.81 | 13.28 |
| 36 | 17.33 | 17.29 | 16.89 | 16.21 | 15.35 | 14.42 | 13.87 |
| 38 | 18.03 | 17.99 | 17.57 | 16.86 | 15.98 | 15.02 | 14.45 |
| 40 | 18.72 | 18.68 | 18.24 | 17.51 | 16.60 | 15.61 | 15.02 |
| 42 | 19.38 | 19.33 | 18.89 | 18.14 | 17.21 | 16.19 | 15.58 |
| 44 | 20.03 | 19.99 | 19.53 | 18.76 | 17.80 | 16.75 | 16.14 |
| 46 | 20.67 | 20.62 | 20.15 | 19.36 | 18.38 | 17.30 | 16.67 |
| 48 | 21.30 | 21.25 | 20.76 | 19.95 | 18.95 | 17.84 | 17.20 |
| 50 | 21.92 | 21.87 | 21.36 | 20.53 | 19.51 | 18.38 | 17.72 |
| 52 | 22.52 | 22.47 | 21.95 | 21.10 | 20.05 | 18.89 | 18.22 |
| 54 | 23.11 | 23.06 | 22.53 | 21.66 | 20.59 | 19.40 | 18.72 |
| 56 | 23.70 | 23.64 | 23.09 | 22.20 | 21.11 | 19.89 | 19.21 |
| 58 | 24.26 | 24.21 | 23.65 | 22.74 | 21.63 | 20.39 | 19.68 |
| 60 | 24.82 | 24.77 | 24.19 | 23.26 | 22.13 | 20.87 | 20.15 |
| 65 | 26.18 | 26.12 | 25.50 | 24.53 | 23.34 | 22.02 | 21.28 |
| 70 | 27.47 | 27.41 | 26.75 | 25.73 | 24.50 | 23.12 | 22.36 |
| 75 | 28.71 | 28.55 | 27.94 | 26.88 | 25.60 | 24.17 | 23.39 |
| 80 | 29.89 | 29.82 | 29.08 | 27.97 | 26.65 | 25.16 | 24.36 |
| 85 | 31.02 | 30.95 | 30.17 | 29.01 | 27.65 | 26.10 | 25.31 |
| 90 | 32.10 | 32.03 | 31.20 | 30.00 | 28.60 | 27.03 | 26.25 |
| 95 | 33.04 | 32.96 | 32.14 | 30.95 | 29.54 | 27.93 | 27.10 |
| 100 | 33.94 | 33.85 | 33.03 | 31.85 | 30.44 | 28.82 | 27.98 |
| 110 | 35.55 | 35.46 | 34.65 | 33.49 | 32.08 | 30.47 | 29.62 |
| 120 | 36.97 | 36.90 | 36.11 | 34.98 | 33.58 | 31.98 | 31.14 |
| 130 | 38.28 | 38.19 | 37.44 | 36.33 | 34.96 | 33.38 | 32.55 |
| 140 | 39.44 | 39.37 | 38.64 | 37.56 | 36.23 | 34.67 | 33.85 |
| 150 | 40.49 | 40.42 | 39.71 | 38.67 | 37.38 | 35.86 | 35.04 |
| 170 | 42.21 | 42.15 | 41.51 | 40.54 | 39.33 | 37.89 | 37.11 |
| 190 | 43.62 | 43.55 | 42.98 | 42.10 | 40.97 | 39.62 | 38.90 |
| 210 | 44.77 | 44.72 | 44.19 | 43.40 | 42.36 | 41.11 | 40.42 |
| 230 | 45.71 | 45.67 | 45.20 | 44.48 | 43.54 | 42.38 | 41.74 |
| 250 | 46.48 | 46.44 | 46.01 | 45.38 | 44.53 | 43.47 | 42.87 |
| 270 | 47.11 | 47.06 | 46.70 | 46.13 | 45.36 | 44.40 | 43.84 |
| 290 | 47.61 | 47.58 | 47.25 | 46.75 | 46.07 | 45.19 | 44.68 |

(table continued on next page)

Table 10-7 (continued)

| t_D | z'_D | | | | | | |
|-------|--------|-------|-------|-------|-------|-------|-------|
| | 0.05 | 0.1 | 0.3 | 0.5 | 0.7 | 0.9 | 1.0 |
| 310 | 48.03 | 48.00 | 47.72 | 47.26 | 46.66 | 45.87 | 45.41 |
| 330 | 48.38 | 48.35 | 48.10 | 47.71 | 47.16 | 46.45 | 46.03 |
| 350 | 48.66 | 48.64 | 48.42 | 48.08 | 47.59 | 46.95 | 46.57 |
| 400 | 49.15 | 49.14 | 48.99 | 48.74 | 48.38 | 47.89 | 47.60 |
| 450 | 49.46 | 49.45 | 49.35 | 49.17 | 48.91 | 48.55 | 48.31 |
| 500 | 49.65 | 49.64 | 49.58 | 49.45 | 49.26 | 48.98 | 48.82 |
| 600 | 49.84 | 49.84 | 49.81 | 49.74 | 49.65 | 49.50 | 49.41 |
| 700 | 49.91 | 49.91 | 49.90 | 49.87 | 49.82 | 49.74 | 49.69 |
| 800 | 49.94 | 49.94 | 49.93 | 49.92 | 49.90 | 49.85 | 49.83 |
| 900 | 49.96 | 49.96 | 49.94 | 49.94 | 49.93 | 49.91 | 49.90 |
| 1000 | 49.96 | 49.96 | 49.96 | 49.96 | 49.94 | 49.93 | 49.93 |
| 1200 | 49.96 | 49.96 | 49.96 | 49.96 | 49.96 | 49.96 | 49.96 |

(text continued from page 693)

Example 10-8

An infinite-acting bottom-water aquifer is characterized by the following properties:

$$r_a = \infty$$

$$\phi = 0.1$$

$$h = 200'$$

$$k_h = 50 \text{ md}$$

$$\mu_w = 0.395 \text{ cp}$$

$$r_e = 2000'$$

$$F_k = 0.04$$

$$c_t = 8 \times 10^{-6} \text{ psi}^{-1}$$

$$\theta = 360^\circ$$

The boundary pressure history is given below:

| Time, days | p, psi |
|------------|--------|
| 0 | 3000 |
| 30 | 2956 |
| 60 | 2917 |
| 90 | 2877 |
| 120 | 2844 |
| 150 | 2811 |
| 180 | 2791 |
| 210 | 2773 |
| 240 | 2755 |

Calculate the cumulative water influx as a function of time by using the bottom-water-drive solution and compare with the edge-water-drive approach.

Solution

Step 1. For an infinite-acting aquifer:

$$r_D = \infty$$

Step 2. Calculate z_D from Equation 10-30.

$$z_D = \frac{200}{2000\sqrt{0.04}} = 0.5$$

Step 3. Calculate the water influx constant B.

$$B = 1.119 (0.1) (200) (8 \times 10^{-6}) (2000)^2 = 716 \text{ bbl/psi}$$

Step 4. Calculate the dimensionless time t_D .

$$t_D = 6.328 \times 10^{-3} \left[\frac{50}{(0.1) (0.395) (8 \times 10^{-6}) (2000)^2} \right] t$$

$$t_D = 0.2503 t$$

Step 5. Calculate the water influx.

| t days | t_D | Δp psi | Bottom-Water Model | | Edge-Water Model | |
|-----------|-------|-------------------|--------------------|-----------------------|------------------|-----------------------|
| | | | W_{eD} | $W_{e'} \text{ Mbbl}$ | W_{eD} | $W_{e'} \text{ Mbbl}$ |
| 0 | 0 | 0 | — | — | — | — |
| 30 | 7.5 | 22 | 5.038 | 79 | 6.029 | 95 |
| 60 | 15.0 | 41.5 | 8.389 | 282 | 9.949 | 336 |
| 90 | 22.5 | 39.5 | 11.414 | 572 | 13.459 | 678 |
| 120 | 30.0 | 36.5 | 14.994 | 933 | 16.472 | 1103 |
| 150 | 37.5 | 33.0 | 16.994 | 1353 | 19.876 | 1594 |
| 180 | 45.0 | 26.5 | 19.641 | 1810 | 22.897 | 2126 |
| 210 | 52.5 | 19.0 | 22.214 | 2284 | 25.827 | 2676 |
| 240 | 60.0 | 18.0 | 24.728 | 2782 | 28.691 | 3250 |

The Carter-Tracy Water Influx Model

Van Everdingen-Hurst methodology provides the exact solution to the radial diffusivity equation and therefore is considered the correct technique for calculating water influx. However, because superposition of solutions is required, their method involves tedious calculations. To reduce the complexity of water influx calculations, Carter and Tracy (1960) proposed a calculation technique that does not require superposition and allows direct calculation of water influx.

The primary difference between the Carter-Tracy technique and the van Everdingen-Hurst technique is that the Carter-Tracy technique assumes constant water influx rates over each finite time interval. Using the Carter-Tracy technique, the cumulative water influx at any time, t_n , can be calculated directly from the previous value obtained at t_{n-1} , or:

$$(W_e)_n = (W_e)_{n-1} + [(t_D)_n - (t_D)_{n-1}] \left[\frac{B \Delta p_n - (W_e)_{n-1} (p'_D)_n}{(p_D)_n - (t_D)_{n-1} (p'_D)_n} \right] \quad (10-34)$$

where B = the van Everdingen-Hurst water influx constant as defined by Equation 10-23

t_D = the dimensionless time as defined by Equation 10-17

n = refers to the *current* time step

$n - 1$ = refers to the *previous* time step

Δp_n = total pressure drop, $p_i - p_n$, psi

p_D = dimensionless pressure

p'_D = dimensionless pressure derivative

Values of the dimensionless pressure p_D as a function of t_D and r_D are tabulated in Chapter 6, Table 6-2. In addition to the curve-fit equations given in Chapter 6 (Equations 6-91 through 6-96), Edwardson and co-authors (1962) developed the following approximation of p_D for an infinite-acting aquifer.

$$p_D = \frac{370.529\sqrt{t_D} + 137.582t_D + 5.69549(t_D)^{1.5}}{328.834 + 265.488\sqrt{t_D} + 45.2157t_D + (t_D)^{1.5}} \quad (10-35)$$

The dimensionless pressure derivative can then be approximated by

$$p'_D = \frac{E}{F} \quad (10-36)$$

$$\begin{aligned} \text{where } E &= 716.441 + 46.7984 (t_D)^{0.5} + 270.038 t_D + 71.0098 (t_D)^{1.5} \\ F &= 1296.86 (t_D)^{0.5} + 1204.73 t_D + 618.618 (t_D)^{1.5} \\ &\quad + 538.072 (t_D)^2 + 142.41 (t_D)^{2.5} \end{aligned}$$

The following approximation could also be used between $t_D > 100$:

$$p_D = 0.5 [\ln (t_D) + 0.80907]$$

with the derivative as given by:

$$p'_D = 1/(2t_D)$$

It should be noted that the Carter-Tracy method is not an exact solution to the diffusivity equation and should be considered an approximation.

Example 10-9

Rework Example 10-7 by using the Carter-Tracy method.

Solution

Example 10-7 shows the following preliminary results:

- Water influx constant $B = 20.4$ bbl/psi
- $t_D = 0.9888$ t

Step 1. For each time step n , calculate the *total* pressure drop $\Delta p_n = p_i - p_n$ and the corresponding t_D

| N | t, days | p_n | Δp_n | t_D |
|---|---------|-------|--------------|-------|
| 0 | 0 | 2500 | 0 | 0 |
| 1 | 182.5 | 2490 | 10 | 180.5 |
| 2 | 365.0 | 2472 | 28 | 361.0 |
| 3 | 547.5 | 2444 | 56 | 541.5 |
| 4 | 730.0 | 2408 | 92 | 722.0 |

Step 2. Since values of t_D are greater than 100, use Equation 6-92 to calculate p_D and its derivative p'_D , i.e.,

$$p_D = 0.5 [\ln (t_D) + 0.80907]$$

$$p'_D = 1/(2 t_D)$$

| N | t | t _D | p _D | p _D ' |
|---|-------|----------------|----------------|------------------------|
| 0 | 0 | 0 | — | — |
| 1 | 182.5 | 180.5 | 3.002 | 2.770×10^{-3} |
| 2 | 365 | 361.0 | 3.349 | 1.385×10^{-3} |
| 3 | 547.5 | 541.5 | 3.552 | 0.923×10^{-3} |
| 4 | 730.0 | 722.0 | 3.696 | 0.693×10^{-3} |

Step 3. Calculate cumulative water influx by applying Equation 10-33.

• **W_e after 182.5 days:**

$$W_e = 0 + [180.5 - 0] \left[\frac{(20.4)(10) - (0)(2.77 \times 10^{-3})}{3.002 - (0)(2.77 \times 10^{-3})} \right]$$

$$W_e = 12,266 \text{ bbl}$$

• **W_e after 365 days:**

$$W_e = 12,266 + [361 - 180.5] \left[\frac{(20.4)(28) - (12,266)(1.385 \times 10^{-3})}{3.349 - (180.5)(1.385 \times 10^{-3})} \right]$$

$$= 42,546 \text{ bbl}$$

• **W_e after 547.5 days:**

$$W_e = 42,546 + [541.5 - 361] \left[\frac{(20.4)(56) - (42,546)(0.923 \times 10^{-3})}{3.552 - (361)(0.923 \times 10^{-3})} \right]$$

$$W_e = 104,406$$

• **W_e after 720 days:**

$$W_e = 104,406 + [722 - 541.5] \left[\frac{(20.4)(92) - (104,406)(0.693 \times 10^{-3})}{3.696 - (541.5)(0.693 \times 10^{-3})} \right]$$

$$W_e = 202,477 \text{ bbl}$$

The following table compares results of the Carter-Tracy water influx calculations with those of the van Everdingen-Hurst method.

| Time, month | Carter-Tracy W_{er} bbl | Van Everdingen-Hurst W_{er} bbl |
|-------------|------------------------------|--------------------------------------|
| 0 | 0 | 0 |
| 6 | 12,266 | 7080 |
| 12 | 42,546 | 32,435 |
| 18 | 104,400 | 85,277 |
| 24 | 202,477 | 175,522 |

The above comparison indicates that the Carter-Tracy method considerably overestimates the water influx. This is due, however, to the fact that a large time-step of 6 months was used in the Carter-Tracy method to determine the water influx. Accuracy of the Carter-Tracy method can be increased substantially by restricting the time step used in performing the water influx calculations to less than 30 days, i.e. $\Delta t = 30$ days. Recalculating the water influx on a monthly basis produces an excellent match with the van Everdingen-Hurst method as shown below.

| Time months | Time days | p psi | Dp psi | t_D | p_D | p_D' | Carter- Tracy | van Everdingen- Hurst |
|----------------|--------------|------------|-------------|---------|-------|---------|------------------|--------------------------|
| | | | | | | | W_e bbl | W_e bbl |
| 0 | 0 | 2500.0 | 0.00 | 0 | 0.00 | 0 | 0.0 | 0 |
| 1 | 30 | 2498.9 | 1.06 | 30.0892 | 2.11 | 0.01661 | 308.8 | |
| 2 | 61 | 2497.7 | 2.31 | 60.1784 | 2.45 | 0.00831 | 918.3 | |
| 3 | 91 | 2496.2 | 3.81 | 90.2676 | 2.66 | 0.00554 | 1860.3 | |
| 4 | 122 | 2494.4 | 5.56 | 120.357 | 2.80 | 0.00415 | 3171.7 | |
| 5 | 152 | 2492.4 | 7.55 | 150.446 | 2.91 | 0.00332 | 4891.2 | |
| 6 | 183 | 2490.2 | 9.79 | 180.535 | 3.00 | 0.00277 | 7057.3 | 7088.9 |
| 7 | 213 | 2487.7 | 12.27 | 210.624 | 3.08 | 0.00237 | 9709.0 | |
| 8 | 243 | 2485.0 | 15.00 | 240.713 | 3.15 | 0.00208 | 12,884.7 | |
| 9 | 274 | 2482.0 | 17.98 | 270.802 | 3.21 | 0.00185 | 16,622.8 | |
| 10 | 304 | 2478.8 | 21.20 | 300.891 | 3.26 | 0.00166 | 20,961.5 | |
| 11 | 335 | 2475.3 | 24.67 | 330.981 | 3.31 | 0.00151 | 25,938.5 | |
| 12 | 365 | 2471.6 | 28.38 | 361.070 | 3.35 | 0.00139 | 31,591.5 | 32,438.0 |
| 13 | 396 | 2467.7 | 32.34 | 391.159 | 3.39 | 0.00128 | 37,957.8 | |
| 14 | 426 | 2463.5 | 36.55 | 421.248 | 3.43 | 0.00119 | 45,074.5 | |
| 15 | 456 | 2459.0 | 41.00 | 451.337 | 3.46 | 0.00111 | 52,978.6 | |
| 16 | 487 | 2454.3 | 45.70 | 481.426 | 3.49 | 0.00104 | 61,706.7 | |
| 17 | 517 | 2449.4 | 50.64 | 511.516 | 3.52 | 0.00098 | 71,295.3 | |
| 18 | 547 | 2444.3 | 55.74 | 541.071 | 3.55 | 0.00092 | 81,578.8 | 85,552.0 |
| 19 | 578 | 2438.8 | 61.16 | 571.130 | 3.58 | 0.00088 | 92,968.2 | |
| 20 | 608 | 2433.2 | 66.84 | 601.190 | 3.60 | 0.00083 | 105,323 | |
| 21 | 638 | 2427.2 | 72.75 | 631.249 | 3.63 | 0.00079 | 118,681 | |
| 22 | 669 | 2421.1 | 78.92 | 661.309 | 3.65 | 0.00076 | 133,076 | |
| 23 | 699 | 2414.7 | 85.32 | 691.369 | 3.67 | 0.00072 | 148,544 | |
| 24 | 730 | 2408.0 | 91.98 | 721.428 | 3.70 | 0.00069 | 165,119 | 175,414.0 |

Fetkovich's Method

Fetkovich (1971) developed a method of describing the approximate water influx behavior of a finite aquifer for radial and linear geometries. In many cases, the results of this model closely match those determined using the van Everdingen-Hurst approach. The Fetkovich theory is much simpler, and, like the Carter-Tracy technique, this method does not require the use of superposition. Hence, the application is much easier, and this method is also often utilized in numerical simulation models.

Fetkovich's model is based on the premise that the productivity index concept will adequately describe water influx from a finite aquifer into a hydrocarbon reservoir. That is, the water influx rate is directly proportional to the pressure drop between the average aquifer pressure and the pressure at the reservoir-aquifer boundary. The method neglects the effects of any transient period. Thus, in cases where pressures are changing rapidly at the aquifer/reservoir interface, predicted results may differ somewhat from the more rigorous van Everdingen-Hurst or Carter-Tracy approaches. In many cases, however, pressure changes at the waterfront are gradual and this method offers an excellent approximation to the two methods discussed above.

This approach begins with two simple equations. The first is the productivity index (PI) equation for the aquifer, which is analogous to the PI equation used to describe an oil or gas well:

$$e_w = \frac{dW_e}{dt} = J(\bar{p}_a - p_r) \quad (10-37)$$

where e_w = water influx rate from aquifer, bbl/day

J = productivity index for the aquifer, bbl/day/psi

\bar{p}_a = average aquifer pressure, psi

p_r = inner aquifer boundary pressure, psi

The second equation is an aquifer material balance equation for a constant compressibility, which states that the amount of pressure depletion in the aquifer is directly proportional to the amount of water influx from the aquifer, or:

$$W_e = c_t W_i (p_i - \bar{p}_a) f \quad (10-38)$$

where W_i = initial volume of water in the aquifer, bbl

c_t = total aquifer compressibility, $c_w + c_f$, psi^{-1}

p_i = initial pressure of the aquifer, psi

$f = \theta/360$

Equation 10-37 suggests that the maximum possible water influx occurs if $p_a = 0$, or:

$$W_{ei} = c_t W_i p_i f \quad (10-39)$$

Combining Equation 10-38 with 10-37 gives:

$$\bar{p}_a = p_i \left(1 - \frac{W_e}{c_t W_i p_i} \right) = p_i \left(1 - \frac{W_e}{W_{ei}} \right) \quad (10-40)$$

Equation 10-37 provides a simple expression to determine the average aquifer pressure \bar{p}_a after removing W_e bbl of water from the aquifer to the reservoir, i.e., cumulative water influx.

Differentiating Equation 10-39 with respect to time gives:

$$\frac{dW_e}{dt} = - \frac{W_{ei}}{p_i} \frac{d\bar{p}_a}{dt} \quad (10-41)$$

Fetkovich combined Equation 10-40 with 10-36 and integrated to give the following form:

$$W_e = \frac{W_{ei}}{p_i} (p_i - p_r) \exp\left(\frac{-J p_i t}{W_{ei}}\right) \quad (10-42)$$

where W_e = cumulative water influx, bbl

p_r = reservoir pressure, i.e., pressure at the oil- or gas-water contact

t = time, days

Equation 10-41 has no practical applications since it was derived for a constant inner boundary pressure. To use this solution in the case in which the boundary pressure is varying continuously as a function of time, the superposition technique must be applied. Rather than using superposition, Fetkovich suggested that, if the reservoir-aquifer boundary pressure history is divided into a finite number of time intervals, the incremental water influx during the n^{th} interval is:

$$(\Delta W_e)_n = \frac{W_{ei}}{p_i} [(\bar{p}_a)_{n-1} - (\bar{p}_r)_n] \left[1 - \exp\left(-\frac{J p_i \Delta t_n}{W_{ei}}\right) \right] \quad (10-43)$$

where $(\bar{p}_a)_{n-1}$ is the average aquifer pressure at the end of the previous time step. This average pressure is calculated from Equation 10-39 as:

$$(\bar{p}_a)_{n-1} = p_i \left(1 - \frac{(W_e)_{n-1}}{W_{ei}} \right) \quad (10-44)$$

The average reservoir boundary pressure $(\bar{p}_r)_n$ is estimated from:

$$(\bar{p}_r)_n = \frac{(P_r)_n + (p_r)_{n-1}}{2} \quad (10-45)$$

The productivity index J used in the calculation is a function of the geometry of the aquifer. Fetkovich calculated the productivity index from Darcy's equation for bounded aquifers. Lee and Wattenbarger (1996) pointed out that Fetkovich's method can be extended to infinite-acting aquifers by requiring that the ratio of water influx rate to pressure drop be approximately constant throughout the productive life of the reservoir. The productivity index J of the aquifer is given by the following expressions.

| Type of Outer Aquifer Boundary | J for Radial Flow, bbl/day/psi | J for Linear Flow, bbl/day/psi | Equation # |
|--------------------------------|--|---|------------|
| Finite, no flow | $J = \frac{0.00708 \text{ kh f}}{m [\ln e_D - 0.75]}$ | $J = \frac{0.003381 \text{ kwh}}{mL}$ | (10-45) |
| Finite, constant pressure | $J = \frac{0.00708 \text{ kh f}}{m [\ln (r_D)]}$ | $J = \frac{0.001127 \text{ k wh}}{mL}$ | (10-46) |
| Infinite | $J = \frac{0.00708 \text{ kh f}}{m \ln (a/r_e)}$ $a = \sqrt{0.0142 \text{ kt} / (f m c_t)}$ | $J = \frac{0.001 \text{ k wh}}{\sqrt{0.0633 \text{ kt} / (f m c_t)}}$ | (10-47) |

where w = width of the linear aquifer

L = length of the linear aquifer

r_D = dimensionless radius, r_a/r_e

k = permeability of the aquifer, md
 t = time, days
 θ = encroachment angle
 h = thickness of the aquifer
 $f = \theta/360$

The following steps describe the methodology of using Fetkovich's model in predicting the cumulative water influx.

Step 1. Calculate initial volume of water in the aquifer from:

$$W_i = \frac{\pi}{5.615} (r_a^2 - r_e^2) h \phi$$

Step 2. Calculate the maximum possible water influx W_{ei} by applying Equation 10-38, or:

$$W_{ei} = c_t W_i p_i f$$

Step 3. Calculate the productivity index J based on the boundary conditions and aquifer geometry.

Step 4. Calculate the incremental water influx $(\Delta W_e)_n$ from the aquifer during the n^{th} time interval by using Equation 10-42. For example, during the first time interval Δt_1 :

$$(\Delta W_e)_1 = \frac{W_{ei}}{p_i} [p_i - (\bar{p}_r)_1] \left[1 - \exp\left(\frac{-J p_i \Delta t_1}{W_{ei}}\right) \right]$$

with

$$(\bar{p}_r)_1 = \frac{p_i + (p_r)_1}{2}$$

For the second time interval Δt_2

$$(\Delta W_e)_2 = \frac{W_{ei}}{p_i} [(\bar{p}_a)_1 - (\bar{p}_r)_2] \left[1 - \exp\left(\frac{-J p_i \Delta t_2}{W_{ei}}\right) \right]$$

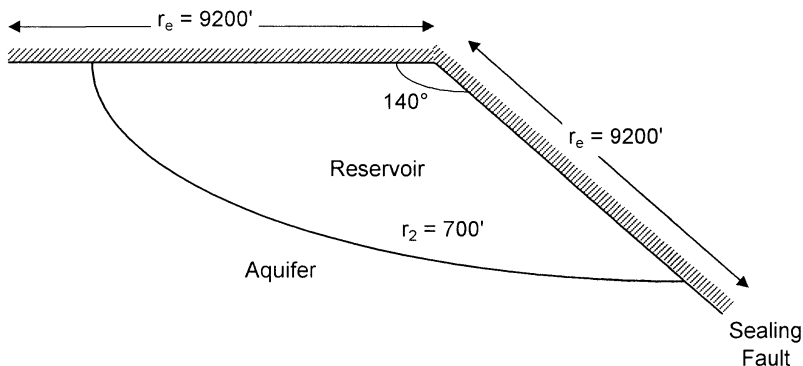


Figure 10-17. Aquifer-reservoir geometry for Example 10-10.

where $(\bar{p}_a)_1$ is the average aquifer pressure at the end of the first period and removing $(\Delta W_e)_1$ barrels of water from the aquifer to the reservoir. From Equation 10-43:

$$(\bar{p}_a)_1 = p_i \left(1 - \frac{(\Delta W_e)_1}{W_{ei}} \right)$$

Step 5. Calculate the cumulative (total) water influx at the end of any time period from:

$$W_e = \sum_{i=1}^n (\Delta W_e)_i$$

Example 10-10²

Using Fetkovich's method, calculate the water influx as a function of time for the following reservoir-aquifer and boundary pressure data:

| | | |
|-------------------------------|---------------------------------|------------------------------|
| $p_i = 2740$ psi | $h = 100'$ | $c_t = 7 \times 10^{-6}$ psi |
| $\mu_w = 0.55$ cp | $k = 200$ md | $\theta = 140^\circ$ |
| reservoir area = 40,363 acres | aquifer area = 1,000,000 acres. | |

²Data of this example are given by L. P. Dake, *Fundamentals of Reservoir Engineering*, Elsevier Publishing Company, 1978.

| Time, days | p_r , psi |
|------------|-------------|
| 0 | 2740 |
| 365 | 2500 |
| 730 | 2290 |
| 1095 | 2109 |
| 1460 | 1949 |

Figure 10-17 shows the wedge reservoir-aquifer system with an encroachment angle of 140° .

Solution

Step 1. Calculate the reservoir radius r_e :

$$r_e = \left(\frac{140}{360} \right) \sqrt{\frac{(2374)(43,560)}{\pi}} = 9200 \text{ ft}$$

Step 2. Calculate the equivalent aquifer radius r_a :

$$r_a = \left(\frac{140}{360} \right) \sqrt{\frac{(1,000,000)(43,560)}{\pi}} = 46,000 \text{ ft}$$

Step 3. Calculate the dimensionless radius r_D .

$$\begin{aligned} r_D &= r_a / r_e \\ &= 46,000 / 9200 = 5 \end{aligned}$$

Step 4. Calculate initial water in place W_i .

$$\begin{aligned} W_i &= \pi(r_a^2 - r_e^2) h \phi / 5.615 \\ &= \frac{\pi(46,000^2 - 9200^2)(100)(0.25)}{5.615} = 28.41 \text{ MMM bbl} \end{aligned}$$

Step 5. Calculate W_{ei} from Equation 10-38.

$$W_{ei} = c_t W_i p_i f$$

$$W_{ei} = 7 \times 10^{-6} (28.41 \times 10^9) (2740) \left(\frac{140}{360} \right) = 211.9 \text{ MM bbl}$$

Step 6. Calculate the productivity index J of the radial aquifer from Equation 10-45.

$$J = \frac{0.00708(200)(100)\left(\frac{140}{360}\right)}{0.55 \ln(5)} = 116.5 \text{ bbl/day/psi}$$

$$\text{Therefore, } Jp_i/W_{ci} = (116.5 \times 2740)/(211.9 \times 10^6) = 1.506 \times 10^{-3}$$

Since the time step Δt is fixed at 365 days, then

$$1 - e^{-Jp_i \Delta t/W_{ci}} = 1 - e^{-1.506 \times 10^{-3} \times 365} = 0.4229$$

Equation 10-42 can be reduced to:

$$(\Delta W_e)_n = \frac{211.9 \times 10^6}{2740} [(\bar{p}_a)_{n-1} - (\bar{p}_r)_n]^{(0.4229)}$$

$$(\Delta W_e)_n = 32,705 [(\bar{p}_a)_{n-1} - (\bar{p}_r)_n]$$

Step 7. Calculate cumulative water influx as shown in the following table:

| n | t days | p_r | $(\bar{p}_r)_n$ | $(\bar{p}_a)_{n-1}$ | $(\bar{p}_a)_{n-1} - (\bar{p}_r)_n$ | $(\Delta W_e)_n$ MM bbl | $(W_e)_n$ MM bbl |
|---|-----------|-------|-----------------|---------------------|-------------------------------------|----------------------------|---------------------|
| 0 | 0 | 2740 | 2740 | 2740 | 0 | 0 | 0 |
| 1 | 365 | 2500 | 2620 | 2740 | 120 | 3.925 | 3.925 |
| 2 | 730 | 2290 | 2395 | 2689 | 294 | 9.615 | 13.540 |
| 3 | 1095 | 2109 | 2199 | 2565 | 366 | 11.970 | 25.510 |
| 4 | 1460 | 1949 | 2029 | 2409 | 381 | 12.461 | 37.971 |

PROBLEMS

1. Calculate the cumulative water influx that results from a pressure drop of 200 psi at the oil-water contact with an encroachment angle of 50° . The reservoir-aquifer system is characterized by the following properties:

| | Reservoir | Aquifer |
|---------------------------|--------------------|--------------------|
| radius, ft | 6000 | 20,000 |
| porosity | 0.18 | 0.15 |
| c_f , psi^{-1} | 4×10^{-6} | 3×10^{-6} |
| c_w , psi^{-1} | 5×10^{-6} | 4×10^{-6} |
| h, ft | 25 | 20 |

2. An active water-drive oil reservoir is producing under the steady-state flowing conditions. The following data are available:

$$\begin{array}{lll}
 p_i = 4000 \text{ psi} & Q_w = 0 & R_s = 500 \text{ scf/STB} \\
 Q_o = 40,000 \text{ STB/day} & p = 3000 \text{ psi} & T = 140^\circ\text{F} \\
 \text{GOR} = 700 \text{ scf/STB} & B_o = 1.3 \text{ bbl/STB} & B_w = 1.0 \text{ bbl/STB} \\
 z = 0.82 & &
 \end{array}$$

Calculate Schilthuis' water influx constant.

3. The pressure history of a water-drive oil reservoir is given below:

| t, days | p, psi |
|---------|--------|
| 0 | 4000 |
| 120 | 3950 |
| 220 | 3910 |
| 320 | 3880 |
| 420 | 3840 |

The aquifer is under a steady-state flowing condition with an estimated water influx constant of 80 bbl/day/psi. Using the steady-state model, calculate and plot the cumulative water influx as a function of time.

4. A water-drive reservoir has the following boundary pressure history:

| Time, months | Boundary pressure, psi |
|--------------|------------------------|
| 0 | 2610 |
| 6 | 2600 |
| 12 | 2580 |
| 18 | 2552 |
| 24 | 2515 |

The aquifer-reservoir system is characterized by the following data:

| | Reservoir | Aquifer |
|---------------------------|----------------------|----------------------|
| radius, ft | 2000 | ∞ |
| h, ft | 25 | 30 |
| k, md | 60 | 80 |
| ϕ , % | 17 | 18 |
| μ_w , cp | 0.55 | 0.85 |
| c_w , psi^{-1} | 0.7×10^{-6} | 0.8×10^{-6} |
| c_f , psi^{-1} | 0.2×10^{-6} | 0.3×10^{-6} |

If the encroachment angle is 360° , calculate the water influx as a function of time by using:

- a. The van Everdingen-Hurst method
- b. The Carter-Tracy method

5. The following table summarizes the original data available on the West Texas water-drive reservoir:

| | Oil Zone | Aquifer |
|----------------------------------|--------------------|--------------------|
| Geometry | Circle | Semi-circle |
| Area, acres | 640 | Infinite |
| Initial reservoir pressure, psia | 4000 | 4000 |
| Initial oil saturation | 0.80 | 0 |
| Porosity, % | 22 | — |
| B_{oi} , bbl/STB | 1.36 | — |
| B_{wi} , bbl/STB | 1.00 | 1.05 |
| c_o , psi^{-1} | 6×10^{-6} | — |
| c_w , psi^{-1} | 3×10^{-6} | 7×10^{-6} |

The aquifer geological data estimate the water influx constant at 551 bbl/psi. After 1,120 days of production, the reservoir average pressure has dropped to 3,800 psi and the field has produced 860,000 STB of oil. The field condition after 1,120 days of production is given below:

$$\begin{aligned}
 p &= 3800 \text{ psi} \\
 N_p &= 860,000 \text{ STB} \\
 B_o &= 1.34 \text{ bbl/STB} \\
 B_w &= 1.05 \text{ bbl/STB} \\
 W_e &= 991,000 \text{ bbl} \\
 t_D &= 32.99 \text{ (dimensionless time after 1120 days)} \\
 W_p &= 0 \text{ bbl}
 \end{aligned}$$

It is expected that the average reservoir pressure will drop to 3,400 psi after 1,520 days (i.e., from the start of production). Calculate the cumulative water influx after 1,520 days.

6. A wedge reservoir-aquifer system with an encroachment angle of 60° has the following boundary pressure history:

| Time, days | Boundary Pressure, psi |
|------------|------------------------|
| 0 | 2850 |
| 365 | 2610 |
| 730 | 2400 |
| 1095 | 2220 |
| 1460 | 2060 |

Given:

$$\begin{aligned}
 h &= 120' & c_f &= 5 \times 10^{-6} \text{ psi}^{-1} & c_w &= 4 \times 10^{-6} \text{ psi}^{-1} \\
 \mu_w &= 0.7 \text{ cp} & k &= 60 \text{ md} & \phi &= 12\% \\
 \text{reservoir area} &= 40,000 \text{ acres} & \text{aquifer area} &= 980,000 \text{ acres} & T &= 140^\circ\text{F}
 \end{aligned}$$

Calculate the cumulative influx as a function of time by using Fetkovich's method.

REFERENCES

- Allard, D. R., and Chen, S. M., "Calculation of Water Influx for Bottom Water Drive Reservoirs," *SPE Reservoir Engineering*, May 1988, pp. 369–379.
- Carter, R. D., and Tracy, G. W., "An Improved Method for Calculations Water Influx," *Trans. AIME*, 1960.
- Chatas, A., "A Practical Treatment of Nonsteady-State Flow Problems in Reservoir Systems," *Petroleum Engineering*, May 1953, 25, No. 5, B-42; No. 6, June, p. B-38; No. 8, August, p. B-44.
- Coats, K., "A Mathematical Model for Water Movement about Bottom-Water-Drive Reservoirs," *SPE Jour.*, March 1962, pp. 44–52; *Trans. AIME*, p. 225.
- Craft, B., and Hawkins, M., *Applied Reservoir Engineering*. Prentice Hall, 1959.
- Craft, B., Hawkins, M., and Terry, R., *Applied Petroleum Reservoir Engineering*, 2nd ed. Prentice Hall, 1991.
- Dake, L. P., *Fundamentals of Reservoir Engineering*. Amsterdam: Elsevier, 1978.
- Dake, L., *The Practice of Reservoir Engineering*. Amsterdam: Elsevier, 1994.
- Edwardson, M. et al., "Calculation of Formation Temperature Disturbances Caused by Mud Circulation," *JPT*, April 1962, pp. 416–425; *Trans. AIME*, p. 225.
- Fetkovich, M. J., "A Simplified Approach to Water Influx Calculations—Finite Aquifer Systems," *JPT*, July 1971, pp. 814–828.

11. Hurst, W., "Water Influx into a Reservoir and its Application to the Equation of Volumetric Balance," *Trans. AIME*, Vol. 151, pp. 57, 1643.
12. Lee, J., and Wattenbarger, R., *Gas Reservoir Engineering*. SPE Textbook Series, Vol. 5, SPE, Dallas, TX, 1996.
13. Schilthuis, R., "Active Oil and Reservoir Energy," *Trans. AIME*, 1936, pp. 37, 118.
14. Van Everdingen, A., and Hurst, W., "The Application of the Laplace Transformation to Flow Problems in Reservoirs," *Trans. AIME*, 1949, pp. 186, 305.



C H A P T E R 11

OIL RECOVERY MECHANISMS AND THE MATERIAL BALANCE EQUATION

Each reservoir is composed of a unique combination of geometric form, geological rock properties, fluid characteristics, and primary drive mechanism. Although no two reservoirs are identical in all aspects, they can be grouped according to the primary recovery mechanism by which they produce. It has been observed that each drive mechanism has certain typical performance characteristics in terms of:

- Ultimate recovery factor
- Pressure decline rate
- Gas-oil ratio
- Water production

The recovery of oil by any of the natural drive mechanisms is called **primary recovery**. The term refers to the production of hydrocarbons from a reservoir without the use of any process (such as fluid injection) to supplement the natural energy of the reservoir.

The two main objectives of this chapter are to:

1. Introduce and give a detailed discussion of the various primary recovery mechanisms and their effects on the overall performance of oil reservoirs.

2. Provide the basic principles of the material balance equation and other governing relationships that can be used to predict the volumetric performance of oil reservoirs.

PRIMARY RECOVERY MECHANISMS

For a proper understanding of reservoir behavior and predicting future performance, it is necessary to have knowledge of the driving mechanisms that control the behavior of fluids within reservoirs. The overall performance of oil reservoirs is largely determined by the nature of the energy, i.e., driving mechanism, available for moving the oil to the wellbore. There are basically six driving mechanisms that provide the natural energy necessary for oil recovery:

- Rock and liquid expansion drive
- Depletion drive
- Gas-cap drive
- Water drive
- Gravity drainage drive
- Combination drive

These driving mechanisms are discussed as follows.

Rock and Liquid Expansion

When an oil reservoir initially exists at a pressure higher than its bubble-point pressure, the reservoir is called an **undersaturated-oil reservoir**. At pressures above the bubble-point pressure, crude oil, connate-water, and rock are the only materials present. As the reservoir pressure declines, the rock and fluids expand due to their individual compressibilities. The reservoir rock compressibility is the result of two factors:

- Expansion of the individual rock grains
- Formation compaction

Both of the above two factors are the results of a decrease of fluid pressure within the pore spaces, and both tend to reduce the pore volume through the reduction of the porosity.

As the expansion of the fluids and reduction in the pore volume occur with decreasing reservoir pressure, the crude oil and water will be forced

out of the pore space to the wellbore. Because liquids and rocks are only slightly compressible, the reservoir will experience a rapid pressure decline. The oil reservoir under this driving mechanism is characterized by a constant gas-oil ratio that is equal to the gas solubility at the bubble point pressure.

This driving mechanism is considered the least efficient driving force and usually results in the recovery of only a small percentage of the total oil-in-place.

The Depletion-Drive Mechanism

This driving form may also be referred to by the following various terms:

- Solution gas drive
- Dissolved gas drive
- Internal gas drive

In this type of reservoir, the principal source of energy is a result of gas liberation from the crude oil and the subsequent expansion of the solution gas as the reservoir pressure is reduced. As pressure falls below the bubble-point pressure, gas bubbles are liberated within the microscopic pore spaces. These bubbles expand and force the crude oil out of the pore space as shown conceptually in Figure 11-1.

Cole (1969) suggests that a depletion-drive reservoir can be identified by the following characteristics:

- **Reservoir pressure:** The reservoir pressure declines rapidly and continuously. This reservoir pressure behavior is attributed to the fact that no extraneous fluids or gas caps are available to provide a replacement of the gas and oil withdrawals.
- **Water production:** The absence of a water drive means there will be little or no water production with the oil during the entire producing life of the reservoir.
- **Gas-oil ratio:** A depletion-drive reservoir is characterized by a rapidly increasing gas-oil ratio from all wells, regardless of their structural position. After the reservoir pressure has been reduced below the bubble-point pressure, gas evolves from solution throughout the reservoir. Once the gas saturation exceeds the critical gas saturation, free gas begins to flow toward the wellbore and the gas-oil ratio increases. The

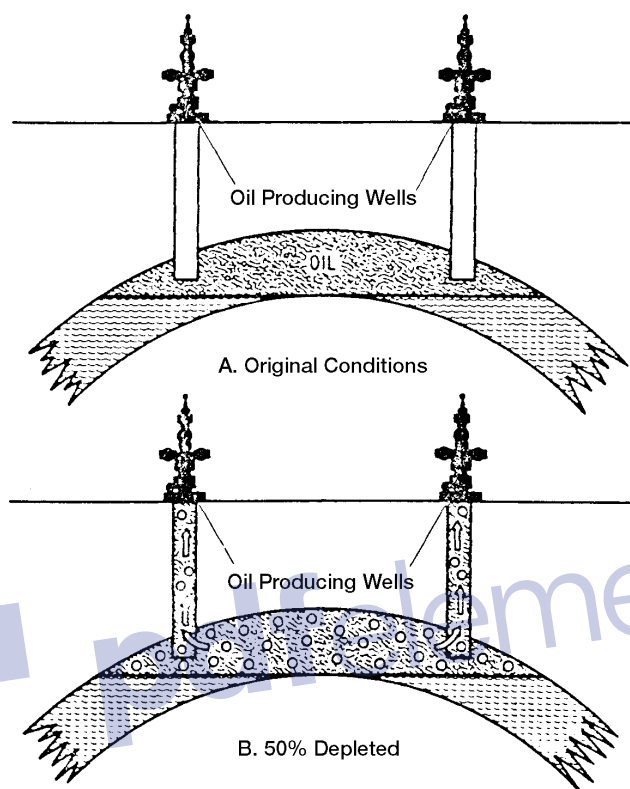


Figure 11-1. Solution-gas-drive reservoir. (After Clark, N. J., *Elements of Petroleum Reservoirs*, SPE, 1969.)

gas will also begin a vertical movement due to the gravitational forces, which may result in the formation of a secondary gas cap. Vertical permeability is an important factor in the formation of a secondary gas cap.

- **Ultimate oil-recovery:** Oil production by depletion drive is usually the least efficient recovery method. This is a direct result of the formation of gas saturation throughout the reservoir. Ultimate oil recovery from depletion-drive reservoirs may vary from less than 5% to about 30%. The low recovery from this type of reservoirs suggests that large quantities of oil remain in the reservoir and, therefore, depletion-drive reservoirs are considered the best candidates for secondary recovery applications.

The above characteristic trends occurring during the production life of depletion-drive reservoirs are shown in Figure 11-2 and summarized below:

| Characteristics | Trend |
|--------------------|--|
| Reservoir pressure | Declines rapidly and continuously |
| Gas-oil ratio | Increases to maximum and then declines |
| Water production | None |
| Well behavior | Requires pumping at early stage |
| Oil recovery | 5% to 30% |

Gas-Cap Drive

Gas-cap-drive reservoirs can be identified by the presence of a gas cap with little or no water drive as shown in Figure 11-3.

Due to the ability of the gas cap to expand, these reservoirs are characterized by a slow decline in the reservoir pressure. The natural energy available to produce the crude oil comes from the following two sources:

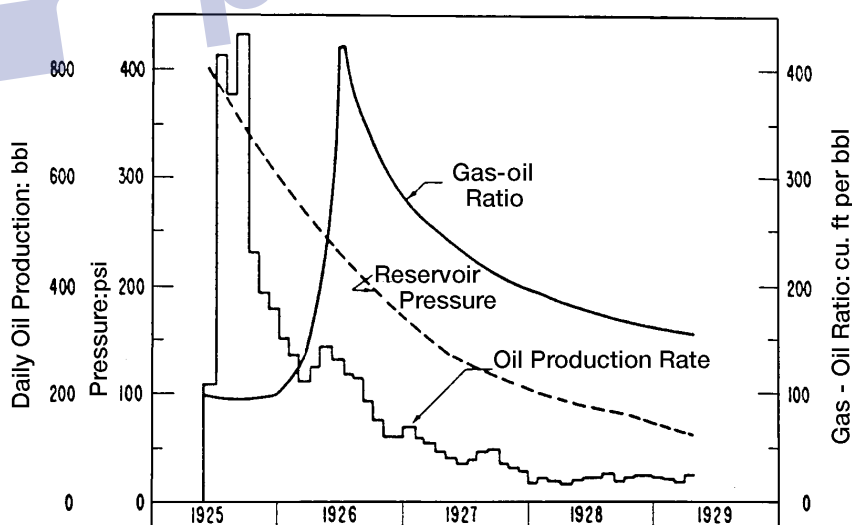


Figure 11-2. Production data of a solution-gas-drive reservoir. (After Clark, N. J., Elements of Petroleum Reservoirs, SPE, 1969.)

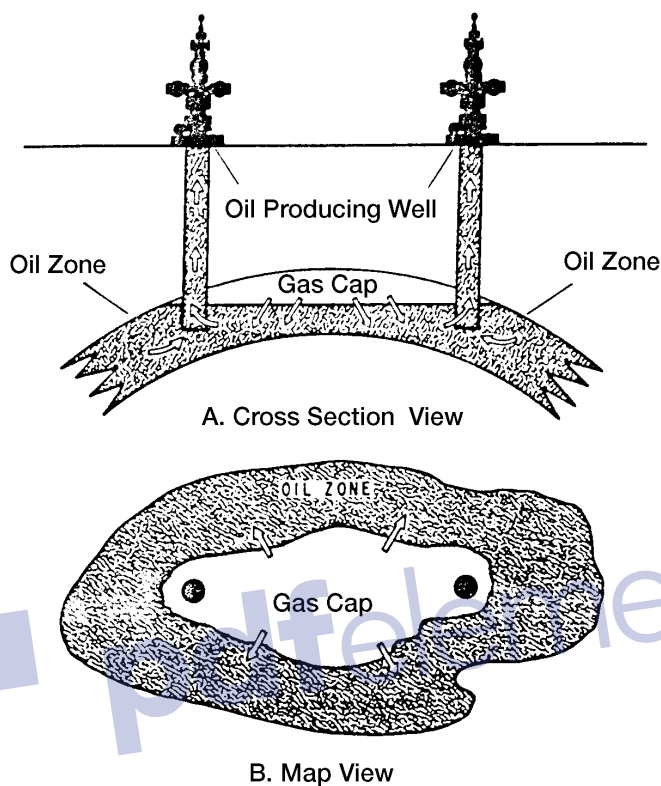


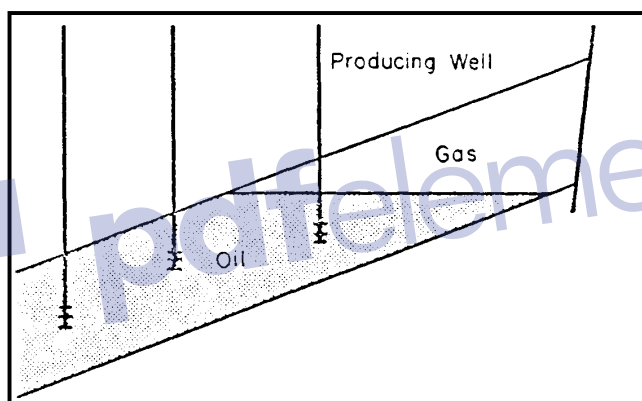
Figure 11-3. Gas-cap-drive reservoir. (After Clark, N. J., *Elements of Petroleum Reservoirs, SPE, 1969.*)

- Expansion of the gas-cap gas
- Expansion of the solution gas as it is liberated

Cole (1969) and Clark (1969) presented a comprehensive review of the characteristic trends associated with gas-cap-drive reservoirs. These characteristic trends are summarized below:

- **Reservoir pressure:** The reservoir pressure falls slowly and continuously. Pressure tends to be maintained at a higher level than in a depletion-drive reservoir. The degree of pressure maintenance depends upon the volume of gas in the gas cap compared to the oil volume.
- **Water production:** Absent or negligible water production.

- **Gas-oil ratio:** The gas-oil ratio rises continuously in up-structure wells. As the expanding gas cap reaches the producing intervals of upstructure wells, the gas-oil ratio from the affected wells will increase to high values.
- **Ultimate oil recovery:** Oil recovery by gas-cap expansion is actually a frontal drive displacing mechanism that, therefore, yields a considerably larger recovery efficiency than that of depletion-drive reservoirs. This larger recovery efficiency is also attributed to the fact that no gas saturation is being formed throughout the reservoir at the same time. Figure 11-4 shows the relative positions of the gas-oil contact at different times in the producing life of the reservoir. The expected oil recovery ranges from 20% to 40%.



A. Initial fluid distribution.

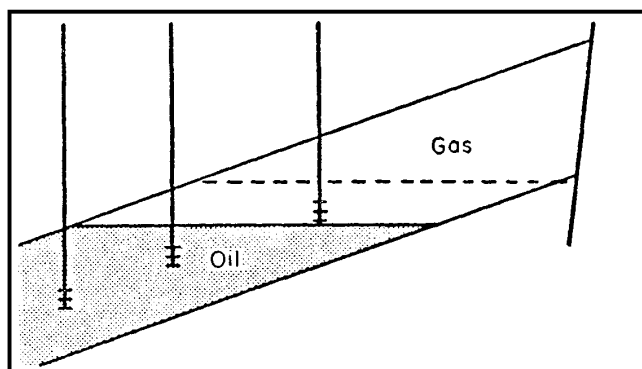


Figure 11-4. Gas-cap-drive reservoir. (After Cole, F., Reservoir Engineering Manual, Gulf Publishing Company, 1969.)

- **Well behavior:** Because of effects of gas-cap expansion on maintaining reservoir pressure and the effect of decreased liquid column weight as it is produced out of the well, gas-cap-drive reservoirs tend to flow longer than depletion-drive reservoirs.

The ultimate oil recovery from a gas-cap-drive reservoir will vary depending largely on the following six important parameters:

Size of the Original Gas Cap

As shown graphically in Figure 11-5, the ultimate oil recovery increases with increasing the size of the gas cap.

Vertical Permeability

Good vertical permeability will permit the oil to move downward with less bypassing of gas.

Oil Viscosity

As the oil viscosity increases, the amount of gas bypassing will also increase, which leads to a lower oil recovery.

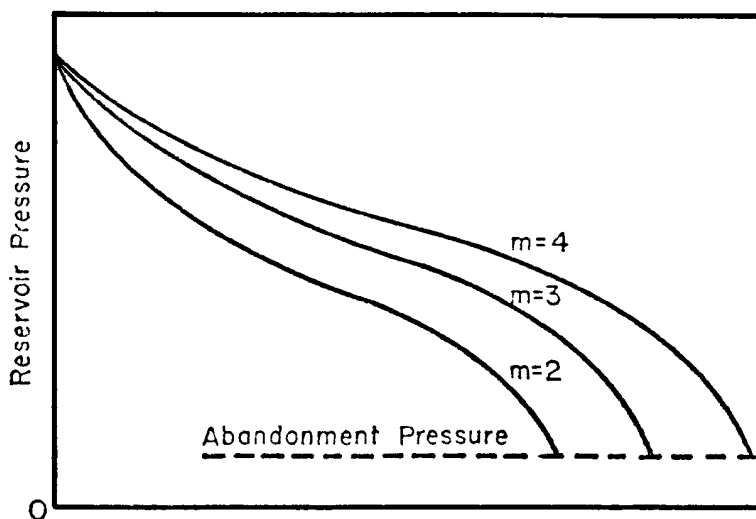


Figure 11-5. Effect of gas-cap size on ultimate oil recovery. (After Cole, F., Reservoir Engineering Manual, Gulf Publishing Company, 1969.)

Degree of Conservation of the Gas

In order to conserve gas, and thereby increase ultimate oil recovery, it is necessary to shut-in the wells that produce excessive gas.

Oil Production Rate

As the reservoir pressure declines with production, solution gas evolves from the crude oil and the gas saturation increases continuously. If the gas saturation exceeds the critical gas saturation, the evolved gas begins to flow in the oil zone. As a result of creating a mobile gas phase in the oil zone, the following two events will occur:

- The effective permeability to oil will be decreased as a result of the increased gas saturation.
- The effective permeability to gas will be increased, thereby increasing the flow of gas.

The formation of the free gas saturation in the oil zone cannot be prevented without resorting to pressure maintenance operations. Therefore, in order to achieve maximum benefit from a gas-cap-drive-producing mechanism, gas saturation in the oil zone must be kept to an absolute minimum. This can be accomplished by taking advantage of gravitational segregation of the fluids. In fact, an efficiently operated gas-cap-drive reservoir must also have an efficient gravity segregation drive. As the gas saturation is formed in the oil zone it must be allowed to migrate upstructure to the gas cap. Thus, a gas-cap-drive reservoir is in reality a combination-driving reservoir, although it is not usually considered as such.

Lower producing rates will permit the maximum amount of free gas in the oil zone to migrate to the gas cap. Therefore, gas-cap-drive reservoirs are rate sensitive, as lower producing rates will usually result in increased recovery.

Dip Angle

The size of the gas cap, a measure of reservoir energy available to produce the oil, will in large part determine the recovery percent to be expected. Such recovery normally will be 20% to 40% of the original oil-in-place; if some other features are present to assist, however, such as a steep angle of dip that allows good oil drainage to the bottom of the

structure, considerably higher recoveries (up to 60% or greater) may be obtained. Conversely, extremely thin oil columns (where early breakthrough of the advancing gas cap occurs in producing wells) may limit oil recovery to lower figures regardless of the size of the gas cap. Figure 11-6 shows a typical production and pressure data for a gas-cap-drive reservoir.

The Water-Drive Mechanism

Many reservoirs are bounded on a portion or all of their peripheries by water bearing rocks called aquifers. The aquifers may be so large compared to the reservoir they adjoin as to appear infinite for all practical purposes, and they may range down to those so small as to be negligible in their effects on the reservoir performance.

The aquifer itself may be entirely bounded by impermeable rock so that the reservoir and aquifer together form a closed (volumetric) unit. On the other hand, the reservoir may be outcropped at one or more places where it may be replenished by surface water as shown schematically in Figure 11-7.

It is common to speak of edge water or bottom water in discussing water influx into a reservoir. Bottom water occurs directly beneath the oil and edge water occurs off the flanks of the structure at the edge of the oil

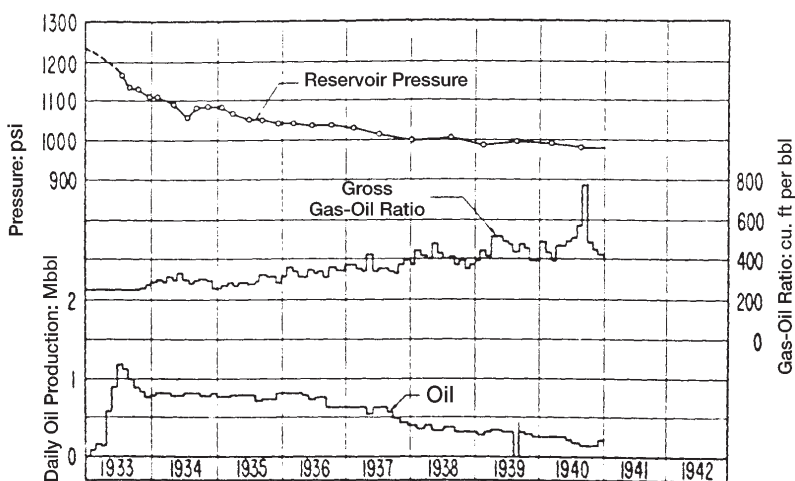


Figure 11-6. Production data for a gas-cap-drive reservoir. (After Clark, N. J., Elements of Petroleum Reservoirs, SPE, 1969. Courtesy of API.)

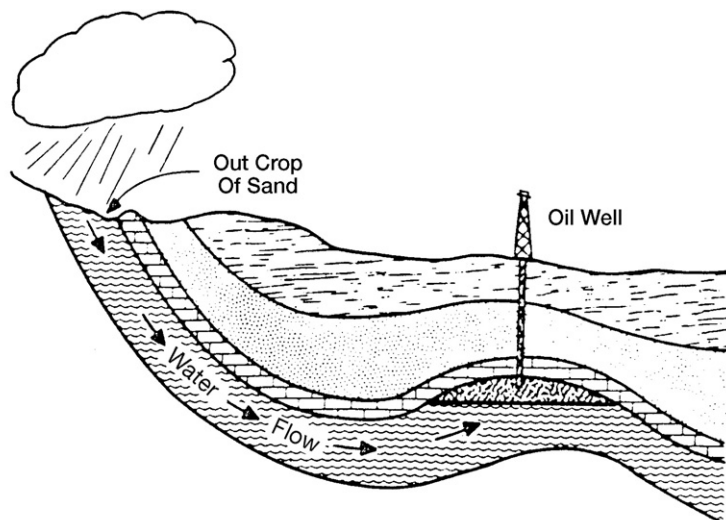


Figure 11-7. Reservoir having artesian water drive. (After Clark, N. J., *Elements of Petroleum Reservoirs, SPE, 1969.*)

as illustrated in Figure 11-8. Regardless of the source of water, the water drive is the result of water moving into the pore spaces originally occupied by oil, replacing the oil and displacing it to the producing wells.

Cole (1969) presented the following discussion on the characteristics that can be used for identification of the water-driving mechanism:

Reservoir Pressure

The reservoir pressure decline is usually very gradual. Figure 11-9 shows the pressure-production history of a typical water-drive reservoir.

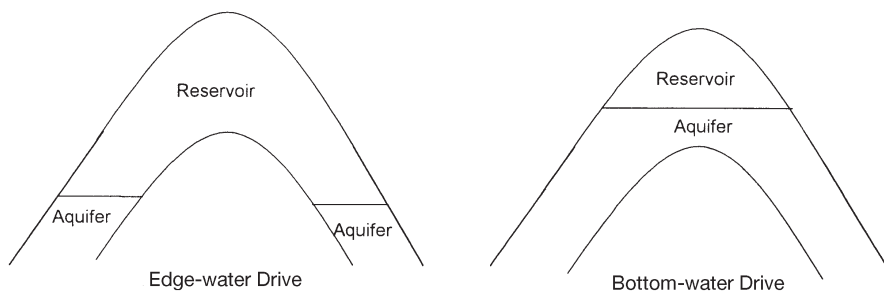


Figure 11-8. Aquifer geometries.

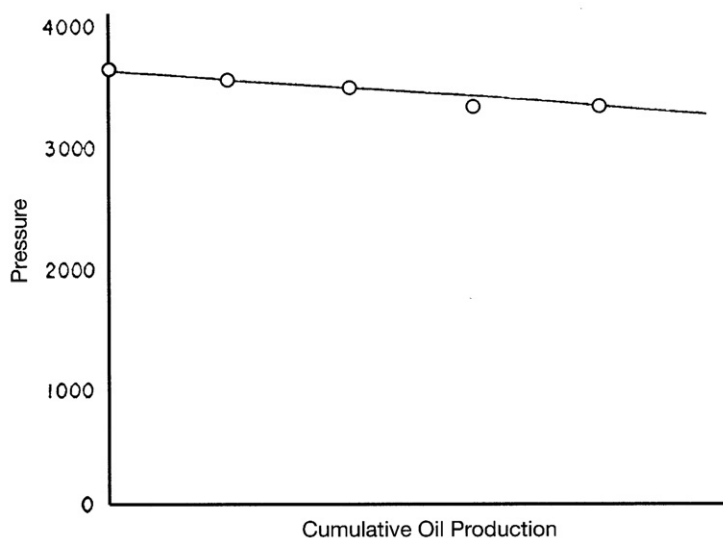


Figure 11-9. Pressure-production history for a water-drive reservoir.

It is not uncommon for many thousands of barrels of oil to be produced for each pound per square inch drop in reservoir pressure. The reason for the small decline in reservoir pressure is that oil and gas withdrawals from the reservoir are replaced almost volume for volume by water encroaching into the oil zone.

Several large oil reservoirs in the Gulf Coast areas of the United States have such active water drives that the reservoir pressure has declined only about 1 psi per million barrels of oil produced. Although pressure history is normally plotted versus cumulative oil production, it should be understood that total reservoir fluid withdrawals are the really important criteria in the maintenance of reservoir pressure. In a water-drive reservoir, only a certain number of barrels of water can move into the reservoir as a result of a unit pressure drop within the reservoir.

Since the principal income production is from oil, if the withdrawals of water and gas can be minimized, then the withdrawal of oil from the reservoir can be maximized with minimum pressure decline. Therefore, it is extremely important to reduce water and gas production to an absolute minimum. This can usually be accomplished by shutting in wells producing large quantities of these fluids and, where possible, transferring their allowables to other wells producing with lower water-oil or gas-oil ratios.

Water Production

Early excess water production occurs in structurally low wells. This is characteristic of a water-drive reservoir, and, provided the water is encroaching in a uniform manner, nothing can or should be done to restrict this encroachment, as the water will probably provide the most efficient displacing mechanism possible.

If the reservoir has one or more lenses of very high permeability, then the water may be moving through this more permeable zone. In this case, it may be economically feasible to perform remedial operations to shut off this permeable zone producing water. It should be realized that in most cases the oil that is being recovered from a structurally low well will be recovered from wells located higher on the structure and any expenses involved in remedial work to reduce the water-oil ratio of structurally low wells may be needless expenditures.

Gas-Oil Ratio

There is normally little change in the producing gas-oil ratio during the life of the reservoir. This is especially true if the reservoir does not have an initial free gas cap. Pressure will be maintained as a result of water encroachment and therefore there will be relatively little gas released from this solution.

Ultimate Oil Recovery

Ultimate recovery from water-drive reservoirs is usually much larger than recovery under any other producing mechanism. Recovery is dependent upon the efficiency of the flushing action of the water as it displaces the oil. In general, as the reservoir heterogeneity increases, the recovery will decrease, due to the uneven advance of the displacing water.

The rate of water advance is normally faster in the zones of high permeability. This results in earlier high water-oil ratios and consequent earlier economic limits. Where the reservoir is more or less homogeneous, the advancing water front will be more uniform, and when the economic limit, due primarily to high water-oil ratio, has been reached, a greater portion of the reservoir will have been contacted by the advancing water.

Ultimate oil recovery is also affected by the degree of activity of the water drive. In a very active water drive where the degree of pressure maintenance is good, the role of solution gas in the recovery process is

reduced to almost zero, with maximum advantage being taken of the water as a displacing force. This should result in maximum oil recovery from the reservoir. The ultimate oil recovery normally ranges from 35% to 75% of the original oil-in-place.

The characteristic trends of a water-drive reservoir are shown graphically in Figure 11-10 and are summarized below:

| Characteristics | Trends |
|-----------------------|---|
| Reservoir pressure | Remains high |
| Surface gas-oil ratio | Remains low |
| Water production | Starts early and increases to appreciable amounts |
| Well behavior | Flow until water production gets excessive |
| Expected oil recovery | 35% to 75% |

The Gravity-Drainage-Drive Mechanism

The mechanism of gravity drainage occurs in petroleum reservoirs as a result of differences in densities of the reservoir fluids. The effects of gravitational forces can be simply illustrated by placing a quantity of crude oil and a quantity of water in a jar and agitating the contents. After agitation, the jar is placed at rest, and the denser fluid (normally water)

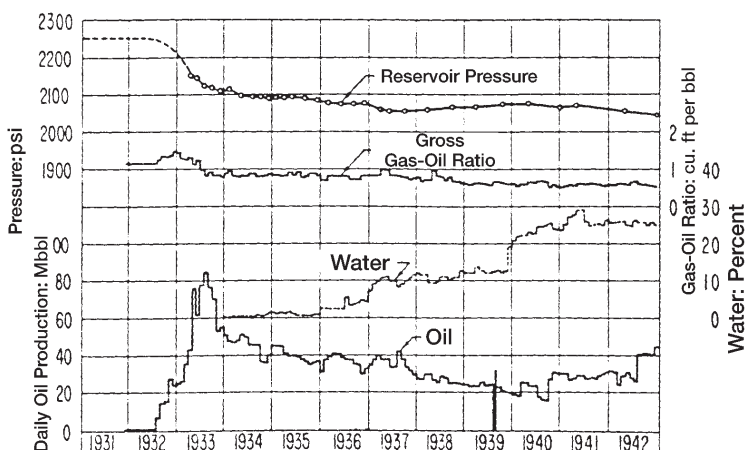


Figure 11-10. Production data for a water-drive reservoir. (After Clark, N. J., Elements of Petroleum Reservoirs, SPE, 1969. Courtesy of API.)

will settle to the bottom of the jar, while the less dense fluid (normally oil) will rest on top of the denser fluid. The fluids have separated as a result of the gravitational forces acting on them.

The fluids in petroleum reservoirs have all been subjected to the forces of gravity, as evidenced by the relative positions of the fluids, i.e., gas on top, oil underlying the gas, and water underlying oil. The relative positions of the reservoir fluids are shown in Figure 11-11. Due to the long periods of time involved in the petroleum accumulation-and-migration process, it is generally assumed that the reservoir fluids are in equilibrium. If the reservoir fluids are in equilibrium, then the gas-oil and oil-water contacts should be essentially horizontal. Although it is difficult to determine precisely the reservoir fluid contacts, best available data indicate that, in most reservoirs, the fluid contacts actually are essentially horizontal.

Gravity segregation of fluids is probably present to some degree in all petroleum reservoirs, but it may contribute substantially to oil production in some reservoirs.

Cole (1969) stated that reservoirs operating largely under a gravity-drainage-producing mechanism are characterized by:

- Reservoir Pressure

Variable rates of pressure decline, depending principally upon the amount of gas conservation. Strictly speaking, where the gas is conserved and reservoir pressure is maintained, the reservoir would be operating

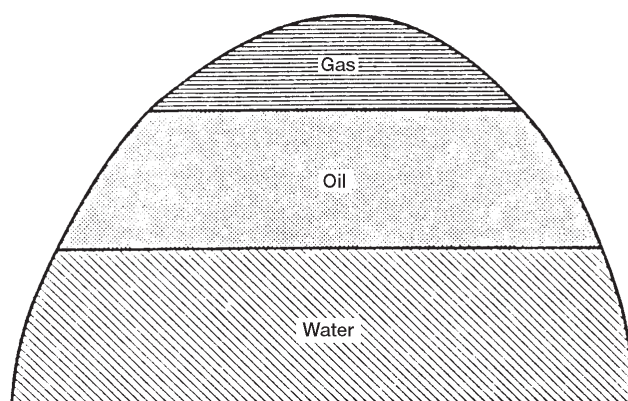


Figure 11-11. Initial fluids distribution in an oil reservoir.

under combined gas-cap drive and gravity-drainage mechanisms. Therefore, for the reservoir to be operating solely as a result of gravity drainage, the reservoir would show a rapid pressure decline. This would require the upstructure migration of the evolved gas where it later would be produced from structurally high wells, resulting in rapid loss of pressure.

- Gas-Oil Ratio

Low gas-oil ratio from structurally low wells. This is caused by migration of the evolved gas upstructure due to gravitational segregation of the fluids. On the other hand, the structurally high wells will experience an increasing gas-oil ratio as a result of the upstructure migration of the gas released from the crude oil.

- Secondary Gas Cap

Formation of a secondary gas cap in reservoirs that initially were undersaturated. Obviously the gravity-drainage mechanism does not become operative until reservoir pressure has declined below the saturation pressure, since above the saturation pressure there will be no free gas in the reservoir.

- Water Production

Little or no water production. Water production is indicative of a water drive.

Ultimate Oil Recovery

Ultimate recovery from gravity-drainage reservoirs will vary widely, due primarily to the extent of depletion by gravity drainage alone. Where gravity drainage is good, or where producing rates are restricted to take maximum advantage of the gravitational forces, recovery will be high. There are reported cases where recovery from gravity-drainage reservoirs has exceeded 80% of the initial oil-in-place. In other reservoirs where depletion drive also plays an important role in the oil recovery process, the ultimate recovery will be less.

In operating a gravity-drainage reservoir, it is essential that the oil saturation in the vicinity of the wellbore must be maintained as high as possible. There are two basic reasons for this requirement:

- A high oil saturation means a higher oil flow rate
- A high oil saturation means a lower gas flow rate

If the evolved gas migrates upstructure instead of toward the wellbore, then a high oil saturation in the vicinity of the wellbore can be maintained.

In order to take maximum advantage of the gravity-drainage-producing mechanism, wells should be located as structurally low as possible. This will result in maximum conservation of the reservoir gas. A typical gravity-drainage reservoir is shown in Figure 11-12.

Factors that affect ultimate recovery from gravity-drainage reservoirs are:

- Permeability in the direction of dip
- Dip of the reservoir
- Reservoir producing rates
- Oil viscosity
- Relative permeability characteristics

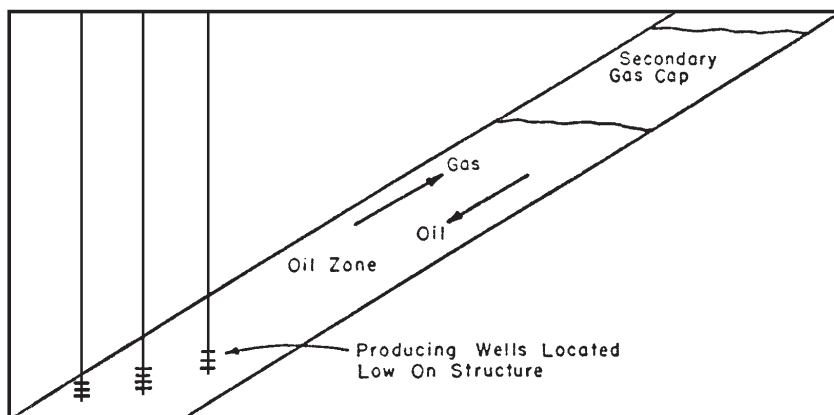


Figure 11-12. Gravity-drainage reservoir. (After Cole, F., Reservoir Engineering Manual, Gulf Publishing Company, 1969.)

Cole (1969) presented the following complete treatment of the above listed factors.

Permeability in the Direction of Dip

Good permeability in the direction of migration of the oil is a prerequisite for efficient gravity drainage. For example, a reservoir with little structural relief that also contained many more or less continuous shale “breaks” could probably not be operated under gravity drainage because the oil could not flow to the base of the structure.

Dip of the Reservoir

In most reservoirs, the permeability in the direction of dip is considerably larger than the permeability transverse to the direction of dip. Therefore, as the dip of the reservoir increases, the oil and gas can flow along the direction of dip (which is also the direction of greatest permeability) and still achieve their desired structural position.

Reservoir-Producing Rates

Since the gravity-drainage rate is limited, the reservoir-producing rates should be limited to the gravity-drainage rate, and then maximum recovery will result. If the reservoir-producing rate exceeds the gravity-drainage rate, the depletion-drive-producing mechanism will become more significant with a consequent reduction in ultimate oil recovery.

Oil Viscosity

Oil viscosity is important because the gravity-drainage rate is dependent upon the viscosity of the oil. In the fluid flow equations, the flow rate increases as the viscosity decreases. Therefore, the gravity-drainage rate will increase as the reservoir oil viscosity decreases.

Relative Permeability Characteristics

For an efficient gravity-drive mechanism to be operative, the gas must flow upstructure while the oil flows downstructure. Although this situation involves counterflow of the oil and gas, both fluids are flowing and, therefore, relative permeability characteristics of the formation are very important.

The Combination-Drive Mechanism

The driving mechanism most commonly encountered is one in which both water and free gas are available in some degree to displace the oil toward the producing wells. The most common type of drive encountered, therefore, is a combination-drive mechanism as illustrated in Figure 11-13.

Two combinations of driving forces can be present in combination-drive reservoirs. These are (1) depletion drive and a weak water drive and; (2) depletion drive with a small gas cap and a weak water drive. Then, of course, gravity segregation can play an important role in any of the aforementioned drives.

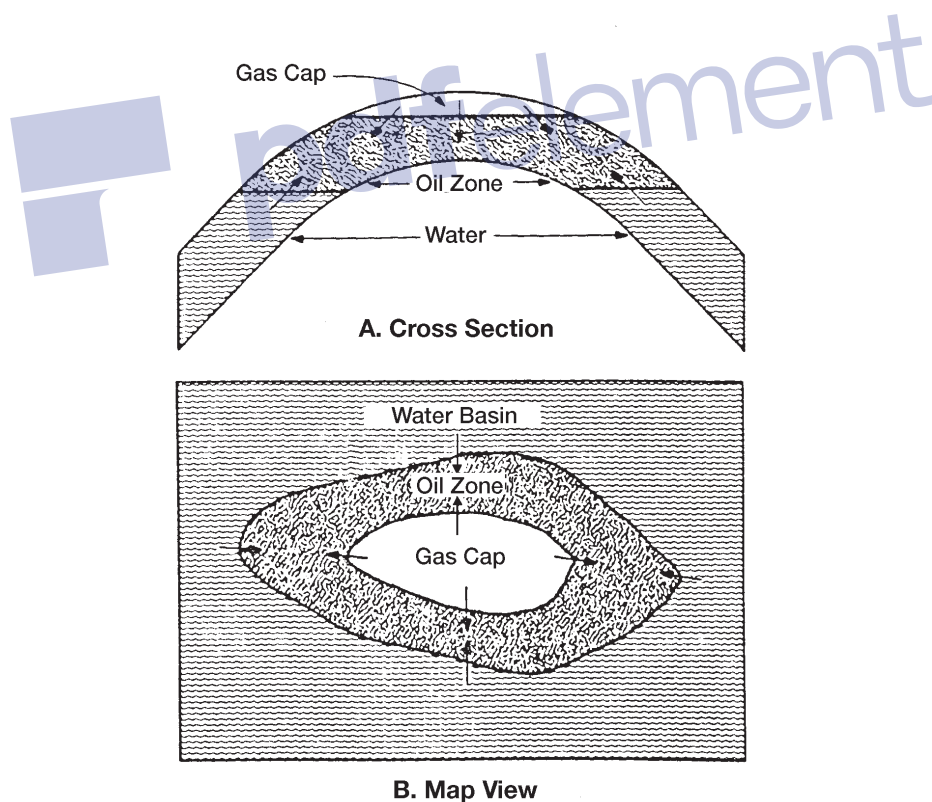


Figure 11-13. Combination-drive reservoir. (After Clark, N. J., *Elements of Petroleum Reservoirs*, SPE, 1969.)

Combination-drive reservoirs can be recognized by the occurrence of a combination of some of the following factors:

- a. Relatively rapid pressure decline. Water encroachment and/or external gas-cap expansion are insufficient to maintain reservoir pressures.
- b. Water encroaching slowly into the lower part of the reservoir. Structurally low producing wells will exhibit slowly increasing water producing rates.
- c. If a small gas cap is present the structurally high wells will exhibit continually increasing gas-oil ratios, provided the gas cap is expanding. It is possible that the gas cap will shrink due to production of excess free gas, in which case the structurally high wells will exhibit a **decreasing** gas-oil ratio. This condition should be avoided whenever possible, as large volumes of oil can be lost as a result of a shrinking gas cap.
- d. A substantial percentage of the total oil recovery may be due to the depletion-drive mechanism. The gas-oil ratio of structurally low wells will also continue to increase due to evolution of solution gas throughout the reservoir, as pressure is reduced.
- e. Ultimate recovery from combination-drive reservoirs is usually greater than recovery from depletion-drive reservoirs but less than recovery from water-drive or gas-cap-drive reservoirs. Actual recovery will depend upon the degree to which it is possible to reduce the magnitude of recovery by depletion drive. In most combination-drive reservoirs, it will be economically feasible to institute some type of pressure maintenance operation, either gas injection, water injection, or both gas and water injection, depending upon the availability of the fluids.

THE MATERIAL BALANCE EQUATION

The material balance equation (MBE) has long been recognized as one of the basic tools of reservoir engineers for interpreting and predicting reservoir performance. The MBE, when properly applied, can be used to:

- Estimate initial hydrocarbon volumes in place
- Predict future reservoir performance
- Predict ultimate hydrocarbon recovery under various types of primary driving mechanisms

The equation is structured to simply keep inventory of all materials entering, leaving, and accumulating in the reservoir. The concept of the material balance equation was presented by Schilthuis in 1941. In its simplest form, the equation can be written on a volumetric basis as:

$$\text{Initial volume} = \text{volume remaining} + \text{volume removed}$$

Since oil, gas, and water are present in petroleum reservoirs, the material balance equation can be expressed for the total fluids or for any one of the fluids present.

Before deriving the material balance, it is convenient to denote certain terms by symbols for brevity. The symbols used conform where possible to the standard nomenclature adopted by the Society of Petroleum Engineers.

| | |
|------------|--|
| p_i | Initial reservoir pressure, psi |
| p | Volumetric average reservoir pressure |
| Δp | Change in reservoir pressure = $p_i - p$, psi |
| p_b | Bubble point pressure, psi |
| N | Initial (original) oil-in-place, STB |
| N_p | Cumulative oil produced, STB |
| G_p | Cumulative gas produced, scf |
| W_p | Cumulative water produced, bbl |
| R_p | Cumulative gas-oil ratio, scf/STB |
| GOR | Instantaneous gas-oil ratio, scf/STB |
| R_{si} | Initial gas solubility, scf/STB |
| R_s | Gas solubility, scf/STB |
| B_{oi} | Initial oil formation volume factor, bbl/STB |
| B_o | Oil formation volume factor, bbl/STB |
| B_{gi} | Initial gas formation volume factor, bbl/scf |
| B_g | Gas formation volume factor, bbl/scf |
| W_{inj} | Cumulative water injected, STB |
| G_{inj} | Cumulative gas injected, scf |
| W_e | Cumulative water influx, bbl |
| m | Ratio of initial gas-cap gas reservoir volume to initial reservoir oil volume, bbl/bbl |
| G | Initial gas-cap gas, scf |
| P.V | Pore volume, bbl |
| c_w | Water compressibility, psi^{-1} |
| c_f | Formation (rock) compressibility, psi^{-1} |

Several of the material balance calculations require the total pore volume (P.V) as expressed in terms of the initial oil volume N and the volume of the gas cap. The expression for the total pore volume can be

derived by conveniently introducing the parameter m into the relationship as follows:

Defining the ratio m as:

$$m = \frac{\text{Initial volume of gas cap}}{\text{Volume of oil initially in place}} = \frac{G B_{gi}}{N B_{oi}}$$

Solving for the volume of the gas cap gives:

$$\text{Initial volume of the gas cap} = G B_{gi} = m N B_{oi}$$

The total volume of the hydrocarbon system is then given by:

$$\text{Initial oil volume} + \text{initial gas cap volume} = (P.V) (1 - S_{wi})$$

$$N B_{oi} + m N B_{oi} = (P.V) (1 - S_{wi})$$

or

$$P.V = \frac{N B_{oi} (1 + m)}{1 - S_{wi}} \quad (11-1)$$

where S_{wi} = initial water saturation

N = initial oil-in-place, STB

$P.V$ = total pore volume, bbl

m = ratio of initial gas-cap gas reservoir volume to initial reservoir oil volume, bbl/bbl

Treating the reservoir pore as an idealized container as illustrated in Figure 11-14, volumetric balance expressions can be derived to account for all volumetric changes which occur during the natural productive life of the reservoir.

The MBE can be written in a generalized form as follows:

Pore volume occupied by the oil initially in place at p_i

+

Pore volume occupied by the gas in the gas cap at p_i

=

Pore volume occupied by the remaining oil at p

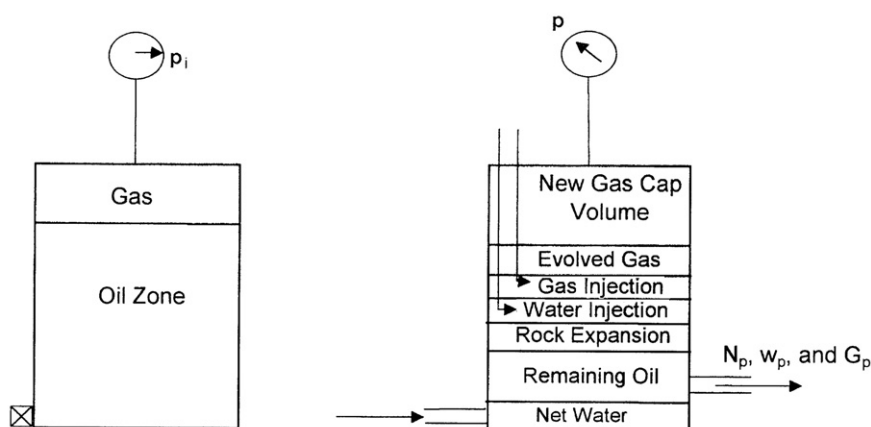


Figure 11-14. Tank-model concept.

$$\begin{aligned}
 &+ \text{Pore volume occupied by the gas in the gas cap at } p \\
 &+ \text{Pore volume occupied by the evolved solution gas at } p \\
 &+ \text{Pore volume occupied by the net water influx at } p \\
 &+ \text{Change in pore volume due to connate-water expansion and pore} \\
 &\text{volume reduction due to rock expansion} \\
 &+ \text{Pore volume occupied by the injected gas at } p \\
 &+ \text{Pore volume occupied by the injected water at } p
 \end{aligned} \tag{11-2}$$

The above nine terms composing the MBE can be separately determined from the hydrocarbon PVT and rock properties, as follows:

Pore Volume Occupied by the Oil Initially in Place

$$\text{Volume occupied by initial oil-in-place} = N B_{oi} \tag{11-3}$$

where N = oil initially in place, STB

B_{oi} = oil formation volume factor at initial reservoir pressure p_i ,
bbl/STB

Pore Volume Occupied by the Gas in the Gas Cap

$$\text{Volume of gas cap} = m N B_{oi} \quad (11-4)$$

where m is a dimensionless parameter and defined as the ratio of gas-cap volume to the oil zone volume.

Pore Volume Occupied by the Remaining Oil

$$\text{Volume of the remaining oil} = (N - N_p) B_o \quad (11-5)$$

where N_p = cumulative oil production, STB

B_o = oil formation volume factor at reservoir pressure p , bbl/STB

Pore Volume Occupied by the Gas Cap at Reservoir Pressure p

As the reservoir pressure drops to a new level p , the gas in the gas cap expands and occupies a larger volume. Assuming no gas is produced from the gas cap during the pressure decline, the new volume of the gas cap can be determined as:

$$\text{Volume of the gas cap at } p = \left[\frac{m N B_{oi}}{B_{gi}} \right] B_g \quad (11-6)$$

where B_{gi} = gas formation volume factor at initial reservoir pressure, bbl/scf

B_g = current gas formation volume factor, bbl/scf

Pore Volume Occupied by the Evolved Solution Gas

This volumetric term can be determined by applying the following material balance on the solution gas:

$$\begin{aligned} \left[\begin{array}{c} \text{volume of the evolved} \\ \text{solution gas} \end{array} \right] &= \left[\begin{array}{c} \text{volume of gas initially} \\ \text{in solution} \end{array} \right] \\ &\quad - \left[\begin{array}{c} \text{volume of gas} \\ \text{produced} \end{array} \right] \\ &\quad - \left[\begin{array}{c} \text{volume of gas} \\ \text{remaining in solution} \end{array} \right] \end{aligned}$$

or

$$\left[\begin{array}{c} \text{volume of the evolved} \\ \text{solution gas} \end{array} \right] = [N R_{si} - N_p R_p - (N - N_p) R_s] B_g \quad (11-7)$$

where N_p = cumulative oil produced, STB

R_p = net cumulative produced gas-oil ratio, scf/STB

R_s = current gas solubility factor, scf/STB

B_g = current gas formation volume factor, bbl/scf

R_{si} = gas solubility at initial reservoir pressure, scf/STB

Pore Volume Occupied by the Net Water Influx

$$\text{net water influx} = W_e - W_p B_w \quad (11-8)$$

where W_e = cumulative water influx, bbl

W_p = cumulative water produced, STB

B_w = water formation volume factor, bbl/STB

Change in Pore Volume Due to Initial Water and Rock Expansion

The component describing the reduction in the hydrocarbon pore volume due to the expansion of initial (connate) water and the reservoir rock cannot be neglected for an undersaturated-oil reservoir. The water compressibility c_w and rock compressibility c_f are generally of the same order of magnitude as the compressibility of the oil. The effect of these two components, however, can be generally neglected for the gas-cap-drive reservoir or when the reservoir pressure drops below the bubble-point pressure.

The compressibility coefficient c , which describes the changes in the volume (expansion) of the fluid or material with changing pressure, is given by:

$$c = \frac{-1}{V} \frac{\partial V}{\partial p}$$

or

$$\Delta V = V c \Delta p$$

where ΔV represents the net changes or expansion of the material as a result of changes in the pressure. Therefore, the reduction in the pore volume due to the expansion of the connate-water in the oil zone and the gas cap is given by:

$$\text{Connate-water expansion} = [(\text{pore volume}) S_{wi}] c_w \Delta p$$

Substituting for the pore volume (P.V) with Equation 11-1 gives:

$$\text{Expansion of connate water} = \frac{N B_{oi} (1 + m)}{1 - S_{wi}} S_{wi} c_w \Delta p \quad (11-9)$$

where Δp = change in reservoir pressure, $(p_i - p)$

c_w = water compressibility coefficient, psi^{-1}

m = ratio of the volume of the gas-cap gas to the reservoir oil volume, bbl/bbl

Similarly, the reduction in the pore volume due to the expansion of the reservoir rock is given by:

$$\text{Change in pore volume} = \frac{N B_{oi} (1 + m)}{1 - S_{wi}} c_f \Delta p \quad (11-10)$$

Combining the expansions of the connate-water and formation as represented by Equations 11-9 and 11-10 gives:

Total changes in the pore volume

$$= N B_{oi} (1 + m) \left(\frac{S_{wi} c_w + c_f}{1 - S_{wi}} \right) \Delta p \quad (11-11)$$

Pore Volume Occupied by the Injection Gas and Water

Assuming that G_{inj} volumes of gas and W_{inj} volumes of water have been injected for pressure maintenance, the total pore volume occupied by the two injected fluids is given by:

$$\text{Total volume} = G_{inj} B_{ginj} + W_{inj} B_w \quad (11-12)$$

where G_{inj} = cumulative gas injected, scf
 B_{ginj} = injected gas formation volume factor, bbl/scf
 W_{inj} = cumulative water injected, STB
 B_w = water formation volume factor, bbl/STB

Combining Equations 11-3 through 11-12 with Equation 11-2 and rearranging gives:

$$N = \frac{N_p B_o + (G_p - N_p R_s) B_g - (W_e - W_p B_w) - G_{inj} B_{ginj} - W_{inj} B_w}{(B_o - B_{oi}) + (R_{si} - R_s) B_g + m B_{oi} \left[\frac{B_g}{B_{gi}} - 1 \right] + B_{oi} (1 + m) \left[\frac{S_{wi} c_w + c_f}{1 - S_{wi}} \right] \Delta p} \quad (11-13)$$

where N = initial oil-in-place, STB
 G_p = cumulative gas produced, scf
 N_p = cumulative oil produced, STB
 R_{si} = gas solubility at initial pressure, scf/STB
 m = ratio of gas-cap gas volume to oil volume, bbl/bbl
 B_{gi} = gas formation volume factor at p_i , bbl/scf
 B_{ginj} = gas formation volume factor of the injected gas, bbl/scf

The cumulative gas produced G_p can be expressed in terms of the cumulative gas-oil ratio R_p and cumulative oil produced N_p by:

$$G_p = R_p N_p \quad (11-14)$$

Combining Equation 11-14 with Equation 11-13 gives:

$$N = \frac{N_p [B_o + (R_p - R_s) B_g] - (W_e - W_p B_w) - G_{inj} B_{ginj} - W_{inj} B_w}{(B_o - B_{oi}) + (R_{si} - R_s) B_g + m B_{oi} \left[\frac{B_g}{B_{gi}} - 1 \right] + B_{oi} (1 + m) \left[\frac{S_{wi} c_w + c_f}{1 - S_{wi}} \right] \Delta p} \quad (11-15)$$

The above relationship is referred to as the **material balance equation** (MBE). A more convenient form of the MBE can be determined by introducing the concept of the total (two-phase) formation volume factor B_t into the equation. This oil PVT property is defined as:

$$B_t = B_o + (R_{si} - R_s) B_g \quad (11-16)$$

Introducing B_t into Equation 11-15 and assuming, for the sake of simplicity, no water or gas injection gives:

$$N = \frac{N_p [B_t + (R_p - R_{si})B_g] - (W_e - W_p B_w)}{(B_t - B_{ti}) + m B_{ti} \left[\frac{B_g}{B_{gi}} - 1 \right] + B_{ti} (1 + m) \left[\frac{S_{wi} c_w + c_f}{1 - S_{wi}} \right] \Delta p} \quad (11-17)$$

where S_{wi} = initial water saturation

R_p = cumulative produced gas-oil ratio, scf/STB

Δp = change in the volumetric average reservoir pressure, psi

In a combination-drive reservoir where all the driving mechanisms are simultaneously present, it is of practical interest to determine the relative magnitude of each of the driving mechanisms and its contribution to the production.

Rearranging Equation 11-17 gives:

$$\frac{N(B_t - B_{ti})}{A} + \frac{NmB_{ti}(B_g - B_{gi})/B_{gi}}{A} + \frac{W_e - W_p B_w}{A} + \frac{NB_{oi}(1 + m) \left[\frac{c_w S_{wi} + c_f}{1 - S_{wi}} \right] (p_i - p)}{A} = 1 \quad (11-18)$$

with the parameter A as defined by:

$$A = N_p [B_t + (R_p - R_{si}) B_g] \quad (11-19)$$

Equation 11-18 can be abbreviated and expressed as:

$$DDI + SDI + WDI + EDI = 1.0 \quad (11-20)$$

where DDI = depletion-drive index

SDI = segregation (gas-cap)-drive index

WDI = water-drive index

EDI = expansion (rock and liquid)-drive index

The four terms of the left-hand side of Equation 11-20 represent the major primary driving mechanisms by which oil may be recovered from oil reservoirs. As presented earlier in this chapter, these driving forces are:

a. Depletion Drive. Depletion drive is the oil recovery mechanism wherein the production of the oil from its reservoir rock is achieved by the expansion of the original oil volume with all its original dissolved gas. This driving mechanism is represented mathematically by the first term of Equation 11-18 or:

$$DDI = N (B_t - B_{ti})/A \quad (11-21)$$

where DDI is termed the **depletion-drive index**.

b. Segregation Drive. Segregation drive (gas-cap drive) is the mechanism wherein the displacement of oil from the formation is accomplished by the expansion of the original free gas cap. This driving force is described by the second term of Equation 11-18, or:

$$SDI = [N m B_{ti} (B_g - B_{gi})/B_{gi}]/A \quad (11-22)$$

where SDI is termed the **segregation-drive index**.

c. Water Drive. Water drive is the mechanism wherein the displacement of the oil is accomplished by the net encroachment of water into the oil zone. This mechanism is represented by the third term of Equation 11-18 or:

$$WDI = (W_e - W_p B_w)/A \quad (11-23)$$

where WDI is termed the **water-drive index**.

d. Expansion Drive. For undersaturated-oil reservoirs with no water influx, the principal source of energy is a result of the rock and fluid expansion. Where all the other three driving mechanisms are contributing to the production of oil and gas from the reservoir, the contribution of the rock and fluid expansion to the oil recovery is too small and essentially negligible and can be ignored.

Cole (1969) pointed out that since the sum of the driving indexes is equal to one, it follows that if the magnitude of one of the index terms is reduced, then one or both of the remaining terms must be correspondingly increased. An effective water drive will usually result in maximum recovery from the reservoir. Therefore, if possible, the reservoir should be operated to yield a maximum water-drive index and minimum values for the depletion-drive index and the gas-cap-drive index. Maximum advantage should be taken of the most efficient drive available, and where the water drive is too weak to provide an effective displacing force, it may be possible to utilize the displacing energy of the gas cap. In any event, the depletion-drive index should be maintained as low as possible at all times, as this is normally the most inefficient driving force available.

Equation 11-20 can be solved at any time to determine the magnitude of the various driving indexes. The forces displacing the oil and gas from the reservoir are subject to change from time to time and for this reason Equation 11-20 should be solved periodically to determine whether there has been any change in the driving indexes. Changes in fluid withdrawal rates are primarily responsible for changes in the driving indexes. For example, reducing the oil-producing rate could result in an increased water-drive index and a correspondingly reduced depletion-drive index in a reservoir containing a weak water drive. Also, by shutting in wells producing large quantities of water, the water-drive index could be increased, as the net water influx (gross water influx minus water production) is the important factor.

When the reservoir has a very weak water drive but a fairly large gas cap, the most efficient reservoir producing mechanism may be the gas cap, in which case a large gas-cap-drive index is desirable. Theoretically, recovery by gas-cap drive is independent of producing rate, as the gas is readily expansible. Low vertical permeability could limit the rate of expansion of the gas cap, in which case the gas-cap-drive index would be rate sensitive. Also, gas coning into producing wells will reduce the effectiveness of the gas-cap expansion due to the production of free gas. Gas coning is usually a rate sensitive phenomenon; the higher the producing rates, the greater the amount of coning.

An important factor in determining the effectiveness of a gas-cap drive is the degree of conservation of the gas-cap gas. As a practical matter, it will often be impossible, because of royalty owners or lease agreements, to completely eliminate gas-cap gas production. Where free gas is being produced, the gas-cap-drive index can often be markedly increased by

shutting in high gas-oil ratio wells and, if possible, transferring their allowables to other low gas-oil ratio wells.

Figure 11-15 shows a set of plots that represent various driving indexes for a combination-drive reservoir. At point A, some of the structurally low wells are reworked to reduce water production. This resulted in an effective increase in the water-drive index. At point B, workover operations are complete; water-, gas-, and oil-producing rates are relatively stable; and the driving indexes show no change. At point C, some of the wells which have been producing relatively large, but constant, volumes of water are shut-in, which results in an increase in the water-drive index. At the same time, some of the upstructure, high gas-oil ratio wells have been shut-in and their allowables transferred to wells lower on the structure producing with normal gas-oil ratios. At point D, gas is being returned to the reservoir, and the gas-cap-drive index is exhibiting a decided increase.

The water-drive index is relatively constant, although it is decreasing somewhat, and the depletion-drive index is showing a marked decline. This is indicative of a more efficient reservoir operation, and, if the depletion-drive index can be reduced to zero, relatively good recovery can be expected from the reservoir. Of course, to achieve a zero-depletion-drive index would require the complete maintenance of reservoir pressure, which is often difficult to accomplish. It can be noted from Figure 11-15 that the sum of the various indexes of drive is always equal to one.

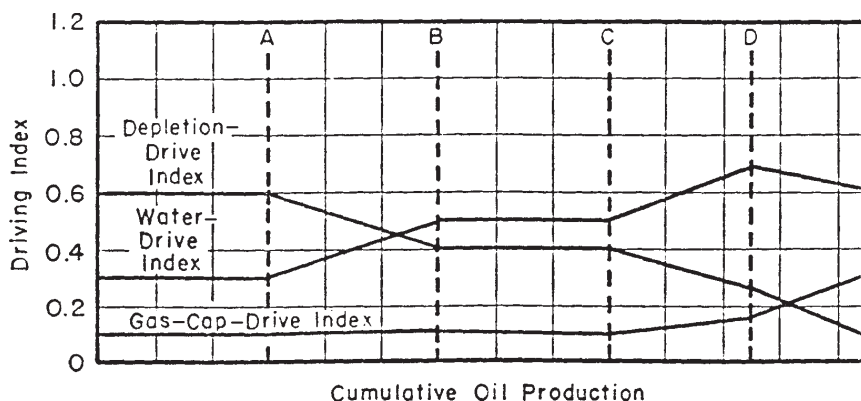


Figure 11-15. Driving indexes in a combination-drive reservoir. (After Clark, N. J., *Elements of Petroleum Reservoirs*, SPE, 1969.)

Example 11-1

A combination-drive reservoir contains 10 MMSTB of oil initially in place. The ratio of the original gas-cap volume to the original oil volume, i.e., m , is estimated as 0.25. The initial reservoir pressure is 3,000 psia at 150°F. The reservoir produced 1 MMSTB of oil, 1,100 MMscf of 0.8 specific gravity gas, and 50,000 STB of water by the time the reservoir pressure dropped to 2,800 psi. The following PVT is available:

| | 3000 psi | 2800 psi |
|-----------------|----------|----------|
| B_o , bbl/STB | 1.58 | 1.48 |
| R_s , scf/STB | 1040 | 850 |
| B_g , bbl/scf | 0.00080 | 0.00092 |
| B_t , bbl/STB | 1.58 | 1.655 |
| B_w , bbl/STB | 1.000 | 1.000 |

The following data are also available:

$$S_{wi} = 0.20 \quad c_w = 1.5 \times 10^{-6} \text{ psi}^{-1} \quad c_f = 1 \times 10^{-6} \text{ psi}^{-1}$$

Calculate:

- Cumulative water influx
- Net water influx
- Primary driving indexes at 2,800 psi

Solution

Because the reservoir contains a gas cap, the rock and fluid expansion can be neglected, i.e., set c_f and $c_w = 0$. For illustration purposes, however, the rock and fluid expansion term will be included in the calculations.

Part A. Cumulative water influx

Step 1. Calculate cumulative gas-oil ratio R_p :

$$R_p = \frac{1100 \times 10^6}{1 \times 10^6} = 1100 \text{ scf/STB}$$

Step 2. Arrange Equation 11-17 to solve for W_e :

$$W_e = N_p [B_t + (R_p - R_{si}) B_g] - N \left[(B_g - B_{ti}) + m B_{ti} \left(\frac{B_g}{B_{gi}} - 1 \right) + B_{ti} (1 + m) \left(\frac{S_{wi} c_w + c_f}{1 - S_{wi}} \right) \Delta p \right] + W_p B_{wp}$$

$$\begin{aligned} W_e &= 10^6 [1.655 + (1100 - 1040) 0.00092] \\ &\quad - 10^7 \left[(1.655 - 1.58) + 0.25 (1.58) \left(\frac{0.00092}{0.00080} - 1 \right) \right. \\ &\quad \left. + 1.58 (1 + 0.25) \left(\frac{0.2 (1.5 \times 10^{-6})}{1 - 0.2} \right) (3000 - 2800) \right] + 50,000 \\ &= 411,281 \text{ bbl} \end{aligned}$$

Neglecting the rock and fluid expansion term, the cumulative water influx is 417,700 bbl.

Part B. Net water influx

$$\text{Net water influx} = W_e - W_p B_w = 411,281 - 50,000 = 361,281 \text{ bbl}$$

Part C. Primary recovery indexes

Step 1. Calculate the parameter A by using Equation 11-19:

$$A = 10^6 [1.655 + (1100 - 1040) 0.00092] = 1,710,000$$

Step 2. Calculate DDI, SDI, and WDI by applying Equations 11-21 through 11-23, respectively:

$$\text{DDI} = \frac{10 \times 10^6 (1.655 - 1.58)}{1,710,000} = 0.4385$$

$$\text{SDI} = \frac{10 \times 10^6 (0.25) (1.58) (0.00092 - 0.0008) / 0.0008}{1,710,000} = 0.3465$$

$$\text{WDI} = \frac{411,281 - 50,000}{1,710,000} = 0.2112$$

$$\text{EDI} = 1 - 0.4385 - 0.3465 - 0.2112 = 0.0038$$

where EDI is termed the **expansion-drive index**.

These calculations show that the 43.85% of the recovery was obtained by depletion drive, 34.65% by gas-cap drive, 21.12% by water drive, and only 0.38% by connate-water and rock expansion. The results suggest that the expansion-drive index (EDI) term can be neglected in the presence of a gas cap or when the reservoir pressure drops below the bubble-point pressure. In high pore volume compressibility reservoirs, such as chalks and unconsolidated sands, however, the energy contribution of the rock and water expansion cannot be ignored even at high gas saturations.

Example 11-2

The Big Butte field is a combination-drive reservoir. The current reservoir pressure is estimated at 2,500 psi. The reservoir production data and PVT information are given below:

| | Initial Reservoir Condition | Current Reservoir Condition |
|---------------------------------|-----------------------------|-----------------------------|
| p, psi | 3000 | 2500 |
| B _o , bbl/STB | 1.35 | 1.33 |
| R _s , scf/STB | 600 | 500 |
| N _p , MMSTB | 0 | 5 |
| G _p , MMMscf | | 5.5 |
| B _w , bbl/STB | 1.00 | 1.00 |
| W _e , MMbbl | 0 | 3 |
| W _p , MMbbl | 0 | 0.2 |
| B _g , bbl/scf | 0.0011 | 0.0015 |
| c _f , c _w | 0 | 0 |

The following additional information is available:

Volume of bulk oil zone = 100,000 ac-ft

Volume of bulk gas zone = 20,000 ac-ft

Calculate the initial oil-in-place.

Solution

Step 1. Assuming the same porosity and connate-water for the oil and gas zones, calculate m :

$$m = \frac{20,000}{100,000} = 0.2$$

Step 2. Calculate the cumulative gas-oil ratio R_p :

$$R_p = \frac{5.5 \times 10^9}{5 \times 10^6} = 1100 \text{ scf/STB}$$

Step 3. Solve for the initial oil-in-place by applying Equation 11-15:

$$N = \frac{5 \times 10^6 [1.33 + (1100 - 500)0.0015] - (3 \times 10^6 - 0.2 \times 10^6)}{(1.35 - 1.33) + (600 - 500)0.0015 + (0.2)(1.35) \left[\frac{0.0015}{0.0011} - 1 \right]}$$

$$= 31.14 \text{ MMSTB}$$

Basic Assumptions in the MBE

The material balance equation calculation is based on changes in reservoir conditions over discrete periods of time during the production history. The calculation is most vulnerable to many of its underlying assumptions early in the depletion sequence when fluid movements are limited and pressure changes are small. Uneven depletion and partial reservoir development compound the accuracy problem.

The basic assumptions in the material balance equation (MBE) are as follows:

- **Constant temperature.** Pressure-volume changes in the reservoir are assumed to occur without any temperature changes. If any temperature changes occur, they are usually sufficiently small to be ignored without significant error.
- **Pressure equilibrium.** All parts of the reservoir have the same pressure, and fluid properties are therefore constant throughout. Minor variations in the vicinity of the well bores may usually be ignored. Substantial pressure variation across the reservoir may cause excessive calculation error.

It is assumed that the PVT samples or data sets represent the actual fluid compositions and that reliable and representative laboratory procedures have been used. Notably, the vast majority of material balances assume that differential depletion data represent reservoir flow and that separator flash data may be used to correct for the wellbore transition to surface conditions. Such “black oil” PVT treatments relate volume changes to temperature and pressure only. They lose validity in cases of volatile oil or gas condensate reservoirs where compositions are also important. Special laboratory procedures may be used to improve PVT data for volatile fluid situations.

Constant reservoir volume. Reservoir volume is assumed to be constant except for those conditions of rock and water expansion or water influx that are specifically considered in the equation. The formation is considered to be sufficiently competent that no significant volume change will occur through movement or reworking of the formation due to overburden pressure as the internal reservoir pressure is reduced. The constant volume assumption is also related to an area of interest to which the equation is applied. If the focus is on some part of a reservoir system, except for specific exterior flow terms it is assumed that the particular portion is encased in no-flow boundaries.

Reliable production data. All production data should be recorded with respect to the same time period. If possible, gas-cap- and solution-gas production records should be maintained separately.

Gas and oil gravity measurements should be recorded in conjunction with the fluid volume data. Some reservoirs require a more detailed analysis and that the material balance be solved for volumetric segments. The produced fluid gravities will aid in the selection of the volumetric segments and also in the averaging of fluid properties. There are essentially three types of production data that must be recorded in order to use the MBE in performing reliable reservoir calculations. These are:

- **Oil-production data**, even for non-interest properties, which can usually be obtained from various sources and are usually fairly reliable.
- **Gas-production data**, which are becoming more available and reliable as the market value of this commodity increases; unfortunately, these data will often be more questionable where gas is flared.
- **The water-production term**, which need represent only the net withdrawals of water; therefore, where subsurface disposal of produced brine is to the same source formation, most of the error due to poor data will be eliminated.

A source of error is often introduced in the MBE calculations when determining the average reservoir pressure and the associated problem of correctly weighting or averaging the individual well pressures. An example of such a problem is when the producing formations are composed of two or more zones of different permeabilities. In this case, the pressures are generally higher in the zone of low permeability, and because the measured pressures are nearer to those in high-permeability zones, the measured static pressures tend to be lower and the reservoir behaves as if it contained less oil. Schilthuis (1941) explained this phenomenon by referring to the oil in the more permeable zones as **active oil** and by observing that the *calculated active oil usually increases with time* because the oil and gas in low-permeability zones slowly expand to offset the pressure decline. This is also true for fields that are not fully developed, because the average pressure can be that of only the developed portion, whereas the pressure is higher in the undeveloped portions.

Craft et al. (1991) pointed out that the effect of pressure errors on the calculated values of initial oil and water influx depends on the size of the errors in relation to the reservoir pressure decline. Notice that the pressure enters the MBE mainly when determining the PVT differences in terms of the following:

- $(B_o - B_{oi})$
- $(B_g - B_{gi})$
- $(R_{si} - R_s)$

Because water influx and gas cap expansion tend to offset pressure decline, the pressure errors are more serious than for the undersaturated reservoirs. In the case of very active water drives or gas caps that are large compared with the oil zone, the MBE usually produces considerable errors when determining the initial oil-in-place because of the very small pressure decline.

Dake (1994) points out that there are two “necessary” conditions that must be satisfied for a meaningful application of the MBE to a reservoir; these are as follows:

1. There should be adequate data collection in terms of production pressure and PVT, both in frequency and quality for proper use of the MBE.
2. It must be possible to define an average reservoir pressure trend as a function of time or production for the field.

Establishing an average pressure-decline trend can be possible even if there are large pressure differences across the field under normal conditions. Averaging **individual well pressure** declines can possibly be used to determine a uniform trend in the entire reservoir. The concept of average well pressure and its use in determining the reservoir volumetric average pressure was introduced in Chapter 6, as illustrated by Figure 6-24. This illustration shows that if $(\bar{P})_j$ and V_j represent the pressure and volume drained by the j th well, the volumetric average pressure of the entire reservoir can be estimated from:

$$\bar{p}_r = \frac{\sum_j (\bar{p} V)_j}{\sum_j V_j}$$

in which

V_j = pore volume of the j th well drainage volume

$(\bar{P})_j$ = Volumetric average pressure *within the j th drainage volume*

In practice, the V_i values are difficult to determine and, therefore, it is common to use individual wells' flow rates, q_i , in determining the average reservoir pressure from individual wells' average drainage pressure. From the definition of the isothermal compressibility coefficient:

$$c = \frac{1}{V} \frac{\partial V}{\partial P}$$

Differentiating this equation with time gives:

$$\frac{\partial p}{\partial t} = \frac{1}{c V} \frac{\partial V}{\partial t}$$

or:

$$\frac{\partial p}{\partial t} = \frac{1}{c V} (q)$$

The last expression suggests that for a reasonably constant c at the time of measurement,

$$V \propto \frac{q}{\partial p / \partial t}$$

Since the flow rates are measured on a routing basis throughout the lifetime of the field, the average reservoir pressure can be alternatively

expressed in terms of the individual wells' average drainage-pressure-decline rates and fluid-flow rates by:

$$\bar{p}_r = \frac{\sum_j [(\bar{p}q)_j / (\partial \bar{p} / \partial t)_j]}{\sum_j [q_j / (\partial \bar{p} / \partial t)_j]}$$

However, since the MBE is usually applied at regular intervals of 3–6 months (i.e., $\Delta t = 3\text{--}6$ months), throughout the life of the field, the average field pressure can be expressed in terms of the incremental net change in underground fluid withdrawal, $\Delta(F)$, as follows:

$$\bar{p}_r = \frac{\sum_j \frac{\bar{p}_j \Delta(F)_j}{\Delta \bar{p}_j}}{\sum_j \frac{\Delta(F)_j}{\Delta \bar{p}_j}}$$

where the total underground fluid withdrawal at times t and $t + \Delta t$ are given by:

$$F_t = \int_0^t [Q_o B_o + Q_w B_w + (Q_g - Q_o R_s - Q_w R_{sw}) B_g] dt$$

$$F_{t+\Delta t} = \int_0^{t+\Delta t} [Q_o B_o + Q_w B_w + (Q_g - Q_o R_s - Q_w R_{sw}) B_g] dt$$

with:

$$\Delta(F) = F_{t+\Delta t} - F_t$$

where R_s = gas solubility, scf/STB

R_{sw} = gas solubility in the water, scf/STB

B_g = gas formation volume factor, bbl/scf

Q_o = oil flow rate, STB/day

q_o = oil flow rate, bbl/day

Q_w = water flow rate, STB/day

q_w = water flow rate, bbl/day

Q_g = gas flow rate, scf/day

For a volumetric reservoir with total fluid production and initial reservoir pressure as the only available data, the average pressure can be *roughly approximated* by using the following expression:

$$\bar{p}_r = p_i - \left[\frac{5.371 \times 10^{-6} F_t}{c_t (Ah\phi)} \right]$$

with the total fluid production, F_t , as defined above by:

$$F_t = \int_0^t [Q_o B_o + Q_w B_w + (Q_g - Q_o R_s - Q_w R_{sw}) B_g] dt$$

where A = well or reservoir drainage area, acres

h = thickness, ft

c_t = total compressibility coefficient, psi^{-1}

ϕ = porosity, fraction

p_i = initial reservoir pressure, psi

The last expression can be employed in an incremental manner, from time t to $t + \Delta t$, by:

$$(\bar{p}_r)_{t+\Delta t} = (\bar{p}_r)_t - \left[\frac{5.371 \times 10^{-6} \Delta F}{c_t (Ah\phi)} \right]$$

with:

$$\Delta(F) = F_{t+\Delta t} - F_t$$

The MBE as an Equation of a Straight Line

An insight into the general MBE, i.e., Equation 11-15, may be gained by considering the physical significance of the following groups of terms of which it is comprised:

- $N_p [B_o + (R_p - R_s) B_g]$ Represents the reservoir volume of cumulative oil and gas produced.
- $[W_e - W_p B_w]$ Refers to the net water influx that is retained in the reservoir.
- $[G_{inj} B_{ginj} + W_{inj} B_w]$ This pressure maintenance term represents cumulative fluid injection in the reservoir.

- $[m B_{oi} (B_g/B_{gi} - 1)]$ Represents the net expansion of the gas cap that occurs with the production of N_p stock-tank barrels of oil (as expressed in bbl/STB of original oil-in-place).

There are essentially three unknowns in Equation 11-15:

- The original oil-in-place N
- The cumulative water influx W_e
- The original size of the gas cap as compared to the oil zone size m

In developing a methodology for determining the above three unknowns, Havlena and Odeh (1963) expressed Equation 11-15 in the following form:

$$N_p [B_o + (R_p - R_s)B_g] + W_p B_w = N[(B_o - B_{oi}) + (R_{si} - R_s)B_g] + m N B_{oi} \left(\frac{B_g}{B_{gi}} - 1 \right) + N (1 + m) B_{oi} \left[\frac{c_w S_{wi} + c_f}{1 + S_{wi}} \right] \Delta p + W_e + W_{inj} B_w + G_{inj} B_{ginj} \quad (11-24)$$

Havlena and Odeh further expressed Equation 11-24 in a more condensed form as:

$$F = N [E_o + m E_g + E_{f,w}] + (W_e + W_{inj} B_w + G_{inj} B_{ginj})$$

Assuming, for the purpose of simplicity, that no pressure maintenance by gas or water injection is being considered, the above relationship can be further simplified and written as:

$$F = N [E_o + m E_g + E_{f,w}] + W_e \quad (11-25)$$

in which the terms F , E_o , E_g , and $E_{f,w}$ are defined by the following relationships:

- F represents the underground withdrawal and is given by:

$$F = N_p [B_o + (R_p - R_s) B_g] + W_p B_w \quad (11-26)$$

In terms of the two-phase formation volume factor B_t , the underground withdrawal F can be written as:

$$F = N_p [B_t + (R_p - R_{si}) B_g] + W_p B_w \quad (11-27)$$

- E_o describes the expansion of oil and its originally dissolved gas and is expressed in terms of the oil formation volume factor as:

$$E_o = (B_o - B_{oi}) + (R_{si} - R_s) B_g \quad (11-28)$$

Or equivalently, in terms of B_t :

$$E_o = B_t - B_{ti} \quad (11-29)$$

- E_g is the term describing the expansion of the gas-cap gas and is defined by the following expression:

$$E_g = B_{oi} [(B_g/B_{gi}) - 1] \quad (11-30)$$

In terms of the two-phase formation volume factor B_t , essentially $B_{ti} = B_{oi}$ or:

$$E_g = B_{ti} [(B_g/B_{gi}) - 1]$$

- $E_{f,w}$ represents the expansion of the initial water and the reduction in the pore volume and is given by:

$$E_{f,w} = (1 + m)B_{oi} \left[\frac{c_w S_{wi} + c_f}{1 - S_{wi}} \right] \Delta p \quad (11-31)$$

Havlena and Odeh examined several cases of varying reservoir types with Equation 11-25 and pointed out that the relationship can be rearranged into the form of a straight line. For example, in the case of a reservoir which has no initial gas cap (i.e., $m = 0$) or water influx (i.e., $W_e = 0$), and negligible formation and water compressibilities (i.e., c_f and $c_w = 0$), Equation 11-25 reduces to:

$$F = N E_o$$

The above expression suggests that a plot of the parameter F as a function of the oil expansion parameter E_o would yield a straight line with a slope N and intercept equal to zero.

The Straight-Line Solution Method to the MBE

The straight-line solution method requires the plotting of a variable group versus another variable group, with the variable group selection depending on the mechanism of production under which the reservoir is producing. The most important aspect of this method of solution is that it

attaches significance to the sequence of the plotted points, the direction in which they plot, and to the shape of the resulting plot.

The significance of the straight-line approach is that the sequence of plotting is important and if the plotted data deviate from this straight line, there is some reason for it. This significant observation will provide the engineer with valuable information that can be used in determining the following unknowns:

- Initial oil-in-place N
- Size of the gas cap m
- Water influx W_e
- Driving mechanism

The applications of the straight-line form of the MBE in solving reservoir engineering problems are presented next to illustrate the usefulness of this particular form. Six cases of applications are presented:

1. Case 1: Determination of N in volumetric undersaturated reservoirs
2. Case 2: Determination of N in volumetric saturated reservoirs
3. Case 3: Determination of N and m in gas-cap-drive reservoirs
4. Case 4: Determination of N and W_e in water-drive reservoirs
5. Case 5: Determination of N , m , and W_e in combination-drive reservoirs
6. Case 6: Determination of average reservoir pressure, \bar{p}

The remainder of this chapter is devoted to illustrations of the use of the straight-line solution method in determining N , m , and W_e for different reservoir mechanisms.

Case 1. Volumetric Undersaturated-Oil Reservoirs

Assuming no water or gas injection, the linear form of the MBE as expressed by Equation 11-25 can be written as:

$$F = N [E_o + m E_g + E_{f,w}] + W_e \quad (11-32)$$

Several terms in the above relationship may disappear when imposing the conditions associated with the assumed reservoir-driving mechanism. For a volumetric and undersaturated reservoir, the conditions associated with a driving mechanism are:

- $W_e = 0$, since the reservoir is volumetric
- $m = 0$, since the reservoir is undersaturated

- $R_s = R_{si} = R_p$, since all produced gas is dissolved in the oil

Applying the above conditions on Equation 11-32 gives:

$$F = N (E_o + E_{f,w}) \quad (11-33)$$

or

$$N = \frac{F}{E_o + E_{f,w}} \quad (11-34)$$

where N = initial oil-in-place, STB

$$F = N_p B_o + W_p B_w \quad (11-35)$$

$$E_o = B_o - B_{oi} \quad (11-36)$$

$$E_{f,w} = B_{oi} \left[\frac{c_w S_w + c_f}{1 - S_{wi}} \right] \Delta p \quad (11-37)$$

$$\Delta p = p_i - \bar{p}_r$$

p_i = initial reservoir pressure

\bar{p}_r = volumetric average reservoir pressure

When a new field is discovered, one of the first tasks of the reservoir engineer is to determine if the reservoir can be classified as a volumetric reservoir, i.e., $W_e = 0$. The classical approach of addressing this problem is to assemble all the necessary data (i.e., production, pressure, and PVT) that are required to evaluate the right-hand side of Equation 11-36. The term $F/(E_o + E_{f,w})$ for each pressure and time observation is plotted versus cumulative production N_p or time, as shown in Figure 11-16. Dake (1994) suggests that such a plot can assume two various shapes, which are:

- All the calculated points of $F/(E_o + E_{f,w})$ lie on a horizontal straight line (see Line A in Figure 11-16). Line A in the plot implies that the reservoir can be classified as a volumetric reservoir. This defines a purely depletion-drive reservoir whose energy derives solely from the expansion of the rock, connate-water, and the oil. Furthermore, the ordinate value of the plateau determines the initial oil-in-place N .
- Alternately, the calculated values of the term $F/(E_o + E_{f,w})$ rise, as illustrated by the curves B and C, indicating that the reservoir has been

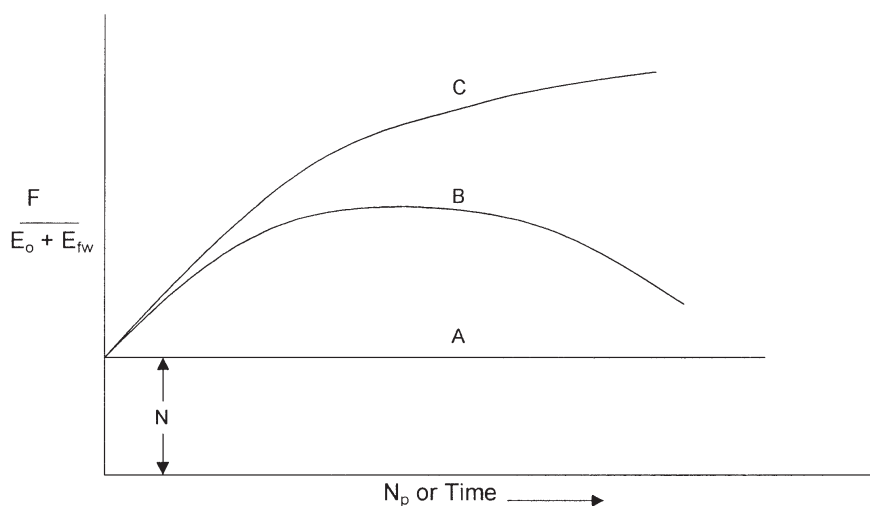


Figure 11-16. Classification of the reservoir.

energized by water influx, abnormal pore compaction, or a combination of these two. Curve C in Figure 11-16 might be for a strong water-drive field in which the aquifer is displacing an infinite acting behavior, whereas B represents an aquifer whose outer boundary has been felt and the aquifer is depleting in unison with the reservoir itself. The downward trend in points on curve B as time progresses denotes the diminishing degree of energizing by the aquifer. Dake (1994) points out that in water-drive reservoirs, the shape of the curve, i.e., $F/(E_o + E_{f,w})$ vs. time, is highly rate dependent. For instance, if the reservoir is producing at a higher rate than the water-influx rate, the calculated values of $F/(E_o + E_{f,w})$ will dip downward revealing a lack of energizing by the aquifer, whereas, if the rate is decreased, the reverse happens and the points are elevated.

Similarly, Equation 11-33 could be used to verify the characteristic of the reservoir-driving mechanism and to determine the initial oil-in-place. A plot of the underground withdrawal F versus the expansion term $(E_o + E_{f,w})$ should result in a straight line going through the origin with N being the slope. It should be noted that the origin is a “must” point; thus, one has a fixed point to guide the straight-line plot (as shown in Figure 11-17).

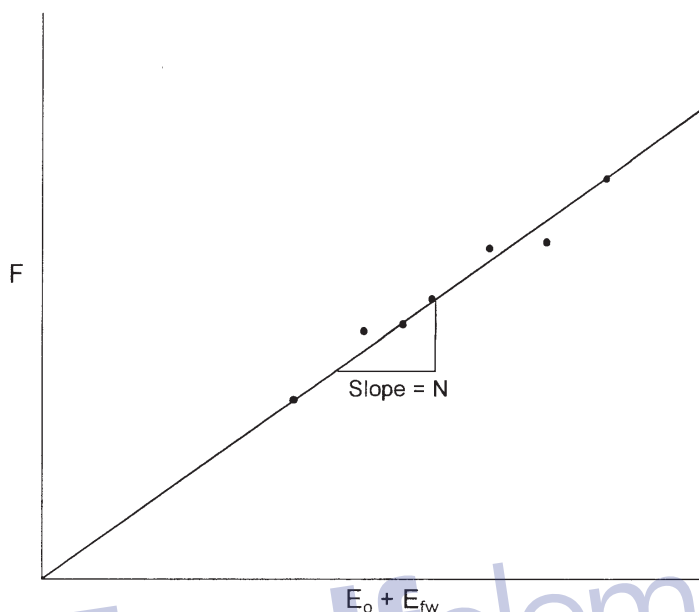


Figure 11-17. Underground withdrawal vs. $E_o + E_{fw}$.

This interpretation technique is useful in that, if the linear relationship is expected for the reservoir and yet the actual plot turns out to be non-linear, then this deviation can itself be diagnostic in determining the actual drive mechanisms in the reservoir.

A linear plot of the underground withdrawal F versus $(E_o + E_{f,w})$ indicates that the field is producing under volumetric performance, i.e., no water influx, and strictly by pressure depletion and fluid expansion. On the other hand, a nonlinear plot indicates that the reservoir should be characterized as a water-drive reservoir.

Example 11-3

The Virginia Hills Beaverhill Lake field is a volumetric undersaturated reservoir. Volumetric calculations indicate the reservoir contains 270.6 MMSTB of oil initially in place. The initial reservoir pressure is 3685 psi. The following additional data are available:

$$\begin{array}{lll}
 S_{wi} = 24\% & c_w = 3.62 \times 10^{-6} \text{ psi}^{-1} & c_f = 4.95 \times 10^{-6} \text{ psi}^{-1} \\
 B_w = 1.0 \text{ bbl/STB} & p_b = 1500 \text{ psi} &
 \end{array}$$

The field production and PVT data are summarized below:

| Volumetric Average Pressure | No. of Producing Wells | B_o bbl/STB | N_p MSTB | W_p MSTB |
|--------------------------------|---------------------------|------------------|---------------|---------------|
| 3685 | 1 | 1.3102 | 0 | 0 |
| 3680 | 2 | 1.3104 | 20.481 | 0 |
| 3676 | 2 | 1.3104 | 34.750 | 0 |
| 3667 | 3 | 1.3105 | 78.557 | 0 |
| 3664 | 4 | 1.3105 | 101.846 | 0 |
| 3640 | 19 | 1.3109 | 215.681 | 0 |
| 3605 | 25 | 1.3116 | 364.613 | 0 |
| 3567 | 36 | 1.3122 | 542.985 | 0.159 |
| 3515 | 48 | 1.3128 | 841.591 | 0.805 |
| 3448 | 59 | 1.3130 | 1273.530 | 2.579 |
| 3360 | 59 | 1.3150 | 1691.887 | 5.008 |
| 3275 | 61 | 1.3160 | 2127.077 | 6.500 |
| 3188 | 61 | 1.3170 | 2575.330 | 8.000 |

Calculate the initial oil-in-place by using the MBE and compare with the volumetric estimate of N .

Solution

Step 1. Calculate the initial water and rock expansion term $E_{f,w}$ from Equation 11-37:

$$E_{f,w} = 1.3102 \left[\frac{3.62 \times 10^{-6} (0.24) + 4.95 \times 10^{-6}}{1 - 0.24} \right] \Delta p$$

$$E_{f,w} = 10.0 \times 10^{-6} (3685 - \bar{p}_r)$$

Step 2. Construct the following table:

| \bar{p}_r , psi | F , Mbbl Equation 10-35 | E_o , bbl/STB Equation 10-36 | Δp | $E_{f,w}$ | $E_o + E_{f,w}$ |
|-------------------|------------------------------|-----------------------------------|------------|----------------------|-----------------|
| 3685 | — | — | 0 | 0 | — |
| 3680 | 26.84 | 0.0002 | 5 | 50×10^{-6} | 0.00025 |
| 3676 | 45.54 | 0.0002 | 9 | 90×10^{-6} | 0.00029 |
| 3667 | 102.95 | 0.0003 | 18 | 180×10^{-6} | 0.00048 |
| 3664 | 133.47 | 0.0003 | 21 | 210×10^{-6} | 0.00051 |
| 3640 | 282.74 | 0.0007 | 45 | 450×10^{-6} | 0.00115 |

(table continued on next page)

| \bar{p}_r , psi | F, Mbbbl Equation 10-35 | E_o , bbl/STB Equation 10-36 | Δp | $E_{f,w}$ | $E_o + E_{f,w}$ |
|-------------------|----------------------------|-----------------------------------|------------|-----------------------|-----------------|
| 3605 | 478.23 | 0.0014 | 80 | 800×10^{-6} | 0.00220 |
| 3567 | 712.66 | 0.0020 | 118 | 1180×10^{-6} | 0.00318 |
| 3515 | 1105.65 | 0.0026 | 170 | 1700×10^{-6} | 0.00430 |
| 3448 | 1674.72 | 0.0028 | 237 | 2370×10^{-6} | 0.00517 |
| 3360 | 2229.84 | 0.0048 | 325 | 3250×10^{-6} | 0.00805 |
| 3275 | 2805.73 | 0.0058 | 410 | 4100×10^{-6} | 0.00990 |
| 3188 | 3399.71 | 0.0068 | 497 | 4970×10^{-6} | 0.01170 |

Step 3. Plot the underground withdrawal term F against the expansion term ($E_o + E_{f,w}$) on a Cartesian scale, as shown in Figure 11-18.

Step 4. Draw the best straight line through the points and determine the slope of the line and the volume of the active initial oil-in-place as:

$$N = 257 \text{ MMSTB}$$

It should be noted that the value of the initial oil-in-place as determined from the MBE is referred to as the effective or active initial oil-in-place. This value is usually smaller than that of the volumetric estimate due to oil being trapped in undrained fault compartments or low-permeability regions of the reservoir.

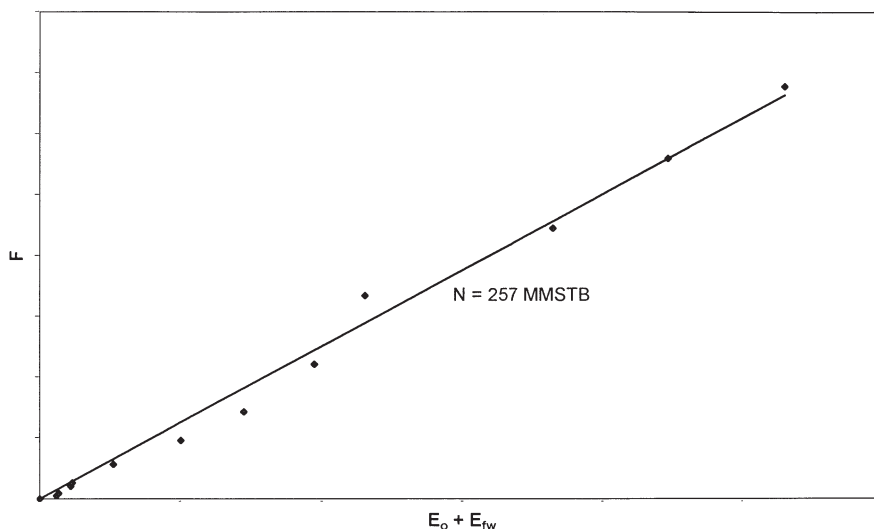


Figure 11-18. F vs. ($E_o + E_{f,w}$) for Example 11-3.

Case 2. Volumetric Saturated-Oil Reservoirs

An oil reservoir that originally exists at its bubble-point pressure is referred to as a saturated-oil reservoir. The main driving mechanism in this type of reservoir results from the liberation and expansion of the solution gas as the pressure drops below the bubble-point pressure. The only unknown in a volumetric saturated-oil reservoir is the initial oil-in-place N . Assuming that the water and rock expansion term $E_{f,w}$ is negligible in comparison with the expansion of solution gas, Equation 11-32 can be simplified as:

$$F = N E_o \quad (11-38)$$

where the underground withdrawal F and the oil expansion E_o were defined previously by Equations 11-26 and 11-28 or Equations 11-27 and 11-29 to give:

$$F = N_p [B_t + (R_p - R_{si}) B_g] + W_p B_w$$

$$E_o = B_t - B_{ti}$$

Equation 11-38 indicates that a plot of the underground withdrawal F , evaluated by using the actual reservoir production data, as a function of the fluid expansion term E_o , should result in a straight line going through the origin with a slope of N .

The above interpretation technique is useful in that, if a simple linear relationship such as Equation 11-38 is expected for a reservoir and yet the actual plot turns out to be nonlinear, then this deviation can itself be diagnostic in determining the actual drive mechanisms in the reservoir. For instance, Equation 11-38 may turn out to be nonlinear because there is an unsuspected water influx into the reservoir helping to maintain the pressure.

It should be pointed out that, as the reservoir pressure continues to decline below the bubble-point and with the increasing volume of the liberated gas, it reaches the time where the saturation of the liberated gas exceeds the critical gas saturation. As a result, the gas will start to be produced in disproportionate quantities to the oil. At this stage of depletion, there is little that can be done to avert this situation during the primary production phase. As indicated earlier, the primary recovery from these types of reservoirs seldom exceeds 30%. However, under very favorable conditions, the oil and gas might separate, with the gas moving structurally updip in the reservoir; this might lead to preservation of the natur-

al energy of the reservoir with a consequent improvement in overall oil recovery. Water injection is traditionally used by the oil industry to maintain the pressure above the bubble-point pressure or alternatively to pressurize the reservoir to the bubble-point pressure. In such types of reservoirs, as the reservoir pressure drops below the bubble-point pressure, some volume of the liberated gas will remain in the reservoir as a free gas. This volume, expressed in scf, is given by Equation 11-7 as:

$$\left[\text{Volume of the free gas in scf} \right] = N R_{si} - (N - N_p) R_s - N_p R_p$$

However, the total volume of the liberated gas at any depletion pressure is given by

$$\left[\begin{array}{l} \text{Total volume of the} \\ \text{liberated gas, in scf} \end{array} \right] = N R_{si} - (N - N_p) R_s$$

Therefore, the fraction of the total solution gas that has been retained in the reservoir as a free gas, α_g , at any depletion stage is then given by:

$$\alpha_g = \frac{N R_{si} - (N - N_p) R_s - N_p R_p}{N R_{si} - (N - N_p) R_s} = 1 - \left[\frac{N_p R_p}{N R_{si} - (N - N_p) R_s} \right]$$

Alternatively, it can be expressed as a fraction of the total initial gas in solution, by

$$\alpha_{gi} = \frac{N R_{si} - (N - N_p) R_s - N_p R_p}{N R_{si}} = 1 - \left[\frac{(N - N_p) R_s + N_p R_p}{N R_{si}} \right]$$

The calculation of the changes in the fluid saturations with declining reservoir pressure is an integral part of using the MBE. The remaining volume of each phase can be determined by calculating the saturation of each phase as:

$$\text{Oil saturation: } S_o = \frac{\text{oil volume}}{\text{pore volume}}$$

$$\text{Water saturation: } S_w = \frac{\text{water volume}}{\text{pore volume}}$$

$$\text{Gas saturation: } S_g = \frac{\text{gas volume}}{\text{pore volume}}$$

and:

$$S_o + S_w + S_g = 1.0$$

If we consider a volumetric saturated-oil reservoir that contains N stock-tank barrels of oil at the initial reservoir pressure p_i (i.e., p_b), the initial oil saturation at the bubble-point pressure is given by:

$$S_{oi} = 1 - S_{wi}$$

From the definition of oil saturation:

$$\frac{\text{oil volume}}{\text{pore volume}} = \frac{N B_{oi}}{\text{pore volume}} = 1 - S_{wi}$$

or

$$\text{pore volume} = \frac{N B_{oi}}{1 - S_{wi}}$$

If the reservoir has produced N_p stock-tank barrels of oil, the remaining oil volume is given by:

$$\text{Remaining oil volume} = (N - N_p) B_o$$

This indicates that for a volumetric-type oil reservoir, the oil saturation at any depletion state below the bubble-point pressure can be represented by:

$$S_o = \frac{\text{oil volume}}{\text{pore volume}} = \frac{(N - N_p) B_o}{\left(\frac{N B_{oi}}{1 - S_{wi}} \right)}$$

Rearranging gives:

$$S_o = (1 - S_{wi}) \left(1 - \frac{N_p}{N} \right) \frac{B_o}{B_{oi}}$$

As the solution gas evolves from the oil with declining reservoir pressure, the gas saturation (assuming constant water saturation, S_{wi}) is simply given as

$$S_g = 1 - S_{wi} - S_o$$

or

$$S_g = 1 - S_{wi} - \left[(1 - S_{wi}) \left(1 - \frac{N_p}{N} \right) \frac{B_o}{B_{oi}} \right]$$

Simplifying gives

$$S_g = (1 - S_{wi}) \left[1 - \left(1 - \frac{N_p}{N} \right) \frac{B_o}{B_{oi}} \right]$$

Another important function of the MBE is history-matching the production-pressure data of individual wells. Once the reservoir pressure declines below the bubble-point pressure, it is essential to perform the following tasks:

- Generating the pseudo-relative permeability ratio, k_{rg}/k_{ro} for the entire reservoir or for individual wells' drainage areas
- Assessing the solution gas driving efficiency
- Examining the field gas-oil ratio (GOR) as compared to the laboratory solution gas solubility, R_s to define the bubble-point pressure and critical gas saturation

The instantaneous GOR, as discussed earlier, is given by:

$$\text{GOR} = \frac{Q_g}{Q_o} = R_s + \left(\frac{k_{rg}}{k_{ro}} \right) \left(\frac{\mu_o B_o}{\mu_g B_g} \right)$$

This can be arranged to solve for the relative permeability ratio, k_{rg}/k_{ro} to give:

$$\left(\frac{k_{rg}}{k_{ro}} \right) = (\text{GOR} - R_s) \left(\frac{\mu_g B_g}{\mu_o B_o} \right)$$

One of the most practical applications of the MBE is its ability to generate the field relative permeability ratio as a function of gas saturation, which can be used to adjust the laboratory core relative permeability data. *The main advantage of the field- or well-generated relative permeability ratio is that it incorporates some of the complexities of reservoir heterogeneity and degree of the segregation of the oil and the evolved gas.*

It should be noted that the laboratory relative permeability data apply to an **un-segregated** reservoir, one that has no change in fluid saturation

with height. The laboratory relative permeability is most suitable for applications with the zero-dimensional tank model. For a reservoir with complete gravity segregation, it is possible to generate a pseudo-relative permeability ratio, k_{rg}/k_{ro} . A complete segregation means that the upper part of the reservoir contains gas and immobile oil, that is, residual oil, S_{or} , while the lower part contains oil and immobile gas that exists at critical saturation, S_{gc} . Vertical communication implies that as the gas evolves in the lower region, any gas with saturation above S_{gc} moves upward rapidly and leaves that region, while in the upper region any oil above S_{or} drains downward and moves into the lower region. On the basis of these assumptions, Poston (1987) proposed the following two relationships:

$$\frac{k_{rg}}{k_{ro}} = \frac{(S_g - S_{gc})(k_{rg})_{or}}{(S_o - S_{or})(k_{ro})_{gc}}$$

$$k_{ro} = \left[\frac{S_o - S_{or} (k_{rg})_{or}}{1 - S_w - S_{gc} - S_{or}} \right] (k_{ro})_{gc}$$

where

$(k_{ro})_{gc}$ = relative permeability to oil at critical gas saturation

$(k_{go})_{or}$ = relative permeability to gas at residual oil saturation

If the reservoir is initially undersaturated (i.e., $p_i > p_b$), the reservoir pressure will continue to decline with production, and it eventually reaches the bubble-point pressure. It is recommended the material calculations be performed in two stages; first from p_i to p_b , and second from p_b to different depletion pressures p . As the pressure declines from p_i to p_b , the following changes will occur as a result:

1. Based on the water compressibility, c_w , the connate-water will expand, resulting in an increase in the connate-water saturation (provided that there is no water production)
2. Based on the formation compressibility, c_f , a reduction (compaction) in the entire reservoir pore volume

Therefore, there are several volumetric calculations that must be performed to reflect the reservoir condition at the bubble-point pressure. These calculations are based on defining the following parameters:

- Initial oil-in-place at p_i , known as N_i , with *initial* oil and water saturations of S_{oi}^i and S_{wi}^i

- Cumulative oil produced at the bubble-point pressure, N_{pb}
- Oil remaining at the bubble-point pressure, that is, *initial* oil at the bubble-point:

$$N_b = N_i - N_{pb}$$

- Total pore volume at the bubble-point pressure, $(P.V)_b$:

$(P.V)_b$ = remaining oil volume + connate-water volume + connate-water expansion – reduction in P.V due to compaction

$$(P.V)_b = (N_i - N_{pb})B_{ob} + \left[\frac{N_i B_{oi}}{1 - S_{wi}} \right] S_{wi} + \left[\frac{N_i B_{oi}}{1 - S_{wi}} \right] (p_i - p_b)(-c_f + c_w S_{wi}')$$

Simplifying gives:

$$(P.V)_b = (N_i - N_{pb})B_{ob} + \left[\frac{N_i B_{oi}}{1 - S_{wi}} \right] [S_{wi}' + (p_i - p_b)(-c_f + c_w S_{wi}')]$$

- *Initial* oil and water saturations *at the bubble-point pressure*, S_{oi} and S_{wi} :

$$S_{oi} = \frac{(N_i - N_{pb})B_{ob}}{(P.V)_b} = \frac{(N_i - N_{pb})B_{ob}}{(N_i - N_{pb})B_{ob} + \left[\frac{N_i B_{oi}}{1 - S_{wi}} \right] [S_{wi}' + (p_i - p_b)(-c_f + c_w S_{wi}')]}$$

$$S_{wi} = \frac{\left[\frac{N_i B_{oi}}{1 - S_{wi}} \right] [S_{wi}' + (p_i - p_b)(-c_f + c_w S_{wi}')]}{(N_i - N_{pb})B_{ob} + \left[\frac{N_i B_{oi}}{1 - S_{wi}} \right] [S_{wi}' + (p_i - p_b)(-c_f + c_w S_{wi}')]} = 1 - S_{oi}$$

- Oil saturation, S_o , at any pressure below p_b is given by:

$$S_o = \frac{(N_i - N_p)B_o}{(P.V)_b} = \frac{(N_i - N_p)B_o}{(N_i - N_{pb})B_{ob} + \left[\frac{N_i B_{oi}}{1 - S_{wi}} \right] [S_{wi}' + (p_i - p_b)(-c_f + c_w S_{wi}')]}$$

Gas saturation, S_g at any pressure below p_b , assuming no water production, is given by:

$$S_g = 1 - S_o - S_{wi}$$

- where N_i = initial oil-in-place at p_i , i.e., $p_i > p_b$, STB
 N_b = initial oil-in-place at the bubble-point pressure, STB
 N_{pb} = cumulative oil production at the bubble-point pressure, STB
 S_{oi} = oil saturation at p_i , $p_i > p_b$
 S_{oi} = initial oil saturation at p_b
 S_{wi} = water saturation at p_i , $p_i > p_b$
 S_{wi} = initial water saturation at p_b

It is very convenient also to qualitatively represent the fluid production graphically by employing the concept of the **bubble map**. The bubble map essentially illustrates the growing size of the drainage area of a production well. The drainage area of each well is represented by a circle with an oil bubble radius, r_{ob} , as follows:

$$r_{ob} = \sqrt{\frac{5.615 N_p}{\pi \phi h \left(\frac{1 - S_{wi}}{B_{oi}} - \frac{S_o}{B_o} \right)}}$$

This expression is based on the assumption that the saturation is evenly distributed throughout a homogeneous drainage area, where

- r_{ob} = oil bubble radius, ft
 N_p = well current cumulative oil production, bbl
 S_o = current oil saturation

Similarly, the growing bubble of the reservoir free gas can be described graphically after calculation of the gas bubble radius, r_{gb} , of:

$$r_{gb} = \sqrt{\frac{5.615 [N R_{si} - (N - N_p) R_s - N_p R_p] B_g}{\pi \phi h (1 - S_o - S_{wi})}}$$

- where r_{gb} = gas bubble radius, ft
 N_p = well current cumulative oil production, bbl
 B_g = current gas formation volume factor, bbl/scf
 S_o = current oil saturation

Case 3. Gas-Cap-Drive Reservoirs

For a reservoir in which the expansion of the gas-cap gas is the predominant driving mechanism and assuming that the natural water influx is negligible ($W_e = 0$), the effect of water and pore compressibilities can

be considered negligible. Under these conditions, the Havlena-Odeh material balance can be expressed as:

$$F = N [E_o + m E_g] \quad (11-39)$$

where E_g is defined by Equation 11-30 as:

$$E_g = B_{oi} [(B_g/B_{gi}) - 1]$$

The way in which Equation 11-39 can be used depends on the number of unknowns in the equation. There are three possible unknowns in Equation 11-39:

- N is unknown, m is known
- m is unknown, N is known
- N and m are unknown

The practical use of Equation 11-39 in determining the three possible unknowns is presented below:

a. Unknown N , known m :

Equation 11-39 indicates that a plot of F versus $(E_o + m E_g)$ on a Cartesian scale would produce a straight line through the origin with a slope of N , as shown in Figure 11-19. In making the plot, the underground withdrawal F can be calculated at various times as a function of the production terms N_p and R_p .

Conclusion: $N = \text{Slope}$

b. Unknown m , known N :

Equation 11-39 can be rearranged as an equation of straight line, to give:

$$\left(\frac{F}{N} - E_o \right) = m E_g \quad (11-40)$$

The above relationship shows that a plot of the term $(F/N - E_o)$ versus E_g would produce a straight line with a slope of m . One advantage of this particular arrangement is that the straight line must pass through the origin which, therefore, acts as a control point. Figure 11-20 shows an illustration of such a plot.

Conclusion: $m = \text{Slope}$

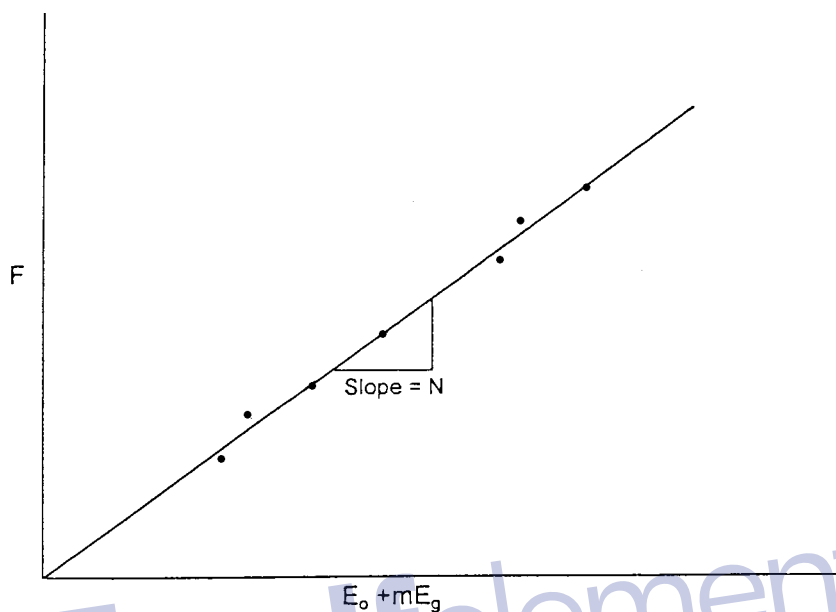


Figure 11-19. F vs. $E_o + mE_g$.

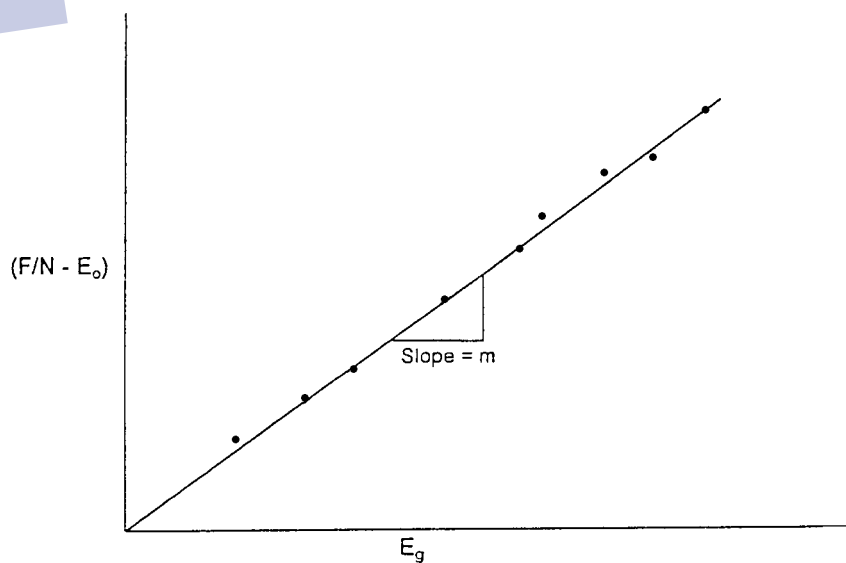


Figure 11-20. $(F/N - E_o)$ vs. E_g .

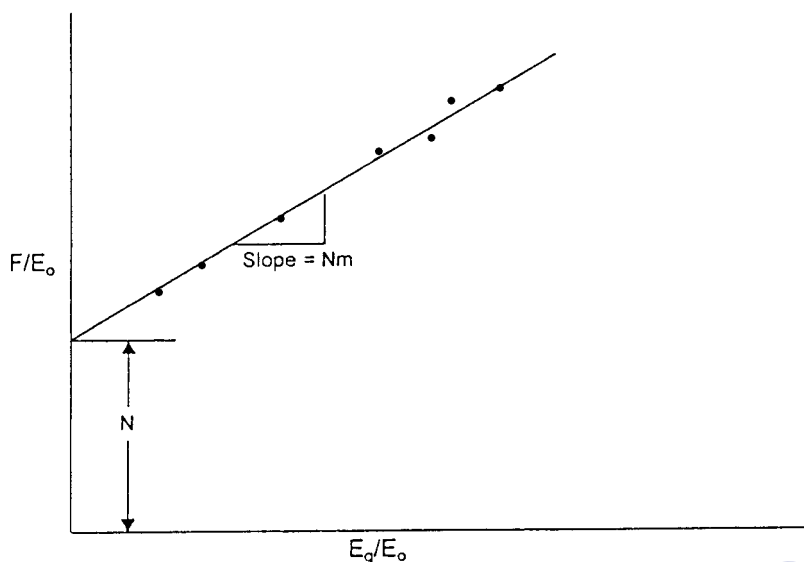


Figure 11-21. F/E_o vs. E_g/E_o .

c. N and m are Unknown

If there is uncertainty in both the values of N and m , Equation 11-39 can be re-expressed as:

$$\frac{F}{E_o} = N + mN \left(\frac{E_g}{E_o} \right) \quad (11-41)$$

A plot of F/E_o versus E_g/E_o should then be linear with intercept N and slope mN . This plot is illustrated in Figure 11-21.

Conclusions: N = Intercept
 mN = Slope
 m = Slope/intercept

Example 11-4¹

The production history and the PVT data of a gas-cap-drive reservoir are given below:

¹After Economides, M., and Hill, D., *Petroleum Production Systems*, Prentice Hall, 1993.

| Date | \bar{p} psi | N_p MSTB | G_p Mscf | B_t bbl/STB | B_g bbl/scf |
|--------|------------------|---------------|---------------|------------------|------------------|
| 5/1/89 | 4415 | — | — | 1.6291 | 0.00077 |
| 1/1/91 | 3875 | 492.5 | 751.3 | 1.6839 | 0.00079 |
| 1/1/92 | 3315 | 1015.7 | 2409.6 | 1.7835 | 0.00087 |
| 1/1/93 | 2845 | 1322.5 | 3901.6 | 1.9110 | 0.00099 |

The initial gas solubility R_{si} is 975 scf/STB. Estimate the initial oil and gas-in-place.

Solution

Step 1. Calculate the cumulative produced gas-oil ratio R_p

| \bar{p} | G_p Mscf | N_p MSTB | $R_p = G_p/N_p$ scf/STB |
|-----------|---------------|---------------|----------------------------|
| 4415 | — | — | — |
| 3875 | 751.3 | 492.5 | 1525 |
| 3315 | 2409.6 | 1015.7 | 2372 |
| 2845 | 3901.6 | 1322.5 | 2950 |

Step 2. Calculate F , E_o , and E_g :

| p | F | E_o | E_g |
|------|---------------------|--------|--------|
| 3875 | 2.04×10^6 | 0.0548 | 0.0529 |
| 3315 | 8.77×10^6 | 0.1540 | 0.2220 |
| 2845 | 17.05×10^6 | 0.2820 | 0.4720 |

Step 3. Calculate F/E_o and E_g/E_o

| p | F/E_o | E_g/E_o |
|------|--------------------|-----------|
| 3875 | 3.72×10^7 | 0.96 |
| 3315 | 5.69×10^7 | 1.44 |
| 2845 | 6.00×10^7 | 1.67 |

Step 4. Plot (F/E_o) versus (E_g/E_o) as shown in Figure 11-22 to give:

- Intercept = $N = 9$ MMSTB
- Slope = $N m = 3.1 \times 10^7$

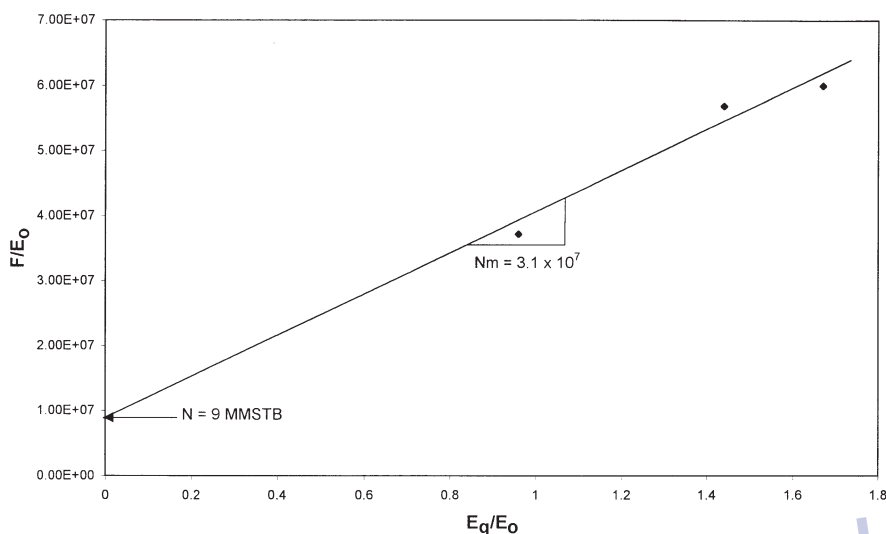


Figure 11-22. Calculation of m and N for Example 11-4.

Step 5. Calculate m :

$$m = 3.1 \times 10^7 / (9 \times 10^6) = 3.44$$

Step 6. Calculate initial gas-in-place G :

$$m = \frac{GB_{gi}}{NB_{oi}}$$

$$G = \frac{(3.44)(9 \times 10^6)(1.6291)}{0.00077} = 66 \text{ MMMscf}$$

Case 4. Water-Drive Reservoirs

In a water-drive reservoir, identifying the type of the aquifer and characterizing its properties are perhaps the most challenging tasks involved in conducting a reservoir engineering study. Yet, without an accurate description of the aquifer, future reservoir performance and management cannot be properly evaluated.

The full MBE can be expressed again as:

$$F = N(E_o + m E_g + E_{f,w}) + W_e$$

Dake (1978) points out that the term $E_{f,w}$ can frequently be neglected in water-drive reservoirs. This is not only for the usual reason that the water and pore compressibilities are small, but also because a water influx helps to maintain the reservoir pressure and, therefore, the Δp appearing in the $E_{f,w}$ term is reduced, or

$$F = N (E_o + m E_g) + W_e \quad (11-42)$$

If, in addition, the reservoir has an initial gas cap, then Equation 11-42 can be further reduced to:

$$F = N E_o + W_e \quad (11-43)$$

Dake (1978) points out that in attempting to use the above two equations to match the production and pressure history of a reservoir, the greatest uncertainty is always the determination of the water influx W_e . In fact, in order to calculate the influx the engineer is confronted with what is inherently the greatest uncertainty in the whole subject of reservoir engineering. The reason is that the calculation of W_e requires a mathematical model which itself relies on the knowledge of aquifer properties. These, however, are seldom measured since wells are not deliberately drilled into the aquifer to obtain such information.

For a water-drive reservoir with no gas cap, Equation 11-43 can be rearranged and expressed as:

$$\frac{F}{E_o} = N + \frac{W_e}{E_o} \quad (11-44)$$

Several water influx models have been described in Chapter 10, including the:

- Pot-aquifer model
- Schilthuis steady-state method
- Van Everdingen-Hurst model

The use of these models in connection with Equation 11-44 to simultaneously determine N and W_e is described below.

The Pot-Aquifer Model in the MBE

Assume that the water influx could be properly described using the simple pot-aquifer model given by Equation 10-5 as:

$$W_e = (c_w + c_f) W_i f (p_i - p) \quad (11-45)$$

$$f = \frac{(\text{encroachment angle})^\circ}{360^\circ} = \frac{\theta}{360^\circ}$$

$$W_i = \left[\frac{\pi(r_a^2 - r_e^2) h \phi}{5.615} \right]$$

where r_a = radius of the aquifer, ft

r_e = radius of the reservoir, ft

h = thickness of the aquifer, ft

ϕ = porosity of the aquifer

θ = encroachment angle

c_w = aquifer water compressibility, psi^{-1}

c_f = aquifer rock compressibility, psi^{-1}

W_i = initial volume of water in the aquifer, bbl

Since the aquifer properties c_w , c_f , h , r_a , and θ are seldom available, it is convenient to combine these properties and treat as one unknown K . Equation 11-45 can be rewritten as:

$$W_e = K \Delta p \quad (11-46)$$

Combining Equation 11-46 with Equation 11-44 gives:

$$\frac{F}{E_o} = N + K \left(\frac{\Delta p}{E_o} \right) \quad (11-47)$$

Equation 11-47 indicates that a plot of the term (F/E_o) as a function of $(\Delta p/E_o)$ would yield a straight line with an intercept of N and slope of K , as illustrated in Figure 11-23.

The Steady-State Model in the MBE

The steady-state aquifer model as proposed by Schilthuis (1936) is given by:

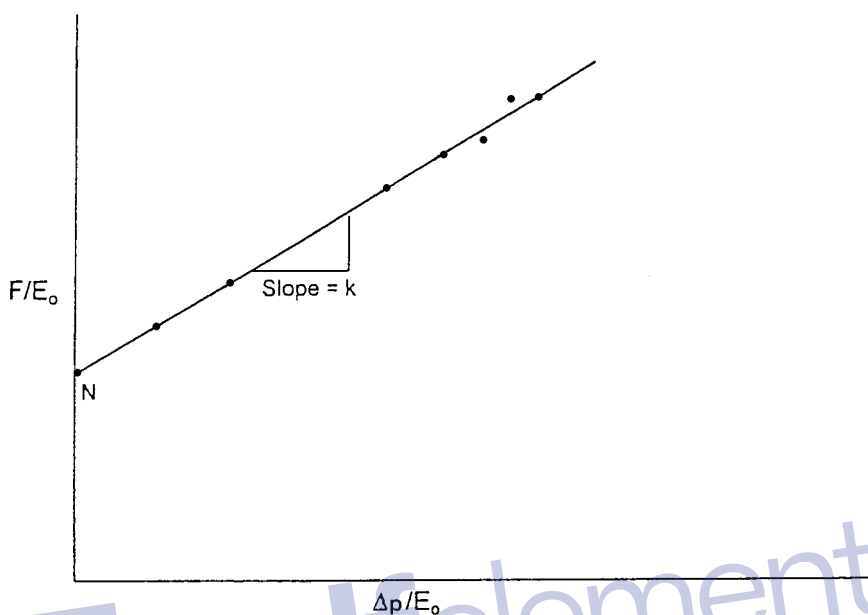


Figure 11-23. F/E_o vs. $\Delta p/E_o$.

$$W_e = C \int_0^t (p_i - p) dt \quad (11-48)$$

where W_e = cumulative water influx, bbl

C = water influx constant, bbl/day/psi

t = time, days

p_i = initial reservoir pressure, psi

p = pressure at the oil-water contact at time t , psi

Combining Equation 11-48 with Equation 11-44 gives:

$$\frac{F}{E_o} = N + C \left(\frac{\int_0^t (p_i - p) dt}{E_o} \right) \quad (11-49)$$

Plotting (F/E_o) versus $\int_0^t (p_i - p) dt/E_o$ results in a straight line with an intercept that represents the initial oil-in-place N and a slope that describes the water influx C as shown in Figure 11-24.

The Unsteady-State Model in the MBE

The van Everdingen-Hurst unsteady-state model is given by:

$$W_e = B \Sigma \Delta p W_{eD} \quad (11-50)$$

with

$$B = 1.119 \phi c_t r_c^2 h f$$

Van Everdingen and Hurst presented the dimensionless water influx W_{eD} as a function of the dimensionless time t_D and dimensionless radius r_D that are given by:

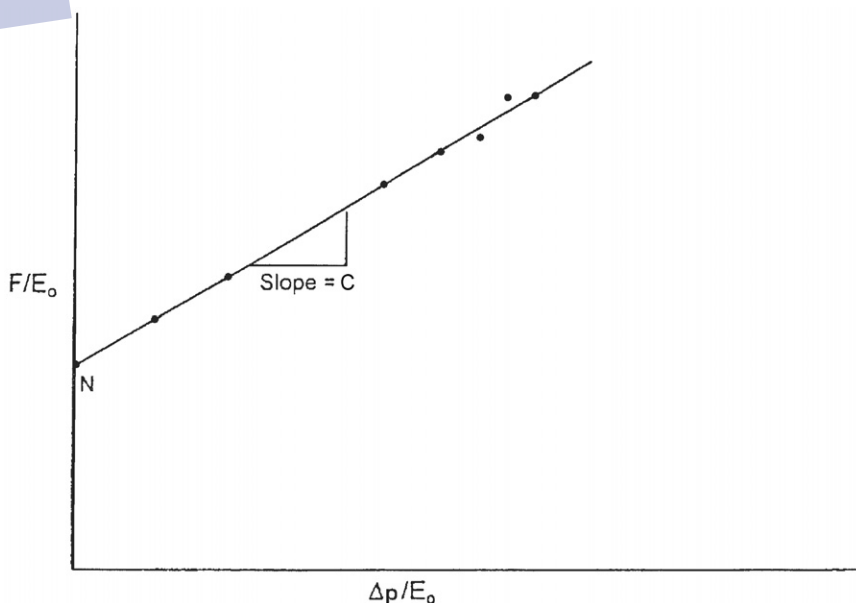


Figure 11-24. Graphical determination of N and C .

$$t_D = 6.328 \times 10^{-3} \frac{kt}{\phi \mu_w c_t r_e^2}$$

$$r_D = \frac{r_a}{r_e}$$

$$c_t = c_w + c_f$$

where t = time, days

k = permeability of the aquifer, md

ϕ = porosity of the aquifer

μ_w = viscosity of water in the aquifer, cp

r_a = radius of the aquifer, ft

r_e = radius of the reservoir, ft

c_w = compressibility of the water, psi^{-1}

Combining Equation 11-50 with Equation 11-44 gives:

$$\frac{F}{E_o} = N + B \left(\frac{\sum \Delta p W_{eD}}{E_o} \right) \quad (11-51)$$

The proper methodology of solving the above linear relationship is summarized in the following steps.

Step 1. From the field past production and pressure history, calculate the underground withdrawal F and oil expansion E_o .

Step 2. Assume an aquifer configuration, i.e., linear or radial.

Step 3. Assume the aquifer radius r_a and calculate the dimensionless radius r_D .

Step 4. Plot (F/E_o) versus $(\sum \Delta p W_{eD})/E_o$ on a Cartesian scale. If the assumed aquifer parameters are correct, the plot will be a straight line with N being the intercept and the water influx constant B being the slope. It should be noted that four other different plots might result. These are:

- Complete random scatter of the individual points, which indicates that the calculation and/or the basic data are in error.

- A systematically upward curved line, which suggests that the assumed aquifer radius (or dimensionless radius) is too small.
- A systematically downward curved line, indicating that the selected aquifer radius (or dimensionless radius) is too large.
- An s-shaped curve indicates that a better fit could be obtained if a linear water influx is assumed.

Figure 11-25 shows a schematic illustration of Havlena-Odeh (1963) methodology in determining the aquifer fitting parameters.

Example 11-5

The material balance parameters, the underground withdrawal F , and oil expansion E_o of a saturated-oil reservoir (i.e., $m = 0$) are given below:

| p | F | E_o |
|------|---------------------|--------|
| 3500 | — | — |
| 3488 | 2.04×10^6 | 0.0548 |
| 3162 | 8.77×10^6 | 0.1540 |
| 2782 | 17.05×10^6 | 0.2820 |

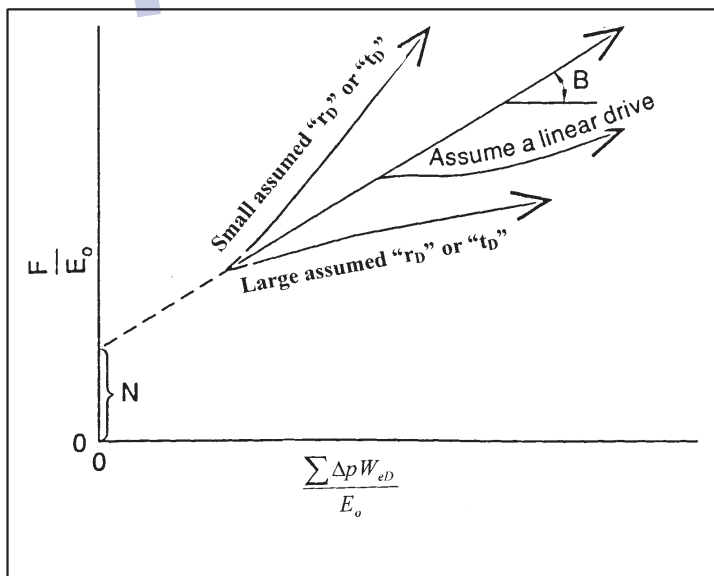


Figure 11-25. Havlena and Odeh straight-line plot. (After Havlena and Odeh, 1963.)

Assuming that the rock and water compressibilities are negligible, calculate the initial oil-in-place.

Solution

Step 1. The most important step in applying the MBE is to verify that no water influx exists. Assuming that the reservoir is volumetric, calculate the initial oil-in-place N by using every individual production data point in Equation 11-38, or:

$$N = F/E_o$$

| F | E_o | $N = F/E_o$ |
|---------------------|--------|-------------|
| 2.04×10^6 | 0.0548 | 37 MMSTB |
| 8.77×10^6 | 0.1540 | 57 MMSTB |
| 17.05×10^6 | 0.2820 | 60 MMSTB |

Step 2. The above calculations show the calculated values of the initial oil-in-place are increasing (as shown graphically in Figure 11-26), which indicates a water encroachment, i.e., water-drive reservoir.

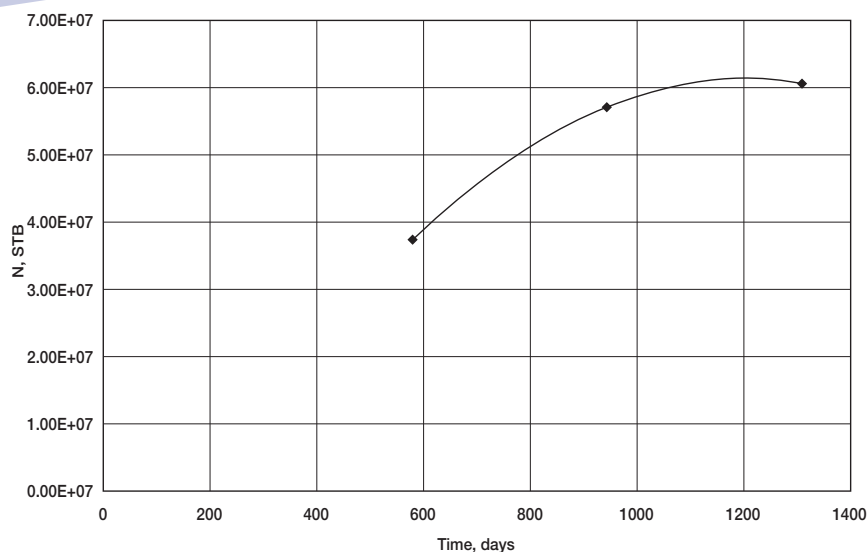


Figure 11-26. Indication of water influx.

Step 3. For simplicity, select the pot-aquifer model to represent the water encroachment calculations in the MBE as given by Equation 11-47, or:

$$\frac{F}{E_o} = N + K \left(\frac{\Delta p}{E_o} \right)$$

Step 4. Calculate the terms (F/E_o) and $(\Delta p/E_o)$ of Equation 11-47.

| p | Δp | F | E_o | F/E_o | $\Delta p/E_o$ |
|------|------------|---------------------|--------|---------------------|----------------|
| 3500 | 0 | — | — | — | — |
| 3488 | 12 | 2.04×10^6 | 0.0548 | 37.23×10^6 | 219.0 |
| 3162 | 338 | 8.77×10^6 | 0.1540 | 56.95×10^6 | 2194.8 |
| 2782 | 718 | 17.05×10^6 | 0.2820 | 60.46×10^6 | 2546 |

Step 5. Plot (F/E_o) versus $(\Delta p/E_o)$, as shown in Figure 11-27, and determine the intercept and the slope.

Intercept = $N = 35$ MMSTB

Slope = $K = 9983$

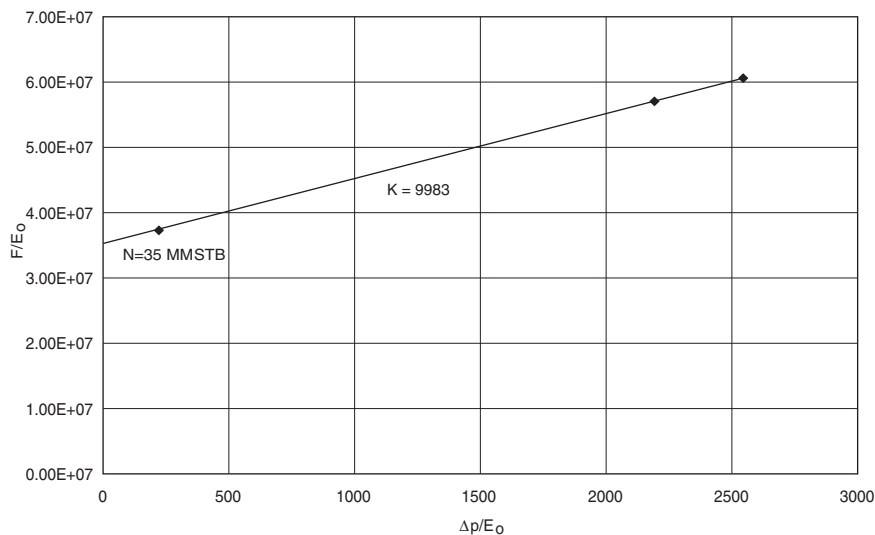


Figure 11-27. F/E_o versus $\Delta p/E_o$.

Case 5. Combination-Drive Reservoirs

This relatively complicated case involves the determination of the following three unknowns:

- Initial oil-in-place, N
- Size of the gas cap, m
- Water influx, W_e

The general MBE that includes these three unknowns is given by Equation 11-32:

$$F = N (E_o + mE_g) + W_e$$

Where the variables constituting the above expressions are defined by

$$\begin{aligned} F &= N_p [B_o + (R_p - R_s) B_g] + W_p B_w \\ &= N_p [B_t + (R_p - R_s) B_g] + W_p B_w \end{aligned}$$

$$\begin{aligned} E_o &= (B_o + B_{oi}) + (R_{si} - R_s) B_g \\ &= B_t + B_{ti} \end{aligned}$$

$$E_g = B_{oi} [(B_g/B_{gi}) - 1]$$

Havlena and Odeh differentiated Equation 11-32 with respect to pressure and rearranged the resulting equation to eliminate m , to give:

$$\frac{F E_g' - F' E_g}{E_o E_g' - E_o' E_g} = N + \frac{W_e E_g' - W_e' E_g}{E_o E_g' - E_o' E_g}$$

in which the primes denote derivatives with respect to pressure, that is,

$$E_g' = \frac{\partial E_g}{\partial p} = \left(\frac{B_{oi}}{B_{gi}} \right) \frac{\partial B_g}{\partial p} \approx \left(\frac{B_{oi}}{B_{gi}} \right) \frac{\Delta B_g}{\Delta p}$$

$$E_o' = \frac{\partial E_o}{\partial p} = \frac{\partial B_t}{\partial p} \approx \frac{\Delta B_t}{\Delta p}$$

$$F' = \frac{\partial F}{\partial p} \approx \frac{\Delta F}{\Delta p}$$

$$W_e' = \frac{\partial W_e}{\partial p}$$

A plot of the left-hand side of the equation versus the second term on the right for a selected aquifer model should, if the choice is correct, provide a straight line with unit slope whose intercept on the ordinate gives the initial oil-in-place, N . Having correctly determined N and W_e , Equation 11-32 can be solved directly for m , to give:

$$m = \frac{F - N E_o - W_e}{N E_g}$$

Notice that all the given derivatives can be evaluated numerically using one of the finite difference techniques: forward, backward, or central difference formula.

Case 6. Average Reservoir Pressure

To gain an understanding of the behavior of a reservoir with free gas, for example, solution gas drive or gas-cap drive, it is essential that every effort be made to determine reservoir pressures with accuracy. In the absence of reliable pressure data, the MBE can be used to estimate average reservoir pressure if accurate values of m and N are available from volumetric calculations. The general MBE is given by Equation 11-39 as:

$$F = N[E_o + m E_g]$$

Solving Equation 11-39 for the average pressure using the production history of the field involves the following graphical procedure:

- Step 1.* Select the time at which the average reservoir pressure is to be determined and obtain the corresponding production data, N_p , G_p , and R_p .
- Step 2.* Assume several average reservoir pressure values and determine the left-hand side, F , of Equation 11-39 at each assumed pressure:

$$F = N_p [B_o + (R_p - R_s) B_g] + W_p B_w$$

- Step 3.* Using the same assumed average reservoir pressure values as in Step 2, calculate the right-hand side of Equation 11-39:

$$\text{RHS} = N[E_o + m E_g]$$

where

$$E_o = (B_o - B_{oi}) + (R_{si} - R_s) B_g$$

$$E_g = B_{oi} [(B_g/B_{gi}) - 1]$$

Step 4. Plot the left-hand and right-hand sides of the MBE as calculated in Steps 2 and 3, on Cartesian paper, as a function of assumed average pressure. The point of intersection gives the average reservoir pressure that corresponds to the selected time of Step 1.

Step 5. Repeat Steps 1 through 4 to estimate reservoir pressure at each selected depletion time.

Tracy's Form of the Material Balance Equation

Neglecting the formation and water compressibilities, the general material balance equation as expressed by Equation 11-13 can be reduced to the following:

$$N = \frac{N_p B_o + (G_p - N_p R_s) B_g - (W_e - W_p B_w)}{(B_o - B_{oi}) + (R_{si} - R_s) B_g + m B_{oi} \left[\frac{B_g}{B_{gi}} - 1 \right]} \quad (11-52)$$

Tracy (1955) suggested that the above relationship can be rearranged into a more usable form as:

$$N = N_p \Phi_o + G_p \Phi_g + (W_p B_w - W_e) \Phi_w \quad (11-53)$$

where Φ_o , Φ_g , and Φ_w are considered PVT related properties that are functions of pressure and defined by:

$$\Phi_o = \frac{B_o - R_s B_g}{\text{Den}} \quad (11-54)$$

$$\Phi_g = \frac{B_g}{\text{Den}} \quad (11-55)$$

$$\phi_w = \frac{1}{\text{Den}} \quad (11-56)$$

with

$$\text{Den} = (B_o - B_{oi}) + (R_{si} - R_s)B_g + mB_{oi} \left[\frac{B_g}{B_{gi}} - 1 \right] \quad (11-57)$$

where Φ_o = oil PVT function

Φ_g = gas PVT function

Φ_w = water PVT function

Figure 11-28 gives a graphical presentation of the behavior of Tracy's PVT functions with changing pressure.

Notice that Φ_o is negative at low pressures and all Φ functions are approaching infinity at bubble-point pressure. Tracy's form is valid only for initial pressures equal to bubble-point pressure and cannot be used at pressures above bubble-point. Furthermore, the shape of the Φ function curves illustrates that small errors in pressure and/or production can cause large errors in calculated oil-in-place at pressures near the bubble-point.

Steffensen (1992), however, pointed out that Tracy's equation uses the oil formation volume factor at the bubble-point pressure B_{ob} for the initial B_{oi} , which causes all the PVT functions to become infinity at the bubble-point pressure. Steffensen suggested that Tracy's equation could be extended for applications above the bubble-point pressure, i.e., for undersaturated-oil reservoirs, by simply using the value of B_o at the initial reservoir pressure. He concluded that Tracy's methodology could predict reservoir performance for the entire pressure range from any initial pressure down to abandonment.

The following example is given by Tracy (1955) to illustrate his proposed approach.

Example 11-6

The production history of a saturated-oil reservoir is as follows:

| Pressure, psia | Cumulative Oil, MSTB | Cumulative Gas, MMscf |
|----------------|----------------------|-----------------------|
| 1690 | 0 | 0 |
| 1600 | 398 | 38.6 |
| 1500 | 1570 | 155.8 |
| 1100 | 4470 | 803 |

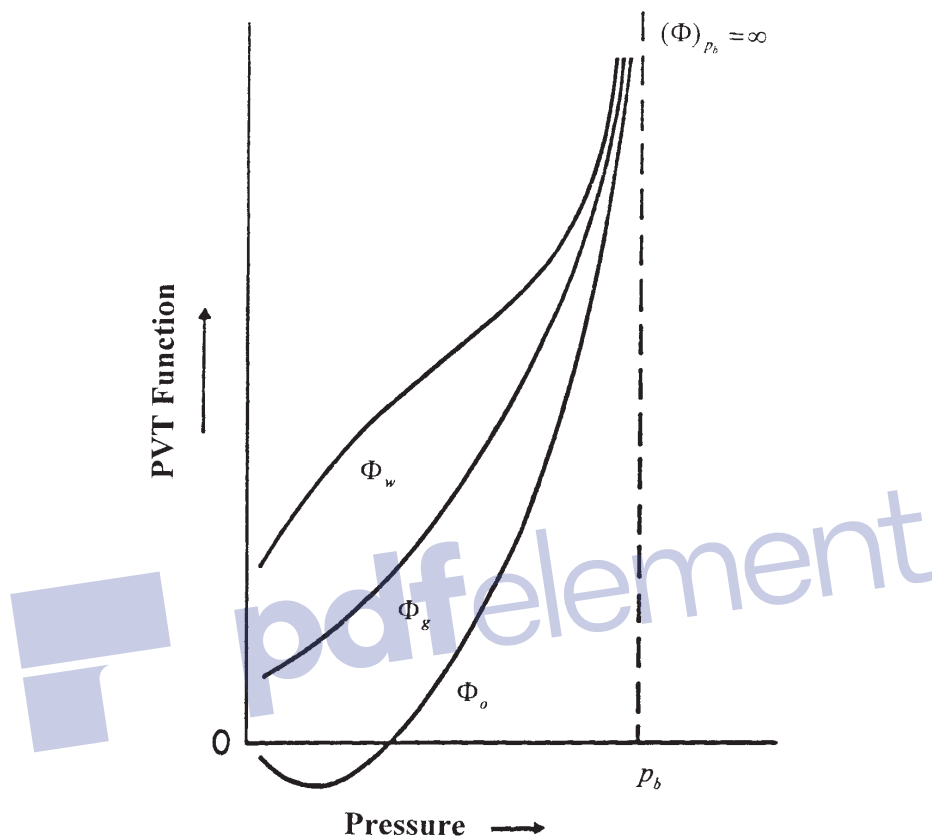


Figure 11-28. Tracy's PVT functions.

The calculated values of the PVT functions are given below:

| Pressure, psia | Φ_o | Φ_g |
|----------------|----------|----------|
| 1600 | 36.60 | 0.4000 |
| 1500 | 14.30 | 0.1790 |
| 1100 | 2.10 | 0.0508 |

Calculate the oil-in-place N .

Solution

The calculations can be conveniently performed in following table:

| p , psia | N_p , MSTB | G_p , MMscf | $(N_p \Phi_o)$ | $(G_p \Phi_g)$ | N , STB |
|------------|--------------|---------------|---------------------|---------------------|---------------------|
| 1600 | 398 | 38.6 | 14.52×10^6 | 15.42×10^6 | 29.74×10^6 |
| 1500 | 155.8 | 155.8 | 22.45×10^6 | 27.85×10^6 | 50.30×10^6 |
| 1100 | 803.0 | 803.0 | 9.39×10^6 | 40.79×10^6 | 50.18×10^6 |

The above results show that the original oil-in-place in this reservoir is approximately 50 MMSTB of oil. The calculation at 1600 psia is a good example of the sensitivity of such a calculation near the bubble-point pressure. Since the last two values of the original oil-in-place agree so well, the first calculation is probably wrong.

PROBLEMS

- Given the following data on an oil reservoir:

| | Oil | Aquifer |
|------------------------|------------------|----------------|
| Geometry | circle | semi-circle |
| Encroachment angle | — | 180° |
| Radius, ft | 4000 | 80,000 |
| Flow regime | semisteady-state | unsteady-state |
| Porosity | — | 0.20 |
| Thickness, ft | — | 30 |
| Permeability, md | 200 | 50 |
| Viscosity, cp | 1.2 | 0.36 |
| Original pressure | 3800 | 3800 |
| Current pressure | 3600 | — |
| Original volume factor | 1.300 | 1.04 |
| Current volume factor | 1.303 | 1.04 |
| Bubble-point pressure | 3000 | — |

The field has been on production for 1120 days and has produced 800,000 STB of oil and 60,000 STB of water. Water and formation compressibilities are estimated to 3×10^{-6} and 3.5×10^{-6} psi^{-1} , respectively. Calculate the original oil-in-place.

- The following rock- and fluid-properties data are available on the Nameless Fields:

Reservoir area = 1000 acres porosity = 10% thickness = 20'

$$T = 140^{\circ}\text{F} \quad s_{wi} = 20\%$$

$$p_i = 4000 \text{ psi} \quad p_b = 4000 \text{ psi}$$

The gas compressibility factor and relative permeability ratio are given by the following expressions:

$$z = 0.8 - 0.00002 (p - 4000)$$

$$\frac{k_{rg}}{k_{ro}} = 0.00127 e^{17.269 S_g}$$

The production history of the field is given below:

| | 4000 psi | 3500 psi | 3000 psi |
|-----------------|----------|----------|----------|
| μ_o , cp | 1.3 | 1.25 | 1.2 |
| μ_g , cp | — | 0.0125 | 0.0120 |
| B_o , bbl/STB | 1.4 | 1.35 | 1.30 |
| R_s , scf/STB | — | — | 450 |
| GOR, scf/STB | 600 | — | 1573 |

Subsurface information indicates that there is no aquifer and has been no water production.

Calculate:

- Remaining oil-in-place at 3,000 psi
 - Cumulative gas produced at 3,000 psi
3. The following PVT and production history data are available on an oil reservoir in West Texas:

Original oil-in-place = 10 MMSTB
 Initial water saturation = 22%
 Initial reservoir pressure = 2496 psia
 Bubble-point pressure = 2496 psi

| Pressure psi | B_o bbl/STB | R_s scf/STB | B_g bbl/scf | μ_o cp | μ_g cp | GOR scf/STB |
|-----------------|------------------|------------------|------------------|---------------|---------------|----------------|
| 2496 | 1.325 | 650 | 0.000796 | 0.906 | 0.016 | 650 |
| 1498 | 1.250 | 486 | 0.001335 | 1.373 | 0.015 | 1360 |
| 1302 | 1.233 | 450 | 0.001616 | 1.437 | 0.014 | 2080 |

The cumulative gas-oil ratio at 1,302 psi is recorded at 953 scf/STB.
 Calculate:

- a. Oil saturation at 1,302 psia
 - b. Volume of the free gas in the reservoir at 1,302 psia
 - c. Relative permeability ratio (k_g/k_o) at 1,302 psia
4. The Nameless Field is an undersaturated-oil reservoir. The crude oil system and rock type indicate that the reservoir is highly compressible. The available reservoir and production data are given below:

$$S_{wi} = 0.25 \quad \phi = 20\% \quad \text{Area} = 1000 \text{ acres}$$

$$h = 70' \quad T = 150^\circ\text{F}$$

Bubble-point pressure = 3500 psia

| | Original Condition | Current Conditions |
|-----------------|--------------------|--------------------|
| Pressure, psi | 5000 | 4500 |
| B_o , bbl/STB | 1.905 | 1.920 |
| R_s , scf/STB | 700 | 700 |
| N_p , MSTB | 0 | 610.9 |

Calculate the cumulative oil production at 3,900 psi. The PVT data show that the oil formation volume factor is equal to 1.938 bbl/STB at 3,900 psia.

5. The following data² are available on a gas-cap-drive reservoir:

| Pressure (psi) | N_p (MMSTB) | R_p (scf/STB) | B_o (RB/STB) | R_s (scf/STB) | B_g (RB/scf) |
|----------------|---------------|-----------------|----------------|-----------------|----------------|
| 3330 | | | 1.2511 | 510 | 0.00087 |
| 3150 | 3.295 | 1050 | 1.2353 | 477 | 0.00092 |
| 3000 | 5.903 | 1060 | 1.2222 | 450 | 0.00096 |
| 2850 | 8.852 | 1160 | 1.2122 | 425 | 0.00101 |
| 2700 | 11.503 | 1235 | 1.2022 | 401 | 0.00107 |
| 2550 | 14.513 | 1265 | 1.1922 | 375 | 0.00113 |
| 2400 | 17.730 | 1300 | 1.1822 | 352 | 0.00120 |

Calculate the initial oil and free gas volumes.

6. The Wildcat Reservoir was discovered in 1980. This reservoir had an initial reservoir pressure of 3,000 psia, and laboratory data indicated a bubble-point pressure of 2,500 psi. The following additional data are available:

²Dake, L. P., *Fundamentals of Reservoir Engineering*, Elsevier Publishing Co., Amsterdam, 1978.

| | |
|--------------------------|-------------|
| Area | = 700 acres |
| Thickness | = 35 ft |
| Porosity | = 20% |
| Temperature | = 150°F |
| API gravity | = 50° |
| Specific gravity of gas | = 0.72 |
| Initial water saturation | = 25% |

Average isothermal oil compressibility above the bubble point = $18 \times 10^{-6} \text{ psi}^{-1}$

Calculate the volume of oil initially in place at 3,000 psi as expressed in STB.

REFERENCES

1. Clark, N., *Elements of Petroleum Reservoirs*. Dallas, TX: SPE, 1969.
2. Cole, F., *Reservoir Engineering Manual*. Houston, TX: Gulf Publishing Co., 1969.
3. Craft, B. C., and Hawkins, M. (Revised by Terry, R. E.), *Applied Petroleum Reservoir Engineering*, 2nd ed. Englewood Cliffs, NJ: Prentice Hall, 1991.
4. Dake, L. P., *Fundamentals of Reservoir Engineering*. Amsterdam: Elsevier, 1978.
5. Dake, L., *The Practice of Reservoir Engineering*. Amsterdam: Elsevier, 1994.
6. Economides, M., and Hill, D., *Petroleum Production System*. Prentice Hall, 1993.
7. Havlena, D., and Odeh, A. S., "The Material Balance as an Equation of a Straight Line," *JPT*, August 1963, pp. 896–900.
8. Havlena, D., and Odeh, A. S., "The Material Balance as an Equation of a Straight Line, Part II—Field Cases," *JPT*, July 1964, pp. 815–822.
9. Schilthuis, R., "Active Oil and Reservoir Energy," *Trans. AIME*, 1936, Vol. 118, p. 33.
10. Steffensen, R., "Solution-Gas-Drive Reservoirs," *Petroleum Engineering Handbook*, Chapter 37. Dallas: SPE, 1992.
11. Tracy, G., "Simplified Form of the MBE," *Trans. AIME*, 1955, Vol. 204, pp. 243–246.
12. Van Everdingen, A., and Hurst, W., "The Application of the Laplace Transformation to Flow Problems in Reservoirs," *Trans. AIME*, 1949, p. 186.

C H A P T E R 1 2

PREDICTING OIL RESERVOIR PERFORMANCE

Most reservoir engineering calculations involve the use of the material balance equation. Some of the most useful applications of the MBE require the concurrent use of fluid flow equations, e.g., Darcy's equation. Combining the two concepts would enable the engineer to predict the reservoir future production performance as a function of time. Without the fluid flow concepts, the MBE simply provides performance as a function of the average reservoir pressure. Prediction of the reservoir future performance is ordinarily performed in the following two phases:

Phase 1. Predicting cumulative hydrocarbon production as a function of declining reservoir pressure. This stage is accomplished without regard to:

- Actual number of wells
- Location of wells
- Production rate of individual wells
- Time required to deplete the reservoir

Phase 2. The second stage of prediction is the time-production phase. In these calculations, the reservoir performance data, as calculated from Phase 1, are correlated with time. It is necessary in this phase to account for the number of wells and the productivity of each well.

PHASE 1. RESERVOIR PERFORMANCE PREDICTION METHODS

The material balance equation in its various mathematical forms as presented in Chapter 11 is designed to provide estimates of the initial oil-in-place N , size of the gas cap m , and water influx W_e . To use the MBE to predict the reservoir future performance, it requires two additional relations:

- Equation of producing (instantaneous) gas-oil ratio
- Equation for relating saturations to cumulative oil production

These auxiliary mathematical expressions are presented as follows.

Instantaneous Gas-Oil Ratio

The produced gas-oil ratio (GOR) at any particular time is the ratio of the standard cubic feet of *total* gas being produced at any time to the stock-tank barrels of oil being produced at that same instant. Hence, the name *instantaneous gas-oil ratio*. Equation 6-54 in Chapter 6 describes the GOR mathematically by the following expression:

$$\text{GOR} = R_s + \left(\frac{k_{rg}}{k_{ro}} \right) \left(\frac{\mu_o B_o}{\mu_g B_g} \right) \quad (12-1)$$

where GOR = instantaneous gas-oil ratio, scf/STB

R_s = gas solubility, scf/STB

k_{rg} = relative permeability to gas

k_{ro} = relative permeability to oil

B_o = oil formation volume factor, bbl/STB

B_g = gas formation volume factor, bbl/scf

μ_o = oil viscosity, cp

μ_g = gas viscosity, cp

The instantaneous GOR equation is of fundamental importance in reservoir analysis. The importance of Equation 12-1 can appropriately be discussed in conjunction with Figures 12-1 and 12-2.

These illustrations show the history of the gas-oil ratio of a hypothetical depletion-drive reservoir that is typically characterized by the following points:

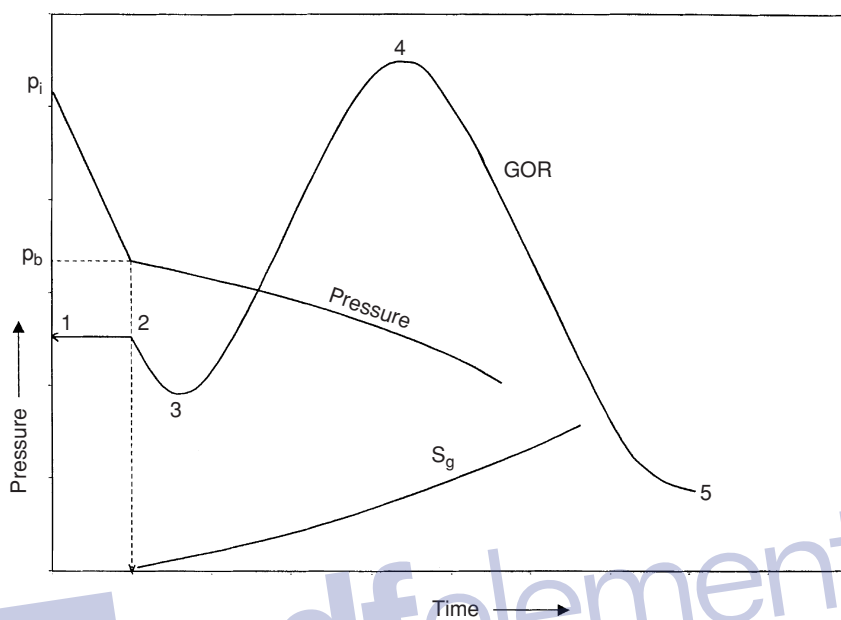


Figure 12-1. Characteristics of solution-gas-drive reservoirs.

Point 1. When the reservoir pressure p is above the bubble-point pressure p_b , there is no free gas in the formation, i.e., $k_{rg} = 0$, and therefore:

$$\text{GOR} = R_{si} = R_{sb} \quad (12-2)$$

The gas-oil ratio remains constant at R_{si} until the pressure reaches the bubble-point pressure at Point 2.

Point 2. As the reservoir pressure declines below p_b , the gas begins to evolve from solution and its saturation increases. This free gas, however, cannot flow until the gas saturation S_g reaches the critical gas saturation S_{gc} at Point 3. From Point 2 to Point 3, the instantaneous GOR is described by a decreasing gas solubility as:

$$\text{GOR} = R_s \quad (12-3)$$

Point 3. At Point 3, the free gas begins to flow with the oil and the values of GOR are progressively increasing with the declining reservoir pressure to Point 4. During this pressure decline period, the GOR is described by Equation 12-1, or:

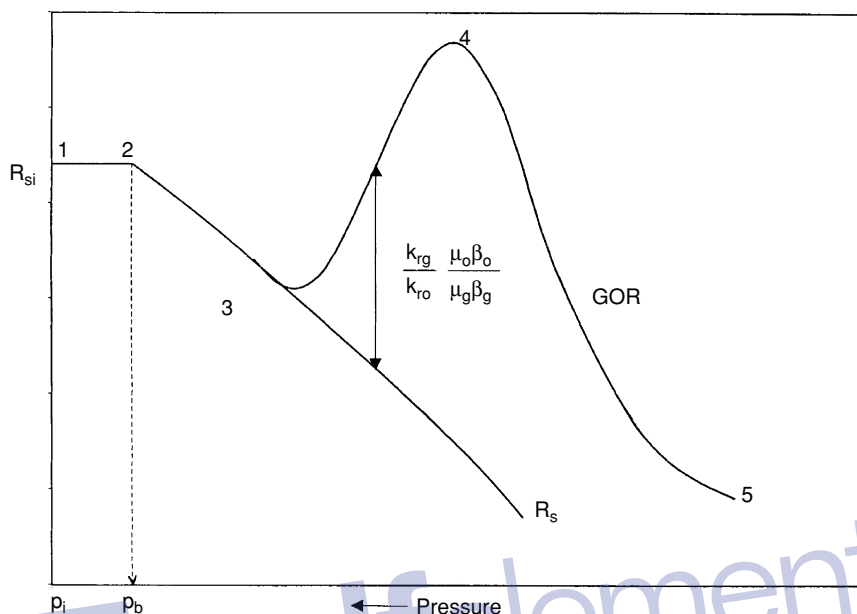


Figure 12-2. History of GOR and R_s for a solution-gas-drive reservoir.

$$\text{GOR} = R_s + \left(\frac{k_{rg}}{k_{ro}} \right) \left(\frac{\mu_o B_o}{\mu_g B_g} \right)$$

Point 4. At Point 4, the maximum GOR is reached due to the fact that the supply of gas has reached a maximum and marks the beginning of the *blow-down* period to Point 5.

Point 5. This point indicates that all the producible free gas has been produced and the GOR is essentially equal to the gas solubility and continues to Point 6.

There are three types of gas-oil ratios, all expressed in scf/STB, which must be clearly distinguished from each other. These are:

- Instantaneous GOR (defined by Equation 12-1)
- Solution GOR
- Cumulative GOR

The solution gas-oil ratio is a PVT property of the crude oil system. It is commonly referred to as *gas solubility* and denoted by R_s . It measures the tendency of the gas to dissolve in or evolve from the oil with changing pressures. It should be pointed out that as long as the evolved gas remains immobile, i.e., gas saturation S_g is less than the critical gas saturation, the instantaneous GOR is equal to the gas solubility, i.e.:

$$\text{GOR} = R_s$$

The cumulative gas-oil ratio R_p , as defined previously in the material balance equation, should be clearly distinguished from the producing (instantaneous) gas-oil ratio (GOR). The cumulative gas-oil ratio is defined as:

$$R_p = \frac{\text{cumulative (TOTAL) gas produced}}{\text{cumulative oil produced}}$$

or

$$R_p = \frac{G_p}{N_p}$$

(12-4)

where R_p = cumulative gas-oil ratio, scf/STB

G_p = cumulative gas produced, scf

N_p = cumulative oil produced, STB

The cumulative gas produced G_p is related to the instantaneous GOR and cumulative oil production by the expression:

$$G_p = \int_0^{N_p} (\text{GOR}) dN_p \quad (12-5)$$

Equation 12-5 simply indicates that the cumulative gas production at any time is essentially the area under the curve of the GOR versus N_p relationship, as shown in Figure 12-3.

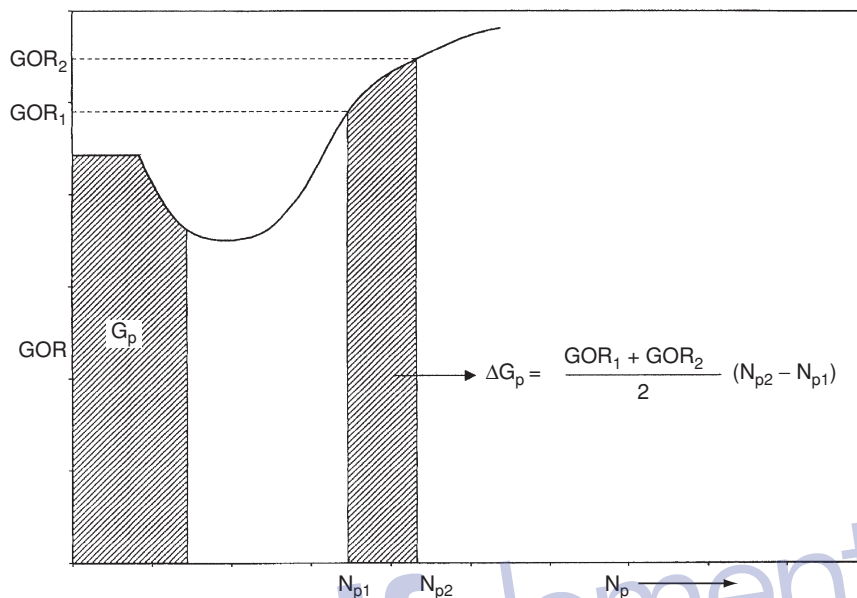


Figure 12-3. Relationship between GOR and G_p .

The incremental cumulative gas produced ΔG_p between N_{p1} , and N_{p2} is then given by:

$$\Delta G_p = \int_{N_{p1}}^{N_{p2}} (\text{GOR}) dN_p \quad (12-6)$$

The above integral can be approximated by using the trapezoidal rule, to give:

$$\Delta G_p = \left[\frac{(\text{GOR})_1 + (\text{GOR})_2}{2} \right] (N_{p2} - N_{p1})$$

or

$$\Delta G_p = (\text{GOR})_{\text{avg}} \Delta N_p$$

Equation 12-5 can then be approximated as:

$$G_p = \sum_o (GOR)_{avg} \Delta N_p \quad (12-7)$$

Example 12-1

The following production data are available on a depletion-drive reservoir:

| p psi | GOR scf/STB | N _p MMSTB |
|------------------------|----------------|-------------------------|
| 2925 (p _i) | 1340 | 0 |
| 2600 | 1340 | 1.380 |
| 2400 | 1340 | 2.260 |
| 2100 (p _i) | 1340 | 3.445 |
| 1800 | 1936 | 7.240 |
| 1500 | 3584 | 12.029 |
| 1200 | 6230 | 15.321 |

Calculate cumulative gas produced G_p and cumulative gas-oil ratio at each pressure.

Solution

Step 1. Construct the following table:

| p psi | GOR scf/STB | (GOR) _{avg} scf/STB | N _p MMSTB | ΔN _p MMSTB | ΔG _p MMscf | G _p MMscf | R _p scf/STB |
|----------|----------------|---------------------------------|-------------------------|--------------------------|--------------------------|-------------------------|---------------------------|
| 2925 | 1340 | 1340 | 0 | 0 | 0 | 0 | — |
| 2600 | 1340 | 1340 | 1.380 | 1.380 | 1849 | 1849 | 1340 |
| 2400 | 1340 | 1340 | 2.260 | 0.880 | 1179 | 3028 | 1340 |
| 2100 | 1340 | 1340 | 3.445 | 1.185 | 1588 | 4616 | 1340 |
| 1800 | 1936 | 1638 | 7.240 | 3.795 | 6216 | 10,832 | 1496 |
| 1500 | 3584 | 2760 | 12.029 | 4.789 | 13,618 | 24,450 | 2033 |
| 1200 | 6230 | 4907 | 15.321 | 3.292 | 16,154 | 40,604 | 2650 |

The Reservoir Saturation Equations

The saturation of a fluid (gas, oil, or water) in the reservoir is defined as the volume of the fluid divided by the pore volume, or:

$$S_o = \frac{\text{oil volume}}{\text{pore volume}} \quad (12-8)$$

$$S_w = \frac{\text{water volume}}{\text{pore volume}} \quad (12-9)$$

$$S_g = \frac{\text{gas volume}}{\text{pore volume}} \quad (12-10)$$

$$S_o + S_w + S_g = 1.0 \quad (12-11)$$

Consider a volumetric oil reservoir with no gas cap that contains N stock-tank barrels of oil at the initial reservoir pressure p_i . Assuming no water influx gives:

$$S_{oi} = 1 - S_{wi}$$

where the subscript i indicates initial reservoir condition. From the definition of oil saturation:

$$1 - S_{wi} = \frac{N B_{oi}}{\text{pore volume}}$$

or

$$\text{pore volume} = \frac{N B_{oi}}{1 - S_{wi}} \quad (12-12)$$

If the reservoir has produced N_p stock-tank barrels of oil, the remaining oil volume is given by:

$$\text{remaining oil volume} = (N - N_p) B_o \quad (12-13)$$

Substituting Equations 12-13 and 12-12 into Equation 12-8 gives:

$$S_o = \frac{(N - N_p) B_o}{\left(\frac{N B_{oi}}{1 - S_{wi}} \right)} \quad (12-14)$$

or

$$S_o = (1 - S_{wi}) \left(1 - \frac{N_p}{N} \right) \frac{B_o}{B_{oi}} \quad (12-15)$$

$$S_g = 1 - S_o - S_{wi} \quad (12-16)$$

Example 12-2

A volumetric solution-gas-drive reservoir has an initial water saturation of 20%. The initial oil formation volume factor is reported at 1.5 bbl/STB. When 10% of the initial oil was produced, the value of B_o decreased to 1.38. Calculate the oil saturation and gas saturation.

Solution

From Equation 12-5

$$S_o = (1 - 0.2)(1 - 0.1) \left(\frac{1.38}{1.50} \right) = 0.662$$

$$S_g = 1 - 0.662 - 0.20 = 0.138$$

It should be pointed out that the values of the relative permeability ratio k_{rg}/k_{ro} as a function of oil saturation can be generated by using the actual field production as expressed in terms of N_p , GOR, and PVT data. The proposed methodology involves the following steps:

Step 1. Given the actual field cumulative oil production N_p and the PVT data as a function of pressure, calculate the oil and gas saturations from Equations 12-15 and 12-16, i.e.:

$$S_o = (1 - S_{wi}) \left(1 - \frac{N_p}{N} \right) \frac{B_o}{B_{oi}}$$

$$S_g = 1 - S_o - S_{wi}$$

Step 2. Using the actual field instantaneous GORs, solve Equation 12-1 for the relative permeability ratio as:

$$\frac{k_{rg}}{k_{ro}} = (GOR - R_s) \left(\frac{\mu_g B_g}{\mu_o B_o} \right) \quad (12-17)$$

Step 3. Plot (k_{rg}/k_{ro}) versus S_o on a semilog paper.

Equation 12-15 suggests that all the remaining oil saturation be distributed uniformly throughout the reservoir. If water influx, gas-cap expansion, or gas-cap shrinking has occurred, the oil saturation equation, i.e., Equation 12-15, must be adjusted to account for oil trapped in the invaded regions.

Oil saturation adjustment for water influx

The proposed oil saturation adjustment methodology is illustrated in Figure 12-4 and described by the following steps:

Step 1. Calculate the pore volume in the water-invaded region, as:

$$W_e - W_p B_w = (P.V.)_{water} (1 - S_{wi} - S_{orw})$$

Solving for the pore volume of water-invaded zone $(P.V.)_{water}$ gives:

$$(P.V.)_{water} = \frac{W_e - W_p B_w}{1 - S_{wi} - S_{orw}} \quad (12-18)$$

where $(P.V.)_{water}$ = pore volume in water-invaded zone, bbl
 S_{orw} = residual oil saturated in the imbibition water-oil system

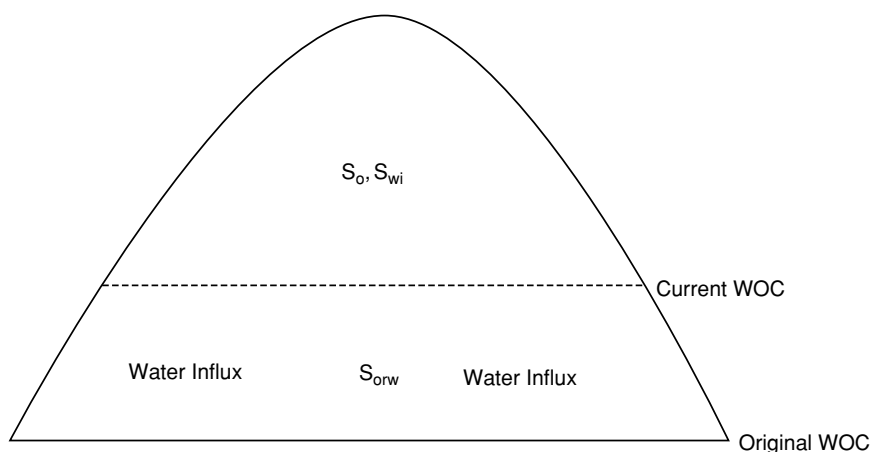


Figure 12-4. Oil saturation adjusted for water influx.

Step 2. Calculate oil volume in the water-invaded zone, or:

$$\text{volume of oil} = (P.V)_{\text{water}} S_{\text{orw}} \quad (12-19)$$

Step 3. Adjust Equation 12-14 to account for the trapped oil by using Equations 12-18 and 12-19:

$$S_o = \frac{(N - N_p) B_o - \left[\frac{W_e - W_p B_w}{1 - S_{wi} - S_{orw}} \right] S_{orw}}{\left(\frac{N B_{oi}}{1 - S_{wi}} \right) - \left[\frac{W_e - W_p B_w}{1 - S_{wi} - S_{orw}} \right]} \quad (12-20)$$

Oil saturation adjustment for gas-cap expansion

The oil saturation adjustment procedure is illustrated in Figure 12-5 and summarized below:

Step 1. Assuming no gas is produced from the gas cap, calculate the net expansion of the gas cap, from:

$$\text{Expansion of the gas cap} = m N B_{oi} \left(\frac{B_g}{B_{gi}} - 1 \right) \quad (12-21)$$

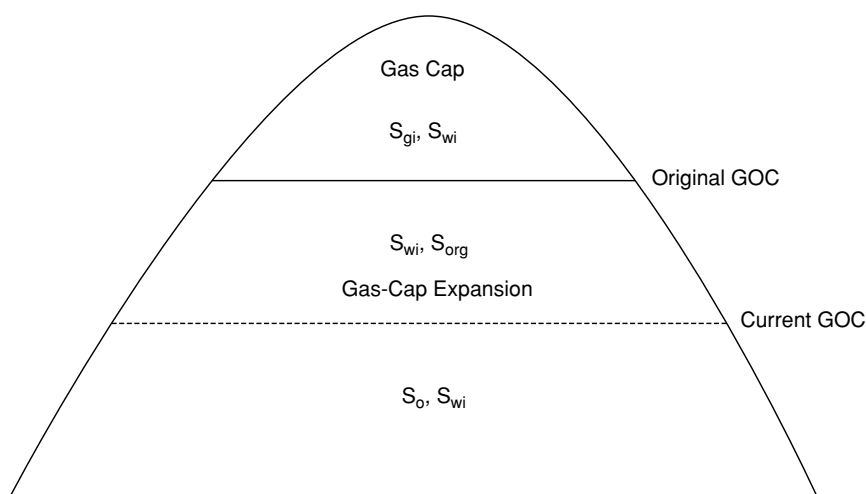


Figure 12-5. Oil saturation adjustment for gas-cap expansion.

Step 2. Calculate the pore volume of the gas-invaded zone, $(P.V)_{\text{gas}}$, by solving the following simple material balance:

$$mNB_{\text{oi}} \left(\frac{B_g}{B_{\text{gi}}} - 1 \right) = (P.V)_{\text{gas}} (1 - S_{\text{wi}} - S_{\text{org}})$$

or

$$(P.V)_{\text{gas}} = \frac{mNB_{\text{oi}} \left(\frac{B_g}{B_{\text{gi}}} - 1 \right)}{1 - S_{\text{wi}} - S_{\text{org}}} \quad (12-22)$$

where $(P.V)_{\text{gas}}$ = pore volume of the gas-invaded zone
 S_{org} = residual oil saturation in gas-oil system

Step 3. Calculate the volume of oil in the gas-invaded zone.

$$\text{oil volume} = (P.V)_{\text{gas}} S_{\text{org}} \quad (12-23)$$

Step 4. Adjust Equation 12-14 to account for the trapped oil in the gas expansion zone by using Equations 12-22 and 12-23, to give:

$$S_o = \frac{(N - N_p)B_o - \left[\frac{mNB_{oi} \left(\frac{B_g}{B_{gi}} - 1 \right)}{1 - S_{wi} - S_{org}} \right] S_{org}}{\left(\frac{NB_{oi}}{1 - S_{wi}} \right) - \left[\frac{mNB_{oi}}{1 - S_{wi} - S_{org}} \right] \left(\frac{B_g}{B_{gi}} - 1 \right)} \quad (12-24)$$

Oil saturation adjustment for combination drive

For a combination-drive reservoir, i.e., water influx and gas cap, the oil saturation equation as given by Equation 12-14 can be adjusted to account for both driving mechanisms, as:

$$S_o = \frac{(N - N_p)B_o - \left[\frac{mNB_{oi} \left(\frac{B_g}{B_{gi}} - 1 \right) S_{org}}{1 - S_{wi} - S_{org}} + \frac{(W_e - W_p)S_{orw}}{1 - S_{wi} - S_{orw}} \right]}{\frac{NB_{oi}}{1 - S_{wi}} - \left[\frac{mNB_{oi} \left(\frac{B_g}{B_{gi}} - 1 \right)}{1 - S_{wi} - S_{org}} + \frac{W_e - W_p}{1 - S_{wi} - S_{orw}} B_w \right]} \quad (12-25)$$

Oil saturation adjustment for shrinking gas cap

Cole (1969) points out that the control of the gas-cap size is very often a reliable guide to the efficiency of reservoir operations. A shrinking gas cap will cause the loss of a substantial amount of oil, which might otherwise be recovered. Normally, there is little or no oil saturation in the gas cap, and if the oil migrates into the original gas zone, there will necessarily

be some residual oil saturation remaining in this portion of the gas cap at abandonment. The magnitude of this loss may be quite large, depending upon the:

- Area of the gas-oil contact
- Rate of gas-cap shrinkage
- Relative permeability characteristics
- Vertical permeability

A shrinking gas cap can be controlled by either shutting in wells that are producing large quantities of gas-cap gas or by returning some of the produced gas back to the gas cap portion of the reservoir. In many cases, the shrinkage cannot be completely eliminated by shutting in wells, as there is a practical limit to the number of wells that can be shut-in. The amount of oil lost by the shrinking gas cap can be very well the engineer's most important economic justification for the installation of gas return facilities.

The difference between the original volume of the gas cap and the volume occupied by the gas cap at any subsequent time is a measure of the volume of oil that has migrated into the gas cap. If the size of the original gas cap is $m N B_{oi}$, then the expansion of the original free gas resulting from reducing the pressure from p_i to p is:

$$\text{Expansion of the original gas cap} = m N B_{oi} [(B_g/B_{gi}) - 1]$$

where $m N B_{oi}$ = original gas-cap volume, bbl

B_g = gas FVF, bbl/scf

If the gas cap is shrinking, then the volume of the produced gas must be larger than the gas-cap expansion. All of the oil that moves into the gas cap will not be lost, as this oil will also be subject to the various driving mechanisms. Assuming no original oil saturation in the gas zone, the oil that will be lost is essentially the residual oil saturation remaining at abandonment. If the cumulative gas production from the gas cap is G_{pc} scf, the volume of the gas-cap shrinkage as expressed in barrels is equal to:

$$\text{Gas-cap shrinkage} = G_{pc} B_g - m N B_{oi} [(B_g/B_{gi}) - 1]$$

From the volumetric equation:

$$G_{pc} B_g - m N B_{oi} [(B_g/B_{gi}) - 1] = 7758 A h \phi (1 - S_{wi} - S_{gr})$$

where A = average cross-sectional area of the gas-oil contact, acres

h = average change in depth of the gas-oil contact, feet

S_{gr} = residual gas saturation in the shrinking zone

The volume of oil lost as a result of oil migration to the gas cap can also be calculated from the volumetric equation as follows:

$$\text{Oil lost} = 7758 A h \phi S_{org}/B_{oa}$$

where S_{org} = residual oil saturation in the gas-cap shrinking zone

B_{oa} = oil FVF at abandonment

Combining the above relationships and eliminating the term $7,758 A h \phi$, give the following expression for estimating the volume of oil in barrels lost in the gas cap:

$$\text{Oil lost} = \frac{\left[G_{pc} B_g - m N B_{oi} \left(\frac{B_g}{B_{gi}} - 1 \right) \right] S_{org}}{(1 - S_{wi} - S_{gr}) B_{oa}}$$

where G_{pc} = cumulative gas production for the gas cap, scf

B_g = gas FVF, bbl/scf

All the methodologies that have been developed to predict the future reservoir performance are essentially based on employing and combining the above relationships that include the:

- MBE
- Saturation equations
- Instantaneous GOR
- Equation relating the cumulative gas-oil ratio to the instantaneous GOR

Using the above information, it is possible to predict the field primary recovery performance with declining reservoir pressure. There are three

methodologies that are widely used in the petroleum industry to perform a reservoir study. These are:

- Tracy's method
- Muskat's method
- Turner's method

These methods yield essentially the same results when small intervals of pressure or time are used. The methods can be used to predict the performance of a reservoir under any driving mechanism, including:

- Solution-gas drive
- Gas-cap drive
- Water drive
- Combination drive

The practical use of all the techniques is illustrated in predicting the primary recovery performance of a volumetric solution-gas-drive reservoir. Using the appropriate saturation equation, e.g., Equation 12-20 for a water-drive reservoir, any of the available reservoir prediction techniques could be applied to other reservoirs operating under different driving mechanisms.

The following two cases of the solution-gas-drive reservoir are considered:

- Undersaturated-oil reservoirs
- Saturated-oil reservoirs

Undersaturated-Oil Reservoirs

When the reservoir pressure is above the bubble-point pressure of the crude oil system, the reservoir is considered undersaturated. The general material balance is expressed in Chapter 11 by Equation 11-15.

$$N = \frac{N_p [B_o + (R_p - R_s)B_g] - (W_e - W_p B_w) - G_{inj} B_{ginj} - W_{inj} B_{wi}}{(B_o - B_{oi}) + (R_{si} - R_s)B_g + mB_{oi} \left[\frac{B_g}{B_{gi}} - 1 \right] + B_{oi} (1 + m) \left[\frac{S_{wi} c_w + c_f}{1 - S_{wi}} \right] \Delta p}$$

For a volumetric undersaturated reservoir with no fluid injection, the following conditions are observed:

$$\begin{aligned}m &= 0 \\W_e &= 0 \\R_s &= R_{si} = R_p\end{aligned}$$

Imposing the above conditions on the MBE reduces the equation to the following simplified form:

$$N = \frac{N_p B_o}{(B_o - B_{oi}) + B_{oi} \left[\frac{S_{wi} c_w + c_f}{1 - S_{wi}} \right] \Delta p} \quad (12-26)$$

with

$$\Delta p = p_i - p$$

where p_i = initial reservoir pressure
 p = current reservoir pressure

Hawkins (1955) introduced the oil compressibility c_o into the MBE to further simplify the equation. The oil compressed is defined in Chapter 2 by:

$$c_o = \frac{1}{B_{oi}} \frac{B_o - B_{oi}}{\Delta p}$$

Rearranging gives:

$$B_o - B_{oi} = c_o B_{oi} \Delta p$$

Combining the above expression with Equation 12-26 gives:

$$N = \frac{N_p B_o}{c_o B_{oi} \Delta p + B_{oi} \left[\frac{S_{wi} c_w + c_f}{1 - S_{wi}} \right] \Delta p} \quad (12-27)$$

The denominator of the above equation can be written as:

$$B_{oi} \left[c_o + \frac{S_{wi} c_w}{1 - S_{wi}} + \frac{c_f}{1 - S_{wi}} \right] \Delta p \quad (12-28)$$

Since there are only two fluids in the reservoir, i.e., oil and water, then:

$$S_{oi} + S_{wi} = 1$$

Equation 12-28 can then be expressed as:

$$B_{oi} \left[\frac{S_{oi} c_o + S_{wi} c_w + c_f}{1 - S_{wi}} \right] \Delta p$$

The term between the two brackets is called the effective compressibility and defined by Hawkins (1955) as:

$$c_e = \frac{S_{oi} c_o + S_{wi} c_w + c_f}{1 - S_{wi}} \quad (12-29)$$

Combining Equations 12-27, 12-28, and 12-29, the MBE above the bubble-point pressure becomes:

$$N = \frac{N_p B_o}{B_{oi} c_e \Delta p} = \frac{N_p B_o}{B_{oi} c_e (P_i - P)} \quad (12-30)$$

Equation 12-30 can be expressed as an equation of a straight line by:

$$P = P_i - \left[\frac{1}{N B_{oi} c_e} \right] N_p B_o \quad (12-31)$$

Figure 12-6 indicates that the reservoir pressure will decrease linearly with cumulative reservoir voidage $N_p B_o$.

Rearranging Equation 12-31 and solving for the cumulative oil production N_p gives:

$$N_p = N c_e \left(\frac{B_o}{B_{oi}} \right) \Delta p \quad (12-32)$$

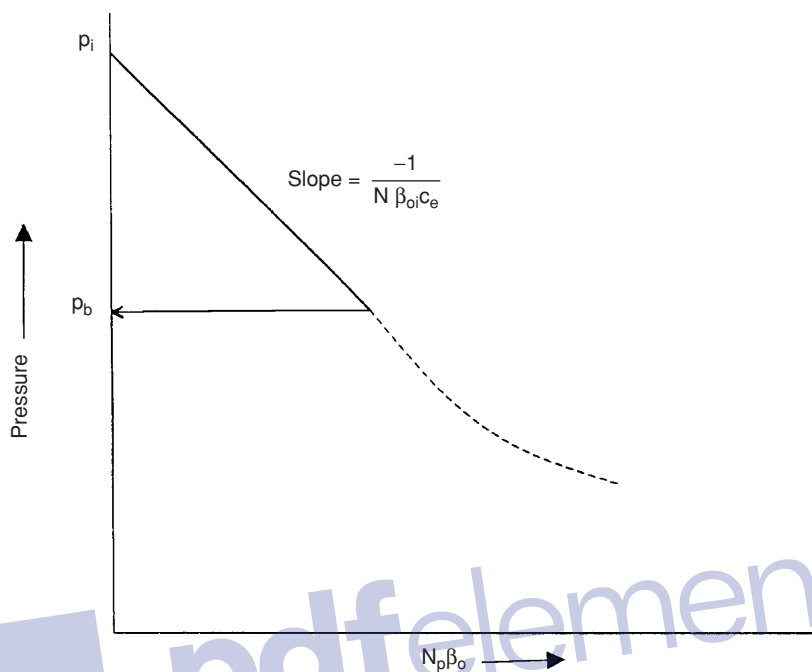


Figure 12-6. Pressure voidage relationship.

The calculation of future reservoir production, therefore, does not require a trial-and-error procedure, but can be obtained directly from the above expression.

Example 12-3

The following data are available on a volumetric undersaturated-oil reservoir:

$$\begin{array}{lll}
 p_i = 4000 \text{ psi} & p_b = 3000 \text{ psi} & N = 85 \text{ MMSTB} \\
 c_f = 5 \times 10^{-6} \text{ psi}^{-1} & c_o = 15 \times 10^{-6} \text{ psi}^{-1} & c_w = 3 \times 10^{-6} \text{ psi}^{-1} \\
 S_{wi} = 30\% & B_{oi} = 1.40 \text{ bbl/STB} &
 \end{array}$$

Estimate cumulative oil production when the reservoir pressure drops to 3,500 psi. The oil formation volume factor at 3,500 psi is 1.414 bbl/STB.

Solution

Step 1. Determine the effective compressibility from Equation 12-29.

$$c_e = \frac{(0.7)(15 \times 10^{-6}) + (0.3)(3 \times 10^{-6}) + 5 \times 10^{-6}}{1 - 0.3}$$

$$= 23.43 \times 10^{-6} \text{ psi}^{-1}$$

Step 2. Estimate N_p from Equation 12-32.

$$N_p = (85 \times 10^{-6})(23.43 \times 10^{-6}) \left(\frac{1.411}{1.400} \right) (4000 - 3500)$$

$$= 985.18 \text{ MSTB}$$

Saturated-Oil Reservoirs

If the reservoir originally exists at its bubble-point pressure, the reservoir is referred to as a saturated-oil reservoir. This is considered as the second type of the solution-gas-drive reservoir. As the reservoir pressure declines below the bubble-point, the gas begins to evolve from solution. The general MBE may be simplified by assuming that the expansion of the gas is much greater than the expansion of rock and initial water and, therefore, can be neglected. For a volumetric and saturated-oil reservoir with no fluid injection, the MBE can be expressed by:

$$N = \frac{N_p B_o + (G_p - N_p R_s) B_g}{(B_o - B_{oi}) + (R_{si} - R_s) B_g} \quad (12-33)$$

The above material balance equation contains two unknowns, which are:

- Cumulative oil production N_p
- Cumulative gas production G_p

The following reservoir and PVT data must be available in order to predict the primary recovery performance of a depletion-drive reservoir in terms of N_p and G_p :

a. Initial oil-in-place N

Generally, the volumetric estimate of in-place oil is used in calculating the performance. Where there is sufficient solution-gas-drive history,

however, this estimate may be checked by calculating a material-balance estimate.

b. Hydrocarbon PVT data

Since differential gas liberation is assumed to best represent the conditions in the reservoir, differential laboratory PVT data should be used in reservoir material balance. The flash PVT data are then used to convert from reservoir conditions to stock-tank conditions.

If laboratory data are not available, reasonable estimates may sometimes be obtained from published correlations. If differential data are not available, the flash data may be used instead; however, this may result in large errors for high-solubility crude oils.

c. Initial fluid saturations

Initial fluid saturations obtained from a laboratory analysis of core data are preferred; however, if these are not available, estimates in some cases may be obtained from a well-log analysis or may be obtained from other reservoirs in the same or similar formations.

d. Relative permeability data

Generally, laboratory-determined k_g/k_o and k_{ro} data are averaged to obtain a single representative set for the reservoir. If laboratory data are not available, estimates in some cases may be obtained from other reservoirs in the same or similar formations.

Where there is sufficient solution-gas-drive history for the reservoir, calculate (k_{rg}/k_{ro}) values versus saturation from Equations 12-15 and 12-17, i.e.:

$$S_o = (1 - S_{wi}) (1 - N_p/N) (B_o/B_{oi})$$

$$k_{rg}/k_{ro} = (GOR - R_s) (\mu_g B_g/\mu_o B_o)$$

The above results should be compared with the averaged laboratory relative permeability data. This may indicate a needed adjustment in the early data and possibly an adjustment in the overall data.

All the techniques that are used to predict the future performance of a reservoir are based on combining the appropriate MBE with the instantaneous GOR using the proper saturation equation. The calculations are repeated at a series of assumed reservoir pressure drops. These calculations are usually based on one stock-tank barrel of oil-in-place at the

bubble-point pressure, i.e., $N = 1$. This avoids carrying large numbers in the calculation procedure and permits calculations to be made on the basis of the fractional recovery of initial oil-in-place.

There are several widely used techniques that were specifically developed to predict the performance of solution-gas-drive reservoirs, including:

- Tracy's method
- Muskat's method
- Tarner's method

These methodologies are presented below.

Tracy's Method

Tracy (1955) suggests that the general material balance equation can be rearranged and expressed in terms of three functions of PVT variables. Tracy's arrangement is given in Chapter 11 by Equation 11-53 and is repeated here for convenience:

$$N = N_p \Phi_o + G_p \Phi_g + (W_p B_w - W_e) \Phi_w \quad (12-34)$$

where Φ_o , Φ_g , and Φ_w are considered PVT-related properties that are functions of pressure and defined by:

$$\Phi_o = \frac{B_o - R_s B_g}{\text{Den}}$$

$$\Phi_g = \frac{B_g}{\text{Den}}$$

$$\Phi_w = \frac{1}{\text{Den}}$$

with

$$\text{Den} = (B_o - B_{oi}) + (R_{si} - R_s) B_g + m B_{oi} \left[\frac{B_g}{B_{gi}} - 1 \right] \quad (12-35)$$

For a solution-gas-drive reservoir, Equations 12-34 and 12-35 are reduced to the following expressions, respectively:

$$N = N_p \Phi_o + G_p \Phi_g \quad (12-36)$$

and

$$\text{Den} = (B_o - B_{oi}) + (R_{si} - R_s) B_g \quad (12-37)$$

Tracy's calculations are performed in series of pressure drops that proceed from a known reservoir condition at the previous reservoir pressure p^* to the new assumed lower pressure p . The calculated results at the new reservoir pressure become "known" at the next assumed lower pressure.

In progressing from the conditions at any pressure p^* to the lower reservoir pressure p , consider that the incremental oil and gas production are ΔN_p and ΔG_p , or:

$$N_p = N_p^* + \Delta N_p \quad (12-38)$$

$$G_p = G_p^* + \Delta G_p \quad (12-39)$$

where N_p^* , G_p^* = "known" cumulative oil and gas production at previous pressure level p^*

N_p , G_p = "unknown" cumulative oil and gas at new pressure level p

Replacing N_p and G_p in Equation 12-36 with those of Equations 12-38 and 12-39 gives:

$$N = (N_p^* + \Delta N_p) \Phi_o + (G_p^* + \Delta G_p) \Phi_g \quad (12-40)$$

Define the average instantaneous GOR between the two pressures p^* and p by:

$$(\text{GOR})_{\text{avg}} = \frac{\text{GOR}^* + \text{GOR}}{2} \quad (12-41)$$

The incremental cumulative gas production ΔG_p can be approximated by Equation 12-7 as:

$$\Delta G_p = (\text{GOR})_{\text{avg}} \Delta N_p \quad (12-42)$$

Replacing ΔG_p in Equation 12-40 with that of 12-41 gives:

$$N = [N_p^* + \Delta N_p] \Phi_o + [G_p^* + \Delta N_p (GOR)_{avg}] \Phi_g \quad (12-43)$$

If Equation 12-43 is expressed for $N = 1$, the cumulative oil production N_p and cumulative gas production G_p become fractions of initial oil-in-place. Rearranging Equation 12-43 gives:

$$\Delta N_p = \frac{1 - (N_p^* \Phi_o + G_p^* \Phi_g)}{\Phi_o + (GOR)_{avg} \Phi_g} \quad (12-44)$$

Equation 12-44 shows that there are essentially two unknowns, the incremental cumulative oil production ΔN_p and the average gas-oil ratio $(GOR)_{avg}$.

Tracy suggested the following alternative technique for solving Equation 12-44.

Step 1. Select an average reservoir pressure p .

Step 2. Calculate the values of the PVT functions Φ_o and Φ_g .

Step 3. Estimate the GOR at p .

Step 4. Calculate the average instantaneous GOR $(GOR)_{avg} = (GOR^* + GOR)/2$.

Step 5. Calculate the incremental cumulative oil production ΔN_p from Equation 12-44 as:

$$\Delta N_p = \frac{1 - (N_p^* \Phi_o + G_p^* \Phi_g)}{\Phi_o + (GOR)_{avg} \Phi_g}$$

Step 6. Calculate cumulative oil production N_p :

$$N_p = N_p^* + \Delta N_p$$

Step 7. Calculate the oil and gas saturations at selected average reservoir pressure by using Equations 12-15 and 12-16, as:

$$S_o = (1 - S_{wi}) (1 - N_p) (B_o/B_{oi})$$

$$S_g = 1 - S_o - S_{wi}$$

Step 8. Obtain the relative permeability ratio k_{rg}/k_{ro} at S_g .

Step 9. Calculate the instantaneous GOR from Equation 12-1.

$$\text{GOR} = R_s + (k_{rg}/k_{ro}) (\mu_o B_o/\mu_g B_g)$$

Step 10. Compare the estimated GOR in Step 3 with the calculated GOR in Step 9. If the values are within the acceptable tolerance, proceed to the next step. If not within the tolerance, set the estimated GOR equal to the calculated GOR and repeat the calculations from Step 3.

Step 11. Calculate the cumulative gas production.

$$G_p = G_p^* + \Delta N_p (\text{GOR})_{\text{avg}}$$

Step 12. Since results of the calculations are based on 1 STB of oil initially in place, a final check on the accuracy of the prediction should be made on the MBE, or:

$$N_p \Phi_o + G_p \Phi_g = 1 \pm \text{tolerance}$$

Step 13. Repeat from Step 1.

As the calculation progresses, a plot of GOR versus pressure can be maintained and extrapolated as an aid in estimating GOR at each new pressure.

Example 12-4¹

The following PVT data characterize a solution-gas-drive reservoir.

¹The example data and solution are given by Economides, M., Hill, A., and Economides, C., *Petroleum Production System*, Prentice Hall Petroleum Engineering series, 1994.

The relative permeability data are shown in Figure 12-7.

| p psi | B_o bbl/STB | B_g bbl/scf | R_s scf/STB |
|----------|------------------|----------------------|------------------|
| 4350 | 1.43 | 6.9×10^{-4} | 840 |
| 4150 | 1.420 | 7.1×10^{-4} | 820 |
| 3950 | 1.395 | 7.4×10^{-4} | 770 |
| 3750 | 1.380 | 7.8×10^{-4} | 730 |
| 3550 | 1.360 | 8.1×10^{-4} | 680 |
| 3350 | 1.345 | 8.5×10^{-4} | 640 |

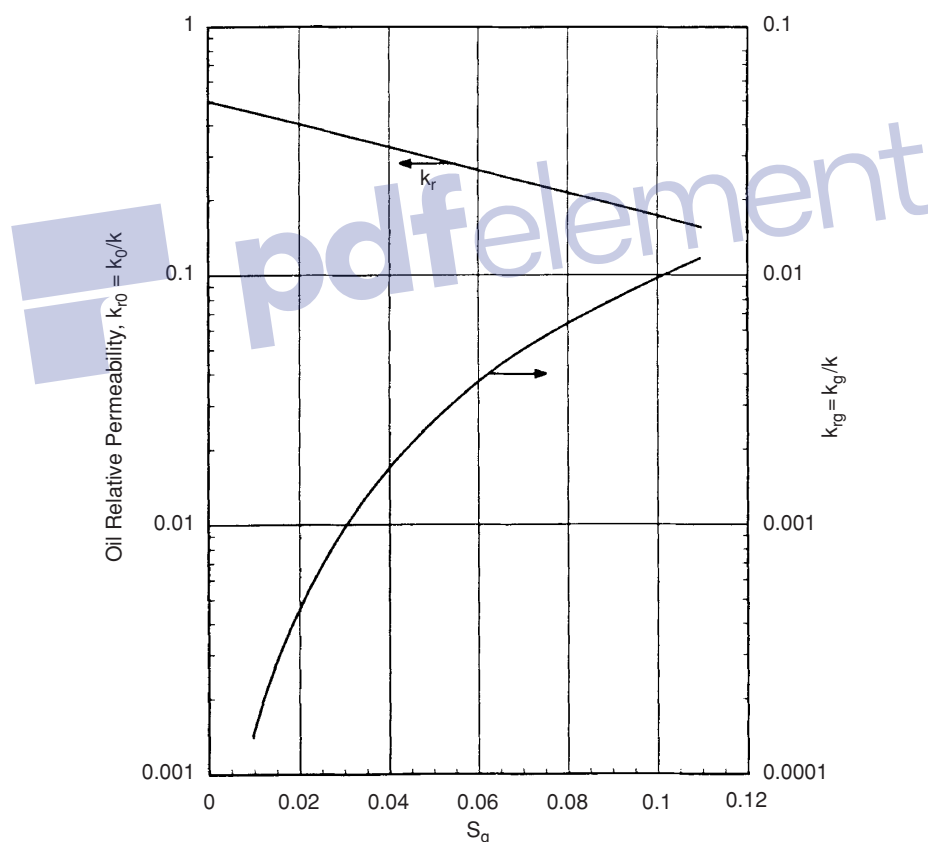


Figure 12-7. Relative permeability data for Example 12-3. (After Economides, M., et al., *Petroleum Production Systems*, Prentice Hall Petroleum Engineers Series, 1994.)

The following additional data are available:

$$p_i = p_b = 4350 \text{ psi} \quad S_{wi} = 30\% \quad N = 15 \text{ MMSTB}$$

Predict the cumulative oil and gas production to 3,350 psi.

Solution

A sample of the Tracy's calculation procedure is performed at 4,150 psi.

Step 1. Calculate Tracy's PVT functions at 4,150.

- Calculate the term Den from Equation 12-37

$$\text{Den} = (B_o - B_{oi}) + (R_{si} - R_s) B_g$$

$$\text{Den} = (1.42 - 1.43) + (840 - 820) (7.1 \times 10^{-4}) = 0.0042$$

- Calculate Φ_o and Φ_g

$$\Phi_o = (B_o - R_s B_g) / \text{Den}$$

$$\Phi_o = [1.42 - (820) (7.1 \times 10^{-4})] / 0.0042 = 199$$

$$\Phi_g = B_g / \text{Den}$$

$$= 7.1 \times 10^{-4} / 0.0042 = 0.17$$

Similarly, these PVT variables are calculated for all other pressures to give:

| p | Φ_o | Φ_g |
|------|----------|----------|
| 4350 | — | — |
| 4150 | 199 | 0.17 |
| 3950 | 49 | 0.044 |
| 3750 | 22.6 | 0.022 |
| 3550 | 13.6 | 0.014 |
| 3350 | 9.42 | 0.010 |

Step 2. Assume a value for the GOR at 4,150 psi as 850 scf/STB.

Step 3. Calculate the average GOR.

$$(\text{GOR})_{\text{avg}} = \frac{840 + 850}{2} = 845 \text{ scf/STB}$$

Step 4. Calculate the incremental cumulative oil production ΔN_p .

$$\Delta N_p = \frac{1 - 0}{199 + (845)(0.17)} = 0.00292 \text{ STB}$$

Step 5. Calculate the cumulative oil production N_p .

$$N_p = N_p^* + \Delta N_p$$

$$N_p = 0 + 0.00292 = 0.00292$$

Step 6. Calculate oil and gas saturations.

$$S_o = (1 - N_p) (B_o/B_{oi}) (1 - S_{wi})$$

$$S_o = (1 - 0.00292) (1.42/1.43) (1 - 0.3) = 0.693$$

$$S_g = 1 - S_{wi} - S_o$$

$$S_g = 1 - 0.3 - 0.693 = 0.007$$

Step 7. Determine the relative permeability ratio k_{rg}/k_{ro} from Figure 12-7, to give:

$$k_{rg}/k_{ro} = 8 \times 10^{-5}$$

Step 8. Using $\mu_o = 1.7$ cp and $\mu_g = 0.023$ cp, calculate the instantaneous GOR.

$$\text{GOR} = 820 + (1.7 \times 10^{-4}) \frac{(1.7)(1.42)}{(0.023)(7.1 \times 10^{-4})} = 845 \text{ scf/STB}$$

which agrees with the assumed value.

Step 9. Calculate cumulative gas production.

$$G_p = 0 + (0.00292) (850) = 2.48$$

Complete results of the method are shown below:

| \bar{p} | ΔN_p | N_p | (GOR) _{avg} | ΔG_p | G_p scf/STB | $N_p = 15 \times 10^6$ N STB | $G_p = 15 \times 10^6$ N scf |
|-----------|--------------|---------|----------------------|--------------|------------------|---------------------------------|---------------------------------|
| 4350 | — | — | — | — | — | — | — |
| 4150 | 0.00292 | 0.00292 | 845 | 2.48 | 2.48 | 0.0438×10^6 | 37.2×10^6 |
| 3950 | 0.00841 | 0.0110 | 880 | 7.23 | 9.71 | 0.165×10^6 | 145.65×10^6 |
| 3750 | 0.0120 | 0.0230 | 1000 | 12 | 21.71 | 0.180×10^6 | 325.65×10^6 |
| 3550 | 0.0126 | 0.0356 | 1280 | 16.1 | 37.81 | 0.534×10^6 | 567.15×10^6 |
| 3350 | 0.011 | 0.0460 | 1650 | 18.2 | 56.01 | 0.699×10^6 | 840×10^6 |

Muskat's Method

Muskat (1945) expressed the material balance equation for a depletion-drive reservoir in the following differential form:

$$\frac{dS_o}{dp} = \frac{\frac{S_o B_g}{B_o} \frac{dR_s}{dp} + \frac{S_o k_{rg} \mu_o}{B_o k_{ro} \mu_g} \frac{dB_o}{dp} + (1 - S_o - S_{wc}) B_g \frac{d(1/B_g)}{dp}}{1 + \frac{\mu_o k_{rg}}{\mu_g k_{ro}}} \quad (12-45)$$

with

$$\Delta S_o = S_o^* - S_o$$

$$\Delta p = p^* - p$$

where S_o^* , p^* = oil saturation and average reservoir pressure at the beginning of the pressure step

S_o , p = oil saturation and average reservoir pressure at the end of the time step

R_s = gas solubility, scf/STB

B_g = gas formation volume factor, bbl/scf

Craft, Hawkins, and Terry (1991) suggested the calculations can be greatly facilitated by computing and preparing in advance in graphical form the following pressure dependent groups:

$$X(p) = \frac{B_g}{B_o} \frac{dR_s}{dp} \quad (12-46)$$

$$Y(p) = \frac{1}{B_o} \frac{\mu_o}{\mu_g} \frac{dB_o}{dp} \quad (12-47)$$

$$Z(p) = B_g \frac{d(1/B_g)}{dp} \quad (12-48)$$

Introducing the above pressure dependent terms into Equation 12-45, gives:

$$\left(\frac{\Delta S_o}{\Delta p} \right) = \frac{S_o X(p) + S_o \frac{k_{rg}}{k_{ro}} Y(p) + (1 - S_o - S_{wc}) Z(p)}{1 + \frac{\mu_o}{\mu_g} \frac{k_{rg}}{k_{ro}}} \quad (12-49)$$

Craft, Hawkins, and Terry (1991) proposed the following procedure for solving Muskat's equation for a given pressure drop Δp , i.e., $(p^* - p)$:

Step 1. Prepare a plot of k_{rg}/k_{ro} versus gas saturation.

Step 2. Plot R_s , B_o , and $(1/B_g)$ versus pressure and determine the slope of each plot at selected pressures, i.e., dB_o/dp , dR_s/dp , and $d(1/B_g)/dp$.

Step 3. Calculate the pressure dependent terms $X(p)$, $Y(p)$, and $Z(p)$ that correspond to the selected pressures in Step 2.

Step 4. Plot the pressure dependent terms as a function of pressure, as illustrated in Figure 12-8.

Step 5. Graphically determine the values of $X(p)$, $Y(p)$, and $Z(p)$ that correspond to the pressure p .

Step 6. Solve Equation 12-49 for $(\Delta S_o/\Delta p)$ by using the oil saturation S_o^* at the beginning of the pressure drop interval p^* .

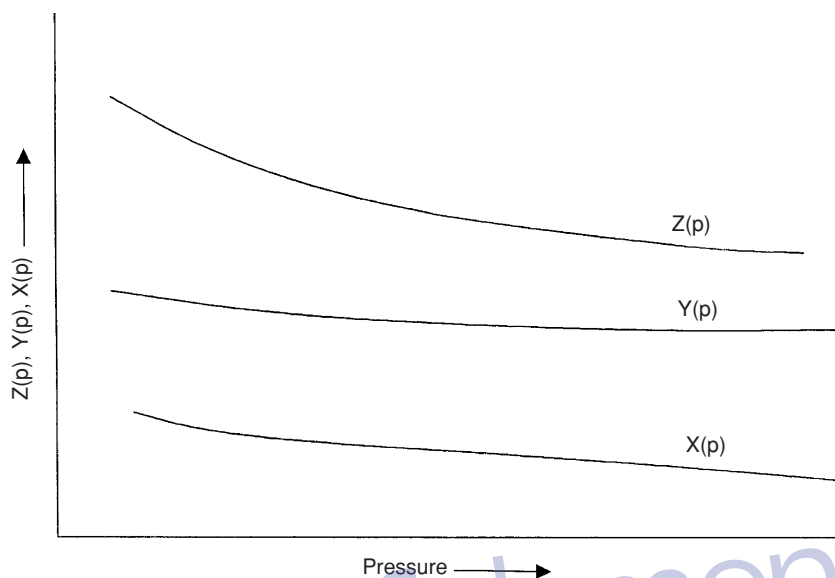


Figure 12-8. Pressure dependant terms vs. p .

Step 7. Determine the oil saturation S_o at the average reservoir pressure p , from:

$$S_o = S_o^* - (p^* - p) \left(\frac{\Delta S_o}{\Delta p} \right) \quad (12-50)$$

Step 8. Using the S_o from Step 7 and the pressure p , recalculate $(\Delta S_o/\Delta p)$ from Equation 12-49.

Step 9. Calculate the average value for $(\Delta S_o/\Delta p)$ from the two values obtained in Steps 6 and 8, or:

$$\left(\frac{\Delta S_o}{\Delta p} \right)_{\text{avg}} = \frac{1}{2} \left[\left(\frac{\Delta S_o}{\Delta p} \right)_{\text{step 6}} + \left(\frac{\Delta S_o}{\Delta p} \right)_{\text{step 8}} \right]$$

Step 10. Using $(\Delta S_o/\Delta p)_{\text{avg}}$, solve for the oil saturation S_o from:

$$S_o = S_o^* - (p^* - p) \left(\frac{\Delta S_o}{\Delta p} \right)_{\text{avg}} \quad (12-51)$$

This value of S_o becomes S_o^* for the next pressure drop interval.

Step 11. Calculate gas saturation S_g by:

$$S_g = 1 - S_{wi} - S_o$$

Step 12. Using the saturation equation, i.e., Equation 12-15, solve for the cumulative oil production.

$$N_p = N \left[1 - \left(\frac{B_{oi}}{B_o} \right) \left(\frac{S_o}{1 - S_{wi}} \right) \right] \quad (12-52)$$

Step 13. Calculate the cumulative gas production by using Equations 12-40 and 12-41.

Step 14. Repeat Steps 5 through 13 for all pressure drops of interest.

Example 12-5²

A volumetric depletion-drive reservoir exists at its bubble-point pressure of 2,500 psi. Detailed fluid property data are listed by Craft and his coauthors and given here at only two pressures.

| Fluid Property | $p_b = 2500$ psi | $p = 2300$ psi |
|-----------------|------------------|----------------|
| B_o , bbl/STB | 1.498 | 1.463 |
| R_s , scf/STB | 721 | 669 |
| B_g , bbl/scf | 0.001048 | 0.001155 |
| μ_o , cp | 0.488 | 0.539 |
| μ_g , cp | 0.0170 | 0.0166 |
| X (p) | 0.00018 | 0.00021 |
| Y (p) | 0.00328 | 0.00380 |
| Z (p) | 0.00045 | 0.00050 |

²Craft, B. C., Hawkins, M., Terry, R., *Applied Petroleum Reservoir Engineering*, 2nd ed. Prentice Hall, 1991.

The following additional information is available:

$$N = 56 \text{ MMSTB} \quad S_{wi} = 20\% \quad S_{oi} = 80\%$$

| S_g | k_{rg}/k_{ro} |
|-------|-----------------|
| 0.10 | 0.010 |
| 0.20 | 0.065 |
| 0.30 | 0.200 |
| 0.50 | 2.000 |
| 0.55 | 3.000 |
| 0.57 | 5.000 |

Calculate the cumulative oil production for a pressure drop of 200 psi, i.e., at 2,300 psi.

Solution

Step 1. Using the oil saturation at the beginning of the pressure interval, i.e., $S_o^* = 0.8$, calculate (k_{rg}/k_{ro}) to give:

$$k_{rg}/k_{ro} = 0.0 \text{ (No free gas initially in place.)}$$

Step 2. Evaluate $(\Delta S_o/\Delta p)$ by applying Equation 12-49.

$$\left(\frac{\Delta S_o}{\Delta p} \right) = \frac{(0.8)(0.00018) + 0 + 0}{1 + 0} = 0.000146$$

Step 3. Estimate the oil saturation at $p = 2,300$ psi from Equation 12-51.

$$S_o = 0.8 - 200(0.000146) = 0.7709$$

Step 4. Recalculate $(\Delta S_o/\Delta p)$ by using $S_o = 0.7709$ and the pressure dependent terms at 2,300 psi.

$$\left(\frac{\Delta S_o}{\Delta p} \right) = \frac{0.7709(0.00021) + 0.7709(0.00001)0.0038 + (1 - 0.2 - 0.7709)0.0005}{1 + \left(\frac{0.539}{0.0166} \right)(0.00001)}$$

$$\left(\frac{\Delta S_o}{\Delta p} \right) = 0.000173$$

Step 5. Calculate the average $(\Delta S_o/\Delta p)$.

$$\left(\frac{\Delta S_o}{\Delta p}\right)_{\text{avg}} = \frac{0.000146 + 0.000173}{2} = 0.000159$$

Step 6. Calculate $S_o = 0.8 - (2500 - 2300)(0.000159) = 0.7682$.

Step 7. Calculate gas saturation.

$$S_g = 1 - 0.2 - 0.7682 + 0.0318$$

Step 8. Calculate cumulative oil production at 2,300 psi by using Equation 12-52.

$$N_p = 56 \times 10^6 \left[1 - \left(\frac{1.498}{1.463}\right) \left(\frac{0.7682}{1-0.2}\right) \right] = 939,500 \text{ STB}$$

Step 9. Calculate k_{rg}/k_{ro} at 2,300 psi, to give $k_{rg}/k_{ro} = 0.00001$.

Step 10. Calculate the instantaneous GOR at 2,300 psi.

$$\text{GOR} = 669 + 0.00001 \frac{(0.539)(1.463)}{(0.0166)(0.001155)} = 669 \text{ scf/STB}$$

Step 11. Calculate cumulative gas production.

$$G_p = \left(\frac{669 + 669}{2}\right) 939,500 = 629 \text{ MMscf}$$

It should be stressed that this method is based on the assumption of uniform oil saturation in the whole reservoir and that the solution will therefore break down when there is appreciable gas segregation in the formation. It is therefore applicable only when permeabilities are relatively low.

Tarner's Method

Tarner (1944) suggests an iterative technique for predicting cumulative oil production N_p and cumulative gas production G_p as a function of

reservoir pressure. The method is based on solving the material-balance equation and the instantaneous gas-oil ratio equation simultaneously for a given reservoir pressure drop from p_1 to p_2 . It is accordingly assumed that the cumulative oil and gas production has increased from N_{p1} and G_{p1} to N_{p2} and G_{p2} . To simplify the description of the proposed iterative procedure, the stepwise calculation is illustrated for a volumetric saturated-oil reservoir. It should be pointed out that Tarner's method could be extended to predict the volumetric behavior of reservoirs under different driving mechanisms.

Step 1. Select a future reservoir pressure p_2 below the initial (current) reservoir pressure p_1 and obtain the necessary PVT data. Assume that the cumulative oil production has increased from N_{p1} to N_{p2} . It should be pointed out that N_{p1} and G_{p1} are set equal to zero at the initial reservoir pressure, i.e., bubble-point pressure.

Step 2. Estimate or guess the cumulative oil production N_{p2} at p_2 .

Step 3. Calculate the cumulative gas production G_{p2} by rearranging the MBE, i.e., Equation 12-33, to give:

$$G_{p2} = N \left[(R_{si} - R_s) - \frac{B_{oi} - B_o}{B_g} \right] - N_{p2} \left[\frac{B_o}{B_g} - R_s \right] \quad (12-53)$$

Equivalently, the above relationship can be expressed in terms of the two-phase (total) formation volume factor B_t as:

$$G_{p2} = \frac{N(B_t - B_{ti}) - N_{p2}(B_t - R_{si}B_g)}{B_g} \quad (12-54)$$

where B_g = gas formation volume factor at p_2 , bbl/scf
 B_o = oil formation volume factor at p_2 , bbl/STB
 B_t = two-phase formation volume factor at p_2 , bbl/STB
 N = initial oil-in-place, STB

Step 4. Calculate the oil and gas saturations at the assumed cumulative oil production N_{p2} and the selected reservoir pressure p_2 by applying Equations 12-15 and 12-16 respectively, or:

$$S_o = (1 - S_{wi}) \left[1 - \frac{N_{p2}}{N} \right] \left(\frac{B_o}{B_{oi}} \right)$$

$$S_g = 1 - S_o - S_{wi}$$

where B_o = initial oil formation volume factor at p_1 , bbl/STB

B_o = oil formation volume factor at p_2 , bbl/STB

S_g = gas saturation at p_2

B_o = oil saturation at p_2

Step 5. Using the available relative permeability data, determine the relative permeability ratio k_{rg}/k_{ro} that corresponds to the gas saturation at p_2 and compute the instantaneous $(GOR)_2$ at p_2 from Equation 12-1, as:

$$(GOR)_2 = R_s + \left(\frac{k_{rg}}{k_{ro}} \right) \left(\frac{\mu_o B_o}{\mu_g B_g} \right) \quad (12-55)$$

It should be noted that all the PVT data in the expression must be evaluated at the assumed reservoir pressure p_2 .

Step 6. Calculate again the cumulative gas production G_{p2} at p_2 by applying Equation 12-7, or:

$$G_{p2} = (G_{p1}) + \left[\frac{(GOR)_1 + (GOR)_2}{2} \right] [N_{p2} - N_{p1}] \quad (12-56)$$

in which $(GOR)_1$ represents the instantaneous GOR at p_1 . If p_1 represents the initial reservoir pressure, then set $(GOR)_1 = R_{si}$.

Step 7. The total gas produced G_{p2} during the first prediction period as calculated by the material balance equation is compared to the total gas produced as calculated by the GOR equation. These two equations provide the two independent methods required for determining the total gas produced. Therefore, if the cumulative gas production G_{p2} as calculated from Step 3 agrees with the value of Step 6, the assumed value of N_{p2} is correct and a new

pressure may be selected and Steps 1 through 6 are repeated. Otherwise, assume another value of N_{p2} and repeat Steps 2 through 6.

Step 8. In order to simplify this iterative process, three values of N_p can be assumed, which yield three different solutions of cumulative gas production for each of the equations (i.e., MBE and GOR equation). When the computed values of G_{p2} are plotted versus the assumed values of N_{p2} , the resulting two curves (one representing results of Step 3 and the one representing Step 5) will intersect. This intersection indicates the cumulative oil and gas production that will satisfy both equations.

It should be pointed out that it may be more convenient to assume values of N_p as a fraction of the initial oil-in-place N . For instance, N_p could be assumed as $0.01 N$, rather than as 10,000 STB. In this method, a true value of N is not required. Results of the calculations would be, therefore, in terms of STB of oil produced per STB of oil initially in place and scf of gas produced per STB of oil initially in place.

To illustrate the application of Tarner's method, Cole (1969) presented the following example:

Example 12-6

A saturated-oil reservoir has a bubble-point pressure of 2,100 psi at 175°F. The initial reservoir pressure is 2,925 psi. The following data summarize the rock and fluid properties of the field:

Original oil-in-place = 10 MMSTB

Connate-water saturation = 15%

Porosity = 12%

$$c_w = 3.6 \times 10^{-6} \text{ psi}^{-1}$$

$$c_f = 4.9 \times 10^{-6} \text{ psi}^{-1}$$

Basic PVT Data

| p, psi | B_o , bbl/STB | B_{tr} , bbl/STB | R_{sr} , scf/STB | B_g , bbl/scf | μ_o/μ_g |
|--------|-----------------|--------------------|--------------------|-----------------|---------------|
| 2925 | 1.429 | 1.429 | 1340 | — | — |
| 2100 | 1.480 | 1.480 | 1340 | 0.001283 | 34.1 |
| 1800 | 1.468 | 1.559 | 1280 | 0.001518 | 38.3 |
| 1500 | 1.440 | 1.792 | 1150 | 0.001853 | 42.4 |

Relative Permeability Ratio

| S_{or} % | k_{rg}/k_{ro} |
|------------|-----------------|
| 81 | 0.018 |
| 76 | 0.063 |
| 60 | 0.85 |
| 50 | 3.35 |
| 40 | 10.2 |

Predict cumulative oil and gas production at 2,100, 1,800, and 1,500 psi.

Solution

The required calculations will be performed under the following two different driving mechanisms:

- During the reservoir pressure declines from the initial reservoir pressure of 2,925 to the bubble-point pressure of 2,100 psi, the reservoir is considered undersaturated and, therefore, the MBE can be used directly to calculate cumulative production without resorting to the iterative technique.
- For reservoir pressures below the bubble-point pressure, the reservoir is treated as a saturated-oil reservoir and Turner's method may be applied.

Phase 1: Oil recovery prediction above the bubble-point pressure

Step 1. Arrange the MBE (Equation 11-32) and solve for the cumulative oil as:

$$N_p = \frac{N[E_o + E_{f,w}]}{B_o} \quad (12-57)$$

where

$$E_{f,w} = B_{oi} \left[\frac{c_w S_w + c_f}{1 - S_{wi}} \right] (p_i - p)$$

$$E_o = B_o - B_{oi}$$

Step 2. Calculate the two expansion factors E_o and $E_{f,w}$ for the pressure declines from 2,925 to 2,100 psi:

$$E_o = 1.480 - 1.429 = 0.051$$

$$E_{f,w} = 1.429 \left[\frac{(3.6 \times 10^{-6})(0.15) + (4.9 \times 10^{-6})}{1 - 0.15} \right] = 9.1456 \times 10^{-6}$$

Step 3. Calculate cumulative oil and gas production when the reservoir pressure declines from 2,925 to 2,100 psi by applying Equation 12-57, to give:

$$N_p = \frac{10 \times 10^6 [0.051 + 9.1456 \times 10^{-6}]}{1.48} = 344,656 \text{ STB}$$

At or above the bubble-point pressure, the producing gas-oil ratio is equal to the gas solubility at the bubble-point and, therefore, the cumulative gas production is given by:

$$G_p = N_p R_{si}$$

$$G_p = (344,656) (1340) = 462 \text{ MMscf}$$

Step 4. Determine remaining oil-in-place at 2,100 psi.

$$\text{Remaining oil-in-place} = 10,000,000 - 344,656 = 9,655,344 \text{ STB}$$

This remaining oil-in-place is considered as the initial oil-in-place during the reservoir performance below the saturation pressure, i.e.:

$$N = 9,655,344 \text{ STB}$$

$$N_p = 0.0 \text{ STB}$$

$$G_p = 0.0 \text{ scf}$$

$$R_{si} = 1340 \text{ scf/STB}$$

$$B_{oi} = 1.489 \text{ bbl/STB}$$

$$B_{ti} = 1.489 \text{ bbl/STB}$$

$$B_{gi} = 0.001283 \text{ bbl/scf}$$

Phase 2: Oil recovery prediction above the bubble-point pressure

First prediction period at 1,800 psi:

Step 1. Assume $N_p = 0.01 N$ and apply Equation 12-54 to solve for G_p .

$$G_p = \frac{N(1.559 - 1.480) - (0.01N)(1.559 - 1340 \times 0.001518)}{0.001518} = 55.17 N$$

Step 2. Calculate the oil saturation, to give:

$$S_o = (1 - S_{wi}) \left(1 - \frac{N_p}{N} \right) \frac{B_o}{B_{oi}} = (1 - 0.15) \left(1 - \frac{0.01N}{N} \right) \frac{1.468}{1.480} = 0.835$$

Step 3. Determine the relative permeability ratio k_{rg}/k_{ro} from the available data to give:

$$k_{rg}/k_{ro} = 0.0100$$

Step 4. Calculate the instantaneous GOR at 1,800 psi by applying Equation 12-55 to give:

$$GOR = 1280 + 0.0100(38.3) \left(\frac{1.468}{0.001518} \right) = 1650 \text{ scf/STB}$$

Step 5. Solve again for the cumulative gas production by using the average GOR and applying Equation 12-56 to yield:

$$G_p = 0 + \frac{1340 + 1650}{2} (0.01N - 0) = 14.95N$$

Step 6. Since the cumulative gas production as calculated by the two independent methods (Step 1 and Step 5) do not agree, the calculations must be repeated by assuming a different value for N_p and plotting results of the calculation. The final results as summarized below show the cumulative gas and oil production as the pressure declines from the bubble-point pressure. It should be pointed out that the cumulative production above the bubble-point pressure must be included when reporting the *total* cumulative oil and gas production.

| Pressure | N_p | Actual N_p , STB | G_p | Actual G_p , MMscf |
|----------|----------|--------------------|---------|----------------------|
| 1800 | 0.0393 N | 379,455 | 64.34 N | 621.225 |
| 1500 | 0.0889 N | 858,360 | 136.6 N | 1318.92 |

PHASE 2. RELATING RESERVOIR PERFORMANCE TO TIME

All reservoir performance techniques show the relationship of cumulative oil production and the instantaneous GOR as a function of average reservoir pressure. These techniques, however, do not relate the cumulative oil production N_p and cumulative gas production G_p with time. Figure 12-9 shows a schematic illustration of the predicted cumulative oil production with reservoir pressure.

The time required for production can be calculated by applying the concept of the inflow performance relation (IPR) in conjunction with the

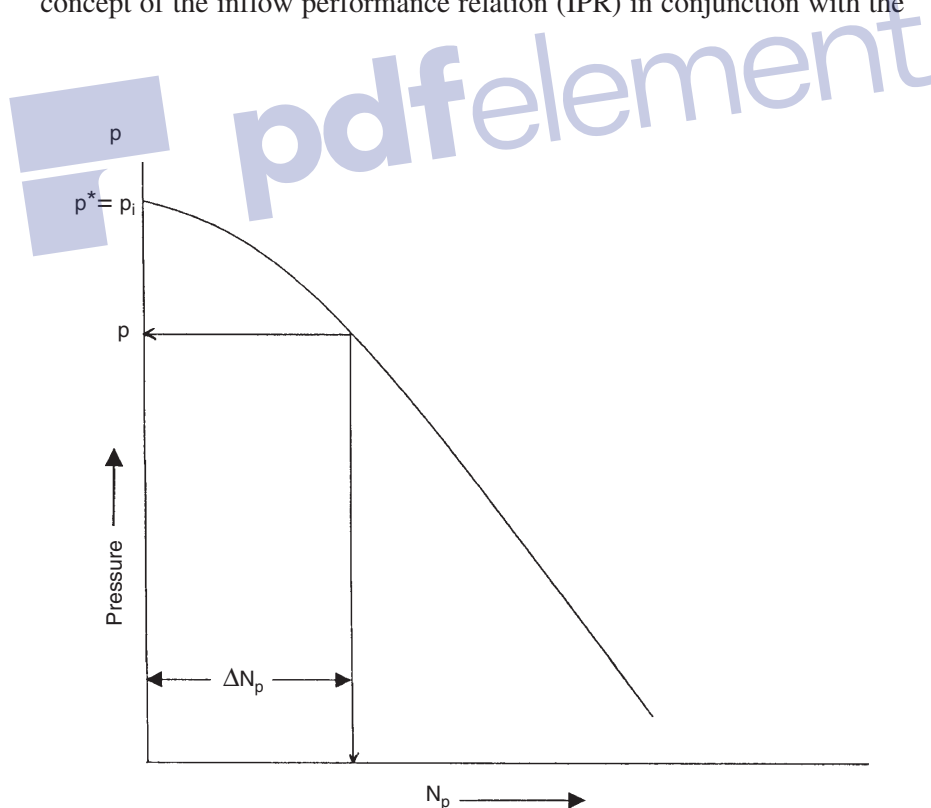
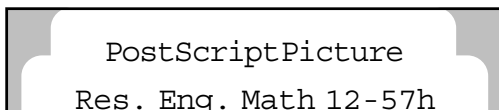


Figure 12-9. Cumulative production as a function of average reservoir pressure.

MBE predictions. Vogel (1969) expressed the well's inflow performance relationship by Equation 7-9, or:



The following methodology can be employed to correlate the predicted cumulative field production with time t .

Step 1. Plot the predicted cumulative oil production N_p as a function of average reservoir pressure p as shown in Figure 12-9.

Step 2. Construct the IPR curve for each well in field at the initial average reservoir pressure p^* . Calculate the oil flow rate for the entire field by taking the summation of the flow rates. Plot the flow rates as shown schematically in Figure 12-10 for two hypothetical wells and establish the IPR for the field.

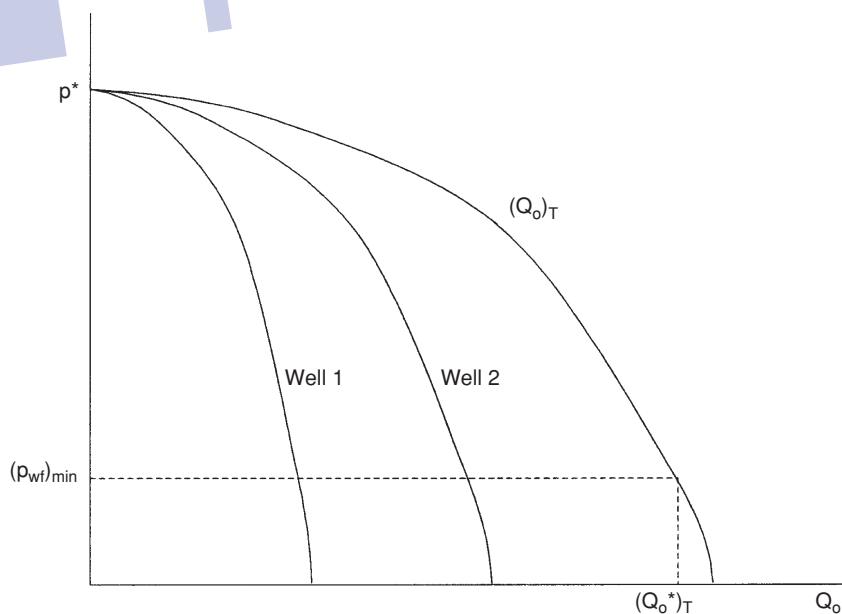


Figure 12-10. Overall field IPR at current pressure.

Step 3. Using the minimum bottom-hole flowing pressure $(p_{wf})_{min}$, determine the total field flow rate $(Q_o)_T^*$.

Step 4. Select a future average reservoir pressure p and determine the future IPR for each well in the field. Construct the field IPR curve as shown in Figure 12-11.

Step 5. Using the minimum p_{wf} , determine the field total oil flow rate $(Q_o)_T$.

Step 6. Calculate the average field production rate $(\bar{Q}_o)_T$.

$$(\bar{Q}_o)_T = \frac{(Q_o)_T + (Q_o)_T^*}{2}$$

Step 7. Calculate the time Δt required for the incremental oil production ΔN_p during the first pressure drop interval, i.e., from p^* to p , by:

$$\Delta t = \frac{\Delta N_p}{(\bar{Q}_o)_T}$$

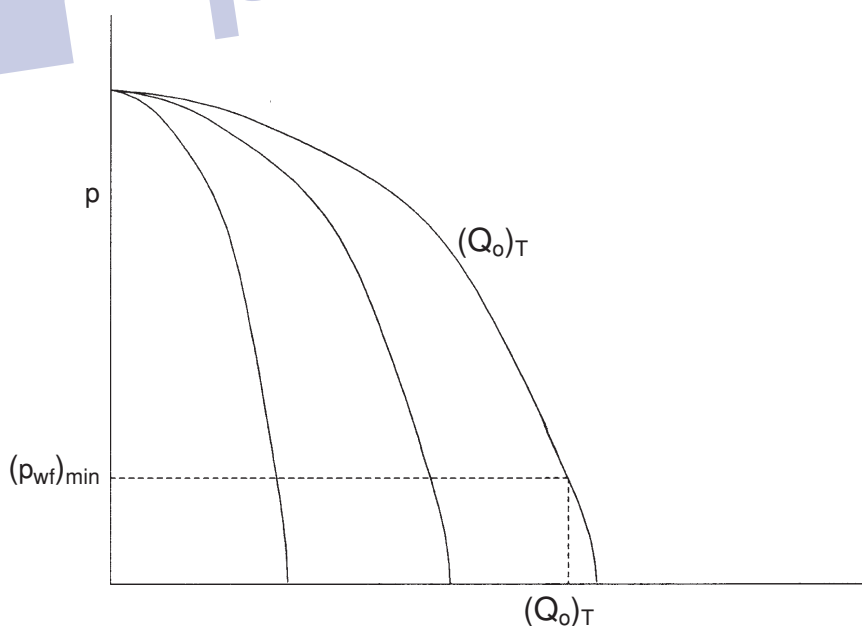


Figure 12-11. Future field IPR.

Step 8. Repeat the above steps and calculate the total time t to reach an average reservoir pressure p by:

$$t = \Sigma \Delta t$$

PROBLEMS

1. Determine the fractional oil recovery, during depletion down to bubble-point pressure, for the reservoir whose PVT parameters are listed in Table 3-7 and for which:

$$c_w = 3.5 \times 10^{-6} \text{ psi}^{-1} \quad c_f = 3.5 \times 10^{-6} \text{ psi}^{-1} \quad S_{wc} = 0.20$$

2. The Big Butte field is a depletion-drive reservoir that contains 25 MMSTB of oil initially in place. Tables 3-4 through 3-7 show the experimental PVT data of the crude oil system. The initial reservoir pressure is recorded as 1,936 psi at 247°F. The relative permeability ratio k_{rg}/k_{ro} is given by:

$$k_{rg}/k_{ro} = 0.007 e^{11.513 S_g}$$

Given

$$S_{or} = 35\% \quad S_{gc} = 3\% \quad S_{wi} = 25\%$$

and using a pressure drop increment of 200 psi, predict the reservoir future performance in terms of:

- Cumulative oil production N_p
- Cumulative gas production G_p
- Oil saturation S_o
- Gas saturation S_g
- Instantaneous GOR
- Cumulative producing gas-oil ratio R_p

Plot results of the calculations to an abandonment pressure of 500 psi. Use the following three methods:

1. Tracy's method
2. Muskat's method
3. Tarner's method

REFERENCES

1. Cole, F., *Reservoir Engineering Manual*. Houston: Gulf Publishing Company, 1969.
2. Craft, B. C., and Hawkins, M. (revised by Terry, R. E.), *Applied Petroleum Reservoir Engineering*, 2nd ed. Englewood Cliffs, NJ: Prentice Hall, 1991.
3. Dake, L. P., *Fundamentals of Reservoir Engineering*. Amsterdam: Elsevier, 1978.
4. Economides, M., Hill, A., and Economides, C., *Petroleum Production Systems*. Englewood Cliffs, NJ: Prentice Hall, 1994.
5. Havlena, D., and Odeh, A. S., "The Material Balance as an Equation of a Straight Line," *JPT*, August 1963, pp. 896–900.
6. Havlena, D., and Odeh, A. S., "The Material Balance as an Equation of a Straight Line. Part II—Field Cases," *JPT*, July 1964, pp. 815–822.
7. Hawkins, M., "Material Balances in Expansion Type Reservoirs Above Bubble-Point," SPE Transactions Reprint Series No. 3, 1955, pp. 36–40.
8. Muskat, M., "The Production Histories of Oil Producing Gas-Drive Reservoirs," *Journal of Applied Physics*, 1945, Vol. 16, p. 167.
9. Tamer, J., "How Different Size Gas Caps and Pressure Maintenance Programs Affect Amount of Recoverable Oil," *Oil Weekly*, June 12, 1944, Vol. 144.
10. Tracy, G., "Simplified Form of the MBE," *Trans. AIME*, 1955, Vol. 204, pp. 243–246.
11. Vogel, J. V., "Inflow Performance Relationships for Three-Phase Flow," SPE Paper 25458 presented at the SPE Production Operations Symposium, Oklahoma City, March 21–23, 1993.

C H A P T E R 1 3

GAS RESERVOIRS

Reservoirs containing only free gas are termed gas reservoirs. Such a reservoir contains a mixture of hydrocarbons, which exists wholly in the gaseous state. The mixture may be a *dry*, *wet*, or *condensate* gas, depending on the composition of the gas, along with the pressure and temperature at which the accumulation exists.

Gas reservoirs may have water influx from a contiguous water-bearing portion of the formation or may be volumetric (i.e., have no water influx).

Most gas engineering calculations involve the use of gas formation volume factor B_g and gas expansion factor E_g . Both factors are defined in Chapter 2 by Equations 2-52 through 2-56. Those equations are summarized below for convenience:

- Gas formation volume factor B_g is defined as the actual volume occupied by n moles of gas at a specified pressure and temperature, divided by the volume occupied by the same amount of gas at standard conditions. Applying the real gas equation-of-state to both conditions gives:

$$B_g = \frac{p_{sc}}{T_{sc}} \frac{zT}{p} = 0.02827 \frac{zT}{p} \quad (13-1)$$

- The gas expansion factor is simply the reciprocal of B_g , or:

$$E_g = \frac{T_{sc}}{p_{sc}} \frac{p}{zT} = 35.37 \frac{p}{zT} \quad (13-2)$$

where B_g = gas formation volume factor, ft³/scf
 E_g = gas expansion factor, scf/ft³

This chapter presents two approaches for estimating initial gas-in-place G , gas reserves, and the gas recovery for volumetric and water-drive mechanisms:

- Volumetric method
- Material balance approach

THE VOLUMETRIC METHOD

Data used to estimate the gas-bearing reservoir PV include, but are not limited to, well logs, core analyses, bottom-hole pressure (BHP), and fluid sample information, along with well tests. These data typically are used to develop various subsurface maps. Of these maps, structural and stratigraphic cross-sectional maps help to establish the reservoir's areal extent and to identify reservoir discontinuities, such as pinch-outs, faults, or gas-water contacts. Subsurface contour maps, usually drawn relative to a known or marker formation, are constructed with lines connecting points of equal elevation and therefore portray the geologic structure. Subsurface isopachous maps are constructed with lines of equal net gas-bearing formation thickness. With these maps, the reservoir PV can then be estimated by planimetry the areas between the isopachous lines and using an approximate volume calculation technique, such as the pyramidal or trapezoidal method.

The volumetric equation is useful in reserve work for estimating gas-in-place at any stage of depletion. During the development period before reservoir limits have been accurately defined, it is convenient to calculate gas-in-place per acre-foot of bulk reservoir rock. Multiplication of this unit figure by the best available estimate of bulk reservoir volume then gives gas-in-place for the lease, tract, or reservoir under consideration. Later in the life of the reservoir, when the reservoir volume is defined and performance data are available, volumetric calculations provide valuable checks on gas-in-place estimates obtained from material balance methods.

The equation for calculating gas-in-place is:

$$G = \frac{43,560 Ah\phi(1 - S_{wi})}{B_{gi}} \quad (13-3)$$

where G = gas-in-place, scf
 A = area of reservoir, acres
 h = average reservoir thickness, ft
 ϕ = porosity
 S_{wi} = water saturation, and
 B_{gi} = gas formation volume factor, ft³/scf

This equation can be applied at both initial and abandonment conditions in order to calculate the recoverable gas.

Gas produced = Initial gas – Remaining gas

or

$$G_p = 43,560 Ah\phi(1 - S_{wi}) \left(\frac{1}{B_{gi}} - \frac{1}{B_{ga}} \right) \quad (13-4)$$

where B_{ga} is evaluated at abandonment pressure. Application of the volumetric method assumes that the pore volume occupied by gas is constant. If water influx is occurring, A , h , and S_w will change.

Example 13-1

A gas reservoir has the following characteristics:

$A = 3000$ acres $h = 30$ ft $\phi = 0.15$ $S_{wi} = 20\%$
 $T = 150^\circ\text{F}$ $p_i = 2600$ psi

| | p | z |
|--|----------|----------|
| | 2600 | 0.82 |
| | 1000 | 0.88 |
| | 400 | 0.92 |

Calculate cumulative gas production and recovery factor at 1,000 and 400 psi.

Solution

Step 1. Calculate the reservoir pore volume P.V.

$$P.V = 43,560 Ah\phi$$

$$P.V = 43,560 (3000) (30) (0.15) = 588.06 \text{ MMft}^3$$

Step 2. Calculate B_g at every given pressure by using Equation 13-1.

| p | z | $B_g, \text{ft}^3/\text{scf}$ |
|------|------|-------------------------------|
| 2600 | 0.82 | 0.0054 |
| 1000 | 0.88 | 0.0152 |
| 400 | 0.92 | 0.0397 |

Step 3. Calculate initial gas-in-place at 2,600 psi.

$$G = 588.06 (10^6) (1 - 0.2)/0.0054 = 87.12 \text{ MMMscf}$$

Step 4. Since the reservoir is assumed volumetric, calculate the remaining gas at 1,000 and 400 psi.

- Remaining gas at 1,000 psi

$$G_{1000 \text{ psi}} = 588.06(10^6) (1 - 0.2)/0.0152 = 30.95 \text{ MMMscf}$$

- Remaining gas at 400 psi

$$G_{400 \text{ psi}} = 588.06(10^6) (1 - 0.2)/0.0397 = 11.95 \text{ MMMscf}$$

Step 5. Calculate cumulative gas production G_p and the recovery factor RF at 1,000 and 400 psi.

- At 1,000 psi:

$$G_p = (87.12 - 30.95) \times 10^9 = 56.17 \text{ MMM scf}$$

$$RF = \frac{56.17 \times 10^9}{87.12 \times 10^9} = 64.5\%$$

- At 400 psi:

$$G_p = (87.12 - 11.95) \times 10^9 = 75.17 \text{ MMMscf}$$

$$\text{RF} = \frac{75.17 \times 10^9}{87.12 \times 10^9} = 86.3\%$$

The recovery factors for volumetric gas reservoirs will range from 80% to 90%. If a strong water drive is present, trapping of residual gas at higher pressures can reduce the recovery factor substantially, to the range of 50% to 80%.

THE MATERIAL BALANCE METHOD

If enough production-pressure history is available for a gas reservoir, the initial gas-in-place G , the initial reservoir pressure p_i , and the gas reserves can be calculated without knowing A , h , ϕ , or S_w . This is accomplished by forming a mass or mole balance on the gas as:

$$n_p = n_i - n_f \quad (13-5)$$

where n_p = moles of gas produced

n_i = moles of gas initially in the reservoir

n_f = moles of gas remaining in the reservoir

Representing the gas reservoir by an idealized gas container, as shown schematically in Figure 13-1, the gas moles in Equation 13-5 can be replaced by their equivalents using the real gas law to give:

$$\frac{p_{sc} G_p}{R T_{sc}} = \frac{p_i V}{z_i R T} - \frac{p[V - (W_e - W_p)]}{z R T} \quad (13-6)$$

where p_i = initial reservoir pressure

G_p = cumulative gas production, scf

p = current reservoir pressure

V = original gas volume, ft^3

z_i = gas deviation factor at p_i

z = gas deviation factor at p

T = temperature, $^\circ\text{R}$

W_e = cumulative water influx, ft^3

W_p = cumulative water production, ft^3

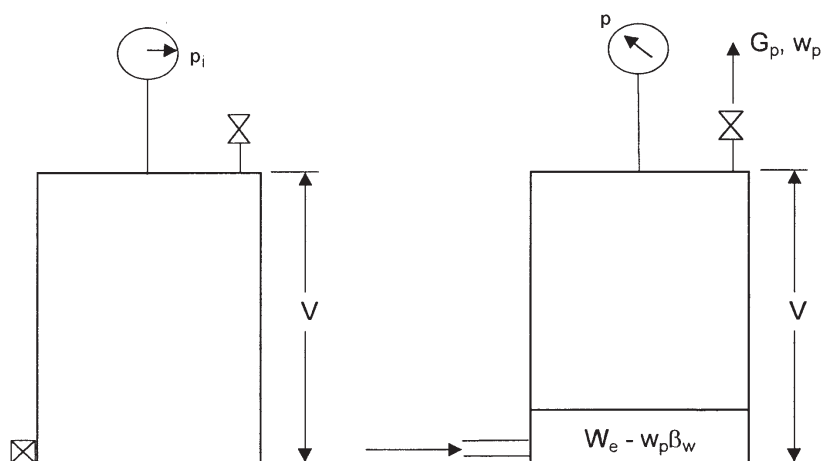


Figure 13-1. Idealized water-drive gas reservoir.

Equation 13-6 is essentially the general material balance equation (MBE). Equation 13-6 can be expressed in numerous forms depending on the type of the application and the driving mechanism. In general, dry gas reservoirs can be classified into two categories:

- Volumetric gas reservoirs
- Water-drive gas reservoirs

The remainder of this chapter is intended to provide the basic background in natural gas engineering. There are several excellent textbooks that comprehensively address this subject, including the following:

- Ikoku, C., *Natural Gas Reservoir Engineering*, 1984
- Lee, J. and Wattenbarger, R., *Gas Reservoir Engineering*, SPE, 1996

Volumetric Gas Reservoirs

For a volumetric reservoir and assuming no water production, Equation 13-6 is reduced to:

$$\frac{p_{sc} G_p}{T_{sc}} = \left(\frac{p_i}{z_i T} \right) V - \left(\frac{p}{z T} \right) V \quad (13-7)$$

Equation 13-7 is commonly expressed in the following two forms:

Form 1. In terms of p/z

Rearranging Equation 13-7 and solving for p/z gives:

$$\frac{p}{z} = \frac{p_i}{z_i} - \left(\frac{p_{sc} T}{T_{sc} V} \right) G_p \quad (13-8)$$

Equation 13-8 is an equation of a straight line when (p/z) is plotted versus the cumulative gas production G_p , as shown in Figure 13-2. This straight-line relationship is perhaps one of the most widely used relationships in gas-reserve determination.

The straight-line relationship provides the engineer with the reservoir characteristics:

- Slope of the straight line is equal to:

$$\text{slope} = \frac{p_{sc} T}{T_{sc} V} \quad (13-9)$$

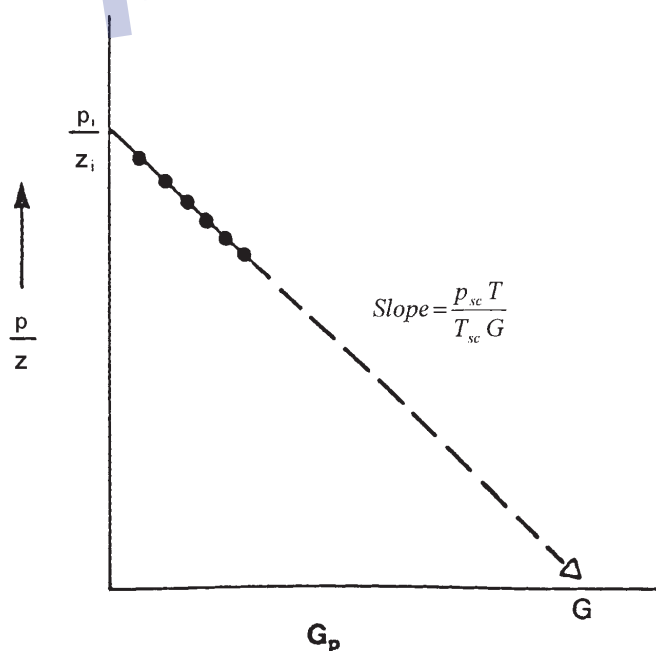


Figure 13-2. Gas material balance equation.

The original gas volume V can be calculated from the slope and used to determine the areal extent of the reservoir from:

$$V = 43,560 Ah \phi (1 - S_{wi}) \quad (13-10)$$

where A is the reservoir area in acres.

- Intercept at $G_p = 0$ gives p_i/z_i
- Intercept at $p/z = 0$ gives the gas initially in place G in scf
- Cumulative gas production or gas recovery at any pressure

Example 13-2¹

A volumetric gas reservoir has the following production history.

| Time, t years | Reservoir Pressure, p psia | z | Cumulative Production, G_p MMMscf |
|--------------------|---------------------------------|-------|--|
| 0.0 | 1798 | 0.869 | 0.00 |
| 0.5 | 1680 | 0.870 | 0.96 |
| 1.0 | 1540 | 0.880 | 2.12 |
| 1.5 | 1428 | 0.890 | 3.21 |
| 2.0 | 1335 | 0.900 | 3.92 |

The following data are also available:

$$\begin{aligned} \phi &= 13\% \\ S_{wi} &= 0.52 \\ A &= 1060 \text{ acres} \\ h &= 54 \text{ ft} \\ T &= 164^\circ\text{F} \end{aligned}$$

Calculate the gas initially in place volumetrically and from the MBE.

Solution

Step 1. Calculate B_{gi} from Equation 13-1.

$$B_{gi} = 0.02827 \frac{(0.869)(164 + 460)}{1798} = 0.00853 \text{ ft}^3/\text{scf}$$

¹After Ikoku, C., *Natural Gas Reservoir Engineering*, John Wiley & Sons, 1984.

Step 2. Calculate the gas initially in place volumetrically by applying Equation 13-3.

$$G = 43,560 (1060) (54) (0.13) (1 - 0.52)/0.00853 = 18.2 \text{ MMMscf}$$

Step 3. Plot p/z versus G_p as shown in Figure 13-3 and determine G .

$$G = 14.2 \text{ MMMscf}$$

This checks the volumetric calculations.

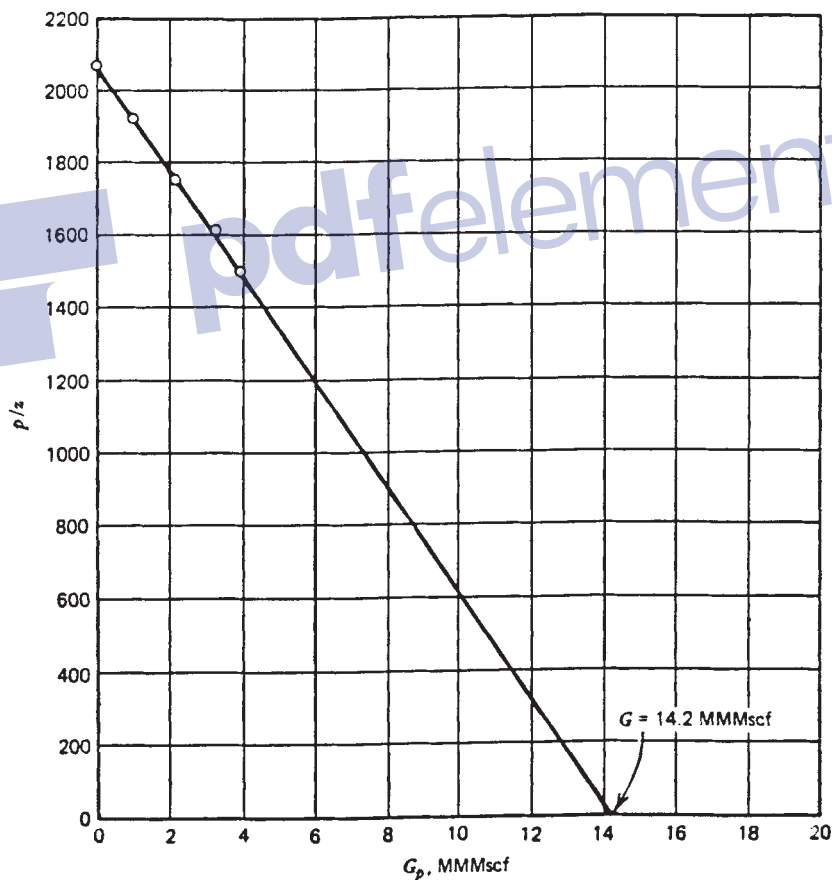


Figure 13-3. Relationship of p/z vs. G_p for Example 13-2.

The initial reservoir gas volume V can be expressed in terms of the volume of gas at standard conditions by:

$$V = B_g G = \left(\frac{p_{sc} z_i T}{T_{sc} p_i} \right) G$$

Combining the above relationship with that of Equation 13-8 gives:

$$\frac{p}{z} = \frac{p_i}{z_i} - \left[\left(\frac{p_i}{z_i} \right) \frac{1}{G} \right] G_p \quad (13-11)$$

This relationship can be expressed in a more simplified form as:

$$\frac{p}{z} = \frac{p_i}{z_i} - [m] G_p$$

where the coefficient m is essentially constant and represents the resulting straight line when P/Z is plotted against G_p . The slope, m is defined by:

$$m = \left(\frac{p_i}{z_i} \right) \frac{1}{G}$$

Equivalently, m is defined by Equation 13-9 as:

$$m = \frac{T p_{sc}}{T_{sc} V}$$

where

G = Original gas-in-place, scf

V = Original gas-in-place, ft³

Again, Equation 13-11 shows that for a volumetric reservoir, the relationship between (p/z) and G_p is essentially linear. This popular equation indicates that by extrapolation of the straight line to abscissa, i.e., at $p/z = 0$, will give the value of the gas initially in place as $G = G_p$.

The graphical representation of Equation 13-11 can be used to detect the presence of water influx, as shown graphically in Figure 13-4. When the plot of (p/z) versus G_p deviates from the linear relationship, it indicates the presence of water encroachment.

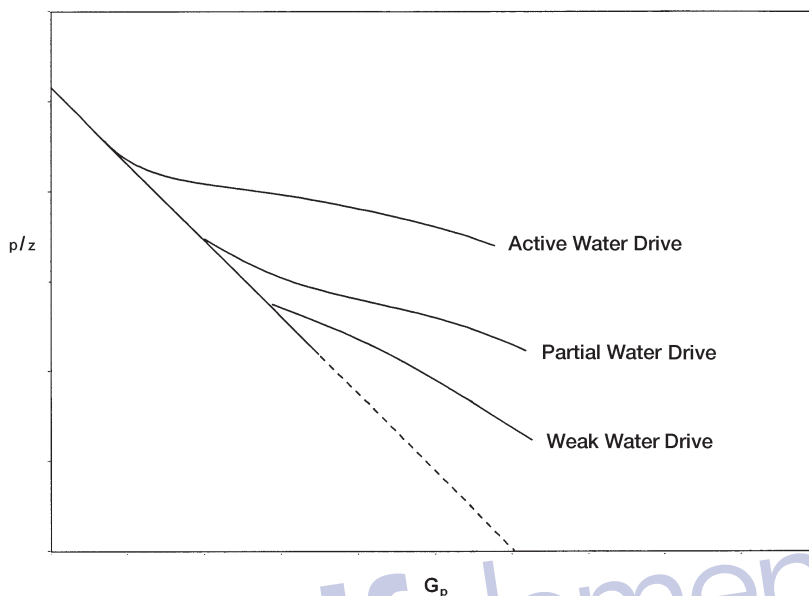


Figure 13-4. Effect of water drive on p/z vs. G_p relationship.

Many other graphical methods have been proposed for solving the gas MBE that are useful in detecting the presence of water influx. One such graphical technique is called the **energy plot**, which is based on arranging Equation 13-11 and taking the logarithm of both sides to give:

$$\log \left[1 - \frac{z_i p}{p_i z} \right] = \log G_p - \log G \quad (13-12)$$

Figure 13-5 shows a schematic illustration of the plot.

From Equation 13-12, it is obvious that a plot of $[1 - (z_i p)/(p_i z)]$ versus G_p on log-log coordinates will yield a straight line with a slope of one (45° angle). An extrapolation to one on the vertical axis ($p = 0$) yields a value for initial gas-in-place, G . The graphs obtained from this type of analysis have been referred to as *energy plots*. They have been found to be useful in detecting water influx early in the life of a reservoir. If W_e is not zero, the slope of the plot will be less than one, and will also decrease with time, since W_e increases with time. An increasing slope can only occur as a result of either gas leaking from the reservoir or bad data,

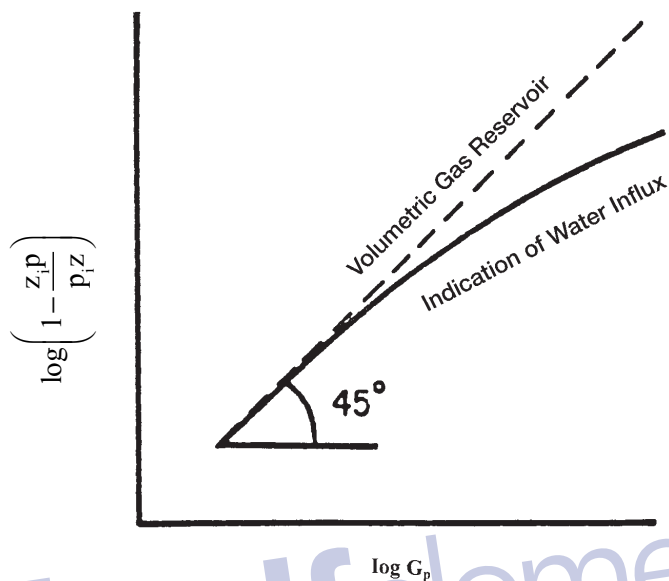


Figure 13-5. An energy plot.

since the increasing slope would imply that the gas-occupied pore volume was increasing with time.

It should be pointed out that the average field, $(p/Z)_{\text{Field}}$, can be estimated from the individual wells' p/Z versus G_P performance by applying the following relationship:

$$\left(\frac{p}{Z}\right)_{\text{Field}} = \frac{p_i}{Z_i} - \frac{\sum_{j=1}^n (G_P)_j}{\sum_{j=1}^n \left[\frac{G_P}{\frac{p_i}{Z_i} - \frac{p}{Z}} \right]_j}$$

The summation Σ is taking over the total number n of the field gas wells, that is, $j = 1, 2, \dots, n$. The total field performance in terms of $(p/Z)_{\text{Field}}$ versus $(G_P)_{\text{Field}}$ can then be constructed from the estimated

values of the field p/Z and actual total field production, that is, $(p/Z)_{\text{Field}}$ versus ΣG_p . The above equation is applicable as long as all wells are producing with defined static boundaries, that is, under pseudosteady-state conditions.

When using the MBE for reserve analysis for an entire reservoir that is characterized by a distinct lack of pressure equilibrium throughout, the following average reservoir pressure decline, $(p/Z)_{\text{Field}}$, can be used:

$$\left(\frac{p}{Z}\right)_{\text{Field}} = \frac{\sum_{j=1}^n \left(\frac{p \Delta G_p}{\Delta p}\right)_j}{\sum_{j=1}^n \left(\frac{\Delta G_p}{\Delta p / Z}\right)_j}$$

where Δp and ΔG_p are the incremental pressure difference and cumulative production, respectively.

The gas recovery factor (RF) at any depletion pressure is defined as the cumulative gas produced, G_p , at this pressure divided by the gas initially in place, G :

$$\text{RF} = \frac{G_p}{G}$$

Introducing the gas RF to Equation 8-60 gives

$$\frac{p}{Z} = \frac{p_i}{Z_i} \left[1 - \frac{G_p}{G}\right]$$

or

$$\frac{p}{Z} = \frac{p_i}{Z_i} [1 - \text{RF}]$$

Solving for the recovery factor at any depletion pressure gives:

$$\text{RF} = 1 - \left[\frac{Z_i}{Z} \frac{p}{p_i}\right]$$

Form 2. In terms of B_g

From the definition of the gas formation volume factor, it can be expressed as:

$$B_{gi} = \frac{V}{G}$$

Combining the above expression with Equation 13-1 gives:

$$\frac{p_{sc}}{T_{sc}} \frac{z_i T}{p_i} = \frac{V}{G} \quad (13-13)$$

where V = volume of gas originally in place, ft^3

G = volume of gas originally in place, scf

p_i = original reservoir pressure

z_i = gas compressibility factor at p_i

Equation 13-13 can be combined with Equation 13-7, to give:

$$G = \frac{G_p B_g}{B_g - B_{gi}} \quad (13-14)$$

Equation 13-14 suggests that to calculate the initial gas volume, the only information required is production data, pressure data, gas specific gravity for obtaining z -factors, and reservoir temperature. Early in the producing life of a reservoir, however, the denominator of the right-hand side of the material balance equation is very small, while the numerator is relatively large. A small change in the denominator will result in a large discrepancy in the calculated value of initial gas-in-place. Therefore, the material balance equation should not be relied on early in the producing life of the reservoir.

Material balances on volumetric gas reservoirs are simple. Initial gas-in-place may be computed from Equation 13-14 by substituting cumulative gas produced and appropriate gas formation volume factors at corresponding reservoir pressures during the history period. If successive calculations at various times during the history give consistent values for initial gas-in-place, the reservoir is operating under volumetric control and computed G is reliable, as shown in Figure 13-6. Once G has been determined and the absence of water influx established in this fashion,

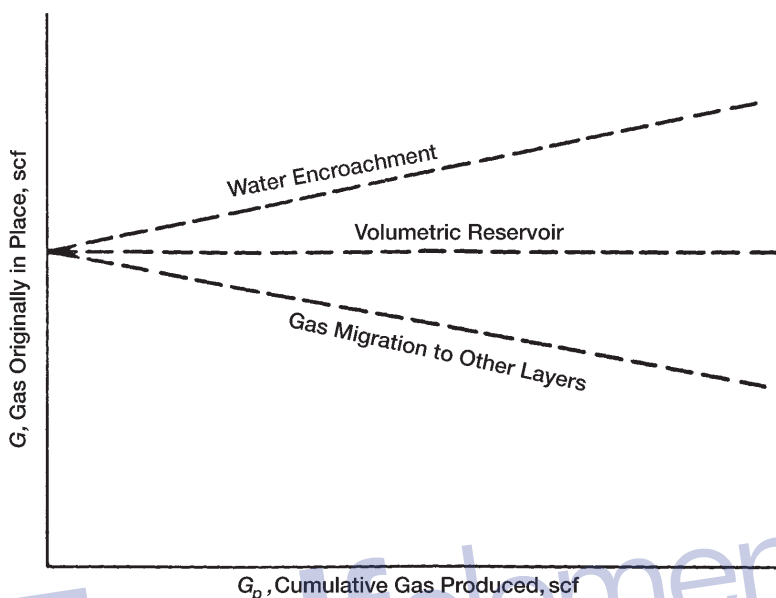


Figure 13-6. Graphical determination of the gas initially in place G .

the same equation can be used to make future predictions of cumulative gas production function of reservoir pressure.

Ikoku (1984) points out that successive application of Equation 13-14 will normally result in increasing values of the gas initially in place G with time if water influx is occurring. If there is gas leakage to another zone due to bad cement jobs or casing leaks, however, the computed value of G may decrease with time.

Example 13-3

After producing 360 MMscf of gas from a volumetric gas reservoir, the pressure has declined from 3,200 psi to 3,000 psi, given:

$$B_{gi} = 0.005278 \text{ ft}^3/\text{scf}$$

$$B_g = 0.005390 \text{ ft}^3/\text{scf}$$

- Calculate the gas initially in place.
- Recalculate the gas initially in place assuming that the pressure measurements were incorrect and the true average pressure is 2,900 psi. The gas formation volume factor at this pressure is 0.00558 ft³/scf.

Solution

a. Using Equation 13-14, calculate G.

$$G = \frac{360 \times 10^6 (0.00539)}{0.00539 - 0.005278} = 17.325 \text{ MMMscf}$$

b. Recalculate G by using the correct value of B_g .

$$G = \frac{360 \times 10^6 (0.00668)}{0.00558 - 0.005278} = 6.652 \text{ MMMscf}$$

Thus, an error of 100 psia, which is only 3.5% of the total reservoir pressure, resulted in an increase in calculated gas-in-place of approximately 160%, a 2½-fold increase. Note that a similar error in reservoir pressure later in the producing life of the reservoir will not result in an error as large as that calculated early in the producing life of the reservoir.

Water-Drive Gas Reservoirs

If the gas reservoir has a water drive, then there will be two unknowns in the material balance equation, even though production data, pressure, temperature, and gas gravity are known. These two unknowns are initial gas-in-place and cumulative water influx. In order to use the material balance equation to calculate initial gas-in-place, some independent method of estimating W_e , the cumulative water influx, must be developed as discussed in Chapter 11.

Equation 13-14 can be modified to include the cumulative water influx and water production to give:

$$G = \frac{G_p B_g - (W_e - W_p B_w)}{B_g - B_{gi}} \quad (13-15)$$

The above equation can be arranged and expressed as:

$$G + \frac{W_e}{B_g - B_{gi}} = \frac{G_p B_g + W_p B_w}{B_g - B_{gi}} \quad (13-16)$$

Equation 13-16 reveals that for a volumetric reservoir, i.e., $W_e = 0$, the right-hand side of the equation will be constant regardless of the amount

of gas G_p that has been produced. For a water-drive reservoir, the values of the right-hand side of Equation 13-16 will continue to increase because of the $W_e/(B_g - B_{gi})$ term. A plot of several of these values at successive time intervals is illustrated in Figure 13-7. Extrapolation of the line formed by these points back to the point where $G_p = 0$ shows the true value of G , because when $G_p = 0$, then $W_e/(B_g - B_{gi})$ is also zero.

This graphical technique can be used to estimate the value of W_e , because at any time the difference between the horizontal line (i.e., true value of G) and the sloping line $[G + (W_e)/(B_g - B_{gi})]$ will give the value of $W_e/(B_g - B_{gi})$.

Because gas often is bypassed and trapped by the encroaching water, recovery factors for gas reservoirs with water drive can be significantly lower than for volumetric reservoirs produced by simple gas expansion. In addition, the presence of reservoir heterogeneities, such as low-permeability stringers or layering, may reduce gas recovery further. As noted previously, ultimate recoveries of 80% to 90% are common in volumetric gas reservoirs, while typical recovery factors in water-drive gas reservoirs can range from 50% to 70%.

Because gas often is bypassed and trapped by encroaching water, recovery factors for gas reservoirs with water drive can be significantly lower than for volumetric reservoirs produced by simple gas expansion. In addition, the presence of reservoir heterogeneities, such as low-permeability stringers or layering, may reduce gas recovery further. As noted previously,

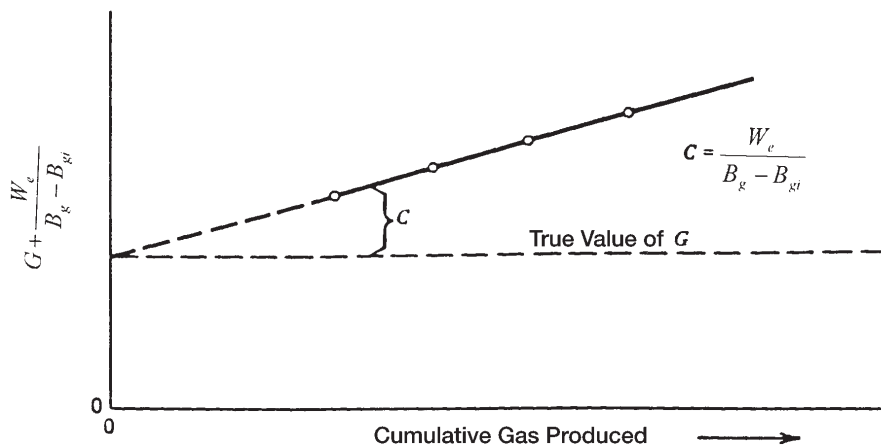


Figure 13-7. Effect of water influx on calculating the gas initially in place.

ultimate recoveries of 80% to 90% are common in volumetric gas reservoirs, while typical recovery factors in water-drive gas reservoirs can range from 50% to 70%. The amount of gas that is trapped in a region that has been flooded by water encroachment can be estimated by defining the following characteristic reservoir parameters and taking the steps outlined below:

(P.V) = reservoir pore volume, ft³

(P.V)_{water} = pore volume of the water-invaded zone, ft³

S_{grw} = residual gas saturation to water displacement

S_{wi} = initial water saturation

G = gas initially in place, scf

G_p = cumulative gas production at depletion pressure p, scf

B_{gi} = initial gas formation volume factor, ft³/scf

B_g = gas formation volume factor at depletion pressure p, ft³/scf

Z = gas deviation factor at depletion pressure p

Step 1. Express the reservoir pore volume, (P.V), in terms of the initial gas-in-place, G, as follows:

$$G B_{gi} = (P.V) (1 - S_{wi})$$

Solving for the reservoir pore volume gives:

$$(P.V) = \frac{G B_{gi}}{1 - S_{wi}}$$

Step 2. Calculate the pore volume in the water-invaded zone:

$$W_e - W_p B_w = (P.V)_{water} (1 - S_{wi} - S_{grw})$$

Solving for the pore volume of the water-invaded zone, (P.V)_{water}, gives:

$$(P.V)_{water} = \frac{W_e - W_p B_w}{1 - S_{wi} - S_{grw}}$$

Step 3. Calculate trapped gas volume in the water-invaded zone, or:

$$\text{Trapped gas volume} = (P.V)_{\text{water}} S_{\text{grw}}$$

$$\text{Trapped gas volume} = \left[\frac{W_e - W_p B_w}{1 - S_{\text{wi}} - S_{\text{grw}}} \right] S_{\text{grw}}$$

Step 4. Calculate the number n of moles of gas trapped in the water-invaded zone by using the equation of state, or:

$$p (\text{Trapped gas volume}) = Z n R T$$

Solving for n gives:

$$n = \frac{p \left[\frac{W_e - W_p B_w}{1 - S_{\text{wi}} - S_{\text{grw}}} \right] S_{\text{grw}}}{Z R T}$$

which indicates that the higher the pressure, the greater the quantity of trapped gas. Dake (1994) points out that if the pressure is reduced by rapid gas withdrawal, the volume of gas trapped in each individual pore space, that is, S_{grw} , will remain unaltered, but its quantity, n , will be reduced.

Step 5. The gas saturation at any pressure can be adjusted to account for the trapped gas, as follows:

$$S_g = \frac{\text{remaining gas volume} - \text{trapped gas volume}}{\text{reservoir pore volume} - \text{pore volume of water invaded zone}}$$

$$S_g = \frac{(G - G_p) B_g - \left[\frac{W_e - W_p B_w}{1 - S_{\text{wi}} - S_{\text{grw}}} \right] S_{\text{grw}}}{\left(\frac{G B_{\text{gi}}}{1 - S_{\text{wi}}} \right) - \left[\frac{W_e - W_p B_w}{1 - S_{\text{wi}} - S_{\text{grw}}} \right]}$$

MATERIAL BALANCE EQUATION AS A STRAIGHT LINE

Havlena and Odeh (1963) expressed the material balance in terms of gas production, fluid expansion, and water influx as:

$$\text{Underground withdrawal} = \text{Gas expansion} + \text{Water expansion/pore compaction} + \text{Water influx}$$

or

$$G_p B_g + W_p B_w = G(B_g - B_{gi}) + G B_{gi} \frac{(c_w S_{wi} + c_f)}{1 - S_{wi}} \Delta p + W_e B_w \quad (13-17)$$

Using the nomenclature of Havlena and Odeh, as described in Chapter 11, gives:

$$F = G(E_g + E_{f,w}) + W_e B_w \quad (13-18)$$

with the terms F , E_g , and $E_{f,w}$ as defined by:

- Underground fluid withdrawal F :

$$F = G_p B_g + W_p B_w \quad (13-19)$$

- Gas expansion E_g :

$$E_g = B_g - B_{gi} \quad (13-20)$$

- Water and rock expansion $E_{f,w}$:

$$E_{f,w} = B_{gi} \frac{(c_w S_{wi} + c_f)}{1 - S_{wi}} \quad (13-21)$$

Assuming that the rock and water expansion term $E_{f,w}$ is negligible in comparison with the gas expansion E_g , Equation 13-18 is reduced to:

$$F = G E_g + W_e B_w \quad (13-22)$$

Finally, dividing both sides of the equation by E_g gives:

$$\frac{F}{E_g} = G + \frac{W_e B_w}{E_g} \quad (13-23)$$

Using the production, pressure, and PVT data, the left-hand side of this expression should be plotted as a function of the cumulative gas production, G_p . This is simply for display purposes to inspect its variation during depletion. Plotting F/E_g versus production time or pressure decline, Δp , can be equally illustrative.

Dake (1994) presented an excellent discussion of the strengths and weaknesses of the MBE as a straight line. He points out that the plot will have one of the three shapes depicted in Figure 13-8. If the reservoir is of the volumetric depletion type, $W_e = 0$, then the values of F/E_g evaluated, say, at six monthly intervals, should plot as a straight line parallel to the abscissa—whose ordinate value is the GIIP.

Alternatively, if the reservoir is affected by natural water influx, then the plot of F/E_g will usually produce a concave downward shaped arc

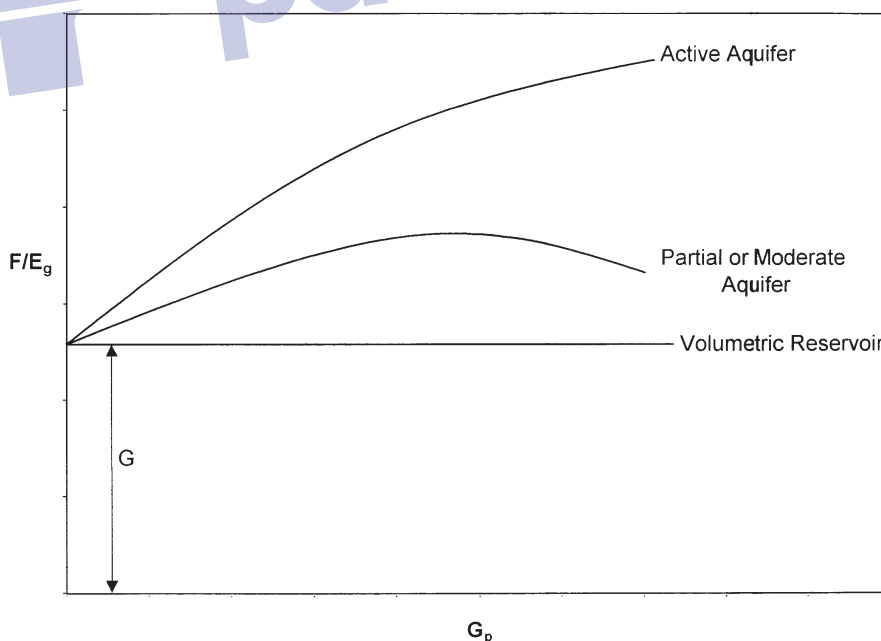


Figure 13-8. Defining the reservoir-driving mechanism.

whose exact form is dependent upon the aquifer size and strength and the gas off-take rate. Backward extrapolation of the F/E_g trend to the ordinate should nevertheless provide an estimate of the GIIP ($W_e \sim 0$); however, the plot can be highly nonlinear in this region yielding a rather uncertain result. The main advantage in the F/E_g versus G_p plot is that it is much more sensitive than other methods in establishing whether the reservoir is being influenced by natural water influx or not.

The graphical presentation of Equation 13-23 is illustrated by Figure 13-9. A graph of F/E_g vs. $\Sigma \Delta p W_{eD}/E_g$ yields a straight line, provided the unsteady-state influx summation, $\Sigma \Delta p W_{eD}$, is accurately assumed. The resulting straight line intersects the y-axis at the initial gas-in-place G and has a slope equal to the water influx constant B .

Nonlinear plots will result if the aquifer is improperly characterized. A systematic upward or downward curvature suggests that the summation term is too small or too large, respectively, while an S-shaped curve indicates that a linear (instead of a radial) aquifer should be assumed. The points should plot sequentially from left to right. A reversal of this

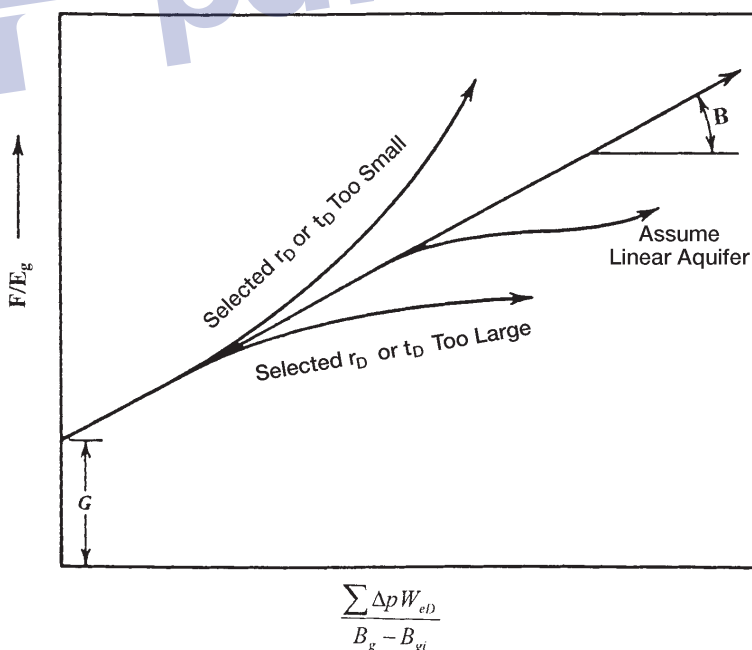


Figure 13-9. Havlena-Odeh MBE plot for a gas reservoir.

plotting sequence indicates that an unaccounted aquifer boundary has been reached and that a smaller aquifer should be assumed in computing the water influx term.

A linear infinite system rather than a radial system might better represent some reservoirs, such as reservoirs formed as fault blocks in salt domes. The van Everdingen-Hurst dimensionless water influx W_{eD} is replaced by the square root of time as:

$$W_e = C \sum \Delta p_n \sqrt{t - t_n} \quad (13-24)$$

where C = water influx constant ft^3/psi

t = time (any convenient units, i.e., days, year)

The water influx constant C must be determined by using the past production and pressure of the field in conjunction with Havlena-Odeh methodology. For the linear system, the underground withdrawal F is plotted versus $[\sum \Delta p_n zt - t_n/(B - B_{gi})]$ on a Cartesian coordinate graph. The plot should result in a straight line with G being the intercept and the water influx constant C being the slope of the straight line.

To illustrate the use of the linear aquifer model in the gas MBE as expressed as an equation of straight line, i.e., Equation 13-23, Havlena and Odeh proposed the following problem.

Example 13-4

The volumetric estimate of the gas initially in place for a dry-gas reservoir ranges from 1.3 to 1.65×10^{12} scf. Production, pressures, and pertinent gas expansion term, i.e., $E_g = B_g - B_{gi}$, are presented in Table 13-1. Calculate the original gas-in-place G .

Solution

Step 1. Assume volumetric gas reservoir.

Step 2. Plot (p/z) versus G_p or $G_p B_g/(B_g - B_{gi})$ versus G_p .

Step 3. A plot of $G_p B_g/(B_g - B_{gi})$ vs. $G_p B_g$ showed an upward curvature, as shown in Figure 13-10, indicating water influx.

Table 13-1
Havlena-Odeh Dry-Gas Reservoir Data for Example 13-4

| Time (months) | Average Reservoir Pressure (psi) | $E_g =$ $(B_g - B_{gi}) \times 10^{-6}$ (ft ³ /scf) | $F =$ $(G_b B_g) \times 10^6$ (ft ³) | $\frac{\sum \Delta p_n z t - t_n}{B_g - B_{gi}}$ (10 ⁶) | $\frac{F/E_g =}{G_p B_g}$ $\frac{B_g - B_{gi}}{(10^{12})}$ |
|------------------|---|--|--|--|---|
| 0 | 2883 | 0.0 | — | — | — |
| 2 | 2881 | 4.0 | 5.5340 | 0.3536 | 1.3835 |
| 4 | 2874 | 18.0 | 24.5967 | 0.4647 | 1.3665 |
| 6 | 2866 | 34.0 | 51.1776 | 0.6487 | 1.5052 |
| 8 | 2857 | 52.0 | 76.9246 | 0.7860 | 1.4793 |
| 10 | 2849 | 68.0 | 103.3184 | 0.9306 | 1.5194 |
| 12 | 2841 | 85.0 | 131.5371 | 1.0358 | 1.5475 |
| 14 | 2826 | 116.5 | 180.0178 | 1.0315 | 1.5452 |
| 16 | 2808 | 154.5 | 240.7764 | 1.0594 | 1.5584 |
| 18 | 2794 | 185.5 | 291.3014 | 1.1485 | 1.5703 |
| 20 | 2782 | 212.0 | 336.6281 | 1.2426 | 1.5879 |
| 22 | 2767 | 246.0 | 392.8592 | 1.2905 | 1.5970 |
| 24 | 2755 | 273.5 | 441.3134 | 1.3702 | 1.6136 |
| 26 | 2741 | 305.5 | 497.2907 | 1.4219 | 1.6278 |
| 28 | 2726 | 340.0 | 556.1110 | 1.4672 | 1.6356 |
| 30 | 2712 | 373.5 | 613.6513 | 1.5174 | 1.6430 |
| 32 | 2699 | 405.0 | 672.5969 | 1.5714 | 1.6607 |
| 34 | 2688 | 432.5 | 723.0868 | 1.6332 | 1.6719 |
| 36 | 2667 | 455.5 | 771.4902 | 1.7016 | 1.6937 |

Step 4. Assuming a linear water influx, plot $G_p B_g / (B_g - B_{gi})$ versus

$$\left[\sum \Delta p_n \sqrt{t - t_n} \right] / (B_g - B_{gi}) \text{ as shown in Figure 13-11.}$$

Step 5. As evident from Figure 13-11, the necessary straight-line relationship is regarded as satisfactory evidence of the presence of a linear aquifer.

Step 6. From Figure 13-11, determine the original gas-in-place G and the linear water influx constant C as:

$$G = 1.325 \times 10^{12} \text{ scf}$$

$$C = 212.7 \times 10^3 \text{ ft}^3/\text{psi}$$

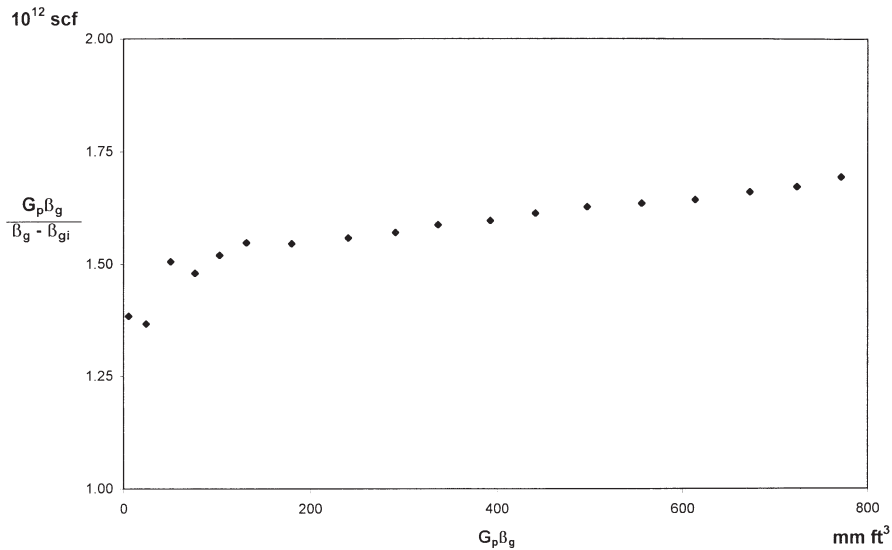


Figure 13-10. Indication of the water influx.

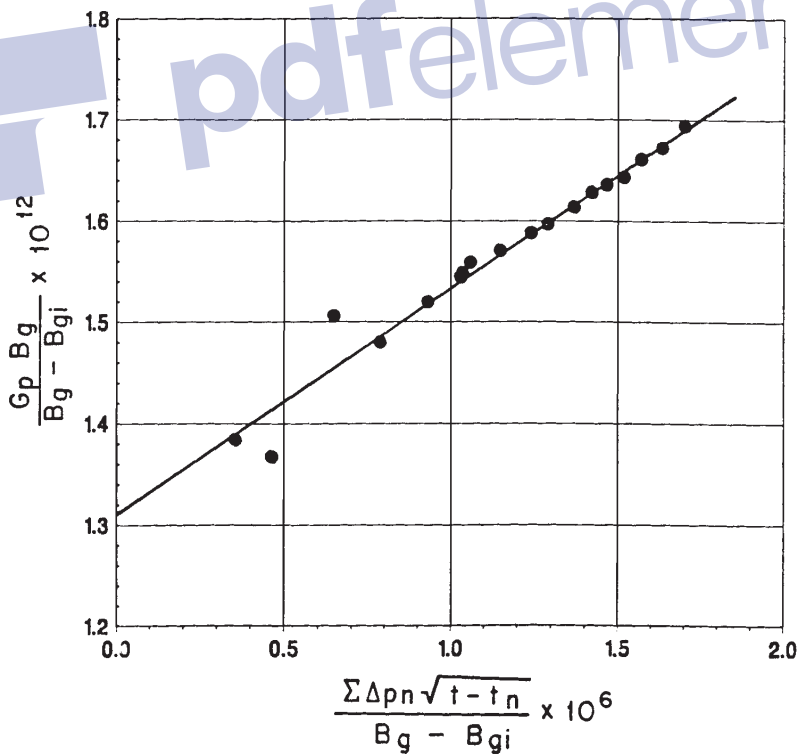


Figure 13-11. Havlena-Odeh MBE plot for Example 13-4.

ABNORMALLY PRESSURED GAS RESERVOIRS

Hammerlindl (1971) pointed out that in abnormally high-pressure volumetric gas reservoirs, two distinct slopes are evident when the plot of p/z versus G_p is used to predict reserves because of the formation and fluid compressibility effects as shown in Figure 13-12. The final slope of the p/z plot is steeper than the initial slope; consequently, reserve estimates based on the early life portion of the curve are erroneously high. The initial slope is due to gas expansion and significant pressure maintenance brought about by formation compaction, crystal expansion, and water expansion. At an approximately normal pressure gradient, the formation compaction is essentially complete and the reservoir assumes the characteristics of a normal gas expansion reservoir. This accounts for the second slope. Most early decisions are made based on the early life extrapolation of the p/z plot; therefore, the effects of hydrocarbon

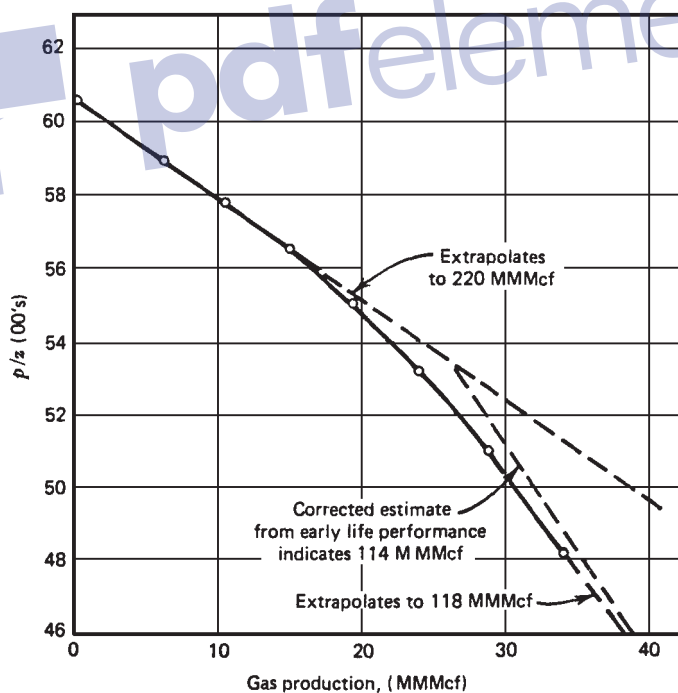


Figure 13-12. P/z versus cumulative production. North Ossum Field, Lafayette Parish, Louisiana NS2B Reservoir. (After Hammerlindl.)

pore volume change on reserve estimates, productivity, and abandonment pressure must be understood.

All gas reservoir performance is related to effective compressibility, not gas compressibility. When the pressure is abnormal and high, effective compressibility may equal two or more times that of gas compressibility. If effective compressibility is equal to twice the gas compressibility, then the first cubic foot of gas produced is due to 50% gas expansion and 50% formation compressibility and water expansion. As the pressure is lowered in the reservoir, the contribution due to gas expansion becomes greater because gas compressibility is approaching effective compressibility. Using formation compressibility, gas production, and shut-in bottom-hole pressures, two methods are presented for correcting the reserve estimates from the early life data (assuming no water influx).

Roach (1981) proposed a graphical technique for analyzing abnormally pressured gas reservoirs. The MBE as expressed by Equation 13-17 may be written in the following form for a volumetric gas reservoir:

$$(p/z)c_t = (p_i/z_i) - \left[1 - \frac{G_p}{G} \right] \quad (13-25)$$

where

$$c_t = 1 - \frac{(c_f + c_w S_{wi})(p_i - p)}{1 - S_{wi}} \quad (13-26)$$

Defining the rock expansion term E_R as:

$$E_R = \frac{c_f + c_w S_{wi}}{1 - S_{wi}} \quad (13-27)$$

Equation 13-26 can be expressed as:

$$c_t = 1 - E_R (p_i - p) \quad (13-28)$$

Equation 13-25 indicates that plotting $(p/z)c_t$ versus cumulative gas production on Cartesian coordinates results in a straight line with an x-intercept at the original gas-in-place and a y-intercept at the original p/z . Since c_t is unknown and must be found by choosing the compressibility values resulting in the best straight-line fit, this method is a trial-and-error procedure.

Roach used the data published by Duggan (1972) for the Mobil-David Anderson gas field to illustrate the application of Equations 13-25 and 13-28 to determine graphically the gas initially in place. Duggan reported that the reservoir had an initial pressure of 9,507 psig at 11,300 ft. Volumetric estimates of original gas-in-place indicated that the reservoir contains 69.5 MMMscf. The historical p/z versus G_p plot produced an initial gas-in-place of 87 MMMscf, as shown in Figure 13-13.

Using the trial-and-error approach, Roach showed that a value of the rock expansion term E_R of 18.5×10^{-6} would result in a straight line with a gas initially in place of 75 MMMscf, as shown in Figure 13-13.

To avoid the trial-and-error procedure, Roach proposed that Equations 13-25 and 13-28 can be combined and expressed in a linear form by:

$$\alpha = \left(\frac{1}{G}\right)\beta - E_R \quad (13-29)$$

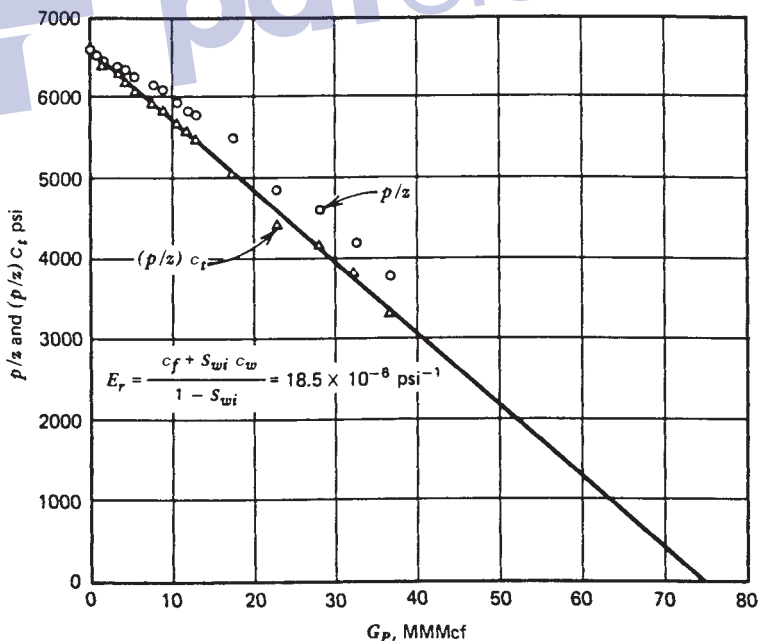


Figure 13-13. Mobil-David Anderson "L" p/z versus cumulative production. (After Roach.)

with

$$\alpha = \frac{[(p_i/z_i)/(p/z)] - 1}{(p_i - p)} \quad (13-30)$$

$$\beta = \frac{(p_i/z_i)(p/z)}{(p_i - p)} \quad (13-31)$$

where G = initial gas-in-place, scf
 E_R = rock expansion term, psi^{-1}
 S_{wi} = initial water saturation

Roach (1981) shows that a plot of α versus β will yield a straight line with slope $1/G$ and y-intercept $= -E_R$. To illustrate his proposed methodology, he applied Equation 13-29 to the Mobil-David gas field as shown in Figure 13-14. The slope of the straight line gives $G = 75.2 \text{ MMMscf}$ and the intercept gives $E_R = 18.5 \times 10^{-6}$.

Begland and Whitehead (1989) proposed a method to predict the percent recovery of volumetric, high-pressure gas reservoirs from the initial pressure to the abandonment pressure with only initial reservoir data. The proposed technique allows the pore volume and water compressibilities to be pressure-dependent. The authors derived the following form of the MBE for a volumetric gas reservoir:

$$r = \frac{G_p}{G} = \frac{B_g - B_{gi}}{B_g} + \frac{B_{gi} S_{wi} \left[\frac{B_{tw}}{B_{twi}} - 1 + \frac{c_f (p_i - p)}{S_{wi}} \right]}{1 - S_{wi} B_g} \quad (13-32)$$

where r = recovery factor
 B_g = gas formation volume factor, bbl/scf
 c_f = formation compressibility, psi^{-1}
 B_{tw} = two-phase water formation volume factor, bbl/STB
 B_{twi} = initial two-phase water formation volume factor, bbl/STB

The water two-phase FVF is determined from:

$$B_{tw} = B_w + B_g (R_{swi} - R_{sw}) \quad (13-33)$$

where R_{sw} = gas solubility in the water phase, scf/STB
 B_w = water FVF, bbl/STB

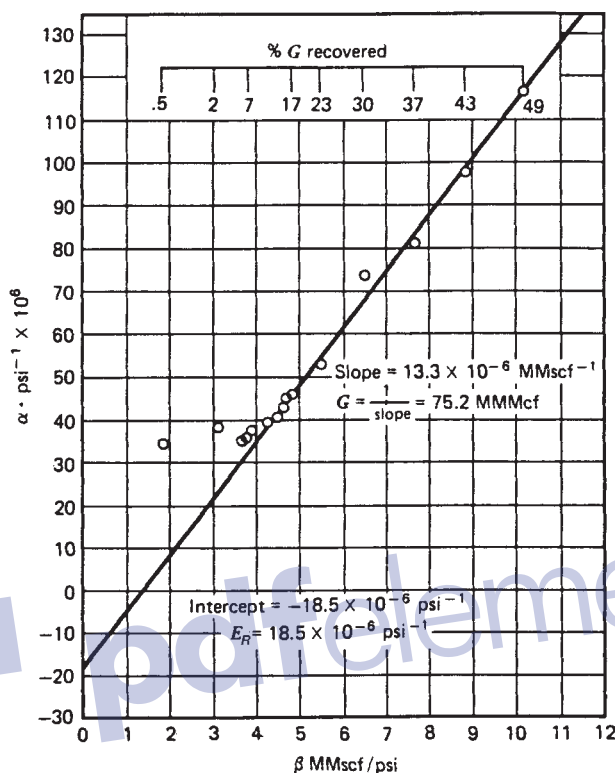


Figure 13-14. Mobil-David Anderson "L" gas material balance. (After Roach.)

The following three assumptions are inherent in Equation 13-32:

- A volumetric, single-phase gas reservoir
- No water production
- The formation compressibility c_f remains constant over the pressure drop ($p_i - p$)

The authors point out that the changes in water compressibility c_w are implicit in the change of B_{tw} with pressure as determined by Equation 13-33.

Begland and Whitehead suggest that because c_f is pressure-dependent, Equation 13-32 is not correct as reservoir pressure declines from the initial pressure to some value several hundred psi lower. The pressure dependence of c_f can be accounted for in Equation 13-32 and is solved in an incremental manner.

Effect of Gas Production Rate on Ultimate Recovery

Volumetric gas reservoirs are essentially depleted by expansion and, therefore, the ultimate gas recovery is independent of the field production rate. The gas saturation in this type of reservoir is never reduced; only the number of pounds of gas occupying the pore spaces is reduced. Therefore, it is important to reduce the abandonment pressure to the lowest possible level. In closed-gas reservoirs, it is not uncommon to recover as much as 90% of the initial gas-in-place.

Cole (1969) points out that for water-drive gas reservoirs, recovery may be rate dependent. There are two possible influences that producing rate may have on ultimate recovery. First, in an active water-drive reservoir, the abandonment pressure may be quite high, sometimes only a few psi below initial pressure. In such a case, the number of pounds of gas remaining in the pore spaces at abandonment will be relatively great.

The encroaching water, however, reduces the initial gas saturation. Therefore, the high abandonment pressure is somewhat offset by the reduction in initial gas saturation. If the reservoir can be produced at a rate greater than the rate of water influx rate, without water coning, then a high producing rate could result in maximum recovery by taking advantage of a combination of reduced abandonment pressure and reduction in initial gas saturation. Second, the water coning problems may be very severe in gas reservoirs, in which case it will be necessary to restrict withdrawal rates to reduce the magnitude of this problem.

Cole suggests that the recovery from water-drive gas reservoirs is substantially less than recovery from closed-gas reservoirs. As a rule of thumb, recovery from a water-drive reservoir will be approximately 50% to 80% of the initial gas-in-place. The structural location of producing wells and the degree of water coning are important considerations in determining ultimate recovery.

A set of circumstances could exist—such as the location of wells very high on the structure with very little coning tendencies—where water-drive recovery would be greater than depletion-drive recovery. Abandonment pressure is a major factor in determining recovery efficiency, and permeability is usually the most important factor in determining the magnitude of the abandonment pressure. Reservoirs with low permeability will have higher abandonment pressures than reservoirs with high permeability. A certain minimum flow rate must be sustained, and a higher permeability will permit this minimum flow rate at a lower pressure.

Tight Gas Reservoirs

Gas reservoirs with permeabilities of less than 0.1 md are considered “tight gas” reservoirs. They present unique problems to reservoir engineers when applying the MBE to predict the gas-in-place and recovery performance.

The use of the conventional material balance in terms of the p/Z plot is a powerful tool for evaluating the performance of gas reservoirs. For a volumetric gas reservoir, the MBE is expressed in different forms that will produce a linear relationship between p/Z versus the cumulative gas production, G_p . Two such forms are given by Equation 13-11:

$$\frac{p}{Z} = \frac{p_i}{Z_i} - \left[\left(\frac{p_i}{Z_i} \right) \frac{1}{G} \right] G_p$$

Simplified:

$$\frac{p}{Z} = \frac{p_i}{Z_i} \left[1 - \frac{G_p}{G} \right]$$

The MBE as expressed by either of these equations is very simple to apply because it is not dependent on flow rates, reservoir configuration, rock properties, or well details. However, there are fundamental assumptions that must be satisfied when applying the equation, including the following:

- There is uniform saturation throughout the reservoir at any time.
- There is little or no pressure variation within the reservoir.
- The reservoir can be represented by a single weighted-average pressure at any time.
- The reservoir is represented by a tank, i.e., constant drainage area, of homogeneous properties.

Payne (1996) pointed out that the assumption of uniform pressure distributions is required to ensure that pressure measurements taken at different well locations represent true average reservoir pressures. This assumption implies that the average reservoir pressure to be used in the MBE can be described with one pressure value. In high-permeability reservoirs, small pressure gradients exist away from the wellbore, and the average reservoir pressure estimates can be readily made with short-term shut-in buildups or static pressure surveys.

Unfortunately, the concept of the straight-line p/Z plot as described by the conventional MBE fails to produce this linear behavior when applied to tight gas reservoirs that have not established a constant drainage area. Payne (1996) suggests that the essence of the errors associated with the use of p/Z plots in tight gas reservoirs is that substantial pressure gradients exist within the formation, resulting in a violation of the basic tank assumption. These gradients manifest themselves in terms of scattered, generally curved, and rate-dependent p/Z plot behavior. This nonlinear behavior of p/Z plots, as shown in Figure 13-15, may significantly underestimate gas initially in place (GIIP) when interpreting by the conventional straight-line method. Figure 13-15a reveals that the reservoir pressure declines very rapidly, as the area surrounding the well cannot be recharged as fast as it is depleted by the well. This early, rapid pressure decline is seen often in tight gas reservoirs and is an indication that the use of p/Z plot analysis may be inappropriate. It is quite apparent that the use of early points would dramatically underestimate GIIP, as shown in Figure 13-15a for the Waterton gas field, which has an apparent GIIP of 7.5 Bm^3 . However, late time production and pressure data show a nearly double GIIP of 16.5 Bm^3 , as shown in Figure 13-15b.

The main problem with tight gas reservoirs is the difficulty of accurately estimating the average reservoir pressure required for p/Z plots as a function of G_p or time. If the pressures obtained during shut-in do not

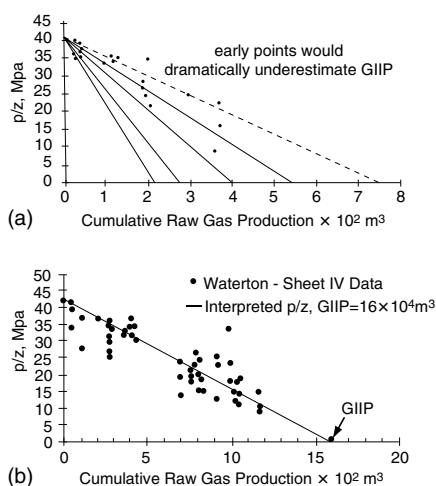


Figure 13-15. (a) Real-life example of p/Z plot from Sheet IVc in the Waterton Gas Field. (b) Real-life example of p/Z plot from Sheet IV in the Waterton Gas Field.

reflect the average reservoir pressure, the resulting analysis will be inaccurate. In tight gas reservoirs, excessive shut-in times of months or years may be required to obtain accurate estimates of average reservoir pressure. The minimum shut-in time required to obtain a reservoir pressure that represents the average reservoir pressure must be at least equal to the time it takes to reach the pseudosteady-state, t_{pss} . This time, for a well in the center of a circular or square drainage area, is given by:

$$t_{pss} = \frac{15.8\phi\mu_{gi}c_{ti}A}{k}$$

with

$$c_{ti} = S_{wi}c_{wi} + S_g c_{gi} + c_f$$

where t_{pss} = stabilization (pseudosteady-state) time, days

c_{ti} = total compressibility coefficient at initial pressure, psi^{-1}

c_{wi} = water compressibility coefficient at initial pressure, psi^{-1}

c_f = formation compressibility coefficient, psi^{-1}

c_{gi} = gas compressibility coefficient at initial pressure, psi^{-1}

ϕ = porosity, fraction

Since most tight gas reservoirs are hydraulically fractured, Earlougher (1977) proposed the following expression for estimating the minimum shut-in time to reach the semisteady-state:

$$t_{pss} = \frac{474\phi\mu_g c_t x_f^2}{k}$$

where x_f = fracture half-length, ft

k = permeability, md

Example 13-5

Estimate the time required for a shut-in gas well to reach its 40-acre drainage area. The well is located in the center of a square-drainage boundary with the following properties:

$$\begin{aligned}\phi &= 14\% \\ \mu_{gi} &= 0.016 \text{ cp} \\ c_{ti} &= 0.0008 \text{ psi}^{-1} \\ A &= 40 \text{ acres} \\ K &= 0.1 \text{ md}\end{aligned}$$

Solution

Calculate the stabilization time by applying Earlougher's equation to give:

$$t_{\text{pss}} = \frac{474\phi\mu_g c_i x_f^2}{k}$$

$$t_{\text{pss}} = \frac{15.8 (0.14) (0.016) (0.0008) (40) (43,650)}{0.1} = 493 \text{ days}$$

This example indicates that an excessive shut-in time of approximately 16 months is required to obtain a reliable average reservoir pressure.

Unlike curvature in the p/Z plot, which can be caused by

- An aquifer
- An oil leg
- Formation compressibility, or
- Liquid condensation

scatter in the p/Z plot is diagnostic of substantial reservoir pressure gradients. Hence, if substantial scatter is seen in a p/Z plot, the tank assumption is being violated and the plot should not be used to determine the GIP. One obvious solution to the material balance problem in tight gas reservoirs is the use of a numerical simulator. Two other relatively new approaches to solving the material balance problem that can be used if reservoir simulation software is not available are:

- The compartmental reservoir approach
- The combined decline-curve and type-curve approach

These two methodologies are discussed next.

Compartmental Reservoir Approach

A compartmental reservoir is defined as a reservoir that consists of two or more distinct regions that are allowed to communicate. Each compartment or “tank” is described by its own material balance, which is coupled to the material balance of the neighboring compartments through influx or efflux gas across the common boundaries. Payne (1996) and Hagoort and Hoogstra (1999) proposed two different robust and rigorous schemes for the numerical solution of the material balance equations of compartmental gas reservoirs. The main difference between the two approaches is that Payne solves for the pressure in each compartment **explicitly** and Hagoort and Hoogstra do so **implicitly**. However, *both schemes* employ the following basic approach:

- Divide the reservoir into a number of compartments with each compartment containing one or more production wells that are proximate and that measure consistent reservoir pressures. The initial division should be made with as few tanks as possible, and each compartment should have different dimensions in terms of length L , width W , and height h .
- Each compartment must be characterized by a historical production and pressure decline data as a function of time.
- If the initial division is not capable of matching the observed pressure decline, additional compartments can be added either by subdividing the previously defined tanks or by adding tanks that do not contain drainage points, that is, production wells.

The practical application of the compartmental reservoir approach is illustrated by the following two methods:

- Payne’s method
- Hagoort–Hoogstra method

Payne’s Method

Rather than using the conventional single-tank MBE in describing the performance of tight gas reservoirs, Payne (1996) suggests a different approach that is based on subdividing the reservoir into a number of tanks, that is, compartments, which are allowed to communicate. Such compartments can either be depleted directly by wells or indirectly through other tanks. Flow rate between tanks is set proportionally to either the difference in the squares of tank pressure or the difference in pseudo-pressures, $m(p)$. To illustrate the concept, consider a reservoir that consists of two compartments, 1 and 2, as shown schematically in Figure 13-16.

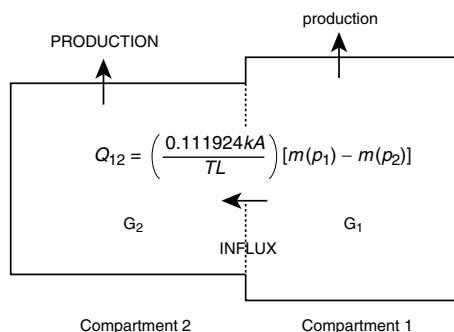


Figure 13-16. Schematic representation of compartmental reservoir consisting of two reservoir compartments separated by a permeable boundary.

Initially, that is, before the start of production, the two compartments are in equilibrium, with the same initial reservoir pressure. Gas production can be produced from either one or both compartments. With gas production, the pressures in the reservoir compartments will decline at different rates depending on the production rate from each compartment and the crossflow rate between the two compartments. Adopting the convention that influx is positive if gas flows from compartment 1 into compartment 2, the linear gas flow rate between the two compartments in terms of gas pseudo-pressure is given by Equation 6-23 from Chapter 6:

$$Q_{12} = \left(\frac{0.111924kA}{TL} \right) [m(p_1) - m(p_2)]$$

where Q_{12} = flow rate between the two compartments, scf/day

$m(p_1)$ = gas pseudo-pressure in compartment (tank) 1, psi²/cp

$m(p_2)$ = gas pseudo-pressure in compartment (tank) 2, psi²/cp

k = permeability, md

L = distance between the center of the two compartments, ft

A = cross-sectional area, width \times height, ft²

T = temperature, °R

This equation can be expressed in a more compacted form by including a “communication factor,” C_{12} , between the two compartments:

$$Q_{12} = C_{12} [m(p_1) - m(p_2)] \quad (13-34)$$

The C_{12} between the two compartments is computed by calculating the individual communication factor for each compartment and employing an averaging technique. The communication factor for each of the compartments is as follows:

$$\text{For compartment 1: } C_1 = \frac{0.111924k_1 A_1}{T L_1}$$

$$\text{For compartment 2: } C_2 = \frac{0.111924k_2 A_2}{T L_2}$$

And the communication factor between the two compartments, C_{12} , is given by the following harmonic average technique:

$$C_{12} = \frac{2C_1 C_2}{(C_1 + C_2)}$$

where

C_{12} = communication factor between two compartments, scf/day/psi²/cp

C_1 = communication factor for compartment 1, scf/day/psi²/cp

C_2 = communication factor for compartment 2, scf/day/psi²/cp

L_1 = length of compartment 1, ft

L_2 = length of compartment 2, ft

A_1 = cross-sectional area of compartment 1, ft²

A_2 = cross-sectional area of compartment 2, ft²

The cumulative gas influx, G_{p12} , from compartment 1 to compartment 2 is given by the integration of flow rate over time t as:

$$G_{p12} = \int_0^t Q_{12} dt = \sum_0^t (\Delta Q_{12}) \Delta t \quad (13-35)$$

Payne proposes that **individual** compartment pressures are determined by assuming a straight-line relationship of p/Z versus G_{pt} , with the total gas production, G_{pt} , from an individual compartment as defined by the following expression:

$$G_{pt} = G_p + G_{p12}$$

where G_p is cumulative gas produced from wells in the compartment and G_{p12} is the cumulative gas efflux/influx between the connected compartments. Solving Equation 8-59 for the pressure in each compartment and assuming a positive flow from compartment 1 to compartment 2 gives:

$$p_1 = \left(\frac{p_i}{Z_i} \right) Z_1 \left[1 - \frac{G_{p1} + G_{p12}}{G_1} \right] \quad (13-36)$$

$$p_2 = \left(\frac{p_i}{Z_i} \right) Z_2 \left[1 - \frac{G_{p2} - G_{p12}}{G_2} \right] \quad (13-37)$$

with:

$$G_1 = 43,560 A_1 h_1 \phi_1 (1 - S_{wi}) / B_{gi} \quad (13-38)$$

$$G_2 = 43,560 A_2 h_2 \phi_2 (1 - S_{wi}) / B_{gi} \quad (13-39)$$

where G_1 = initial gas-in-place in compartment 1, scf

G_2 = initial gas-in-place in compartment 2, scf

G_{p1} = **actual** cumulative gas production from compartment 1, scf

G_{p2} = **actual** cumulative gas production from compartment 2, scf

A_1 = areal extent of compartment 1, acres

A_2 = areal extent of compartment 2, acres

h_1 = average thickness of compartment 1, ft

h_2 = average thickness of compartment 2, ft

B_{gi} = initial gas formation volume factor, ft³/scf

ϕ_1 = average porosity in compartment 1

ϕ_2 = average porosity in compartment 2

The subscripts 1 and 2 denote the two compartments 1 and 2, while the subscript i refers to an initial condition. The required input data for Payne's method are as follows:

- Amount of gas contained in each tank, that is, tank dimensions, porosity, and saturation
- Inter-compartment communication factors, C_{12}
- Initial pressure in each compartment
- Production data profiles from the individual tanks

Payne's technique is performed fully explicit in time. At each time step, the pressures in various tanks are calculated, yielding a pressure profile that can be matched to the actual pressure decline. The specific steps of this iterative method are summarized below:

Step 1. Prepare the available gas properties data in tabulated and graphical forms including:

- Z versus p
- μ_g versus p
- $2p/(\mu_g Z)$ versus p
- $m(p)$ versus p

Step 2. Divide the reservoir into compartments and determine the dimensions of each compartments in terms of:

- Length, L
- Height, h
- Width, W
- Cross-sectional area, A

Step 3. For each compartment, determine the initial gas-in-place, G. Assuming two compartments, for example, then calculate G_1 and G_2 from Equations 13-38 and 13-39.

$$G_1 = 43,560 A_1 h_1 \phi_1 (1-S_{wi}) / B_{gi}$$

$$G_2 = 43,560 A_2 h_2 \phi_2 (1-S_{wi}) / B_{gi}$$

Step 4. For each compartment, make a plot of p/Z vs. G_p that can be constructed by simply drawing a straight line between p_i/Z_i with initial gas-in-place in both compartments, G_1 and G_2 .

Step 5. Calculate the communication factors for each compartment and between compartments. For two compartments:

$$C_1 = \frac{0.111924 k_1 A_1}{T L_1}$$

$$C_2 = \frac{0.111924 k_2 A_2}{T L_2}$$

$$C_{12} = \frac{2 C_1 C_2}{(C_1 + C_2)}$$

Step 6. Select a small time step, Δt , and determine the corresponding *actual* cumulative gas production, G_p , from each compartment. Assign $G_p = 0$ if the compartment does not include a well.

Step 7. Assume (guess) the pressure distributions throughout the selected compartmental system and determine the gas deviation factor, Z , at each pressure. For a two-compartment system, let the initial values be denoted by p_1^k and p_2^k .

Step 8. Using the assumed values of pressure, p_1^k and p_2^k , determine the corresponding $m(p_1)$ and $m(p_2)$ from the data of Step 1.

Step 9. Calculate the gas influx rate, Q_{12} , and cumulative gas influx G_{p12} by applying Equations 13-34 and 13-35, respectively.

$$Q_{12} = C_{12} [m(p_1) - m(p_2)]$$

$$G_{p12} = \int_0^t Q_{12} dt = \sum_0^t (\Delta Q_{12}) \Delta t$$

Step 10. Substitute the values of G_{p12} , Z -factor, and actual values of G_{p1} and G_{p2} , in Equations 13-36 and 13-37 to calculate the pressure in each compartment, denoted by p_1^{k+1} and p_2^{k+1} .

$$p_1^{k+1} = \left(\frac{p_i}{Z_i} \right) Z_1 \left(1 - \frac{G_{p1} + G_{p12}}{G_1} \right)$$

$$p_2^{k+1} = \left(\frac{p_i}{Z_i} \right) Z_2 \left(1 - \frac{G_{p2} - G_{p12}}{G_2} \right)$$

Step 11. Compare the assumed and calculated values, $|p_1^k - p_1^{k+1}|$ and $|p_2^k - p_2^{k+1}|$. If a satisfactory match is achieved within a tolerance of 5–10 psi for all the pressure values, then Steps 3 through 7 are repeated at a new time level with corresponding historical gas

production data. If the match is not satisfactory, repeat the iterative cycle of Steps 4 through 7 and set $p_1^k = p_1^{k+1}$ and $p_2^k = p_2^{k+1}$.

Step 12. Repeat Steps 6 through 11 to produce a pressure-decline profile for each compartment that can be compared with the actual pressure profile for each compartment or that from Step 4.

Performing a material-balance history match consists of varying the number of compartments required, the dimension of the compartments, and the communication factors until an acceptable match of the pressure decline is obtained. The improved accuracy in estimating the original gas-in-place, resulting from determining the optimum number and size of compartments, stems from the ability of the proposed method to incorporate reservoir pressure gradients, which are completely neglected in the single-tank conventional p/Z plot method.

Hagoort–Hoogstra Method

Based on Payne's method, Hagoort and Hoogstra (1999) developed a numerical method to solve the MBE of compartmental gas reservoirs that employs an implicit, iterative procedure, and that recognizes the pressure dependency of the gas properties. The iterative technique relies on adjusting the size of the compartments and the transmissibility values to match the historical pressure data for each compartment as a function of time. Referring to Figure 13-16, the authors assume a thin permeable layer with a transmissibility of Γ_{12} separating the two compartments. Hagoort and Hoogstra expressed the instantaneous gas influx through the thin permeable layer by Darcy's equation, as given by (in Darcy's units):

$$Q_{12} = \frac{\Gamma_{12} (p_1^2 - p_2^2)}{2 p_1 (\mu_g B_g)_{\text{avg}}}$$

where Γ_{12} = the transmissibility between compartments

The gas influx between compartments can be obtained by modifying Equation 6-23 in Chapter 6 to give:

$$Q_{12} = \frac{0.111924 \Gamma_{12} (p_1^2 - p_2^2)}{TL} \quad (13-40)$$

with

$$\Gamma_{12} = \frac{\Gamma_1 \Gamma_2 (L_1 + L_2)}{L_1 \Gamma_2 + L_2 \Gamma_1} \quad (13-41)$$

$$\Gamma_1 = \left[\frac{kA}{Z\mu_g} \right]_1 \quad (13-42)$$

$$\Gamma_2 = \left[\frac{kA}{Z\mu_g} \right]_2 \quad (13-43)$$

where Q_{12} = influx gas rate, scf/day

L = distance between the centers of compartment 1 and 2, ft

A = cross-sectional area, ft²

μ_g = gas viscosity, cp

Z = gas deviation factor

k = permeability, md

p = pressure, psia

T = temperature, °R

L_1 = length of compartment 1, ft

L_2 = length of compartment 2, ft

The subscripts 1 and 2 refer to compartments 1 and 2, respectively.

The material balance for the two reservoir compartments can be modified to include the gas influx from compartment 1 to compartment 2:

$$\frac{p_1}{Z_1} = \frac{p_1}{Z_1} \left(1 - \frac{G_{p1} + G_{p12}}{G_1} \right) \quad (13-44)$$

$$\frac{p_2}{Z_2} = \frac{p_1}{Z_1} \left(1 - \frac{G_{p2} - G_{p12}}{G_2} \right) \quad (13-45)$$

where p_1 = initial reservoir pressure, psi

Z_1 = initial gas deviation factor

G_p = actual (historical) cumulative gas production, scf

G_1, G_2 = initial gas-in-place in compartments 1 and 2, scf

G_{p12} = cumulative gas influx from compartment 1 to 2, scf as given in Equation 13-35

Again, subscripts 1 and 2 represent compartments 1 and 2, respectively.

To solve the material balance equations as represented by the relationships in Equations 13-45 and 13-46 for the two unknowns p_1 and p_2 , the two expressions can be arranged to equate to zero, as follows:

$$F_1(p_1, p_2) = p_1 - \left(\frac{p_i}{Z_i} \right) Z_1 \left(1 - \frac{G_{p1} + G_{p12}}{G_1} \right) = 0 \quad (13-46)$$

$$F_2(p_1, p_2) = p_2 - \left(\frac{p_i}{Z_i} \right) Z_2 \left(1 - \frac{G_{p2} - G_{p12}}{G_2} \right) = 0 \quad (13-47)$$

The general methodology of applying the method is very similar to that of Payne's and involves the following specific steps:

Step 1. Prepare the available data on gas properties in tabulated and graphical forms that include Z versus p and μ_g versus p

Step 2. Divide the reservoir into compartments and determine the dimensions of each compartment in terms of

- Length, L
- Height, h
- Width, W
- Cross-sectional area, A

Step 3. For each compartment, determine the initial gas-in-place, G . For clarity, assume two gas compartments and calculate G_1 and G_2 from Equations 13-38 and 13-39.

$$G_1 = 43,560 A_1 h_1 \phi_1 (1 - S_{wi}) / B_{gi}$$

$$G_2 = 43,560 A_2 h_2 \phi_2 (1 - S_{wi}) / B_{gi}$$

Step 4. For each compartment, make a plot of p/Z versus G_p that can be constructed by simply drawing a straight line between p_i/Z_i with initial gas-in-place in both compartments, G_1 and G_2 .

Step 5. Calculate the transmissibility by applying Equation 13-41.

Step 6. Select a time step, Δt , and determine the corresponding actual cumulative gas production G_{p1} and G_{p2} .

Step 7. Calculate the gas influx rate, Q_{12} , and cumulative gas influx, G_{p12} , by applying Equations 13-40 and 13-35, respectively.

$$Q_{12} = \frac{0.111924 \Gamma_{12} (p_1^2 - p_2^2)}{TL}$$

$$G_{p12} = \int_0^t Q_{12} dt = \sum_0^t (\Delta Q_{12}) \Delta t$$

Step 8. Start the iterative solution by assuming initial estimates of the pressure for compartments 1 and 2 (i.e., p_1^k and p_2^k). Using Newton and Raphson's iterative scheme, calculate new improved values of the pressure p_1^{k+1} and p_2^{k+1} by solving the following linear equations as expressed in a matrix form:

$$\begin{bmatrix} p_1^{k+1} \\ p_2^{k+1} \end{bmatrix} = \begin{bmatrix} p_1^k \\ p_2^k \end{bmatrix} - \begin{bmatrix} \frac{\partial F_1(p_1^k, p_2^k)}{\partial p_1} & \frac{\partial F_1(p_1^k, p_2^k)}{\partial p_2} \\ \frac{\partial F_2(p_1^k, p_2^k)}{\partial p_1} & \frac{\partial F_2(p_1^k, p_2^k)}{\partial p_2} \end{bmatrix}^{-1} \begin{bmatrix} -F_1(p_1^k, p_2^k) \\ -F_2(p_1^k, p_2^k) \end{bmatrix}$$

where the superscript “-1” denotes the inverse of the matrix. The partial derivatives in this system of equations can be expressed in analytical form by differentiating Equations 8-140 and 8-141 with respect to p_1 and p_2 . During an iterative cycle, the derivatives are evaluated at the updated new pressures, i.e., p_1^{k+1} and p_2^{k+1} . The iteration is stopped when $|p_1^{k+1} - p_1^k|$ and $|p_2^{k+1} - p_2^k|$ are less than a certain pressure tolerance, that is, 5–10 psi.

Step 9. Generate the pressure profile as a function of time for each compartment by repeating Steps 2 and 3.

$$\frac{p_1}{Z_1} = \frac{p_i}{Z_i} \left(1 - \frac{G_{p1} + G_{p12}}{G_1} \right)$$

where p_1 = initial reservoir pressure, psi

Z_1 = initial gas deviation factor

G_p = actual (historical) cumulative gas production, scf

G_1, G_2 = initial gas-in-place in compartment 1 and 2, scf

G_{p12} = cumulative gas influx from compartment 1 to 2 in scf, as given in Equation 13-35

Step 10. Repeat Steps 6 through 11 to produce a pressure decline profile for each compartment that can be compared with the actual pressure profile for each compartment or that from step 4.

Compare the calculated pressure profiles with those of the observed pressures. If a match has not been achieved, adjust the size and number of compartments (i.e., initial gas-in-place) and repeat Steps 2 through 10.

Shallow Gas Reservoirs

Tight shallow gas reservoirs present a number of unique challenges in determining reserves accurately. Traditional methods such as decline analysis and material balance are inaccurate owing to the formation's low permeability and the usually poor-quality pressure data. The low permeabilities cause long transient periods that are not separated early from production decline with conventional decline analysis, resulting in lower confidence in selecting the appropriate decline characteristics, which affects recovery factors and remaining reserves significantly. In an excellent paper by West and Cochrane (1995), the authors used the Medicine Hat field in Western Canada as an example of these types of reservoirs and developed a methodology called the Extended Material Balance (EMB) technique, to evaluate gas reserves and potential infill drilling.

The Medicine Hat field is a tight, shallow gas reservoir producing from multiple highly interbedded, silty sand formations with poor permeabilities of < 0.1 md. This poor permeability is the main characteristic of these reservoirs that affects conventional decline analysis. Owing to these low permeabilities, and in part to commingled multilayer production effects, wells experience long transient periods before they begin experiencing the

pseudosteady-state flow that represents the decline portion of their lives. One of the principal assumptions often neglected when conducting decline analysis is that pseudosteady-state must have been achieved. The initial transient production trend of a well or group of wells is not indicative of the long-term decline of the well. Distinguishing the transient production of a well from its pseudosteady-state production is often difficult, and this can lead to errors in determining the decline characteristic (exponential, hyperbolic, or harmonic) of a well. Figure 13-17 shows the production history from a tight, shallow gas well and illustrates the difficulty in selecting the correct decline. Another characteristic of tight, shallow gas reservoirs that affects conventional decline analysis is that constant reservoir conditions, an assumption required for conventional decline analysis, do not exist because of increasing drawdown, changing operating strategies, erratic development, and deregulation.

Material balance is affected by tight, shallow gas reservoirs because the pressure data are limited, of poor quality, and not representative of a majority of the wells. Because the risk of drilling dry holes is low and drillstem tests (DSTs) are not cost-effective in the development of shallow gas, DST data are very limited. Reservoir pressures are recorded only for government-designated “control” wells, which account for only 5% of all wells. Shallow gas produces from multiple formations, and production from these formations is typically commingled, exhibiting some degree of pressure equalization. Unfortunately, the control wells are segregated by tubing/packers, and consequently, the control-well pressure data are not representative of most commingled wells. In addition, pressure monitoring has been very inconsistent. Varied measurement points (downhole or

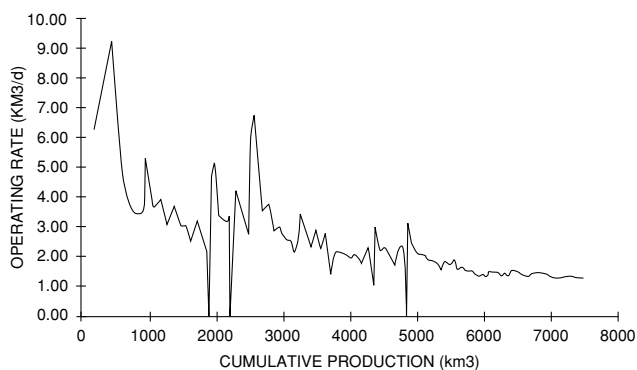


Figure 13-17. Production history for a typical Medicine Hat property (Permission to copy SPE, copyright SPE 1995).

wellhead), inconsistent shut-in times, and different analysis types (e.g., buildup and static gradient) make quantitative pressure-tracking difficult. As Figure 13-18 shows, both of these problems result in a scatter of data, which makes material balance extremely difficult.

Wells in the Medicine Hat shallow gas area are generally cased, perforated, and fractured in one, two, or all three formations, as ownerships vary not only areally but between formations. The Milk River and Medicine Hat formations are usually produced commingled. Historically, the Second White Specks formation has been segregated from the other two; recently, however, commingled production from all three formations has been approved. Spacing for shallow gas is usually two to four wells per section. As a result of the poor reservoir quality and low pressure, well productivity is very low. Initial rates rarely exceed 700 Mscf/day. Current average production per well is approximately 50 Mscf/day for a three-formation completion. There are approximately 24,000 wells producing from the Milk River formation in Southern Alberta and Saskatchewan with total estimated gas reserves of 5.3 Tscf. West and Cochrane's EMB technique was developed to determine gas reserves in 2,300 wells in the Medicine Hat field.

The EMB technique is essentially an iterative process for obtaining a suitable p/Z versus G_p line for a reservoir where pressure data are inadequate. It combines the principles of volumetric gas depletion with the gas-deliverability (back-pressure) equation. The deliverability equation for radial flow of gas describes the relationship between the pressure differential in the wellbore and the gas flow rate from the well:

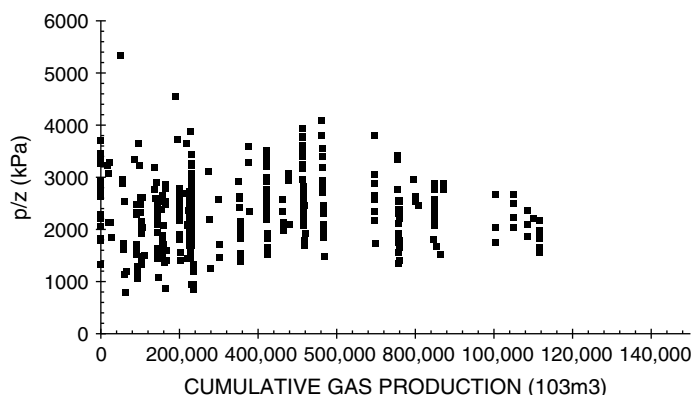


Figure 13-18. Scatter pressure data for a typical Medicine Hat property (Permission to copy SPE, copyright SPE 1995).

$$Q_g = C [p_r^2 - p_{wf}^2]^n$$

Owing to the very low production rates from the wells in Medicine Hat shallow gas, a laminar flow regime exists, which can be described with an exponent $n = 1$. The terms making up the coefficient C in the back-pressure equation are either fixed reservoir parameters (kh , r_e , r_w , and T) that do not vary with time or terms that fluctuate with pressure, temperature, and gas composition, for example, μ_g and Z . The performance coefficient “ C ” is given by:

$$C = \frac{kh}{1422 T \mu_g Z [\ln(r_e / r_w) - 0.5]}$$

Because the original reservoir pressure in these shallow formations is low, the differences between initial and abandonment pressures are not significant and the variation in the pressure-dependent terms over time can be assumed negligible. C may be considered constant for a given Medicine Hat shallow gas reservoir over its life. With these simplifications for shallow gas, the deliverability equation becomes:

$$Q_g = C [p_r^2 - p_{wf}^2]$$

The sum of the instantaneous production rates with time will yield the relationship between G_p and reservoir pressure, similar to the material balance equation. By use of this common relationship, with the unknowns being reservoir pressure, p , and the performance coefficient, C , the EMB method involves iterating to find the correct p/Z versus G_p relationship to give a constant C with time. The proposed iterative method is applied as outlined in the following steps:

Step 1. To avoid calculating individual reserves for each of the 2,300 wells, West and Cochrane grouped wells by formation and by date on production. The authors verified this simplification on a test group by ensuring that the reserves from the group of wells yielded the same results as the sum of the individual well reserves. These groupings were used for each of the 10 properties, and the results of the groupings combined to give a property production forecast. Also, to estimate the reservoir decline characteristics more accurately, the rates were normalized to reflect changes in the bottom-hole flowing pressure (BHFP).

- Step 2.* Using the gas specific gravity and reservoir temperature, calculate the gas deviation factor, Z , as a function of pressure and plot p/Z versus p on a Cartesian scale.
- Step 3.* An initial estimate for the p/Z variation with G_p is made by guessing an initial pressure, p_i , and a linear slope, m , of Equation 13-11:

$$\frac{p}{Z} = \frac{p_i}{Z_i} - [m]G_p$$

with the slope m defined by:

$$m = \left(\frac{p_i}{Z_i} \right) \frac{1}{G}$$

- Step 4.* Starting at the initial production date for the property, the p/Z versus time relationship is established by simply substituting the actual cumulative production, G_p , into the MBE with estimated slope m and p_i because actual cumulative production G_p versus time is known. The reservoir pressure, p , can then be constructed as a function of time from the plot of p/Z as a function of p , that is, Step 2.

- Step 5.* Knowing the actual production rates, Q_g , and bottom-hole flowing pressures, p_{wf} , for each monthly time interval and having estimated reservoir pressures, p , from Step 3, C is calculated for each time interval with:

$$C = \frac{Q_g}{p^2 - p_{wf}^2}$$

- Step 6.* C is plotted against time. If C is not constant (i.e., the plot is not a horizontal line), a new p/Z versus G_p is guessed and the process is repeated from Step 3 through Step 5.
- Step 7.* Once a constant C solution is obtained, the representative p/Z relationship has been defined for reserves determination.

Use of the EMB method in the Medicine Hat shallow gas makes the fundamental assumptions (1) that the gas pool depletes volumetrically (i.e., there is no water influx) and (2) that all wells behave like an average well with the same deliverability constant, turbulence constant, and BHFP, which is a reasonable assumption given the number of wells in the area, the homogeneity of the rocks, and the observed well production trends.

In the EMB evaluation, West and Cochrane point out that wells for each property were grouped according to their producing interval so that the actual production from the wells could be related to a particular reservoir pressure trend. When calculating the coefficient C , as outlined above, a total C based on grouped production was calculated and then divided by the number of wells producing in a given time interval to give an average C value. The average C value was used to calculate an average permeability/thickness, kh , for comparison with actual kh data obtained through buildup analysis for the reservoir, as follows:

$$kh = 1422 T \mu_g Z [\ln(r_e / r_w) - 0.5] C$$

For that reason, kh versus time, instead of C versus time, was plotted in the method. Figure 13-19 shows a flat kh versus time profile indicating a valid p/Z versus G_p relationship.

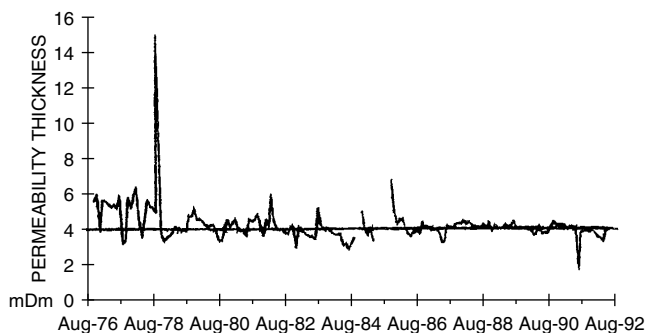


Figure 13-19. Example for a successful EMB solution-flat kh profile (Permission to copy SPE, copyright SPE 1995).

PROBLEMS

1. The following information is available on a volumetric gas reservoir:

| | |
|--------------------------------------|------------------|
| Initial reservoir temperature, T_i | = 155°F |
| Initial reservoir pressure, p_i | = 3500 psia |
| Specific gravity of gas, γ_g | = 0.65 (air = 1) |
| Thickness of reservoir, h | = 20 ft |
| Porosity of the reservoir, ϕ | = 10% |
| Initial water saturation, S_{wi} | = 25% |

After producing 300 MMscf, the reservoir pressure declined to 2,500 psia. Estimate the areal extent of this reservoir.

2. The following pressures and cumulative production data² are available for a natural gas reservoir:

| Reservoir Pressure, psia | Gas Deviation Factor, z | Cumulative Production, MMMscf |
|--------------------------|---------------------------|-------------------------------|
| 2080 | 0.759 | 0 |
| 1885 | 0.767 | 6.873 |
| 1620 | 0.787 | 14.002 |
| 1205 | 0.828 | 23.687 |
| 888 | 0.866 | 31.009 |
| 645 | 0.900 | 36.207 |

- Estimate the initial gas-in-place.
 - Estimate the recoverable reserves at an abandonment pressure of 500 psia. Assume $z_a = 1.00$.
 - What is the recovery factor at the abandonment pressure of 500 psia?
3. A gas field with an active water drive showed a pressure decline from 3,000 to 2,000 psia over a 10-month period. From the following production data, match the past history and calculate the original hydrocarbon gas in the reservoir. Assume $z = 0.8$ in the range of reservoir pressures and $T = 140^\circ\text{F}$.

| Data | | | | | |
|---------------|------|------|-------|-------|-------|
| t , months | 0 | 2.5 | 5.0 | 7.5 | 10.0 |
| p , psia | 3000 | 2750 | 2500 | 2250 | 2000 |
| G_p , MMscf | 0 | 97.6 | 218.9 | 355.4 | 500.0 |

²Ikoku, C., *Natural Gas Reservoir Engineering*, John Wiley and Sons, 1984.

4. A volumetric gas reservoir produced 600 MMscf of 0.62 specific gravity gas when the reservoir pressure declined from 3,600 to 2,600 psi. The reservoir temperature is reported at 140°F. Calculate:
- Gas initially in place
 - Remaining reserves to an abandonment pressure of 500 psi
 - Ultimate gas recovery at abandonment
5. The following information on a water-drive gas reservoir is given:

Bulk volume = 100,000 acre-ft

Gas gravity = 0.6

Porosity = 15%

$S_{wi} = 25\%$

$T = 140^\circ\text{F}$

$p_i = 3500$ psi

Reservoir pressure has declined to 3,000 psi while producing 30 MMMscf of gas and no water production. Calculate cumulative water influx.

6. The pertinent data for the Mobil-David field are given below.

$$G = 70 \text{ MMMscf} \quad p_i = 9507 \text{ psi} \quad \phi = 24\% \quad S_{wi} = 35\%$$

$$c_w = 401 \times 10^{-6} \text{ psi}^{-1} \quad c_f = 3.4 \times 10^{-6} \text{ psi}^{-1} \quad \gamma_g = 0.94 \quad T = 266^\circ\text{F}$$

For this volumetric abnormally pressured reservoir, calculate and plot cumulative gas production as a function of pressure.

7. The Big Butte field is a volumetric dry-gas reservoir with a recorded initial pressure of 3,500 psi at 140°F. The specific gravity of the produced gas is measured at 0.65. The following reservoir data are available from logs and core analysis:

Reservoir area = 1500 acres

Thickness = 25 ft

Porosity = 15%

Initial water saturation = 20%

Calculate:

- Initial gas in place as expressed in scf
- Gas viscosity at 3,500 psi and 140°F

REFERENCES

1. Begland, T., and Whitehead, W., "Depletion Performance of Volumetric High-Pressured Gas Reservoirs," *SPE Reservoir Engineering*, August 1989, pp. 279–282.
2. Cole, F. W., *Reservoir Engineering Manual*. Houston: Gulf Publishing Co., 1969.
3. Dake, L., *The Practice of Reservoir Engineering*. Amsterdam: Elsevier Publishing Company, 1994.
4. Duggan, J. O., "The Anderson 'L'—An Abnormally Pressured Gas Reservoir in South Texas," *Journal of Petroleum Technology*, February 1972, Vol. 24, No. 2, pp. 132–138.
5. Hagoort, J., and Hoogstra, R., "Numerical Solution of the Material Balance Equations of Compartmented Gas Reservoirs," *SPE Reservoir Eval. & Eng.* 2 (4), August 1999.
6. Hagoort, J., Sinke, J., Dros, B., and Nieuwland, F., "Material Balance Analysis of Faulted and Stratified Tight Gas Reservoirs," SPE 65179, SPE European Petroleum Conference, Paris, France, October 2000.
7. Hammerlindl, D. J., "Predicting Gas Reserves in Abnormally Pressured Reservoirs," SPE Paper 3479 presented at the 46th Annual Fall Meeting of SPE, New Orleans, October 1971.
8. Havlena, D., and Odeh, A. S., "The Material Balance as an Equation of a Straight Line," *Trans. AIME*, Part 1: 228 I-896 (1963); Part 2: 231 I-815 (1964).
9. Ikoku, C., *Natural Gas Reservoir Engineering*. John Wiley & Sons, Inc., 1984.
10. Payne, D. A., "Material Balance Calculations in Tight Gas Reservoirs: The Pitfalls of p/Z Plots and a More Accurate Technique," *SPE Reservoir Engineering*, November 1996.
11. Roach, R. H., "Analyzing Geopressured Reservoirs—A Material Balance Technique," SPE Paper 9968, Society of Petroleum Engineers of AIME, Dallas, December 1981.
12. Van Everdingen, A. F., and Hurst, W., "Application of Laplace Transform to Flow Problems in Reservoirs," *Trans. AIME*, 1949, Vol. 186, pp. 305–324B.
13. West, S., "Reserve Determination Using Type Curve Matching and Extended Material Balance Methods in The Medicine Hat Shallow Gas Field," SPE 28609, The 69th Annual Technical Conference, New Orleans, LA, September 25–28, 1994.

C H A P T E R 1 4

PRINCIPLES OF WATERFLOODING

The terms primary oil recovery, secondary oil recovery, and tertiary (enhanced) oil recovery are traditionally used to describe hydrocarbons recovered according to the method of production or the time at which they are obtained.

Primary oil recovery describes the production of hydrocarbons under the natural driving mechanisms present in the reservoir without supplementary help from injected fluids such as gas or water. In most cases, the natural driving mechanism is a relatively inefficient process and results in a low overall oil recovery. The lack of sufficient natural drive in most reservoirs has led to the practice of supplementing the natural reservoir energy by introducing some form of artificial drive, the most basic method being the injection of gas or water.

Secondary oil recovery refers to the additional recovery that results from the conventional methods of water-injection and immiscible gas injection. Usually, the selected secondary recovery process follows the primary recovery but it can also be conducted concurrently with the primary recovery. Waterflooding is perhaps the most common method of secondary recovery. However, before undertaking a secondary recovery project, it should be clearly proven that the natural recovery processes are insufficient; otherwise there is a risk that the substantial capital investment required for a secondary recovery project may be wasted.

Tertiary (enhanced) oil recovery is that additional recovery over and above what could be recovered by primary and secondary recovery methods. Various methods of enhanced oil recovery (EOR) are essentially

designed to recover oil, commonly described as residual oil, left in the reservoir after both primary and secondary recovery methods have been exploited to their respective economic limits. Figure 14-1 illustrates the concept of the three oil recovery categories.

FACTORS TO CONSIDER IN WATERFLOODING

Thomas, Mahoney, and Winter (1989) pointed out that in determining the suitability of a candidate reservoir for waterflooding, the following reservoir characteristics must be considered:

- Reservoir geometry
- Fluid properties
- Reservoir depth
- Lithology and rock properties
- Fluid saturations

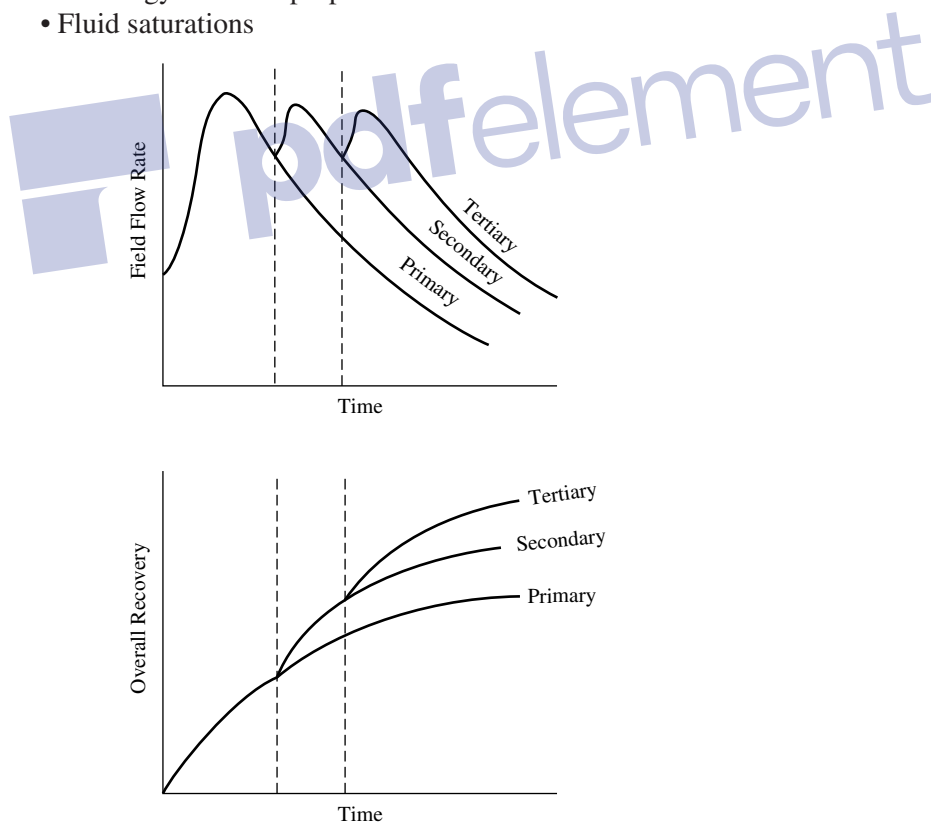


Figure 14-1. Oil recovery categories.

- Reservoir uniformity and pay continuity
- Primary reservoir-driving mechanisms

Each of these topics is discussed in detail in the following subsections.

Reservoir Geometry

The areal geometry of the reservoir will influence the location of wells and, if offshore, will influence the location and number of platforms required. The reservoir's geometry will essentially dictate the methods by which a reservoir can be produced through water-injection practices.

An analysis of reservoir geometry and past reservoir performance is often important when defining the presence and strength of a natural water drive and, thus, when defining the need to supplement the natural injection. If a water-drive reservoir is classified as an active water drive, injection may be unnecessary.

Fluid Properties

The physical properties of the reservoir fluids have pronounced effects on the suitability of a given reservoir for further development by waterflooding. The viscosity of the crude oil is considered the most important fluid property that affects the degree of success of a waterflooding project. The oil viscosity has the important effect of determining the mobility ratio that, in turn, controls the sweep efficiency.

Reservoir Depth

Reservoir depth has an important influence on both the technical and economic aspects of a secondary or tertiary recovery project. Maximum injection pressure will increase with depth. The costs of lifting oil from very deep wells will limit the maximum economic water-oil ratios that can be tolerated, thereby reducing the ultimate recovery factor and increasing the total project operating costs. On the other hand, a shallow reservoir imposes a restraint on the injection pressure that can be used, because this must be less than fracture pressure. In waterflood operations, there is a critical pressure (approximately 1 psi/ft of depth) that, if exceeded, permits the injecting water to expand openings along fractures or to create fractures. This results in the channeling of the injected water or the bypassing of large portions of the reservoir matrix. Consequently, an operational pressure gradient of 0.75 psi/ft of depth normally is allowed to provide a sufficient margin of safety to prevent pressure parting.

Lithology and Rock Properties

Thomas et al. (1989) pointed out that lithology has a profound influence on the efficiency of water-injection in a particular reservoir. Reservoir lithology and rock properties that affect flood ability and success are:

- Porosity
- Permeability
- Clay content
- Net thickness

In some complex reservoir systems, only a small portion of the total porosity, such as fracture porosity, will have sufficient permeability to be effective in water-injection operations. In these cases, a water-injection program will have only a minor impact on the matrix porosity, which might be crystalline, granular, or vugular in nature.

Although evidence suggests that the clay minerals present in some sands may clog the pores by swelling and deflocculating when water-flooding is used, no exact data are available as to the extent to which this may occur.

Tight (low-permeability) reservoirs or reservoirs with thin net thickness possess water-injection problems in terms of the desired water-injection rate or pressure. Note that the water-injection rate and pressure are roughly related by the following expression:

$$p_{inj} \propto \frac{i_w}{hk}$$

where p_{inj} = water-injection pressure

i_w = water-injection rate

h = net thickness

k = absolute permeability

The above relationship suggests that to deliver a desired daily injection rate of i_w in a tight or thin reservoir, the required injection pressure might exceed the formation fracture pressure.

Fluid Saturations

In determining the suitability of a reservoir for waterflooding, a high oil saturation that provides a sufficient supply of recoverable oil is the primary criterion for successful flooding operations. Note that higher oil saturation at the beginning of flood operations increases the oil mobility that, in turn, gives higher recovery efficiency.

Reservoir Uniformity and Pay Continuity

Substantial reservoir uniformity is one of the major physical criteria for successful waterflooding. For example, if the formation contains a stratum of limited thickness with a very high permeability (i.e., **thief zone**), rapid channeling and bypassing will develop. Unless this zone can be located and shut off, the producing water-oil ratios will soon become too high for the flooding operation to be considered profitable.

The lower depletion pressure that may exist in the highly permeable zones will also aggravate the water-channeling tendency due to the high-permeability variations. Moreover, these thief zones will contain less residual oil than the other layers, and their flooding will lead to relatively lower oil recoveries than other layers.

Areal continuity of the pay zone is also a prerequisite for a successful waterflooding project. Isolated lenses may be effectively depleted by a single well completion, but a flood mechanism requires that both the injector and producer be present in the lens. Breaks in pay continuity and reservoir anisotropy caused by depositional conditions, fractures, or faulting need to be identified and described before determining the proper well spanning and the suitable flood pattern orientation.

Primary Reservoir-Driving Mechanisms

As described in Chapter 11, six driving mechanisms basically provide the natural energy necessary for oil recovery:

- Rock and liquid expansion
- Solution gas drive
- Gas-cap drive
- Water drive
- Gravity drainage drive
- Combination drive

The recovery of oil by any of the above driving mechanisms is called *primary recovery*. The term refers to the production of hydrocarbons from a reservoir without the use of any process (such as water-injection) to supplement the natural energy of the reservoir. The primary drive mechanism and anticipated ultimate oil recovery should be considered when reviewing possible waterflood prospects. The approximate oil recovery range is tabulated below for various driving mechanisms. Note that these calculations are approximate and, therefore, oil recovery may fall outside these ranges.

| Driving Mechanism | Oil Recovery Range, % |
|---------------------------|-----------------------|
| Rock and liquid expansion | 3–7 |
| Solution gap | 5–30 |
| Gas cap | 20–40 |
| Water drive | 35–75 |
| Gravity drainage | <80 |
| Combination drive | 30–60 |

Water-drive reservoirs that are classified as strong water-drive reservoirs are not usually considered to be good candidates for waterflooding because of the natural ongoing water influx. However, in some instances a natural water drive could be supplemented by water-injection in order to:

- Support a higher withdrawal rate
- Better distribute the water volume to different areas of the field to achieve more uniform areal coverage
- Better balance voidage and influx volumes

Gas-cap reservoirs are not normally good waterflood prospects because the primary mechanism may be quite efficient without water-injection. In these cases, gas injection may be considered in order to help maintain pressure. Smaller gas-cap drives may be considered as waterflood prospects, but the existence of the gas cap will require greater care to prevent migration of displaced oil into the gas cap. This migration would result in a loss of recoverable oil due to the establishment of residual oil saturation in pore volume, which previously had none. If a gas cap is repressured with water, a substantial volume may be required for this purpose, thereby lengthening the project life and requiring a higher vol-

ume of water. However, the presence of a gas cap does not always mean that an effective gas-cap drive is functioning. If the vertical communication between the gas cap and the oil zone is considered poor due to low vertical permeability, a waterflood may be appropriate in this case. Analysis of past performance, together with reservoir geology studies, can provide insight as to the degree of effective communication. Natural permeability barriers can often restrict the migration of fluids to the gas cap. It may also be possible to use selective plugging of input wells to restrict the loss of injection fluid to the gas cap.

Solution-gas-drive mechanisms generally are considered the best candidates for waterfloods. Because the primary recovery will usually be low, the potential exists for substantial additional recovery by water-injection. In effect, we hope to create an artificial water-drive mechanism. The typical range of water-drive recovery is approximately double that of solution gas drive. As a general guideline, waterfloods in solution gas-drive reservoirs frequently will recover an additional amount of oil equal to primary recovery.

Volumetric undersaturated-oil reservoirs producing above the bubble-point pressure must depend on rock and liquid expansion as the main driving mechanism. In most cases, this mechanism will not recover more than about 5% of the original oil-in-place. These reservoirs will offer an opportunity for greatly increasing recoverable reserves if other conditions are favorable.

OPTIMUM TIME TO WATERFLOOD

The most common procedure for determining the optimum time to start waterflooding is to calculate:

- Anticipated oil recovery
- Fluid production rates
- Monetary investment
- Availability and quality of the water supply
- Costs of water treatment and pumping equipment
- Costs of maintenance and operation of the water installation facilities
- Costs of drilling new injection wells or converting existing production wells into injectors

These calculations should be performed for several assumed times and the net income for each case determined. The scenario that maximizes the profit and perhaps meets the operator's desirable goal is selected.

Cole (1969) lists the following factors as being important when determining the reservoir pressure (or time) to initiate a secondary recovery project:

- **Reservoir oil viscosity.** Water-injection should be initiated when the reservoir pressure reaches its bubble-point pressure since the oil viscosity reaches its minimum value at this pressure. The mobility of the oil will increase with decreasing oil viscosity, which in turns improves the sweeping efficiency.
- **Free gas saturation.** (1) In **water-injection projects.** It is desirable to have initial gas saturation, possibly as much as 10%. This will occur at a pressure that is below the bubble-point pressure. (2) In **gas injection projects.** Zero gas saturation in the oil zone is desired. This occurs while reservoir pressure is at or above bubble-point pressure.
- **Cost of injection equipment.** This is related to reservoir pressure, and at higher pressures, the cost of injection equipment increases. Therefore, a low reservoir pressure at initiation of injection is desirable.
- **Productivity of producing wells.** A high reservoir pressure is desirable to increase the productivity of producing wells, which prolongs the flowing period of the wells, decreases lifting costs, and may shorten the overall life of the project.
- **Effect of delaying investment on the time value of money.** A delayed investment in injection facilities is desirable from this standpoint.
- **Overall life of the reservoir.** Because operating expenses are an important part of total costs, the fluid injection process should be started as early as possible.

Some of these six factors act in opposition to others. Thus the actual pressure at which a fluid injection project should be initiated will require optimization of the various factors in order to develop the most favorable overall economics.

The principal requirement for a successful fluid injection project is that sufficient oil must remain in the reservoir after primary operations have ceased to render economic the secondary recovery operations. This high residual oil saturation after primary recovery is essential not only because there must be a sufficient volume of oil left in the reservoir, but also because of relative permeability considerations. A high oil relative permeability, i.e., high oil saturation, means more oil recovery with less production of the displacing fluid. On the other hand, low oil saturation means a low oil relative permeability with more production of the displacing fluid at a given time.

EFFECT OF TRAPPED GAS ON WATERFLOOD RECOVERY

Numerous experimental and field studies have been conducted to study the effect of the presence of initial gas saturation on waterflood recovery. Early research indicated that the waterflooding of a linear system results in the formation of an oil bank, or zone of increased oil saturation, ahead of the injection water. The moving oil bank will displace a portion of the free water ahead of it, trapping the rest as a residual gas. An illustration of the water saturation profile is shown schematically in Figure 14-2. Several authors have shown through experiments that oil recovery by water is improved as a result of the establishment of **trapped gas saturation**, S_{gt} , in the reservoir.

Willhite (1986) and Craig (1971) indicate that, in some instances, oil recovery can be increased if the reservoir pressure is carefully controlled so as to leave *optimum* trapped gas saturation within the oil bank. The idea is to reduce the residual oil saturation value, S_{or} , by an amount equal to the trapped gas saturation. For example, if the residual oil saturation is 35% and if a trapped gas saturation can be maintained at 5%, the residual oil saturation would be 30%. In this case, S_{or} would be reduced by 14.3%. However, selecting and maintaining the optimum reservoir pressure to maintain this critical gas saturation is difficult to achieve in practice.

The theory of this phenomenon of improving overall oil recovery when initial gas exists at the start of the flood is not well established;

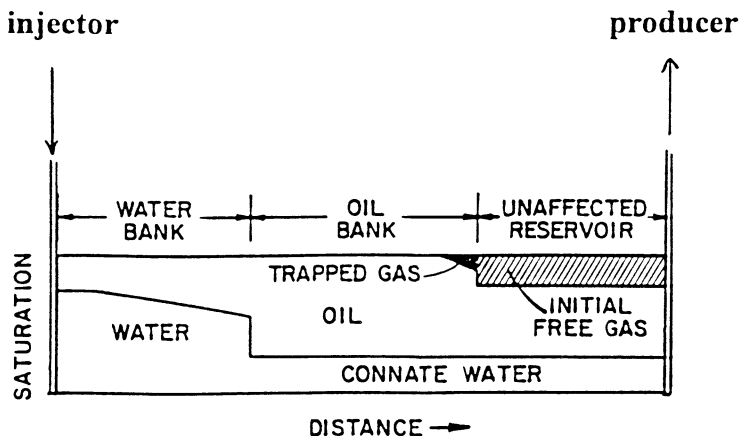


Figure 14-2. Water saturation profile during a waterflood.

however, Cole (1969) proposed the following two different theories that perhaps provide insight into this phenomenon.

First Theory

Cole (1969) postulates that since the interfacial tension of a gas-oil system is less than the interfacial tension of a gas-water system, in a three-phase system containing gas, water, and oil, the reservoir fluids will tend to arrange themselves in a minimum energy relationship. In this case, this would dictate that the gas molecules enclose themselves in an oil “blanket.” This increases the effective size of any oil globules, which have enclosed some gas. When the oil is displaced by water, the oil globules are reduced to some size dictated by the flow mechanics. If a gas bubble existed on the inside of the oil globule, the amount of residual oil left in the reservoir would be reduced by the size of the gas bubble within the oil globule. As illustrated in Figure 14-3, the external diameters of the residual oil globules are the same in both views. However, in view b, the center of the residual oil globule is not oil, but gas. Therefore, in view b, the actual residual oil saturation is reduced by the size of the gas bubble within the oil globule.

Second Theory

Cole (1969) points out that reports on other laboratory experiments have noted the increased recovery obtained by flooding cores with air

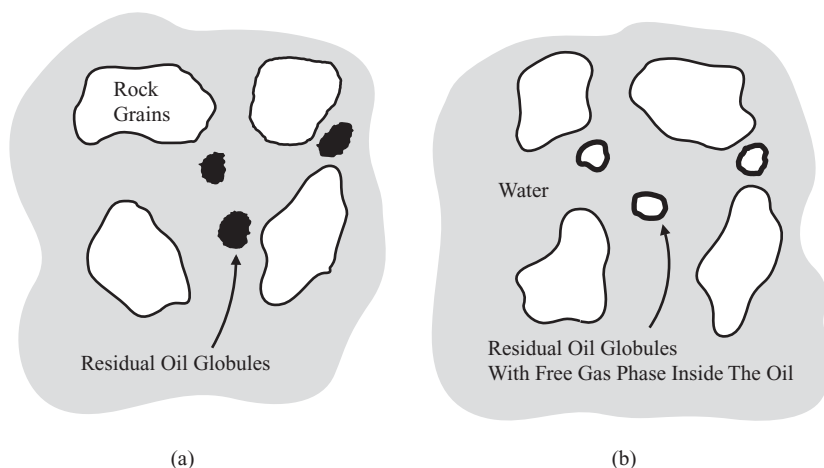


Figure 14-3. Effect of free gas saturation on S_{or} (first theory). (After Cole, F., 1969.)

after waterflooding. These cores were classified as water-wet at the time the laboratory experiments were conducted. On the basis of these experiments, it was postulated that the residual oil saturation was located in the larger pore spaces, since the water would be preferentially pulled into the smaller pore spaces by capillary action in the water-wet sandstone. At a later time, when air was flooded through the core, it moved preferentially through the larger pore spaces since it was nonwetting. However, in passing through these large pore spaces, the air displaced some of the residual oil left by water displacement.

This latter theory is more nearly compatible with fluid flow observations, because the gas saturation does not have to exist inside the oil phase. If this theory were correct, the increased recovery due to the presence of free gas saturation could be explained quite simply for water-wet porous media. As the gas saturation formed, it displaced oil from the larger pore spaces, because it is more nonwetting to the reservoir rock than the oil. Then, as water displaced the oil from the reservoir rock, the amount of residual oil left in the larger pore spaces would be reduced because of occupancy of a portion of this space by gas. This phenomenon is illustrated in Figure 14-4. In view a, there is no free gas saturation and the residual oil occupies the larger pore spaces. In view b, free gas saturation is present and this free gas now occupies a portion of the space originally occupied by the oil. The combined residual saturations of oil and gas in view b are approximately equal to the residual oil saturation of view a.

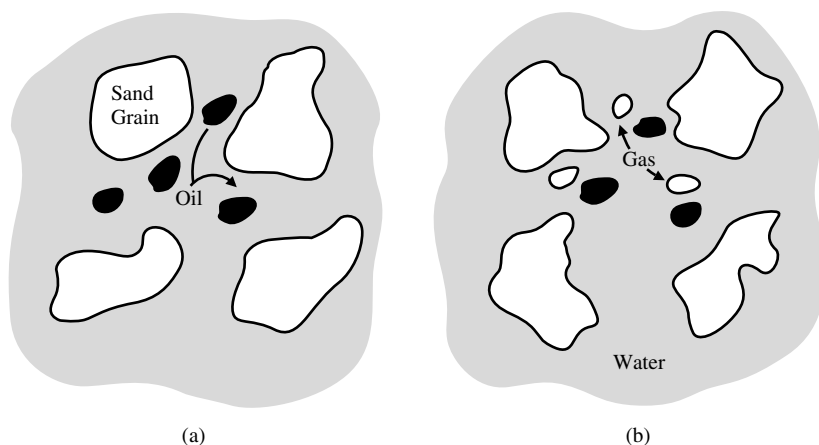


Figure 14-4. Effect of free gas saturation on S_{or} (second theory). (After Cole, F., 1969.)

Craig (1971) presented two graphical correlations that are designed to account for the reduction in the residual oil saturation due to the presence of the trapped gas. The first graphical correlation, shown in Figure 14-5, correlates the trapped gas saturation (S_{gt}) as a function of the initial gas saturation (S_{gi}). The second correlation as presented in Figure 14-6 illustrates the effect of the trapped gas saturation on the reduction in residual oil saturation (ΔS_{or}) for preferentially water-wet rock. The two graphic correlations can be expressed mathematically by the following two expressions:

$$S_{gt} = a_1 + a_2 S_{gi} + a_3 S_{gi}^2 + a_4 S_{gi}^3 + \frac{a_5}{S_{gi}} \quad (14-1)$$

and

$$\Delta S_{or} = a_1 + a_2 S_{gt} + a_3 S_{gt}^2 + a_4 S_{gt}^3 + \frac{a_5}{S_{gt}} \quad (14-2)$$

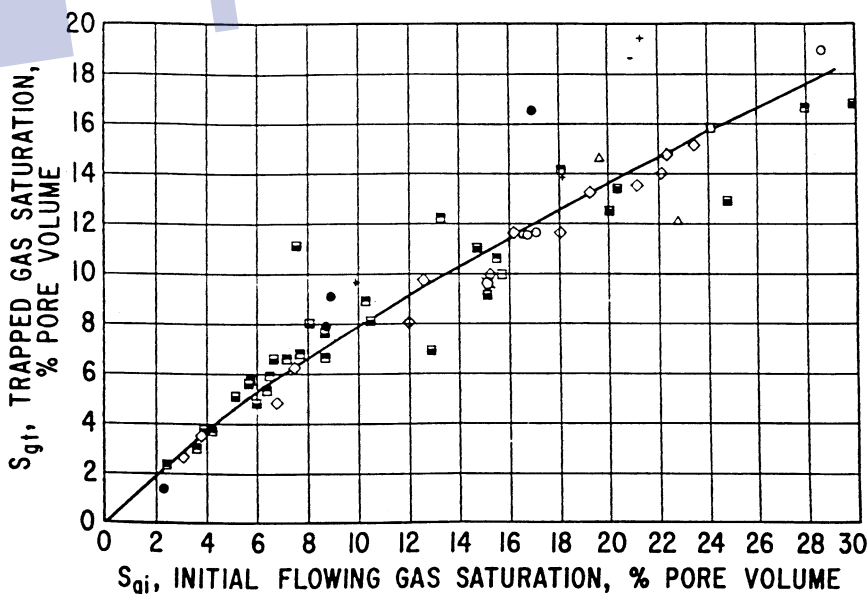


Figure 14-5. Relation between S_{gi} and S_{gt} . (Permission to publish by the Society of Petroleum Engineers.)

where S_{gi} = initial gas saturation

S_{gt} = trapped gas saturation

ΔS_{or} = reduction in residual oil saturation

Values of coefficients a_1 through a_5 for both expressions are tabulated below:

| Coefficients | Equation 14-1 | Equation 14-2 |
|--------------|-----------------------------|-----------------------------|
| a_1 | 0.030517211 | 0.026936065 |
| a_2 | 0.4764700 | 0.41062853 |
| a_3 | 0.69469046 | 0.29560322 |
| a_4 | -1.8994762 | -1.4478797 |
| a_5 | $-4.1603083 \times 10^{-4}$ | $-3.0564771 \times 10^{-4}$ |

Example 14-1

An oil reservoir is being considered for further development by initiating a waterflooding project. The oil-water relative permeability data indicate that the residual oil saturation is 35%. It is projected that the initial gas saturation at the start of the flood is approximately 10%. Calculate the anticipated reduction in residual oil, ΔS_{or} , due to the presence of the initial gas at the start of the flood.

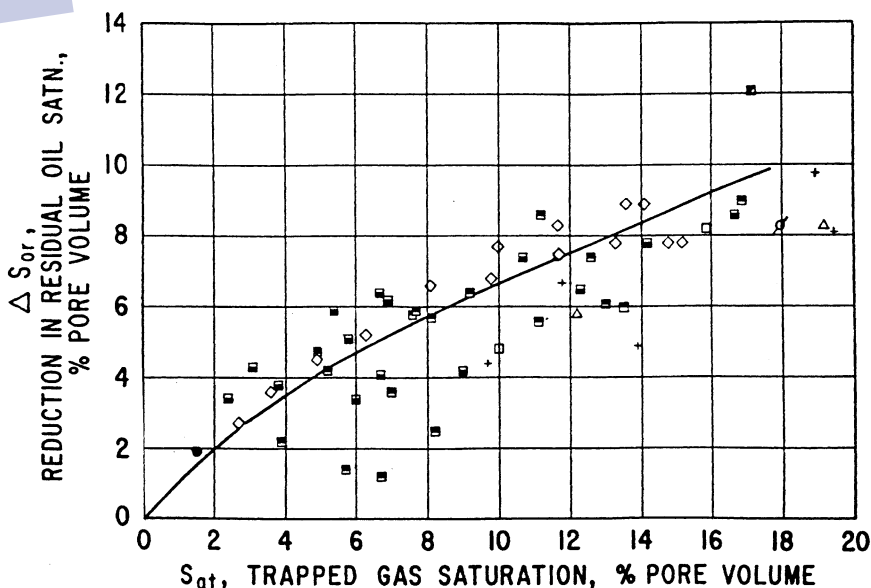


Figure 14-6. Effect of S_{gt} on waterflood recovery. (Permission to publish by the Society of Petroleum Engineers.)

Solution

Step 1. From Figure 14-5 or Equation 14-1, determine the trapped gas saturation, to give:

$$S_{gt} = 8\%$$

Step 2. Estimate the reduction in the residual oil saturation from Figure 14-6 or Equation 14-2, to give:

$$\Delta S_{or} = 5.7\%$$

Therefore, new residual oil saturation is:

$$S_{or} = 33\%$$

Khelil (1983) suggests that waterflood recovery can possibly be improved if a so-called “optimum gas saturation” is present at the start of the flood. This optimum gas saturation is given by:

$$(S_g)_{opt} = \frac{0.001867k^{0.634} B_o^{0.902}}{\left(\frac{S_o}{\mu_o}\right)^{0.352} \left(\frac{S_{wi}}{\mu_w}\right)^{0.166} \phi^{1.152}} \quad (14-3)$$

where $(S_g)_{opt}$ = optimum gas saturation, fraction
 S_o , S_{wi} = oil and initial water saturations, fraction
 μ_o , μ_w = oil and water viscosities, cp
 k = absolute permeability, md
 B_o = oil formation volume factor, bbl/STB
 ϕ = porosity, fraction

The above correlation is not explicit and must be used in conjunction with the *material balance equation* (MBE). The proposed methodology of determining $(S_g)_{opt}$ is based on calculating the gas saturation as a function of reservoir pressure (or time) by using both the MBE and Equation 14-3. When the gas saturation as calculated by the two equations is identical, this gas saturation is identified as $(S_g)_{opt}$.

Example 14-2

An absolute permeability of 33 md, porosity of 25%, and an initial water saturation of 30% characterize a saturated oil reservoir that exists at its bubble-point pressure of 1,925 psi. The water viscosity is treated as

a constant with a value of 0.6 cp. Results of the material balance calculations are given below:

| Pressure, psi | Bo, bbl/STB | μ_o , cp | S _o | S _g = 1 - S _o - S _{wi} |
|---------------|-------------|--------------|----------------|---|
| 1925 | 1.333 | 0.600 | 0.700 | 0.000 |
| 1760 | 1.287 | 0.625 | 0.628 | 0.072 |
| 1540 | 1.250 | 0.650 | 0.568 | 0.132 |
| 1342 | 1.221 | 0.700 | 0.527 | 0.173 |

Using the above data, calculate the optimum gas saturation.

Solution

| Pressure, psi | Bo, bbl/STB | μ_o , cp | MBE, S _o | S _g | Equation 14-3 (S _g) _{opt} |
|---------------|-------------|--------------|---------------------|----------------|---|
| 1925 | 1.333 | 0.600 | 0.700 | 0.000 | — |
| 1760 | 1.287 | 0.625 | 0.628 | 0.072 | 0.119 |
| 1540 | 1.250 | 0.650 | 0.568 | 0.132 | 0.122 |
| 1342 | 1.221 | 0.700 | 0.527 | 0.173 | |

The calculated value of (S_g)_{opt} at 1,540 psi agrees with the value of S_g as calculated from the MBE. Thus, to obtain the proposed additional recovery benefit, the primary depletion should be terminated at a pressure of 1,540 psi and water-injection initiated.

The injection into a solution gas-drive reservoir usually occurs at injection rates that cause repressurization of the reservoir. If pressure is high enough, the trapped gas will dissolve in the oil with no effect on subsequent residual oil saturations. It is of interest to estimate what pressure increases would be required in order to dissolve the trapped gas in the oil system. The pressure is essentially defined as the “new” bubble-point pressure (P_b^{new}). As the pressure increases to the new bubble-point pressure, the trapped gas will dissolve in the oil phase with a subsequent increase in the gas solubility from R_s to R_s^{new}. As illustrated in Figure 14-7, the new gas solubility can be estimated as the sum of the volumes of the dissolved gas and the trapped gas in the reservoir divided by the volume of stock-tank oil in the reservoir, or:

$$R_s^{\text{new}} = \frac{\left[\frac{(S_o)(\text{Pore volume})}{B_o} \right] R_s + \left[\frac{(S_{gt})(\text{Pore volume})}{B_g} \right]}{\frac{(S_o)(\text{Pore volume})}{B_o}}$$

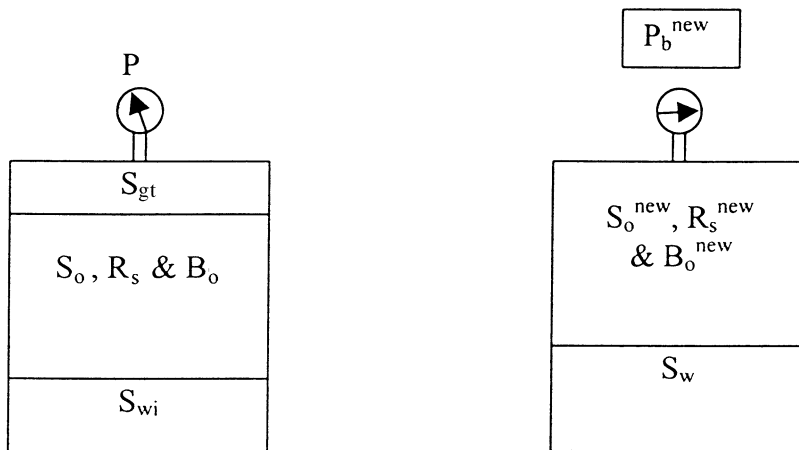


Figure 14-7. Variable bubble-point pressures.

Simplifying gives:

$$R_s^{\text{new}} = R_s + \left(\frac{S_{\text{gt}}}{S_o} \right) \left(\frac{B_o}{B_g} \right) \quad (14-4)$$

where R_s^{new} = gas solubility at the “new” bubble-point pressure, scf/STB

R_s = gas solubility at current pressure p , scf/STB

B_g = gas formation volume factor, bbl/scf

B_o = oil formation volume factor, bbl/STB

S_{gt} = trapped gas saturation

The pressure that corresponds to the new gas solubility (R_s^{new}) on the R_s vs. p relationship is then identified as the pressure at which the trapped gas will completely dissolve in the oil phase.

Example 14-3

The Big Butte Field is a solution gas-drive reservoir that is under consideration for a waterflood project. The volumetric calculations of the field indicate that the areal extent of the field is 1,612.6 acres. The field is characterized by the following properties:

| | |
|-----------------------------------|------------|
| Thickness h | = 25 ft |
| Porosity ϕ | = 15% |
| Initial water saturation S_{wi} | = 20% |
| Initial pressure p_i | = 2377 psi |

Results from the MBE in terms of cumulative oil production N_p as a function of reservoir pressure p are given below:

| Pressure, psi | N_p , MMSTB |
|---------------|---------------|
| 2377 | 0 |
| 2250 | 1.10 |
| 1950 | 1.76 |
| 1650 | 2.64 |
| 1350 | 3.3 |

The PVT properties of the crude oil system are tabulated below:

| Pressure, psi | B_o , bbl/STB | R_s , scf/STB | B_g , bbl/scf |
|---------------|-----------------|-----------------|-----------------|
| 2377 | 1.706 | 921 | — |
| 2250 | 1.678 | 872 | 0.00139 |
| 1950 | 1.555 | 761 | 0.00162 |
| 1650 | 1.501 | 657 | 0.00194 |
| 1350 | 1.448 | 561 | 0.00240 |
| 1050 | 1.395 | 467 | 0.00314 |
| 750 | 1.336 | 375 | 0.00448 |
| 450 | 1.279 | 274 | 0.00754 |

Assume that the waterflood will commence when the reservoir pressure declines to 1,650 psi; find the pressure that is required to dissolve the trapped gas.

Solution

Step 1. Calculate initial oil-in-place N :

$$N = 7758 A h \phi (1 - S_{wi})/B_{oi}$$

$$N = 7758 (1612.6) (25) (0.15) (1 - 0.2)/1.706 = 22 \text{ MMSTB}$$

Step 2. Calculate remaining oil saturation by applying Equation 12-5 at 1,650 psi:

$$S_o = (1 - S_{wi}) \left(1 - \frac{N_p}{N} \right) \left(\frac{B_o}{B_{oi}} \right)$$

$$S_o = (1 - 0.2) \left(1 - \frac{2.64}{22} \right) \left(\frac{1.501}{1.706} \right) = 0.619$$

Step 3. Calculate gas saturation at 1,650 psi:

$$S_g = 1 - S_o - S_{wi}$$

$$S_g = 1 - 0.619 - 0.2 = 0.181$$

Step 4. Calculate the trapped gas saturation from Figure 14-5 or Equation 14-1, to give:

$$S_{gt} = 12.6\%$$

Step 5. Calculate the gas solubility when all the trapped gas is dissolved in the oil by applying Equation 14-4:

$$R_s^{\text{new}} = 657 + \left(\frac{0.126}{0.619} \right) \left(\frac{1.501}{0.00194} \right) = 814 \text{ scf/STB}$$

Step 6. Enter the tabulated PVT data with the new gas solubility of 814 scf/STB and find the corresponding pressure of approximately 2,140 psi. This pressure is identified as the pressure that is required to dissolve the trapped gas.

SELECTION OF FLOODING PATTERNS

One of the first steps in designing a waterflooding project is flood pattern selection. The objective is to select the proper pattern that will provide the injection fluid with the maximum possible contact with the crude oil system. This selection can be achieved by (1) converting existing production wells into injectors or (2) drilling infill injection wells. When making the selection, the following factors must be considered:

- Reservoir heterogeneity and directional permeability
- Direction of formation fractures
- Availability of the injection fluid (gas or water)
- Desired and anticipated flood life
- Maximum oil recovery
- Well spacing, productivity, and injectivity

In general, the selection of a suitable flooding pattern for the reservoir depends on the number and location of existing wells. In some cases, producing wells can be converted to injection wells while in other cases it may be necessary or desirable to drill new injection wells. Essentially four types of well arrangements are used in fluid injection projects:

- Irregular injection patterns
- Peripheral injection patterns
- Regular injection patterns
- Crestal and basal injection patterns

Irregular Injection Patterns

Willhite (1986) points out that surface or subsurface topology and/or the use of slant-hole drilling techniques may result in production or injection wells that are not uniformly located. In these situations, the region affected by the injection well could be different for every injection well. Some small reservoirs are developed for primary production with a limited number of wells and when the economics are marginal, perhaps only a few production wells are converted into injectors in a nonuniform pattern. Faulting and localized variations in porosity or permeability may also lead to irregular patterns.

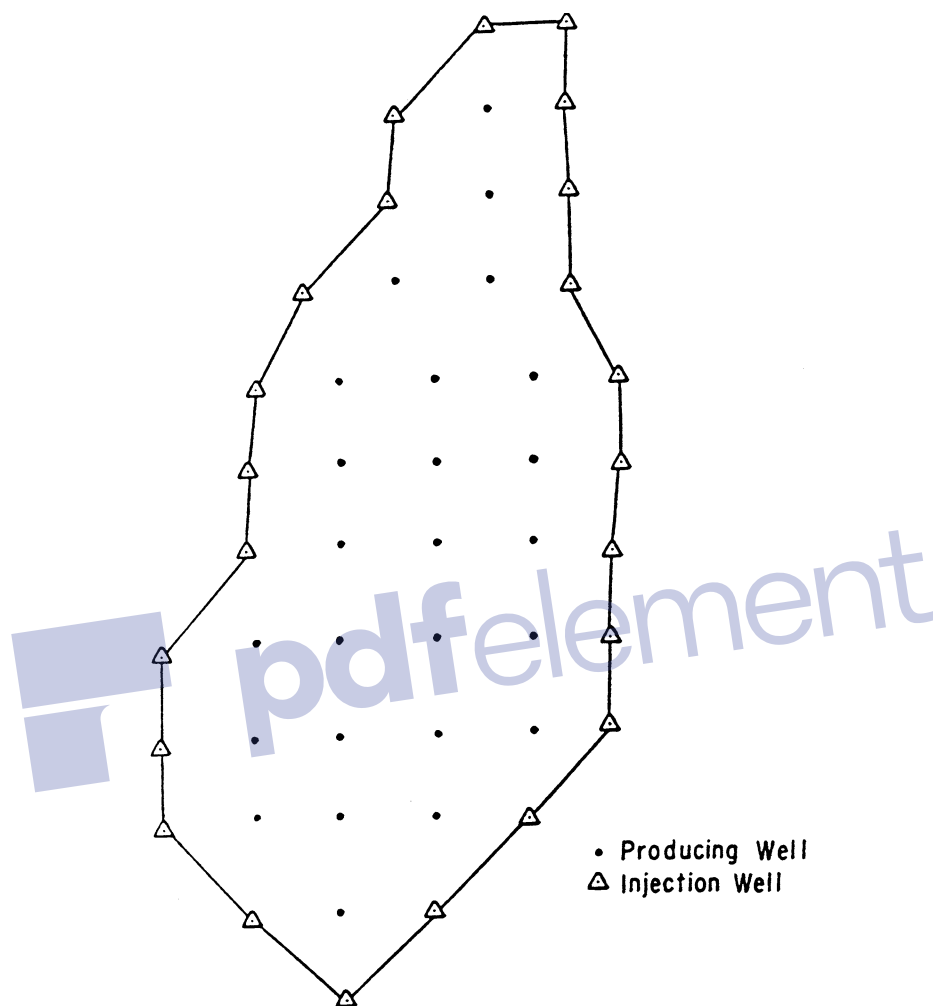


Figure 14-8. Typical peripheral waterflood. (After Cole, F., 1969.)

Peripheral Injection Patterns

In peripheral flooding, the injection wells are located at the external boundary of the reservoir and the oil is displaced toward the interior of the reservoir, as shown in Figure 14-8. Craig (1971), in an excellent review of the peripheral flood, points out the following main characteristics of the flood:

- The peripheral flood generally yields a maximum oil recovery with a minimum of produced water.
- The production of significant quantities of water can be delayed until only the last row of producers remains.
- Because of the unusually small number of injectors compared with the number of producers, it takes a long time for the injected water to fill up the reservoir gas space. The result is a delay in the field response to the flood.
- For a successful peripheral flood, the formation permeability must be large enough to permit the movement of the injected water at the desired rate over the distance of several well spacings from injection wells to the last line of producers.
- To keep injection wells as close as possible to the waterflood front without bypassing any movable oil, watered-out producers may be

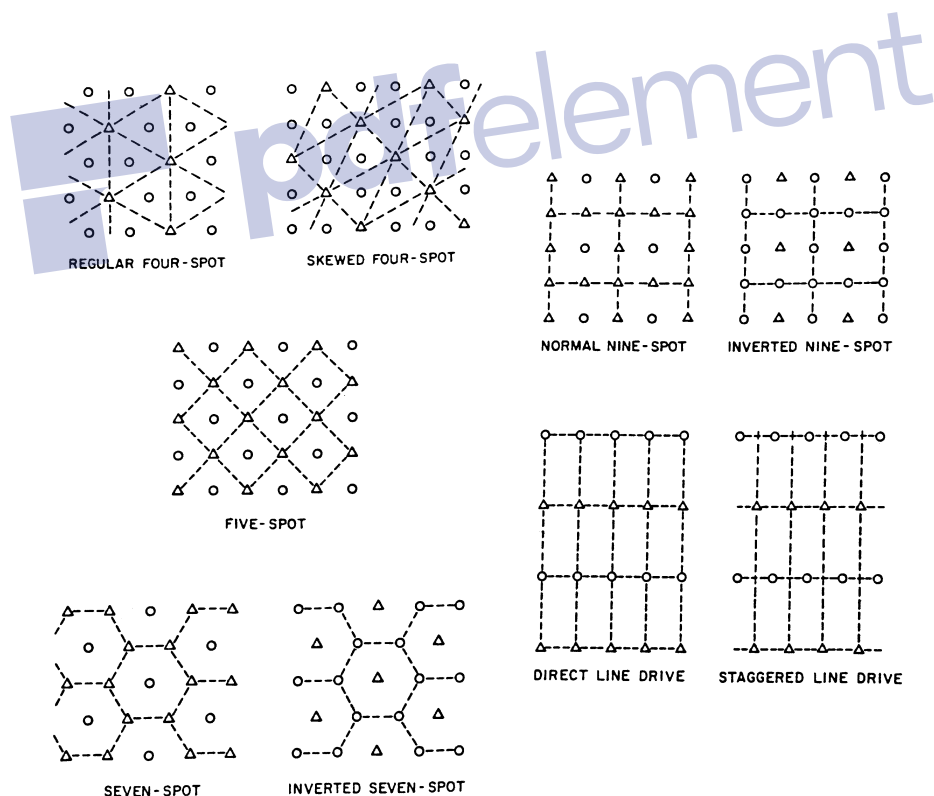


Figure 14-9. Flood patterns. (Permission to publish by the Society of Petroleum Engineers.)

converted into injectors. However, moving the location of injection wells frequently requires laying longer surface water lines and adding costs.

- Results from peripheral flooding are more difficult to predict. The displacing fluid tends to displace the oil bank past the inside producers, which are thus difficult to produce.
- Injection rates are generally a problem because the injection wells continue to push the water greater distances.

Regular Injection Patterns

Due to the fact that oil leases are divided into square miles and quarter square miles, fields are developed in a very regular pattern. A wide variety of injection-production well arrangements have been used in injection projects. The most common patterns, as shown in Figure 14-9, are the following:

- **Direct line drive.** The lines of injection and production are directly opposed to each other. The pattern is characterized by two parameters: a = distance between wells of the same type, and d = distance between lines of injectors and producers.
- **Staggered line drive.** The wells are in lines as in the direct line, but the injectors and producers are no longer directly opposed but laterally displaced by a distance of $a/2$.
- **Five spot.** This is a special case of the staggered line drive in which the distance between all like wells is constant, i.e., $a = 2d$. Any four injection wells thus form a square with a production well at the center.
- **Seven spot.** The injection wells are located at the corner of a hexagon with a production well at its center.
- **Nine spot.** This pattern is similar to that of the five spot but with an extra injection well drilled at the middle of each side of the square. The pattern essentially contains eight injectors surrounding one producer.

The patterns termed **inverted** have only one injection well per pattern. This is the difference between **normal** and **inverted** well arrangements. Note that the four-spot and inverted seven-spot patterns are identical.

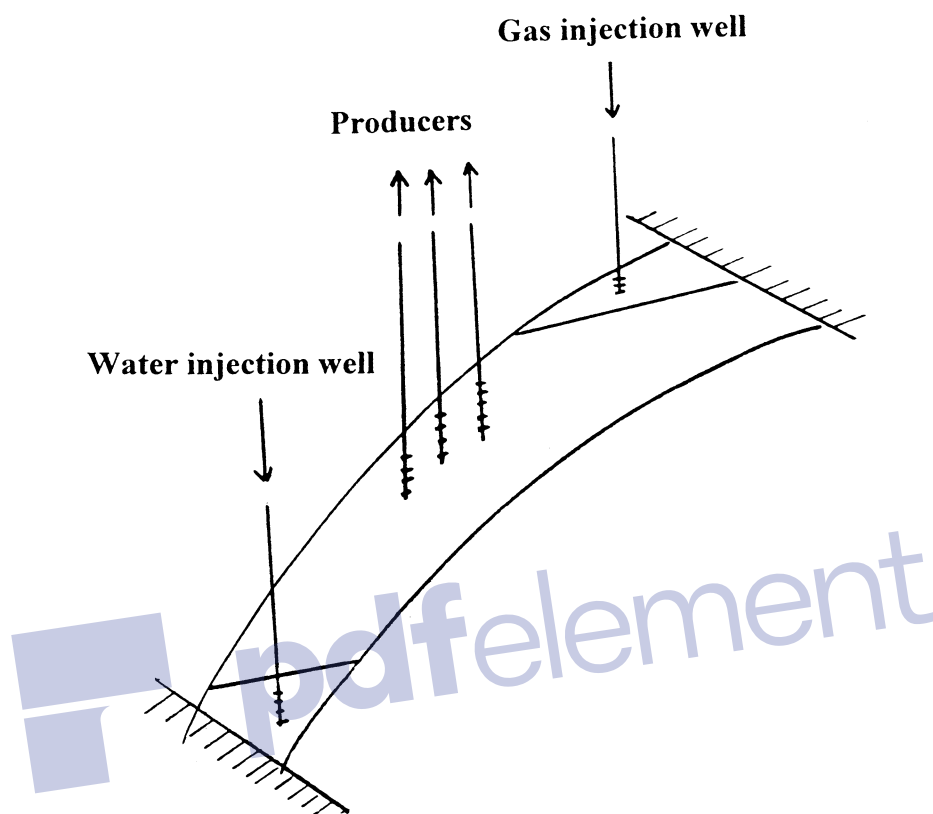


Figure 14-10. Well arrangements for dipping reservoirs.

Crestal and Basal Injection Patterns

In crestal injection, as the name implies, the injection is through wells located at the top of the structure. Gas injection projects typically use a crestal injection pattern. In basal injection, the fluid is injected at the bottom of the structure. Many water-injection projects use basal injection patterns with additional benefits being gained from gravity segregation. A schematic illustration of the two patterns is shown in Figure 14-10.

OVERALL RECOVERY EFFICIENCY

The overall recovery factor (efficiency) RF of any secondary or tertiary oil recovery method is the product of a combination of three individual efficiency factors as given by the following generalized expression:

$$RF = E_D E_A E_V \quad (14-5)$$

In terms of cumulative oil production, Equation 14-5 can be written as:

$$N_P = N_S E_D E_A E_V \quad (14-6)$$

where RF = overall recovery factor

N_S = initial oil-in-place at the start of the flood, STB

N_P = cumulative oil produced, STB

E_D = displacement efficiency

E_A = areal sweep efficiency

E_V = vertical sweep efficiency

The displacement efficiency E_D is the fraction of movable oil that has been displaced from the swept zone at any given time or pore volume injected. Because an immiscible gas injection or waterflood will always leave behind some residual oil, E_D will always be less than 1.0.

The areal sweep efficiency E_A is the fractional area of the pattern that is swept by the displacing fluid. The major factors determining areal sweep are:

- Fluid mobilities
- Pattern type
- Areal heterogeneity
- Total volume of fluid injected

The vertical sweep efficiency E_V is the fraction of the vertical section of the pay zone that is contacted by injected fluids. The vertical sweep efficiency is primarily a function of:

- Vertical heterogeneity
- Degree of gravity segregation
- Fluid mobilities
- Total volume injection

Note that the product of $E_A E_V$ is called the **volumetric sweep efficiency** and represents the overall fraction of the flood pattern that is contacted by the injected fluid.

In general, reservoir heterogeneity probably has more influence than any other factor on the performance of a secondary or tertiary injection project. The most important two types of heterogeneity affecting sweep efficiencies, E_A and E_V , are the reservoir vertical heterogeneity and areal heterogeneity.

- **Vertical heterogeneity** is by far the most significant parameter influencing the vertical sweep and in particular its degree of variation in the vertical direction. A reservoir may exhibit many different layers in the vertical section that have highly contrasting properties. This stratification can result from many factors, including change in depositional environment, change in depositional source, or particle segregation. Water injected into a stratified system will preferentially enter the layers of highest permeability and will move at a higher velocity. Consequently, at the time of water breakthrough in higher-permeability zones, a significant fraction of the less-permeable zones will remain unflooded. Although a flood will generally continue beyond breakthrough, the economic limit is often reached at an earlier time.
- **Areal heterogeneity** includes areal variation in formation properties (e.g., h , k , ϕ , S_{wc}), geometrical factors such as the position, any sealing nature of faults, and boundary conditions due to the presence of an aquifer or gas cap. Operators spend millions of dollars coring, logging, and listing appraisal wells, all of which permits direct observation of vertical heterogeneity. Therefore, if the data are interpreted correctly, it should be possible to quantify the vertical sweep, E_V , quite accurately. Areal, of course, matters are much more uncertain since methods of defining heterogeneity are indirect, such as attempting to locate faults from well testing analysis. Consequently, the areal sweep efficiency is to be regarded as the unknown in reservoir-development studies.

All three efficiency factors (i.e., E_D , E_A , and E_V) are variables that increase during the flood and reach maximum values at the economic limit of the injection project. Each of the three efficiency factors is discussed individually and methods of estimating these efficiencies are presented.

I. DISPLACEMENT EFFICIENCY

As defined previously, displacement efficiency is the fraction of movable oil that has been recovered from the swept zone at any given time. Mathematically, the displacement efficiency is expressed as:

$$E_D = \frac{\text{Volume of oil at start of flood} - \text{Remaining oil volume}}{\text{Volume of oil at start of flood}}$$

$$E_D = \frac{(\text{Pore volume})\left(\frac{S_{oi}}{B_{oi}}\right) - (\text{Pore volume})\left(\frac{\bar{S}_o}{B_o}\right)}{(\text{Pore volume})\left(\frac{S_{oi}}{B_{oi}}\right)}$$

or

$$E_D = \frac{\frac{S_{oi}}{B_{oi}} - \frac{\bar{S}_o}{B_o}}{\frac{S_{oi}}{B_{oi}}} \quad (14-7)$$

where S_{oi} = initial oil saturation at start of flood

B_{oi} = oil FVF at start of flood, bbl/STB

\bar{S}_o = average oil saturation in the flood pattern at a particular point during the flood

Assuming a constant oil formation volume factor during the flood life, Equation 14-7 is reduced to:

$$E_D = \frac{S_{oi} - \bar{S}_o}{S_{oi}} \quad (14-8)$$

where the initial oil saturation S_{oi} is given by:

$$S_{oi} = 1 - S_{wi} - S_{gi}$$

However, in the swept area, the gas saturation is considered zero, thus:

$$\bar{S}_o = 1 - \bar{S}_w$$

The displacement efficiency E_D can be expressed more conveniently in terms of water saturation by substituting the above relationships into Equation 14-8, to give:

$$E_D = \frac{\bar{S}_w - S_{wi} - S_{gi}}{1 - S_{wi} - S_{gi}} \quad (14-9)$$

where \bar{S}_w = average water saturation in the swept area

S_{gi} = initial gas saturation at the start of the flood

S_{wi} = initial water saturation at the start of the flood

If no initial gas is present at the start of the flood, Equation 14-9 is reduced to:

$$E_D = \frac{\bar{S}_w - S_{wi}}{1 - S_{wi}} \quad (14-10)$$

The displacement efficiency E_D will continually increase at different stages of the flood, i.e., with increasing \bar{S}_w . Equation 14-8 or 14-10 suggests that E_D reaches its maximum when the average oil saturation in the area of the flood pattern is reduced to the residual oil saturation S_{or} or, equivalently, when $\bar{S}_w = 1 - S_{or}$.

Example 14-4

A saturated oil reservoir is under consideration to be waterflooded immediately after drilling and completion. Core analysis tests indicate that the initial and residual oil saturations are 70% and 35%, respectively. Calculate the displacement efficiency when the oil saturation is reduced to 65%, 60%, 55%, 50%, and 35%. Assume that B_o will remain constant throughout the project life.

Solution

Step 1. Calculate initial water saturation:

$$S_{wi} = 1 - 0.7 = 0.3$$

Step 2. Calculate E_D from Equation 14-10:

$$E_D = \frac{\bar{S}_w - S_{wi}}{1 - S_{wi}}$$

| \bar{S}_o | $\bar{S}_w = 1 - \bar{S}_o$ | $E_D = \frac{\bar{S}_w - S_{wi}}{1 - S_{wi}}$ |
|-----------------|-----------------------------|---|
| 0.65 | 0.35 | 0.071 |
| 0.60 | 0.40 | 0.142 |
| 0.55 | 0.45 | 0.214 |
| 0.50 | 0.50 | 0.286 |
| $S_{or} = 0.35$ | 0.65 | 0.500 (maximum) |

Example 14-4 shows that E_D will continually increase with increasing water saturation in the reservoir. The problem, of course, lies with developing an approach for determining the increase in the average water saturation in the swept area as a function of cumulative water injected (or injection time). Buckley and Leverett (1942) developed a well-established theory, called the *frontal displacement theory*, which provides the basis for establishing such a relationship. This classic theory consists of two equations:

- Fractional flow equation
- Frontal advance equation

The frontal displacement theory and its main two components are discussed next.

Fractional Flow Equation

The development of the fractional flow equation is attributed to Leverett (1941). For two immiscible fluids, oil and water, the fractional flow of water, f_w (or any immiscible displacing fluid), is defined as the water flow rate divided by the total flow rate, or:

$$f_w = \frac{q_w}{q_t} = \frac{q_w}{q_w + q_o} \quad (14-11)$$

where f_w = fraction of water in the flowing stream, i.e., water cut, bbl/bbl
 q_t = total flow rate, bbl/day
 q_w = water flow rate, bbl/day
 q_o = oil flow rate, bbl/day

Consider the steady-state flow of two immiscible fluids (oil and water) through a tilted-linear porous media as shown in Figure 14-11. Assuming a homogeneous system, Darcy's equation can be applied for each of the fluids:

$$q_o = \frac{-k_o A}{\mu_o} \left[\frac{\partial P_o}{\partial x} + g \rho_o \sin(\alpha) \right] \quad (14-12)$$

$$q_w = \frac{-k_w A}{\mu_w} \left[\frac{\partial P_w}{\partial x} + g \rho_w \sin(\alpha) \right] \quad (14-13)$$

where subscripts o, w = oil and water

k_o, k_w = effective permeability

μ_o, μ_w = viscosity

p_o, p_w = pressure

ρ_o, ρ_w = density

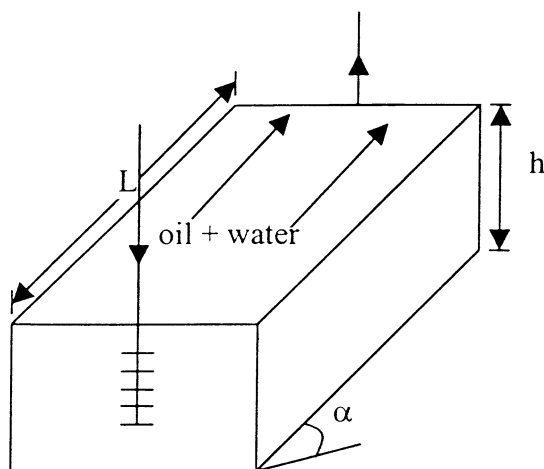


Figure 14-11. Linear displacement in a tilted system.

A = cross-sectional area

x = distance

α = dip angle

$\sin(\alpha)$ = **positive** for updip flow and
negative for downdip flow

Rearranging Equations 14-12 and 14-13 gives:

$$\frac{q_o \mu_o}{Ak_o} = -\frac{\partial p_o}{\partial x} - g \rho_o \sin(\alpha)$$

$$\frac{q_w \mu_w}{Ak_w} = -\frac{\partial p_w}{\partial x} - g \rho_w \sin(\alpha)$$

Subtracting the above two equations yields:

$$\frac{q_w \mu_w}{Ak_w} - \frac{q_o \mu_{ow}}{Ak_o} = \left(\frac{\partial p_o}{\partial x} - \frac{\partial p_w}{\partial x} \right) - g(\rho_w - \rho_o) \sin \alpha \quad (14-14)$$

From the definition of the capillary pressure p_c :

$$P_c = p_o - p_w$$

Differentiating the above expression with respect to the distance x gives:

$$\frac{\partial p_c}{\partial x} = \frac{\partial p_o}{\partial x} - \frac{\partial p_w}{\partial x} \quad (14-15)$$

Combining Equation 14-15 with 14-16 gives:

$$\frac{q_w \mu_w}{Ak_w} - \frac{q_o \mu_o}{Ak_o} = \frac{\partial p_c}{\partial x} - g \Delta \rho \sin(\alpha) \quad (14-16)$$

where $\Delta \rho = \rho_w - \rho_o$. From the water cut equation, i.e., Equation 14-11:

$$q_w = f_w q_t \text{ and } q_o = (1 - f_w) q_t \quad (14-17)$$

Replacing q_o and q_w in Equation 14-16 with those of Equation 14-17 gives:

$$f_w = \frac{1 + \left(\frac{k_o A}{\mu_o q_t} \right) \left[\frac{\partial p_c}{\partial x} - g \Delta \rho \sin(\alpha) \right]}{1 + \frac{k_o \mu_w}{k_w \mu_o}}$$

In field units, the above equation can be expressed as:

$$f_w = \frac{1 + \left(\frac{0.001127 k_o A}{\mu_o q_t} \right) \left[\frac{\partial p_c}{\partial x} - 0.433 \Delta \rho \sin(\alpha) \right]}{1 + \frac{k_o \mu_w}{k_w \mu_o}} \quad (14-18)$$

where f_w = fraction of water (water cut), bbl/bbl

k_o = effective permeability of oil, md

k_w = effective permeability of water, md

$\Delta \rho$ = water-oil density differences, g/cm³

k_w = effective permeability of water, md

q_t = total flow rate, bbl/day

μ_o = oil viscosity, cp

μ_w = water viscosity, cp

A = cross-sectional area, ft²

Noting that the relative permeability ratios $k_{ro}/k_{rw} = k_o/k_w$ and, for two-phase flow, the total flow rate q_t are essentially equal to the water-injection rate, i.e., $i_w = q_t$, Equation 14-18 can be expressed more conveniently in terms of k_{ro}/k_{rw} and i_w as:

$$f_w = \frac{1 + \left(\frac{0.001127 (k k_{ro}) A}{\mu_o i_w} \right) \left[\frac{\partial p_c}{\partial x} - 0.433 \Delta \rho \sin(\alpha) \right]}{1 + \frac{k_{ro} \mu_w}{k_{rw} \mu_o}} \quad (14-19)$$

where i_w = water-injection rate, bbl/day
 f_w = water cut, bbl/bbl
 k_{ro} = relative permeability to oil
 k_{rw} = relative permeability to water
 k = absolute permeability, md

The fractional flow equation as expressed by the above relationship suggests that for a given rock-fluid system, all the terms in the equation are defined by the characteristics of the reservoir, except:

- water-injection rate, i_w
- water viscosity, μ_w
- direction of the flow, i.e., updip or downdip injection

Equation 14-19 can be expressed in a more generalized form to describe the fractional flow of any displacement fluid as:

$$f_D = \frac{1 + \left(\frac{0.001127(kk_{rD})A}{\mu_o i_D} \right) \left[\frac{\partial p_c}{\partial x} - 0.433 \Delta \rho \sin(\alpha) \right]}{1 + \frac{k_{ro} \mu_D}{k_{rD} \mu_o}} \quad (14-20)$$

where the subscript D refers to the displacement fluid and $\Delta \rho$ is defined as:

$$\Delta \rho = \rho_D - \rho_o$$

For example, when the displacing fluid is immiscible gas, then:

$$f_g = \frac{1 + \left(\frac{0.001127(kk_{rg})A}{\mu_o i_g} \right) \left[\frac{\partial p_c}{\partial x} - 0.433(\rho_g - \rho_o) \sin(\alpha) \right]}{1 + \frac{k_{ro} \mu_g}{k_{rg} \mu_o}} \quad (14-21)$$

The effect of capillary pressure is usually neglected because the capillary pressure gradient is generally small and, thus, Equations 14-19 and 14-21 are reduced to:

$$f_w = \frac{1 - \left(\frac{0.001127(kk_{ro})A}{\mu_o i_w} \right) [0.433(\rho_w - \rho_o) \sin(\alpha)]}{1 + \frac{k_{ro} \mu_w}{k_{rw} \mu_o}} \quad (14-22)$$

and

$$f_g = \frac{1 - \left(\frac{0.001127(kk_{ro})A}{\mu_o i_g} \right) [0.433(\rho_g - \rho_o) \sin(\alpha)]}{1 + \frac{k_{ro} \mu_g}{k_{rg} \mu_o}}$$

where i_g = gas injection rate, bbl/day

μ_g = gas viscosity, cp

ρ_g = gas density, g/cm³

From the definition of water cut, i.e., $f_w = q_w/(q_w + q_o)$, we can see that the limits of the water cut are 0% and 100%. At the irreducible (connate) water saturation, the water flow rate q_w is zero and, therefore, the water cut is 0%. At the residual oil saturation point, S_{or} , the oil flow rate is zero and the water cut reaches its upper limit of 100%. The shape of the water cut versus water saturation curve is characteristically S-shaped, as shown in Figure 14-12. The limits of the f_w curve (0 and 1) are defined by the end points of the relative permeability curves.

The implications of the above discussion are also applied to defining the relationship that exists between f_g and gas saturation, as shown in Figure 14-12.

Note that, in general, any influences that cause the fractional flow curve to shift upward (i.e., increase in f_w or f_g) will result in a *less efficient displacement* process. It is essential, therefore, to determine the effect of various component parts of the fractional flow equation on the displacement efficiency. Note that for any two immiscible fluids, e.g., water and oil, the fraction of the oil (oil cut) f_o flowing at any point in the reservoir is given by:

$$f_o + f_w = 1 \quad \text{or} \quad f_o = 1 - f_w$$

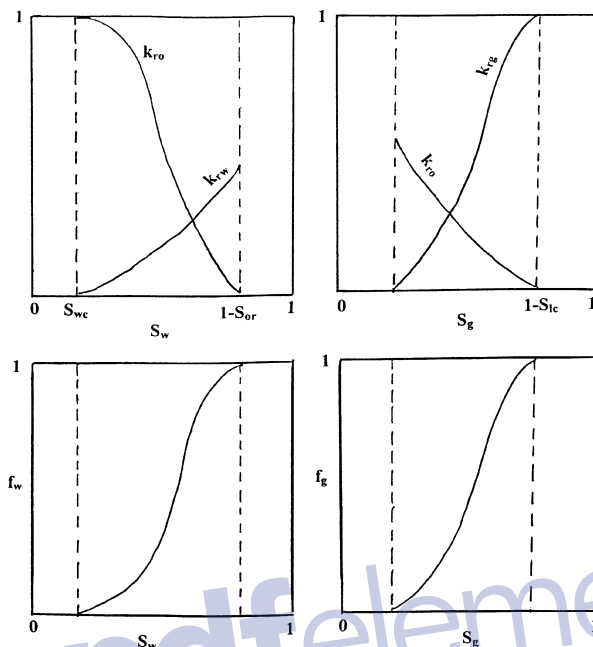


Figure 14-12. Fractional flow curves a function of saturations.

The above expression indicates that during the displacement of oil by waterflood, an **increase in f_w** at any point in the reservoir will cause a proportional **decrease in f_o and oil mobility**. Therefore, the objective is to select the proper injection scheme that could possibly reduce the water fractional flow. This can be achieved by investigating the effect of the injected water viscosity, formation dip angle, and water-injection rate on the water cut. The overall effect of these parameters on the water fractional flow curve are discussed next.

Effect of Water and Oil Viscosities

Figure 14-13 shows the general effect of oil viscosity on the fractional flow curve for both water-wet and oil-wet rock systems. This illustration reveals that regardless of the system wettability, a higher oil viscosity results in an upward shift (an increase) in the fractional flow curve. The apparent effect of the water viscosity on the water fractional flow is clearly indicated by examining Equation 14-22. Higher injected water viscosities will result in an increase in the value of the

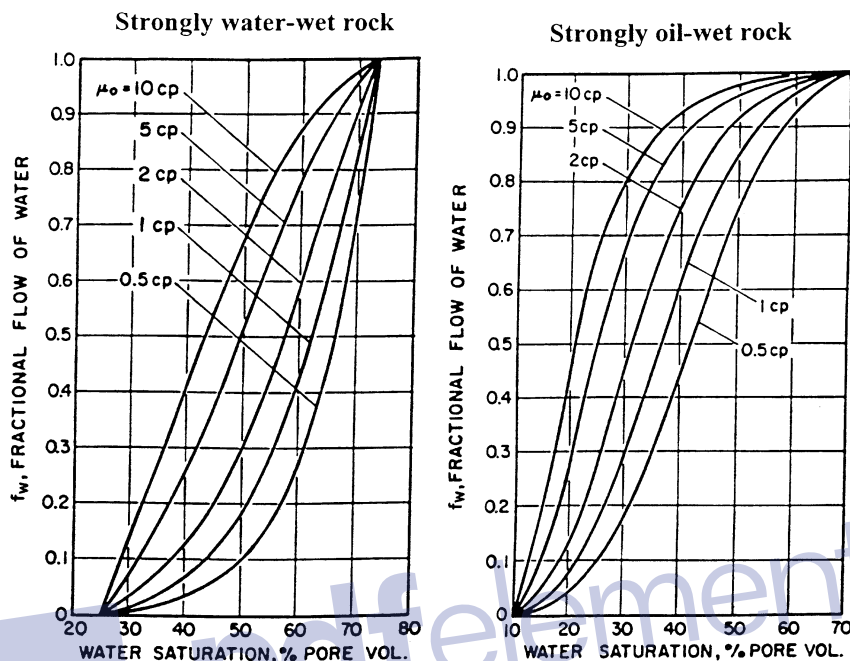


Figure 14-13. Effect of oil viscosity on f_w .

denominator of Equation 14-22 with an overall reduction in f_w (i.e., a downward shift).

Effect of Dip Angle and Injection Rate

To study the effect of the formation dip angle α and the injection rate on the displacement efficiency, consider the water fractional flow equation as represented by Equation 14-22. Assuming a constant injection rate and realizing that $(\rho_w - \rho_o)$ is always positive and in order to isolate the effect of the dip angle and injection rate on f_w , Equation 14-22 is expressed in the following simplified form:

$$f_w = \frac{1 - \left[X \frac{\sin(\alpha)}{i_w} \right]}{1 + Y} \quad (14-23)$$

where the variables X and Y are a collection of different terms that are all considered positives and given by:

$$X = \frac{(0.001127)(0.433)(k k_{ro})A(\rho_w - \rho_o)}{\mu_o}$$

$$Y = \frac{k_{ro} \mu_w}{k_{rw} \mu_o}$$

- Updip flow, i.e., $\sin(\alpha)$ is positive. Figure 14-14 shows that when the water displaces oil *updip* (i.e., injection well is located *down*dip), a more efficient performance is obtained. This improvement is due to the fact that the term $X \sin(\alpha)/i_w$ will always remain positive, which leads

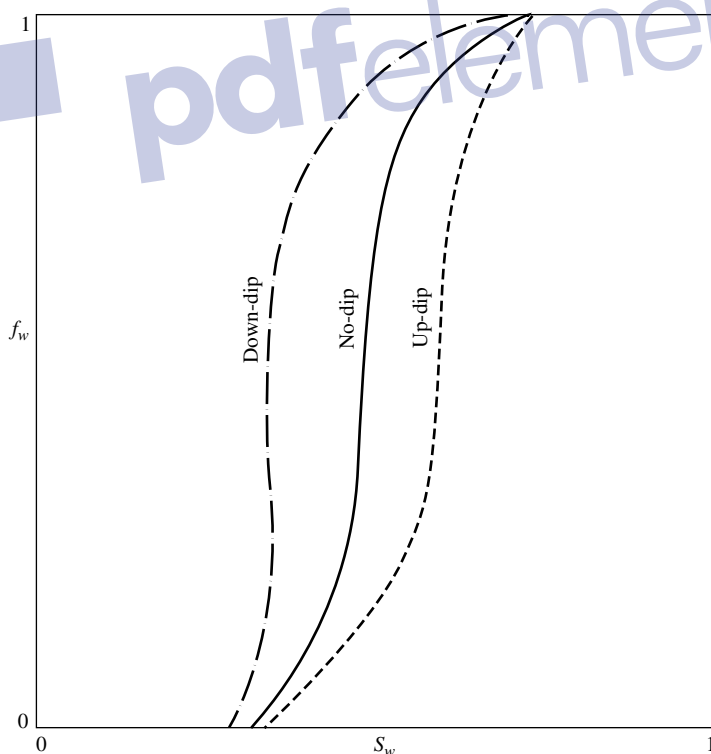


Figure 14-14. Effect of dip angle on f_w .

to a decrease (downward shift) in the f_w curve. Equation 14-23 also reveals that a *lower water-injection rate* i_w is desirable since the numerator $1 - [X \sin(\alpha)/i_w]$ of Equation 14-23 will decrease with a lower injection rate i_w , resulting in an overall downward shift in the f_w curve.

- Downdip flow, i.e., $\sin(\alpha)$ is negative. When the oil is displaced *downdip* (i.e., injection well is located updip), the term $X \sin(\alpha)/i_w$ will always remain negative and, therefore, the numerator of Equation 14-23 will be $1 + [X \sin(\alpha)/i_w]$, i.e.:

$$f_w = \frac{1 + \left[X \frac{\sin(\alpha)}{i_w} \right]}{1 + Y}$$

which causes an increase (upward shift) in the f_w curve. It is beneficial, therefore, when injection wells are located at the top of the structure to inject the water at a higher injection rate to improve the displacement efficiency.

It is interesting to reexamine Equation 14-23 when displacing the oil *downdip*. Combining the product $X \sin(\alpha)$ as C , Equation 14-23 can be written:

$$f_w = \frac{1 + \left(\frac{C}{i_w} \right)}{1 + Y}$$

The above expression shows that the possibility exists that the water cut f_w could reach a value greater than unity ($f_w > 1$) if:

$$\frac{C}{i_w} > Y$$

This could only occur when displacing the oil *downdip* at a low water-injection rate i_w . The resulting effect of this possibility is called a **counterflow**, where the oil phase is moving in a direction opposite to that of the water (i.e., oil is moving upward and the water downward). When the water-injection wells are located at the top of a tilted formation, the injection rate must be high to avoid oil migration to the top of the formation.

Note that for a horizontal reservoir, i.e., $\sin(\alpha) = 0$, the injection rate has no effect on the fractional flow curve. When the dip angle α is zero, Equation 14-22 is reduced to the following simplified form:

$$f_w = \frac{1}{1 + \left(\frac{k_{ro} \mu_w}{k_{rw} \mu_o} \right)} \quad (14-24)$$

In waterflooding calculations, the reservoir water cut f_w and the water-oil ratio WOR are both traditionally expressed in two different units: bbl/bbl and STB/STB. The interrelationships that exist between these two parameters are conveniently presented below, where

Q_o = oil flow rate, STB/day

q_o = oil flow rate, bbl/day

Q_w = water flow rate, STB/day

q_w = water flow rate, bbl/day

WOR_s = surface water-oil ratio, STB/STB

WOR_r = reservoir water-oil ratio, bbl/bbl

f_{ws} = surface water cut, STB/STB

f_w = reservoir water cut, bbl/bbl

i) Reservoir f_w – Reservoir WOR_r Relationship

$$f_w = \frac{q_w}{q_w + q_o} = \frac{\left(\frac{q_w}{q_o} \right)}{\left(\frac{q_w}{q_o} \right) + 1}$$

Substituting for WOR gives:

$$f_w = \frac{WOR_r}{WOR_r + 1} \quad (14-25)$$

Solving for WOR_r gives:

$$WOR_r = \frac{1}{\frac{1}{f_w} - 1} = \frac{f_w}{1 - f_w} \quad (14-26)$$

ii) Reservoir f_w – Surface WOR_s Relationship

By definition:

$$f_w = \frac{q_w}{q_w + q_o} = \frac{Q_w B_w}{Q_w B_w + Q_o B_o} = \frac{\left(\frac{Q_w}{Q_o}\right) B_w}{\left(\frac{Q_w}{Q_o}\right) B_w + B_o}$$

Introducing the surface WOR_s into the above expression gives:

$$f_w = \frac{B_w WOR_s}{B_w WOR_s + B_o} \quad (14-27)$$

Solving for WOR_s yields:

$$WOR_s = \frac{B_o}{B_w \left(\frac{1}{f_w} - 1\right)} = \frac{B_o f_w}{B_w (1 - f_w)} \quad (14-28)$$

iii) Reservoir WOR_r – Surface WOR_s Relationship

From the definition of WOR :

$$WOR_r = \frac{q_w}{q_o} = \frac{Q_w B_w}{Q_o B_o} = \frac{\left(\frac{Q_w}{Q_o}\right) B_w}{B_o}$$

Introducing the surface WOR_s into the above expression gives:

$$WOR_r = (WOR)_s \left(\frac{B_w}{B_o}\right) \quad (14-29)$$

or

$$WOR_s = (WOR)_r \left(\frac{B_o}{B_w}\right)$$

iv) Surface f_{ws} – Surface WOR_s Relationship

$$f_{ws} = \frac{Q_w}{Q_w + Q_o} = \frac{\left(\frac{Q_w}{Q_o}\right)}{\left(\frac{Q_w}{Q_o}\right) + 1}$$

or

$$f_{ws} = \frac{WOR_s}{WOR_s + 1} \quad (14-30)$$

v) Surface f_{ws} – Reservoir f_w Relationship

$$f_{ws} = \frac{B_o}{B_w \left(\frac{1}{f_w} - 1\right) + B_o} \quad (14-31)$$

Example 14-5

Use the relative permeability as shown in Figure 14-15 to plot the fractional flow curve for a linear reservoir system with the following properties:

| | | | |
|-----------|-------------------------|------------------------|---------------------------|
| Dip angle | = 0 | Absolute permeability | = 50 md |
| B_o | = 1.20 bbl/STB | B_w | = 1.05 bbl/STB |
| ρ_o | = 45 lb/ft ³ | ρ_w | = 64.0 lb/ft ³ |
| μ_w | = 0.5 cp | Cross-sectional area A | = 25,000 ft ² |

Perform the calculations for the following values of oil viscosity: $\mu_o = 0.5$, 1.0, 5, and 10 cp.

Solution

For a horizontal system, Equation 14-24 can be used to calculate f_w as a function of saturation.

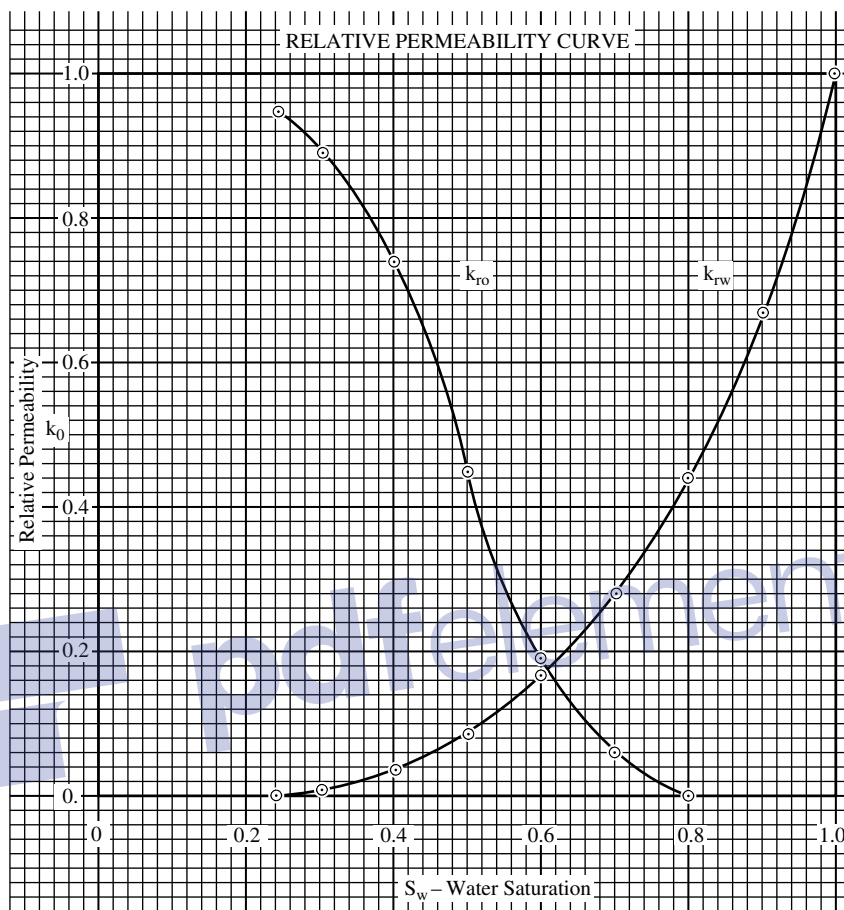


Figure 14-15. Relative permeability curves for Example 14-5.

$$f_w = \frac{1}{1 + \frac{k_{ro} \mu_w}{k_{rw} \mu_o}}$$

| S_w | k_{ro} | k_{rw} | k_{ro}/k_{rw} | f_w | | | |
|-------|----------|----------|-----------------|-------------|-------------|-----------|------------|
| | | | | $\mu_o=0.5$ | $\mu_o=1.0$ | $\mu_o=5$ | $\mu_o=10$ |
| 0.24 | 0.95 | 0.00 | 00 | 0 | 0 | 0 | 0 |
| 0.30 | 0.89 | 0.01 | 89.0 | 0.011 | 0.022 | 0.101 | 0.183 |
| 0.40 | 0.74 | 0.04 | 18.5 | 0.051 | 0.098 | 0.351 | 0.519 |
| 0.50 | 0.45 | 0.09 | 5.0 | 0.17 | 0.286 | 0.667 | 0.800 |
| 0.60 | 0.19 | 0.17 | 1.12 | 0.47 | 0.641 | 0.899 | 0.947 |
| 0.65 | 0.12 | 0.28 | 0.43 | 0.70 | 0.823 | 0.459 | 0.979 |
| 0.70 | 0.06 | 0.22 | 0.27 | 0.79 | 0.881 | 0.974 | 0.987 |
| 0.75 | 0.03 | 0.36 | 0.08 | 0.93 | 0.962 | 0.992 | 0.996 |
| 0.78 | 0.00 | 0.41 | 0 | 1.00 | 1.000 | 1.000 | 1.000 |

Results of the above example are documented graphically in Figure 14-16, which shows the apparent effect of oil viscosity on the fractional flow curve.

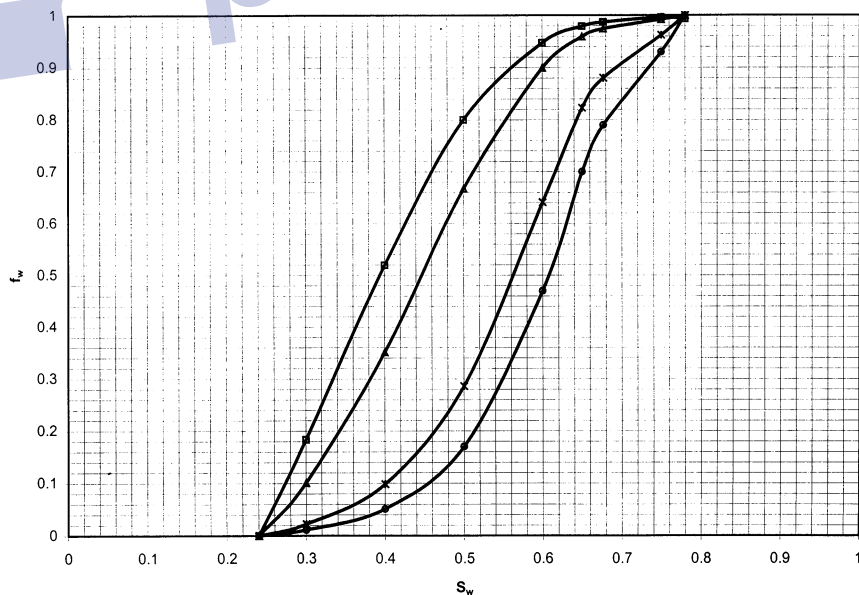


Figure 14-16. Effect of μ_o on f_w .

Example 14-6

The linear system in Example 14-5 is under consideration for a waterflooding project with a water-injection rate of 1,000 bbl/day. The oil viscosity is considered constant at 1.0 cp. Calculate the fractional flow curve for the reservoir dip angles of 10, 20, and 30°, assuming (a) updip displacement and (b) downdip displacement.

Solution

Step 1. Calculate the density difference ($\rho_w - \rho_o$) in g/cm³:

$$(\rho_w - \rho_o) = (64 - 45) / 62.4 = 0.304 \text{ g/cm}^3$$

Step 2. Simplify Equation 14-22 by using the given fixed data:

$$f_w = \frac{1 - \frac{0.001127(50k_{ro})(25,000)}{(1)(1000)} [0.433(0.304) \sin(\alpha)]}{1 + \left(\frac{0.5}{1}\right) \left(\frac{k_{ro}}{k_{rw}}\right)}$$

$$f_w = \frac{1 - 0.185 k_{ro} [\sin(\alpha)]}{1 + 0.5 \left(\frac{k_{ro}}{k_{rw}}\right)}$$

For updip displacement, **sin(α) is positive**, therefore:

$$f_w = \frac{1 - 0.185 k_{ro} \sin(\alpha)}{1 + 0.5 \left(\frac{k_{ro}}{k_{rw}}\right)}$$

For downdip displacement, **sin(α) is negative**, therefore:

$$f_w = \frac{1 + 0.185 k_{ro} \sin(\alpha)}{1 + 0.5 \left(\frac{k_{ro}}{k_{rw}}\right)}$$

Step 3. Perform the fractional flow calculations in the following tabulated form:

| S_w | k_{ro} | k_{ro}/k_{rw} | f_w , Updip Displacement | | | f_w , Downdip Displacement | | |
|-------|----------|-----------------|----------------------------|-------|-------|------------------------------|-------|-------|
| | | | 10° | 20° | 30° | 10° | 20° | 30° |
| 0.24 | 0.95 | 00 | 0 | 0 | 0 | 0 | 0 | 0 |
| 0.30 | 0.89 | 89 | 0.021 | 0.021 | 0.020 | 0.023 | 0.023 | 0.024 |
| 0.40 | 0.74 | 18.5 | 0.095 | 0.093 | 0.091 | 0.100 | 0.102 | 0.104 |
| 0.50 | 0.45 | 5.0 | 0.282 | 0.278 | 0.274 | 0.290 | 0.294 | 0.298 |
| 0.60 | 0.19 | 1.12 | 0.637 | 0.633 | 0.630 | 0.645 | 0.649 | 0.652 |
| 0.65 | 0.12 | 0.43 | 0.820 | 0.817 | 0.814 | 0.826 | 0.830 | 0.832 |
| 0.70 | 0.06 | 0.27 | 0.879 | 0.878 | 0.876 | 0.883 | 0.884 | 0.886 |
| 0.75 | 0.03 | 0.08 | 0.961 | 0.960 | 0.959 | 0.962 | 0.963 | 0.964 |
| 0.78 | 0.00 | 0 | 1.000 | 1.000 | 1.000 | 1.000 | 1.000 | 1.000 |

The fractional flow equation, as discussed in the previous section, is used to determine the water cut f_w at any point in the reservoir, assuming that the water saturation at the point is known. The question, however, is how to determine the water saturation at this particular point. The answer is to use the **frontal advance equation**. The frontal advance equation is designed to determine the water saturation profile in the reservoir at any give time during water-injection.

Frontal Advance Equation

Buckley and Leverett (1942) presented what is recognized as the basic equation for describing two-phase, immiscible displacement in a linear system. The equation is derived based on developing a material balance for the displacing fluid as it flows through any given element in the porous media:

$$\begin{aligned} \text{Volume entering the element} - \text{Volume leaving the element} \\ = \text{change in fluid volume} \end{aligned}$$

Consider a differential element of porous media, as shown in Figure 14-17, having a differential length dx , an area A , and a porosity ϕ . During a differential time period dt , the total volume of water entering the element is given by:

$$\text{Volume of water entering the element} = q_t f_w dt$$

The volume of water leaving the element has a differentially smaller water cut ($f_w - df_w$) and is given by:

$$\text{Volume of water leaving the element} = q_t (f_w - df_w) dt$$

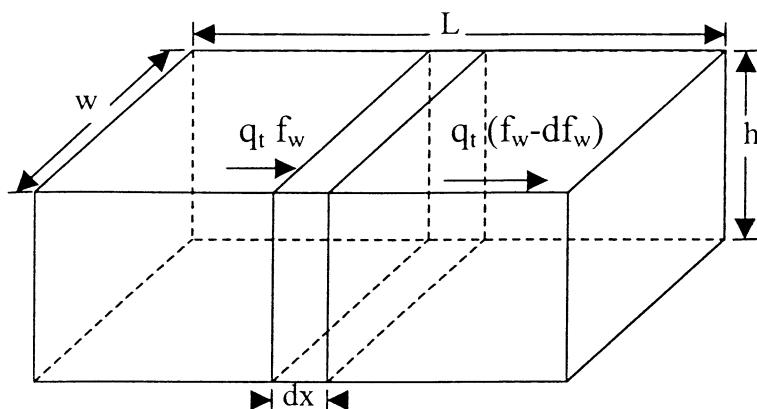


Figure 14-17. Water flow through a linear differential element.

Subtracting the above two expressions gives the accumulation of the water volume within the element in terms of the differential changes of the saturation df_w :

$$q_t f_w dt - q_t (f_w - df_w) dt = A \phi (dx) (dS_w) / 5.615$$

Simplifying:

$$q_t df_w dt = A \phi (dx) (dS_w) / 5.615$$

Separating the variables gives:

$$\left(\frac{dx}{dt} \right)_{S_w} = (v)_{S_w} = \left(\frac{5.615 q_t}{\phi A} \right) \left(\frac{df_w}{dS_w} \right)_{S_w} \quad (14-32)$$

where $(v)_{S_w}$ = velocity of any specified value of S_w , ft/day

A = cross-sectional area, ft^2

q_t = total flow rate (oil + water), bbl/day

$(df_w/dS_w)_{S_w}$ = slope of the f_w vs. S_w curve at S_w

The above relationship suggests that the velocity of any specific water saturation S_w is directly proportional to the value of the slope of the f_w vs. S_w curve, evaluated at S_w . Note that for two-phase flow, the total flow rate q_t is essentially equal to the injection rate i_w , or:

$$\left(\frac{dx}{dt} \right)_{S_w} = (v)_{S_w} = \left(\frac{5.615 i_w}{\phi A} \right) \left(\frac{df_w}{dS_w} \right)_{S_w} \quad (14-33)$$

where i_w = water-injection rate, bbl/day.

To calculate the total distance any specified water saturation will travel during a total time t , Equation 14-33 must be integrated:

$$\int_0^x dx = \left(\frac{5.615i_w}{\phi A} \right) \left(\frac{df_w}{dS_w} \right) \int_0^t dt$$

or

$$(x)_{S_w} = \left(\frac{5.615i_w t}{\phi A} \right) \left(\frac{df_w}{dS_w} \right) \quad (14-34)$$

Equation 14-34 can also be expressed in terms of total volume of water injected by recognizing that under a constant water-injection rate, the cumulative water injected is given by:

$$W_{inj} = t i_w$$

or

$$(x)_{S_w} = \frac{5.615W_{inj}}{\phi A} \left(\frac{df_w}{dS_w} \right)_{S_w} \quad (14-35)$$

where i_w = water-injection rate, bbl/day

W_{inj} = cumulative water injected, bbl

t = time, day

$(x)_{S_w}$ = distance from the injection for any given saturation S_w , ft

Equation 14-35 also suggests that the position of any value of water saturation S_w at given cumulative water injected W_{inj} is proportional to the slope (df_w/dS_w) for this particular S_w . At any given time t , the water saturation profile can be plotted by simply determining the slope of the f_w curve at each selected saturation and calculating the position of S_w from Equation 14-35.

Figure 14-18 shows the typical S shape of the f_w curve and its derivative curve. However, a mathematical difficulty arises when using the derivative curve to construct the water saturation profile at any given time. Suppose we want to calculate the positions of two different saturations (shown in Figure 14-18 as saturations A and B) after W_{inj} barrels of water have been injected in the reservoir. Applying Equation 14-35 gives:

$$(x)_A = \frac{5.615W_{inj}}{\phi A} \left(\frac{df_w}{dS_w} \right)_A$$

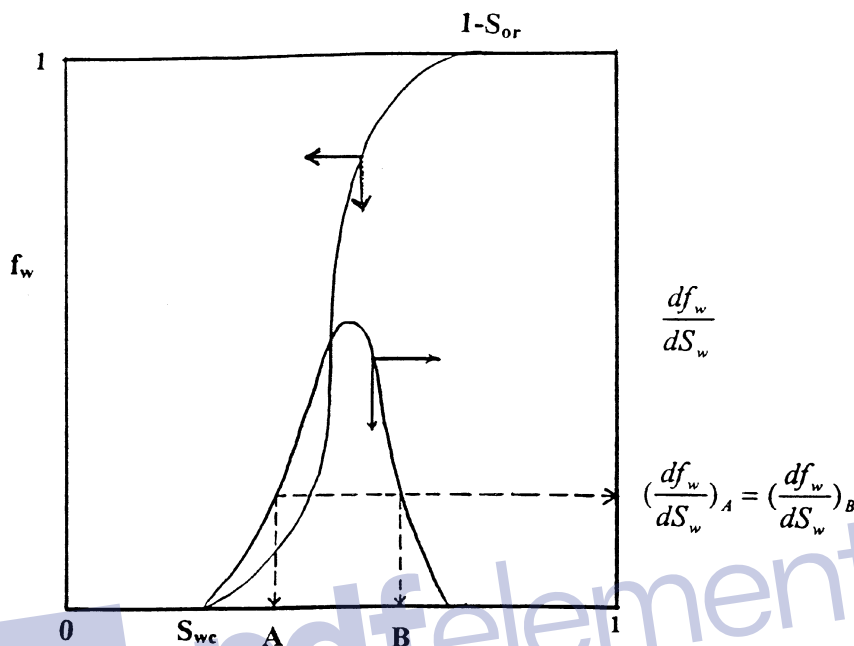


Figure 14-18. The f_w curve with its saturation derivative curve.

$$(x)_B = \frac{5.615W_{inj}}{\phi A} \left(\frac{df_w}{dS_w} \right)_B$$

Figure 14-18 indicates that both derivatives are identical, i.e., $(df_w/dS_w)_A = (df_w/dS_w)_B$, which implies that multiple water saturations can coexist at the same position—but this is physically impossible. Buckley and Leverett (1942) recognized the physical impossibility of such a condition. They pointed out that this apparent problem is due to the neglect of the capillary pressure gradient term in the fractional flow equation. This capillary term is given by:

$$\text{Capillary term} = \left(\frac{0.001127k_o A}{\mu_o i_w} \right) \left(\frac{dP_c}{dx} \right)$$

Including the above capillary term when constructing the fractional flow curve would produce a graphical relationship that is characterized by the following two segments of lines, as shown in Figure 14-19:

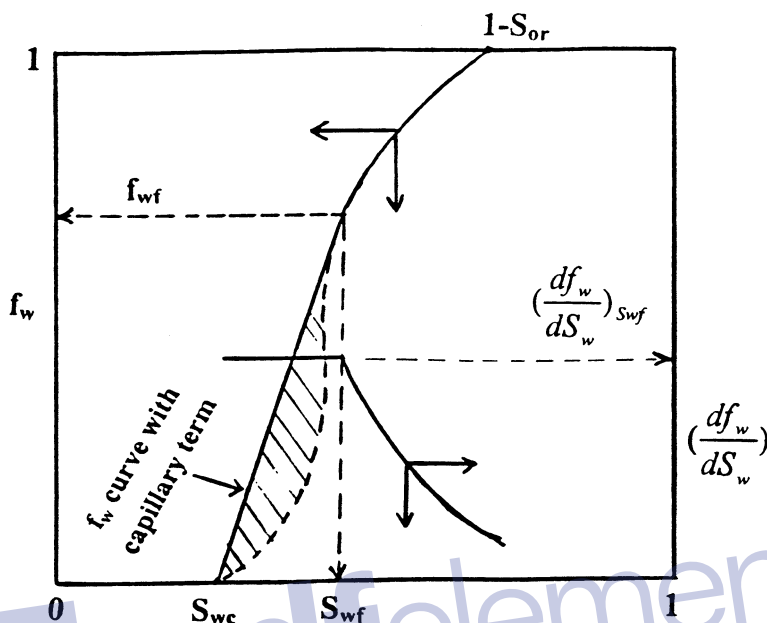


Figure 14-19. Effect of the capillary term on the f_w curve.

- A straight line segment with a constant slope of $(df_w/dS_w)_{S_{wf}}$ from S_{wc} to S_{wf}
- A concaving curve with decreasing slopes from S_{wf} to $(1 - S_{or})$

Terwilliger et al. (1951) found that at the lower range of water saturations between S_{wc} and S_{wf} , all saturations move at the same velocity as a function of time and distance. Notice that all saturations in that range have the same value for the slope and, therefore, the same velocity as given by Equation 14-33:

$$(v)_{S_w < S_{wf}} = \left(\frac{5.615 i_w}{\phi A} \right) \left(\frac{df_w}{dS_w} \right)_{S_{wf}}$$

We can also conclude that all saturations in this particular range will travel the same distance x at any particular time, as given by Equation 14-34 or 14-35:

$$(x)_{S_w < S_{wf}} = \left(\frac{5.615 i_w t}{\phi A} \right) \left(\frac{df_w}{dS_w} \right)_{S_{wf}}$$

The result is that the water saturation profile will maintain a constant shape over the range of saturations between S_{wc} and S_{wf} with time. Terwilliger and his coauthors termed the reservoir-flooded zone with this range of saturations the **stabilized zone**. They define the stabilized zone as that particular saturation interval (i.e., S_{wc} to S_{wf}) where all points of saturation travel at the same velocity. Figure 14-20 illustrates the concept of the stabilized zone. The authors also identified another saturation zone between S_{wf} and $(1 - S_{or})$, where the velocity of any water saturation is variable. They termed this zone the **nonstabilized zone**.

Experimental core flood data show that the actual water saturation profile during waterflooding is similar to that of Figure 14-20. There is a distinct front, or **shock front**, at which the water saturation abruptly increases from S_{wc} to S_{wf} . Behind the flood front there is a gradual increase in saturations from S_{wf} up to the maximum value of $1 - S_{or}$. Therefore, the saturation S_{wf} is called the water saturation at the front or, alternatively, the water saturation of the stabilized zone.

Welge (1952) showed that by drawing a straight line from S_{wc} (or from S_{wi} if it is different from S_{wc}) *tangent* to the fractional flow curve, the saturation value at the tangent point is equivalent to that at the front S_{wf} .

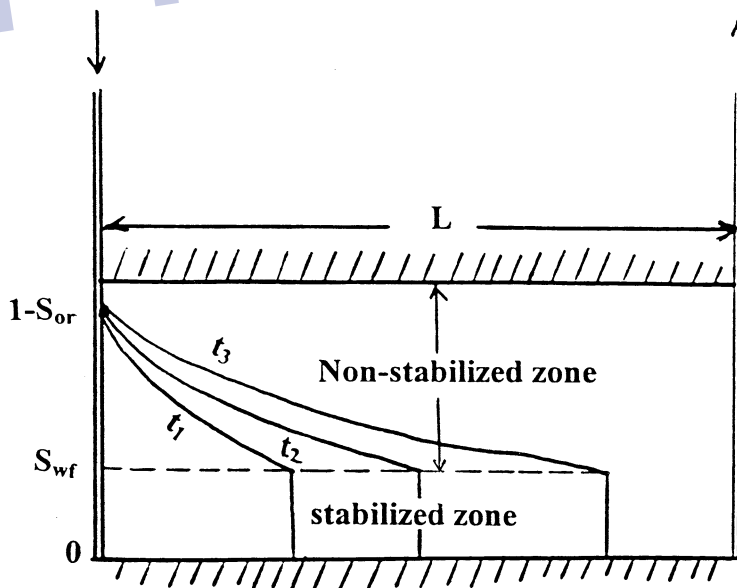


Figure 14-20. Water saturation profile as a function of distance and time.

The coordinate of the point of tangency represents also the value of the water cut at the leading edge of the water front f_{wf} .

From the above discussion, the water saturation profile at any given time t_1 can be easily developed as follows:

Step 1. Ignoring the capillary pressure term, construct the fractional flow curve, i.e., f_w vs. S_w .

Step 2. Draw a straight line tangent from S_{wi} to the curve.

Step 3. Identify the point of tangency and read off the values of S_{wf} and f_{wf} .

Step 4. Calculate graphically the slope of the tangent as $(df_w/dS_w)_{S_{wf}}$.

Step 5. Calculate the distance of the leading edge of the water front from the injection well by using Equation 14-34, or:

$$(x)_{S_{wf}} = \left(\frac{5.615 i_w t_1}{\phi A} \right) \left(\frac{df_w}{dS_w} \right)_{S_{wf}}$$

Step 6. Select several values for water saturation S_w greater than S_{wf} and determine $(df_w/dS_w)_{S_w}$ by graphically drawing a tangent to the f_w curve at each selected water saturation (as shown in Figure 14-21).

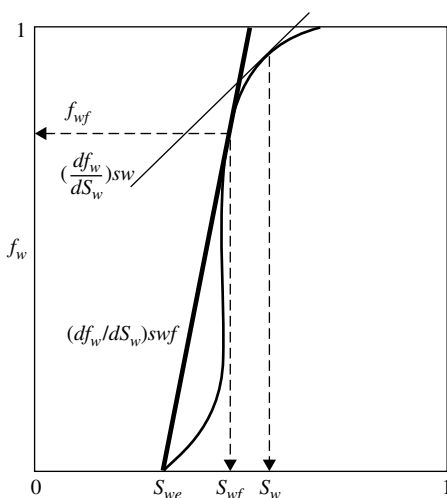


Figure 14-21. Fractional flow curve.

Step 7. Calculate the distance from the injection well to each selected saturation by applying Equation 14-36, or:

$$(x)_{S_w} = \left(\frac{5.615 i_w t_1}{\phi A} \right) \left(\frac{df_w}{dS_w} \right)_{S_w}$$

Step 8. Establish the water saturation profile after t_1 days by plotting results obtained in Step 7.

Step 9. Select a new time t_2 and repeat Steps 5 through 7 to generate a family of water saturation profiles as shown schematically in Figure 14-20.

Some erratic values of $(df_w/dS_w)_{S_w}$ might result when determining the slope graphically at different saturations. A better way is to determine the derivative mathematically by recognizing that the relative permeability ratio (k_{ro}/k_{rw}) can be expressed by Equation 5-29 of Chapter 5 as:

$$\frac{k_{ro}}{k_{rw}} = a e^{bS_w} \quad (14-36)$$

Notice that the slope b in the above expression has a negative value. The above expression can be substituted into Equation 14-26 to give:

$$f_w = \frac{1}{1 + \left(\frac{\mu_w}{\mu_o} \right) a e^{bS_w}} \quad (14-37)$$

The derivative of $(df_w/dS_w)_{S_w}$ may be obtained mathematically by differentiating the above equation with respect to S_w to give:

$$\left(\frac{df_w}{dS_w} \right)_{S_w} = \frac{- \left(\frac{\mu_w}{\mu_o} \right) a b e^{bS_w}}{\left[1 + \left(\frac{\mu_w}{\mu_o} \right) a e^{bS_w} \right]^2} \quad (14-38)$$

The data in the following example, as given by Craft and Hawkins (1959), are used to illustrate one of the practical applications of the frontal displacement theory.

Example 14-7

The following data are available for a linear-reservoir system:

| | | | | | | | | | | | |
|-----------------|-------|-------|------|------|------|------|------|------|------|------|------|
| S_w | 0.25 | 0.30 | 0.35 | 0.40 | 0.45 | 0.50 | 0.55 | 0.60 | 0.65 | 0.70 | 0.75 |
| k_{ro}/k_{rw} | 30.23 | 17.00 | 9.56 | 5.38 | 3.02 | 1.70 | 0.96 | 0.54 | 0.30 | 0.17 | 0.10 |

| | |
|--|----------------|
| Oil formation volume factor B_o | = 1.25 bbl/STB |
| Water formation volume factor B_w | = 1.02 bbl/STB |
| Formation thickness h | = 20 ft |
| Cross-sectional area A | = 26,400 ft |
| Porosity ϕ | = 25% |
| Injection rate i_w | = 900 bbl/day |
| Distance between producer and injector L | = 600 ft |
| Oil viscosity μ_o | = 2.0 cp |
| Water viscosity μ_w | = 1.0 cp |
| Dip angle α | = 0° |
| Connate water saturation S_{wc} | = 20% |
| Initial water saturation S_{wi} | = 20% |
| Residual water saturation S_{or} | = 20% |

Calculate and plot the water saturation profile after 60, 120, and 240 days.

Solution

Step 1. Plot the relative permeability ratio k_{ro}/k_{rw} vs. water saturation on a semi log paper and determine the coefficients a and b of Equation 14-36, as shown in Figure 14-22, to give:

$$a = 537.59 \quad \text{and} \quad b = -11.51$$

Therefore,

$$\frac{k_{ro}}{k_{rw}} = 537.59e^{-11.51S_w}$$

Step 2. Assume several values of water saturation and calculate the fractional flow curve at its derivatives by applying Equations 14-37 and 14-38:

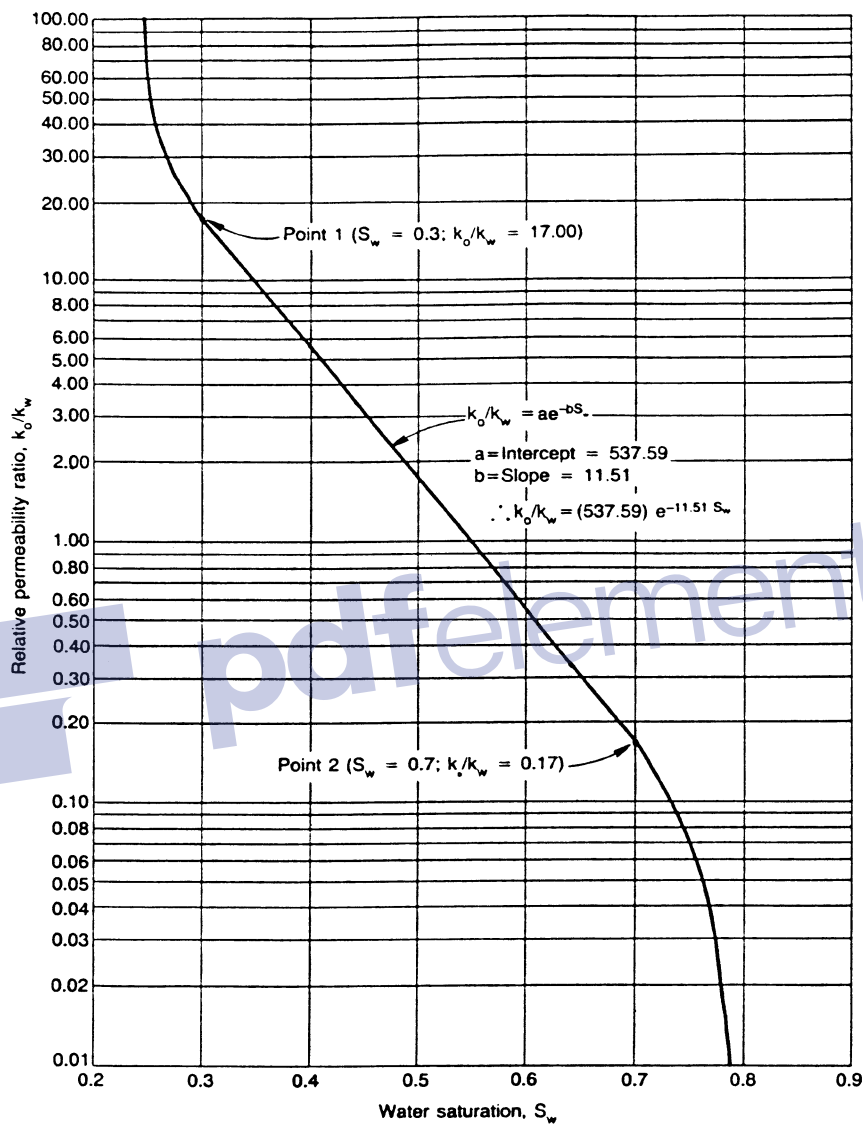


Figure 14-22. Relative permeability ratio.

| S_w | k_{ro}/k_{rw} | f_w , Equation 14-37 | (df_w/dS_w) , Equation 14-38 |
|-------|-----------------|------------------------|--------------------------------|
| 0.25 | 30.23 | 0.062 | 0.670 |
| 0.30 | 17.00 | 0.105 | 1.084 |
| 0.35 | 9.56 | 0.173 | 1.647 |
| 0.40 | 5.38 | 0.271 | 2.275 |
| 0.45 | 3.02 | 0.398 | 2.759 |
| 0.50 | 1.70 | 0.541 | 2.859 |
| 0.55 | 0.96 | 0.677 | 2.519 |
| 0.60 | 0.54 | 0.788 | 1.922 |
| 0.65 | 0.30 | 0.869 | 1.313 |
| 0.70 | 0.17 | 0.922 | 0.831 |
| 0.75 | 0.10 | 0.956 | 0.501 |

Step 3. Plot f_w and (df_w/S_w) vs. S_w on a Cartesian scale as shown in Figure 14-23. Draw a straight line from S_{wc} and tangent to the f_w curve. Determine the coordinates of point of tangency and the slope of the tangent $(df_w/dS_w)_{S_{wf}}$ to give:

$$(S_{wf}, f_{wf}) = (0.596, 0.48) \quad \text{and} \quad \left(\frac{df_w}{dS_w} \right)_{S_{wf}} = 1.973$$

This means that the leading edge of the water front (stabilized zone) has a constant saturation of 0.596 and water cut of 78%.

Step 4. When constructing the water saturation profile, it should be noted that **no water saturation with a value less than S_{wf} , i.e., 59.6%, exists behind the leading edge of the water bank.** Assume water saturation values in the range of S_{wf} to $(1 - S_{or})$, i.e., 59.6% to 75%, and calculate the water saturation profile as a function of time by using Equation 14-36:

$$(x)_{S_w} = \left(\frac{5.615i_w t}{\phi A} \right) \left(\frac{df_w}{dS_w} \right)_{S_w}$$

$$(x)_{S_w} = \left(\frac{(5.615)(900)t}{(0.25)(26,400)} \right) \left(\frac{df_w}{dS_w} \right)_{S_w}$$

$$(x)_{S_w} = (0.77t) \left(\frac{df_w}{dS_w} \right)_{S_w}$$

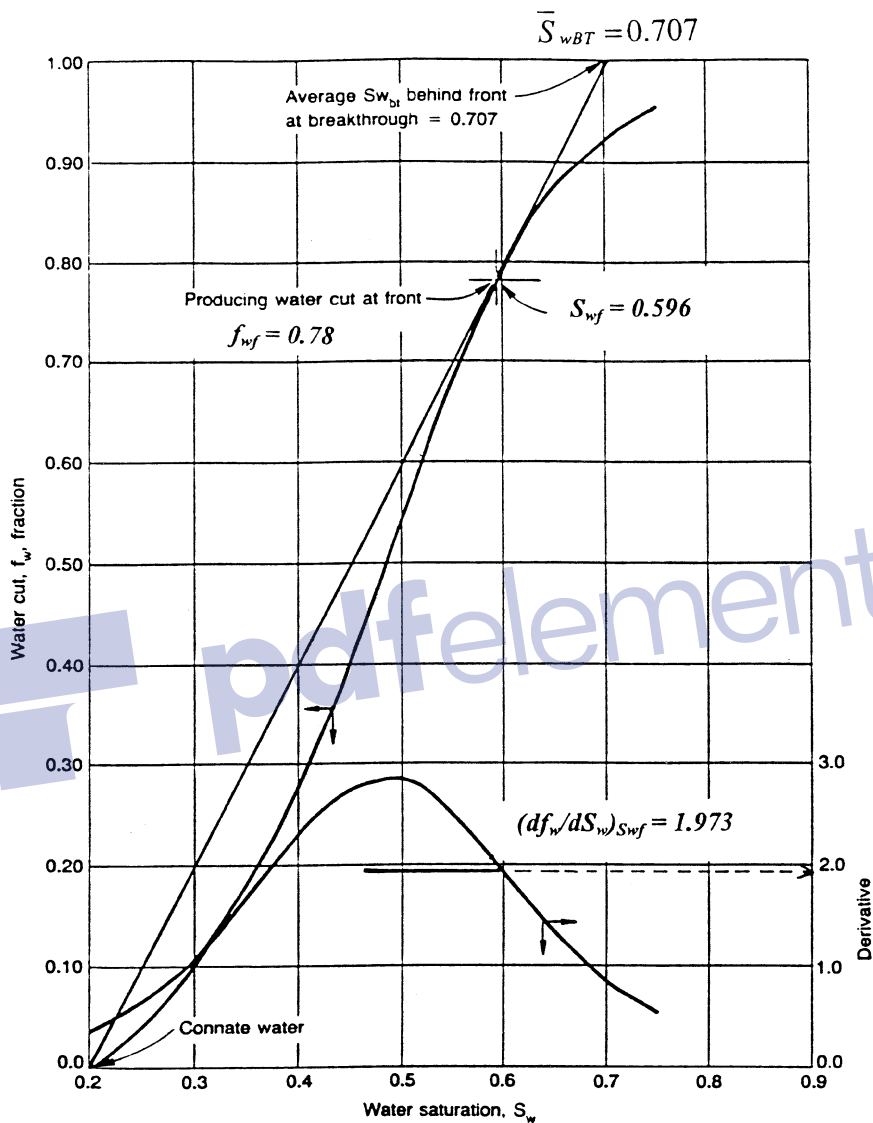


Figure 14-23. Water cut curve and its derivative.

| Assumed S_w | (df_w/dS_w) | $x = 0.77t(df/dS_w)$ $t = 60$ days | $x = 0.77t(df/dS_w)$ $t = 120$ days | $x = 0.77t(df/dS_w)$ $t = 240$ days |
|---------------|---------------|---------------------------------------|--|--|
| 0.596 | 1.973 | 91 | 182 | 365 |
| 0.60 | 1.922 | 88 | 177 | 353 |
| 0.65 | 1.313 | 60 | 121 | 241 |
| 0.70 | 0.831 | 38 | 76 | 153 |
| 0.75 | 0.501 | 23 | 46 | 92 |

Step 5. Plot the water saturation profile as a function of distance and time, as shown in Figure 14-24.

The above example shows that after 240 days of water-injection, the leading edge of the water front has moved 365 feet from the injection well (235 feet from the producer). The water front (leading edge) will eventually reach the production well and water breakthrough occurs.

The example also indicates that at water breakthrough, the leading edge of the water front would have traveled exactly the entire distance between the two wells, i.e., 600 feet. Therefore, to determine the time to breakthrough, t_{BT} , simply set $(x)_{S_{wf}}$ equal to the distance between the injector and producer L in Equation 14-34 and solve for the time:

$$L = \left(\frac{5.615i_w t_{BT}}{\phi A} \right) \left(\frac{df_w}{dS_w} \right)_{S_{wf}}$$

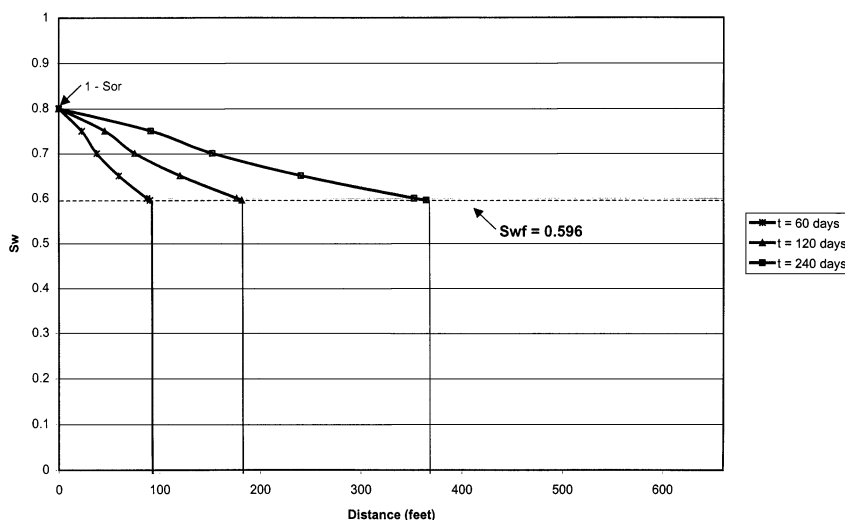


Figure 14-24. Water saturation profile for Example 14-7.

Note that the pore volume (PV) is given by:

$$(PV) = \frac{\phi AL}{5.615}$$

Combining the above two expressions and solving for the time to breakthrough t_{BT} gives:

$$t_{BT} = \left[\frac{(PV)}{i_w} \right] \frac{1}{\left(\frac{df_w}{dS_w} \right)_{S_{wf}}} \quad (14-39)$$

where t_{BT} = time to breakthrough, day

PV = total flood pattern pore volume, bbl

L = distance between the injector and producer, ft

Assuming a constant water-injection rate, the cumulative water injected at breakthrough is calculated from Equation 14-39 as:

$$W_{iBT} = i_w t_{BT} = \frac{(PV)}{\left(\frac{df_w}{dS_w} \right)_{S_{wf}}} \quad (14-40)$$

where W_{iBT} = cumulative water injected at breakthrough, bbl

$\left(\frac{\phi AL}{5.615} \right)$ = total flood pattern pore volume, bbl

It is convenient to express the cumulative water injected in terms of pore volumes injected, i.e., dividing W_{inj} by the reservoir total pore volume. Conventionally, Q_i refers to the total pore volumes of water injected. From Equation 14-40, Q_i at breakthrough is:

$$Q_{iBT} = \frac{W_{iBT}}{(PV)} = \frac{1}{\left(\frac{df_w}{dS_w} \right)_{S_{wf}}} \quad (14-41)$$

where Q_{iBT} = cumulative pore volumes of water injected at breakthrough

PV = total flood pattern pore volume, bbl

Example 14-8

Using the data given in Example 14-7, calculate:

- Time to breakthrough
- Cumulative water injected at breakthrough
- Total pore volumes of water injected at breakthrough

Solution

Step 1. Calculate the reservoir pore volume:

$$(PV) = \frac{(0.25)(26,400)(660)}{5.615} = 775,779 \text{ bbl}$$

Step 2. Calculate the time to breakthrough from Equation 14-39:

$$t_{BT} = \frac{(PV)}{i_w} \frac{1}{\left(\frac{df_w}{dS_w}\right)_{S_{wf}}}$$

$$t_{BT} = \left(\frac{775,779}{900}\right) \left(\frac{1}{1.973}\right) = 436.88 \text{ days}$$

Step 3. Determine cumulative water injected at breakthrough:

$$W_{iBT} = i_w t_{BT}$$

$$W_{iBT} = (900)(436.88) = 393,198 \text{ bbl}$$

Step 4. Calculate total pore volumes of water injected at breakthrough:

$$Q_{iBT} = \frac{1}{\left(\frac{df_w}{dS_w}\right)_{S_{wf}}}$$

$$Q_{iBT} = \frac{1}{1.973} = 0.507 \text{ pore volumes}$$

A further discussion of Equation 14-40 is needed to better understand the significance of the Buckley and Leverett (1942) frontal advance theory. Equation 14-40, which represents cumulative water injected at breakthrough, is given by:

$$W_{iBT} = (PV) \frac{1}{\left(\frac{df_w}{dS_w} \right)_{S_{wf}}} = (PV) Q_{iBT}$$

If the tangent to the fractional flow curve is extrapolated to $f_w = 1$ with a corresponding water saturation of S_w^* (as shown in Figure 14-25), then the slope of the tangent can be calculated numerically as:

$$\left(\frac{df_w}{dS_w} \right)_{S_{wf}} = \frac{1-0}{S_w^* - S_{wi}}$$

Combining the above two expressions gives:

$$W_{iBT} = (PV)(S_w^* - S_{wi}) = (PV) Q_{iBT}$$

The above equation suggests that the water saturation value denoted as S_w^* must be the average water saturation at breakthrough, or:

$$W_{iBT} (PV) (\bar{S}_{wBT} - S_{wi}) = (PV) Q_{iBT} \quad (14-42)$$

where \bar{S}_{wBT} = average water saturation in the reservoir at breakthrough

PV = flood pattern pore volume, bbl

W_{iBT} = cumulative water injected at breakthrough, bbl

S_{wi} = initial water saturation

Two important points **must be** considered when determining \bar{S}_{wBT} :

1. When drawing the tangent, the line must be originated from the initial water saturation S_{wi} if it is different from the connate-water saturation S_{wc} , as shown in Figure 14-26.

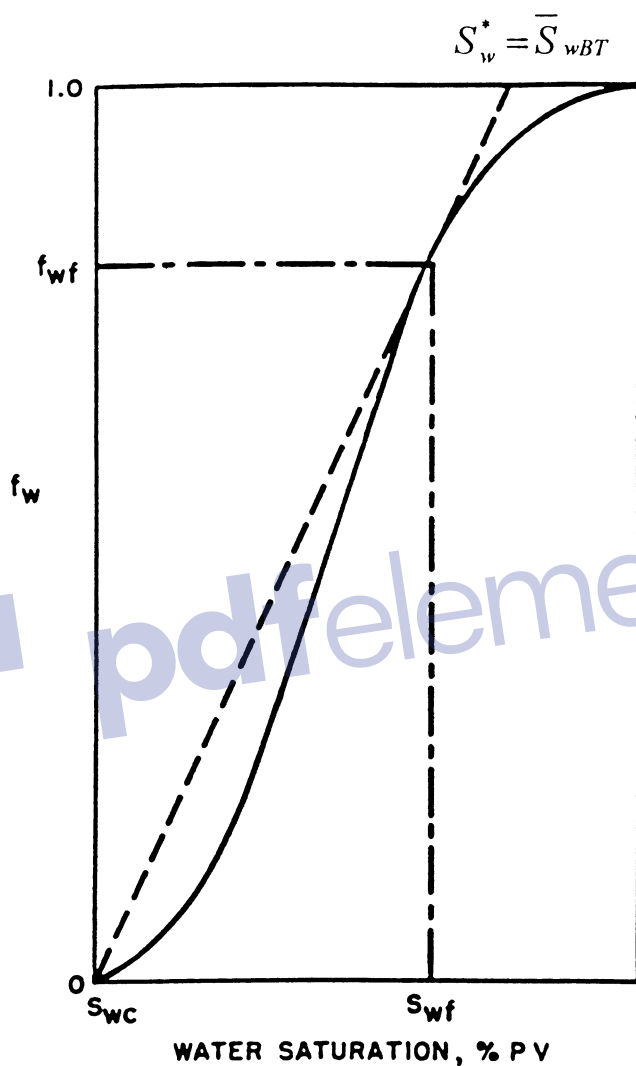


Figure 14-25. Average water saturation at breakthrough.

- When considering the areal sweep efficiency E_A and vertical sweep efficiency E_V , Equation 14-42 should be expressed as:

$$W_{iBT} = (PV)(\bar{S}_{wBT} - S_{wi})E_{ABT}E_{VBT} \quad (14-43)$$

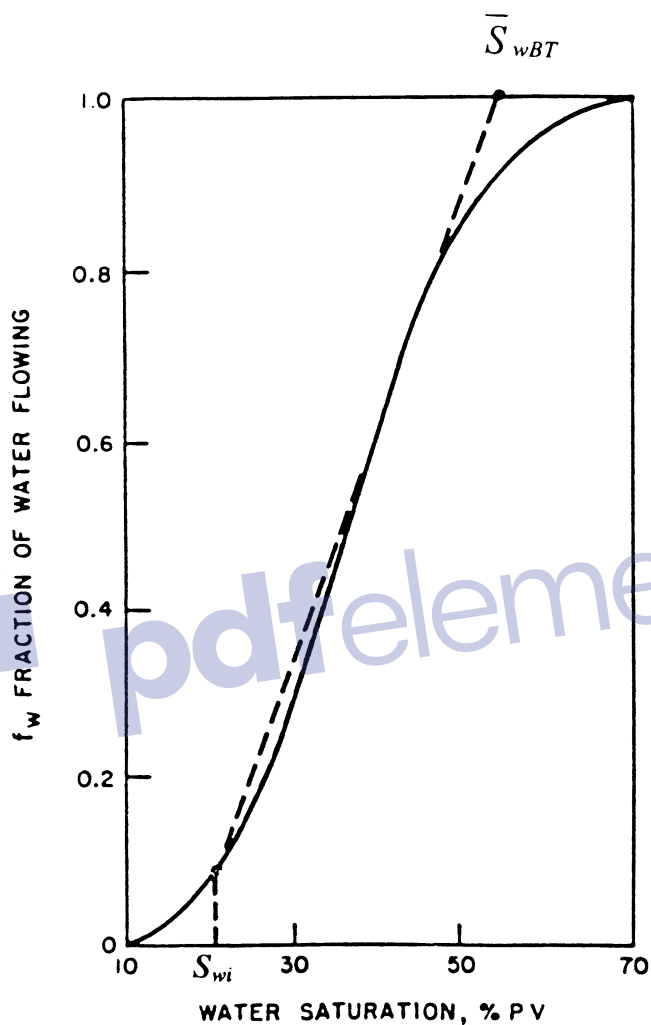


Figure 14-26. Tangent from S_{wi} .

or equivalently as:

$$W_{iBT} = (PV)Q_{iBT}E_{ABT}E_{VBT} \quad (14-44)$$

where E_{ABT} and E_{VBT} are the areal and vertical sweep efficiencies at breakthrough (as discussed later in the chapter). Note that the average water saturation in the swept area would remain constant with a value of

\bar{S}_{wBT} until breakthrough occurs, as illustrated in Figure 14-27. At the time of breakthrough, the flood front saturation S_{wf} reaches the producing well and the water cut increases suddenly from zero to f_{wf} . At breakthrough, S_{wf} and f_{wf} are designated \bar{S}_{wBT} and f_{wBT} .

After breakthrough, the water saturation and the water cut at the producing well gradually increase with continuous injection of water, as shown in Figure 14-28. Traditionally, the produced well is designated as well 2 and, therefore, the water saturation and water cut at the producing well are denoted as S_{w2} and f_{w2} , respectively.

Welge (1952) illustrated that when the water saturation at the producing well reaches any assumed value S_{w2} after breakthrough, the fractional flow curve can be used to determine:

- Producing water cut f_{w2}
- Average water saturation in the reservoir \bar{S}_{w2}
- Cumulative water injected in pore volumes, i.e., Q_i

As shown in Figure 14-29, the author pointed out that drawing a tangent to the fractional flow curve at **any** assumed value of S_{w2} greater than S_{wf} has the following properties:

1. The value of the fractional flow at the point of tangency corresponds to the well producing water cut f_{w2} , as expressed in bbl/bbl.

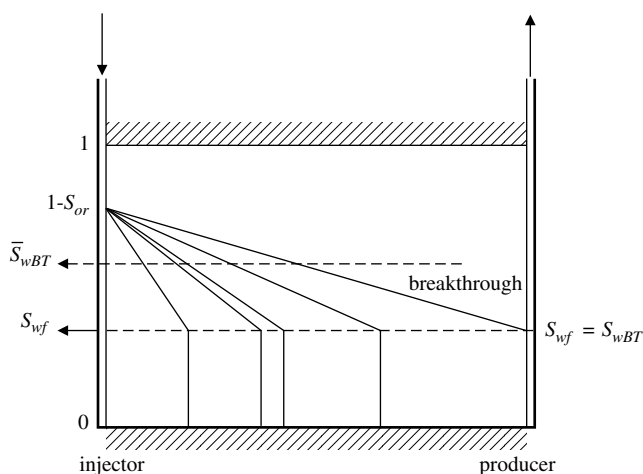


Figure 14-27. Average water saturation before breakthrough.

2. The saturation at which the tangent intersects $f_w = 1$ is the average water saturation \bar{S}_{w2} in the swept area. Mathematically, the average water saturation is determined from:

$$\bar{S}_{w2} = S_{w2} + \frac{1 - f_{w2}}{\left(\frac{df_w}{dS_w}\right)_{S_{w2}}} \quad (14-45)$$

3. The reciprocal of the slope of the tangent is defined as the cumulative pore volumes of water injected Q_i at the time when the water saturation reaches S_{w2} at the producing well, or:

$$Q_i = \frac{1}{\left(\frac{df_w}{dS_w}\right)_{S_{w2}}} \quad (14-46)$$

4. The cumulative water injected when the water saturation at the producing well reaches S_{w2} is given by:

$$W_{inj} = (PV)Q_i E_A E_V \quad (14-47)$$

or equivalently as:

$$W_{inj} = (PV)(\bar{S}_{w2} - S_{wi})E_A E_V + W_p B_N \quad (14-48)$$

where: W_{inj} = cumulative water injected, bbl

(PV) = pattern pore volume, bbl

E_A = areal sweep efficiency

E_V = vertical sweep efficiency

5. For a constant injection rate i_w , the total time t to inject W_{inj} barrels of water is given by:

$$t = \frac{W_{inj}}{i_w} \quad (14-49)$$

Example 14-9

Using the data given in Example 14-7 for the linear reservoir system, calculate the following when the water saturation at the producing well reaches 0.70 (i.e., $S_{w2} = 0.7$):

- reservoir water cut in bbl/bbl
- surface water cut in STB/STB
- reservoir water-oil ratio in bbl/bbl
- surface water-oil ratio in STB/STB
- average water saturation in the swept area
- pore volumes of water injected
- cumulative water injected in bbl

Assume that the areal and vertical sweep efficiency are 100%, i.e., $E_A = 1.0$ and $E_V = 1.0$.

Solution

- Results of Example 14-7 indicate that at a water saturation value of 70%, the corresponding water cut f_w is 0.922, therefore:

$$f_{w2} = 0.922 \text{ bbl/bbl}$$

- Calculate the surface water cut by applying Equation 14-31:

$$f_{ws} = \frac{B_o}{B_w \left(\frac{1}{f_w} - 1 \right) + B_o}$$

$$f_{ws} = \frac{1.25}{1.02 \left(\frac{1}{0.922} - 1 \right) + 1.25} = 0.935 \text{ STB/STB}$$

- Determine the producing water-oil ratio by using Equation 14-26:

$$\text{WOR}_r = \frac{f_w}{1 - f_w}$$

$$\text{WOR}_r = \frac{0.922}{1 - 0.922} = 11.82 \text{ bbl/bbl}$$

d. Apply Equation 14-29 to determine the surface water-oil ratio:

$$\text{WOR}_s = \frac{B_o \text{WOR}_r}{B_w}$$

$$\text{WOR}_s = \frac{(1.25)(11.82)}{1.02} = 14.49 \text{ STB/STB}$$

e. Draw a tangent to the fractional flow curve at the coordinate of the point $(S_w, f_w) = (0.7, 0.922)$ and extrapolate to $f_w = 1.0$ to give a corresponding $\bar{S}_{w2} = 0.794$. Equivalently, the average water saturation can be calculated by determining the slope of the tangent and applying Equation 14-45, to give:

$$\left(\frac{df_w}{dS_w} \right)_{S_{w2}} = 0.831$$

$$\bar{S}_{w2} = 0.70 + \frac{1 - 0.922}{0.831} = 0.794$$

f. From Equation 14-46, the cumulative pore volume of water injected is the reciprocal of the slope of the tangent line:

$$Q_i = 1/0.831 = 1.203$$

g. Calculate cumulative water injected by applying Equation 14-47:

$$W_{inj} = (PV)(Q_i)E_A E_V$$

$$W_{inj} = (775,779)(1.203)(1)(1) = 933,262 \text{ bbl}$$

Oil Recovery Calculations

The main objective of performing oil recovery calculations is to generate a set of performance curves under a specific water-injection scenario. A set of performance curves is defined as the graphical presentation of the time-related oil recovery calculations in terms of:

- Oil production rate, Q_o
- Water production rate, Q_w
- Surface water-oil ratio, WOR_s
- Cumulative oil production, N_p
- Recovery factor, RF

- Cumulative water production, W_p
- Cumulative water injected, W_{inj}
- Water-injection pressure, p_{inj} (discussed later in the chapter)
- Water-injection rate, i_w (discussed later in the chapter)

In general, oil recovery calculations are divided into two parts: (1) before breakthrough calculations and (2) after breakthrough calculations. Regardless of the stage of the waterflood, i.e., before or after breakthrough, the cumulative oil production is given previously by Equation 14-6 as:

$$N_p = N_S E_D E_A E_V$$

where N_p = cumulative oil production, STB
 N_S = initial oil-in-place at start of the flood, STB
 E_D = displacement efficiency
 E_A = areal sweep efficiency
 E_V = vertical sweep efficiency

As defined by Equation 14-10 when $S_{gi} = 0$, the displacement efficiency is given by:

$$E_D = \frac{\bar{S}_w - S_{wi}}{1 - S_{wi}}$$

At breakthrough, the E_D can be calculated by determining the average water saturation at breakthrough:

$$E_{DBT} = \frac{\bar{S}_{wBT} - S_{wi}}{1 - S_{wi}} \quad (14-50)$$

where E_{DBT} = displacement efficiency at breakthrough
 \bar{S}_{wBT} = average water saturation at breakthrough

The cumulative oil production at breakthrough is then given by:

$$(N_p)_{BT} = N_S E_{DBT} E_{ABT} E_{VBT} \quad (14-51)$$

where $(N_p)_{BT}$ = cumulative oil production at breakthrough, STB
 E_{ABT} , E_{VBT} = areal and vertical sweep efficiencies at breakthrough

Assuming E_A and E_V are 100%, Equation 14-51 is reduced to:

$$(N_p)_{BT} = N_S E_{DBT} \quad (14-52)$$

Before breakthrough occurs, the oil recovery calculations are simple when assuming that **no free gas exists at the start of the flood, i.e., $S_{gi} = 0$** . The cumulative oil production is simply equal to the volume of water injected with no water production during this phase ($W_p = 0$ and $Q_w = 0$).

Oil recovery calculations after breakthrough are based on determining E_D at various assumed values of water saturations at the producing well. The specific steps of performing complete oil recovery calculations are composed of three stages:

1. Data preparation
2. Recovery performance to breakthrough
3. Recovery performance after breakthrough

Stage 1: Data Preparation

Step 1. Express the relative permeability data as relative permeability ratio k_{ro}/k_{rw} and plot their values versus their corresponding water saturations on a semi log scale.

Step 2. Assuming that the resulting plot of relative permeability ratio, k_{ro}/k_{rw} vs. S_w , forms a straight-line relationship, determine values of the coefficients a and b of the straight line (see Example 14-7). Express the straight-line relationship in the form given by Equation 14-36, or:

$$\frac{k_{ro}}{k_{rw}} = ae^{bS_w}$$

Step 3. Calculate and plot the fractional flow curve f_w , allowing for gravity effects if necessary, but neglecting the capillary pressure gradient.

Step 4. Select several values of water saturations between S_{wf} and $(1 - S_{or})$ and determine the slope (df_w/dS_w) at each saturation. The numerical calculation of each slope as expressed by Equation 14-38 provides consistent values as a function of saturation, or:

$$\left(\frac{df_w}{dS_w}\right) = \frac{-\left(\frac{\mu_w}{\mu_o}\right)abe^{bS_w}}{\left[1 + \left(\frac{\mu_w}{\mu_o}\right)ae^{bS_w}\right]^2}$$

Step 5. Prepare a plot of the calculated values of the slope (df_w/dS_w) versus S_w on a Cartesian scale and draw a smooth curve through the points.

Stage 2: Recovery Performance to Breakthrough ($S_{gi} = 0, E_A, E_V = 100\%$)

Step 1. Draw a tangent to the fractional flow curve as originated from S_{wi} and determine:

- Point of tangency with the coordinate (S_{wf}, f_{wf})
- Average water saturation at breakthrough \bar{S}_{wBT} by extending the tangent line to $f_w = 1.0$
- Slope of the tangent line $\left(\frac{df_w}{dS_w}\right)_{S_{wf}}$

Step 2. Calculate pore volumes of water injected at breakthrough by using Equation 14-41:

$$Q_{iBT} = \frac{1}{\left(\frac{df_w}{dS_w}\right)_{S_{wf}}} = (\bar{S}_{wBT} - S_{wi})$$

Step 3. Assuming E_A and E_V are 100%, calculate cumulative water injected at breakthrough by applying Equation 14-42:

$$W_{iBT} = (PV)(\bar{S}_{wBT} - S_{wi})$$

or equivalently:

$$W_{iBT} = (PV)Q_{iBT}$$

Step 4. Calculate the displacement efficiency at breakthrough by applying Equation 14-50:

$$E_{DBT} = \frac{\bar{S}_{wBT} - S_{wi}}{1 - S_{wi}}$$

Step 5. Calculate cumulative oil production at breakthrough from Equation 14-52:

$$(N_p)_{BT} = N_s E_{DBT}$$

Step 6. Assuming a constant water-injection rate, calculate time to breakthrough from Equation 14-40:

$$t_{BT} = \frac{W_{iBT}}{i_w}$$

Step 7. Select several values of injection time less than the breakthrough time, i.e., $t < t_{BT}$, and set:

$$W_{inj} = i_w t$$

$$Q_o = i_w / B_o$$

$$WOR = 0$$

$$W_p = 0$$

$$N_p = \frac{i_w t}{B_o} = \frac{W_{inj}}{B_o}$$

Step 8. Calculate the surface water-oil ratio WOR_s exactly at breakthrough by using Equation 14-28:

$$WOR_s = \frac{B_o}{B_w \left(\frac{1}{f_{wBT}} - 1 \right)}$$

where f_{wBT} is the water cut at breakthrough (notice that $f_{wBT} = f_{wf}$).

Note that WOR_s as calculated from the above expression is only correct when **both** the areal sweep efficiency E_A and vertical sweep efficiency E_V are 100%.

Stage 3: Recovery Performance After Breakthrough ($S_{gi} = 0$, E_A , $E_V = 100\%$)

The recommended methodology of calculating recovery performance after breakthrough is based on selecting several values of water saturations around the producing well, i.e., S_{w2} , and determining the corresponding average reservoir water saturation \bar{S}_{w2} for each S_{w2} . The specific steps that are involved are summarized below:

- Step 1.* Select six to eight different values of S_{w2} (i.e., S_w at the producing well) between S_{wBT} and $(1 - S_{or})$ and determine (df_w/dS_w) values corresponding to these S_{w2} points.
- Step 2.* For each selected value of S_{w2} , calculate the corresponding reservoir water cut and average water saturation from Equations 14-37 and 14-45:

$$f_{w2} = \frac{1}{1 + \left(\frac{\mu_w}{\mu_o}\right) a e^{b S_{w2}}}$$

$$\bar{S}_{w2} = S_{w2} + \frac{1 - f_{w2}}{\left(\frac{df_w}{dS_w}\right)_{S_{w2}}}$$

- Step 3.* Calculate the displacement efficiency E_D for each selected value of S_{w2} :

$$E_D = \frac{\bar{S}_{w2} - S_{wi}}{1 - S_{wi}}$$

- Step 4.* Calculate cumulative oil production N_p for each selected value of S_{w2} from Equation 14-6, or:

$$N_p = N_s E_D E_A E_V$$

Assuming E_A and E_V are equal to 100%, then:

$$N_p = N_s E_D$$

- Step 5.* Determine pore volumes of water injected, Q_i , for each selected value of S_{w2} from Equation 14-46:

$$Q_i = \frac{1}{\left(\frac{df_w}{dS_w}\right)_{S_{w2}}}$$

- Step 6.* Calculate cumulative water injected for each selected value of S_{w2} by applying Equation 14-47 or 14-48:

$$W_{inj} = (PV)Q_i \quad \text{or} \quad W_{inj} = (PV)(\bar{S}_{w2} - S_{wi})$$

Notice that E_A and E_V are set equal to 100%.

Step 7. Assuming a constant water-injection rate i_w , calculate the time t to inject W_{inj} barrels of water by applying Equation 14-49:

$$t = \frac{W_{inj}}{i_w}$$

Step 8. Calculate cumulative water production W_p at any time t from the material balance equation, which states that the cumulative water injected at any time will displace an equivalent volume of oil and water, or:

$$W_{inj} = N_p B_o + W_p B_w$$

Solving for W_p gives:

$$W_p = \frac{W_{inj} - N_p B_o}{B_w} \quad (14-53)$$

or equivalently in a more generalized form:

$$W_p = \frac{W_{inj} - (\bar{S}_{w2} - S_{wi})(PV)E_A E_V}{B_w} \quad (14-54)$$

We should emphasize that all of the above derivations are based on the assumption that **no free gas exists from the start of the flood till abandonment.**

Step 9. Calculate the surface water-oil ratio WOR_s that corresponds to each value of f_{w2} (as determined in Step 2) from Equation 14-28:

$$WOR_s = \frac{B_o}{B_w \left(\frac{1}{f_{w2}} - 1 \right)}$$

Step 10. Calculate the oil and water flow rates from the following derived relationships:

$$i_w = Q_o B_o + Q_w B_w$$

Introducing the surface water-oil ratio into the above expression gives:

$$i_w = Q_o B_o + Q_o WOR_s B_w$$

Solving for Q_o gives:

$$Q_o = \frac{i_w}{B_o + B_w \text{WOR}_s} \quad (14-55)$$

and

$$Q_w = Q_o \text{WOR}_s \quad (14-56)$$

where Q_o = oil flow rate, STB/day

Q_w = water flow rate, STB/day

i_w = water-injection rate, bbl/day

Step 11. The preceding calculations as described in Steps 1 through 10 can be organized in the following tabulated form:

| S_{w2} | $F_{w2} (df_w/dS_w)$ | \bar{S}_{w2} | E_D | N_p | Q_i | W_{inj} | t | W_p | WOR_s | Q_o | Q_w |
|----------------|----------------------|----------------|-----------|-----------|-----------|-----------|-----------|----------|----------------|---------|---------|
| S_{wBT} | f_{wBT} | \cdot | S_{wBT} | E_{DBT} | N_{pBT} | Q_{iBT} | W_{iBT} | t_{BT} | 0 | \cdot | \cdot |
| \cdot | \cdot | \cdot | \cdot | \cdot | \cdot | \cdot | \cdot | \cdot | \cdot | \cdot | \cdot |
| \cdot | \cdot | \cdot | \cdot | \cdot | \cdot | \cdot | \cdot | \cdot | \cdot | \cdot | \cdot |
| $(1 - S_{or})$ | 1.0 | \cdot | \cdot | \cdot | \cdot | \cdot | \cdot | \cdot | 100% | 0 | \cdot |

Step 12. Express the results in a graphical form.

Example 14-10

The data of Example 14-7 are reproduced here for convenience:

| | | | | | | | | | | | |
|-----------------|-------|-------|-------|-------|-------|-------|-------|-------|-------|-------|-------|
| S_w | 0.25 | 0.30 | 0.35 | 0.40 | 0.45 | 0.50 | 0.55 | 0.60 | 0.65 | 0.70 | 0.75 |
| k_{ro}/k_{rw} | 30.23 | 17.00 | 9.56 | 5.38 | 3.02 | 1.70 | 0.96 | 0.54 | 0.30 | 0.17 | 0.10 |
| f_w | 0.062 | 0.105 | 0.173 | 0.271 | 0.398 | 0.541 | 0.677 | 0.788 | 0.869 | 0.922 | 0.956 |
| df_w/dS_w | 0.670 | 10.84 | 1.647 | 2.275 | 2.759 | 2.859 | 2.519 | 1.922 | 1.313 | 0.831 | 0.501 |

$$\mu_o = 2.0 \text{ cp}$$

$$\mu_w = 1.0 \text{ cp}$$

$$B_o = 1.25 \text{ bbl/STB}$$

$$B_w = 1.02 \text{ bbl/STB}$$

$$\phi = 25\%$$

$$h = 20 \text{ ft}$$

$$S_{wi} = 20\%$$

$$S_{or} = 20\%$$

$$i_w = 900 \text{ bbl/day}$$

$$(PV) = 775,779 \text{ bbl}$$

$$N_s = 496,449 \text{ STB}$$

$$E_A = 100\%$$

$$E_V = 100\%$$

Predict the waterflood performance to abandonment at a WOR_s of 45 STB/STB.

Solution

Step 1. Plot f_w vs. S_w as shown in Figure 14-30 and construct the tangent to the curve. Extrapolate the tangent to $f_w=1.0$ and determine:

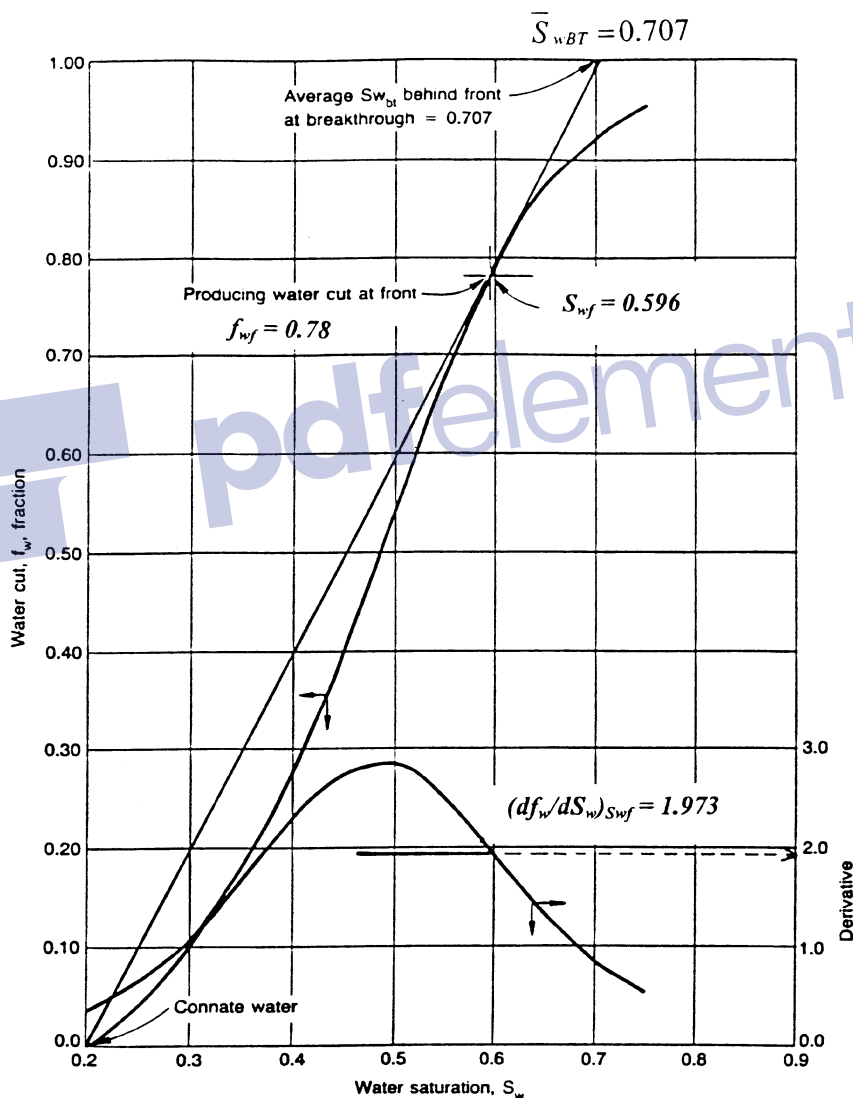


Figure 14-30. Fractional flow curve for Example 14-10.

$$\begin{aligned}
 S_{wf} = S_{wBT} &= 0.596 \\
 f_{wf} = f_{wBT} &= 0.780 \\
 (df_w/dS_w)_{swf} &= 1.973 \\
 \underline{Q}_{iBT} &= 1/1.973 = 0.507 \\
 \underline{S}_{wBT} &= 0.707
 \end{aligned}$$

Step 2. Calculate E_{DBT} by using Equation 14-50:

$$E_{DBT} = \frac{0.707 - 0.20}{1 - 0.20} = 0.634$$

Step 3. Calculate $(N_p)_{BT}$ by applying Equation 14-52:

$$(N_p)_{BT} = 496,499 (0.634) = 314,780 \text{ STB}$$

Step 4. Calculate cumulative water injected at breakthrough from Equation 14-42:

$$W_{iBT} = 775,779(0.507) = 393,198 \text{ bbl}$$

Step 5. Calculate the time to breakthrough:

$$t_{BT} = \frac{393,198}{900} = 436.88 \text{ days}$$

Step 6. Calculate WOR_s exactly at breakthrough by applying Equation 14-28:

$$WOR_s = \frac{1.25}{1.02 \left(\frac{1}{0.78} - 1 \right)} = 4.34 \text{ STB/STB}$$

Step 7. Describe the recovery performance to breakthrough in the following tabulated form:

| t , days | $W_{inj} = 900 t$ | $N_p = \frac{W_{inj}}{B_o}$ | $Q_o = \frac{i_w}{B_o}$ | WOR_s | $Q_w = Q_o WOR_s$ | W_p |
|------------|-------------------|-----------------------------|-------------------------|---------|-------------------|-------|
| 0 | 0 | 0 | 0 | 0 | 0 | 0 |
| 100.0 | 90,000 | 72,000 | 720 | 0 | 0 | 0 |
| 200.0 | 180,000 | 144,000 | 720 | 0 | 0 | 0 |
| 300.0 | 270,000 | 216,000 | 720 | 0 | 0 | 0 |
| 400.0 | 360,000 | 288,000 | 720 | 0 | 0 | 0 |
| 436.88 | 393,198 | 314,780 | 720 | 4.34 | 3125 | 0 |

Step 8. Following the computational procedure as outlined for recovery performance after breakthrough, construct the following table:

| S_{w2} | f_{w2} | df_w/dS_w | Q_i | \bar{S}_{w2} | E_D | N_p | W_{inj} | t , days | W_p | WOR_s | Q_o | Q_w |
|----------|----------|-------------|-------|----------------|-------|---------|-----------|------------|-----------|---------|-------|-------|
| 0.598 | 0.784 | 1.948 | 0.513 | 0.709 | 0.636 | 315,773 | 397,975 | 442 | 82,202 | 4.45 | 155 | 690 |
| 0.600 | 0.788 | 1.922 | 0.520 | 0.710 | 0.638 | 316,766 | 403,405 | 448 | 86,639 | 4.56 | 153 | 698 |
| 0.700 | 0.922 | 0.831 | 1.203 | 0.794 | 0.743 | 368,899 | 933,262 | 1,037 | 564,363 | 14.49 | 56 | 814 |
| 0.800 | 0.974 | 0.293 | 3.407 | 0.889 | 0.861 | 427,486 | 2,643,079 | 2,937 | 2,215,593 | 45.91 | 19 | 859 |

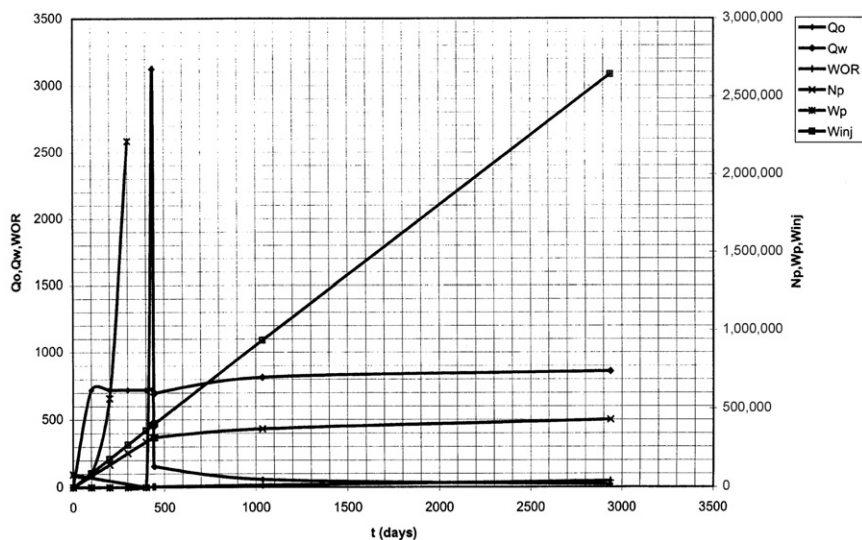


Figure 14-31. Performance curves of Example 14-10.

Step 9. Express graphically results of the calculations as a set of performance curves, as shown in Figure 14-31.

II. AREAL SWEEP EFFICIENCY

The areal sweep efficiency E_A is defined as the fraction of the total flood pattern that is contacted by the displacing fluid. It increases steadily with injection from zero at the start of the flood until breakthrough occurs, after which E_A continues to increase at a slower rate.

The areal sweep efficiency depends basically on the following three main factors:

1. Mobility ratio M
2. Flood pattern
3. Cumulative water injected W_{inj}
4. Pressure distribution between injectors and producers
5. Directional permeability

Correlations of sweep efficiency as a function of mobility ratio will be presented in a subsequent section for several well patterns. If directional permeability trends can be identified, injection and production wells can be arranged to take advantage of the trends to enhance areal sweep efficiency. It is also possible to maximize areal sweep through a careful management of pressure distribution and proper injection–production pattern selection.

Mobility Ratio

In general, the mobility of any fluid λ is defined as the ratio of the effective permeability of the fluid to the fluid viscosity, i.e.:

$$\lambda_o = \frac{k_o}{\mu_o} = \frac{k k_{ro}}{\mu_o} \quad (14-57)$$

$$\lambda_w = \frac{k_w}{\mu_w} = \frac{k k_{rw}}{\mu_w} \quad (14-58)$$

$$\lambda_g = \frac{k_g}{\mu_g} = \frac{k k_{rg}}{\mu_g} \quad (14-59)$$

where λ_o , λ_w , λ_g = mobility of oil, water, and gas, respectively

k_o, k_w, k_g = effective permeability to oil, water, and gas, respectively
 k_{ro}, k_{rw} = relative permeability to oil, water, and gas, respectively
 k = absolute permeability

The fluid mobility as defined mathematically by the above three relationships indicates that λ is a strong function of the fluid saturation. The mobility ratio M is defined as the mobility of the *displacing fluid* to the mobility of the *displaced fluid*, or:

$$M = \frac{\lambda_{\text{displacing}}}{\lambda_{\text{displaced}}}$$

For waterflooding then:

$$M = \frac{\lambda_w}{\lambda_o}$$

Substituting for λ :

$$M = \frac{k k_{rw}}{\mu_w} \frac{\mu_o}{k k_{ro}}$$

Simplifying gives:

$$M = \frac{k_{rw}}{k_{ro}} \frac{\mu_o}{\mu_w} \quad (14-60)$$

Muskat (1946) points out that in calculating M by applying Equation 14-60, the following concepts must be employed in determining k_{ro} and k_{rw} :

- **Relative permeability of oil k_{ro} .** Because the displaced oil is moving ahead of the water front in the noninvaded portion of the pattern, as shown schematically in Figure 14-32, k_{ro} must be evaluated at the initial water saturation S_{wi} .
- **Relative permeability of water k_{rw} .** The displacing water will form a water bank that is characterized by an average water saturation of \bar{S}_{wBT} in the swept area. This average saturation will remain constant until breakthrough, after which the average water saturation will continue to increase (as denoted by \bar{S}_{w2}). The mobility ratio, therefore, can be expressed more explicitly under two different stages of the flood:

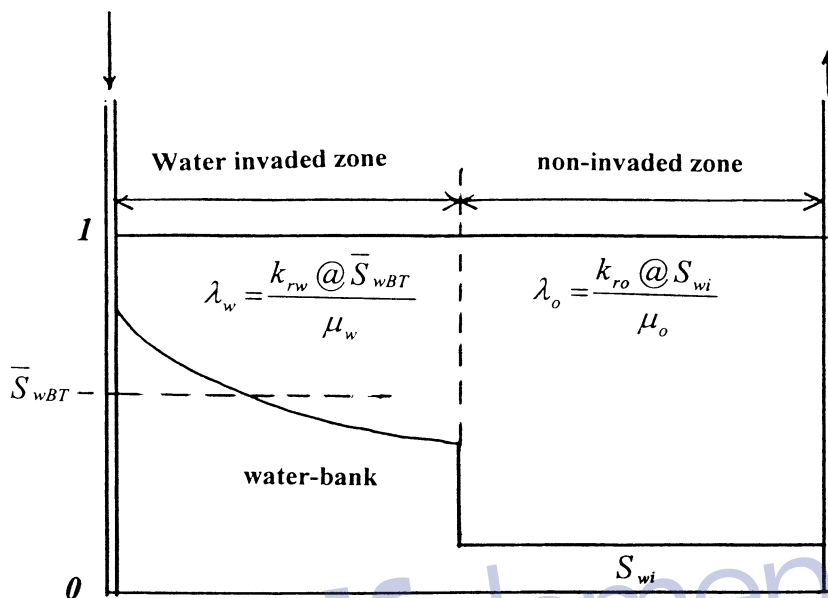


Figure 14-32. Oil and water mobilities to breakthrough.

From the start to breakthrough:

$$M = \frac{k_{rw} @ \bar{S}_{wBT} \mu_0}{k_{ro} @ S_{wi} \mu_w} \quad (14-61)$$

where $k_{rw} @ \bar{S}_{wBT}$ = relative permeability of water at \bar{S}_{wBT}
 $k_{ro} @ S_{wi}$ = relative permeability of oil at S_{wi}

The above relationship indicates that the mobility ratio will remain constant from the start of the flood until breakthrough occurs.

After breakthrough:

$$M = \frac{k_{rw} @ \bar{S}_{w2} \mu_0}{k_{ro} @ S_{wi} \mu_w} \quad (14-62)$$

Equation 14-62 indicates that the mobility of the water k_{rw}/μ_w will increase after breakthrough due to the continuous increase in the average water saturation \bar{S}_{w2} . This will result in a proportional increase in the mobility ratio M after breakthrough, as shown in Figure 14-33.

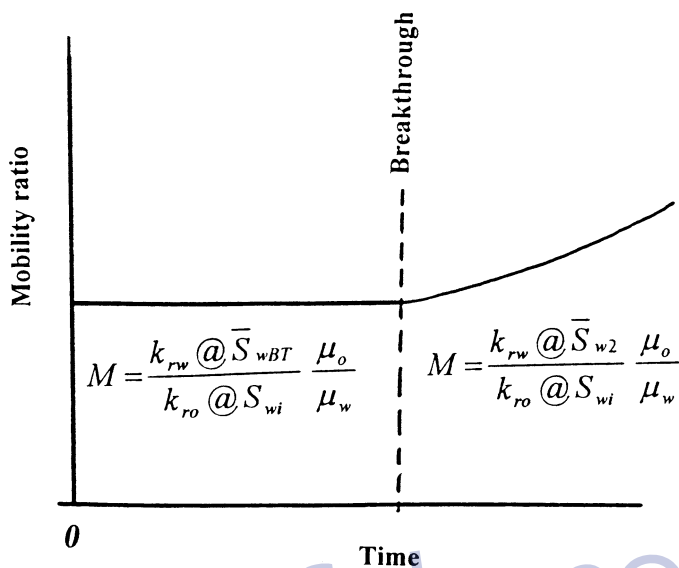


Figure 14-33. Mobility ratio versus time relationship.

In general, if no further designation is applied, the term **mobility ratio** refers to the mobility ratio before breakthrough.

Flood Patterns

In designing a waterflood project, it is common practice to locate injection and producing wells in a regular geometric pattern so that a symmetrical and interconnected network is formed. As shown previously in Figure 14-9, regular flood patterns include these:

- Direct line drive
- Staggered line drive
- Five spot
- Seven spot
- Nine spot

By far the most used pattern is the five spot and, therefore, most of the discussion in the remainder of the chapter will focus on this pattern.

Craig et al. (1955) performed experimental studies on the influence of fluid mobilities on the areal sweep efficiency resulting from water or gas

injection. Craig and his co-investigators used horizontal laboratory models representing a quadrant of five spot patterns. Areal sweep efficiencies were determined from x-ray shadowgraphs taken during various stages of the displacement as illustrated in Figure 14-34. Two mobility ratios, 1.43 and 0.4, were used in the study.

Figure 14-34 shows that at the start of the flood, the water front takes on a cylindrical form around the injection point (well). As a result of the continuous injection, pressure distribution and corresponding streamlines are developed between the injection and production wells. However, various streamlines have different lengths with the shortest streamline being the direct line between the injector and producer. The pressure gradient along this line is the highest that causes the injection fluid to flow faster along the shortest streamline than the other lines. The water front gradually begins to deform from the cylindrical form and cusp into the production well as water breakthrough occurs. The effect of the mobility ratio on the areal sweep efficiency is apparent by examining Figure 14-34. This figure shows that at breakthrough, only 65% of the flood pattern area has been contacted (swept) by the injection fluid with a mobility ratio of 1.43 and 82.8% when the mobility ratio is 0.4. This contacted fraction when water breakthrough occurs is

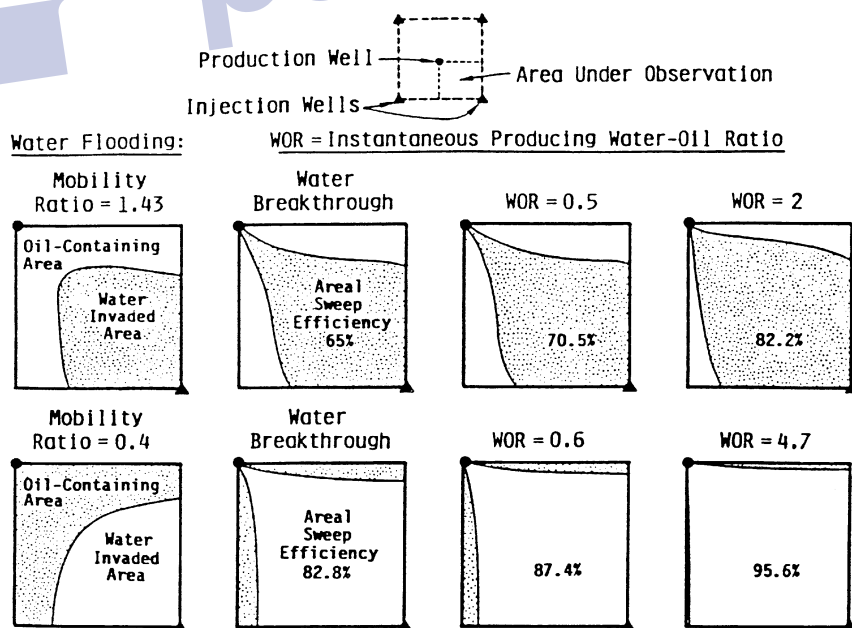


Figure 14-34. X-ray shadowgraphs of flood progress. (Permission to publish by the Society of Petroleum Engineers.)

defined as the **areal sweep efficiency at breakthrough**, as denoted by E_{ABT} . In general, **lower mobility ratios would increase the areal sweep efficiency and higher mobility ratios would decrease the E_A** . Figure 14-34 also shows that with continued injection after breakthrough, the areal sweep efficiency continues to increase until it eventually reaches 100%.

Cumulative Water Injected

Continued injection after breakthrough can result in substantial increases in recovery, especially in the case of an adverse mobility ratio. The work of Craig et al. (1955) has shown that significant quantities of oil may be swept by water after breakthrough. It should be pointed out that the higher the mobility ratio, the more important is the “after-breakthrough” production.

Areal Sweep Prediction Methods

Methods of predicting the areal sweep efficiency are essentially divided into the following three phases of the flood:

- Before breakthrough
- At breakthrough
- After breakthrough

Phase 1: Areal Sweep Efficiency Before Breakthrough

The areal sweep efficiency before breakthrough is simply proportional to the volume of water injected and is given by:

$$E_A = \frac{W_{inj}}{(PV)(\bar{S}_{wBT} - S_{wi})} \quad (14-63)$$

where W_{inj} = cumulative water injected, bbl
 (PV) = flood pattern pore volume, bbl

Phase 2: Areal Sweep Efficiency at Breakthrough

Craig (1955) proposed a graphical relationship that correlates the areal sweep efficiency at breakthrough E_{ABT} with the mobility ratio for the five-spot pattern. The correlation, as shown in Figure 14-35, closely simulates flooding operations and is probably the most representative of actual waterfloods. The graphical illustration of areal sweep efficiency as

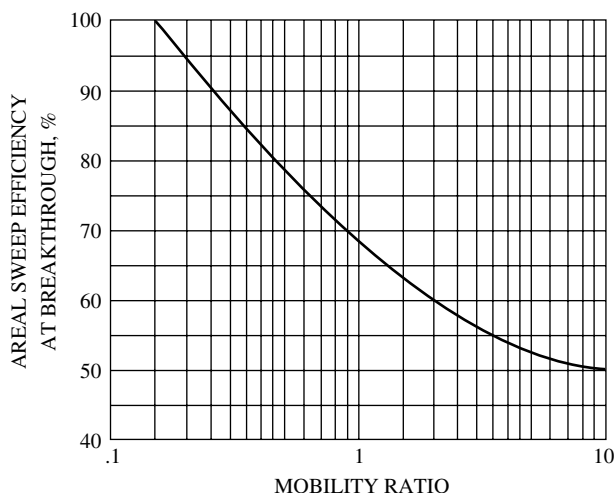


Figure 14-35. Areal sweep efficiency at breakthrough. (Permission to publish by the Society of Petroleum Engineers.)

a strong function of mobility ratio shows that a change in the mobility ratio from 0.15 to 10.0 would change the breakthrough areal sweep efficiency from 100% to 50%. Willhite (1986) presented the following mathematical correlation, which closely approximates the graphical relationship presented in Figure 14-35:

$$E_{ABT} = 0.54602036 + \frac{0.03170817}{M} + \frac{0.30222997}{e^M} - 0.00509693M \quad (14-64)$$

where E_{ABT} = areal sweep efficiency at breakthrough
 M = mobility ratio

Phase 3: Areal Sweep Efficiency After Breakthrough

In the same way that displacement efficiency E_D increases after breakthrough, the areal sweep efficiency also increases due to the gradual increase in the total swept area with continuous injection. Dyes et al. (1954) correlated the increase in the areal sweep efficiency after breakthrough with the ratio of water volume injected at any time after breakthrough, W_{inj} , to water volume injected at breakthrough, W_{iBT} , as given by:

$$E_A = E_{ABT} + 0.633 \log\left(\frac{W_{inj}}{W_{iBT}}\right) \quad (14-65)$$

or

$$E_A = E_{ABT} + 0.2749 \ln\left(\frac{W_{inj}}{W_{iBT}}\right) \quad (14-66)$$

where E_A = areal sweep efficiency after breakthrough
 W_{inj} = cumulative water injected
 W_{iBT} = cumulative water injected at breakthrough

The authors also presented a graphical relationship that relates the areal sweep efficiency with the reservoir water cut f_w and the reciprocal of mobility ratio $1/M$ as shown in Figure 14-36. Fassihi (1986) used a nonlinear regression model to reproduce the data of Figure 14-36 by using the following expression:

$$E_A = \frac{1}{1 + A} \quad (14-67)$$

with

$$A = [a_1 \ln(M + a_2) + a_3] f_w + a_4 \ln(M + a_5) + a_6$$

The coefficient of Equation 14-67 for patterns such as the five spot, staggered line drive, and direct line drive are given below:

| Coefficients in Areal Sweep Efficiency Correlations | | | |
|---|-----------|-------------|----------------|
| Coefficient | Five Spot | Direct Line | Staggered Line |
| a_1 | -0.2062 | -0.3014 | -0.2077 |
| a_2 | -0.0712 | -0.1568 | -0.1059 |
| a_3 | -0.511 | -0.9402 | -0.3526 |
| a_4 | 0.3048 | 0.3714 | 0.2608 |
| a_5 | 0.123 | -0.0865 | 0.2444 |
| a_6 | 0.4394 | 0.8805 | 0.3158 |

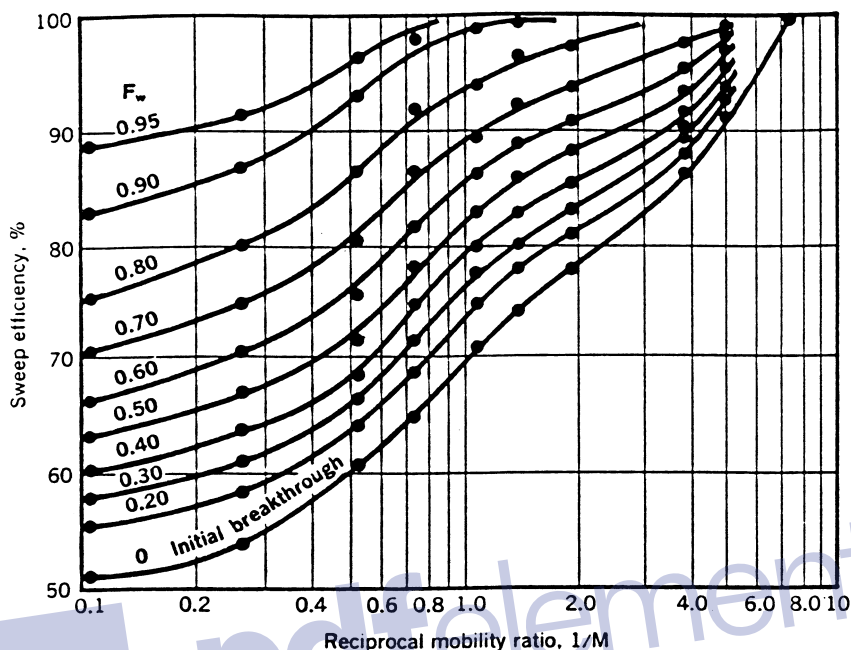


Figure 14-36. Areal sweep efficiency as a function of $1/M$ and f_w . (Permission to publish by the Society of Petroleum Engineers.)

Craig (1971) proposed that for a given value of E_{ABT} for a five-spot flood pattern, the ratio Q_i/Q_{iBT} that corresponds to W_{inj}/W_{iBT} could be determined mathematically by evaluating the following expression:

$$\frac{Q_i}{Q_{iBT}} = 1 + E_{ABT} \int_1^x \left(\frac{1}{E_A} \right) dx$$

with

$$x = \frac{W_{inj}}{W_{iBT}}$$

where Q_i = total pore volumes of water injected any time after breakthrough = $1/(df_w/dS_w)_{S_w2}$

Q_{iBT} = total pore volumes of water injected at water breakthrough = $1/(df_w/dS_w)_{S_wf}$

Values of W_i/W_{iBT} at which $E_A = 100$ percent

2.978 2.872 2.769 2.670 2.575 2.483 2.394 2.309 2.226 2.147

| W_i/W_{iBT} | E_{ABT} percent | | | | | | | | | |
|---------------|-------------------|-------|-------|-------|-------|-------|-------|-------|-------|-------|
| | 80. | 81. | 82. | 83. | 84. | 85. | 86. | 87. | 88. | 89. |
| 1.0 | 1.000 | 1.000 | 1.000 | 1.000 | 1.000 | 1.000 | 1.000 | 1.000 | 1.000 | 1.000 |
| 1.2 | 1.194 | 1.194 | 1.194 | 1.194 | 1.194 | 1.194 | 1.194 | 1.194 | 1.194 | 1.194 |
| 1.4 | 1.377 | 1.378 | 1.378 | 1.378 | 1.378 | 1.379 | 1.379 | 1.379 | 1.379 | 1.379 |
| 1.6 | 1.553 | 1.553 | 1.554 | 1.555 | 1.555 | 1.555 | 1.556 | 1.556 | 1.557 | 1.557 |
| 1.8 | 1.722 | 1.723 | 1.724 | 1.725 | 1.725 | 1.726 | 1.727 | 1.728 | | |
| 2.0 | 1.886 | 1.887 | 1.888 | 1.890 | | | | | | |
| 2.2 | 2.045 | | | | | | | | | |

Values of W_i/W_{iBT} at which $E_A = 100$ percent

2.070 1.996 1.925 1.856 1.790 1.726 1.664 1.605 1.547 1.492

| W_i/W_{iBT} | E_{ABT} percent | | | | | | | | | |
|---------------|-------------------|-------|-------|-------|-------|-------|-------|-------|-------|-------|
| | 90. | 91. | 92. | 93. | 94. | 95. | 96. | 97. | 98. | 99. |
| 1.0 | 1.000 | 1.000 | 1.000 | 1.000 | 1.000 | 1.000 | 1.000 | 1.000 | 1.000 | 1.000 |
| 1.2 | 1.194 | 1.195 | 1.195 | 1.195 | 1.195 | 1.195 | 1.195 | 1.195 | 1.195 | 1.195 |
| 1.4 | 1.380 | 1.380 | 1.380 | 1.380 | 1.381 | | | | | |
| 1.6 | 1.558 | | | | | | | | | |

Values of W_i/W_{iBT} at which $E_A = 100$ percent

1.439 1.387 1.338 1.290 1.244 1.199 1.157 1.115 1.075 1.037

Willhite (1986) proposed an analytical expression for determining the value of the ratio (Q_i/Q_{iBT}) at any value of (W_{inj}/W_{iBT}) for a given E_{ABT} :

$$\frac{Q_i}{Q_{iBT}} = 1 + a_1 e^{-a_1} [Ei(a_2) - Ei(a_1)] \quad (14-68)$$

where

$$a_1 = 3.65 E_{ABT}$$

$$a_2 = a_1 + \ln \frac{W_{inj}}{W_{iBT}}$$

and $Ei(x)$ is the Ei function as approximated by:

$$Ei(x) = 0.57721557 + \ln(x) + \sum_{n=1}^{\infty} \frac{x^n}{n(n!)}$$

To include the areal sweep efficiency in waterflooding calculations, the proposed methodology is divided into the following three phases:

1. Initial calculations
2. Recovery performance calculations to breakthrough
3. Recovery performance calculations after breakthrough

The specific steps of each of the above three phases are summarized below.

Phase 1: Initial Calculations ($S_{gi} = 0$, $EV = 100\%$)

Step 1. Express the relative permeability data as relative permeability ratios and plot them versus their corresponding water saturations on a semi-log scale. Describe the resulting straight line by the following relationship:

$$\frac{k_{ro}}{k_{rw}} = a e^{bS_w}$$

Step 2. Calculate and plot f_w versus S_w .

Step 3. Draw a tangent to the fractional flow curve as originated from S_{wi} and determine:

- Point of tangency (S_{wf} , f_{wf}), i.e., (S_{wBT} , f_{wBT})
- Average water saturation at breakthrough \bar{S}_{wBT}
- Slope of the tangent $\left(\frac{df_w}{dS_w}\right)_{S_{wf}}$

Step 4. Using S_{wi} and \bar{S}_{wBT} , determine the corresponding values of k_{ro} and k_{rw} . Designate these values $k_{ro}@S_{wBT}$ and $k_{rw}@S_{wBT}$, respectively.

Step 5. Calculate the mobility ratio as defined by Equation 14-61:

$$M = \frac{k_{rw}@S_{wBT}}{k_{ro}@S_{wi}} \frac{\mu_o}{\mu_w}$$

- Step 6.* Select several water saturations S_{w2} between S_{wf} and $(1 - S_{or})$ and numerically or graphically determine the slope $\left(\frac{df_w}{dS_w}\right)_{S_{w2}}$ at each saturation.
- Step 7.* Plot $\left(\frac{df_w}{dS_w}\right)_{S_{w2}}$ versus S_{w2} on a Cartesian scale.

Phase 2: Recovery Performance to Breakthrough

Assuming that the vertical sweep efficiency E_V and initial gas saturation S_{gi} are 100% and 0%, respectively, the required steps to complete the calculations of this phase are summarized below:

Step 1. Calculate the areal sweep efficiency at breakthrough E_{ABT} from Figure 14-35 or Equation 14-64.

Step 2. Calculate pore volumes of water injected at breakthrough by applying Equation 14-41:

$$Q_{iBT} = \frac{1}{\left(\frac{df_w}{dS_w}\right)_{S_{wf}}} = (\bar{S}_{wBT} - S_{wi})$$

Step 3. Calculate cumulative water injected at breakthrough W_{iBT} from Equation 14-43 or 14-44:

$$W_{iBT} = (PV)(\bar{S}_{wBT} - S_{wi})E_{ABT} = (PV)(Q_{iBT})E_{ABT}$$

Step 4. Assuming a constant water-injection rate i_w , calculate time to breakthrough t_{BT} :

$$t_{BT} = \frac{W_{iBT}}{i_w}$$

Step 5. Calculate the displacement efficiency at breakthrough E_{DBT} from Equation 14-50:

$$E_{DBT} = \frac{\bar{S}_{wBT} - S_{wi}}{1 - S_{wi}}$$

Step 6. Compute the cumulative oil production at breakthrough from Equation 14-51:

$$(N_p)_{BT} = N_S E_{DBT} E_{ABT}$$

Notice that when $S_{gi} = 0$, the cumulative oil produced at breakthrough is equal to cumulative water injected at breakthrough, or:

$$(N_p)_{BT} = \frac{W_{iBT}}{B_o}$$

Step 7. Divide the interval between 0 and W_{iBT} into any arbitrary number of increments and set the following production data for each increment:

$$Q_o = i_w/B_o$$

$$Q_w = 0$$

$$WOR = 0$$

$$N_p = W_{inj}/B_o$$

$$W_p = 0$$

$$t = W_{inj}/i_w$$

Step 8. Express Steps 1 through 7 in the following tabulated form:

| W_{inj} | $t = W_{inj}/i_w$ | $N_p = W_{inj}/B_o$ | $Q_o = i_w/B_o$ | WOR_s | $Q_w = Q_o WOR_s$ | W_p |
|-----------|-------------------|---------------------|-----------------|---------|-------------------|-------|
| 0 | 0 | 0 | 0 | 0 | 0 | 0 |
| • | • | • | • | 0 | 0 | 0 |
| • | • | • | • | 0 | 0 | 0 |
| • | • | • | • | 0 | 0 | 0 |
| W_{iBT} | t_{BT} | $(N_p)_{BT}$ | • | WOR_s | • | 0 |

Phase 3: Recovery Performance After Breakthrough ($S_{gi} = 0$, $EV = 100\%$)

Craig et al. (1955) point out that after water breakthrough, the displacing fluid continues to displace more oil from the already swept zone (behind the front) and from newly swept regions in the pattern. Therefore, the producing water-oil ratio WOR is estimated by separating the displaced area into two distinct zones:

1. Previously swept area of the flood pattern
2. Newly swept zone that is defined as the region that was just swept by the displacing fluid

The previously swept area contains all reservoir regions where water saturation is greater than S_{wf} and continues to produce both oil and water. With continuous water-injection, the injected water contacts more regions as the area sweep efficiency increases. This newly swept zone is assumed to produce only oil. Craig et al. (1955) developed an approach for determining the producing WOR that is based on estimating the incremental oil produced, $(\Delta N_p)_{\text{newly}}$, from the newly swept region for 1 bbl of total production. The authors proposed that the incremental oil produced from the newly swept zone is given by:

$$(\Delta N_p)_{\text{newly}} = E\lambda \quad (14-69)$$

with

$$E = \frac{S_{wf} - S_{wi}}{E_{\text{ABT}}(\bar{S}_{\text{wBT}} - S_{wi})}$$

$$\lambda = 0.2749 \left(\frac{W_{\text{iBT}}}{W_{\text{inj}}} \right)$$

Notice that the parameter E is constant, whereas the parameter λ is decreasing with continuous water-injection. Craig et al. (1955) expressed the producing water-oil ratio as:

$$\text{WOR}_s = \frac{f_{w2} (1 - (\Delta N_p)_{\text{newly}})}{1 - [f_{w2} (1 - (\Delta N_p)_{\text{newly}})]} \left(\frac{B_o}{B_w} \right) \quad (14-70)$$

where WOR_s = surface water-oil ratio, STB/STB

W_{iBT} = cumulative water injected at breakthrough, bbl

W_{inj} = cumulative water injected at any time after breakthrough, bbl

f_{w2} = water cut at the producing well, bbl/bbl

Note that when the areal sweep efficiency E_A reaches 100%, the incremental oil produced from the newly swept areal is zero, i.e., $(\Delta N_P)_{\text{newly}} = 0$, which reduces the above expression to Equation 14-28:

$$\text{WOR}_s = \frac{f_{w2}}{1-f_{w2}} \left(\frac{B_o}{B_w} \right) = \frac{B_o}{B_w \left(\frac{1}{f_{w2}} - 1 \right)}$$

The recommended methodology for predicting the recovery performance after breakthrough is summarized in the following steps:

Step 1. Select several values of $W_{\text{inj}} > W_{\text{iBT}}$.

Step 2. Assuming constant injection rate i_w , calculate the time t required to inject W_{inj} barrels of water.

Step 3. Calculate the ratio $W_{\text{inj}}/W_{\text{iBT}}$ for each selected W_{inj} .

Step 4. Calculate the areal sweep efficiency E_A at each selected W_{inj} by applying Equation 14-65 or 14-66:

$$E_A = E_{\text{ABT}} + 0.633 \log \left(\frac{W_{\text{inj}}}{W_{\text{iBT}}} \right) = E_{\text{ABT}} + 0.2749 \ln \left(\frac{W_{\text{inj}}}{W_{\text{iBT}}} \right)$$

Step 5. Calculate the ratio Q_i/Q_{iBT} that corresponds to each $W_{\text{inj}}/W_{\text{iBT}}$ from Table 14-1. The ratio Q_i/Q_{iBT} is a function of E_{ABT} and $W_{\text{inj}}/W_{\text{iBT}}$.

Step 6. Determine the total pore volumes of water injected by multiplying each ratio of Q_i/Q_{iBT} (obtained in Step 5) by Q_{iBT} , or:

$$Q_i = \left(\frac{Q_i}{Q_{\text{iBT}}} \right) Q_{\text{iBT}}$$

Step 7. From the definition of Q_i , as expressed by Equation 14-46, determine the slope $(df_w/dS_w)_{S_{w2}}$ for each value of Q_i by:

$$\left(\frac{df_w}{dS_w} \right)_{S_{w2}} = \frac{1}{Q_i}$$

Step 8. Read the value of S_{w2} , i.e., water saturation at the producing well, that corresponds to each slope from the plot of $(df_w/dS_w)_{S_{w2}}$ vs. S_{w2} (see Phase 1, Step 7).

Step 9. Calculate the reservoir water cut at the producing well f_{w2} for each S_{w2} from Equation 14-24 or 14-37.

$$f_{w2} = \frac{1}{1 + \frac{\mu_w}{\mu_o} \frac{k_{ro}}{k_{rw}}}$$

or

$$f_{w2} = \frac{1}{1 + \left(\frac{\mu_w}{\mu_o}\right) a e^{bS_{w2}}}$$

Step 10. Determine the average water saturation in the swept area \bar{S}_{w2} by applying Equation 14-45:

$$\bar{S}_{w2} = S_{w2} + \frac{1 - f_{w2}}{\left(\frac{df_w}{dS_w}\right)_{S_{w2}}}$$

Step 11. Calculate the displacement efficiency E_D for each \bar{S}_{w2} :

$$E_D = \frac{\bar{S}_{w2} - S_{wi}}{1 - S_{wi}}$$

Step 12. Calculate cumulative oil production from Equation 14-6:

$$N_p = N_s E_D E_A E_V$$

For 100% vertical sweep efficiency:

$$N_p = N_s E_D E_A$$

Example 14-11¹

An oil reservoir is under consideration for waterflooding. The relative permeability data and the corresponding water cut are given below:

| | | | | | | | | | |
|----------|-------|--------|--------|--------|--------|--------|--------|--------|--------|
| S_w | 0.100 | 0.300 | 0.400 | 0.450 | 0.500 | 0.550 | 0.600 | 0.650 | 0.700 |
| k_{ro} | 1.000 | 0.373 | 0.210 | 0.148 | 0.100 | 0.061 | 0.033 | 0.012 | 0.000 |
| k_{rw} | 0.000 | 0.070 | 0.169 | 0.226 | 0.300 | 0.376 | 0.476 | 0.600 | 0.740 |
| f_w | 0.000 | 0.2729 | 0.6168 | 0.7533 | 0.8571 | 0.9250 | 0.9665 | 0.9901 | 1.0000 |

Reservoir properties are as follows:

| | |
|-----------------------------|----------|
| Flood area, acres | = 40 |
| Thickness, ft | = 5 |
| Average permeability, md | = 31.5 |
| Porosity, % | = 20 |
| Initial water saturation, % | = 10 |
| Connate water saturation, % | = 10 |
| Current gas saturation, % | = 0 |
| Water viscosity, cp | = 0.5 |
| Oil viscosity, cp | = 1.0 |
| Reservoir pressure, psi | = 1000 |
| Constant B_o , bbl/STB | = 1.20 |
| Flood pattern | = 5 spot |
| Wellbore radius, ft | = 1.0 |

Predict the recovery performance under a constant water-injection rate of 269 bbl/day.

¹From Craig, *The Reservoir Engineering Aspects of Waterflooding*, Dallas: Society of Petroleum Engineers, 1971, p. 116.

Solution

Phase 1. Initial Calculations

Step 1. Calculate pore volume and oil volume at start of flood:

$$(PV) = 7758(40)(5)(0.20) = 310,320\text{bbl}$$

$$N_s = 310,320(1 - 0.1)/1.20 = 232,740\text{STB}$$

Step 2. Plot f_w vs. S_w on a Cartesian scale, as shown in Figure 14-37, and determine:

$$S_{wf} = S_{wBT} = 0.469 \quad Q_{iBT} = \frac{1}{2.16} = 0.463$$

$$f_{wf} = f_{wBT} = 0.798 \quad \bar{S}_{wBT} = 0.563$$

$$(df_w/dS_w)_{S_{wf}} = 2.16$$

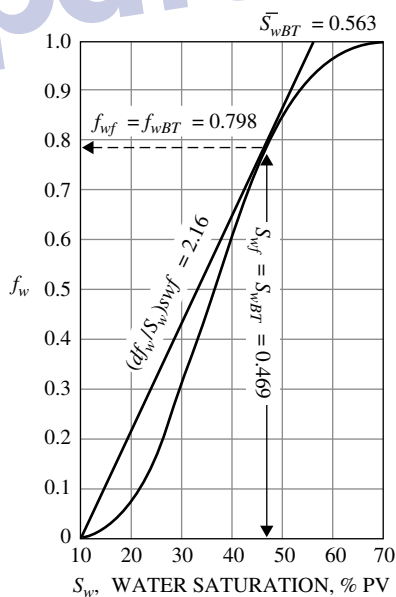


Figure 14-37. The f_w curve for Example 14-11. (Permission to publish by the Society of Petroleum Engineers.)

Step 3. Determine k_{ro} and k_{rw} at S_{wi} and \bar{S}_{wBT} from the relative permeability data, to give:

$$k_{ro} @ 0.1 = 1.00$$

$$k_{rw} @ 0.563 = 0.40$$

Step 4. Calculate the mobility ratio M from Equation 14-61:

$$M = \frac{0.4}{1.0} \frac{1.0}{0.5} = 0.8$$

Step 5. Calculate the areal sweep efficiency at breakthrough from Equation 14-64 or Figure 14-35:

$$E_{ABT} = 0.71702$$

Step 6. Select several values of S_{w2} between 0.469 and 0.700 and determine the slope, graphically or numerically, at each selected saturation:

| S_{w2} | f_{w2} | df_w/dS_w |
|----------|----------|-------------|
| 0.469 | 0.798 | 2.16 |
| 0.495 | 0.848 | 1.75 |
| 0.520 | 0.888 | 1.41 |
| 0.546 | 0.920 | 1.13 |
| 0.572 | 0.946 | 0.851 |
| 0.597 | 0.965 | 0.649 |
| 0.622 | 0.980 | 0.477 |
| 0.649 | 0.990 | 0.317 |
| 0.674 | 0.996 | 0.195 |
| 0.700 | 1.000 | 0.102 |

Step 7. Plot df_w/dS_w vs. S_{w2} as shown in Figure 14-38.

Phase 2. Calculation of Recovery Performance to Breakthrough

Step 1. Calculate Q_{iBT} using Equation 14-41:

$$Q_{iBT} = (\bar{S}_{wBT} - S_{wi})$$

$$Q_{iBT} = (0.563 - 0.1) = 0.463$$

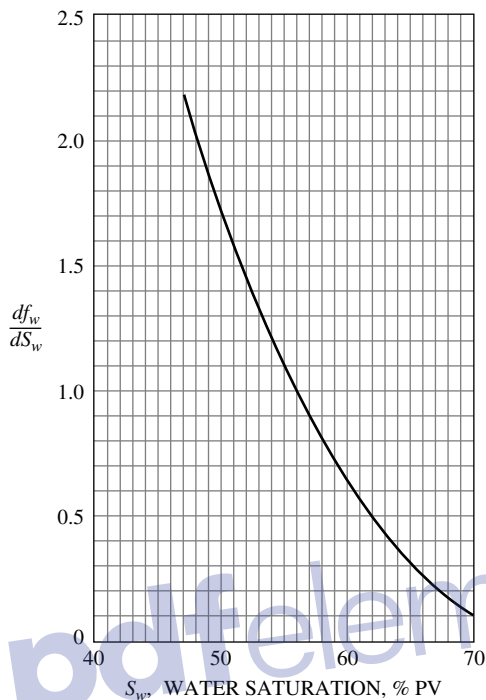


Figure 14-38. Derivative curve for Example 14-11. (Permission to publish by the Society of Petroleum Engineers.)

Step 2. Calculate cumulative water injected at breakthrough from Equation 14-43 or 14-44:

$$W_{iBT} = (PV)Q_{iBT}E_{ABT}$$

$$W_{iBT} = (310,320)(0.463)(0.71702) = 103,020 \text{ bbl}$$

Step 3. Calculate time to breakthrough:

$$t_{BT} = W_{iBT}/i_w$$

$$t_{BT} = 103,020 / 269 = 383 \text{ days}$$

Step 4. Calculate the displacement efficiency at breakthrough E_{DAB} from Equation 14-50:

$$E_{DBT} = \frac{\bar{S}_{wBT} - S_{wi}}{1 - S_{wi}}$$

$$E_{DBT} = \frac{0.563 - 0.1}{1 - 0.1} = 0.5144$$

Step 5. Calculate cumulative oil production at breakthrough by using Equation 14-51.

$$(N_p)_{BT} = N_s E_{DBT} E_{ABT}$$

$$(N_p)_{BT} = (232,740)(0.5144)(0.717) = 85,850 \text{ STB}$$

Notice that when $S_{gi} = 0$, the cumulative water injected at breakthrough W_{iBT} will displace an equivalent volume of oil, i.e.:

$$(N_p)_{BT} = \frac{W_{iBT}}{B_o} = \frac{103,020}{1.2} = 85,850 \text{ STB}$$

Step 6. Calculate the surface water cut WOR_s exactly at breakthrough from Equation 14-70:

$$E = \frac{S_{wf} - S_{wi}}{E_{ABT}(\bar{S}_{wBT} - S_{wi})} = \frac{0.469 - 0.1}{0.717(0.563 - 0.1)} = 1.1115$$

$$\lambda = 0.2749 \left(\frac{W_{iBT}}{W_{inj}} \right) = 0.2749 \left(\frac{103,020}{103,020} \right) = 0.2749$$

$$(\Delta N_p)_{newly} = E\lambda = (1.1115)(0.2749) = 0.30555$$

$$WOR_s = \frac{f_{wf} \left[1 - (\Delta N_p)_{newly} \right]}{1 - f_{wf} \left[1 - (\Delta N_p)_{newly} \right]} \left(\frac{B_o}{B_w} \right) = \frac{0.798[1 - 0.30555]}{1 - 0.798[1 - 0.30555]} \left(\frac{1.2}{1} \right)$$

$$= 1.49 \text{ STB / STB}$$

| (1) | (2) | (3) | (4) | (5) | (6) | (7) | (8) | (9) | (10) | (11) | (12) | (13) | (14) | (15) | (16) |
|-----------|---------------------------|--------------------------|-----------|----------------------|--|----------------------------------|------------|-----------|----------------|----------|-----------|-----------|-----------|-----------|-------|
| W_{inj} | $t = \frac{W_{inj}}{I_w}$ | $\frac{W_{inj}}{W_{RT}}$ | E_A | $\frac{Q_i}{Q_{RT}}$ | $\left(\frac{Q_i}{Q_{RT}}\right)^{RT} = \frac{1}{Q_i}$ | $\left(\frac{df_w}{ds_w}\right)$ | S_{w2} | f_{w2} | \bar{S}_{w2} | E_b | N_p | W_p | WOR_s | Q_o | Q_w |
| (Assumed) | (days) | | Eq. 14-65 | Table 14-1 | | Fig. 14-38 | Fig. 14-37 | Eq. 14-45 | Eq. 14-10 | Eq. 14-6 | Eq. 14-53 | Eq. 14-70 | Eq. 14-55 | Eq. 14-56 | |
| 103,020 | 383 | 1.0 | 0.717 | 1.000 | 0.463 | 2.159 | 0.470 | 0.800 | 0.563 | 0.514 | 85,850 | 0 | 1.49 | 99.6 | 149.4 |
| 123,620 | 460 | 1.2 | 0.767 | 1.193 | 0.552 | 1.810 | 0.492 | 0.843 | 0.579 | 0.532 | 100,292 | 3270 | 2.03 | 83.3 | 169.1 |
| 144,230 | 536 | 1.4 | 0.809 | 1.375 | 0.636 | 1.570 | 0.507 | 0.870 | 0.590 | 0.544 | 106,986 | 15,847 | 2.55 | 71.73 | 182.9 |
| 164,830 | 613 | 1.6 | 0.846 | 1.548 | 0.717 | 1.394 | 0.524 | 0.893 | 0.601 | 0.557 | 113,820 | 28,246 | 3.12 | 62.3 | 194.4 |
| 185,440 | 689 | 1.8 | 0.879 | 1.715 | 0.794 | 1.259 | 0.534 | 0.905 | 0.610 | 0.567 | 119,559 | 41,969 | 3.63 | 55.7 | 202.2 |
| 206,040 | 766 | 2.0 | 0.906 | 1.875 | 0.869 | 1.151 | 0.543 | 0.920 | 0.613 | 0.570 | 128,417 | 51,940 | 4.24 | 49.4 | 209.5 |
| 257,550 | 958 | 2.5 | 0.969 | 2.256 | 1.046 | 0.956 | 0.562 | 0.937 | 0.628 | 0.587 | 136,618 | 93,608 | 5.56 | 39.8 | 221.3 |
| 309,060 | 1149 | 3.0 | 1.000 | 2.619 | 1.214 | 0.823 | 0.575 | 0.944 | 0.637 | 0.597 | 138,946 | 142,325 | 22.33 | 11 | 255 |
| 412,080 | 1532 | 4.0 | 1.000 | 3.336 | 1.545 | 0.647 | 0.597 | 0.963 | 0.653 | 0.614 | 142,902 | 240,598 | 31.23 | 8 | 259 |
| 515,100 | 1915 | 5.0 | 1.000 | 4.053 | 1.877 | 0.533 | 0.611 | 0.973 | 0.660 | 0.622 | 144,764 | 341,383 | 43.24 | 6 | 262 |
| 618,120 | 2298 | 6.0 | 1.000 | 4.770 | 2.208 | 0.453 | 0.622 | 0.980 | 0.664 | 0.627 | 145,928 | 443,006 | 58.8 | 4 | 264 |
| 824,160 | 3064 | 8 | 1.000 | 6.204 | 2.872 | 0.348 | 0.637 | 0.985 | 0.676 | 0.640 | 148,954 | 645,415 | 78.8 | 3 | 265 |
| 1,030,200 | 3830 | 10 | 1.000 | 7.638 | 3.536 | 0.283 | 0.650 | 0.990 | 0.683 | 0.648 | 150,816 | 849,221 | 119 | 2 | 267 |
| 1,545,300 | 5745 | 15 | 1.000 | 11.223 | 5.199 | 0.192 | 0.677 | 0.995 | 0.697 | 0.663 | 154,307 | 1,360,132 | 239 | 1 | 268 |

Step 7. Set up the following table to describe the oil recovery performance to breakthrough (remember, $S_{gi} = 0$):

| W_{inj} | $t = \frac{W_{inj}}{i_w}$ | $N_p = \frac{W_{inj}}{B_o}$ | $Q_o = \frac{i_w}{B_o}$ | WOR_s | $Q_w = Q_o WOR_s$ | W_p |
|-----------|---------------------------|-----------------------------|-------------------------|---------|-------------------|-------|
| bbl | days | STB | STB | STB/STB | STB/day | STB |
| 0 | 0 | 0 | 0 | 0 | 0 | 0 |
| 20,000 | 74.34 | 16,667 | 224 | 0 | 0 | 0 |
| 40,000 | 148.7 | 33,333 | 224 | 0 | 0 | 0 |
| 60,000 | 223.0 | 50,000 | 224 | 0 | 0 | 0 |
| 80,000 | 297.4 | 66,667 | 224 | 0 | 0 | 0 |
| 103,020 | 383.0 | 85,850 | 224 | 1.49 | 334 | 0 |

Phase 3. Oil Recovery Calculations After Breakthrough

A step-by-step description of the oil recovery calculations as well as a convenient worksheet to perform the computations after breakthrough are given below:

Column 1: Select several values of W_{inj} .

Column 2: For a constant injection rate, calculate the time t required to W_{inj} barrels of water.

Column 3: Divide values of W_{inj} in Column 1 by W_{iBT} .

Column 4: Calculate E_A from Equation 14-65 for value of W_{inj}/W_{iBT} .

Column 5: Determine the values of the ratio Q_i/Q_{iBT} from Table 14-1 for each value of W_{inj}/W_{iBT} in Column 4.

Column 6: Obtain Q_i by multiplying Column 5 by Q_{iBT} .

Column 7: The term $(df_w/dS_w)_{S_{w2}}$ is the reciprocal of Column 6, i.e., $1/Q_i$.

Column 8: Determine the value of S_{w2} from the plot of df_w/dS_w vs. S_w as given in Figure 14-38.

Column 9: Calculate the value of f_{w2} that corresponds to each value of S_{w2} in Column 8 by using Equation 14-24 or Figure 14-37.

Column 10: Calculate the average water saturation in the swept area \bar{S}_{w2} by applying Equation 14-45.

Column 11: Calculate the displacement efficiency E_D by using Equation 14-10 for each value of \bar{S}_{w2} in Column 10.

Column 12: Calculate cumulative oil production N_p by using Equation 14-53.

Column 13: Calculate the cumulative water production W_p from Equation 14-53.

Column 14: Calculate the surface water-oil ratio WOR_s from Equation 14-70.

Column 15: Calculate the oil flow rate Q_o by using Equation 14-55.

Column 16: Determine the water flow rate Q_w by multiplying Column 14 by Column 15.

Results of the above waterflooding calculations are expressed graphically in Figure 14-39.

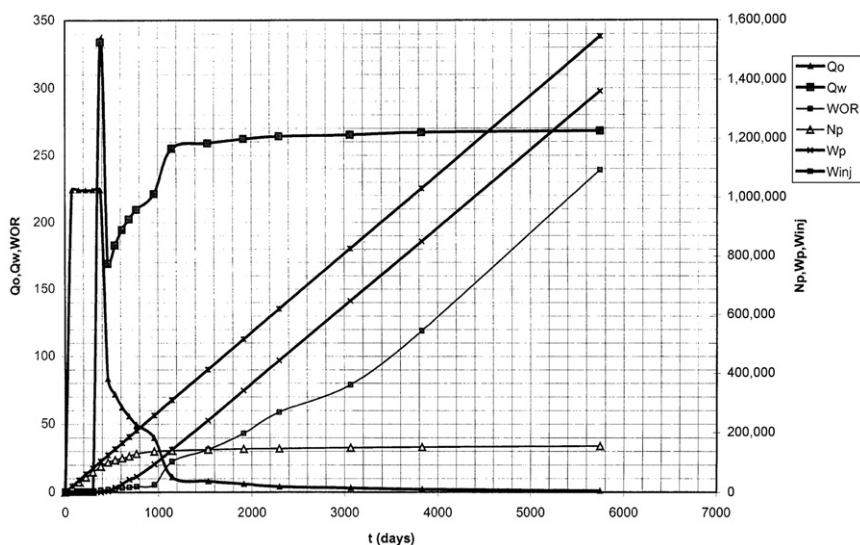


Figure 14-39. Performance curves for Example 14-11.

Note that all the areal sweep efficiency correlations that have been presented thus far are based on idealized cases with severe imposed assumptions on the physical characteristics of the reservoir. These assumptions include:

- Uniform isotropic permeability distribution
- Uniform porosity distribution
- No fractures in reservoir
- Confined patterns
- Uniform saturation distribution
- Off-pattern wells

To understand the effect of eliminating any of the above assumptions on the areal sweep efficiency, it has been customary to employ laboratory models to obtain more generalized numerical expressions. However, it is virtually impossible to develop a generalized solution when eliminating all or some of the above assumptions.

Landrum and Crawford (1960) have studied the effects of directional permeability on waterflood areal sweep efficiency. Figures 14-40 and 14-41 illustrate the impact of directional permeability variations on areal sweep efficiency for a line drive and five-spot pattern flood.

Two key elements affect the performance of waterflooding that must be included in recovery calculations: (1) water-injection rate, i.e., fluid injectivity, and (2) effect of initial gas saturation on the recovery performance.

These key elements are discussed next.

Fluid Injectivity

Injection rate is a key economic variable that must be considered when evaluating a waterflooding project. The waterflood project's life and, consequently, the economic benefits will be directly affected by the rate at which fluid can be injected and produced. Estimating the injection rate is also important for the proper sizing of injection equipment and pumps. Although injectivity can be best determined from small-scale pilot floods, empirical methods for estimating water injectivity for regular pattern floods have been proposed by Muskat (1948) and Deppe (1961). The authors derived their correlations based on the following assumptions:

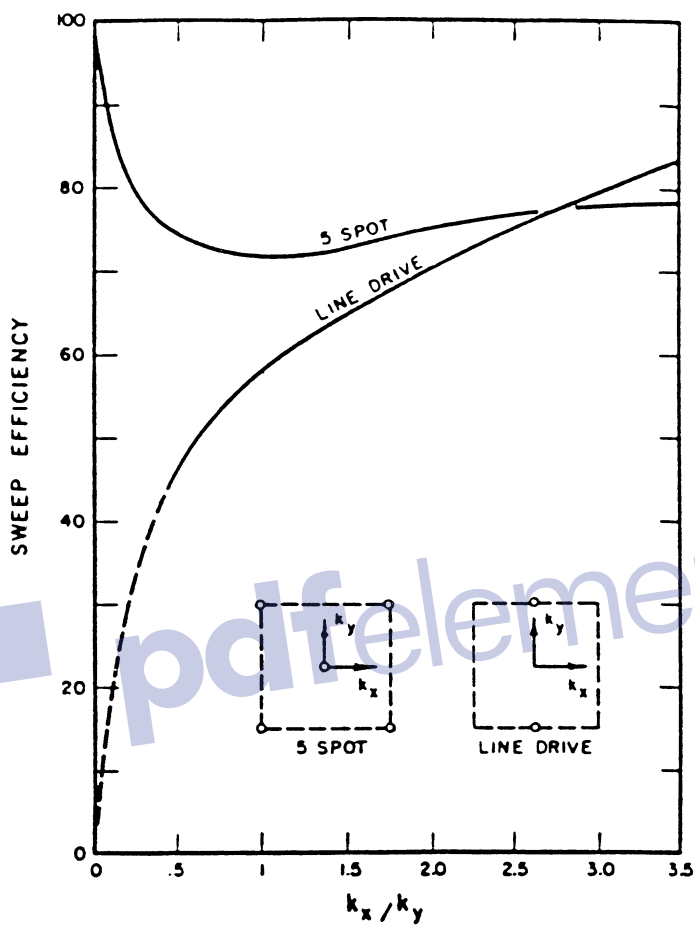


Figure 14-40. Effect of directional permeability on E_A . (Permission to publish by the Society of Petroleum Engineers.)

- Steady-state conditions
- No initial gas saturation
- Mobility ratio of unity

Water injectivity is defined as the ratio of the water-injection to the pressure difference between the injector and producer, or:

$$I = \frac{i_w}{\Delta P}$$

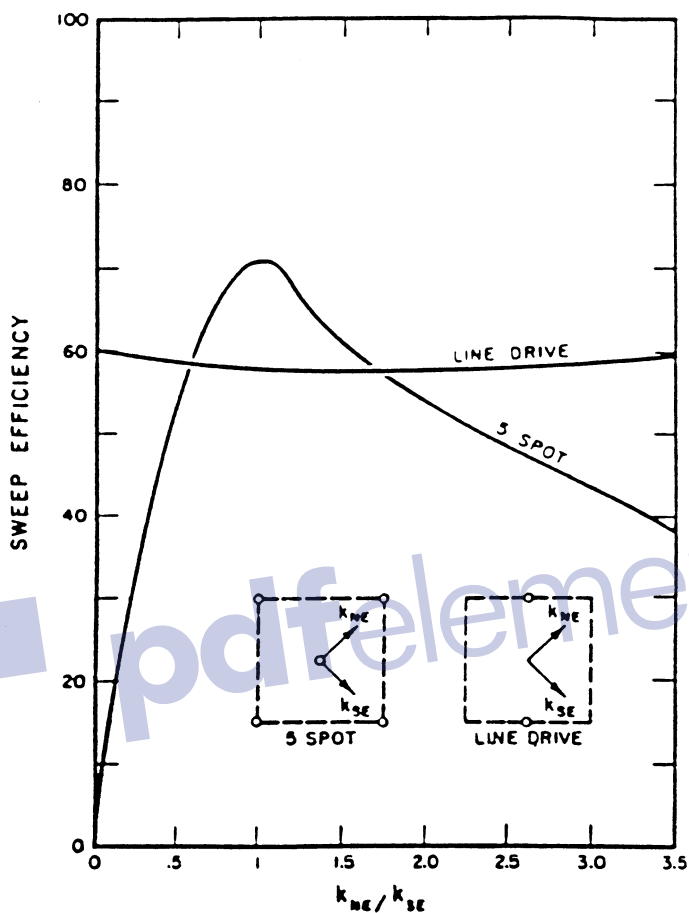


Figure 14-41. Effect of directional permeability on E_A . (Permission to publish by the Society of Petroleum Engineers.)

where I = injectivity, bbl/day/psi

i_w = injection rate, bbl/day

ΔP = difference between injection pressure and producing well bottom-hole flowing pressure.

When the injection fluid has the same mobility as the reservoir oil (mobility ratio $M = 1$), the initial injectivity at the start of the flood is referred to as I_{base} , or:

$$I_{\text{base}} = \frac{i_{\text{base}}}{\Delta P_{\text{base}}}$$

where i_{base} = initial (base) water-injection rate, bbl/day
 ΔP_{base} = initial (base) pressure difference between injector and producer

For a five-spot pattern that is completely filled with oil, i.e., $S_{\text{gi}} = 0$, Muskat (1948) proposed the following injectivity equation:

$$I_{\text{base}} = \frac{0.003541 h k k_{\text{ro}} \Delta P_{\text{base}}}{\mu_{\text{o}} \left[\ln \frac{d}{r_{\text{w}}} - 0.619 \right]} \quad (14-71)$$

or

$$\left(\frac{i}{\Delta P} \right)_{\text{base}} = \frac{0.003541 h k k_{\text{ro}}}{\mu_{\text{o}} \left[\ln \frac{d}{r_{\text{w}}} - 0.619 \right]} \quad (14-72)$$

where i_{base} = base (initial) water-injection rate, bbl/day
 h = net thickness, ft
 k = absolute permeability, md
 k_{ro} = oil relative permeability as evaluated at S_{wi}
 ΔP_{base} = base (initial) pressure difference, psi
 d = distance between injector and producer, ft
 r_{w} = wellbore radius, ft

Several studies have been conducted to determine the fluid injectivity at mobility ratios other than unity. All of the studies concluded the following:

- At favorable mobility ratios, i.e., $M < 1$, the fluid injectivity declines as the areal sweep efficiency increases.
- At unfavorable mobility ratios, i.e., $M > 1$, the fluid injectivity increases with increasing areal sweep efficiency.

Caudle and Witte (1959) used the results of their investigation to develop a mathematical expression that correlates the fluid injectivity with the

mobility ratio and areal sweep efficiency for five-spot patterns. The correlation may only be used in a *liquid-filled system*, i.e., $S_{gi} = 0$. The authors presented their correlation in terms of the **conductance ratio** γ , which is defined as the ratio of the fluid injectivity at any stage of the flood to the initial (base) injectivity, i.e.:

$$\gamma = \frac{\text{Fluid injectivity at any stage of the flood}}{\text{Base (initial) fluid injectivity}}$$

$$\gamma = \frac{\left(\frac{i_w}{\Delta P}\right)}{\left(\frac{i}{\Delta P}\right)_{\text{base}}} \quad (14-73)$$

Caudle and Witte presented the variation in the conductance ratio with EA and M in graphical form as shown in Figure 14-42. Note again that if an initial gas is present, the Caudle-Witte conductance ratio will not be applicable until the gas is completely dissolved or the system becomes liquid filled (fill-up occurs). The two possible scenarios for the practical use of Equation 14-73 follow:

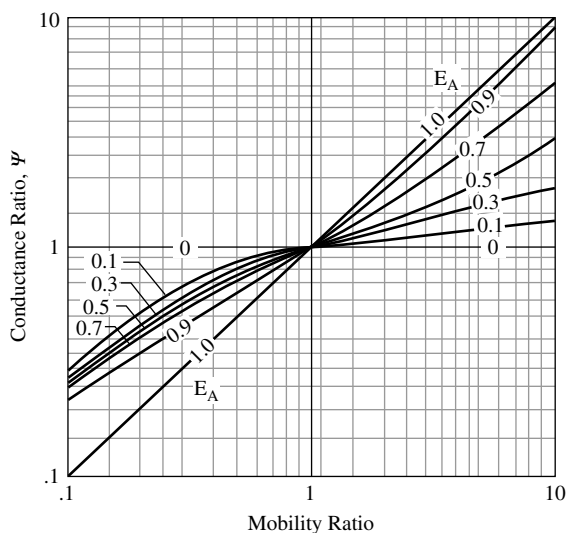


Figure 14-42. Conductance ratio curve. (Permission to publish by the Society of Petroleum Engineers.)

Scenario 1: Constant Injection Pressure and Variable Injection Rate

At constant injection pressure, i.e., $\Delta P_{\text{base}} = \Delta P$, the conductance ratio as expressed by Equation 14-73 can be written as:

$$\gamma = \frac{i_w}{i_{\text{base}}}$$

or

$$i_w = \gamma i_{\text{base}} \quad (14-74)$$

where i_w = water-injection rate, bbl/day
 i_{base} = base (initial) water-injection rate, bbl/day

Scenario 2: Constant Injection Rate and Variable Injection Pressure

When the water-injection rate is considered constant, i.e., $i_w = i_{\text{base}}$, the conductive ratio is expressed as:

$$\gamma = \frac{\Delta P_{\text{base}}}{\Delta P}$$

or

$$\Delta P = \frac{\Delta P_{\text{base}}}{\gamma} \quad (14-75)$$

where ΔP_{base} = initial (base) pressure difference, psi
 ΔP = pressure difference at any stage of flood, psi

The usefulness of the conductance ratio in determining the pressure and injectivity behavior of the five-spot system can be best described by the following example.

Example 14-12

Estimate the water-injection rate for the waterflood in Example 14-11 at 60,000 and 144,230 bbl of water injected. Assume that the pressure between the injector and producer will remain constant at 3,000 psi.

Solution

Step 1. Calculate the distance between the injector and producer as shown in Figure 14-43, to give:

$$d = \sqrt{(660)^2 + (660)^2} = 933 \text{ ft}$$

Step 2. Calculate the initial (base) injection rate from Equation 14-71:

$$i_w = \frac{0.003541(5)(31.5)(1)(3000)}{(1)\left(\ln \frac{933}{1} - 0.619\right)} = 269.1 \text{ bbl/day}$$

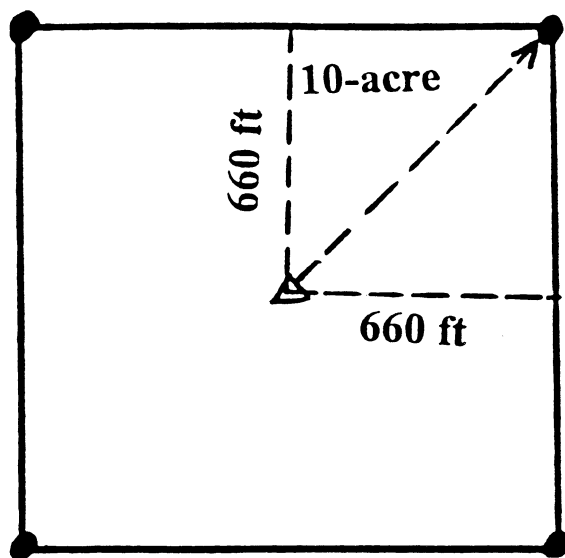


Figure 14-43. Forty-acre, five-spot spacing.

Step 3. Notice that the cumulative water injected of 60,000 bbl is less than the amount of cumulative water injected at breakthrough of 103,020 bbl; therefore, $M = 0.8$ (remains constant until breakthrough) and E_A from Equation 14-63 is:

$$E_A = \frac{60,000}{(310,320)(0.563 - 0.10)} = 0.418$$

Step 4. Calculate the conductance ratios from Figure 14-42, to give $\gamma = 0.92$.

Step 5. Calculate the water-injection rate when the cumulative water injected reaches 60,000 bbl from Equation 14-74:

$$i_w = (269.1)(0.92) = 247.6 \text{ bbl/day}$$

Step 6. After breakthrough when the cumulative water injected reaches 144,230 barrels of water, the average water saturation in the swept area is 59% (see Example 14-11), or

$$\bar{S}_{w2} = 0.59$$

Step 7. Determine the water relative permeability k_{rw} at 0.59 water saturation (data of Example 14-11), to give $k_{rw} = 0.45$.

Step 8. Calculate the mobility ratio after breakthrough when $W_{inj} = 144,230$ from Equation 14-62:

$$M = \frac{0.45}{1} \frac{1}{0.5} = 0.9$$

Step 9. Calculate the areal sweep efficiency when $W_{inj} = 144,230$ from Equation 14-65: $E_A = 0.845$.

Step 10. Determine the conductance ratio from Figure 14-42: $\gamma = 0.96$.

Step 11. Calculate the water-injection rate from Equation 14-76:

$$i_w = (269.1) (0.96) = 258.3 \text{ bbl/day}$$

The conductance ratio can be expressed more conveniently in a mathematical form as follows. For an areal sweep efficiency of 100%, i.e., $E_A = 1.0$:

$$\gamma = M \quad (14-76)$$

where γ = conductance ratio
 M = mobility ratio

For $1 < E_A < 100\%$:

$$\gamma = a_1 + (a_2 + a_3 E_A) M^{(a_4 + a_5 E_A)} + a_6 \left(\frac{M}{E_A} \right)^2 + a_7 M \quad (14-77)$$

where the coefficients a_1 through a_7 are given below:

| Coefficients | $M < 1$ | $M > 1$ |
|--------------|---------------|---------------|
| a_1 | 0.060635530 | 0.4371235 |
| a_2 | -2.039996000 | 0.5804613 |
| a_3 | 0.025367490 | -0.004392097 |
| a_4 | 1.636640000 | 0.01001704 |
| a_5 | -0.624070600 | 1.28997700 |
| a_6 | -0.0002522163 | 0.00002379785 |
| a_7 | 2.958276000 | -0.015038340 |

Effect of Initial Gas Saturation

When a solution-gas-drive reservoir is under consideration for waterflooding, substantial gas saturation usually exists in the reservoir at the start of the flood. It is necessary to inject a volume of water that approaches the volume of the pore space occupied by the free gas before the oil is produced. This volume of water is called the **fill-up volume**. During the waterflood process, a portion of the initial free gas will usually be displaced by the leading edge of the oil bank due to the favorable mobility ratio between the displacing oil and the displaced gas. This will occur if the initial gas saturation exceeds its critical saturation S_{gc} . It should be noted that the increase in the oil saturation in the oil bank is

exactly equal to the decrease in the initial gas saturation S_{gi} . Also, the increase in oil saturation in the oil bank is the result of water displacing oil from the water zone. The buildup or increase in the oil saturation in the oil zone is sometimes called an “oil resaturation effect.” During this resaturation process, oil displaced from the water zone resaturates pore space in the oil bank previously filled with free gas. During the resaturation process, the oil displaced from the water zone is *not produced*. It is simply displaced from the water zone to a different part of the reservoir, that is, the oil bank. The resaturation process is also referred to as the “gas fill-up” process. With continued water-injection, the leading edge of the oil bank reaches the producing well, and that marks the end of the fill-up period, referred to as “fill-up time.” Because economic considerations dictate that waterflooding should occur at the highest possible injection rates, the associated increase in the reservoir pressure might be sufficient to redissolve all of the trapped gas S_{gt} back in solution. Willhite (1986) points out that relatively small increases in pressure frequently are required to redissolve the trapped gas (see Figure 14-2). Thus, in waterflooding calculations, it is usually assumed that the trapped (residual) gas saturation is zero. A description of the displacement mechanism occurring under a five-spot pattern will indicate the nature of other secondary recovery operations. The five-spot pattern uses a producing well and four injection wells. The four injectors drive the crude oil inward to the centrally located producer. If only one five-spot pattern exists, the ratio of injection to producing wells is 4:1; however, on a full-field scale it includes a large number of adjacent five spots. In such a case, the number of injection wells compared to producing wells approaches a 1:1 ratio.

At the start of the waterflood process in a solution-gas-drive reservoir, the selected flood pattern is usually characterized by a high initial gas saturation of S_{gi} and remaining liquid saturations of S_{oi} and S_{wi} . When initial gas saturation exists in the reservoir, Craig, Geffen, and Morse (1955) developed a methodology that is based on dividing the flood performance into four stages. The method, known as the CGM method after the authors, was developed from experimental data in horizontal laboratory models representing a quadrant of a five spot. Craig et al. identified the following four stages of the waterflood as:

1. Start—interference
2. Interference—fill-up
3. Fill-up—water breakthrough
4. Water breakthrough—end of the project

A detailed description of each stage of the flood is illustrated schematically in Figures 14-44 through 14-46 and described below:

Stage 1: Start—Interference

At the start of the water-injection process in the selected pattern area of a solution-gas-drive reservoir, high gas saturation usually exists in the flood area as shown schematically in Figure 14-44. The current oil production at the start of the flood is represented by point **A** on the conventional flow rate–time curve of Figure 14-45. After the injection is initiated and a certain amount of water injected, an area of high water saturation called the **water bank** is formed around the injection well at the start of the flood. This stage of the injection is characterized by a **radial flow** system for both the displacing water and displaced oil. With continuous water-injection, the water bank grows radially and displaces the oil phase that forms a region of high oil saturation that forms an **oil bank**. This radial flow continues until the oil banks, formed around adjacent injectors, meet. The place where adjacent oil banks meet is termed **interference**, as shown schematically in Figure 14-46. During this stage of the flood, the condition around the producer is similar to that of the beginning of the flood, i.e., no changes are seen in the well flow rate Q_o as indicated in Figure 14-45 by point **B**. Craig, Geffen, and Morse (1955) summarized the computational steps during this stage of the flood, where radial flow prevails, in the following manner:

Step 1. Calculate the cumulative water injected to interference W_{ii} from the following expression:

$$W_{ii} = \frac{\pi h \phi S_{gi} r_{ei}^2}{5.615} \quad (14-78)$$

where W_{ii} = cumulative water injected to interference, bbl
 S_{gi} = initial gas saturation
 ϕ = porosity
 r_{ei} = half the distance between adjacent injectors, ft

Step 2. Assume several successive values of cumulative water injected W_{inj} , ranging between 0 and W_{ii} , and calculate the water-injection rate at each assumed value of W_{inj} from:

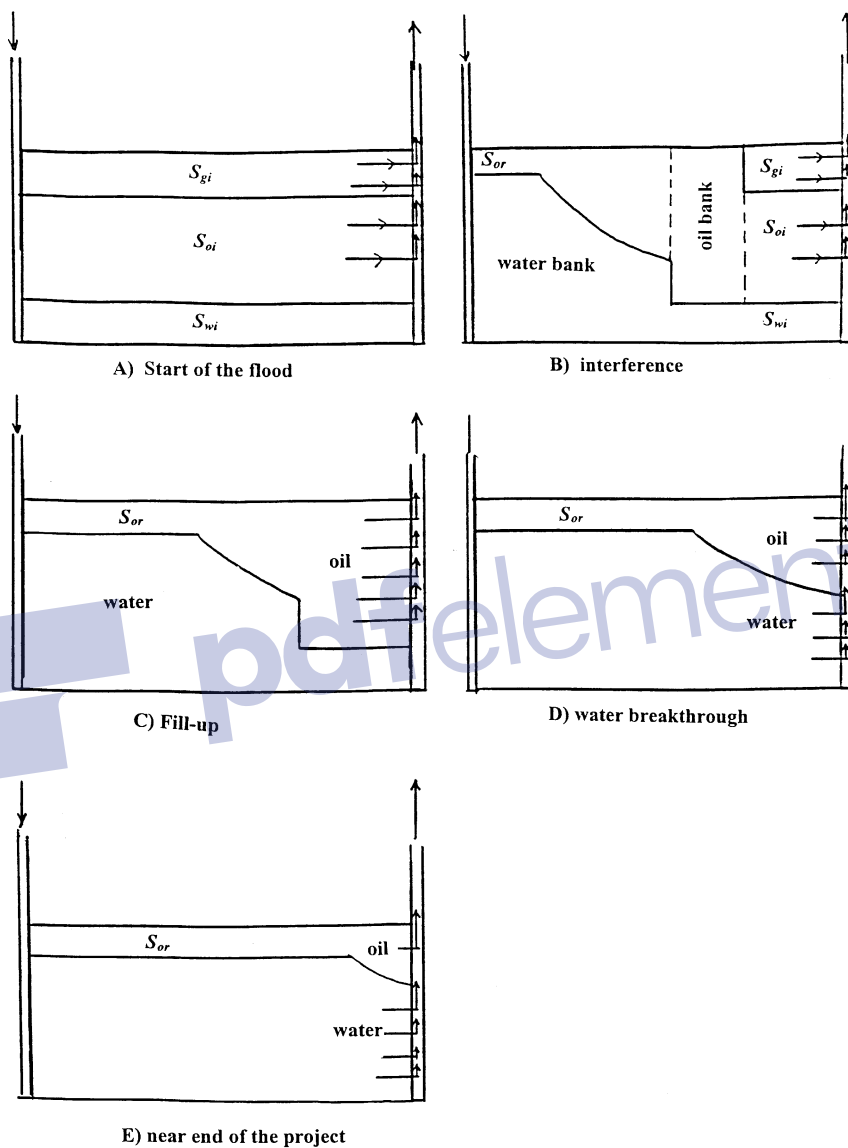


Figure 14-44. Stages of waterflooding.

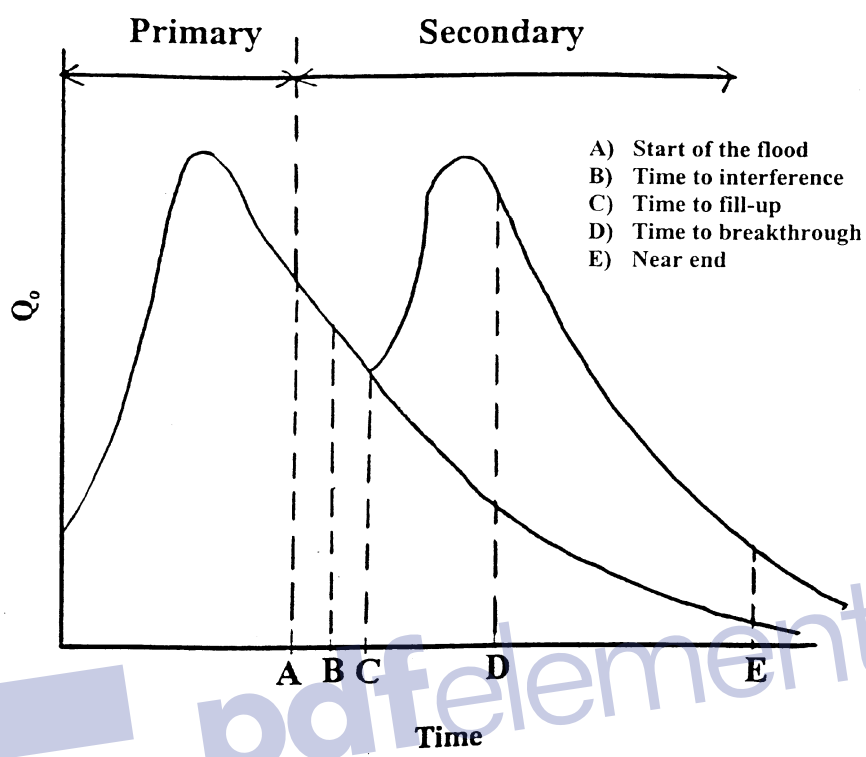


Figure 14-45. Predicted production history.

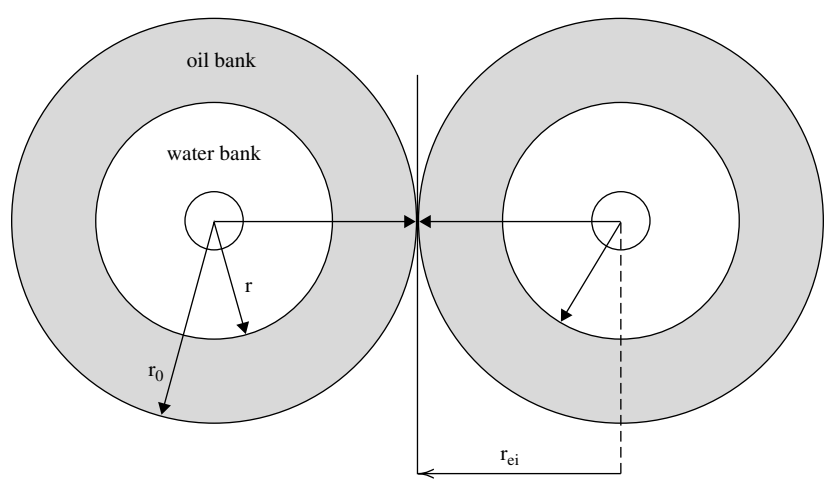


Figure 14-46. Interference of oil banks.

$$i_w = \frac{0.00707 h k \Delta P}{\left(\frac{\mu_w}{k_{rw}} \ln \frac{r}{r_w} + \frac{\mu_o}{k_{ro}} \ln \frac{r_o}{r} \right)} \quad (14-79)$$

where i_w = water-injection, bbl/day

ΔP = pressure difference between injector and producer, psi

k = absolute permeability, md

k_{ro} = relative permeability of oil at S_{wi}

k_{rw} = relative permeability of water at \bar{S}_{wBT}

r_o = outer radius of the oil bank, ft

r = outer radius of the water bank, ft

r_w = wellbore radius, ft

The outer radii of the oil and water banks are calculated from:

$$r_o = \sqrt{\frac{5.615 W_{inj}}{\pi h \phi S_{gi}}} \quad (14-80)$$

$$r = r_o \sqrt{\frac{S_{gi}}{\bar{S}_{wBT} - S_{wi}}} \quad (14-81)$$

The flood performance from the start to interference, i.e., Stage 1, is further discussed in the following example.

Example 14-13

Use the data given in Example 14-11 and determine the performance of the flood from the start to interference. The following additional data are available to reflect the assumption that a free gas exists at the start of the flood:

Initial oil saturation $S_{oi} = 0.75$

Initial gas saturation $S_{gi} = 0.15$

Initial water saturation $S_{wi} = 0.10$

Constant pressure difference $\Delta P = 3000$ psi

Half distance between injectors $r_{ci} = 660$ ft

Distance between injector and producer $d = 932$ ft

Mobility ratio $M = 0.8$

$E_{ABT} = 0.717$

$Q_{iBT} = 0.463$

Pore volume = 310,320 bbl

Solution

Step 1. Calculate stock-tank oil-in-place at start of flood, N_S :

$$N_S = \frac{(PV)S_{oi}}{B_{oi}} = \frac{(310,320)(1 - 0.15 - 0.10)}{1.20} = 193,950 \text{ STB}$$

Step 2. Calculate injected water at interference W_{ii} from Equation 14-78:

$$W_{ii} = \frac{\pi h \phi S_{gi} r_{ei}^2}{5.615} = \frac{\pi(5)(0.20)(0.15)(660)^2}{5.615} = 36,572 \text{ bbl}$$

Step 3. Simplify the calculations by expressing outer radii of the oil and water banks (Equations 14-80 and 14-81) as follows:

$$r_o = \sqrt{\frac{5.615 W_{inj}}{\pi h \phi S_{gi}}} = \sqrt{\frac{5.615 W_{inj}}{\pi(5)(0.2)(0.15)}} = 3.452 \sqrt{W_{inj}}$$

$$r = r_o \sqrt{\frac{S_{gi}}{S_{wBT} - S_{wi}}} = r_o \sqrt{\frac{0.15}{0.563 - 0.10}} = 0.562 r_o$$

Step 4. Express the injectivity equation as represented by Equation 14-79 by:

$$i_w = \frac{0.00707 h k \Delta P}{\left(\frac{\mu_w}{k_{rw}} \ln \frac{r}{r_w} + \frac{\mu_o}{k_{ro}} \ln \frac{r_o}{r} \right)} = \frac{0.00707(5)(31.5)(3000)}{\frac{0.5}{0.4} \ln \left(\frac{r}{1} \right) + \frac{1.0}{1.0} \ln \left(\frac{r_o}{r} \right)}$$

$$i_w = \frac{3,340}{1.25 \ln(r) + \ln \left(\frac{r_o}{r} \right)}$$

Step 5. Perform the required calculation for “stage one” in the following tabulated form:

| W_{inj} (Assume) | r_o | r | i_w | $(i_w)_{avg}$ | $\Delta t = \Delta W_{inj} / (i_w)_{avg}$ | $t = \Sigma(\Delta t)$ |
|-----------------------|-------|-------|-------|---------------|---|------------------------|
| 500 | 77.2 | 43.9 | 631.1 | | 0.79 | 0.79 |
| 5,000 | 244.1 | 138 | 496.2 | 563.8 | 7.98 | 8.77 |
| 10,000 | 345.2 | 196.5 | 466.2 | 481.2 | 10.39 | 19.16 |
| 15,000 | 422.8 | 240.7 | 450.3 | 458.3 | 10.91 | 30.07 |
| 20,000 | 488.2 | 277.9 | 439.6 | 445.0 | 11.24 | 41.31 |
| 25,000 | 545.8 | 310.7 | 431.7 | 435.7 | 11.48 | 52.79 |
| 30,000 | 597.9 | 340.3 | 425.5 | 428.6 | 11.67 | 64.61 |
| 35,000 | 645.8 | 367.6 | 420.3 | 422.9 | 11.82 | 76.43 |
| 36,572 | 660 | 375.7 | 418.9 | 419.6 | 3.75 | 80.18 |

The above calculations indicate that time to interference t_{ii} will occur at 80.18 days after the start of the flood with a water-injection rate at interference i_{wi} of 418.9 bbl/day. Prior to oil bank interference, the injection rate i_w (or injectivity $i_w/\Delta P$) decreases because the radii of the oil and water banks, i.e., r_o and r , are continuously increasing. Notice that the **reservoir will not respond to the waterflood during this stage**. This delay in the reservoir response is mainly due to the fact that the injected water and the displaced oil are essentially moved to fill up part of the gas pore space. As described previously in Example 14-11, an immediate reservoir response to the waterflood can **only** occur when no gas exists at the start of the flood, i.e., $S_{gi} = 0$.

Stage 2: Interference—Fill-Up

This stage describes the period from interference until the fill-up of the preexisting gas space. **Fill-up** is the start of the oil production response as illustrated in Figure 14-44 and by point **C** on Figure 14-45. The flow during this time is not strictly radial and is generally complex to quantify mathematically. Therefore, the flood performance can only be determined at the time of fill-up.

The required performance calculations at the fill-up are summarized in the following steps:

Step 1. Calculate the cumulative water injected at fill-up W_{if} by applying the following expression:

$$W_{if} = (PV)S_{gi} \quad (14-82)$$

where W_{if} = cumulative water injected at fill-up, bbl
 (PV) = total flood pattern pore volume, bbl
 S_{gi} = initial gas saturation

The above equation suggests that while fill-up is occurring, the oil production rate is either zero or negligible, compared with the water-injection rate. If the oil production rate Q_o prior to fill-up is significant, the cumulative water injected at the fill-up W_{if} must be increased by the total volume of oil produced from the start of injection to fill-up, i.e.:

$$W_{if} = (PV)S_{gi} + \frac{N_p}{B_o} \quad (14-83)$$

where N_p = cumulative oil production from start of flood to fill-up, STB
 B_o = oil formation volume factor, bbl/bbl

Equation 14-83 indicates that the fill-up time will also increase; in addition, it causes the fill-up time calculation to be iterative.

Step 2. Calculate the areal sweep efficiency at fill-up by using Equation 14-63, or:

$$E_A = \frac{W_{inj}}{(PV)(\bar{S}_{wBT} - S_{wi})}$$

at fill-up:

$$E_A = \frac{W_{if}}{(PV)(\bar{S}_{wBT} - S_{wi})}$$

Step 3. Using the mobility ratio and the areal sweep efficiency at fill-up, determine the conductance ratio γ from Figure 14-42 or Equation 14-77. Note that the conductance ratio can only be determined when the flood pattern is completely filled with liquids, which occurs at the fill-up stage.

Step 4. For a constant pressure difference, the initial (base) water-injection rate i_{base} from Equation 14-71 is:

$$i_{\text{base}} = \frac{0.003541 h k k_{\text{ro}} \Delta P}{\mu_o \left[\ln \frac{d}{r_w} - 0.619 \right]}$$

Step 5. Calculate the water-injection at fill-up i_{wf} and thereafter from Equation 14-74:

$$i_{\text{wf}} = \gamma i_{\text{base}}$$

The above expression is only valid when the system is filled with liquid, i.e., from the fill-up point and thereafter.

Step 6. Calculate the incremental time occurring from interference to fill-up from:

$$\Delta t = \frac{W_{\text{if}} - W_{\text{ii}}}{\frac{i_{\text{wi}} + i_{\text{wf}}}{2}}$$

The above expression suggests that the **fill-up will occur after interference.**

Example 14-14

Using the data given from Example 14-13, calculate the flood performance at fill-up. Results of Example 14-13 show:

- Time to interference $t_{\text{ii}} = 80.1$ days
- Cumulative water injected to interference $W_{\text{ii}} = 36,572$ bbl
- Water-injection rate at interference $i_{\text{wi}} = 418.9$ bbl/day

Solution

Step 1. Calculate the cumulative water injected at fill-up from Equation 14-81:

$$W_{\text{if}} = (PV)S_{\text{gi}} = 310,320(0.15) = 46,550 \text{ bbl}$$

Step 2. Calculate the areal sweep efficiency at fill-up from Equation 14-63:

$$E_A = \frac{W_{inj}}{(PV)(\bar{S}_{wBT} - S_{wi})} = \frac{W_{inj}}{310,320(0.563 - 0.10)} = \frac{W_{inj}}{143,678}$$

at fill-up:

$$E_A = \frac{W_{if}}{143,678} = \frac{46,550}{143,678} = 0.324$$

Step 3. Given a mobility ratio M of 0.8 (Example 14-11) and E_A of 0.324, calculate the conductance ratio at the fill-up from Figure 14-42: $\gamma = 0.96$.

Step 4. Calculate the initial (base) injection rate from Equation 14-71:

$$i_{base} = \frac{0.003541(5)(31.5)(1)(3,000)}{(1.0)\left(\ln \frac{932}{1} - 0.619\right)} = 269.1 \text{ bbl/day}$$

Step 5. Calculate the water-injection rate at fill-up i_{wf} from Equation 14-74:

$$i_{wf} = \gamma i_{base} = (0.96)(269.1) = 258.2 \text{ bbl/day}$$

Step 6. Calculate the average water-injection rate from interference to fill-up:

$$(i_w)_{avg} = \frac{i_{wi} + i_{wf}}{2} = \frac{418.9 + 258.2}{2} = 338.55 \text{ bbl/day}$$

Step 7. Calculate the incremented time occurring from interference to fill-up:

$$\Delta t = \frac{W_{if} - W_{ii}}{(i_w)_{avg}} = \frac{46,550 - 36,572}{338.55} = 29.5 \text{ days}$$

Thus, the time to fill-up t_f is:

$$t_f = 80.2 + 29.5 = 109.7 \text{ days}$$

Stage 3: Fill-up—Water Breakthrough

The time to fill-up, as represented by point **C** on Figures 14-44 and 14-45, marks the following four events:

1. No free gas remaining in the flood pattern
2. Arrival of the oil-bank front to the production well
3. Flood pattern response to the waterflooding
4. Oil flow rate Q_o equal to the water-injection rate i_w

During this stage, the oil production rate is essentially equal to the injection due to the fact that no free gas exists in the swept flood area. With continuous water-injection, the leading edge of the water bank eventually reaches the production well, as shown in Figure 14-44, and marks the time to breakthrough. At breakthrough the water production rises rapidly.

The waterflood performance calculations are given by the following steps:

Step 1. Calculate cumulative water injected at breakthrough by using Equation 14-43 or 14-44 :

$$W_{iBT} = (PV)(\bar{S}_{wBT} - S_{wi})E_{ABT} = (PV)(Q_{iBT})E_{ABT}$$

Step 2. Assume several values of cumulative water injected W_{inj} between W_{if} and W_{iBT} and calculate the areal sweep efficiency at each W_{inj} from Equation 14-63:

$$E_A = \frac{W_{inj}}{(PV)(\bar{S}_{wBT} - S_{wi})}$$

Step 3. Determine the conductance ratio γ for each assumed value of W_{inj} from Figure 14-42.

Step 4. Calculate the water-injection rate at each W_{inj} by applying Equation 14-74:

$$i_w = \gamma i_{base}$$

Step 5. Calculate the oil flow rate Q_o during this stage from:

$$Q_o = \frac{i_w}{B_o} \quad (14-84)$$

Step 6. Calculate cumulating oil production N_P from the following expression:

$$N_P = \frac{W_{inj} - W_{if}}{B_o} \quad (14-85)$$

Example 14-15

Using the data given in Example 14-14, calculate the flood performance from the fill-up to breakthrough. Results of Example 14-14 show:

- Cumulative water injected to fill-up $W_{if} = 46,550$ bbl
- Water-injection rate at fill-up $i_{wf} = 358.2$ bbl/day
- Time to fill-up $t_f = 109.7$ days

Solution

Step 1. Calculate cumulative water injected at breakthrough from Equation 14-43:

$$W_{iBT} = 310,320(0.563 - 0.1)(0.717) = 103,020 \text{ bbl}$$

Step 2. Perform the required computations in the following tabulated form:

| (1) W_{inj} (Assume) | (2) E_A | (3) γ | (4) i_w | (5) $(i_w)_{avg}$ | (6) $\Delta t = \frac{\Delta W_{inj}}{(i_w)_{avg}}$ | (7) $t = \Sigma \Delta t$ | (8) $Q_o = i_w/B_o$ | (9) $N_p = (W_{inj} - W_{if})/B_o$ |
|------------------------------|--------------|-----------------|--------------|----------------------|--|------------------------------|------------------------|---------------------------------------|
| 46,550 | 0.324 | 0.96 | 258.6 | | | 109.7 | 215.5 | 0 |
| 50,000 | 0.348 | 0.95 | 255.6 | 257.1 | 13.27 | 123.0 | 213.0 | 2844 |
| 60,000 | 0.418 | 0.94 | 253.0 | 254.3 | 39.32 | 162.3 | 210.8 | 11,177 |
| 70,000 | 0.487 | 0.94 | 253.0 | 253.0 | 39.53 | 201.8 | 210.8 | 19,511 |
| 80,000 | 0.557 | 0.93 | 251.7 | 251.7 | 39.73 | 241.6 | 208.6 | 27,844 |
| 90,000 | 0.626 | 0.92 | 247.6 | 249.0 | 40.16 | 281.7 | 206.3 | 36,177 |
| 100,000 | 0.696 | 0.92 | 247.6 | 247.6 | 40.39 | 322.1 | 206.3 | 44,511 |
| 103,020 | 0.717 | 0.91 | 244.9 | 246.3 | 12.26 | 334.4 | 204.1 | 47,027 |

The above calculations indicate that the time to breakthrough will occur after 334.4 days from the start of flood with cumulative oil produced of 47,027 STB.

Stage 4: Water Breakthrough—End of the Project

After breakthrough, the water-oil ratio increases rapidly with a noticeable decline in the oil flow rate as shown in Figure 14-45 by point **D**. The swept area will continue to increase as additional water is injected. The

incrementally swept area will contribute additional oil production, while the previously swept area will continue to produce both oil and water.

As represented by Equation 14-70, the WOR is calculated on the basis of the amounts of oil and water flowing from the swept region and the oil displaced from the newly swept portion of the pattern. It is assumed the oil from the newly swept area is displaced by the water saturation just behind the stabilized zone, i.e., S_{wf} .

The calculations during the fourth stage of the waterflooding process are given below:

Step 1. Assume several values for the ratio W_{inj}/W_{iBT} that correspond to the values given in Table 14-1, i.e., 1, 1.2, 1.4, etc.

Step 2. Calculate the cumulative water injected for each assumed ratio of (W_{inj}/W_{iBT}) from:

$$W_{inj} = \left(\frac{W_{inj}}{W_{iBT}} \right) W_{iBT}$$

Step 3. Calculate the areal sweep efficiency at each assumed (W_{inj}/W_{iBT}) from Equation 14-65:

$$E_A = E_{ABT} + 0.633 \log \left(\frac{W_{inj}}{W_{iBT}} \right)$$

Step 4. Calculate the ratio (Q_i/Q_{iBT}) that corresponds to each value of (W_{inj}/W_{iBT}) from Table 14-1 or Equation 14-69.

Step 5. Determine the total pore volumes of water injected by multiplying each ratio of Q_i/Q_{iBT} by Q_{iBT} , or:

$$Q_i = \left(\frac{Q_i}{Q_{iBT}} \right) Q_{iBT}$$

Step 6. From the definition of Q_i , as expressed by Equation 14-46, determine the slope $(df_w/dS_w)_{Sw2}$ for each value of Q_i by:

$$\left(\frac{df_w}{dS_w} \right)_{Sw2} = \frac{1}{Q_i}$$

Step 7. Read the value of S_{w2} , i.e., water saturation at the producing well, that corresponds to each slope from the plot of $(df_w/dS_w)S_{w2}$ vs. S_{w2} (see Example 14-11).

Step 8. Calculate the reservoir water cut at the producing well f_{w2} for each S_{w2} from Equation 14-24 or 14-37:

$$f_{w2} = \frac{1}{1 + \frac{\mu_w}{\mu_o} \frac{k_{ro}}{k_{rw}}}$$

or

$$f_{w2} = \frac{1}{1 + \left(\frac{\mu_w}{\mu_o}\right) a e^{b S_{w2}}}$$

Step 9. Determine the average water saturation in the swept area \bar{S}_{w2} by applying Equation 14-45:

$$\bar{S}_{w2} = S_{w2} + \frac{1 - f_{w2}}{\left(\frac{df_w}{dS_w}\right)_{S_{w2}}}$$

Step 10. Calculate the surface water-oil ratio WOR_s that corresponds to each value of f_{w2} by applying Equation 14-70:

$$WOR_s = \frac{f_{w2} \left[1 - (\Delta N_P)_{\text{newly}} \right]}{1 - f_{w2} \left[1 - (\Delta N_P)_{\text{newly}} \right]} \left(\frac{B_o}{B_w} \right)$$

Step 11. Craig, Geffen, and Morse (1955) point out when calculating cumulative oil production during this stage that one must account for the oil lost to the unswept area of the flood pattern. To account for the lost oil, the authors proposed the following expression:

$$N_P = N_S E_D E_A - \frac{(PV)(1 - E_A) S_{gi}}{B_o} \quad (14-86)$$

where E_D is the displacement efficiency and is given by Equation 14-9 as:

$$E_D = \frac{\bar{S}_w - S_{wi} - S_{gi}}{1 - S_{wi} - S_{gi}}$$

Step 12. Calculate cumulative water from the expression:

$$\text{Water produced} = \text{Water injected} - \text{Oil produced} \\ - \text{Fill-up volume}$$

or

$$W_p = \frac{w_{inj} - N_p B_o - (PV)S_{gi}}{B_w}$$

Step 13. Calculate $k_{rw} \bar{S}_{w2}$ at and determine the mobility ratio **M after breakthrough** from Equation 14-62:

$$M = \frac{k_{rw} @ \bar{S}_{w2} \left(\frac{\mu_o}{\mu_w} \right)}{k_{ro} @ S_{wi} \left(\frac{\mu_o}{\mu_w} \right)}$$

Step 14. Calculate the conductance ratio γ from Figure 14-42.

Step 15. Determine the water-injection rate from Equation 14-74

$$i_w = \gamma i_{base}$$

Step 16. Calculate the oil and water production rates from Equations 14-55 and 14-56, respectively:

$$Q_o = \frac{i_w}{B_o + B_w WOR_s}$$

$$Q_w = Q_o WOR_s$$

Example 14-16

Complete the waterflooding performance calculation for Example 14-11 by predicting the performance of a producing WOR of 50 STB/STB, given:

| | | |
|-----------------|---|-------------|
| W_{iBT} | = | 103,020 bbl |
| $(N_p)_{BT}$ | = | 47,027 bbl |
| t_{BT} | = | 334.4 days |
| E_{ABT} | = | 0.717 |
| S_{wf} | = | 0.469 |
| \bar{S}_{wBT} | = | 0.563 |
| S_{wi} | = | 0.10 |

Solution

The required calculations are conveniently performed in the following worksheet:

| (1) W_{inj}/W_{iBT} (Assume) | (2) $W_{inj} =$ (1) $\times W_{iBT}$ | (3) E_A Eq. 14-65 | (4) Q_i/Q_{iBT} Table 14-1 | (5) $Q_i =$ (4) $\times Q_{iBT}$ | (6) $df_w/dS_w =$ $1/Q_i$ | (7) S_{w2} Fig. 14-38 | (8) f_{w2} Fig. 14-37 | (9) \bar{S}_{w2} Eq. 14-45 |
|--|---|------------------------------|---------------------------------------|---|---------------------------------|----------------------------------|-----------------------------------|---------------------------------------|
| 1.0 | 103,020 | 0.717 | 1.000 | 0.463 | 2.159 | 0.470 | 0.800 | 0.563 |
| 1.2 | 123,620 | 0.767 | 1.193 | 0.552 | 1.810 | 0.492 | 0.843 | 0.579 |
| 1.4 | 144,230 | 0.809 | 1.375 | 0.636 | 1.570 | 0.507 | 0.870 | 0.590 |
| 1.6 | 164,830 | 0.8462 | 1.548 | 0.717 | 1.394 | 0.524 | 0.893 | 0.601 |
| 1.8 | 185,440 | 0.879 | 1.715 | 0.794 | 1.259 | 0.534 | 0.905 | 0.610 |
| 2.0 | 206,040 | 0.906 | 1.875 | 0.869 | 1.151 | 0.543 | 0.920 | 0.613 |
| 2.5 | 257,550 | 0.969 | 2.256 | 1.046 | 0.956 | 0.562 | 0.937 | 0.628 |
| 3.0 | 309,060 | 1.000 | 2.619 | 1.214 | 0.823 | 0.575 | 0.949 | 0.637 |
| 4.0 | 412,080 | 1.000 | 3.336 | 1.545 | 0.647 | 0.597 | 0.963 | 0.653 |
| 5.0 | 515,100 | 1.000 | 4.053 | 1.877 | 0.533 | 0.611 | 0.973 | 0.660 |
| 6.0 | 618,120 | 1.000 | 4.770 | 2.208 | 0.453 | 0.622 | 0.980 | 0.664 |
| (10) $(\Delta N_p)_{newly}$ Eq. 14-69 | (11) WOR_S Eq. 14-70 | (12) E_D Eq. 14-9 | (13) N_p Eq. 14-86 | (14) W_p Eq. 14-87 | (15) $k_{rw} @ \bar{S}_{w2}$ | (16) M Eq. 14-62 | (17) γ Fig. 14-42 | (18) i_w Eq. 14-76 |
| 0.3056 | 1.5* | 0.4173 | 47,027 | 0 | 0.400 | 0.800 | 0.91 | 244.9 |
| 0.2545 | 2.03 | 0.4387 | 56,223 | 9604 | 0.430 | 0.860 | 0.94 | 252.9 |
| 0.2182 | 2.55 | 0.4533 | 63,716 | 21,223 | 0.450 | 0.900 | 0.96 | 258.3 |
| 0.1910 | 3.12 | 0.4680 | 70,816 | 33,303 | 0.480 | 0.960 | 0.98 | 263.7 |
| 0.1697 | 3.63 | 0.480 | 77,138 | 46,326 | 0.500 | 1.000 | 1.0 | 269.1 |
| 0.1528 | 4.24 | 0.484 | 81,400 | 61,812 | 0.510 | 1.020 | 1.02 | 274.5 |
| 0.1223 | 5.56 | 0.504 | 93,518 | 98,780 | 0.542 | 1.084 | 1.08 | 287.9 |
| 0.000 | 22.3 [†] | 0.516 | 100,078 | 142,418 | 0.560 | 1.120 | 1.12 | 301.4 |
| 0.0000 | 31.2 | 0.5373 | 104,209 | 240,481 | 0.600 | 1.200 | 1.20 | 322.9 |
| 0.0000 | 43.2 | 0.5467 | 106,032 | 341,314 | 0.625 | 1.250 | 1.25 | 336.4 |
| 0.0000 | 58.8 | 0.5520 | 107,060 | 443,100 | 0.635 | 1.270 | 1.27 | 341.8 |

| (19) | (20) | (21) | (22) | (23) | (24) |
|---------------|------------------|-----------------------------------|--------------------------------|--------------------|--------------------------|
| $(i_w)_{avg}$ | ΔW_{inj} | $\frac{\Delta t}{(20) \div (19)}$ | $t = \Sigma(\Delta t)$ days | Q_o Eq. 14-55 | $Q_w = (11) \times (22)$ |
| | | | 334.4 | 90.7 | 136.1 |
| 248.9 | 20,600 | 82.7 | 417.1 | 78.6 | 159.6 |
| 255.6 | 20,610 | 80.6 | 497.7 | 69.6 | 177.5 |
| 261.0 | 20,600 | 79.0 | 576.5 | 61.5 | 191.9 |
| 266.4 | 20,610 | 77.3 | 663.8 | 56.5 | 205.1 |
| 271.8 | 20,600 | 75.9 | 729.7 | 51.5 | 218.4 |
| 282.2 | 51,510 | 183.0 | 912.7 | 43.1 | 239.6 |
| 295.6 | 103,020 | 349.0 | 1261.7 | 12.8 | 285.4 |
| 312.7 | 103,020 | 330.0 | 1591.5 | 9.9 | 308.9 |
| 330.6 | 103,020 | 312.0 | 1903.5 | 7.6 | 328.3 |
| 339.1 | 103,020 | 305.0 | 2208.3 | 5.7 | 335.2 |

*Equation 14-70.

†Equation 14-20.

To illustrate the use of Equation 14-70 in calculating the WOR_s values of column 11, the value of the surface water-oil ratio when W_{inj}/W_{iBT} reaches 2 bbl/bbl is calculated below:

Step 1. Calculate the coefficient E , which remains constant for all the values of W_{inj}/W_{iBT} :

$$E = \frac{S_{wf} - S_{wi}}{E_{ABT}(\bar{S}_{wBT} - S_{wi})} = \frac{0.469 - 0.1}{0.717(0.563 - 0.1)} = 1.1115$$

Step 2. Calculate the parameter λ :

$$\lambda = 0.2749 \left(\frac{W_{iBT}}{W_{inj}} \right) = 0.2749 \left(\frac{1}{2} \right) = 0.13745$$

Step 3. Calculate the incremental oil produced from the newly swept area when $(W_{inj}/W_{iBT}) = 2$ from Equation 14-69:

$$(\Delta N_p)_{newly} = E \lambda = (1.1115)(0.13745) = 0.1528 \text{ bbl/bbl}$$

Step 4. Calculate WOR_s from Equation 14-70:

$$WOR_s = \frac{0.920(1 - 0.1528)}{1 - 0.920(1 - 0.1528)} \left(\frac{1.20}{1.00} \right) = 4.24 \text{ STB/STB}$$

Figure 14-47 documents results of Examples 14-15 and 14-16 graphically.

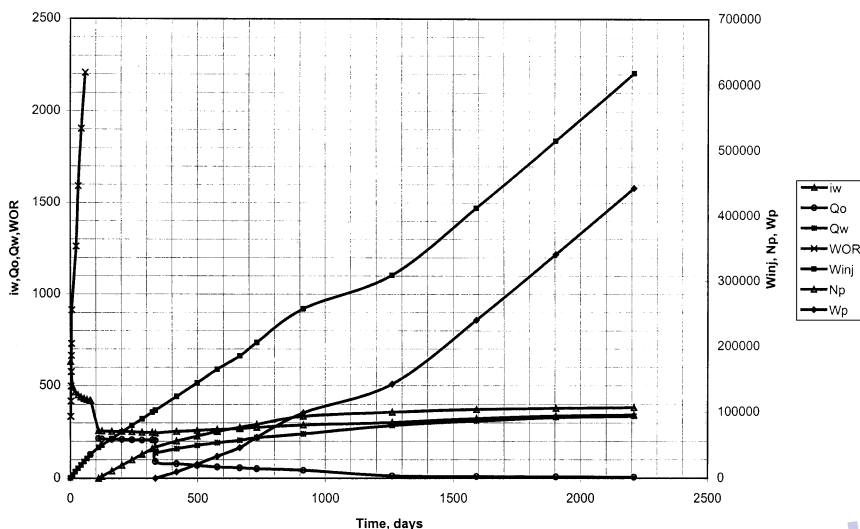


Figure 14-47. Performance curves for Example 14-16.

Water Fingering and Tonguing

In thick, dipping formations containing heavy viscous oil, water tends to advance as a “tongue” at the bottom of the pay zone. Similarly, displacement of oil with a gas will result in the gas attempting to overrun the oil due to gravity differences unless stopped by a shale barrier within the formation or by a low overall effective vertical permeability. In linear laboratory experiments, it was observed that the fluid interface remains horizontal and independent of fluid velocity when the viscosities of the two phases are equal. If the oil and water have different viscosities, the original horizontal interface will become tilted.

In a dipping reservoir, Dake (1978) developed a gravity segregation model that allows the calculation of the critical injection rate i_{crit} that is required to propagate a stable displacement. The condition for stable displacement is that the angle between the fluid interface and the direction of flow should remain constant throughout the displacement as shown in Figure 14-48. Dake introduced the two parameters, the dimensionless gravity number “G” and the end-point mobility ratio M^* , that can be used to define the stability of displacement. These two parameters are defined by the following relationships:

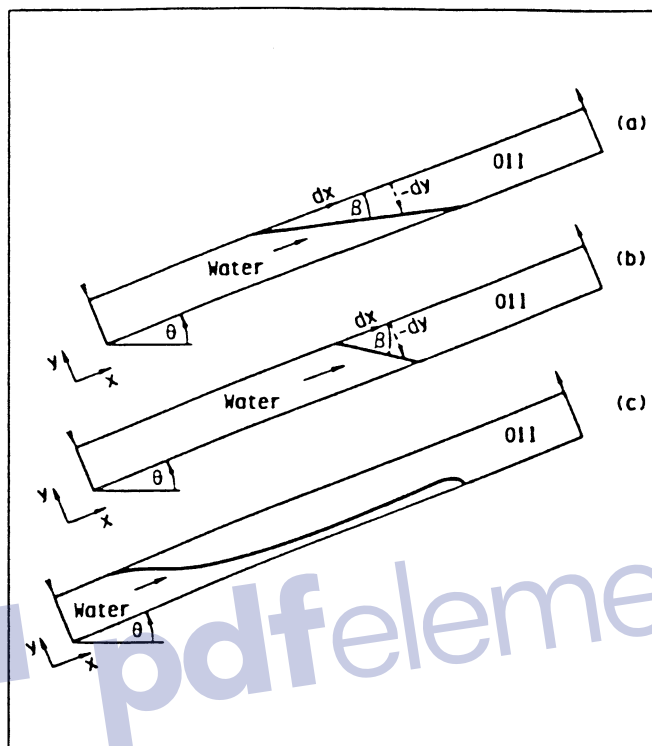


Figure 14-48. Stable and unstable displacement in gravity segregated displacement: (a) stable: $G > m - 1$, $M > 1$, and $\beta < \theta$; (b) stable: $G > M - 1$, $M < 1$, $\beta > \theta$; and (c) unstable: $G < M - 1$. (Courtesy of Elsevier.)

1. **Dimensionless gravity number.** The dimensionless gravity number G is given by:

$$G = \frac{7.853 \times 10^{-6} k k_{rw} A (\rho_w - \rho_o) \sin(\theta)}{i_w \mu_w} \quad (14-87)$$

where k = absolute permeability, md
 k_{rw} = relative permeability to water as evaluated at S_{or}
 A = cross-sectional area
 ρ_w = water density, lb/ft³
 θ = dip angle

2. **End-point mobility ratio.** The end-point mobility ratio M^* is defined by:

$$M^* = \frac{k_{rw} @ S_{or} \mu_o}{k_{ro} @ S_{wi} \mu_w} \quad (14-88)$$

Dake used the above two parameters to define the following stability criteria:

- **If $M^* > 1$.** The displacement is stable if $G > (M^* - 1)$, in which case the fluid interface angle $\beta < \theta$. The displacement is unstable if $G < (M^* - 1)$.
- **If $M^* = 1$.** This is a very favorable condition, because there is no tendency for the water to bypass the oil. The displacement is considered unconditionally stable and is characterized by the fact that the interface rises horizontally in the reservoir, i.e., $\beta = \theta$.
- **If $M^* < 1$.** When the end-point mobility ratio M^* is less than unity, the displacement is characterized as unconditionally stable displacement with $\beta > \theta$ (Figure 14-48b).

The author also defined the critical flow rate, i_{crit} by:

$$i_{crit} = \frac{7.853 \times 10^{-6} k k_{rw} A (\rho_w - \rho_o) \sin(\alpha)}{\mu_w (M^* - 1)} \quad (14-89)$$

- where i_{crit} = critical water-injection rate, bbl/day
 k_{rw} = relative permeability to water @ S_{or}
 μ_w = water viscosity, cp
 k = absolute permeability, md
 θ = dip angle

Duke (1978) pointed out that in horizontal or relatively low dip reservoirs with favorable mobility ratios, the fluid interface angle β can be estimated from the following expression:

$$\tan(\beta) = \frac{127,608 i_w \left(\frac{\mu_w}{K_{rw}} - \frac{\mu_o}{K_{ro}} \right)}{A k (\rho_o - \rho_w)}$$

Practical units, as previously defined, are used in the above equation.

Example 14-17

A tilted linear reservoir is under consideration for waterflooding. The rock and fluid properties are given below:

- Cross-sectional area $A = 31,250 \text{ ft}^2$
- Absolute permeability $k = 70 \text{ md}$
- Dip angle $\theta = 20^\circ$
- Water density $\rho_w = 63 \text{ lb/ft}^3$
- Oil density $\rho_o = 35 \text{ lb/ft}^3$
- Water viscosity $\mu_w = 0.5 \text{ cp}$
- Oil viscosity $\mu_o = 3.0 \text{ cp}$
- $k_{rw} @ S_{or} = 0.35$
- $k_{ro} @ S_{wi} = 1.00$
- Water-injection rate = 800 bbl/day

Calculate the critical water-injection rate for water displacing oil updip.

Solution

Step 1. Calculate the end-point mobility ratio from Equation 14-88:

$$M^* = \frac{0.35 \cdot 3.0}{1.00 \cdot 0.5} = 2.0$$

Step 2. Calculate the critical injection rate by using Equation 14-89:

$$i_{\text{crit}} = \frac{7.853 \times 10^{-6} (70)(0.35)(31,250)(63 - 35) \sin(20)}{0.5(2.1 - 1)} = 106 \text{ bbl/day}$$

The above example indicates that the water-injection rate must be 106 bbl/day to ensure a stable displacement, which, when compared with the proposed injection rate of 800 bbl/day, is perhaps not economically feasible to maintain.

Dake (1978) and Willhite (1986) presented a comprehensive treatment of water displacement under segregated flow conditions.

III. VERTICAL SWEEP EFFICIENCY

The vertical sweep efficiency, E_v , is defined as the fraction of the vertical section of the pay zone that is the injection fluid. This particular sweep efficiency depends primarily on (1) the mobility ratio and (2) total

volume injected. As a consequence of the nonuniform permeabilities, any injected fluid will tend to move through the reservoir with an irregular front. In the more permeable portions, the injected water will travel more rapidly than in the less permeable zone.

Perhaps the area of the greatest uncertainty in designing a waterflood is the quantitative knowledge of the permeability variation within the reservoir. The degree of permeability variation is considered by far the most significant parameter influencing the vertical sweep efficiency.

To calculate the vertical sweep efficiency, the engineer must be able to address the following three problems:

1. How to describe and define the permeability variation in mathematical terms
2. How to determine the minimum number of layers that are sufficient to model the performance of the fluid
3. How to assign the proper average rock properties for each layer (called the **zonation problem**)

A complete discussion of the above three problems is given below.

Reservoir Vertical Heterogeneity

As pointed out in Chapter 4, one of the first problems encountered by the reservoir engineer is that of organizing and utilizing the large amount of data available from core and well logging analyses. Although porosity and connate-water saturation may vary aurally and vertically within a reservoir, the most important rock property variation to influence waterflood performance is permeability. Permeabilities pose particular problems because they usually vary by more than an order of magnitude between different strata.

Dykstra and Parsons (1950) introduced the concept of the permeability variation V , which is designed to describe the **degree of heterogeneity** within the reservoir. The value of this uniformity coefficient ranges between zero for a completely homogeneous system and one for a completely heterogeneous system. Example 4-18 of Chapter 4 illustrates the required computational steps for determining the coefficient V that is given by Equation 4-70, as:

$$V = \frac{k_{50} - k_{84.1}}{k_{50}}$$

To further illustrate the use of the Dykstra and Parsons permeability variation, Craig (1971) proposed a hypothetical reservoir that consists of 10 wells (wells A through J) with detailed permeability data given for each well, as shown in Table 14-2. Each well is characterized by 10 values of permeability with each value representing 1 ft of pay.

Arranging all of these permeability values, i.e., the entire 100 permeability values, from maximum to minimum, Craig (1971) obtained the permeability distribution as shown in the log-probability scale of Figure 14-49. The resulting permeability distribution indicates that this hypothetical reservoir is characterized by a permeability variation of 70%, or:

$$V = \frac{k_{50} - k_{84.1}}{k_{50}} = \frac{10 - 3}{10} = 0.7$$

Table 14-2
Ten-Layer Hypothetical Reservoir
(Permission to publish by the Society of Petroleum Engineers)

| CORE ANALYSIS FOR HYPOTHETICAL RESERVOIR | | | | | | | | | | |
|---|-------|-------|------|------|------|------|-------|------|------|------|
| Cores from 10 Wells, A Through J; Each Permeability Value (md) Represents 1 ft of Pay | | | | | | | | | | |
| Depth (ft) | A | B | C | D | E | F | G | H | I | J |
| 6791 | 2.9 | 7.4 | 30.4 | 3.8 | 8.6 | 14.5 | 39.9 | 2.3 | 12.0 | 29.0 |
| 6792 | 11.3 | 1.7 | 17.6 | 24.6 | 5.5 | 5.3 | 4.8 | 3.0 | 0.6 | 99.0 |
| 6793 | 2.1 | 21.2 | 4.4 | 2.4 | 5.0 | 1.0 | 3.9 | 8.4 | 8.9 | 7.6 |
| 6794 | 167.0 | 1.2 | 2.6 | 22.0 | 11.7 | 6.7 | 74.0 | 25.5 | 1.5 | 5.9 |
| 6795 | 3.6 | 920.0 | 37.0 | 10.4 | 16.5 | 11.0 | 120.0 | 4.1 | 3.5 | 33.5 |
| 6796 | 19.5 | 26.6 | 7.8 | 32.0 | 10.7 | 10.0 | 19.0 | 12.4 | 3.3 | 6.5 |
| 6797 | 6.9 | 3.2 | 13.1 | 41.8 | 9.4 | 12.9 | 55.2 | 2.0 | 5.2 | 2.7 |
| 6798 | 50.4 | 35.2 | 0.8 | 18.4 | 20.1 | 27.8 | 22.7 | 47.4 | 4.3 | 66.0 |
| 6799 | 16.0 | 71.5 | 1.8 | 14.0 | 84.0 | 15.0 | 6.0 | 6.3 | 44.5 | 5.7 |
| 6800 | 23.5 | 13.5 | 1.5 | 17.0 | 9.8 | 8.1 | 15.4 | 4.6 | 9.1 | 60.0 |

Minimum Number of Layers

Based on a computer study, Craig (1971) outlined some guidelines for selecting the minimum number of layers needed to predict the performance of a reservoir under waterflooding operation. The author simulated the performance of a waterflood five-spot pattern that is composed of 100 layers with permeability variations ranging from 0.4 to 0.8. The minimum number of layers required to match results of the 100-layer model was

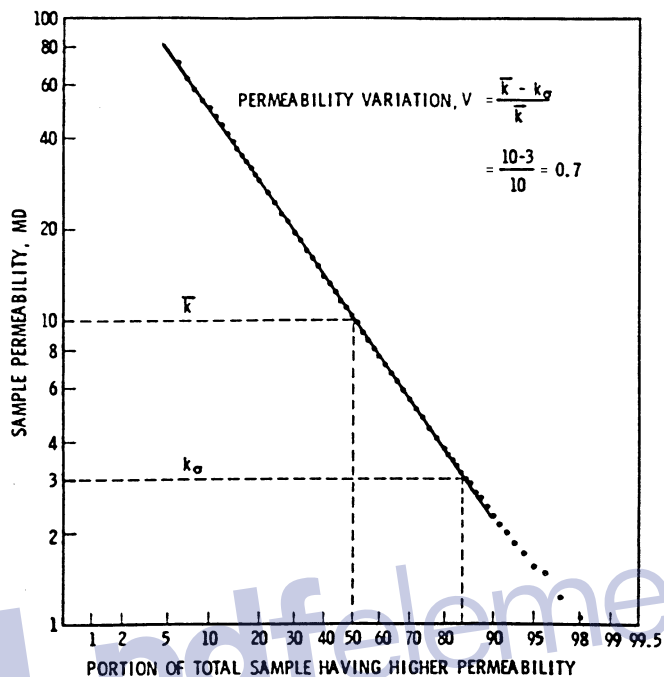


Figure 14-49. Determination of permeability variation for the hypothetical reservoir. (Permission to publish by the Society of Petroleum Engineers.)

determined as a function of mobility ratio M and permeability variation V . Tables 14-3 through 14-5 summarize results of these simulations and provide a guide to selection of the number of layers for five-spot patterns.

Table 14-3
Minimum Number of Layers for WOR > 2.5
 (Permission to publish by the Society of Petroleum Engineers)

| Mobility Ratio | Permeability Variation | | | | | | | |
|----------------|------------------------|-----|-----|-----|-----|-----|-----|-----|
| | 0.1 | 0.2 | 0.3 | 0.4 | 0.5 | 0.6 | 0.7 | 0.8 |
| 0.05 | 1 | 1 | 2 | 4 | 10 | 20 | 20 | 20 |
| 0.1 | 1 | 1 | 2 | 4 | 10 | 20 | 100 | 100 |
| 0.2 | 1 | 1 | 2 | 4 | 10 | 20 | 100 | 100 |
| 0.5 | 1 | 2 | 2 | 4 | 10 | 20 | 100 | 100 |
| 1.0 | 1 | 3 | 3 | 4 | 10 | 20 | 100 | 100 |
| 2.0 | 2 | 4 | 4 | 10 | 20 | 50 | 100 | 100 |
| 5.0 | 2 | 5 | 10 | 20 | 50 | 100 | 100 | 100 |

Table 14-4
Minimum Number of Layers for WOR > 5
(Permission to publish by the Society of Petroleum Engineers)

| Mobility Ratio | Permeability Variation | | | | | | | |
|----------------|------------------------|-----|-----|-----|-----|-----|-----|-----|
| | 0.1 | 0.2 | 0.3 | 0.4 | 0.5 | 0.6 | 0.7 | 0.8 |
| 0.05 | 1 | 1 | 2 | 4 | 5 | 10 | 10 | 20 |
| 0.1 | 1 | 1 | 2 | 4 | 10 | 10 | 10 | 100 |
| 0.2 | 1 | 1 | 2 | 4 | 10 | 10 | 20 | 100 |
| 0.5 | 1 | 2 | 2 | 4 | 10 | 10 | 20 | 100 |
| 1.0 | 1 | 2 | 3 | 4 | 10 | 10 | 20 | 100 |
| 2.0 | 2 | 3 | 4 | 5 | 10 | 10 | 50 | 100 |
| 5.0 | 2 | 4 | 5 | 10 | 20 | 100 | 100 | 100 |

Table 14-5
Minimum Number of Layers for WOR > 10
(Permission to publish by the Society of Petroleum Engineers)

| Mobility Ratio | Permeability Variation | | | | | | | |
|----------------|------------------------|-----|-----|-----|-----|-----|-----|-----|
| | 0.1 | 0.2 | 0.3 | 0.4 | 0.5 | 0.6 | 0.7 | 0.8 |
| 0.05 | 1 | 1 | 1 | 2 | 4 | 5 | 10 | 20 |
| 0.1 | 1 | 1 | 1 | 2 | 5 | 5 | 10 | 20 |
| 0.2 | 1 | 1 | 2 | 3 | 5 | 5 | 10 | 20 |
| 0.5 | 1 | 1 | 2 | 3 | 5 | 5 | 10 | 20 |
| 1.0 | 1 | 1 | 2 | 3 | 5 | 10 | 10 | 50 |
| 2.0 | 1 | 2 | 3 | 4 | 10 | 10 | 20 | 100 |
| 5.0 | 1 | 3 | 4 | 5 | 10 | 100 | 100 | 100 |

Example 14-18

A reservoir is under consideration for waterflooding. The heterogeneity of the reservoir is described by a permeability variation V of 40%. The mobility ratio is determined as 2.0. Determine the minimum number of layers required to perform waterflooding calculations.

Solution

Table 14-4 shows that the minimum number of layers required to match the performance of the 100-layer computer model with a producing WOR above 10 STB/STB is 4 layers.

The Zonation Problem

In waterflooding calculations, it is frequently desirable to divide the reservoir into a number of layers that have equal thickness but different permeabilities and porosities. Traditionally, two methods are used in the industry to assign the proper average permeability for each layer: (1) the positional method or (2) the permeability ordering method.

Positional Method

The positional method describes layers according to their relative location within the vertical rock column. This method assumes that the injected fluid remains in the same elevation (layer) as it moves from the injector to the producer. Miller and Lents (1966) successfully demonstrated this concept in predicting the performance of the Bodcaw Reservoir Cycling Project. The authors proposed that the average permeability in a selected layer (elevation) should be calculated by applying the geometric-average permeability as given by Equation 4-54 or 4-55:

$$k_{\text{avg}} = \exp \left[\frac{\sum_{i=1}^n h_i \ln(k_i)}{\sum_{i=1}^n h_i} \right]$$

If all the thicknesses are equal, then:

$$k_{\text{avg}} = (k_1 k_2 k_3 \dots k_n)^{1/n}$$

Example 14-19

Using the core analysis data given in Table 14-2 for the 10-well system, assign the proper average permeability for each layer if the reservoir is divided into:

- a. 10 equal-thickness layers, each with a 1-ft thickness
- b. 5 equal-thickness layers, each with a 2-ft thickness

Solution

- a. Using the positional method approach and applying Equation 4-55, calculate the permeability for each 1-ft layer:

$$\text{Layer 1} = [(2.9)(7.4)(30.4)(3.8)(8.6)(14.5)(39.9)(2.3)(12.0)(29.0)]^{1/10} = 10 \text{ md}$$

A similar approach for calculating the permeability for the remaining layers yields:

| Layer # | Permeability, md |
|---------|------------------|
| 1 | 10.0 |
| 2 | 6.8 |
| 3 | 4.7 |
| 4 | 10.4 |
| 5 | 20.5 |
| 6 | 12.1 |
| 7 | 8.6 |
| 8 | 18.4 |
| 9 | 14.3 |
| 10 | 10.9 |

- b. Five equal-thickness layers:

Step 1. Calculate the arithmetic-average permeability for each layer per location:

| Depth | A | B | C | D | E | F | G | H | I | J |
|---------|-------|--------|-------|-------|-------|-------|-------|-------|-------|-------|
| 6791–92 | 7.10 | 4.55 | 24.00 | 14.20 | 7.05 | 9.90 | 22.35 | 2.65 | 6.30 | 64.00 |
| 93–94 | 84.55 | 11.20 | 3.50 | 12.20 | 8.35 | 3.85 | 38.95 | 16.95 | 5.20 | 6.75 |
| 95–96 | 11.55 | 473.30 | 22.40 | 21.20 | 13.60 | 10.50 | 69.50 | 8.25 | 3.40 | 20.00 |
| 97–98 | 28.65 | 19.20 | 6.95 | 30.10 | 14.75 | 20.35 | 38.95 | 24.70 | 4.75 | 34.35 |
| 99–00 | 19.75 | 42.50 | 1.65 | 15.50 | 46.90 | 13.05 | 10.70 | 5.45 | 26.80 | 32.85 |

Step 2. Use the geometric-average method to calculate the permeability in each layer:

$$\text{Layer 1} = [(7.1)(4.5)(24.0)(14.2)(7.05)(9.9)(22.35)(2.65)(6.3)(64.0)]^{1/10} = 10.63$$

Remaining layers are treated in the same fashion to give:

| Layer # | Permeability, md |
|---------|------------------|
| 1 | 10.63 |
| 2 | 11.16 |
| 3 | 20.70 |
| 4 | 18.77 |
| 5 | 15.26 |

Permeability Ordering Method

The permeability ordering method is essentially based on the Dykstra and Parsons (1950) permeability sequencing technique. The core analysis permeabilities are arranged in a decreasing permeability order and a plot like that shown in Figure 14-49 is made. The probability scale is divided into equal-percent increments with each increment representing a layer. The permeability for each layer is assigned to the permeability value that **corresponds to the midpoint of each interval.**

Example 14-20

For the 10-layer system of Example 14-19, determine the permeability for each layer by using the permeability ordering approach.

Solution

From Figure 14-49, determine the permeability for each of the 10 layers by reading the permeability at the following midpoints: 5%, 15%, 25%, 35%, 45%, 55%, 65%, 75%, 85%, and 95%:

| Layer #1 | Permeability Ordering | Positional Approach |
|----------|-----------------------|---------------------|
| 1 | 84.0 | 10.0 |
| 2 | 37.0 | 6.8 |
| 3 | 23.5 | 4.7 |
| 4 | 16.5 | 10.4 |
| 5 | 12.0 | 20.5 |
| 6 | 8.9 | 12.1 |
| 7 | 6.5 | 8.6 |
| 8 | 4.6 | 18.4 |
| 9 | 3.0 | 14.3 |
| 10 | 1.5 | 10.9 |

Porosity assignments for the selected reservoir layers may also be treated in a similar manner to that of the permeability ordering approach. All porosity measurements are arranged in decreasing order and a plot of the porosity versus percentage of thickness with greater porosity is made on a Cartesian-probability scale (rather than a log-probability scale). The porosity of each layer can then be obtained for each interval of thickness selected.

The permeability ordering technique is perhaps the most widely used approach in the petroleum industry when determining the vertical sweep efficiency.

Calculation of Vertical Sweep Efficiency

Basically two methods are traditionally used in calculating the vertical sweep efficiency EV: (1) Stiles' method and (2) the Dykstra-Parsons method. These two methods assume that the reservoir is composed of an idealized layered system, as shown schematically in Figure 14-50. The layered system is selected based on the permeability ordering approach with layers arranged in order of descending permeability. The common assumptions of both methods are:

- No cross-flow between layers
- Immiscible displacement
- Linear flow
- The distance water has traveled through each layer is proportional to the permeability of the layer
- Piston-like displacement

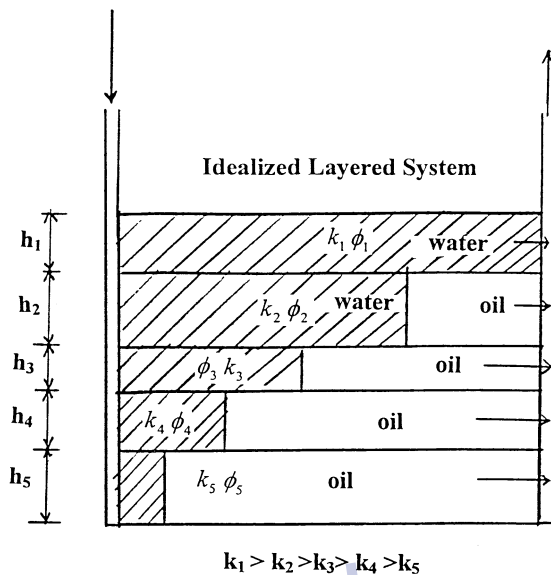


Figure 14-50. Idealized layered system.

The basic idea used in Stiles' method and the Dykstra-Parsons method is to determine the frontal position in each layer at the time water breakthrough occurs in successive layers. If the flow capacity of each layer is defined by the product of permeability and thickness, i.e., kh , then the water and oil flow rates from all layers can be calculated to yield the producing water-oil ratio.

Stiles' Method

Stiles (1949) proposed an approach that takes into account the effect of permeability variations in predicting the performance of waterfloods. Stiles assumes that in a layered system, the water breakthrough occurs in a sequence that starts in the layer with the highest permeability. Assuming that the reservoir is divided into n layers that are arranged in a descending permeability order with breakthrough occurring in a layer i , all layers from 1 to i have already been swept by water. The remaining layers obviously have not reached breakthrough.

The method assumes that there is piston-like displacement of oil, so that after water breakthrough in a layer, *only* water is produced from this layer. After water breakthrough, the producing *WOR* is given by:

$$\text{WOR} = \left[\frac{C}{1-C} \right] \left[\frac{k_{rw} \mu_o B_o}{k_{ro} \mu_w B_w} \right]$$

where C is the fraction of the total flow capacity represented by layers that have water breakthrough.

Based on the above concept, Stiles proposed that the vertical sweep efficiency can be calculated from the following expression:

$$E_v = \frac{k_i \sum_{j=1}^i h_j + \sum_{j=i+1}^n (kh)_j}{k_i h_t} \quad (14-90)$$

where i = breakthrough layer, i.e., $i = 1, 2, 3, \dots, n$

n = total number of layers

E_v = vertical sweep efficiency

h_t = total thickness, ft

h_i = layer thickness, ft

If the values of the porosity vary between layers, Equation 14-90 can be written:

$$E_v = \frac{\left(\frac{k}{\phi} \right)_i \sum_{j=1}^i (\phi h)_j + \sum_{j=i+1}^n (kh)_j}{\left(\frac{k}{\phi} \right)_i \sum_{j=1}^n (\phi h)_j} \quad (14-91)$$

Stiles also developed the following expression for determining the surface water-oil ratio as breakthrough occurs in any layer:

$$\text{WOR}_s = A \left[\frac{\sum_{j=1}^i (kh)_j}{\sum_{j=i+1}^n (kh)_j} \right] \quad (14-92)$$

with

$$A = \frac{k_{rw} \mu_o B_o}{k_{ro} \mu_w B_w} \quad (14-93)$$

where WOR_s = surface water-oil ratio, STB/STB
 k_{rw} = relative permeability to water at S_{or}
 k_{ro} = relative permeability to oil at S_{wi}

Both the vertical sweep efficiency and surface WOR equations are used simultaneously to describe the sequential breakthrough as it occurs in layer 1 through layer n. It is usually convenient to represent the results of these calculations graphically in terms of $\log(WOR_s)$ as a function of E_V .

Example 14-21

The Dykstra and Parsons (1950) permeability ordering approach is used to describe a reservoir by the following five-layer system:

| Layer | k, md | h, ft |
|-------|-------|-------|
| 1 | 120 | 15 |
| 2 | 90 | 15 |
| 3 | 70 | 10 |
| 4 | 55 | 10 |
| 5 | 30 | 10 |

The reservoir is under consideration for further development by water-injection. The following additional information is available:

$$\begin{aligned}
 k_{rw}@S_{or} &= 0.3 \\
 k_{ro}@S_{wi} &= 0.9 \\
 \mu_o &= 2.0 \text{ cp} \\
 \mu_w &= 0.5 \text{ cp} \\
 B_o &= 1.20 \text{ bbl/STB} \\
 B_w &= 1.01 \text{ bbl/STB} \\
 h_t &= 60 \text{ ft}
 \end{aligned}$$

Calculate the vertical sweep efficiency and surface water-oil ratio using Stiles' method:

Solution

Step 1. Calculate parameter A using Equation 14-93:

$$A = \frac{0.3 (2.0)(1.20)}{0.9 (0.5)(1.01)} = 1.584$$

Step 2. Calculate E_V and WOR_s when breakthrough occurs in the first layer, i.e., $i = 1$, by applying Equations 14-90 and 14-92:

$$E_V = \frac{k_i \sum_{j=1}^i h_j \sum_{j=2}^5 (kh)_j}{k_i h_t}$$

$$E_V = \frac{k_1 h_1 + [k_2 h_2 + k_3 h_3 + k_4 h_4 + k_5 h_5]}{k_1 h_t}$$

$$E_V = \frac{(120)(15) + [(90)(15) + (70)(10) + (55)(10) + (30)(10)]}{(120)(60)} = 0.653$$

$$WOR_s = (1.584) \frac{\sum_{j=1}^1 (kh)_j}{\sum_{j=2}^5 (kh)_j}$$

$$WOR_s = (1.584) \frac{(kh)_1}{(kh)_2 + (kh)_3 + (kh)_4 + (kh)_5}$$

$$WOR_s = (1.584) \frac{(120)(15)}{(90)(15) + (70)(10) + (55)(10) + (30)(10)}$$

$$= 0.983 \text{ STB} / \text{STB}$$

Step 3. Calculate E_V and WOR_s when water breakthrough occurs in the second layer, i.e., $i = 2$:

$$E_V = \frac{k_2 \sum_{j=1}^2 h_j + \sum_{j=3}^5 (kh)_j}{k_2 h_t}$$

$$E_V = \frac{k_2 (h_1 + h_2) + [(kh)_3 + (kh)_4 + (kh)_5]}{k_2 h_t}$$

$$E_V = \frac{90(15 + 15) + [(70)(10) + (55)(10) + (30)(10)]}{(90)(60)} = 0.787$$

$$\text{WOR}_s = (1.584) \frac{\sum_{j=1}^2 (kh)_j}{\sum_{j=3}^5 (kh)_j}$$

$$\text{WOR}_s = (1.584) \frac{(kh)_1 + (kh)_2}{(kh)_3 + (kh)_4 + (kh)_5}$$

$$\text{WOR}_s = (1.584) \frac{(120)(15) + (90)(15)}{(70)(10) + (55)(10) + (30)(10)} = 3.22 \text{ STB/STB}$$

Step 4. The required calculations can be performed more conveniently in the following worksheet:

| (1) | (2) | (3) | (4) | (5) | (6) | (7) | (8) | (9) | (10) | | |
|-------|-------|-------|--------------|------------------|-----------|------------------|-----------|--|---|--|--|
| Layer | k_i | h_i | Σh_i | $k_i \Sigma h_i$ | $k_i h_i$ | $\Sigma k_i h_i$ | $h_i k_i$ | $E_v = \frac{(5) + [\text{sum} + (7)]}{(8)}$ | $\text{WOR}_s = 1.584 \left[\frac{(7)}{\text{sm} \cdot (7)} \right]$ | | |
| 1 | 120 | 15 | 15 | 1800 | 1800 | 1800 | 7200 | 0.653 | 0.983 | | |
| 2 | 90 | 15 | 30 | 2700 | 1350 | 3150 | 5400 | 0.787 | 3.22 | | |
| 3 | 70 | 10 | 40 | 2800 | 700 | 3850 | 4200 | 0.869 | 7.17 | | |
| 4 | 55 | 10 | 50 | 2750 | 550 | 4400 | 3300 | 0.924 | 23.23 | | |
| 5 | 30 | 10 | 60 | 1800 | 300 | 4700 | 1800 | 1.000 | — | | |
| | | | | sum = 4700 | | | | | | | |

Figure 14-51 shows the resulting relationship between the vertical sweep efficiency and producing WOR. The curve can be extended to WOR = 0 to give the vertical sweep efficiency at breakthrough E_v .

The Dykstra-Parsons Method

Dykstra and Parsons (1950) correlated the vertical sweep efficiency with the following parameters:

- Permeability variation V
- Mobility ratio M
- Water-oil ratio WOR_r as expressed in bbl/bbl

The authors presented their correlation in a graphical form for water-oil ratios of 0.1, 0.2, 0.5, 1, 2, 5, 10, 25, 50, and 100 bbl/bbl. Figure 14-52 shows Dykstra and Parsons' graphical correlation for a WOR of 50 bbl/bbl. Using a regression analysis model, de Souza and Brigham

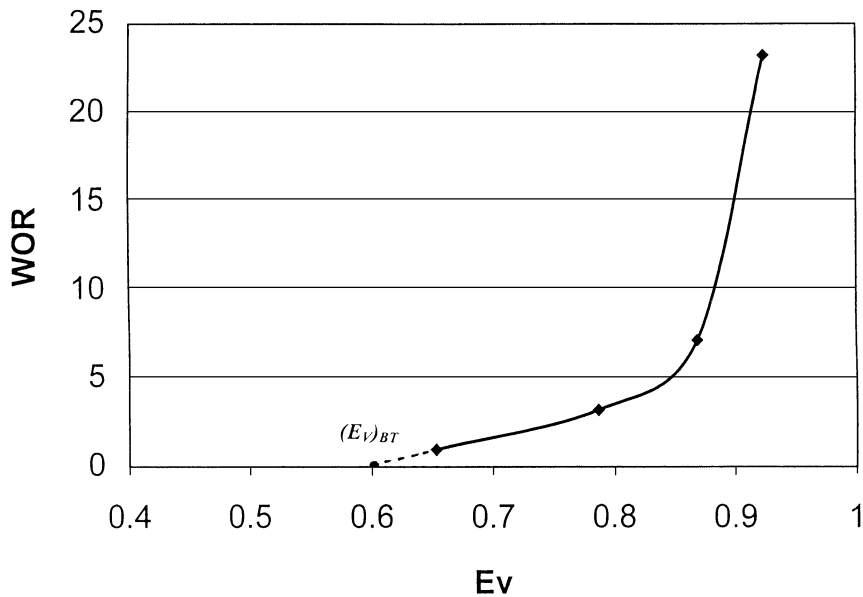


Figure 14-51. WOR vs. E_v .

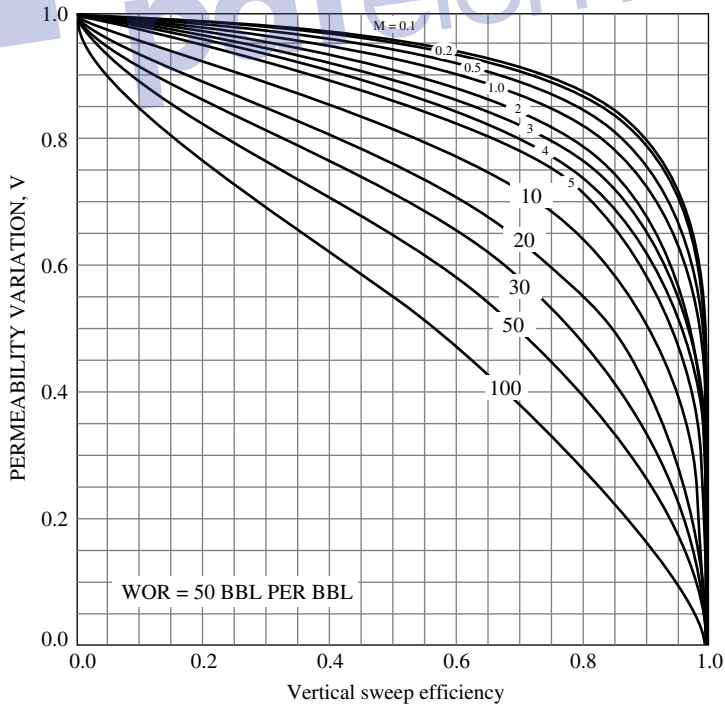


Figure 14-52. Vertical sweep efficiency curves for WOR = 50. (Permission to publish by the Society of Petroleum Engineers.)

(1981) grouped the vertical sweep efficiency curves for $0 \leq M \leq 10$ and $0.3 \leq V \leq 0.8$ into one curve as shown in Figure 14-53. The authors used a combination of WOR, V, and M to define the correlation parameter Y of Figure 14-53:

$$Y = \frac{(\text{WOR} + 0.4)(18.948 - 2.499V)}{(M - 0.8094V + 1.137)10^x} \quad (14-94)$$

with

$$x = 1.6453V^2 + 0.935V - 0.6891 \quad (14-95)$$

The specific steps involved in determining the vertical sweep efficiency as a function of water-oil ratios are summarized below:

1. Calculate the mobility ratio M and permeability variation V.
2. Select several values for the WOR, e.g., 1, 2, 5, 10, and calculate the correlating parameter Y at each selected WOR.
3. Enter Figure 14-53 with each value of Y and determine the corresponding values of the vertical sweep efficiency E_V .
4. Plot WOR versus E_V .

To further simplify the calculations for determining E_V , Fassihi (1986) curve-fitted the graph of Figure 14-53 and proposed the following non-linear function, which can be solved iteratively for the vertical sweep efficiency E_V :

$$a_1 E_V^{a_2} (1 - E_V)^{a_3} - Y = 0 \quad (14-96)$$

where $a_1 = 3.334088568$

$a_2 = 0.7737348199$

$a_3 = 1.225859406$

The Newton-Raphson method is perhaps the appropriate technique for solving Equation 14-96. To avoid the iterative process, the following expression could be used to estimate the vertical sweep efficiency using the correlating parameter Y:

$$E_V = a_1 + a_2 \ln(Y) + a_3 [\ln(Y)]^2 + a_4 [\ln(Y)]^3 + a_5 / \ln(Y) + a_6 Y$$

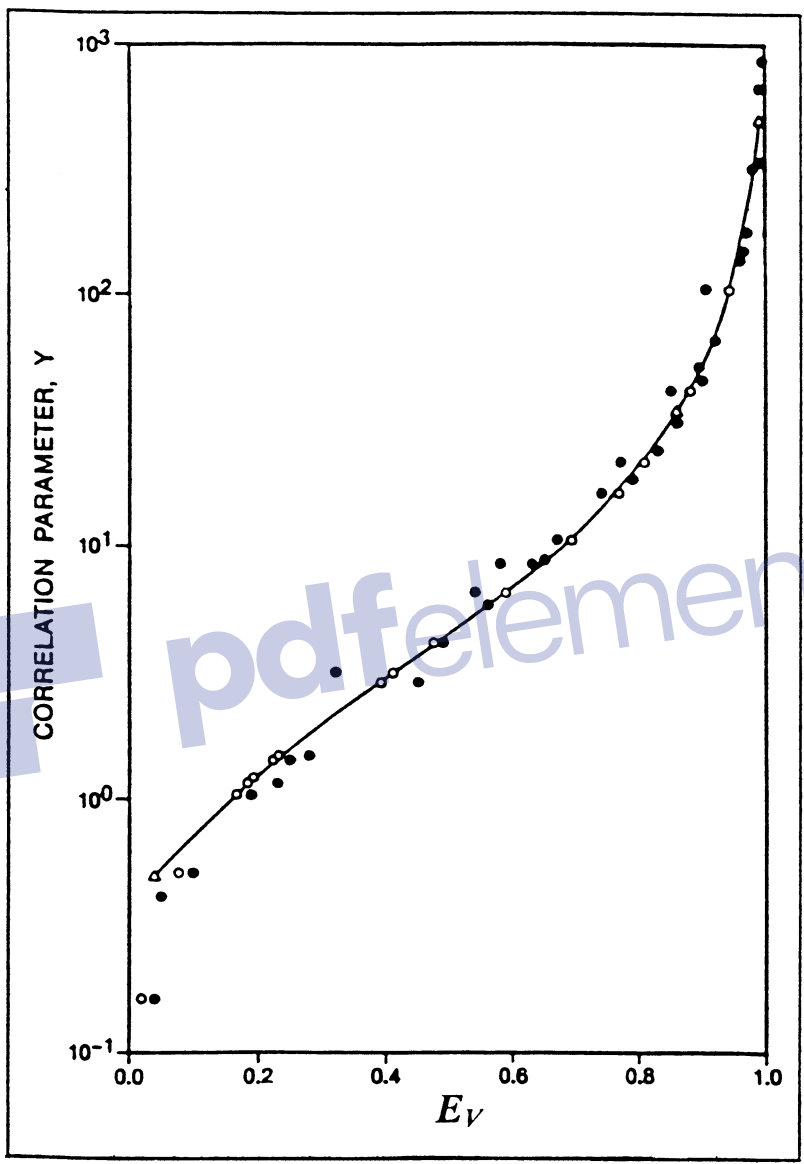


Figure 14-53. E_V versus the correlating parameter Y . (Permission to publish by the Society of Petroleum Engineers.)

with the coefficients a_1 through a_6 as given by:

$$\begin{aligned} a_1 &= 0.19862608 & a_2 &= 0.18147754 \\ a_3 &= 0.01609715 & a_4 &= -4.6226385 \times 10^{-3} \\ a_5 &= -4.2968246 \times 10^{-4} & a_6 &= 2.7688363 \times 10^{-4} \end{aligned}$$

Example 14-22

A layered reservoir is characterized by a permeability variation V of 0.8. Calculate the vertical sweep efficiency E_V when the producing water-oil ratio reaches 50 bbl/bbl assuming a mobility ratio of 10.0.

Solution

Step 1. Calculate the parameter x by applying Equation 14-95:

$$x = 1.6453(0.8)^2 + 0.9735(0.8) - 0.6891 = 1.1427$$

Step 2. Calculate the correlation parameter Y from Equation 14-96:

$$Y = \frac{(50 + 0.4)[18.948 - 2.499(0.8)]}{[10 - 0.8094(0.8) + 1.137]10^{1.1427}} = 5.863$$

Step 3. From Figure 14-53, determine E_V to give:

$$E_V = 0.56$$

METHODS OF PREDICTING RECOVERY PERFORMANCE FOR LAYERED RESERVOIRS

To account for the reservoir vertical heterogeneity when predicting reservoir performance, the reservoir is represented by a series of layers with no vertical communication, i.e., no cross-flow between layers. Each layer is characterized by a thickness h , permeability k , and porosity ϕ . The heterogeneity of the entire reservoir is usually described by the permeability variation parameter V . Three of the methods that are designed to predict the performance of layered reservoirs are discussed below.

Simplified Dykstra-Parsons Method

Dykstra and Parsons (1950) proposed a correlation for predicting waterflood oil recovery that uses the mobility ratio, permeability variation, and producing water-oil ratio as correlating parameters. Johnson (1956) developed a simplified graphical approach for the Dykstra and Parsons method that is based on predicting the overall oil recovery R at water-oil ratios of 1, 5, 25, and 100 bbl/bbl. Figure 14-54 shows the proposed graphical charts for the four selected WOR_s . The correlating parameters shown in Figure 14-54 are:

R = overall oil recovery factor

S_{wi} = initial water saturation

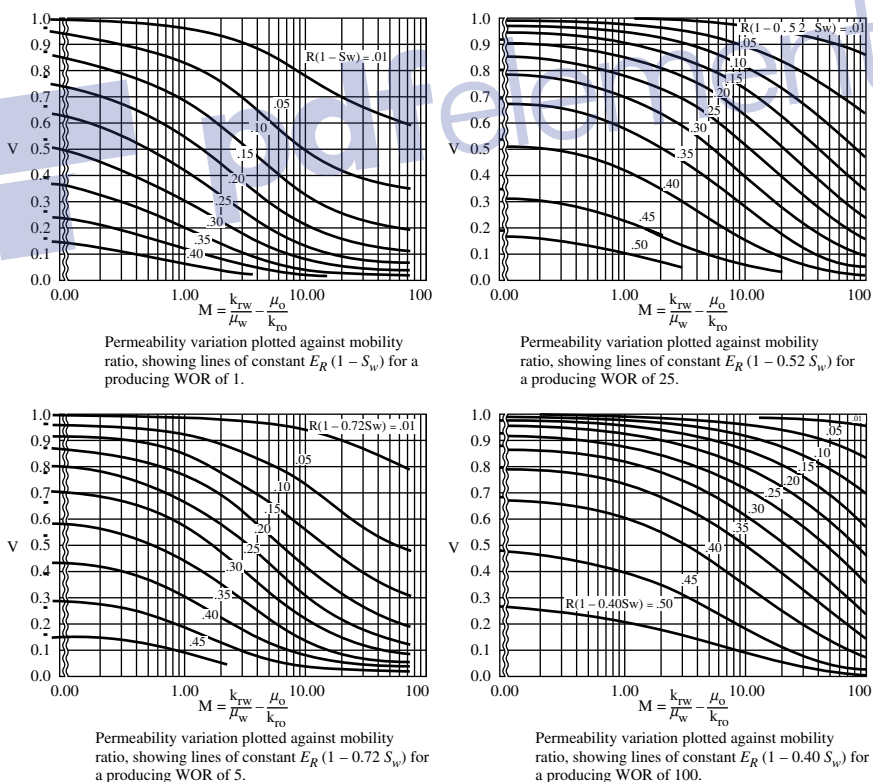


Figure 14-54. Simplified Dykstra and Parsons curves. (Permission to publish by the Society of Petroleum Engineers.)

M = mobility ratio

V = permeability variation

The practical application of the simplified Dykstra and Parsons method is outlined below:

1. Calculate the permeability variation V and mobility ratio M.
2. Using the permeability ratio and mobility ratio, calculate the overall oil recovery factor R from the four charts at WOR of 1, 5, 25, 100 bbl/bbl. For example, to determine the oil recovery factor when the WOR reaches 5 bbl/bbl for a flood pattern that is characterized by a V and M of 0.5 and 2, respectively:
 - Enter the appropriate graph with these values, i.e., 0.5 and 2.
 - The point of intersection shows that $R(1 - 0.72 S_{wi}) = 0.25$.
 - If the initial water saturation S_{wi} is 0.21, solve for the recovery factor to give $R = 0.29$.
3. Calculate the cumulative oil production N_P at each of the four water-oil ratios, i.e., 1, 5, 25, and 100 bbl/bbl, from:

$$N_P = N_S R$$

4. If the water-oil ratio is plotted against the oil recovery on semi log paper and a Cartesian scale, the oil recovery at breakthrough can be found by extrapolating the line to a very low value of WOR, as shown schematically in Figure 14-55.

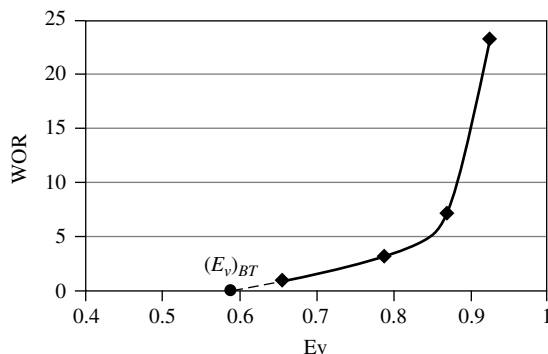


Figure 14-55. WOR versus E_v relationship.

5. For a constant injection rate, adding the fill-up volume W_{if} to the cumulative oil produced at breakthrough and dividing by the injection rate can estimate the time to breakthrough.
6. The cumulative water produced at any given value of WOR is obtained by finding the area under the curve of WOR versus N_p , as shown schematically in Figure 14-56.
7. The cumulative water injected at any given value of WOR is calculated by adding cumulative oil produced to the produced water and fill-up volume, or:

$$W_{inj} = N_p B_o + W_p B_w + W_{if}$$

Example 14-23

A reservoir is characterized by the following parameters:

Initial oil-in-place, $N_S = 12$ MMSTB

Permeability variation, $V = 0.8$

Mobility ratio, $M = 2.0$

Initial water saturation, $S_{wi} = 0.25$

Predict the cumulative oil production as a function of the producing water-oil ratio.

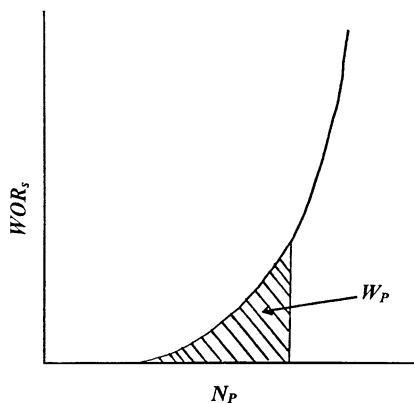


Figure 14-56. Cumulative water production from WOR vs. N_p curve.

Solution

Using Johnson's graphical approach, perform the required calculations in the following worksheet:

| WOR | Figure 14-54 | R | $N_p = N_s R$ |
|-----|------------------------------|-------|---------------|
| 1 | $R(1 - S_{wi}) = 0.049$ | 0.065 | 0.78 MMSTB |
| 5 | $R(1 - 0.72 S_{wi}) = 0.100$ | 0.122 | 1.464 MMSTB |
| 25 | $R(1 - 0.32 S_{wi}) = 0.200$ | 0.217 | 2.604 MMSTB |
| 100 | $R(1 - 0.40 S_{wi}) = 0.377$ | 0.419 | 5.028 MMSTB |

Modified Dykstra-Parsons Method

Felsenthal, Cobb, and Heuer (1962) extend the work of Dykstra and Parsons to account for the presence of initial gas saturation at the start of flood. Assuming a constant water-injection rate i_w , the method is summarized in the following steps:

- Step 1.* Perform the following preliminary calculations to determine:
- Pore volume PV and oil-in-place at start of flood N_s
 - Water cut f_w as a function of S_w
 - Slope (df_w/dS_w) as a function of S_w
 - Average water saturation at breakthrough \bar{S}_{wBT}
 - Mobility ratio M from Equation 14-61
 - Displacement sweep efficiency at breakthrough E_{DBT} from Equation 14-9
 - Areal sweep efficiency at breakthrough E_{ABT} from Equation 14-64
 - Permeability variation V from Equation 14-70
 - Fill-up volume W_{if} from Equation 14-82
- Step 2.* Using Equations 14-94 and 14-96, calculate the vertical sweep efficiency at assumed water-oil ratios of 1, 2, 5, 10, 15, 20, 25, 50, and 100 bbl/bbl.
- Step 3.* Plot WOR versus E_v on a Cartesian scale, as shown schematically in Figure 14-55, and determine the vertical sweep efficiency at breakthrough E_{vBT} by extrapolating the WOR versus E_v curve to $WOR = 0$.

Step 4. Calculate cumulative water injected at breakthrough by using Equation 14-43:

$$W_{iBT} = (PV)(\bar{S}_{wBT} - S_{wi})E_{ABT}E_{VBT}$$

where W_{iBT} = cumulative water injected at breakthrough, bbl

PV = pattern pore volume

E_{VBT} = vertical sweep efficiency at breakthrough

E_{ABT} = areal sweep efficiency at breakthrough

Step 5. Calculate cumulative oil produced at breakthrough from the following expression:

$$(N_P)_{BT} = \frac{W_{iBT} - W_{if}E_{VBT}}{B_o} \quad (14-97)$$

Step 6. Calculate the time to breakthrough t_{BT} from:

$$t_{BT} = \frac{W_{iBT}}{i_w}$$

Step 7. Assume several values for water-oil ratios WOR_r , e.g., 1, 2, 5, 10, 15, 20, 25, 50, and 100 bbl/bbl.

Step 8. Determine E_V for each assumed value of WOR (see Step 3).

Step 9. Convert the assumed values of WOR_r to water cut f_{w2} and surface WOR from Equations 14-25 and 14-29, respectively:

$$f_{w2} = \frac{WOR_r}{WOR_r + 1}$$

$$WOR_s = WOR_r \left(\frac{B_o}{B_w} \right)$$

where f_{w2} = water cut at the sand face of producer, bbl/bbl

WOR_s = surface water-oil ratio, STB/STB

WOR_r = reservoir water-oil ratio, bbl/bbl

Step 10. Determine the water saturation S_{w2} for each value of f_{w2} from the water cut curve.

- Step 11.* Using Equation 14-67 or Figure 14-36, determine the areal sweep efficiency E_A for each value of f_{w2} .
- Step 12.* Using Equation 14-67 or Figure 14-36, determine the areal sweep efficiency E_A for each value of f_{w2} .
- Step 13.* Determine the average water saturation \bar{S}_{w2} for each value of f_{w2} from Equation 14-45.
- Step 14.* Calculate the displacement efficiency E_D for each \bar{S}_{w2} in step 13 by applying Equation 14-9.
- Step 15.* Calculate cumulative oil production for each WOR from:

$$N_p = N_s E_D E_A E_V - \frac{(PV) S_{gi} (1 - E_A E_V)}{B_o} \quad (14-98)$$

- Step 16.* Plot the cumulative oil production N_p versus WOR_s on Cartesian coordinate paper, as shown schematically in Figure 14-56, and calculate the area under the curve at several values of WOR_s . The area under the curve represents the cumulative water production W_p at any specified WOR_s , i.e., $(W_p)_{WOR}$.

- Step 17.* Calculate the cumulative water injected W_{inj} at each selected WOR from:

$$W_{inj} = (N_p)_{WOR} B_o + (W_p)_{WOR} B_w + (PV) S_{gi} (E_v)_{WOR} \quad (14-99)$$

where W_{inj} = cumulative water injected, bbl

S_{gi} = initial gas saturation

$(N_p)_{WOR}$ = cumulative oil production when the water-oil ratio reaches WOR, STB

$(E_v)_{WOR}$ = vertical sweep efficiency when the water-oil ratio reaches WOR

- Step 18.* Calculate the time to inject W_{inj} :

$$t = \frac{W_{inj}}{i_w}$$

- Step 19.* Calculate the oil and water flow rates from Equations 14-55 and 14-56, respectively:

$$Q_o = \frac{i_w}{B_o + B_w \text{WOR}_S}$$

$$Q_w = Q_o \text{WOR}_S$$

Craig-Geffen-Morse Method

With the obvious difficulty of incorporating the vertical sweep efficiency in oil recovery calculations, Craig et al. (1955) proposed performing the calculations for only one selected layer in the multilayered system. The selected layer, identified as the **base layer**, is considered to have a 100% vertical sweep efficiency. The performance of each of the remaining layers can be obtained by “sliding the timescale” as summarized in the following steps:

Step 1. Divide the reservoir into the appropriate number of layers.

Step 2. Calculate the performance of a single layer, i.e., the base layer, for example, layer n .

Step 3. Plot cumulative liquid volumes (N_p , W_p , W_{inj}) and liquid rates (Q_o , Q_w , i_w) as a function of time t for the base layer, i.e., layer n .

Step 4. For each layer (including the base layer n) obtain:

- (k / ϕ)
- (ϕh)
- $(k h)$

Step 5. To obtain the performance of layer i , select a succession of times t and obtain plotted values N_p^* , W_p^* , W_{inj}^* , Q_o^* , Q_w^* , and i_w^* by reading the graph of Step 3 at time t^* :

$$t_i^* = t \frac{\left(\frac{k}{\phi}\right)_i}{\left(\frac{k}{\phi}\right)_n} \quad (14-100)$$

Then calculate the performance of layer i at any time t from:

$$N_p = N_p^* \frac{(\phi h)_i}{(\phi h)_n} \quad (14-101)$$

$$W_p = W_p^* \frac{(\phi h)_i}{(\phi h)_n} \quad (14-102)$$

$$W_{inj} = W_{inj}^* \frac{(\phi h)_i}{(\phi h)_n} \quad (14-103)$$

$$Q_o = Q_o^* \frac{(k/\phi)_i}{(k/\phi)_n} \quad (14-104)$$

$$Q_w = Q_w^* \frac{(k/\phi)_i}{(k/\phi)_n} \quad (14-105)$$

$$i_w = i_w^* \frac{(k/\phi)_i}{(k/\phi)_n} \quad (14-106)$$

where

n = base layer

i = layer i

N_p^* , W_p^* , W_{inj}^* = volumes at t^*

Q_o^* , Q_w^* , and i_w^* = rates at t^*

Step 6. The composite performance of the flood pattern at time t is obtained by summation of individual layer values.

Example 14-24

Results of Example 14-16 are shown graphically in Figure 14-47. Assume that the reservoir has an *additional* four layers that are characterized by the following properties:

| Layer | k , md | h , ft | ϕ |
|---------------------|----------|----------|--------|
| “Original (base)” 1 | 31.5 | 5 | 0.20 |
| 2 | 20.5 | 5 | 0.18 |
| 3 | 16.0 | 4 | 0.15 |
| 4 | 13.0 | 3 | 0.14 |
| 5 | 10.9 | 2 | 0.10 |

Calculate N_p , W_p , W_{inj} , Q_o , Q_w , and i_w for the remaining four layers at $t = 730$ days.

Solution

Step 1. Calculate k/ϕ , ϕh , and kh for each layer.

| Layer | k/ϕ | ϕh | kh |
|-------|----------|----------|-------|
| 1 | 157.5 | 1.00 | 157.5 |
| 2 | 113.9 | 0.90 | 102.5 |
| 3 | 106.7 | 0.60 | 64.0 |
| 4 | 92.8 | 0.42 | 39.3 |
| 5 | 109.0 | 0.20 | 21.8 |

Step 2. At $t = 730$, calculate t^* :

| Layer | $\frac{(k/\phi)_i}{(k/\phi)_n}$ | $t^* = 730 \left[\frac{(k/\phi)_i}{(k/\phi)_n} \right]$ |
|-------|---------------------------------|--|
| 1 | 1.000 | 730 |
| 2 | 0.723 | 528 |
| 3 | 0.677 | 495 |
| 4 | 0.589 | 430 |
| 5 | 0.692 | 505 |

Step 3. Read the values of N_p^* , W_p^* , W_{inj}^* , Q_o^* , Q_w^* , and i_w^* at each t^* from Figure 14-47:

| Layer | t^* | N_p^* | W_p^* | W_{inj}^* | Q_o^* | Q_w^* | i_w^* |
|-------|-------|---------|---------|-------------|---------|---------|---------|
| 1 | 730 | 81,400 | 61,812 | 206,040 | 51.5 | 218.4 | 274.5 |
| 2 | 528 | 68,479 | 19,954 | 153,870 | 65 | 191 | 261 |
| 3 | 495 | 63,710 | 21,200 | 144,200 | 68 | 175 | 258 |
| 4 | 430 | 57,000 | 9620 | 124,000 | 75 | 179 | 254 |
| 5 | 505 | 74,763 | 41,433 | 177,696 | 58 | 200 | 267 |

Step 4. Calculate N_p , W_p , W_{inj} , Q_o , Q_w , and i_w for each layer after 730 days by applying Equations 14-101 through 14-106:

| Layer | $(\phi h)_i/(\phi h)_1$ | N_p | W_p | W_{inj} |
|-------|-------------------------|---------|--------|-----------|
| 1 | 1.00 | 81,400 | 61,812 | 206,040 |
| 2 | 0.90 | 61,631 | 11,972 | 138,483 |
| 3 | 0.60 | 38,226 | 12,720 | 86,520 |
| 4 | 0.42 | 23,940 | 4040 | 52,080 |
| 5 | 0.20 | 14,953 | 8287 | 35,539 |
| Total | | 220,150 | 98,831 | 466,582 |

| Layer | $(\phi h)_i/(\phi h)_1$ | Q_o | Q_w | i_w |
|-------|-------------------------|-------|-------|-------|
| 1 | 1.000 | 51.5 | 218.4 | 274.5 |
| 2 | 0.651 | 42.3 | 124.3 | 169.9 |
| 3 | 0.406 | 27.6 | 71.1 | 104.7 |
| 4 | 0.250 | 18.8 | 44.8 | 63.5 |
| 5 | 0.138 | 8.0 | 27.6 | 36.8 |
| Total | | 148.2 | 486.2 | 649.4 |

$$\text{Producing WOR} = \frac{486.2}{148.2} = 3.28 \text{ STB / STB.}$$

Step 5. Steps 2 and 3 are repeated for a succession of times t and the composite reservoir performance curves are generated to describe the entire reservoir performance.

In addition to the previously discussed methods of predicting waterflood performance, there are empirical prediction methods that provide estimates of ultimate waterflood recovery factors. Based on 73 sandstone reservoirs, Guthrie and Greenberger (1963) developed an empirical expression that correlates the recovery factor with

- Permeability, k , md
- Porosity, ϕ , as a fraction
- Oil viscosity, μ_o , cp
- Connate water saturation, S_{wc} , as a fraction
- Reservoir thickness, h , ft

The empirical equation for predicting the waterflood ultimate recovery factor (RF) takes the form:

$$\text{RF} = 0.2719 \log k + 0.25569 S_{wc} - 0.1355 \log \mu_o - 1.538 \phi - 0.0008488h + 0.11403$$

Arps (1967) statistically correlated the recovery factor as a function of the initial pressure p_i and pressure at depletion p_a by the following relationship:

$$\text{RF} = 54.898 \left[\frac{\phi(1-S_{wi})}{B_{oi}} \right]^{0.0422} \left[\frac{\mu_{wi} k}{\mu_{oi}} \right]^{0.077} (S_w)^{-0.1903} \left(\frac{P_i}{P_a} \right)^{-0.2159}$$

If the relative permeability data are available, the ultimate waterflood recovery can be estimated by applying the following steps:

Step 1. Using the relative permeability data, plot k_{rw}/k_{ro} versus S_w on a semi log paper and draw a straight line or a smooth curve through the data points.

Step 2. Estimate the economic water cut or WOR, $(WOR)_{econ}$.

Step 3. Solve for the water-oil relative permeability ratio from the following relationship:

$$\left(\frac{k_{rw}}{k_{ro}} \right) = \frac{\mu_w B_w}{\mu_o B_o} (WOR)_{econ}$$

Step 4. Enter the relative permeability ratio curve (constructed in Step 1) with the cumulative value of k_{rw}/k_{ro} and determine the corresponding value of water saturation, S_w .

Step 5. Assuming that no free gas exists at the economic WOR and there is no significant change in either oil viscosity or the oil formation volume factor, calculate the remaining oil saturation S_{or} from

$$S_{or} = 1 - S_w$$

Step 6. Estimate the maximum possible recovery, N_p .

$$N_p = \frac{(P.V)(S_{oi} - S_{or})}{B_o}$$

where S_{oi} = initial oil saturated at start of flood

P.V = pore volume, bbl

This value of N_p represents the maximum possible recovery because it assumes that at floodout the entire reservoir has been contacted and swept by the injected water.

WATERFLOOD SURVEILLANCE

An essential key to a successful waterflooding project is a well-planned and well-executed program of surveillance and monitoring. Production

curves are very valuable tools for monitoring and detecting changes in well and reservoir performance. Production performance can provide clues as to the nature of reservoir behavior. To be meaningful, production curves require accurate and regular production well tests since fluids produced from the field are annually allocated to individual wells based on these tests. It is important to consider the following items in the design and implementation of a comprehensive waterflood surveillance program.

- Accurate record-keeping of each injector's and producer's data performance in terms of:
 - Injection and production rates
 - Bottom-hole pressures
 - Fluid profiles, for example, water and oil cut, WOR, GOR, etc.
- Monthly comparison of actual and predicted performance
- Estimate of sweep efficiency and oil recovery at various stages of depletion
- Performance and operating conditions of facilities
- Accurate and detailed reservoir description
- Water quality and treating
- Economic surveillance
- Diagnosis of existing/potential problems and their solutions

As a general objective, a surveillance program should allow for the maximum oil recovery to be achieved at the lowest WOR and operation cost. From a reservoir viewpoint, this can be achieved by maximizing the water recovery factors, which are primarily controlled by the three main efficiency factors (E_A , E_Y , and E_D) with a minimum amount of injected water. There are useful plotting and diagnostic techniques and procedures that are designed to supplement prediction methods and assist in quantifying the flood performance. Some of these techniques are briefly discussed here.

Bubble Maps

This pictorial display shows the location of various flood fronts. The maps allow visual differentiation between areas of the reservoirs that have and have not been swept by injected water. The outer radii of the oil and water banks are given by Equations 14-80 and 14-81 as:

$$r_o = \sqrt{\frac{5.615 W_{inj}}{\pi \phi h S_{gi}}}$$

$$r = r_o \sqrt{\frac{S_{gi}}{S_{wBT} - S_{wi}}}$$

where r_o = outer radius of oil bank

r = outer radius of water bank

The bubble map can be used to identify areas that are not flooded and areas with infill drilling opportunities.

Hall Plot

Hall (1963) presented a methodology for analyzing injection well data that is based on a plot of cumulative pressure versus cumulative injection. The required data include:

- Average monthly bottom-hole injection pressures P_{inj} , however, well-head injection pressures can be used if they are correctly converted to bottom-hole pressures by accounting for the hydraulic head and friction losses in the tubing
- Average reservoir pressure, \bar{p}
- Monthly injection volumes
- Injection days for the month

The methodology assumes that the steady-state injection rate is preserved such that the injection rate can be expressed by Darcy's equation:

$$i_w = \frac{0.00708 k h (p_{inj} - \bar{p})}{\mu_w \left[\ln \left(\frac{r_e}{r_w} \right) - 0.75 + s \right]}$$

Assuming k , b , μ , r_c , r_w , and s are constant, the last equation is reduced to

$$i_w = A(p_{inj} - \bar{p})$$

where

$$A = \frac{0.00708 kh}{\mu_w \left[\ln \left(\frac{r_c}{r_w} \right) - 0.75 + s \right]}$$

or

$$(p_{inj} - \bar{p}) = \frac{i_w}{A}$$

Integrating both sides of this equation with respect to time gives

$$\int_0^t (p_{inj} - \bar{p}) dt = \frac{1}{A} \int_0^t i_w dt$$

The integral on the right hand side is essentially the cumulative water injected W_{inj} at any time t , or

$$\int_0^t (p_{inj} - \bar{p}) dt = \frac{W_{inj}}{A} \quad (14-107)$$

where p_{inj} = monthly average injection pressure, psi

\bar{p} = monthly average reservoir pressure, psi

W_{inj} = cumulative volume water injected at time t , bbl

Equation 14-107 suggests that a plot of the integral term $\int_0^t (p_{inj} - \bar{p}) dt$ versus the cumulative water injected, W_{inj} , on a Cartesian scale would produce a straight line with a slope of $1/A$. This graph is called a Hall

Plot. If the parameters k , h , r_e , r_w , μ , and s are constants, then the value of A is also constant and yields a straight line with a constant slope of $1/A$. However, if these parameters change, A will also change and thus the slope of the Hall Plot will change. These changes in the slope can provide a wealth of information regarding the characteristic of an injection well, as shown in Figure 14-57.

Early in the life of an injection well, the water-zone radius will increase with time, causing the slope to curve concavely upward, as shown by segment ab in Figure 14-57. After fill-up, line bA indicates stable or normal injection. An increasing slope that is concave upward generally indicates a positive skin or poor water quality (line D). Similar slopes may occur if a well treatment is designed to improve effective volumetric sweep. In this case, however, the slope will first increase and then stay constant. Line B indicates a decreasing slope, indicating negative skin or injection above parting pressure. The injection under the latter condition can be verified by running step-rate tests. A very low slope value, as shown by line bC , is an indication of possible channeling or out-of-zone injection.

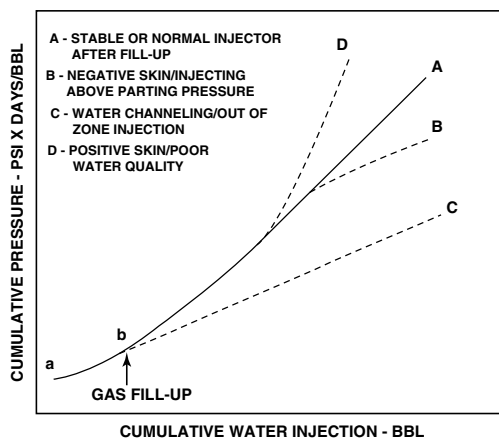


Figure 14-57. Typical Hall Plot for various conditions. (Permission to publish by the SPE.)

Example 14-25

Using the following data on an injection well, prepare and discuss a Hall Plot.

| Month | p_{inj} , psi | \bar{p} , psi | Δt , days | i_w , bbl/month |
|-------|-----------------|-----------------|-------------------|-------------------|
| 1 | 2600 | 1509 | 11 | 11,000 |
| 2 | 2635 | 1511 | 28 | 28,000 |
| 3 | 2652 | 1513 | 30 | 30,000 |
| 4 | 2658 | 1516 | 16 | 16,000 |
| 5 | 2667 | 1518 | 31 | 31,000 |
| 6 | 2683 | 1521 | 28 | 28,000 |

Solution

Step 1. Approximate the integral of Equation 14-107 as follows:

$$\int_0^t (p_{inj} - \bar{p}) dt \cong \sum_0^t (\Delta p \Delta t)$$

where

$$\Delta p = p_{inj} - \bar{p}$$

Δt = number of injection days for the month

Step 2. Prepare the following table.

| Month | $\Delta p = p_{inj} - \bar{p}$ | Δt , day | $\Delta P \cdot \Delta t$ psi-day | $\Sigma \Delta P \Delta t$ | i_w bbl/ month | W_{inj} bbl |
|-------|--------------------------------|------------------|--------------------------------------|----------------------------|---------------------|---------------|
| 1 | 1091 | 11 | 12×10^3 | 12×10^3 | 11,000 | 11,000 |
| 2 | 1124 | 28 | 31.47×10^3 | 44.47×10^3 | 28,000 | 39,000 |
| 3 | 1139 | 30 | 34.17×10^3 | 78.64×10^3 | 30,000 | 64,000 |
| 4 | 1142 | 16 | 18.27×10^3 | 96.91×10^3 | 16,000 | 85,000 |
| 5 | 1149 | 31 | 35.62×10^3 | 132.53×10^3 | 31,000 | 116,000 |
| 6 | 1162 | 28 | 32.53×10^3 | 165.06×10^3 | 28,000 | 144,000 |

Step 3. Plot $\Sigma \Delta p \Delta t$ versus W_{inj} on a Cartesian scale as shown in Figure 14-58.

It should be pointed out that the changes in the Hall Plot will occur gradually, as in production-decline analysis. The increase in the slope could indicate a positive skin or poor-quality injection water.

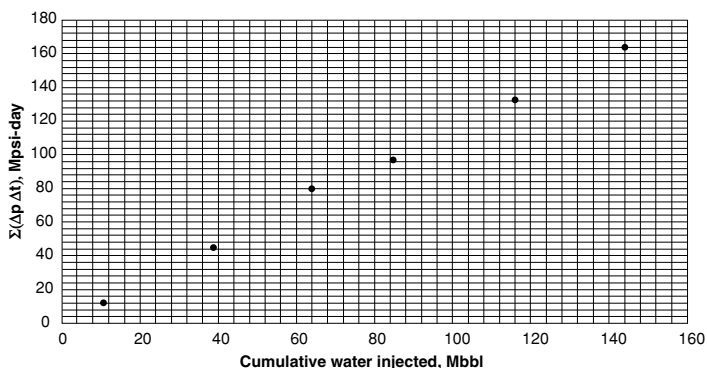


Figure 14-58. Hall Plot for Example 14-25.

The X-Plot

Because the traditional method of extrapolating the part production performance on the graph of water cut versus cumulative oil is often complicated, Ershaghi and Omoregie (1978) suggested an alternative method of analyzing waterflood performance. Their method is a graphical technique that is referred to as the X-plot. The authors defined variable X mathematically as follows:

$$X = \frac{1}{f_w} - \ln \left(\frac{1}{f_w} - 1 \right)$$

with

$$f_w = \frac{Q_w}{Q_w + Q_o} = \frac{WOR}{WOR + 1}$$

Ershaghi and Omoregie observed that plotting the recovery factor, RF, or cumulative oil production, N_p versus variable X will yield a straight line that can be extrapolated at the economic water cut limit to project the ultimate waterflood oil recovery.

In the absence of layering effects, a linear plot is obtained for water cut values above 50%. The formation of a straight line indicates that the performance is being controlled by the relative permeability ratio characteristics of the reservoir. Ershaghi et al. (1987) developed a procedure to

estimate cumulative water injected (in a pattern waterflood or the entire field) from the slope of the $X-N_p$ plot. The authors indicated that the cumulative water injected, W_{inj} , when the water cut reaches a value of f_w can be estimated from

$$W_{inj} = \frac{B_{oi}}{m' f_w (1 - f_w)}$$

where $m' =$ slope of X versus N_p , 1/STB

$B_{oi} =$ formation volume factor at start of flood, bbl/STB

$W_{inj} =$ cumulative water injected, bbl

$f_w =$ water cut

The authors demonstrated their technique through a simulated flood example; using the following data:

- Five-spot pattern
- Area = 40 acres
- Injection rate = 600 bbl/dat
- $Q = 150$ bbl/dat/well
- Thickness = 28 ft
- $S_{wi} = 0.191$
- $B_{oi} = 1.258$
- Porosity = 25%

Other given data include total injection time, observed water cut, and cumulative oil production. A plot of the variable X versus N_p , as shown graphically in Figure 14-59, produced a straight line with the following slope:

$$m' = 1.88 \times 10^{-5}$$

The cumulative water injected at any value of water cut can be calculated from

$$W_{inj} = \frac{B_{oi}}{m' f_w (1 - f_w)} = \frac{1.258}{1.88 \times 10^{-5} f_w (1 - f_w)}$$

The cumulative water injected or *water influx* can be calculated by using the observed production data, as shown in the following table:

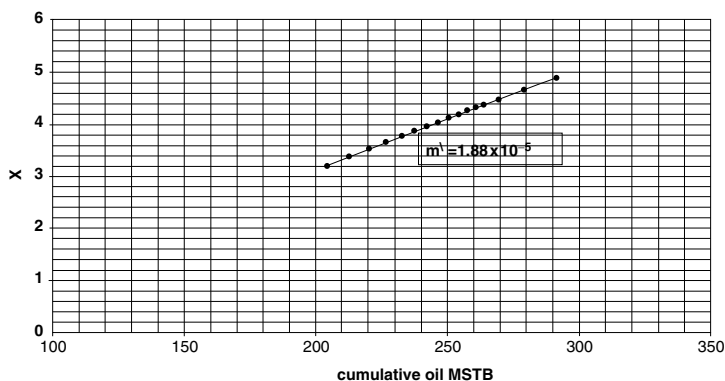


Figure 14-59. X-plot of a simulated waterflood.

PERFORMANCE OF THE SIMULATED WATERFLOOD

| Year | Water cut, f_w | $X = 1/f_w - \ln(1/f_w - 1)$ | Cumulative oil, N_p (STB) | W_{inj} , MMbbl |
|------|---------------------|------------------------------|--------------------------------|-------------------|
| 3.0 | 0.8881 | 3.1975 | 204,228 | 0.673 |
| 3.5 | 0.9066 | 3.3758 | 212,776 | 0.7902 |
| 4.0 | 0.9200 | 3.5293 | 220,109 | 0.909 |
| 4.5 | 0.9295 | 3.6549 | 226,530 | 1.021 |
| 5.0 | 0.9369 | 3.7652 | 232,747 | 1.132 |
| 5.5 | 0.9429 | 3.8647 | 237,406 | 1.243 |
| 6.0 | 0.9478 | 3.9541 | 242,106 | 1.352 |
| 6.5 | 0.9520 | 4.0378 | 246,422 | 1.464 |
| 7.0 | 0.9556 | 4.1158 | 250,409 | 1.577 |
| 7.5 | 0.9586 | 4.1854 | 254,113 | 1.686 |
| 8.0 | 0.9614 | 4.2553 | 257,570 | 1.803 |
| 8.5 | 0.9637 | 4.3166 | 260,810 | 1.913 |
| 9.0 | 0.9657 | 4.3720 | 263,864 | 2.020 |
| 10.0 | 0.9691 | 4.4775 | 269,506 | 2.235 |
| 12.0 | 0.9742 | 4.6577 | 279,288 | 2.662 |
| 15 | 0.9794 | 4.8877 | 291,259 | 3.316 |

An improved graphical technique for the recovery factor plot was suggested by Robertson (1986). In this approach, a special coordinate system (Figure 14-60) was devised to directly plot the water cut f_w versus cumulative oil production. In such a plot, no conversion to the X parameter is required.

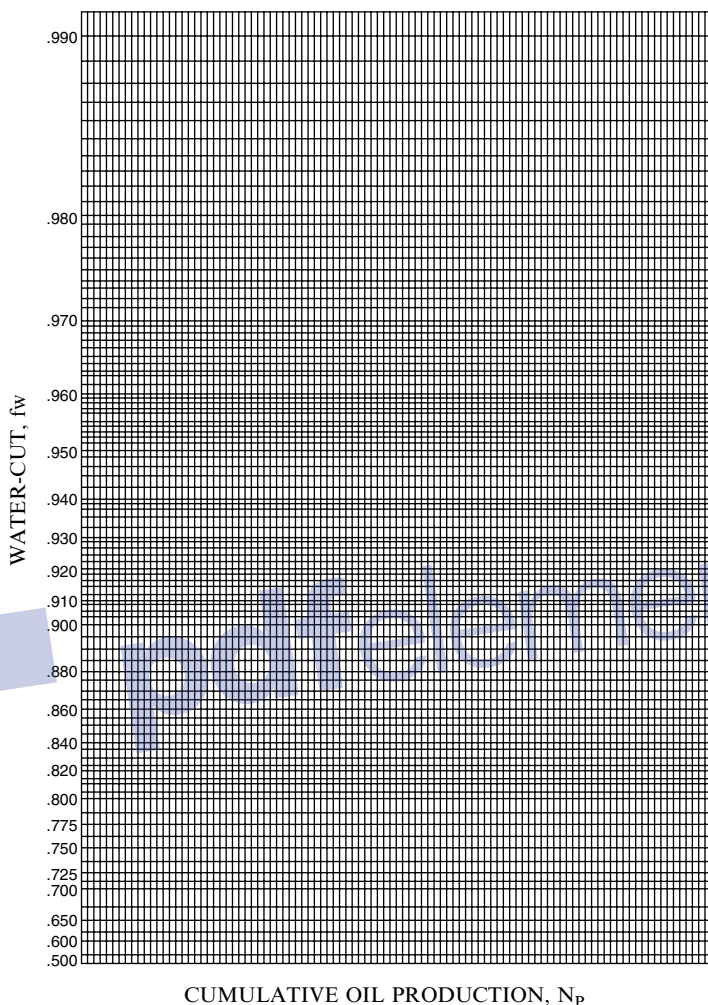
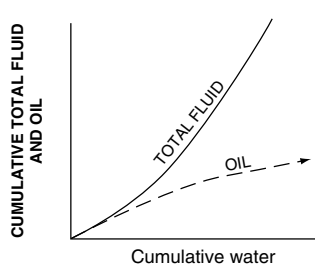


Figure 14-60. Special graph for plotting water cut f_w versus cumulative oil production. (Permission to publish by the SPE.)

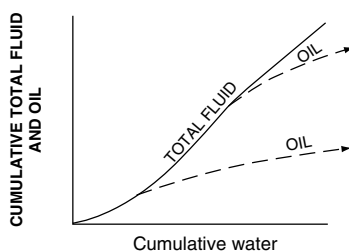
Production Curves

Plotting both cumulative *total* fluid production and cumulative oil production versus cumulative water-injection can be a useful diagnostic tool for understanding the performance of the flood as it progresses. Thakur (1991) illustrated various examples of waterflood performances, as shown in Figure 14-61.



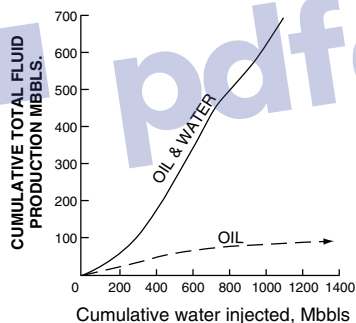
SLOPE OF TOTAL FLUID CURVE

- (1) 45 DEGREES INDICATES INJECTION EQUALS WITHDRAWALS.
- (2) LESS THAN 45 DEGREES INDICATES FILLUP OR FLUID LEAVING PATTERN.
- (3) GREATER THAN 45 DEGREES INDICATES WITHDRAWALS EXCEED INJECTION.



DEVIATION OF OIL AND TOTAL FLUID CURVE

- (1) DEVIATION AT LOW CUMULATIVE INDICATES EARLY WATER BREAKTHRU.
- (2) SLOPE OF OIL CURVE INDICATES WHAT THE INCREMENTAL SUPPLEMENTAL RECOVERY MIGHT BE WITH CONTINUED INJECTION, WITH PRESENT INJECTION PRODUCTION CONFIGURATIONS.



EXAMPLE FROM A NORTH TEXAS WATERFLOOD ILLUSTRATES EARLY WATER BREAKTHROUGH AND POOR RECOVERY.

Figure 14-61. Cumulative water-injection vs. cumulative total fluid and cumulative oil. (Permission to publish by the SPE.)

Pattern Balancing

Balancing injection and production rates can significantly enhance the profitability of a waterflood project by:

- Minimizing or migrating across pattern boundaries
- Improving the capture of the mobilized oil
- Reducing the volume of recycled water
- Increasing sweep efficiency
- Providing more opportunity to increase oil recovery

In balanced patterns, important events such as fill-up or water breakthrough for the various patterns should occur at the same time.

Several authors have suggested that the injection rate in each pattern should be in proportion to the displaceable hydrocarbon pore volume, V_D . V_D is defined as:

$$V_D = V_p(1 - S_{wc} - S_{or})$$

where V_D = displaceable hydrocarbon pore volume, bblu

V_p = pore volume, bbl

S_{wc} = connate-water saturation, fraction

S_{or} = residual oil saturation, fraction

The fraction of total field injection into an individual pattern is then given by:

$$(i_w)_{\text{pattern}} \left[\frac{(V_D)_{\text{pattern}}}{(V_D)_{\text{field}}} \right] (i_w)_{\text{field}}$$

where $(i_w)_{\text{pattern}}$ = injection rate in the pattern, bbl/day

$(i_w)_{\text{field}}$ = total target field injection rate, bbl/day

$(V_D)_{\text{field}}$ = total field pore volume, bbl

Based on the basic principles of waterflood and the volumetric material balances, the confinement of the injected water and displaced fluid to the flood pattern can be roughly estimated by calculating the confinement factor, CF, as defined by:

$$CF = \frac{\left[1 + \frac{N_p B_o}{V_p (1 - S_{wi})} \right] + \sqrt{\left[1 + \frac{N_p B_o}{V_p (1 - S_{wi})} \right]^2 - \frac{4(W_{inj} - W_p)}{V_p (1 - S_{wi})}}}{2}$$

or, alternatively, in terms of the recovery factor, RF, as:

$$CF = \frac{\left[1 + RF \right] + \sqrt{\left(1 + RF \right)^2 - \frac{4(W_{inj} - W_p)}{V_p (1 - S_{wi})}}}{2}$$

where RF = recovery factor

CF = confinement factor

V_p = flood area pore volume, bbl

S_{wi} = water saturation at start of flood

N_p = cumulative oil produced, STB

B_o = oil formation volume factor, bbl/STB

W_{inj} = cumulative water injected, bbl

W_p = cumulative water produced, bbl

It should be pointed out that the above expression is only valid after free gas fill-up. The CF provides an indication of the loss of the injection water or displaced fluid outside the flood area or indicates the inflow of oil or water from outside the flood area, or numerically,

CF = 1.0, indicates confined flood

CF < 1.0, indicates migration or loss outside the flood area

CF > 1.0, indicates inflow from outside the flood area

The concept of the CF can be illustrated graphically, as shown in Figure 14-62.

Volumetric Sweep Efficiency

The volumetric sweep efficiency, designated as E_{VOL} , is the percentage of the total reservoir contacted by the injected fluid. This efficiency is

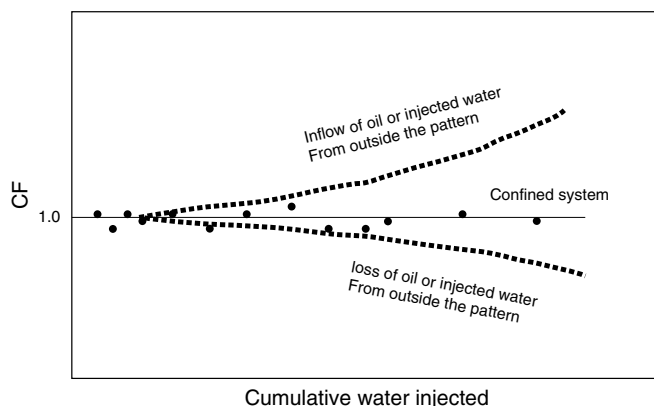


Figure 14-62. Conformance factor vs. Cumulative water injected.

commonly called “**fluid conformance**” and is the resulting product of E_A and E_V at any time during the waterflood process:

$$E_{VOL} = E_A E_V$$

The E_{vol} provides an indication of the fraction of the reservoir that has been swept or not swept by the injected water. The volumetric sweep efficiency quantitatively reflects the potential for additional oil recovery that exists in the unswept portion of the reservoir. This important waterflood surveillance parameter can be roughly estimated after the **gas fill-up** with the assumption of negligible changes in B_o from the following expression.

$$E_{vol} = \left[\frac{B_o}{(P.V)(1 - S_{wi} - S_{or})} \right] N_p + \frac{S_{gi}}{1 - S_{wi} - S_{or}}$$

where E_{vol} = volumetric sweep efficiency

S_{wi} = water saturation at the start of the waterflood

P.V = pore volume, bbls

S_{or} = residual oil solution

S_{gi} = gas saturation at the start of the flood

N_p = cumulative oil produced at any time during the fluid

Therefore, after the fill-up, the equation indicates that a plot of the E_{vol} as a function of the historical oil products N_p would produce a straight line of the following form:

$$E_{VOL} = a N_p + b$$

Where the slope “a” and intercept “b” are given by:

$$a = \frac{B_o}{(P.V)(1 - S_{or} - S_{wi})}$$

$$b = \frac{S_{gi}}{1 - S_{gi} - S_{wi}}$$

Example 14-26

A multilayered reservoir is under waterflood. The following data are available at the start of the flood.

$$S_{wi} = 20\%$$

$$\phi = 15\%$$

$$S_{or} = 30\%$$

$$S_{gi} = 15\%$$

$$B_o = 1.2 \text{ bbl/STB}$$

$$h = 29 \text{ ft}$$

$$A = 6000 \text{ acres}$$

The available historical production data are listed below.

| Time, years | N_p , MMSTB |
|-------------|---------------|
| 2 | 11 |
| 5 | 14.3 |
| 8 | 16.5 |
| 11 | 18.6 |
| 16 | 21.9 |

Assuming that the projected ultimate waterflood recovery factor is 25% when reaching the economic WOR limit, determine whether an opportunity exists to increase recovery beyond the projected estimate through an infill drilling or an injection well realignment program.

Solution

Step 1. Calculate the pore volume (P.V), initial oil-in-place at start of the waterflood N , and the projected ultimate oil production from:

$$P.V = 7758Ah\phi$$

$$P.V = 7758 (6000) (29) (0.15) = 202.484 \text{ MMBBL}$$

$$N = \frac{(P.V)(1 - S_{wi} - S_{gi})}{B_o} = \frac{202.484(1 - 0.2 - 0.15)}{1.2} = 109.68 \text{ MMSTB}$$

$$N_p = (RF) (N) = (0.25) (109.68) = 27.42 \text{ MMSTB}$$

Step 2. Calculate the coefficients “a” and “b” of the volumetric sweep efficiency equation from:

$$a = \frac{B_o}{(P.V)(1 - S_{or} - S_{wi})}$$

$$a = \frac{1.20}{(202.486 \times 10^{-6})(1 - 0.3 - 0.2)} = 0.01185 \times 10^6$$

$$b = \frac{S_{gi}}{1 - S_{or} - S_{wi}}$$

$$b = \frac{0.15}{1 - 0.3 - 0.2} = 0.3$$

Step 3. Calculate the volumetric sweep efficiency as a function of cumulative oil after gas fill-up from:

$$E_{VOL} = a N_P + b$$

$$E_{VOL} = 0.01185 \times 10^{-6} N_P + 0.3$$

| N_P , MMSTB | E_{VOL} , % |
|---------------|---------------|
| 11.0 | 43.0 |
| 14.3 | 46.9 |
| 16.5 | 49.5 |
| 18.6 | 52.1 |
| 21.9 | 56.0 |
| 27.42 | 62.5 |

Step 4. The current volumetric sweep efficiency after producing 21.9 MMSTB is 56% of the projected ultimate value of 62.5%. This suggests that approximately 37.5% of the reservoir will not have been swept by the injected water when reaching the economic limit.

Step 5. Assuming that by infill drilling and pattern realignment, the volumetric sweep efficiency can be increased to 80%, the expected recovery would be:

$$N_p = \frac{E_{VOL} - b}{a}$$

$$N_p = \frac{0.80 - 0.03}{0.01185 \times 10^{-6}} = 42.19 \text{ MMSTB}$$

an increase of 14.77 MMSTB over the ultimate projected recovery.

It should be pointed out that the use of the E_{VOL} equation provides only a rough estimate of the volumetric efficiency with the following limitations:

- Use after gas fill-up
- Accuracy of S_{gi} , S_{or} , and S_{wi}
- Accuracy of the pore volume

PROBLEMS

1. A saturated oil reservoir exists at its bubble-point pressure of 2,840 psi. The following pressure-production data are given:

| P | N_p , STB | G_p , Mscf | B_t , bbl/STB | B_g , ft ³ /scf | R_s , scf/STB |
|------|-------------|--------------|-----------------|------------------------------|-----------------|
| 2840 | 0 | 0 | 1.528 | — | 827 |
| 2660 | 36,933 | 37,851 | 1.563 | 0.00618 | 772 |
| 2364 | 65,465 | 74,137 | 1.636 | 0.00680 | 680 |
| 2338 | 75,629 | 91,910 | 1.648 | 0.00691 | 675 |
| 2375 | 85,544 | 115,256 | 1.634 | 0.00674 | 685 |
| 2305 | 96,100 | 148,200 | 1.655 | 0.00702 | 665 |

The following information is also available:

$$S_{wi} = 25\% \text{ and } S_{or} = 35\%.$$

- a. Calculate the reduction in the residual gas saturation if a waterflooding project were to start at 2,364 psi.
- b. Calculate the injection that is required to dissolve the trapped gas.

2. The relative permeability data for a core sample taken from the Vu-Villa Field are given below:

| S_w | k_{rw} | k_{ro} |
|-------|----------|----------|
| 0.16 | 0 | 1.00 |
| 0.20 | 0.0008 | 0.862 |
| 0.26 | 0.0030 | 0.670 |
| 0.32 | 0.0090 | 0.510 |
| 0.40 | 0.024 | 0.330 |
| 0.50 | 0.064 | 0.150 |
| 0.60 | 0.140 | 0.040 |
| 0.66 | 0.211 | 0.010 |
| 0.72 | 0.30 | 0.00 |
| 1.00 | 1.00 | 0.00 |

$$S_{wi} = 0.16$$

$$\mu_o = 2.00 \text{ cp}$$

$$S_{or} = 0.28$$

$$\rho_w = 1.0 \text{ g/cm}^3$$

$$\mu_w = 0.75 \text{ cp}$$

$$\rho_o = 0.83 \text{ g/cm}^3$$

- Neglecting gravity and capillary pressure terms, develop the fractional flow curve.
- Assuming a water-injection rate of $0.08 \text{ bbl/day/ft}^2$ and a dip angle of 15° , develop the fractional flow curve.
- Determine from both curves:
 - f_w at the front
 - S_w at the front, i.e., S_{wf}
 - Average water saturation behind the front

3. A linear reservoir system is characterized by the following data:

$$L = 500 \text{ ft} \quad A = 10,000 \text{ ft}^2 \quad S_{wi} = 24\% \quad B_w = 1.01 \text{ bbl/STB}$$

$$S_{or} = 20\% \quad i_w = 100 \text{ ft}^3/\text{hr} \quad B_o = 1.25 \text{ bbl/STB} \quad \phi = 15\%$$

| S_w | f_w |
|-------|--------|
| 0.30 | 0.0181 |
| 0.40 | 0.082 |
| 0.50 | 0.247 |
| 0.60 | 0.612 |
| 0.70 | 0.885 |
| 0.75 | 0.952 |
| 0.80 | 1.000 |

Determine:

- a. Water saturation profile after 10, 100, and 300 hr
 - b. Oil recovery at breakthrough
 - c. Time to breakthrough
 - d. Cumulative water injected at breakthrough
4. The following relative permeability data² are available on a rock sample taken from the R-Field:

| S_w | k_{rw} | k_{ro} |
|-------|----------|----------|
| 0.25 | 0.00 | 0.495 |
| 0.35 | 0.015 | 0.327 |
| 0.40 | 0.030 | 0.260 |
| 0.45 | 0.068 | 0.200 |
| 0.50 | 0.110 | 0.148 |
| 0.55 | 0.149 | 0.102 |
| 0.60 | 0.213 | 0.064 |
| 0.65 | 0.277 | 0.032 |
| 0.70 | 0.350 | 0.000 |

Additional data:

| | | |
|-----------------------------|-----------------------------|-----------------------------|
| $S_{wi} = 25\%$ | $S_{oi} = 75\%$ | $S_{gi} = 0\%$ |
| $B_o = 1.2 \text{ bbl/STB}$ | $B_w = 1.0 \text{ bbl/STB}$ | $\mu_w = 0.90 \text{ cp}$ |
| $\mu_o = 10.0 \text{ cp}$ | $A = 28,934 \text{ ft}^2$ | $i_w = 100 \text{ bbl/day}$ |
| $E_A = 100\%$ | $E_V = 100\%$ | Area = 10 acres |
| $h = 31 \text{ ft}$ | $k = 50 \text{ md}$ | |

Distance between injector and producer = 467 ft.

- a. Calculate the water saturation profile after 100, 200, 500, 1,000, 2,000, and 5,000 days. Plot your results.
- b. Calculate the mobility ratio.
- c. Calculate the time to breakthrough
- d. Calculate and plot N_p , Q_o , Q_w , and W_{inj} as a function of time.

²Data from *Reservoir Engineering Manual*, Cole, Houston, TX: Gulf Publishing Company, 1969.

5. An oil reservoir is under consideration for waterflooding. The relative permeability data are given by the following expression:

$$k_{rw} = 0.4(1 - S_{wD})^2$$

$$k_{ro} = 0.3(S_{wD})^{2.5}$$

where

$$S_{wD} = \frac{S_w - S_{wi}}{1 - S_{or} - S_{wi}}$$

Other reservoir data are given below:

| | |
|-----------------|----------------|
| Flood pattern | = Five-spot |
| Flood area | = 40 acres |
| Oil viscosity | = 2 cp |
| Water viscosity | = 0.5 cp |
| B_o | = 1.3 bbl/STB |
| B_w | = 1.05 bbl/STB |
| S_{oi} | = 0.75 |
| S_{wi} | = 0.25 |
| S_{or} | = 0.35 |
| S_{wi} | = 0.25 |
| ϕ | = 15% |
| k | = 50 md |
| r_w | = 0.3 ft |
| h | = 20 ft |
| P_i | = 1000 psi |
| E_V | = 100% |

Assuming a constant water-injection rate of 800 bbl/day, predict the recovery performance and express results in a graphical form.

6. An oil reservoir is under consideration for further development by water-injection. The relative permeability data are given below:

| | | | | | | |
|----------|------|------|------|------|------|------|
| S_w | 0.10 | 0.20 | 0.30 | 0.40 | 0.70 | 0.85 |
| k_{rw} | 0.00 | 0.00 | 0.02 | 0.05 | 0.35 | 0.60 |
| k_{ro} | 1.00 | 0.93 | 0.60 | 0.35 | 0.05 | 0.00 |

Additional data are given below:

| | |
|---------------------------------|-----------------------|
| Flood pattern | = Five-spot |
| Absolute permeability | = 70 md |
| Thickness | = 20 ft |
| Porosity | = 15% |
| S_{gi} | = 15% |
| S_{wi} | = 20% |
| μ_o | = 3.1 cp |
| μ_w | = 1.0 cp |
| B_o | = 1.25 bbl/STB |
| B_w | = 1.01 bbl/STB |
| Pattern area | = 40 acres |
| r_w | = 1.0 ft |
| $\Delta p = (P_{inj} - P_{wf})$ | = 1000 psi (constant) |

- Calculate and plot the reservoir performance during the following stages:
 - Start—interference
 - Interference—fill-up
 - Fill-up—breakthrough
 - After breakthrough
- Show on your graph time to: interference, fill-up, and breakthrough.
- Plot water injectivity and areal sweep efficiency as a function of time.

7. The following core analysis is available on a reservoir that is being considered for a waterflooding project:

| Sample | h, ft | k, md |
|--------|-------|-------|
| 1 | 2 | 14 |
| 2 | 2 | 39 |
| 3 | 1 | 108 |
| 4 | 2 | 77 |
| 5 | 2 | 28 |
| 6 | 1 | 212 |
| 7 | 1 | 151 |
| 8 | 3 | 10 |
| 9 | 2 | 20 |
| 10 | 3 | 55 |

Other data:

$$i_w = 1000 \text{ bbl/day}$$

$$\mu_o = 9.0 \text{ cp}$$

$$\mu_w = 0.95 \text{ cp}$$

$$M = 4.73$$

$$N_s = 6 \text{ MMSTB}$$

$$B_o = 1.02 \text{ bbl/STB}$$

$$B_w = 1.00 \text{ bbl/STB}$$

$$S_{wi} = 0.2$$

$$S_{oi} = 0.8$$

Using the simplified Dykstra-Parsons method, determine the following recovery parameters as a function of time:

- Q_o
- Q_w
- WOR
- N_p
- W_p

Show your results graphically.

8. The following core and relative permeability data are given:

| Depth, ft | k, md |
|-----------|-------|
| 4100–4101 | 295 |
| 2 | 762 |
| 3 | 88 |
| 4 | 87 |
| 5 | 148 |
| 6 | 71 |
| 7 | 62 |
| 8 | 187 |
| 9 | 349 |
| 10 | 77 |
| 11 | 127 |
| 12 | 161 |
| 13 | 50 |
| 14 | 58 |
| 15 | 109 |
| 16 | 228 |
| Depth, ft | k, md |
| 17 | 282 |
| 18 | 776 |
| 19 | 87 |
| 20 | 47 |
| 21 | 16 |
| 22 | 35 |
| 23 | 47 |
| 24 | 54 |
| 25 | 273 |
| 26 | 454 |
| 27 | 308 |
| 28 | 159 |
| 29 | 178 |

| S_w | k_{rw} | k_{ro} |
|-------|----------|----------|
| 0.10 | 0.00 | 0.96 |
| 0.20 | 0.00 | 0.89 |
| 0.24 | 0.00 | 0.80 |
| 0.30 | 0.01 | 0.60 |
| 0.40 | 0.03 | 0.30 |
| 0.50 | 0.06 | 0.12 |
| 0.60 | 0.12 | 0.06 |
| 0.70 | 0.19 | 0.015 |
| 0.76 | 0.25 | 0.00 |
| 0.80 | 0.32 | 0.00 |
| 0.90 | 0.65 | 0.00 |

$$\begin{aligned}
 S_{oi} &= 0.59 & \mu_o &= 40.34 \text{ cp} \\
 S_{wi} &= 0.24 & \mu_w &= 0.82 \text{ cp} \\
 S_{gi} &= 0.17 & B_o &= 1.073 \text{ bbl/STB} \\
 h &= 29 \text{ ft} & B_w &= 1.00 \text{ bbl/STB} \\
 A &= 40 \text{ acres} & \phi &= 19\%
 \end{aligned}$$

Using the modified Dykstra-Parsons method, generate the performance curves for this reservoir under a constant water-injection rate of 700 bbl/day.

9. Using Stiles' and the Dykstra-Parsons methods, calculate the vertical sweep efficiency as a function of producing water-oil ratio, given:

| Layer | h, ft | k, md |
|-------|-------|-------|
| 1 | 2 | 5.0 |
| 2 | 2 | 7.0 |
| 3 | 2 | 11.0 |
| 4 | 2 | 4.0 |
| 5 | 2 | 14.0 |
| 6 | 2 | 21.0 |
| 7 | 2 | 68.0 |
| 8 | 2 | 13.0 |

$$\begin{aligned}
 \mu_o &= 8.0 \text{ cp} \\
 \mu_w &= 0.9 \text{ cp} \\
 M &= 1.58 \\
 k_{ro} &= 0.45
 \end{aligned}$$

$$k_{rw} = 0.08$$

$$\phi = 15\%$$

$$B_o = 1.2 \text{ bbl/STB}$$

$$B_w = \text{bbl/STB}$$

Show your results graphically.

10. An oil reservoir is characterized by the following six-layer system:

| Layer | h, ft | k, md | ϕ |
|-------|-------|-------|--------|
| 1 | 10 | 50 | 0.20 |
| 2 | 10 | 40 | 0.16 |
| 3 | 5 | 35 | 0.12 |
| 4 | 5 | 30 | 0.12 |
| 5 | 5 | 25 | 0.10 |
| 6 | 5 | 20 | 0.10 |

The first layer is identified as the *base layer* with the following relative permeability data:

| | | | | | | | | | | | | |
|----------|------|------|------|------|------|------|------|------|-------|------|------|------|
| S_w | 0.0 | 0.1 | 0.2 | 0.3 | 0.4 | 0.5 | 0.6 | 0.7 | 0.75 | 0.8 | 0.9 | 1.00 |
| k_{rw} | 0 | 0 | 0 | 0 | 0.04 | 0.11 | 0.20 | 0.30 | 0.36 | 0.44 | 0.68 | 1.00 |
| k_{ro} | 1.00 | 1.00 | 1.00 | 1.00 | 0.94 | 0.80 | 0.44 | 0.16 | 0.045 | 0 | 0 | 0 |

The other rock and fluid properties are given below:

$$S_{oi} = 0.65$$

$$S_{wi} = 0.30$$

$$S_{gi} = 0.05$$

$$\mu_o = 1.5 \text{ cp}$$

$$\mu_w = 0.8 \text{ cp}$$

$$B_o = 1.2 \text{ bbl/STB}$$

$$B_w = 1.01 \text{ bbl/STB}$$

$$N_S = 12 \text{ MMSTB}$$

$$\text{Constant } (P_{inj} - P_{wf}) = 950 \text{ psi}$$

$$\text{Wellbore radius} = 0.3 \text{ ft}$$

- Generate the performance curves for the base layer.
- Generate the composite (overall) performance curves for the reservoir.

REFERENCES

1. Buckley, S., and Leverett, M., "Mechanism of Fluid Displacement in Sands," *Trans. AIME*, 1962, Vol. 146, p. 107.
2. Caudle, B., and Witte, M., "Production Potential Changes During Sweep-out in a Five-Spot System," *Trans. AIME*, 1959, Vol. 216, pp. 446–448.
3. Cole, F., *Reservoir Engineering Manual*. Houston, TX: Gulf Publishing Company, 1969.
4. Craft, B., and Hawkins, M., *Applied Petroleum Reservoir Engineering*. Englewood Cliffs, NJ: Prentice Hall, 1959.
5. Craig, Jr., F. F., *The Reservoir Engineering Aspects of Waterflooding*. Dallas: Society of Petroleum Engineers of AIME, 1971.
6. Craig, F., Geffen, T., and Morse, R., "Oil Recovery Performance of Pattern Gas or Water-Injection Operations from Model Tests," *JPT*, Jan. 1955, pp. 7–15, *Trans. AIME*, p. 204.
7. Dake, L., *Fundamentals of Reservoir Engineering*. Amsterdam: Elsevier Scientific Publishing Company, 1978.
8. Deppe, J., "Injection Rates—The Effect of Mobility Ratio, Areal Sweep, and Pattern," *SPEJ*, June 1961, pp. 81–91.
9. de Souza, A., and Brigham, W., "A Study on Dykstra–Parsons Curves," TR29. Palo Alto, CA: Stanford University Petroleum Research Institute, 1981.
10. Dyes, A., Caudle, B., and Erickson, R., "Oil Production After Breakthrough as Influenced by Mobility Ratio," *JPT*, April 1954, pp. 27–32; *Trans. AIME*, p. 201.
11. Dykstra, H., and Parsons, R., "The Prediction of Oil Recovery by Water Flood," in *Secondary Recovery of Oil in the United States*, 2nd ed. Washington, DC: American Petroleum Institute, 1950, pp. 160–174.
12. Fassihi, M., "New Correlations for Calculation of Vertical Coverage and Areal Sweep Efficiency," *SPERE*, Nov. 1986, pp. 604–606.
13. Felsenthal, M., Cobb, T., and Heur, G., "A Comparison of Waterflooding Evaluation Methods," SPE Paper 332 presented at the SPE 5th Biennial Secondary Recovery Symposium, Wichita Falls, TX, May 7, 1962.
14. Johnson, C., "Prediction of Oil Recovery by Waterflood—A Simplified Graphical Treatment of the Dykstra-Parsons Method," *Trans. AIME*, 1956, Vol. 207, pp. 345–346.
15. Khelil, C., "A Correlation of Optimum Free Gas Saturation," SPE Paper 01983, 1983.

16. Landrum, B., and Crawford, P., "Effect of Directional Permeability on Sweep Efficiency and Production Capacity," *JPT*, Nov. 1960, pp. 67–71.
17. Miller, M., and Lents, M., "Performance of Bodcaw Reservoir, Cotton Valley Field Cycling Project, New Methods of Predicting Gas-Condensate Reservoirs," *SPEJ*, Sep. 1966, p. 239.
18. Muskat, M., *Flow of Homogeneous Fluids Through Porous Systems*. Ann Arbor, MI: J. W. Edwards, 1946.
19. Muskat, M., "The Theory of Nine-Spot Flooding Networks," *Prod. Monthly*, March 1948, Vol. 13, No. 3, p. 14.
20. Stiles, W., "Use of Permeability Distribution in Waterflood Calculations," *Trans. AIME*, 1949, Vol. 186, p. 9.
21. Terwilliger, P., Wilsey, L., Hall, H., Bridges, P., and Morse, R., "An Experimental and Theoretical Investigation of Gravity Drainage Performance," *Trans. AIME*, 1951, Vol. 192, pp. 285–296.
22. Thomas, C. E., Mahoney, C. F., and Winter, G. W., *Petroleum Engineering Handbook*. Dallas: Society of Petroleum Engineers, 1989.
23. Welge, H., "A Simplified Method for Computing Oil Recovery By Gas or Water Drive," *Trans. AIME*, 1952, pp. 91–98.
24. Willhite, G. P., *Waterflooding*. Dallas: Society of Petroleum Engineers, 1986.

C H A P T E R 1 5

VAPOR-LIQUID PHASE EQUILIBRIA

A phase is defined as that part of a system that is uniform in physical and chemical properties, homogeneous in composition, and separated from other coexisting phases by definite boundary surfaces. The most important phases occurring in petroleum production are the hydrocarbon liquid phase and the gas phase. Water is also commonly present as an additional liquid phase. These can coexist in equilibrium when the variables describing change in the entire system remain constant with time and position. The chief variables that determine the state of equilibrium are system temperature, system pressure, and composition.

The conditions under which these different phases can exist are a matter of considerable practical importance in designing surface separation facilities and developing compositional models. These types of calculations are based on the concept of equilibrium ratios.

VAPOR PRESSURE

A system that contains only one component is considered the simplest type of hydrocarbon system. The word *component* refers to the number of molecular or atomic species present in the substance. A single-component system is composed entirely of one kind of atom or molecule. We often use the word *pure* to describe a single-component system. The qualitative understanding of the relationship that exists

between temperature T , pressure p , and volume V of pure components can provide an excellent basis for understanding the phase behavior of complex hydrocarbon mixtures.

Consider a closed evacuated container that has been partially filled with a pure component in the liquid state. The molecules of the liquid are in constant motion with different velocities. When one of these molecules reaches the liquid surface, it may possess sufficient kinetic energy to overcome the attractive forces in the liquid and pass into the vapor spaces above. As the number of molecules in the vapor phase increases, the rate of return to the liquid phase also increases. A state of equilibrium is eventually reached when the number of molecules leaving and returning is equal. The molecules in the vapor phase obviously exert a pressure on the wall of the container and this pressure is defined as the vapor pressure, p_v . As the temperature of the liquid increases, the average molecular velocity increases with a larger number of molecules possessing sufficient energy to enter the vapor phase. As a result, the vapor pressure of a pure component in the liquid state increases with increasing temperature.

A method that is particularly convenient for expressing the vapor pressure of pure substances as a function of temperature is shown in Figure 15-1. The chart, known as the *Cox chart*, uses a logarithmic scale for the vapor pressure and an entirely arbitrary scale for the temperature in $^{\circ}\text{F}$. The vapor pressure curve for any particular component, as shown in Figure 15-1, can be defined as the dividing line between the area where vapor and liquid exists. If the system pressure exists at its vapor pressure, two phases can coexist in equilibrium. Systems represented by points located below that vapor pressure curve are composed only of the vapor phase. Similarly, points above the curve represent systems that exist in the liquid phase. These statements can be conveniently summarized by the following expressions:

- $p < p_v \rightarrow$ system is entirely in the vapor phase
- $p > p_v \rightarrow$ system is entirely in the liquid phase
- $p = p_v \rightarrow$ vapor and liquid coexist in equilibrium

where p is the pressure exerted on the pure component. Note that the above expressions are valid only if the system temperature T is below the critical temperature T_c of the substance.

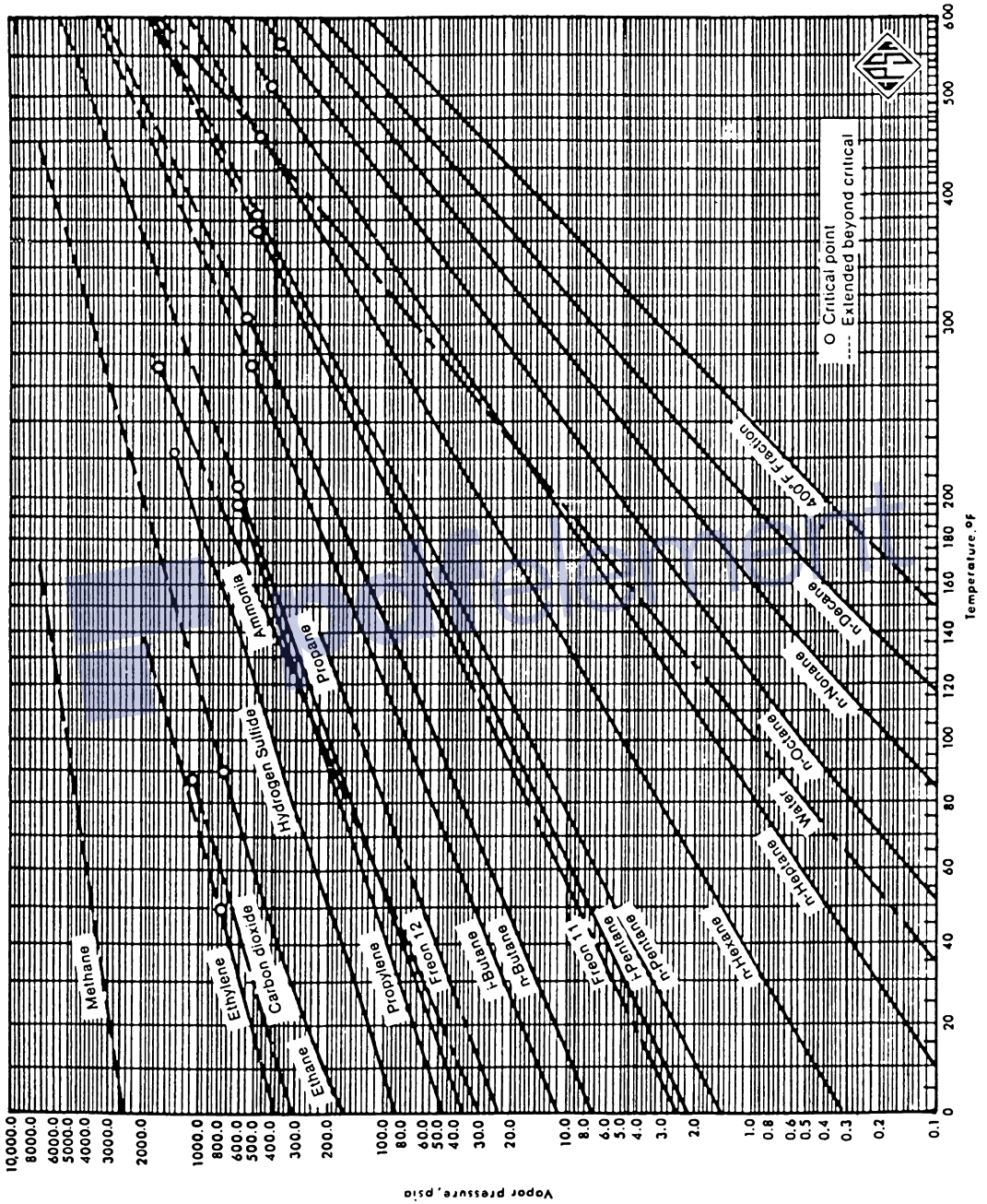


Figure 15-1. Vapor pressures for hydrocarbon components. (Courtesy of the Gas Processors Suppliers Association, Engineering Book, 10th Ed., 1987.)

The vapor pressure chart allows a quick determination of p_v of a pure component at a specific temperature. For computer and spreadsheet applications, however, an equation is more convenient. Lee and Kesler (1975) proposed the following generalized vapor pressure equation:

$$p_v = p_c \exp(A + \omega B)$$

with

$$A = 5.92714 - \frac{6.09648}{T_r} - 1.2886 \ln(T_r) + 0.16934(T_r)^6$$

$$B = 15.2518 - \frac{15.6875}{T_r} - 13.4721 \ln(T_r) + 0.4357(T_r)^6$$

where p_v = vapor pressure, psi

p_c = critical pressure, psi

T_r = reduced temperature (T / T_c)

T = system temperature, °R

T_c = critical temperature, °R

ω = acentric factor

EQUILIBRIUM RATIOS

In a multicomponent system, the equilibrium ratio K_i of a given component is defined as the ratio of the mole fraction of the component in the gas phase y_i to the mole fraction of the component in the liquid phase x_i . Mathematically, the relationship is expressed as:

$$K_i = \frac{y_i}{x_i} \quad (15-1)$$

where K_i = equilibrium ratio of component i

y_i = mole fraction of component i in the gas phase

x_i = mole fraction of component i in the liquid phase

At pressures below 100 psia, Raoult's and Dalton's laws for ideal solutions provide a simplified means of predicting equilibrium ratios. Raoult's law states that the partial pressure p_i of a component in a multicomponent

system is the product of its mole fraction in the liquid phase x_i and the vapor pressure of the component p_{vi} , or:

$$p_i = x_i p_{vi} \quad (15-2)$$

where p_i = partial pressure of a component i , psia
 p_{vi} = vapor pressure of component i , psia
 x_i = mole fraction of component i in the liquid phase

Dalton's law states that the partial pressure of a component is the product of its mole fraction in the gas phase y_i and the total pressure of the system p , or:

$$p_i = y_i p \quad (15-3)$$

where p = total system pressure, psia.

At equilibrium and in accordance with the above stated laws, the partial pressure exerted by a component in the gas phase must be equal to the partial pressure exerted by the same component in the liquid phase. Therefore, equating the equations describing the two laws yields:

$$x_i p_{vi} = y_i p$$

Rearranging the above relationship and introducing the concept of the equilibrium ratio gives:

$$\frac{y_i}{x_i} = \frac{p_{vi}}{p} = K_i \quad (15-4)$$

Equation 15-4 shows that for ideal solutions and regardless of the overall composition of the hydrocarbon mixture, the equilibrium ratio is only a function of the system pressure p and the temperature T since the vapor pressure of a component is only a function of temperature (see Figure 15-1).

It is appropriate at this stage to introduce and define the following nomenclatures:

- z_i = mole fraction of component in the entire hydrocarbon mixture
- n = total number of moles of the hydrocarbon mixture, lb-mol
- n_L = total number of moles in the liquid phase
- n_v = total number of moles in the vapor (gas) phase

By definition:

$$n = n_L + n_v \quad (15-5)$$

Equation 15-5 indicates that the total number of moles in the system is equal to the total number of moles in the liquid phase plus the total number of moles in the vapor phase. A material balance on the i 'th component results in:

$$z_i n = x_i n_L + y_i n_v \quad (15-6)$$

where $z_i n$ = total number of moles of component i in the system
 $x_i n_L$ = total number of moles of component i in the liquid phase
 $y_i n_v$ = total number of moles of component i in the vapor phase

Also by the definition of mole fraction, we may write:

$$\sum_i z_i = 1 \quad (15-7)$$

$$\sum_i x_i = 1 \quad (15-8)$$

$$\sum_i y_i = 1 \quad (15-9)$$

It is convenient to perform all phase-equilibria calculations on the basis of 1 mol of the hydrocarbon mixture, i.e., $n = 1$. That assumption reduces Equations 15-5 and 15-6 to:

$$n_L + n_v = 1 \quad (15-10)$$

$$x_i n_L + y_i n_v = z_i \quad (15-11)$$

Combining Equations 15-4 and 15-11 to eliminate y_i from Equation 15-11 gives:

$$x_i n_L + (x_i K_i) n_v = z_i$$

Solving for x_i yields:

$$x_i = \frac{z_i}{n_L + n_v K_i} \quad (15-12)$$

Equation 15-11 can also be solved for y_i by combining it with Equation 15-4 to eliminate x_i :

$$y_i = \frac{z_i K_i}{n_L + n_v K_i} = x_i K_i \quad (15-13)$$

Combining Equation 15-12 with 15-8 and Equation 15-13 with 15-19 results in:

$$\sum_i x_i = \sum_i \frac{z_i}{n_L + n_v K_i} = 1 \quad (15-14)$$

$$\sum_i y_i = \sum_i \frac{z_i K_i}{n_L + n_v K_i} = 1 \quad (15-15)$$

since

$$\sum_i y_i - \sum_i x_i = 0$$

Therefore,

$$\sum_i \frac{z_i K_i}{n_L + n_v K_i} - \sum_i \frac{z_i}{n_L + n_v K_i} = 0$$

or

$$\sum_i \frac{z_i (K_i - 1)}{n_L + n_v K_i} = 0$$

Replacing n_L with $(1 - n_v)$ yields:

$$f(n_v) = \sum_i \frac{z_i (K_i - 1)}{n_v (K_i - 1) + 1} = 0 \quad (15-16)$$

The above set of equations provides the necessary phase relationships to perform volumetric and compositional calculations on a hydrocarbon system. These calculations are referred to as *flash calculations* and are discussed next.

FLASH CALCULATIONS

Flash calculations are an integral part of all reservoir and process engineering calculations. They are required whenever it is desirable to know the amounts (in moles) of hydrocarbon liquid and gas coexisting in a reservoir or a vessel at a given pressure and temperature. These calculations are also performed to determine the composition of the existing hydrocarbon phases.

Given the overall composition of a hydrocarbon system at a specified pressure and temperature, flash calculations are performed to determine:

- Moles of the gas phase n_v
- Moles of the liquid phase n_L
- Composition of the liquid phase x_i
- Composition of the gas phase y_i

The computational steps for determining n_L , n_v , y_i , and x_i of a hydrocarbon mixture with a known overall composition of z_i and characterized by a set of equilibrium ratios K_i are summarized in the following steps:

Step 1. Calculation of n_v : Equation 15-16 can be solved for n_v by using the Newton-Raphson iteration techniques. In applying this iterative technique:

- Assume any arbitrary value of n_v between 0 and 1, e.g., $n_v = 0.5$. A good assumed value may be calculated from the following relationship, providing that the values of the equilibrium ratios are accurate:

$$n_v = A/(A - B)$$

$$\text{where } A = \sum_i [z_i(K_i - 1)]$$

$$B = \sum_i [z_i(K_i - 1)/K_i]$$

- Evaluate the function $f(n_v)$ as given by Equation 15-16 using the assumed value of n_v .

- If the absolute value of the function $f(n_v)$ is smaller than a pre-set tolerance, e.g., 10^{-15} , then the assumed value of n_v is the desired solution.
- If the absolute value of $f(n_v)$ is greater than the preset tolerance, then a new value of n_v is calculated from the following expression:

$$(n_v)_n = n_v - f(n_v)/f'(n_v)$$

with

$$f' = -\sum_i \left[\frac{z_i(K_i - 1)^2}{[n_v(K_i - 1) + 1]^2} \right]$$

where $(n_v)_n$ is the new value of n_v to be used for the next iteration.

- The above procedure is repeated with the new values of n_v until convergence is achieved.

Step 2. Calculation of n_L : Calculate the number of moles of the liquid phase from Equation 15-10, to give:

$$n_L = 1 - n_v$$

Step 3. Calculation of x_i : Calculate the composition of the liquid phase by applying Equation 15-12:

$$x_i = \frac{z_i}{n_L + n_v K_i}$$

Step 4. Calculation of y_i : Determine the composition of the gas phase from Equation 15-13:

$$y_i = \frac{z_i K_i}{n_L + n_v K_i} = x_i K_i$$

Example 15-1

A hydrocarbon mixture with the following overall composition is flashed in a separator at 50 psia and 100°F.

| Component | z_i |
|--------------------|-------|
| C ₃ | 0.20 |
| i - C ₄ | 0.10 |
| n - C ₄ | 0.10 |
| i - C ₅ | 0.20 |
| n - C ₅ | 0.20 |
| C ₆ | 0.20 |

Assuming an ideal solution behavior, perform flash calculations.

Solution

Step 1. Determine the vapor pressure for the Cox chart (Figure 15-1) and calculate the equilibrium ratios from Equation 15-4.

| Component | z_i | p_{vi} at 100°F | $K_i = p_{vi}/50$ |
|--------------------|-------|-------------------|-------------------|
| C ₃ | 0.20 | 190 | 3.80 |
| i - C ₄ | 0.10 | 72.2 | 1.444 |
| n - C ₄ | 0.10 | 51.6 | 1.032 |
| i - C ₅ | 0.20 | 20.44 | 0.4088 |
| n - C ₅ | 0.20 | 15.57 | 0.3114 |
| C ₆ | 0.20 | 4.956 | 0.09912 |

Step 2. Solve Equation 15-16 for n_v by using the Newton-Raphson method, to give:

| Iteration | n_v | $f(n_v)$ |
|-----------|------------|------------|
| 0 | 0.08196579 | 3.073 E-02 |
| 1 | 0.1079687 | 8.894 E-04 |
| 2 | 0.1086363 | 7.60 E-07 |
| 3 | 0.1086368 | 1.49 E-08 |
| 4 | 0.1086368 | 0.0 |

Step 3. Solve for n_L :

$$n_L = 1 - n_v$$

$$n_L = 1 - 0.1086368 = 0.8913631$$

Step 4. Solve for x_i and y_i to yield:

| Component | z_i | K_i | $x_i = z_i / (0.8914 + 0.1086K_i)$ | $y_i = x_i K_i$ |
|-----------|-------|---------|------------------------------------|-----------------|
| C_3 | 0.20 | 3.80 | 0.1534 | 0.5829 |
| i - C_4 | 0.10 | 1.444 | 0.0954 | 0.1378 |
| n - C_4 | 0.10 | 1.032 | 0.0997 | 0.1029 |
| i - C_5 | 0.20 | 0.4088 | 0.2137 | 0.0874 |
| n - C_5 | 0.20 | 0.3114 | 0.2162 | 0.0673 |
| C_6 | 0.20 | 0.09912 | 0.2216 | 0.0220 |

Notice that for a binary system, i.e., two-component system, flash calculations can be performed without restoring to the above iterative technique by applying the following steps:

Step 1. **Solve for the composition of the liquid phase x_i .** From equations 15-8 and 15-9:

$$\sum_i x_i = x_1 + x_2 = 1$$

$$\sum_i y_i = y_1 + y_2 = K_1 x_1 + K_2 x_2 = 1$$

Solving the above two expressions for the liquid compositions x_1 and x_2 gives:

$$x_1 = \frac{1 - K_2}{K_1 - K_2}$$

and

$$x_2 = 1 - x_1$$

where x_1 = mole fraction of the first component in the liquid phase

x_2 = mole fraction of the second component in the liquid phase

K_1 = equilibrium ratio of the first component

K_2 = equilibrium ratio of the second component

Step 2. Solve for the composition of the gas phase y_i . From the definition of the equilibrium ratio, calculate the composition of the gas as follows:

$$y_1 = x_1 K_1$$

$$y_2 = x_2 K_2 = 1 - y_1$$

Step 3. Solve for the number of moles of the vapor phase n_v . Arrange Equation 15-12 to solve for n_v , to give:

$$n_v = \frac{z_1 - x_1}{x_1(K_1 - 1)}$$

and

$$n_l = 1 - n_v$$

where z_1 = mole fraction of the first component in the entire system

x_1 = mole fraction of the first component in the liquid phase

K_1 = equilibrium ratio of the first component

K_2 = equilibrium ratio of the second component

EQUILIBRIUM RATIOS FOR REAL SOLUTIONS

The equilibrium ratios, which indicate the partitioning of each component between the liquid phase and gas phase, as calculated by Equation 15-4 in terms of vapor pressure and system pressure, proved to be inadequate. The basic assumptions behind Equation 15-4 are that:

- The vapor phase is an ideal gas as described by Dalton's law.
- The liquid phase is an ideal solution as described by Raoult's law.

The above combination of assumptions is unrealistic and results in inaccurate predictions of equilibrium ratios at high pressures.

For a real solution, the equilibrium ratios are no longer a function of the pressure and temperature alone, but also a function of the composition of the hydrocarbon mixture. This observation can be stated mathematically as:

$$K_i = K(p, T, z_i)$$

Numerous methods have been proposed for predicting the equilibrium ratios of hydrocarbon mixtures. These correlations range from a simple mathematical expression to a complicated expression containing several composition-dependent variables. The following methods are presented:

- Wilson's correlation
- Standing's correlation
- Convergence pressure method
- Whitson and Torp correlation

Wilson's Correlation

Wilson (1968) proposed a simplified thermodynamic expression for estimating K values. The proposed expression has the following form:

$$K_i = \frac{p_{ci}}{p} \exp \left[5.37(1 + \omega_i) \left(1 - \frac{T_{ci}}{T} \right) \right] \quad (15-17)$$

where p_{ci} = critical pressure of component i, psia

p = system pressure, psia

T_{ci} = critical temperature of component i, °R

T = system temperature, °R

ω_i = acentric factor of component i

The above relationship generates reasonable values for the equilibrium ratio when applied at low pressures.

Standing's Correlation

Hoffmann et al. (1953), Brinkman and Sicking (1960), Kehn (1964), and Dykstra and Mueller (1965) suggested that any pure hydrocarbon or

nonhydrocarbon component could be uniquely characterized by combining its boiling-point temperature, critical temperature, and critical pressure into a characterization parameter that is defined by the following expression:

$$F_i = b_i [1/T_{bi} - 1/T] \quad (15-18)$$

with

$$b_i = \frac{\log(p_{ci}/14.7)}{[1/T_{bi} - 1/T_{ci}]} \quad (15-19)$$

where F_i = component characterization factor
 T_{bi} = normal boiling point of component i , °R

Standing (1979) derived a set of equations that fit the equilibrium ratio data of Katz and Hachmuth (1937) at pressures of less than 1,000 psia and temperatures below 200°F. The proposed form of the correlation is based on an observation that plots of $\log(K_i p)$ vs. F_i at a given pressure often form straight lines. The basic equation of the straight-line relationship is given by:

$$\log(K_i p) = a + cF_i$$

Solving for the equilibrium ratio K_i gives:

$$K_i = \frac{1}{p} 10^{(a+cF_i)} \quad (15-20)$$

where the coefficients a and c are the intercept and the slope of the line, respectively.

From a total of six isobar plots of $\log(K_i p)$ vs. F_i for 18 sets of equilibrium ratio values, Standing correlated the coefficients a and c with the pressure, to give:

$$a = 1.2 + 0.00045p + 15(10^{-8})p^2 \quad (15-21)$$

$$c = 0.89 - 0.00017p - 3.5(10^{-8})p^2 \quad (15-22)$$

Standing pointed out that the predicted values of the equilibrium ratios of N_2 , CO_2 , H_2S , and C_1 through C_6 can be improved considerably by

changing the correlating parameter b_i and the boiling point of these components. The author proposed the following modified values:

| Component | b_i | T_{bi} °R |
|---------------------|-------|-------------|
| N ₂ | 470 | 109 |
| CO ₂ | 652 | 194 |
| H ₂ S | 1136 | 331 |
| C ₁ | 300 | 94 |
| C ₂ | 1145 | 303 |
| C ₃ | 1799 | 416 |
| i - C ₄ | 2037 | 471 |
| n - C ₄ | 2153 | 491 |
| i - C ₅ | 2368 | 542 |
| n - C ₅ | 2480 | 557 |
| C ₆ * | 2738 | 610 |
| n - C ₆ | 2780 | 616 |
| n - C ₇ | 3068 | 669 |
| n - C ₈ | 3335 | 718 |
| n - C ₉ | 3590 | 763 |
| n - C ₁₀ | 3828 | 805 |

*Lumped Hexanes-fraction.

When making flash calculations, the question of the equilibrium ratio to use for the lumped heptanes-plus fraction always arises. One rule of thumb proposed by Katz and Hachmuth (1937) is that the K value for C₇₊ can be taken as 15% of the K of C₇, or:

$$K_{C_{7+}} = 0.15K_{C_7}$$

Standing (1979) offered an alternative approach for determining the K value of the heptanes and heavier fractions. By imposing experimental equilibrium ratio values for C₇₊ on Equation 15-20, Standing calculated the corresponding characterization factors F_i for the plus fraction. The calculated F_i values were used to specify the pure normal paraffin hydrocarbon having the K value of the C₇₊ fraction.

Standing suggested the following computational steps for determining the parameters b and T_b of the heptanes-plus fraction.

Step 1. Determine, from the following relationship, the number of carbon atoms n of the normal paraffin hydrocarbon having the K value of the C₇₊ fraction,

$$n = 7.30 + 0.0075(T - 460) + 0.0016p \quad (15-23)$$

Step 2. Calculate the correlating parameter b and the boiling point T_b from the following expression:

$$b = 1013 + 324n - 4.256n^2 \quad (15-24)$$

$$T_b = 301 + 59.85n - 0.971n^2 \quad (15-25)$$

The above calculated values can then be used in Equation 15-18 to evaluate F_i for the heptanes-plus fraction, i.e., $F_{C_{7+}}$. It is also interesting to note that experimental phase equilibria data suggest that the equilibrium ratio for carbon dioxide can be closely approximated by the following relationship:

$$K_{CO_2} = \sqrt{K_{C_1} K_{C_2}}$$

where K_{CO_2} = equilibrium ratio of CO_2

K_{C_1} = equilibrium ratio of methane

K_{C_2} = equilibrium ratio of ethane

Example 15-2

A hydrocarbon mixture with the following composition is flashed at 1,000 psia and 150°F.

| Component | z_i |
|-----------|-------|
| CO_2 | 0.009 |
| N_2 | 0.003 |
| C_1 | 0.535 |
| C_2 | 0.115 |
| C_3 | 0.088 |
| $i - C_4$ | 0.023 |
| $n - C_4$ | 0.023 |
| $i - C_5$ | 0.015 |
| $n - C_5$ | 0.015 |
| C_6 | 0.015 |
| C_{7+} | 0.159 |

If the molecular weight and specific gravity of C_{7+} are 150.0 and 0.78, respectively, calculate the equilibrium ratios by using:

- Wilson's correlation
- Standing's correlation

Solution

Step 1. Calculate the critical pressure, critical temperature, and acentric factor of C_{7+} by using the characterization method of Riazi and Daubert discussed in Chapter 1. Example 1-1, page 27, gives:

$$T_c = 1139.4^\circ\text{R}, \quad p_c = 320.3 \text{ psia}, \quad \omega = 0.5067$$

Step 2. Apply Equation 15-17 to give:

| Component | P_c , psia | T_c , °R | ω | $K_i = \frac{P_{ci}}{1000} \exp\left[5.37(1 + \omega_i)\left(1 - \frac{T_{ci}}{610}\right)\right]$ |
|------------------|--------------|------------|----------|--|
| CO ₂ | 1071 | 547.9 | 0.225 | 2.0923 |
| N ₂ | 493 | 227.6 | 0.040 | 16.343 |
| C ₁ | 667.8 | 343.37 | 0.0104 | 7.155 |
| C ₂ | 707.8 | 550.09 | 0.0986 | 1.236 |
| C ₃ | 616.3 | 666.01 | 0.1542 | 0.349 |
| i-C ₄ | 529.1 | 734.98 | 0.1848 | 0.144 |
| n-C ₄ | 550.7 | 765.65 | 0.2010 | 0.106 |
| i-C ₅ | 490.4 | 829.1 | 0.2223 | 0.046 |
| n-C ₅ | 488.6 | 845.7 | 0.2539 | 0.036 |
| C ₆ | 436.9 | 913.7 | 0.3007 | 0.013 |
| C ₇₊ | 320.3 | 1139.4 | 0.5069 | 0.00029 |

b.

Step 1. Calculate coefficients a and c from Equations 15-21 and 15-22 to give:

$$a = 1.2 + 0.00045(1000) + 15(10^{-8})(1000)^2 = 1.80$$

$$c = 0.89 - 0.00017(1000) - 3.5(10^{-8})(1000)^2 = 0.685$$

Step 2. Calculate the number of carbon atoms n from Equation 15-23 to give:

$$n = 7.3 + 0.0075(150) + 0.0016(1000) = 10.025$$

Step 3. Determine the parameter b and the boiling point T_b for the hydrocarbon component with n carbon atoms by using Equations 15-24 and 15-25 to yield:

$$b = 1013 + 324(10.025) - 4.256(10.025)^2 = 3833.369$$

$$T_b = 301 + 59.85(10.025) - 0.971(10.025)^2 = 803.41^\circ\text{R}$$

Step 4. Apply Equation 15-20, to give:

| Component | b_i | T_{bi} | F_i Eq. 15-18 | K_i Eq. 15-20 |
|--------------------|----------|----------|--------------------|--------------------|
| CO ₂ | 652 | 194 | 2.292 | 2.344 |
| N ₂ | 470 | 109 | 3.541 | 16.811 |
| C ₁ | 300 | 94 | 2.700 | 4.462 |
| C ₂ | 1145 | 303 | 1.902 | 1.267 |
| C ₃ | 1799 | 416 | 1.375 | 0.552 |
| i - C ₄ | 2037 | 471 | 0.985 | 0.298 |
| n - C ₄ | 2153 | 491 | 0.855 | 0.243 |
| i - C ₅ | 2368 | 542 | 0.487 | 0.136 |
| n - C ₅ | 2480 | 557 | 0.387 | 0.116 |
| C ₆ | 2738 | 610 | 0 | 0.063 |
| C ₇₊ | 3833.369 | 803.41 | - 1.513 | 0.0058 |

Convergence Pressure Method

Early high-pressure phase-equilibria studies have revealed that when a hydrocarbon mixture of a fixed overall composition is held at a constant temperature as the pressure increases, the equilibrium values of all components converge toward a common value of unity at certain pressure. This pressure is termed the convergence pressure P_k of the hydrocarbon mixture. The convergence pressure is essentially used to correlate the effect of the composition on equilibrium ratios.

The concept of the convergence pressure can be better appreciated by examining Figure 15-2. The figure shows a schematic diagram of a typical set of equilibrium ratios plotted versus pressure on log-log paper for a hydrocarbon mixture held at a constant temperature. The illustration shows a tendency of the equilibrium ratios to converge isothermally to a value of $K_i = 1$ for all components at a specific pressure, i.e., convergence pressure. A different hydrocarbon mixture may exhibit a different convergence pressure.

The Natural Gas Processors Suppliers Association (NGPSA) correlated a considerable quantity of K-factor data as a function of temperature, pressure, component identity, and convergence pressure. These correlation charts were made available through the NGPSA's *Engineering Data Book* and are considered to be the most extensive set of published equilibrium ratios for hydrocarbons. They include the K values for a number of convergence pressures, specifically 800, 1,000, 1,500, 2,000, 3,000, 5,000, and 10,000 psia. Equilibrium ratios for methane through decane and for a convergence pressure of 5,000 psia are given in Appendix A.

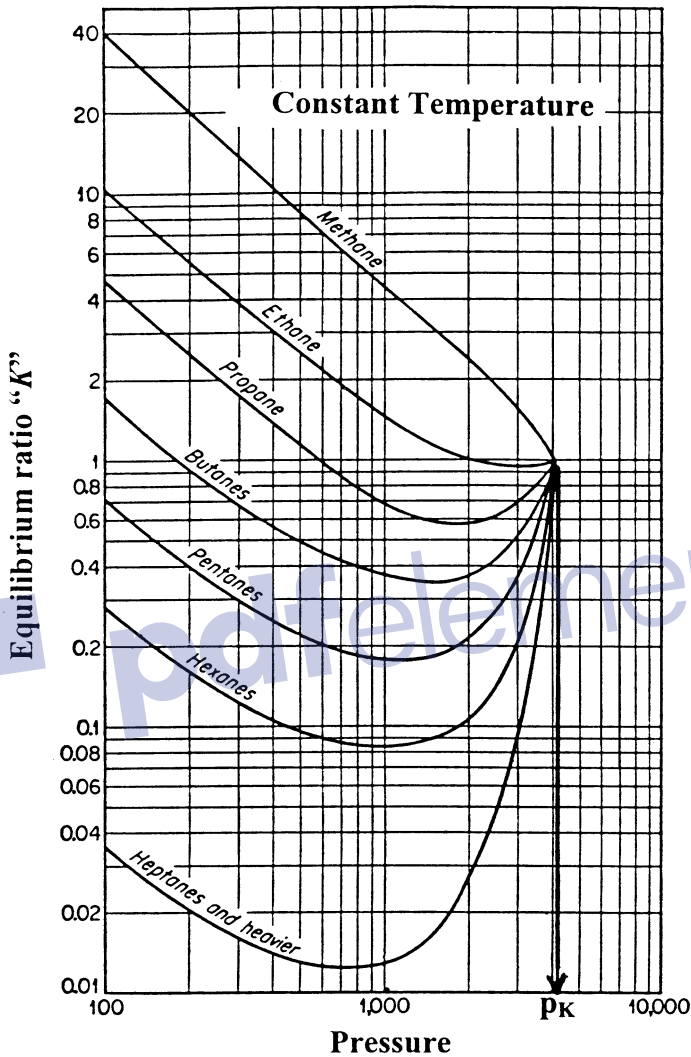


Figure 15-2. Equilibrium ratios for a hydrocarbon system.

Several investigators observed that for hydrocarbon mixtures with convergence pressures of 4,000 psia or greater, the values of the equilibrium ratio are essentially the same for hydrocarbon mixtures with system pressures of less than 1,000 psia. This observation led to the conclusion that the overall composition of the hydrocarbon mixture has little effect on equilibrium ratios when the system pressure is less than 1,000 psia.

The problem with using the NGPSA equilibrium ratio graphical correlations is that the convergence pressure must be known before selecting the appropriate charts. Three of the methods of determining the convergence pressure are discussed next.

Hadden's Method

Hadden (1953) developed an iterative procedure for calculating the convergence pressure of the hydrocarbon mixture. The procedure is based on forming a "binary system" that describes the entire hydrocarbon mixture. One of the components in the binary system is selected as the lightest fraction in the hydrocarbon system and the other is treated as a "pseudo-component" that lumps all the remaining fractions. The binary system concept uses the binary system convergence pressure chart, as shown in Figure 15-3, to determine the p_k of the mixture at the specified temperature.

The equivalent binary system concept employs the following steps for determining the convergence pressure:

- Step 1.* Estimate a value for the convergence pressure.
- Step 2.* From the appropriate equilibrium ratio charts, read the K values of each component present in the mixture by entering the charts with the system pressure and temperature.
- Step 3.* Perform flash calculations using the calculated K values and system composition.
- Step 4.* Identify the lightest hydrocarbon component that comprises at least 0.1 mol % in the liquid phase.
- Step 5.* Convert the liquid mole fraction to a weight fraction.
- Step 6.* Exclude the lightest hydrocarbon component, as identified in Step 4, and normalize the weight fractions of the remaining components.

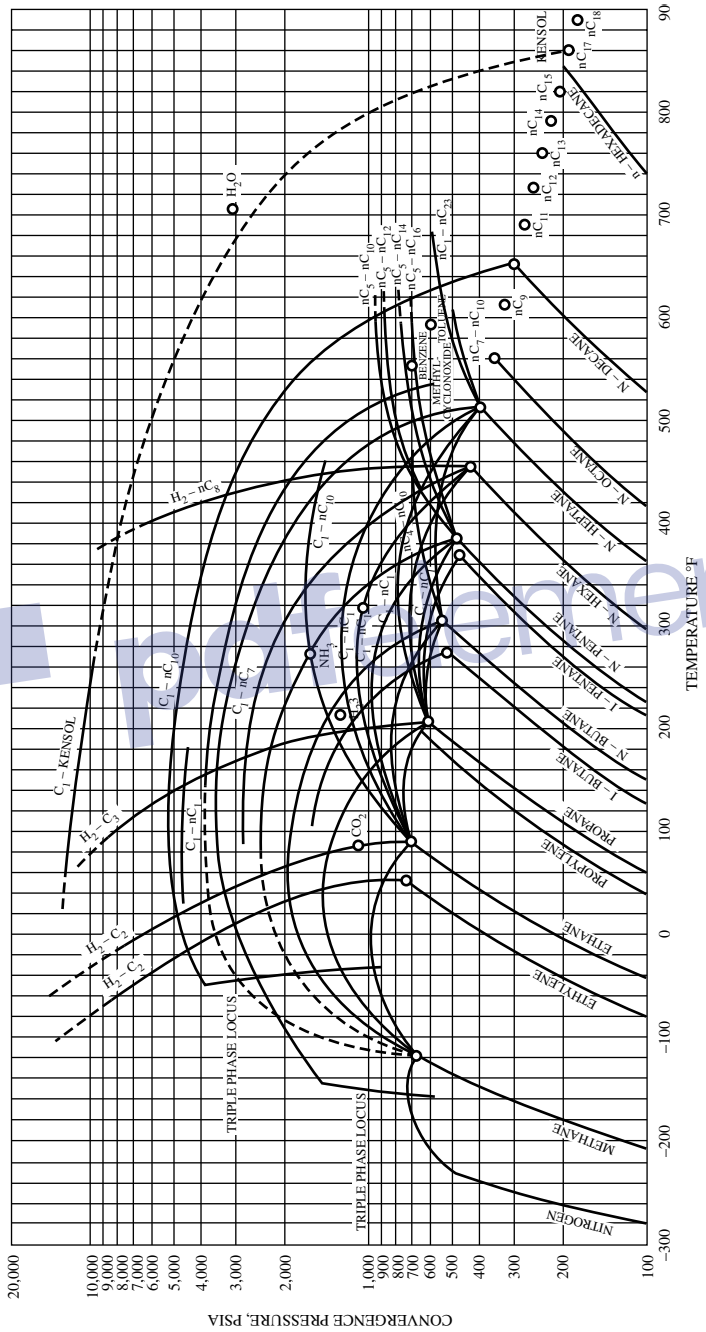


Figure 15-3. Convergence pressures for binary systems. (Courtesy of the Gas Processors Suppliers Association, Engineering Data Book, 10th Ed., 1987.)

Step 7. Calculate the weight average critical temperature and pressure of the lumped components (pseudo-component) from the following expressions:

$$T_{pc} = \sum_{i=2} w_i^* T_{ci}$$

$$p_{pc} = \sum_{i=2} w_i^* p_{ci}$$

where w_i^* = normalized weight fraction of component i
 T_{pc} = pseudo-critical temperature, °R
 p_{pc} = pseudo-critical pressure, psi

Step 8. Enter Figure 15-3 with the critical properties of the pseudo-component and trace the critical locus of the binary consisting of the light component and the pseudo-component.

Step 9. Read the new convergence pressure (ordinate) from the point at which the locus crosses the temperature of interest.

Step 10. If the calculated new convergence pressure is not reasonably close to the assumed value, repeat Steps 2 through 9.

Note that when the calculated new convergence pressure is between values for which charts are provided, interpolation between charts might be necessary. If the K values do not change rapidly with the convergence pressure, i.e., $p_k \gg p$, then the set of charts nearest to the calculated p_k may be used.

Standing's Method

Standing (1977) suggested that the convergence pressure can be roughly correlated linearly with the molecular weight of the heptanes-plus fraction. Whitson and Torp (1981) expressed this relationship by the following equation:

$$p_k = 60M_{C_{7+}} - 4200 \quad (15-26)$$

where $M_{C_{7+}}$ is the molecular weight of the heptanes-plus fraction.

Rzasa's Method

Rzasa, Glass, and Opfell (1952) presented a simplified graphical correlation for predicting the convergence pressure of light hydrocarbon mixtures. They used the temperature and the product of the molecular weight and specific gravity of the heptanes-plus fraction as correlating parameters. The graphical illustration of the proposed correlation is shown in Figure 15-4.

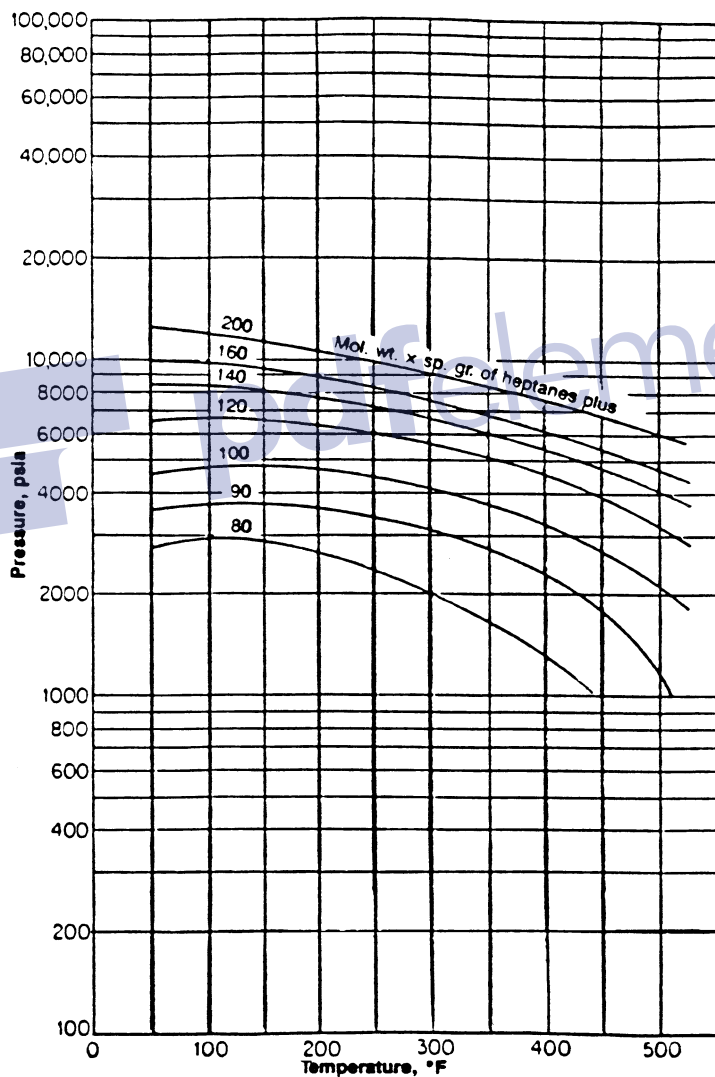


Figure 15-4. Rzasa's convergence pressure correlation. (Courtesy of the American Institute of Chemical Engineers.)

The graphical correlation is expressed mathematically by the following equation:

$$p_k = -2381.8542 + 46.341487[M\gamma]_{C_{7+}} + \sum_{i=1}^3 a_i \left[\frac{(M\gamma)_{C_{7+}}}{T - 460} \right]^i \quad (15-27)$$

where $(M)_{C_{7+}}$ = molecular weight of C_{7+}

$(\gamma)_{C_{7+}}$ = specific gravity of C_{7+}

T = temperature, °R

$a_1 - a_3$ = coefficients of the correlation with the following values:

$$a_1 = 6124.3049$$

$$a_2 = -2753.2538$$

$$a_3 = 415.42049$$

The above mathematical expression can be used for determining the convergence pressure of hydrocarbon mixtures at temperatures in the range of 50 to 300°F.

Whitson and Torp Correlation

Whitson and Torp (1981) reformulated Wilson's equation (Equation 15-17) to yield accurate results at higher pressures. Wilson's equation was modified by incorporating the convergence pressure into the correlation, to give:

$$K_i = \left(\frac{p_{ci}}{p_k} \right)^{A-1} \left(\frac{p_{ci}}{p} \right) \exp \left[5.37A(1 + \omega_i) \left(1 - \frac{T_{ci}}{T} \right) \right] \quad (15-28)$$

with

$$A = 1 - \left(\frac{p}{p_k} \right)^{0.7}$$

where p = system pressure, psig

p_k = convergence pressure, psig

T = system temperature, °R

ω_i = acentric factor of component i

Example 15-3

Rework Example 15-2 and calculate the equilibrium ratios using the Whitson and Torp method.

Solution

Step 1. Determine the convergence pressure from Equation 15-27 to give $P_k = 9473.89$.

Step 2. Calculate the coefficient A:

$$A = 1 - \left(\frac{1000}{9474} \right)^{0.7} = 0.793$$

Step 3. Calculate the equilibrium ratios from Equation 15-28 to give:

| Component | P_{cr} psia | T_{cr} °R | ω | $K_i = \left(\frac{P_{ci}}{9474} \right)^{0.793} \frac{P_i}{1000} \exp \left[5.37A(1 + \omega_i) \left(1 - \frac{T_i}{610} \right) \right]$ |
|--------------------|------------------|----------------|----------|--|
| CO ₂ | 1071 | 547.9 | 0.225 | 2.9 |
| N ₂ | 493 | 227.6 | 0.040 | 14.6 |
| C ₁ | 667.8 | 343.37 | 0.0104 | 7.6 |
| C ₂ | 707.8 | 550.09 | 0.0968 | 2.1 |
| C ₃ | 616.3 | 666.01 | 0.1524 | 0.7 |
| i - C ₄ | 529.1 | 734.98 | 0.1848 | 0.42 |
| n - C ₄ | 550.7 | 765.65 | 0.2010 | 0.332 |
| i - C ₅ | 490.4 | 829.1 | 0.2223 | 0.1749 |
| n - C ₅ | 488.6 | 845.7 | 0.2539 | 0.150 |
| C ₆ | 436.9 | 913.7 | 0.3007 | 0.0719 |
| C ₇₊ | 320.3 | 1139.4 | 0.5069 | 0.683(10 ⁻³) |

EQUILIBRIUM RATIOS FOR THE PLUS FRACTION

The equilibrium ratios of the plus fraction often behave in a manner different from the other components of a system. This is because the plus fraction in itself is a mixture of components. Several techniques have been proposed for estimating the K value of the plus fractions. Some of these techniques are presented here.

Campbell's Method

Campbell (1976) proposed that the plot of the log of K_i versus T_{ci}^2 for each component is a linear relationship for any hydrocarbon system. Campbell suggested that by drawing the best straight line through the points for propane through hexane components, the resulting line can be extrapolated to obtain the K value of the plus fraction. He pointed out that the plot of $\log K_i$ versus $1/T_{bi}$ of each heavy fraction in the mixture is also a straight-line relationship. The line can be extrapolated to obtain the equilibrium ratio of the plus fraction from the reciprocal of its average boiling point.

Winn's Method

Winn (1954) proposed the following expression for determining the equilibrium ratio of heavy fractions with a boiling point above 210°F.

$$K_{C_+} = \frac{K_{C_7}}{(K_{C_2}/K_{C_7})^b} \quad (15-29)$$

where K_{C_+} = value of the plus fraction
 K_{C_7} = K value of n-heptane at system pressure, temperature, and convergence pressure

K_{C_2} = K value of ethane
 b = volatility exponent

Winn correlated, graphically, the volatility component b of the heavy fraction, with the atmosphere boiling point, as shown in Figure 15-5.

This graphical correlation can be expressed mathematically by the following equation:

$$b = a_1 + a_2(T_b - 460) + a_3(T - 460)^2 + a_4(T_b - 460)^3 + a_5/(T - 460) \quad (15-30)$$

where T_b = boiling point, °R

$a_1 - a_5$ = coefficients with the following values:

$$\begin{aligned} a_1 &= 1.6744337 \\ a_2 &= -3.4563079 \times 10^{-3} \\ a_3 &= 6.1764103 \times 10^{-6} \\ a_4 &= 2.4406839 \times 10^{-6} \\ a_5 &= 2.9289623 \times 10^2 \end{aligned}$$

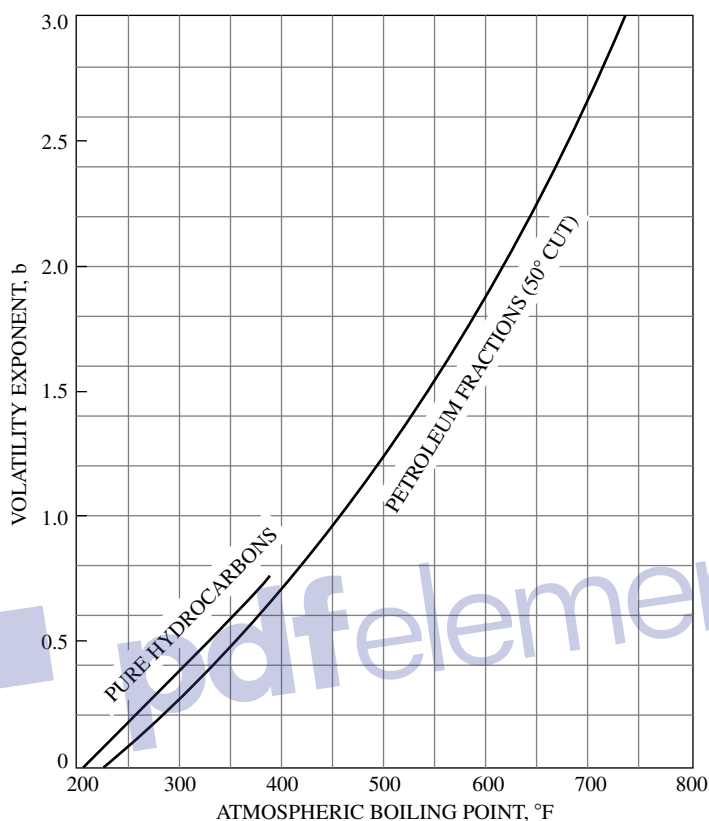


Figure 15-5. Volatility exponent. (Courtesy of the Petroleum Refiner.)

Katz's Method

Katz et al. (1957) suggested that a factor of 0.15 times the equilibrium ratio for the heptane component will give a reasonably close approximation to the equilibrium ratio for heptanes and heavier. This suggestion is expressed mathematically by the following equation:

$$K_{C_{7+}} = 0.15K_{C_7} \quad (15-31)$$

APPLICATIONS OF THE EQUILIBRIUM RATIO IN RESERVOIR ENGINEERING

The vast amount of experimental and theoretical work that has been performed on equilibrium ratio studies indicates their importance in solving phase equilibrium problems in reservoir and process engineering. Some of their practical applications are discussed next.

Dew-Point Pressure

The dew-point pressure p_d of a hydrocarbon system is defined as the pressure at which an infinitesimal quantity of liquid is in equilibrium with a large quantity of gas. For a total of 1 lb-mol of a hydrocarbon mixture, i.e., $n = 1$, the following conditions are applied at the dew-point pressure:

$$\begin{aligned}n_L &= 0 \\n_v &= 1\end{aligned}$$

Under these conditions, the composition of the vapor phase y_i is equal to the overall composition z_i . Applying the above constraints to Equation 15-14 yields:

$$\sum_i \frac{z_i}{K_i} \quad (15-32)$$

where z_i = total composition of the system under consideration.

The solution of Equation 15-32 for the dew-point pressure p_d involves a trial-and-error process. The process is summarized in the following steps:

Step 1. Assume a trial value of p_d . A good starting value can be obtained by applying Wilson's equation (Equation 15-17) for calculating K_i to Equation 15-32 to give:

$$\sum_i \left[\frac{z_i}{\frac{p_{ci}}{p_d} \exp \left[5.37(1 + \omega_i) \left(1 - \frac{T_{ci}}{T} \right) \right]} \right] = 1$$

Solving for p_d yields:

$$\text{initial } p_d = \frac{1}{\sum_i \left[\frac{z_i}{p_{ci} \exp \left[5.37(1 + \omega_i) \left(1 - \frac{T_{ci}}{T} \right) \right]} \right]} \quad (15-33)$$

Another simplified approach for estimating the dew-point pressure is to treat the hydrocarbon mixture as an ideal system with the equilibrium ratio K_i as given by Equation (15-4):

$$K_i = \frac{p_{vi}}{p}$$

Substituting the above expression into Equation (15-29) gives:

$$\sum_i \left[z_i \left(\frac{p_d}{p_{vi}} \right) \right] = 1.0$$

Solving for p_d yields:

$$\text{initial } p_d = \frac{1}{\sum_{i=1} \left(\frac{z_i}{p_{vi}} \right)}$$

Step 2. Using the assumed dew-point pressure, calculate the equilibrium ratio, K_i , for each component at the system temperature.

Step 3. Compute the summation of Equation 15-33.

Step 4. If the sum is less than 1, Steps 2 and 3 are repeated at a higher initial value of pressure; conversely, if the sum is greater than 1, repeat the calculations with a lower initial value of p_d . The correct value of the dew-point pressure is obtained when the sum is equal to 1.

Example 15-4

A natural gas reservoir at 250°F has the following composition:

| Component | z_i |
|--------------------|-------|
| C ₁ | 0.80 |
| C ₂ | 0.05 |
| C ₃ | 0.04 |
| i - C ₄ | 0.03 |
| n - C ₄ | 0.02 |
| i - C ₅ | 0.03 |
| n - C ₅ | 0.02 |
| C ₆ | 0.005 |
| C ₇₊ | 0.005 |

If the molecular weight and specific gravity of C₇₊ are 140 and 0.8, calculate the dew-point pressure.

Solution

Step 1. Calculate the convergence pressure of the mixture from Rzasas's correlation, i.e., Equation 15-27, to give:

$$p_k = 5000 \text{ psia}$$

Step 2. Determine an initial value for the dew-point pressure from Equation 15-33 to give:

$$p_d = 207 \text{ psia}$$

Step 3. Using the K-value curves in Appendix A, solve for the dew-point pressure by applying the iterative procedure outlined previously, and by using Equation 15-32, to give:

| Component | z_i | K_i at 207 psia | z_i/K_i | K_i at 300 psia | z_i/K_i | K_i at 222.3 psia | z_i/K_i |
|-----------|-------|-------------------------|-----------|----------------------|-----------|---------------------------|-----------|
| C_1 | 0.78 | 19 | 0.0411 | 13 | 0.06 | 18 | 0.0433 |
| C_2 | 0.05 | 6 | 0.0083 | 4.4 | 0.0114 | 5.79 | 0.0086 |
| C_3 | 0.04 | 3 | 0.0133 | 2.2 | 0.0182 | 2.85 | 0.0140 |
| i - C_4 | 0.03 | 1.8 | 0.0167 | 1.35 | 0.0222 | 1.75 | 0.0171 |
| n - C_4 | 0.02 | 1.45 | 0.0138 | 1.14 | 0.0175 | 1.4 | 0.0143 |
| i - C_5 | 0.03 | 0.8 | 0.0375 | 0.64 | 0.0469 | 0.79 | 0.0380 |
| n - C_5 | 0.02 | 0.72 | 0.0278 | .55 | 0.0364 | 0.69 | 0.029 |
| C_6 | 0.005 | 0.35 | 0.0143 | 0.275 | 0.0182 | 0.335 | 0.0149 |
| C_{7+} | 0.02 | 0.255* | 0.7843 | 0.02025* | 0.9877 | 0.0243* | 0.8230 |
| | | | 0.9571 | | 1.2185 | | 1.0022 |

*Equation 15-29

The dew-point pressure is therefore 222 psia at 250°F.

Bubble-Point Pressure

At the bubble-point, p_b , the hydrocarbon system is essentially liquid, except for an infinitesimal amount of vapor. For a total of 1 lb-mol of the hydrocarbon mixture, the following conditions are applied at the bubble-point pressure:

$$n_L = 1$$

$$n_v = 0$$

Obviously, under the above conditions, $x_i = z_i$. Applying the above constraints to Equation 15-15 yields:

$$\sum_i (z_i K_i) = 1 \quad (15-34)$$

Following the procedure outlined in the dew-point pressure determination, Equation 15-34 is solved for the bubble-point pressure p_b by assuming various pressures and determining the pressure that will produce K values that satisfy Equation 15-34.

During the iterative process, if:

$$\sum_i (z_i K_i) < 1 \rightarrow \text{the assumed pressure is high}$$

$$\sum_i (z_i K_i) > 1 \rightarrow \text{the assumed pressure is low}$$

Wilson's equation can be used to give a good starting value for the iterative process:

$$\sum_i \left[z_i \frac{p_{ci}}{p_b} \exp \left[5.37(1 + \omega) \left(1 - \frac{T_{ci}}{T} \right) \right] \right] = 1$$

Solving for the bubble-point pressure gives:

$$p_b = \sum_i \left[z_i p_{ci} \exp \left[5.37(1 + \omega) \left(1 - \frac{T_{ci}}{T} \right) \right] \right] \quad (15-35)$$

Assuming an ideal solution behavior, an initial guess for the bubble-point pressure can also be calculated by replacing the K_i in Equation 15-34 with that of Equation 15-4 to give:

$$\sum_i \left[z_i \left(\frac{p_{vi}}{p_b} \right) \right] = 1$$

or

$$p_b = \sum_i (z_i p_{vi}) \quad (15-36)$$

Example 15-5

A crude oil reservoir has a temperature of 200°F and a composition as given below. Calculate the bubble-point pressure of the oil.

| Component | x_i |
|--------------------|-------|
| C ₁ | 0.42 |
| C ₂ | 0.05 |
| C ₃ | 0.05 |
| i - C ₄ | 0.03 |
| n - C ₄ | 0.02 |
| i - C ₅ | 0.01 |
| n - C ₅ | 0.01 |
| C ₆ | 0.01 |
| C ₇₊ | 0.40* |

$$*(M)_{C_7} = 216.0$$

$$(\gamma)_{C_7} = 0.8605$$

$$(T_b)_{C_7} = 977^\circ R$$

Solution

Step 1. Calculate the convergence pressure of the system by using Standing's correlation (Equation 15-26):

$$p_k = (60)(216) - 4200 = 8760 \text{ psia}$$

Step 2. Calculate the critical pressure and temperature by the Riazi and Daubert equation (Equation 1-2), to give:

$$p_c = 230.4 \text{ psia}$$

$$T_c = 1279.8^\circ R$$

Step 3. Calculate the acentric factor by employing the Edmister correlation (Equation 1-3) to yield:

$$\omega = 0.653$$

Step 4. Estimate the bubble-point pressure from Equation 15-35 to give:

$$p_b = 3924 \text{ psia}$$

Step 5. Employing the iterative procedure outlined previously and using the Whitson and Torp equilibrium ratio correlation gives:

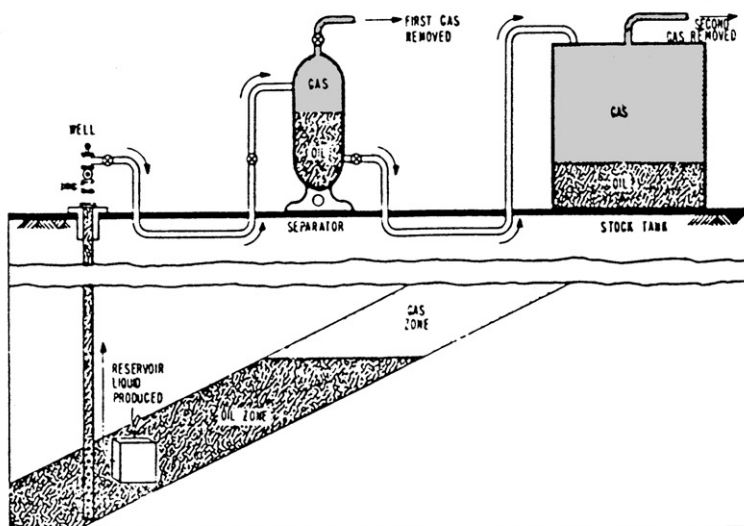
| Component | z_i | K_i at 3924 psia | $z_i K_i$ | K_i at 3950 psia | $z_i K_i$ | K_i at 4,329 psia | $z_i K_i$ |
|--------------------|-------|--------------------------|-----------|--------------------------|-----------|---------------------------|-----------|
| C ₁ | 0.42 | 2.257 | 0.9479 | 2.242 | 0.9416 | 2.0430 | 0.8581 |
| C ₂ | 0.05 | 1.241 | 0.06205 | 2.137 | 0.0619 | 1.1910 | 0.0596 |
| C ₃ | 0.05 | 0.790 | 0.0395 | 0.7903 | 0.0395 | 0.793 | 0.0397 |
| i - C ₄ | 0.03 | 0.5774 | 0.0173 | 0.5786 | 0.0174 | 0.5977 | 0.0179 |
| n - C ₄ | 0.02 | 0.521 | 0.0104 | 0.5221 | 0.0104 | 0.5445 | 0.0109 |
| i - C ₅ | 0.01 | 0.3884 | 0.0039 | 0.3902 | 0.0039 | 0.418 | 0.0042 |
| n - C ₅ | 0.01 | 0.3575 | 0.0036 | 0.3593 | 0.0036 | 0.3878 | 0.0039 |
| C ₆ | 0.01 | 0.2530 | 0.0025 | 0.2549 | 0.0025 | 0.2840 | 0.0028 |
| C ₇₊ | 0.40 | 0.227 | 0.0091 | 0.0232 | 0.00928 | 0.032 | 0.0138 |
| Σ | | | 1.09625 | | 1.09008 | | 1.0099 |

The calculated bubble-point pressure is 4,330 psia.

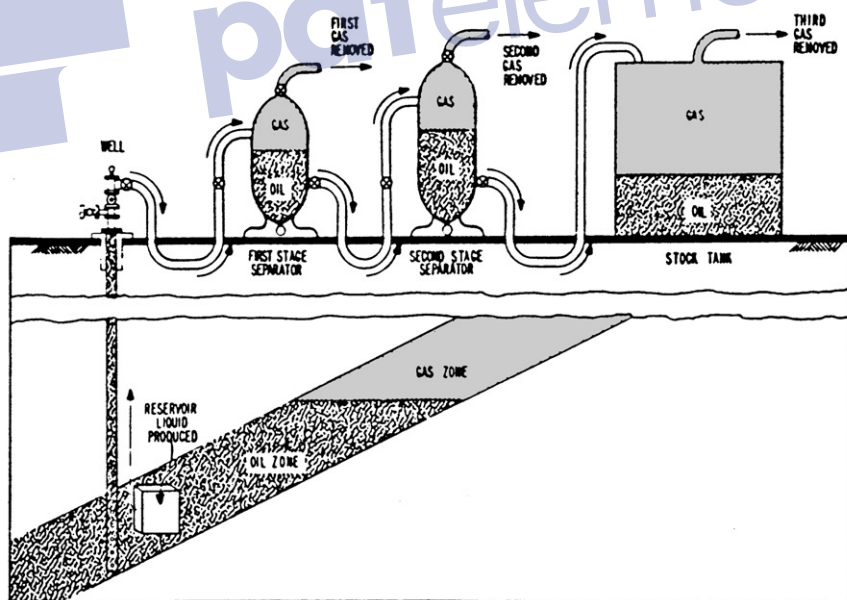
Separator Calculations

Produced reservoir fluids are complex mixtures of different physical characteristics. As a wellstream flows from the high-temperature, high-pressure petroleum reservoir, it experiences pressure and temperature reductions. Gases evolve from the liquids and the wellstream changes in character. The physical separation of these phases is by far the most common of all field-processing operations and one of the most critical. The manner in which the hydrocarbon phases are separated at the surface influences the stock-tank oil recovery. The principal means of surface separation of gas and oil is the conventional stage separation.

Stage separation is a process in which gaseous and liquid hydrocarbons are flashed (separated) into vapor and liquid phases by two or more separators. These separators are usually operated in series at consecutively lower pressures. Each condition of pressure and temperature at which hydrocarbon phases are flashed is called a *stage of separation*. Examples of one- and two-stage separation processes are shown in Figure 15-6. Traditionally, the stock-tank is normally considered a separate stage of separation. Mechanically, there are two types of gas-oil separation: (1) differential separation and (2) flash or equilibrium separation.



One-stage separation



Two-stage separation

Figure 15-6. Schematic drawing of one- and two-stage separation processes. (After Clark, 1951.)

To explain the various separation processes, it is convenient to define the composition of a hydrocarbon mixture by three groups of components:

1. The very volatile components (“lights”), such as nitrogen, methane, and ethane
2. The components of intermediate volatility (“intermediates”), such as propane through hexane
3. The components of less volatility, or the “heavies,” such as heptane and heavier components

In the differential separation, the liberated gas (which is composed mainly of lighter components) is removed from contact with the oil as the pressure on the oil is reduced. As pointed out by Clark (1960), when the gas is separated in this manner, the maximum amount of heavy and intermediate components will remain in the liquid, minimum shrinkage of the oil will occur, and, therefore, greater stock-tank oil recovery will occur. This is due to the fact that the gas liberated earlier at higher pressures is not present at lower pressures to attract the intermediate and heavy components and pull them into the gas phase.

In the flash (equilibrium) separation, the liberated gas remains in contact with oil until its instantaneous removal at the final separation pressure. A maximum proportion of intermediate and heavy components is attracted into the gas phase by this process, and this results in a maximum oil shrinkage and, thus, a lower oil recovery.

In practice, the differential process is introduced first in field separation when gas or liquid is removed from the primary separator. In each subsequent stage of separation, the liquid initially undergoes a flash liberation followed by a differential process as actual separation occurs. As the number of stages increases, the differential aspect of the overall separation becomes greater.

The purpose of stage separation then is to reduce the pressure on the produced oil in steps so that more stock-tank oil recovery will result. Separator calculations are basically performed to determine:

- Optimum separation conditions: separator pressure and temperature
- Compositions of the separated gas and oil phases
- Oil formation volume factor
- Producing gas-oil ratio
- API gravity of the stock-tank oil

Note that if the separator pressure is high, large amounts of light components will remain in the liquid phase at the separator and be lost along with other valuable components to the gas phase at the stock tank. On the other hand, if the pressure is too low, large amounts of light components will be separated from the liquid and they will attract substantial quantities of intermediate and heavier components. An intermediate pressure, called *optimum separator pressure*, should be selected to maximize the oil volume accumulation in the stock tank. This optimum pressure will also yield:

- A maximum stock-tank API gravity
- A minimum oil formation volume factor (i.e., less oil shrinkage)
- A minimum producing gas-oil ratio (gas solubility)

The concept of determining the optimum separator pressure by calculating the API gravity, B_o , and R_s is shown graphically in Figure 15-7. The computational steps of the separator calculations are described below in conjunction with Figure 15-8, which schematically shows a bubble-point reservoir flowing into a surface separation unit consisting of n stages operating at successively lower pressures.

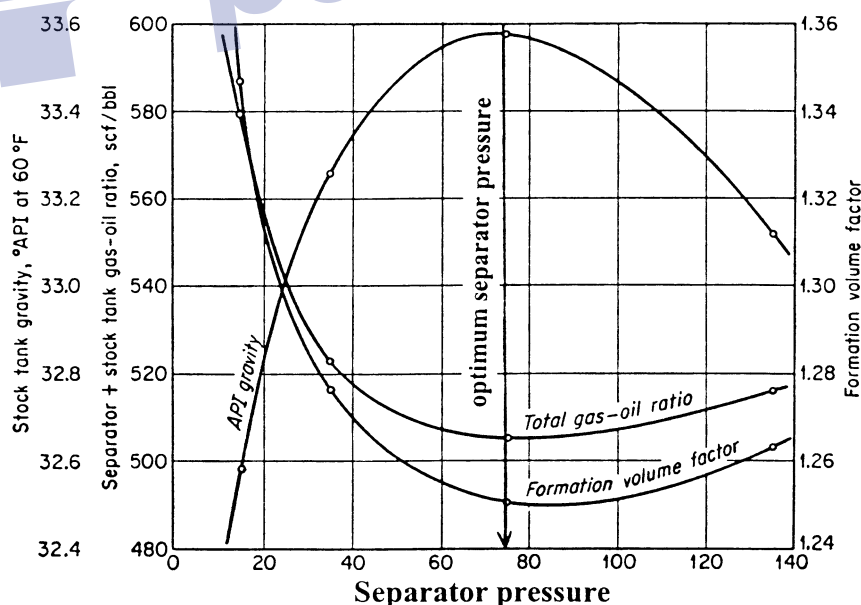


Figure 15-7. Effect of separator pressure on API, B_o , and GOR. (After Amyx, Bass, and Whiting, 1960.)

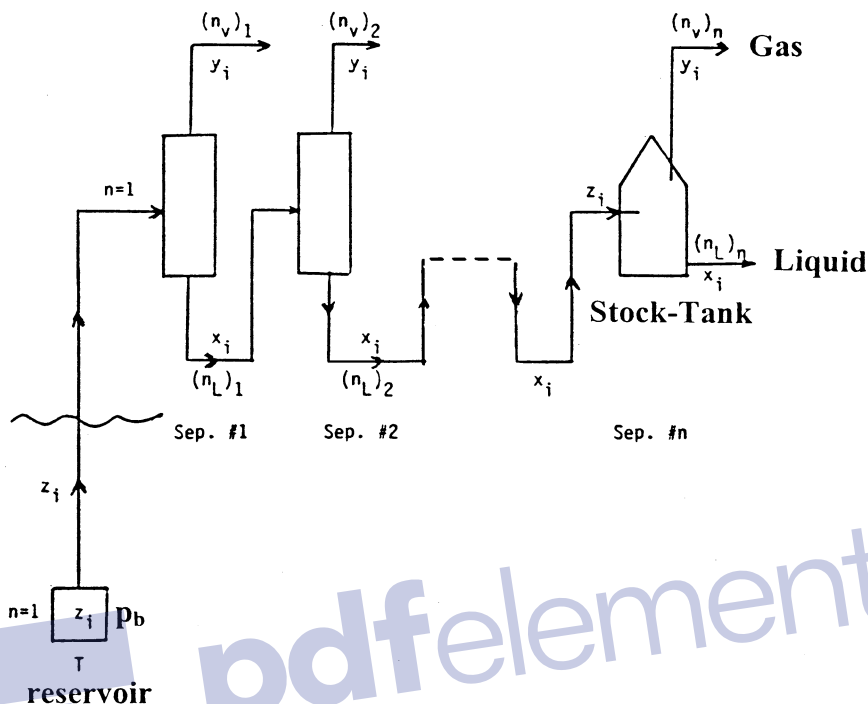


Figure 15-8. Schematic illustration of n separation stages.

Step 1. Calculate the volume of oil occupied by 1 lb-mol of crude at the reservoir pressure and temperature. This volume, denoted V_o , is calculated by recalling and applying the equation that defines the number of moles to give:

$$n = \frac{m}{M_a} = \frac{\rho_o V_o}{M_a} = 1$$

Solving for the oil volume gives:

$$V_o = \frac{M_a}{\rho_o} \quad (15-37)$$

where m = total weight of 1 lb-mol of crude oil, lb/mol

V_o = volume of 1 lb-mol of crude oil at reservoir conditions, ft^3/mol

M_a = apparent molecular weight

ρ_o = density of the reservoir oil, lb/ft^3

Step 2. Given the composition of the feed stream z_i to the first separator and the operating conditions of the separator, i.e., separator pressure and temperature, calculate the equilibrium ratios of the hydrocarbon mixture.

Step 3. Assuming a total of 1 mol of the feed entering the first separator and using the above calculated equilibrium ratios, perform flash calculations to obtain the compositions and quantities, in moles, of the gas and the liquid leaving the first separator. Designating these moles as $(n_L)_1$ and $(n_v)_1$, the actual number of moles of the gas and the liquid leaving the first separation stage are:

$$[n_{v1}]_a = (n)(n_v)_1 = (1)(n_v)_1$$

$$[n_{L1}]_a = (n)(n_L)_1 = (1)(n_L)_1$$

where $[n_{v1}]_a$ = actual number of moles of vapor leaving the first separator

$[n_{L1}]_a$ = actual number of moles of liquid leaving the first separator

Step 4. Using the composition of the liquid leaving the first separator as the feed for the second separator, i.e., $z_i = x_i$, calculate the equilibrium ratios of the hydrocarbon mixture at the prevailing pressure and temperature of the separator.

Step 5. Based on 1 mol of the feed, perform flash calculations to determine the compositions and quantities of the gas and liquid leaving the second separation stage. The actual number of moles of the two phases are then calculated from:

$$[n_{v2}]_a = [n_{L1}]_a (n_v)_2 = (1)(n_L)_1 (n_v)_2$$

$$[n_{L2}]_a = [n_{L1}]_a (n_L)_2 = (1)(n_L)_1 (n_L)_2$$

where $[n_{v2}]_a, [n_{L2}]_a$ = actual moles of gas and liquid leaving separator 2

$(n_v)_2, (n_L)_2$ = moles of gas and liquid as determined from flash calculations

Step 6. The previously outlined procedure is repeated for each separation stage, including the stock-tank storage, and the calculated moles and compositions are recorded. The total number of moles of gas off all stages are then calculated as:

$$(n_v)_t = \sum_{i=1}^n (n_{va})_i = (n_v)_1 + (n_L)_1 (n_v)_2 + (n_L)_1 (n_L)_2 (n_v)_3 + \dots + (n_L)_1 \dots (n_L)_{n-1} (n_v)_n$$

In a more compacted form, the above expression can be written:

$$(n_v)_t = (n_v)_1 + \sum_{i=2}^n \left[(n_v)_i \prod_{j=1}^{i-1} (n_L)_j \right] \quad (15-38)$$

where $(n_v)_t$ = total moles of gas off all stages, lb-mol/mol of feed
 n = number of separation stages

Total moles of liquid remaining in the stock-tank can also be calculated as:

$$(n_L)_{st} = n_{L1} n_{L2} \dots n_{Ln}$$

or

$$(n_L)_{st} = \prod_{i=1}^n (n_L)_i \quad (15-39)$$

where

$(n_L)_{st}$ = number of moles of liquid remaining in the stock tank
 $(n_L)_i$ = moles of liquid off i th stage

Step 7. Calculate the volume, in scf, of all the liberated solution gas from:

$$V_g = 379.4 (n_v)_t \quad (15-40)$$

where V_g = total volume of the liberated solution gas scf/mol of feed.

Step 8. Determine the volume of stock-tank oil occupied by $(n_L)_{st}$ moles of liquid from:

$$(V_o)_{st} = \frac{(n_L)_{st} (M_a)_{st}}{(\rho_o)_{st}} \quad (15-41)$$

where $(V_o)_{st}$ = volume of stock-tank oil, ft³/mol of feed
 $(M_a)_{st}$ = apparent molecular weight of the stock-tank oil
 $(\rho_o)_{st}$ = density of the stock-tank oil, lb/ft³

Step 9. Calculate the specific gravity and the API gravity of the stock-tank oil by applying these expressions:

$$\gamma_o = \frac{(\rho_o)_{st}}{62.4}$$

$$^\circ\text{API} = \frac{141.5}{\gamma_o} - 131.5$$

Step 10. Calculate the total gas-oil ratio (or gas solubility R_s):

$$\text{GOR} = \frac{V_g}{(V_o)_{st} / 5.615} = \frac{(5.615)(379.4)(n_v)_t}{(n_L)_{st} (M)_{st} / (\rho_o)_{st}}$$

$$\text{GOR} = \frac{2130.331(n_v)_t (\rho_o)_{st}}{(n_L)_{st} (M)_{st}} \quad (15-42)$$

where GOR = gas-oil ratio, scf/STB.

Step 11. Calculate the oil formation volume factor from the relationship:

$$B_o = \frac{V_o}{(V_o)_{st}}$$

Combining Equations 15-37 and 15-41 with the above expression gives:

$$B_o = \frac{M_a (\rho_o)_{st}}{\rho_o (n_L)_{st} (M_a)_{st}}$$

where B_o = oil formation volume factor, bbl/STB
 M_a = apparent molecular weight of the feed
 $(M_a)_{st}$ = apparent molecular weight of the stock-tank oil
 ρ_o = density of crude oil at reservoir conditions, lb/ft³

The separator pressure can be optimized by calculating the API gravity, GOR, and B_o in the manner outlined above at different assumed pressures. The optimum pressure corresponds to a maximum in the API gravity and a minimum in gas-oil ratio and oil formation volume factor.

Example 15-6

A crude oil, with the composition given below, exists at its bubble-point pressure of 1,708.7 psia and at a temperature of 131°F. The crude oil is flashed through two-stage and stock-tank separation facilities. The operating conditions of the three separators are:

| Separator | Pressure, psia | Temperature, °F |
|------------|----------------|-----------------|
| 1 | 400 | 72 |
| 2 | 350 | 72 |
| Stock-tank | 14.7 | 60 |

The composition of the crude oil is given below:

| Component | z_i |
|--------------------|--------|
| CO ₂ | 0.0008 |
| N ₂ | 0.0164 |
| C ₁ | 0.2840 |
| C ₂ | 0.0716 |
| C ₃ | 0.1048 |
| i - C ₄ | 0.0420 |
| n - C ₄ | 0.0420 |
| i - C ₅ | 0.0191 |
| n - C ₅ | 0.0191 |
| C ₆ | 0.0405 |
| C ₇₊ | 0.3597 |

The molecular weight and specific gravity of C₇₊ are 252 and 0.8429. Calculate B_o , R_S , stock-tank density, and the API gravity of the hydrocarbon system.

Solution

Step 1. Calculate the apparent molecular weight of the crude oil to give $M_a = 113.5102$.

Step 2. Calculate the density of the bubble-point crude oil by using the Standing and Katz correlation to yield $\rho_o = 44.794 \text{ lb/ft}^3$.

Step 3. Flash the original composition through the first separator by generating the equilibrium ratios by using the Standing correlation (Equation 15-20) to give:

| Component | z_i | K_i | x_i | y_i |
|--------------------|--------|--------|--------|--------|
| CO ₂ | 0.0008 | 3.509 | 0.0005 | 0.0018 |
| N ₂ | 0.0164 | 39.90 | 0.0014 | 0.0552 |
| C ₁ | 0.2840 | 8.850 | 0.089 | 0.7877 |
| C ₂ | 0.0716 | 1.349 | 0.0652 | 0.0880 |
| C ₃ | 0.1048 | 0.373 | 0.1270 | 0.0474 |
| i - C ₄ | 0.0420 | 0.161 | 0.0548 | 0.0088 |
| n - C ₄ | 0.0420 | 0.120 | 0.0557 | 0.0067 |
| i - C ₅ | 0.0191 | 0.054 | 0.0259 | 0.0014 |
| n - C ₅ | 0.0191 | 0.043 | 0.0261 | 0.0011 |
| C ₆ | 0.0405 | 0.018 | 0.0558 | 0.0010 |
| C ₇₊ | 0.3597 | 0.0021 | 0.4986 | 0.0009 |

with $n_L = 0.7209$ and $n_V = 0.29791$.

Step 4. Use the calculated liquid composition as the feed for the second separator and flash the composition at the operating condition of the separator.

| Component | z_i | K_i | x_i | y_i |
|--------------------|--------|---------|--------|--------|
| CO ₂ | 0.0005 | 3.944 | 0.0005 | 0.0018 |
| N ₂ | 0.0014 | 46.18 | 0.0008 | 0.0382 |
| C ₁ | 0.089 | 10.06 | 0.0786 | 0.7877 |
| C ₂ | 0.0652 | 1.499 | 0.0648 | 0.0971 |
| C ₃ | 0.1270 | 0.4082 | 0.1282 | 0.0523 |
| i - C ₄ | 0.0548 | 0.1744 | 0.0555 | 0.0097 |
| n - C ₄ | 0.0557 | 0.1291 | 0.0564 | 0.0072 |
| i - C ₅ | 0.0259 | 0.0581 | 0.0263 | 0.0015 |
| n - C ₅ | 0.0261 | 0.0456 | 0.0264 | 0.0012 |
| C ₆ | 0.0558 | 0.0194 | 0.0566 | 0.0011 |
| C ₇₊ | 0.4986 | 0.00228 | 0.5061 | 0.0012 |

with $n_L = 0.9851$ and $n_V = 0.0149$.

Step 5. Repeat the above calculation for the stock-tank stage to give:

| Component | z_i | K_i | x_i | y_i |
|--------------------|--------|---------|---------|--------|
| CO ₂ | 0.0005 | 81.14 | 0.000 | 0.0014 |
| N ₂ | 0.0008 | 1159 | 0.000 | 0.026 |
| C ₁ | 0.0784 | 229 | 0.0011 | 0.2455 |
| C ₂ | 0.0648 | 27.47 | 0.0069 | 0.1898 |
| C ₃ | 0.1282 | 6.411 | 0.0473 | 0.3030 |
| i - C ₄ | 0.0555 | 2.518 | 0.0375 | 0.0945 |
| n - C ₄ | 0.0564 | 1.805 | 0.0450 | 0.0812 |
| i - C ₅ | 0.0263 | 0.7504 | 0.0286 | 0.0214 |
| n - C ₅ | 0.0264 | 0.573 | 0.02306 | 0.0175 |
| C ₆ | 0.0566 | 0.2238 | 0.0750 | 0.0168 |
| C ₇₊ | 0.5061 | 0.03613 | 0.7281 | 0.0263 |

with $n_L = 0.6837$ and $n_v = 0.3163$.

Step 6. Calculate the actual number of moles of the liquid phase at the stock-tank conditions from Equation 15-39:

$$(n_L)_{st} = (1)(0.7209)(0.9851)(0.6837) = 0.48554$$

Step 7. Calculate the total number of moles of the liberated gas from the entire surface separation system:

$$n_v = 1 - (n_L)_{st} = 1 - 0.48554 = 0.51446$$

Step 8. Calculate apparent molecular weight of the stock-tank oil from its composition to give $(M_a)_{st} = 200.6$.

Step 9. Calculate the density of the stock-tank oil by using the Standing correlation to give:

$$(\rho_o)_{st} = 50.920$$

$$\gamma = 50.920/62.4 = 0.816 \quad 60^\circ/60^\circ$$

Step 10. Calculate the API gravity of the stock-tank oil:

$$API = (141.5/0.816) - 131.5 = 41.9$$

Step 11. Calculate the gas solubility from Equation 15-42 to give:

$$R_s = \frac{2130.331(0.51446)(50.92)}{0.48554(200.6)} = 573.0 \text{ scf/STB}$$

Step 12. Calculate B_o from Equation 15-43 to give:

$$B_o = \frac{(113.5102)(50.92)}{(44.794)(0.48554)(200.6)} = 1.325 \text{ bbl/STB}$$

To optimize the operating pressure of the separator, the above steps should be repeated several times under different assumed pressures and the results, in terms of API, B_o , and R_s , should be expressed graphically and used to determine the optimum pressure.

Note that at **low pressures**, e.g., $p < 1,000$, equilibrium ratios are nearly independent of the overall composition z_i or the convergence pressure and can be considered only a function pressure and temperature. Under this condition, i.e, $p < 1,000$, the equilibrium ratio for any component i can be expressed as:

$$K_i = \frac{A_i}{p}$$

The temperature-dependent coefficient A_i is a characterization parameter of component i that accounts for the physical properties of the component. The above expression suggests that the K_i varies linearly at a constant temperature with $1/p$. For example, suppose that a hydrocarbon mixture exists at 300 psi and 100°F. Assume that the mixture contains methane and we want to estimate the equilibrium ratio of methane (or any other components) when the mixture is flashed at 100 psi and at the same temperature of 100°F. The recommended procedure is summarized in the following steps:

Step 1. Because at low pressure the equilibrium ratio is considered independent of the overall composition of the mixture, use the equilibrium ratio charts of Appendix A to determine the K_i value of methane at 300 psi and 100°F:

$$K_{C_1} = 10.5$$

Step 2. Calculate the characterization parameter A_i of methane from the above proposed relationship:

$$10.5 = \frac{A_i}{500}$$

$$A_i = (10.5)(500) = 5250$$

Step 3. Calculate the K_i of methane at 100 psi and 100°F from:

$$K_{C_1} = \frac{3,150}{100} = 31.5$$

In many low-pressure applications of flash calculations at constant temperature, it might be possible to characterize the entire hydrocarbon mixture as a binary system, i.e., two-component system. Because methane exhibits a linear relationship with pressure of a wide range of pressure values, one of the components that forms the binary system should be methane. The main advantage of such a binary system is the simplicity of performing flash calculations because it does not require an iterative technique.

Reconsider Example 15-6 where flash calculations were performed on the entire system at 400 psia and 72°F. To perform flash calculations on the feed for the second separator at 350 psi and 72°F, follow these steps:

Step 1. Select methane as one of the binary systems with the other component defined as ethane-plus, i.e., C_{2+} , which lumps the remaining components. Results of Example 15-6 show:

- $K_{C_1} = 8.85$
- $y_{C_1} = 0.7877$
- $x_{C_2} = 0.089$
- $y_{C_{2+}} = 1.0 - 0.7877 = 0.2123$
- $x_{C_{2+}} = 1.0 - 0.089 = 0.911$

Step 2. From the definition of the equilibrium ratio, calculate the K value of C_{2+} :

$$K_{C_{2+}} = \frac{y_{C_{2+}}}{x_{C_{2+}}} = \frac{0.2123}{0.9110} = 0.2330$$

Step 3. Calculate the characterization parameter A_i for methane and C_{2+} :

$$A_{C_1} = K_{C_1} p = (8.85)(400) = 3540$$

$$A_{C_{2+}} = K_{C_{2+}} p = (0.233)(400) = 93.2$$

The equilibrium ratio for each of the two components (at a constant temperature) can then be described by:

$$K_{C_1} = \frac{3540}{p}$$

$$K_{C_{2+}} = \frac{93.2}{p}$$

Step 4. Calculate the K_i value for each component at the second separator pressure of 350 psi:

$$K_{C_1} = \frac{3540}{350} = 10.11$$

$$K_{C_{2+}} = \frac{93.2}{350} = 0.266$$

Step 5. Using the flash calculations procedure as outlined previously for a binary system, calculate the composition and number of moles of the gas and liquid phase at 350 psi:

- Solve for x_{C_1} and $x_{C_{2+}}$:

$$x_{C_1} = \frac{1 - K_2}{K_1 - K_2} = \frac{1.0 - 0.266}{10.11 - 0.266} = 0.0746$$

$$x_{C_{2+}} = 1 - x_{C_1} = 1.0 - 0.0746 = 0.9254$$

- Solve for y_{C_1} and $y_{C_{2+}}$:

$$y_{C_1} = x_{C_1} K_1 = (0.0746)(10.11) = 0.754$$

$$y_{C_{2+}} = 1 - y_{C_1} = 1.0 - 0.754 = 0.246$$

- Solve for number of moles of the vapor and liquid phase:

$$n_v = \frac{z_1 - x_1}{x_1(K_1 - 1)} = \frac{0.089 - 0.0746}{0.0746(10.11 - 1)} = 0.212$$

$$n_L = 1 - n_v = 1.0 - 0.212 = 0.788$$

The above calculations are considered meaningless without converting moles of liquid n_i into volume, which requires the calculation of the liquid density at separator pressure and temperature. Notice:

$$V = \frac{n_L M_a}{\rho_o}$$

where M_a is the apparent molecular weight of the separated liquid and is given by (for a binary system):

$$M_a = x_{C_1} M_{C_1} + x_{C_{2+}} M_{C_{2+}}$$

Density Calculations

The calculation of crude oil density from its composition is an important and integral part of performing flash calculations. The best known and most widely used calculation methods are those of Standing-Katz (1942) and Alani-Kennedy (1960). These two methods are presented below:

The Standing-Katz Method

Standing and Katz (1942) proposed a graphical correlation for determining the density of hydrocarbon liquid mixtures. The authors developed the correlation from evaluating experimental, compositional, and density data on 15 crude oil samples containing up to 60 mol% methane. The proposed method yielded an average error of 1.2% and maximum error of 4% for the data on these crude oils. The original correlation did not have a procedure for handling significant amounts of nonhydrocarbons.

The authors expressed the density of hydrocarbon liquid mixtures as a function of pressure and temperature by the following relationship:

$$\rho_o = \rho_{sc} + \Delta\rho_p - \Delta\rho_T$$

where ρ_o = crude oil density at p and T, lb/ft³

ρ_{sc} = crude oil density (with all the dissolved solution gas) at standard conditions, i.e., 14.7 psia and 60°F, lb/ft³

$\Delta\rho_p$ = density correction for compressibility of oils, lb/ft³

$\Delta\rho_T$ = density correction for thermal expansion of oils, lb/ft³

Standing and Katz correlated graphically the liquid density at standard conditions with:

- The density of the propane-plus fraction $\rho_{C_{3+}}$
- The weight percent of methane in the entire system $(m_{C_1})_{C_{1+}}$
- The weight percent of ethane in the ethane-plus $(m_{C_2})_{C_{2+}}$

This graphical correlation is shown in Figure 15-9. The following are the specific steps in the Standing and Katz procedure of calculating the liquid density at a specified pressure and temperature.

Step 1. Calculate the total weight and the weight of each component in 1 lb-mol of the hydrocarbon mixture by applying the following relationships:

$$m_i = x_i M_i$$

$$m_t = \sum x_i M_i$$

where m_i = weight of component i in the mixture, lb/lb-mol
 x_i = mole fraction of component i in the mixture
 M_i = molecular weight of component i
 m_t = total weight of 1 lb-mol of the mixture, lb/lb-mol

Step 2. Calculate the weight percent of methane in the entire system and the weight percent of ethane in the ethane-plus from the following expressions:

$$(m_{C_1})_{C_{1+}} = \left[\frac{x_{C_1} M_{C_1}}{\sum_{i=1}^n x_i M_i} \right] 100 = \left[\frac{m_{C_1}}{m_t} \right] 100$$

and

$$(m_{C_2})_{C_{2+}} = \left[\frac{m_{C_2}}{m_{C_{2+}}} \right] 100 = \left[\frac{m_{C_2}}{m_t - m_{C_1}} \right] 100$$

where $(m_{C_1})_{C_{1+}}$ = weight percent of methane in the entire system
 m_{C_1} = weight of methane in 1 lb-mol of the mixture, i.e., $x_{C_1} M_{C_1}$
 $(m_{C_2})_{C_{2+}}$ = weight percent of ethane in ethane-plus
 m_{C_2} = weight of ethane in 1 lb-mol of the mixture, i.e., $x_{C_2} M_{C_2}$
 M_{C_1} = molecular weight of methane
 M_{C_2} = molecular weight of ethane

Step 3. Calculate the density of the propane-plus fraction at standard conditions by using the following equations:

$$\rho_{C_{3+}} = \frac{m_{C_{3+}}}{V_{C_{3+}}} = \frac{\sum_{i=C_3}^n x_i M_i}{\sum_{i=C_3}^n \frac{x_i M_i}{\rho_{oi}}}$$

with

$$m_{C_{3+}} = \sum_{i=C_3} x_i M_i$$

$$V_{C_{3+}} = \sum_{i=C_3} V_i = \sum_{i=C_3} \frac{m_i}{\rho_{oi}}$$

where $\rho_{C_{3+}}$ = density of the propane and heavier components, lb/ft³

$m_{C_{3+}}$ = weight of the propane and heavier fractions, lb/lb-mol

$V_{C_{3+}}$ = volume of the propane-plus fraction, ft³/lb-mol

V_i = volume of component i in 1 lb-mol of the mixture

m_i = weight of component i , i.e., $x_i M_i$, lb/lb-mole

ρ_{oi} = density of component i at standard conditions, lb/ft³

Density values for pure components are tabulated in Table 1-2 in Chapter 1, but the density of the plus fraction must be measured.

Step 4. Using Figure 15-9, enter the $\rho_{C_{3+}}$ value into the left ordinate of the chart and move horizontally to the line representing $(m_{C_2})_{C_{2+}}$; then drop vertically to the line representing $(m_{C_1})_{C_{1+}}$. The density of the oil at standard condition is read on the right side of the chart. Standing (1977) expressed the graphical correlation in the following mathematical form:

$$\rho_{sc} = \rho_{C_{2+}} \left[1 - 0.012(m_{C_1})_{C_{1+}} - 0.000158(m_{C_1})_{C_{1+}}^2 \right] \\ + 0.0133(m_{C_1})_{C_{1+}} + 0.00058(m_{C_1})_{C_{2+}}^2$$

with

$$\rho_{C_{2+}} = \rho_{C_{3+}} \left[1 - 0.01386(m_{C_2})_{C_{2+}} - 0.000082(m_{C_2})_{C_{2+}}^2 \right] \\ + 0.379(m_{C_2})_{C_{2+}} + 0.0042(m_{C_2})_{C_{2+}}^2$$

where $\rho_{C_{2+}}$ = density of ethane-plus fraction.

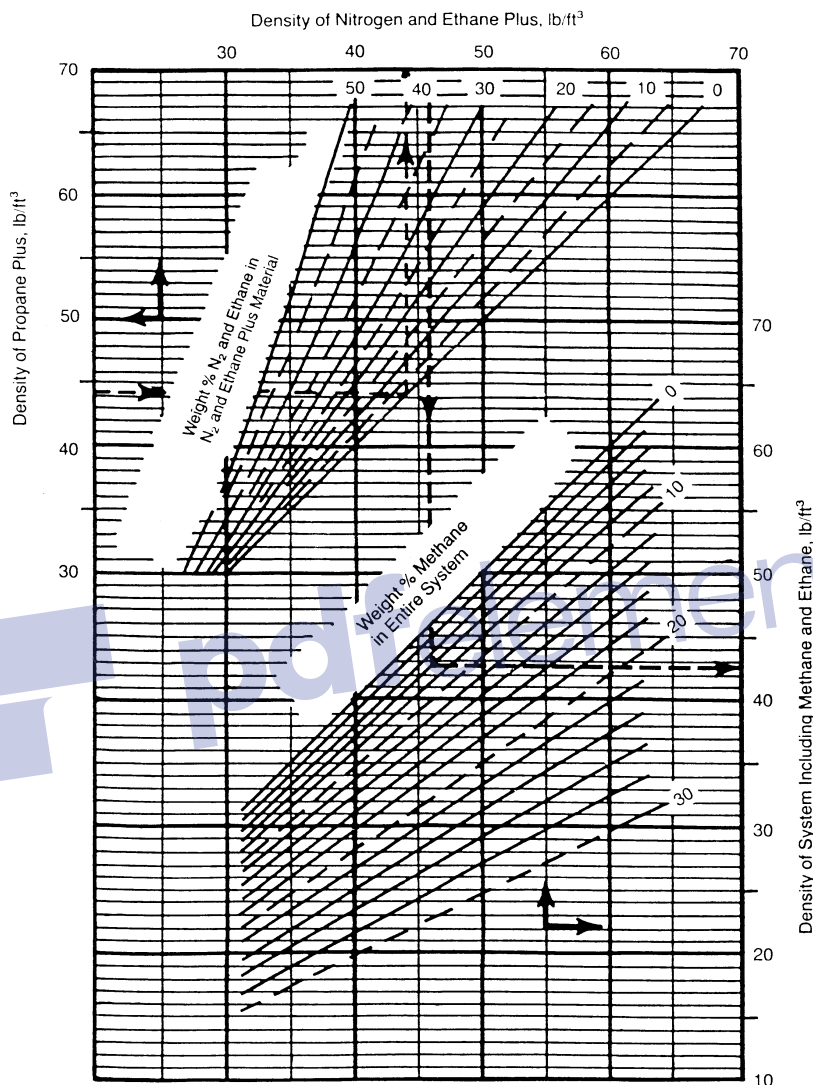


Figure 15-9. Standing and Katz density correlation. (Courtesy of the Gas Processors Suppliers Association, Engineering Data Book, 10th ed., 1987.)

Step 5. Correct the density at standard conditions to the actual pressure by reading the additive pressure correction factor, $\Delta\rho_p$, from Figure 15-10, or using the following expression:

$$\Delta\rho_p = \left[0.000167 + (0.016181)10^{-0.0425p_{sc}} \right] p - (10^{-8}) \left[0.299 + (263)10^{-0.0603p_{sc}} \right] p^2$$

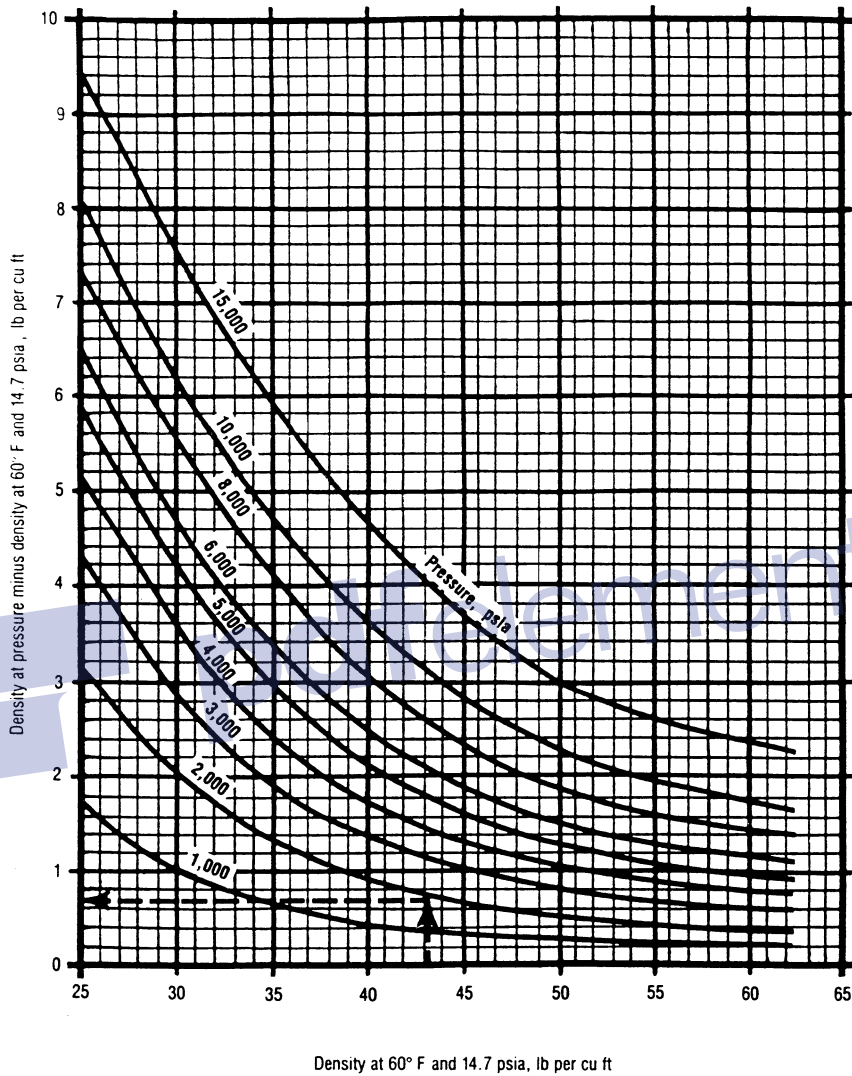


Figure 15-10. Density correction for compressibility of crude oils. (Courtesy of the Gas Processors Suppliers Association, Engineering Data Book, 10th ed., 1987.)

Step 6. Correct the density at 60°F and pressure to the actual temperature by reading the thermal expansion correction term, $\Delta\rho_T$, from Figure 15-11, or from:

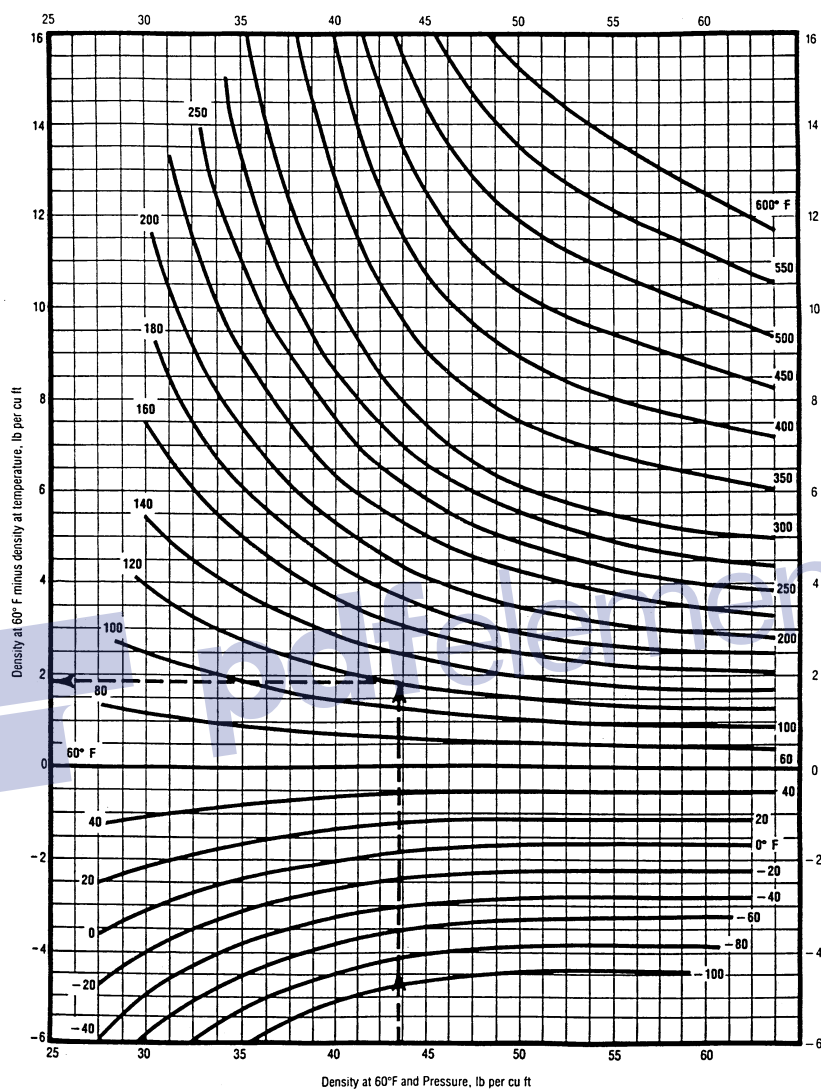


Figure 15-11. Density correction for isothermal expansion of crude oils. (Courtesy of the Gas Processors Suppliers Association, Engineering Data Book, 10th ed., 1987.)

$$\Delta\rho_T = (T - 520) \left[0.0133 + 152.4(\rho_{sc} + \Delta\rho_p)^{-2.45} \right] - (T - 520)^2 \left[8.1(10^{-6}) - (0.0622)10^{-0.0764(\rho_{sc} + \Delta\rho_p)} \right]$$

where T is the system temperature in °R.

Example 15-7

A crude oil system has the following composition.

| Component | x_i |
|-----------------|-------|
| C ₁ | 0.45 |
| C ₂ | 0.05 |
| C ₃ | 0.05 |
| C ₄ | 0.03 |
| C ₅ | 0.01 |
| C ₆ | 0.01 |
| C ₇₊ | 0.40 |

If the molecular weight and specific gravity of C₇₊ fractions are 215 and 0.87, respectively, calculate the density of the crude oil at 4,000 psia and 160°F by using the Standing and Katz method.

Solution

| Component | x_i | M_i | $m_i = x_i M_i$ | ρ_{oi} , lb/ft ^{3*} | $V_i = m_i / \rho_{oi}$ |
|-----------------|-------|-------|-----------------|-----------------------------------|-------------------------|
| C ₁ | 0.45 | 16.04 | 7.218 | — | — |
| C ₂ | 0.05 | 30.07 | 1.5035 | — | — |
| C ₃ | 0.05 | 44.09 | 2.2045 | 31.64 | 0.0697 |
| C ₄ | 0.03 | 58.12 | 1.7436 | 35.71 | 0.0488 |
| C ₅ | 0.01 | 72.15 | 0.7215 | 39.08 | 0.0185 |
| C ₆ | 0.01 | 86.17 | 0.8617 | 41.36 | 0.0208 |
| C ₇₊ | 0.40 | 215.0 | 86.00 | 54.288 [†] | 1.586 |
| | | | | $m_t = 100.253$ | $V_{C_{3+}} = 1.7418$ |

* From Table 1-2.

[†] $\rho_{C_{7+}} = (0.87)(62.4) = 54.288$.

Step 1. Calculate the weight percent of C₁ in the entire system and the weight percent of C₂ in the ethane-plus fraction:

$$(m_{C_1})_{C_{1+}} = \left[\frac{7.218}{100.253} \right] 100 = 7.2\%$$

$$(m_{C_2})_{C_{2+}} = \left[\frac{1.5035}{100.253 - 7.218} \right] 100 = 1.616\%$$

Step 2. Calculate the density of the propane-plus fraction:

$$\rho_{C_{3+}} = \frac{100.253 - 7.218 - 1.5035}{1.7418} = 52.55 \text{ lb/ft}^3$$

Step 3. Determine the density of the oil at standard conditions from Figure 15-9:

$$\rho_{sc} = 47.5 \text{ lb/ft}^3$$

Step 4. Correct for the pressure by using Figure 15-10:

$$\Delta\rho_p = 1.18 \text{ lb/ft}^3$$

Density of the oil at 4,000 psia and 60°F is then calculated by the expression:

$$\rho_{p,60} = \rho_{sc} + \Delta\rho_p = 47.5 + 1.18 = 48.68 \text{ lb/ft}^3$$

Step 5. From Figure 15-11, determine the thermal expansion correction factor:

$$\Delta\rho_T = 2.45 \text{ lb/ft}^3$$

Step 6. The required density at 4,000 psia and 160°F is:

$$\rho_0 = 48.68 - 2.45 = 46.23 \text{ lb/ft}^3$$

The Alani-Kennedy Method

Alani and Kennedy (1960) developed an equation to determine the molar liquid volume V_m of pure hydrocarbons over a wide range of temperature and pressure. The equation was then adopted to crude oils with the heavy hydrocarbons expressed as a heptanes-plus fraction, i.e., C_{7+} .

The Alani-Kennedy equation is similar in form to the van der Waals equation, which takes the following form:

$$V_m^3 - \left[\frac{RT}{p} + b \right] V_m^2 + \frac{aV_m}{p} - \frac{ab}{p} = 0 \quad (15-43)$$

where R = gas constant, 10.73 psia ft³/lb-mol °R

T = temperature, °R

p = pressure, psia

V_m = molecular volume, ft³/lb-mol

a, b = constants for pure substances

Alani and Kennedy considered the constants a and b to be functions of temperature and proposed these expressions for calculating the two parameters:

$$a = Ke^{n/T}$$

$$b = mT + c$$

where K , n , m , and c are constants for each pure component. Values of these constants are tabulated in Table 15-1. Table 15-1 contains no constants from which the values of the parameters a and b for heptanes-plus can be calculated. Therefore, Alani and Kennedy proposed the following equations for determining a and b of C_{7+} .

Table 15-1
Alani and Kennedy Coefficients

| Components | K | n | $m \times 10^4$ | c |
|--------------------|------------|------------|-----------------|------------|
| C_1 70° – 300°F | 9160.6413 | 61.893223 | 3.3162472 | 0.50874303 |
| C_1 301° – 460°F | 147.47333 | 3247.4533 | -14.072637 | 1.8326659 |
| C_2 100° – 249°F | 46,709.573 | -404.48844 | 5.1520981 | 0.52239654 |
| C_2 250° – 460°F | 17,495.343 | 34.163551 | 2.8201736 | 0.62309877 |
| C_3 | 20,247.757 | 190.24420 | 2.1586448 | 0.90832519 |
| i – C_4 | 32,204.420 | 131.63171 | 3.3862284 | 1.1013834 |
| n – C_4 | 33,016.212 | 146.15445 | 2.902157 | 1.1168144 |
| i – C_5 | 37,046.234 | 299.62630 | 2.1954785 | 1.4364289 |
| n – C_5 | 37,046.234 | 299.62630 | 2.1954785 | 1.4364289 |
| n – C_6 | 52,093.006 | 254.56097 | 3.6961858 | 1.5929406 |
| H_2S^* | 13,200.00 | 0 | 17.900 | 0.3945 |
| N_2^* | 4300.00 | 2.293 | 4.490 | 0.3853 |
| CO_2^* | 8166.00 | 126.00 | 1.8180 | 0.3872 |

* Values for nonhydrocarbon components as proposed by Lohrenz et al. (1964).

$$\ln(a_{C_{7+}}) = 3.8405985(10^{-3})(M)_{C_{7+}} - 9.5638281(10^{-4})\left(\frac{M}{\gamma}\right)_{C_{7+}}$$

$$+ \frac{261.80818}{T} + 7.3104464(10^{-6})(M)_{C_{7+}}^2 + 10.753517$$

$$b_{C_{7+}} = 0.03499274(M)_{C_{7+}} - 7.275403(\gamma)_{C_{7+}} + 2.232395(10^{-4})T$$

$$- 0.016322572\left(\frac{M}{\gamma}\right)_{C_{7+}} + 6.2256545$$

where $M_{C_{7+}}$ = molecular weight of C_{7+}
 $\gamma_{C_{7+}}$ = specific gravity of C_{7+}
 $a_{C_{7+}}$, $b_{C_{7+}}$ = constants of the heptanes-plus fraction
 T = temperature in °R

For hydrocarbon mixtures, the values of a and b of the mixture are calculated using the following mixing rules:

$$a_m = \sum_{i=1}^{C_{7+}} a_i x_i$$

$$b_m = \sum_{i=1}^{C_{7+}} b_i x_i$$

where the coefficients a_i and b_i refer to pure hydrocarbons at existing temperature, and x_i is the mole fraction in the mixture. The values of a_m and b_m are then used in Equation 15-43 to solve for the molar volume V_m . The density of the mixture at pressure and temperature of interest is determined from the following relationship:

$$\rho_o = \frac{M_a}{V_m}$$

where ρ_o = density of the crude oil, lb/ft³
 M_a = apparent molecular weight, i.e., $M_a = \sum x_i M_i$
 V_m = molar volume, ft³/lb-mol

The Alani and Kennedy method for calculating the density of liquids is summarized in the following steps:

Step 1. Calculate the constants a and b for each pure component from:

$$a = Ke^{n/T}$$

$$b = mT + c$$

Step 2. Determine $a_{C_{7+}}$ and $b_{C_{7+}}$.

Step 3. Calculate the values of coefficients a_m and b_m .

Step 4. Calculate molar volume V_m by solving Equation 15-43 for the smallest real root:

$$V_m^3 - \left[\frac{RT}{p} + b_m \right] V_m^2 + \frac{a_m V_m}{p} - \frac{a_m b_m}{p} = 0$$

Step 5. Compute the apparent molecular weight, M_a .

Step 6. Determine the density of the crude oil from:

$$\rho_0 = \frac{M_a}{V_m}$$

Example 15-8

A crude oil system has the composition:

| Component | x_i |
|--------------------|--------|
| CO ₂ | 0.0008 |
| N ₂ | 0.0164 |
| C ₁ | 0.2840 |
| C ₂ | 0.0716 |
| C ₃ | 0.1048 |
| i - C ₄ | 0.0420 |
| n - C ₄ | 0.0420 |
| i - C ₅ | 0.0191 |
| n - C ₅ | 0.0191 |
| C ₆ | 0.0405 |
| C ₇₊ | 0.3597 |

The following additional data are given:

$$M_{C_{7+}} = 252$$

$$\gamma_{C_{7+}} = 0.8424$$

$$\text{Pressure} = 1708.7 \text{ psia}$$

$$\text{Temperature} = 591^\circ\text{R}$$

Calculate the density of the crude oil.

Solution

Step 1. Calculate the parameters $a_{C_{7+}}$ and $b_{C_{7+}}$:

$$a_{C_{7+}} = 229,269.9$$

$$b_{C_{7+}} = 4.165811$$

Step 2. Calculate the mixture parameters a_m and b_m :

$$a_m = \sum_{i=1}^{C_{7+}} a_i x_i$$

$$a_m = 99,111.71$$

$$b_m = \sum_{i=1}^{C_{7+}} b_i x_i$$

$$b_m = 2.119383$$

Step 3. Solve Equation 15-43 for the molar volume:

$$V_m^3 - \left[\frac{RT}{p} + b_m \right] V_m^2 + \frac{a_m V_m}{p} - \frac{a_m b_m}{p} = 0$$

$$V_m = 2.528417$$

Step 4. Determine the apparent molecular weight of this mixture:

$$M_a = \sum x_i M_i$$

$$M_a = 113.5102$$

Step 5. Compute the density of the oil system:

$$\rho_0 = \frac{M_a}{V_m}$$

$$\rho_0 = \frac{113.5102}{2.528417} = 44.896 \text{ lb/ft}^3$$

EQUATIONS OF STATE

An equation of state (EOS) is an analytical expression relating the pressure p to the temperature T and the volume V . A proper description of this PVT relationship for real hydrocarbon fluids is essential in determining the volumetric and phase behavior of petroleum reservoir fluids and in predicting the performance of surface separation facilities.

The best known and the simplest example of an equation of state is the ideal gas equation, expressed mathematically by the expression:

$$p = \frac{RT}{V} \quad (15-44)$$

where V = gas volume in cubic feet per 1 mol of gas. This PVT relationship is only used to describe the volumetric behavior of real hydrocarbon gases at pressures close to the atmospheric pressure for which it was experimentally derived.

The extreme limitations of the applicability of Equation 15-44 prompted numerous attempts to develop an equation of state (EOS) suitable for describing the behavior of real fluids at extended ranges of pressures and temperatures.

The main objective of this chapter is to review developments and advances in the field of empirical cubic equations of state and demonstrate their applications in petroleum engineering.

The Van der Waals Equation of State

In developing the ideal gas EOS (Equation 15-44), two assumptions were made:

- **First assumption:** The volume of the gas molecules is insignificant compared to the volume of the container and distance between the molecules.
- **Second assumption:** There are no attractive or repulsive forces between the molecules or the walls of the container.

Van der Waals (1873) attempted to eliminate these two assumptions by developing an empirical equation of state for real gases. In his attempt to eliminate the first assumption, van der Waals pointed out that the gas molecules occupy a significant fraction of the volume at higher pressures and proposed that the volume of the molecules, as denoted by the

parameter b , be subtracted from the actual molar volume V in Equation 15-44, to give:

$$p = \frac{RT}{V - b}$$

where the parameter b is known as the co-volume and is considered to reflect the volume of molecules. The variable V represents the actual volume in cubic feet per 1 mol of gas.

To eliminate the second assumption, van der Waals subtracted a corrective term, as denoted by a/V^2 , from the above equation to account for the attractive forces between molecules. In a mathematical form, van der Waals proposed the following expression:

$$p = \frac{RT}{V - b} - \frac{a}{V^2} \quad (15-45)$$

where p = system pressure, psia

T = system temperature, °R

R = gas constant, 10.73 psi-ft³/lb-mol = °R

V = volume, ft³/mol

The two parameters a and b are constants characterizing the molecular properties of the individual components. The symbol a is considered a measure of the intermolecular attractive forces between the molecules. Equation 15-45 shows the following important characteristics:

1. At low pressures, the volume of the gas phase is large in comparison with the volume of the molecules. The parameter b becomes negligible in comparison with V and the attractive forces term a/V^2 becomes insignificant; therefore, the van der Waals equation reduces to the ideal gas equation (Equation 15-44).
2. At high pressure, i.e., $p \rightarrow \infty$, volume V becomes very small and approaches the value b , which is the actual molecular volume.

The van der Waals or any other equation of state can be expressed in a more generalized form as follows:

$$p = P_{\text{repulsive}} - P_{\text{attractive}}$$

where the repulsive pressure term $p_{\text{repulsive}}$ is represented by the term $RT/(V - b)$ and the attractive pressure term $p_{\text{attractive}}$ is described by a/V^2 .

In determining the values of the two constants a and b for any pure substance, van der Waals observed that the critical isotherm has a horizontal slope and an inflection point at the critical point, as shown in Figure 15-12. This observation can be expressed mathematically as follows:

$$\left[\frac{\partial p}{\partial V} \right]_{T_c, p_c} = 0, \quad \left[\frac{\partial^2 p}{\partial V^2} \right]_{T_c, p_c} = 0 \quad (15-46)$$

Differentiating Equation 15-45 with respect to the volume at the critical point results in:

$$\left[\frac{\partial p}{\partial V} \right]_{T_c, p_c} = \frac{-RT_c}{(V_c - b)^3} + \frac{2a}{V_c^3} = 0 \quad (15-47)$$

$$\left[\frac{\partial^2 p}{\partial V^2} \right]_{T_c, p_c} = \frac{2RT_c}{(V_c - b)^3} + \frac{6a}{V_c^4} = 0 \quad (15-48)$$

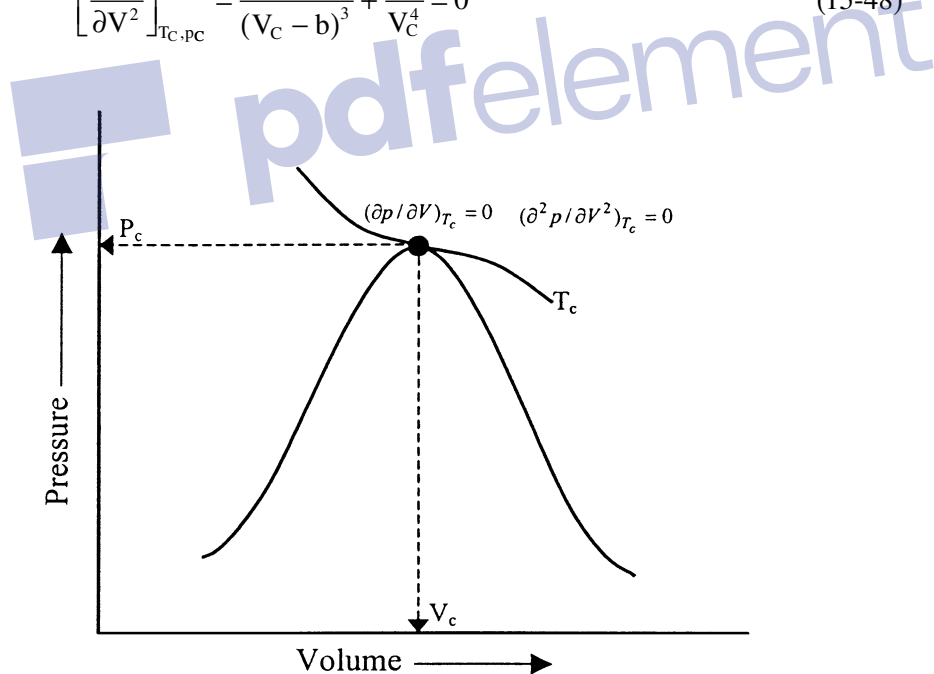


Figure 15-12. An idealized pressure-volume relationship for a pure compound.

Solving Equations 15-47 and 15-48 simultaneously for the parameters a and b gives:

$$b = \left(\frac{1}{3}\right)V_c \quad (15-49)$$

$$a = \left(\frac{8}{9}\right)RT_c V_c \quad (15-50)$$

Equation 15-49 suggests that the volume of the molecules b is approximately 0.333 of the critical volume V_c of the substance. Experimental studies reveal that the co-volume b is in the range of 0.24 to 0.28 of the critical volume and pure component.

By applying Equation 15-45 to the critical point (i.e., by setting $T = T_c$, $p = p_c$, and $V = V_c$) and combining with Equations 15-49 and 15-50, we get:

$$p_c V_c = (0.375)RT_c \quad (15-51)$$

Equation 15-51 shows that regardless of the type of substance, the van der Waals EOS produces a universal critical gas compressibility factor Z_c of 0.375. Experimental studies show that Z_c values for substances range between 0.23 and 0.31.

Equation 15-51 can be combined with Equations 15-49 and 15-50 to give a more convenient and traditional expression for calculating the parameters a and b to yield:

$$a = \Omega_a \frac{R^2 T_c^2}{p_c} \quad (15-52)$$

$$b = \Omega_b \frac{RT_c}{p_c} \quad (15-53)$$

where R = gas constant, 10.73 psia-ft³/lb-mol-°R
 p_c = critical pressure, psia
 T_c = critical temperature, °R
 Ω_a = 0.421875
 Ω_b = 0.125

Equation 15-45 can also be expressed in a cubic form in terms of the volume V as follows:

$$V^3 - \left(b + \frac{RT}{p}\right)V^2 + \left(\frac{a}{p}\right)V - \left(\frac{ab}{p}\right) = 0 \quad (15-54)$$

Equation 15-54 is usually referred to as the van der Waals two-parameter cubic equation of state. The term *two-parameter* refers to the parameters a and b . The term *cubic equation of state* implies an equation that, if expanded, would contain volume terms to the first, second, and third power.

Perhaps the most significant feature of Equation 15-54 is its ability to describe the liquid-condensation phenomenon and the passage from the gas to the liquid phase as the gas is compressed. This important feature of the van der Waals EOS is discussed below in conjunction with Figure 15-13.

Consider a pure substance with a p - V behavior as shown in Figure 15-13. Assume that the substance is kept at a constant temperature T below its critical temperature. At this temperature, Equation 15-54 has three real roots (volumes) for each specified pressure p . A typical solution of Equation 15-54 at constant temperature T is shown graphically by the dashed isotherm: the constant temperature curve DWEZB in Figure 15-13. The three values of V are the intersections B , E , and D on the horizontal line, corresponding to a fixed value of the pressure. This dashed calculated line (DWEZB) then appears to give a continuous

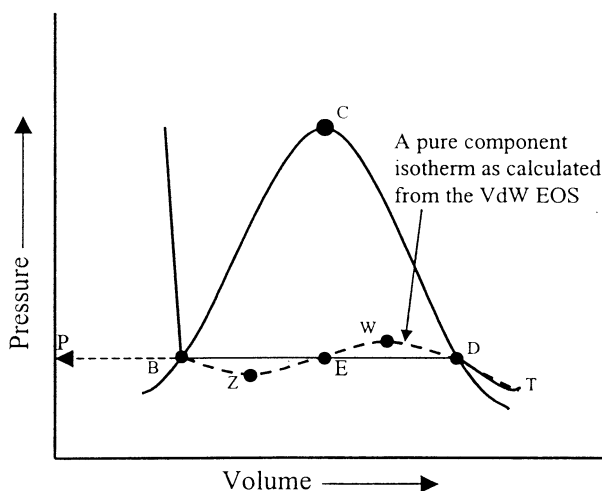


Figure 15-13. Pressure-volume diagram for a pure component.

transition from the gaseous phase to the liquid phase, but in reality, the transition is abrupt and discontinuous, with both liquid and vapor existing along the straight horizontal line DB. Examining the graphical solution of Equation 15-54 shows that the largest root (volume), as indicated by point D, corresponds to the volume of the saturated vapor, while the smallest positive volume, as indicated by point B, corresponds to the volume of the saturated liquid. The third root, point E, has no physical meaning. Note that these values become identical as the temperature approaches the critical temperature T_c of the substance.

Equation 15-54 can be expressed in a more practical form in terms of the compressibility factor Z . Replacing the molar volume V in Equation 15-54 with ZRT/p gives:

$$Z^3 - (1 + B)Z^2 + AZ - AB = 0 \quad (15-55)$$

where

$$A = \frac{ap}{R^2T^2} \quad (15-56)$$

$$B = \frac{bp}{RT} \quad (15-57)$$

Z = compressibility factor

p = system pressure, psia

T = system temperature, °R

Equation 15-55 yields one real root¹ in the one-phase region and three real roots in the two-phase region (where system pressure equals the vapor pressure of the substance). In the latter case, the largest root corresponds to the compressibility factor of the vapor phase Z^V , while the smallest positive root corresponds to that of the liquid Z^L .

An important practical application of Equation 15-55 is for calculating density calculations, as illustrated in the following example.

Example 15-9

A pure propane is held in a closed container at 100°F. Both gas and liquid are present. Calculate, by using the van der Waals EOS, the density of the gas and liquid phases.

¹ In some supercritical regions, Equation 15-55 can yield three real roots for Z . From the three real roots, the largest root is the value of the compressibility with physical meaning.

Solution

Step 1. Determine the vapor pressure p_v of the propane from the Cox chart. This is the only pressure at which two phases can exist at the specified temperature:

$$p_v = 185 \text{ psi}$$

Step 2. Calculate parameters a and b from Equations 15-52 and 15-53, respectively.

$$a = \Omega_a \frac{R^2 T_c^2}{P_c}$$

$$a = 0.421875 \frac{(10.73)^2 (666)^2}{616.3} = 34,957.4$$

and

$$b = \Omega_b \frac{RT_c}{P_c}$$

$$b = 0.125 \frac{10.73(666)}{616.3} = 1.4494$$

Step 3. Compute coefficients A and B by applying Equations 15-56 and 15-57, respectively.

$$A = \frac{ap}{R^2 T^2}$$

$$A = \frac{(34,957.4)(185)}{(10.73)^2 (560)^2} = 0.179122$$

$$B = \frac{bp}{RT}$$

$$B = \frac{(1.4494)(185)}{(10.73)(560)} = 0.044625$$

Step 4. Substitute the values of A and B into Equation 15-55 to give:

$$Z^3 - (1+B)Z^2 + AZ - AB = 0$$

$$Z^3 - 1.044625Z^2 + 0.179122Z - 0.007993 = 0$$

Step 5. Solve the above third-degree polynomial by extracting the largest and smallest roots of the polynomial by using the appropriate direct or iterative method to give:

$$Z^v = 0.72365$$

$$Z^L = 0.07534$$

Step 6. Solve for the density of the gas and liquid phases by using Equation 2-17:

$$\rho_g = \frac{pM}{Z^v RT}$$

$$\rho_g = \frac{(185)(44.0)}{(0.72365)(10.73)(560)} = 1.87 \text{ lb/ft}^3$$

and

$$\rho_L = \frac{pM}{Z^L RT}$$

$$\rho_L = \frac{(185)(44)}{(0.07534)(10.73)(560)} = 17.98 \text{ lb/ft}^3$$

The van der Waals equation of state, despite its simplicity, provides a correct description, at least qualitatively, of the PVT behavior of substances in the liquid and gaseous states. Yet it is not accurate enough to be suitable for design purposes.

With the rapid development of computers, the EOS approach for the calculation of physical properties and phase equilibria proved to be a powerful tool, and much energy was devoted to the development of new and accurate equations of state. These equations, many of them a modification of the van der Waals equation of state, range in complexity from simple expressions containing 2 or 3 parameters to complicated forms containing more than 50 parameters. Although the complexity of any equation of state presents no computational problem, most authors prefer to retain the simplicity found in the van der Waals cubic equation while improving its accuracy through modifications.

All equations of state are generally developed for pure fluids first, and then extended to mixtures through the use of mixing rules. These mixing

rules are simply means of calculating mixture parameters equivalent to those of pure substances.

Redlich-Kwong Equation of State

Redlich and Kwong (1949) demonstrated that by a simple adjustment, the van der Waals attractive pressure term a/V^2 could considerably improve the prediction of the volumetric and physical properties of the vapor phase. The authors replaced the attractive pressure term with a generalized temperature dependence term. Their equation has the following form:

$$p = \frac{RT}{V - b} - \frac{a}{V(V + b)\sqrt{T}} \quad (15-58)$$

where T is the system temperature in $^{\circ}\text{R}$.

Redlich and Kwong (1949), in their development of the equation, noted that as the system pressure becomes very large, i.e., $p \rightarrow \infty$, the molar volume V of the substance shrinks to about 26% of its critical volume regardless of the system temperature. Accordingly, they constructed Equation 15-58 to satisfy the following condition:

$$b = 0.26V_c \quad (15-59)$$

Imposing the critical point conditions (as expressed by Equation 15-46) on Equation 15-58 and solving the resulting equations simultaneously gives:

$$a = \Omega_a \frac{R^2 T_c^{2.5}}{p_c} \quad (15-60)$$

$$b = \Omega_b \frac{RT_c}{p_c} \quad (15-61)$$

where $\Omega_a = 0.42747$ and $\Omega_b = 0.08664$. Equating Equation 15-61 with 15-59 gives:

$$p_c V_c = 0.333RT_c \quad (15-62)$$

Equation 15-62 shows that the Redlich-Kwong EOS produces a universal critical compressibility factor (Z_c) of 0.333 for all substances. As indicated earlier, the critical gas compressibility ranges from 0.23 to 0.31 for most of the substances.

Replacing the molar volume V in Equation 15-58 with ZRT/p gives:

$$Z^3 - Z^2 + (A - B - B^2)Z - AB = 0 \quad (15-63)$$

where

$$A = \frac{ap}{R^2T^{2.5}} \quad (15-64)$$

$$B = \frac{bp}{RT} \quad (15-65)$$

As in the van der Waals EOS, Equation 15-63 yields one real root in the one-phase region (gas-phase region or liquid-phase region), and three real roots in the two-phase region. In the latter case, the **largest root** corresponds to the compressibility factor of the gas phase Z^V while the **smallest positive root** corresponding to that of the liquid Z^L .

Example 15-10

Rework Example 15-9 by using the Redlich-Kwong equation of state.

Solution

Step 1. Calculate the parameters a , b , A , and B :

$$a = 0.42747 \frac{(10.73)^2 (666)^{2.5}}{616.3} = 914,110.1$$

$$b = 0.08664 \frac{(10.73)(666)}{616.3} = 1.0046$$

$$A = \frac{(914,110.1)(185)}{(10.73)^2 (560)^{2.5}} = 0.197925$$

$$B = \frac{(1.0046)(185)}{(10.73)(560)} = 0.03093$$

Step 2. Substitute parameters A and B into Equation 15-63, and extract the largest and the smallest root, to give:

$$Z^3 - Z^2 + 0.1660384Z - 0.0061218 = 0$$

$$\text{Largest root } Z^V = 0.802641$$

$$\text{Smallest root } Z^L = 0.0527377$$

Step 3. Solve for the density of the liquid phase and gas phase:

$$\rho = \frac{pM}{ZRT}$$

$$\rho^L = \frac{(185)(44)}{(0.0527377)(10.73)(560)} = 25.7 \text{ lb/ft}^3$$

$$\rho^v = \frac{(185)(44)}{(0.802641)(10.73)(560)} = 1.688 \text{ lb/ft}^3$$

Redlich and Kwong extended the application of their equation to hydrocarbon liquid or gas mixtures by employing the following mixing rules:

$$a_m = \left[\sum_{i=1}^n x_i \sqrt{a_i} \right]^2 \quad (15-66)$$

$$b_m = \sum_{i=1}^n [x_i b_i] \quad (15-67)$$

where n = number of components in mixture

a_i = Redlich-Kwong a parameter for the i 'th component as given by Equation 15-60

b_i = Redlich-Kwong b parameter for the i 'th component as given by Equation 15-61

a_m = parameter a for mixture

b_m = parameter b for mixture

x_i = mole fraction of component i in the liquid phase

To calculate a_m and b_m for a hydrocarbon gas mixture with a composition of y_i , use Equations 15-66 and 15-67 and replace x_i with y_i :

$$a_m = \left[\sum_{i=1}^n y_i \sqrt{a_i} \right]^2$$

$$b_m = \sum_{i=1}^n [y_i b_i]$$

Equation 15-63 gives the compressibility factor of the gas phase or the liquid with the coefficients A and B as defined by Equations 15-64 and 15-65.

The application of the Redlich-Kwong equation of state for hydrocarbon mixtures can be best illustrated through the following two examples.

Example 15-11

Calculate the density of a crude oil with the following composition at 4,000 psia and 160°F. Use the Redlich-Kwong EOS.

| Component | x_i | M | p_c | T_c |
|--------------------|-------|--------|-------|--------|
| C ₁ | 0.45 | 16.043 | 666.4 | 343.33 |
| C ₂ | 0.05 | 30.070 | 706.5 | 549.92 |
| C ₃ | 0.05 | 44.097 | 616.0 | 666.06 |
| n - C ₄ | 0.03 | 58.123 | 527.9 | 765.62 |
| n - C ₅ | 0.01 | 72.150 | 488.6 | 845.8 |
| C ₆ | 0.01 | 84.00 | 453 | 923 |
| C ₇₊ | 0.40 | 215 | 285 | 1287 |

Solution

Step 1. Determine the parameters a_i and b_i for each component by using Equations 15-60 and 15-61.

| Component | a_i | b_i |
|-----------------|------------|-----------|
| C ₁ | 161,044.3 | 0.4780514 |
| C ₂ | 493,582.7 | 0.7225732 |
| C ₃ | 914,314.8 | 1.004725 |
| C ₄ | 1,449,929 | 1.292629 |
| C ₅ | 2,095,431 | 1.609242 |
| C ₆ | 2,845,191 | 1.945712 |
| C ₇₊ | 1.022348E7 | 4.191958 |

Step 2. Calculate the mixture parameters a_m and b_m from Equations 15-66 and 15-67 to give:

$$a_m = \left[\sum_{i=1}^n x_i \sqrt{a_i} \right]^2 = 2,591,967$$

and

$$b_m = \sum_{i=1}^n [x_i b_i] = 2.0526$$

Step 3. Compute the coefficients A and B by using Equations 15-64 and 15-65 to produce:

$$A = \frac{a_m p}{R^2 T^{2.5}} = \frac{2,591,967(4000)}{10.73^2 (620)^{2.5}} = 9.406539$$

$$B = \frac{b_m p}{RT} = \frac{2.0526(4000)}{10.73(620)} = 1.234049$$

Step 4. Solve Equation 15-63 for the largest positive root to yield:

$$Z^3 - Z^2 + 6.93845Z - 11.60813 = 0$$

$$Z^L = 1.548126$$

Step 5. Calculate the apparent molecular weight of the crude oil:

$$M_a = \sum x_i M_i$$

$$M_a = 100.2547$$

Step 6. Solve for the density of the crude oil:

$$\rho^L = \frac{p M_a}{Z^L R T}$$

$$\rho^L = \frac{(4000)(100.2547)}{(10.73)(620)(1.548120)} = 38.93 \text{ lb/ft}^3$$

Notice that liquid density, as calculated by Standing's correlation, gives a value of 46.23 lb/ft³.

Example 15-12

Calculate the density of a gas phase with the following composition at 4,000 psia and 160°F. Use the Redlich-Kwong EOS.

| Component | y_i | M | P_c | T_c |
|-----------------|-------|--------|-------|--------|
| C ₁ | 0.86 | 16.043 | 666.4 | 343.33 |
| C ₂ | 0.05 | 30.070 | 706.5 | 549.92 |
| C ₃ | 0.05 | 44.097 | 616.0 | 666.06 |
| C ₄ | 0.02 | 58.123 | 527.9 | 765.62 |
| C ₅ | 0.01 | 72.150 | 488.6 | 845.8 |
| C ₆ | 0.005 | 84.00 | 453 | 923 |
| C ₇₊ | 0.005 | 215 | 285 | 1287 |

Solution

Step 1. Calculate a_m and b_m by using Equations 15-66 and 15-67 to give:

$$a_m = \left[\sum_{i=1}^n y_i \sqrt{a_i} \right]^2$$

$$a_m = 241,118$$

$$b_m = \sum b_i x_i$$

$$b_m = 0.5701225$$

Step 2. Calculate the coefficients A and B by applying Equations 15-64 and 15-65 to yield:

$$A = \frac{a_m P}{R^2 T^{2.5}} = \frac{241,118(4000)}{10.73^2 (620)^{2.5}} = 0.8750$$

$$B = \frac{b_m P}{RT} = \frac{0.5701225(4000)}{10.73(620)} = 0.3428$$

Step 3. Solve Equation 15-63 for Z^V to give:

$$Z^3 - Z^2 + 0.414688Z - 0.29995 = 0$$

$$Z^V = 0.907$$

Step 4. Calculate the apparent density of the gas mixture:

$$M_a = \sum y_i M_i = 20.89$$

$$\rho^v = \frac{p M_a}{Z^V R T}$$

$$\rho^v = \frac{(4000)(20.89)}{(10.73)(620)(0.907)} = 13.85 \text{ lb/ft}^3$$

Soave-Redlich-Kwong Equation of State and Its Modifications

One of the most significant milestones in the development of cubic equations of state was the publication by Soave (1972) of a modification to the evaluation of parameter a in the attractive pressure term of the Redlich-Kwong equation of state (Equation 15-68). Soave replaced the term $a/T^{0.5}$ in Equation 15-58 with a more generalized **temperature-dependent term**, as denoted by $(a\alpha)$, to give:

$$p = \frac{RT}{V - b} - \frac{a\alpha}{V(V + b)} \quad (15-68)$$

where α is a dimensionless factor that becomes unity at $T = T_c$. At temperatures other than critical temperature, the parameter α is defined by the following expression:

$$\alpha = [1 + m(1 - \sqrt{T_r})]^2 \quad (15-69)$$

The parameter m is correlated with the acentric factor to give:

$$m = 0.480 + 1.574\omega - 0.176\omega^2 \quad (15-70)$$

where T_r = reduced temperature T/T_c
 ω = acentric factor of the substance
 T = system temperature, °R

For any pure component, the constants a and b in Equation 15-68 are found by imposing the classical van der Waals critical point constraints (Equation 15-46) on Equation 15-68, and solving the resulting equations, to give:

$$a = \Omega_a \frac{R^2 T_c^2}{p_c} \quad (15-71)$$

$$b = \Omega_b \frac{RT_c}{p_c} \quad (15-72)$$

where Ω_a and Ω_b are the Soave-Redlich-Kwong (SRK) dimensionless pure component parameters and have the following values:

$$\Omega_a = 0.42747 \quad \text{and} \quad \Omega_b = 0.08664$$

Edmister and Lee (1986) showed that the two parameters a and b can be determined more conveniently by considering the critical isotherm:

$$(V - V_c)^3 = V^3 - [3V_c]V^2 + [3V_c^2]V - V_c^3 = 0 \quad (15-73)$$

Equation 15-27 can also be put into a cubic form to give:

$$V^3 - \left[\frac{RT}{p} \right] V^2 + \left[\frac{a\alpha}{p} - \frac{bRT}{p} - b^2 \right] V - \left[\frac{(a\alpha)b}{p} \right] = 0 \quad (15-74)$$

At the critical point, the coefficient $\alpha = 1$ and the above two expressions are essentially identical. Equating the like terms gives:

$$3V_c = \frac{RT_c}{p_c} \quad (15-75)$$

$$3V_c^2 = \frac{a}{p_c} - \frac{bRT_c}{p_c} - b^2 \quad (15-76)$$

and

$$V_c^3 = \frac{ab}{p_c} \quad (15-77)$$

Solving the above equations for parameters a and b yields expressions for the parameters as given by Equations 15-71 and 15-72.

Equation 15-75 indicates that the SRK equation of state gives a universal critical gas compressibility factor of 0.333. Combining Equation 15-34 with 15-72 gives:

$$b = 0.26V_c$$

Introducing the compressibility factor Z into Equation 15-33 by replacing the molar volume V in the equation with (ZRT/p) and rearranging gives:

$$Z^3 - Z^2 + (A - B - B^2)Z - AB = 0 \quad (15-78)$$

with

$$A = \frac{(a\alpha)p}{(RT)^2} \quad (15-79)$$

$$B = \frac{bp}{RT} \quad (15-80)$$

where p = system pressure, psia
 T = system temperature, °R
 R = 10.730 psia ft³/lb-mol-°R

Example 15-13

Rework Example 15-9 and solve for the density of the two phases by using the SRK EOS.

Solution

Step 1. Determine the critical pressure, critical temperature, and acentric factor from Table 1-2 of Chapter 1 to give:

$$\begin{aligned}T_c &= 666.01^\circ\text{R} \\ p_c &= 616.3 \text{ psia} \\ \omega &= 0.1524\end{aligned}$$

Step 2. Calculate the reduced temperature.

$$T_r = 560/666.01 = 0.8408$$

Step 3. Calculate the parameter m by applying Equation 15-70 to yield:

$$\begin{aligned}m &= 0.480 + 1.574\omega - 0.176\omega^2 \\ m &= 0.480 + 1.574(0.1524) - 0.176(1.524)^2 = 0.7051\end{aligned}$$

Step 4. Solve for the parameter a by using Equation 15-69 to give:

$$\alpha = \left[m + (1 - \sqrt{T_r}) \right]^2 = 1.120518$$

Step 5. Compute the coefficients a and b by applying Equations 15-71 and 15-72 to yield:

$$\begin{aligned}a &= 0.42747 \frac{10.73^2 (666.01)^2}{616.3} = 35,427.6 \\ b &= 0.08664 \frac{10.73(666.01)}{616.3} 1.00471\end{aligned}$$

Step 6. Calculate the coefficients A and B from Equations 15-79 and 15-80, to produce:

$$A = \frac{(a\alpha)p}{R^2T^2}$$

$$A = \frac{(35,427.6)(1.120518)185}{10.73^2(560)^2} = 0.203365$$

$$B = \frac{bp}{RT}$$

$$B = \frac{(1.00471)(185)}{(10.73)(560)} = 0.034658$$

Step 7. Solve Equation 15-78 for Z^L and Z^V :

$$Z^3 - Z^2 + (A - B - B^2)Z + AB = 0$$

$$Z^3 - Z^2 + (0.203365 - 0.034658 - 0.034658^2)Z + (0.203365)(0.034658) = 0$$

Solving the above third-degree polynomial gives:

$$Z^L = 0.06729$$

$$Z^V = 0.80212$$

Step 8. Calculate the gas and liquid density to give:

$$\rho = \frac{pM}{ZRT}$$

$$\rho^v = \frac{(185)(44.0)}{(0.802121)(10.73)(560)} = 1.6887 \text{ lb/ft}^3$$

$$\rho^L = \frac{(185)(44.0)}{(0.06729)(10.73)(560)} = 20.13 \text{ lb/ft}^3$$

To use Equation 15-78 with mixtures, mixing rules are required to determine the terms $(a\alpha)$ and b for the mixtures. Soave adopted the following mixing rules:

$$(a\alpha)_m = \sum_i \sum_j [x_i x_j \sqrt{a_i a_j \alpha_i \alpha_j} (1 - k_{ij})] \quad (15-81)$$

$$b_m = \sum_i [x_i b_i] \quad (15-82)$$

with

$$A = \frac{(a\alpha)_m p}{(RT)^2} \quad (15-83)$$

and

$$B = \frac{b_m P}{RT} \quad (15-84)$$

The parameter k_{ij} is an empirically determined correction factor (called the binary interaction coefficient) that is designed to characterize any binary system formed by component i and component j in the hydrocarbon mixture.

These binary interaction coefficients are used to model the intermolecular interaction through empirical adjustment of the $(a\alpha)_m$ term as represented mathematically by Equation 15-81. They are dependent on the difference in molecular size of components in a binary system and they are characterized by the following properties:

- The interaction between hydrocarbon components increases as the relative difference between their molecular weights increases:

$$k_{i, j+1} > k_{i, j}$$

- Hydrocarbon components with the same molecular weight have a binary interaction coefficient of zero:

$$k_{i, i} = 0$$

- The binary interaction coefficient matrix is symmetric:

$$k_{j, i} = k_{i, j}$$

Slot-Petersen (1987) and Vidal and Daubert (1978) presented a theoretical background to the meaning of the interaction coefficient and techniques for determining their values. Graboski and Daubert (1978) and Soave (1972) suggested that no binary interaction coefficients are required for hydrocarbon systems. However, with nonhydrocarbons present, binary interaction parameters can greatly improve the volumetric and phase behavior predictions of the mixture by the SRK EOS.

In solving Equation 15-73 for the compressibility factor of the liquid phase, the composition of the liquid x_i is used to calculate the coefficients A and B of Equations 15-83 and 15-84 through the use of the mixing rules as described by Equations 15-81 and 15-82. For determining the compressibility factor of the gas phase Z^g , the above outlined procedure is used with composition of the gas phase y_i replacing x_i .

Example 15-14

A two-phase hydrocarbon system exists in equilibrium at 4,000 psia and 160°F. The system has the following composition:

| Component | x_i | y_i |
|-----------------|-------|-------|
| C ₁ | 0.45 | 0.86 |
| C ₂ | 0.05 | 0.05 |
| C ₃ | 0.05 | 0.05 |
| C ₄ | 0.03 | 0.02 |
| C ₅ | 0.01 | 0.01 |
| C ₆ | 0.01 | 0.005 |
| C ₇₊ | 0.40 | 0.005 |

The heptanes-plus fraction has the following properties:

$$M = 215$$

$$p_c = 285 \text{ psia}$$

$$T_c = 700^\circ\text{F}$$

$$\omega = 0.52$$

Assuming $k_{ij} = 0$, calculate the density of each phase by using the SRK EOS.

Solution

Step 1. Calculate the parameters α , a , and b by applying Equations 15-64, 15-71, and 15-72.

| Component | α_i | a_i | b_i |
|-----------------|------------|-----------|--------|
| C ₁ | 0.6869 | 8689.3 | 0.4780 |
| C ₂ | 0.9248 | 21,040.8 | 0.7725 |
| C ₃ | 1.0502 | 35,422.1 | 1.0046 |
| C ₄ | 1.1616 | 52,390.3 | 1.2925 |
| C ₅ | 1.2639 | 72,041.7 | 1.6091 |
| C ₆ | 1.3547 | 94,108.4 | 1.9455 |
| C ₇₊ | 1.7859 | 232,367.9 | 3.7838 |

Step 2. Calculate the mixture parameters $(a\alpha)_m$ and b_m for the gas phase and liquid phase by applying Equations 15-81 and 15-82 to give:

- **For the gas phase using y_i :**

$$(\alpha\alpha)_m = \sum_i \sum_j \left[y_i y_j \sqrt{a_i a_j \alpha_i \alpha_j} (1 - k_{ij}) \right] = 9219.3$$

$$b_m = \sum_i [y_i b_i] = 0.5680$$

- **For the liquid phase using x_i :**

$$(\alpha\alpha)_m = \sum_i \sum_j \left[x_i x_j \sqrt{a_i a_j \alpha_i \alpha_j} (1 - k_{ij}) \right] = 104,362.9$$

$$b_m = \sum_i [x_i b_i] = 0.18893$$

Step 3. Calculate the coefficients A and B for each phase by applying Equations 15-83 and 15-84 to yield:

- **For the gas phase:**

$$A = \frac{(\alpha\alpha)_m p}{R^2 T^2} = \frac{(9219.3)(4000)}{(10.73)^2 (620)^2} = 0.8332$$

$$B = \frac{b_m p}{RT} = \frac{(0.5680)(4000)}{(10.73)(620)} = 0.3415$$

- **For the liquid phase:**

$$A = \frac{(\alpha\alpha)_m p}{R^2 T^2} = \frac{(104,362.9)(4000)}{(10.73)^2 (620)^2} = 9.4324$$

$$B = \frac{b_m p}{RT} = \frac{(1.8893)(4000)}{(10.73)(620)} = 1.136$$

Step 4. Solve Equation 15-78 for the compressibility factor of the gas phase to produce:

$$Z^3 - Z^2 + (A - B - B^2)Z + AB = 0$$

$$Z^3 - Z^2 + (0.8332 - 0.3415 - 0.3415^2)Z + (0.8332)(0.3415) = 0$$

Solving the above polynomial for the largest root gives:

$$Z^v = 0.9267$$

Step 5. Solve Equation 15-78 for the compressibility factor of the liquid phase to produce:

$$Z^3 - Z^2 + (A - B - B^2)Z + AB = 0$$

$$Z^3 - Z^2 + (9.4324 - 1.136 - 1.136^2)Z + (9.4324)(1.136) = 0$$

Solving the above polynomial for the smallest root gives:

$$Z^L = 1.4121$$

Step 6. Calculate the apparent molecular weight of the gas phase and liquid phase from their composition, to yield:

- **For the gas phase:**

$$M_a = \sum y_i M_i = 20.89$$

- **For the liquid phase:**

$$M_a = \sum x_i M_i = 100.25$$

Step 7. Calculate the density of each phase:

$$\rho = \frac{pM_a}{RTZ}$$

- **For the gas phase:**

$$\rho^v = \frac{(4000)(20.89)}{(10.73)(620)(0.9267)} = 13.556 \text{ lb/ft}^3$$

- **For the liquid phase:**

$$\rho^L = \frac{(4000)(100.25)}{(10.73)(620)(1.4121)} = 42.68 \text{ lb/ft}^3$$

It is appropriate at this time to introduce and define the concept of the fugacity and the fugacity coefficient of the component. The **fugacity** f is a measure of the molar Gibbs energy of a real gas. It is evident from the definition that the fugacity has the units of pressure; in fact, the fugacity may be looked on as a vapor pressure modified to correctly represent the escaping tendency of the molecules from one phase into the other. In a mathematical form, the fugacity of a pure component is defined by the following expression:

$$f = p \exp \left[\int_0^p \left(\frac{Z-1}{p} \right) dp \right] \quad (15-85)$$

where f = fugacity, psia
 p = pressure, psia
 Z = compressibility factor

The ratio of the fugacity to the pressure, i.e., f/p , is called the **fugacity coefficient** Φ and is calculated from Equation 15-85 as:

$$\frac{f}{p} = \Phi = \exp \left[\int_0^p \left(\frac{Z-1}{p} \right) dp \right]$$

Soave applied the above-generalized thermodynamic relationship to Equation 15-68 to determine the fugacity coefficient of a pure component:

$$\ln \left(\frac{f}{p} \right) = \ln(\Phi) = Z - 1 - \ln(Z - B) - \frac{A}{B} \ln \left[\frac{Z + B}{Z} \right] \quad (15-86)$$

In practical petroleum engineering applications, we are concerned with the phase behavior of the hydrocarbon liquid mixture, which, at a specified pressure and temperature, is in equilibrium with a hydrocarbon gas mixture at the same pressure and temperature.

The component fugacity in each phase is introduced to develop a criterion for thermodynamic equilibrium. Physically, the fugacity of a component i in one phase with respect to the fugacity of the component in a second phase is a measure of the potential for transfer of the component between phases. The phase with the lower component fugacity accepts the component from the phase with a higher component fugacity. Equal fugacities of a component in the two phases results in a zero net transfer. A zero transfer for all components implies a hydrocarbon system that is in thermodynamic equilibrium. Therefore, the condition of the thermodynamic equilibrium can be expressed mathematically by:

$$f_i^v = f_i^l \quad 1 \leq i \leq n \quad (15-87)$$

where f_i^v = fugacity of component i in the gas phase, psi
 f_i^l = fugacity of component i in the liquid phase, psi
 n = number of components in the system

The fugacity coefficient of component i in a hydrocarbon liquid mixture or hydrocarbon gas mixture is a function of:

- System pressure
- Mole fraction of the component
- Fugacity of the component

For a component i in the gas phase, the fugacity coefficient is defined as:

$$\Phi_i^y = \frac{f_i^y}{y_i p} \quad (15-88)$$

For a component i in the liquid phase, the fugacity coefficient is:

$$\Phi_i^l = \frac{f_i^l}{x_i p} \quad (15-89)$$

where Φ_i^y = fugacity coefficient of component i in the vapor phase
 Φ_i^l = fugacity coefficient of component i in the liquid phase

It is clear that at equilibrium $f_i^l = f_i^y$, the equilibrium ratio K_i as previously defined by Equation 15-1, i.e., $K_i = y_i/x_i$, can be redefined in terms of the fugacity of components as:

$$K_i = \frac{[f_i^l/(x_i p)]}{[f_i^y/(y_i p)]} = \frac{\Phi_i^l}{\Phi_i^y} \quad (15-90)$$

Reid, Prausnitz, and Sherwood (1977) defined the fugacity coefficient of component i in a hydrocarbon mixture by the following generalized thermodynamic relationship:

$$\ln(\Phi_i) = \left(\frac{1}{RT} \right) \left[\int_v^\infty \left(\frac{\partial p}{\partial n_i} - \frac{RT}{V} \right) dV \right] - \ln(Z) \quad (15-91)$$

where V = total volume of n moles of the mixture

n_i = number of moles of component i

Z = compressibility factor of the hydrocarbon mixture

By combining the above thermodynamic definition of the fugacity with the SRK EOS (Equation 15-68), Soave proposed the following expression for the fugacity coefficient of component i in the liquid phase:

$$\ln(\Phi_i^L) = \frac{b_i(Z^L - 1)}{b_m} - \ln(Z^L - B) - \left(\frac{A}{B}\right) \left[\frac{2\Psi_i}{(a\alpha)_m} - \frac{b_i}{b_m} \right] \ln \left[1 + \frac{B}{Z^L} \right] \quad (15-92)$$

where

$$\Psi_i = \sum_j \left[x_j \sqrt{a_i a_j \alpha_i \alpha_j} (1 - k_{ij}) \right] \quad (15-93)$$

$$(a\alpha)_m = \sum_i \sum_j \left[x_i x_j \sqrt{a_i a_j \alpha_i \alpha_j} (1 - k_{ij}) \right] \quad (15-94)$$

Equation 15-92 is also used to determine the fugacity coefficient of a component in the gas phase Φ_i^y by using the composition of the gas phase y_i in calculating A, B, Z^y , and other composition-dependent terms, or:

$$\ln(\Phi_i^y) = \frac{b_i(Z^y - 1)}{b_m} - \ln(Z^y - B) - \left(\frac{A}{B}\right) \left[\frac{2\Psi_i}{(a\alpha)_m} - \frac{b_i}{b_m} \right] \ln \left[1 + \frac{B}{Z^y} \right]$$

where

$$\Psi_i = \sum_j \left[y_j \sqrt{a_i a_j \alpha_i \alpha_j} (1 - k_{ij}) \right]$$

$$(a\alpha)_m = \sum_i \sum_j \left[y_i y_j \sqrt{a_i a_j \alpha_i \alpha_j} (1 - k_{ij}) \right]$$

Modifications of the SRK EOS

To improve the pure component vapor pressure predictions by the SRK equation of state, Graboski and Daubert (1978) proposed a new expression for calculating parameter m of Equation 15-70. The proposed relationship originated from analyses of extensive experimental data for pure hydrocarbons. The relationship has the following form:

$$m = 0.48508 + 1.55171\omega - 0.15613\omega^2 \quad (15-95)$$

Sim and Daubert (1980) pointed out that because the coefficients of Equation 15-95 were determined by analyzing vapor pressure data of low-molecular-weight hydrocarbons it is unlikely that Equation 15-95 will suffice for high-molecular-weight petroleum fractions. Realizing that the acentric factors for the heavy petroleum fractions are calculated from an equation such as the Edmister correlation or the Lee and Kessler (1975) correlation, the authors proposed the following expressions for determining the parameter m :

- If the acentric factor is determined by using the Edmister correlation, then:

$$m = 0.431 + 1.57\omega_i - 0.161\omega_i^2 \quad (15-96)$$

- If the acentric factor is determined by using the Lee and Kessler correction, then:

$$m = 0.315 + 1.60\omega_i - 0.166\omega_i^2 \quad (15-97)$$

Elliot and Daubert (1985) stated that the optimal binary interaction coefficient k_{ij} would minimize the error in the representation of all thermodynamic properties of a mixture. Properties of particular interest in phase equilibrium calculations include bubble-point pressure, dew-point pressure, and equilibrium ratios. The authors proposed a set of relationships for determining interaction coefficients for asymmetric mixtures² that contain methane, N₂, CO₂, and H₂S. Referring to the principal component as i and the other fraction as j , Elliot and Daubert proposed the following expressions:

- For N₂ systems:

$$k_{ij} = 0.107089 + 2.9776k_{ij}^\infty \quad (15-98)$$

- For CO₂ systems:

$$k_{ij} = 0.08058 - 0.77215k_{ij}^\infty - 1.8404(k_{ij}^\infty)^2 \quad (15-99)$$

- For H₂S systems:

$$k_{ij} = 0.07654 + 0.017921k_{ij}^\infty \quad (15-100)$$

- For methane systems with compounds of 10 carbons or more:

$$k_{ij} = 0.17985 - 2.6958k_{ij}^\infty - 10.853(k_{ij}^\infty)^2 \quad (15-101)$$

where

$$k_{ij}^\infty = \frac{-(\epsilon_i - \epsilon_j)^2}{2\epsilon_i\epsilon_j} \quad (15-102)$$

² An asymmetric mixture is defined as one in which two of the components are considerably different in their chemical behavior. Mixtures of methane with hydrocarbons of 10 or more carbon atoms can be considered asymmetric. Mixtures containing gases such as nitrogen or hydrogen are asymmetric.

and

$$\epsilon_i = \frac{0.480453\sqrt{a_i}}{b_i} \quad (15-103)$$

The two parameters a_i and b_i in Equation 15-103 were previously defined by Equations 15-71 and 15-72.

The major drawback in the SRK EOS is that the critical compressibility factor takes on the unrealistic universal critical compressibility of 0.333 for all substances. Consequently, the molar volumes are typically overestimated and, hence, densities are underestimated.

Peneloux et al. (1982) developed a procedure for improving the volumetric predictions of the SRK EOS by introducing a volume correction parameter c_i into the equation. This third parameter does not change the vapor-liquid equilibrium conditions determined by the unmodified SRK equation, i.e., the equilibrium ratio K_i , but it modifies the liquid and gas volumes. The proposed methodology, known as the **volume translation method**, uses the following expressions:

$$V_{\text{corr}}^L = V^L - \sum_i (x_i c_i) \quad (15-104)$$

$$V_{\text{corr}}^V = V^V - \sum_i (y_i c_i) \quad (15-105)$$

where V^L = uncorrected liquid molar volume, i.e., $V^L = Z^L RT/p$, ft^3/mol

V^V = uncorrected gas molar volume $V^V = Z^V RT/p$, ft^3/mol

V_{corr}^L = corrected liquid molar volume, ft^3/mol

V_{corr}^V = corrected gas molar volume, ft^3/mol

x_i = mole fraction of component i in the liquid phase

y_i = mole fraction of component i in the gas phase

The authors proposed six different schemes for calculating the correction factor c_i for each component. For petroleum fluids and heavy hydrocarbons, Peneloux and coworkers suggested that the best correlating parameter for the correction factor c_i is the Rackett compressibility factor Z_{RA} . The correction factor is then defined mathematically by the following relationship:

$$c_i = 4.43797878(0.29441 - Z_{RA}) T_{ci} / p_{ci} \quad (15-106)$$

where c_i = correction factor for component i , $\text{ft}^3/\text{lb-mol}$

T_{ci} = critical temperature of component i , $^{\circ}\text{R}$

p_{ci} = critical pressure of component i , psia

The parameter Z_{RA} is a unique constant for each compound. The values of Z_{RA} are in general not much different from those of the critical compressibility factors Z_c . If their values are not available, Peneloux et al. (1982) proposed the following correlation for calculating c_i :

$$c_i = (0.0115831168 + 0.411844152\omega) \left(\frac{T_{ci}}{p_{ci}} \right) \quad (15-107)$$

where ω_i = acentric factor of component i .

Example 15-15

Rework Example 15-14 by incorporating the Peneloux volume correction approach in the solution. Key information from Example 15-14 includes:

- For gas: $Z^V = 0.9267$, $\text{Ma} = 20.89$
- For liquid: $Z^L = 1.4121$, $\text{Ma} = 100.25$
- $T = 160^{\circ}\text{F}$, $p = 4000$ psi

Solution

Step 1. Calculate the correction factor c_i using Equation 15-107:

| Component | c_i | x_i | $c_i x_i$ | y_i | $c_i y_i$ |
|-----------|---------|-------|-----------|-------|-----------|
| C_1 | 0.00839 | 0.45 | 0.003776 | 0.86 | 0.00722 |
| C_2 | 0.03807 | 0.05 | 0.001903 | 0.05 | 0.00190 |
| C_3 | 0.07729 | 0.05 | 0.003861 | 0.05 | 0.00386 |
| C_4 | 0.1265 | 0.03 | 0.00379 | 0.02 | 0.00253 |
| C_5 | 0.19897 | 0.01 | 0.001989 | 0.01 | 0.00198 |
| C_6 | 0.2791 | 0.01 | 0.00279 | 0.005 | 0.00139 |
| C_{7+} | 0.91881 | 0.40 | 0.36752 | 0.005 | 0.00459 |
| sum | | | 0.38564 | | 0.02349 |

Step 2. Calculate the uncorrected volume of the gas and liquid phase by using the compressibility factors as calculated in Example 15-14:

$$V^v = \frac{(10.73)(620)(0.9267)}{4000} = 1.54119 \text{ ft}^3/\text{mol}$$

$$V^L = \frac{(10.73)(620)(1.4121)}{4000} = 2.3485 \text{ ft}^3/\text{mol}$$

Step 3. Calculate the corrected gas and liquid volumes by applying Equations 15-104 and 15-105:

$$V_{\text{corr}}^L = V^L - \sum_i (x_i c_i) = 2.3485 - 0.38564 = 1.962927 \text{ ft}^3/\text{mol}$$

$$V_{\text{corr}}^v = V^v - \sum_i (y_i c_i) = 1.54119 - 0.02349 = 1.5177 \text{ ft}^3/\text{mol}$$

Step 4. Calculate the corrected compressibility factors:

$$Z_{\text{corr}}^v = \frac{(4000)(1.5177)}{(10.73)(620)} = 0.91254$$

$$Z_{\text{corr}}^L = \frac{(4000)(1.962927)}{(10.73)(620)} = 1.18025$$

Step 5. Determine the corrected densities of both phases:

$$\rho = \frac{pM_a}{RTZ}$$

$$\rho^v = \frac{(4000)(20.89)}{(10.73)(620)(0.91254)} = 13.767 \text{ lb/ft}^3$$

$$\rho^L = \frac{(4000)(100.25)}{(10.73)(620)(1.18025)} = 51.07 \text{ lb/ft}^3$$

Peng-Robinson Equation of State and Its Modifications

Peng and Robinson (1976a) conducted a comprehensive study to evaluate the use of the SRK equation of state for predicting the behavior of naturally occurring hydrocarbon systems. They illustrated the need for an improvement in the ability of the equation of state to predict liquid densities and other fluid properties particularly in the vicinity of the critical region. As a basis for creating an improved model, Peng and Robinson proposed the following expression:

$$p = \frac{RT}{V-b} - \frac{a\alpha}{(V+b)^2 - cb^2}$$

where a , b , and α have the same significance as they have in the SRK model, and the parameter c is a whole number optimized by analyzing the values of the two terms Z_c and b/V_c as obtained from the equation. It is generally accepted that Z_c should be close to 0.28 and that b/V_c should be approximately 0.26. An optimized value of $c = 2$ gave $Z_c = 0.307$ and $(b/V_c) = 0.253$. Based on this value of c , Peng and Robinson proposed the following equation of state:

$$p = \frac{RT}{V-b} - \frac{a\alpha}{V(V+b) + b(V-b)} \quad (15-108)$$

Imposing the classical critical point conditions (Equation 15-46) on Equation 15-108 and solving for parameters a and b yields:

$$a = \Omega_a \frac{R^2 T_c^2}{p_c} \quad (15-109)$$

$$b = \Omega_b \frac{RT_c}{p_c} \quad (15-110)$$

where $\Omega_a = 0.45724$ and $\Omega_b = 0.07780$. This equation predicts a universal critical gas compressibility factor Z_c of 0.307 compared to 0.333 for the SRK model. Peng and Robinson also adopted Soave's approach for calculating the temperature-dependent parameter α :

$$\alpha = [1 + m(1 - \sqrt{T_r})]^2 \quad (15-111)$$

where

$$m = 0.3796 + 1.54226\omega - 0.2699\omega^2$$

Peng and Robinson (1978) proposed the following modified expression for m that is recommended for heavier components with acentric values $\omega > 0.49$:

$$m = 0.379642 + 1.48503\omega - 0.1644\omega^2 + 0.016667\omega^3 \quad (15-112)$$

Rearranging Equation 15-108 into the compressibility factor form gives:

$$Z^3 + (B-1)Z^2 + (A-3B^2-2B)Z - (AB-B^2-B^3) = 0 \quad (15-113)$$

where A and B are given by Equations 15-79 and 15-80 for pure components and by Equations 15-83 and 15-84 for mixtures.

Example 15-16

Using the composition given in Example 15-14, calculate the density of the gas phase and liquid phase by using the Peng-Robinson EOS. Assume $k_{ij} = 0$.

Solution

Step 1. Calculate the mixture parameters $(a\alpha)_m$ and b_m for the gas and liquid phase, to give:

- **For the gas phase:**

$$(a\alpha)_m = \sum_i \sum_j [y_i y_j \sqrt{a_i a_j \alpha_i \alpha_j} (1 - k_{ij})] = 10,423.54$$

$$b_m = \sum_i (y_i b_i) = 0.862528$$

- **For the liquid phase:**

$$(a\alpha)_m = \sum_i \sum_j [x_i x_j \sqrt{a_i a_j \alpha_i \alpha_j} (1 - k_{ij})] = 107,325.4$$

$$b_m = \sum_i (y_i b_i) = 1.69543$$

Step 2. Calculate the coefficients A and B, to give:

- **For the gas phase:**

$$A = \frac{(a\alpha)_m P}{R^2 T^2} = \frac{(10,423.54)(4000)}{(10.73)^2 (620)^2} = 0.94209$$

$$B = \frac{b_m P}{RT} = \frac{(0.862528)(4000)}{(10.73)(620)} = 0.30669$$

- **For the liquid phase:**

$$A = \frac{(a\alpha)_m P}{R^2 T^2} = \frac{(107,325.4)(4000)}{(10.73)^2 (620)^2} = 9.700183$$

$$B = \frac{b_m P}{RT} = \frac{(1.636543)(4000)}{(10.73)(620)} = 1.020078$$

Step 3. Solve Equation 15-113 for the compressibility factor of the gas phase and the liquid phase to give:

$$Z^3 + (B-1)Z^2 + (A-3B^2-2B)Z - (AB-B^2-B^3) = 0$$

- **For the gas phase:** Substituting for $A = 0.94209$ and $B = 0.30669$ in the above equation gives:

$$Z^v = 0.8625$$

- **For the liquid phase:** Substituting for $A = 9.700183$ and $B = 1.020078$ in the above equation gives:

$$Z^L = 1.2645$$

Step 4. Calculate the density of both phases:

$$\rho^v = \frac{(4,000)(20.89)}{(10.73)(620)(0.8625)} = 14.566 \text{ lb/ft}^3$$

$$\rho^L = \frac{(4,000)(100.25)}{(10.73)(620)(1.2645)} = 47.67 \text{ lb/ft}^3$$

Applying the thermodynamic relationship, as given by Equation 15-86, to Equation 15-109 yields the following expression for the fugacity of a pure component:

$$\ln\left(\frac{f}{p}\right) = \ln(\Phi) = Z - 1 - \ln(Z - B) - \left[\frac{A}{2\sqrt{2}B}\right] \ln\left[\frac{Z + (1 + \sqrt{2})B}{Z + (1 - \sqrt{2})B}\right] \quad (15-114)$$

The fugacity coefficient of component i in a hydrocarbon liquid mixture is calculated from the following expression:

$$\ln\left(\frac{f^L}{x_i p}\right) = \ln(\Phi_i^L) = \frac{b_i(Z^L - 1)}{b_m} - \ln(Z^L - B) - \left[\frac{A}{2\sqrt{2}B}\right] \left[\frac{2\Psi_i}{(a\alpha)_m} - \frac{b_i}{b_m}\right] \ln\left[\frac{Z^L + (1 + \sqrt{2})B}{Z^L - (1 - \sqrt{2})B}\right] \quad (15-115)$$

where the mixture parameters b_m , B , A , Ψ_i , and $(a\alpha)_m$ are as defined previously.

Equation 15-115 is also used to determine the fugacity coefficient of any component in the gas phase by replacing the composition of the liquid phase x_i with the composition of the gas phase y_i in calculating the composition-dependent terms of the equation, or:

$$\ln\left(\frac{f^v}{y_i p}\right) = \ln(\Phi_i^v) = \frac{b_i(Z^v - 1)}{b_m} - \ln(Z^v - B) - \left[\frac{A}{2\sqrt{2}B}\right] \left[\frac{2\Psi_i}{(a\alpha)_m} - \frac{b_i}{b_m}\right] \ln\left[\frac{Z^v + (1 + \sqrt{2})B}{Z^v - (1 - \sqrt{2})B}\right]$$

The set of binary interaction coefficients k_{ij} on page 1117 is traditionally used when predicting the volumetric behavior of a hydrocarbon mixture with the Peng and Robinson (PR) equation of state.

To improve the predictive capability of the PR EOS when describing mixtures containing N_2 , CO_2 , and CH_4 , Nikos et al. (1986) proposed a generalized correlation for generating the binary interaction coefficient k_{ij} . The authors correlated these coefficients with system pressure, temperature, and the acentric factor. These generalized correlations were originated with all the binary experimental data available in the literature. The authors proposed the following generalized form for k_{ij} :

$$k_{ij} = \delta_2 T_{ij}^2 + \delta_1 T_{ij} + \delta_0 \quad (15-116)$$

where i refers to the principal components N_2 , CO_2 , or CH_4 ; and j refers to the other hydrocarbon component of the binary. The acentric factor-dependent coefficients δ_0 , δ_1 , and δ_2 are determined for each set of binaries by applying the following expressions:

- **For nitrogen-hydrocarbons:**

$$\delta_0 = 0.1751787 - 0.7043 \log(\omega_j) - 0.862066 [\log(\omega_i)]^2 \quad (15-117)$$

$$\delta_1 = -0.584474 + 1.328 \log(\omega_j) + 2.035767 [\log(\omega_i)]^2 \quad (15-118)$$

and

$$\delta_2 = 2.257079 + 7.869765 \log(\omega_j) + 13.50466 [\log(\omega_i)]^2 + 8.3864 [\log(\omega)]^3 \quad (15-119)$$

They also suggested the following pressure correction:

$$k'_{ij} = k_{ij} (1.04 - 4.2 \times 10^{-5} p) \quad (15-120)$$

where p is the pressure in pounds per square inch.

- **For methane-hydrocarbons:**

$$\delta_0 = -0.01664 - 0.37283 \log(\omega_j) + 1.31757 [\log(\omega_i)]^2 \quad (15-121)$$

$$\delta_1 = 0.48147 + 3.35342 \log(\omega_j) - 1.0783 [\log(\omega_i)]^2 \quad (15-122)$$

Binary Interaction Coefficients* k_{ij} for the Peng and Robinson EOS

| | CO ₂ | N ₂ | H ₂ S | C ₁ | C ₂ | C ₃ | i-C ₄ | n-C ₄ | i-C ₅ | n-C ₅ | C ₆ | C ₇ | C ₈ | C ₉ | C ₁₀ |
|------------------|-----------------|----------------|------------------|----------------|----------------|----------------|------------------|------------------|------------------|------------------|----------------|----------------|----------------|----------------|-----------------|
| CO ₂ | 0 | 0 | 0.135 | 0.105 | 0.130 | 0.125 | 0.120 | 0.115 | 0.115 | 0.115 | 0.115 | 0.115 | 0.115 | 0.115 | 0.115 |
| N ₂ | 0 | 0 | 0.130 | 0.025 | 0.010 | 0.090 | 0.095 | 0.095 | 0.100 | 0.100 | 0.110 | 0.115 | 0.120 | 0.120 | 0.125 |
| H ₂ S | | | 0 | 0.070 | 0.085 | 0.080 | 0.075 | 0.075 | 0.070 | 0.070 | 0.070 | 0.060 | 0.060 | 0.060 | 0.055 |
| C ₁ | | | | 0 | 0.005 | 0.010 | 0.035 | 0.025 | 0.050 | 0.030 | 0.030 | 0.035 | 0.040 | 0.040 | 0.045 |
| C ₂ | | | | | 0 | 0.005 | 0.005 | 0.010 | 0.020 | 0.020 | 0.020 | 0.020 | 0.020 | 0.020 | 0.020 |
| C ₃ | | | | | | 0 | 0.000 | 0.000 | 0.015 | 0.015 | 0.010 | 0.005 | 0.005 | 0.005 | 0.005 |
| i-C ₄ | | | | | | | 0 | 0.005 | 0.005 | 0.005 | 0.005 | 0.005 | 0.005 | 0.005 | 0.005 |
| n-C ₄ | | | | | | | | 0 | 0.005 | 0.005 | 0.005 | 0.005 | 0.005 | 0.005 | 0.005 |
| i-C ₅ | | | | | | | | | 0 | 0.000 | 0.000 | 0.000 | 0.000 | 0.000 | 0.000 |
| n-C ₅ | | | | | | | | | | 0 | 0.000 | 0.000 | 0.000 | 0.000 | 0.000 |
| C ₆ | | | | | | | | | | | 0 | 0.000 | 0.000 | 0.000 | 0.000 |
| C ₇ | | | | | | | | | | | | 0 | 0.000 | 0.000 | 0.000 |
| C ₈ | | | | | | | | | | | | | 0 | 0.000 | 0.000 |
| C ₉ | | | | | | | | | | | | | | 0 | 0.000 |
| C ₁₀ | | | | | | | | | | | | | | | 0 |

* Notice that $k_{ij} = k_{ji}$.

and

$$\delta_2 = -0.4114 - 3.5072 \log(\omega_j) - 1.0783 [\log(\omega_1)]^2 \quad (15-123)$$

• **For CO₂-hydrocarbons:**

$$\delta_0 = 0.4025636 + 0.1748927 \log(\omega_j) \quad (15-124)$$

$$\delta_1 = -0.94812 - 0.6009864 \log(\omega_j) \quad (15-125)$$

and

$$\delta_2 = 0.741843368 + 0.441775 \log(\omega_j) \quad (15-126)$$

For the CO₂ interaction parameters, the following pressure correction is suggested:

$$k'_{ij} = k_{ij} (1.044269 - 4.375 \times 10^{-5} p) \quad (15-127)$$

Stryjek and Vera (1986) proposed an improvement in the reproduction of vapor pressures of pure components by the PR EOS in the reduced temperature range from 0.7 to 1.0 by replacing the m term in Equation 15-111 with the following expression:

$$m_0 = 0.378893 + 1.4897153 - 0.17131848\omega^2 + 0.0196554\omega^3 \quad (15-128)$$

To reproduce vapor pressures at reduced temperatures below 0.7, Stryjek and Vera further modified the m parameter in the PR equation by introducing an adjustable parameter m_1 characteristic of each compound to Equation 15-111. They proposed the following generalized relationship for the parameter m :

$$m = m_0 + [m_1 (1 + \sqrt{T_r})(0.7 - T_r)] \quad (15-129)$$

where T_r = reduced temperature of the pure component

m_0 = defined by Equation 15-128

m_1 = adjustable parameter

For all components with a reduced temperature above 0.7, Stryjek and Vera recommended setting $m_1 = 0$. For components with a reduced temperature greater than 0.7, the optimum values of m_1 for compounds of industrial interest are tabulated below:

Parameter m_1 of Pure Compounds

| Compound | m_1 | Compound | m_1 |
|----------------|----------|-------------|---------|
| Nitrogen | 0.01996 | Nonane | 0.04104 |
| Carbon dioxide | 0.04285 | Decane | 0.04510 |
| Water | -0.06635 | Undecane | 0.02919 |
| Methane | -0.00159 | Dodecane | 0.05426 |
| Ethane | 0.02669 | Tridecane | 0.04157 |
| Propane | 0.03136 | Tetradecane | 0.02686 |
| Butane | 0.03443 | Pentadecane | 0.01892 |
| Pentane | 0.03946 | Hexadecane | 0.02665 |
| Hexane | 0.05104 | Heptadecane | 0.04048 |
| Heptane | 0.04648 | Octadecane | 0.08291 |
| Octane | 0.04464 | | |

Due to the totally empirical nature of the parameter m_1 , Stryjek and Vera (1986) could not find a generalized correlation for m_1 in terms of pure component parameters. They pointed out that the values of m_1 given above should be used without changes.

Jhaveri and Youngren (1984) pointed out that when applying the Peng-Robinson equation of state to reservoir fluids, the error associated with the equation in the prediction of gas-phase Z factors ranged from 3% to 5%, and the error in the liquid density predictions ranged from 6% to 12%. Following the procedure proposed by Peneloux and coworkers (see the SRK EOS), Jhaveri and Youngren introduced the volume correction parameter c_i to the PR EOS. This third parameter has the same units as the second parameter b_i of the unmodified PR equation and is defined by the following relationship:

$$c_i = S_i b_i \quad (15-130)$$

where S_i = dimensionless parameter and is called the shift parameter
 b_i = Peng-Robinson co-volume as given by Equation 15-110

The volume correction parameter c_i does not change the vapor-liquid equilibrium conditions, i.e., equilibrium ratio K_i . The corrected hydrocarbon phase volumes are given by the following expressions:

$$V_{\text{corr}}^L = V^L - \sum_{i=1} (x_i c_i)$$

$$V_{\text{corr}}^V = V^V - \sum_{i=1} (y_i c_i)$$

where V^L, V^V = volumes of the liquid phase and gas phase as calculated by unmodified PR EOS, ft³/mol
 $V_{\text{corr}}^L, V_{\text{corr}}^V$ = corrected volumes of the liquid and gas phase

Whitson and Brule (2000) point out that the volume translation (correction) concept can be applied to any two-constant cubic equation, thereby eliminating the volumetric deficiency associated with application of EOS. Whitson and Brule extended the work of Jhaveri and Youngren (1984) and proposed the following shift parameters for selected pure components:

Shift Parameters for the PR EOS and SRK EOS

| Compound | PR EOS | SRK EOS |
|---------------------|---------|---------|
| N ₂ | -0.1927 | -0.0079 |
| CO ₂ | -0.0817 | 0.0833 |
| H ₂ S | -0.1288 | 0.0466 |
| C ₁ | -0.1595 | 0.0234 |
| C ₂ | -0.1134 | 0.0605 |
| C ₃ | -0.0863 | 0.0825 |
| i - C ₄ | -0.0844 | 0.0830 |
| n - C ₄ | -0.0675 | 0.0975 |
| i - C ₅ | -0.0608 | 0.1022 |
| n - C ₅ | -0.0390 | 0.1209 |
| n - C ₆ | -0.0080 | 0.1467 |
| n - C ₇ | 0.0033 | 0.1554 |
| n - C ₈ | 0.0314 | 0.1794 |
| n - C ₉ | 0.0408 | 0.1868 |
| n - C ₁₀ | 0.0655 | 0.2080 |

Jhaveri and Youngren (1984) proposed the following expression for calculating the shift parameter for the C₇₊:

$$S = 1 - \frac{d}{(M)^e}$$

where M = molecular weight of the heptanes-plus fraction
d, e = positive correlation coefficients

The authors proposed that in the absence of the experimental information needed for calculating e and d, the power coefficient e can be set equal to 0.2051 and the coefficient d adjusted to match the C₇₊ density with the values of d ranging from 2.2 to 3.2. In general, the following values may be used for C₇₊ fractions:

| Hydrocarbon Family | d | e |
|--------------------|-------|--------|
| Paraffins | 2.258 | 0.1823 |
| Naphthenes | 3.044 | 0.2324 |
| Aromatics | 2.516 | 0.2008 |

To use the Peng and Robinson equation of state to predict the phase and volumetric behavior of mixtures, one must be able to provide the critical pressure, the critical temperature, and the acentric factor for each component in the mixture. For pure compounds, the required properties are well defined and known. Nearly all naturally occurring petroleum fluids contain a quantity of heavy fractions that are not well defined. These heavy fractions are often lumped together as the heptanes-plus fraction. The problem of how to adequately characterize the C_{7+} fractions in terms of their critical properties and acentric factors has been long recognized in the petroleum industry. Changing the characterization of C_{7+} fractions present in even small amounts can have a profound effect on the PVT properties and the phase equilibria of a hydrocarbon system as predicted by the Peng and Robinson equation of state.

The usual approach for such situations is to “tune” the parameters in the EOS in an attempt to improve the accuracy of prediction. During the tuning process, the critical properties of the heptanes-plus fraction and the binary interaction coefficients are adjusted to obtain a reasonable match with experimental data available on the hydrocarbon mixture.

Recognizing that the inadequacy of the predictive capability of the PR EOS lies with the improper procedure for calculating the parameters a , b , and α of the equation for the C_{7+} fraction, Ahmed (1991) devised an approach for determining these parameters from the following two readily measured physical properties of C_{7+} : molecular weight, M_{7+} , and specific gravity, γ_{7+} .

The approach is based on generating 49 density values for the C_{7+} by applying the Riazi and Daubert correlation. These values were subsequently subjected to 10 temperature and 10 pressure values in the range of 60 to 300°F and 14.7 to 7,000 psia, respectively. The Peng and Robinson EOS was then applied to match the 4,900 generated density values by optimizing the parameters a , b , and α using a nonlinear regression model. The optimized parameters for the heptanes-plus fraction are given by the following expressions.

For the parameter a of C_{7+} :

$$\alpha = \left[1 + m \left(1 - \sqrt{\frac{520}{T}} \right) \right]^2 \quad (15-131)$$

with m defined by:

$$m = \frac{D}{A_0 + A_1 D} + A_2 M_{7+} + A_3 M_{7+}^2 + \frac{A_4}{M_{7+}} + A_5 \gamma_{7+} + A_6 \gamma_{7+}^2 + \frac{A_7}{\gamma_{7+}} \quad (15-132)$$

with the parameter D defined by the ratio of the molecular weight to the specific gravity of the heptanes-plus fraction, or:

$$D = \frac{M_{7+}}{\gamma_{7+}}$$

where M_{7+} = molecular weight of C_{7+}

γ_{7+} = specific gravity of C_{7+}

$A_0 - A_7$ = coefficients as given in Table 15-2

For the parameters a and b of C_{7+} , the following generalized correlation is proposed:

$$a \text{ or } b = \left[\sum_{i=0}^3 (A_i D^i) \right] + \frac{A_4}{D} \left[\sum_{i=5}^6 (A_i \gamma_{7+}^{i-4}) \right] + \frac{A_7}{\gamma_{7+}} \quad (15-133)$$

The coefficients A_0 through A_7 are included in Table 15-2.

To further improve the predictive capability of the Peng-Robinson EOS, the author optimized coefficients a , b , and m for nitrogen, CO_2 , and methane by matching 100 Z-factor values for each of these components. Using a nonlinear regression model, the following optimized values are recommended:

Table 15-2 Coefficients for Equations 15-132 and 15-133

| Coefficient | a | b | m |
|-------------|----------------------------|-----------------------------|-----------------------------|
| A_0 | -2.433525×10^7 | -6.8453198 | -36.91776 |
| A_1 | 8.3201587×10^3 | 1.730243×10^{-2} | $-5.2393763 \times 10^{-2}$ |
| A_2 | -0.18444102×10^2 | $-6.2055064 \times 10^{-6}$ | 1.7316235×10^{-2} |
| A_3 | 3.6003101×10^{-2} | 9.0910383×10^{-9} | $-1.3743308 \times 10^{-5}$ |
| A_4 | 3.4992796×10^7 | 13.378898 | 12.718844 |
| A_5 | 2.838756×10^7 | 7.9492922 | 10.246122 |
| A_6 | -1.1325365×10^7 | -3.1779077 | -7.6697942 |
| A_7 | 6.418828×10^6 | 1.7190311 | -2.6078099 |

| Component | a | b | m in Eq. 15-131 |
|-----------------|-------------------------|------------|-----------------|
| CO ₂ | 1.499914×10^4 | 0.41503575 | -0.73605717 |
| N ₂ | 4.5693589×10^3 | 0.4682582 | -0.97962859 |
| C ₁ | 7.709708×10^3 | 0.46749727 | -0.549765 |

To provide the modified PR EOS with a consistent procedure for determining the binary interaction coefficient k_{ij} , the following computational steps are proposed:

Step 1. Calculate the binary interaction coefficient between methane and the heptanes-plus fraction from:

$$k_{c_1-c_{7+}} = 0.00189T - 1.167059$$

where the temperature T is in °R.

Step 2. Set:

$$\begin{aligned} k_{\text{CO}_2-\text{N}_2} &= 0.12 \\ k_{\text{CO}_2-\text{hydrocarbon}} &= 0.10 \\ k_{\text{N}_2-\text{hydrocarbon}} &= 0.10 \end{aligned}$$

Step 3. Adopting the procedure recommended by Petersen (1989), calculate the binary interaction coefficients between components heavier than methane (e.g., C₂, C₃) and the heptanes-plus fraction from:

$$k_{C_n-C_{7+}} = 0.8k_{C_{(n-1)}-C_{7+}}$$

where n is the number of carbon atoms of component C_n; e.g.:

Binary interaction coefficient between C₂ and C₇₊ is

$$k_{C_2-C_{7+}} = 0.8 k_{C_1-C_{7+}}$$

Binary interaction coefficient between C₃ and C₇₊ is

$$k_{C_3-C_{7+}} = 0.8 k_{C_2-C_{7+}}$$

Step 4. Determine the remaining k_{ij} from:

$$k_{ij} = k_{i-C_{7+}} \left[\frac{(M_j)^5 - (M_i)^5}{(M_{C_{7+}})^5 - (M_i)^5} \right]$$

where M is the molecular weight of any specified component.

For example, the binary interaction coefficient between propane C₃ and butane C₄ is:

$$k_{C_3-C_4} = k_{C_3-C_{7+}} \left[\frac{(M_{C_4})^5 - (M_{C_3})^5}{(M_{C_{7+}})^5 - (M_{C_3})^5} \right]$$

APPLICATIONS OF THE EQUATION OF STATE IN PETROLEUM ENGINEERING

Determination of the Equilibrium Ratios

A flow diagram is presented in Figure 15-14 to illustrate the procedure of determining equilibrium ratios of a hydrocarbon mixture. For this type of calculation, the system temperature T , the system pressure p , and the overall composition of the mixture z_i must be known. The procedure is summarized in the following steps in conjunction with Figure 15-14.

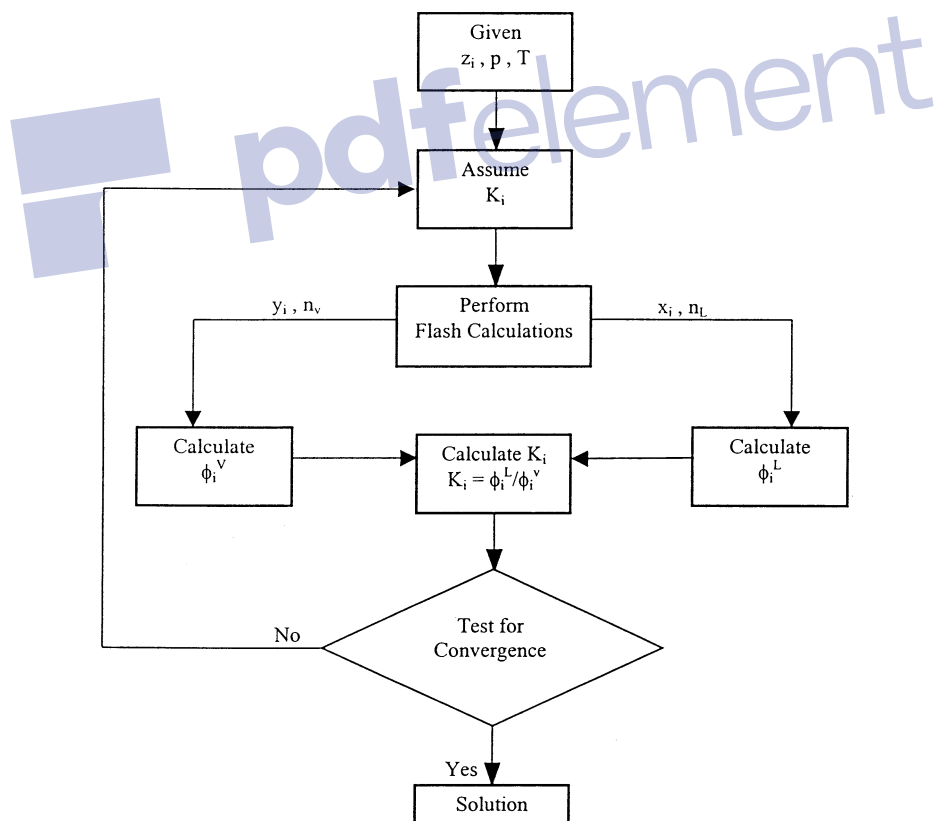


Figure 15-14. Flow diagram of the equilibrium ratio determination by an equation of state.

Step 1. Assume an initial value of the equilibrium ratio for each component in the mixture at the specified system pressure and temperature. Wilson's equation can provide the starting K_i values.

$$K_i^A = \frac{P_{ci}}{p} \exp[5.37(1 + \omega_i)(1 - T_{ci}/T)]$$

where K_i^A = assumed equilibrium ratio of component i .

Step 2. Using the overall composition and the assumed K values, perform flash calculations to determine x_i , y_i , n_L , and n_V .

Step 3. Using the calculated composition of the liquid phase x_i , determine the fugacity coefficient Φ_i^L for each component in the liquid phase.

Step 4. Repeat Step 3 using the calculated composition of the gas phase y_i to determine Φ_i^V .

Step 5. Calculate the new set of equilibrium ratios from:

$$K_i = \frac{\Phi_i^L}{\Phi_i^V}$$

Step 6. Check for the solution by applying the following constraint:

$$\sum_{i=1}^n [K_i / K_i^A - 1]^2 \leq \epsilon$$

where ϵ = preset error tolerance, e.g., 0.0001
 n = number of components in the system

If the above conditions are satisfied, then the solution has been reached. If not, steps 1 through 6 are repeated by using the calculated equilibrium ratios as initial values.

Determination of the Dew-Point Pressure

A saturated vapor exists for a given temperature at the pressure at which an infinitesimal amount of liquid first appears. This pressure is referred to as the dew-point pressure p_d . The dew-point pressure of a mixture is described mathematically by the following two conditions:

$$y_i = z_i \quad 1 \leq i \leq n \quad (15-134)$$

$$n_v = 1$$

and:

$$\sum_{i=1}^n \left[\frac{z_i}{K_i} \right] = 1 \quad (15-135)$$

Applying the definition of K_i in terms of the fugacity coefficient to Equation 15-135 gives:

$$\sum_{i=1}^n \left[\frac{z_i}{k_i} \right] = \sum_{i=1}^n \left[\frac{z_i}{(\Phi_i^L / \Phi_i^V)} \right] = \sum_{i=1}^n \left[\left(\frac{z_i}{\Phi_i^L} \right) \frac{f_i^V}{z_i p_d} \right] = 1$$

or

$$p_d = \sum_{i=1}^n \left[\frac{f_i^V}{\Phi_i^L} \right]$$

The above equation is arranged to give:

$$f(p_d) = \sum_{i=1}^n \left[\frac{f_i^V}{\Phi_i^L} \right] - p_d = 0 \quad (15-136)$$

where p_d = dew-point pressure, psia

f_i^V = fugacity of component i in the vapor phase, psia

Φ_i^L = fugacity coefficient of component i in the liquid phase

Equation 15-136 can be solved for the dew-point pressure by using the Newton-Raphson iterative method. To use the iterative method, the derivative of Equation 15-136 with respect to the dew-point pressure p_d is required. This derivative is given by the following expression:

$$\frac{\partial f}{\partial p_d} = \sum_{i=1}^n \left[\frac{\Phi_i^L (\partial f_i^V / \partial p_d) - f_i^V (\partial \Phi_i^L / \partial p_d)}{(\Phi_i^L)^2} \right] - 1 \quad (15-137)$$

The two derivatives in the above equation can be approximated numerically as follows:

$$\frac{\partial f^V}{\partial p_d} = \left[\frac{f_i^V(p_d + \Delta p_d) - f_i^V(p_d - \Delta p_d)}{2\Delta p_d} \right] \quad (15-138)$$

and

$$\frac{\partial f_i^L}{\partial p_d} = \left[\frac{\Phi_i^L(p_d + \Delta p_d) - \Phi_i^L(p_d - \Delta p_d)}{2\Delta p_d} \right] \quad (15-139)$$

where Δp_d = pressure increment, 5 psia, for example

$f_i^Y(p_d + \Delta p_d)$ = fugacity of component i at $(p_d + \Delta p_d)$

$f_i^Y(p_d - \Delta p_d)$ = fugacity of component i at $(p_d - \Delta p_d)$

$\Phi_i^L(p_d + \Delta p_d)$ = fugacity coefficient of component i at $(p_d + \Delta p_d)$

$\Phi_i^L(p_d - \Delta p_d)$ = fugacity coefficient of component i at $(p_d - \Delta p_d)$

Φ_i^L = fugacity coefficient of component i at p_d

The computational procedure of determining p_d is summarized in the following steps:

Step 1. Assume an initial value for the dew-point pressure p_d^A .

Step 2. Using the assumed value of p_d^A , calculate a set of equilibrium ratios for the mixture by using any of the previous correlations, e.g., Wilson's correlation.

Step 3. Calculate the composition of the liquid phase, i.e., composition of the droplets of liquid, by applying the mathematical definition of K_i , to give:

$$x_i = \frac{z_i}{K_i}$$

Note that $y_i = z_i$.

Step 4. Calculate f_i^Y using the composition of the gas phase z_i and Φ_i^L using the composition of liquid phase x_i at the following three pressures:

- p_d^A
- $p_d^A + \Delta p_d$
- $p_d^A - \Delta p_d$

where p_d^A is the assumed dew-point pressure and Δp_d is a selected pressure increment of 5 to 10 psi.

Step 5. Evaluate the function $f(p_d)$, i.e., Equation 15-136, and its derivative by using Equations 15-137 through 15-139.

Step 6. Using the values of the function $f(p_d)$ and the derivative $\partial f/\partial p_d$ as determined in step 5, calculate a new dew-point pressure by applying the Newton-Raphson formula:

$$p_d = p_d^A - f(p_d)/[\partial f/\partial p_d] \quad (15-140)$$

Step 7. The calculated value of p_d is checked numerically against the assumed value by applying the following condition:

$$|p_d - p_d^A| \leq 5$$

If the above condition is met, then the correct dew-point pressure p_d has been found. Otherwise, Steps 3 through 6 are repeated by using the calculated p_d as the new value for the next iteration. A set of equilibrium ratios must be calculated at the new assumed dew-point pressure from:

$$k_i = \frac{\Phi_i^L}{\Phi_i^V}$$

Determination of the Bubble-Point Pressure

The bubble-point pressure p_b is defined as the pressure at which the first bubble of gas is formed. Accordingly, the bubble-point pressure is defined mathematically by the following equations:

$$x_i = z_i \quad 1 \leq i \leq n \quad (15-141)$$

$$n_L = 1.0$$

and

$$\sum_{i=1}^n [z_i K_i] = 1 \quad (15-142)$$

Introducing the concept of the fugacity coefficient into Equation 15-142 gives:

$$\sum_{i=1}^n \left[z_i \frac{\Phi_i^L}{\Phi_i^V} \right] = \sum_{i=1}^n \left[z_i \frac{\left(\frac{f_i^L}{z_i p_b} \right)}{\Phi_i^V} \right] = 1$$

Rearranging,

$$p_b = \sum_{i=1}^n \left[\frac{f_i^L}{\Phi_i^V} \right]$$

or

$$f(p_b) = \sum_{i=1}^n \left[\frac{f_i^L}{\Phi_i^V} \right] - p_b = 0 \quad (15-143)$$

The iteration sequence for calculation of p_b from the above function is similar to that of the dew-point pressure, which requires differentiating the above function with respect to the bubble-point pressure, or:

$$\frac{\partial f}{\partial p_b} = \sum_{i=1}^n \left[\frac{\Phi_i^V (\partial f_i^L / \partial p_b) - f_i^L (\partial \Phi_i^V / \partial p_b)}{(\Phi_i^V)^2} \right] - 1 \quad (15-144)$$

Three-Phase Equilibrium Calculations

Two- and three-phase equilibria occur frequently during the processing of hydrocarbon and related systems. Peng and Robinson (1976b) proposed a three-phase equilibrium calculation scheme of systems that exhibit a water-rich liquid phase, a hydrocarbon-rich liquid phase, and a vapor phase.

Applying the principle of mass conservation to 1 mol of a water-hydrocarbon in a three-phase state of thermodynamic equilibrium at a fixed temperature T and pressure p gives:

$$n_L + n_w + n_v = 1 \quad (15-145)$$

$$n_L x_i + n_w x_{wi} + n_v y_i = z_i \quad (15-146)$$

$$\sum_i^n x_i = \sum_{i=1}^n x_{wi} = \sum_{i=1}^n y_i = \sum_{i=1}^n z_i = 1 \quad (15-147)$$

where n_L, n_w, n_v = number of moles of the hydrocarbon-rich liquid, the water-rich liquid, and the vapor, respectively
 x_i, x_{wi}, y_i = mole fraction of component i in the hydrocarbon-rich liquid, the water-rich liquid, and the vapor, respectively.

The equilibrium relations between the compositions of each phase are defined by the following expressions:

$$K_i = \frac{y_i}{x_i} = \frac{\Phi_i^L}{\Phi_i^V} \quad (15-148)$$

and

$$K_{wi} = \frac{y_i}{x_{wi}} = \frac{\Phi_i^W}{\Phi_i^V} \quad (15-149)$$

where K_i = equilibrium ratio of component i between vapor and hydrocarbon-rich liquid

K_{wi} = equilibrium ratio of component i between the vapor and water-rich liquid

Φ_i^L = fugacity coefficient of component i in the hydrocarbon-rich liquid

Φ_i^V = fugacity coefficient of component i in the vapor phase

Φ_i^W = fugacity coefficient of component i in the water-rich liquid

Combining Equations 15-145 through 15-149 gives the following conventional nonlinear equations:

$$\sum_{i=1} x_i = \sum_{i=1} \left[\frac{z_i}{n_L(1 - K_i) + n_w \left(\frac{K_i}{K_{wi}} - K_i \right) + K_i} \right] = 1 \quad (15-150)$$

$$\sum_{i=1} x_{wi} = \sum_{i=1} \left[\frac{z_i (K_i / K_{wi})}{n_L(1 - K_i) + n_w \left(\frac{K_i}{K_{wi}} - K_i \right) + K_i} \right] = 1 \quad (15-151)$$

$$\sum_{i=1} y_i = \sum_{i=1} \left[\frac{z_i K_i}{n_L(1 - K_i) + n_w \left(\frac{K_i}{K_{wi}} - K_i \right) + K_i} \right] = 1 \quad (15-152)$$

Assuming that the equilibrium ratios between phases can be calculated, the above equations are combined to solve for the two unknowns n_L and n_w , and hence x_i , x_{wi} , and y_i . It is the nature of the specific equilibrium calculation that determines the appropriate combination of Equations

15-150 through 15-152. The combination of the above three expressions can then be used to determine the phase and volumetric properties of the three-phase system.

There are essentially three types of phase behavior calculations for the three-phase system:

1. Bubble-point prediction
2. Dew-point prediction
3. Flash calculation

Peng and Robinson (1980) proposed the following combination schemes of Equations 15-150 through 15-152.

- **For the bubble-point pressure determination:**

$$\sum_i x_i - \sum_i x_{wi} = 0 \quad \left[\sum_i y_i \right] - 1 = 0$$

Substituting Equations 15-150 through 15-152 in the above relationships gives:

$$f(n_L, n_w) = \sum_i \left[\frac{z_i (1 - K_i/K_{wi})}{n_L (1 - K_i) + n_w (K_i/K_{wi} - K_i) + K_i} \right] = 0 \quad (15-153)$$

and

$$g(n_L, n_w) = \sum_i \left[\frac{z_i K_i}{n_L (1 - K_i) + n_w (K_i/K_{wi} - K_i) + K_i} \right] - 1 = 0 \quad (15-154)$$

- **For the dew-point pressure:**

$$\sum_i x_{wi} - \sum_i y_i = 0 \quad \left[\sum_i x_i \right] - 1 = 0$$

Combining with Equations 15-150 through 15-152 yields:

$$f(n_L, n_w) = \sum_i \left[\frac{z_i K_i (1/K_{wi} - 1)}{n_L (1 - K_i) + n_w (K_i/K_{wi} - K_i) + K_i} \right] = 0 \quad (15-155)$$

and

$$g(n_L, n_w) = \sum_i \left[\frac{z_i}{n_L (1 - K_i) + n_w (K_i/K_{wi} - K_i) + K_i} \right] - 1 = 0 \quad (15-156)$$

• **For flash calculations:**

$$\sum_i x_i - \sum_i y_i = 0 \quad \left[\sum_i x_{wi} \right] - 1 = 0$$

or

$$f(n_L, n_w) = \sum_i \left[\frac{z_i (1 - K_i)}{n_L (1 - K_i) + n_w (K_i / K_{wi} - K_i) + K_i} \right] = 0 \quad (15-157)$$

and

$$g(n_L, n_w) = \sum_i \left[\frac{z_i K_i / K_{wi}}{n_L (1 - K_i) + n_w (K_i / K_{wi} - K_i) + K_i} \right] - 1.0 = 0 \quad (15-158)$$

Note that in performing any of the above property predictions, we always have two unknown variables, n_L and n_w , and between them, two equations. Providing that the equilibrium ratios and the overall composition are known, the equations can be solved simultaneously by using the appropriate iterative technique, e.g., the Newton-Raphson method. The application of this iterative technique for solving Equations 15-157 and 15-158 is summarized in the following steps:

Step 1. Assume initial values for the unknown variables n_L and n_w .

Step 2. Calculate new values of n_L and n_w by solving the following two linear equations:

$$\begin{bmatrix} n_L \\ n_w \end{bmatrix}^{\text{new}} = \begin{bmatrix} n_L \\ n_w \end{bmatrix} - \begin{bmatrix} \partial f / \partial n_L & \partial f / \partial n_w \\ \partial g / \partial n_L & \partial g / \partial n_w \end{bmatrix}^{-1} \begin{bmatrix} f(n_L, n_w) \\ g(n_L, n_w) \end{bmatrix}$$

where $f(n_L, n_w)$ = value of the function $f(n_L, n_w)$ as expressed by Equation 15-157

$g(n_L, n_w)$ = value of the function $g(n_L, n_w)$ as expressed by Equation 15-158

The first derivative of the above functions with respect to n_L and n_w are given by the following expressions:

$$\begin{aligned}
 (\partial f / \partial n_L) &= \sum_{i=1} \left[\frac{-z_i(1-K_i)^2}{\left[n_L(1-K_i) + n_w(K_i/K_{wi} - K_i) + K_i \right]^2} \right] \\
 (\partial f / \partial n_w) &= \sum_{i=1} \left[\frac{-z_i(1-K_i)(K_i/K_{wi} - K_i)}{\left[n_L(1-K_i) + n_w(K_i/K_{wi} - K_i) + K_i \right]^2} \right] \\
 (\partial g / \partial n_L) &= \sum_{i=1} \left[\frac{-z_i(K_i/K_{wi})(1-K_i)}{\left[n_L(1-K_i) + n_w(K_i/K_{wi} - K_i) + K_i \right]^2} \right] \\
 (\partial g / \partial n_w) &= \sum_{i=1} \left[\frac{-z_i(K_i K_{wi})(K_i/K_{wi} - K_i)}{\left[n_L(1-K_i) + n_w(K_i/K_{wi} - K_i) + K_i \right]^2} \right]
 \end{aligned}$$

Step 3. The new calculated values of n_L and n_w are then compared with the initial values. If no changes in the values are observed, then the correct values of n_L and n_w have been obtained. Otherwise, the above steps are repeated with the new calculated values used as initial values.

Peng and Robinson (1980) proposed two modifications when using their equation of state for three-phase equilibrium calculations. The first modification concerns the use of the parameter α as expressed by Equation 15-111 for the water compound. Peng and Robinson suggested that when the reduced temperature of this compound is less than 0.85, the following equation is applied:

$$\alpha = [1.0085677 + 0.82154(1 - T_r^{0.5})]^2 \quad (15-159)$$

where T_r is the reduced temperature $(T/T_c)_{H_2O}$ of the water component.

The second modification concerns the application of Equation 15-81 for the water-rich liquid phase. A temperature-dependent binary interaction coefficient was introduced into the equation to give:

$$(\alpha\alpha)_m = \sum_i \sum_j [x_{wi}x_{wj}(a_i a_j \alpha_i \alpha_j)^{0.5} (1 - \tau_{ij})] \quad (15-160)$$

where τ_{ij} is a temperature-dependent binary interaction coefficient. Peng and Robinson proposed graphical correlations for determining this parameter for each aqueous binary pair. Lim et al. (1984) expressed these

graphical correlations mathematically by the following generalized equation:

$$\tau_{ij} = a_1 \left[\frac{T}{T_{ci}} \right]^2 \left[\frac{p_{ci}}{p_{cj}} \right]^2 + a_2 \left[\frac{T}{T_{ci}} \right] \left[\frac{p_{ci}}{p_{cj}} \right] + a_3 \quad (15-161)$$

where T = system temperature, °R

T_{ci} = critical temperature of the component of interest, °R

p_{ci} = critical pressure of the component of interest, psia

p_{cj} = critical pressure of the water compound, psia

Values of the coefficients a_1 , a_2 , and a_3 of the above polynomial are given below for selected binaries:

| Component i | a_1 | a_2 | a_3 |
|-------------|---------|--------|--------|
| C_1 | 0 | 1.659 | -0.761 |
| C_2 | 0 | 2.109 | -0.607 |
| C_3 | -18.032 | 9.441 | -1.208 |
| $n - C_4$ | 0 | 2.800 | -0.488 |
| $n - C_6$ | 49.472 | -5.783 | -0.152 |

For selected nonhydrocarbon components, values of interaction parameters are given by the following expressions:

• **For N_2 - H_2O binary:**

$$\tau_{ij} = 0.402(T/T_{ci}) - 1.586 \quad (15-162)$$

where τ_{ij} = binary parameter between nitrogen and the water compound

T_{ci} = critical temperature of nitrogen, °R

• **For CO_2 - H_2O binary:**

$$\tau_{ij} = -0.074 \left[\frac{T}{T_{ci}} \right]^2 + 0.478 \left[\frac{T}{T_{ci}} \right] - 0.503 \quad (15-163)$$

where T_{ci} is the critical temperature of CO_2 .

In the course of making phase equilibrium calculations, it is always desirable to provide initial values for the equilibrium ratios so the iterative

procedure can proceed as reliably and rapidly as possible. Peng and Robinson (1980) adopted Wilson's equilibrium ratio correlation to provide initial K values for the hydrocarbon-vapor phase.

$$K_i = p_{ci}/p \exp[5.3727(1 + \omega_i)(1 - T_{ci}/T)]$$

while for the water-vapor phase, Peng and Robinson proposed the following expression:

$$K_{wi} = 10^6 [p_{ci}T/(T_{ci}P)]$$

Vapor Pressure from Equation of State

The calculation of the vapor pressure of a pure component through an EOS is usually made by the same trial-and-error algorithms used to calculate vapor-liquid equilibria of mixtures. Soave (1972) suggests that the van der Waals (vdW), Soave-Redlich-Kwong (SRK), and the Peng-Robinson (PR) equations of state can be written in the following generalized form:

$$p = \frac{RT}{v - b} - \frac{a\alpha}{v^2 + \mu vb + wb^2} \quad (15-164)$$

with

$$a = \Omega_a \frac{R^2 T_c^2}{P_c}$$

$$b = \Omega_b \frac{RT_c}{P_c}$$

where the values of μ , w , Ω_a , and Ω_b for three different equations of state are given below:

| EOS | μ | w | Ω_a | Ω_b |
|-----|-------|-----|------------|------------|
| vdW | 0 | 0 | 0.421875 | 0.125 |
| SRK | 1 | 0 | 0.42748 | 0.08664 |
| PR | 2 | -1 | 0.45724 | 0.07780 |

Soave (1972) introduced the reduced pressure p_r and reduced temperature T_r to the above equations to give:

$$A = \frac{a\alpha p}{R^2 T^2} = \Omega_a \frac{\alpha p_r}{T_r} \quad (15-165)$$

$$B = \frac{bp}{RT} = \Omega_b \frac{p_r}{T_r} \quad (15-166)$$

and

$$\frac{A}{B} = \frac{\Omega_a}{\Omega_b} \left(\frac{\alpha}{T_r} \right) \quad (15-167)$$

where:

$$p_r = p / p_c$$

$$T_r = T / T_c$$

In the cubic form and in terms of the Z factor, the above three equations of state can be written:

$$\text{vdW: } Z^3 - Z^2(1+B) + ZA - AB = 0$$

$$\text{SRK: } Z^3 - Z^2 + Z(A - B - B^2) - AB = 0 \quad (15-168)$$

$$\text{PR: } Z^3 - Z^2(1-B) + Z(A - 3B^2 - 2B) - (AB - B^2 - B^3) = 0$$

and the pure component fugacity coefficient is given by:

$$\text{VdW: } \ln(f/p) = Z - 1 - \ln(Z - B) - \frac{A}{Z}$$

$$\text{SRK: } \ln(f/p) = Z - 1 - \ln(Z - B) - \left(\frac{A}{B} \right) \ln \left(1 + \frac{B}{Z} \right)$$

$$\text{PR: } \ln(f/p) = Z - 1 - \ln(Z - B) - \left(\frac{A}{2\sqrt{2}B} \right) \ln \left(\frac{Z + (1 + \sqrt{2})B}{Z - (1 - \sqrt{2})B} \right)$$

A typical iterative procedure for the calculation of pure component vapor pressure at any temperature T through one of the above EOS is summarized below:

Step 1. Calculate the reduced temperature, i.e., $T_r = T/T_c$.

Step 2. Calculate the ratio A/B from Equation 15-167.

- Step 3.* Assume a value for B.
- Step 4.* Solve Equation (15-168) and obtain Z^L and Z^V , i.e., smallest and largest roots, for both phases.
- Step 5.* Substitute Z^L and Z^V into the pure component fugacity coefficient and obtain $\ln(f/p)$ for both phases.
- Step 6.* Compare the two values of f/p . If the isofugacity condition is not satisfied, assume a new value of B and repeat Steps 3 through 6.
- Step 7.* From the final value of B, obtain the vapor pressure from Equation 15-166, or:

$$B = \Omega_b \frac{(p_v/p_c)}{T_r}$$

Solving for p_v gives

$$p_v = \frac{BT_r P_c}{\Omega_b}$$

SPLITTING AND LUMPING SCHEMES OF THE PLUS FRACTION

The hydrocarbon plus fractions that comprise a significant portion of naturally occurring hydrocarbon fluids create major problems when predicting the thermodynamic properties and the volumetric behavior of these fluids by equations of state. These problems arise due to the difficulty of properly characterizing the plus fractions (heavy ends) in terms of their critical properties and acentric factors.

Whitson (1980) and Maddox and Erbar (1982, 1984), among others, have shown the distinct effect of the heavy fractions characterization procedure on PVT relationship prediction by equations of state. Usually, these undefined plus fractions, commonly known as the C_{7+} fractions, contain an undefined number of components with a carbon number higher than 6. Molecular weight and specific gravity of the C_{7+} fraction may be the only measured data available.

In the absence of detailed analytical data for the plus fraction in a hydrocarbon mixture, erroneous predictions and conclusions can result if the plus fraction is used directly as a single component in the mixture

phase behavior calculations. Numerous authors have indicated that these errors can be substantially reduced by “splitting” or “breaking down” the plus fraction into a manageable number of fractions (pseudo-components) for equation of state calculations.

The problem, then, is how to adequately split a C_{7+} fraction into a number of psuedo-components characterized by:

- Mole fractions
- Molecular weights
- Specific gravities

These characterization properties, when properly M_{7+} combined, should match the measured plus fraction properties, i.e., $(M)_{7+}$ and $(\gamma)_{7+}$.

Splitting Schemes

Splitting schemes refer to the procedures of dividing the heptanes-plus fraction into hydrocarbon groups with a single carbon number (C_7 , C_8 , C_9 , etc.) and are described by the same physical properties used for pure components.

Several authors have proposed different schemes for extending the molar distribution behavior of C_{7+} , i.e., the molecular weight and specific gravity. In general, the proposed schemes are based on the observation that lighter systems such as condensates usually exhibit exponential molar distribution, while heavier systems often show left-skewed distributions. This behavior is shown schematically in Figure 15-15.

Three important requirements should be satisfied when applying any of the proposed splitting models:

1. The sum of the mole fractions of the individual pseudo-components is equal to the mole fraction of C_{7+} .
2. The sum of the products of the mole fraction and the molecular weight of the individual pseudo-components is equal to the product of the mole fraction and molecular weight of C_{7+} .
3. The sum of the product of the mole fraction and molecular weight divided by the specific gravity of each individual component is equal to that of C_{7+} .

The above requirements can be expressed mathematically by the following relationship:

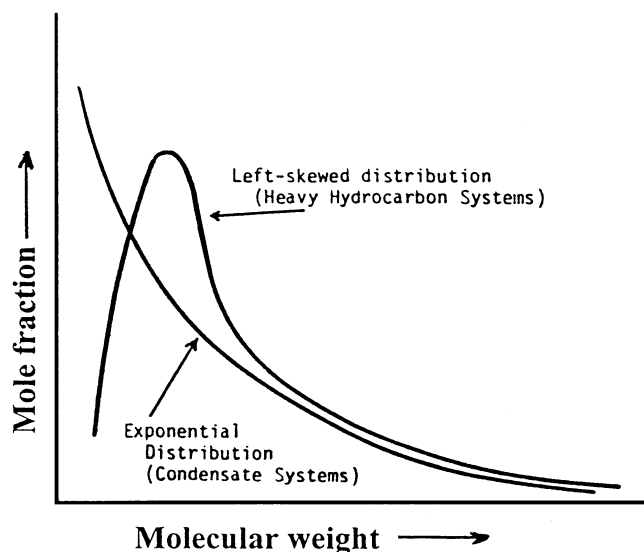


Figure 15-15. Exponential and left-skewed distribution functions.

$$\sum_{n=7}^{N_+} z_n = z_{7+} \quad (15-169)$$

$$\sum_{n=7}^{N_+} [z_n M_n] = z_{7+} M_{7+} \quad (15-170)$$

$$\sum_{n=7}^{N_+} \frac{z_n M_n}{\gamma_n} = \frac{z_{7+} M_{7+}}{\gamma_{7+}} \quad (15-171)$$

where z_{7+} = mole fraction of C_{7+}
 n = number of carbon atoms
 N_+ = last hydrocarbon group in C_{7+} with n carbon atoms, e.g.,
 20+
 z_n = mole fraction of pseudo-component with n carbon atoms
 M_{7+}, γ_{7+} = measure of molecular weight and specific gravity of C_{7+}
 M_n, γ_n = molecular weight and specific gravity of the pseudo-
 component with n carbon atoms

Several splitting schemes have been proposed recently. These schemes, as discussed below, are used to predict the compositional distribution of the heavy plus fraction.

Katz's Method

Katz (1983) presented an easy-to-use graphical correlation for breaking down into pseudo-components the C_{7+} fraction present in condensate systems. The method was originated by studying the compositional behavior of six condensate systems using detailed extended analysis. On a semi log scale, the mole percent of each constituent of the C_{7+} fraction versus the carbon number in the fraction was plotted. The resulting relationship can be conveniently expressed mathematically by the following expression:

$$z_n = 1.38205z_{7+}e^{-0.25903n} \quad (15-172)$$

where z_{7+} = mole fracture of C_{7+} in the condensate system

n = number of carbon atoms of the psuedo-component

z_n = mole fraction of the pseudo-component with number of carbon atoms of n

Equation 15-172 is repeatedly applied until Equation 15-169 is satisfied. The molecular weight and specific gravity of the last pseudo-component can be calculated from Equations 15-170 and 15-171, respectively.

The computational procedure of Katz's method is best explained through the following example.

Example 15-17

A naturally occurring condensate gas system has the following composition:

| Component | z_i |
|-----------|--------|
| C_1 | 0.9135 |
| C_2 | 0.0403 |
| C_3 | 0.0153 |
| i - C_4 | 0.0039 |
| n - C_4 | 0.0043 |
| i - C_5 | 0.0015 |
| n - C_5 | 0.0019 |
| C_6 | 0.0039 |
| C_{7+} | 0.0154 |

The molecular weight and specific gravity of C_{7+} are 141.25 and 0.797, respectively.

- Using Katz's splitting scheme, extend the compositional distribution of C_{7+} to the pseudo-fraction C_{16+} .
- Calculate M , γ , T_b , p_c , T_c , and ω of C_{16+} .

Solution

- Applying Equation 15-172 with $z_{7+} = 0.0154$ gives

| n | Experimental z_n | Equation 15-172 z_n |
|-----|--------------------|-----------------------|
| 7 | 0.00361 | 0.00347 |
| 8 | 0.00285 | 0.00268 |
| 9 | 0.00222 | 0.00207 |
| 10 | 0.00158 | 0.001596 |
| 11 | 0.00121 | 0.00123 |
| 12 | 0.00097 | 0.00095 |
| 13 | 0.00083 | 0.00073 |
| 14 | 0.00069 | 0.000566 |
| 15 | 0.00050 | 0.000437 |
| 16+ | 0.00094 | 0.001671* |

*This value is obtained by applying Equation 15-169, i.e., $0.0154 - \sum_{n=7}^{15} z_n = 0.001671$.

-

Step 1. Calculate the molecular weight and specific gravity of C_{16+} by solving Equations 15-170 and 15-171 for these properties:

$$M_{16+} = z_{7+}M_{7+} - \left[\left(\frac{1}{z_{16+}} \right) \sum_{n=7}^{15} (z_n \cdot M_n) \right]$$

and

$$\gamma_{16+} = \frac{z_{16+}M_{16+}}{(z_{7+}M_{7+}/\gamma_{7+})} - \sum_{n=7}^{15} \left(\frac{z_n M_n}{\gamma_n} \right)$$

where M_n , γ_n = molecular weight and specific gravity of the hydrocarbon group with n carbon atoms. The calculations are performed in the following tabulated form:

| n | z_n | M_n (Table 1-1) | $z_n M_n$ | γ_n (Table 1-1) | $z_n \cdot M/\gamma_n$ |
|-----|----------|----------------------|-----------|---------------------------|------------------------|
| 7 | 0.00347 | 96 | 0.33312 | 0.727 | 0.4582 |
| 8 | 0.00268 | 107 | 0.28676 | 0.749 | 0.3829 |
| 9 | 0.00207 | 121 | 0.25047 | 0.768 | 0.3261 |
| 10 | 0.001596 | 134 | 0.213864 | 0.782 | 0.27348 |
| 11 | 0.00123 | 147 | 0.18081 | 0.793 | 0.22801 |
| 12 | 0.00095 | 161 | 0.15295 | 0.804 | 0.19024 |
| 13 | 0.00073 | 175 | 0.12775 | 0.815 | 0.15675 |
| 14 | 0.000566 | 190 | 0.10754 | 0.826 | 0.13019 |
| 15 | 0.000437 | 206 | 0.09002 | 0.836 | 0.10768 |
| 16+ | 0.001671 | — | — | — | — |
| | | | 1.743284 | | 2.25355 |

$$M_{16+} = \frac{(0.0154)(141.25) - 1.743284}{0.001671} = 258.5$$

$$\gamma_{16+} = \frac{(0.001671)(258.5)}{(0.0154)(141.25)} - 2.25355 = 0.908$$

Step 2. Calculate the boiling points, critical pressure, and critical temperature of C_{16+} by using the Riazi-Daubert correlation to give:

$$T_b = 1136^\circ\text{R}$$

$$p_c = 215 \text{ psia}$$

$$T_c = 1473^\circ\text{R}$$

Step 3. Calculate the acentric factor of C_{16+} by applying the Edmister correlation to give $\omega = 0.684$.

Lohrenz's Method

Lohrenz et al. (1964) proposed that the heptanes-plus fraction could be divided into pseudo-components with carbon numbers ranging from 7 to 40. They mathematically stated that the mole fraction z_n is related to its number of carbon atoms n and the mole fraction of the hexane fraction z_6 by the expression:

$$z_n = z_6 e^{A(n-6)^2 + B(n-6)} \quad (15-173)$$

The constants A and B are determined such that the constraints given by Equations 15-169 through 15-171 are satisfied.

The use of Equation 15-173 assumes that the individual C_{7+} components are distributed through the hexane mole fraction and tail off to an extremely small quantity of heavy hydrocarbons.

Example 15-18

Rework Example 15-17 by using the Lohrenz splitting scheme and assuming that a partial molar distribution of C_{7+} is available. The composition is given below:

| Component | z_i |
|-----------|---------|
| C_1 | 0.9135 |
| C_2 | 0.0403 |
| C_3 | 0.0153 |
| i - C_4 | 0.0039 |
| n - C_4 | 0.0043 |
| i - C_5 | 0.0015 |
| n - C_5 | 0.0019 |
| C_6 | 0.0039 |
| C_7 | 0.00361 |
| C_8 | 0.00285 |
| C_9 | 0.00222 |
| C_{10} | 0.00158 |
| C_{11+} | 0.00514 |

Solution

Step 1. Determine the coefficients A and B of Equation 15-173 by the least-squares fit to the mole fractions C_6 through C_{10} to give $A = 0.03453$ and $B = 0.08777$.

Step 2. Solve for the mole fraction of C_{10} through C_{15} by applying Equation 15-173 and setting $z_6 = 0.0039$:

| Component | Experimental z_n | Equation 15-173 z_n |
|------------------|--------------------|-----------------------|
| C ₇ | 0.00361 | 0.00361 |
| C ₈ | 0.00285 | 0.00285 |
| C ₉ | 0.00222 | 0.00222 |
| C ₁₀ | 0.00158 | 0.00158 |
| C ₁₁ | 0.00121 | 0.00106 |
| C ₁₂ | 0.00097 | 0.00066 |
| C ₁₃ | 0.00083 | 0.00039 |
| C ₁₄ | 0.00069 | 0.00021 |
| C ₁₅ | 0.00050 | 0.00011 |
| C ₁₆₊ | 0.00094 | 0.00271* |

*Obtained by applying Equation 15-169.

Step 3. Calculate the molecular weight and specific gravity of C₁₆₊ by applying Equations 15-170 and 15-171 to give $(M)_{16+} = 233.3$ and $(\gamma)_{16+} = 0.943$.

Step 4. Solve for T_b , p_c , T_c , and ω by applying the Riazi–Daubert and Edmister correlations, to give:

$$\begin{aligned} T_b &= 1103^\circ\text{R} \\ p_c &= 251 \text{ psia} \\ T_c &= 1467^\circ\text{R} \\ \omega &= 0.600 \end{aligned}$$

Pedersen's Method

Pedersen et al. (1982) proposed that, for naturally occurring hydrocarbon mixtures, an exponential relationship exists between the mole fraction of a component and the corresponding carbon number. They expressed this relationship mathematically in the following form:

$$z_n = e^{(n-A)/B} \quad (15-174)$$

where A and B are constants.

For condensates and volatile oils, Pedersen and coworkers suggested that A and B can be determined by a least-squares fit to the molar distribution of the lighter fractions. Equation 15-174 can then be used to calculate

the molar content of each of the heavier fractions by extrapolation. The classical constraints as given by Equations 15-169 through 15-171 are also imposed.

Example 15-19

Rework Example 15-18 using the Pedersen splitting correlation.

Solution

Step 1. Calculate coefficients A and B by the least-squares fit to the molar distribution of C₆ through C₁₀ to give A = -14.404639 and B = -3.8125739.

Step 2. Solve for the mole fraction of C₁₀ through C₁₅ by applying Equation 15-176.

| Component | Experimental z_n | Calculated z_n |
|------------------|--------------------|------------------|
| C ₇ | 0.000361 | 0.00361 |
| C ₈ | 0.00285 | 0.00285 |
| C ₉ | 0.00222 | 0.00222 |
| C ₁₀ | 0.00158 | 0.00166 |
| C ₁₁ | 0.00121 | 0.00128 |
| C ₁₂ | 0.00097 | 0.00098 |
| C ₁₃ | 0.00083 | 0.00076 |
| C ₁₄ | 0.00069 | 0.00058 |
| C ₁₅ | 0.00050 | 0.00045 |
| C ₁₆₊ | 0.00094 | 0.00101* |

*From Equation 15-169.

Ahmed's Method

Ahmed et al. (1985) devised a simplified method for splitting the C₇₊ fraction into pseudo-components. The method originated from studying the molar behavior of 34 condensate and crude oil systems through detailed laboratory compositional analysis of the heavy fractions. The only required data for the proposed method are the molecular weight and the total mole fraction of the heptanes-plus fraction.

The splitting scheme is based on calculating the mole fraction z_n at a progressively higher number of carbon atoms. The extraction process

continues until the sum of the mole fraction of the pseudo-components equals the total mole fraction of the heptanes-plus (z_{7+}).

$$z_n = z_{n+} \left[\frac{M_{(n+1)+} - M_{n+}}{M_{(n+1)+} - M_n} \right] \quad (15-175)$$

where z_n = mole fraction of the pseudo-component with a number of carbon atoms of n (z_7, z_8, z_9 , etc.)

M_n = molecular weight of the hydrocarbon group with n carbon atoms as given in Table 1-1 in Chapter 1

M_{n+} = molecular weight of the $n+$ fraction as calculated by the following expression:

$$M_{(n+1)+} = M_{7+} + S(n - 6) \quad (15-176)$$

where n is the number of carbon atoms and S is the coefficient of Equation 15-178 with these values:

| Number of Carbon Atoms | Condensate Systems | Crude Oil Systems |
|------------------------|--------------------|-------------------|
| $n \leq 8$ | 15.5 | 16.5 |
| $n > 8$ | 17.0 | 20.1 |

The stepwise calculation sequences of the proposed correlation are summarized in the following steps:

- Step 1.* According to the type of hydrocarbon system under investigation (condensate or crude oil), select appropriate values for the coefficients.
- Step 2.* Knowing the molecular weight of C_{7+} fraction (M_{7+}), calculate the molecular weight of the octanes-plus fraction (M_{8+}) by applying Equation 15-176.
- Step 3.* Calculate the mole fraction of the heptane fraction (z_7) using Equation 15-175.
- Step 4.* Apply Steps 2 and 3 repeatedly for each component in the system (C_8, C_9 , etc.) until the sum of the calculated mole fractions is equal to the mole fraction of C_{7+} of the system.

The splitting scheme is best explained through the following example.

Example 15-20

Rework Example 15-19 using Ahmed's splitting method.

Solution

Step 1. Calculate the molecular weight of C_{8+} by applying Equation 15-176:

$$M_{8+} = 141.25 + 15.5(7 - 6) = 156.75$$

Step 2. Solve for the mole fraction of heptane (z_7) by applying Equation 15-175:

$$z_7 = z_{7+} \left[\frac{M_{8+} - M_{7+}}{M_{8+} - M_7} \right] = 0.0154 \left[\frac{156.75 - 141.25}{156.75 - 96} \right] = 0.00393$$

Step 3. Calculate the molecular weight of C_{9+} from Equation 15-178:

$$M_{9+} = 141.25 + 15.5(8 - 6) = 172.25$$

Step 4. Determine the mole fraction of C_8 from Equation 15-177:

$$z_8 = z_{8+} \left[\frac{(M_{9+} - M_{8+})}{(M_{9+} - M_8)} \right]$$

$$z_8 = (0.0154 - 0.00393) \left[\frac{(172.5 - 156.75)}{(172.5 - 107)} \right]$$

$$= 0.00276$$

Step 5. This extracting method is repeated as outlined in the above steps to give:

| Component | n | M_{n+} Equation 15-176 | M_n (Table 1-1) | z_n Equation 15-175 |
|-----------|-----|-----------------------------|----------------------|--------------------------|
| C_7 | 7 | 141.25 | 96 | 0.000393 |
| C_8 | 8 | 156.25 | 107 | 0.00276 |
| C_9 | 9 | 175.25 | 121 | 0.00200 |
| C_{10} | 10 | 192.25 | 134 | 0.00144 |
| C_{11} | 11 | 209.25 | 147 | 0.00106 |
| C_{12} | 12 | 226.25 | 161 | 0.0008 |
| C_{13} | 13 | 243.25 | 175 | 0.00061 |
| C_{14} | 14 | 260.25 | 190 | 0.00048 |
| C_{15} | 15 | 277.25 | 206 | 0.00038 |
| C_{16+} | 16+ | 294.25 | 222 | 0.00159* |

*Calculated from Equation 15-169.

Step 6. The boiling point, critical properties, and the acentric factor of C_{16+} are then determined by using the appropriate methods, where

$$\begin{aligned}M &= 222 \\ \gamma &= 0.856 \\ T_b &= 1174.6^\circ\text{R} \\ p_c &= 175.9 \text{ psia} \\ T_c &= 1449.3^\circ\text{R} \\ \omega &= 0.742\end{aligned}$$

Lumping Schemes

The large number of components necessary to describe the hydrocarbon mixture for accurate phase behavior modeling frequently burdens EOS calculations. Often, the problem is either lumping together the many experimentally determined fractions, or modeling the hydrocarbon system when the only experimental data available for the C_{7+} fraction are the molecular weight and specific gravity.

Generally, with a sufficiently large number of pseudo-components used in characterizing the heavy fraction of a hydrocarbon mixture, a satisfactory prediction of the PVT behavior by the equation of state can be obtained. However, in compositional models, the cost and computing time can increase significantly with the increased number of components in the system. Therefore, strict limitations are placed on the maximum number of components that can be used in compositional models and the original components have to be lumped into a smaller number of pseudo-components.

The term *lumping* or *pseudoization* then denotes the reduction in the number of components used in EOS calculations for reservoir fluids. This reduction is accomplished by employing the concept of the pseudo-component. The pseudo-component denotes a group of pure components lumped together and represented by a single component.

Several problems are associated with “regrouping” the original components into a smaller number without losing the predicting power of the equation of state. These problems include:

- How to select the groups of pure components to be represented by one pseudo-component each
- What mixing rules should be used for determining the EOS constants (p_c , T_c , and ω) for the new lumped pseudo-components

Several unique techniques have been published that can be used to address the above lumping problems, notably the methods proposed by:

- Lee et al. (1979)
- Whitson (1980)
- Mehra et al. (1983)
- Montel and Gouel (1984)
- Schlijper (1984)
- Behrens and Sandler (1986)
- Gonzalez, Colonomos, and Rusinek (1986)

Several of these techniques are presented in the following discussion.

Whitson's Lumping Scheme

Whitson (1980) proposed a regrouping scheme whereby the compositional distribution of the C_{7+} fraction is reduced to only a few multiple-carbon-number (MCN) groups. Whitson suggested that the number of MCN groups necessary to describe the plus fraction is given by the following empirical rule:

$$N_g = \text{Int}[1 + 3.3 \log(N - n)] \quad (15-177)$$

where N_g = number of MCN groups

Int = integer

N = number of carbon atoms of the last component in the hydrocarbon system

n = number of carbon atoms of the first component in the plus fraction, i.e., $n = 7$ for C_{7+}

The integer function requires that the real expression evaluated inside the brackets be rounded to the nearest integer. Whitson pointed out that for black-oil systems, one could reduce the calculated value of N_g .

The molecular weights separating each MCN group are calculated from the following expression:

$$M_I = M_{C7} \left(\frac{M_{N+}}{M_{C7}} \right)^{I/N_g} \quad (15-178)$$

where $(M)_{N+}$ = molecular weight of the last reported component in the extended analysis of the hydrocarbon system

$$M_{C7} = \text{molecular weight of } C_7$$

$$I = 1, 2, \dots, N_g$$

Components with a molecular weight falling within the boundaries of M_{I-1} to M_I are included in the I 'th MCN group. Example 15-21 illustrates the use of Equations 15-177 and 15-178.

Example 15-21

Given the following compositional analysis of the C_{7+} fraction in a condensate system, determine the appropriate number of pseudo-components forming in the C_{7+} .

| Component | z_i |
|-----------|----------|
| C_7 | 0.00347 |
| C_8 | 0.00268 |
| C_9 | 0.00207 |
| C_{10} | 0.001596 |
| C_{11} | 0.00123 |
| C_{12} | 0.00095 |
| C_{13} | 0.00073 |
| C_{14} | 0.000566 |
| C_{15} | 0.000437 |
| C_{16+} | 0.001671 |

$$M_{16+} = 259.$$

Solution

Step 1. Determine the molecular weight of each component in the system:

| Component | z_i | M_i |
|-----------|----------|-------|
| C_7 | 0.00347 | 96 |
| C_8 | 0.00268 | 107 |
| C_9 | 0.00207 | 121 |
| C_{10} | 0.001596 | 134 |
| C_{11} | 0.00123 | 147 |
| C_{12} | 0.00095 | 161 |
| C_{13} | 0.00073 | 175 |
| C_{14} | 0.000566 | 190 |
| C_{15} | 0.000437 | 206 |
| C_{16+} | 0.001671 | 259 |

Step 2. Calculate the number of pseudo-components from Equation 15-178:

$$N_g = \text{Int}[1 + 3.3 \log(16 - 7)]$$

$$N_g = \text{Int}[4.15]$$

$$N_g = 4$$

Step 3. Determine the molecular weights separating the hydrocarbon groups by applying Equation 15-179:

$$M_1 = 96 \left[\frac{259}{96} \right]^{1/4}$$

$$M_1 = 96 [2.698]^{1/4}$$

| i | (M) _i |
|---|------------------|
| 1 | 123 |
| 2 | 158 |
| 3 | 202 |
| 4 | 259 |

- **First pseudo-component:** The first pseudo-component includes all components with a molecular weight in the range of 96 to 123. This group then includes C₇, C₈, and C₉.
- **Second pseudo-component:** The second pseudo-component contains all components with a molecular weight higher than 123 to a molecular weight of 158. This group includes C₁₀ and C₁₁.
- **Third pseudo-component:** The third pseudo-component includes components with a molecular weight higher than 158 to a molecular weight of 202. Therefore, this group includes C₁₂, C₁₃, and C₁₄.
- **Fourth pseudo-component:** This pseudo-component includes all the remaining components, i.e., C₁₅ and C₁₆₊.

| Group I | Component | z_i | z_i |
|---------|------------------|----------|----------|
| 1 | C ₇ | 0.00347 | 0.00822 |
| | C ₈ | 0.00268 | |
| | C ₉ | 0.00207 | |
| 2 | C ₁₀ | 0.001596 | 0.002826 |
| | C ₁₁ | 0.00123 | |
| 3 | C ₁₂ | 0.00095 | 0.002246 |
| | C ₁₃ | 0.00073 | |
| | C ₁₄ | 0.000566 | |
| 4 | C ₁₅ | 0.000437 | 0.002108 |
| | C ₁₆₊ | 0.001671 | |

It is convenient at this stage to present the mixing rules that can be employed to characterize the pseudo-component in terms of its pseudo-physical and pseudo-critical properties. Because there are numerous ways to mix the properties of the individual components, all giving different properties for the pseudo-components, the choice of a correct mixing rule is as important as the lumping scheme. Some of these mixing rules are given next.

Hong's Mixing Rules

Hong (1982) concluded that the weight fraction average w_i is the best mixing parameter in characterizing the C₇₊ fractions by the following mixing rules:

- Pseudo-critical pressure $p_{cL} = \sum_{i=1}^L w_i p_{ci}$
- Pseudo-critical temperature $T_{cL} = \sum_{i=1}^L w_i T_{ci}$
- Pseudo-critical volume $V_{cL} = \sum_{i=1}^L w_i V_{ci}$
- Pseudo-acentric factor $\omega_L = \sum_{i=1}^L [\phi_i \omega_i]$
- Pseudo-molecular weight $M_L = \sum_{i=1}^L w_i M_i$
- Binary interaction coefficient $K_{kl} = 1 - \sum_{i=1}^L \sum_{j=1}^L w_i w_j (1 - k_{ij})$

with:

$$w_i = \frac{z_i M_i}{\sum_L z_i M_i}$$

where: w_i = average weight fraction

K_{kL} = binary interaction coefficient between the k 'th component and the lumped fraction

The subscript L in the above relationship denotes the lumped fraction.

Lee's Mixing Rules

Lee et al. (1979), in their proposed regrouping model, employed Kay's mixing rules as the characterizing approach for determining the properties of the lumped fractions. Defining the normalized mole fraction of the component i in the lumped fraction as:

$$\phi_i = z_i / \sum_L z_i$$

the following rules are proposed:

$$M_L = \sum_L \phi_i M_i \quad (15-179)$$

$$\gamma_L = M_L / \sum_L [\phi_i M_i / \gamma_i] \quad (15-180)$$

$$V_{cL} = \sum_L [\phi_i M_i V_{ci} / M_L] \quad (15-181)$$

$$p_{cL} = \sum_L [\phi_i p_{ci}] \quad (15-182)$$

$$T_{cL} = \sum_L [\phi_i T_{ci}] \quad (15-183)$$

$$\omega_L = \sum_L [\phi_i \omega_i] \quad (15-184)$$

Example 15-22

Using Lee's mixing rules, determine the physical and critical properties of the four pseudo-components in Example 15-21.

Solution

Step 1. Assign the appropriate physical and critical properties to each component:

| Group | Comp. | z_i | z_i | M_i | γ_i | V_{ci} | p_{ci} | T_{ci} | ω_i |
|-------|------------------|----------|----------|-------|------------|---------------------|------------------|----------|-------------------|
| 1 | C ₇ | 0.00347 | | 96* | 0.272* | 0.06289* | 453* | 985* | 0.280* |
| | C ₈ | 0.00268 | 0.00822 | 107 | 0.748 | 0.06264 | 419 | 1036 | 0.312 |
| | C ₉ | 0.00207 | | 121 | 0.768 | 0.06258 | 383 | 1058 | 0.348 |
| 2 | C ₁₀ | 0.001596 | 0.002826 | 134 | 0.782 | 0.06273 | 351 | 1128 | 0.385 |
| | C ₁₁ | 0.00123 | | 147 | 0.793 | 0.06291 | 325 | 1166 | 0.419 |
| 3 | C ₁₂ | 0.00095 | | 161 | 0.804 | 0.06306 | 302 | 1203 | 0.454 |
| | C ₁₃ | 0.00073 | 0.002246 | 175 | 0.815 | 0.06311 | 286 | 1236 | 0.484 |
| | C ₁₄ | 0.000566 | | 190 | 0.826 | 0.06316 | 270 | 1270 | 0.516 |
| 4 | C ₁₅ | 0.000437 | 0.002108 | 206 | 0.826 | 0.06325 | 255 | 1304 | 0.550 |
| | C ₁₆₊ | 0.001671 | | 259 | 0.908 | 0.0638 [†] | 215 [†] | 1467 | 0.68 [†] |

*From Table 1-1.

[†]Calculated.

Step 2. Calculate the physical and critical properties of each group by applying Equations 15-179 through 15-184 to give:

| Group | Z_i | M_i | γ_i | V_{ci} | p_{ci} | T_{ci} | ω_i |
|-------|----------|-------|------------|----------|----------|----------|------------|
| 1 | 0.00822 | 105.9 | 0.746 | 0.0627 | 424 | 1020 | 0.3076 |
| 2 | 0.002826 | 139.7 | 0.787 | 0.0628 | 339.7 | 1144.5 | 0.4000 |
| 3 | 0.002246 | 172.9 | 0.814 | 0.0631 | 288 | 1230.6 | 0.4794 |
| 4 | 0.002108 | 248 | 0.892 | 0.0637 | 223.3 | 1433 | 0.6531 |

PROBLEMS

1. A hydrocarbon system has the following composition:

| Component | z_i |
|--------------------|-------|
| C ₁ | 0.30 |
| C ₂ | 0.10 |
| C ₃ | 0.05 |
| i - C ₄ | 0.03 |
| n - C ₄ | 0.03 |
| i - C ₅ | 0.02 |
| n - C ₅ | 0.02 |
| C ₆ | 0.05 |
| C ₇₊ | 0.40 |

Given the following additional data:

System pressure = 2100 psia
 System temperature = 150°F
 Specific gravity of C₇₊ = 0.80
 Molecular weight of C₇₊ = 140

Calculate the equilibrium ratios of the above system.

2. A well is producing oil and gas with the compositions given below at a gas-oil ratio of 500 scf/STB:

| Component | x_i | y_i |
|--------------------|-------|-------|
| C ₁ | 0.35 | 0.60 |
| C ₂ | 0.08 | 0.10 |
| C ₃ | 0.07 | 0.10 |
| n - C ₄ | 0.06 | 0.07 |
| n - C ₅ | 0.05 | 0.05 |
| C ₆ | 0.05 | 0.05 |
| C ₇₊ | 0.34 | 0.05 |

Given the following additional data:

Current reservoir pressure = 3000 psia
 Bubble-point pressure = 2800 psia
 Reservoir temperature = 120°F
 M of C₇₊ = 125
 Specific gravity of C₇₊ = 0.823

Calculate the composition of the reservoir fluid.

3. A saturated hydrocarbon mixture with the composition given below exists in a reservoir at 234°F:

| Component | z_i |
|-----------------|--------|
| C ₁ | 0.3805 |
| C ₂ | 0.0933 |
| C ₃ | 0.0885 |
| C ₄ | 0.0600 |
| C ₅ | 0.0378 |
| C ₆ | 0.0356 |
| C ₇₊ | 0.3043 |

Calculate:

- The bubble-point pressure of the mixture
 - The compositions of the two phases if the mixture is flashed at 500 psia and 150°F
 - The density of the liquid phase
 - The compositions of the two phases if the liquid from the first separator is further flashed at 14.7 psia and 60°F
 - The oil formation volume factor at the bubble-point pressure
 - The original gas solubility
 - The oil viscosity at the bubble-point pressure
4. A crude oil exists in a reservoir at its bubble-point pressure of 2,520 psig and a temperature of 180°F. The oil has the following composition:

| Component | x_i |
|--------------------|--------|
| CO ₂ | 0.0044 |
| N ₂ | 0.0045 |
| C ₁ | 0.3505 |
| C ₂ | 0.0464 |
| C ₃ | 0.0246 |
| i - C ₄ | 0.0683 |
| n - C ₄ | 0.0083 |
| i - C ₅ | 0.0080 |
| n - C ₅ | 0.0080 |
| C ₆ | 0.0546 |
| C ₇₊ | 0.4824 |

The molecular weight and specific gravity of C_{7+} are 225 and 0.8364. The reservoir contains initially 12 MMbbl of oil. The surface facilities consist of two separation stages connecting in series. The first separation stage operates at 500 psig and 100°F. The second stage operates under standard conditions.

- a. Characterize C_{7+} in terms of its critical properties, boiling point, and acentric factor.
 - b. Calculate the initial oil-in-place in STB.
 - c. Calculate the standard cubic feet of gas initially in solution.
 - d. Calculate the composition of the free gas and the composition of the remaining oil at 2,495 psig, assuming the overall composition of the system will remain constant.
5. A pure n-butane exists in the two-phase region at 120°F. Calculate the density of the coexisting phase by using the following equations of state:
- a. Van der Waals
 - b. Redlich-Kwong
 - c. Soave-Redlich-Kwong
 - d. Peng-Robinson
6. A crude oil system with the following composition exists at its bubble-point pressure of 3,250 psia and 155°F:

| Component | x_i |
|-----------|-------|
| C_1 | 0.42 |
| C_2 | 0.08 |
| C_3 | 0.06 |
| C_4 | 0.02 |
| C_5 | 0.01 |
| C_6 | 0.04 |
| C_{7+} | 0.37 |

If the molecular weight and specific gravity of the heptanes-plus fraction are 225 and 0.823, respectively, calculate the density of the crude oil by using:

- a. Van der Waals EOS
- b. Redlich-Kwong EOS

- c. SRR EOS
- d. PR EOS

7. Calculate the vapor pressure of propane at 100°F by using:

- a. Van der Waals EOS
- b. SRK EOS
- c. PR EOS

Compare the results with that obtained from the Cox chart.

8. A natural gas exists at 2,000 psi and 150°F. The gas has the following composition:

| Component | y_i |
|--------------------|-------|
| C ₁ | 0.80 |
| C ₂ | 0.10 |
| C ₃ | 0.07 |
| i - C ₄ | 0.02 |
| n - C ₄ | 0.01 |

Calculate the density of the gas using the following equations of state:

- a. VdW
 - b. RK
 - c. SRK
 - d. PR
9. The heptanes-plus fraction in a condensate gas system is characterized by a molecular weight and specific gravity of 190 and 0.8, respectively. The mole fraction of the C₇₊ is 0.12. Extend the molar distribution of the plus fraction to C₂₀₊ by using:
- a. Katz's method
 - b. Ahmed's method

Determine the critical properties of C₂₀₊.

10. A naturally occurring crude oil system has a heptanes-plus fraction with the following properties:

$$M_{7+} = 213$$

$$\gamma_{7+} = 0.8405$$

$$x_{7+} = 0.3497$$

Extend the molar distribution of the plus fraction to C_{25+} and determine the critical properties and acentric factor of the last component.

11. A crude oil system has the following composition:

| Component | x_i |
|-----------|--------|
| C_1 | 0.3100 |
| C_2 | 0.1042 |
| C_3 | 0.1187 |
| C_4 | 0.0732 |
| C_5 | 0.0441 |
| C_6 | 0.0255 |
| C_{7+} | 0.3243 |

The molecular weight and specific gravity of C_{7+} are 215 and 0.84, respectively.

- Extend the molar distribution of C_{7+} to C_{20+} .
- Calculate the appropriate number of pseudo-components necessary to adequately represent the composition from C_7 to C_{20+} and characterize the resulting pseudo-components in terms of:

- Molecular weight
- Specific gravity
- Critical properties
- Acentric factor

REFERENCES

- Ahmed, T., "A Practical Equation of State," *SPE*, Feb. 1991, Vol. 291, pp. 136–137.
- Ahmed, T., Cady, G., and Story, A., "A Generalized Correlation for Characterizing the Hydrocarbon Heavy Fractions," SPE Paper 14266 presented at

- the SPE 60th Annual Technical Conference, Las Vegas, NV, Sep. 22–25, 1985.
3. Alani, G. H., and Kennedy, H. T., "Volume of Liquid Hydrocarbons at High Temperatures and Pressures," *Trans. AIME*, 1960, Vol. 219, pp. 288–292.
 4. Amyx, J., Bass, D., and Whitney, R., *Petroleum Reservoir Engineering*. New York: McGraw-Hill Book Company, 1960.
 5. Behrens, R., and Sandler, S., "The Use of Semi-Continuous Description to Model the C₇₊ Fraction in Equation of State Calculation," SPE/DOE Paper 14925 presented at the 5th Annual Symposium on EOR, Tulsa, OK, April 20–23, 1986.
 6. Brinkman, F. H., and Sicking, J. N., "Equilibrium Ratios for Reservoir Studies," *Trans. AIME*, 1960, Vol. 219, pp. 313–319.
 7. Campbell, J. M., *Gas Conditioning and Processing*, Vol. 1. Norman, OK: Campbell Petroleum Series, 1976.
 8. Chueh, P., and Prausnitz, J., "Vapor-Liquid Equilibria at High Pressures: Calculation of Critical Temperatures, Volumes, and Pressures of Nonpolar Mixtures," *AIChE Journal*, 1967, Vol. 13, No. 6, pp. 1107–1112.
 9. Clark, N., *Elements of Petroleum Reservoirs*. Dallas: Society of Petroleum Engineers, 1960.
 10. Clark, N., "A Review of Reservoir Engineering," *World Oil*, June 1951.
 11. Dykstra, H., and Mueller, T. D., "Calculation of Phase Composition and Properties for Lean- or Enriched-Gas Drive," *SPEJ*, Sep. 1965, pp. 239–246.
 12. Edmister, W., and Lee, B., *Applied Hydrocarbon Thermodynamics*, Vol. 1, 2nd ed. Houston: Gulf Publishing Company, 1986, p. 52.
 13. Elliot, J., and Daubert, T., "Revised Procedure for Phase Equilibrium Calculations with Soave Equation of State," *Ind. Eng. Chem. Process Des. Dev.*, 1985, Vol. 23, pp. 743–748.
 14. Gibbons, R., and Laughton, A., "An Equation of State for Polar and Non-Polar Substances and Mixtures," *J. Chem. Soc.*, 1984, Vol. 80, pp. 1019–1038.
 15. Gonzalez, E., Colonomos, P., and Rusinek, I., "A New Approach for Characterizing Oil Fractions and for Selecting Pseudo-Components of Hydrocarbons," *Canadian JPT*, March-April 1986, pp. 78–84.
 16. Graboski, M. S., and Daubert, T. E., "A Modified Soave Equation of State for Phase Equilibrium Calculations 1. Hydrocarbon System," *Ind. Eng. Chem. Process Des. Dev.*, 1978, Vol. 17, pp. 443–448.
 17. Hadden, J. T., "Convergence Pressure in Hydrocarbon Vapor-Liquid Equilibria," *Chem. Eng. Progr. Symposium Ser.*, 1953, Vol. 49, No. 7, p. 53.

18. Hariu, O., and Sage, R., "Crude Split Figured by Computer," *Hydrocarbon Process.*, April 1969, pp. 143–148.
19. Heyen, G., "A Cubic Equation of State with Extended Range of Application," paper presented at 2nd World Congress Chemical Engineering, Montreal, Oct. 4–9, 1983.
20. Hoffmann, A. E., Crump, J. S., and Hocott, R. C., "Equilibrium Constants for a Gas-Condensate System," *Trans. AIME*, 1953, Vol. 198, pp. 1–10.
21. Hong, K. C., "Lumped-Component Characterization of Crude Oils for Compositional Simulation," SPE/DOE Paper 10691 presented at the 3rd Joint Symposium on EOR, Tulsa, OK, April 4–7, 1982.
22. Jhaveri, B. S., and Youngren, G. K., "Three-Parameter Modification of the Peng-Robinson Equation of State to Improve Volumetric Predictions," SPE Paper 13118 presented at the 1984 SPE Annual Technical Conference, Houston, Sep. 16–19.
23. Katz, D. L., and Hachmuth, K. H., "Vaporization Equilibrium Constants in a Crude Oil-Natural Gas System," *Ind. Eng. Chem.*, 1937, Vol. 29, p. 1072.
24. Katz, D., et al., "Overview of Phase Behavior of Oil and Gas Production," *JPT*, June 1983, pp. 1205–1214.
25. Katz, D., et al., *Handbook of Natural Gas Engineering*. New York: McGraw-Hill Book Company, 1959.
26. Kehn, D. M., "Rapid Analysis of Condensate Systems by Chromatography," *JPT*, April 1964, pp. 435–440.
27. Kubic, W. L. J., "A Modification of the Martin Equation of State for Calculating Vapor-Liquid Equilibria," *Fluid Phase Equilibria*, 1982, Vol. 9, pp. 79–97.
28. Lee, B., and Kesler, G., "A Generalized Thermodynamic Correlation Based on Three-Parameter Corresponding States," *AIChE Journal*, May 1975, Vol. 21, No. 3, pp. 510–527.
29. Lee, S., et al., "Experimental and Theoretical Studies on the Fluid Properties Required for Simulation of Thermal Processes," SPE Paper 8393 presented at the SPE 54th Annual Technical Conference, Las Vegas, NV, Sep. 23–26, 1979.
30. Lim, D., et al., "Calculation of Liquid Dropout for Systems Containing Water," SPE Paper 13094 presented at the SPE 59th Annual Technical Conference, Houston, Sep. 16–19, 1984.
31. Lohrenz, J., Bray, B. G., and Clark, C. R., "Calculating Viscosities of Reservoir Fluids from Their Compositions," *JPT*, Oct. 1964, p. 1171; *Trans. AIME*, Vol. 231.

32. Maddox, R. N., and Erbar, J. H., "Improve P-V-T Predictions," *Hydrocarbon Process.*, January 1984, pp. 119–121.
33. Maddox, R. N., and Erbar, J. H., *Gas Conditioning and Processing, Vol. 3—Advanced Techniques and Applications*. Norman, OK: Campbell Petroleum Series, 1982.
34. Mehra, R., et al., "A Statistical Approach for Combining Reservoir Fluids into Pseudo Components for Compositional Model Studies," SPE Paper 11201 presented at the SPE 57th Annual Meeting, New Orleans, Sep. 26–29, 1983.
35. Montel, F., and Gouel, P., "A New Lumping Scheme of Analytical Data for Composition Studies," SPE Paper 13119 presented at the SPE 59th Annual Technical Conference, Houston, Sep. 16–19, 1984.
36. Nikos, V., et al., "Phase Behavior of Systems Comprising North Sea Reservoir Fluids and Injection Gases," *JPT*, Nov. 1986, pp. 1221–1233.
37. Patel, N., and Teja, A., "A New Equation of State for Fluids and Fluid Mixtures," *Chem. Eng. Sci.*, 1982, Vol. 37, No. 3, pp. 463–473.
38. Pedersen, K., Thomassen, P., and Fredenslund, A., "Phase Equilibria and Separation Processes," Report SEP 8207. Denmark: Institute for Kemiteknik, Denmark Tekniske Hojskole (July 1982).
39. Peneloux, A., Rauzy, E., and Freze, R., "A Consistent Correlation for Redlich–Kwong–Soave Volumes," *Fluid Phase Equilibria*, 1982, Vol. 8, pp. 7–23.
40. Peng, D., and Robinson, D., "Two and Three Phase Equilibrium Calculations for Coal Gasification and Related Processes," ACS Symposium Series, No. 133, *Thermodynamics of Aqueous Systems with Industrial Applications*. Washington, DC: American Chemical Society, 1980.
41. Peng, D., and Robinson, D., "A New Two Constant Equation of State," *Ind. Eng. Chem. Fund.*, 1976a, Vol. 15, No. 1, pp. 59–64.
42. Peng, D., and Robinson, D., "Two and Three Phase Equilibrium Calculations for Systems Containing Water," *Canadian J. Chem. Eng.*, 1976b, Vol. 54, pp. 595–598.
43. Peterson, C. S., "A Systematic and Consistent Approach to Determine Binary Interaction Coefficients for the Peng-Robinson Equations of State," *SPE*, Nov. 1989, pp. 488–496.
44. Redlich, O., and Kwong, J., "On the Thermodynamics of Solutions. An Equation of State. Fugacities of Gaseous Solutions," *Chem. Rev.*, 1949, Vol. 44, pp. 233–247.

45. Reid, R., Prausnitz, J. M., and Sherwood, T., *The Properties of Gases and Liquids, Third Edition*. New York: McGraw-Hill Book Company, 1977, p. 21.
46. Robinson, D. B., and Peng, D. Y., "The Characterization of the Heptanes and Heavier Fractions," *Research Report 28*, Tulsa: GPA, 1978.
47. Rzasas, M. J., Glass, E. D., and Opfell, J. B., "Prediction of Critical Properties and Equilibrium Vaporization Constants for Complex Hydrocarbon Systems," *Chem. Eng. Progr. Symposium Ser.*, 1952, Vol. 48, No. 2, p. 28.
48. Schlijper, A. G., "Simulation of Compositional Process: The Use of Pseudo-Components in Equation of State Calculations," SPE/DOE Paper 12633 presented at the SPE/DOE 4th Symposium on EOR, Tulsa, OK, April 15–18, 1984.
49. Schmidt, G., and Wenzel, H., "A Modified Van der Waals Type Equation of State," *Chem. Eng. Sci.*, 1980, Vol. 135, pp. 1503–1512.
50. Sim, W. J., and Daubert, T. E., "Prediction of Vapor-Liquid Equilibria of Undefined Mixtures," *Ind. Eng. Chem. Process Des. Dev.*, 1980, Vol. 19, No. 3, pp. 380–393.
51. Slot-Petersen, C., "A Systematic and Consistent Approach to Determine Binary Interaction Coefficients for the Peng-Robinson Equation of State," SPE Paper 16941 presented at the SPE 62 Annual Technical Conference, Dallas, Sep. 27–30, 1987.
52. Soave, G., "Equilibrium Constants from a Modified Redlich–Kwong Equation of State," *Chem. Eng. Sci.*, 1972, Vol. 27, pp. 1197–1203.
53. Spencer, C., Daubert, T., and Danner, R., "A Critical Review of Correlations for the Critical Properties of Defined Mixtures," *AIChE Journal*, 1973, Vol. 19, No. 3, pp. 522–527.
54. Standing, M. B., "A Set of Equations for Computing Equilibrium Ratios of a Crude Oil/Natural Gas System at Pressures Below 1,000 psia," *JPT*, Sep. 1979, pp. 1193–1195.
55. Standing, M. B., *Volumetric and Phase Behavior of Oil Field Hydrocarbon Systems*. Dallas: Society of Petroleum Engineers of AIME, 1977.
56. Standing, M. B., and Katz, D. L., "Density of Crude Oils Saturated with Natural Gas," *Trans. AIME*, 1942, Vol. 146, pp. 159–165.
57. Stryjek, R., and Vera, J. H., "PRSV: An Improvement to the Peng-Robinson Equation of State for Pure Compounds and Mixtures," *Canadian J. Chem. Eng.*, April 1986, Vol. 64, pp. 323–333.
58. Valderrama, J., and Cisternas, L., "A Cubic Equation of State for Polar and Other Complex Mixtures," *Fluid Phase Equilibria*, 1986, Vol. 29, pp. 431–438.

59. Van der Waals, J. D., "On the Continuity of the Liquid and Gaseous State," Ph.D. Dissertation, Sigthoff, Leiden, 1873.
60. Vidal, J., and Daubert, T., "Equations of State—Reworking the Old Forms," *Chem. Eng. Sci.*, 1978, Vol. 33, pp. 787–791.
61. Whitson, C., "Characterizing Hydrocarbon Plus Fractions," EUR Paper 183 presented at the European Offshore Petroleum Conference, London, Oct. 21–24, 1980.
62. Whitson, C. H., and Torp, S. B., "Evaluating Constant Volume Depletion Data," SPE Paper 10067 presented at the SPE 56th Annual Fall Technical Conference, San Antonio, TX, Oct. 5-7, 1981.
63. Willman, B. T., and Teja, B. T., "Continuous Thermodynamics of Phase Equilibria Using a Multivariable Distribution Function and an Equation of State," *AIChE Journal*, Dec. 1986, Vol. 32, No. 12, pp. 2067–2078.
64. Wilson, G., "A Modified Redlich–Kwong EOS, Application to General Physical Data Calculations," Paper 15C presented at the Annual AIChE National Meeting, Cleveland, OH, May 4–7, 1968.
65. Winn, F. W., "Simplified Nomographic Presentation, Hydrocarbon Vapor–Liquid Equilibria," *Chem. Eng. Progr. Symposium Ser.*, 1954, Vol. 33, No. 6, pp. 131–135.
66. Whitson, C., and Brule, M., *Phase Behavior*. Richardson, TX: Society of Petroleum Engineers, Inc., 2000.

C H A P T E R 1 6

ANALYSIS OF DECLINE AND TYPE CURVES

Production-decline analysis is the analysis of past trends of declining production performance, that is, rate versus time and rate versus cumulative production plots, for wells and reservoirs. From about 1975 to 2005, various methods were developed for estimating reserves in tight gas reservoirs. These methods range from the basic material balance equation to decline- and type-curve analysis techniques. There are two kinds of decline-curve analysis techniques, namely,

- The classical curve fit of historical production data
- The type-curve matching technique

Some graphical solutions use a combination of decline curves and type curves with varying limitations. General principles of both types and methods of combining both approaches to determine gas reserves are briefly presented in this chapter.

DECLINE-CURVE ANALYSIS

Decline curves are one of the most extensively used forms of data analysis employed in evaluating gas reserves and predicting future production. The decline-curve analysis technique is based on the assumption that past production trends and their controlling factors will continue in the future and, therefore, can be extrapolated and described by a mathematical expression.

The method of extrapolating a “trend” for the purpose of estimating future performance must satisfy the condition that the factors that caused changes in past performance, for example, decline in the flow rate, will operate in the same way in the future. These decline curves are characterized by three factors:

- Initial production rate, or the rate at some particular time
- Curvature of the decline
- Rate of decline

These factors are a complex function of numerous parameters within the reservoir, wellbore, and surface-handling facilities.

Ikoku (1984) presented a comprehensive and rigorous treatment of production-decline-curve analysis. He pointed out that the following three conditions must be considered in production-decline-curve analysis:

1. Certain conditions must prevail before we can analyze a production-decline curve with any degree of reliability. The production must have been stable over the period being analyzed; that is, a flowing well must have been produced with constant choke size or constant well-head pressure and a pumping well must have been pumped off or produced with constant fluid level. These indicate that the well must have been produced at capacity under a given set of conditions. The production decline observed should truly reflect reservoir productivity and not be the result of an external cause, such as a change in production conditions, well damage, production controls, or equipment failure.
2. Stable reservoir conditions must also prevail in order to extrapolate decline curves with any degree of reliability. This condition will normally be met as long as the producing mechanism is not altered. However, when an action is taken to improve the recovery of gas, such as infill drilling, fluid injection, fracturing, or acidizing, decline-curve analysis can be used to estimate the performance of the well or reservoir in the absence of the change and compare it to the actual performance with the change. This comparison will enable us to determine the technical and economic success of our efforts.
3. Production-decline-curve analysis is used in the evaluation of new investments and the audit of previous expenditures. Associated with this is the sizing of equipment and facilities such as pipelines, plants, and treating facilities. Also associated with the economic analysis is the determination of reserves for a well, lease, or field. This is an inde-

pendent method of reserve estimation, the result of which can be compared to volumetric or material-balance estimates.

Arps (1945) proposed that the “curvature” in the production-rate-versus-time curve can be expressed mathematically by a member of the hyperbolic family of equations. Arps recognized the following three types of rate-decline behavior:

- Exponential decline
- Harmonic decline
- Hyperbolic decline

Each type of decline curve has a different curvature, as shown in Figure 16-1. This figure depicts the characteristic shape of each type of decline when the flow rate is plotted versus time or versus cumulative production on **Cartesian, semi log, and log-log scales**. The main characteristics of these decline curves can be used to select the flow-rate-decline model that is appropriate for describing the rate-time relationship of the hydrocarbon system:

- **For exponential decline:** A straight-line relationship will result when the flow rate versus time is plotted on a semi log scale and also when

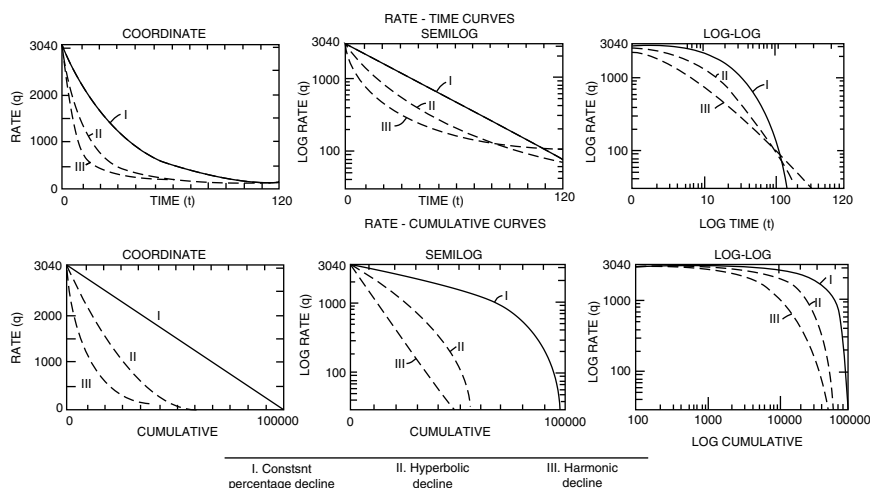


Figure 16-1. Classification of production decline curves. (After Arps, J.J. “Estimation of Primary Oil Reserves,” *Courtesy of Trans., AIME*, vol. 207, 1956).

the flow rate versus cumulative production is plotted on a Cartesian scale.

- **For harmonic decline:** Rate versus cumulative production is a straight line on a semi log scale; all other types of decline curves have some curvature. There are several shifting techniques that are designed to straighten out the curve that results from plotting flow rate versus time on a log-log scale.
- **For hyperbolic decline:** None of the above plotting scales, that is, Cartesian, semi log, or log-log, will produce a straight-line relationship for a hyperbolic decline. However, if the flow rate is plotted versus time on log-log paper, the resulting curve can be straightened out with shifting techniques.

Nearly all conventional decline-curve analysis is based on empirical relationships of production rate versus time, given by Arps (1945) as follows:

$$q_t = \frac{q_i}{(1 + bD_i t)^{1/b}} \quad (16-1)$$

where q_t = gas flow rate at time t , MMscf/day

q_i = initial gas flow rate, MMscf/day

t = time, days

D_i = initial decline rate, day⁻¹

b = Arps' decline-curve exponent

The mathematical description of these production-decline curves is greatly simplified by the use of the instantaneous (nominal) decline rate, D . This decline rate is defined as the rate of change of the natural logarithm of the production rate, that is, $\ln(q)$, with respect to time, t , or

$$D = -\frac{d(\ln q)}{dt} = -\frac{1}{q} \frac{dq}{dt} \quad (16-2)$$

The minus sign has been added because dq and dt have opposite signs and it is convenient to have D always positive. Notice that the decline-rate equation, Equation 16-2, describes the instantaneous changes in the slope of the curvature, dq/dt , with the change in the flow rate, q , over time.

The parameters determined from the classical fit of the historical data, namely the decline rate, D , and the exponent, b , can be used to predict future production. This type of decline-curve analysis can be applied to **individual wells or the entire reservoir**. The accuracy of the entire-reservoir application is sometimes even better than for individual wells due to smoothing of the rate data. Based on the type of rate-decline behavior of the hydrocarbon system, the value of b ranges from 0 to 1, and, accordingly, Arps' equation can be conveniently expressed in the following three forms:

| Case | b | Rate-Time Relationship |
|--------------------|---------|---------------------------------|
| Exponential | $b = 0$ | $q_t = q_i \exp(-D_i t)$ (16-3) |

| | | |
|-------------------|-------------|--|
| Hyperbolic | $0 < b < 1$ | $q_t = \frac{q_i}{(1 + b D_i t)^{1/b}}$ (16-4) |
|-------------------|-------------|--|

| | | |
|-----------------|---------|--|
| Harmonic | $b = 1$ | $q_t = \frac{q_i}{(1 + D_i t)}$ (16-5) |
|-----------------|---------|--|

Figure 16-2 illustrates the general shape of the three curves at different possible values of b . These mathematical relations can be applied equally for gas and oil reservoirs.

It should be pointed out that these three forms of decline-curve equations are *applicable ONLY when the well/reservoir is under pseudosteady (semi steady)-state flow conditions, that is, boundary-dominated flow conditions*. Arps' equation has been often misused to model the performance of oil and gas wells whose flow regimes are in a transient state. As presented in Chapter 6, when a well is first open to flow, it is in a transient (unsteady-state) condition. It remains in this condition until the production from the well affects the total reservoir system by reaching its drainage boundary, at which time the well is said to be flowing in a pseudosteady-state or **boundary-dominated flow condition**. The following is a list of inherent assumptions that must be satisfied before performance of rate-time decline-curve analysis:

- The well is draining a constant drainage area, that is, the well is in a boundary-dominated flow condition.

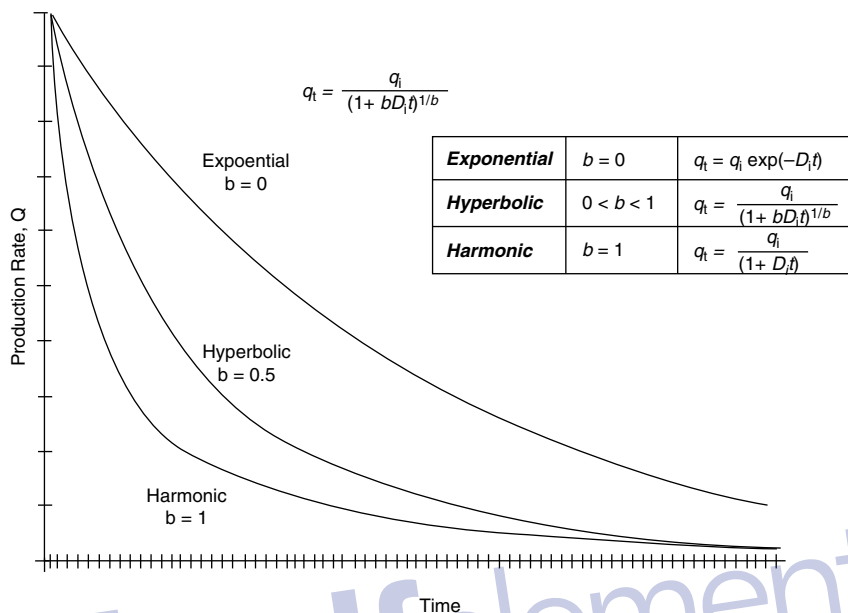


Figure 16-2. Decline curve-rate/time (exponential, harmonic, hyperbolic).

- The well is produced at or near capacity.
- The well is produced at a **constant bottom-hole pressure**.

Again, these three conditions must be satisfied before any of the decline-curve analysis methods is applied to describe the production performance of a reservoir. In most cases, tight gas wells are producing at capacity and approach a constant bottom-hole pressure if produced at a constant line pressure. However, it can be extremely difficult to determine when a tight gas well has defined its drainage area and thus to identify the start of the pseudosteady-state flow condition.

The area under the decline curve of q versus time between the times t_1 and t_2 is a measure of the cumulative oil or gas production during this period. Dealing with gas reservoirs, the cumulative gas production, G_p , can be expressed mathematically:

$$G_p = \int_{t_1}^{t_2} q_t dt \quad (16-6)$$

Replacing the flow rate, q_t , in the above equation with the three individual expressions that describe types of decline curves (Equations 16-3, 16-4, and 16-5), and integrating gives the following:

$$\text{Exponential } b = 0: \quad G_{p(t)} = \frac{(q_i - q_t)}{D_i} \quad (16-7)$$

$$\text{Hyperbolic } 0 < b < 1: \quad G_{p(t)} = \left[\frac{(q_i)}{D_i (1-b)} \right] \left[1 - \left(\frac{q_t}{q_i} \right)^{1-b} \right] \quad (16-8)$$

$$\text{Harmonic } b = 1: \quad G_{p(t)} = \left(\frac{q_i}{D_i} \right) \ln \left(\frac{q_i}{q_t} \right) \quad (16-9)$$

where $G_{p(t)}$ = cumulative gas production at time t , MMscf

q_i = initial gas flow rate at time $t = 0$, MMscf/unit time

t = time, unit time

q_t = gas flow rate at time t , MMscf/unit time

D_i = nominal (initial) decline rate, 1/unit time

All the expressions given by Equations 16-3 through 16-9 require **consistent units**. Any convenient unit of time can be used, but, again, care should be taken to make certain that the time unit of the gas flow rates, q_i and q_t , matches the time unit of the decline rate, D_i , for example, for flow rate q in scf/month or STB/month with D_i in month⁻¹.

Note that the traditional Arps decline-curve analysis, as given in Equations 16-7 through 16-9, gives a reasonable estimation of reserve but also has its failings, the most important one being that it *completely ignores the flowing pressure data*. As a result, it can underestimate or overestimate the reserves. The practical applications of these three commonly used decline curves for gas reservoirs are as follows:

Exponential Decline, $b = 0$

The graphical presentation of this type of decline curve indicates that a plot of q_t versus t on a semi log scale or a plot of q_t versus $G_{p(t)}$ on a Cartesian scale will produce linear relationships that can be described mathematically by

$$q_t = q_i \exp(-D_i t)$$

or linearly as

$$\ln(q_t) = \ln(q_i) - D_i t$$

Similarly,

$$G_{p(t)} = \frac{q_i - q_t}{D_i}$$

or linearly as

$$q_t = q_i - D_i G_{p(t)}$$

This type of decline curve is perhaps the simplest to use and perhaps the most conservative. It is widely used in the industry for the following reasons:

- Many wells follow a constant decline rate over a great portion of their productive life and will deviate significantly from this trend toward the end of this period.
- The mathematics involved, as described by the line expressions just given, are easier to apply than those for the other line types.

Assuming that the historical production from a well or field is recognized by its exponential production-decline behavior, the following steps summarize the procedure to predict the behavior of the well or the field as a function of time.

Step 1. Plot q_t versus G_p on a Cartesian scale and q_t versus t on semi log paper.

Step 2. For both plots, draw the best straight line through the points.

Step 3. Extrapolate the straight line on q_t versus G_p to $G_p = 0$, which intercepts the y-axis with a flow rate value that is identified as q_i .

Step 4. Calculate the initial decline rate, D_i , by selecting a point on the Cartesian straight line with a coordinate of (q_t, G_{pt}) or on a semi-log line with a coordinate of (q_t, t) and solve for D_i by applying Equation 16-5 or Equation 16-7.

$$D_i = \frac{\ln(q_i/q_t)}{t} \quad (16-10)$$

or equivalently as

$$D_i = \frac{q_i - q_t}{G_{p(t)}} \quad (16-11)$$

If the method of least squares is used to determine the decline rate by analyzing all of the production data, then

$$D_i = \frac{\sum_t [t \ln(q_i/q_t)]}{\sum_t t^2} \quad (16-12)$$

or equivalently as

$$D_i = \frac{n \sum_t (q_i G_{p(t)}) - \left[\left(\sum_t q_t \right) \left(\sum_t G_{p(t)} \right) \right]}{n \sum_t (G_{p(t)})^2 - \left(\sum_t G_{p(t)} \right)^2} \quad (16-13)$$

where n is the number of data points.

Step 5. Calculate the time it will take to reach the economic flow rate, q_a (or any rate) and corresponding cumulative gas production from Equations 16-3 and 16-7.

$$t_a = \frac{\ln(q_i/q_a)}{D_i}$$

$$G_{pa} = \frac{q_i - q_a}{t_a}$$

where G_{pa} = cumulative gas production when reaching the economic flow rate or at abandonment, MMscf
 q_i = initial gas flow rate at time $t = 0$, MMscf/unit time

- t = abandonment time, unit time
 q_a = economic (abandonment) gas flow rate, MMscf/unit time
 D_i = nominal (initial) decline rate, 1/time unit

Example 16-1

The following production data are available from a dry gas field:

| q_t , MMscf/day | G_p , MMscf | q_t , MMscf/day | G_p , MMscf |
|-------------------|---------------|-------------------|---------------|
| 320 | 16,000 | 208 | 304,000 |
| 336 | 32,000 | 197 | 352,000 |
| 304 | 48,000 | 184 | 368,000 |
| 309 | 96,000 | 176 | 384,000 |
| 272 | 160,000 | 184 | 400,000 |
| 248 | 240,000 | | |

Estimate

- (a) The future cumulative gas production when the gas flow rate reaches 80 MMscf/day
 (b) *Extra* time to reach 80 MMscf/day

Solution

Part a

- Step 1.* A plot of G_p versus q_t on a Cartesian scale, as shown in Figure 16-3, produces a straight line indicating an exponential decline.
- Step 2.* From the graph, cumulative gas production is 633,600 MMscf at $q_t = 80$ MMscf/day, indicating an extra production of $633.6 - 400.0 = 233.6$ MMMscf.
- Step 3.* The intercept of the straight line with the y-axis gives a value of $q_i = 344$ MMscf/day.
- Step 4.* Calculate the initial (nominal) decline rate D_i by selecting a point *on* the straight line and solving for D_i by applying Equation 16-11. Selecting a $G_{p(t)}$ of 352 MMscf, at a q_t of 197 MMscf/day, gives

$$D_i = \frac{q_i - q_t}{G_{p(t)}} = \frac{344 - 197}{352,000} = 0.000418 \text{ day}^{-1}$$

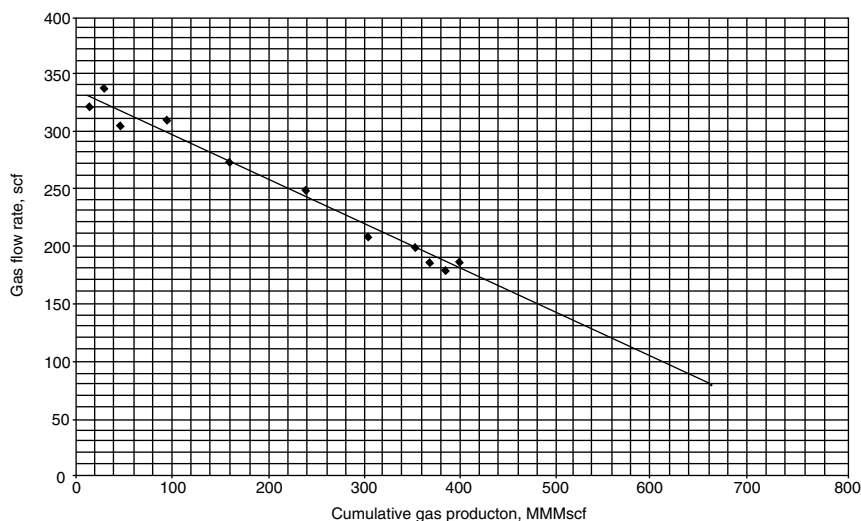


Figure 16-3. Decline curve data for Example 16-1.

It should be pointed out that the monthly and yearly nominal decline, that is, D_{im} and D_{iy} , respectively, can be determined as

$$D_{im} = (0.000418) (30.4) = 0.0126 \text{ month}^{-1}$$

$$D_{iy} = (0.0126) (12) = 0.152 \text{ year}^{-1}$$

Using the least-squares approach from Equation 16-13 gives

$$D_i = \frac{n \sum_t (q_t G_{p(t)}) - [(\sum_t q_t)(\sum_t G_{p(t)})]}{n \sum_t (G_{p(t)})^2 - (\sum_t G_{p(t)})^2}$$

$$D_i = \frac{5.55104(10^9) - 6.5712(10^9)}{8.3072(10^{12}) - 5.760(10^{12})} = 0.000401 \text{ day}^{-1}$$

Part b

To calculate the extra time to reach 80 MMscf/day, apply the following steps:

Step 1. Calculate the time to reach the last recorded flow rate, 184 MMscf, using Equation 16-10:

$$t_a = \frac{\ln(q_i/q_a)}{D_i} = \frac{\ln(344/184)}{0.000401} = 1560 \text{ days} = 4.275 \text{ year}$$

Step 2. Calculate the total time to reach a gas flow rate of 80 MMscf/day:

$$t = \frac{\ln(344/80)}{0.000401} = 3637 \text{ days} = 9.966 \text{ years}$$

Step 3. Extra time = 9.966 – 4.275 = 5.691 years

Example 16-2

A gas well has the following production history:

| Date | Time t , months | q_r , MMscf/month |
|---------|-------------------|---------------------|
| 1-1-02 | 0 | 1240 |
| 2-1-02 | 1 | 1193 |
| 3-1-02 | 2 | 1148 |
| 4-1-02 | 3 | 1104 |
| 5-1-02 | 4 | 1066 |
| 6-1-02 | 5 | 1023 |
| 7-1-02 | 6 | 986 |
| 8-1-02 | 7 | 949 |
| 9-1-02 | 8 | 911 |
| 10-1-02 | 9 | 880 |
| 11-1-02 | 10 | 843 |
| 12-1-02 | 11 | 813 |
| 1-1-03 | 12 | 782 |

- Use the first six months of the production history data to determine the coefficient of the decline-curve equation.
- Predict flow rates and cumulative gas production from August 1, 2002 through January 1, 2003.
- Assuming that the economic limit is 30 MMscf/month, estimate the time to reach the economic limit and the corresponding cumulative gas production.

Solution

Part a

Step 1. A plot of q_t versus t on a semi log scale, as shown in Figure 16-4, indicates an exponential decline.

Step 2. Determine the initial decline rate, D_i , by selecting a point on the straight line and substituting the coordinates of the point in Equation 16-10 to give

$$D_i = \frac{\ln(q_i/q_t)}{t} = \frac{\ln(1240/986)}{6} = 0.0382 \text{ month}^{-1}$$

Alternatively, using the least-squares method as expressed by Equation 16-12 gives

$$D_i = \frac{\sum_t [t \ln(q_i/q_t)]}{\sum_t t^2}$$

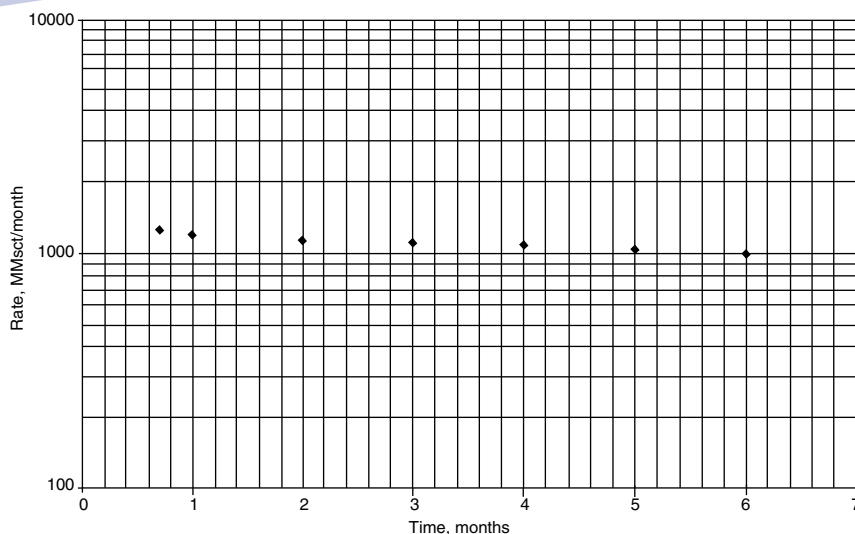


Figure 16-4. Decline-curve data for Example 16-2.

$$D_i = \frac{1 \times 0.0386 + 2 \times 0.0771 + 3 \times 0.116 + 4 \times 0.151 + 5 \times 0.192 + 6 \times 0.229}{1^2 + 2^2 + 3^2 + 4^2 + 5^2 + 6^2}$$

$$\neq \frac{3.48325}{91} = 0.0383 \text{ month}^{-1}$$

Part b

Use Equations 16-3 and 16-7 to calculate q_t and $G_{p(t)}$, and tabulate the results as follows:

$$q_t = q_i \exp(-D_i t) = 1240 \exp(-0.0383 t)$$

$$G_{p(t)} = \frac{(q_i - q_t)}{D_i} = \frac{(q_i - q_t)}{0.0383}$$

| Date | Time, months | Actual q_t , MMscf/month | Calculated q_t , MMscf/month | $G_{p(t)}$, MMscf/month |
|---------|--------------|----------------------------|--------------------------------|--------------------------|
| 2-1-02 | 1 | 1193 | 1193 | 1217 |
| 3-1-02 | 2 | 1148 | 1149 | 2387 |
| 4-1-02 | 3 | 1104 | 1105 | 3514 |
| 5-1-02 | 4 | 1066 | 1064 | 4599 |
| 6-1-02 | 5 | 1023 | 1026 | 4643 |
| 7-1-02 | 6 | 986 | 986 | 6647 |
| 8-1-02 | 7 | 949 | 949 | 7614 |
| 9-1-02 | 8 | 911 | 913 | 8545 |
| 10-1-02 | 9 | 880 | 879 | 9441 |
| 11-1-02 | 10 | 843 | 846 | 10,303 |
| 12-1-02 | 11 | 813 | 814 | 11,132 |
| 1-1-03 | 12 | 782 | 783 | 11,931 |

Part c

Apply Equations 16-10 and 16-11 to calculate the time, t_a , to reach an economic flow rate, q_a , of 30 MMscf/month, and the corresponding reserves, G_{pa} :

$$t_a = \frac{\ln(q_i/q_a)}{D_i} = \frac{\ln(1240/30)}{0.0383} = 97 \text{ months} = 8 \text{ year}$$

$$G_{pa} = \frac{q_i - q_a}{t_a} = \frac{(1240 - 30)10^6}{0.0383} = 31.6 \text{ MMMscf}$$

Harmonic Decline, $b = 1$

The production-recovery performance of a hydrocarbon system that follows a harmonic decline (i.e., $b = 1$ in Equation 16-1) is described by Equations 16-5 and 16-9.

$$q_t = \frac{q_i}{1 + D_i t}$$

$$G_{p(t)} = \left(\frac{q_i}{D_i} \right) \ln \left(\frac{q_i}{q_t} \right)$$

These two expressions can be rearranged and expressed as follows:

$$\frac{1}{q_t} = \frac{1}{q_i} + \left(\frac{D_i}{q_i} \right) t \quad (16-14)$$

$$\ln(q_t) = \ln(q_i) - \left(\frac{D_i}{q_i} \right) G_{p(t)} \quad (16-15)$$

The basic two plots for harmonic decline-curve analysis are based on these two relationships. Equation 16-14 indicates that a plot of $1/q_t$ versus t on a Cartesian scale will yield a straight line with a slope of (D_i/q_i) and an intercept of $1/q_i$. Equation 16-15 suggests a plot of q_t versus $G_{p(t)}$ on a semi log scale and will yield a straight line with a negative slope of $(-D_i/q_i)$ and an intercept of q_i . The method of least squares can also be used to calculate the decline rate, D_i , to give

$$D_i = \frac{\sum_t \left(\frac{t q_i}{q_t} \right) - \sum_t t}{\sum_t t^2}$$

Other relationships that can be derived from Equations 16-14 and 16-15 include the time to reach the economic flow rate, q_a (or any flow rate), and the corresponding cumulative gas production, $G_{p(a)}$:

$$t_a = \frac{q_i - q_a}{q_a D_i} \quad (16-16)$$

$$G_{p(a)} = \left(\frac{q_i}{D_i} \right) \ln \left(\frac{q_a}{q_t} \right)$$

Hyperbolic Decline, $0 < b < 1$

The two governing relationships for a reservoir or a well whose production follows the hyperbolic decline behavior are given by Equations 16-4 and 16-8:

$$q_t = \frac{q_i}{(1 + bD_i t)^{1/b}}$$

$$G_{p(t)} = \left[\frac{q_i}{D_i(1-b)} \right] \left[1 - \left(\frac{q_t}{q_i} \right)^{1-b} \right]$$

The following simplified iterative method is designed to determine D_i and b from the historical production data.

- Step 1.* Plot q_t versus t on a semi log scale and draw a *smooth curve* through the points.
- Step 2.* Extend the curve to intercept the y-axis at $t = 0$ and read q_i .
- Step 3.* Select the other end-point of the smooth curve, record the coordinates of the point, and refer to it as (t_2, q_2) .
- Step 4.* Determine the coordinate of the middle point on the smooth curve that corresponds to (t_1, q_1) with the value of q_1 , as obtained from the following expression:

$$q_1 = \sqrt{q_i q_2} \quad (16-17)$$

The corresponding value of t_1 is read from the smooth curve at q_1 .

Step 5. Solve the following equation iteratively for b :

$$f(b) = t_2 \left(\frac{q_i}{q_1} \right)^b - t_1 \left(\frac{q_i}{q_2} \right)^b - (t_2 - t_1) = 0 \quad (16-18)$$

The Newton-Raphson iterative method can be employed to solve the previous nonlinear function by using the following recursion technique:

$$b^{k+1} = b^k - \frac{f(b^k)}{f'(b^k)} \quad (16-19)$$

where the derivative, $f'(b^k)$, is given by

$$f'(b^k) = t_2 \left(\frac{q_i}{q_1} \right)^{b^k} \ln \left(\frac{q_i}{q_1} \right) - t_1 \left(\frac{q_i}{q_2} \right)^{b^k} \ln \left(\frac{q_i}{q_2} \right) \quad (16-20)$$

Starting with an initial value of $b = 0.5$, that is, $b^k = 0.5$, the method will usually converge after 4–5 iterations when the convergence criterion is set at $[b^{k+1} - b^k] \leq 10^{-6}$.

Step 6. Solve for D_i with Equation 16-4, by using the calculated value of b from Step 5 and the coordinate of a point on the smooth graph, for example, (t_2, q_2) , to give

$$D_i = \frac{(q_i/q_2)^b - 1}{b t_2} \quad (16-21)$$

The next example illustrates the proposed methodology for determining b and D_i .

Example 16-3

The following production data were reported by Ikoku (1984) for a gas well:

| Date | Time, years | q_t , MMscf/day | $G_{p(t)}$, MMscf |
|-------------|-------------|-------------------|--------------------|
| Jan 1, 1979 | 0.0 | 10.00 | 0.00 |
| Jul 1, 1979 | 0.5 | 8.40 | 1.67 |
| Jan 1, 1980 | 1.0 | 7.12 | 3.08 |
| Jul 1, 1980 | 1.5 | 6.16 | 4.30 |
| Jan 1, 1981 | 2.0 | 5.36 | 5.35 |
| Jul 1, 1981 | 2.5 | 4.72 | 6.27 |
| Jan 1, 1982 | 3.0 | 4.18 | 7.08 |
| Jul 1, 1982 | 3.5 | 3.72 | 7.78 |
| Jan 1, 1983 | 4.0 | 3.36 | 8.44 |

Estimate the future production performance for the next 16 years.

Solution

Step 1. Determine the type of decline that adequately represents the historical data. This can be done by constructing the following two plots:

- Plot q_t versus t on a semi log scale, as shown in Figure 16-5. The plot does not yield a straight line, and, thus, the decline is *not exponential*.
- Plot q_t versus $G_{p(t)}$ on a semi log scale, as shown in Figure 16-6. The plot again does not produce a straight line, and, therefore, the decline is *not harmonic*.

The two generated plots indicate that the decline must be hyperbolic.

Step 2. From Figure 16-5, determine the initial flow rate, q_i , by extending the smooth curve to intercept with the y-axis, at $t = 0$, to give

$$q_i = 10 \text{ MMscf/day}$$

Step 3. Select the coordinate of the other end-point on the smooth curve as (t_2, q_2) , to give

$$t_2 = 4 \text{ years and } q_2 = 3.36 \text{ MMscf/day}$$

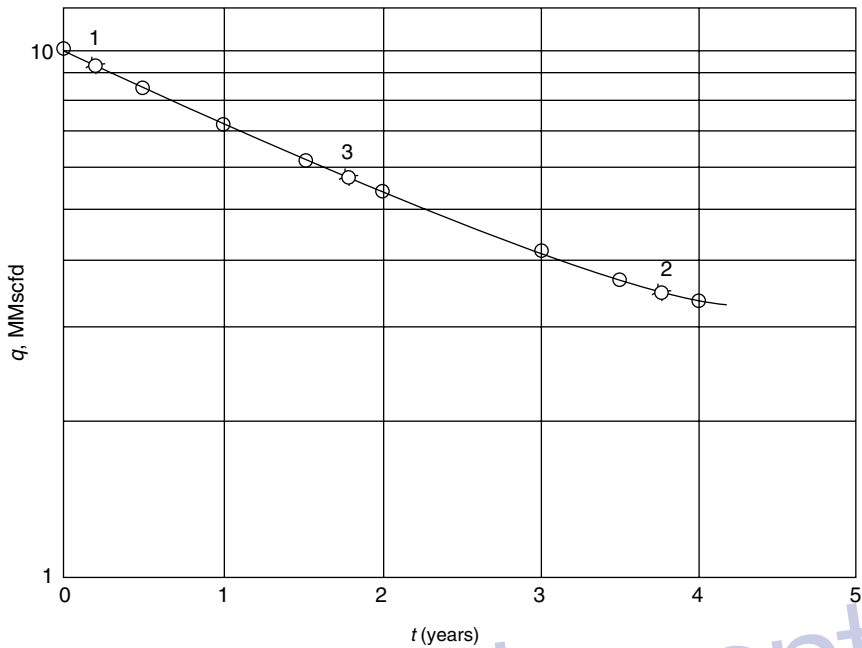


Figure 16-5. Rate-time plot for Example 16-3.

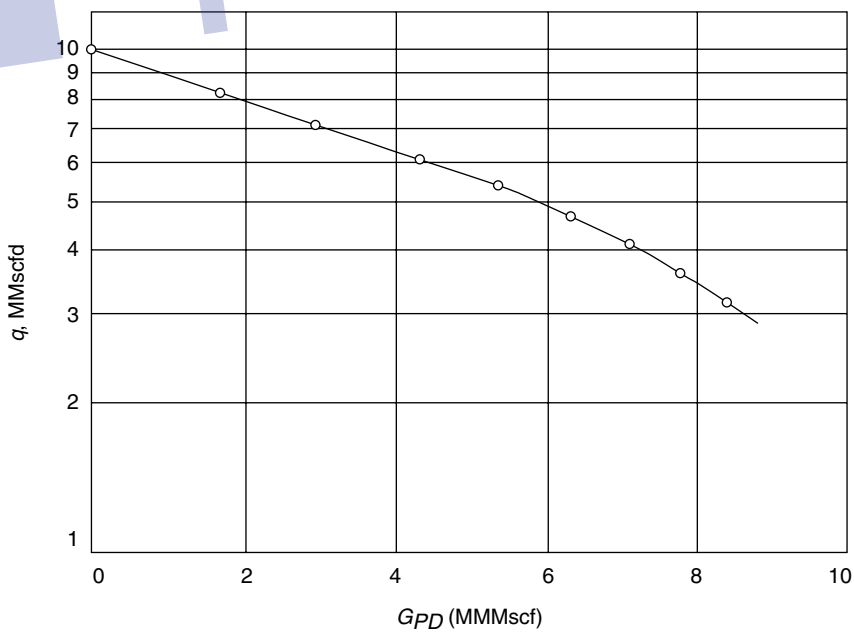


Figure 16-6. Rate-cumulative plot for Example 16-3.

Step 4. Calculate q_1 from Equation 16-17 and determine the corresponding time:

$$q_1 = \sqrt{q_i q_2} = \sqrt{(10)(3.36)} = 5.8 \text{ MMscf/day}$$

the corresponding time $t_1 = 1.719$ years

Step 5. Given $b = 0.5$, solve Equation 16-18 iteratively for b :

$$f(b) = t_2 \left(\frac{q_i}{q_1} \right)^b - t_1 \left(\frac{q_i}{q_2} \right)^b - (t_2 - t_1)$$

$$f(b) = 4(1.725)^b - 1.719(2.976)^b - 2.26$$

and

$$f'(b^k) = t_2 \left(\frac{q_i}{q_1} \right)^{b^k} \ln \left(\frac{q_i}{q_1} \right) - t_1 \left(\frac{q_i}{q_2} \right)^{b^k} \ln \left(\frac{q_i}{q_2} \right)$$

$$f'(b^k) = 2.18 (1.725)^{b^k} - 1.875 (2.976)^{b^k}$$

with

$$b^{k+1} = b^k - \frac{f(b^k)}{f'(b^k)}$$

It is convenient to perform the iterative method by constructing the following table:

| k | b^k | $f(b^k)$ | $f'(b^k)$ | b^{k+1} |
|-----|----------|------------------------|-----------|-----------|
| 0 | 0.500000 | $7.57 (10^{-3})$ | -0.36850 | 0.520540 |
| 1 | 0.520540 | $-4.19 (10^{-4})$ | -0.40950 | 0.519517 |
| 2 | 0.519517 | $-1.05 (10^{-6})$ | -0.40746 | 0.519514 |
| 3 | 0.519514 | -6.87×10^{-9} | -0.40745 | 0.519514 |

The method converges after 3 iterations with a value of $b = 0.5195$.

Step 6. Solve for D_i by using Equation 16-21.

$$D_i = \frac{(q_i/q_2)^b - 1}{b t_2} = \frac{(10/3.36)^{0.5195} - 1}{(0.5195)(4)} = 0.3668 \text{ year}^{-1}$$

or, on a monthly basis,

$$D_{im} = 0.3668/12 = 0.0306 \text{ month}^{-1}$$

or, on a daily basis,

$$D_{id} = 0.3668/365 = 0.001 \text{ day}^{-1}$$

Step 7. Use Equations 16-4 and 16-8 to predict the future production performance of the gas well. Notice that in Equation 16-4 the denominator contains $D_i t$ and, therefore, the product must be dimensionless, or

$$q_t = \frac{10(10^6)}{[1 + 0.5195 D_i t]^{(1/0.5195)}} = \frac{(10)(10^6)}{[1 + 0.5195 (0.3668)(t)]^{(1/0.5195)}}$$

where q_t = flow rate, MMscf/day

t = time, years

D_i = decline rate, year⁻¹

In Equation 16-8, the time basis in q_i is expressed in days and, therefore, D_i must be expressed in day⁻¹, or

$$G_{p(t)} = \left[\frac{q_i}{D_i(1-b)} \right] \left[1 - \left(\frac{q_t}{q_i} \right)^{1-b} \right]$$

$$G_{p(t)} = \left[\frac{(10)(10^6)}{(0.001)(1-0.5195)} \right] \left[1 - \left(\frac{q_t}{(10)(10^6)} \right)^{1-0.5195} \right]$$

The results of Step 7 are tabulated below and shown graphically in Figure 16-7.

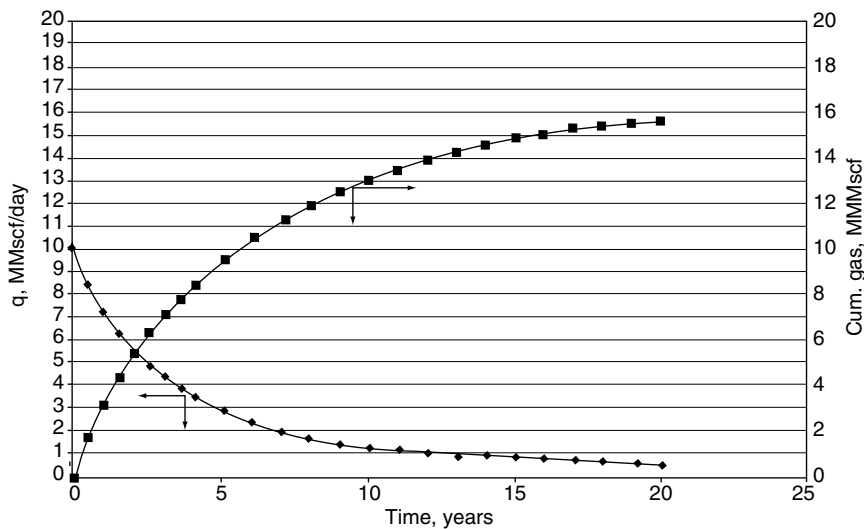


Figure 16-7. Decline-curve data for Example 3-18.

| Time, years | Actual q , MMscf/day | Calculated q , MMscf/day | Actual cumulative gas, MMscf | Calculated cumulative gas, MMscf |
|-------------|------------------------|----------------------------|------------------------------|----------------------------------|
| 0 | 10 | 10 | 0 | 0 |
| 0.5 | 8.4 | 8.392971 | 1.67 | 1.671857 |
| 1 | 7.12 | 7.147962 | 3.08 | 3.08535 |
| 1.5 | 6.16 | 6.163401 | 4.3 | 4.296641 |
| 2 | 5.36 | 5.37108 | 5.35 | 5.346644 |
| 2.5 | 4.72 | 4.723797 | 6.27 | 6.265881 |
| 3 | 4.18 | 4.188031 | 7.08 | 7.077596 |
| 3.5 | 3.72 | 3.739441 | 7.78 | 7.799804 |
| 4 | 3.36 | 3.36 | 8.44 | 8.44669 |
| 5 | | 2.757413 | | 9.557617 |
| 6 | | 2.304959 | | 10.477755 |
| 7 | | 1.956406 | | 11.252814 |
| 8 | | 1.68208 | | 11.914924 |
| 9 | | 1.462215 | | 12.487334 |
| 10 | | 1.283229 | | 12.987298 |
| 11 | | 1.135536 | | 13.427888 |
| 12 | | 1.012209 | | 13.819197 |
| 13 | | 0.908144 | | 14.169139 |
| 14 | | 0.819508 | | 14.484015 |
| 15 | | 0.743381 | | 14.768899 |
| 16 | | 0.677503 | | 15.027928 |
| 17 | | 0.620105 | | 15.264506 |
| 18 | | 0.569783 | | 15.481464 |
| 19 | | 0.525414 | | 15.681171 |
| 20 | | 0.486091 | | 15.86563 |

Gentry (1972) developed a graphical method for the coefficients b and D_i , as shown in Figures 16-8 and 16-9. Arps' decline-curve exponent, b , is expressed in Figure 16-8 in terms of the ratios q_i/q and $G_p/(t q_i)$, with an upper limit for q_i/q of 100. To determine the exponent b , enter the graph with the abscissa with a value of $G_p/(t q_i)$ that corresponds to the last data point on the decline curve and enter the coordinate with the value of the ratio of initial production rate to last production rate on the decline curve, q_i/q . The exponent b is read by the intersection of these two values. The initial decline rate, D_i , can be determined from Figure 16-9 by entering the coordinate with the value of q_i/q and moving to the right to the curve that corresponds to the value of b . The initial decline rate, D_i , can be obtained by reading the value on the abscissa divided by the time t from q_i to q .

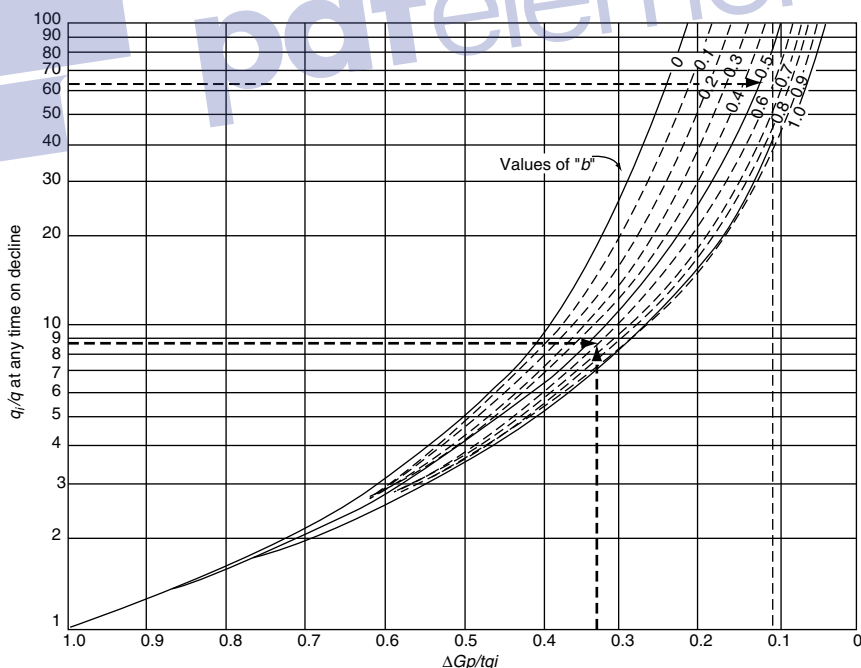


Figure 16-8. Relationship between production rate and cumulative production. (After Gentry, 1972.)

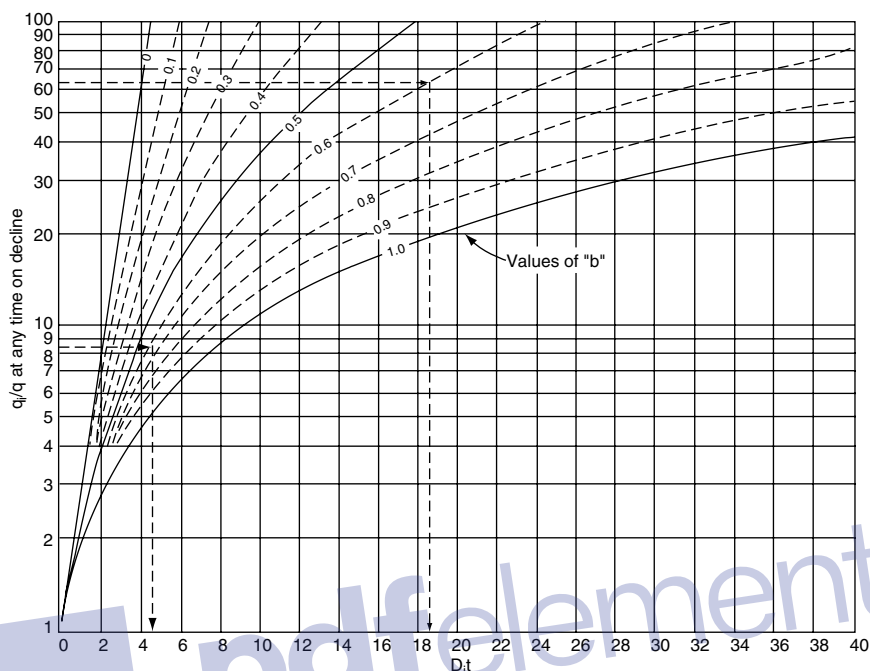


Figure 16-9. Relationship between production rate and time. (After Gentry, 1972.)

Example 16-4

Using the data given in Example 8-18, recalculate the coefficients b and D_i by using Gentry's graphs.

Solution

Step 1. Calculate the ratios q_i/q and $G_p/(t q_i)$:

$$q_i/q = 10/3.36 = 2.98$$

$$G_p/(t q_i) = 8440/[(4 \times 365)(10)] = 0.58$$

Step 2. Enter Figure 16-9 with the values of 2.98 and 0.5 to give

$$D_i t = 1.5$$

Solving for D_i gives

$$D_i = 1.5/4 = 0.38 \text{ year}^{-1}$$

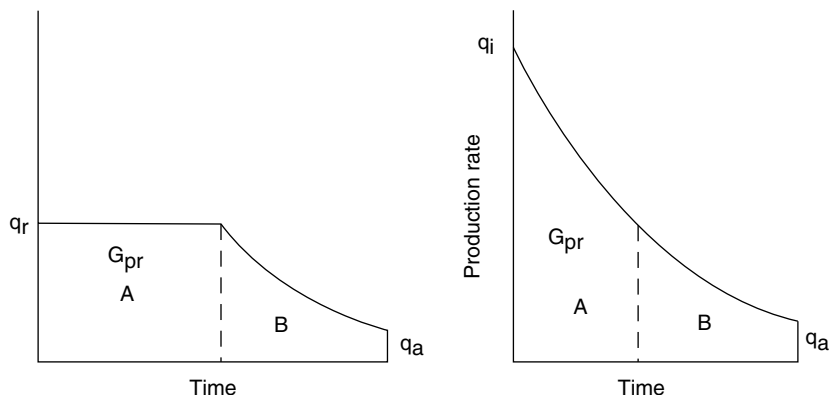


Figure 16-10. Estimation of the effect of restricting maximum production rate.

In many cases gas wells are not produced at their full capacity during their early life for various reasons, such as limited capacity of flow lines, transportation, low demands, or other types of restrictions. Figure 16-10 illustrates a model for estimating the time pattern of production where the rate is restricted.

Figure 16-10 shows that the well produces at a restricted flow rate of q_r for a total time of t_r with a cumulative production of G_{pr} . The proposed methodology of estimating the restricted time, t_r , is to set the total cumulative production, $G_{p(t_r)}$, that would have occurred under normal decline from the initial well capacity, q_i , down to q_r equal to G_{pr} . Eventually, the well will reach the time t_r where it begins to decline with a behavior similar to that of other wells in the area. The proposed method for predicting the decline-rate behavior for a well under restricted flow is based on the assumption that the following data are available and applicable to the well:

- Coefficients of Arps' equation, that is, D_i and b , by analogy with other wells
- Abandonment (economic) gas flow rate, q_a
- Ultimate recoverable reserves, G_{pa}
- Allowable (restricted) flow rate, q_r

The methodology is summarized in the following steps:

Step 1. Calculate the initial well flow capacity, q_i , that would have occurred with no restrictions, as follows:

- For Exponential: $q_i = G_{pa} D_i + q_a$ (16-22)

- For Harmonic: $q_i = q_r \left[1 + \frac{D_i G_{pa}}{q_r} - \ln \left(\frac{q_r}{q_a} \right) \right]$ (16-23)

- For Hyperbolic:

$$q_i = \left[(q_r)^b + \frac{D_i b G_{pa}}{(q_r)^{1-b}} - \frac{b (q_r)^b}{1-b} \left[1 - \left(\frac{q_a}{q_r} \right)^{1-b} \right] \right]^{1/b}$$
 (16-24)

Step 2. Calculate the cumulative gas production during the restricted-flow-rate period:

- For Exponential: $G_{pr} = \frac{q_i - q_r}{D_i}$ (16-25)

- For Harmonic: $G_{pr} = \left(\frac{q_i}{D_i} \right) \ln \left(\frac{q_i}{q_r} \right)$ (16-26)

- For Hyperbolic: $G_{pr} = \left[\frac{q_i}{D_i (1-b)} \right] \left[1 - \left(\frac{q_r}{q_i} \right)^{1-b} \right]$ (16-27)

Step 3. Regardless of the type of decline, calculate the total time of the restricted flow rate from

$$t_r = \frac{G_{pr}}{q_r}$$
 (16-28)

Step 4. Generate the well-production performance as a function of time by applying the appropriate decline relationships, as given by Equations 16-3 through 16-14.

Example 16-5

The volumetric calculations on a gas well show that the ultimate recoverable reserves, G_{pa} , are 25 MMMscf of gas. By analogy with other wells in the area, the following data are assigned to the well.

- Exponential decline
- Allowable (restricted) production rate $q_r = 425$ MMscf/month
- Economic limit $q_a = 30$ MMscf/month
- Nominal decline rate = 0.044 month^{-1}

Calculate the yearly production performance of the well.

Solution

Step 1. Estimate the initial flow rate, q_i , from Equation 16-22:

$$q_i = G_{pa} D_i + q_a = (0.044)(25,000) + 30 = 1,130 \text{ MMscf/month}$$

Step 2. Calculate the cumulative gas production during the restricted flow period by using Equation 16-25.

$$G_{pr} = \frac{q_i - q_r}{D_i} = \frac{1130 - 425}{0.044} = 16.023 \text{ MMscf}$$

Step 3. Calculate the total time of the restricted flow from Equation 16-28:

$$t_r = \frac{G_{pr}}{q_r} = \frac{16,023}{425} = 37.7 \text{ months} = 3.14 \text{ years}$$

Step 4. The yearly production during the first 3 years is

$$q = (425) (12) = 5100 \text{ MMscf/year}$$

The fourth year is divided into 1.68 months, that is, 0.14 years (of constant production) plus 10.32 months of declining production; therefore, cumulative gas production during the first 1.68 months:

$$G_{P \text{ during } 1.68 \text{ months}} = (1.68) (425) = 714 \text{ MMscf}$$

At the end of the fourth year:

$$q_t = q_i \exp(-D_i t) = 425 \exp[-0.044 (10.32)] = 270 \text{ MMscf/month}$$

and cumulative gas production for the last 10.32 months:

$$G_{p(t)} = \frac{(q_i - q_t)}{D_i} = \frac{425 - 270}{0.044} = 3523 \text{ MMscf}$$

Total production for the fourth year = 714 + 3523 = 4237 MMscf

| Year | Production, MMscf/year |
|------|------------------------|
| 1 | 5100 |
| 2 | 5100 |
| 3 | 5100 |
| 4 | 4237 |

The flow rate at the end of the fourth year, 270 MMscf/month, is set equal to the *initial flow rate at the beginning of the fifth year*. The flow rate at the end of the fifth year, q_{end} , is calculated from Equation 16-25 as

$$q_{\text{end}} = q_i \exp[-D_i (12)] = 270 \exp[-0.044 (12)] = 159 \text{ MMscf/month}$$

with a cumulative gas production of

$$G_p = \frac{q_i - q_{\text{end}}}{D_i} = \frac{270 - 159}{0.044} = 2523 \text{ MMscf}$$

For the sixth year,

$$q_{\text{end}} = 159 \exp[-0.044 (12)] = 94 \text{ MMscf/month}$$

$$G_p = \frac{159 - 94}{0.044} = 1482 \text{ MMscf}$$

Results of this procedure are then tabulated:

| t, years | Q _i , MMscf/month | Q _{end} , MMscf/month | Yearly Production, MMscf/year | Cumulative Production, MMMscf |
|----------|------------------------------|--------------------------------|-------------------------------|-------------------------------|
| 1 | 425 | 425 | 5100 | 5.100 |
| 2 | 425 | 425 | 5100 | 10.200 |
| 3 | 425 | 425 | 5100 | 15.300 |
| 4 | 425 | 270 | 4237 | 19.537 |
| 5 | 270 | 159 | 2523 | 22.060 |
| 6 | 159 | 94 | 1482 | 23.542 |
| 7 | 94 | 55 | 886 | 24.428 |
| 8 | 55 | 33 | 500 | 24.928 |

Reinitialization of Data

Fetkovich (1971) points out that there are several obvious situations where rate–time data must be reinitialized for reasons that include among others,

- The drive or production mechanism has changed
- An abrupt change in the number of wells on a lease or a field due to infill drilling
- Changing the size of tubing would change q_i and also the decline exponent, b

Provision of a well is not limited by tubing or equipment; the effects of stimulation will result in a change in deliverability, q_i , and possibly the remaining recoverable gas. However, the decline exponent, b , normally can be assumed constant. Fetkovich et al. (1996) suggested a rule-of-thumb equation to approximate an increase in rate due to stimulation:

$$(q_i)_{\text{new}} = \left[\frac{7 + s_{\text{old}}}{7 + s_{\text{new}}} \right] (q_t)_{\text{old}}$$

where $(q_t)_{\text{old}}$ = producing rate just prior to stimulation
 s = skin factor

Arps' equation (Equation 16-1) can be expressed as

$$q_t = \frac{(q_i)_{\text{new}}}{(1 + bt(D_i)_{\text{new}})^{1/b}}$$

with

$$(D_i)_{\text{new}} = \frac{(q_i)_{\text{new}}}{(1 - b)G}$$

where G = gas-in-place, scf

TYPE-CURVE ANALYSIS

The type-curve analysis approach was introduced to the petroleum industry by Agarwal et al. (1970) as a valuable tool when used in conjunction with conventional semi log plots. A **type curve** is a graphical representation of the theoretical solutions to flow equations. **Type-curve analysis** consists of finding the theoretical type curve that “matches” the actual response from a test well and the reservoir when subjected to changes in production rates or pressures. The match can be found graphically by physical superposition of a graph of actual test data on a similar graph of type curve(s) and searching for the type curve that provides the best match. Since type curves are plots of theoretical solutions to transient and pseudosteady-state flow equations, they are usually presented in terms of dimensionless variables, for example,

- dimensionless pressure, p_D
- dimensionless time, t_D
- dimensionless radius, r_D , and
- dimensionless wellbore storage, C_D

rather than real variables (e.g., Δp , t , r , and C). The reservoir and well parameters, such as permeability and skin, can then be calculated from the dimensionless parameters defining that type curve.

Any variable can be made “dimensionless” when multiplied by a group of constants with opposite dimensions, but the choice of this group will depend on the type of problem to be solved. For example, to create the dimensionless pressure drop, p_D , the actual pressure drop Δp in psi is multiplied by **group A** with units of psi^{-1} , or

$$p_D = A \Delta p$$

Finding a group A that makes a variable **dimensionless** is derived from equations that describe reservoir fluid flow. To introduce this concept,

recall Darcy's equation (Chapter 6), which describes the radial, incompressible, steady-state flow as expressed by

$$Q = \left[\frac{k h}{141.2 B \mu [\ln(r_e / r_{wa}) - 0.5]} \right] \Delta p \quad (16-29)$$

where r_{wa} is the apparent (effective) wellbore radius, as defined by Equation 6-152 in terms of the skin factors by

$$r_{wa} = r_w e^{-s}$$

Group A can be then defined by rearranging Darcy's equation as:

$$\ln\left(\frac{r_e}{r_{wa}}\right) - \frac{1}{2} = \left[\frac{k h}{141.2 Q B \mu} \right] \Delta p$$

Because the left-hand side of the previous equation is dimensionless, the right-hand side must be accordingly dimensionless. This suggests that the term $([kh/(141.2 Q B \mu)])$ is essentially a group A with units of psi^{-1} that defines the dimensionless variable p_D , or

$$p_D = \left[\frac{k h}{141.2 Q B \mu} \right] \Delta p \quad (16-30)$$

Taking the logarithm of both sides of the above equation gives

$$\log(p_D) = \log(\Delta p) + \log\left(\frac{k h}{141.2 Q B \mu}\right) \quad (16-31)$$

where Q = flow rate, STB/day

B = formation, volume factor, bbl/STB

μ = viscosity, cp

For a constant flow rate, Equation 16-31 indicates that the logarithm of dimensionless pressure drop, $\log(p_D)$, will differ from the logarithm of *actual* pressure drop, $\log(\Delta p)$, by a constant amount:

$$\log\left(\frac{k h}{141.2 Q B \mu}\right)$$

Similarly, the dimensionless time, t_D , is given in Chapter 6 by Equation 6-87 as

$$t_D = \left[\frac{0.0002637k}{\phi \mu c_t r_w^2} \right] t$$

Taking the logarithm of both sides of the above equation gives

$$\log(t_D) = \log(t) + \log \left[\frac{0.0002637k}{\phi \mu c_t r_w^2} \right] \quad (16-32)$$

where t = time, hours

c_t = total compressibility coefficient, psi^{-1}

ϕ = porosity

Hence, a graph of $\log(\Delta p)$ versus $\log(t)$ will have an identical shape (i.e., parallel) to a graph of $\log(p_D)$ versus $\log(t_D)$, although the curve will be shifted by $\log[kh/(141.2QB\mu)]$ vertically in pressure and $\log[0.0002637k/(\phi \mu c_t r_w^2)]$ horizontally in time. This concept is illustrated in Figure 16-11.

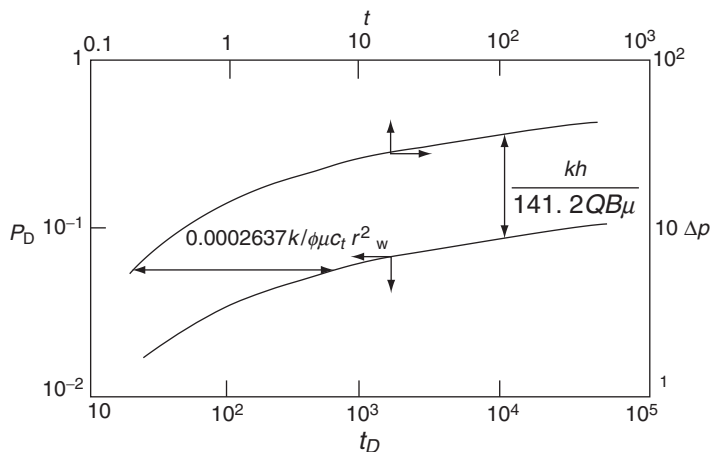


Figure 16-11. Concept of type curves.

Not only do these two curves have the same shape, but if they are *moved relative to each other until they coincide or “match,”* the vertical and horizontal displacements required to achieve the **match** are related to these constants in Equations 16-31 and 16-32. Once these constants are determined from the vertical and horizontal displacements, it is possible to estimate reservoir properties such as permeability and porosity. This process of matching two curves through the vertical and horizontal displacements and determining the reservoir or well properties is called type-curve matching.

Consider the Ei-function solution to the diffusivity equations, as given in Chapter 6 by Equation 6-78:

$$p(r, t) = p_i + \left[\frac{70.6 Q B \mu}{k h} \right] \text{Ei} \left[\frac{-948 \phi \mu c_t r^2}{k t} \right]$$

This relationship can be expressed in a dimensionless form by manipulation of the expression, to give

$$\frac{p_i - p(r, t)}{\left[\frac{141.2 Q_o B_o \mu_o}{k h} \right]} = -\frac{1}{2} \text{Ei} \left[\frac{-(r/r_w)^2}{4 \left(\frac{0.0002637 k t}{\phi \mu c_t r_w^2} \right)} \right]$$

From the definition of the dimensionless variables p_D , t_D , and r_D , this relation can be expressed in terms of these dimensionless variables:

$$p_D = -\frac{1}{2} \text{Ei} \left(-\frac{r_D^2}{4 t_D} \right) \quad (16-33)$$

It should be noted that when $t_D/r_D^2 > 25$, Equation 16-33 can be approximated by

$$p_D = \frac{1}{2} \left[\ln \frac{t_D}{r_D^2} + 0.080907 \right]$$

Notice that

$$\frac{t_D}{r_D^2} = \left[\frac{0.0002637 k}{\phi \mu c_t r^2} \right] t$$

Taking the logarithm of both sides of the above equation gives

$$\log\left(\frac{t_D}{r_D^2}\right) = \log\left[\frac{0.0002637k}{\phi\mu c_t r^2}\right] + \log(t) \quad (16-34)$$

Equations 16-31 and 16-34 indicate that a graph of $\log(\Delta p)$ versus $\log(t)$ will have an *identical shape* (i.e., will be parallel) to a graph of $\log(p_D)$ versus $\log(t_D/r_D^2)$, although the curve will be shifted by $\log(kh/141.2QB\mu)$ vertically in pressure and $\log(0.0002637k/\phi\mu c_t r^2)$ horizontally in time. When these two curves are moved relative to each other until they coincide or “match,” the vertical and horizontal movements, in mathematical terms, are given by

$$\left(\frac{p_D}{\Delta p}\right)_{MP} = \frac{kh}{141.2QB\mu} \quad (16-35)$$

and

$$\left(\frac{t_D/r_D^2}{t}\right)_{MP} = \frac{0.0002637k}{\phi\mu c_t r^2} \quad (16-36)$$

The subscript “MP” denotes a **match point**.

A more practical solution to the diffusivity equation, then, is a plot of the dimensionless p_D versus t_D/r_D^2 , as shown in Figure 16-12, which can be used to determine the pressure at any time and distance from the producing well. Figure 16-12 is basically a type curve that is mostly used in interference tests when analyzing pressure-response data in a shut-in observation well at a distance r from an active producer or injector well.

In general, the type-curve approach employs the flowing procedure that will be illustrated by the use of Figure 16-12:

Step 1. Select the proper type curve (e.g., Figure 16-12).

Step 2. Place a tracing paper over Figure 16-12 and construct a log-log scale that has the same dimensions as those of the type curve. This can be achieved by tracing the major and minor grid lines from the type curve to the tracing paper.

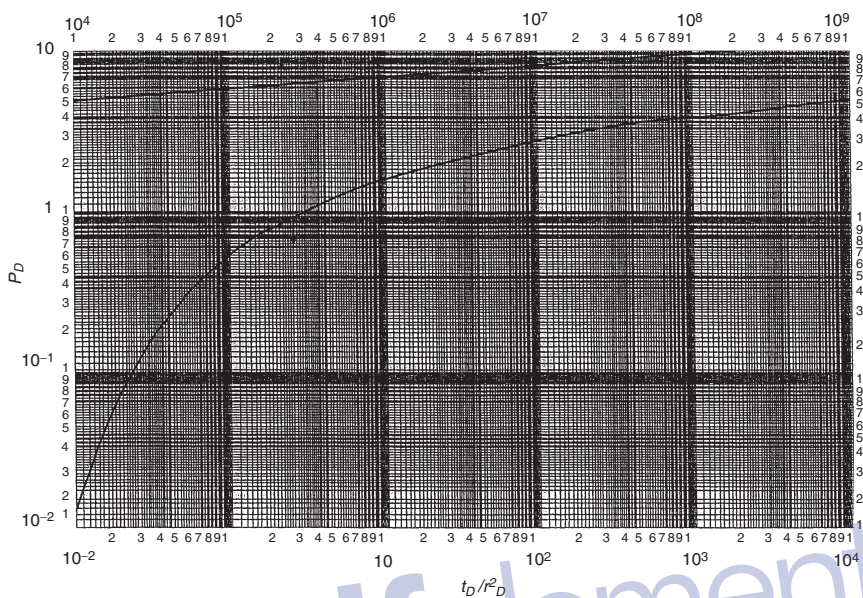


Figure 16-12. Dimensionless pressure for a single well in an infinite system, no wellbore storage, no skin. Exponential-integral solution. (After Earlougher, R. *Advances in Well Test Analysis*) (Permission to publish by the SPE, copyright SPE, 1977).

- Step 3.* Plot the well-test data in terms of Δp versus t on the tracing paper.
- Step 4.* Overlay the tracing paper on the type curve and slide the actual data plot, keeping the x- and y-axes of both graphs parallel, until the actual data point curve coincides with or matches the type curve.
- Step 5.* Select any arbitrary match point (MP), such as an intersection of major grid lines, and record $(\Delta p)_{MP}$ and $(t)_{MP}$ from the actual data plot and the corresponding values of $(p_D)_{MP}$ and $(t_D/r_D^2)_{MP}$ from the type curve.
- Step 6.* Using the match point, calculate the properties of the reservoir.

Example 16-5 illustrates the convenience of using the type-curve approach in an interference test for 48 hours followed by a falloff period for 100 hours.

Example 16-6¹

During an interference test, water was injected at 170 bbl/day for 48 hours in an injection well. The pressure response in an observation well 119 ft away from the injector is as follows:

| t, hours | p, psig | $\Delta p_{ws} = p_i - p$, psi |
|----------|----------------|---------------------------------|
| 0 | $p_i = 0$ | 0 |
| 4.3 | 22 | -22 |
| 21.6 | 82 | -82 |
| 28.2 | 95 | -95 |
| 45.0 | 119 | -119 |
| 48.0 | injection ends | |
| 51.0 | 109 | -109 |
| 69.0 | 55 | -55 |
| 73.0 | 47 | -47 |
| 93.0 | 32 | -32 |
| 142.0 | 16 | -16 |
| 148.0 | 15 | -15 |

Other given data include the following:

| | |
|------------------------------|--|
| Initial pressure, p_i | = 0 psi |
| Water FVF, B_w | = 1.00 bbl/STB |
| Total compressibility, c_t | = 9.0×10^{-6} psi ⁻¹ |
| Formation thickness, h | = 45 ft |
| Water viscosity, μ_w | = 1.3 cp |
| Injection rate, q | = -170 bbl/day |

Calculate the reservoir permeability and porosity.

Solution

Step 1. Figure 16-13 shows a plot of the well-test data during the injection period (48 hours) in terms of Δp versus t on a tracing paper with the same scale dimensions as in Figure 16-12. Using the overlay technique with the vertical and horizontal movements, find the segment of the type curve that matches the actual data.

¹ This example problem and the solution procedure were given by Earlougher, R., "Advanced Well Test Analysis," SPE Monograph Series, SPE, Dallas, TX (1977).

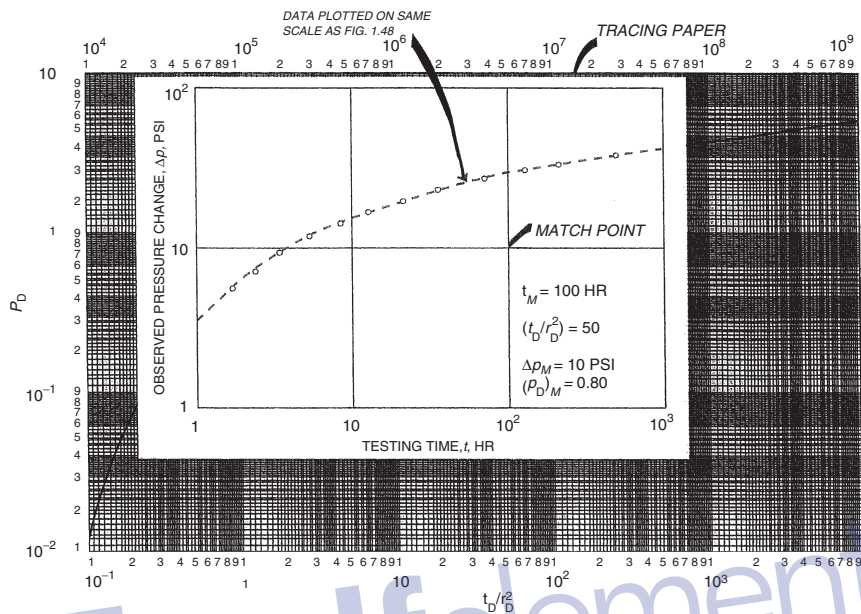


Figure 16-13. Illustration of type curve matching for an interference test using the type curve. (After Earlougher, R., *Advances in Well Test Analysis*) (Permission to publish by the SPE, copyright SPE, 1977).

Step 2. Select *any point* on the graph to be defined as a match point, as shown in Figure 16-13. Record $(\Delta p)_{MP}$ and $(t)_{MP}$ from the actual data plot and the corresponding values of $(p_D)_{MP}$ and $(t_D/r_D^2)_{MP}$ from the type curve, to give

- Type-curve match values:

$$(p_D)_{MP} = 0.96, (t_D/r_D^2)_{MP} = 0.94$$

- Actual data match values:

$$(\Delta p)_{MP} = -100 \text{ psig}, (t)_{MP} = 10 \text{ hours}$$

Step 3. Using Equations 16-35 and 16-36, solve for the permeability and porosity:

$$k = \frac{141.2QB\mu}{h} \left(\frac{p_D}{\Delta p} \right)_{MP} = \frac{141.2(-170)(1.0)(1.0)}{45} \left(\frac{0.96}{-100} \right)_{MP}$$

$$= 5.1 \text{ md}$$

and:

$$\phi = \frac{0.0002637k}{\mu c_t r^2 [(t_D/r_D^2)/t]_{MP}} = \frac{0.0002637(5.1)}{(1.0)(9.0 \times 10^{-6})(119)^2 [0.94/10]_{MP}}$$

$$= 0.11$$

To fully understand the power and convenience of using the dimensionless concept approach in solving engineering problems, consider the following example.

Example 16-7

An oil well is producing under transient (unsteady-state) flow conditions. The following properties are given:

$$p_i = 3500 \text{ psi}$$

$$B = 1.44 \text{ bbl/STB}$$

$$c_t = 17.6 \times 10^{-6} \text{ psi}^{-1}$$

$$\phi = 15\%$$

$$\mu = 1.3 \text{ cp}$$

$$h = 20 \text{ ft}$$

$$Q = 360 \text{ STB/day}$$

$$k = 22.9 \text{ md}$$

$$s = 0$$

- (a) Calculate the pressure at radii of 10 ft and 100 ft for the flowing times 0.1, 0.5, 1.0, 2.0, 5.0, 10, 20, 50, and 100 hours. Plot $[p_i - p(r,t)]$ versus (t/r^2) on a log-log scale.
- (b) Present the data from part a in terms of $[p_i - p(r,t)]$ versus (t/r^2) on a log-log scale.

Solution

During transient flow, Equation 6-78 is designed to describe the pressure at any radius r and any time t , as given by

$$p(r,t) = p_i + \left[\frac{70.6 QB\mu}{kh} \right] \text{Ei} \left[\frac{-948\phi\mu c_t r^2}{kt} \right]$$

or

$$p_i - p(r,t) = \left[\frac{-70.6 (360) (1.444) (1.3)}{(22.9) (20)} \right] \text{Ei} \left[\frac{-948 (0.15) (1.3) (17.6 \times 10^{-6}) r^2}{(22.9)t} \right]$$

$$p_i - p(r,t) = -104 \operatorname{Ei} \left[-0.0001418 \frac{r^2}{t} \right]$$

Values of “ $p_i - p(r,t)$ ” are presented as a function of time and radius (i.e., at $r = 10$ feet and 100 feet) in the following table and graphically in Figure 16-14.

| Assumed t, hours | r = 10 feet | | | r = 100 feet | | |
|---------------------|------------------|-------------------------------------|-------------------------|------------------|-------------------------------------|-------------------------|
| | t/r ² | Ei[-0.0001418 r ² /t] | p _i - p(r,t) | t/r ² | Ei[-0.0001418 r ² /t] | p _i - p(r,t) |
| 0.1 | 0.001 | -1.51 | 157 | 0.00001 | 0.00 | 0 |
| 0.5 | 0.005 | -3.02 | 314 | 0.00005 | -0.19 | 2 |
| 1.0 | 0.010 | -3.69 | 384 | 0.00010 | -0.12 | 12 |
| 2.0 | 0.020 | -4.38 | 455 | 0.00020 | -0.37 | 38 |
| 5.0 | 0.050 | -5.29 | 550 | 0.00050 | -0.95 | 99 |
| 10.0 | 0.100 | -5.98 | 622 | 0.00100 | -1.51 | 157 |
| 20.0 | 0.200 | -6.67 | 694 | 0.00200 | -2.14 | 223 |
| 50.0 | 0.500 | -7.60 | 790 | 0.00500 | -3.02 | 314 |
| 100.0 | 1.000 | -8.29 | 862 | 0.01000 | -3.69 | 386 |

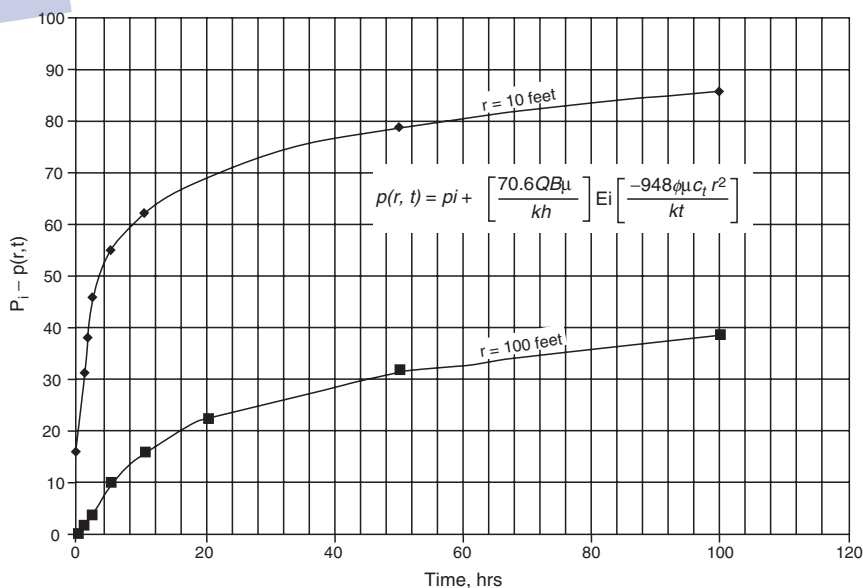


Figure 16-14. Pressure profile at 10 feet and 100 feet as a function of time.

Figure 16-14 shows different curves for the two radii. Obviously, the same calculations can be repeated for any number of radii and, consequently, the same number of curves will be generated. However, the solution can be greatly simplified by examining Figure 16-15. This plot shows that when the pressure difference $p_i - p(r,t)$ is plotted versus t/r^2 , the data for both radii form a common curve. In fact, the pressure difference for any reservoir radius will plot on this exact same curve.

For example, in the same reservoir, to calculate the pressure p at 150 feet after 200 hours of transient flow:

$$t/r^2 = 200/150^2 = 0.0089$$

From Figure 16-15:

$$p_i - p(r,t) = 370 \text{ psi}$$

Thus,

$$p(r,t) = p_i - 370 = 5000 - 370 = 4630 \text{ psi}$$

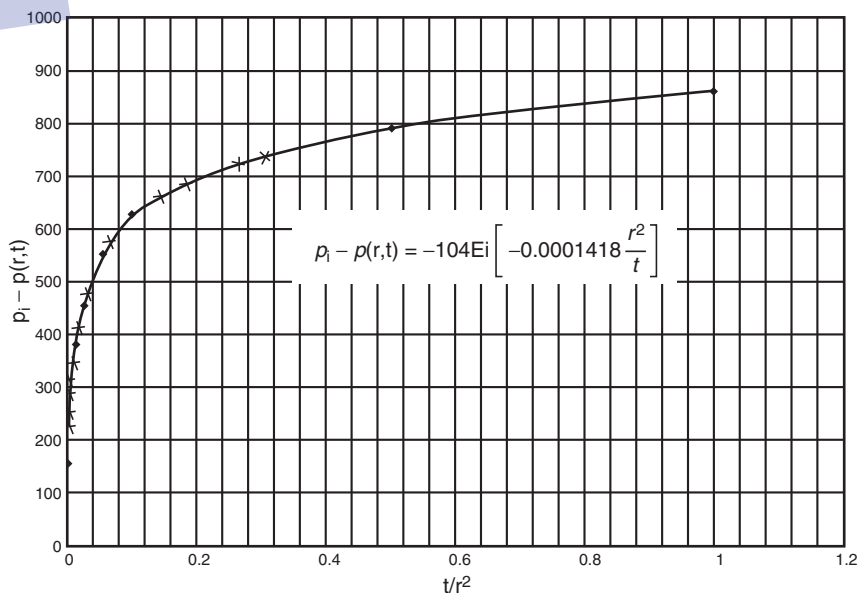


Figure 16-15. Pressure profile at 10 feet and 100 feet as a function of t/r^2 .

Several investigators have employed the dimensionless-variables approach to determine reserves and to describe the recovery performance of hydrocarbon systems with time, notably the following:

- Fetkovich (1980)
- Carter (1985)
- Palacio and Blasingame (1993)
- Mattar and Anderson's *Flowing Material Balance* (2003)
- Anash et al. (2000)
- Decline-curve analysis for fractured reservoirs

All the methods are based on defining a set of decline-curve dimensionless variables that includes:

- Decline-curve dimensionless rate, q_{Dd}
- Decline-curve dimensionless cumulative production, Q_{Dd}
- Decline-curve dimensionless time, t_{Dd}

The aforementioned methods were developed with the objective of providing the engineer with an additional convenient tool for estimating reserves and determining other reservoir properties for oil and gas wells using the available performance data. A review of these methods and their practical applications is given next.

1. Fetkovich Type Curve

Type-curve matching is an advanced form of decline analysis proposed by Fetkovich (1980). The author proposed that the concept of the dimensionless-variables approach can be extended for use in decline-curve analysis to simplify the calculations. He introduced the variables for decline-curve dimensionless flow rate, q_{dD} , and decline-curve dimensionless time, t_{dD} , that are used in all decline-curve and type-curve analysis techniques. Arps' relationships can thus be expressed in the following dimensionless forms:

- **Hyperbolic:**
$$\frac{q_t}{q_i} = \frac{1}{[1 + b D_i t]^{1/b}}$$

In a dimensionless form:

$$q_{Dd} = \frac{1}{[1 + b t_{Dd}]^{1/b}} \quad (16-37)$$

where the decline-curve dimensionless variables q_{Dd} and t_{Dd} are defined by

$$q_{Dd} = \frac{q_t}{q_i} \quad (16-38)$$

$$t_{Dd} = D_i t \quad (16-39)$$

- **Exponential:** $\frac{q_t}{q_i} = \frac{1}{\exp[D_i t]}$

Similarly, $q_{Dd} = \frac{1}{\exp[t_{Dd}]}$ (16-40)

- **Harmonic:** $\frac{q_t}{q_i} = \frac{1}{1 + D_i t}$

or $q_{Dd} = \frac{1}{1 + t_{Dd}}$ (16-41)

where q_{Dd} and t_{Dd} are the decline-curve dimensionless variables, as defined by Equations 16-38 and 16-39, respectively.

During the **boundary-dominated flow period**, that is, steady-state or semisteady-state flowing conditions, Darcy's equation can be used to describe the initial flow rate, q_i :

$$q_i = \frac{0.00708 k h \Delta p}{B \mu \left[\ln \left(\frac{r_e}{r_{wa}} \right) \right] - \frac{1}{2}} = \frac{k h (p_i - p_{wf})}{141.2 B \mu \left[\ln \left(\frac{r_e}{r_{wa}} \right) - \frac{1}{2} \right]}$$

where q = flow rate, STB/day

B = formation, volume factor, bbl/STB

μ = viscosity, cp

k = permeability, md

h = thickness, ft

r_e = drainage radius, ft

r_{wa} = apparent (effective) wellbore radius, ft

The ratio r_e/r_{wa} is commonly referred to as the dimensionless drainage radius r_D :

$$r_D = r_e / r_{wa} \quad (16-42)$$

with

$$r_{wa} = r_w e^{-s}$$

The ratio r_e/r_{wa} in Darcy's equation can be replaced with r_D to give

$$q_i = \frac{k h (p_i - p_{wf})}{141.2 B \mu \left[\ln(r_D) - \frac{1}{2} \right]}$$

Rearranging Darcy's equation gives

$$\left[\frac{141.2 B \mu}{k h \Delta p} \right] q_i = \frac{1}{\ln(r_D) - \frac{1}{2}}$$

It is obvious that the right-hand side of the previous equation is dimensionless, which indicates that the left-hand side of the equation is also dimensionless. This relationship thus defines the dimensionless rate q_D as follows:

$$q_D = \frac{141.2 B \mu q_i}{k h \Delta p} = \frac{1}{\ln(r_D) - \frac{1}{2}} \quad (16-43)$$

Recall the dimensionless form of the diffusivity equation from Chapter 6, Equation 6-90:

$$\frac{\partial^2 p_D}{\partial r_D^2} + \frac{1}{r_D} \frac{\partial p_D}{\partial r_D} = \frac{\partial p_D}{\partial t_D}$$

Fetkovich (1980) demonstrated that the analytical solutions to these equations, the transient-flow diffusivity equation and the pseudosteady-state decline-curve equation, could be combined and presented in a family of log-log dimensionless curves. To develop this link between the two flow regimes, Fetkovich expressed the decline-curve dimensionless variables

q_{Dd} and t_{Dd} in terms of the transient dimensionless rate q_D and time t_D . Combining Equation 16-38 with Equation 16-43 gives

$$q_{Dd} = \frac{q_t}{q_i} = \frac{q_t}{\frac{k h (p_i - p)}{141.2 B \mu \left[\ln(r_D) - \frac{1}{2} \right]}}$$

or

$$q_{Dd} = \dot{q}_D \left[\ln(r_D) - \frac{1}{2} \right]$$

Fetkovich expressed the decline-curve dimensionless time t_{Dd} in terms of the transient dimensionless time t_D in this way:

$$t_{Dd} = \frac{t_D}{\frac{1}{2} [r_D^2 - 1] \left[\ln(r_D) - \frac{1}{2} \right]} \quad (16-44)$$

Replacing the dimensionless time t_D with Equation 6-87 gives

$$t_{Dd} = \frac{1}{\frac{1}{2} [r_D^2 - 1] \left[\ln(r_D) - \frac{1}{2} \right]} \left[\frac{0.006328 t}{\phi(\mu c_t) r_{wa}^2} \right] \quad (16-45)$$

Although Arps' exponential and hyperbolic equations were developed empirically on the basis of production data, Fetkovich was able to give a physical basis to Arps' coefficients. Equations 16-39 and 16-46 indicate that the initial decline rate, D_i , can be defined mathematically by the following expression:

$$D_i = \frac{1}{\frac{1}{2} [r_D^2 - 1] \left[\ln(r_D) - \frac{1}{2} \right]} \left[\frac{0.006328}{\phi(\mu c_t) r_{wa}^2} \right] \quad (16-46)$$

Fetkovich arrived at his unified type curve, as shown in Figure 16-16, by solving the dimensionless form of the diffusivity equation using the constant-terminal solution approach for several assumed values of r_D and

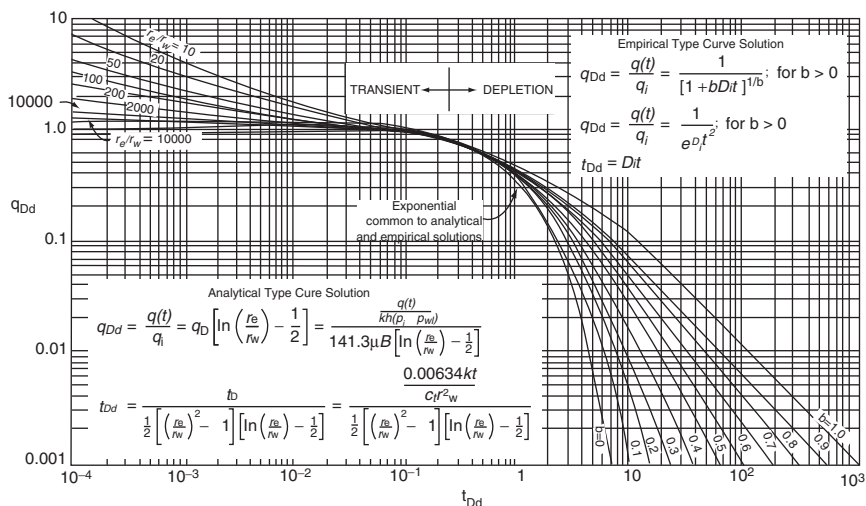


Figure 16-16. Fetkovich type curves. (After Fetkovich, 1980, JPT June 1980, copyright SPE 1980.)

t_{Dd} and the solution to Equation 16-37 as a function of t_{Dd} for several values of b ranging from 0 to 1.

Notice for Figure 16-16 that all curves coincide and become indistinguishable at $t_{Dd} \approx 0.3$. Any data existing before a t_{Dd} of 0.3 will appear to represent exponential decline regardless of the true value of b and, thus, will plot as a straight line on a semi log scale. With regard to the initial rate q_i , it is not the actual producing rate at early time; it is very specifically a pseudosteady-state rate at the surface. This pseudo-state rate can be substantially less than the actual early time transient flow rates that would be produced from low-permeability wells with large negative skins.

The basic steps used in Fetkovich type-curve matching of declining rate-time data are as follows:

- Step 1.* Plot the historical flow rate, q_t , versus time, t , in any convenient units on log-log paper or tracing paper with the same logarithmic cycles as in the Fetkovich type curve.
- Step 2.* Place the tracing-paper data plot over the type curve and slide the tracing paper with plotted data, keeping the coordinate axes parallel, until the actual data points match one of the type curves with a specific value of b .

Because decline type-curve analysis is based on boundary-dominated flow conditions, there is no basis for choosing the proper b values for future boundary-dominated production if only transient data are available. In addition, because of the similarity of curve shapes, unique type-curve matches are difficult to obtain with transient data only. If it is apparent that boundary-dominated (i.e., pseudosteady-state) data are present and can be matched on a curve for a particular value of b , the actual curve can simply be extrapolated following the trend of the type curve into the future.

Step 3. From the match of the particular type curve of Step 2, record values of the reservoir dimensionless radius r_e/r_{wa} and the parameter b .

Step 4. Select any convenient match point on the actual data plot (q_t and t)_{mp} and the corresponding values lying beneath that point on the type-curve grid (q_{Dd} , t_{Dd})_{mp}.

Step 5. Calculate the initial surface gas flow rate, q_i , at $t = 0$ from the rate match point:

$$q_i = \left[\frac{q_t}{q_{Dd}} \right]_{mp} \quad (16-47)$$

Step 6. Calculate the initial decline rate, D_i , from the time match point:

$$D_i = \left[\frac{t_{Dd}}{t} \right]_{mp} \quad (16-48)$$

Step 7. Using the value of r_e/r_{wa} from Step 3 and the calculated value of q_i , calculate the formation permeability, k , by applying Darcy's equation in one of the following three forms:

- Pseudo-pressure form:

$$k = \frac{1422 T [\ln(r_e/r_{wa}) - 0.5] q_i}{h [m(p_i) - m(p_{wf})]} \quad (16-49)$$

- Pressure-squared form:

$$k = \frac{1422 T (\mu_g Z)_{\text{avg}} [\ln(r_c/r_{\text{wa}}) - 0.5] q_i}{h (p_i^2 - p_{\text{wf}}^2)} \quad (16-50)$$

- Pressure-approximation form:

$$k = \frac{141.2 (10^3) T (\mu_g B_g) [\ln(r_c/r_{\text{wa}}) - 0.5] q_i}{h (p_i - p_{\text{wf}})} \quad (16-51)$$

where k = permeability, md

p_i = initial pressure, psia

p_{wf} = bottom-hole flowing pressure, psia

$m(p)$ = pseudo-pressure, psi^2/cp

q_i = initial gas flow rate, Mscf/day

T = temperature, °R

h = thickness, ft

μ_g = gas viscosity, cp

Z = gas deviation factor

B_g = gas formation volume factor, bbl/scf

Step 8. Determine the reservoir pore volume (PV) of the well drainage area at the beginning of the boundary-dominated flow from the following expression:

$$\text{PV} = \frac{56.54 T}{(\mu_g c_t)_i [m(p_i) - m(p_{\text{wf}})]} \left(\frac{q_i}{D_i} \right) \quad (16-52)$$

or, in terms of pressure squared,

$$\text{PV} = \frac{28.27 T (\mu_g Z)_{\text{avg}}}{(\mu_g c_t)_i [p_i^2 - p_{\text{wf}}^2]} \left(\frac{q_i}{D_i} \right) \quad (16-53)$$

with

$$r_c = \sqrt{\frac{(\text{PV})}{\pi h \phi}} \quad (16-54)$$

$$A = \frac{\pi r_e^2}{43,560} \quad (16-55)$$

where PV = pore volume, ft³

ϕ = porosity, fraction

μ_g = gas viscosity, cp

c_t = total compressibility coefficient, psi⁻¹

q_i = initial gas rate, Mscf/day

D_i = decline rate, day⁻¹

r_e = drainage radius of the well, ft

A = drainage area, acres

subscripts

_i = initial

_{avg} = average

Step 9. Calculate the skin factor, s , from the r_e/r_{wa} matching parameter and the calculated values of A and r_e from Step 8.

$$s = \ln \left[\left(\frac{r_e}{r_{wa}} \right)_{mp} \left(\frac{r_w}{r_e} \right) \right] \quad (16-56)$$

Step 10. Calculate the initial gas-in-place, G , from

$$G = \frac{(PV)[1 - S_w]}{5.615 B_{gi}} \quad (16-57)$$

The initial gas-in-place can also be estimated from the following relationship:

$$G = \frac{q_i}{D_i(1 - b)} \quad (16-58)$$

where G = initial gas-in-place, scf

S_w = initial water saturation

B_{gi} = gas formation volume factor at P_i , bbl/scf

PV = pore volume, ft³

An inherent problem when applying decline-curve analysis is having sufficient rate–time data to determine a unique value for b as shown in the Fetkovich type curve. It illustrates that the shorter the producing time, the

more the b value curves approach one another, which leads to the difficulty of obtaining a unique match. Arguably, applying the type-curve approach with only three years of production history may not be possible for some pools. Unfortunately, since time is plotted on a log scale, the production history becomes compressed so that even when incremental history is added, it may still be difficult to differentiate and clearly identify the appropriate decline exponent b .

The following example illustrates the use of the type-curve approach to determine reserves and other reservoir properties.

Example 16-8

Well A is a low-permeability gas well located in West Virginia. It produces from the Onondaga chert, which has been hydraulically fractured with 50,000 gal of 3% gelled acid and 30,000 lb of sand. A conventional Horner analysis of pressure buildup data on the well indicated the following:

$$\begin{aligned} p_i &= 3268 \text{ psia} \\ m(P_i) &= 794.8 (10^6) \text{ psi}^2/\text{cp} \\ k &= 0.082 \text{ md} \\ s &= -5.4 \end{aligned}$$

Fetkovich et al. (1987) provided the following additional data on the gas well:

$$\begin{aligned} p_{wf} &= 500 \text{ psia} \\ \mu_{gi} &= 0.0172 \text{ cp} \\ T &= 620^\circ\text{R} \\ \phi &= 0.06 \\ S_w &= 0.35 \\ m(P_{wf}) &= 20.8 (10^6) \text{ psi}^2/\text{cp} \\ c_{ti} &= 177 (10^{-6}) \text{ psi}^{-1} \\ h &= 70 \text{ ft} \\ B_{gi} &= 0.000853 \text{ bbl/scf} \\ r_w &= 0.35 \text{ ft} \end{aligned}$$

The rate-time data from the past 8 years were plotted and matched to an r_c/r_{wa} stem of 20 and b of 0.5, as shown in Figure 16-17. The resulting match point has the following coordinates:

$$\begin{aligned} q_t &= 1000 \text{ Mscf/day} \\ t &= 100 \text{ days} \\ q_{Dd} &= 0.58 \\ t_{Dd} &= 0.126 \end{aligned}$$

ED: 8 or eight?

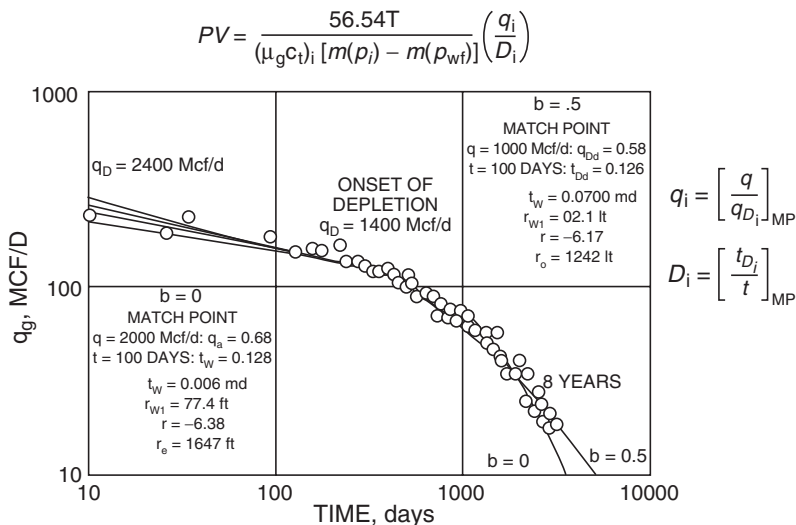


Figure 16-17. West Virginia gas well A type curve fit. (Copyright SPE 1987.)

Using the given data, calculate

- Permeability, k
- Drainage area, A
- Skin factor, s
- Gas-in-place, G

Solution

Step 1. Using the match point, calculate q_i and D_i by applying Equations 16-48 and 16-49, respectively.

$$q_i = \left[\frac{q_t}{q_{Dt}} \right]_{mp}$$

$$q_i = \frac{1000}{0.58} = 1724.1 \text{ Mscf/day}$$

and:

$$D_i = \left[\frac{t_{Dd}}{t} \right]_{mp}$$

$$D_i = \frac{0.126}{100} = 0.00126 \text{ day}^{-1}$$

Step 2. Calculate the permeability, k , from Equation 16-50:

$$k = \frac{1422 T [\ln(r_e/r_{wa}) - 0.5] q_i}{h [m(p_i) - m(p_{wf})]}$$

$$k = \frac{1422(620) [\ln(20) - 0.5] (1724.1)}{(70) [794.8 - 20.8] (10^6)} = 0.07 \text{ md}$$

Step 3. Calculate the reservoir pore volume of the well drainage area using Equation 16-53:

$$PV = \frac{56.54 T}{(\mu_g c_t)_i [m(p_i) - m(p_{wf})]} \left(\frac{q_i}{D_i} \right)$$

$$PV = \frac{(56.54) (620)}{(0.0172) (177) (10^{-6}) [794.8 - 20.8] (10^6)} \frac{1724.1}{0.00126}$$

$$= 20.36 \times 10^6 \text{ ft}^3$$

Step 4. Calculate the drainage radius and area by applying Equations 16-55 and 16-56:

$$r_e = \sqrt{\frac{(PV)}{\pi h \phi}}$$

$$r_e = \sqrt{\frac{(20.36) 10^6}{\pi (70)(0.06)}} = 1242 \text{ ft}$$

and:

$$A = \frac{\pi r_e^2}{43,560}$$

$$A = \frac{\pi(1,242)^2}{43,560} = 111 \text{ acres}$$

Step 5. Determine the skin factor from Equation 16-57:

$$s = \ln \left[\left(\frac{r_e}{r_{wa}} \right)_{mp} \left(\frac{r_w}{r_e} \right) \right]$$

$$s = \ln \left[(20) \left(\frac{0.35}{1242} \right) \right] = -5.18$$

Step 6. Calculate the initial gas-in-place using Equation 16-58:

$$G = \frac{(PV)[1 - S_w]}{5.615 B_{gi}}$$

$$G = \frac{(20.36)(10^6)[1 - 0.35]}{(5.615)(0.000853)} = 2.763 \text{ Bscf}$$

The initial gas G can also be estimated from Equation 16-59, to give

$$G = \frac{q_i}{D_i(1 - b)}$$

$$G = \frac{1.7241(10^6)}{0.00126(1 - 0.5)} = 2.737 \text{ Bscf}$$

Limits of Exponent b and Decline Analysis of Stratified No-Crossflow Reservoirs

Most reservoirs consist of several layers with varying reservoir properties. No-crossflow reservoirs are perhaps the most prevalent and important, so reservoir heterogeneity is of considerable significance in long-term prediction and reserve estimates. In layered reservoirs with crossflow, adjacent layers can simply be combined into a single equivalent layer that can be described as a homogeneous layer by averaging reservoir properties of the crossflowing layers. As shown later in this section, the decline-curve exponent, b , for a single homogeneous layer ranges between 0 and a maximum value of 0.5. For layered no-crossflow systems, values of b range between 0.5 and 1 and therefore can be used to identify the stratification. These separated layers might have the greatest potential for increasing current production and recoverable reserves.

Recall the back-pressure equation, Equation (16-5):

$$q_g = C(p_r^2 - p_{wf}^2)^n$$

where n = back-pressure curve exponent

C = performance coefficient

p_r = reservoir pressure

Fetkovich (1996) suggested that the Arps decline exponent b and the decline rate can be expressed in terms of the exponent n as follows:

$$b = \frac{1}{2n} \left[(2n - 1) - \left(\frac{p_{wf}}{p_i} \right)^2 \right] \quad (16-59)$$

$$D_i = 2n \left(\frac{q_i}{G} \right) \quad (16-60)$$

where G is the initial gas-in-place.

Equation 16-60 indicates that as the reservoir pressure, p_i , approaches p_{wf} with depletion, all the nonexponential decline ($b \neq 0$) will shift toward exponential decline ($b = 0$) as depletion proceeds. Equation 16-60 also suggests that if the well is producing at a very low bottom-hole flowing

pressure (i.e., $p_{wf} = 0$ or $p_{wf} < p_i$), the equation can be reduced to the following expression:

$$b = 1 - \frac{1}{2n} \quad (16-61)$$

The exponent n from a gas well back-pressure performance curve can therefore be used to calculate or estimate b and D_i . Equation 16-61 provides the physical limits of b , which is between 0 and 0.5, over the accepted theoretical range of n , which is between 0.5 and 1.0 for a single-layer homogeneous system, as shown in the following table:

| n | b |
|------------------|-----|
| (high k) 0.50 | 0.0 |
| 0.56 | 0.1 |
| 0.62 | 0.2 |
| 0.71 | 0.3 |
| 0.83 | 0.4 |
| (low k) 1.00 | 0.5 |

However, the harmonic decline exponent, $b = 1$, cannot be obtained from the back-pressure exponent. The b value of 0.4 should be considered a good limiting value for gas wells when not clearly defined by actual production data.

The following is a tabulation of the values of b that should be expected for homogeneous single-layer or layered crossflow systems.

| b | System Characterization and Identification |
|-----------------|---|
| 0.0 | <ul style="list-style-type: none"> • Gas wells undergoing liquid loading • Wells with high back pressure • High-pressure gas • Low-pressure gas with a back-pressure curve exponent of $n \approx 0.5$ • Poor waterflood performance (oil wells) • Gravity drainage with no solution gas (oil wells) • Solution gas drive with unfavorable k_g/k_o (oil wells) |
| 0.3 | <ul style="list-style-type: none"> • Typical for solution-gas-drive reservoirs |
| 0.4 – 0.5 | <ul style="list-style-type: none"> • Typical for gas wells, $b = 0.5$ for $p_{wf} \approx 0$; $b = 0.4$ for $p_{wf} \approx 0.1p_i$ |
| 0.5 | <ul style="list-style-type: none"> • Gravity drainage WITH solution gas and for water-drive oil reservoirs |
| Undeterminable | <ul style="list-style-type: none"> • Constant-rate or increasing-rate production period • Flow rates are all in transient or infinite-acting period |
| $0.5 < b < 0.9$ | <ul style="list-style-type: none"> • Layered or composite reservoir |

The significance of the b value is that for a single-layer reservoir, the value of b will lie between 0 and 0.5. With layered no-crossflow performance, however, the b value can be between 0.5 and 1.0. As pointed out by Fetkovich (1997), the further the b value is driven toward 1.0, the more unrecovered reserves remain in the tight low-permeability layer and the greater potential there is to increase production and recoverable reserves through stimulation of the low-permeability layer. This suggests that decline-curve analysis can be used to recognize and identify layered no-crossflow performance using only readily available historical production data. *Recognition of the layers that are not being adequately drained compared to other layers, that is, differential depletion, is where the opportunity lies.* Stimulation of the less-productive layers can allow an increase in both production and reserves. Figure 16-18 represents the standard Arps depletion/decline curves, as presented by Fetkovich (1997). Ten curves are shown, each described by a b value that ranges between 0 and 1 in increments of 0.1. All of the values have meaning and should be understood for the proper application of decline-curve analysis. *When decline-curve analysis yields a b value greater than 0.5 (layered no-crossflow production), it is inaccurate to simply make a prediction from the match-point values.* This is because the match point represents a best fit of the surface production data, which include production

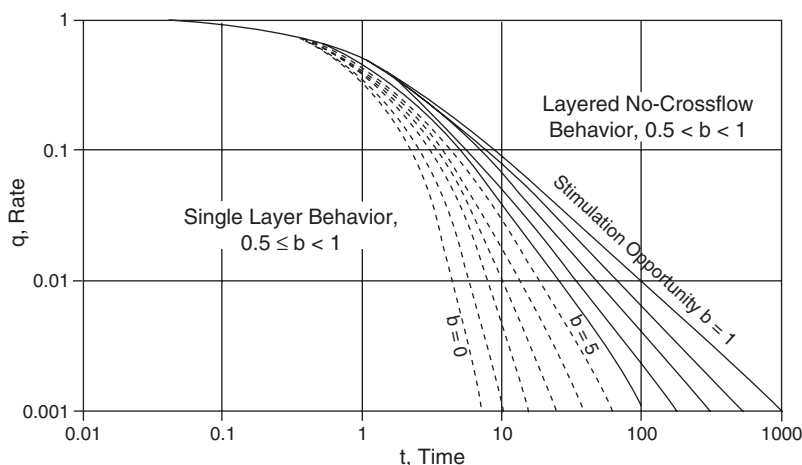


Figure 16-18. Depletion decline curves. (After Fetkovich, 1997, copyright SPE 1997.)

data from all layers. Multiple combinations of layer production values can give the same composite curve and, therefore, unrealistic forecasts in late time may be generated.

To demonstrate the effect of the layered no-crossflow reservoir system on the exponent b , Fetkovich et al. (1990) evaluated the production-depletion performance of a two-layered gas reservoir producing from two noncommunicated layers. The field produces from 10 wells and contains an estimated 1.5 Bscf gas initially in place at an initial reservoir pressure of 428 psia. The reservoir has a gross thickness of 350 ft and a shale barrier with an average thickness of 50 ft that is clearly identified across the field and separates the two layers. Core data indicate a bimodal distribution with a permeability ratio between 10:1 and 20:1.

A type-curve analysis and regression fit of the total field composite $\log(q_i)$ versus $\log(t)$ yielded $b = 0.89$, which is identical to all values obtained from individual well analysis. To provide a quantitative analysis and an early recognition of a non-crossflow layered reservoir, Fetkovich (1980) expressed the rate-time equation for a gas well in terms of the back-pressure exponent, n , with a constant p_{wf} of 0. The derivation is based on a combination of Arps' hyperbolic equation with the material balance equation (i.e., p/z versus G_p) and back-pressure equation to give the following:

- For $0.5 < n < 1$, $0 < b < 0.5$:

$$q_t = \frac{q_i}{\left[1 + (2n - 1)\left(\frac{q_i}{G}\right)t\right]^{\frac{2n}{2n-1}}} \quad (16-62)$$

$$G_{p(t)} = G \left\{ 1 - \left[1 + (2n - 1)\left(\frac{q_i}{G}\right)t\right]^{\frac{1}{1-2n}} \right\} \quad (16-63)$$

- For $n = 0.5$, $b = 0$:

$$q_t = q_i \exp \left[-\left(\frac{q_i}{G}\right)t \right] \quad (16-64)$$

$$G_{p(t)} = G \left[1 - \exp \left[- \left(\frac{q_i}{G} \right) t \right] \right] \quad (16-65)$$

- For $n = 1$, $b = 0.5$:

$$q_t = \frac{q_i}{\left[1 + \left(\frac{q_i}{G} \right) t \right]^2} \quad (16-66)$$

$$G_{p(t)} = G - \frac{G}{1 + \left(\frac{q_i}{G} \right) t} \quad (16-67)$$

These relationships are based on $P_{wf} = 0$, which implies that $q_i = q_{i\max}$, as given by

$$q_i = q_{i\max} = \frac{k h p_i^2}{1422 T (\mu_g Z)_{\text{avg}} [\ln(r_c/r_w) - 0.75 + s]} \quad (16-68)$$

where

$q_{i\max}$ = stabilized absolute open-flow potential, i.e., at $P_{wf} = 0$, Mscf/day

G = initial gas-in-place, Mscf

q_t = gas flow rate at time t , Mscf/day

t = time

$G_{p(t)}$ = cumulative gas production at time t , Mscf

For a commingled well producing from two layers at a constant P_{wf} , the total flow rate $(q_t)_{\text{total}}$ is essentially the sum of the flow rates from all layers, or

$$(q_t)_{\text{total}} = (q_t)_1 + (q_t)_2$$

where the subscripts 1 and 2 represent the more permeable layer and less permeable layer, respectively. For a hyperbolic exponent of $b = 0.5$, Equation 16-67 can be substituted into the above expression to give

$$\frac{(q_{\max})_{\text{total}}}{\left[1 + t \left(\frac{q_{\max}}{G}\right)_{\text{total}}\right]^2} = \frac{(q_{\max})_1}{\left[1 + t \left(\frac{q_{\max}}{G}\right)_1\right]^2} + \frac{(q_{\max})_2}{\left[1 + t \left(\frac{q_{\max}}{G}\right)_2\right]^2} \quad (16-69)$$

Equation 16-70 indicates that only if $\left(\frac{q_{\max}}{G}\right)_1 = \left(\frac{q_{\max}}{G}\right)_2$ will the value of $b = 0.5$ for each layer yield a composite rate–time value of $b = 0.5$.

Mattar and Anderson (2003) presented an excellent review of methods that are available for analyzing production data using traditional and modern type curves. Basically, modern type-curve analysis methods incorporate the flowing pressure data along with production rates, and they use the analytical solutions to calculate hydrocarbon in place. Two important features of modern decline analysis that improve upon the traditional techniques are as follows:

- **Normalization of rates using flowing pressure drop:** Plotting a normalized rate ($q/\Delta p$) enables the effects of back-pressure changes to be accommodated in the reservoir analysis.
- **Handling the change in gas compressibility with pressure:** Using pseudo-time as the time function, instead of real time, enables the gas material balance to be handled rigorously as the reservoir pressure declines with time.

2. Carter Type Curve

Fetkovich originally developed his type curves for gas and oil wells that are producing at constant pressures. Carter (1985) presented a new set of type curves developed exclusively for the analysis of gas rate data. Carter noted that the changes in fluid properties with pressure significantly affect reservoir performance predictions. Of utmost importance is the variation in the gas viscosity–compressibility product, $\mu_g c_g$, which was ignored by Fetkovich. Carter developed another set of decline curves for boundary-dominated flow that uses a new correlating parameter, λ , to represent the changes in $\mu_g c_g$ during depletion. The λ parameter, called the “dimensionless drawdown correlating parameter,”

is designated to reflect the magnitude of pressure drawdown on $\mu_g c_g$ and defined as follows:

$$\lambda = \frac{(\mu_g c_g)_i}{(\mu_g c_g)_{\text{avg}}} \quad (16-70)$$

or, equivalently,

$$\lambda = \frac{(\mu_g c_g)_i}{2} \left[\frac{m(p_i) - m(p_{wf})}{\frac{p_i}{Z_i} - \frac{p_{wf}}{Z_{wf}}} \right] \quad (16-71)$$

where

c_g = gas compressibility coefficient, psi^{-1}

$m(p)$ = real gas pseudo-pressure, psi^2/cp

p_{wf} = bottom-hole flowing pressure, psi

p_i = initial pressure, psi

μ_g = gas viscosity, cp

Z = gas deviation factor

For $\lambda = 1$, it indicates a negligible drawdown effect and corresponds to the $b = 0$ on the Fetkovich exponential decline curve. Values of λ range between 0.55 and 1.0. The type curves presented by Carter are based on four specially defined dimensionless parameters:

- Dimensionless time, t_D
- Dimensionless rate, q_D
- Dimensionless geometry parameter, η , which characterizes the dimensionless radius, r_{eD} , and flow geometry
- Dimensionless drawdown correlating parameter, λ

Carter used a finite-difference radial-gas model to generate the data used to construct the type curves shown in Figure 16-19.

The following steps summarize the type-curve matching procedure.

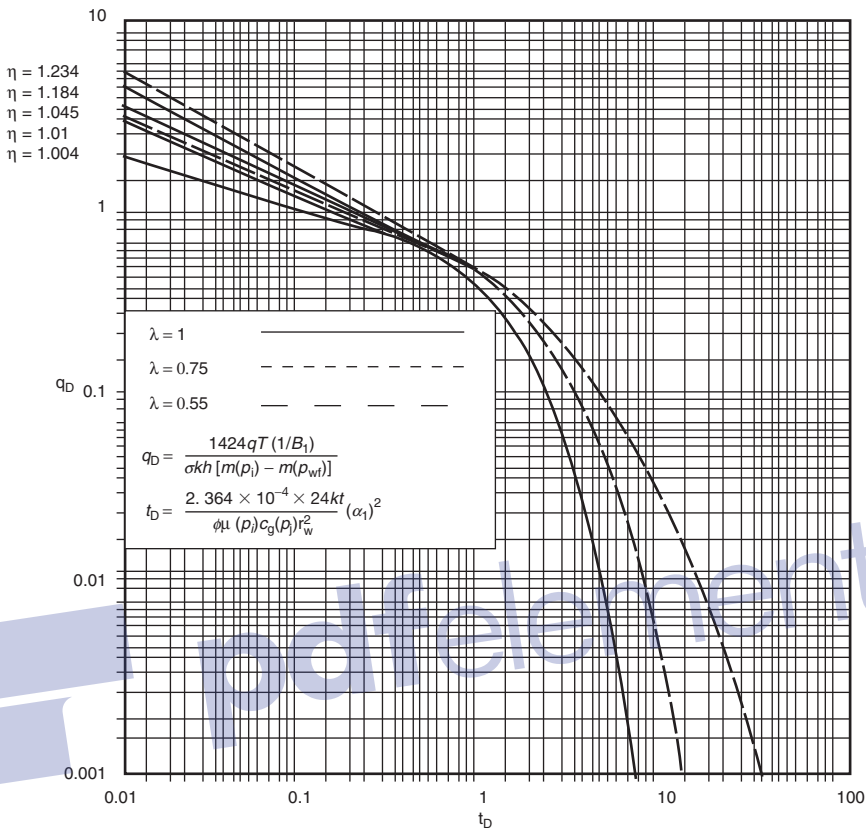


Figure 16-19. Radial-linear gas reservoir type curves. (After Carter, SPEJ 1985, copyright SPE 1985.)

Step 1. Using Equation 16-71 or Equation 16-72, calculate the parameter λ .

$$\lambda = \frac{(\mu_g c_g)_i}{(\mu_g c_g)_{\text{avg}}}$$

or

$$\lambda = \frac{(\mu_g c_g)_i}{2} \left[\frac{m(p_i) - m(p_{wf})}{\frac{p_i}{Z_i} - \frac{p_{wf}}{Z_{wf}}} \right]$$

Step 2. Plot gas rate, q , in Mscf/day or MMscf/day as a function of time (t) in days using the same log-log scale as the type curves. If actual rate values are erratic or fluctuate, it may be best to obtain averaged values of rate by determining the slope of straight lines drawn through adjacent points spaced at regular intervals on the plot of cumulative production, G_p , versus time. That is, slope = $dG_p/dt = q_g$. The resulting plot of q_g versus t should be made on tracing paper or on a transparency so that it can be laid over the type curves for matching.

Step 3. Match the rate data to a type curve corresponding to the computed value of λ in Step 1. If the computed value of λ is not one of the values for which a type curve is shown, the needed curve can be obtained by interpolation and graphical construction.

Step 4. From the match, values of $(q_D)_{mp}$ and $(t_D)_{mp}$ corresponding to specific values for $(q)_{mp}$ and $(t)_{mp}$ are recorded. A value for the dimensionless geometry parameter η is also obtained from the match. It is strongly emphasized that **late-time** data points (boundary-dominated, pseudosteady-state flow condition) are to be matched in preference to **early-time** data points (unsteady-state flow condition) because matching some early rate data often will be impossible.

Step 5. Estimate the gas that would be recoverable if the average reservoir pressure were reduced from its initial value to P_{wf} from the following expression:

$$\Delta G = G_i - G_{P_{wf}} = \frac{(q t)_{mp}}{(q_D t_D)_{mp}} \frac{\eta}{\lambda} \quad (16-72)$$

Step 6. Calculate the initial gas-in-place, G_i , from

$$G_i = \left[\frac{\frac{p_i}{Z_i}}{\frac{p_i}{Z_i} - \frac{p_{wf}}{Z_{wf}}} \right] \Delta G \quad (16-73)$$

Step 7. Estimate the drainage area of the gas well from

$$A = \frac{B_{gi} G_i}{43,560 \phi h (1 - s_{wi})} \quad (16-74)$$

where B_{gi} = gas formation volume factor at P_i , ft³/scf

A = drainage area, acres

h = thickness, ft

ϕ = porosity

S_{wi} = initial water saturation

Example 16-9

The following production and reservoir data were used by Carter (1985) to illustrate the proposed calculation procedure.

| p, psia | μ_{gr} , cp | Z |
|---------|-----------------|--------|
| 1 | 0.0143 | 1.0000 |
| 601 | 0.0149 | 0.9641 |
| 1201 | 0.0157 | 0.9378 |
| 1801 | 0.0170 | 0.9231 |
| 2401 | 0.0188 | 0.9207 |
| 3001 | 0.0208 | 0.9298 |
| 3601 | 0.0230 | 0.9486 |
| 4201 | 0.0252 | 0.9747 |
| 4801 | 0.0275 | 1.0063 |
| 5401 | 0.0298 | 1.0418 |

$$p_i = 5400 \text{ psia}$$

$$T = 726^\circ\text{R}$$

$$\phi = 0.070$$

$$\lambda = 0.55$$

$$p_{wf} = 500 \text{ psi}$$

$$h = 50 \text{ ft}$$

$$S_{wi} = 0.50$$

| Time, days | q_t , MMscf/day |
|------------|-------------------|
| 1.27 | 8.300 |
| 10.20 | 3.400 |
| 20.50 | 2.630 |
| 40.90 | 2.090 |

| Time, days | q_t , MMscf/day |
|------------|-------------------|
| 81.90 | 1.700 |
| 163.80 | 1.410 |
| 400.00 | 1.070 |
| 800.00 | 0.791 |
| 1600.00 | 0.493 |
| 2000.00 | 0.402 |
| 3000.00 | 0.258 |
| 5000.00 | 0.127 |
| 10,000.00 | 0.036 |

Calculate the initial gas-in-place and the drainage area.

Solution

Step 1. The calculated value of λ is given as 0.55 and, therefore, the type curve for a λ value of 0.55 can be used directly from Figure 16-19.

Step 2. Plot the production data, as shown in Figure 16-20, on the same log-log scale as Figure 16-16 and determine the match points of the following:

$$\begin{aligned}(q)_{mp} &= 1.0 \text{ MMscf/day} \\ (t)_{mp} &= 1000 \text{ days} \\ (q_D)_{mp} &= 0.605 \\ (t_D)_{mp} &= 1.1 \\ \eta &= 1.045\end{aligned}$$

Step 3. Calculate ΔG from Equation 16-73.

$$\Delta G = G_i - G_{p_{wf}} = \frac{(q t)_{mp}}{(q_D t_D)_{mp}} \frac{\eta}{\lambda}$$

$$\Delta G = \frac{(1) (1000)}{(0.605) (1.1)} \frac{1.045}{0.55} = 2860 \text{ MMscf}$$

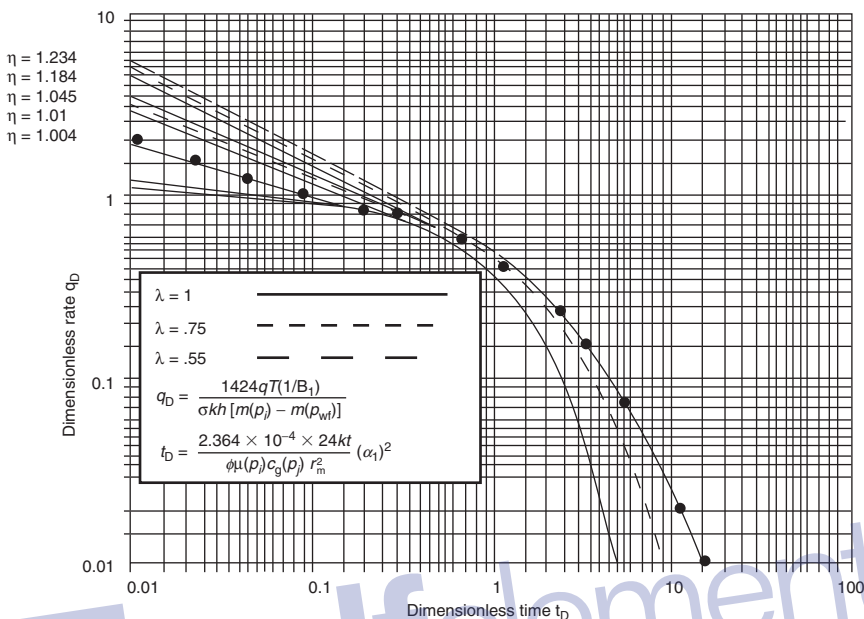


Figure 16-20. Carter type curves for Example 16-7.

Step 4. Estimate the initial gas-in-place by applying Equation 16-74:

$$G_i = \left[\frac{\frac{p_i}{Z_i}}{\frac{p_i}{Z_i} - \frac{p_{wf}}{Z_{wf}}} \right] \Delta G$$

$$G_i = \left[\frac{\frac{5400}{1.0418}}{\frac{5400}{1.0418} - \frac{500}{0.970}} \right] 2860 = 3176 \text{ MMscf}$$

Step 5. Calculate the gas formation volume factor, B_{gi} , at p_i :

$$B_{gi} = 0.0287 \frac{Z_i T}{p_i} = 0.0287 \frac{(1.0418)(726)}{5400} = 0.00396 \text{ ft}^3/\text{scf}$$

Step 6. Determine the drainage area from Equation 16-75:

$$A = \frac{B_{gi} G_i}{43,560 \phi h (1 - s_{wi})}$$

$$A = \frac{0.00396 (3176) (10^6)}{43,560 (0.070) (50) (1 - 0.50)} = 105 \text{ acres}$$

3. Palacio-Blasingame Type Curve

Palacio and Blasingame (1993) presented an innovative technique for converting gas well production data with variable rates and bottom-hole flowing pressures into “equivalent constant-rate liquid data” that allows the liquid solutions to be used to model gas flow. The reasoning for this approach is that the constant-rate type-curve solutions for liquid flow problems are well established from the traditional well-test analysis approach. The new solution for the gas problem is based on a material-balance-like time function and an algorithm that allows the following three things:

- The use of **decline curves that are specifically developed for liquids**
- Modeling of actual **variable rate–variable pressure** drop production conditions
- Explicit computation of **gas-in-place**

Under pseudosteady-state flow conditions, Equation 6-137 in Chapter 6 describes the radial flow of slightly compressible liquids:

$$p_{wf} = \left[p_i - \frac{0.23396 Q B t}{A h \phi c_t} \right] - \frac{162.6 Q B \mu}{k h} \log \left[\frac{4A}{1.781 C_A r_w^2} \right]$$

where

k = permeability, md

A = drainage area, ft²

C_A = shape factor

Q = flow rate, STB/day

t = time, hrs

c_t = total compressibility coefficient, psi⁻¹

Expressing the time t in days and converting from log to a natural logarithm, \ln , the above relation can be written as follows:

$$\frac{p_i - p_{wf}}{q} = \frac{\Delta p}{q} = 70.6 \frac{B\mu}{kh} \ln \left[\frac{4A}{1.781 C_A r_{wa}^2} \right] + \left[\frac{5.615 B}{A h \phi C_t} \right] t \quad (16-75)$$

or more conveniently as

$$\frac{\Delta p}{q} = b_{pss} + m t \quad (16-76)$$

The above expressions suggest that, under a pseudosteady-state flowing condition, a plot of $\Delta p/q$ versus t on a Cartesian scale would yield a straight line with an intercept of b_{pss} and slope of m :

$$\text{Intercept: } b_{pss} = 70.6 \frac{B\mu}{kh} \ln \left[\frac{4A}{1.781 C_A r_{wa}^2} \right] \quad (16-77)$$

$$\text{Slope: } m = \frac{5.615 B}{A h \phi C_t} \quad (16-78)$$

where b_{pss} = constant in the pseudosteady-state (pss) equation

t = time, days

k = permeability, md

A = drainage area, ft^2

q = flow rate, STB/day

B = formation volume factor, bbl/STB

C_A = shape factor

c_t = total compressibility, psi^{-1}

r_{wa} = apparent (effective) wellbore radius, ft

For a gas system flowing under pseudosteady-state conditions, Equation 6-139 in Chapter 6 describes the flow as follows:

$$\frac{m(p_i) - m(p_{wf})}{q} = \frac{\Delta m(p)}{q} = \frac{711T}{kh} \left(\ln \frac{4A}{1.781 C_A r_{wa}^2} \right) + \left[\frac{56.54T}{\phi(\mu_g c_g)_i A h} \right] t \quad (16-79)$$

and in a linear form as

$$\frac{\Delta m(p)}{q} = b_{\text{pss}} + mt \quad (16-80)$$

Similarly to the liquid system, Equation 16-81 indicates that a plot of $\Delta m(p)/q$ versus t will form a straight line with the following features:

$$\text{Intercept: } b_{\text{pss}} = \frac{711 T}{kh} \left(\ln \frac{4A}{1.781 C_A r_{\text{wa}}^2} \right)$$

$$\text{Slope: } m = \frac{56.54 T}{(\mu_g c_t)_i (\phi hA)} = \frac{56.54 T}{(\mu_g c_t)_i (\text{pore volume})}$$

where q = flow rate, Mscf/day

A = drainage area, ft^2

T = temperature, $^\circ\text{R}$

t = flow time, days

The linkage that allows for the conversion of gas-production data into equivalent constant-rate liquid data is based on the use of a new time function called **pseudo-equivalent time** or **normalized material balance pseudo-time**, defined as follows:

$$t_a = \frac{(\mu_g c_g)_i}{q_t} \int_0^t \left[\frac{q_t}{\bar{\mu}_g \bar{c}_g} \right] dt = \frac{(\mu_g c_g)_i}{q_t} \frac{Z_i G}{2p_i} [m(\bar{p}_i) - m(\bar{p})] \quad (16-81)$$

where

t_a = pseudo-equivalent (normalized material balance) time, days

t = time, days

G = original gas-in-place, Mscf

q_t = gas flow rate at time t , Mscf/day

p = average pressure, psi

μ_g = gas viscosity at \bar{p} , cp

\bar{c}_g = gas compressibility at \bar{p} , psi^{-1}

$\bar{m}(p)$ = normalized gas pseudo-pressure, psi^2/cp

In order to perform decline-curve analysis under variable rates and pressures, the authors derived a theoretical expression for decline-curve analysis that combines the following elements:

- Material balance relation
- Pseudosteady-state equation
- Normalized material balance time function, t_a

to give the following relationship:

$$\left[\frac{q_g}{\bar{m}(p_i) - \bar{m}(p_{wf})} \right] b_{pss} = \frac{1}{1 + \left(\frac{m}{b_{pss}} \right) t_a} \quad (16-82)$$

where $\bar{m}(p)$ is the normalized pseudo-pressure as defined by

$$\bar{m}(p_i) = \frac{\mu_{gi} Z_i}{p_i} \int_0^{p_i} \left[\frac{p}{\mu_g Z} \right] dp \quad (16-83)$$

$$\bar{m}(p) = \frac{\mu_{gi} Z_i}{p_i} \int_0^p \left[\frac{p}{\mu_g Z} \right] dp \quad (16-84)$$

and

$$m = \frac{1}{G c_{ti}} \quad (16-85)$$

$$b_{pss} = \frac{70.6 \mu_{gi} B_{gi}}{k_g h} \left[\ln \left(\frac{4A}{1.781 C_A r_{wa}^2} \right) \right] \quad (16-86)$$

where G = original gas-in-place, Mscf

c_{gi} = gas compressibility at p_i , psi^{-1}

c_{ti} = total system compressibility at P_i , psi^{-1}

q_g = gas flow rate, Mscf/day

k_g = effective permeability to gas, md

$\bar{m}(p)$ = normalized pseudo-pressure, psia

p_i = initial pressure
 r_{wa} = effective (apparent) wellbore radius, ft
 B_{gi} = gas formation volume factor at p_i , bbl/Mscf

Notice that Equation 16-83 is essentially expressed in the same dimensionless form as the Fetkovich equation (Equation 16-39), or

$$q_{Dd} = \frac{1}{1 + (t_a)_{Dd}} \quad (16-87)$$

with

$$q_{Dd} = \left[\frac{q_g}{\bar{m}(p_i) - \bar{m}(p_{wf})} \right] b_{pss} \quad (16-88)$$

$$(t_a)_{Dd} = \left(\frac{m}{b_{pss}} \right) t_a \quad (16-89)$$

It must be noted that the q_{Dd} definition is now in terms of normalized pseudo-pressures, and the modified dimensionless decline time function, $(t_a)_{Dt}$, is not in terms of real time but in terms of the material balance pseudo-time. Also notice that Equation 16-89 traces the path of a harmonic decline on the Fetkovich type curve with a hyperbolic exponent of $b = 1$.

However, there is a computational problem when applying Equation 16-82 because it requires the value of the average pressure \bar{p} , which is itself a function of G . Therefore the solution of Equation 16-83 is not direct and requires employing a numerical iterative method. The recommended solution procedure is based on a re-arranging of Equation 16-83 in the following familiar form of linear relationship:

$$\frac{\bar{m}(p_i) - \bar{m}(p)}{q_g} = b_{pss} + m t_a \quad (16-90)$$

The iterative procedure for determining G and \bar{p} is shown in the following steps:

Step 1. Using the available gas properties, step up a table of Z , μ , p/Z , $(p/Z\mu)$ versus p for the gas system.

| Time | p | Z | μ | p/Z | $p/(Z\mu)$ |
|------|-------|-------|---------|-----------|----------------|
| 0 | p_i | Z_i | μ_i | p_i/Z_i | $p_i/(Z\mu)_i$ |
| • | • | • | • | • | • |
| • | • | • | • | • | • |
| • | • | • | • | • | • |

Step 2. Plot $(p/Z\mu)$ versus p on a Cartesian scale and numerically determine the area under the curve for several values of p . Multiply each area by $(Z_i\mu_i/p_i)$ to give the normalized pseudo-pressure as follows:

$$\bar{m}(p) = \frac{\mu_{gi} Z_i}{p_i} \int_0^p \left[\frac{p}{\mu_g Z} \right] dp$$

The required calculations of this step can be performed in the following tabulated form:

| p | area = $\int_0^p \left[\frac{p}{\mu_g Z} \right] dp$ | $\bar{m}(p) = (\text{area}) \frac{\mu_{gi} Z_i}{p_i}$ |
|-------|---|---|
| 0 | 0 | 0 |
| • | • | • |
| • | • | • |
| p_i | • | • |

Step 3. Make plots of $\bar{m}(p)$ and p/Z versus p on a Cartesian scale.

Step 4. Assume a value for the initial gas-in-place, G

Step 5. For each production data point of G_p and t , calculate \bar{p}/\bar{Z} from the gas material balance equation, Equation 16-21:

$$\frac{\bar{p}}{\bar{Z}} = \frac{p_i}{Z_i} \left(1 - \frac{G_p}{G} \right)$$

Step 6. From the plot generated in Step 3, enter the graph of p versus p/Z with *each* value of the ratio \bar{p}/\bar{Z} and determine the value of the corresponding average reservoir pressure \bar{p} . For each value of the average reservoir pressure \bar{p} , determine the values $\bar{m}(\bar{p})$ for each \bar{p} .

Step 7. For *each* production data point, calculate t_a by applying Equation 16-82.

$$t_a = \frac{(\mu_g c_g)_i}{q_i} \frac{Z_i G}{2p_i} [\bar{m}(p_i) - \bar{m}(\bar{p})]$$

The calculation of t_a can be conveniently performed in the following tabulated form:

| T | q_i | G_p | \bar{p} | $\bar{m}(\bar{p})$ | $t_a = \frac{(\mu_g c_g)_i}{q_i} \frac{Z_i G}{2p_i} [\bar{m}(p_i) - \bar{m}(\bar{p})]$ |
|-----|-------|-------|-----------|--------------------|--|
| • | • | • | • | • | • |
| • | • | • | • | • | • |
| • | • | • | • | • | • |

Step 8. Based on the linear relationship given by Equation 16-91, plot $[\bar{m}(p_i) - \bar{m}(\bar{p})]/q_g$ versus t_a on a Cartesian scale and determine the slope, m .

Step 9. Recalculate the initial gas-in-place, G , by using the value m from Step 8 and applying Equation 16-86 to give

$$G = \frac{1}{c_{gi} m}$$

Step 10. The new value of G from Step 9 is used for the next iteration, i.e., starting from Step 5, and this process could continue until some convergence tolerance for G is met.

Palacio and Blasingame developed a modified Fetkovich-Carter type curve, as shown in Figure 16-21, to allow the performance of constant-rate

and constant-pressure gas flow solutions, the traditional Arps curve stems. To obtain a more accurate match to decline type curves than using flow-rate data alone, the authors introduced the following two complementary plotting functions:

- Integral function $(q_{Dd})_i$

$$(q_{Dd})_i = \frac{1}{t_a} \int_0^{t_a} \left(\frac{q_g}{\bar{m}(p_i) - \bar{m}(p_{wf})} \right) dt_a \quad (16-91)$$

- Derivative of the integral function $(q_{Dd})_{id}$

$$(q_{Dd})_{id} = \left(\frac{-1}{t_a} \right) \frac{d}{dt_a} \left[\frac{1}{t_a} \int_0^{t_a} \left(\frac{q_g}{\bar{m}(p_i) - \bar{m}(p_{wf})} \right) dt_a \right] \quad (16-92)$$

Both functions can be easily generated by using simple numerical integration and differentiation methods.

To analyze gas-production data, the proposed method involves the following basic steps:

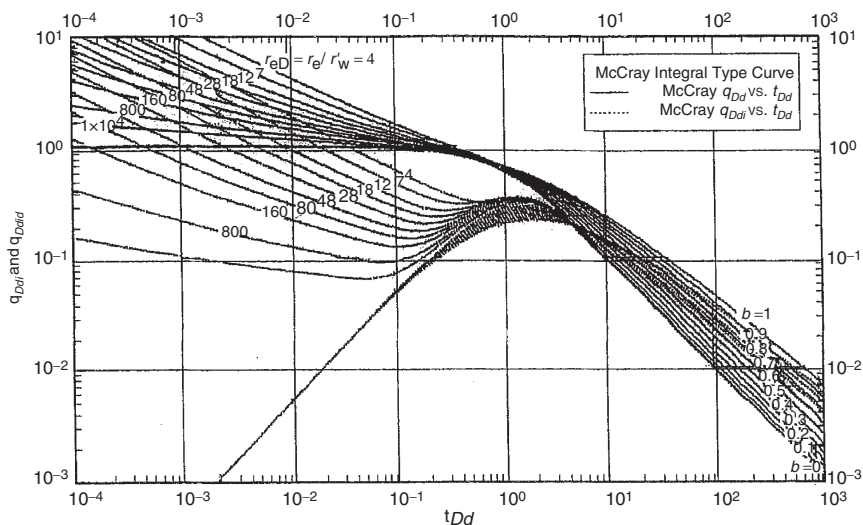


Figure 16-21. Palacio-Blasingame type curve.

Step 1. Calculate the initial gas-in-place, G , as outlined previously.

Step 2. Construct the following table:

| t | q_g | t_a | p_{wf} | $\bar{m}(p_{wf})$ | $\frac{q_g}{\bar{m}(p_i) - \bar{m}(p_{wf})}$ |
|-----|-------|-------|----------|-------------------|--|
| • | • | • | • | • | • |
| • | • | • | • | • | • |
| • | • | • | • | • | • |

Plot $q_g/[\bar{m}(p_i) - \bar{m}(p)]$ versus t_a on a Cartesian scale.

Step 3. Using the well production data as tabulated and plotted in Step 2, compute the two complementary plotting functions, as given by Equations (16-92) and (16-93) as a function of t_a .

$$(q_{Dd})_i = \frac{1}{t_a} \int_0^{t_a} \left(\frac{q_g}{\bar{m}(p_i) - \bar{m}(p_{wf})} \right) dt_a$$

$$(q_{Dd})_{id} = \left(\frac{-1}{t_a} \right) \frac{d}{dt_a} \left[\frac{1}{t_a} \int_0^{t_a} \left(\frac{q_g}{\bar{m}(p_i) - \bar{m}(p_{wf})} \right) dt_a \right]$$

Step 4. Plot both functions, i.e., $(q_{Dd})_i$ and $(q_{Dd})_{id}$, versus t_a on a tracing paper so it can be laid over the type curve of Figure 16-22 for matching.

Step 5. Establish a match point and the corresponding dimensionless radius r_{eD} value to confirm the final value of G and to determine other properties:

$$\bullet \quad G = \frac{1}{c_{ti}} \left[\frac{t_a}{t_{Dd}} \right]_{mp} \left[\frac{(q_{Dd})_i}{q_{Dd}} \right]_{mp} \quad (16-93)$$

$$\bullet \quad A = \frac{5.615 G B_{gi}}{h \phi (1 - S_{wi})}$$

$$\begin{aligned}
 & \bullet r_c = \sqrt{\frac{A}{\pi}} \\
 & \bullet r_{wa} = \frac{r_c}{r_{eD}} \\
 & \bullet s = -\ln\left(\frac{r_{wa}}{r_w}\right) \\
 & \bullet k = \frac{141.2 B_{gi} \mu_{gi}}{h} \left[\ln\left(\frac{r_c}{r_w}\right) - \frac{1}{2} \right] \left[\frac{(q_{Dd})_i}{q_{Dd}} \right]_{mp} \quad (16-94)
 \end{aligned}$$

where G = gas-in-place, Mscf

B_{gi} = gas formation volume factor at p_i , bbl/Mscf

A = drainage area, ft²

s = skin factor

r_{eD} = dimensionless drainage radius

S_{wi} = connate-water saturation

The authors used Fetkovich's West Virginia gas well A, as given in Example 16-6, to demonstrate the use of the proposed type curve. The resulting fit of the data given in Example 16-6 by Palacio and Blasingame is shown in Figure 16-22.

4. Mattar and Anderson's Flowing Material Balance

The flowing material balance method is a new technique that can be used to estimate the original gas-in-place (OGIP). The method, as introduced by Mattar and Anderson (2003), uses the concept of the normalized rate and material balance pseudo-time to create a simple linear plot, which extrapolates to fluids in place. The method uses the available production data in a manner similar to that of Palacio and Blasingame's approach. The authors showed that for a depletion drive gas reservoir flowing under pseudo steady-state conditions, the flow system can be described by the following equation:

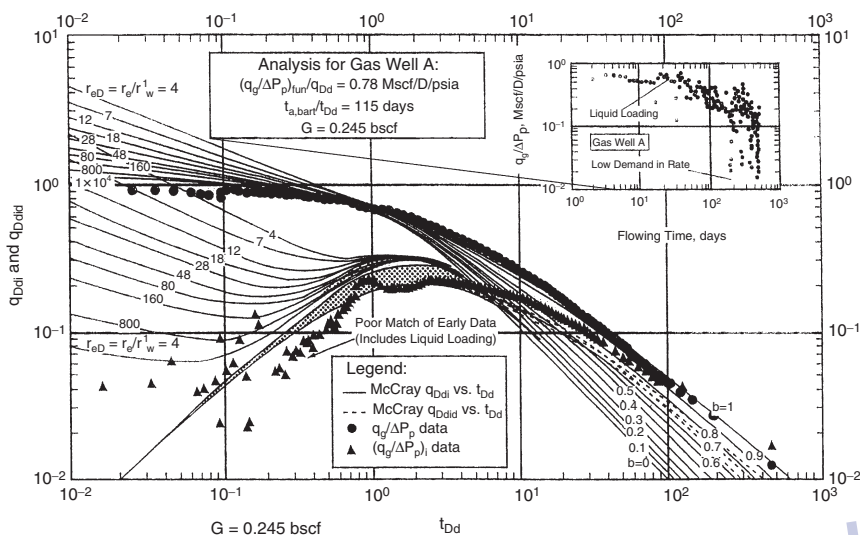


Figure 16-22. Palacio-Blasingame West Virginia gas well example.

$$\frac{q}{m(p_i) - m(p_{wf})} = \frac{q}{\Delta m(p)} = \left(\frac{-1}{G b_{pss}^{\setminus}} \right) Q_N + \frac{1}{b_{pss}^{\setminus}}$$

Q_N is the **normalized** cumulative production, as given by

$$Q_N = \frac{2q_t p_i t_a}{(c_t \mu_i Z_i) \Delta m(p)}$$

And t_a is the Blasingame normalized material balance pseudo-time, as given by

$$t_a = \frac{(\mu_g c_g)_i}{q_t} \frac{Z_i G}{2p_i} [\bar{m}(p_i) - \bar{m}(\bar{p})]$$

The authors defined b_{pss}^{\setminus} as the inverse productivity index, in $\text{psi}^2/\text{cp-MMscf}$, as follows:

$$b_{pss}^{\setminus} = \frac{1.417 \times 10^6 T}{kh} \left[\ln \left(\frac{r_c}{r_{wa}} \right) - \frac{3}{4} \right]$$

where p_i = initial pressure, psi

G = OGIP

r_c = drainage radius, ft

r_{wa} = apparent wellbore radius, ft

Thus, the previous expression suggests that a plot of $q/\Delta m(p)$ versus $[2qp_i t_a / (c_{ti} \mu_i Z_i \Delta m(p))]$ on a Cartesian scale would produce a straight line with the following characteristics:

- x-axis intercept gives gas-in-place, G
- y-axis intercept gives b_{pss}
- Slope gives $(-1/G) b_{pss}$

The specific steps taken in estimating G are summarized below:

Step 1. Using the available gas properties, step up a table of Z , μ , p/Z , $(p/Z\mu)$ versus p for the gas system.

Step 2. Plot $(p/Z\mu)$ versus p on a Cartesian scale and numerically determine the area under the curve for several values of p to give $m(p)$ at each pressure.

Step 3. Assume a value for the initial gas-in-place, G .

Step 4. Using the assumed value of G and for *each* production data point of G_p at time t , calculate \bar{p}/\bar{Z} from the gas material balance equation, Equation 16-21:

$$\frac{\bar{p}}{\bar{Z}} = \frac{p_i}{Z_i} \left(1 - \frac{G_p}{G} \right)$$

Step 5. For *each* production data point of q_t and t , calculate t_a and the normalized cumulative production Q_N :

$$t_a = \frac{(\mu_g c_g)_i}{q_t} \frac{Z_i G}{2p_i} \left[\bar{m}(p_i) - \bar{m}(\bar{p}) \right]$$

$$Q_N = \frac{2q_t p_i t_a}{(c_t \mu_i Z_i) \Delta m(p)}$$

Step 6. Plot $q/\Delta p$ versus Q_N on a Cartesian scale and obtain the best line through the data points. Extrapolate the line to the x-axis and read the OGIP.

Step 7. The new value of G from Step 6 is used for the next iteration, i.e., Step 3, and this process could continue until some convergence tolerance for G is met.

5. Anash et al. Type Curves

The changes in gas properties can significantly affect reservoir performance during depletion; of utmost importance is the variation in the gas viscosity–compressibility product, $\mu_g c_g$, which was ignored by Fetkovich in his development of his type curves. Anash et al. (2000) proposed three functional forms to describe the product, $\mu_g c_t$, as a function of pressure. They conveniently expressed the pressure in a dimensionless form as generated from the gas material balance equation, to give

$$\frac{p}{Z} = \frac{p_i}{Z_i} \left(1 - \frac{G_p}{G} \right)$$

In a dimensionless form, the previous material balance equation is expressed as follows:

$$p_D = (1 - G_{pD})$$

where

$$p_D = \frac{p/Z}{p_i/Z_i} \quad (16-95)$$

$$G_{pD} = \frac{G_p}{G}$$

Anash and co-authors indicated that the product $(\mu_g c_t)$ can be expressed in a **dimensionless ratio** of $(\mu_g c_t)_i/(\mu_g c_t)$ as a function of the dimensionless pressure, p_D , by one of the following three forms:

a) First-order polynomial

The first form is a first-degree polynomial that is adequate in describing the product, $\mu_g c_t$, as a function of pressure at gas-reservoir pressures below

5,000 psi, that is, $p_i < 5000$. The polynomial is expressed in a dimensionless form as

$$\frac{\mu_i c_{ti}}{\mu c_t} = p_D \quad (16-96)$$

where

$$c_{ti} = \text{total system compressibility at } p_i, \text{ psi}^{-1}$$

$$\mu_i = \text{gas viscosity at } p_i, \text{ cp}$$

b) Exponential model

The second form is adequate in describing the product, $\mu_g c_t$, for high-pressure gas reservoirs, that is, $p_i > 8000$ psi.

$$\frac{\mu_i c_{ti}}{\mu c_t} = \beta_0 \exp(\beta_1 p_D) \quad (16-97)$$

i) General polynomial model

A third- or fourth-degree polynomial is considered by the authors a general model that is applicable to all gas-reservoir systems with any range of pressures, as given by

$$\frac{\mu_i c_{ti}}{\mu c_t} = a_0 + a_1 p_D + a_2 p_D^2 + a_3 p_D^3 + a_4 p_D^4 \quad (16-98)$$

The coefficient in Equations 16-98 and 16-99, β_0 , β_1 , a_0 , a_1 , etc., can be determined by plotting the dimensionless ratio $[\mu_i c_{ti}/\mu c_t]$ versus p_D on a Cartesian scale, as shown in Figure 16-23, and using the least-squares regression model to determine the coefficients.

The authors also developed the following fundamental form of the stabilized gas flow equation:

$$\frac{dG_P}{dt} = q_g = \frac{J_g}{c_{ti}} \int_{p_{wD}}^{p_D} \left[\frac{\mu_i c_{ti}}{\mu c_t} \right] dp_D$$

with the dimensionless bottom-hole flowing pressure defined as follows:

$$p_{wD} = \frac{p_{wf}/Z_{wf}}{p_i/Z_i}$$

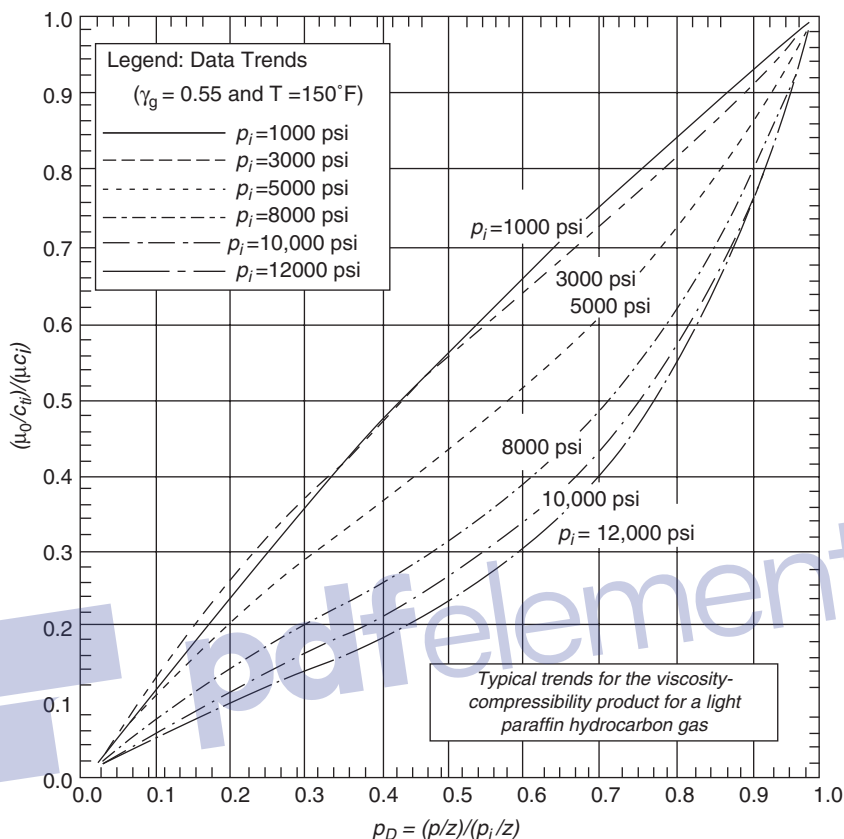


Figure 16-23. Typical distribution of the viscosity-compressibility function. (After Anash et al., 2000.)

where q_g = gas flow rate, scf/day
 p_{wf} = flowing pressure, psia
 Z_{wf} = gas deviation factor at p_{wf}
 J_g = productivity index, scf/day, psia

Anash et al. presented their solutions in a type-curve format in terms of a set of the familiar dimensionless variables, q_{Dd} , t_{Dd} , r_{eD} , and a newly introduced correlating parameter, β , that is a function of the dimensionless pressure. They presented three type-curve sets, as shown in Figures 16-24 through 16-26, one for each of the functional forms selected to

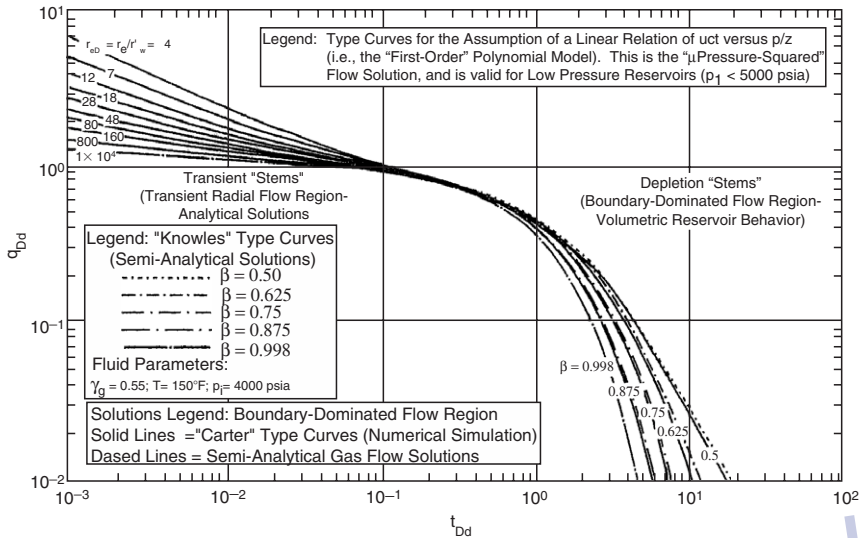


Figure 16-24. "First-order" polynomial solution for real-gas flow under boundary-dominated flow conditions. Solution assumes a μc_t profile that is linear with P_D . (Permission to copy by the SPE, 2000.)

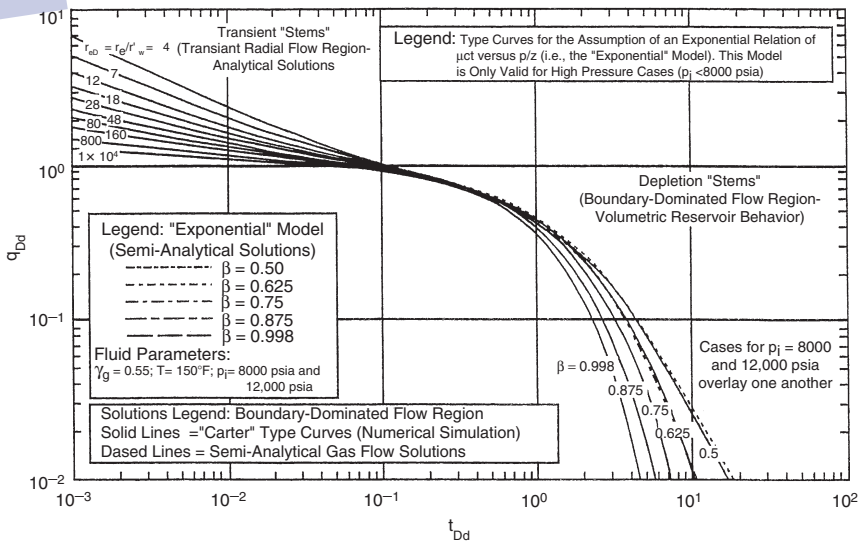


Figure 16-25. "Exponential" solutions for real-gas flow under boundary-dominated flow conditions. (Permission to copy by the SPE, 2000.)

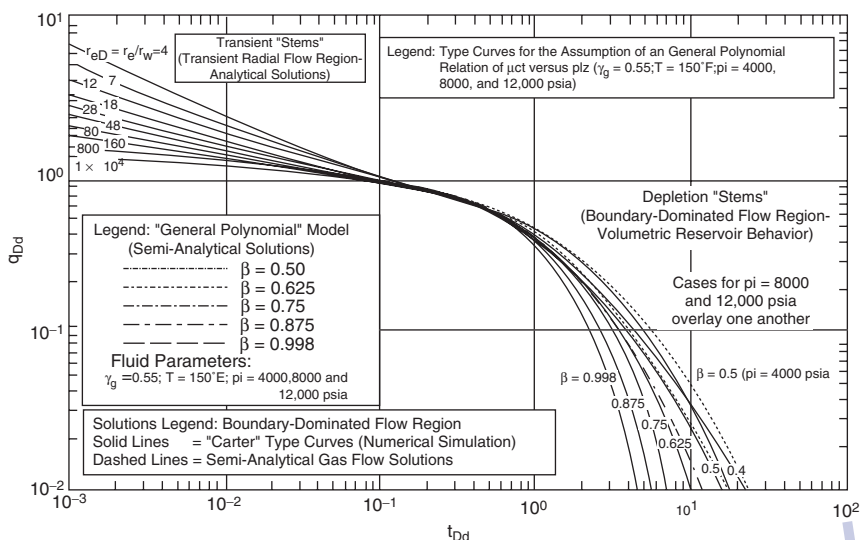


Figure 16-26, “General polydomial” solution for real-gas flow under boundary-dominated flow conditions. (Permission to copy by the SPE, 2000.)

describe the product μc_t (i.e., first-order polynomial, exponential model, or general polynomial).

The methodology of employing the Anash et al. type curve is summarized in the following steps:

Step 1. Using the available gas properties, prepare a plot of $(\mu_i c_{ti}/\mu c_t)$ versus p_D , where

$$p_D = \frac{p/Z}{p_i/Z_i}$$

Step 2. From the generated plot, select the appropriate functional form that describes the resulting curve:

- First-order polynomial

$$\frac{\mu_i c_{ti}}{\mu c_t} = p_D$$

- Exponential model

$$\frac{\mu_i c_{ti}}{\mu c_t} = \beta_o \exp(\beta_1 p_D)$$

- General polynomial model

$$\frac{\mu_i c_{ti}}{\mu c_t} = a_o + a_1 p_D + a_2 p_D^2 + a_3 p_D^3 + a_4 p_D^4$$

Use a regression model (i.e., least-squares) to determine the coefficient of the selected functional form that adequately describes $(\mu_i c_{ti}/\mu c_t)$ versus p_D .

Step 3. Plot the historical flow rate, q_g , versus time, t , on a log-log scale with the same logarithmic cycles as the one given by the selected type curves (i.e., Figures 16-24 through 16-26).

Step 4. Using the type-curve matching technique described previously, select a match point and record

- $(q_g)_{mp}$ and $(q_{Dd})_{mp}$
- $(t)_{mp}$ and $(t_{Dd})_{mp}$
- $(r_{cD})_{mp}$

Step 5. Calculate the dimensionless pressure p_{wD} using the bottom-hole flowing pressure,

$$p_{wD} = \frac{p_{wf}/Z_{wf}}{p_i/Z_i} \quad (16-99)$$

Step 6. Depending on the selected functional form in Step 2, calculate the constant α for the selected functional model:

- For the first-order polynomial

$$\alpha = \frac{1}{2} (1 - p_{wD}^2) \quad (16-100)$$

- For the exponential model

$$\alpha = \frac{\beta_0}{\beta_1} [\exp(\beta_1) - \exp(\beta_1 p_{wD})] \quad (16-101)$$

where β_0 and β_1 are the coefficients of the exponential model.

- For the polynomial function (assuming a fourth-degree polynomial)

$$\alpha = A_0 + A_1 + A_2 + A_3 + A_4 \quad (16-102)$$

where

$$A_0 = -(A_1 p_{wD} + A_2 p_{wD}^2 + A_3 p_{wD}^3 + A_4 p_{wD}^4)$$

$$A_1 = a_0$$

$$A_2 = \frac{a_1}{2}$$

$$A_3 = \frac{a_2}{3}$$

$$A_4 = \frac{a_3}{4}$$

Step 7. Calculate the well **productivity index**, J_g , in scf/day – psia, by using the **flow-rate match point** and the constant α of Step 6 in the following relation:

$$J_g = \frac{C_{ti}}{\alpha} \left(\frac{q_g}{q_{Dd}} \right)_{mp} \quad (16-103)$$

Step 8. Estimate the OGIP, in scf, from the **time match point**:

$$G = \frac{J_g}{C_{ti}} \left(\frac{t}{t_{Dd}} \right)_{mp} \quad (16-104)$$

Step 9. Calculate the reservoir drainage area, A , in ft^2 , from the following expression:

$$A = \frac{5.615 B_{gi} G}{\phi h (1 - S_{wi})} \quad (16-105)$$

where A = drainage area, ft^2

B_{gi} = gas formation volume factor at p_i , bbl/scf

S_{wi} = connate-water saturation

Step 10. Calculate the permeability, k , in md , from the match curve of the **dimensionless drainage radius**, r_{eD} :

$$k = \frac{141.2 \mu_i B_{gi} J_g}{h} \left(\ln[r_{eD}]_{mp} - \frac{1}{2} \right) \quad (16-106)$$

Step 11. Calculate the skin factor from the following relationships:

- Drainage radius $r_e = \sqrt{\frac{A}{\pi}}$ (16-107)

- Apparent wellbore radius $r_{wa} = \frac{r_e}{(r_{eD})_{mp}}$ (16-108)

- Skin factor $s = -\ln\left(\frac{r_{wa}}{r_w}\right)$ (16-109)

Example 16-10

The West Virginia gas well, A, is a vertical gas well that has been hydraulically fractured and is undergoing depletion. The production data were presented by Fetkovich (1980) and used in Example 16-6. A summary of the reservoir and fluid properties is given below:

$$r_w = 0.354 \text{ ft}$$

$$h = 70 \text{ ft}$$

$$\phi = 0.06$$

$$\begin{aligned}
 T &= 160^{\circ}\text{F} \\
 s &= 5.17 \\
 k &= 0.07 \text{ md} \\
 \gamma_g &= 0.57 \\
 B_{gi} &= 0.00071 \text{ bbl/scf} \\
 \mu_{gi} &= 0.0225 \text{ cp} \\
 c_{ti} &= 0.000184 \text{ psi}^{-1} \\
 p_i &= 4175 \text{ psia} \\
 p_{wf} &= 710 \text{ psia} \\
 \alpha &= 0.4855 \text{ (first-order polynomial)} \\
 S_{wi} &= 0.35
 \end{aligned}$$

Solution

Step 1. Figure 16-27 shows the type-curve match of the production data with that of Figure 16-24, to give:

$$(q_{Dd})_{mp} = 1.0$$

$$(q_g)_{mp} = 1.98 \times 10^6 \text{ scf/day}$$

$$(t_{Dd})_{mp} = 1.0$$

$$(t)_{mp} = 695 \text{ days}$$

$$(r_{eD})_{mp} = 28$$

Step 2. Calculate the productivity index from Equation 16-104:

$$J_g = \frac{C_{ti}}{\alpha} \left(\frac{q_g}{(q_{Dd})_{mp}} \right)$$

$$J_g = \frac{0.000184}{0.4855} \left(\frac{1.98 \times 10^6}{1.0} \right) = 743.758 \text{ scf/day} - \text{psi}$$

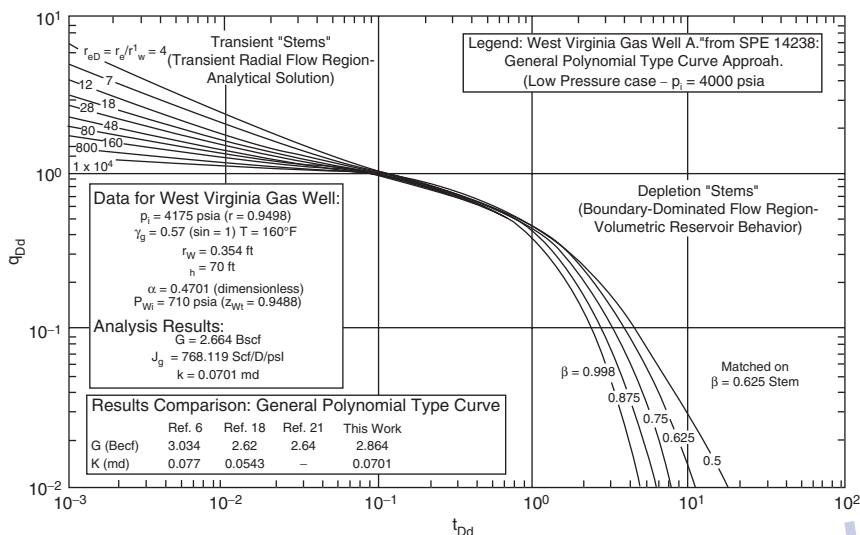


Figure 16-27. Type-curve analysis of West Virginia gas well "A" (SPE 14238). "General polynomial" type-curve analysis approach. (Permission to copy by the SPE, 2000.)

Step 3. Solve from G by applying Equation 16-105:

$$G = \frac{J_g}{C_{ui}} \left(\frac{t}{t_{Dd}} \right)^{mp}$$

$$G = \frac{743.758}{0.0001824} \left(\frac{695}{1.0} \right) = 2.834\beta \text{ scf}$$

Step 4. Calculate the drainage area from Equation 16-106:

$$A = \frac{5.615 B_{gi} G}{\phi h (1 - S_{wi})}$$

$$A = \frac{5.615 (0.00071) (2.834 \times 10^9)}{(0.06) (70) (1 - 0.35)} = 4.1398 \times 10^6 \text{ ft}^2 = 95 \text{ acres}$$

Step 5. Compute the permeability from the match on the $r_{eD} = 28$ transient stem by using Equation 16-107:

$$k = \frac{(141.2)(0.0225)(0.00071)(743.76)}{70} \left(\ln(28) - \frac{1}{2} \right)$$

$$= 0.0679 \text{ md}$$

Step 6. Calculate the skin factor by applying Equations 16-108 and 16-109:

$$\bullet \quad r_c = \sqrt{\frac{A}{\pi}} = \sqrt{\frac{4.1398 \times 10^6}{\pi}} = 1147.9 \text{ ft}$$

$$\bullet \quad r_{wa} = \frac{r_c}{(r_{cD})_{mp}} = \frac{1147.9}{28} = 40.997 \text{ ft}$$

$$\bullet \quad s = -\ln \left(\frac{r_{wa}}{r_w} \right) = -\ln \left(\frac{40.997}{0.354} \right) = -4.752$$

6. Decline-Curve Analysis for Fractured Wells

A fracture is defined as a single crack initiated from the wellbore by hydraulic fracturing. It should be noted that fractures are different from “fissures,” which are the formation of natural fractures. Hydraulically induced fractures are usually vertical, but can be horizontal if the formation is less than about 3,000 ft deep. Vertical fractures are characterized by the following properties:

- Fracture half-length x_f , in ft
- Dimensionless radius r_{cD} , where $r_{cD} = r_c/x_f$
- Fracture height h_f , which is often assumed equal to the formation thickness, in ft
- Fracture permeability k_f , in md
- Fracture width w_f , in ft
- Fracture conductivity F_C , where $F_C = k_f w_f$

The analysis of fractured-well tests deals with the identification of well and reservoir variables that would have an impact on future well performance. However, fractured wells are substantially more complicated. The well-penetrating fracture has unknown geometric features, that is, x_f , w_f , and h_f , and unknown conductivity properties.

Many authors have proposed three transient flow models to consider when analyzing transient pressure data from vertically fractured wells; these are as follows:

- Infinite-conductivity vertical fractures
- Finite-conductivity vertical fractures
- Uniform-flux fractures

Description of these three types of fractures are as follows:

Infinite-Conductivity Vertical Fractures

These fractures are created by conventional hydraulic fracturing and characterized by a very high conductivity, which, for all practical purposes, can be considered infinite. In this case, the fracture acts similarly to a large-diameter pipe with *infinite permeability* and, therefore, there is essentially no pressure drop from the tip of the fracture to the wellbore, that is, no pressure loss in the fracture. This model assumes that the flow into the wellbore is only through the fracture and exhibits three flow periods:

- Fracture linear flow period
- Formation linear flow period
- Infinite-acting pseudo-radial flow period

Several specialized plots are used to identify the start and end of each flow period. For example, an early time log-log plot of Δp versus Δt will exhibit a straight line of half-unit slope. These flow periods associated with infinite conductivity fractures and the diagnostic specialized plots will be discussed later in this section.

Finite-Conductivity Vertical Fractures

These are very long fractures created by massive hydraulic fracture (MHF). These types of fractures need large quantities of propping agent to maintain them open, and, as a result, the fracture permeability, k_f , is lower than that of the infinite-conductivity fractures. These finite-conductivity vertical fractures are characterized by measurable pressure drops in the fracture and, therefore, exhibit unique pressure responses during testing of hydraulically fractured wells. The transient pressure behavior for this system can include the following four sequence flow periods (to be discussed later):

- Initially, linear flow within the fracture
- Next, bilinear flow
- Then, linear flow in the formation
- And eventually, infinite acting pseudo-radial flow

Uniform-Flux Fractures

A uniform flux fracture is one in which the reservoir fluid-flow rate from the formation into the fracture is uniform along the entire fracture length. This model is similar to the infinite-conductivity vertical fracture in several aspects. The difference between these two systems occurs at the boundary of the fracture. The system is characterized by a variable pressure along the fracture and exhibits essentially two flow periods:

- Linear flow
- Infinite-acting pseudo-radial flow

Except for highly propped and conductive fractures, it is thought that the uniform-influx fracture theory better represents reality than the infinite-conductivity fracture; however, the difference between the two is rather small.

The fracture has a much greater permeability than the formation it penetrates; hence, it influences the pressure response of a well test significantly. The general solution for the pressure behavior in a reservoir is expressed in terms of dimensionless variables. The following dimensionless groups are used when analyzing pressure transient data in a hydraulically fractured well:

- Conductivity group: $F_{CD} = \frac{k_f}{k} \frac{w_f}{x_f} = \frac{F_C}{k x_f}$
- Fracture group: $r_{eD} = \frac{r_e}{x_f}$

where x_f = fracture half-length, ft
 w_f = fracture width, ft
 k_f = fracture permeability, md
 k = pre-frac formation permeability, md
 F_C = fracture conductivity, md-ft
 F_{CD} = dimensionless fracture conductivity

Pratikno, Rushing, and Blasingame (2003) developed a new set of type curves specifically for finite-conductivity vertically fractured wells centered in bounded circular reservoirs. The authors used analytical solutions to develop these type curves and to establish a relation for the decline variables.

Recall that the general dimensionless pressure equation for a bounded reservoir during pseudosteady-state flow is given by Equation 6-137:

$$p_D = 2\pi t_{DA} + \frac{1}{2} \left[\ln \left(\frac{A}{r_w^2} \right) \right] + \frac{1}{2} \left[\ln \left(\frac{2.2458}{C_A} \right) \right] + s$$

with the dimensionless time based on the wellbore radius, t_D , or drainage area, t_{DA} , as given by Equations 6-87 and 6-87a:

$$t_D = \frac{0.0002637 kt}{\phi \mu c_t r_w^2}$$

$$t_{DA} = \frac{0.0002637 kt}{\phi \mu c_t A} = t_A \left(\frac{r_w^2}{A} \right)$$

The authors adopted the last form and suggested that, for a well producing under pseudosteady-state at a constant rate with a finite-conductivity fracture in a circular reservoir, the dimensionless pressure drop can be expressed as follows:

$$p_D = 2\pi t_{DA} + b_{Dpss}$$

or

$$b_{Dpss} = p_D - 2\pi t_{DA}$$

where the term b_{Dpss} is the dimensionless pseudosteady-state constant that is independent of time; however, b_{Dpss} is a function of

- the dimensionless radius, r_{eD} , and
- the dimensionless fracture conductivity, F_{CD}

The authors note that, during pseudosteady flow, the equation describing the flow during this period yields constant values for given values of r_{eD} and F_{CD} that are closely given by the following relationship:

$$b_{Dpss} = \ln(r_{eD}) - 0.049298 + \frac{0.43464}{r_{eD}^2} + \frac{a_1 + a_2 u + a_3 u^2 + a_4 u^3 + a_5 u^4}{1 + b_1 u + b_2 u^2 + b_3 u^3 + b_4 u^4}$$

with

$$u = \ln(F_{CD})$$

| | | |
|-------|--------------------|---------------------|
| where | $a_1 = 0.93626800$ | $b_1 = -0.38553900$ |
| | $a_2 = -1.0048900$ | $b_2 = -0.06988650$ |
| | $a_3 = 0.31973300$ | $b_3 = -0.04846530$ |
| | $a_4 = -0.0423532$ | $b_4 = -0.00813558$ |
| | $a_5 = 0.00221799$ | |

Based on the above equations, Pratikno et al. (2003) used Palacio and Blasingame's previously defined functions (i.e., t_a , $(q_{Dd})_i$, and $(q_{Dd})_{id}$) and the parameters r_{cD} and F_{CD} to generate a set of decline curves for a sequence of 13 values for F_{CD} with a sampling of $r_{cD} = 2, 3, 4, 5, 10, 20, 30, 40, 50, 100, 200, 300, 400, 500,$ and $1,000$. Type curves for F_{CD} of $0.1, 1, 10, 100,$ and $1,000$ are shown in Figures 16-28 through 16-32.

The authors recommend the following type-curve matching procedure, which is similar to the methodology used in applying Palacio and Blasingame's type curve:

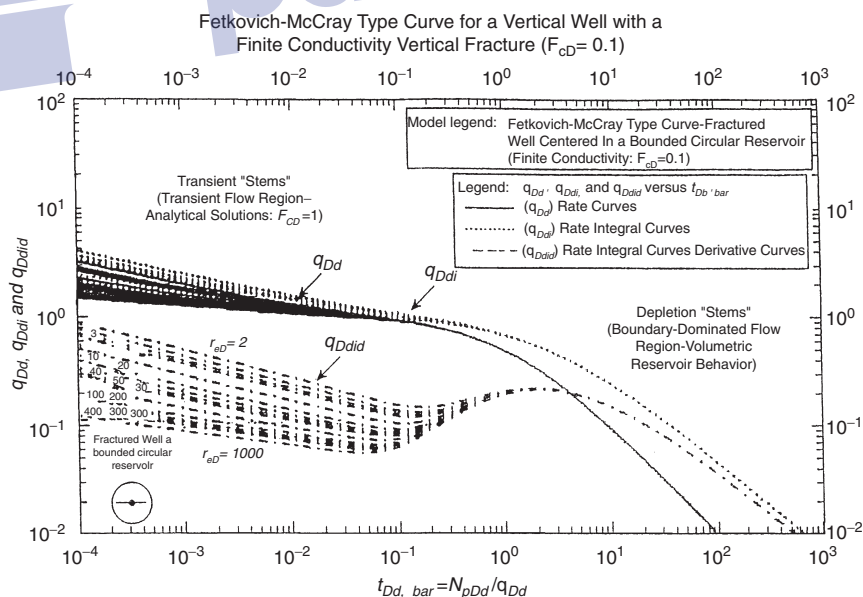


Figure 16-28. Fetkovich-McCray decline type curve-rate versus material balance time format for a well with a finite conductivity vertical fracture ($F_{cD}=0.1$). (Permission to copy by the SPE, 2003.)

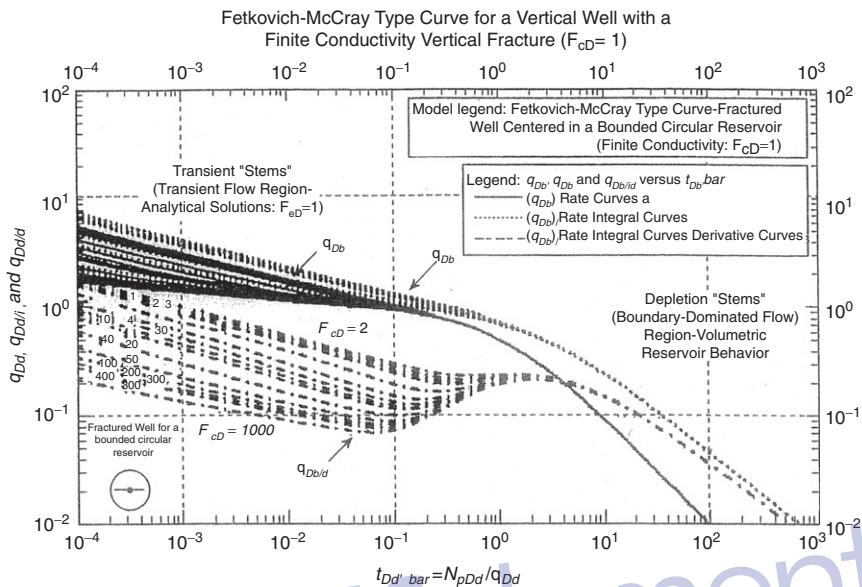


Figure 16-29. Fetkovich-McCray decline type curve–rate versus material balance time format for a well with a finite conductivity vertical fracture ($F_{cD}=1$). (Permission to copy by the SPE, 2003.)

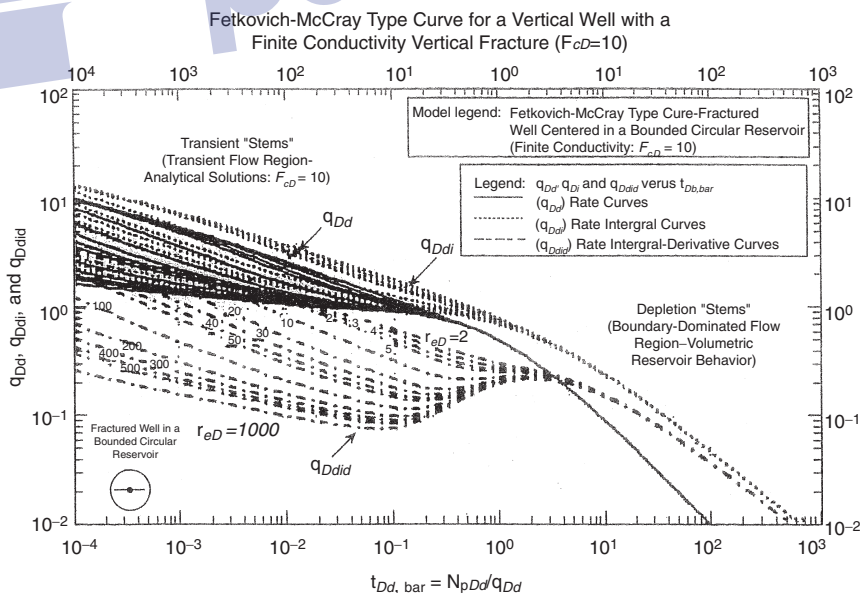


Figure 16-30. Fetkovich-McCray decline type curve–rate versus material balance time format for a well with a finite conductivity vertical fracture ($F_{cD}=10$). (Permission to copy by the SPE, 2003.)

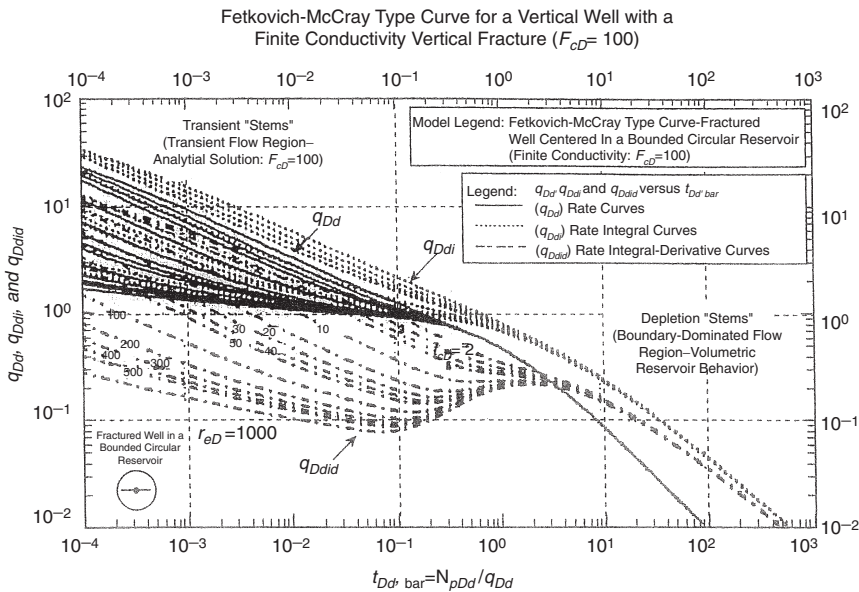


Figure 16-31. Fetkovich-McCray decline type curve-rate versus material balance time format for a well with a finite conductivity vertical fracture ($F_{cD}=100$). (Permission to copy by the SPE, 2003.)

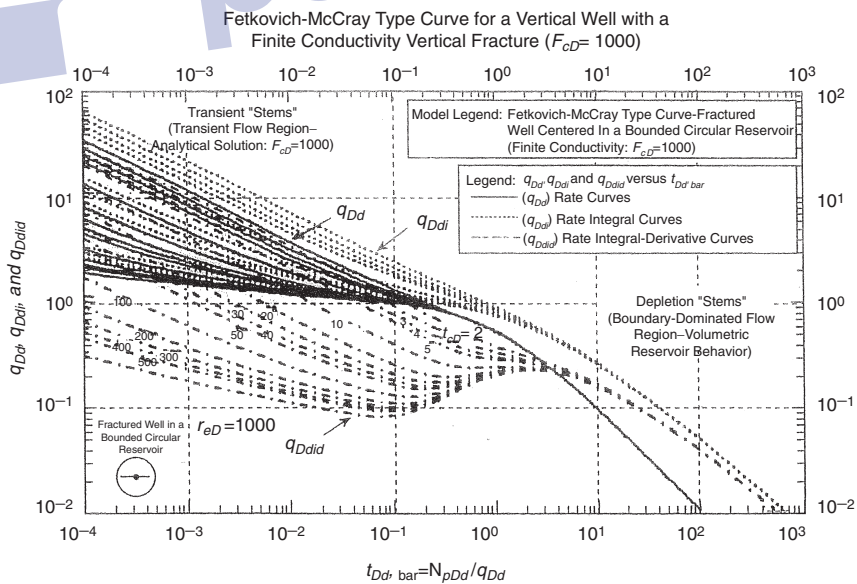


Figure 16-32. Fetkovich-McCray decline type curve-rate versus material balance time format for a well with a finite conductivity vertical fracture ($F_{cD}=1000$). (Permission to copy by the SPE, 2003.)

Step 1. Calculate the dimensionless fracture conductivity, F_{CD} , and the fracture half-length, x_f .

Step 2. Assemble the available well data in terms of bottom-hole pressure and the flow rate, q_t (in STB/day for oil or Mscf/day for gas) as a function of time. Calculate the **material balance pseudotime**, t_a , for each given data point by using the following equations:

- For oil: $t_a = \frac{N_p}{q_t}$
- For gas: $t_a = \frac{(\mu_g c_g)_i}{q_t} \frac{Z_i G}{2p_i} [\bar{m}(p_i) - \bar{m}(p)]$

where $\bar{m}(p_i)$ and $\bar{m}(p)$ are the normalized pseudo-pressures, as defined by Equations 16-84 and 16-85:

$$\bar{m}(p_i) = \frac{\mu_{gi} Z_i}{p_i} \int_0^{p_i} \left[\frac{p}{\mu_g Z} \right] dp$$

$$\bar{m}(p) = \frac{\mu_{gi} Z_i}{p_i} \int_0^p \left[\frac{p}{\mu_g Z} \right] dp$$

Notice that the GOIP must be calculated iteratively, as illustrated previously by Palacio and Blasingame (1993).

Step 3. Using the well-production data tabulated and plotted in Step 2, compute the following three complementary plotting functions:

- Pressure drop normalized rate, q_{Dd}
- Pressure drop normalized rate integral function, $(q_{Dd})_i$
- Pressure drop normalized rate integral–derivative function, $(q_{Dd})_{id}$

For gas:

$$q_{Dd} = \frac{q_g}{\bar{m}(p_i) - \bar{m}(p_{wf})}$$

$$(q_{Dd})_i = \frac{1}{t_a} \int_0^{t_a} \left(\frac{q_g}{\bar{m}(p_i) - \bar{m}(p_{wf})} \right) dt_a$$

$$(q_{Dd})_{id} = \left(\frac{-1}{t_a}\right) \frac{d}{dt_a} \left[\frac{1}{t_a} \int_0^{t_a} \left(\frac{q_g}{\bar{m}(p_i) - \bar{m}(p_{wf})} \right) dt_a \right]$$

- For oil:

$$q_{Dd} = \frac{q_o}{p_i - p_{wf}}$$

$$(q_{Dd})_i = \frac{1}{t_a} \int_0^{t_a} \left(\frac{q_o}{p_i - p_{wf}} \right) dt_a$$

$$(q_{Dd})_{id} = \left(\frac{-1}{t_a}\right) \frac{d}{dt_a} \left[\frac{1}{t_a} \int_0^{t_a} \left(\frac{q_o}{p_i - p_{wf}} \right) dt_a \right]$$

Step 4. Plot the three gas or oil functions, q_{Dd} , $(q_{Dd})_i$, and $(q_{Dd})_{id}$, versus t_a on a tracing paper so that it can be laid over the type curve with the appropriate value of F_{CD} .

Step 5. Establish a match point for each of the three functions (q_{Dd} , $(q_{Dd})_i$, and $(q_{Dd})_{id}$). Once a match is obtained, record the time and rate match points as well as the dimensionless radius value, r_{eD} :

- a) Rate-axis match point Any $(q/\Delta p)_{MP} - (q_{Dd})_{MP}$ pair
- b) Time-axis match point Any $(t)_{MP} - (t_{Dd})_{MP}$ pair
- c) Transient flow stem Select the $(q/\Delta p)$, $(q/\Delta p)_i$

and $(q/\Delta p)_{id}$ functions that best match the transient data stem and record r_{eD} .

Step 6. Solve for b_{Dpss} by using the values of F_{CD} and r_{eD} :

$$u = \ln(F_{CD})$$

$$b_{Dpss} = \ln(r_{eD}) - 0.049298 + \frac{0.43464}{r_{eD}^2} + \frac{a_1 + a_2 u + a_3 u^2 + a_4 u^3 + a_5 u^4}{1 + b_1 u + b_2 u^2 + b_3 u^3 + b_4 u^4}$$

Step 7. Using the results of the match point, estimate the following reservoir properties:

• For gas:
$$G = \frac{1}{c_{ti}} \left[\frac{t_a}{t_{Dd}} \right]_{mp} \left[\frac{(q_g / \Delta m(\bar{p}))}{q_{Dd}} \right]_{mp}$$

$$k_g = \frac{141.2 B_{gi} \mu_{gi}}{h} \left[\frac{(q_g / \Delta m(\bar{p}))_{MP}}{(q_{Dd})_{MP}} \right] b_{Dpss}$$

$$A = \frac{5.615 G B_{gi}}{h \phi (1 - S_{wi})}$$

$$r_c = \sqrt{\frac{A}{\pi}}$$

• For oil:
$$N = \frac{1}{c_t} \left[\frac{t_a}{t_{Dd}} \right]_{mp} \left[\frac{(q_o / \Delta p)_i}{q_{Dd}} \right]_{mp}$$

$$k_o = \frac{141.2 B_{oi} \mu_{goi}}{h} \left[\frac{(q_o / \Delta p)_{MP}}{(q_{Dd})_{MP}} \right] b_{Dpss}$$

$$A = \frac{5.615 N B_{oi}}{h \phi (1 - S_{wi})}$$

$$r_c = \sqrt{\frac{A}{\pi}}$$

where G = gas-in-place, Mscf

N = oil-in-place, STB

B_{gi} = gas formation volume factor at p_i , bbl/Mscf

A = drainage area, ft²

r_c = drainage radius, ft

S_{wi} = connate-water saturation

Step 8. Calculate the fracture half-length, x_f , and compare with Step 1:

$$x_f = \frac{r_c}{r_{eD}}$$

Example 16-11

A Texas field vertical gas well has been hydraulically fractured and is undergoing depletion. A summary of the reservoir and fluid properties is as follows:

$$\begin{aligned} r_w &= 0.333 \text{ ft} \\ h &= 170 \text{ ft} \\ \phi &= 0.088 \\ T &= 300^\circ\text{F} \\ \gamma_g &= 0.70 \\ B_{gi} &= 0.5498 \text{ bbl/Mscf} \\ \mu_{gi} &= 0.0361 \text{ cp} \\ c_{ti} &= 5.1032 \cdot 10^{-5} \text{ psi}^{-1} \\ p_i &= 9330 \text{ psia} \\ p_{wf} &= 710 \text{ psia} \\ S_{wi} &= 0.131 \\ F_{CD} &= 5.0 \end{aligned}$$

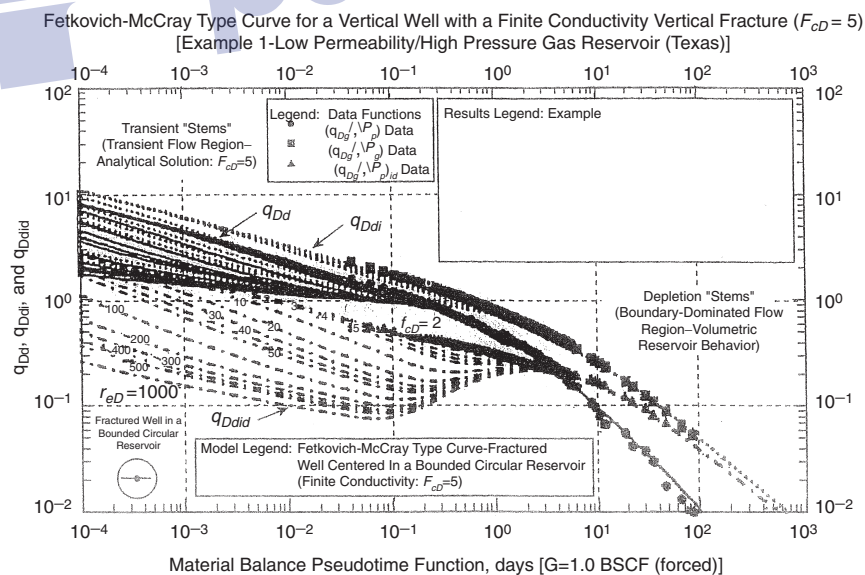


Figure 16-33. Match of production data for Example 1 on the Fetkovich-McCray decline type curve (pseudo-pressure drop normalized rate versus material balance time format) for a well with a finite conductivity vertical fracture ($F_{CD}=5$). (Permission to copy the SPE, 2003.)

Figure 16-33 shows the type-curve match for $F_{CD} = 5$, with the matching points:

$$\begin{aligned}(q_{Dd})_{mp} &= 1.0 \\ [(q_g/\Delta m(\bar{p}))]_{mp} &= 0.89 \text{ Mscf/psi} \\ (t_{Dd})_{mp} &= 1.0 \\ (t_a)_{mp} &= 58 \text{ days} \\ (r_{eD})_{mp} &= 2.0\end{aligned}$$

Perform type-curve analysis on this gas well.

Solution

Step 1. Solve for b_{Dpss} by using the values of F_{CD} and r_{eD} :

$$u = \ln(F_{CD}) = \ln(5) = 1.60944$$

$$b_{Dpss} = \ln(r_{eD}) - 0.049298 + \frac{0.43464}{r_{eD}^2} + \frac{a_1 + a_2 u + a_3 u^2 + a_4 u^3 + a_5 u^4}{1 + b_1 u + b_2 u^2 + b_3 u^3 + b_4 u^4}$$

$$b_{Dpss} = \ln(2) - 0.049298 + \frac{0.43464}{2^2} + \frac{a_1 + a_2 u + a_3 u^2 + a_4 u^3 + a_5 u^4}{1 + b_1 u + b_2 u^2 + b_3 u^3 + b_4 u^4} = 1.0022$$

Step 2. Using the results of the match point, estimate the following reservoir properties:

$$G = \frac{1}{c_{ti}} \left[\frac{t_a}{t_{Dd}} \right]_{mp} \left[\frac{(q_g/\Delta m(\bar{p}))}{q_{Dd}} \right]_{mp}$$

$$G = \frac{1}{5.1032 \times 10^{-5}} \left[\frac{58}{1.0} \right]_{mp} \left[\frac{0.89}{1.} \right]_{mp} = 1.012 \times 10^6 \text{ MMscf}$$

$$k_g = \frac{141.2 B_{gi} \mu_{gi}}{h} \left[\frac{(q_g/\Delta m(\bar{p}))_{MP}}{(q_{Dd})_{MP}} \right] b_{Dpss}$$

$$k_g = \frac{141.2(0.5498)(0.0361)}{170} \left[\frac{0.89}{1.0} \right] 1.00222 = 0.015 \text{ md}$$

$$A = \frac{5.615 \text{ GB}_{gi}}{h\phi(1 - S_{wi})}$$

$$A = \frac{5.615 (1.012 \times 10^6)(0.5498)}{(170)(0.088)(1 - 0.131)} = 240,195 \text{ ft}^2 = 5.51 \text{ acres}$$

$$r_c = \sqrt{\frac{A}{\pi}} = \sqrt{\frac{2401195}{\pi}} = 277 \text{ ft}$$

Step 3. Calculate the fracture half-length, x_f , and compare with Step 1:

$$x_f = \frac{r_c}{r_{eD}} = \frac{277}{2} = 138 \text{ ft}$$

PROBLEMS

1. A gas well has the following production history:

| Date | Time, months | q_t , MMscf/month |
|-----------|--------------|---------------------|
| 1/1/2000 | 0 | 1017 |
| 2/1/2000 | 1 | 978 |
| 3/1/2000 | 2 | 941 |
| 4/1/2000 | 3 | 905 |
| 5/1/2000 | 4 | 874 |
| 6/1/2000 | 5 | 839 |
| 7/1/2000 | 6 | 809 |
| 8/1/2000 | 7 | 778 |
| 9/1/2000 | 8 | 747 |
| 10/1/2000 | 9 | 722 |
| 11/1/2000 | 10 | 691 |
| 12/1/2000 | 11 | 667 |
| 1/1/2001 | 12 | 641 |

- a) Use the first six months of the production history data to determine the coefficient of the decline-curve equation.
 - b) Predict flow rates and cumulative gas production from August 1, 2000 through January 1, 2001.
 - c) Assuming that the economic limit is 20 MMscf/month, estimate the time to reach the economic limit and the corresponding cumulative gas production.
2. The volumetric calculations on a gas well show that the ultimate recoverable reserves, G_{pa} , are 18 MMMscf of gas. By analogy with other wells in the area, the following data are assigned to the well:
- Exponential decline
 - Allowable (restricted) production rate = 425 MMscf/month
 - Economic limit = 20 MMscf/month
 - Nominal decline rate = 0.034 month^{-1}

Calculate the yearly production performance of the well.

3. The following data are available on a gas well's production:

$$p_i = 4100 \text{ psia}$$

$$\phi = 0.10$$

$$p_{wf} = 400 \text{ psi}$$

$$S_{wi} = 0.30$$

$$T = 600^\circ\text{R}$$

$$\gamma_g = 0.65$$

$$h = 40 \text{ ft}$$

| Time, days | q_t , MMscf/day |
|------------|-------------------|
| 0.7874 | 5.146 |
| 6.324 | 2.108 |
| 12.71 | 1.6306 |
| 25.358 | 1.2958 |
| 50.778 | 1.054 |
| 101.556 | 0.8742 |
| 248 | 0.6634 |
| 496 | 0.49042 |
| 992 | 0.30566 |
| 1240 | 0.24924 |
| 1860 | 0.15996 |
| 3100 | 0.07874 |
| 6200 | 0.02232 |

Calculate the GOIP and the drainage area.

REFERENCES

1. Agarwal, R. G., Gardner, D. C., Kleinsteiber, S. W., and Fussell, D. D., "Analyzing Well Production Data Using Combined Type Curve and Decline Curve Analysis Concepts," SPE 49222, SPE Annual Technical Conference and Exhibition, New Orleans, LA, September 1998.
2. Agarwal, R. G., Al-Hussainy, R., and Ramey, H. J. (1970). An Investigation of Wellbore Storage and Skin Effect t in Unsteady Liquid Flow. *SPE J.* September 1970, pp. 279–290.
3. Anash, J., Blasingame, T. A., and Knowles, R. S., "A Semi-Analytic (p/z) Rate–Time Relation for the Analysis and Prediction of Gas Well Performance" (see reference 3), *SPE Reservoir Eval. & Eng.* 3(6), December 2000.
4. Anash, J., Blasingame, T. A., and Knowles, R. S., "A Semi-Analytic (p/z) Rate–Time Relation for the Analysis and Prediction of Gas Well Performance," SPE 35268, SPE Mid-Continent Gas Symposium, Amarillo, TX, April 1996.
5. Arps, J. J., "Analysis of Decline Curves," *Trans. AIME.*, 1945. Volume 160, pp. 228–231.
6. Begland, T., and Whitehead, W., "Depletion Performance of Volumetric High-Pressured Gas Reservoirs," *SPE Reservoir Engineering*, August 1989, pp. 279–282.
7. Blasingame, T. A., and Lee, W. J., "Variable-Rate Reservoir Limits Testing," SPE 15028, SPE Permian Basin Oil & Gas Recovery Conference, Midland, TX, March 1986.
8. Blasingame, T. A., and Lee, W. J., "The Variable-Rate Reservoir Limits Testing of Gas Wells," SPE 17708, SPE Gas Technology Symposium, Dallas, TX, June 1988.
9. Blasingame, T. A., McCray, T. L., and Lee, W. J., "Decline Curve Analysis for Variable Pressure Drop/Variable Flowrate Systems," SPE 21513, SPE Gas Technology Symposium, Houston, TX, January 1991.
10. Carter, R., "Type Curves for Finite Radial and Linear Flow System", *SPE J.* October 1985, pp. 719–728.
11. Chen, H.-Y., and Teufel, L. W., "Estimating Gas Decline Exponent before Decline Curve Analysis," SPE 75693, SPE Gas Technology Symposium, Calgary, Alberta, Canada, April 2002.
12. Chen, H.-Y., and Teufel, L. W., "A New Rate–Time Type Curve for Analysis of Tight-Gas Linear and Radial Flows," SPE 63094, 2000 SPE Annual Technical Conference & Exhibition, Dallas, TX, October 2000.

13. Cox, S. A., Gilbert, J. V., Sutton, R. P., and Stoltz, R. P., "Reserve Analysis for Tight Gas," SPE 78695, Eastern Regional Meeting, Lexington, KY, October 2002.
14. Doublet, L. E., Blasingame, T. A., Pande, P. K., and McCollum, T. J., "Decline Curve Analysis Using Type Curves—Analysis of Oil Well Production Data Using Material Balance Time: Application to Field Cases," SPE 28688, 1994 Petroleum Conference & Exhibition of Mexico, Veracruz, Mexico, October 1994.
15. Earlougher, R. C., Jr., "Advances in Well Test Analysis." SPE of AIME 5, 1977. In *Theory and Practice of the Testing of Gas Wells*, 3 ed. Calgary: Energy Resources Conservation Board, 1975.
16. Engler, T. W., "A New Approach to Gas Material Balance in Tight Gas Reservoirs," SPE 62883, 2000 APE Annual Tech Conference and Exhibition, Dallas, TX, October 2000.
17. Fetkovich, M. J., "Multipoint Testing of Gas Wells," SPE Mid-Continent Section Continuing Education Course of Well Test Analysis, March 17, 1975.
18. Fetkovich, M. J., "Decline Curve Analysis Using Type Curves," SPE 4629, *SPE Journal*, June 1980.
19. Fetkovich, M. J., Vienot, M. E., Johnson, R. D., and Bowman, B. A., "Case Study of a Low-Permeability Volatile Oil Field Using Individual-Well Advanced Decline Curve Analysis," SPE 14237, SPE 60th Annual Tech Conference & Exhibition, Las Vegas, NV, September 1985.
20. Fetkovich, E. J., Fetkovich, M. J., and Fetkovich, M. D., "Useful Concepts for Decline Curve Forecasting, Reserve Estimation, and Analysis," SPE Reservoir Engineering, February 1996.
21. Fetkovich, M. J., Vienot, M. E., Bradley, M. D., and Kiesow, U. G., "Decline Curve Analysis Using Type Curves: Case Histories," SPE 13169, *SPE Formation Evaluation*, December 1987.
22. Fetkovich, M. D., Fetkovich, M. J., Thomas, L. K., and Guerrero, E. T., "Oil and Gas Relative Permeabilities Determined from Rate-Time Performance Data," SPE 15431, SPE 61st Annual Tech Conference & Exhibition, New Orleans, LA, October 1985.
23. Gentry, R. W. "Decline Curve Analysis," *JPT*, January 1972, pp. 38–42.
24. Ikoku, C., *Natural Gas Reservoir Engineering*. John Wiley & Sons, Inc., 1984.
25. Jemert, T. A., "Theory and Application of Polynomial Type Curves," SPE 25876, SPE Rocky Mountain Regional/Low Permeability Reservoirs Symposium, Denver, CO, April 1993.

26. Lee, J., "Well Testing," Society of Petroleum Engineers of AIME, Dallas, TX, 1982.
27. Lord, M. E., and Collins, R. E., "Detecting Compartmented Gas Reservoirs Through Production Performance," SPE 22941, SPE 66th Annual Technical Conference & Exhibition, Dallas, TX, October 1991.
28. McCain, W. D., Voneiff, G. W., Semmelbeck, M. E., and Hunt, E. R., "A Tight Gas Field Study: Carthage (Cotton Valley) Field," SPE 26141, SPE Gas Technology Symposium, Calgary, Alberta, Canada, June 1993.
29. Palacio, C., and Blasingame, T., "Decline-Curve Analysis Using Type-Curve," SPE Paper 25909, Presented at the 1993 SPE Rocky Mountain Regional Meeting, Denver, CO, April 26–28, 1993.
30. Pratikno, H., Rushing, J., and Blasingame, T. A., "Decline Curve Analysis Using Type Curves: Fractured Wells," SPE 84287, SPE Annual Technical Conference, Denver, CO, October 2003.
31. Spivey, J. P., Gatens, J. M., Semmelbeck, M. E., and Lee, W. J., "Integral Type Curves for Advanced Decline Curve Analysis," SPE 24301, SPE Mid-Continent Gas Symposium, Amarillo, TX, April 1992.
32. van Everdingen, A. F., and Hurst, W., "Application of Laplace Transform to Flow Problems in Reservoirs," *Trans. AIME* 186, 1949, pp. 305–324B.
33. Marhaendrajana, T., and Blasingame, T. A., "Decline Curve Analysis Using Type Curves: Evaluation of Well Performance Behavior in a Multiwell Reservoir System," SPE 71517, 2001 SPE Annual Technical Conference & Exhibition, New Orleans, LA, September 2001.
34. Valko, P. P., Doublet, L. E., and Blasingame, T. A., "Development and Application of the Multiwell Productivity Index (MPI)," *SPE Journal* 5(1), March 2000.

C H A P T E R 17

FRACTURED RESERVOIRS

A fundamental property of a reservoir rock is porosity. However, to be an effective reservoir rock, another fundamental property is permeability. Both porosity and permeability are geometric properties of a rock, and both are the result of the rock's lithologic (composition) character. The physical composition and textural properties (geometric properties such as the sizes and shapes of the constituent grains, the process of their packing) of a rock are what is important when discussing reservoir rocks, and not so much the age of the rock. In an excellent paper by Shanley et al. (2004), the authors presented a comprehensive overview of low-permeability gas reservoirs and the underlying petrophysical concepts, and offered additional insights based on their research work. They reiterated the well-known fact that in low-permeability reservoirs, the impact of partial brine saturation and overburden stress on reservoir performance is significant. In low-permeability gas reservoirs, it is not unusual for the effective permeability to gas to be one to three orders of magnitude less than routine permeability. Similarly, effective permeability to brine is such that for many low-permeability reservoirs, water is essentially immobile even at high water saturations. The relative permeability behavior of tight gas reservoirs is characterized by redefining the traditional concepts of critical water saturation S_{wc} (the water saturation at which water ceases to flow), critical gas saturation S_{gc} (the gas saturation at which gas begins to flow), and irreducible water saturation S_{wirr} (the water saturation at which a further increase in capillary pressure produces no additional decrease in water saturation). Figure 17-1 is a schematic illustration of the

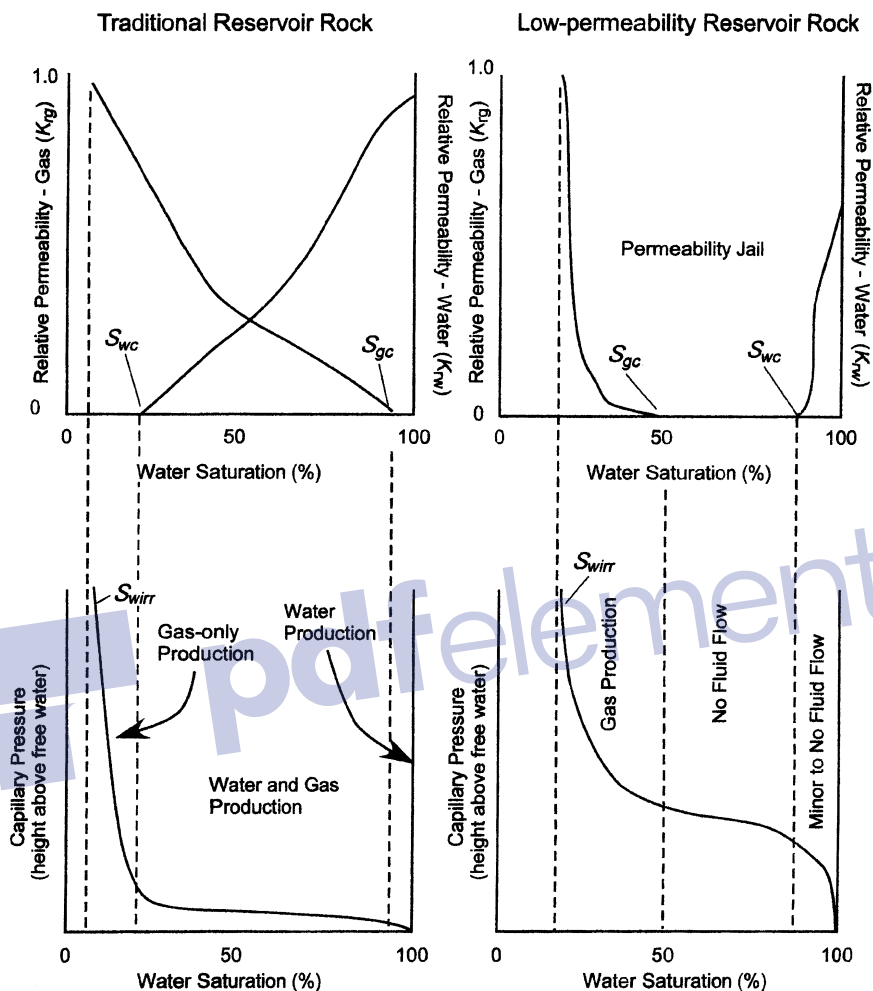


Figure 17-1. Concept of permeability jail.

relationship between capillary pressure and relative permeability in traditional and tight gas reservoirs.

The illustration indicates that in traditional reservoirs, irreducible and critical water saturations are similar. In tight gas reservoirs, however, irreducible and critical water saturations can be significantly different. In traditional reservoirs, there is a wide range of water saturations at which both water and gas can flow. On the other hand, in low-permeability reservoirs, there is a broad range of water saturations at which neither gas nor water

can flow. In some low-permeability reservoirs, there is virtually no mobile water phase even at high water saturations. Shanley et al. (2004) use the term *permeability jail* to describe the saturation region across which there is negligible effective permeability to either water or gas. Failure to fully understand these relationships and associated concepts has led to widespread misunderstanding of how hydrocarbon systems are manifested in low-permeability reservoirs.

This chapter reviews the basic principles of two types of production systems:

- Naturally fractured reservoirs
- Hydraulically fractured wells

NATURALLY FRACTURED RESERVOIRS

Naturally fractured reservoirs represent more than 50% of reservoirs and contribute in a large extent to the worldwide production of oil and gas. These highly heterogeneous reservoirs possess a complex network of several fracture families with different spatial distribution and conductivity. Performing a reservoir characterization study on these naturally fractured systems is a challenging task because they present an extreme property contrast between the two domains it comprises: rock matrix and fractures.

Naturally fractured reservoirs are found in many depositional environments, including:

- Carbonates
- Shales
- Sandstones

The above three sedimentary rocks are so common in reservoirs that it is convenient to think of all sedimentary rocks as being composed of carbonates, shales, and sandstones. Figure 17-2 shows the lithologic relationship of these common rock materials. The nomenclature used is common to hydrocarbon fields and indicates the gradation from one type of rock to another.

A brief description of the above listed fractured systems is given below.

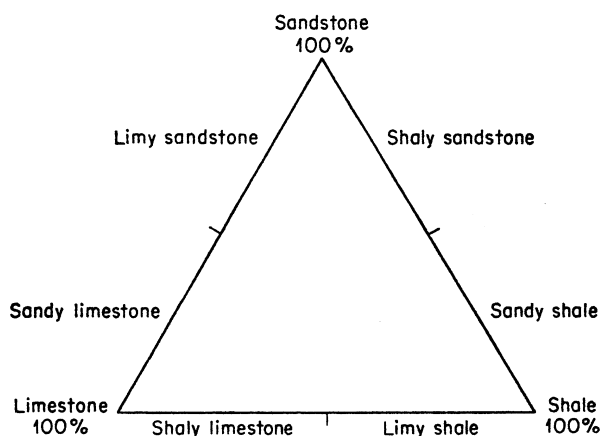


Figure 17-2. Three-component diagram of sedimentary rock constituents.

1. Fractured carbonates

A significant percentage of oil and gas reserves (more than 60% of the world's proven oil reserves and 40% of the world's gas reserves) are trapped in fractured carbonate reservoirs. Although increasing oil and gas production from carbonate reservoirs may not be the only solution to meeting current energy demand, it is clear that these reservoirs will play an increasingly important role in the future of the petroleum industry.

Carbonate reservoirs represent a broader range of producibility than do the more common sandstone reservoirs. The most prolific and sustained production rates come from carbonate reservoirs. But carbonate reservoirs can also be at the other extreme in terms of hydrocarbon production. Many carbonate reservoirs will not yield oil and gas at all unless they are artificially fractured. These reservoirs, because of their complexity and heterogeneity, are considered extremely challenging in terms of accurate recovery prediction. Most carbonate reservoirs are naturally fractured and contain fractures that can range from isolated microscopic fissures to kilometer-wide collections called *fracture swarms* or *corridors*. These fractures create complex paths for fluid movement, which impact reservoir characterization and, ultimately, production performance and total recovery. Fracture corridors consist of thousands of parallel fractures densely packed together to form a volume that typically is a few meters wide, a few tens of meters high, and several hundred meters long. Fracture corridors act as highways for fluid in the reservoir, and knowledge of

their exact position is essential to producing reliable results from reservoir simulation studies on these types of systems.

There are several important factors to note when considering fractures in carbonated reservoirs:

- They typically strike and dip in the same direction.
- Their productivity is related to their density, opening, and connectivity.
- They vary in size, both horizontally and vertically.

Carbonates are limestones, dolomites, and other carbonate rock materials that derive by precipitation. Limestones are typically extensive and massive. A pure limestone or dolomite rarely occurs because of the presence of varying amounts of detrital material.

Carbonate reservoir rocks can be divided into the following lithologic types:

- Oolitic limestone
- Limestone
- Chalk
- Dolomitic limestone
- Dolomite
- Cherty limestone and dolomite

The physical properties of oolitic limestone are largely determined by the depositional environment. The remaining carbonate rocks are largely finely crystalline, and their physical properties depend greatly on such processes as deformation and solution after deposition. A limestone has little resistance to tension, and when it is subjected to tension forces, fractures develop. The subsequent development of fractures allows subsurface water to percolate through these fractures and consequently subject the carbonate material to the processes of secondary solution and deposition.

An example of a carbonate reservoir is the Selma fractured chalk in Gilberttown oil field, Alabama. Figure 17-3 shows a schematic cross section of Gilberttown field. Aguilera (1987) indicated that no matrix porosity was found in the chalk and that fracture porosity was associated with the fault zone. The fracture porosity provided a secondary trap for oil that migrated from lower Eutaw sands. Production from the Selma chalk comes only from wells located in the down-thrown side near the fault.

As shown in Figure 17-3, the dry well encountered a complete section of the Selma chalk but was far from the fault and consequently did not

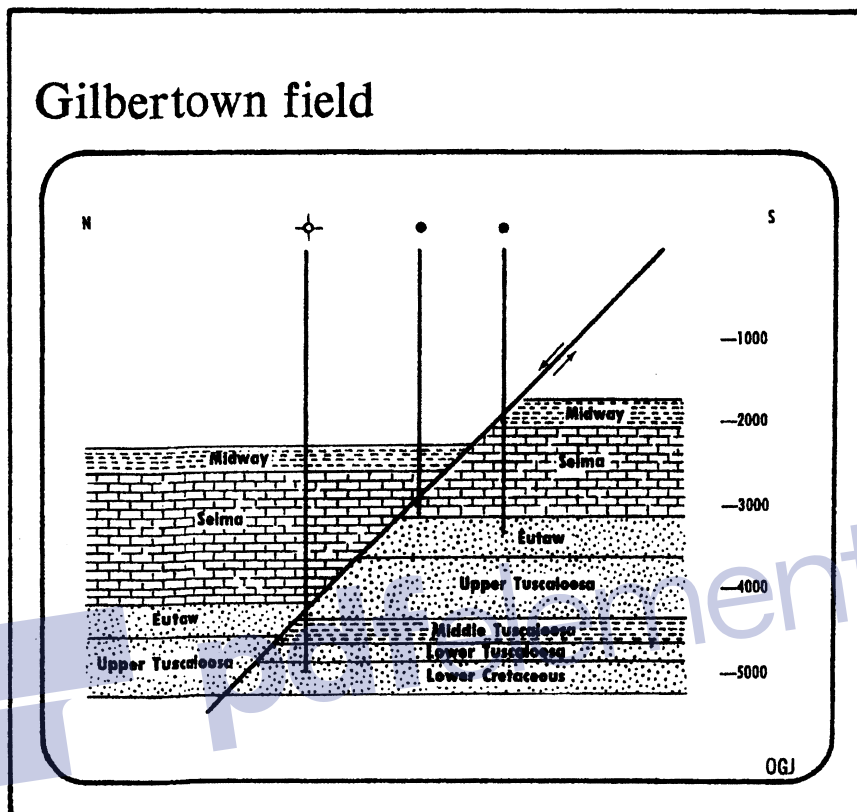


Figure 17-3. Diagrammatic north-south section across Gilberttown field. (After Braunstein, J. "Fracture Controlled Production in Gilberttown Field," *Bulletin, AAPG*, Feb 1953.)

penetrate any fracture. The middle well near the fault produced oil from the fracture Selma chalk. Finally, the well to the right of the fault produced oil from Eutaw sands, but not from the Selma chalk.

Another example of these complex types of reservoirs is the Tamulipas limestone in Mexico. The oil field has produced oil of 12.5°API at rates as high as 30,000 STB/day from a single well. The fracture permeability varies considerably to the extent that wells only 200 ft apart from a producing well are dry.

The Ain Zalah carbonate oil reservoir in Iraq is extremely tight and has very low porosity. However, because of the presence of fractures, the reservoir can produce at high rates during limited periods. It is postulated that hydrocarbon fluid entered the reservoir by upward migration along fractures from a deeper zone, perhaps in the middle of the Cretaceous or

during the Jurassic period. Because the formation had a high degree of fracturing, it was proposed that the pay zones could be drained by two to three wells.

The Kirkuk oil field in Iraq is another interesting example of carbonate reservoirs. The field is classified as a limestone system with a higher than average porosity and varied permeability, which depends on stratigraphy. The fractures at this 61-mi structure are so close that only a few wells located at the base of the highest dome would be enough to drain the entire reservoir with a spacing of approximately 1,280 acres.

2. Fractured shales

Fractured shales have produced gas since the early 1900s along the western margin of the Appalachian Basin. Shale, which consists mainly of consolidated clay-sized particles, is the earth's most common sedimentary rock. Shale looks like the slate of a chalkboard and generally has ultra-low permeability. In oil fields, shale forms the geological seal that retains the oil and gas within producing reservoirs, preventing hydrocarbons from escaping to the surface. In a handful of basins, however, layers of shale, sometimes hundreds of feet thick and covering millions of acres, are both the source and the reservoir for natural gas. These shales have one thing in common: they are rich in organic carbon.

Typically, the methane in organic shales was created in the rock itself over millions of years. This thermogenic gas forms when organic matter left in the rock breaks down under rising temperature. The gas that is generated is then adsorbed onto the organic materials expelled through leaks in the shale, or captured within pores of the shale. In some cases, however, an influx of water and the presence of bacteria will support the generation of biogenic gas.

Although it is difficult to extract, most shale gas is fairly clean and dry. That is because over time, there has been enough heat in the reservoir rock to break down any liquid hydrocarbons. The relative amounts of oil and gas contained in shales are one indication of how much heat has been in the reservoir, and for how long. Thermally mature shales have had enough heat and pressure to produce hydrocarbons. The most thermally mature shales will contain only dry gas. Less mature shales will have wetter gas, and the least thermally mature shales may contain only oil.

In rare cases, the produced methane may have small percentages of carbon dioxide, nitrogen, ethane, and even propane. Carbon dioxide is more commonly found in biogenic gas shales.

Shale gas reservoirs in the United States tend to be found within three depth ranges between 250 and 8,000 ft. The New Albany and Antrim shales, for example, have some 9,000 wells in the range of 250 to 2,000 ft. In the Appalachian Basin shales and the Devonian and Lewis shales, there are about 20,000 wells from 3,000 to 5,000 ft. Although the Barnett and Woodford shales are much deeper, the Caney and Fayetteville shales are from 2,000 to 6,000 ft, with most of the reservoirs between 2,500 and 4,500 ft. A good shale gas prospect has a shale thickness of between 300 and 600 ft.

Shale has such low permeability that it releases gas very slowly, which is why shale is the last major source of nature gas to be developed. The good news is that shale can hold an enormous amount of nature gas. The most prolific shales are relatively flat, thick, and predictable, and the formations are so large that their wells will continue producing gas at a steady rate for decades.

It should be pointed out that the pore spaces in organic shales are not large enough for even methane molecules to flow through easily. However, the rock may contain natural fractures caused by pressure from the overlying rock and natural movement of the earth's crust. Stress loads in the reservoir determine the geometry of the fractures, which are often concentrated in fracture swarms. The gas release is accomplished in the following step-by-step fashion:

- as free gas in the fractures, then
- as adsorbed gas stripped from its adhesion to fracture surfaces, and, finally,
- as adsorbed gas bleeding out of the shale matrix.

The free gas flushes quickly at a high rate, but adsorbed gas is produced slowly in low volumes. Adsorbed gas trickles out at a very steady but extremely slow rate.

Shale oil is another type that is characterized as a fine-grained rock that contains varying amounts of solid organic materials called *kerogen*. When heated to nearly 900°F, the kerogen decomposes into hydrocarbons and carbonaceous residues. The cooled hydrocarbons condense into liquid called *shale oil*. This can be refined into useable fuel. In fact, there was a highly active shale oil industry in the eastern states before Drake's discovery well in Pennsylvania.

Almost two trillion barrels of oil are trapped in shale formations in a 16,000-mi² area that extends into Colorado, Utah, and Wyoming.

Essentially, there are two basic processes for extracting the oil:

- Shale is mined and heated in retorts located above ground to extract the oil.
- After using explosives to create a huge underground cavern of shale rubbles, the shale is heated underground and the oil is pumped from the bottom of the cavern.

Of the various proposed technologies to produce synthetic fuels, shale oil is among those always mentioned as being close to commercialization.

3. Fractured sandstones

The term *sand* refers to a particular grain size (62 μm –2 mm), not to a particular composition. The performance of sandstone as a reservoir rock, including its porosity and permeability, depends on the degree to which it is truly sand. Texture should reflect similar-sized grains, not a combination of coarse and fine-grained material. The best sandstone reservoirs are those that are composed primarily of quartz grains of sand size, silica cement, with minimal fragmented particles. Properties of sandstone reservoirs are assumed to be controlled by depositional environment and diagenesis during subsequent burial. However, open fractures, when present in sandstone reservoirs, can have a significant influence on reservoir flow and performance. These natural fractures not only enhance the overall porosity and permeability of these reservoirs, but also create significant permeability anisotropy, which causes the drainage area around the wells to be elliptical.

The Altamont trend, Uinta basin of Utah, is an example of a fractured sandstone reservoir. Production from this reservoir comes from fine-grained sandstones of Tertiary age and fractured rocks consisting of sandstone, carbonate, and highly calcareous shale. Initial production rates of over 1,000 STB/day are not uncommon in this reservoir, which has low porosity ($\phi \approx 3\%$ –7%) and low absolute permeability ($k < 0.01$ md).

Behavior of Naturally Fractured Reservoirs

Naturally fractured reservoirs contain a substantial amount of the known hydrocarbons worldwide. Naturally fractured reservoirs contain naturally occurring fractures with significant permeability anisotropy. The connected porous space in these reservoirs has been characterized and cat-

egorized by two types of porous media: *matrix* and *fracture*. Because of the different fluid storage and conductivity characteristics of the matrix and fractures, these reservoirs are often called *dual-porosity* reservoirs and described by the following dual-porosity systems:

- Matrix porosity, categorized as primary porosity ϕ_m
- Fracture porosity, categorized as secondary porosity ϕ_f

Primary porosity ϕ_m is established when the sediment is first deposited; thus, it inherits the original characteristic of the rock. It is highly interconnected and usually can be correlated with permeability since it is largely dependent on the geometry, size, and spatial distribution of the grains.

Secondary porosity ϕ_f , also known as induced porosity, is the result of geological processes after the deposition of sedimentary rock and has no direct relation to the form of the sedimentary particles. Most reservoirs with secondary porosity are either limestones or dolomites. In general, secondary porosity is due to solution, recrystallization, fractures, and joints. Essentially, secondary porosity by solution can be generated by percolating acid water, which dissolves mostly limestones and dolomites, thus improving their porosities. Joints or fissures, which occur in massive, extensive formations composed of shale, siltstone, limestone, or dolomite, are generally vertical. Shrinkage cracks are the result of a chemical process (dolomitization) and do not appear to have any preferred orientation.

In general, the matrix has a large bulk porosity and relatively low permeability compared with the fracture, which has a very small bulk porosity and relatively large permeability.

It should be pointed out that the fractures, without consideration of the rest of the reservoir, would have a porosity of 100%; that is, they are entirely void of rock. However, fracture porosity is defined as fracture volume divided by total volume:

$$\phi_f = \frac{\text{fracture volume}}{\text{total volume}} = \frac{V_f}{V_T}$$

Matrix porosity is also defined with respect to total volume. Therefore, matrix porosity is not the same as unfractured core porosity ϕ_{core} measured in the laboratory, that is:

$$\phi_m = \phi_{\text{core}} (1 - \phi_f)$$

Gilman and Kazemi (1983) point out that in naturally fractured systems, the fracture permeability k_f is given by:

$$k_f = \frac{k_e}{\phi_f}$$

where k_e is the effective permeability as calculated from a pressure-buildup test. Another expression that has been used to approximate fracture permeability is given by Poiseuille's law as:

$$k_f = 54 \times 10^9 w_f^2$$

where k_f = fracture permeability, md
 w_f = fracture width, inches

The two expressions just given can be combined to give the correct width to be used in Poiseuille's law as:

$$w_f = \sqrt{\frac{k_e}{54 \times 10^9 \phi_f}}$$

Ramirez et al. (2007) point out that those natural fractures could enhance the ultimate recovery of a given reservoir; however, this depends on the fracture zone architecture. For instance, vertical and subvertical fractures in a reservoir with a high structural relief could enhance gas segregation to the top of the structure to promote efficient gas gravity drainage of oil. On the other hand, fractures can lead to channelization of a reservoir in low-permeability formations, which can lead to early breakthrough of water or gas in production wells. Furthermore, in naturally fractured reservoirs, fluid storativity is mainly associated with the matrix, while high conductivity is associated with the fracture network. Another important characteristic of the fractures is the extremely reduced cross-sectional area open to flow.

Matrix and fractures are connected through large contact surface areas. The mass transfer and flow interaction between these two media depend on several forces, which include fluid expansion, viscous displacement, and capillary and gravity effects. In the matrix, the inertial effects are

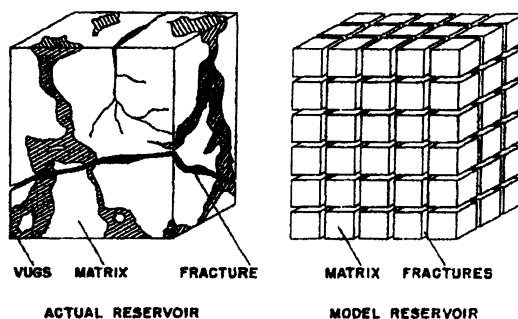


Figure 17-4. Idealization of the heterogeneous porous medium.

rather small because of low velocities, while in the fractures the inertial effects could be very significant because of high velocities. The latter can lead to significant non-Darcy flow effects, at least in the near wellbore region. Given the extreme contrast in the properties of the two media and the heterogeneous nature of the fractures, naturally fractured reservoirs have been the subject of extensive research in the petroleum engineering field.

Several reservoir idealizations of the dual-porosity reservoir systems have been introduced for modeling and describing the fluid flow in naturally fractured reservoirs. Warren and Root (1963) idealized and represented the naturally fractured dual-porosity system by a stack of rectangular blocks, as shown in Figure 17-4. Warren and Root, in developing their proposed model to describe the fluid flow in the idealized fractured system shown in Figure 17-4, employed the following assumptions:

- The rock matrix containing the primary porosity is homogeneous and isotropic, and is contained within a systematic array of identical rectangular parallelepipeds. The matrix is characterized by high storativity and low permeability. Although most of the hydrocarbon is stored in the matrix, the authors assumed that the fluid cannot flow to the well directly; however, the fluid has to enter the fractures and flow to the wellbore.
- The secondary porosity is contained within a system of continuous and uniform fractures that are oriented so that each fracture is parallel to one of the principal axes of permeability. These fractures are uniformly spaced with a constant width. However, different fracture spacing or different width may exist along each of the axes to simulate the proper degree of desired anisotropy.

It should be pointed out that the fracture network is prone to faster depletion with no change in the matrix system pressure. However, upon the establishment of a differential pressure between the matrix and the fracture system, the matrix blocks start discharging fluids to the fractures.

Warren and Root (1963) presented an extensive theoretical work on the behavior of naturally fractured reservoirs. They assume that the formation fluid flows from the matrix system into the fractures under pseudo-steady-state conditions with the fractures acting like conduits to the wellbore. Mathematically, Warren and Roots introduced the matrix–fracture transfer function Γ as defined by the following relationship:

$$\Gamma = \sigma \left(\frac{k_m}{\mu} \right) V (p_m - p_f)$$

where k_m = matrix permeability

σ = block-shape factor

μ = fluid viscosity

V = matrix rock volume

p_m = matrix pressure

p_f = fracture pressure

The shape factor σ is a geometric factor that depends on the geometry and the characteristic shape of the matrix–fissures system, and has the dimension of a reciprocal of the area and is defined by the following expression:

$$\sigma = \frac{A}{Vx}$$

where A = surface area of the matrix block, ft²

V = volume of the matrix block

x = characteristic length of the matrix block, ft

Kazemi (1969) developed a widely used expression for determining the shape factor based on finite-difference as given by:

$$\sigma = 4 \left[\frac{1}{L_x^2} + \frac{1}{L_y^2} + \frac{1}{L_z^2} \right]$$

where L_x , L_y , and L_z represent the dimensions of a matrix block.

In addition to permeability and skin, which control the behavior of double-porosity systems, Warren and Root introduced two other characteristic parameters to describe fully the fluid exchange between the matrix and fractures. These two parameters are called *storativity ratio* ω and *interporosity flow coefficient* λ and defined below:

- a. The dimensionless parameter ω defines the *storativity* of the fractures as a ratio to that of the total reservoir. Mathematically, it is given by:

$$\omega = \frac{(\phi h c_t)_f}{(\phi h c_t)_{f+m}} = \frac{(\phi h c_t)_f}{(\phi h c_t)_f + (\phi h c_t)_m} \quad (17-1)$$

where ω = storativity ratio

h = thickness

c_t = total compressibility, psi^{-1}

ϕ = porosity

The subscripts f and m refer to the fissure and matrix, respectively. A typical range of ω is 0.1 to 0.001.

- b. The second parameter λ is the *interporosity flow coefficient*, which describes the ability of the fluid to flow from the matrix into the fissures, and is defined by the following relationship:

$$\lambda = \sigma \left(\frac{k_m}{k_f} \right) r_w^2 \quad (17-2)$$

where λ = interporosity flow coefficient

k_m = matrix permeability

k_f = fracture permeability

r_w = wellbore radius

σ = block-shape factor

Most of the proposed models assume that the matrix–fissures system can be represented by one the following four block-shape factor geometries:

Cubic matrix blocks separated by fractures with λ as given by:

$$\lambda = \frac{60}{L_m^2} \left(\frac{k_m}{k_f} \right) r_w^2$$

where L_m is the length of a block side.

Spherical matrix blocks separated by fractures with λ as given by

$$\lambda = \frac{15}{r_m^2} \left(\frac{k_m}{k_f} \right) r_w^2$$

where r_m is the radius of the sphere.

Horizontal strata (rectangular slab) matrix blocks separated by fractures with λ as given by:

$$\lambda = \frac{12}{h_f^2} \left(\frac{k_m}{k_f} \right) r_w^2$$

where h_f is the thickness of an individual fracture or high permeability layer.

Vertical cylinder matrix blocks separated by fractures with λ as given by:

$$\lambda = \frac{8}{r_m^2} \left(\frac{k_m}{k_f} \right) r_w^2$$

where r_m is the radius of each cylinder.

In general, the interporosity flow parameter ranges between 10^{-3} and 10^{-9} . Cinco and Samaniego (1981) identified the following two extreme interporosity flow conditions:

Restricted interporosity flow, which corresponds to a high skin between the least permeable media (matrix) and the high permeable media (fissures), and is mathematically equivalent to the pseudosteady-state solution, i.e., the Warren and Root model.

Unrestricted interporosity flow, which corresponds to zero skin between the most and high permeable media and is described as the unsteady-state (transient) solution.

Warren and Root proposed the first identification method of the double-porosity system, as shown by the drawdown semilog plot of Figure 17-5. The curve is characterized by *two parallel straight lines* because of the two separate porosities in the reservoir. Secondary porosity (fissures), having greater transmissivity and being connected to the wellbore,

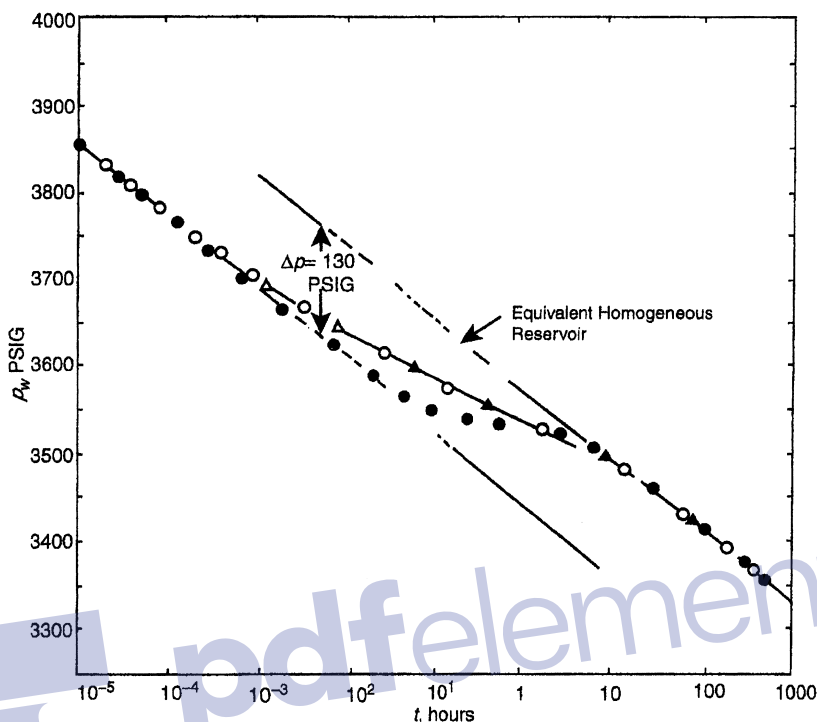


Figure 17-5. Pressure drawdown according to the model by Warren and Root. (Copyright © 1969, SPE, Kazemi, SPEJ.)

responds first as described by the first semilog straight line. Primary porosity (matrix), having a much lower transmissivity, responds much later. The combined effect of the two porosities gives rise to the second semilog straight line. The two straight lines are separated by a transition period during which pressure tends to stabilize.

The first straight line reflects the transient radial flow through the fractures, and thus *its slope is used to determine the system permeability–thickness product*. However, because the fracture storage is small, the fluid in the fractures is quickly depleted with a combined rapid pressure decline in the fractures. This pressure drop in the fracture allows more fluid to flow from the matrix into the fractures, which causes a slowdown in the pressure decline rate (as shown in Figure 17-5 by the transition period). As the matrix pressure approaches the pressure of the fractures, the pressure is stabilized in the two systems and yields the *second semilog straight line*. It should be pointed out that the first semilog straight line may be overshadowed by wellbore storage effects and might not be recognized.

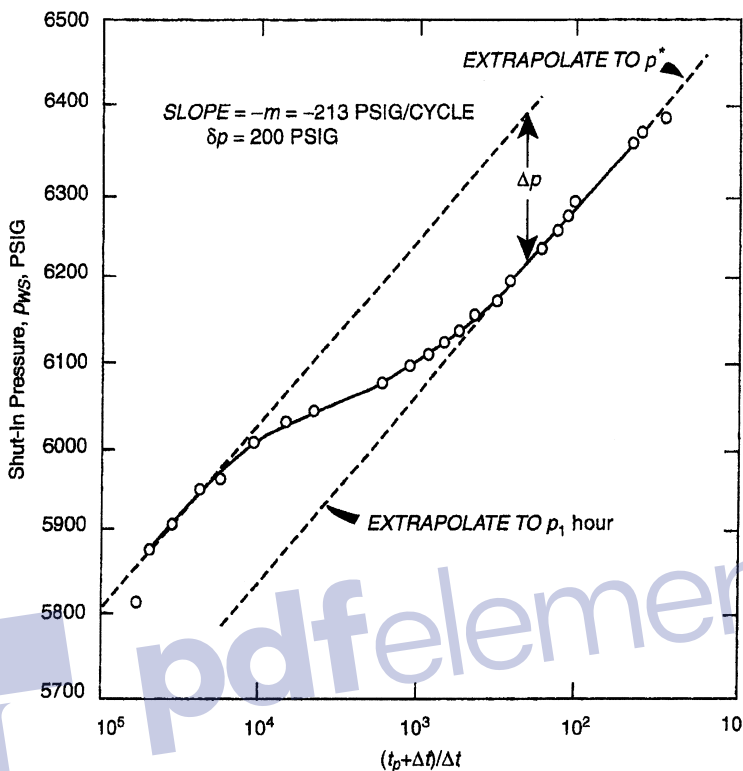


Figure 17-6. Buildup curve from a fractured reservoir. (After Warren and Root, 1963.)

Therefore, in practice, only parameters characterizing the homogeneous behavior of the *total* system $k_f h$ can be obtained.

Figure 17-6 shows the pressure-buildup data for a naturally fractured reservoir. As for the drawdown, wellbore storage effects may obscure the first semilog straight line. If both semilog straight lines develop, analysis of the total permeability–thickness product is estimated from the slope m of either straight line and the use of Equation 6-178 in Chapter 6, that is:

$$(k_f h) = \frac{162.6QB\mu}{m}$$

The skin factor s and the false pressure p^* are calculated by using the second straight line. Warren and Root indicated that the storativity ratio

ω can be determined from the vertical displacement between the two straight lines, identified as Δp in Figures 17-5 and 17-6, by the following expression:

$$\omega = 10^{(-\Delta p/m)} \quad (17-3)$$

Bourdet and Gringarten (1980) indicated that by drawing a horizontal line through the *middle* of the transition curve to intersect with both semilog straight lines, as shown in Figure 17-5 for a pressure drawdown test and Figure 17-6 for a pressure-buildup test, the interporosity flow coefficient λ can then be determined by reading the corresponding time at the *intersection* of either of the two straight lines, e.g., first-line intersection t_1 or second-line intersection t_2 , and applying the following relationships:

For drawdown tests

$$\lambda = \left[\frac{\omega}{1-\omega} \right] \left[\frac{(\phi h c_t)_m \mu r_w^2}{1.781 k_f t_1} \right] \quad (17-4)$$

or

$$\lambda = \left[\frac{\omega}{1-\omega} \right] \left[\frac{(\phi h c_t)_m \mu r_w^2}{1.781 k_f t_2} \right]$$

For buildup tests

$$\lambda = \left[\frac{\omega}{1-\omega} \right] \left[\frac{(\phi h c_t)_m \mu r_w^2}{1.781 k_f t_p} \right] \left(\frac{t_p + \Delta t}{\Delta t} \right)_1$$

or

$$\lambda = \left[\frac{1}{1-\omega} \right] \left[\frac{(\phi h c_t)_m \mu r_w^2}{1.781 k_f t_p} \right] \left(\frac{t_p + \Delta t}{\Delta t} \right)_2$$

where k_f = permeability of the fracture, md

t_p = producing time before shut-in, hours

r_w = wellbore radius, ft

μ = viscosity, cp

The subscripts 1 and 2 (e.g., t_1) refer to the first- and second-line time intersection, respectively, with the horizontal line drawn through the middle of the transition region pressure response during drawdown or buildup tests.

The above relationships indicate that the value of λ is dependent on the value of ω . Since ω is the ratio of fracture to matrix storage, as defined in terms of the *total* isothermal compressibility coefficients of the matrix and fissures by Equation 17-1, it can be expressed as:

$$\omega = \frac{1}{1 + \left[\frac{(\phi h)_m (c_t)_m}{(\phi h)_f (c_t)_f} \right]}$$

The above mathematical expression indicates that storativity ratio ω is also dependent on the PVT properties of the fluid. It is quite possible that when the oil contained in the fracture is below the bubble-point, the oil contained in the matrix is above the bubble-point. Thus, ω is pressure dependent and therefore λ is greater than 10^{-3} , the level of heterogeneity is insufficient for dual-porosity effects to be of importance and the reservoir can be treated with a single porosity.

Example 17-1

Pressure-buildup data as presented by Najurieta (1980) and Sabet (1991) for a double-porosity system are tabulated below:

| Δt (hours) | p_{ws} (psi) | $\frac{t_p + \Delta t}{\Delta t}$ |
|--------------------|----------------|-----------------------------------|
| 0.003 | 6617 | 3,000,000 |
| 0.017 | 6632 | 516,668 |
| 0.033 | 6644 | 358,334 |
| 0.067 | 6650 | 129,168 |
| 0.133 | 6654 | 64,544 |
| 0.267 | 6661 | 32,293 |
| 0.533 | 6666 | 16,147 |
| 1.067 | 6669 | 8074 |
| 2.133 | 6678 | 4038 |
| 4.267 | 6685 | 2019 |
| 8.533 | 6697 | 1010 |
| 17.067 | 6704 | 506 |
| 34.133 | 6712 | 253 |

The following additional reservoir and fluid properties are available:

$$\begin{aligned}
 p_i &= 6789.5 \text{ psi} \\
 p_{wf@\Delta t=0} &= 6352 \text{ psi} \\
 Q_o &= 2554 \text{ STB/day} \\
 B_o &= 2.3 \text{ bbl/STB} \\
 \mu_o &= 1 \text{ cp} \\
 t_p &= 8611 \text{ hours} \\
 r_w &= 0.375 \text{ ft} \\
 c_t &= 8.17 \times 10^{-6} \text{ psi}^{-1} \\
 \phi_m &= 0.21 \\
 k_m &= 0.1 \text{ md} \\
 h_m &= 17 \text{ ft}
 \end{aligned}$$

- Estimate ω and λ
- Storativity of the fractures $(\phi h c_t)_f$

Solution

Step 1. Plot p_{ws} vs $(t_p + \Delta t)/\Delta t$ on a semilog scale as shown in Figure 17-7.

Step 2. Figure 17-7 shows two parallel semilog straight lines with a slope of:

$$m = 32 \text{ psi/cycle}$$

Step 3. Calculate $(k_f h)$ from the slope m to give:

$$(k_f h) = \frac{162.6 Q_o B_o \mu_o}{m} = \frac{162.6(2556)(2.3)}{32} = 29,848.3 \text{ md ft}$$

and

$$k_f = \frac{29,848.3}{17} = 1,756 \text{ md}$$

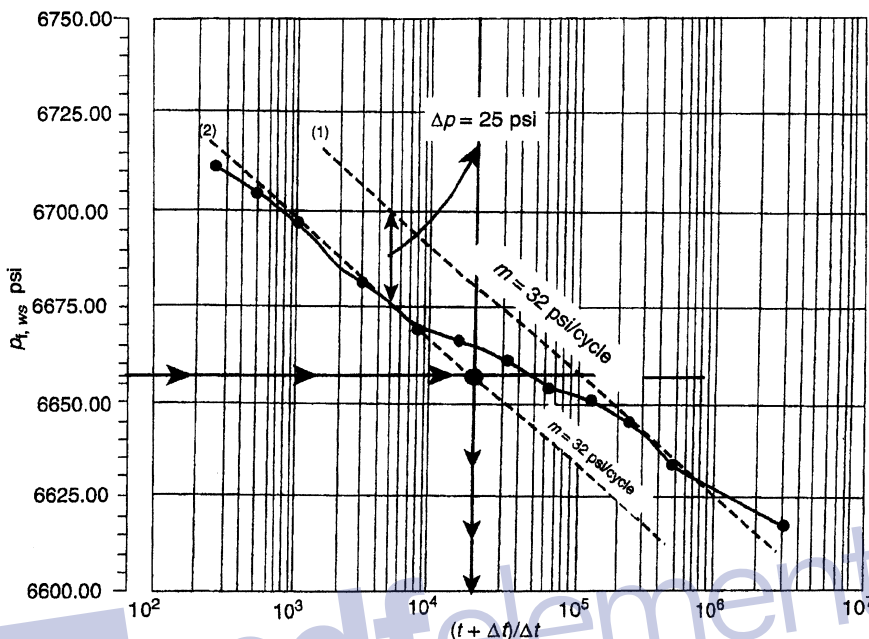


Figure 17-7. Semilog plot of the buildup test data. (After Sabet, 1991.)

Step 4. Determine the vertical distance Δp between the two straight lines to give:

$$\Delta p = 25 \text{ psi}$$

Step 5. Calculate the storativity ratio ω from Equation 17-3 to give:

$$\omega = 10^{(-\Delta p/m)} = 10^{-(25/32)} = 0.165$$

Step 6. Draw a horizontal line through the middle of the transition region to intersect with the two semilog straight lines. Read the corresponding time at the second intersection to give:

$$\left(\frac{t_p + \Delta t}{\Delta t} \right)_2 = 20,000$$

Step 7. Calculate λ from Equation 17-5.

$$\lambda = \left[\frac{1}{1-\omega} \right] \left[\frac{(\phi h c_t)_m \mu r_w^2}{1.781 k_f t_p} \right] \left(\frac{t_p + \Delta t}{\Delta t} \right)_2$$

$$\lambda = \left[\frac{1}{1-0.165} \right] \left[\frac{(0.21)(17)(8.17 \times 10^{-6})(1)(0.375)^2}{1.781(1756)(8611)} \right] (20,000)$$

$$= 3.64 \times 10^{-9}$$

It should be noted that pressure behavior in a naturally fractured reservoir is similar to that obtained in a *layered reservoir with no crossflow*. In fact, in any reservoir system with two predominant rock types, the pressure-buildup behavior is similar to that shown in Figure 17-6.

Gringarten (1987) points out that the two straight lines on the semilog plot may or may not be present depending on the condition of the well and the duration of the test. The author concludes that the semilog plot is not an efficient or sufficient tool for identifying double-porosity behavior. In the semilog plot, as shown in Figure 17-6, the double-porosity behavior yields an S-shape curve with the *initial portion* of the curve representing the homogeneous behavior resulting from depletion in the most permeable medium, e.g., fissures. A *transition period* follows and corresponds to the interporosity flow. Finally, the *last portion* represents the homogeneous behavior of both media when recharge from the least permeable medium (matrix) is fully established and pressure is equalized. The log-log analysis represents a significant improvement over conventional semilog analysis for identifying double-porosity behavior. However, S-shape behavior is difficult to see in highly damaged wells, and well behavior can then be erroneously diagnosed as homogeneous. Furthermore, a similar S-shape behavior may be found in irregularly bounded well drainage systems.

Perhaps the most efficient means of identifying double-porosity systems is by using a pressure-derivative plot. It allows unambiguous identification of the system, provided that the quality of the pressure data is adequate, and, more importantly, an accurate methodology is used in calculating pressure derivatives. Essentially, pressure-derivative analysis involves a log-log plot of the derivative of the pressure with respect to time versus elapsed time. The use of a pressure-derivative type curve offers the following advantages:

- Heterogeneities hardly visible on the conventional plot of well testing data are amplified on the derivative plot.
- Flow regimes have clear characteristic shapes on the derivative plot.
- The derivative plot is able to display in a single graph many separate characteristics that would otherwise require different plots.
- The derivative approach improves the definition of the analysis plots and therefore the quality of the interpretation.

Figure 17-8 shows the combined log–log plot of pressure and its derivative versus time for a dual-porosity system. The derivative plot shows a “minimum” or a “dip” on the pressure-derivative curve caused by the interporosity flow during the transition period. The “minimum” is between two horizontal lines; the first represents the radial flow controlled by the fissures, and the second describes the combined behavior of the double-porosity system. Figure 17-8 shows, at early time, the typical behavior of wellbore storage effects with the deviation from the 45° straight line to a maximum representing wellbore damage. Gringarten (1987) suggests that the shape of the “minimum” depends on the double-porosity behavior. For a restricted interporosity flow, the “minimum” takes a “V-shape” minimum, whereas unrestricted interporosity yields an open “U-shape” minimum.

Based on the Warren and Root double-porosity theory, Bourdet and Gringarten (1980) developed specialized pressure type curves that can be used for analyzing well test data in dual-porosity systems. They showed that double-porosity behavior is controlled by the following independent variables:

- p_D
- t_D/C_D
- $C_D e^{2s}$
- ω
- λe^{-2s}

with the dimensionless time t_D , dimensionless pressure p_D , and dimensionless wellbore-storage coefficient C_D as defined below:

$$t_D = \frac{0.0002637k_f t}{[(\phi\mu c_t)_f + (\phi\mu c_t)_m]\mu r_w^2} = \frac{0.0002637k_f t}{(\phi\mu c_t)_{f+m}\mu r_w^2}$$

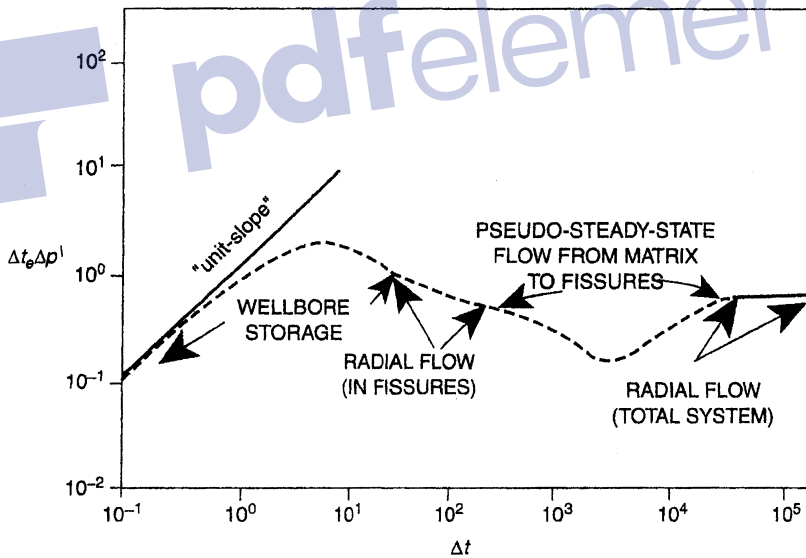
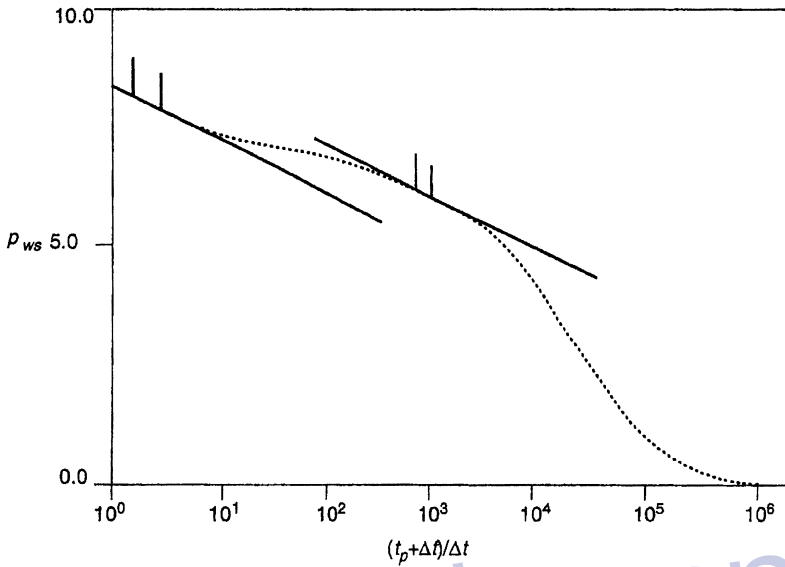


Figure 17-8. Dual-porosity behavior shows as two parallel semilog straight lines on a semilog plot, as a minimum on a derivative plot.

$$p_D = \left[\frac{k_f h}{141.2QB\mu} \right] \Delta p$$

$$C_D = \left[\frac{0.8936}{\phi h c_t r_w^2} \right] C$$

where k = permeability, md

t = time, hours

μ = viscosity, cp

r_w = wellbore radius, ft

C = wellbore storage coefficient, bbl/psi

subscripts:

f = fissure

m = matrix

$f + m$ = total system

D = dimensionless

Bourdet et al. (1984) extended the practical applications of these curves and enhanced their use by introducing the pressure-derivative type curves to the solution. They developed two sets of pressure-derivative type curves as shown in Figures 17-9 and 17-10. The first set (Figure 17-9) is based on the assumption that the interporosity flow obeys the pseudo-steady-state flowing condition, and the other set (Figure 17-10) assumes transient interporosity flow.

The use of either set involves plotting the pressure difference Δp and its derivative versus time on the same size log cycles as the type curve. The pressure difference and its derivative are given by:

For drawdown tests

The pressure difference $\Delta p = p_i - p_{wf}$

The derivative function $t\Delta p' = -t \left(\frac{d(\Delta p)}{d(t)} \right)$

For buildup tests

The pressure difference $\Delta p = p_{ws} - p_{wf@\Delta t=0}$

The derivative function $\Delta t_c \Delta p' = \Delta t \left(\frac{t_p + \Delta t}{\Delta t} \right) \left[\frac{d(\Delta p)}{d(\Delta t)} \right]$

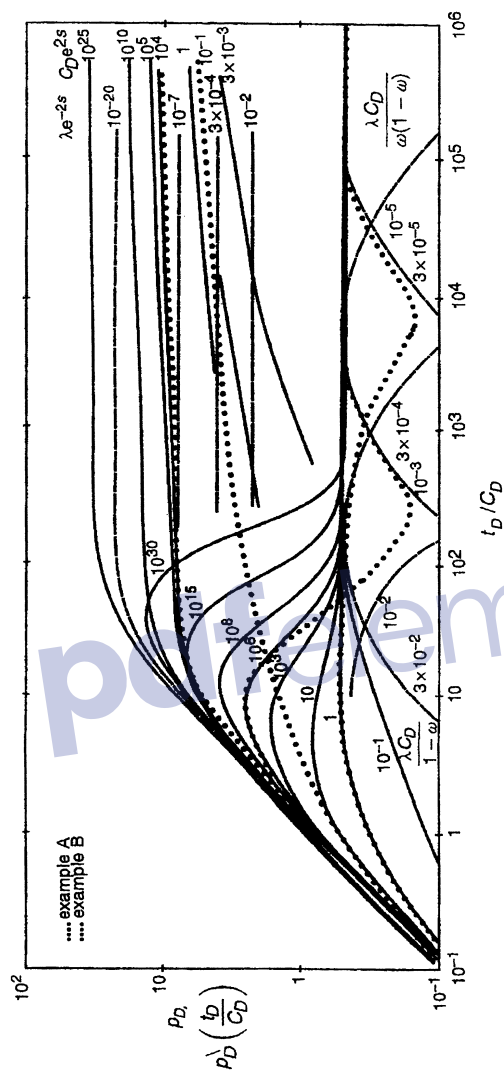


Figure 17-9. Type-curve matching. (Copyright ©1984 World Oil, Bourdet et al., 1984.)

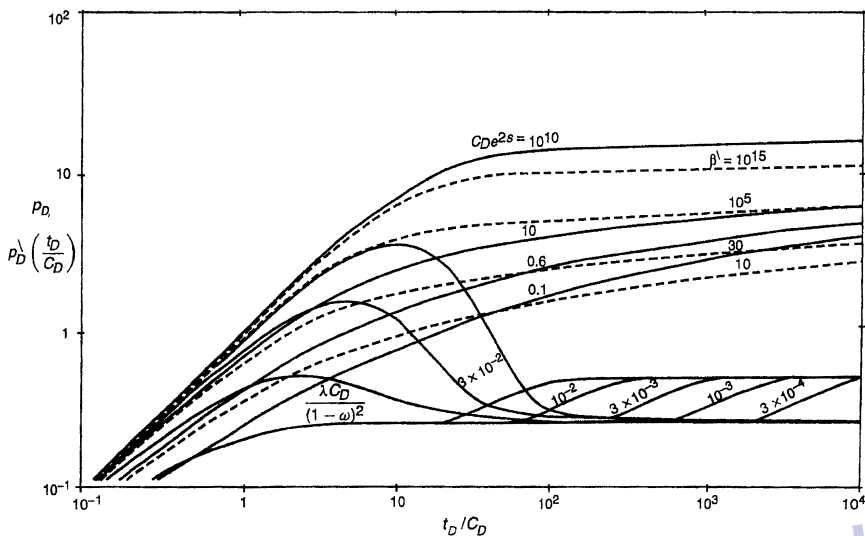


Figure 17-10. Type-curve matching. (Copyright ©1984 World Oil, Bourdet et al., 1984.)

It should be noted that all type-curve solutions are obtained for the drawdown solution. Therefore, these type curves cannot be used for buildup tests without restriction or modification. The only restriction is that the flow period, i.e., t_p , before shut-in must be somewhat large. However, Agarwal (1980) empirically found that by plotting the buildup data ($p_{ws} - p_{wf@\Delta t=0}$) versus **equivalent time** Δt_e instead of the shut-in time Δt , on a log-log scale, the type-curve analysis can be made without the requirement of a long drawdown flowing period before shut-in. Agarwal introduced the **equivalent time** Δt_e as defined by:

$$\Delta t_e = \frac{\Delta t}{1 + \left(\frac{\Delta t}{t_p}\right)} = \left[\frac{\Delta t}{t_p + \Delta t} \right] t_p$$

where Δt = shut-in time, hours

t_p = total flowing time since the last shut-in, hours

Δt_e = Agarwal **equivalent time**, hours

Agarwal's equivalent time Δt_e is simply designed to account for the effects of producing time t_p on a pressure-buildup test. The concept of Δt_e

is that the pressure change $\Delta p = p_{ws} - p_{wf}$ at time Δt during a buildup test is the same as the pressure change $\Delta p = p_i - p_{wf}$ at Δt_e during a drawdown test. Thus, a graph of a buildup test in terms of $p_{ws} - p_{wf}$ versus Δt_e will overlay a graph of pressure change versus flowing time for a drawdown test. Therefore, when applying the type-curve approach in analyzing pressure-buildup data, the actual shut-in time Δt is replaced by the equivalent time Δt_e .

The controlling variables in each of the two type-curve sets, i.e., Figures 17-9 and 17-10, are given below.

1. First type-curve set: Pseudosteady-state interporosity flow

The actual pressure response, i.e., pressure difference Δp , is described by the following three component curves:

1st: At early times, the flow comes from the fissures (most permeable medium) and the actual pressure-difference plot, i.e., Δp curve, matches one of the homogeneous curves that is labeled $(C_D e^{2s})$ with a corresponding value of $(C_D e^{2s})_f$ that describes the *fissure flow*. This value is designated as $[(C_D e^{2s})_f]_M$.

2nd: As the pressure-difference response reaches the transition regime, Δp deviates from the $C_D e^{2s}$ curve and follows one of the transition curves that describe this flow regime by a λe^{-2s} , designated as $[\lambda e^{-2s}]_M$.

3rd: Finally, the pressure-difference response leaves the transition curve and matches a new $C_D e^{2s}$ curve below the first one with a corresponding value of $(C_D e^{2s})_{f+m}$ that describes the *total system* behavior, i.e., matrix and fissures. This value is recorded as $[(C_D e^{2s})_{f+m}]_M$.

On the pressure-derivative response, the storativity ratio ω defines the shape of the derivative curve during the transition regime, which is described by a “depression” or a “minimum.” The duration and depth of the depression are linked by the value of ω ; a small ω produces a long and therefore deep transition. The interporosity coefficient λ is the second parameter defining the position of the time axis of the transition regime. A decrease in the λ value moves the depression to the right side of the plot.

As shown in Figure 17-9, the pressure-derivative plots match on four component curves:

- 1st: The derivative curve follows the fissure flow curve $[(C_D e^{2s})_f]_M$.
 2nd: The derivative curve reaches an early transition period, expressed by a depression, and described by an early transition curve $[\lambda(C_D)_{f+m}/\omega(1-\omega)]_M$.
 3rd: The derivative-pressure curve then matches a late transition curve labeled $[\lambda(C_D)_{f+m}/\omega(1-\omega)]_M$.
 4th: The total system behavior is reached on the 0.5 line.

2. Second type-curve set: Transient interporosity flow

As developed by Bourdet and Gringarten (1980) and expanded by Bourdet et al. (1984) to include the pressure-derivative approach, this type curve is built in the same way as that for the pseudosteady-state interporosity flow. As shown in Figure 17-10, the pressure behavior is defined by three component curves: $(C_D e^{2s})_f$, β^λ , and $(C_D e^{2s})_{f+m}$. The authors defined β^λ as the interporosity dimensionless group and given by:

$$\beta^\lambda = \delta \left[\frac{(C_D e^{2s})_{f+m}}{\lambda e^{-2s}} \right]$$

where the parameter δ is the shape coefficient with assigned values as given below:

- $\delta = 1.0508$, for spherical blocks
 $\delta = 1.8914$, for slab matrix blocks

As the first fissure flow is short lived with transient interporosity flow models, the $(C_D e^{2s})_f$ curves are not seen in practice and therefore have not been included in the derivative curves. The dual-porosity derivative response starts on the derivative of a β^λ transition curve and then follows a late transition curve labeled $\lambda(C_D)_{f+m}/(1-\omega)^2$ until it reaches the total system regime on the 0.5 line.

Bourdet (1985) points out that the pressure-derivative responses during the transition flow regime are very different between the two double-porosity models. With the transient interporosity flow solutions, the transition starts from early time and does not drop to a very low level. With pseudosteady-state interporosity flow, the transition starts later and the shape of the depression is much more pronounced. There is *no lower limit* for the depth of the depression when the flow from the matrix to the

fissures follows the pseudosteady-state model, whereas for the interporosity transient flow, the depth of the depression does not exceed 0.25.

In general, the matching procedure and reservoir parameters estimation as applied to the type curve of Figure 17-10 are summarized by the following steps:

Step 1. Using the actual well test data, calculate the pressure difference Δp and the pressure-derivative plotting functions for every pressure test point.

For drawdown tests

The pressure difference $\Delta p = p_i - p_{wf}$

The derivative function $t\Delta p' = -t \left(\frac{d(\Delta p)}{d(t)} \right)$

For buildup tests

The pressure difference $\Delta p = p_{ws} - p_{wf@ \Delta t=0}$

The derivative function $\Delta t_e \Delta p' = \Delta t \left(\frac{t_p + \Delta t}{\Delta t} \right) \left[\frac{d(\Delta p)}{d(\Delta t)} \right]$

Step 2. On a tracing paper with the same size log cycles as in Figure 17-10, plot the data of Step 1 as a function of flowing time t for drawdown tests or versus equivalent time Δt_e for buildup tests.

Step 3. Place the actual two sets of plots, i.e., Δp and derivative plots, on Figure 17-9 or Figure 17-10 and force a simultaneous match of the two plots to Gringarten–Bourdet type curves. Read the matched derivative curve $[\lambda(C_D)_{f+m}/(1 - \omega)^2]_M$.

Step 4. Choose any point and read its coordinates on both Figures 17-9 and 17-10 to give:

$$(\Delta p, p_D)_{MP} \text{ and } (t \text{ or } \Delta t_e, t_D/C_D)_{MP}$$

Step 5. With the match still maintained, read the values of the curves labeled $(C_D e^{2s})$ which match the initial segment of the curve $[(C_D e^{2s})_f]_M$ and the final segment $[(C_D e^{2s})_{f+m}]_M$ of the data curve.

Step 6. Calculate the well and reservoir parameters from the following relationships:

$$\omega = \frac{[(C_D e^{2s})_{f+m}]_M}{[(C_D e^{2s})_M]} \quad (17-5)$$

$$k_f h = 141.2 Q B \mu \left(\frac{P_D}{\Delta p} \right)_{MP}, \text{ md ft} \quad (17-6)$$

$$C = \left[\frac{0.000295 k_f h}{\mu} \right] \frac{(\Delta t)_{MP}}{(C_D / C_D)_{MP}} \quad (17-7)$$

$$(C_D)_{f+m} = \frac{0.8926 C}{\phi c_t h r_w^2} \quad (17-8)$$

$$s = 0.5 \ln \left[\frac{[(C_D e^{2s})_{f+m}]_M}{(C_D)_{f+m}} \right] \quad (17-9)$$

$$\lambda = \left[\frac{\lambda (C_D)_{f+m}}{(1-\omega)^2} \right]_M \frac{(1-\omega)^2}{(C_D)_{f+m}} \quad (17-10)$$

Selection of the better solution between the pseudosteady-state and the transient interporosity flow is generally straightforward; with the pseudosteady-state model, the drop in the derivative during transition is a function of the transition duration. Long transition regimes, corresponding to small ω values, produce derivative levels much lower than the practical 0.25 limit of the transient solution.

The pressure-buildup data given by Bourdet et al. (1984) and reported by Sabet (1991) are used below as an example to illustrate the use of the pressure-derivative type curves.

Example 17-2

Table 17-1 shows the pressure-buildup and pressure-derivative data for a naturally fractured reservoir. The following flow and reservoir data are also given:

Table 17-1
Pressure Buildup Test, Naturally Fractured Reservoir
(After Sabet, 1991)

| Δt (hour) | Δp_{ws} (psi) | $\frac{t_p + \Delta t}{\Delta t}$ | Slope (psi/hour) | $\Delta p \cdot \frac{t_p + \Delta t}{t_p}$ (psi) |
|-------------------|-----------------------|-----------------------------------|------------------|---|
| 0.00000E+00 | 0.000 | | 3180.10 | |
| 3.48888E-03 | 11.095 | 14,547.22 | 1727.68 | 8.56 |
| 9.04446E-03 | 20.693 | 5612.17 | 847.26 | 11.65 |
| 1.46000E-02 | 25.400 | 3477.03 | 486.90 | 9.74 |
| 2.01555E-02 | 28.105 | 2518.92 | 337.14 | 8.31 |
| 2.57111E-02 | 29.978 | 1974.86 | 257.22 | 7.64 |
| 3.12666E-02 | 31.407 | 1624.14 | 196.56 | 7.10 |
| 3.68222E-02 | 32.499 | 1379.24 | 459.66 | 6.56 |
| 4.23777E-02 | 33.386 | 1198.56 | 127.80 | 6.10 |
| 4.79333E-02 | 34.096 | 1059.76 | 107.28 | 5.64 |
| 5.90444E-02 | 35.288 | 860.52 | 83.25 | 5.63 |
| 7.01555E-02 | 36.213 | 724.39 | 69.48 | 5.36 |
| 8.12666E-02 | 36.985 | 625.49 | 65.97 | 5.51 |
| 9.23777E-02 | 37.718 | 550.38 | 55.07 | 5.60 |
| 0.10349 | 38.330 | 491.39 | 48.83 | 5.39 |
| 0.12571 | 39.415 | 404.71 | 43.65 | 5.83 |
| 0.14793 | 40.385 | 344.07 | 37.16 | 5.99 |
| 0.17016 | 41.211 | 299.25 | 34.38 | 6.11 |
| 0.19238 | 41.975 | 264.80 | 29.93 | 6.21 |
| 0.21460 | 42.640 | 237.49 | 28.85 | 6.33 |
| 0.23682 | 43.281 | 215.30 | 30.96 | 7.12 |
| 0.25904 | 43.969 | 196.92 | 25.78 | 7.39 |
| 0.28127 | 44.542 | 181.43 | 24.44 | 7.10 |
| 0.30349 | 45.085 | 168.22 | 25.79 | 7.67 |
| 0.32571 | 45.658 | 156.81 | 20.63 | 7.61 |
| 0.38127 | 46.804 | 134.11 | 18.58 | 7.53 |
| 0.43628 | 47.836 | 117.18 | 17.19 | 7.88 |
| 0.49298 | 48.791 | 104.07 | 16.36 | 8.34 |
| 0.54793 | 49.700 | 93.62 | 15.14 | 8.72 |
| 0.60349 | 50.541 | 85.09 | 12.50 | 8.44 |
| 0.66460 | 51.305 | 77.36 | 12.68 | 8.48 |
| 0.71460 | 51.939 | 72.02 | 11.70 | 8.83 |
| 0.77015 | 52.589 | 66.90 | 11.14 | 8.93 |
| 0.82571 | 53.208 | 62.46 | 10.58 | 9.11 |
| 0.88127 | 53.796 | 58.59 | 10.87 | 9.62 |
| 0.93682 | 54.400 | 55.17 | 8.53 | 9.26 |
| 0.99238 | 54.874 | 52.14 | 10.32 | 9.54 |
| 1.04790 | 55.447 | 49.43 | 7.70 | 9.64 |
| 1.10350 | 55.875 | 46.99 | 8.73 | 9.26 |
| 1.21460 | 56.845 | 42.78 | 7.57 | 10.14 |

Table 17-1 Continued

| Δt (hour) | Δp_{ws} (psi) | $\frac{t_p + \Delta t}{\Delta t}$ | Slope (psi/hour) | $\Delta p \frac{t_p + \Delta t}{t_p}$ (psi) |
|-------------------|-----------------------|-----------------------------------|-------------------|---|
| 1.32570 | 57.686 | 39.28 | 5.91 | 9.17 |
| 1.43680 | 58.343 | 36.32 | 6.40 | 9.10 |
| 1.54790 | 59.054 | 33.79 | 6.05 | 9.93 |
| 1.65900 | 59.726 | 31.59 | 5.57 | 9.95 |
| 1.77020 | 60.345 | 29.67 | 5.44 | 10.08 |
| 1.88130 | 60.949 | 27.98 | 4.74 | 9.93 |
| 1.99240 | 61.476 | 26.47 | 4.67 | 9.75 |
| 2.10350 | 61.995 | 25.13 | 4.34 | 9.87 |
| 2.21460 | 62.477 | 23.92 | 3.99 | 9.62 |
| 2.43680 | 63.363 | 21.83 | 3.68 | 9.79 |
| 2.69240 | 64.303 | 19.85 | 3.06 ^a | 9.55 ^b |
| 2.91460 | 64.983 | 18.41 | 3.16 | 9.59 |
| 3.13680 | 65.686 | 17.18 | 2.44 | 9.34 |
| 3.35900 | 66.229 | 16.11 | 19.72 | 39.68 |

Adapted from Bourdet et al. (1984).

^a $(64.983 - 64.303)/(2.9146 - 2.69240) = 3.08$.

^b $[(3.68 + 3.06)/2] \times 19.85 \times 2.69240^2/50.75 = 9.55$.

$$Q = 960 \text{ STB/day}$$

$$B_o = 1.28 \text{ bbl/STB}$$

$$c_t = 1 \times 10^{-5} \text{ psi}^{-1}$$

$$\phi = 0.007$$

$$\mu = 1 \text{ cp}$$

$$r_w = 0.29 \text{ ft}$$

$$h = 36 \text{ ft}$$

It is reported that the well was opened to flow at a rate of 2,952 STB/day for 1.33 hours, shut-in for 0.31 hour, opened again at the same rate for 5.05 hours, closed for 0.39 hours, opened for 31.13 hours at the rate of 960 STB/day, and then shut-in for the pressure-buildup test.

Analyze the buildup data and determine the well and reservoir parameters assuming transient interporosity flow.

Solution

Step 1. Calculate the flowing time t_p as follows:

$$\begin{aligned} \text{total oil produced} = N_p &= \frac{2952}{4} [1.33 + 5.05] \\ &+ \frac{960}{24} 31.13 \approx 2030 \text{ STB} \end{aligned}$$

$$t_p = \frac{(24)(2030)}{960} = 50.75 \text{ hours}$$

Step 2. Confirm the double-porosity behavior by constructing Horner's (1967) plot as shown in Figure 17-11. The graph shows the two parallel straight lines confirming the dual-porosity system.

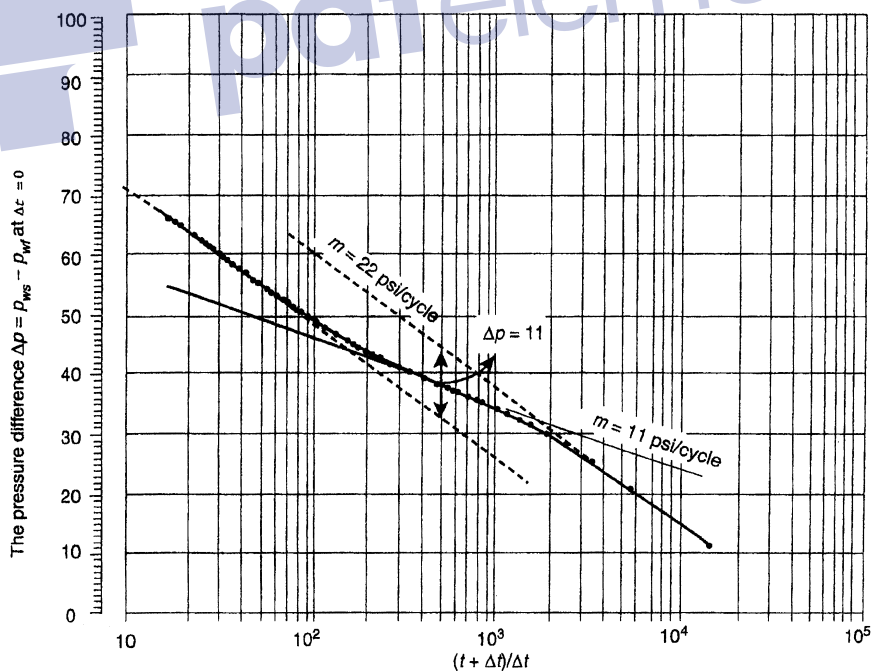


Figure 17-11. The data of the Horner plot. (After Sabet, 1991.)

Step 3. Using the same grid system of Figure 17-10, plot the *actual pressure derivative* versus shut-in time, as shown in Figure 17-12a, and Δp_{ws} versus time, as shown in Figure 17-12b. The 45° line shows that the test was slightly affected by the wellbore storage.

Step 4. Overlay the pressure difference and pressure-derivative plots over the transient interporosity type curve, as shown in Figure 17-13, to give the following matching parameters:

- $\left[\frac{p_D}{\Delta p} \right]_{MP} = 0.053$
- $\left[\frac{t_D/C_D}{\Delta t} \right]_{MP} = 270$
- $\left[\frac{\lambda(C_D)_{f+m}}{(1-\omega)^2} \right]_M = 0.03$
- $[(C_D e^{2s})_f]_M = 33.4$
- $[(C_D e^{2s})_{f+m}]_M = 0.6$

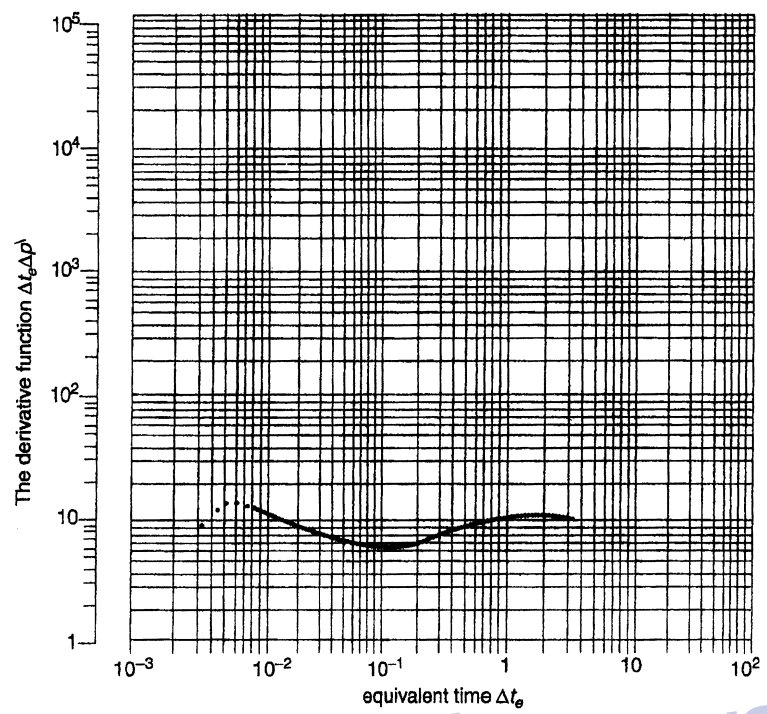
Step 5. Calculate the well and reservoir parameters by applying Equations 17-5 through 17-10, to give:

$$\omega = \frac{[(C_D e^{2s})_{f+m}]_M}{[(C_D e^{2s})_f]_M} = \frac{0.6}{33.4} = 0.018$$

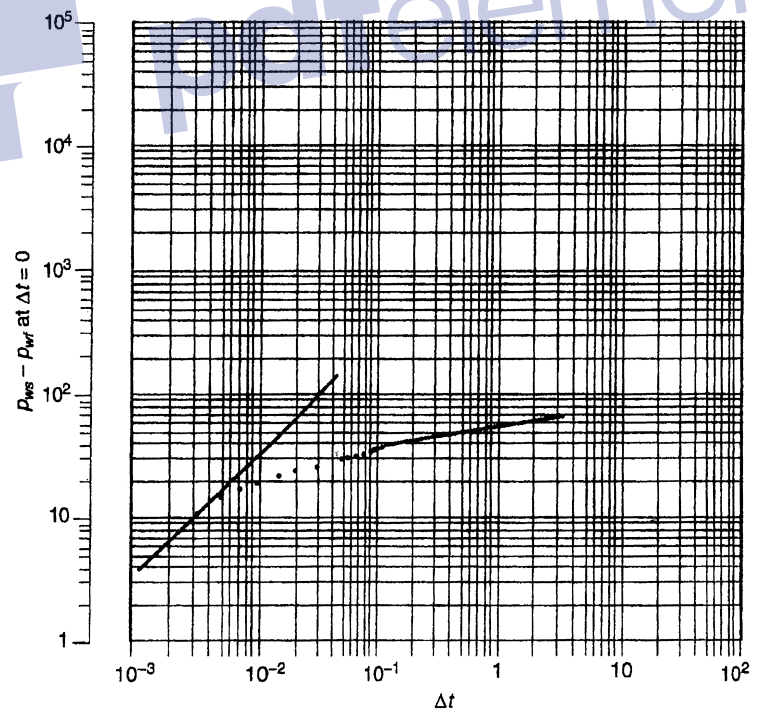
Kazemi (1969) points out that if the vertical separation between the two parallel slopes Δp is less than 100 psi, the calculation of ω by Equation 17-2 will produce a significant error in its values. Figure 17-11 shows that Δp is about 11 psi, and Equation 17-2 gives an *erroneous value* of:

$$\omega = 10^{-(\Delta p/m)} = 10^{-(11/12)} = 0.316$$

$$\begin{aligned} \bullet k_f h &= 141.2QB\mu \left(\frac{p_D}{\Delta p} \right)_{MP} = 141.2(960)(1)(1.28)(0.053) \\ &= 9196 \text{ md ft} \end{aligned}$$



(a)



(b)

Figure 17-12. (a) Derivative function. (b) Log-log plot of Δp versus Δt_e . (After Sabet, 1991.)

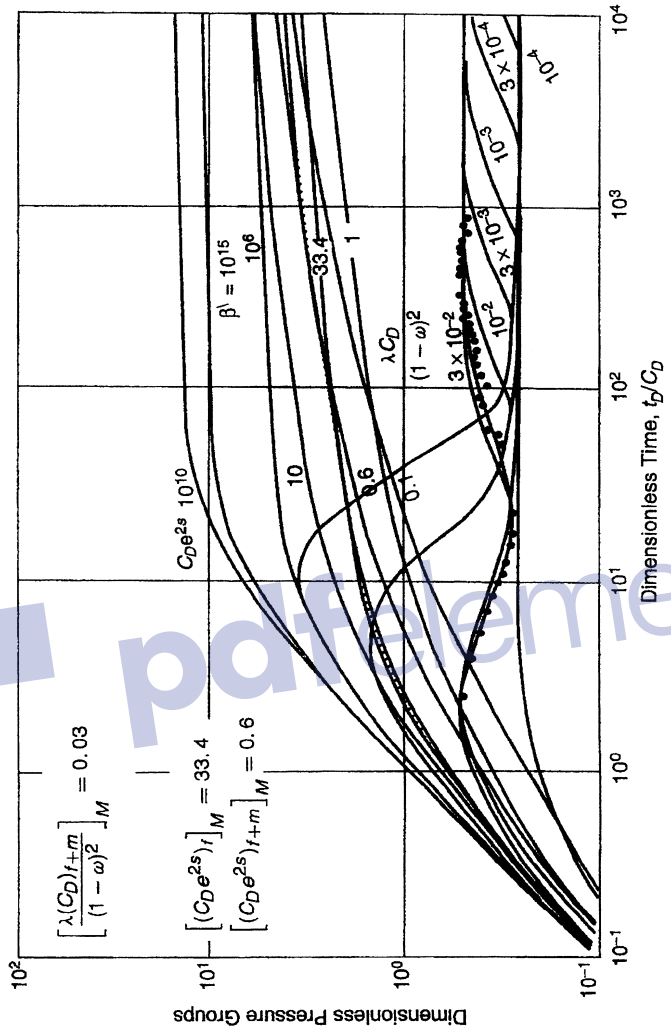


Figure 17-13. Type-curve matching. (Copyright ©1984 World Oil, Bourdet et al., 1984.)

$$C = \left[\frac{0.000295k_f h}{\mu} \right] \frac{(\Delta t)_{MP}}{(C_D/C_D)_{MP}} = \frac{(0.000295)(9196)}{(1.0)(270)} = 0.01 \text{ bbl/psi}$$

$$\bullet (C_D)_{f+m} = \frac{0.8926C}{\phi c_t h r_w^2} = \frac{(0.8936)(0.01)}{(0.07)(1 \times 10^{-5})(36)(90.29)^2} = 4216$$

$$\bullet s = 0.5 \ln \left[\frac{[(C_D e^{2s})_{f+m}]_M}{(C_D)_{f+m}} \right] = 0.5 \ln \left[\frac{0.6}{4216} \right] = -4.4$$

$$\bullet \lambda = \left[\frac{\lambda(C_D)_{f+m}}{(1-\omega)^2} \right]_M \frac{(1-\omega)^2}{(C_D)_{f+m}} = (0.03) \left[\frac{(1-0.018)^2}{4216} \right] = 6.86 \times 10^{-6}$$

HYDRAULICALLY FRACTURED WELLS

Many wells, particularly wells in tight (low-permeability) formations, require hydraulic fracturing to be commercially viable. Interpretation of pressure transient data in hydraulically fractured wells is important for evaluating the success in fracture treatments and predicting the future performance of these types of wells. A well-documented and comprehensive report that overviews theories, design methods, and materials used in a hydraulic fracture treatment was published by the Environmental Protection Agency in June 2004 (EPA, 2004). Hydraulic fracturing is the process of pumping a fluid into a wellbore at an injection rate that is too high for the formation to accept in a radial flow pattern. As the resistance to flow in the formation increases, the pressure in the wellbore increases to a value that exceeds the breakdown pressure of the formation that is open to the wellbore. Once the formation “breaks down,” a crack or fracture is formed, and the injected fluid begins moving down the fracture. In most formations, a single, vertical fracture that propagates in two directions from the wellbore is created. These fracture “wings” are 180° apart and are normally assumed to be identical in shape and size at any point in time. In naturally fractured or cleated formations, such as gas shales or coal seams, it is possible that multiple fractures can be created and propagated during a hydraulic fracture treatment.

Fluid that does not contain any propping agent, often called “pad,” is injected to create a fracture that grows up, out, and down; therefore, the fluid creates a fracture that is wide enough to accept a propping agent.

The purpose of the propping agent is to “prop open” the fracture once the pumping operation ceases, the pressure in the fracture decreases, and the fracture closes. In deep reservoirs, we use human-made ceramic beads to prop open the fracture. In shallow reservoirs, sand is normally used as the propping agent. The sand used as a propping agent in shallow reservoirs, such as coal seams, is mined from certain quarries in the United States. Silica sand is a natural product and will not lead to any environmental concerns that would affect the United States Safe Drinking Water Act.

In general, hydraulic fracture treatments are used to increase the productivity index of a producing well or the injectivity index of an injection well. The productivity index defines the volumes of oil or gas that can be produced at a given pressure differential between the reservoir and the wellbore. The injectivity index refers to how much fluid can be injected into an injection well at a given pressure differential. The EPA (2004) report lists different applications for hydraulic fracturing, such as:

- Increasing the flow rate of oil and/or gas from low-permeability reservoirs
- Increasing the flow rate of oil and/or gas from wells that have been damaged
- Connecting the natural fractures and/or cleats in a formation to the wellbore
- Decreasing the pressure drop around the well to minimize sand production
- Decreasing the pressure drop around the well to minimize problems with asphaltine and/or paraffin deposition
- Increasing the area of drainage or the amount of formation in contact with the wellbore
- Connecting the full vertical extent of a reservoir to a slanted or horizontal well

A low-permeability reservoir has a high resistance to fluid flow. In many formations, chemical and/or physical processes alter the structure of a reservoir rock over geologic time. Sometimes, these diagenetic processes restrict the openings in the rock and reduce the ability of fluids to flow through the rock. Low-permeability rocks are normally excellent candidates for stimulation by hydraulic fracturing.

Regardless of permeability, a reservoir rock can be damaged when a well is drilled through the reservoir and when casing is set and cemented in place. Damage occurs because drilling and/or completion fluids leak

into the reservoir and plug up the pores and pore throats. When the pores are plugged, permeability is reduced, and the fluid flow in this damaged portion of the reservoir may be substantially reduced. Damage can be severe in naturally fractured reservoirs, such as coal seams. To stimulate damaged reservoirs, a short, conductive hydraulic fracture is often the desired solution.

The success or failure of a hydraulic fracture treatment often depends on the quality of the candidate well selected for the treatment. Choosing an excellent candidate for stimulation often ensures success, while choosing a poor candidate normally results in economic failure. To select the best candidate for stimulation, the design engineer must consider many variables. The most critical parameters for hydraulic fracturing are:

- Formation permeability
- *In situ* stress distribution
- Reservoir fluid viscosity
- Skin factor
- Reservoir pressure
- Reservoir depth

If the skin factor is positive, the reservoir is damaged and could possibly be an excellent candidate for stimulation.

The best candidate wells for hydraulic fracturing treatments will have a substantial volume of oil and gas-in-place, and will have a need to increase the productivity index. Such reservoirs will have

- a thick pay zone and
- medium to high pressure, and will either be
- a low-permeability zone or a zone that has been damaged (high skin factor).

Hydraulic fracturing theory and design has been developed by other engineering disciplines. However, certain aspects, such as poroelastic theory, are unique to porous, permeable underground formations. The most important parameters are: Poisson's ratio; Young's modulus; and *in situ* stress.

Poisson's ratio (ν), named after Simeon Poisson, is defined as the ratio of the relative contraction strain (transverse strain) divided by the relative extension strain (or axial strain).

Young's modulus is defined as “the ratio of stress to strain for uniaxial stress.” The theory used to compute fracture dimensions is based upon linear elasticity. To apply this theory, Young’s modulus of the formation is an important parameter.

The modulus of a material is a measure of the stiffness of the material. If the modulus is large, the material is stiff. In hydraulic fracturing, a stiff rock will result in more narrow fractures. If the modulus is low, the fractures will be wider. The modulus of a rock is a function of the lithology, porosity, fluid type, and other variables. Typical ranges for Young’s modulus as a function of lithology are tabulated below.

| Lithology | Young's Modulus (psi) |
|----------------|-----------------------|
| Soft sandstone | $2-5 \times 10^6$ |
| Hard sandstone | $6-10 \times 10^6$ |
| Limestone | $8-12 \times 10^6$ |
| Coal | $0.1-1 \times 10^6$ |
| Shale | $1-10 \times 10^6$ |

In situ stresses. Underground formations are confined and under stress. Figure 17-14 illustrates the local stress state at depth for an element of formation. The stresses can be divided into the following three principal stresses:

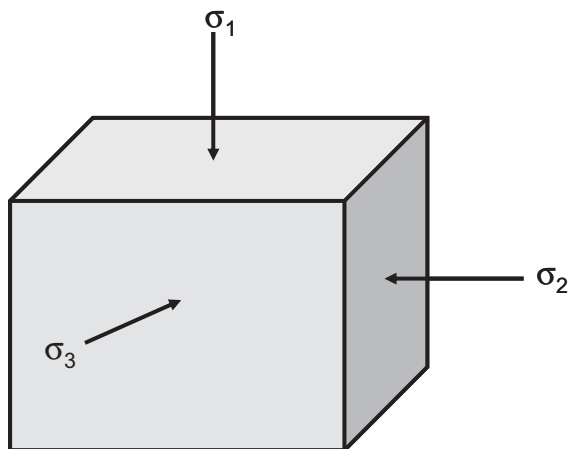


Figure 17-14. Local *in situ* stress at depth.

- the vertical stress σ_1 ,
- the maximum horizontal stress σ_2 , and
- the minimum horizontal stress σ_3 .

where $\sigma_1 > \sigma_2 > \sigma_3$. Depending on geologic conditions, the vertical stress could also be the intermediate (σ_2) or minimum stress (σ_3). These stresses are normally compressive and vary in magnitude throughout the reservoir, particularly in the vertical direction (from layer to layer). The magnitude and direction of the principal stresses are important because they control:

- the pressure required to create and propagate a fracture,
- the shape and vertical extent of the fracture,
- the direction of the fracture, and
- the stresses trying to crush and/or embed the propping agent during production.

A hydraulic fracture will propagate perpendicular to the minimum principal stress (σ_3). If the minimum horizontal stress is σ_3 , the fracture will be vertical. The minimum horizontal stress (*in situ* stress) profile can be calculated from the following expression:

$$\sigma_{\min} \cong \frac{\nu}{1-\nu}(\sigma_{\text{ob}} - \alpha p) + \alpha p$$

where σ_{\min} = the minimum horizontal stress (*in situ* stress)

ν = Poisson's ratio

σ_{ob} = overburden stress

α = poroelastic constant

p = reservoir fluid pressure or pore pressure

Poisson's ratio can be estimated from acoustic log data or from correlations based upon lithology. For coal seams, the value of Poisson's ratio will range from 0.2 to 0.4. The overburden stress can be computed using density log data. Normally, the value for overburden pressure is about 1.1 psi per foot of depth. The reservoir pressure must be measured or estimated.

The poroelastic constant α ranges from 0.5 to 1.0 and is a parameter that describes the "efficiency" of the fluid pressure to counteract the total applied stress. Typically, for hydrocarbon reservoirs, α is about 0.7.

A hydraulic fracture will propagate perpendicular to the least principal stress. In some shallow formations the least principal stress is the overburden stress; thus, the hydraulic fracture will be horizontal. In reservoirs deeper than 1,000 ft or so, the least principal stress will likely be horizontal; thus, the hydraulic fracture will be vertical. The azimuth orientation of the vertical fracture will depend upon the azimuth of the minimum and maximum horizontal stresses.

A fracture is defined as a single crack initiated from the wellbore by hydraulic fracturing. It should be noted that fractures are different from “fissures,” which are the formation of natural fractures. Hydraulically induced fractures are usually vertical, but can be horizontal if the formation is less than approximately 3,000 ft deep. Vertical fractures are characterized by the following properties:

- Fracture half-length x_f , in ft
- Dimensionless radius r_{eD} , where $r_{eD} = r_e/x_f$
- Fracture height h_f , which is often assumed equal to the formation thickness, in ft
- Fracture permeability k_f , in md
- Fracture width w_f , in ft
- Fracture conductivity F_C , where $F_C = k_f w_f$

The analysis of fractured well tests deals with the identification of well and reservoir variables that would have an impact on future well performance. However, fractured wells are substantially more complicated. The well-penetrating fracture has unknown geometric features, i.e., x_f , w_f , and h_f , and unknown conductivity properties.

Gringarten et al. (1974) and Cinco and Samaniego (1981), among others, propose three transient flow models to consider when analyzing transient pressure data from vertically fractured wells. These are: (1) infinite-conductivity vertical fractures; (2) finite-conductivity vertical fractures; (3) uniform-flux fractures.

1. Infinite-conductivity vertical fractures

These fractures are created by conventional hydraulic fracturing and characterized by a very high conductivity, which, for all practical purposes, can be considered infinite. In this case, the fracture acts similarly to a large diameter pipe with *infinite permeability*, and, therefore, there is essentially no pressure drop from the tip of the fracture to the wellbore,

i.e., no pressure loss in the fracture. This model assumes that the flow into the wellbore is only through the fracture and exhibits three flow periods: (1) fractured linear flow period; (2) formation linear flow period; and (3) infinite acting pseudoradial flow period.

Several specialized plots are used to identify the start and end of each flow period. For example, an early time log–log plot of Δp versus Δt will exhibit a straight line of half-unit slope. These flow periods associated with infinite-conductivity fractures, and the diagnostic specialized plots will be discussed later in this section.

2. Finite-conductivity fractures

These are very long fractures created by massive hydraulic fracture (MHF). These types of fractures need large quantities of propping agent to keep them open, resulting in reduced fracture permeability k_f compared with that of the infinite-conductivity fracture. These finite-conductivity vertical fractures are characterized by measurable pressure drops in the fracture and, therefore, exhibit unique pressure responses when testing hydraulically fractured wells. The transient pressure behavior for this system can include the following four sequence flow periods (to be discussed later):

- linear flow within the fracture, followed by
- bilinear flow, then
- linear flow in the formation, and eventually
- infinite acting pseudoradial flow.

3. Uniform-flux fractures

A uniform-flux fracture is one in which the reservoir fluid flow rate from the formation into the fracture is uniform along the entire fracture length. This model is similar to the infinite-conductivity vertical fracture in several aspects. The difference between these two systems occurs at the boundary of the fracture. The system is characterized by a variable pressure along the fracture and exhibits essentially two flow periods: linear flow and infinite acting pseudoradial flow.

Except for highly propped and conductive fractures, it is thought that the uniform-influx fracture theory better represents reality than the infinite-conductivity fracture; however, the difference between the two is rather small.

The fracture has a much greater permeability than the formation it penetrates; hence it influences the pressure response of a well test significantly. The general solution for the pressure behavior in a reservoir is expressed in terms of dimensionless variables. The following dimensionless groups are used when analyzing pressure transient data in a hydraulically fractured well:

$$\text{Diffusivity group: } \eta_{fd} = \frac{k_f \phi c_t}{k \phi_f c_{ft}} \quad (17-11)$$

$$\text{Time group: } t_{Dxf} = \left[\frac{0.0002637k}{\phi \mu c_t x_f^2} \right] t = t_D \left(\frac{r_w^2}{x_f^2} \right) \quad (17-12)$$

$$\text{Conductivity group: } F_{CD} = \frac{k_f w_f}{k x_f} = \frac{F_C}{k x_f} \quad (17-13)$$

$$\text{Storage group: } C_{Df} = \frac{0.8937C}{\phi c_t h x_f^2} \quad (17-14)$$

$$\text{Pressure group: } p_D = \frac{kh\Delta p}{1412QB\mu}; \quad \text{for oil} \quad (17-15)$$

$$p_D = \frac{kh\Delta m(p)}{1424QT}; \quad \text{for gas} \quad (17-16)$$

$$\text{Fracture group: } r_{eD} = \frac{r_e}{x_f}$$

- where x_f = fracture half-length, ft
 w_f = fracture width, ft
 k_f = fracture permeability, md
 k = prefracturing formation permeability, md
 t_{Dxf} = dimensionless time based on the fracture half-length x_f
 t = flowing time in drawdown, Δt or Δt_e in buildup, hours
 T = temperature, °R
 F_C = fracture conductivity, md ft
 F_{CD} = dimensionless fracture conductivity
 η = hydraulic diffusivity
 c_f = total compressibility of the fracture, psi^{-1}

Notice that the above equations are written in terms of the pressure drawdown tests. These equations should be modified for buildup tests by replacing the pressure and time with the appropriate values as shown below:

| Test | Pressure | Time |
|----------|---|----------------------------|
| Drawdown | $\Delta p = p_i - p_{wf}$ | T |
| Buildup | $\Delta p = p_{ws} - p_{wf@\Delta t=0}$ | Δt or Δt_e |

In general, a fracture could be classified as an infinite-conductivity fracture when the dimensionless fracture conductivity F_{CD} is greater than 300. The dimensionless fracture conductivity F_{CD} is defined as the ratio of the ability of the fracture to deliver fluid to the wellbore to the ability of the reservoir to deliver fluid to the fracture. High F_{CD} indicates excessive fracture efficiency and suggests that the fracture capability to deliver reservoir fluids to the wellbore is more efficient than the formation's capability to deliver the same fluids to the fracture.

It should be noted that the fracture conductivity F_C , which is the product of the fracture w_f width times the fracture permeability k_f , will reduce the life of the well because of :

- Increasing stress on fracture

As the well is produced, the effective stress on the proppant agent will normally increase because the value of the bottom-hole pressure will be decreasing.

- Proppant crushing
- Proppant embedment into the formation
- Non-Darcy flow effects
- Damage due to fluid loss additives, i.e., fracturing fluid residue (FFR)

The impact of the FFR on fracture permeability can be estimated by the theoretical model given by Cooke (1973):

$$k_{fd} = k_f \left(\frac{\phi_{fd}}{\phi_f} \right)^3$$

where ϕ_{fd} = fracture porosity after damage

ϕ_f = undamaged original fracture porosity

k_f = undamaged original fracture permeability, md
 k_{fd} = damaged fracture permeability, md

The productivity index of a fractured well J_F can be roughly approximated using the following simple expression:

$$J_F = J \left[\frac{\ln\left(\frac{r_e}{r_w}\right)}{\ln\left(\frac{r_e}{0.5x_f}\right)} \right]$$

where I = productivity index of the well before stimulation

r_w = wellbore radius

r_e = drainage radius

x_f = fracture half-length

There are four flow regimes, as shown conceptually in Figure 17-15, associated with the three types of vertical fractures:

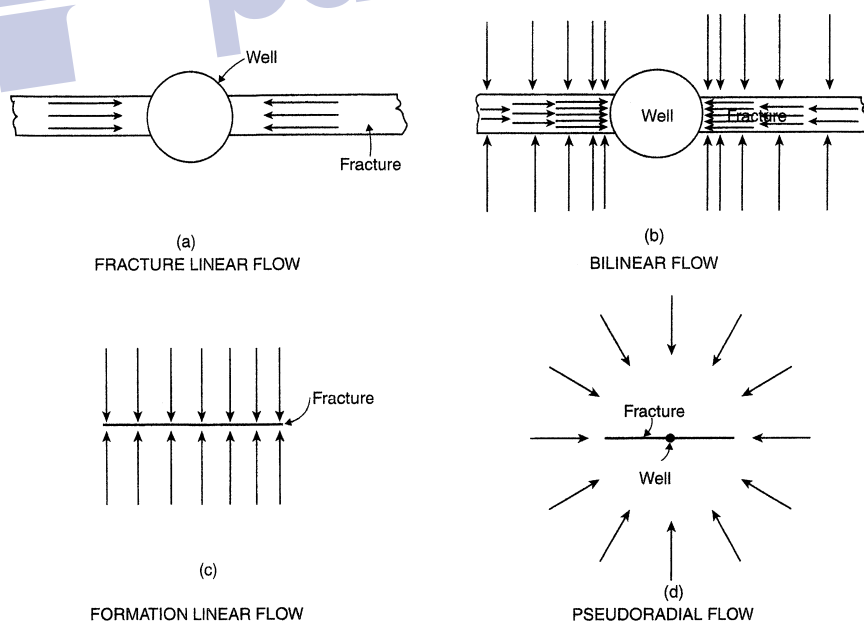


Figure 17-15. Flow periods for a vertically fractured well. (After Cinco and Samaniego, 1981.)

- Fracture linear flow
- Bilinear flow
- Formation linear flow
- Infinite acting pseudoradial flow

These successive flow patterns, often separated by transition periods, can be identified by expressing the pressure transient data in different types of graphs. Some of these graphs are excellent tools for diagnosis and identification of regimes since test data may correspond to different flow periods.

There are specialized graphs of analysis for each flow period that include:

- Graph of Δp versus $\sqrt{\text{time}}$ for linear flow
- Graph of Δp versus $\sqrt[4]{\text{time}}$ for bilinear flow
- Graph of Δp versus $\log(\text{time})$ for infinite acting pseudoradial flow

These types of flow regimes and the diagnostic plots are discussed below.

1. Fracture linear flow

This is the first flow period that occurs in a fractured system. Most of the fluid enters the wellbore during this period as a result of expansion within the fracture; that is, there is negligible fluid coming from the formation. Flow within the fracture and from the fracture to the wellbore during this period is a linear regime and can be described by the diffusivity equation as expressed in a linear form and is applied to both types of flow, i.e., the fracture linear flow and the formation linear flow periods. The pressure transient test data during the linear flow period can be analyzed with a graph of Δp versus $\sqrt{\text{time}}$. Unfortunately, the fracture linear flow occurs at a very early time to be of practical use in well test analyses. However, if the fracture linear flow exists (for fractures with $F_{CD} > 300$), the formation linear flow relationships as given by Equations 17-11 through 17-16 can be used in the exact manner to analyze the pressure data during the formation linear flow.

If fracture linear flow occurs, the flow period is short, as it often is in finite-conductivity fractures with $F_{CD} < 300$, and care must be taken not to misinterpret the early pressure data. It is common in this situation for skin effects or wellbore storage effects to alter pressures to the extent that

the linear flow straight line does not occur or is very difficult to recognize. If the early time slope is used in determining the fracture length, the slope m_{vf} will be erroneously high, the computed fracture length will be unrealistically small, and no quantitative information will be obtained about flow capacity in the fracture. Cinco and Samaniego (1981) observed that this fracture linear flow ends when:

$$t_{Dxf} \approx \frac{0.1(F_{CD})^2}{(\eta_{fD})^2}$$

Because the fracture linear flow period is extremely short, this flow period is often of no practical use in well test analyses.

2. Bilinear flow

This flow period is called bilinear flow because two types of linear flow occur simultaneously. As originally proposed by Cinco and Samaniego (1981), one flow is a linear incompressible flow within the fracture and the other is a linear compressible flow in the formation. Most of the fluid that enters the wellbore during this flow period comes from the formation. Fracture tip effects do not affect well behavior during bilinear flow, and, accordingly, it will not be possible to determine the fracture length from the well bilinear flow period data. However, the actual value of the fracture conductivity F_C can be determined during this flow period. The pressure drop through the fracture is significant for the finite-conductivity case and the bilinear flow behavior is observed; however, the *infinite-conductivity case does not exhibit bilinear flow behavior* because the pressure drop in the fracture is negligible. Thus, identification of the bilinear flow period is important for two reasons:

- It will not be possible to determine a unique fracture length from the well bilinear flow period data. If these data are used to determine the length of the fracture, they will produce a much smaller fracture length than the actual.
- The actual fracture conductivity $k_f w_f$ can be determined from the bilinear flow pressure data.

Cinco and Samaniego (1978, 1981) suggest that during this flow period, the change in the wellbore pressure can be described by the following expressions:

For fractured oil wells

-in terms of dimensionless pressure:

$$p_D = \left[\frac{2.451}{\sqrt{F_{CD}}} \right] (t_{Dxf})^{1/4} \quad (17-17)$$

Taking the logarithm of both sides of Equation 17-17 gives:

$$\log(p_D) = \log \left[\frac{2.451}{\sqrt{F_{CD}}} \right] + 1/4 \log(t_{Dxf}) \quad (17-18)$$

-in terms of pressure:

$$\Delta p = \left[\frac{44.1QB\mu}{h\sqrt{F_C}(\phi\mu c_t k)^{1/4}} \right] t^{1/4} \quad (17-19)$$

or equivalently:

$$\Delta p = m_{bf} t^{1/4}$$

Taking the logarithm of both sides of the above expression gives:

$$\log(\Delta p) = \log(m_{bf}) + \left(\frac{1}{4} \right) \log(t) \quad (17-20)$$

with the bilinear slope m_{bf} as given by:

$$m_{bf} = \left[\frac{44.1QB\mu}{h\sqrt{F_C}(\phi\mu c_t k)^{1/4}} \right]$$

where F_C is the fracture conductivity as defined by:

$$F_C = k_f w_f \quad (17-21)$$

For fractured gas wells

-in a dimensionless form:

$$m_D = \left[\frac{2.451}{\sqrt{F_{CD}}} \right] (t_{Dxf})^{1/4}$$

or

$$\log(m_D) = \log \left[\frac{2.451}{\sqrt{F_{CD}}} \right] + \left(\frac{1}{4} \right) \log(t_{Dxf}) \quad (17-22)$$

-in terms of $m(p)$:

$$\Delta m(p) = \left[\frac{444.6QT}{h\sqrt{F_C}(\phi\mu c_t k)^{1/4}} \right] t^{1/4} \quad (17-23)$$

or equivalently:

$$\Delta m(p) = m_{bf} t^{1/4}$$

Taking the logarithm of both sides gives:

$$\log[\Delta m(p)] = \log(m_{bf}) + \left(\frac{1}{4} \right) \log(t) \quad (17-24)$$

Equations 17-19 and 17-23 indicate that a plot of Δp or $\Delta m(p)$ versus $(\text{time})^{1/4}$ on a Cartesian scale would produce a straight line *passing through the origin* with a slope of m_{bf} (bilinear flow slope) as given by:

For oil

$$m_{bf} = \frac{44.1QB\mu}{h\sqrt{F_C}(\phi\mu c_t k)^{1/4}}$$

The slope can then be used to solve the fracture conductivity F_C , to give:

$$F_C = \left[\frac{44.1QB\mu}{m_{bf}h(\phi\mu c_t k)^{1/4}} \right]^2 \quad (17-25)$$

For gas

$$m_{bf} = \frac{444.6QT}{h\sqrt{F_C}(\phi\mu c_t k)^{1/4}}$$

or

$$F_C = \left[\frac{444.6QT}{m_{bf}h(\phi\mu c_t k)^{1/4}} \right]^2 \quad (17-26)$$

It should be noted that *if the straight-line plot does not pass through the origin*, it indicates an additional pressure drop Δp_s caused by flow restriction within the fracture in the vicinity of the wellbore (choked fracture, where the fracture permeability just away from the wellbore is reduced). Examples of restrictions that cause a loss of production are:

- Inadequate perforations
- Turbulent flow, which can be reduced by increasing the proppant size or concentration
- Overdisplacement of proppant
- Dumping of kill fluid into the fracture

Similarly, Equations 17-20 and 17-24 suggest that a plot of Δp or $\Delta m(p)$ versus (time) on a log–log scale would produce a straight line with a slope of $m_{bf} = 1/4$ and which can be used as a diagnostic tool for bilinear flow detection.

When the bilinear flow ends, the plot will exhibit curvature that could concave upward or downward depending upon the value of the dimensionless fracture conductivity F_{CD} , as shown in Figure 17-16. When the value of F_{CD} is ≤ 1.6 , the curve will concave downward and will concave upward if $F_{CD} > 1.6$. The upward trend indicates that the fracture tip begins to affect wellbore behavior. If the test is not run sufficiently long for bilinear flow to end when $F_{CD} > 1.6$, it is not possible to determine the length of the fracture. When the dimensionless fracture conductivity $F_{CD} \leq 1.6$, it indicates that the fluid flow in the reservoir has changed from a predominantly one-dimensional linear flow to a two-dimensional flow regime. In this particular case, it is not possible to uniquely determine fracture length even if bilinear flow does end during the test.

Cinco and Samaniego (1978, 1981) point out that the dimensionless fracture conductivity F_{CD} can be estimated from the bilinear flow straight line, i.e., Δp versus (time)^{1/4}, by reading the value of the pressure difference Δp at which the line ends Δp_{ebf} , and applying the following approximation:

$$\text{For oil: } F_{CD} = \frac{194.9QB\mu}{kh\Delta p_{ebf}} \quad (17-27)$$

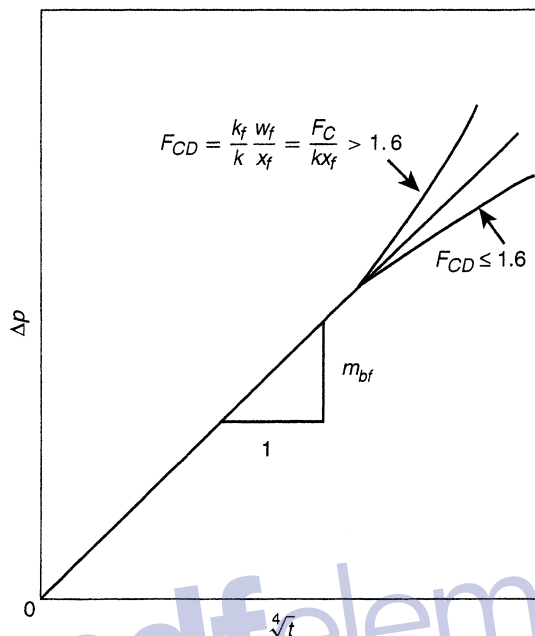


Figure 17-16. Graph for analysis of pressure data of bilinear flow. (After Cinco and Samaniego, 1981.)

$$\text{For gas: } F_{CD} = \frac{1965.1QT}{kh\Delta m(p)_{ebf}} \quad (17-28)$$

where Q = flow rate, STB/day or Mscf/day

T = temperature, °R

The end of the bilinear flow *ebf* straight line depends on the fracture conductivity and can be estimated from the following relationships:

$$\begin{aligned} \text{For } F_{CD} \geq 3: \quad t_{Debf} &\approx \frac{0.1}{(F_{CD})^2} \\ \text{For } 1.6 \leq F_{CD} \leq 3: \quad t_{Debf} &\approx 0.0205[F_{CD} - 1.5]^{-1.53} \\ \text{For } F_{CD} \leq 1.6: \quad t_{Debf} &\approx \left[\frac{4.55}{\sqrt{F_{CD}}} - 2.5 \right]^{-4} \end{aligned}$$

The procedure for analyzing the bilinear flow data is summarized by the following steps:

Step 1. Make a plot of Δp versus time on a log–log scale.

Step 2. Determine if any data fall on a straight line with a $1/4$ slope.

Step 3. If data points fall on a straight line with a $1/4$ slope, re-plot the data in terms of Δp versus $(\text{time})^{1/4}$ on a Cartesian scale and identify those data that form the bilinear straight line.

Step 4. Determine the slope of the bilinear straight line m_{bf} formed in Step 3.

Step 5. Calculate the fracture conductivity $F_C = k_f w_f$ from Equation 17-25 or 17-26, that is:

$$\text{For oil: } F_C = (k_f w_f) = \left[\frac{44.1QB\mu}{m_{bf}h(\phi\mu c_t k)^{1/4}} \right]^2$$

$$\text{For gas: } F_C = (k_f w_f) = \left[\frac{444.6QT}{m_{bf}h(\phi\mu c_t k)^{1/4}} \right]^2$$

Step 6. Read the value of the pressure difference at which the line ends Δp_{ebf} or $\Delta m(p)_{ebf}$.

Step 7. Approximate the dimensionless fracture conductivity from:

$$\text{For oil: } F_{CD} = \frac{194.9QB\mu}{kh\Delta p_{ebf}}$$

$$\text{For gas: } F_{CD} = \frac{1965.1QT}{kg\Delta m(p)_{ebf}}$$

Step 8. Estimate the fracture length from the mathematical definition of F_{CD} as expressed by Equation 17-13 and the value of F_C of Step 5:

$$x_f = \frac{F_C}{F_{CD}k}$$

Example 17-3

A buildup test was conducted on a fractured well producing from a tight gas reservoir. The following reservoir and well parameters are available:

| | |
|---------------------------------|--|
| $Q = 7350$ Mscf/day | $t_p = 2640$ hours |
| $h = 118$ ft | $\phi = 0.10$ |
| $k = 0.025$ md | $\mu = 0.0252$ |
| $T = 690^\circ\text{R}$ | $c_t = 0.129 \times 10^{-3}$ psi ⁻¹ |
| $P_{wf@\Delta t=0} = 1320$ psia | $r_w = 0.28$ ft |

The graphical presentation of the buildup data is given in terms of the log-log plot of $\Delta m(p)$ versus $(\Delta t)^{1/4}$, as shown in Figure 17-17.

Calculate the fracture and reservoir parameters by performing conventional steps.

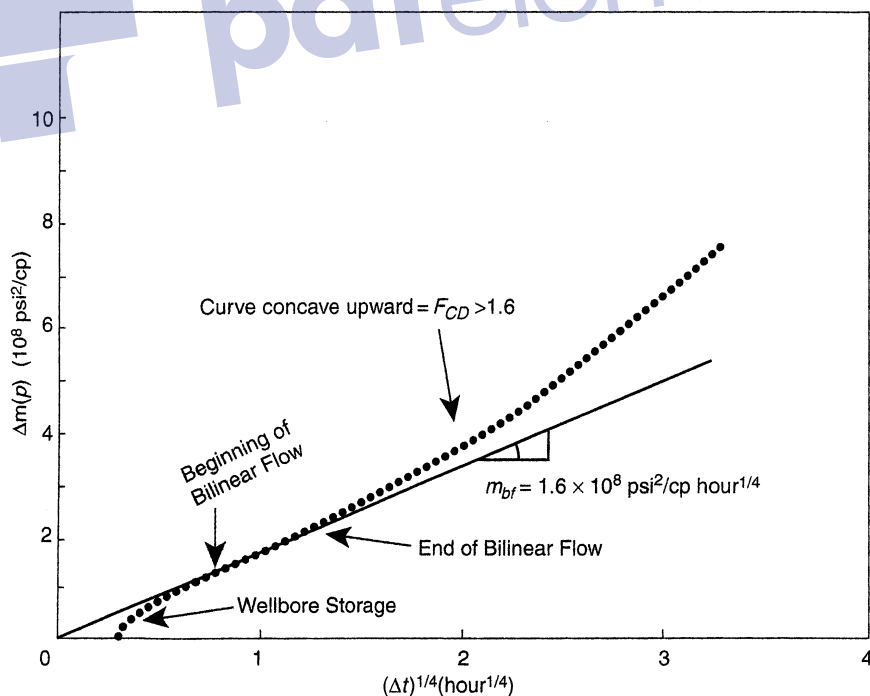


Figure 17-17. Bilinear flow graph for data of Example 1-36. (After Sabet, 1991.)

Solution

Step 1. From the plot of $\Delta m(p)$ versus $(\Delta t)^{1/4}$, in Figure 17-17, determine:

- $m_{bf} = 1.6 \times 10^8 \text{ psi}^2/\text{cp hour}^{1/4}$
- $t_{sbf} \approx 0.35 \text{ hours}$ (*start of bilinear flow*)
- $t_{ebf} \approx 2.5 \text{ hours}$ (*end of bilinear flow*)
- $\Delta m(p)_{ebf} \approx 2.05 \times 10^8 \text{ psi}^2/\text{cp}$

Step 2. Perform the bilinear flow analysis, to give:

- Using Equation 17-26, calculate fracture conductivity F_C .

$$F_C = \left[\frac{444.6QT}{m_{bf}h(\phi\mu c_r k)^{1/4}} \right]^2$$

$$F_C = \left[\frac{444.6(7350)(690)}{(1.62 \times 10^8)(118)[(0.1)(0.0252)(0.129 \times 10^{-3})(0.025)]^{1/4}} \right]^2$$

$$= 154 \text{ md ft}$$

- Calculate the dimensionless conductivity F_{CD} by using Equation 17-28.

$$F_{CD} = \frac{1965.1QT}{kh\Delta m(p)_{ebf}}$$

$$F_{CD} = \frac{1965.1(7350)(690)}{(0.025)(118)(2.02 \times 10^8)} = 16.7$$

- Estimate the fracture half-length from the following Equation

$$x_f = \frac{F_C}{F_{CD}k}$$

$$x_f = \frac{154}{(16.7)(0.025)} = 368 \text{ ft}$$

3. Formation linear flow

At the end of the bilinear flow, there is a transition period after which the fracture tips begin to affect the pressure behavior at the wellbore and a linear flow period might develop. This linear flow period is exhibited by vertical fractures whose dimensionless conductivity is greater than 300, i.e., $F_{CD} > 300$. As in the case of the fracture linear flow, the formation linear flow pressure data collected during this period is a function of the fracture length x_f and fracture conductivity F_C . The pressure behavior during this linear flow period can be described by the diffusivity equation as expressed in linear form, that is:

$$\frac{\partial^2 p}{\partial x^2} = \frac{\phi \mu c_t}{0.002637k} \frac{\partial p}{\partial t}$$

The solution to the above linear diffusivity equation can be applied to both the fracture linear flow and the formation linear flow, with the solution as given in a dimensionless form by:

$$p_D = (\pi t_{Dxf})^{1/2}$$

or in terms of real pressure and time, as:

$$\text{For oil fractured wells: } \Delta p = \left[\frac{4.064QB}{hx_f} \sqrt{\frac{\mu}{k\phi c_t}} \right] t^{1/2}$$

$$\text{In a simplified form as: } \Delta p = (p_{ws} - p_{wf @ \Delta t=0}) = m_{vf} \sqrt{t}$$

$$\text{For gas fractured wells: } \Delta m(p) = \left[\frac{40.925QT}{hx_f} \sqrt{\frac{1}{k\phi \mu c_t}} \right] t^{1/2}$$

$$\text{Equivalently as: } \Delta m(p) = m_{vf} \sqrt{t}$$

The linear flow period may be recognized by pressure data that exhibit a straight line of a half-slope on a log-log plot of Δp versus time, as illustrated in Figure 17-18. Another diagnostic presentation of pressure data points is the plot of Δp or $\Delta m(p)$ versus $\sqrt{\text{time}}$ on a Cartesian scale (as shown in Figure 17-19), which would produce a straight line with a slope of m_{vf} related to the fracture length by the following equations:

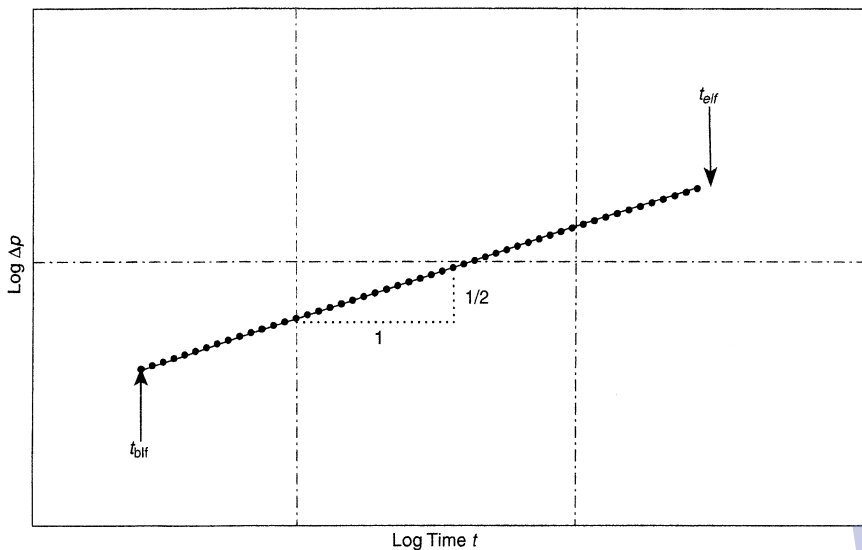


Figure 17-18. Pressure data for a $1/2$ -slope straight line in a log-log graph. (After Cinco and Samaniego, 1981.)

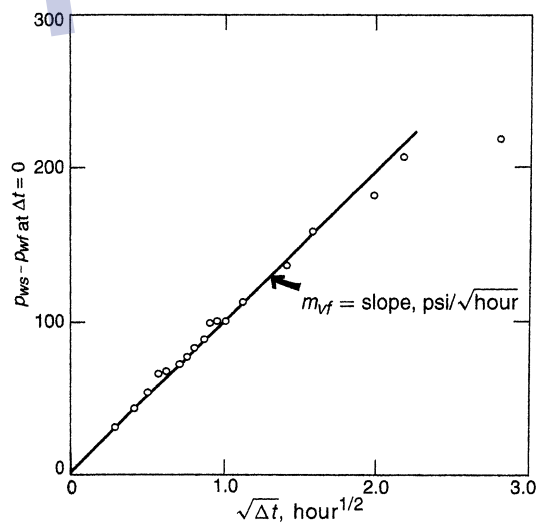


Figure 17-19. Square-root data plot for buildup test.

$$\text{Oil fractured well } x_f = \left[\frac{4.064QB}{m_{vf}h} \right] \sqrt{\frac{\mu}{k\phi c_t}} \quad (17-29)$$

$$\text{Gas fractured well } x_f = \left[\frac{40.925QT}{m_{vf}h} \right] \sqrt{\frac{1}{k\phi\mu c_t}} \quad (17-30)$$

where Q = flow rate, STB/day or Mscf/day

T = temperature, °R

m_{vf} = slope, psi/ $\sqrt{\text{hour}}$ or psi²/cp $\sqrt{\text{hour}}$

k = permeability, md

c_t = total compressibility, psi⁻¹

The straight-line relationships as illustrated by Figures 17-18 and 17-19 provide distinctive and easily recognizable evidence of a fracture. When properly applied, these plots are the best diagnostic tool available for detecting a fracture. In practice, the $1/2$ slope is rarely seen except in fractures with high conductivity. Finite-conductivity fracture responses generally enter a transition period after the bilinear flow (the $1/4$ slope) and reach the infinite acting pseudoradial flow regime before ever achieving a $1/2$ slope (linear flow). For a long duration of wellbore storage effect, the bilinear flow pressure behavior may be masked and data analysis becomes difficult with current interpretation methods.

Agarwal et al. (1979) point out that the pressure data during the transition display a curved portion before straightening to a line of proper slope that represents the fracture linear flow. The duration of the curved portion that represents the transition flow depends on the fracture flow capacity. The lower the fracture flow capacity, the longer the duration of the curved portion. The beginning of formation linear flow, *blf*, depends on F_{CD} and can be approximated from the following relationship:

$$t_{Dblf} \approx \frac{100}{(F_{CD})^2}$$

And the end of this linear flow period *elf* occurs at approximately:

$$t_{Dblf} \approx 0.016$$

Identifying the coordinates of these two points (i.e., beginning and end of the straight line) in terms of time can be used to estimate F_{CD} from:

$$F_{CD} \approx 0.0125 \sqrt{\frac{t_{elf}}{t_{blf}}}$$

where t_{elf} and t_{blf} are given in hours.

4. Infinite acting pseudoradial flow

During this period, the flow behavior is similar to the radial reservoir flow with a negative skin effect caused by the fracture. The traditional semilog and log-log plots of transient pressure data can be used during this period; for example, the drawdown pressure data can be analyzed by using Equations 6-170 through 6-174 of Chapter 6, that is:

$$p_{wf} = p_i - \frac{162.6Q_o B_o \mu}{kh} \left[\log(t) + \log\left(\frac{k}{\phi h c_t r_w^2}\right) - 3.23 + 0.87s \right]$$

or in a linear form as:

$$p_i - p_{wf} = \Delta p = a + m \log(t)$$

with the slope m of:

$$m = \frac{162.6Q_o B_o \mu_o}{kh}$$

Solving for the formation capacity gives:

$$kh = \frac{162.6Q_o B_o \mu_o}{|m|}$$

The skin factor s can be calculated by Equation 6-174:

$$s = 1.151 \left(\frac{p_i - p_{1hr}}{|m|} - \log\left(\frac{k}{\phi \mu c_t r_w^2}\right) + 3.23 \right)$$

If the semilog plot is made in terms of Δp versus t , notice that the slope m is the same when making the semilog plot in terms of p_{wf} versus t , then:

$$s = 1.151 \left(\frac{\Delta p_{1hr}}{|m|} - \log \left(\frac{k}{\phi \mu c_t r_w^2} \right) + 3.23 \right)$$

The Δp_{1hr} can then be calculated from the mathematical definition of the slope m , i.e., rise/run, by using two points on the semilog straight line (conveniently, one point could be Δp at $\log(10)$), to give:

$$m = \frac{\Delta p_{@ \log(10)} - \Delta p_{1hr}}{\log(10) - \log(1)}$$

Solving the above expression for Δp_{1hr} gives:

$$\Delta p_{1hr} = \Delta p_{@ \log(10)} - m \quad (17-31)$$

Again, $\Delta p_{@ \log(10)}$ must be read the corresponding point on the straight line at $\log(10)$ on the x-axis.

Wattenbarger and Ramey (1969) have shown that an approximate relationship exists between the pressure change Δp at the end of the linear flow, i.e., Δp_{elf} , and the beginning of the infinite acting pseudoradial flow Δp_{bsf} , as given by:

$$\Delta p_{bsf} \geq 2\Delta p_{elf} \quad (17-32)$$

The above rule is commonly referred to as the “double Δp rule” and can be obtained from the log–log plot when the $1/2$ slope ends and by reading the value of Δp , that is, Δp_{elf} , at this point. For fractured wells, doubling the value of Δp_{elf} will mark the beginning of the infinite acting pseudoradial flow period. Equivalently, a time rule referred to as the 10 Δt rule can be applied to mark the beginning of pseudoradial flow by:

$$\text{For drawdown: } t_{bsf} \geq 10 t_{elf} \quad (17-33)$$

$$\text{For buildup: } \Delta t_{bsf} \geq 10 \Delta t_{elf} \quad (17-34)$$

The above rule indicates that correct the infinite acting pseudoradial flow occurs 1 log cycle beyond the end of the linear flow. The concept of the above two rules is illustrated graphically in Figure 17-20.

Another approximation that can be used to mark the start of the infinite acting radial flow period for a finite-conductivity fracture is given by:

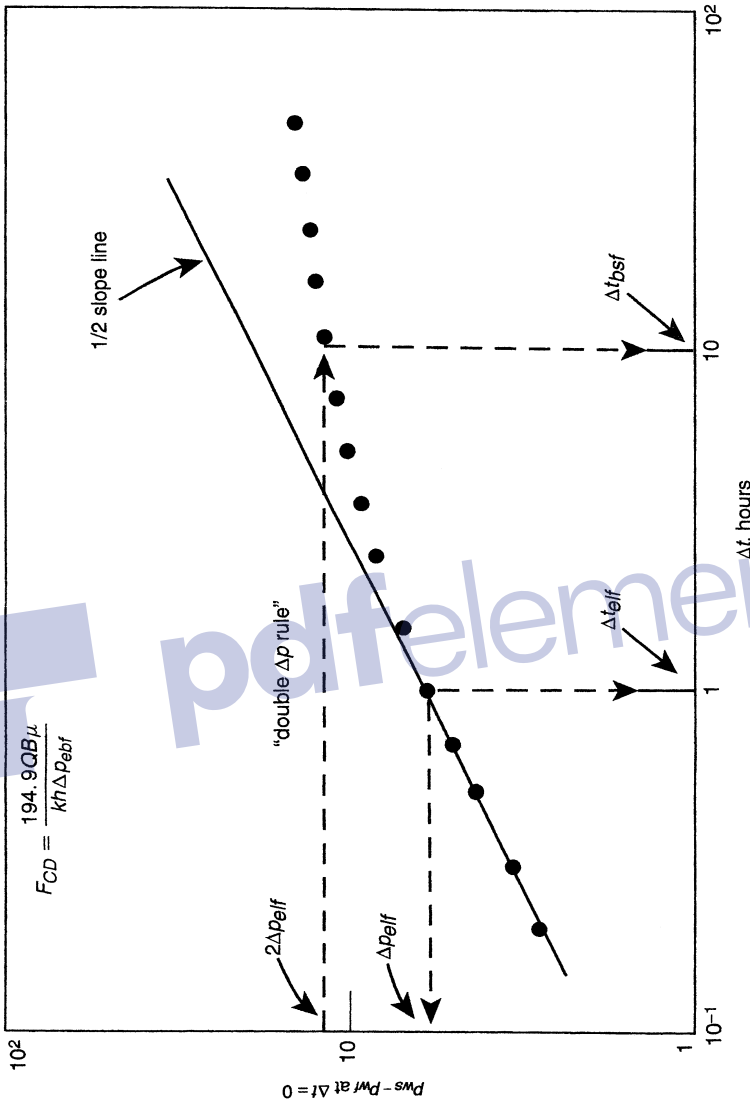


Figure 17-20. Use of the log-log plot to approximate the beginning of pseudoradial flow.

$$t_{Dbs} \approx 5 \exp [-0.5(F_{CD})^{-0.6}], \text{ for } F_{CD} \geq 0.1$$

Sabet (1991) used the following drawdown test data, as originally given by Gringarten et al. (1975), to illustrate the process of analyzing hydraulically fractured well test data.

Example 17-4

The drawdown test data for an infinite-conductivity fractured well are tabulated below:

| t (hour) | p_{wf} (psi) | Δp (psi) | \sqrt{t} hour ^{1/2} |
|------------|----------------|------------------|--------------------------------|
| 0.0833 | 3759.0 | 11.0 | 0.289 |
| 0.1670 | 3755.0 | 15.0 | 0.409 |
| 0.2500 | 3752.0 | 18.0 | 0.500 |
| 0.5000 | 3744.5 | 25.5 | 0.707 |
| 0.7500 | 3741.0 | 29.0 | 0.866 |
| 1.0000 | 3738.0 | 32.0 | 1.000 |
| 2.0000 | 3727.0 | 43.0 | 1.414 |
| 3.0000 | 3719.0 | 51.0 | 1.732 |
| 4.0000 | 3713.0 | 57.0 | 2.000 |
| 5.0000 | 3708.0 | 62.0 | 2.236 |
| 6.0000 | 3704.0 | 66.0 | 2.449 |
| 7.0000 | 3700.0 | 70.0 | 2.646 |
| 8.0000 | 3695.0 | 75.0 | 2.828 |
| 9.0000 | 3692.0 | 78.0 | 3.000 |
| 10.0000 | 3690.0 | 80.0 | 3.162 |
| 12.0000 | 3684.0 | 86.0 | 3.464 |
| 24.0000 | 3662.0 | 108.0 | 4.899 |
| 48.0000 | 3635.0 | 135.0 | 6.928 |
| 96.0000 | 3608.0 | 162.0 | 9.798 |
| 240.0000 | 3570.0 | 200.0 | 14.142 |

Additional reservoir parameters are:

$$\begin{aligned}
 h &= 82 \text{ ft} & \phi &= 0.12 \\
 c_t &= 21 \times 10^{-6} \text{ psi}^{-1} & \mu &= 0.65 \text{ cp} \\
 B_o &= 1.26 \text{ bbl/STB} & r_w &= 0.28 \text{ ft} \\
 Q &= 419 \text{ STB/day} & p_i &= 3770 \text{ psi}
 \end{aligned}$$

Estimate:

- Permeability k
- Fracture half-length x_f
- Skin factor s

Solution

Step 1. Plot:

- Δp versus t on a log-log scale, as shown in Figure 17-21
- Δp versus \sqrt{t} on a Cartesian scale, as shown in Figure 17-22
- Δp versus t on a semilog scale, as shown in Figure 17-23

Step 2. Draw a straight line through the early points representing $\log(\Delta p)$ versus $\log(t)$, as shown in Figure 17-21, and determine the slope

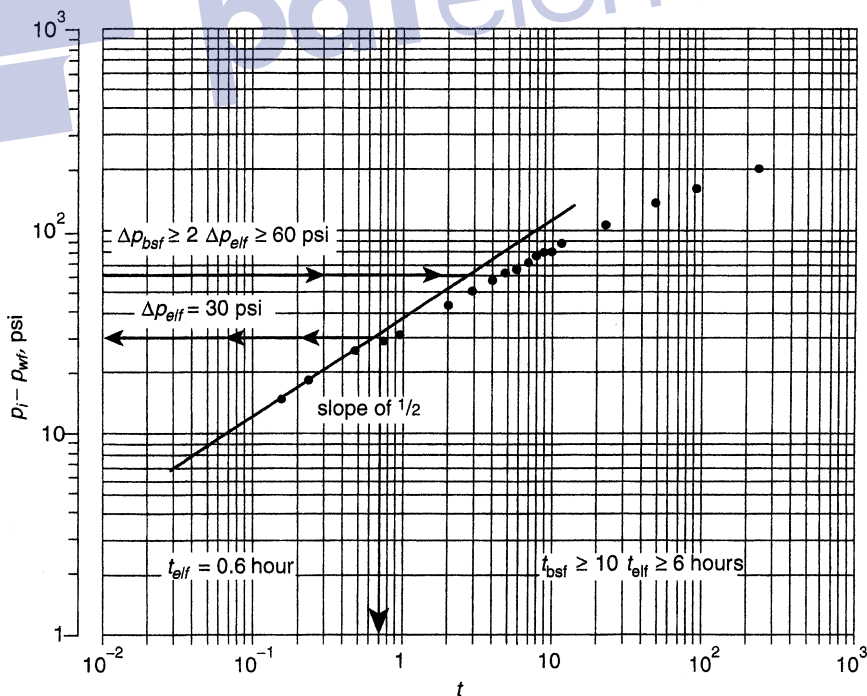


Figure 17-21. Log-log plot, drawdown test data.

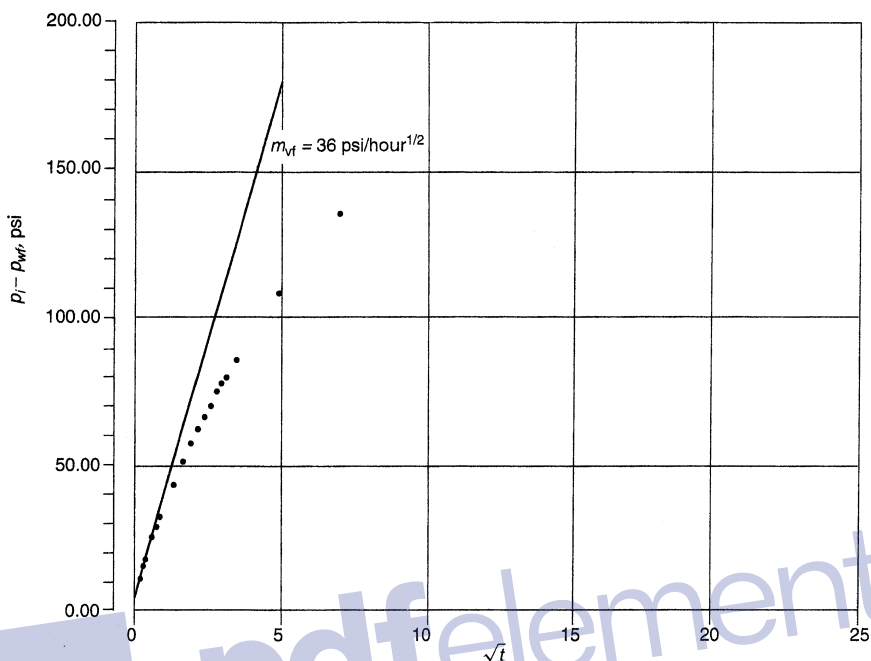


Figure 17-22. Linear flow graph, drawdown test data.

of the line. Figure 17-21 shows a slope of $1/2$ (not 45° angle), indicating linear flow with no wellbore storage effects. This linear flow lasted for approximately 0.6 hour, that is:

$$t_{\text{elf}} = 0.6 \text{ hour}$$

$$\Delta p_{\text{elf}} = 30 \text{ psi}$$

and therefore the beginning of the infinite acting pseudoradial flow can be approximated by the “double Δp rule” or “one-log cycle rule,” i.e., Equations 17-32 and 17-33, to give:

$$t_{\text{bsf}} \geq 10 t_{\text{elf}} \geq 6 \text{ hours}$$

$$\Delta p_{\text{bsf}} \geq 2 \Delta p_{\text{elf}} \geq 60 \text{ psi}$$

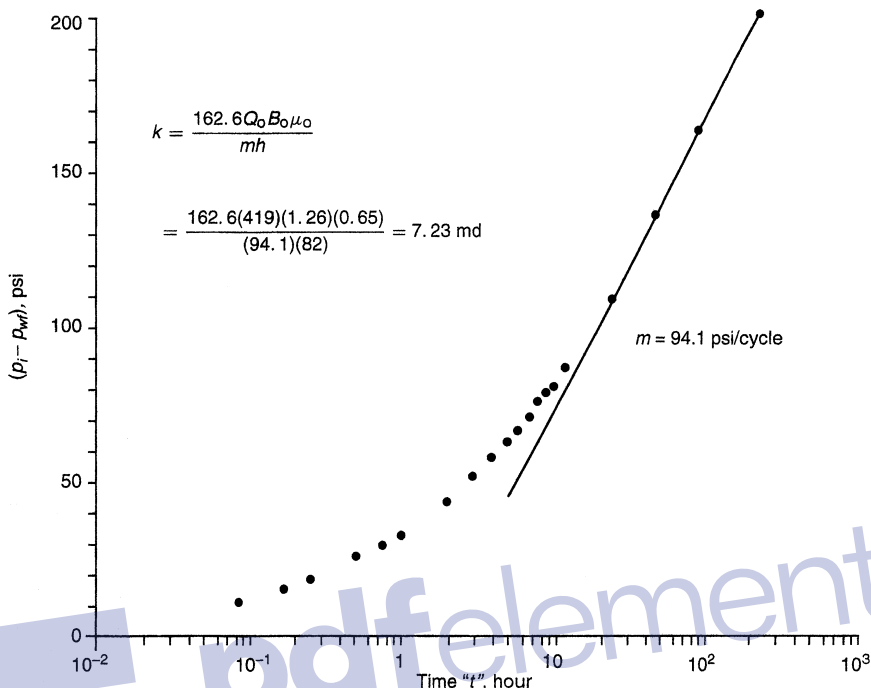


Figure 17-23. Semilog plot, drawdown test data.

Step 3. From the Cartesian scale plot of Δp versus \sqrt{t} , draw a straight line through the early pressure data points representing the first 0.3 hour of the test (as shown in Figure 17-22) and determine the slope of the line, to give:

$$m_{vf} = 36 \text{ psi/hour}^{1/2}$$

Step 4. Determine the slope of the semilog straight line representing the unsteady-state radial flow in Figure 17-23, to give:

$$m = 94.1 \text{ psi/cycle}$$

Step 5. Calculate the permeability k from the slope:

$$k = \frac{162.6 Q_o B_o \mu_o}{m h} = \frac{162.6(419)(1.26)(0.65)}{(94.1)(82)} = 7.23 \text{ md}$$

Step 6. Estimate the length of the fracture half-length from Equation 17-29, to give:

$$x_f = \left[\frac{4.064QB}{m_{vf}h} \right] \sqrt{\frac{\mu}{k\phi c_t}}$$

$$x_f = \left[\frac{4.064(419)(1.26)}{(36)(82)} \right] \sqrt{\frac{0.65}{(7.23)(0.12)(21 \times 10^{-6})}} = 137.3 \text{ ft}$$

Step 7. From the semilog straight line of Figure 17-23, determine Δp at $t = 10$ hours, to give:

$$\Delta p_{@ \Delta t=10} = 71.7 \text{ psi}$$

Step 8. Calculate Δp_{1hr} by applying Equation 17-31.

$$\Delta p_{1hr} = \Delta p_{@ \Delta t=10} - m = 71.7 - 94.1 = -22.4 \text{ psi}$$

Step 9. Solve for the "total" skin factor s , to give:

$$s = 1.151 \left(\frac{\Delta p_{1hr}}{|m|} - \log \left(\frac{k}{\phi \mu c_t r_w^2} \right) + 3.23 \right)$$

$$s = 1.151 \left[\frac{-22.4}{94.1} - \log \left(\frac{7.23}{0.12(0.65)(21 \times 10^{-6})(0.28)^2} \right) + 3.23 \right]$$

$$= -5.5$$

with an apparent wellbore ratio of:

$$r_w^{\lambda} = r_w e^{-s} = 0.28 e^{5.5} = 68.5 \text{ ft}$$

Notice that the *total* skin factor is a composite of effects that include:

$$s = s_d + s_f + s + s_p + s_{sw} + s_r$$

where s_d = skin due to formation and fracture damage
 s_f = skin due to the fracture, large negative value $s_f \ll 0$
 s_t = skin due to turbulence flow
 s_p = skin due to perforations
 s_w = skin due to slanted well
 s_r = skin due to restricted flow

For fractured oil well systems, several of the skin components are negligible or cannot be applied, mainly s_t , s_p , s_{sw} , and s_r ; therefore:

$$s = s_d + s_f$$

or

$$s_d = s - s_f$$

Smith and Cobb (1979) suggest that the best approach for evaluating damage in a fractured well is to use the square root plot. In an ideal well without damage, the square root straight line will extrapolate to p_{wf} at $\Delta t = 0$, i.e., $\Delta p_{wf@ \Delta t=0}$; however, when a well is damaged, the intercept pressure p_{int} will be greater than $p_{wf@ \Delta t=0}$, as illustrated in Figure 17-24. Note that the well shut-in pressure is described by:

$$p_{ws} = p_{wf@ \Delta t=0} + m_{vf} \sqrt{t}$$

Smith and Cobb point out that the total skin factor exclusive of s_f , i.e., $s - s_f$, can be determined from the square root plot by extrapolating the straight line to $\Delta t = 0$ and an intercept pressure p_{int} to give the pressure loss due to skin damage $(\Delta p_s)_d$ as:

$$(\Delta p_s)_d = p_{int} - p_{wf@ \Delta t=0} = \left[\frac{141.2QB\mu}{kh} \right] s_d$$

The above equation indicates that if $p_{int} = p_{wf@ \Delta t=0}$, then the skin due to fracture s_f is equal to the total skin.

It should be pointed out that the external boundary can distort the semilog straight line if the fracture half-length is greater than one-third of the drainage radius. The pressure behavior during this infinite acting period is highly dependent on the fracture length. For relatively short

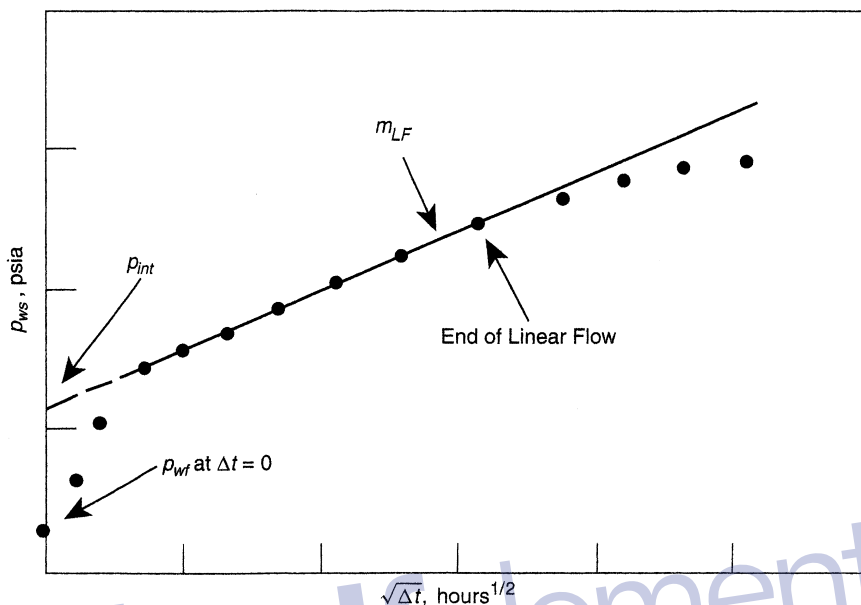


Figure 17-24. Effect of skin on the square root plot.

fractures, the flow is radial but becomes linear as the fracture length increases as it reaches the drainage radius. The external boundary can distort the semilog straight line if the fracture half-length is greater than one-third of the drainage radius. As noted by Russell and Truitt (1964), the slope obtained from the traditional well test analysis of fractured wells is erroneously too small and the calculated value of the slope progressively decreases with increasing fracture length. This dependence of the pressure response on fracture length is illustrated by the theoretical Horner buildup curves given by Russell and Truitt and shown in Figure 17-25. Defining the fracture penetration ratio x_f/x_e as the ratio of the fracture half-length x_f to the half-length x_e of a closed square-drainage area, Figure 17-25 shows the effects of fracture penetration on the slope of the buildup curve. For fractures of small penetration, the slope of the buildup curve is only slightly less than that for the unfractured *radial flow* case. However, the slope of the buildup curve becomes progressively smaller with increasing fracture penetrations. This will result in a calculated flow capacity kh that is too large, an erroneous average pressure, and a skin factor that is too small. Clearly, a modified method for analyzing and

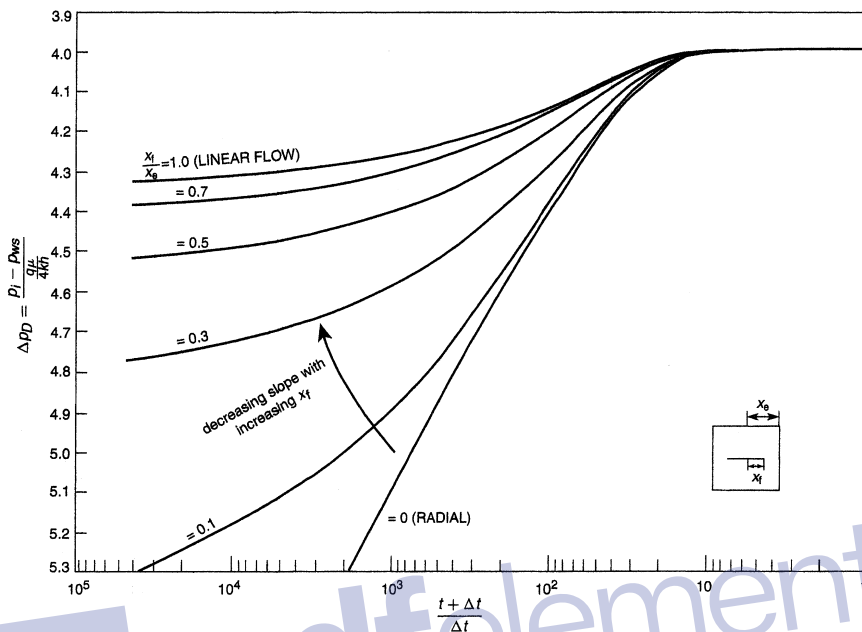


Figure 17-25. Vertically fractured reservoir, calculated pressure-buildup curves. (After Russell and Truitt, 1964.)

interpreting the data must be employed to account for the effect of fracture length on pressure response during the infinite acting flow period. Most of the published correction techniques require the use of iterative procedures. The type-curve matching approach and other specialized plotting techniques have been accepted by the oil industry as accurate and convenient approaches for analyzing pressure data from fractured wells, as briefly discussed below.

An alternate and convenient approach to analyzing fractured well transient test data is type-curve matching. The type-curve matching approach is used by plotting the pressure difference Δp versus time on the same scale as the selected type curve and matching one of the type curves. Gringarten et al. (1974) presented the type curves shown in Figures 17-26 and 17-27 for infinite-conductivity vertical fracture and uniform-flux vertical fracture, respectively, in a square well drainage area. Both figures present log-log plots of the dimensionless pressure drop p_d (equivalently referred to as dimensionless wellbore pressure p_{wd}) versus dimensionless time t_{Dxf} . The fracture solutions show an initial period controlled by linear flow where the pressure is a function of square root of time. On a log-log

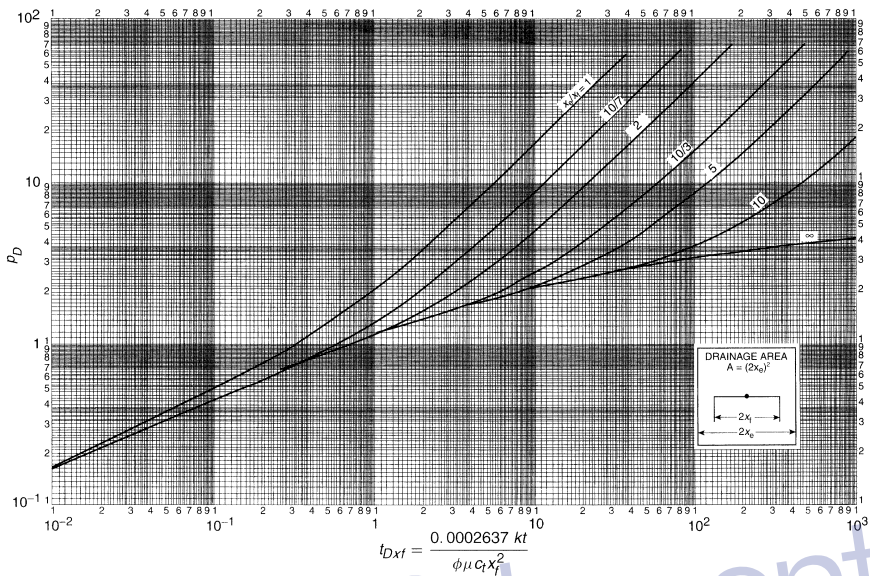


Figure 17-26. Dimensionless pressure for vertically fractured well in the center of a closed square, no wellbore storage, infinite-conductivity fracture. (After Gringarten et al., 1974.)

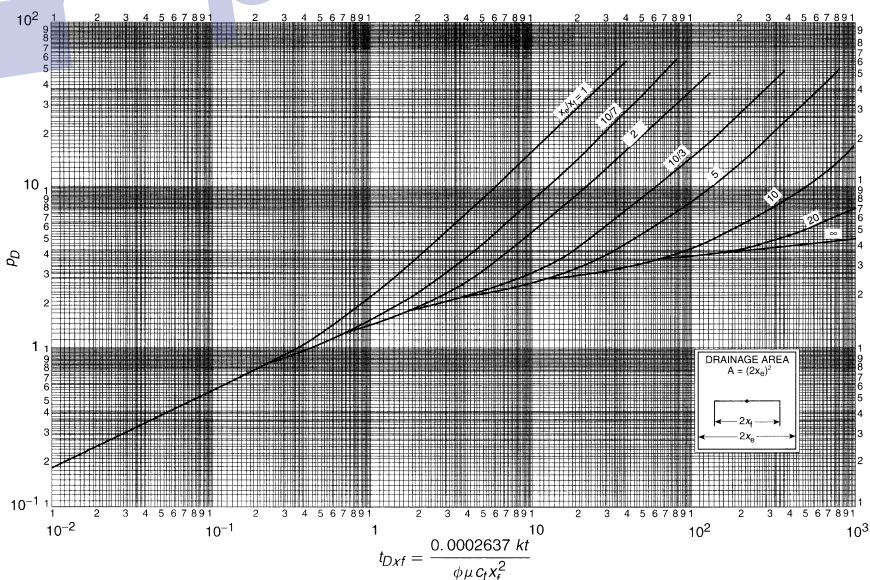


Figure 17-27. Dimensionless pressure for vertically fractured well in the center of a closed square, no wellbore storage, uniform-flux fracture. (After Gringarten et al., 1974.)

coordinate, as indicated before, this flow period is characterized by a straight line with $1/2$ slope. The infinite acting pseudoradial flow occurs at a t_{Dxf} between 1 and 3. Finally, all solutions reach pseudosteady-state.

During the matching process and when a match point is chosen, the dimensionless parameters on the axis of the type curve are used to estimate formation permeability and fracture length from:

$$k = \frac{141.2QB\mu}{h} \left[\frac{p_D}{\Delta p} \right]_{MP} \quad (17-35)$$

$$x_f = \sqrt{\frac{0.0002637k}{\phi\mu C_t} \left(\frac{\Delta t}{t_{Dxf}} \right)_{MP}} \quad (17-36)$$

For large ratios of x_e/x_f , Gringarten and his co-authors suggest that the apparent wellbore radius r'_w can be approximated from:

$$r'_w \approx \frac{x_f}{2} = r_w e^{-s}$$

Thus, the skin factor can be approximated from:

$$s = \ln \left(\frac{2r_w}{x_f} \right) \quad (17-37)$$

Earlougher (1977) points out that if all test data fall on the half-slope line on the $\log \Delta p$ versus \log (time), i.e., the test is not long enough to reach the infinite acting pseudoradial flow period, then the formation permeability k cannot be estimated by either type-curve matching or semilog plot. This situation often occurs in tight gas wells. However, the last point on the $1/2$ slope line, i.e., $(\Delta p)_{Last}$ and $(t)_{Last}$, may be used to estimate an upper limit of the permeability and a minimum fracture length from:

$$k \leq \frac{30.358QB\mu}{h(\Delta p)_{Last}} \quad (17-38)$$

$$x_f \geq \sqrt{\frac{0.01648k(t)_{Last}}{\phi\mu C_t}} \quad (17-39)$$

The two approximations above are only valid for $x_e/x_f \gg 1$ and for infinite-conductivity fractures. For uniform-flux fracture, the constants 30.358 and 0.01648 become 107.312 and 0.001648, respectively.

To illustrate the use of Gringarten–Ramey–Raghavan type curves in analyzing well test data, the following example is presented:

Example 17-5

The pressure-buildup data for an infinite-conductivity fractured well are tabulated below:

| Δt (hours) | P_{ws} | $P_{ws} - P_{wf@\Delta t=0}$ | $(i_p + \Delta t)\Delta t$ |
|--------------------|----------|------------------------------|----------------------------|
| 0.000 | 3420.0 | 0.0 | 0.0 |
| 0.083 | 3431.0 | 11.0 | 93,600.0 |
| 0.167 | 3435.0 | 15.0 | 46,700.0 |
| 0.250 | 3438.0 | 18.0 | 31,200.0 |
| 0.500 | 3444.5 | 24.5 | 15,600.0 |
| 0.750 | 3449.0 | 29.0 | 10,400.0 |
| 1.000 | 3542.0 | 32.0 | 7800.0 |
| 2.000 | 3463.0 | 43.0 | 3900.0 |
| 3.000 | 3471.0 | 51.0 | 2600.0 |
| 4.000 | 3477.0 | 57.0 | 1950.0 |
| 5.000 | 3482.0 | 62.0 | 1560.0 |
| 6.000 | 3486.0 | 66.0 | 1300.0 |
| 7.000 | 3490.0 | 70.0 | 1120.0 |
| 8.000 | 3495.0 | 75.0 | 976.0 |
| 9.000 | 3498.0 | 78.0 | 868.0 |
| 10.000 | 3500.0 | 80.0 | 781.0 |
| 12.000 | 3506.0 | 86.0 | 651.0 |
| 24.000 | 3528.0 | 108.0 | 326.0 |
| 36.000 | 3544.0 | 124.0 | 218.0 |
| 48.000 | 3555.0 | 135.0 | 164.0 |
| 60.000 | 3563.0 | 143.0 | 131.0 |
| 72.000 | 3570.0 | 150.0 | 109.0 |
| 96.000 | 3582.0 | 162.0 | 82.3 |
| 120.000 | 3590.0 | 170.0 | 66.0 |
| 144.000 | 3600.0 | 180.0 | 55.2 |
| 192.000 | 3610.0 | 190.0 | 41.6 |
| 240.000 | 3620.0 | 200.0 | 33.5 |

Other available data:

$$\begin{array}{ll}
 p_i = 3700 & r_w = 0.28 \text{ ft} \\
 \phi = 12\% & h = 82 \text{ ft} \\
 c_t = 21 \times 10^{-6} \text{ psi}^{-1} & \mu = 0.65 \text{ cp} \\
 B = 1.26 \text{ bbl/STB} & Q = 419 \text{ STB/day} \\
 t_p = 7800 \text{ hours} &
 \end{array}$$

Drainage area = 1600 acres (not fully developed)

Calculate:

- Permeability
- Fracture—half-length x_f
- Skin factor

Solution

Step 1. Plot Δp versus Δt on a tracing paper with the same scale as the Gringarten type curve of Figure 17-26. Superimpose the tracing paper on the type curve, as shown in Figure 17-28, with the following match points:

$$\begin{array}{l}
 (\Delta p)_{MP} = 100 \text{ psi} \\
 (\Delta p)_{MP} = 10 \text{ hours} \\
 (p_D)_{MP} = 1.22 \\
 (t_D)_{MP} = 0.68
 \end{array}$$

Step 2. Calculate k and x_f by using Equations 17-35 and 17-36.

$$\begin{aligned}
 k &= \frac{141.2QB\mu}{h} \left[\frac{p_D}{\Delta p} \right]_{MP} = \frac{(141.2)(419)(1.26)(0.65)}{(82)} \left[\frac{1.22}{100} \right] \\
 &= 7.21 \text{ md}
 \end{aligned}$$

$$\begin{aligned}
 x_f &= \sqrt{\frac{0.0002637k}{\phi\mu C_t} \left(\frac{\Delta t}{t_{Dxf}} \right)_{MP}} = \sqrt{\frac{0.0002637(7.21)}{(0.12)(0.65)(21 \times 10^{-6})} \left(\frac{10}{0.68} \right)} \\
 &= 131 \text{ ft}
 \end{aligned}$$

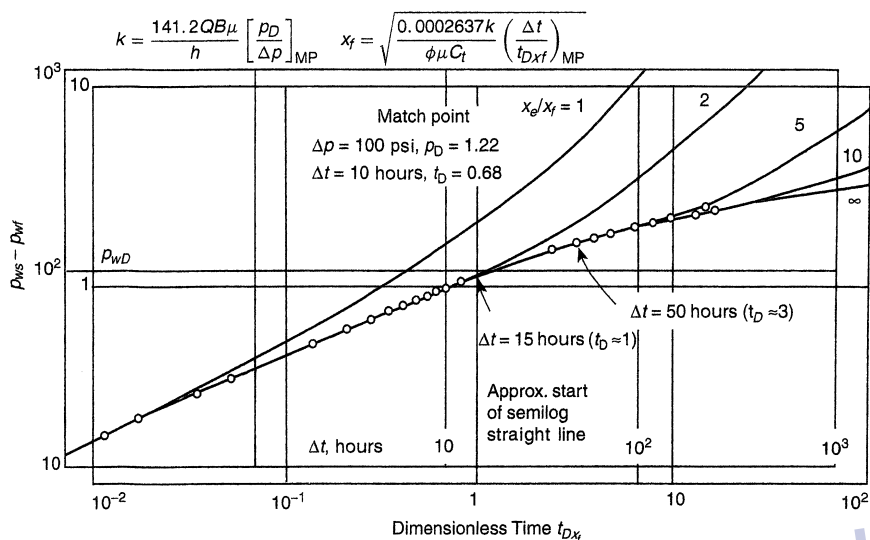


Figure 17-28. Type-curve matching. Data from Example 1-38. (Copyright © 1974 SPE, Gringarten et al., 1974.)

Step 3. Calculate the skin factor by applying Equation 17-37.

$$s = \ln\left(\frac{2r_w}{x_f}\right) = \ln\left[\frac{(2)(0.28)}{131}\right] = 5.46$$

Step 4. Approximate the time that marks the start of the semilog straight line based on the Gringarten et al. criterion, that is:

$$t_{Dxf} = \left[\frac{0.0002637k}{\phi\mu c_t x_f^2}\right] t \geq 3$$

or

$$t \geq \frac{(3)(0.12)(0.68)(21 \times 10^{-6})(131)^2}{(0.0002637)(7.21)} \geq 50 \text{ hours}$$

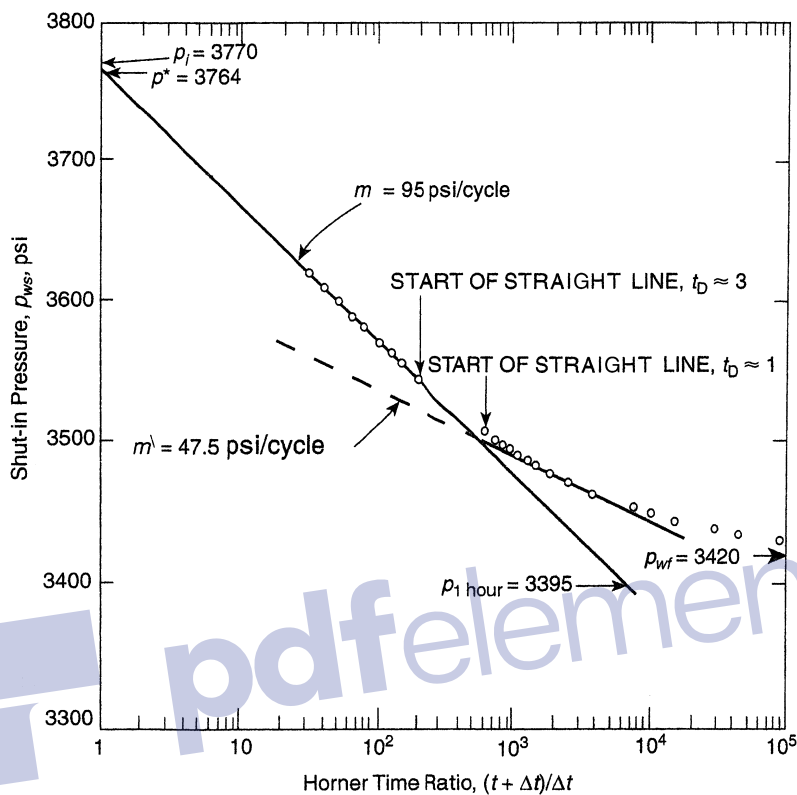


Figure 17-29. Horner graph for a vertical fracture (infinite conductivity).

All the data beyond 50 hours can be used in the conventional Horner plot approach to estimate permeability and skin factor. Figure 17-29 shows a Horner graph with the following results:

$$\begin{aligned}
 m &= 95 \text{ psi/cycle} \\
 p^* &= 3764 \text{ psi} \\
 p_{1 \text{ hr}} &= 3395 \text{ psi} \\
 k &= 7.16 \text{ md} \\
 s &= -5.5 \\
 x_f &= 137 \text{ ft}
 \end{aligned}$$

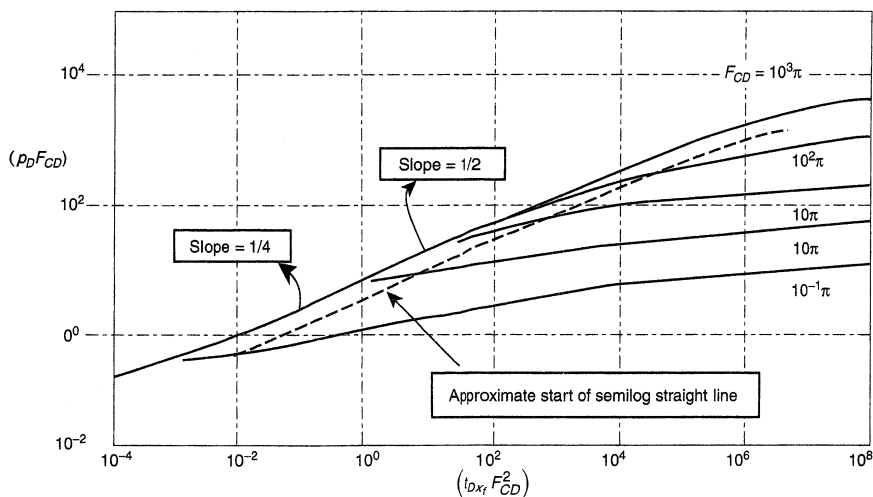


Figure 17-30. Type curve for vertically fractured gas wells graph. (After Cinco and Samaniego, 1981.)

Cinco and Samaniego (1981) developed the type curves shown in Figure 17-30 for finite-conductivity vertical fracture. The proposed type curve is based on the bilinear flow theory and presented in terms of $(p_D F_{CD})$ versus $(t_{Dxf} F_{CD}^2)$ on a log-log scale for various values of F_{CD} ranging from 0.1π to $1,000 \pi$. The main feature of this graph is that for all values of F_{CD} the behavior of the bilinear flow (quarter slope) and the formation linear flow (half-slope) is given by a single curve. Note that there is a transition period between the bilinear and linear flows. The dashed line in Figure 17-30 indicates the approximate start of the infinite acting pseudoradial flow.

The pressure data are plotted in terms of $\log(\Delta p)$ versus $\log(t)$, and the resulting graph is matched to a type curve that is characterized by a dimensionless finite conductivity $(F_{CD})_M$ with match points of:

- $(\Delta p)_{MP}$, $(p_D F_{CD})_{MP}$
- $(t)_{MP}$, $(t_{Dxf} F_{CD}^2)_{MP}$
- End of bilinear flow $(t_{ebf})_{MP}$
- Beginning of formation linear flow $(t_{bif})_{MP}$
- Beginning of semilog straight line $(t_{bssl})_{MP}$

From the above match calculate F_{CD} and x_f :

For oil

$$F_{CD} = \left[\frac{141.2QB\mu}{hk} \right] \frac{(p_D F_{CD})_{MP}}{(\Delta p)_{MP}} \quad (17-40)$$

For gas

$$F_{CD} = \left[\frac{1424QT}{hk} \right] \frac{(p_D F_{CD})_{MP}}{(\Delta m(p))_{MP}} \quad (17-41)$$

The fracture half-length is given by:

$$x_f = \left[\frac{0.0002637k}{\phi\mu c_t} \right] \frac{(t)_{mp} (F_{CD})_M^2}{(t_{Dxf} F_{CD}^2)_{MP}} \quad (17-42)$$

Defining the dimensionless effective wellbore radius r_{wD}^{\setminus} as the ratio of the apparent wellbore radius r_{wD}^{\setminus} to the fracture half-length x_f , i.e., $r_{wD}^{\setminus} = r_w^{\setminus} / x_f$, Cinco and Samaniego (1978, 1981) correlated with the dimensionless fracture conductivity F_{CD} and presented the resulting correlation in a graphical form, as shown in Figure 17-31.

Figure 17-31 indicates that when the dimensionless fracture conductivity is greater than 100, the dimensionless effective wellbore radius r_{wD}^{\setminus}

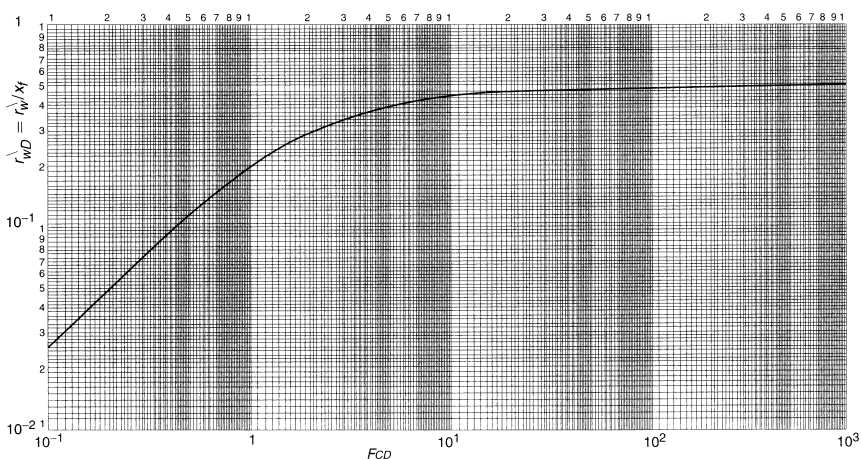


Figure 17-31. Effective wellbore radius versus dimensionless fracture conductivity for a vertical fracture graph. (After Cinco and Samaniego, 1981.)

is independent of the fracture conductivity, with a fixed value of 0.5, i.e., r_{wD}^{λ} for $F_{CD} > 100$. The apparent wellbore radius is expressed in terms of the fracture skin factor s_f by:

$$r_w^{\lambda} = r_w e^{-s_f}$$

Introducing r_{wD}^{λ} into the above expression and solving for s_f gives:

$$s_f = \ln \left[\left(\frac{x_f}{r_w} \right) r_{wD}^{\lambda} \right]$$

for $F_{CD} > 100$, gives:

$$s_f = -\ln \left(\frac{x_f}{2r_w} \right)$$

where s_f = skin due to fracture
 r_w = wellbore radius, ft

It should be kept in mind that specific analysis graphs must be used for different flow regimes to obtain a better estimate of both fracture and reservoir parameters. Cinco and Samaniego (1978, 1981) used the following pressure-buildup data to illustrate the use of their type curve in determining the fracture and reservoir parameters.

Example 17-6

Buildup test data as given in Example 17-3 are given below for convenience.

| | |
|---------------------------------|--|
| $Q = 7350$ Mscf/day | $t_p = 2640$ hours |
| $h = 118$ ft | $\phi = 0.10$ |
| $k = 0.025$ md | $\mu = 0.0252$ |
| $T = 690^\circ\text{R}$ | $c_t = 0.129 \times 10^{-3}$ psi ⁻¹ |
| $p_{wf@\Delta t=0} = 1320$ psia | $r_w = 0.28$ ft |

The graphical presentation of the buildup data is given in the following two forms:

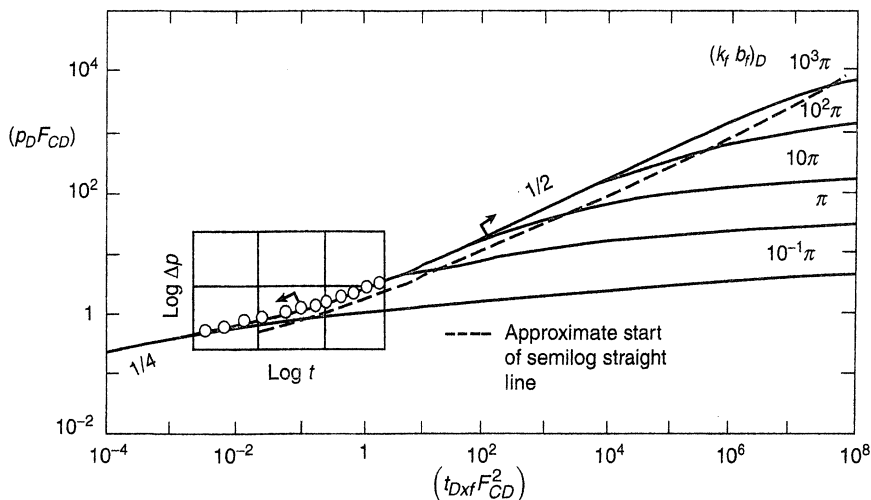


Figure 17-32. Type-curve matching for data in bilinear and transitional flow graph. (After Cinco and Samaniego, 1981.)

- the log–log plot of $\Delta m(p)$ versus $(\Delta t)^{1/4}$, as shown earlier in Figure 17-17,
- the log–log plot of $\Delta m(p)$ versus (Δt) , on the type curve of Figure 17-30, with the resulting match as shown in Figure 17-32.

Calculate the fracture and reservoir parameters by performing conventional and type-curve analyses. Compare the results.

Solution

Step 1. From the plot of $\Delta m(p)$ versus $(\Delta t)^{1/4}$, in Figure 17-17, determine:

- $m_{bf} = 1.6 \times 10^8 \text{ psi}^2/\text{cp hr}^{1/4}$
- $t_{sbf} \approx 0.35 \text{ hrs}$ (start of bilinear flow)
- $t_{ebf} \approx 2.5 \text{ hrs}$ (end of bilinear flow)
- $\Delta m(p)_{ebf} \approx 2.05 \times 10^8 \text{ psi}^2/\text{cp}$

Step 2. Perform the bilinear flow analysis, to give:

- Using Equation 17-26, calculate fracture conductivity F_C .

$$F_C = \left[\frac{444.6QT}{m_{bf} h (\phi \mu c_t k)^{1/4}} \right]^2$$

$$F_C = \left[\frac{444.6(7350)(690)}{(1.62 \times 10^8)(118)[(0.1)(0.0252)(0.129 \times 10^{-3})(0.025)]^{1/4}} \right]^2$$

$$= 154 \text{ md ft}$$

- Calculate the dimensionless conductivity F_{CD} by using Equation 17-28.

$$F_{CD} = \frac{1965.1QT}{kh\Delta m(p)_{\text{ebf}}}$$

$$F_{CD} = \frac{1965.1(7350)(690)}{(0.025)(118)(2.02 \times 10^8)} = 16.7$$

- Estimate the fracture half-length from the following Equation

$$x_f = \frac{F_C}{F_{CD}k}$$

$$x_f = \frac{154}{(16.7)(0.025)} = 368 \text{ ft}$$

- Estimate the dimensionless ratio r_w^λ/x_f from Figure 17-31.

$$\frac{r_w^\lambda}{x_f} \approx 0.46$$

- Calculate the apparent wellbore radius r_w^λ .

$$r_w^\lambda = (0.46)(368) = 169 \text{ ft}$$

- Calculate the apparent skin factor.

$$s = \ln\left(\frac{r_w}{r_w^\lambda}\right) = \ln\left(\frac{0.28}{169}\right) = -6.4$$

Step 3. Perform type-curve analysis:

- Determine match points from Figure 17-29, to give:

$$\Delta m(p)_{MP} = 10^9 \text{ psi}^2/\text{cp}$$

$$(p_D F_{CD})_{MP} = 6.5$$

$$(\Delta t)_{mp} = 1 \text{ hour}$$

$$[t_{Dxf}(F_{CD})^2]_{MP} = 3.69 \times 10^{-2}$$

$$t_{sbf} \approx 0.35 \text{ hour}$$

$$t_{cbf} = 2.5 \text{ hour}$$

- Calculate F_{CD} from Equation 17-41.

$$F_{CD} = \left[\frac{1424(7350)(690)}{(118)(0.025)} \right] \frac{6.5}{(10^9)} = 15.9$$

- Calculate the fracture half-length from Equation 17-42.

$$x_f = \left[\frac{0.0002637(0.025)}{(0.1)(0.0252)(0.129 \times 10^{-3})} \frac{(1)(15.9)^2}{3.69 \times 10^{-2}} \right]^{1/2} = 373 \text{ ft}$$

- Calculate F_C from Equation 17-13.

$$F_C = F_{CD} x_f k = (15.9) (373) (0.025) = 148 \text{ md ft}$$

- Figure 17-27 gives:

$$r_w^\lambda / x_f = 0.46$$

$$r_w^\lambda = (373) (0.46) = 172 \text{ ft}$$

| Test Results | Type-Curve Analysis | Bilinear Flow Analysis |
|---------------|---------------------|------------------------|
| F_C | 148.000 | 154.0 |
| x_f | 373.0 | 368.0 |
| F_{CD} | 15.900 | 16.7 |
| r_w^λ | 172.000 | 169.0 |

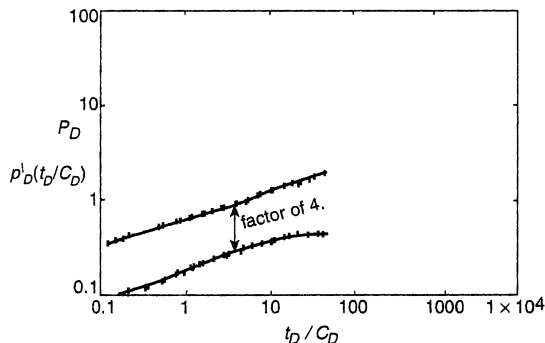


Figure 17-33. Finite-conductivity fracture shows as a $1/2$ slope line on a log-log plot, same on a derivative plot. Separation between pressure and derivative is a factor of 4.

The concept of pressure derivative can be effectively employed for identifying different flow regime periods associated with hydraulically fractured wells. As shown in Figure 17-33, a finite-conductivity fracture shows a $1/4$ straight-line slope for both the pressure difference Δp and its derivative; however, the two parallel lines are separated by a factor of 4. Similarly, for an infinite-conductivity fracture, the two parallel lines representing Δp and its derivative with a $1/2$ slope are separated by a factor of 2 (as shown in Figure 17-34).

In tight reservoirs where the productivity of wells is enhanced by MHF, the resulting fractures are characterized by long vertical fractures with finite conductivities. These wells tend to produce at a constant and low bottom-hole flowing pressure rather than at a constant flow rate. The diagnostic plots and the conventional analysis of bilinear flow data can be used when analyzing well test data under constant flowing pressure. Equations 17-18 through 17-23 can be rearranged and expressed in the following forms:

For fractured oil wells

$$\frac{1}{Q} = \left[\frac{44.1B\mu}{h\sqrt{F_c}(\phi\mu c_t k)^{1/4} \Delta p} \right] t^{1/4}$$

or equivalently:

$$\frac{1}{Q} = m_{br} t^{1/4}$$

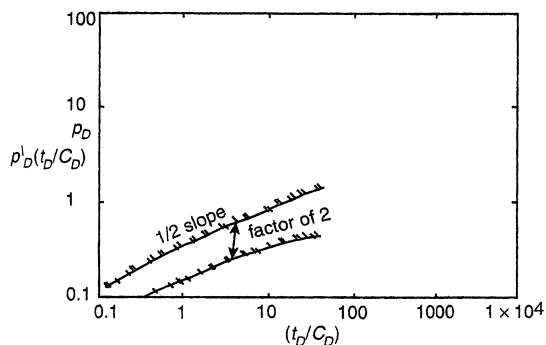


Figure 17-34. Infinite-conductivity fracture shows as a $1/2$ slope line on a log-log plot, same on a derivative plot. Separation between pressure and derivative is a factor of 2.

and

$$\log\left(\frac{1}{Q}\right) = \log(m_{bf}) + 1/4 \log(t)$$

where

$$m_{bf} = \frac{44.1B\mu}{h\sqrt{F_C}(\phi\mu c_t k)^{1/4} \Delta p}$$

$$F_C = k_f w_f = \left[\frac{44.1B\mu}{hm_{bf}(\phi\mu c_t k)^{1/2} \Delta p} \right]^2 \quad (17-43)$$

For fractured gas wells

$$\frac{1}{Q} = m_{bf} t^{1/4}$$

or

$$\log\left(\frac{1}{Q}\right) = \log(m)$$

where

$$m_{bf} = \frac{444.6T}{h\sqrt{F_C}(\phi\mu c_t k)^{1/4} \Delta m(p)}$$

solving for F_C :

$$F_C = \left[\frac{444.6T}{hm_{bf}(\phi\mu c_t k)^{1/4} \Delta m(p)} \right]^2 \quad (17-44)$$

The following procedure can be used to analyze bilinear flow data under a constant flow pressure:

Step 1. Plot $1/Q$ versus t on a log-log scale and determine if any data fall on a straight line of a $1/4$ slope.

Step 2. If any data form a $1/4$ slope in Step 1, plot $1/Q$ versus $t^{1/4}$ on a Cartesian paper and determine the slope m_{bf} .

Step 3. Calculate the fracture conductivity F_C from Equation 17-43 or 17-44:

For oil

$$F_C = \left[\frac{44.1B\mu}{hm_{bf}(\phi\mu c_t k)^{1/4} (p_i - p_{wf})} \right]^2$$

For gas

$$F_C = \left[\frac{444.6T}{hm_{bf}(\phi\mu c_t k)^{1/4} (m(p_i) - m(p_{wf}))} \right]^2$$

Step 4. Determine the value of Q when the bilinear straight line ends and designate it as Q_{ebf} .

Step 5. Calculate F_{CD} from Equation 17-27 or 17-28.

For oil

$$F_{CD} = \frac{194.9Q_{ebf} B\mu}{kh(p_i - p_{wf})}$$

For gas

$$F_{CD} = \frac{1965.1 Q_{cbf} T}{kh(m(p_i) - m(p_{wf}))}$$

Step 6. Estimate the fracture half-length from:

$$x_f = \frac{F_C}{F_{CD} k}$$

Agarwal et al. (1979) presented constant pressure type curves for finite-conductivity fractures, as shown in Figure 17-35. The reciprocal of the dimensionless rate $1/Q_D$ is expressed as a function of dimensionless time t_{Dxf} on a log-log paper, with the dimensionless fracture conductivity F_{CD} as a correlating parameter. The reciprocal dimensionless rate $1/Q_D$ is given by:

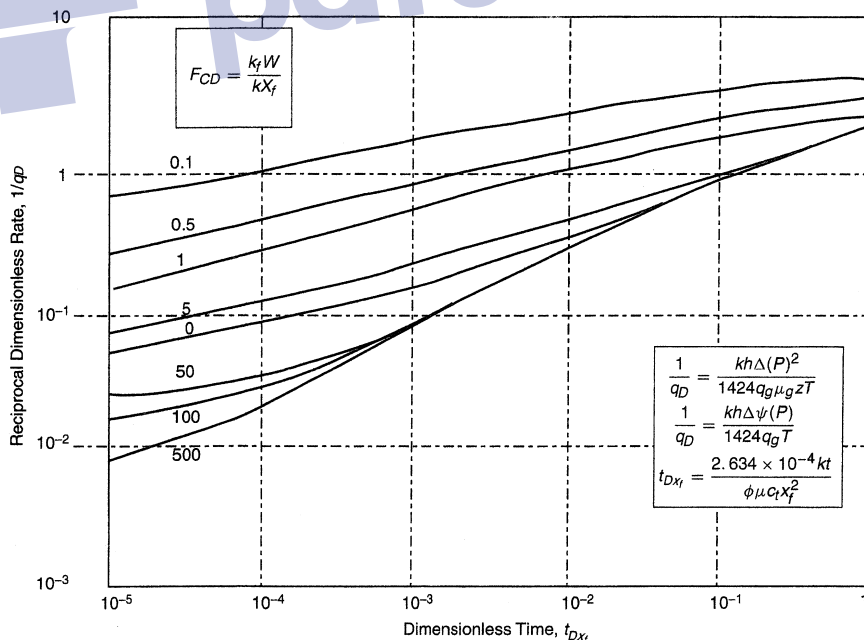


Figure 17-35. Log-log type curves for finite capacity vertical fractures; constant wellbore pressure. (After Agarwal et al., 1979.)

For oil wells

$$\frac{1}{Q_D} = \frac{kh(p_i - p_{wf})}{141.2Q\mu B} \quad (17-45)$$

For gas wells

$$\frac{1}{Q_D} = \frac{kh[m(p_i) - m(p_{wf})]}{1424QT} \quad (17-46)$$

with

$$t_{Dxf} = \frac{0.0002637kt}{\phi(\mu c_t)_i x_f^2} \quad (17-47)$$

where p_{wf} = wellbore pressure, psi

Q = flow rate, STB/day or Mscf/day

T = temperature, °R

t = time, hours

subscripts:

I = initial

D = dimensionless

The following example, as adopted from the Agarwal et al. (1979) paper, illustrates the use of these type curves:

Example 17-7

A prefracturing buildup test was performed on a well producing from a tight gas reservoir to give a formation permeability of 0.0081 md. Following an MHF treatment, the well produced at a constant pressure with recorded rate–time data as given below:

| t (days) | Q (Mscf/day) | 1/Q (day/Mscf) |
|----------|--------------|----------------|
| 20 | 625 | 0.00160 |
| 35 | 476 | 0.00210 |
| 50 | 408 | 0.00245 |
| 100 | 308 | 0.00325 |
| 150 | 250 | 0.00400 |
| 250 | 208 | 0.00481 |
| 300 | 192 | 0.00521 |

The following additional data are available:

$$\begin{array}{ll}
 p_i = 2394 & \Delta m(p) = 396 \times 10^6 \text{ psi}^2/\text{cp} \\
 h = 32 \text{ ft} & \phi = 0.107 \\
 T = 720^\circ R & c_{ti} = 2.34 \times 10^{-4} \text{ psi}^{-1} \\
 \mu_i = 0.0176 \text{ cp} & k = 0.0081 \text{ md}
 \end{array}$$

Calculate:

- Fracture half-length, x_f
- Fracture conductivity, F_C

Solution

Step 1. Plot $1/Q$ versus t on a tracing paper, as shown in Figure 17-36, using the log-log scale of the type curves.

Step 2. We must make use of the available values of k , h , and $\Delta m(p)$ by arbitrarily choosing a convenient value of the flow rate and calculating the corresponding $1/Q_D$. Selecting $Q = 1,000$ Mscf/day, calculate the corresponding value of $1/Q_D$ by applying Equation 6-273, to give:

$$\frac{1}{Q_D} = \frac{kh\Delta m(p)}{1424QT} = \frac{(0.0081)(32)(396 \times 10^6)}{1424(1000)(720)} = 0.1$$

Step 3. Thus, the position of $1/Q = 10^{-3}$ on the y-axis of the tracing paper is fixed in relation to $1/Q_D = 0.1$ on the y-axis of the type-curve graph paper, as shown in Figure 17-37.

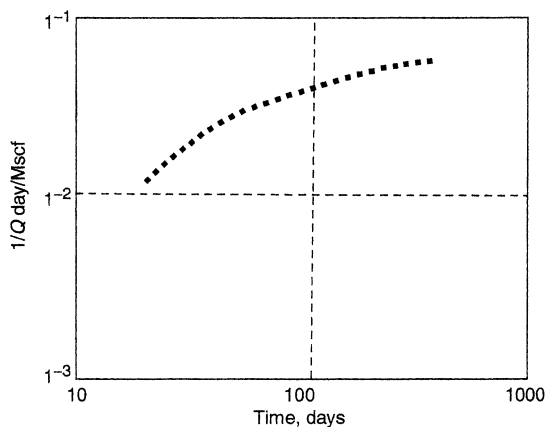


Figure 17-36. Reciprocal smooth rate versus time for MHF, Example 1-42.

Step 4. Move the tracing paper horizontally along the x-axis until a match is obtained, to give:

$$t = 100 \text{ days} = 2400 \text{ hours}$$

$$t_{Dxf} = 2.2 \times 10^{-2}$$

$$F_{CD} = 50$$

Step 5. Calculate the fracture half-length from Equation 17-47.

$$x_f^2 = \left[\frac{0.0002637k}{\phi(\mu c_i)_i} \right] \left(\frac{t}{t_{Dxf}} \right)_{MP}$$

$$x_f^2 = \left[\frac{0.0002637(0.0081)}{(0.107)(0.0176)(2.34 \times 10^{-4})} \right] \left(\frac{2400}{2.2 \times 10^{-2}} \right) = 258,174$$

$$x_f \approx 727 \text{ ft}$$

Thus, the total fracture length

$$2 x_f = 1454 \text{ ft}$$

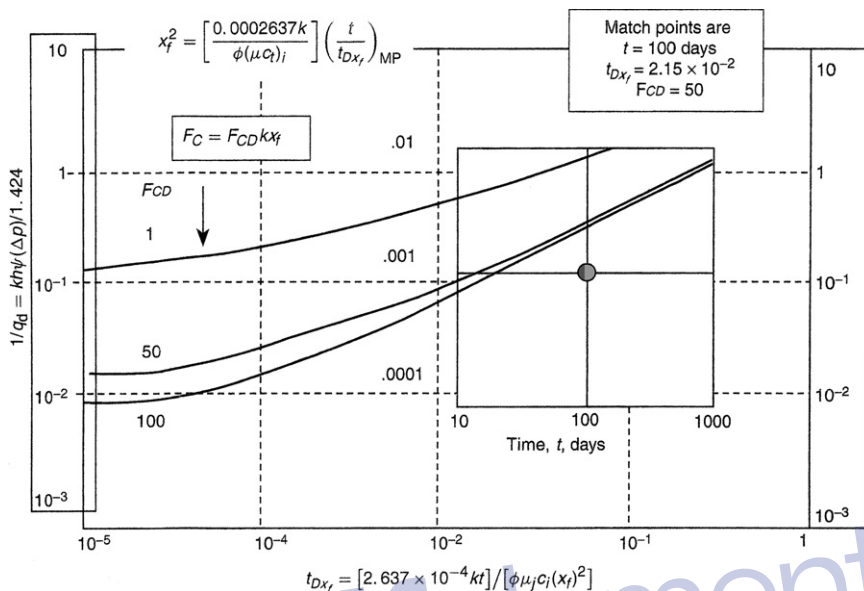


Figure 17-37. Type-curve matching for MHF gas well.

Step 6. Calculate the fracture conductivity F_C from Equation 17-13:

$$F_C = F_{CD} k x_f = (50) (0.0081) (727) = 294 \text{ md ft}$$

It should be pointed out that if the prefracturing buildup test were not available, matching would require shifting the tracing paper along both the x - and y -axes to obtain the proper match. This emphasizes the need for determining kh from a prefracturing test.

REFERENCES

- Abbaszadeh, M., and Kamal, M. M., "Pressure Transient Testing of Water Injection Wells," *SPE Reservoir Eng.*, February 1989, pp. 115–124.
- Agarwal, R. G., "Real Gas Pseudo-Time," SPE Paper 8279, Presented at 54th Annual Technical Conference and Exhibition of the Society of Petroleum Engineers of AIME, Las Vegas, NV, September 1979.
- Agarwal, R. G., "A New Method to Account for Producing Time Effects When Drawdown Type Curves Are Used to Analyze Pressure Buildup and Other Test Data," SPE Paper 9289, Presented at SPE-AIME 55th Annual Technical Conference, Dallas, TX, September 21–24, 1980.

- Agarwal, R. G., Al-Hussainy, R., and Ramey, H. J., Jr., "An Investigation of Wellbore Storage and Skin Effect in Unsteady Liquid Flow: I. Analytical Treatment," *Soc. Pet. Eng. J.*, September 1970, pp. 279–290.
- Agarwal, R. G., Carter, R. D., and Pollock, C. B., "Evaluation and Performance Prediction of Low-Permeability Gas Wells Stimulated by Massive Hydraulic Fracturing," *J. Pet. Tech.*, March 1979, pp. 362–372. Also in SPE Reprint Series No. 9.
- Aguilera, R., "Well Test Analysis of Naturally Fractured Reservoirs," *SPEFEJ*, September 1987, pp. 239–252.
- Al-Hussainy, R., and Ramey, H. J., Jr., "Application of Real Gas Flow Theory to Well Testing and Deliverability Forecasting," *J. Pet. Tech.* (May 1966). In *Theory and Practice of the Testing of Gas Wells*, 3rd ed. Calgary, Canada: Energy Resources Conservation Board, 1975.
- Al-Hussainy, R., Ramey, H. J., Jr., and Crawford, P. B., "The Flow of Real Gases through Porous Media," *Trans. AIME*, 1966, Vol. 237, p. 624.
- Bossie-Codreanu, D., "A Simple Buildup Analysis Method to Determine Well Drainage Area and Drawdown Pressure for a Stabilized Well," SPE Formation Evaluation, September 1989, pp. 418–420.
- Bourdet, D., and Alagoa, A., "New Method Enhances Well Test Interpretation," *World Oil*, September 1984, pp. 37–44.
- Bourdet, D., Alagoa, A., Ayoub, J. A., and Pirard, Y. M., "New Type Curves Aid Analysis of Fissured Zone Well Tests," *World Oil*, April 1984, pp. 111–124.
- Bourdet, D., and Gringarten, A. C., "Determination of Fissure Volume and Block Size in Fractured Reservoirs by Type-Curve Analysis," SPE Paper 9293, Presented at the Annual Technical Conference and Exhibition, Dallas, TX, September 21–24, 1980.
- Bourdet, D., SPE Paper 13628. Presented at the SPE regional meeting in Bakersfield, CA, March 27–29, 1989.
- Bourdet, D., Whittle, T. M., Douglas, A. A., and Pirard, Y. M., "A New Set of Type Curves Simplifies Well Test Analysis," *World Oil*, May 1983, pp. 95–106.
- Chatas, A. T., "A Practical Treatment of Nonsteady-State Flow Problems in Reservoir Systems," *Pet. Eng.*, August 1953, B-44–56.
- Cheng, M. C. Aaron, "A Simple Technique to Determine the Unknown Constant in y or x for Producing y vs. x as a Straight Line in Reservoir Engineering Problems," *J. Pet. Tech.*, May 1982, pp. 1140–1142.
- Cinco, H., and Samaniego, F., "Effect of Wellbore Storage and Damage on the Transient Pressure Behavior for a Well with a Finite Conductivity Vertical Fractures," *SPEJ*, August 1978, pp. 253–266.

- Cinco, H., and Samaniego, F., "Transient Pressure Analysis for Finite Conductivity Fracture Case versus Damage Fracture Case," Soc. Pet. Eng. Paper 10179, 1981.
- Cobb, W. M., Ramey, H. J., Jr., and Miller, F. G., "Well Test Analysis for Wells Producing Commingled Zones," *J. Pet. Tech.*, January 1972, Vol. 24, pp. 27–37.
- Cook, C.E., "Conductivity of Fracture Proppants in Multiple Layers," SPE 4117, *JPT*, May 1973.
- Craft, B., and Hawkins, M., *Applied Petroleum Reservoir Engineering*, Englewood Cliffs, NJ: Prentice-Hall, 1959.
- Craft, B., and Hawkins, M., and Terry, R., *Applied Petroleum Reservoir Engineering*, 2nd ed. Englewood Cliffs, NJ: Prentice Hall, 1990.
- Culham, W. E., "Pressure Buildup Equations for Spherical Flow Regime Problems," *Soc. Pet. Eng. J.*, December 1974, pp. 545–555.
- Dake, L., *Fundamentals of Reservoir Engineering*. Amsterdam: Elsevier, 1978.
- Dake, L. P., *The Practice of Reservoir Engineering*. Amsterdam: Elsevier, 1994.
- Davis, D. H., "Reduction in Permeability with Overburden Pressure," *Trans. AIME*, 1952, Vol. 195, p. 329.
- deSwaan, A., "Analytic Solutions for Determining Naturally Fractured Reservoir Properties by Well Testing," *Soc. Pet. Eng. J.*, June 1976, pp. 117–122.
- Dietz, D. N., "Determination of Average Reservoir Pressure from Buildup Surveys," *J. Pet. Tech.*, Aug. 1965, pp. 955–959; *Trans. AIME*, Vol. 234.
- Donohue, D., and Erkekin, T., "Gas Well Testing, Theory and Practice," *IHRDC*, 1982.
- Earlougher, R. C., Jr., "Advances in Well Test Analysis," Monograph Vol. 5, Society of Petroleum Engineers of AIME, Dallas, TX: Millet the Printer, 1977.
- Earlougher, R. C., Jr., Kersch, K. M., and Kunzman, W. J., "Some Characteristics of Pressure Buildup Behavior in Bounded Multiple Layer Reservoirs without Crossflow," *Jour. Pet. Tech.*, October 1974, pp. 1178–1186.
- Earlougher, R. C., Jr., Ramey, H. J., Jr., Miller, F. G., and Mueller, T. D., "Pressure Distributions in Rectangular Reservoirs," *J. Pet. Tech.*, February 1968, pp. 199–208.
- Economides, C., "Use of the Pressure Derivative for Diagnosing Pressure-Transient Behavior," *JPT*, October 1988.
- Environmental Protection Agency (EPA), "Evaluation of Impacts to Underground Sources of Drinking Water by Hydraulic Fracturing of Coalbed Methane Reservoirs," EPA 816-R-04-003 Report, June 2004.

- van Everdingen, A. F., "The Skin Effect and Its Influence on the Productive Capacity of a Well," *Trans. AIME*, 1953, p. 171.
- van Everdingen, A. F., and Hurst, W., "The Application of the Laplace Transformation to Flow Problems in Reservoirs," *Trans. AIME*, 1949, pp. 186, 305–324.
- Fetkovich, M. J., "The Isochronal Testing of Oil Wells," Paper 4529, Presented at the SPE Annual Meeting, Las Vegas, NV, September 30–October 3, 1973.
- Gilman, J., and Kazemi, H., "Improvements in Simulation of Naturally Fractured Reservoirs," *SPEJ*, August 1983, pp. 695–707.
- Golan, M., and Whitson, C., *Well Performance*, 2nd ed. Englewood Cliffs, NJ: Prentice-Hall, 1986.
- Gringarten, A. C., Bourdet, D. P., Landel, P. A., and Kniazeff, V. J., "A Comparison between Different Skin and Wellbore Storage Type-Curves for Early Time Transient Analysis," SPE Paper 8205, Presented at SPE-AIME 54th Annual Technical Conference, Las Vegas, NV, September 23–25, 1979.
- Gringarten, A. C., Ramey, H. J., Jr., and Raghavan, R., "Unsteady-State Pressure Distributions Created by a Well with a Single Infinite-Conductivity Vertical Fracture," *Soc. Pet. Eng. J.*, August 1974, pp. 347–360.
- Gringarten, A. C., Ramey, H. J., Jr., and Raghavan, R., "Applied Pressure Analysis for Fractured Wells," *J. Pet. Tech.*, July 1975, pp. 887–892.
- Gringarten, A., "Interpretation of Test in Fissured and Multilayered Reservoirs with Double-Porosity Behavior." *JPT*, April, 1984.
- Hassan, A. R., and Kabir, C. S., "Pressure Buildup Analysis: A Simplified Approach," *J. Pet. Tech.*, January 1983, pp. 178–188.
- Horner, D. R., "Pressure Build-Up in Wells," Proc. Third World Pet. Cong., The Hague, 1951, Sec II, 503–523. Also in Reprint Series, No. 9—Pressure Analysis Methods, Society of Petroleum Engineers of AIME, Dallas, TX, 1967, pp. 25–43.
- Hurst, W., "Establishment of the Skin Effect and Its Impediment to Fluid Flow into a Wellbore," *Pet. Eng.*, 1953, Vol. 25, B-6.
- Jargon, J. R., "Effect of Wellbore Storage and Wellbore Damage at the Active Well on Interference Test Analysis," *J. Pet. Tech.*, August 1976, pp. 851–858.
- Jones, S. C., "Using the Inertial Coefficient, b , to Characterize Heterogeneity in Reservoir Rock," Paper SPE 16949, Presented at the 1987 SPE Conference, Dallas, TX, September 27–30.
- Joshi, S., *Horizontal Well Technology*, Pennwell Publishing Company, Tulsa, OK, 1991.

- Kamal, M., and Bigham, W. E., "Pulse Testing Response for Unequal Pulse and Shut-in Periods," *Soc. Pet. Eng. J.*, October 1975, pp. 399–410.
- Kamal, M., Freyder, D., Murray, M., "Use of Transient Testing in Reservoir Management," *JPT*, November 1995.
- Kazemi, H., "Pressure Transient Analysis of Naturally Fractured Reservoirs with Uniform Fracture Distribution," *Soc. Pet. Eng. J.*, December 1969, pp. 451–462.
- Kazemi, H., "Pressure Buildup in Reservoir Limit Testing of Stratified Systems," *J. Pet. Tech.*, April 1970, pp. 503–511; *Trans. AIME*, Vol. 249.
- Kazemi, H., Merrill, L. S., Jr., and Jargon, J. R., "Problems in Interpretation of Pressure Falloff Tests in Reservoirs With and Without Fluid Banks," *J. Pet. Tech.*, September 1972, pp. 1147–1156.
- Kucuk, F., Karakas, M., and Ayestaran, L., "Well Testing and Analysis Techniques for Layered Reservoirs," *SPEFE*, August 1986, pp. 335–341.
- Lee, J. W., *Well Testing*. Dallas, TX: Society of Petroleum Engineers, 1982.
- Lee, J., and Wattenbarger, R., *Gas Reservoir Engineering*. SPE Textbook, Series Vol. 5, SPE, 1996.
- Matthews, C. S., Brons, F., and Hazebroek, P., "A Method for Determination of Average Pressure in a Bounded Reservoir," *Trans. AIME*, Vol. 201, 1954, pp. 182–191. Also in SPE Reprint Series No. 9.
- Matthews, C. S., and Russell, D. G., "Pressure Buildup and Flow Tests in Wells," Monograph Vol. 1, Society of Petroleum Engineers of AIME, Dallas, TX: Millet the Printer, 1967.
- Meunier, D., Wittmann, M. J., and Stewart, G., "Interpretation of Pressure Buildup Test Using In-Situ Measurement of Afterflow," *Jour. Pet. Tech.*, January 1985, pp. 143–152.
- Merrill, L. S., Kazemi, H., and Cogarty, W. B., "Pressure Falloff Analysis in Reservoirs with Fluid Banks," *J. Pet. Tech.*, July 1974, pp. 809–818.
- Miller, C. C., Dyes, A. B., and Hutchinson, C. A., Jr., "The Estimation of Permeability and Reservoir Pressure from Bottom Hole Pressure Buildup Characteristics," *Trans. AIME*, Vol. 189, 1950, pp. 91–104. Also in SPE Reprint Series No. 9.
- Najurieta, H. L., "A Theory for Pressure Transient Analysis in Naturally Fractured Reservoirs," *J. Pet. Tech.*, July 1980, pp. 1241–1250.
- Ramirez, B., Kazemi, H., Ozkan, E., and Atan, S. "A Critical Review for Proper Use of Water/Oil/Gas Transfer Functions in Dual-Porosity NFR," SPE Paper 109295. Presented at the SPE Annual Technical Conference, 11–14 November 2007, Anaheim, CA.

- Russell, D. G., Goodrich, J. H., Perry, G. E., and Bruskotter, J. F., "Methods for Predicting Gas Well Performance," *J. Pet. Tech.*, January 1966, pp. 99–108.
- Russell, D., and Truitt, N., "Transient Pressure Behavior in Vertically Fractured Reservoirs," *JPT*, October 1964.
- Sabet, M. A., *Well Test Analysis*, Gulf Publishing Company, 1991.
- Sabet, M. A., *Well Test Analysis*, Volume 8: Gulf Publishing Company, 1991.
- Shanley, K., Cluff, R., and Robinson, J., "Factors Controlling Prolific Gas Production from Low Permeability Sandstone," *APPG Bulletin*, August 2004, pp. 1083–1121.
- Slider, H. C., *Practical Petroleum Reservoir Engineering Methods*. Tulsa, OK: Petroleum Publishing Co., 1976.
- Smith, J., and Cobb, W., "Pressure Buildup Test in Bounded Reservoirs," *JPT*, August 1979.
- Warren, J. E., and Root, P. J., "The Behavior of Naturally Fractured Reservoirs," *Soc. Pet. Eng. J.*, September 1986, pp. 245–255.
- Wattenbarger, Robert A., and Ramey, H. J., Jr., "Gas Well Testing with Turbulence. Damage and Wellbore Storage," *J. Pet. Tech.*, 1968, pp. 877–887; *Trans. AIME*, p. 243.

APPENDIX

PRESSURE, PSIA →

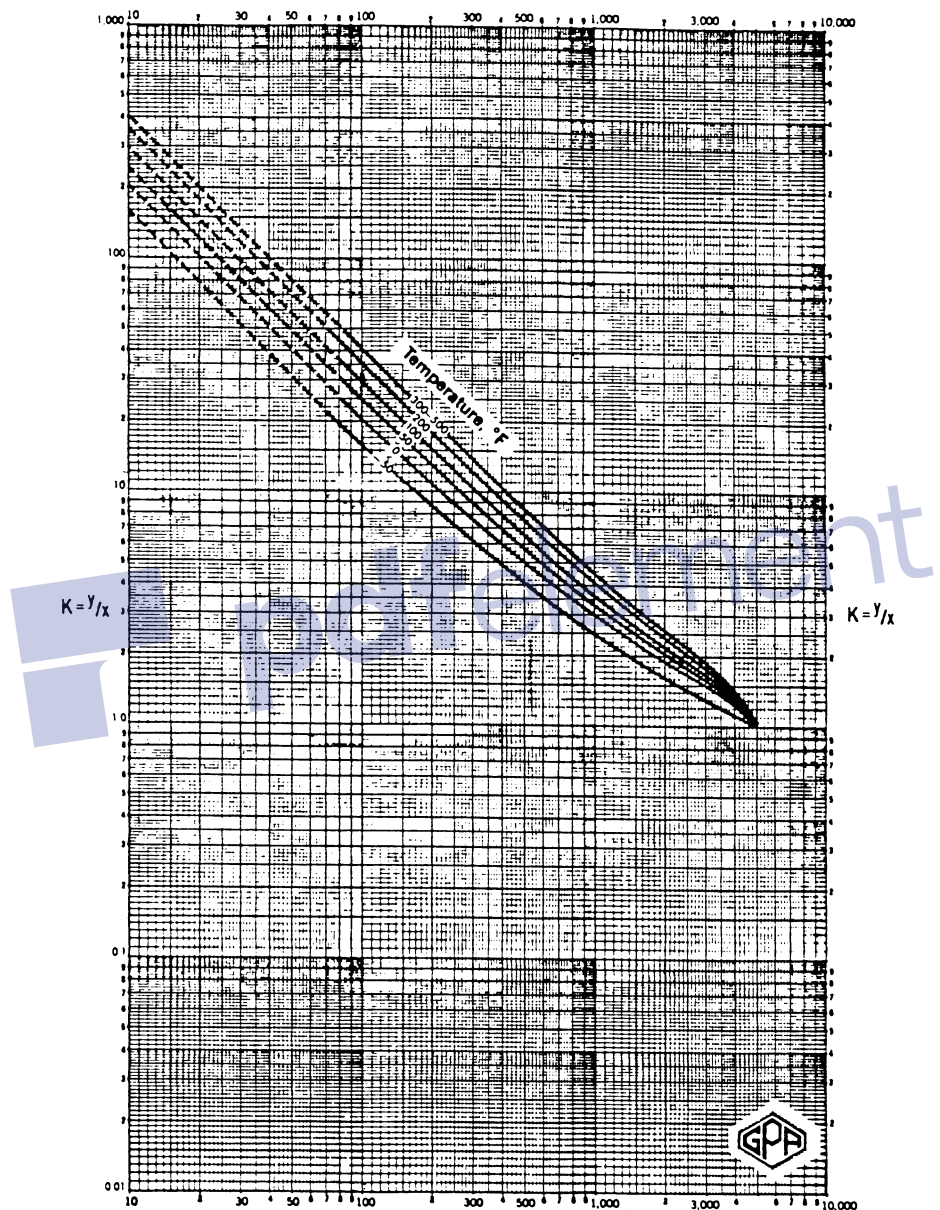


Figure 1. Methane. Conv. press. 5,000 psia. Courtesy of the Gas Processors Suppliers Association. Published in the GPSA Engineering Data Book, Tenth Edition, 1987.

© 2010 Elsevier Inc. All rights reserved.
Doi: 10.1016/C2009-0-30429-8

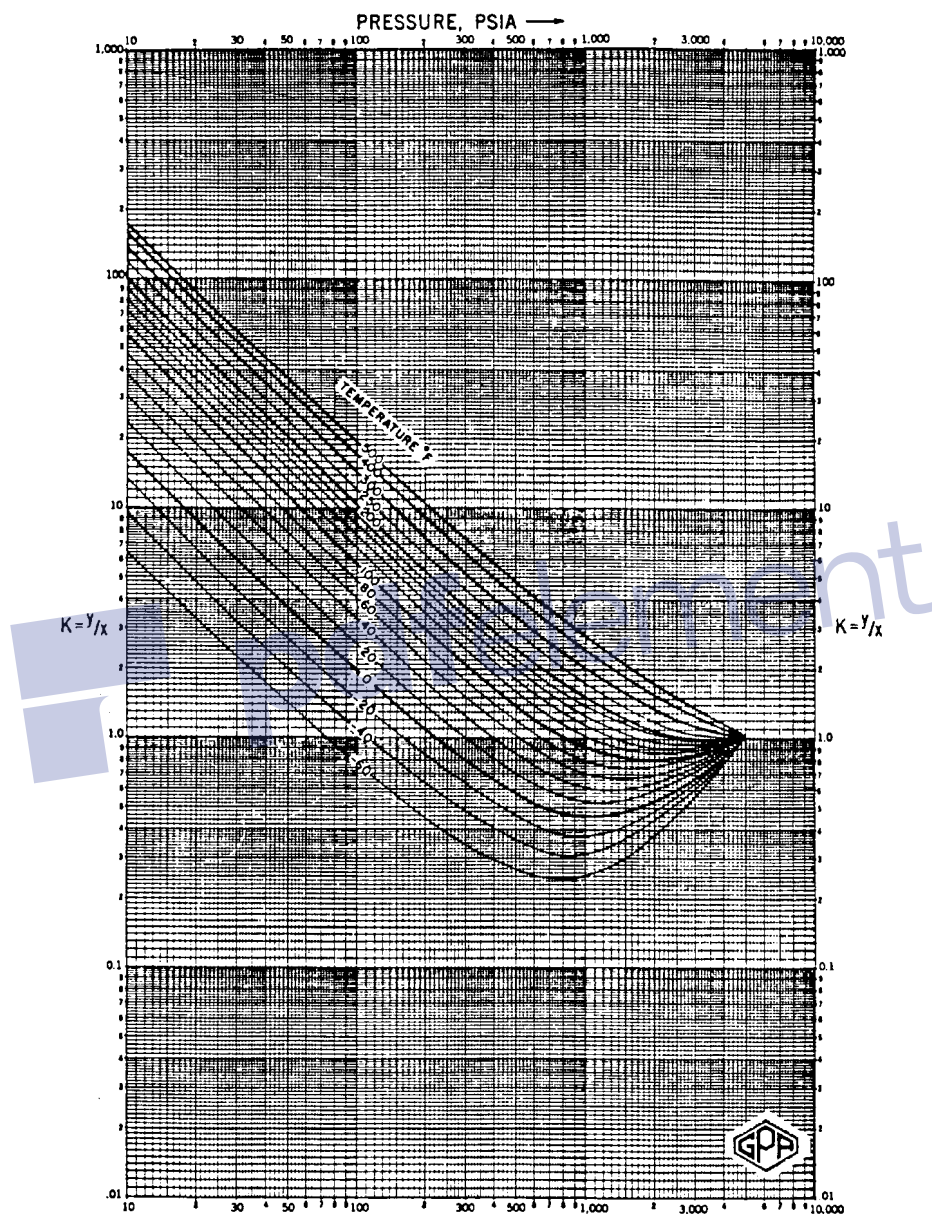


Figure 2. Ethane. Conv. press. 5,000 psia. Courtesy of the Gas Processors Suppliers Association. Published in the GPA Engineering Data Book, Tenth Edition, 1987.

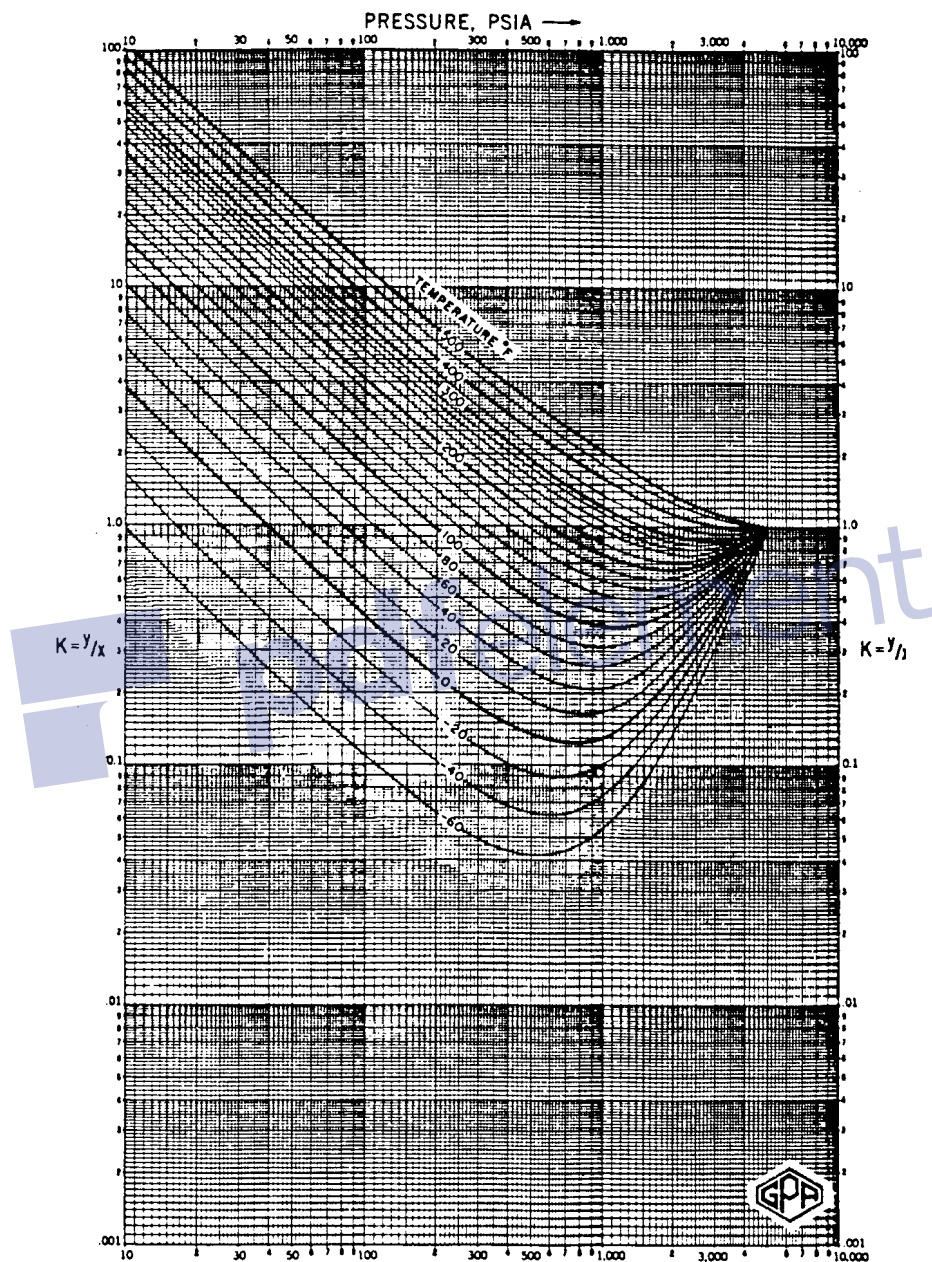


Figure 3. Propane. Conv. press. 5,000 psia. Courtesy of the Gas Processors Suppliers Association. Published in the GPSA Engineering Data Book, Tenth Edition, 1987.

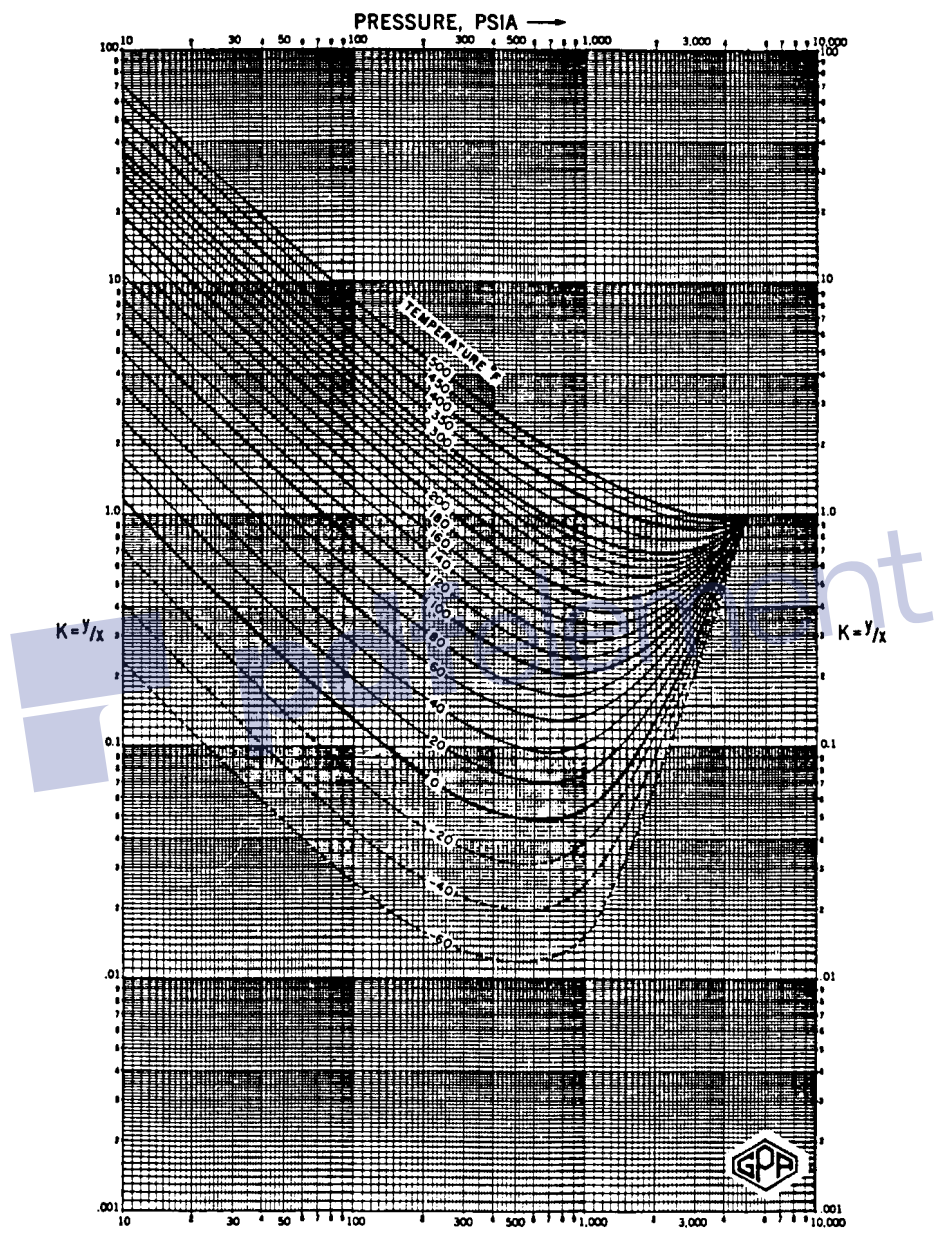


Figure 4. i-Butane. Conv. press. 5,000 psia. Courtesy of the Gas Processors Suppliers Association. Published in the GPSA Engineering Data Book, Tenth Edition, 1987.

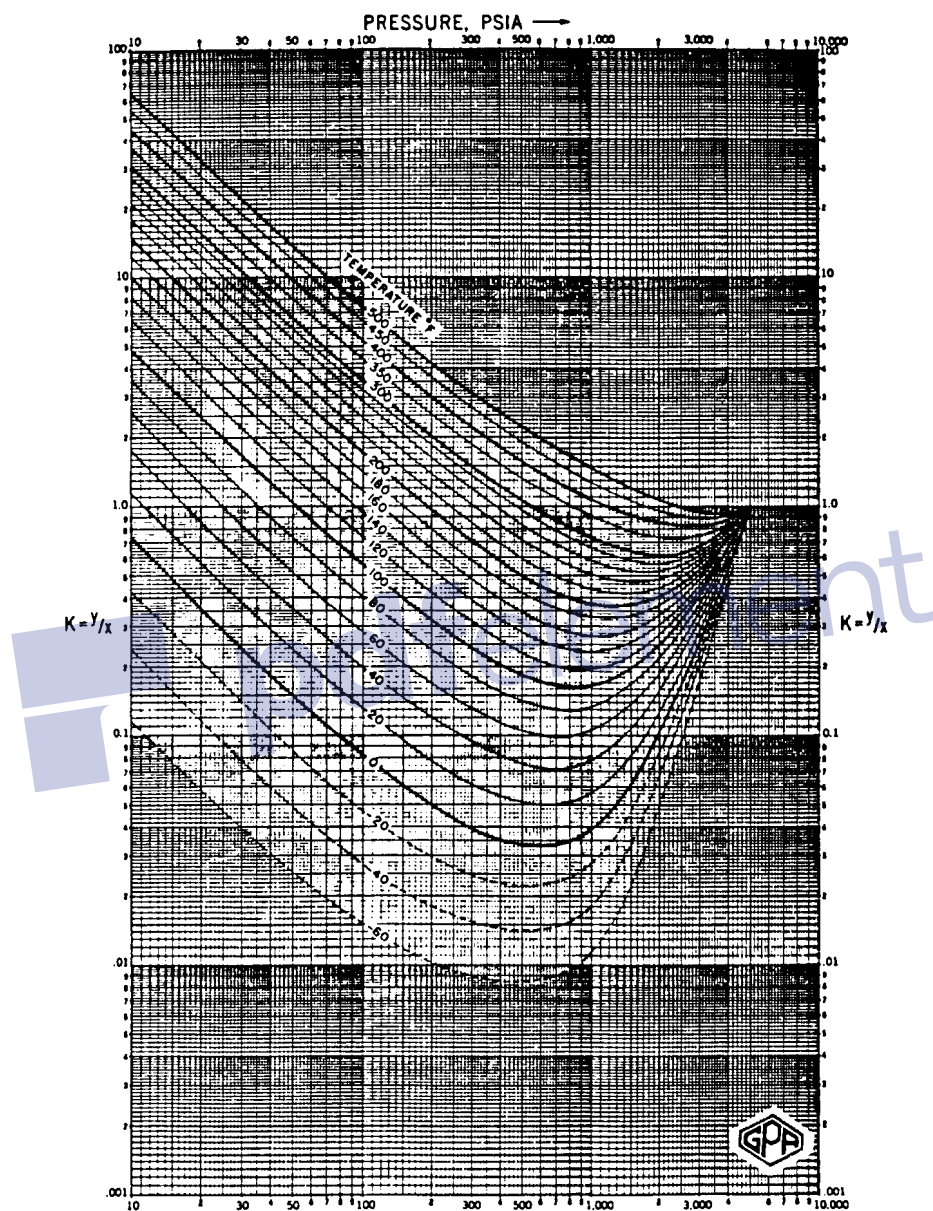


Figure 5. n-Butane. Conv. press. 5,000 psia. Courtesy of the Gas Processors Suppliers Association. Published in the GPSA Engineering Data Book, Tenth Edition, 1987.

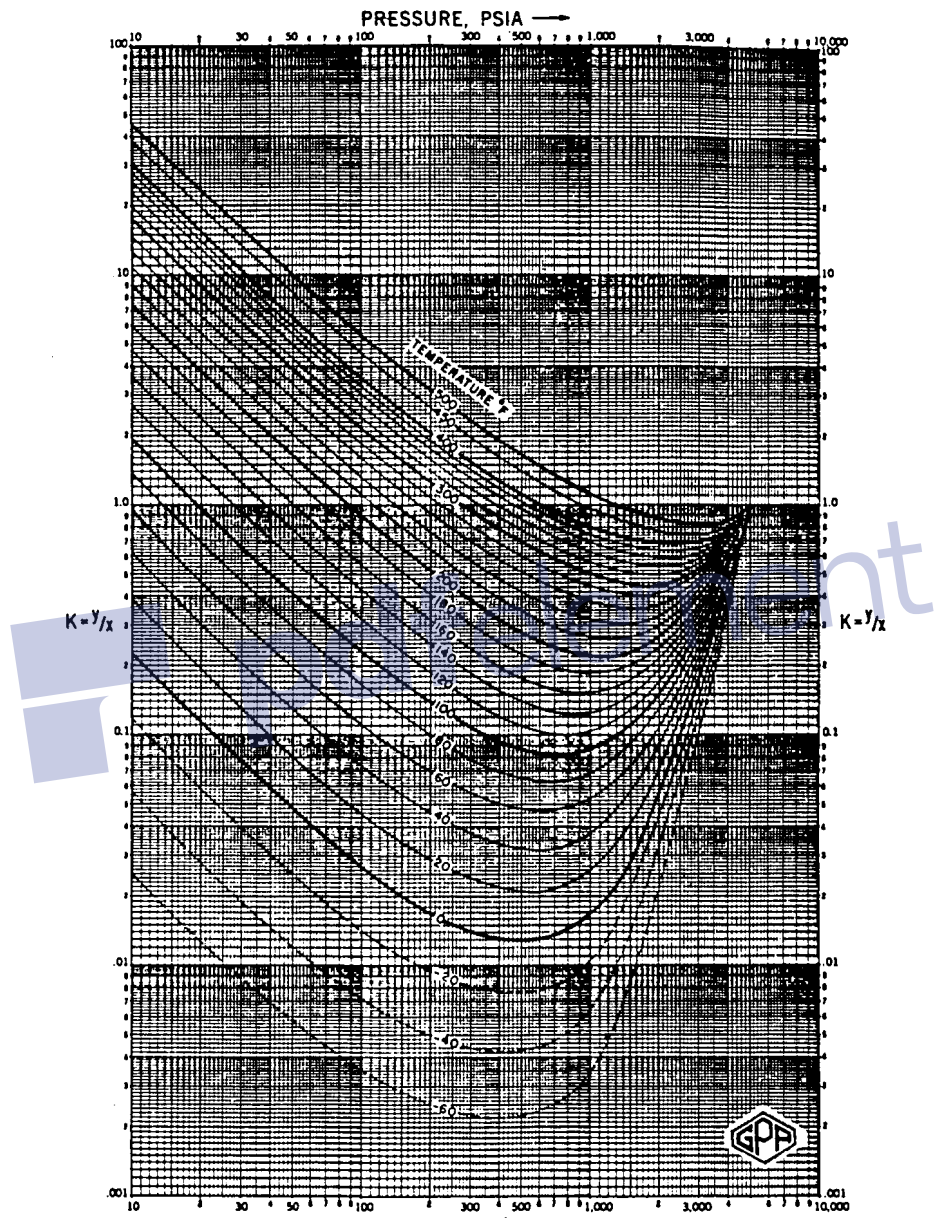


Figure 6. i-Pentane. Conv. press. 5,000 psia. Courtesy of the Gas Processors Suppliers Association. Published in the GPSA Engineering Data Book, Tenth Edition, 1987.

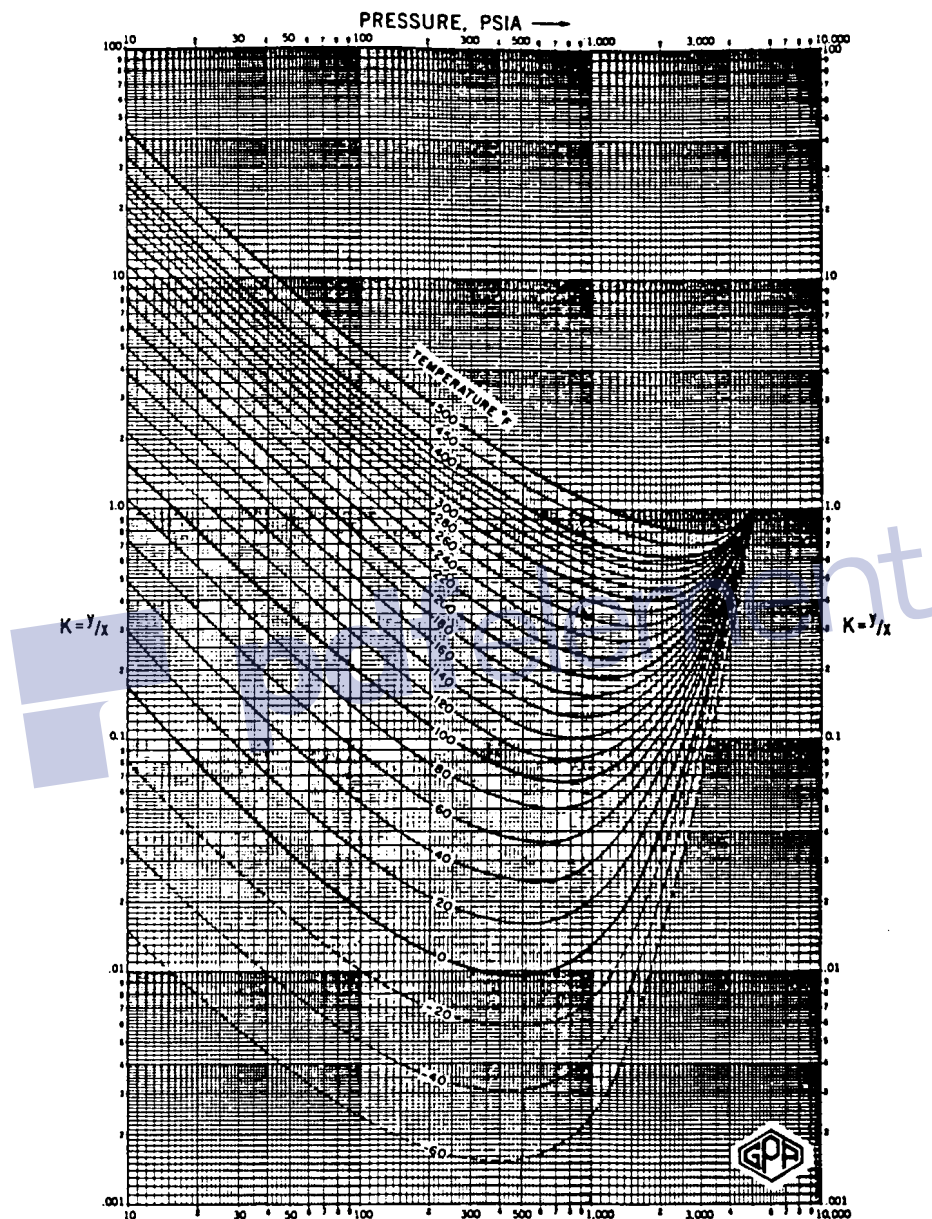


Figure 7. n-Pentane. Conv. press. 5,000 psia. Courtesy of the Gas Processors Suppliers Association. Published in the GPSA Engineering Data Book, Tenth Edition, 1987.

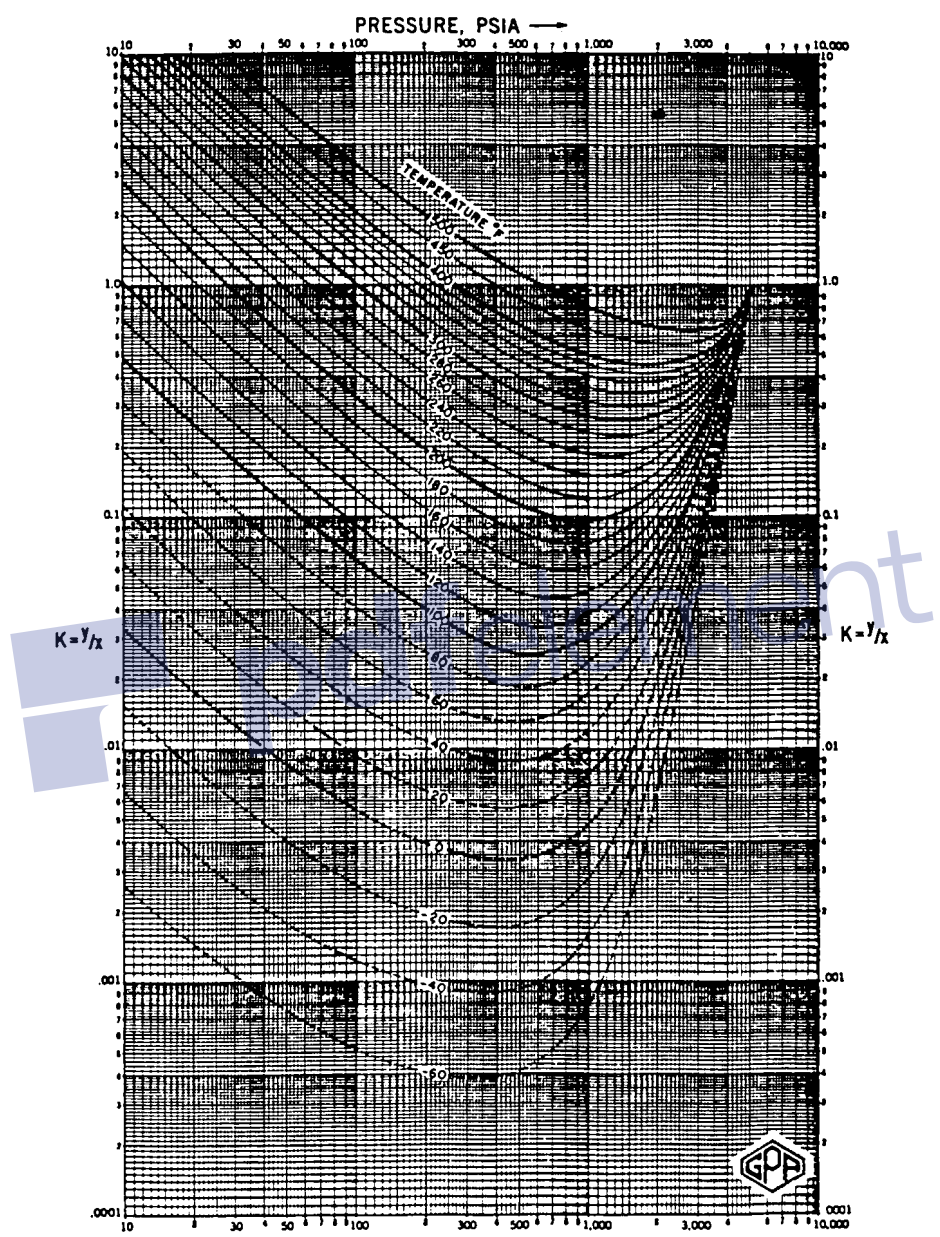


Figure 8. Hexane. Conv. press. 5,000 psia. Courtesy of the Gas Processors Suppliers Association. Published in the GPSA Engineering Data Book, Tenth Edition, 1987.

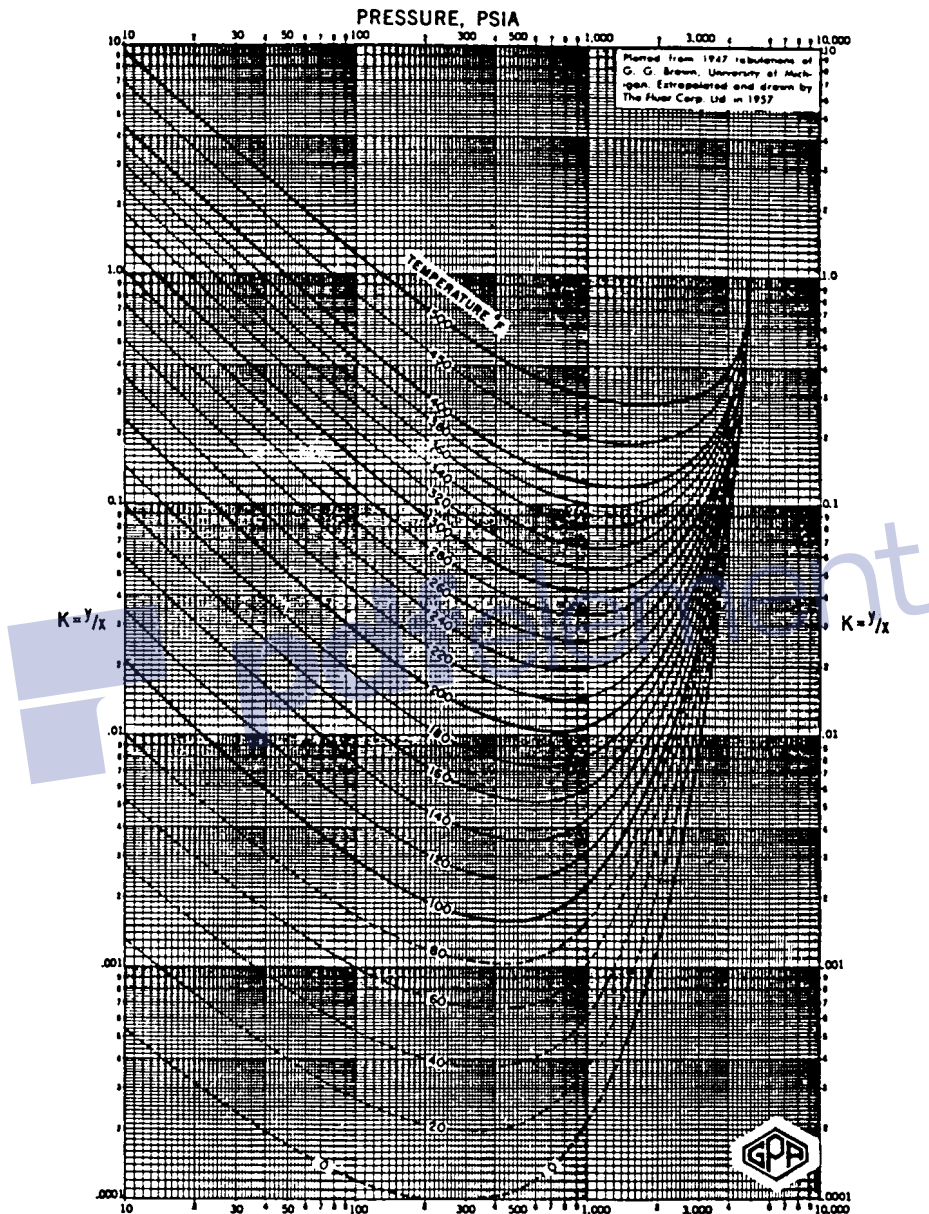


Figure 11. Nonane. Conv. press. 5,000 psia. Courtesy of the Gas Processors Suppliers Association. Published in the GPSA Engineering Data Book, Tenth Edition, 1987.

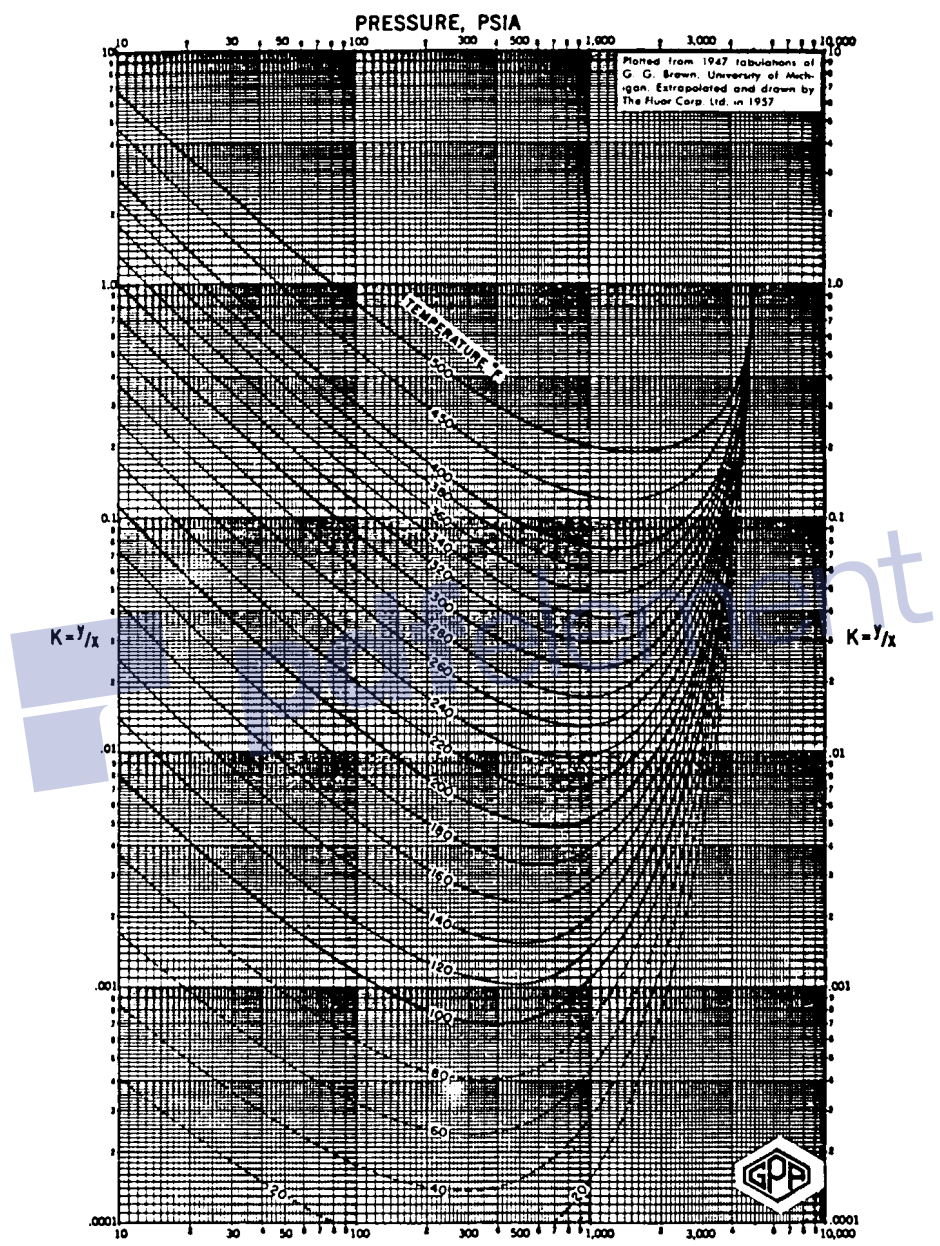


Figure 12. Decane. Conv. press. 5,000 psia. Courtesy of the Gas Processors Suppliers Association. Published in the GPSA Engineering Data Book, Tenth Edition, 1987.

INDEX

A

- Absolute
 - open flow, 488
 - permeability correlations, 250
 - porosity, 190
- Absolute open flow, 488
- Acentric factor, 25
 - correlations, 26
- After-breakthrough production, 976
- Ahmed's splitting scheme, 1215
- Alani-Kennedy equation, 1149
- API gravity, 76
- Apparent molecular weight, 32
- Aquifer, 651
 - boundary conditions, 653
 - classification, 651
 - flow geometry, 653
 - flow regimes, 653
 - prediction models, 655
- Areal sweep efficiency (E_A), 985
- Asymmetric mixture, 1179
- Average reservoir pressure, 419, 770, 866

Averaging

- permeability, 241
- porosity, 184
- relative permeability, 313
- saturation, 197

B

- Back pressure
 - equation, 556
 - plot, 557
- Baurdet and Gringarten model, 1355
- Behavior of real gases, 36
- Bilinear flow, 1386
- Binary interaction coefficient, 1172
- Bottom-water drive, 669, 692
- Breakthrough, 965
- Bubble-point pressure, 86, 871
 - curve, 3
 - definition of, 86
 - methods of determining, 86, 1125, 1198, 1201
 - phase equilibrium, 1179
- Buildup testing, 467

- Bulk compressibility coefficient, 255
- C**
- Campbell's equilibrium ratio method, 1121
- Capillary pressure, 203
curve, 208
definition, 203
hysteresis, 209, 211
- Carter-Tracy water influx model, 718
- Carter type curve, 1291
- Characterizing petroleum fractions, 25
- Combination drive, 801
- Component, 1096
- Compressibility coefficient
bulk, 255
definition, 59
formation, 256
gas, 59
matrix, 255
oil, 98, 148
pore, 255
- Compressibility factor
calculation, 38, 1159
definition, 37
- Compressibility of natural gases, 59
- Concept of permeability jail, 1339
- Condensate
liquid dropout, 182
retrograde, 171
- Conductance ratio, 1016
- Cone, 585
stable, 585
unstable, 585
- Coning, 583
gas, 588
in horizontal wells, 629
in vertical wells, 587
water, 589
- Constant
composition tests, 137, 174
terminal pressure, 384
terminal rate, 384
volume depletion tests, 176
- Convergence pressure, 1113
Hadden's method, 1115
Rzasa's method, 1118
Standing's method, 1117
- Correcting
constant-composition data, 164
differential liberation data, 166
separator data, 169
viscosity data, 167
- Counterflow, 945
- Cox chart, 1097
- Craig-Geffen-Morse oil recovery prediction method, 1065
- Cricondenbar, 3
- Cricondentherm, 3
- Critical
compressibility factor, 26
flow rate, 586
point, 3
pressure, 3
temperature, 3
- Crude oil
density, 97, 141, 1142
gravity, 75
properties, 74
- Cubic equation of state, 1158
- D**
- Dalton's Law, 1099, 1107
- Darcy's Law, 228
- Dead-oil viscosity, 115

- Decline curve analysis, 1235
 - Exponential decline, 1237, 1241
 - Harmonic decline, 1238, 1249
 - Hyperbolic decline, 1238, 1250
 - Deliverability equation, 556
 - Density calculations, 1142
 - Depletion-drive mechanism, 735, 761
 - Desaturating process, 210
 - Dew-point, 11, 1179
 - curve, 3
 - Dew-point pressure, 3, 1179
 - definition of, 1123, 1195
 - methods of determining, 1195, 1201
 - Differential liberation, 149
 - Differential separation, 1130
 - Diffusivity equation, 381
 - Dimensionless
 - diffusivity equation, 395
 - gravity number, 1039
 - pressure, 393
 - radius, 394
 - time, 394
 - Displacement efficiency (E_D), 934
 - Downdip flow, 943
 - Drainage process, 293
 - Drawdown test, 454
 - Driving mechanisms, 761
 - combination, 752
 - depletion, 735
 - gas-cap, 787
 - gravity-drainage, 746
 - solution gas, 735, 761
 - water-drive, 792
 - Dry-gas reservoirs, 15
 - Dykstra-Parsons
 - Modified, 1062
 - oil recovery prediction method, 1059
 - permeability variation method, 1042
 - sequencing technique, 1046
- E**
- E_i -function, 385
 - Edge-water drive, 669
 - Edmister correlation, 1178
 - Effective
 - permeability, 289
 - porosity, 191
 - wellbore radius, 437
 - End-point mobility ratio, 1050
 - Energy plots, 866
 - Equation(s) of state, 1134
 - applications, 1194
 - cubic, 1158
 - Peng-Robinson, 1182, 1203, 1295
 - Redlich-Kwong, 1160
 - Soave-Redlich-Kwong (SRK), 1169, 1205
 - Van der Waals, 1150
 - vapor pressure, 1205
 - Equilibrium ratio, 1099
 - applications, 1122
 - Campbell's method, 1121
 - determination of, 1194
 - Katz's method, 1122
 - phase equilibrium, 1179
 - for plus fractions, 1120
 - for real solutions, 1107
 - three-phase, 1199
 - Winn's method, 1121
 - Equilibrium separation, 1130
 - Equivalent time, 1364
 - Exponential integral, 385
 - Extrapolation of reservoir fluid data, 164

F

Felsenthal, Cobb, and Heuer oil
recovery prediction method,
1062

Fetkovich's

IPR equation, 509

method, 509

Type curve, 1275

Water influx, 722

Fill-up, 1027

Finite-radial reservoir, 398

Flash calculations, 1103, 1202

Flash separation, 1130

Flood patterns, 927

Confinement, 1080

Conformance, 1082

Flow

equations, 340

periods fractured wells,

1384

regimes, 334

Flowing material balance,

1308

Fluids

classification of, 1

injectivity, 1012

properties, 29

Formation compressibility, 254

Correlations, 259

Formation linear flow, 1394

Formation volume factor

gas, 65

oil, 92

Fractional flow equation, 936

Fracture linear flow, 1385

Fractures

Finite-conductivity, 1322

infinite-conductivity, 1322

Uniform-flux, 1323

Fractured

Carbonates, 1341

Reservoirs, 1338

Sandstones, 1346

Shales, 1344

Wells, 1321

Free water level, 213

Frontal advance equation, 952

Frontal displacement theory, 936

Fugacity, 1175

coefficient, 1176

Fundamentals of

reservoir fluid behavior, 1

reservoir fluid flow, 331

rock properties, 189

G

Gas

coning, 583

dry gas, 10, 15

fugacity, 1175

material balance equation,

859

in place, 856

properties, 29

reservoirs, 10, 855

saturation, 873

solubility, 78

viscosity, 68

well performance, 546

wet gas, 10

Gas-cap drive reservoirs, 787

Gas-condensate reservoirs, 10

Gas-oil ratio, 372

Gas solubility correlations, 78

Gas well performance, 546

Geometric

average permeability, 249

shape factor, 1350

- Gravity
 crude oil, 75
 solution gas, 76
 Gravity-drainage reservoirs, 746
- H**
- Hadden's convergence pressure
 method, 1115
 Hall Plot, 1071
 Harmonic average permeability,
 245
 Havlena and Odeh, 772
 Heptanes-plus fraction, 1191, 1207
 Heterogeneity, 261
 vertical, 261
 High shrinkage oil, 6
 Hong's mixing rules, 1222
 Horizontal
 heterogeneity, 261, 274
 well breakthrough, 624
 gas, 577
 oil, 528
 Horner's plot, 470
 Hurst and van Everdingen, 668
 Hurst's steady-state method, 663
 Hydraulically fractured wells,
 1375
- I**
- Image wells, 450
 Imbibition process, 296
 Incompressible fluids, 332
 Infinite
 acting, 374, 396
 acting pseudoradial flow, 1397
 Infinite-conductivity
 fractures, 1381
 vertical fractures, 1380
- Inflow performance relationships
 gas, 547
 oil, 488
 Injection rate, 1012
 Interfacial tension, 200
 Interference, 1012
 Interporosity flow coefficient,
 1351
 IPR, 484, 488
 Fetkovich's, 509
 Standing's, 505
 Vogel's, 493
 Inverse distance method, 276
 Inverse distance squared method,
 277
 Isothermal compressibility
 coefficient
 gas, 59
 oil, 98
 rock, 254
- J**
- J-function, 224
- K**
- Katz's
 equilibrium ratio method, 1122
 splitting scheme, 1210
 Kay's mixing rules, 1223
 Klinkenberg effect, 234
- L**
- Laboratory PVT tests, 136
 routine, 136
 special, 136
 Laminar flow, 342
 Laminar-Inertial-Turbulent, 558

- Layers, minimum number of, 1043
 Lee and Kessler correlation, 1178
 Lee's mixing rules, 1223
 Leverett J-function, 224
 Linear flow, 338
 Liquid dropout, 12
 LIT approach, 558
 Lohrenz's splitting scheme, 1212
 Lorenz coefficient, 268
 Lost oil saturation, 824
 Low-shrinkage oil, 5
 Lumping schemes, 1218
 Whitson's, 1219
- M**
- m(p)-solution method, 405
 Material balance equation (MBE),
 733, 958
 gas, 958
 oil, 733
 straight-line, 772
 Material balance pseudo-time,
 1301
 Matrix compressibility coefficient,
 254
 Maximum liquid dropout, 13
 Method of images, 450
 Mixing rules, 1161, 1222, 1223
 Mobility ratio, 987
 Muskat's material balance method,
 838
- N**
- Natural gases, compressibility of,
 59
 Naturally fractured reservoirs,
 1340
 Near-critical crude oil, 8
 Near-critical gas condensate, 10
 Non-Darcy flow, 438
 Nonstabilized zone, 957
 Normalized material balance
 pseudo-time, 1301
 Normalizing relative permeability,
 313
- O**
- Odeh and Havlena, 772
 Oil formation volume factor, 92
 for undersaturated oils, 103
 Oil material balance equation, 773
 Oil properties, 74
 Oil recovery
 predicting, 81
 Oil reservoirs, 4
 Oil saturation, 824
 Oil saturation adjustment
 for combination drive, 822
 for gas-cap expansion, 820
 for water influx, 819
 Oil viscosity, 115
 Oil-water contact, 213
 Oil well performance, 484
 Optimum gas saturation, 922
 Optimum separator pressure,
 1131
 Ordinary black oil, 4
- P**
- p/z gas equation, 861
 pattern balancing, 1079
 Pedersen's splitting scheme, 1214
 Peng-Robinson equation of state,
 1182, 1203, 1205
 Permeability, 227
 absolute, 227

- averaging, 242
 - effective, 289
 - relative, 288
 - variation, 262
 - Permeability
 - jail, 1339
 - ordering, 1046
 - Phase diagram, 2
 - Phase equilibrium, 1179
 - Plant products, 173
 - Plus fractions, 1191, 1207
 - lumping, 1218
 - splitting, 1208
 - Poisson's ration, 1377
 - Polygon method, 276
 - Pore
 - compressibility coefficient, 255
 - volume, 192
 - Porosity, 190
 - absolute, 190
 - effective, 191
 - Porosity averaging methods, 194
 - Positional permeability variation, 1046
 - Pot aquifer, 655
 - Predicting oil reservoir performance
 - Craig-Geffen-Morse method, 1065
 - Dykstra-Parsons method, 1069, 1062
 - Felsenthal, Cobb, and Heuer method, 1062
 - Muskat's method, 838
 - Turner's method, 843
 - Tracy's method, 831
 - Pressure
 - bubble-point, 3, 86, 1125, 1198, 1201
 - buildup, 467
 - drawdown, 454
 - drop due to skin, 472
 - capillary, 203
 - dew-point, 3, 1123, 1179, 1195, 1201
 - pseudo-critical, 38
 - pseudo reduced, 37
 - separator, 1128
 - squared approximation, 408
 - vapor, 1205
 - Pressure-approximate method, 404
 - Pressure-squared method, 404
 - Pressure-temperature diagram, 2
 - Primary
 - porosity, 1367
 - recovery mechanisms, 761
 - Probability-log scale, 264
 - Productivity index, 473
 - Properties of
 - crude oil systems, 74
 - natural gases, 29
 - rocks, 189
 - water, 124
 - Pseudocritical
 - pressure, 42
 - temperature, 42
 - Pseudoization, 1218
 - Pseudosteady-state flow, 413
- R**
- Radial
 - diffusivity equation, 382
 - flow of gases, 429
 - Raoult's Law, 1099, 1107
 - Real solutions, 1107
 - Redlich-Kwong equation of state, 1162
 - Reduced gas density, 56

- Reduced pressure, 37
 - Reduced temperature, 37
 - Relative oil volume, 141
 - Relative permeability, 288
 - averaging, 313
 - concepts, 288
 - correlations, 296
 - three-phase, 320
 - two-phase, 289
 - Relative total volume, 141
 - Reservoir
 - apparent molecular weight, 32
 - composition of, 137
 - density, 33
 - fluid properties, 29
 - geometry, 336
 - heterogeneity, 261
 - ideal gases, 30
 - specific gravity, 34
 - specific volume, 33
 - standard volume, 33
 - water properties, 122
 - Reservoir drive mechanisms,
 - combination, 752
 - gas-cap, 787
 - solution gas-drive, 735
 - water-drive, 792
 - Reservoirs, classification of, 1
 - Residual oil saturation, 196
 - Retrograde gas reservoirs, 10
 - Riazi and Daubert correlation, 1191
 - Rock
 - compressibility, 254
 - properties, 189
 - Routine laboratory PVT tests, 136
 - Rzasa's convergence pressure method, 1118
- S**
- Saturated oil
 - reservoirs, 4
 - viscosity, 117
 - Saturation, 189
 - averaging, 195
 - critical oil, 196
 - movable oil, 196
 - pressure, 137
 - residual oil, 196
 - trapped gas, 873
 - water, 197
 - Schilthuis's steady-state method, 655, 659
 - Secondary Porosity, 1367
 - Semisteady-state, 336, 414
 - Separator tests, 146, 152
 - Shallow gas reservoirs, 900
 - Shape factor, 423, 466
 - Shock front, 967
 - Shrinking gas cap, 822
 - Skin factor, 431
 - Soave-Redlich-Kwong (SRK)
 - equation of state, 1168
 - modifications of, 1178
 - Splitting schemes, 1108
 - Ahmed's, 1215
 - Lohrenz's, 1212
 - Pedersen's, 1214
 - Stabilized zone, 957
 - Stage separation, 1128
 - Standing-Katz density calculation method, 1142
 - Standing's
 - convergence pressure method, 1117
 - correlation, 1108, 1166
 - IPR equation, 505
 - Steady-state flow, 334, 342

Stiles' permeability variation
 method, 1050
 Stone's I model, 324
 Stone's II model, 326
 Storativity ratio, 1351
 Superposition, 442
 Surface tension, 121, 200

T

Tarner's method, 843
 Three-phase equilibrium, 1199
 Three-phase relative permeability,
 320
 correlations, 322
 Tight gas reservoirs, 866
 Time
 end of infinite-acting, 465
 Total formation volume factor,
 159
 Tounqing, 1038
 Tracy's
 form of the MBE, 803
 method, 831
 Transition zone, 213
 Trapped gas saturation, 873
 Turbulent flow factor, 437
 Two-phase
 Formation volume factor, 108,
 159
 relative correlations, 296
 relative permeability, 289
 z-factor, 178
 Type-curve
 Anash, 1311
 Carter, 1292
 Fetkovich, 1275
 Fractured wells, 1321, 1326
 Palacio-Blasingame, 1299
 Type-curve analysis, 1264

U

Undefined petroleum fractions, 24
 Undersaturated oil
 reservoirs, 4, 825
 viscosity, 117
 Uniform-flux fractures, 1381
 Unsteady-state flow, 373

V

Van der Waals equation of state,
 1149
 Van Everdingen-Hurst's unsteady-
 state model, 668
 Vapor pressure, 1096, 1205
 Vertical
 gas well performance, 546
 heterogeneity, 262
 oil well performance, 484
 sweep efficiency (E_V), 1061
 Viscosity
 dead oil, 115
 gas, 67
 oil, 114
 saturated oil, 117
 undersaturated oil, 119
 water, 125
 Vogel's
 IPR equation, 493
 Volatile crude oil, 6
 Volume translation method, 1180
 Volumetric sweep efficiency, 934

W

Warren and Roots model, 1349
 Water
 properties, 124
 viscosity, 125

- Water coning, 589
 - Water-drive reservoirs, 792
 - gas, 870
 - oil, 792
 - Water fingering, 1038
 - Waterflooding
 - Factors to consider, 910
 - optimum time, 915
 - patterns, 927
 - recovery factor (RF), 932
 - surveillance, 1069
 - trapped gas, 865
 - Water influx, 650
 - Carter-Tracy model, 718
 - Fetkovich's model, 722
 - Water isothermal compressibility, 126
 - Water-oil ratio, 372, 946
 - Waterflood surveillance, 1069
 - Wellbore storage, 460
 - Wet-gas reservoirs, 14
 - Wettability, 199
 - Whitson and Torp correlation, 1119
 - Whitson's lumping scheme, 1219
 - Wilson's correlation, 1108, 1118
 - Winn's equilibrium ratio method, 1121
- X**
- X-plot, 1075
- Y**
- Y-function, 143
 - Young's modulus, 1377
- Z**
- Zonation problem, 1046
 - Z-factor, 37, 151